UCRL-PROC-207967

LAWRENCE
LIVERMORE
NATIONAL
LABORATORY

Short-Pulse Laser-Matter Computational Workshop Proceedings

Richard Town, Max Tabak

November 2, 2004

Short-Pulse Laser-Matter Computational Workshop
Pleasanton, CA, United States
August 25, 2004 through August 27, 2004

Disclaimer

This work was performed under the auspices of the U.S. Department of Energy by the University of California, Lawrence Livermore National Laboratory under Contract No. W-7405-Eng-48.

Introduction

For three days at the end of August 2004 55 plasma scientists met at the Four Points by Sheraton in Pleasanton to discuss some of the critical issues associated with the computational aspects of the interaction of short-pulse high-intensity lasers with matter. The workshop was organized around the following six key areas:

- Laser propagation / interaction through various density plasmas: micro scale.
- Anomalous electron transport effects: From micro to meso scale.
- Electron transport through plasmas: From meso to macro scale.
- Ion beam generation, transport, and focusing.
- "Atomic-scale" electron and proton stopping powers.
- Kα diagnostics.

Each area had a coordinator who drew up a list of questions, moderated discussions, and has written a brief summary of their working groups.

This CD contains the agenda, the workshop questions, the presentations made, and this workshop summary. Please do not reproduce any figures, or presentations without first contacting the first author of the work.

The workshop was made possible by the generous financial support of the *Institute for Laser Science and Applications* and the *Institute for Scientific Computing Research* at the *Lawrence Livermore National Laboratory*.

Laser propagation / interaction through various density plasmas: micro scale – *Chuang Ren (University of Rochester).*

Many important problems in fast ignition are related to laser-plasma interactions. These include:

- laser propagation in the underdense corona plasma;
- laser hole-boring in the overdense plasma;
- laser absorption and energetic electron production at the critical surface; and
- electron transport in the mildly-dense plasma region.

The best-understood and most detailed model for laser-plasma interactions is the explicit particle-in-cell (PIC) model, which is based on the relativistic Newton's equation and Maxwell's equations and resolves the smallest relevant space and time scales. There is a consensus among the PIC community that different PIC codes should give statistically equivalent results when simulating the same problem using the same simulation parameters (such as resolution and number of particle/cell.) However, the PIC model is computationally intensive. Currently it is not feasible to simulate a three-dimensional fast ignition pellet in its entirety. We have to study scaled-down (smaller size and/or two-dimensional) systems. Therefore, it is important to understand how simulation conditions such as system size, dimensionality, and boundary conditions affect simulation results. In the future, devoted experiments with comparable laser and plasma parameters can be done to check the validity of the results from these scaled-down simulations.

Proposed benchmarks:

For all of the following 3 runs, the plasma is at 40 n_c with sharp edges and at an electron temperature of 7 keV. The particle boundary conditions are periodic in the transverse directions and in contact with a thermal bath (maintained at the initial plasma temperature) in the longitudinal direction. The laser wavelength is 1 micron at an intensity of 10^{20} W/cm^2 with a fwhm of 6 micron, and lasts for 1 ps. The field boundary conditions are periodic in the transverse directions and absorbing in the longitudinal direction.

Run 1 (2D): simulation box: 50 micron long and 20 micron wide; plasma: 30 micron long and 20 micron wide.

Run 2 (2D): simulation box: 50 micron long and 40 micron wide; plasma: 30 micron long and 20 micron wide.

Run 3 (3D): simulation box: 40 micron long and 30 micron wide; plasma: 30 micron long and 20 micron wide.

The participants should run these calculations using their standard resolution.

Anomalous electron transport effects: From micro to meso scale – *Hartmut Ruhl (University of Nevada, Reno).*

Electron transport through plasmas: From meso to macro scale – *Roger Evans (AWE/Imperial College London) and Dale Welch (Mission Research Corporation).*

The mesa through macro electron transport group focused primarily on the correct method of initiating the electron beam. Several phenomenological techniques were discussed such as injection at a plane in free space, promotion of ambient electrons, and the use of a ponderomotive force. It was generally agreed that the boundary conditions in the laser-plasma interaction (LPI) region were critical to the problem set up. A two region approach, in which the LPI is simulated in the blow off plasma and hybrid methods are used in the solid density material, being explored with LSP in 3D cylindrical coordinates might be a reasonable intermediate step.

The behavior of the resisitive filamentation instability in very dense collisional plasmas was thought to be important as it may affect the collision frequencies and energy loss rates used in the meso-scale calculations. This might be approached analytically or via a very small scale PIC model.

The experiments described at the session showed a trend for there to be less energy deposited into the bulk of the targets than was expected from the extrapolation of earlier experiments. Inhibition of the electron beam by electric and magnetic fields near the critical density region were one possible explanation and show the need for a self-consistent treatment of the LPI region in the larger scale models. The lack of electron penetration is observed to be accompanied by rapid lateral transport as seen in old CO_2 laser experiments, the role of cones around the laser beam in directing this lateral transport into more useful deposition is of continuing interest. Experimental data remains inconclusive and modeling may help to elucidate the underlying physics.

Results of explicit and hybrid PIC, as well as Vlasov simulation methods, were presented. It was agreed upon that high resolution PIC and Vlasov codes should be used as a check of hybrid PIC models. Sub-grid models for dealing with micro-scale phenomena, such as the Weibel instability, should also be investigated. The implementation of more complex atomic physics, possibly non-LTE, was also identified as an area for future work.

Proposed benchmarks:

We have defined some beam injection conditions for the LSP / hybrid / FP models. Two target materials, say Carbon and Aluminum since they appear to behave quite differently in LSP, and two 'irradiances' say 10^{18} W/cm^2 and 10^{20} W/cm^2. Since most codes do not have a laser deposition package it is necessary to choose the beam parameters. For simplicity the following mono-energetic injection is suggested: 500 keV and 4 x 10^{11} amp cm^{-2} for 10^{18} W/cm^2 with 20% efficiency with a transverse temperature of 50keV; and 5 MeV and 4 x 10^{12} for 10^{20}W/cm^2 with a transverse temperature of 500keV. The injected electron beam should have a spot size of 10 microns Gaussian (FWHM). The temporal pulse shape should be a1ps square with the beam energy constant in time. Treatment of resistivity and EoS is up to the application but we could have Spitzer and perfect gas as a standard comparator.

Ion beam generation, transport, and focusing – *Scott Wilks (Lawrence Livermore National Laboratory)*

The following topics were discussed during the ion beam generation sessions:

- What are the proton generation mechanisms?
  Five mechanisms were identified:
  1) Filamentation in the under-dense plasma.
  2) Light pressure / snowplow.

3) “Bulk” ion heating.
4) Target normal sheath acceleration (TNSA) on the back surface.
5) Self-similar on front surface.

- What are their efficiencies?

  Experimentally it was noted that the efficiency scales with laser energy. Sentoku presented PIC calculations on proton production efficiencies. His simulations showed higher efficiency for shorter pulse lengths for rear-surface acceleration, but the converse for front-surface acceleration.

	E_{max} (MeV)	ΔE (%)	η_{eff} (%)
Pondermotive filamenation	$\sim v^2_p m_i$	~100 (?)	?
Snowplow	$\sim v^2_p m_i$	f_{ion}	f_{ion}
TNSA		10<ΔE<100	~1-20
Self-similar	$\sim c^2_s m_i$	~100	

Where:

$$f_{ion} = 2\sqrt{\frac{n_{cr}}{n_p} \bullet \frac{Zm_e}{m_z} \bullet \frac{I\lambda^2}{2.74\times10^{19}}}$$

$$V_p = \left(\frac{4I}{m_i}\right)^{1/3} \frac{c}{\varpi_p}$$

$$\frac{V_f}{c} = \sqrt{\left(\frac{n_c}{2n_p}\frac{Zm_e}{m_i}\frac{I\lambda^2}{2.74\times10^{19}}\right)} + 1.5U$$

- How sensitive to resolution are the answers?
- What codes can be used?

  A first-cut assessment of code capabilities was undertaken (✓- can be used; X – cannot be used; ? unclear):

Mechanism	PIC	Fluid	Hybrid-PIC	Reduced Description	Fokker-Planck
Pondermotive	✓			X	
Snowplow	✓ ½		✓ ½	X	
Bulk Ion	X	✓		X	
TNSA	✓	✓	✓	?	
Self-similar	✓	✓	✓	?	
Proton transport	✓			✓	
Proton heating	X	X		✓	

- How does electron flow affect proton generation?
- How can we control the generation and focusing of the protons?
- What is the optimum proton energy for radiography?
- What are the qualities that set ions using these mechanisms apart from “standard” ion beams?

- What governs ion flux?
- What is the optimal distance of the "proton lens" from the target?

"Atomic-scale" electron and proton stopping powers – *Claude Deutsch (Université Paris XI)*

The following topics were discussed during the "Atomic-scale" stopping powers session:

- The stopping power of relativistic electron beams (REB) with energies of 1 to10 MeV stopping in pre-compressed DT targets with electron number densities (N_e) greater than 10^{22} cm^{-3};
- The stopping power of non-relativistic (NR) protons with energies of 1 to 100 MeV stopping in similar targets as above;
- Multiple scattering of REB on target ions;
- Multiple scattering of NR protons in thin foils of high Z materials disposed in front of laser proton sources (LPS) (c.f..M.Barriga-Carrasco and G.Maynard in Phys Rev E (to be published));
- Effective Charge Zeff encapsulating dynamical and in-flight correlation effects for REB stopping (cf. C. Thomas at Stanford University); and
- REB and NR proton stopping in strongly magnetized fast ignition targets with magnetic fields of the order of 1 to10 GigaGauss.

These topics were all felt to be of particular relevance to the fast ignition approach to achieving fusion energy.

The working group vigorously discussed these topics and reached the following consensus:

- The target temperature and corresponding electron partial degeneracy have only a small impact (<20%) on REB stopping performances as long as $N_e < 10^{27}$ cm^{-3} (K. Starikov and C. Deutsch Phys Rev E to be published);
- NR proton stopping requires a careful examination of its dependence on target temperature (H. Ruhl et al, U. Nevada, Reno); and
- Effective Zeff(vb) simulated using the LSP code seems to confirm the analytically-predicted enhanced correlated stopping in fast ignition targets (C. Thomas, Stanford University)

However, two issues remain outstanding:

The relative estimates of effective penetration depths (EPD) for REB in terms of their overall ranges was questioned by C K Li from M I T on the basis of his new calculations (to appear in Physics of Plasmas) involving simultaneous estimates of energy loss (mostly on target electron) and angular diffusion through multiple scattering on target ions. Earlier estimates based on separate evaluations of these two mechanisms could be relevant only for very thin targets. Further inquiries are obviously needed to settle this issue on a fundamental science basis. Nonetheless, it should be recalled that those two approaches are not expected to produce EPD differing by more than a factor of two, because the new approach is likely to result in a larger EPD relative to its shorter range when compared to outputs of the previous method. As a result the FIS ignition conditions elaborated by S. Atzeni (PoP Aug 1999) are not expected to be substantially modified.

It was felt that the fast ignition approach based on intense proton beams (cf M.Roth et al PRL jan.01) may have to be seriously modified to prevent too much proton-beam dispersion from multiple scattering in the high Z foil screening the laser-generated proton source. It is recommended to include that foil within the hohlraum to prevent 90 % of the protons miss DT target (M. Barriga-Carrasco and G. Maynard, Phys Rev E, to appear)

Proposed benchmarks:

- REB (E_b=1-50 MeV) effective penetration depths in fast ignition targets with $N_e > 10^{22}$ cm^{-3} and temperatures in the keV range.

- NR proton (E_b=1-100 MeV) ranges in the same fast ignition targets.

- NR proton (E_b=1-100 MeV) multiple scattering on thin foils (20-100 nm) of materials with 6 < Z < 92.

Kα diagnostics – *Mark Foord (Lawrence Livermore National Laboratory)*

The purpose of the K-α diagnostic sessions was to discuss some of the progress being made in modeling K-α emission in short pulse Petawatt laser experiments and to discuss with experimentalist some of their latest results. Hyun-Kyung Chung presented her non-LTE calculations of Cu, which indicated that except in extreme conditions, the ionization balance was typically determined by thermal electron conditions. At electron temperatures between 10-100 eV, which generate only slightly shifted K-α emission spectra, the equilibration times were found to be sub-picosecond and the plasmas reached near LTE ionization values. At kilovolt temperatures, Cu ionized to its He-like ion stage, producing shifted He-α spectra. The ionization times to produce the He-α emission are nearly a picosecond, which seemed consistent with the emission spectra and time-scales of recent RAL experiments.

Hye-Sook Park presented interesting data from a number of her experiments. An important issue for K-α backlighter development is how to maximize the backlighter efficiency on the track towards using higher Z materials needed for producing deeply penetrating high-energy photons. This relates the hot electron energy production generated by the Petawatt laser, the hot electron penetration depth, the degree of ionization of the material, and the self-absorption of the resulting K-α emission. How the overall efficiencies scale with photon energy is not well understood, and will require a strong coupling of experimental and modeling efforts. An interesting result discussed was the efficiency of K-α emission in a silver foil, which varied little with increasing foil thickness. One possibility given was that the insensitivity due to foil thickness may be due to a relatively small (10s of μm) self-absorption depth due to L-shell electrons, and thus the brightness would be determined at least partly due to this fixed self-absorption depth.

Steve Moon discussed interesting Lasnex simulations, which seemed to indicate fast hot thermal conduction on the picosecond timescale, in contrast to experimental results. Mark Foord, Hyun-Kyung Chung, and Mau Chen discussed progress being made in integrating their non-LTE calculations of ionization, fluorescence yields and radiation transport into the PIC-Hybrid simulation code LSP. Using fast tabular look-up routines that are coupled to LSP, the group hopes to be able to model the K-α emission in complex two- and three-dimensional geometries. This work should allow a better understanding of electron transport in solids as well as provide a useful tool for improving the backlighter efficiency in Petawatt laser produced targets.

Short Pulse Laser Matter Computational Workshop Attendees

Afeyan	Bedros	Polymath Research Inc.
Barnard	John	Lawrence Livermore National Laboratory
Bell	Tony	Imperial College
Betti	Riccardo	University of Rochester
Charman	Andrew	University of California, Berkeley
Chung	Hyun-Kyung	Lawrence Livermore National Laboratory
Cottrill	Larissa	Massachusetts Institute of Technology
Deutsch	Claude	Universite Paris XI
Dodd	Evan	Los Alamos National Laboratory
Evans	Roger	AWE / Imperial College
Freeman	Richard	The Ohio State University
Friedman	Alex	Lawrence Livermore National Laboratory
Grote	David	Lawrence Livermore National Laboratory
Hatchett	Steve	Lawrence Livermore National Lab
Hegelich	Bjoern	Los Alamos National Laboratory
Hill	Jeremy	Ohio State University
Hinkel	Denise	Lawrence Livermore National Laboratory
Johzaki	Tomoyuki	Osaka University
Kemp	Andreas	University of Nevada, Reno
Kruer	William	University of California, Davis
Kuba	Jaroslav	Lawrence Livermore National Laboratory
Langdon	Bruce	Lawrence Livermore National Laboratory
Larson	David	Lawrence Livermore National Laboratory
Lasinski	Barbara	Lawrence Livermore National Laboratory
Li	Chikang	Massachusetts Institute of Technology
Libby	Stephen	Lawrence Livermore National Laboratory
Lindl	John	Lawrence Livermore National Laboratory
Lund	Steven	Lawrence Berkeley National Lab
Mason	Rodney	Los Alamos National Laboratory
McCandless	Brian	Lawrence Livermore National Laboratory
Messmer	Peter	Tech-X Corporation
Milovich	Jose	Lawrence Livermore National Laboratory
Moon	Stephen	Lawrence Livermore National Laboratory
Mori	Warren	University of California Los Angeles
Myatt	Jason	Laboratory for Laser Energetics
Noguchi	Koichi	Rice University
Oliver	Bryan	Mission Research Corporation
Ren	Chuang	University of Rochester
Rose	Dave	Mission Research Corporation
Ruhl	Hartmut	University of Nevada
Sakagami	Hitoshi	University of Hyogo
Sefkow	Adam	Princeton Plasma Physics Laboratory
Sentoku	Yasuhiko	Nevada Terawatt Facility
Sharp	William	Lawrence Livermore National Laboratory
Sotnikov	Vladimir	University of Nevada at Reno
Still	Bert	Lawrence Livermore National Laboratory
Stoltz	Peter	Tech-X Corp.
Suter	Larry	Lawrence Livermore National Laboratory
Tabak	Max	Lawrence Livermore National Laboratory
Thomas	Cliff	Stanford University
Tonge	John	University of California, Los Angeles
Town	Richard	Lawrence Livermore National Laboratory
Vay	Jean-Luc	Lawrence Berkeley National Laboratory
Welch	Dale	Mission Research Corporation
Wilks	Scott	Lawrence Livermore National Laboratory

Short-Pulse Laser Matter
Computational Workshop

August 25-27, 2004

Welcome to the Short-Pulse Laser Matter Computational Workshop!

This workshop concentrates on the computational and theoretical aspects of short-pulse laser plasma interactions and will focus on the following six themes:

- Laser propagation / interaction through various density plasmas: micro scale.
- Anomalous electron transport effects: From micro to meso scale.
- Electron transport through plasmas: From meso to macro scale.
- Ion beam generation, transport, and focusing.
- “Atomic-scale” electron and proton stopping powers.
- Kα diagnostics.

Each topic has a coordinator who has drawn up a list of questions that the participants will work on during the next three days.

We would like to thank the Institute for Laser Science and Applications and the Institute for Scientific Computing Research at the Lawrence Livermore National Laboratory for their generous financial support of this workshop.

The level of interest in the workshop has greatly exceeded our expectations. This research area is rapidly evolving and offers many challenging and exciting opportunities. We hope that you will enjoy this workshop and that many long-term collaborations will develop.

Max Tabak and Richard Town

UCRL-BR-20553

General Information:

Meeting Venue:

The workshop will use the San Ramon (A-D) and Livermore (A-B) meeting rooms at the Four Points by Sheraton in Pleasanton. The hotel address is:

Four Points by Sheraton Pleasanton
5115 Hopyard Road
Pleasanton, CA 94588
(925) 460-8800

Messages:

Workshop attendees can be reached by telephone at either the workshop registration desk at (925) 519-2099, or at the reception desk of the Four Points by Sheraton at (925) 460-8800.

Proceedings:

The workshop proceedings will be distributed by CD. In order to produce the proceedings in a timely manner, participants should provide an electronic copy of their presentations on a CD at the registration desk.

Workshop Contacts:

Christine Ynzunza
Lawrence Livermore National Laboratory
P.O. Box 808, L-015
Livermore, CA 94550
Phone: (925) 423-1848
Fax: (925) 422-5102
Email: ynzunza1@llnl.gov

Colleen Camacho
Lawrence Livermore National Laboratory
P.O. Box 808, L-038
Livermore, CA 94550
Phone: (925) 423-6878
Fax: (925) 422-8040
Email: camacho1@llnl.gov

Agenda

Time	Wednesday 8/25		Thursday 8/26		Friday 8/27	
7:45 – 8:30	Registration & Breakfast		Registration & Breakfast		Registration & Breakfast	
8:30 – 10:30	**Applications** *San Ramon A-D*		**Anomalous transport I** *San Ramon A-C*	**Kα diagnostic I** *Livermore A-B*	**Anomalous transport II** *San Ramon A-C*	**Kα diagnostic II** *Livermore A-B*
10:30 – 11:00	Break		Break		Break	
11:00 – 12:30	**Modeling Status** *San Ramon A-D*		**Laser propagation II** *San Ramon A-C*	**Ion Beam generation II** *Livermore A-B*	**Electron transport through plasmas III** *San Ramon A-C*	**Anomalous transport III** *Livermore A-B*
12:30 – 1:30	Lunch		Lunch		Lunch	
1:30 – 3:00	**Laser propagation I** *San Ramon A-C*	**"Atomic-scale" stopping I** *Livermore A-B*	**Electron transport through plasmas II** *San Ramon A-C*	**"Atomic-scale" stopping II** *Livermore A-B*	**Joint Discussions** *San Ramon A-D*	
3:00 – 3:30	Break		Break		Break	
3:30 – 5:30	**Electron transport through plasmas I** *San Ramon A-C*	**Ion Beam generation I** *Livermore A-B*	**Laser propagation III** *San Ramon A-C*	**Ion Beam generation III** *Livermore A-B*	**Joint Discussions** *San Ramon A-D*	
6:00 – 8:00			Working Dinner			

Introductions and Applications

San Ramon A-D: Wed. 8:30 – 10:30

Session chair: ***Warren Mori (UCLA)***

Welcome Address:

Laura Gilliom
University Relations Program
Lawrence Livermore National Laboratory

Presentations:

1. **Fast Ignition – Max Tabak (LLNL)**
2. **Radiography – Hye-Sook Park (LLNL)**
3. **Laboratory Astrophysics – Scott Wilks (LLNL)**

Modeling Status

San Ramon A-D: Wed. 11:00 – 12:30

Session chair: ***Max Tabak (LLNL)***

Presentations:

1. **PIC Calculations – Chuang Ren (University of Rochester)**
2. **Hybrid PIC Calculations – Dale Welch (Mission Research Corp.)**
3. **Atomic Physics Modeling – Steve Libby (LLNL)**

Laser propagation / interaction through various density plasmas: micro scale

San Ramon A-C: Wed. 1:30 – 3:00; Thur. 11:00 – 12:30; 3:30 – 5:30

Coordinator: ***Chuang Ren (University of Rochester)***

Questions:

- **Assess amount of laser beam spray and electron distribution function for different PIC codes / parameters.**
- **How sensitive to resolution are the answers?**
- **What is the effect of background plasma and return currents on laser absorption and electron transport?**

Presentations:

1. **Bedros Afeyan (Polymath Research Inc.)**
2. **Eric Esarey (LBNL)**
3. **Barbara Lasinski (LLNL)**
4. **Jason Myatt (LLE)**
5. **Chuang Ren (University of Rochester)**
6. **Dave Rose (Mission Research Corp.)**
7. **Hitoshi Sakagami (University of Hyogo)**
8. **Yasuhiko Sentoku (Nevada Terawatt Facility)**
9. **Bert Still (LLNL)**
10. **Jean-Luc Vay (LBNL)**
11. **Andrew Charman (UC Berkeley and LBNL)**
12. **Peter Messemer (Tech-X Corporation)**
13. **Claude Deutsch (Université Paris XI)**
14. **Richard Town (LLNL)**

Anomalous electron transport effects: From micro to meso scale

San Ramon A-C: Thur. 8:30 – 10:30; Fri. 8:30 – 10:30; Livermore A-B: Fri. 11:00 – 12:30

Coordinator: ***Hartmut Ruhl (University of Nevada, Reno)***

Questions:

- **What are the dominant electron beam instabilities?**
- **How do the instabilities vary with beam-to-background density ratio?**
- **How do the instabilities vary with the longitudinal and transverse energy spread of the beam?**
- **What resolution is needed to model them?**
- **What are the effects of collisions?**
- **What are the saturation levels?**
- **What is the energy partition between the various components of the plasma?**
- **Can we derive simple formulae for inclusion in hybrid-PIC codes?**

Presentations:

1. **Roger Evans (AWE / Imperial College)**
2. **Andreas Kemp (University of Nevada, Reno)**
3. **Jason Myatt (Laboratory for Laser Energetics)**
4. **Claude Deutsch (Université Paris XI)**

Electron transport through plasmas: From meso to macro scale

San Ramon A-C: Wed. 3:30 – 5:30; Thur. 1:30 – 3:00; Fri. 11:00 – 12:30

Coordinator: *Roger Evans (AWE/Imperial College) and Dale Welch (Mission Research Corp.)*

Questions:

- **How does electron transport depend on:**
  - **the electron beam density and distribution;**
  - **longitudinal and transverse energy spread;**
  - **the background plasma density;**
  - **presence of interfaces; and**
  - **variations in resistivity and EOS models.**
- **How sensitive to resolution are the answers?**
- **How does the sensitivity vary with different models (hybrid PIC; Fokker-Planck; AMR PIC)?**
- **Compare and contrast various computational methods.**
- **Define test problems.**

Presentations:

1. **Larissa Cottrill (LLNL)**
2. **Roger Evans (AWE / Imperial College)**
3. **Tomoyuki Johzaki (Osaka University)**
4. **Andreas Kemp (University of Nevada, Reno)**
5. **Rodney Mason (LANL)**
6. **Jason Myatt (LLE)**
7. **Hartmut Ruhl (University of Nevada)**
8. **Richard Town (LLNL)**
9. **Dale Welch (Mission Research Corp.)**

Ion beam generation, transport, and focusing

Livermore A-B: Wed. 3:30 – 5:30; Thur. 11:00 – 12:30; 3:30 – 5:30

Coordinator: ***Scott Wilks (LLNL)***

Questions:

- **What are the ion beam generation mechanisms?**
- **What are the ion beam generation mechanism efficiencies?**
- **How does the physics change with intensity?**
- **How sensitive to resolution are the answers?**
- **Can hybrid PIC be used?**
- **How does electron flow affect proton generation?**
- **How can we control the generation and focusing of the protons?**

Presentations:

1. **Tony Bell (Imperial College)**
2. **Michael Cuneo (Sandia National Laboratory)**
3. **Andreas Kemp (University of Nevada, Reno)**
4. **Peter Messmer (Tech-X)**
5. **Koichi Noguchi (Rice University)**
6. **Hartmut Ruhl (University of Nevada)**
7. **Richard Town (LLNL)**
8. **Scott Wilks (LLNL)**
9. **Julien Fuchs (University of Nevada, Reno)**

"Atomic-scale" electron and proton stopping powers

Livermore A-B: Wed. 1:30 – 3:00; Thur. 1:30 – 3:00

Coordinator: *Claude Deutsch (Université Paris XI)*

Questions:

- **What are realistic stopping powers / scattering for intense electron / proton beams in dense plasmas?**
- **Relativistic electron stopping in partially degenerate targets. Inference of intrabeam correlations. Multiple scattering contributions to the depth penetration. Collective vs.collisional stopping. Triggering of instabilities.**
- **Non-relativistic proton and ion stopping: in-flight binary correlations, effect of multiple scattering (proton) on hohlraum design.**
- **What are the coherent effects?**

Presentations:

1. **Chikang Li (MIT)**
2. **Peter Stoltz (Tech-X)**
3. **Max Tabak (LLNL)**
4. **Claude Deutsch (Université Paris XI)**
5. **Cliff Thomas (LLNL)**
6. **Julien Fuchs (University of Nevada, Reno)**

Kα diagnostics

Livermore A-B: Thur. 8:30 – 10:30; Fri. 8:30 – 10:30

Coordinator: *Mark Foord (LLNL)*

Questions:

- **How is the atomic physics altered in these extreme states of matter?**
- **How does the atomic physics alter their use as a diagnostic?**
- **Is trapping important?**

Presentations:

1. **Larissa Cottrill (LLNL)**
2. **Stephen Libby (LLNL)**
3. **Hyun Chung (LLNL)**
4. **Cliff Thomas (LLNL)**
5. **Claude Deutsch (Université Paris XI)**

Joint Discussions

San Ramon A-D: Fri. 1:30-3:00; 3:30-5:30

Moderator: *Max Tabak (LLNL)*

Summary of working group sessions:

- **Laser propagation / interaction through various density plasmas: micro scale: *Chuang Ren (University of Rochester)***
- **Anomalous electron transport effects: From micro to meso scale: *Hartmut Ruhl (UN-Reno)***
- **Electron transport through plasmas: From meso to macro scale: *Dale Welch (MRC)***
- **Ion beam generation, transport, and focusing: *Scott Wilks (LLNL)***
- **"Atomic-scale" electron and proton stopping powers: *Claude Deutsch (Université Paris XI)***
- **Kα diagnostics: *Mark Foord (LLNL)***

Electron transport at high laser intensities

Tony Bell, Robert Kingham, Alex Robinson, Mark Sherlock
+ antecedents

Imperial College

Short Pulse Laser -- Solid Interactions

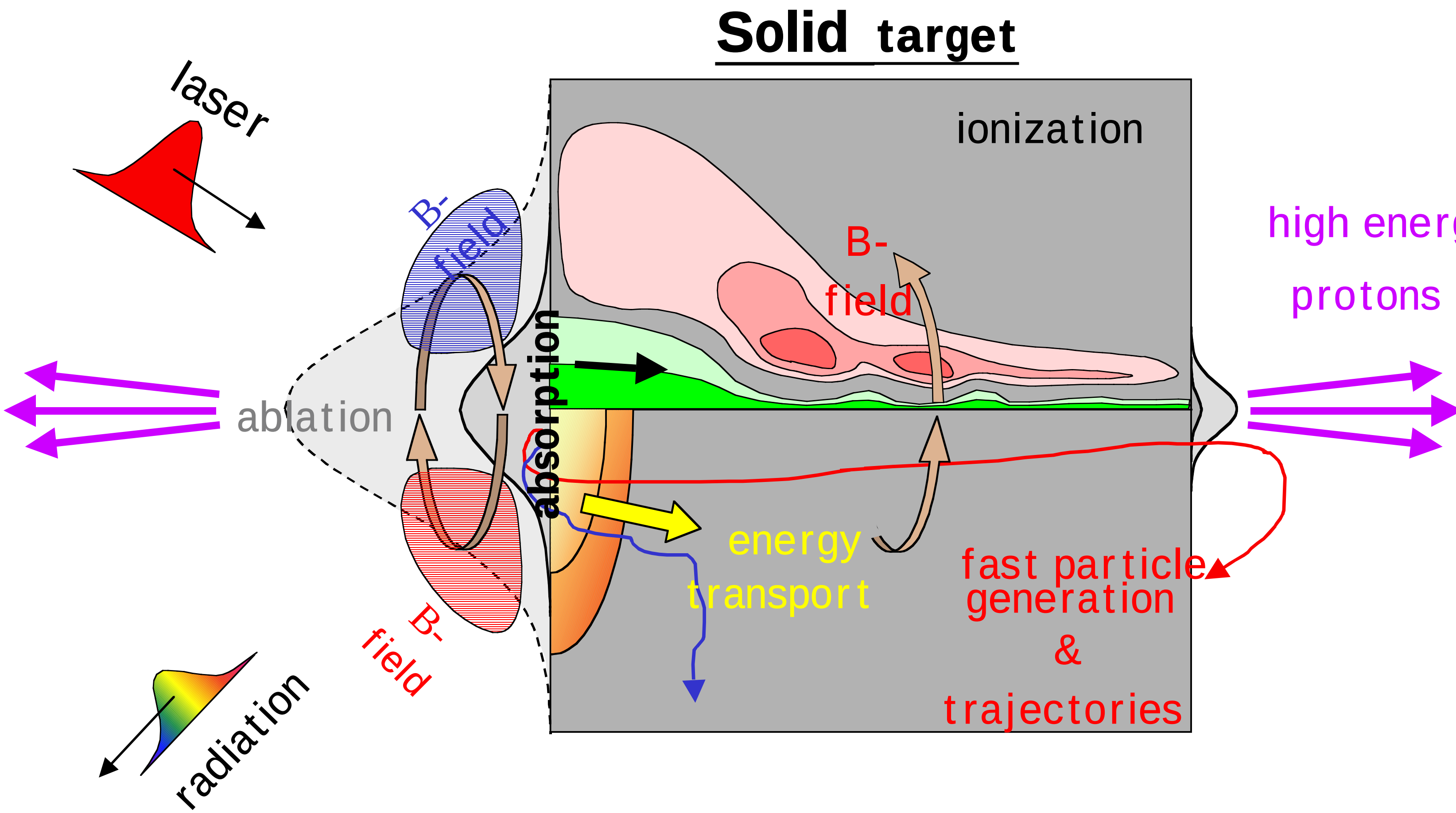

(Robert Kingham)

E has a curl

⇨ Magnetic field

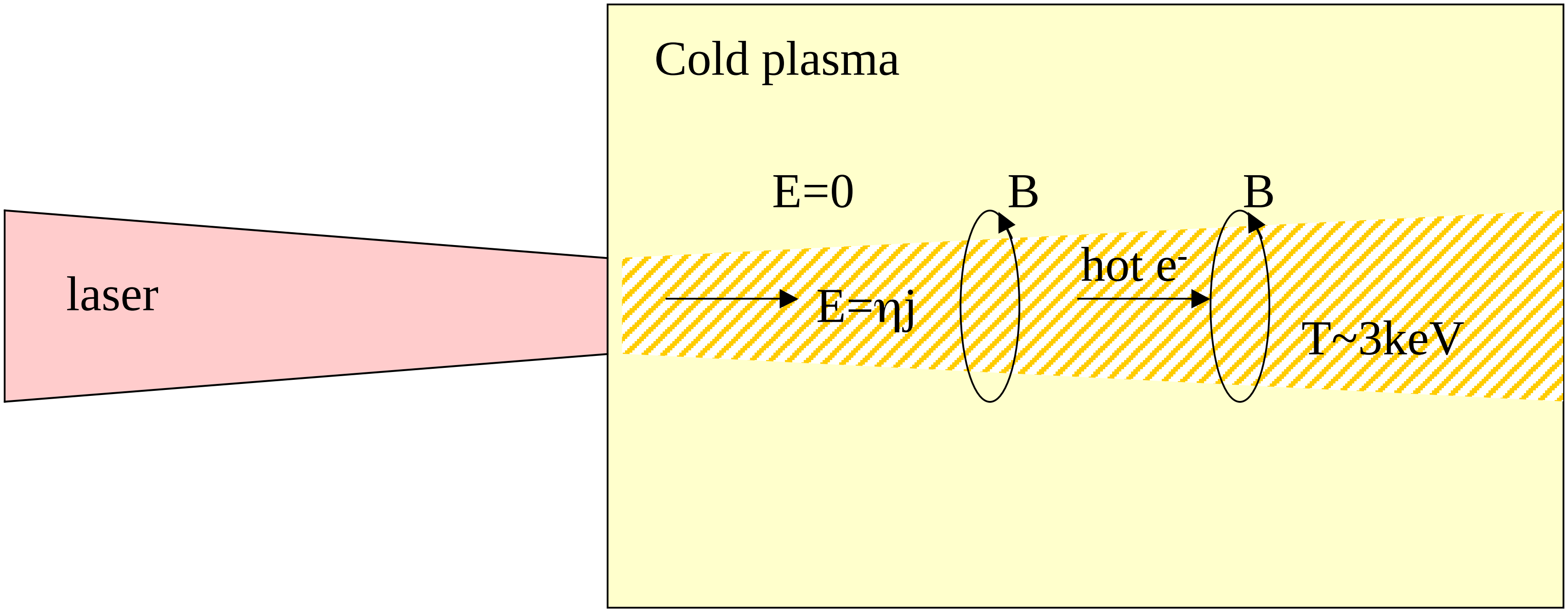

Equation for B

$\text{curl}(B)=\mu_0(j_{hot}+j_{cold})$ ← j_{hot} & j_{cold} don't exactly cancel

$\delta B/\delta t=-\text{curl}(E)$

$E=\eta j_{cold}$

$$\delta B/\delta t = \text{curl}(\eta j_{hot}) - \text{curl}(\ (\eta/\ \mu_0)\ \text{curl}(B)\ )$$

source diffusion of B

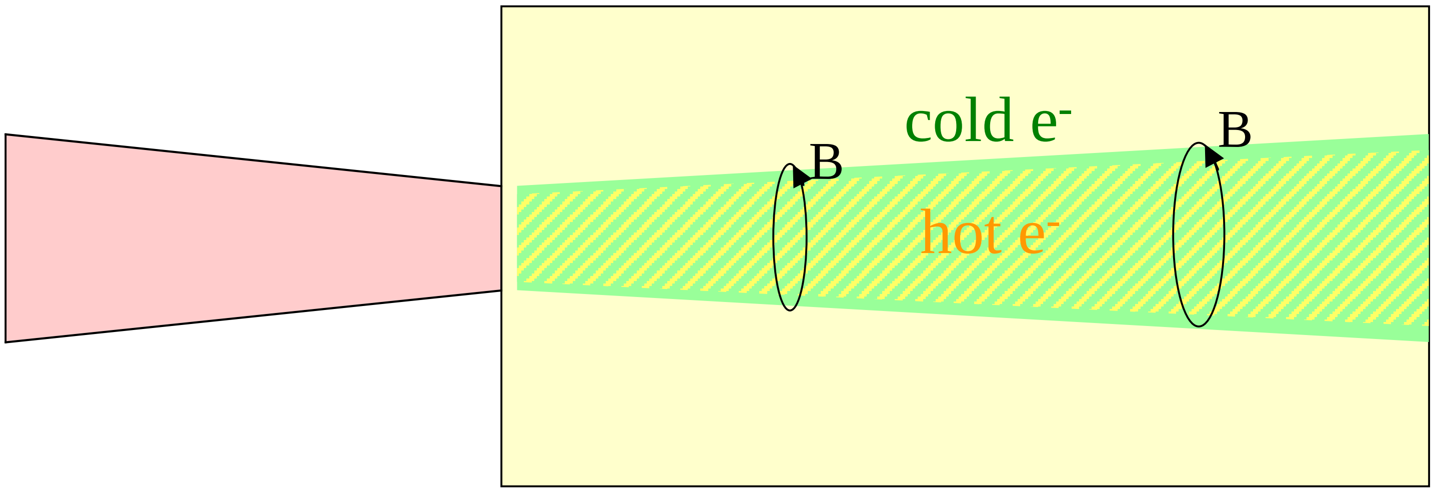

cold e^- return over slightly larger radius

Hybrid code: magnetic field

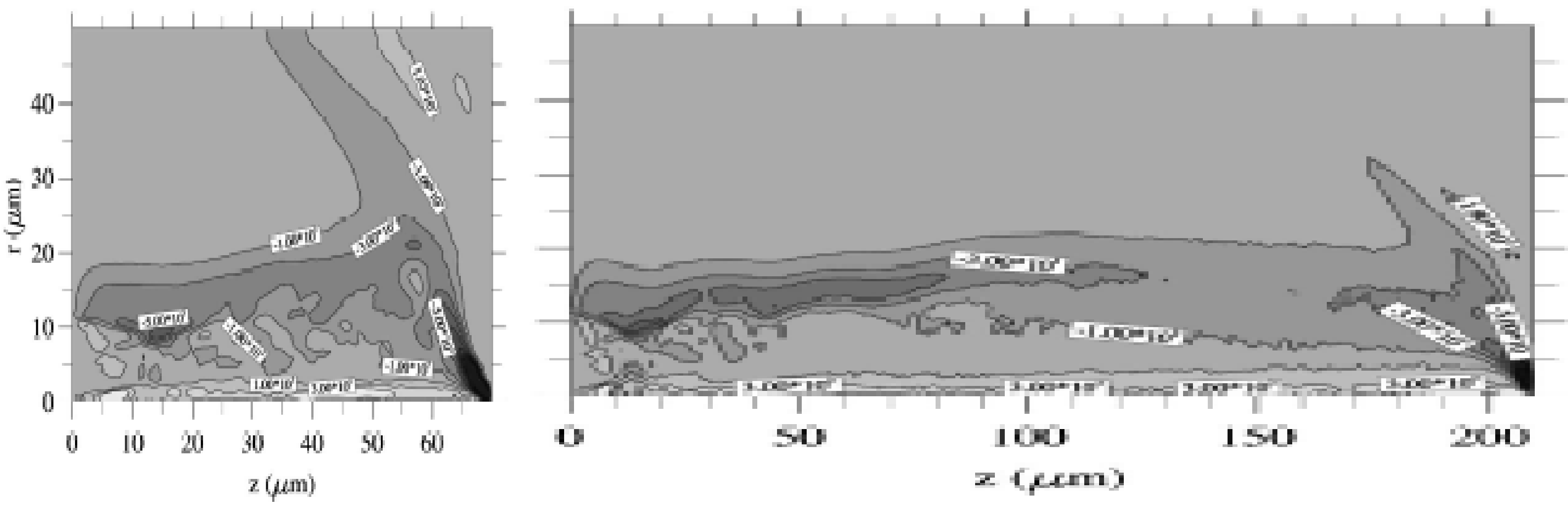

Davies et al, PRE 59, 61032 (1999)

Other geometries

Magnetic field wherever $\mathrm{curl}(\eta j_{hot})$ non-zero

$$\mathrm{curl}(\eta j_{hot}) = \mathrm{grad}(\eta) \times j_{hot} + \eta\, \mathrm{curl}(j_{hot})$$

gradient in resistivity — curl in hot current (as in beam)

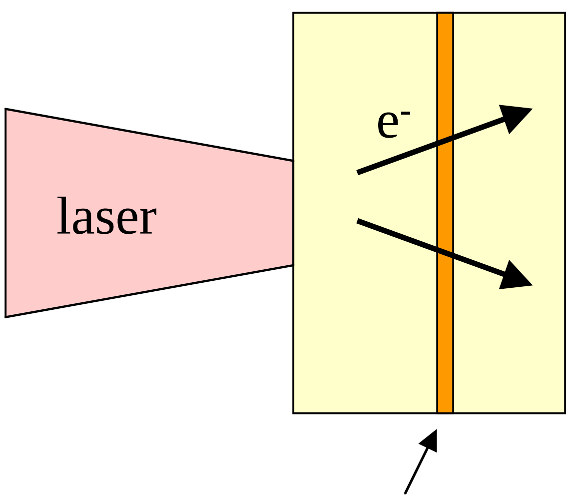

different Z & η

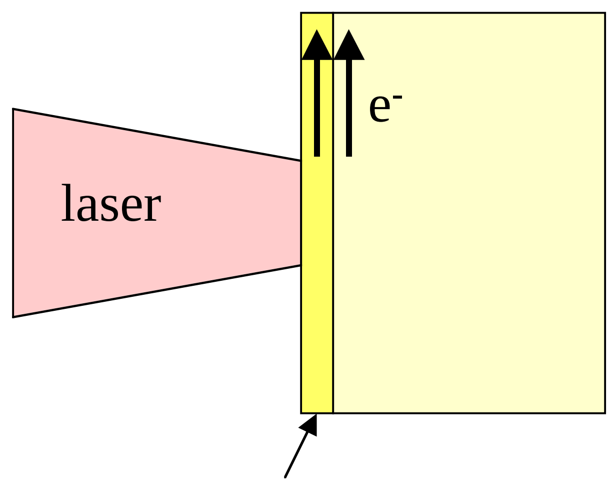

hot corona, different η

Bell et al, PRE 58, 2471 (1998)

KALOS code

Kinetic
a
Laser-plasma
o
Simulation

Expand velocity dist[n] in spherical harmonics

$$f(x,y,v,\theta,\phi,t) = \Sigma\, f_{nm}(x,y,v,t)\, P_n^{|m|}(\cos\theta)\, e^{im\phi}$$

velocity coordinates in 3D

- Any degree of anisotropy by expanding to any order
- Equations very simple – efficient despite small explicit timestep
- Without collisions operates as Vlasov code (efficiently)
- Collisions and B easily included
- Can follow oscillation in laser beam
- Easily parallelised

$$\frac{\partial f_n^m}{\partial t}+\frac{n(n+1)}{2}\upsilon f_n^m-\frac{1}{v^2}\frac{\partial}{\partial v}\left(D_{\parallel}\frac{\partial f_n^m}{\partial v}+Ef_n^m\right)$$

$$f=\sum_{n=0}^{n_{\max}}\sum_{m=-n}^{n}f_n^m(r,z,p)P_n^{|m|}(\cos\vartheta)e^{im\varphi}$$

$$+\omega_x i\left\{mf_n^m\right\}+\omega_r\frac{i}{2}\left\{(n-m)(n+m+1)f_n^{m+1}+f_n^{m-1}\right\}+\omega_z\frac{1}{2}\left\{(n-m)(n+m+1)f_n^{m+1}-f_n^{m-1}\right\}$$

$$=$$

$$-\left(\frac{n-m}{2n-1}\right)v\frac{\partial f_{n-1}^m}{\partial x}-\left(\frac{n+m+1}{2n+3}\right)v\frac{\partial f_{n+1}^m}{\partial x}$$

$$-\frac{v}{2}\left\{\begin{matrix}\frac{1}{2n-1}\left[r^{m-1}\frac{\partial(r^{-m+1}f_{n-1}^{m-1})}{\partial r}-(n-m)(n-m-1)r^{-m-1}\frac{\partial(r^{m+1}f_{n-1}^{m+1})}{\partial r}\right]\\+\frac{1}{2n+3}\left[-r^{m-1}\frac{\partial(r^{-m+1}f_{n+1}^{m-1})}{\partial r}+(n+m+1)(n+m+2)r^{-m-1}\frac{\partial(r^{m+1}f_{n+1}^{m+1})}{\partial r}\right]\end{matrix}\right\}$$

$$-eE_x\left\{\frac{n-m}{2n-1}G_{n-1}^m+\frac{n+m+1}{2n+3}H_{n+1}^m\right\}$$

$$-eE_r\frac{1}{2}\left\{\frac{1}{2n-1}\left[G_{n-1}^{m-1}-(n-m)(n-m-1)G_{n-1}^{m+1}\right]+\frac{1}{2n+3}\left[-H_{n+1}^{m-1}+(n+m+1)(n+m+2)H_{n+1}^{m+1}\right]\right\}$$

$$-eE_\vartheta\frac{i}{2}\left\{\frac{1}{2n-1}\left[-G_{n-1}^{m-1}-(n-m)(n-m-1)G_{n-1}^{m+1}\right]+\frac{1}{2n+3}\left[H_{n+1}^{m-1}+(n+m+1)(n+m+2)H_{n+1}^{m+1}\right]\right\}$$

Advection in momentum due to electric field

$$\frac{\partial f_n^m}{\partial t} = -eE_x \left\{ \frac{n-m}{2n-1} G_{n-1}^m + \frac{n+m+1}{2n+3} H_{n+1}^m \right\}$$

$$-eE_r \frac{1}{2} \left\{ \frac{1}{2n-1} \left[G_{n-1}^{m-1} - (n-m)(n-m-1) G_{n-1}^{m+1} \right] + \frac{1}{2n+3} \left[-H_{n+1}^{m-1} + (n+m+1)(n+m+2) H_{n+1}^{m+1} \right] \right\}$$

$$-eE_\vartheta \frac{i}{2} \left\{ \frac{1}{2n-1} \left[-G_{n-1}^{m-1} - (n-m)(n-m-1) G_{n-1}^{m+1} \right] + \frac{1}{2n+3} \left[H_{n+1}^{m-1} + (n+m+1)(n+m+2) H_{n+1}^{m+1} \right] \right\}$$

$$G_n^m(p) = \frac{\partial f_n^m}{\partial p} - n \frac{f_n^m}{p} = p^n \frac{\partial (p^{-n} f_n^m)}{\partial p}$$

$$H_n^m(p) = \frac{\partial f_n^m}{\partial p} + (n+1) \frac{f_n^m}{p} = \frac{1}{p^{n+1}} \frac{\partial (p^{n+1} f_n^m)}{\partial p}$$

Spatial advection

$$\frac{\partial f_n^m}{\partial t} = -\left(\frac{n-m}{2n-1}\right) v \frac{\partial f_{n-1}^m}{\partial x} - \left(\frac{n+m+1}{2n+3}\right) v \frac{\partial f_{n+1}^m}{\partial x}$$

$$-\frac{v}{2}\left\{\begin{array}{l} \frac{1}{2n-1}\left[r^{m-1} \frac{\partial (r^{-m+1} f_{n-1}^{m-1})}{\partial r} - (n-m)(n-m-1) r^{-m-1} \frac{\partial (r^{m+1} f_{n-1}^{m+1})}{\partial r} \right] \\ + \frac{1}{2n+3}\left[- r^{m-1} \frac{\partial (r^{-m+1} f_{n+1}^{m-1})}{\partial r} + (n+m+1)(n+m+2) r^{-m-1} \frac{\partial (r^{m+1} f_{n+1}^{m+1})}{\partial r} \right] \end{array}\right\}$$

Rotation by magnetic field: $\omega = eB/\gamma m$

$$\frac{\partial f_n^m}{\partial t} = \omega_x i \left\{ m f_n^m \right\}$$

$$+ \omega_r \frac{i}{2} \left\{ (n-m)(n+m+1)\, f_n^{m+1} + f_n^{m-1} \right\}$$

$$+ \omega_z \frac{1}{2} \left\{ (n-m)(n+m+1)\, f_n^{m+1} - f_n^{m-1} \right\}$$

Collisions

$$\frac{\partial f_n^m}{\partial t} = -\frac{n(n+1)}{2}\upsilon_\perp f_n^m + \frac{\upsilon_\parallel}{v^2}\frac{\partial}{\partial v}\left(D_\parallel \frac{\partial f_n^m}{\partial v} + E f_n^m \right)$$

Assumes Rosenbluth potentials dominated by f_0^0

$D_\parallel$ & E are integrals over f_0^0 in velocity space

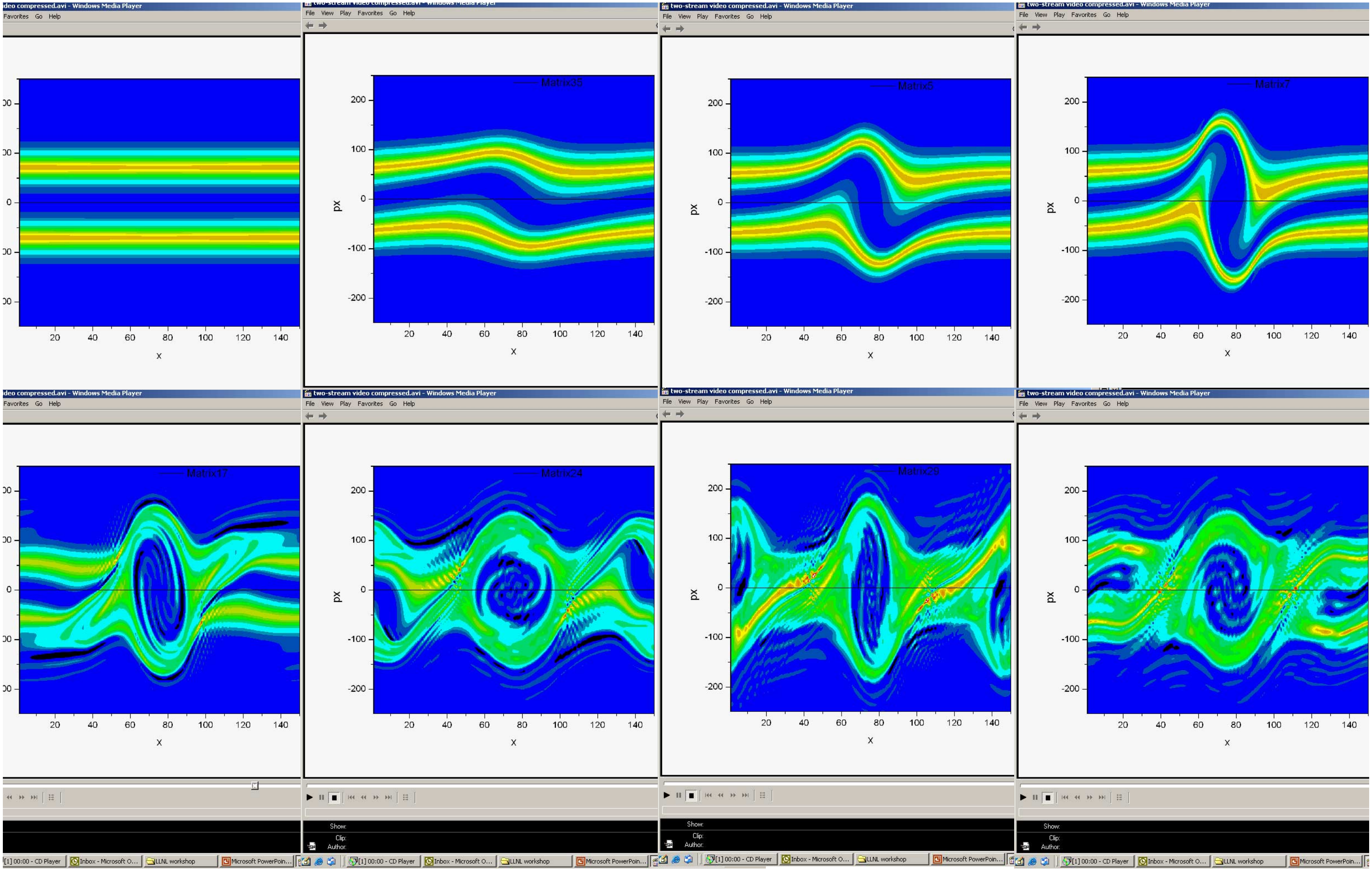

nx=150, np=250, nharmonics=150

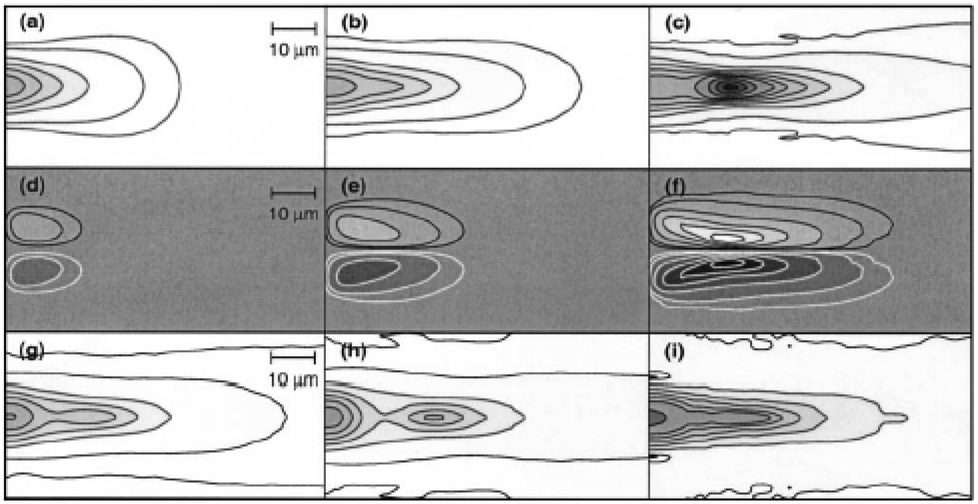

FIG. 1. Spatial plots (close to the axis) of temperature (a)–(c) and (g)–(i) for parameters given in Table I. (d)–(f), respectively, plot the magnetic field for cases (a)–(c). The temperature contour levels are 350, 400, 600, 800, 1000, 1200, 1400, 1800, 2200, and 2600 eV. The magnetic field contour levels are $+/-$ 0.1, 0.2, 0.5, 1.0, 1.5, and 2.0 MG.

TABLE I. Parameters for Fig. 1. Power is the average absorbed power up to that time. T_{max} and B_{max} are calculated by KALOS. B_{est} and F are given by the approximate analytic model with $T_{init} = 1.5$ keV.

Figure	Run	Time fsec	Power TW	T_{max} keV	B_{max} MG	B_{est} MG	Γ	Conditions
(a),(d)	*A*	200	2.1	1.4	0.4	0.5	0.8	Standard
(b),(e)	*A*	400	1.9	1.3	0.8	0.9	1.6	Standard
(c),(f)	*A*	800	1.5	2.8	2.4	1.7	2.9	Standard
(g)	*B*	1200	1.3	1.4	1.5	2.2	1.5	$\vartheta_{1/2} = 33°$
(h)	*C*	2500	0.8	1.5	1.8	2.9	1.1	$\vartheta_{1/2} = 45°$
(i)	*D*	1500	1.2	2.0	0.9	0.7	0.9	Vary T_{fast}, Z, n

KALOS code solves the relativistic VFP equation with Maxwell's equations. It includes electron-electron and electron-ion collisions, field ionization, and collisional ionization.

Not include ion motion or laser absorption. Fast electrons are generated in a "source" region.

We produce fast electrons for 100fs, with a power input of 1TW. The fast electron temperature is 280keV. The fast electron density is controlled via the parameter d_{source} (baseline is 15_m). The simulations were run for 250fs.

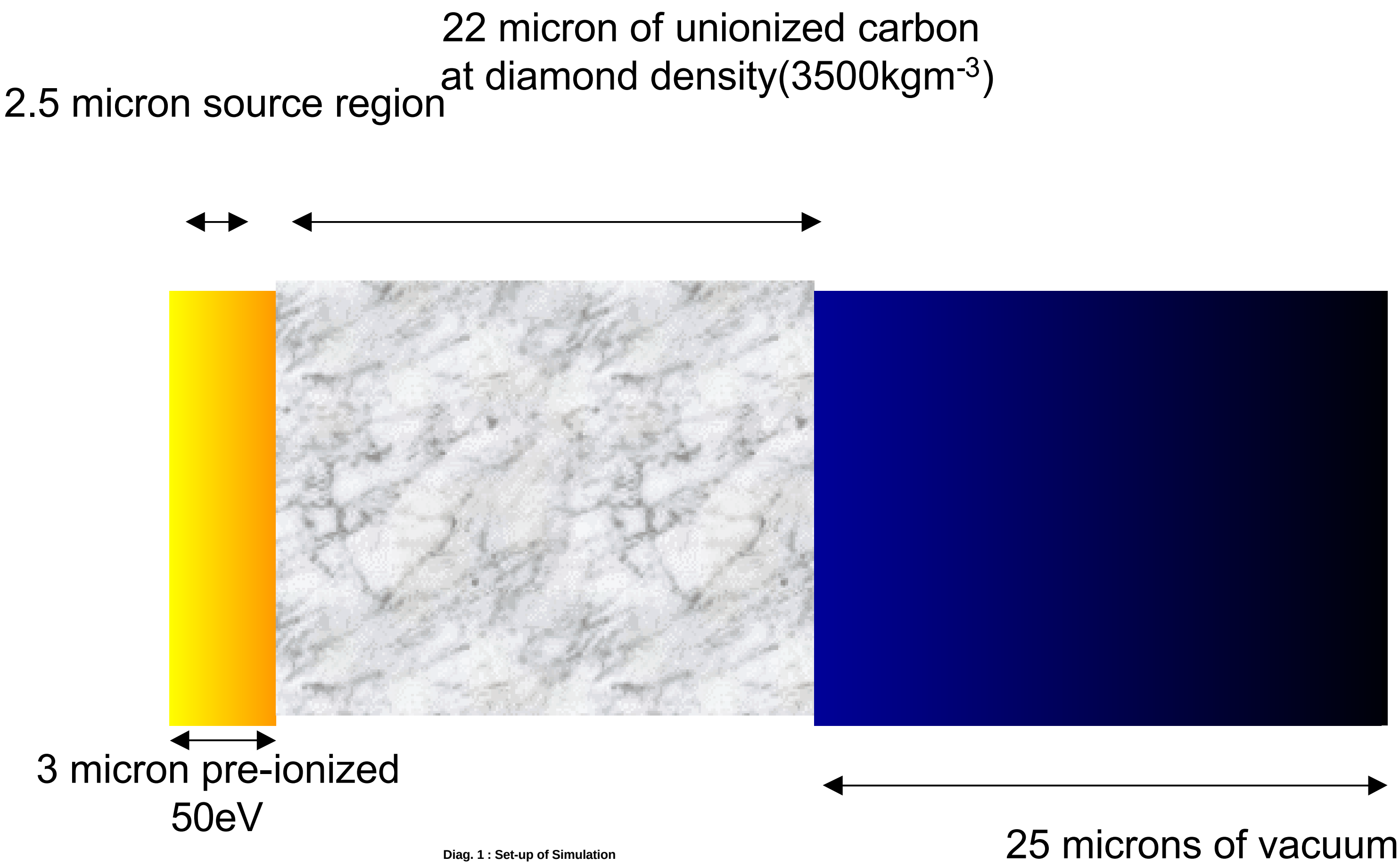

Diag. 1 : Set-up of Simulation

p^2f_0 plot at 180fsec

This is the electron density in the |**p**|-x phase space.

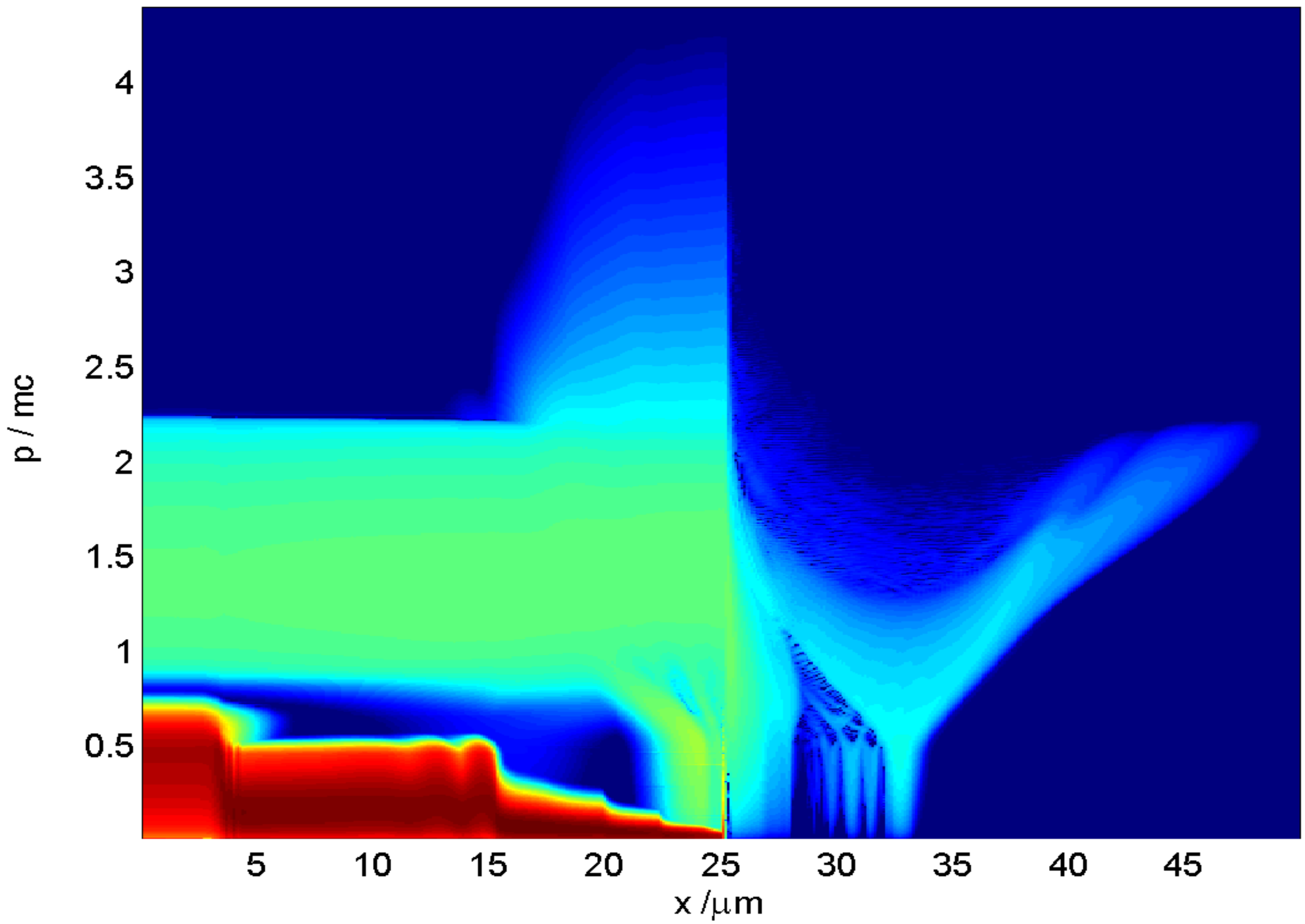

vp^2f_1 plot at 180 fsec

This is the electron flux in the |**p**|-x phase space.

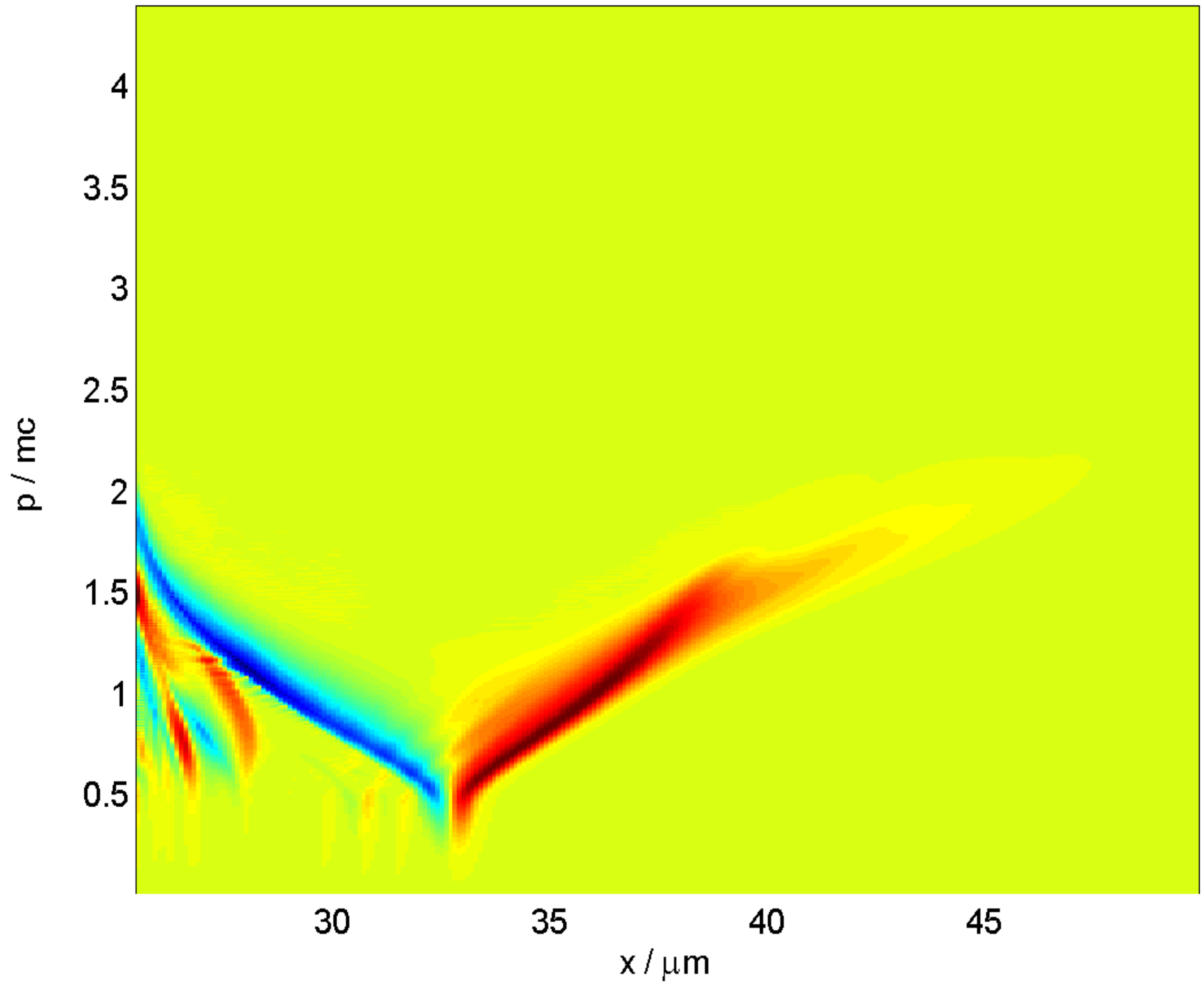

Ion populations in target at 200fs for baseline run.

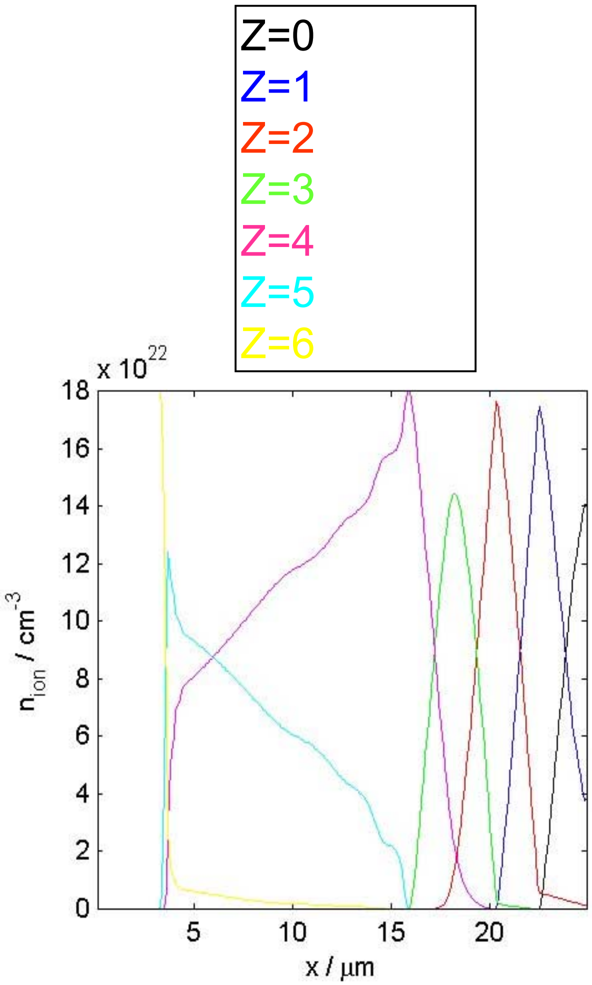

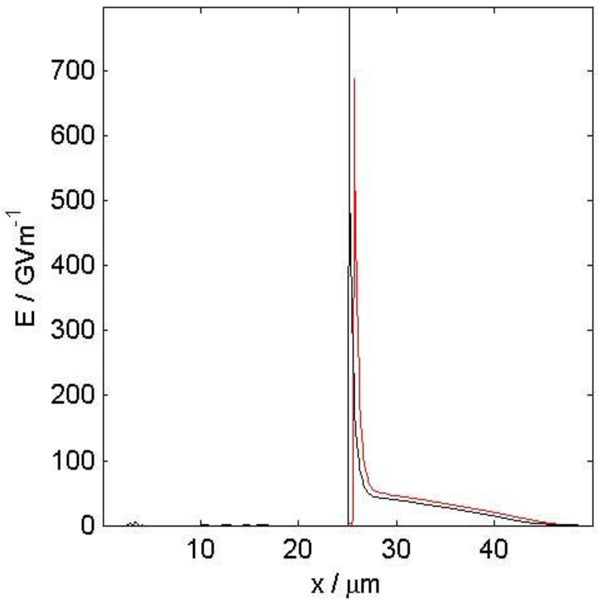

Ionization:

- Pre-ionized targets give different results.
- Due to cold electrons escaping into vacuum.

Electric Field and Potential:

The electric field over time is shown for d_{source} = 15_m and 50_m below.

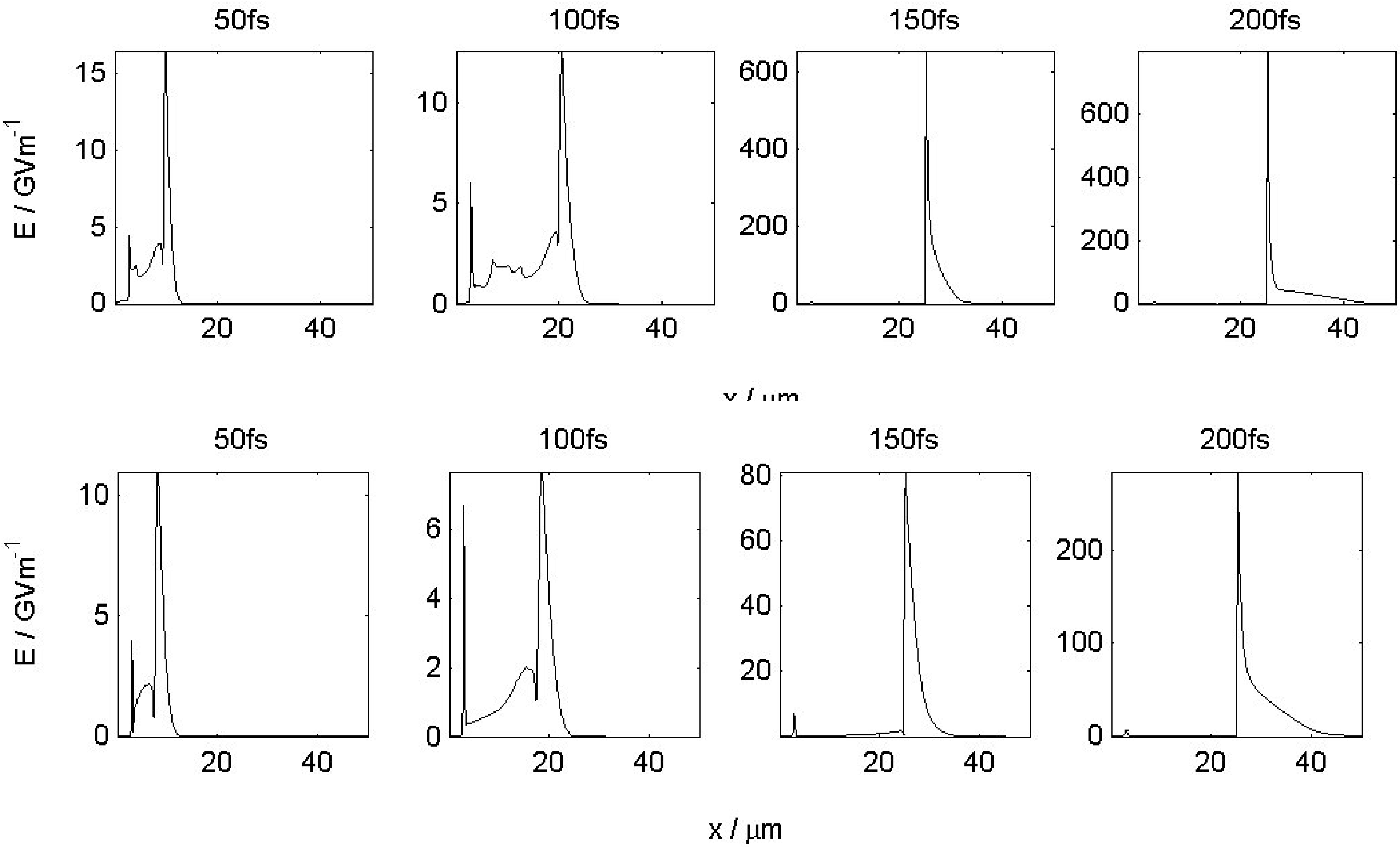

Variation of the max. potential with fast electron density (left) and (right)
Max. field depends on $\sqrt{n_f}$ (n_f proportional to d_{source}^{-2})

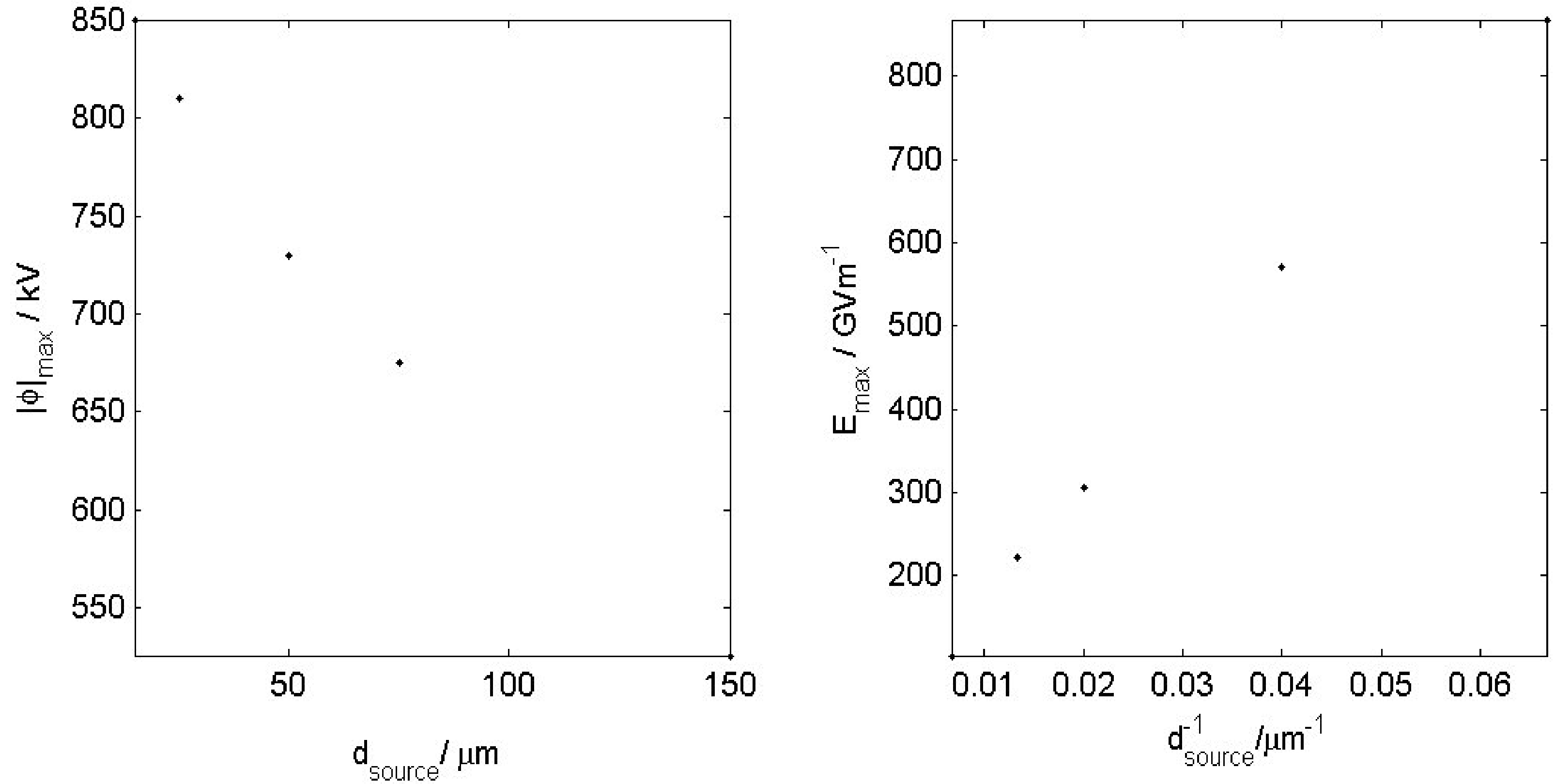

Proton Acceleration:
profile at 200fsec

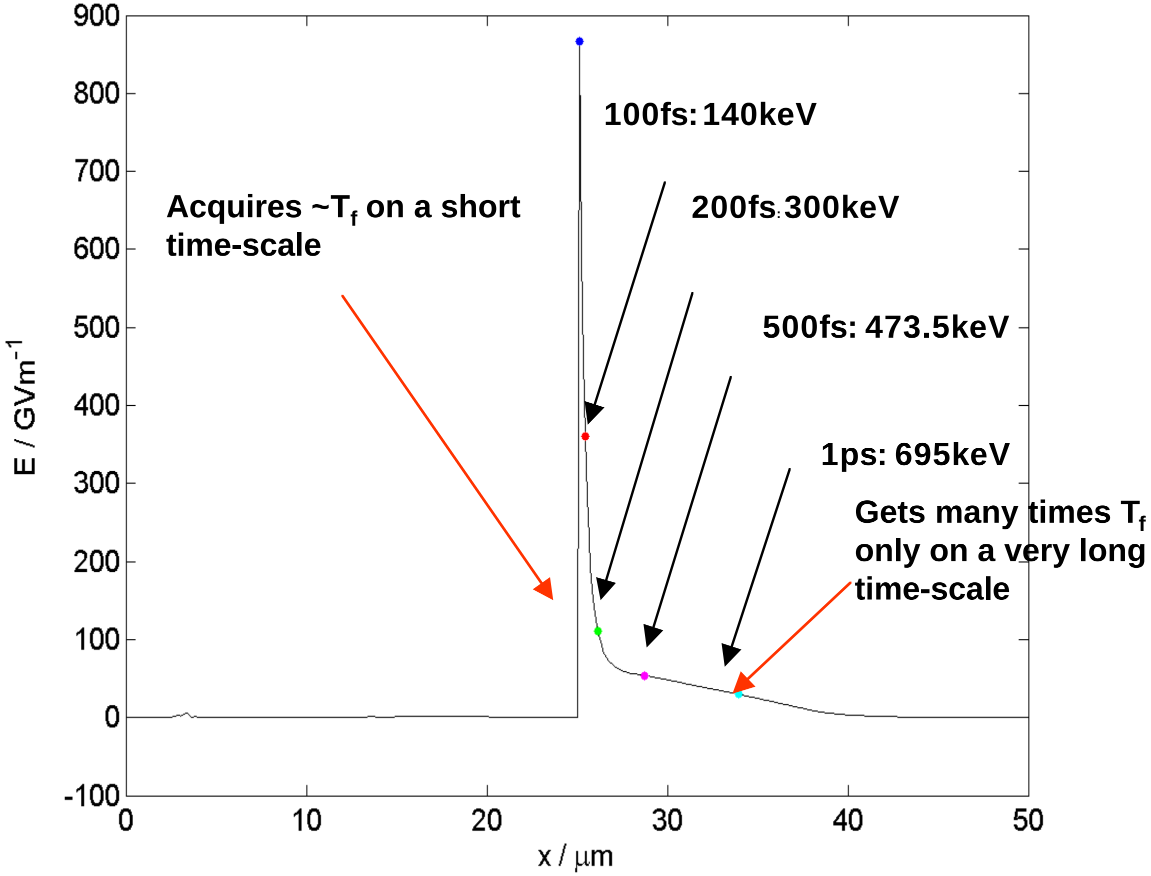

Population Kinetics Capabilities for Short-Pulse Laser-produced plasmas

Hyun-Kyung Chung
LLNL, PAT, V-division

M. H. Chen, M. E. Foord, S. B. Libby, S. J. Moon,
S. C. Wilks and R. W. Lee
LLNL

W. L. Morgan
Kinema Research

August 23-25, 2004

This work was performed under the auspices of the U.S. Department of Energy by University of California, Lawrence Livermore Laboratory under Contract W-7405-Eng-48

Population kinetics modeling **provides** *charge state distributions* **as well as** *level populations*

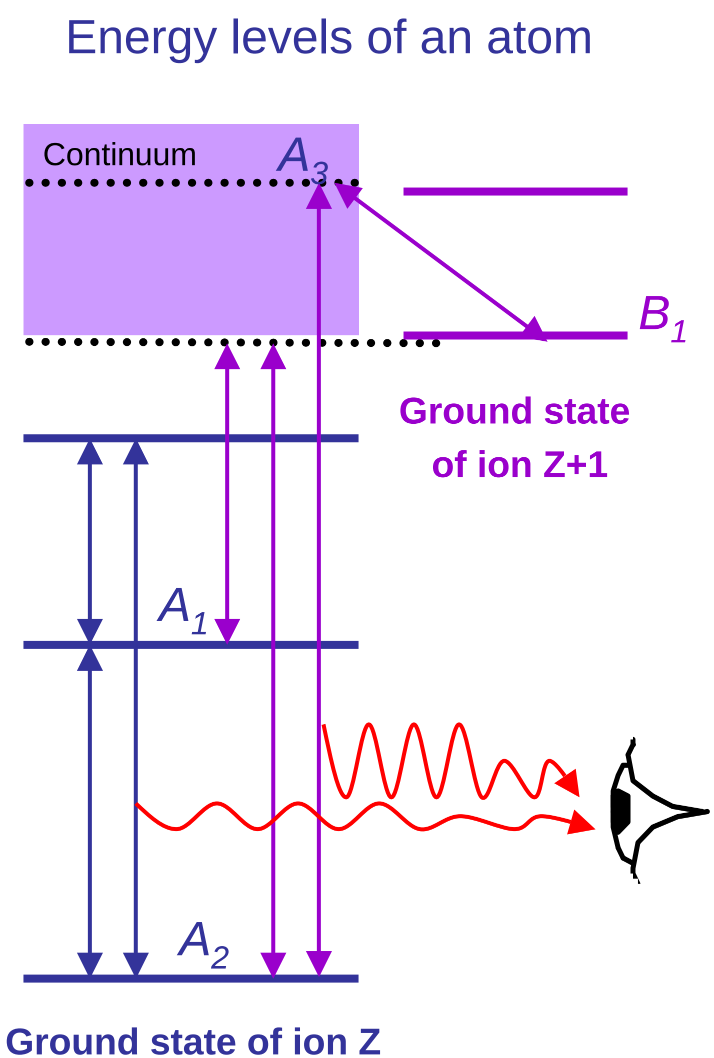

Equation of state (EOS), Conductivity, Opacity, Emissivity, Collisional frequency …..

- **When LTE (Local thermodynamic equilibrium) use , for example,**
  - **Boltzmann distributions for bound states**
  - **Saha equation for ionization distributions**
- **When Non-LTE**
  - **level populations are determined by considering all possible atomic processes**

Developing population kinetics modeling tools: three capabilities for design and analysis of experiments

Design

- **FLYCHK**
  - New simplified ionization balance model that is fast, accurate and easy-to-use for experimental planning
  - Detailed K-shell model (FLY) for H through Fe plasma
- **Ct27**
  - New model to self-consistently treat populations and velocity distributions

Analysis

- **FLYCHK**
  - K-shell spectroscopy for H through Fe plasma measured data analysis
- **HULK**
  - **HUL**LAC-based population **K**inetics code: Revised detailed kinetics modeling tool

Simple but generalized ***population kinetics codes : FLYCHK•Ct27***

- ***Built-in*** **atomic data sets (Hydrogenic model)**
- **Detailed population distributions considering collisional and radiative processes (Non-LTE solutions)**
- **Steady-state, time-dependent, and LTE solutions**
- **Arbitrary electron energy distribution functions with multiple Te option**
- **Atomic model includes the ground state, valence-shell excited levels, and inner shell levels for *all* ion stages from neutral through fully-stripped**
- **Easy and user-friendly interface**

(with an option of detailed K-shell modeling)

- **Accurate built-in atomic data for H, He and Li ions up to Z=26**
- **Spectral intensities and line shapes**

Construction of Hydrogenic models: *simple but complete*

- **Screened hydrogenic model with relativistic corrections to compute energy levels**

$$E_n = -\frac{Q_n^2}{n^2}\left(1+\left[\frac{\alpha Q_n}{n}\right]^2\left[\frac{2n}{n+1}-\frac{3}{4}\right]\right)$$

$$Q_n = Z - 0.5\sigma(n,n)\max(0, P_n - 1) - \sum_{m<n}\sigma(n,m)P_m$$

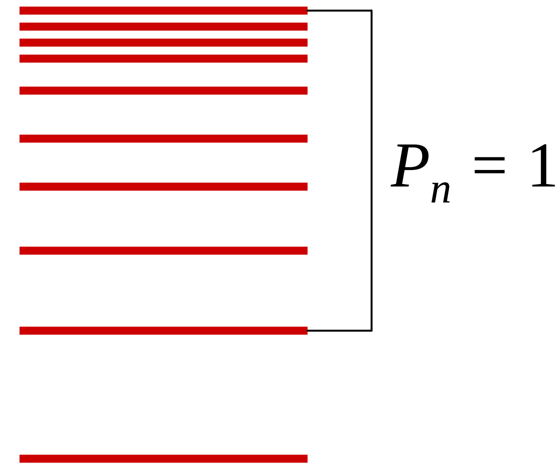

- **Hydrogenic oscillator strengths, f_{ul}**
- **f_{ul} to compute collisional excitation rates**
- **Hydrogenic photoionization cross-sections (Kramer)**
- **Semi-empirical cross-sections for collisional ionization (Lotz)**
- **Hydrogenic dielectronic recombination rates (Burgess-Mertz) or detailed counting of autoionization and electron capture**

FLYCHK: generate a robust, rapid predictor for all Zs

Predictive capability of charge state distribution (CSD)

- **Simple, fool-proof tool needed to help experimentalist design diagnostics**

- **General tool applied to any atom under any condition**

- **Compact module for inclusion in macroscopic codes :**
  Hydrodynamics, PIC (Particle-in-cell) and radiation transport…

- **Initial accurate estimate of ionization distributions necessary for building more sophisticated kinetics model**

New method to include EA and DR processes:
1st Essential element for FLYCHK

- **Excitation following by Autoionization (EA) and its reverse process Dielectronic Recombination (DR) are critical in many kinetics problems**

- **Burgess-Mertz formalism is only valid for coronal lower Z plasmas**

- **EA/DR processes should be in detailed balance for collision-dominated plasmas**

- **EA/DR processes via autoionizing states are modeled within a hydrogenic formalism**

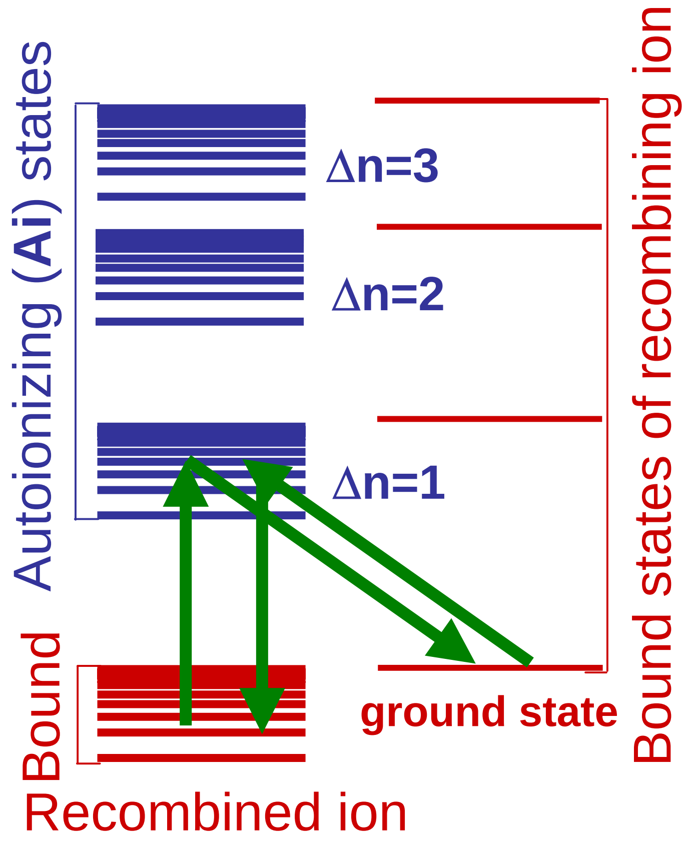

Inner-shell (IS) processes for many-electron ions:
2^{nd} Essential element for FLYCHK

Low Z atom

A promotion of IS electrons leads to states far from continuum limit and rarely matters in CSD

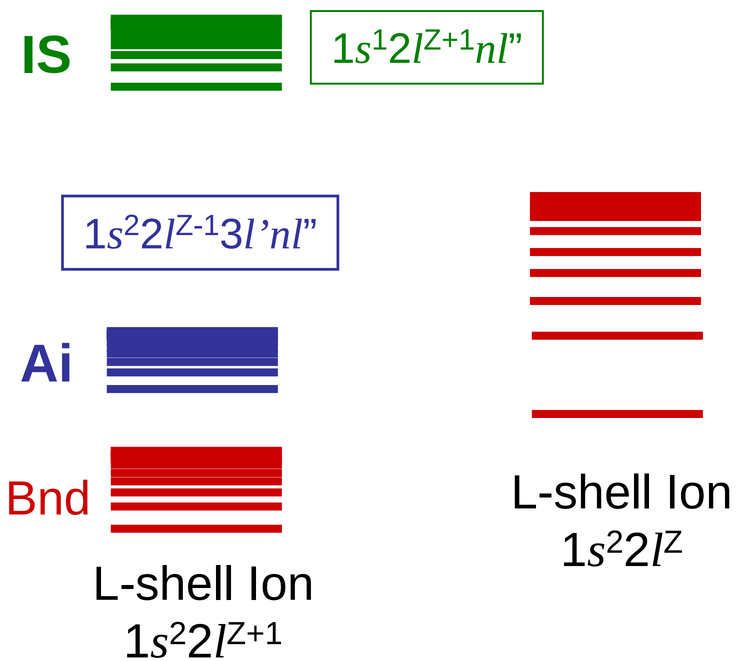

High Z atom

A promotion of IS electrons can lead to states near the continuum limit and hence EA process is critical in CSD

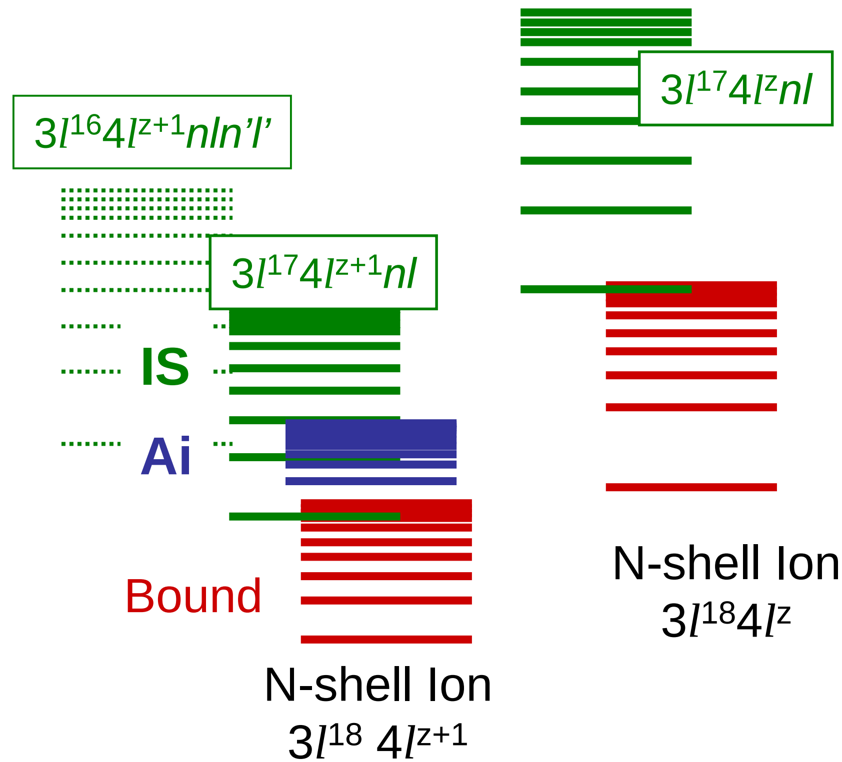

Charge state distributions look extremely promising!

Comparison of **FLYCHK** with measurements and numerous other codes shows excellent agreement for high and low Z

Xenon

$N_i = 4.75 \times 10^{18}$ cm^{-3} $T_e = 415$ eV

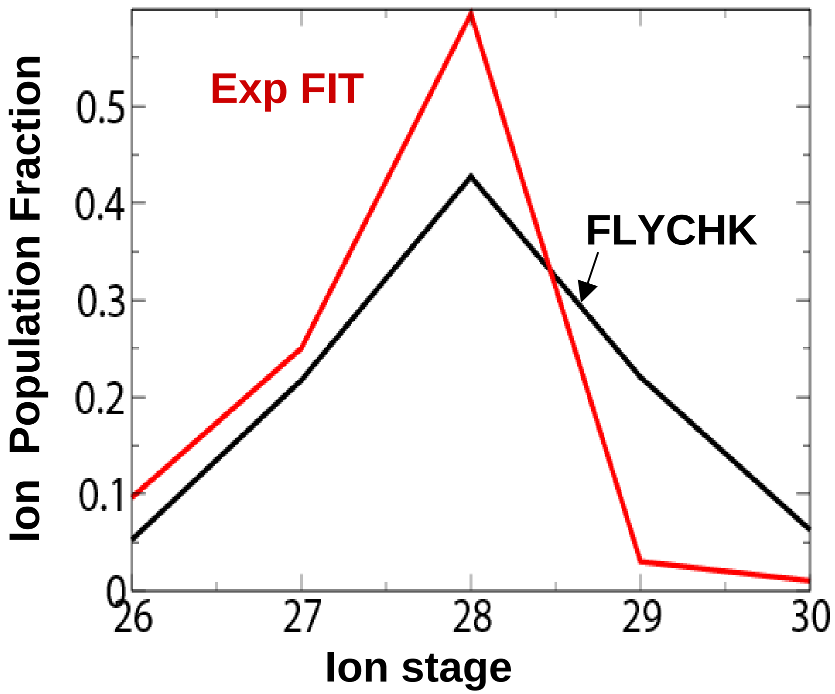

Au

$n_e = 10^{22} cm^{-3}$ $T_e = 750, 1500, 2500$ eV

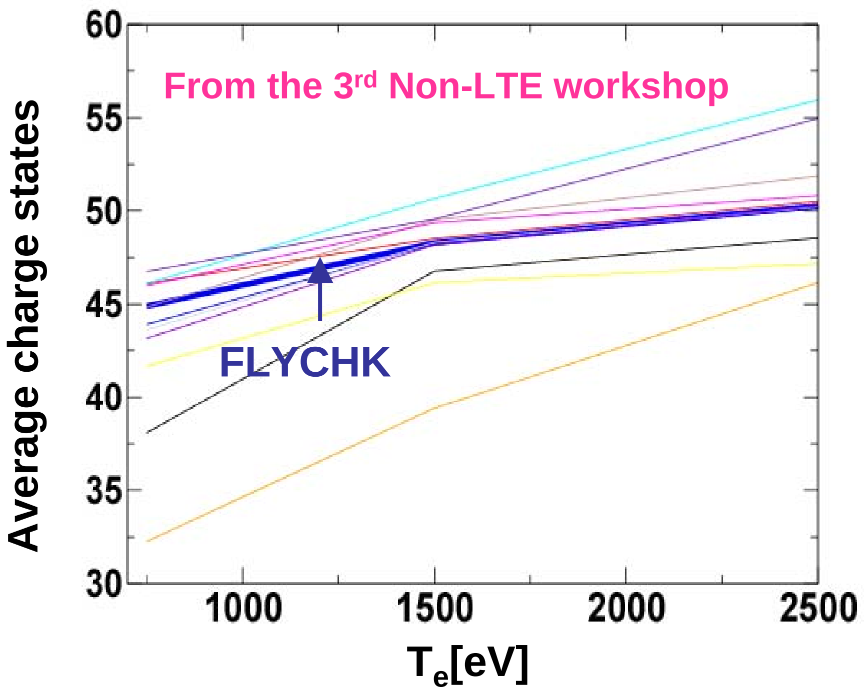

Cases tested include **C, Al, Ar, Ge, Ti, Kr, Xe, Au**

Investigation of ionization processes of short-pulse laser-produced plasmas

1) PIC simulations predict that the electron distributions should be described by multi-temperature Maxwellian.

2) Predicted high-energy electrons induce the inner-shell ionization of K-shell electrons which can be observed in K-α spectra while the laser is on.

3) K- α spectra exhibits shifts and broadening of cold K- α, which gives charge state distributions (CSD) of a plasma.

4) Charge-state distributions are dominated by thermal electron collisions unless hot electrons are predominant.

5) TD-CSD can reach to a steady-state within 1 ps.

6) A relativistic treatment of electron collisions is essential.

1D-PIC simulations show that electron energy distributions are represented by 2 hot electron temperatures

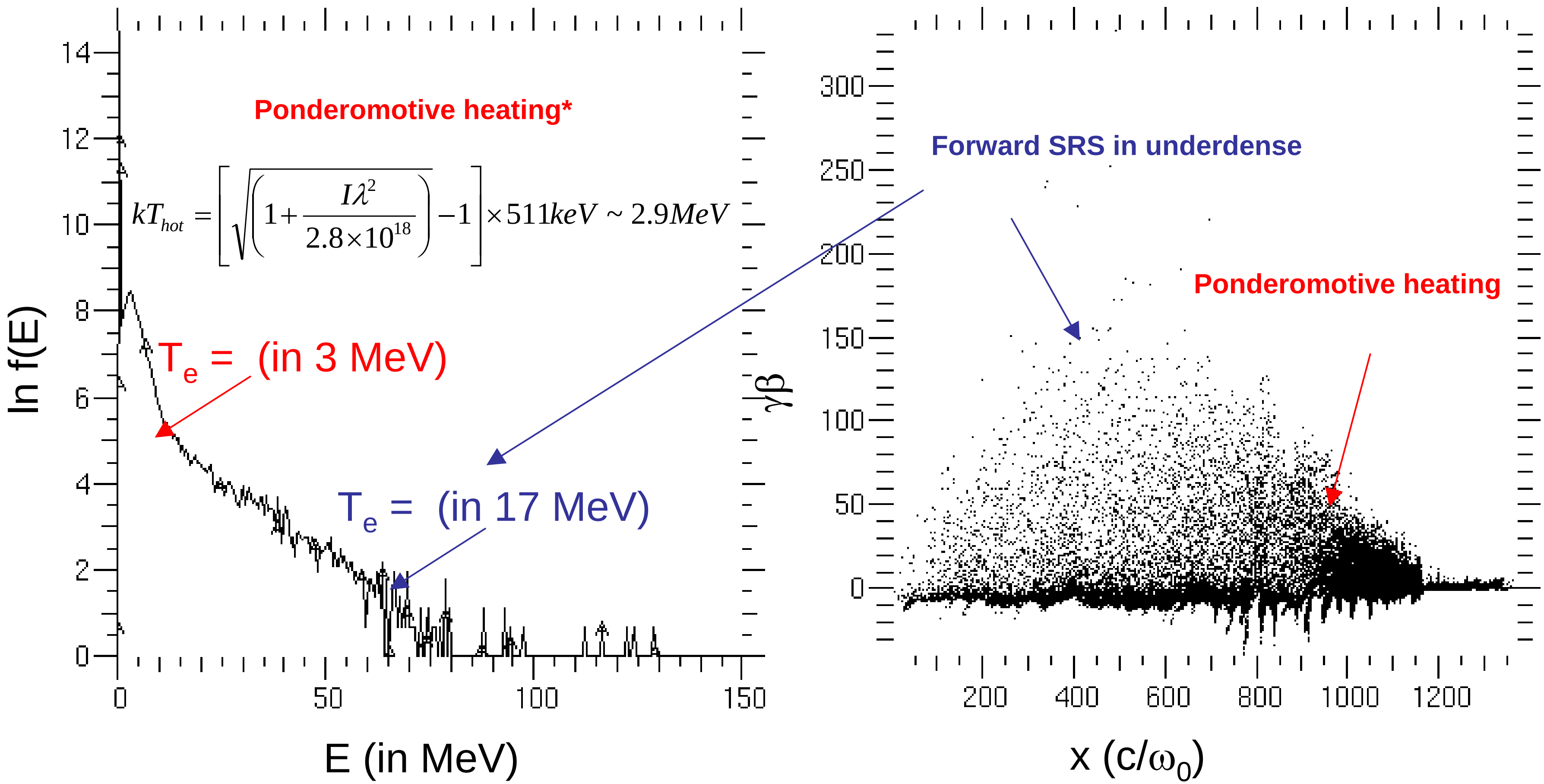

*kT_{hot} scaling from S. C. Wilks and W. L. Kruer,
"Absorption of ultrashort, ultra-intense laser light by Solids and Plasmas", IEEE J. Quant. Elec., **33** 1997.)

Charge state distributions of thermal plasmas with up to 10% of hot electrons of 3MeV remain similar

- CSD is most sensitive to thermal temperatures: 1 keV is required for He-like ion production
- Hot electrons did not make substantial differences :
  - relativistic cross-sections make a difference?
- Time-dependent calculations show that the plasma will reach at its steady-state & LTE values within 1 ps ($N_e=10^{23}cm^{-3}$)

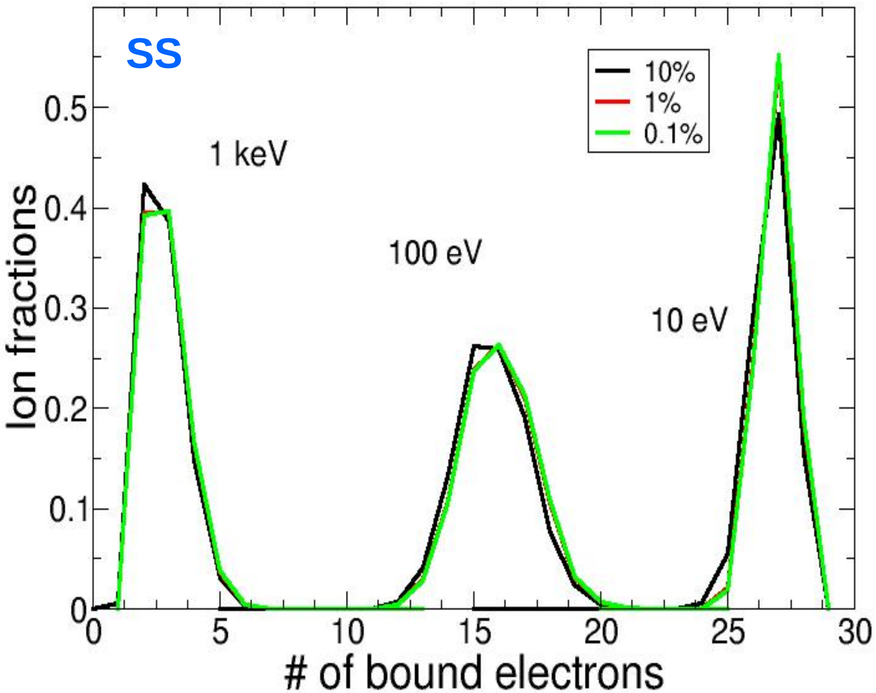

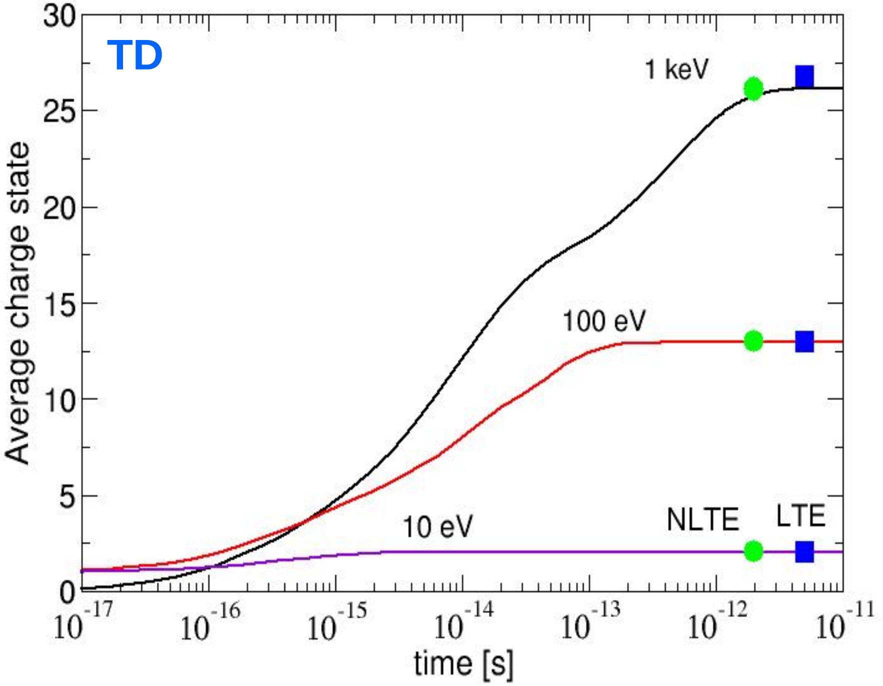

Relativistic ionization cross-sections can lead to a significant increase in ionization processes and K-α lines

Mau's relativistic ionization cross-sections of cupper ions

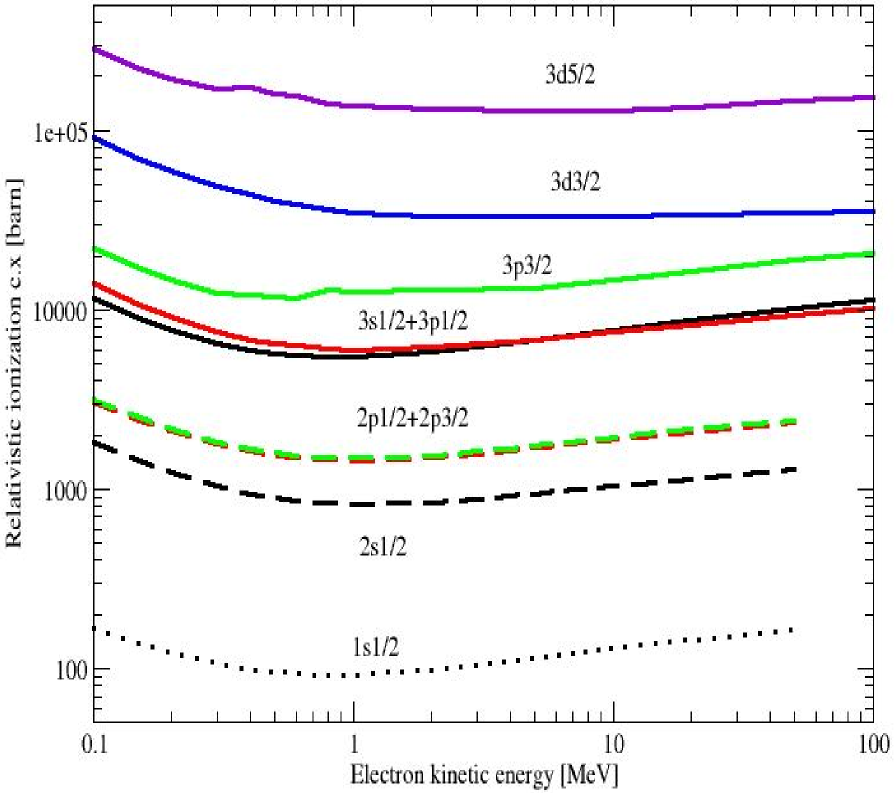

Functional formula of Relativistic ionization cross-sections

$$\sigma \propto \beta^{-2}\left[A\left[\ln\left(\beta^2/\left(1-\beta^2\right)\right)-\beta^2\right]+C\right]$$

J.Scofield, PRA 18,963 (1978)

U.Fano PR 95,1198 (1954)

U.Fano Ann.Rev.Nucl.Sci. 13,1(1963)

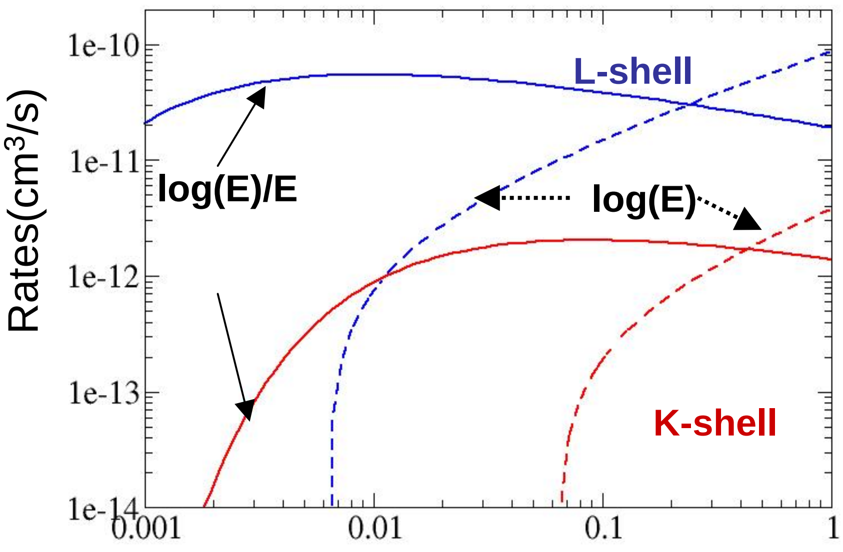

Fitting the Mau's data to give an empirical expression of relativistic ionization cross-sections

K-shell (ΔE=9000 eV)

L-shell (ΔE=1000 eV)

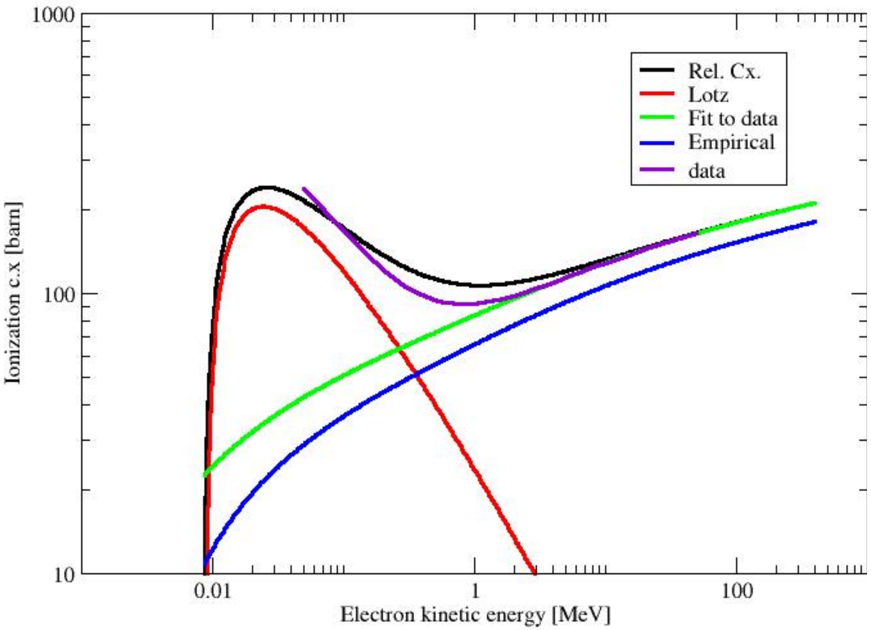

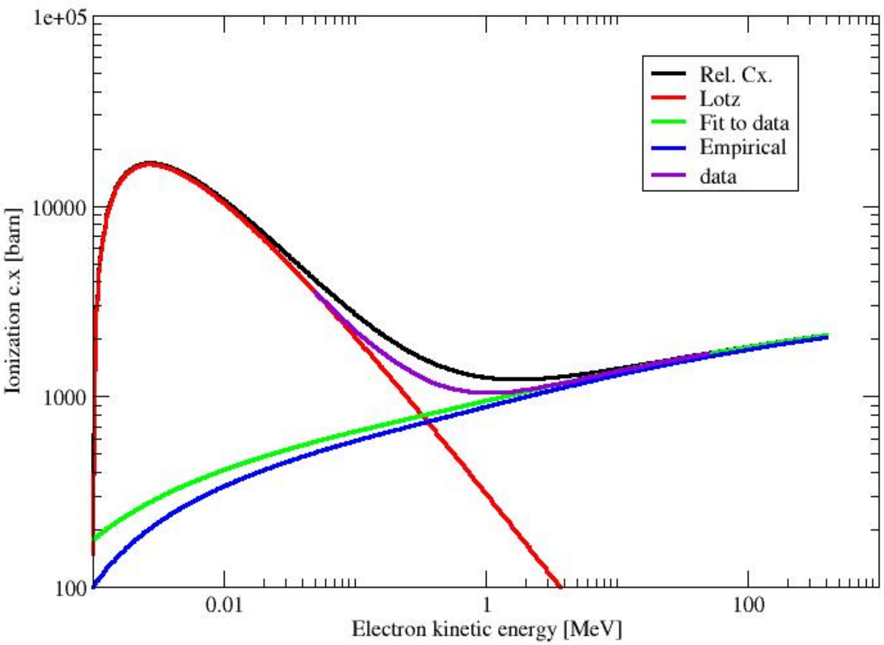

- **A careful study of Mau's relativistic cross-sections of K-, L- and M-shell led to an empirical relationship between ΔE and the fit parameters**

- **For X and Y, two conditions are used:**
  - **At 0.35MeV, the LN portion of c.x is the same as Lotz value**
  - **At IP, the LN portion is 1e5/ΔE barns.**

Relativistic cross-sections can make differences in ionization when relativistic electrons are predominant

Comparisons between non-relativistic (A) and relativistic (B) cases at $N_e=10^{22}$ cm^{-3} for three different hot electron fractions at T_{hot}=3MeV

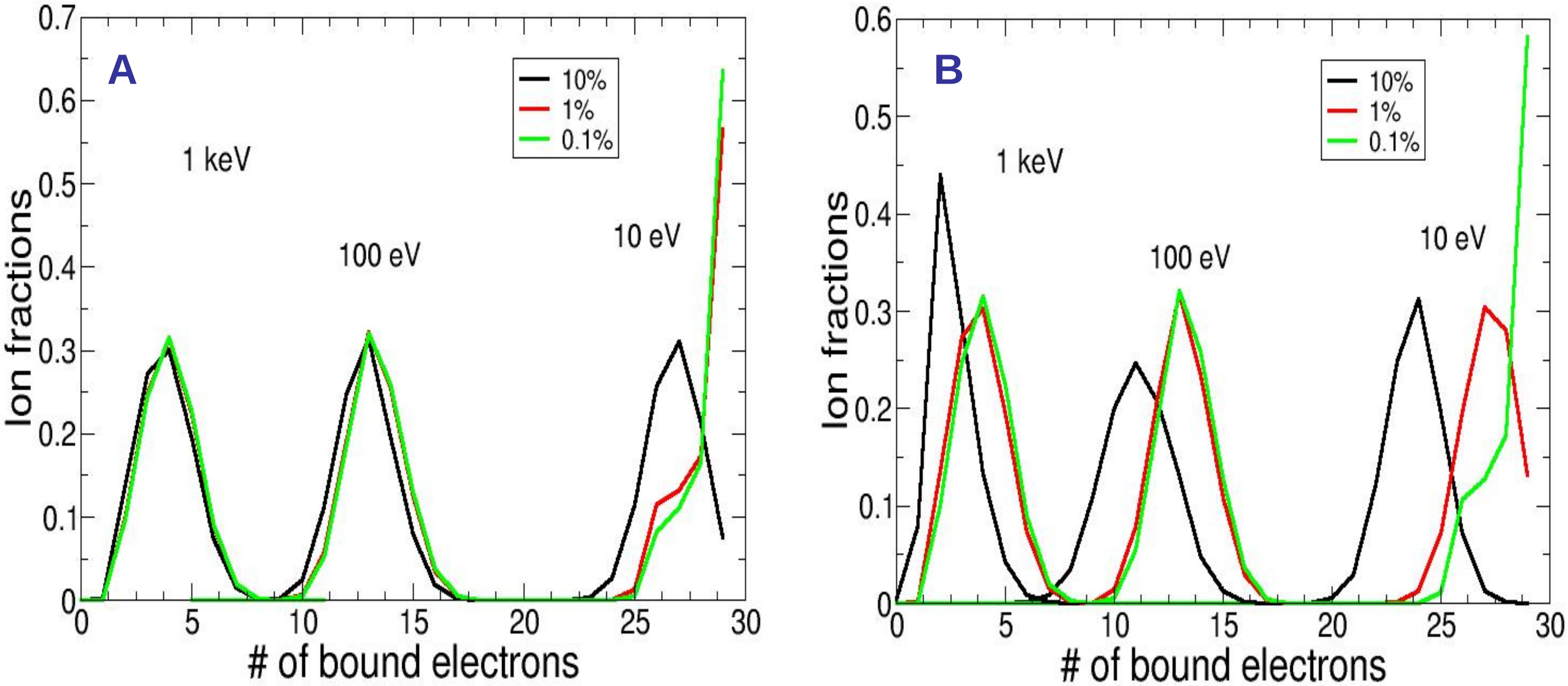

Relativistic cross-sections can make substantial differences in estimating K-α yields

Charge state distributions

T_e=1keV and ρ=0.01 ρ_{solid}

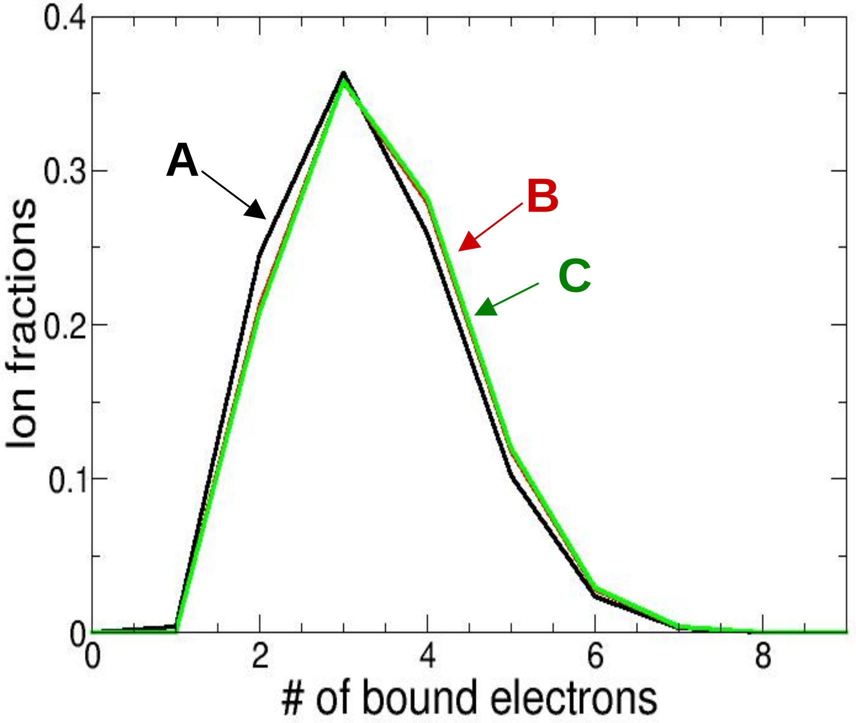

A. Relativistic c.x + 3 MeV (1%)

B. Non-relativistic c.x + 3 MeV(1%)

C. Non-relativistic c.x

K-α spectra

Te=1keV and ρ=0.01 ρ_{solid}

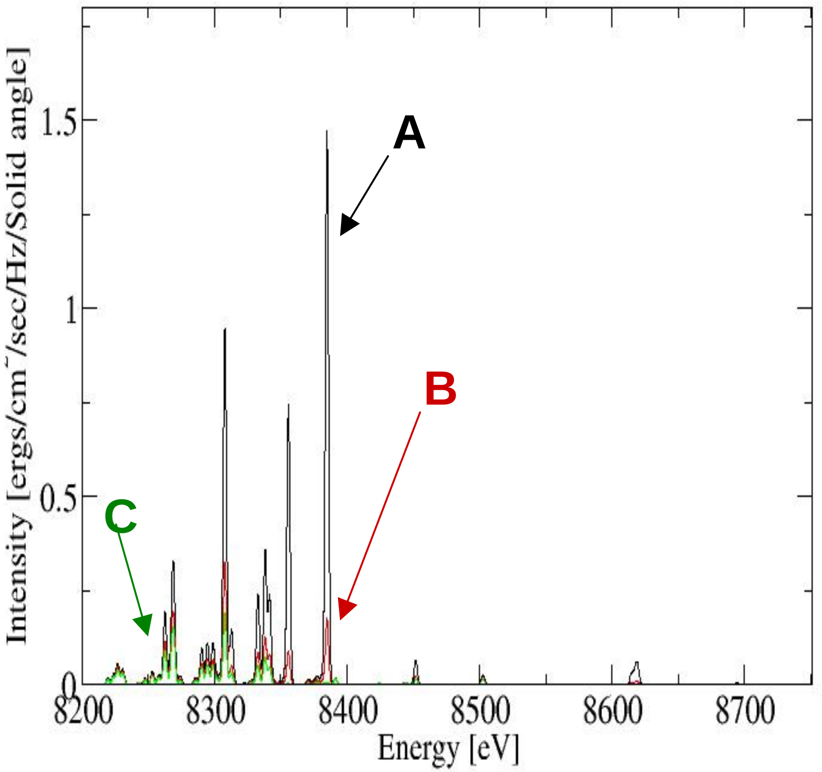

T_e-dependent charge state distributions lead to *shifts and broadening* of K-α emission

Charge state distributions:
Relativistic cross-sections with
1% of 3 MeV hot electrons

K-α spectra for ρ=0.01 ρ_{solid}
T_e: 50, 100, 500, 700 eV, 1keV

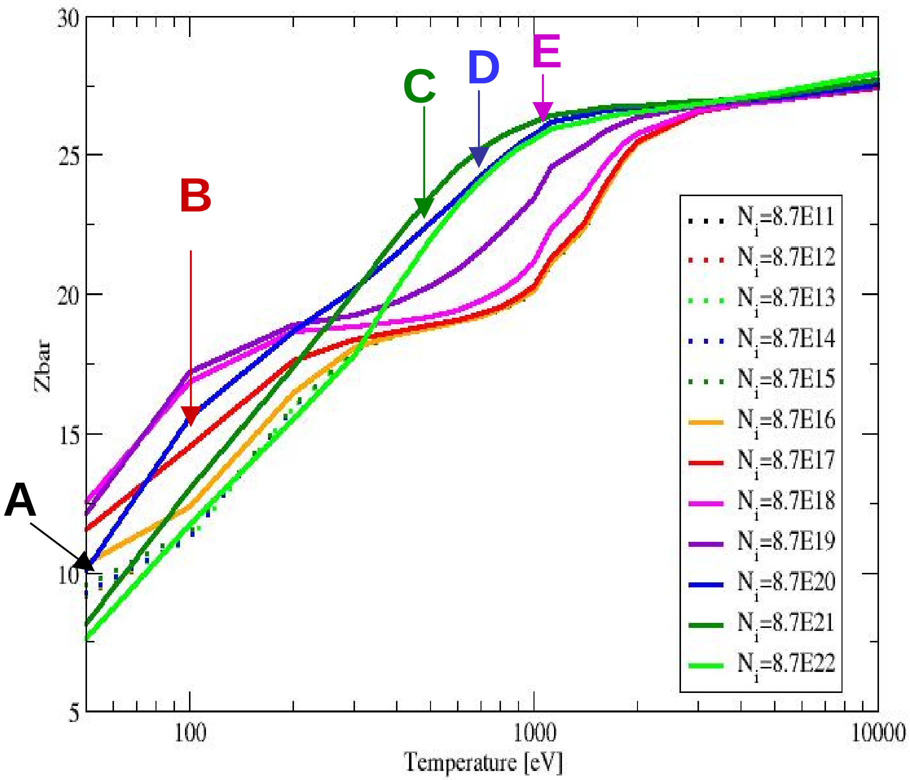

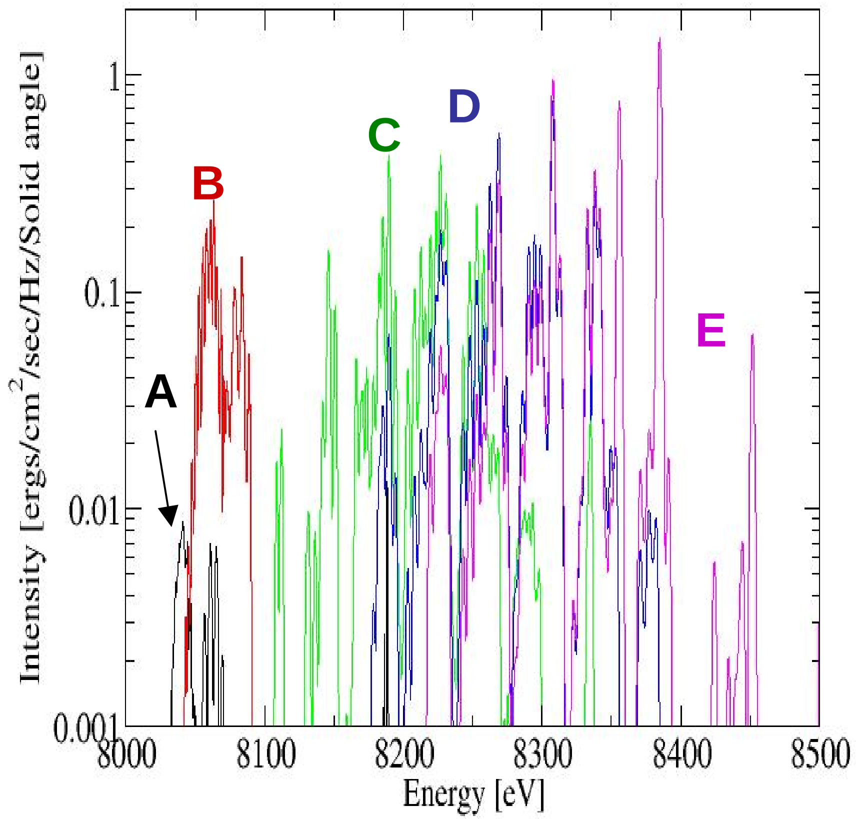

Investigation of K-α production: non-thermal electron diagnostic??

If thermal T_e is sufficiently low, K-α emission is solely dependent on non-thermal electron ionization processes.

T_e=100 eV and 0.1ρ_{solid} | T_e=500 eV and 0.1ρ_{solid} | T_e=1 keV and 0.1ρ_{solid}

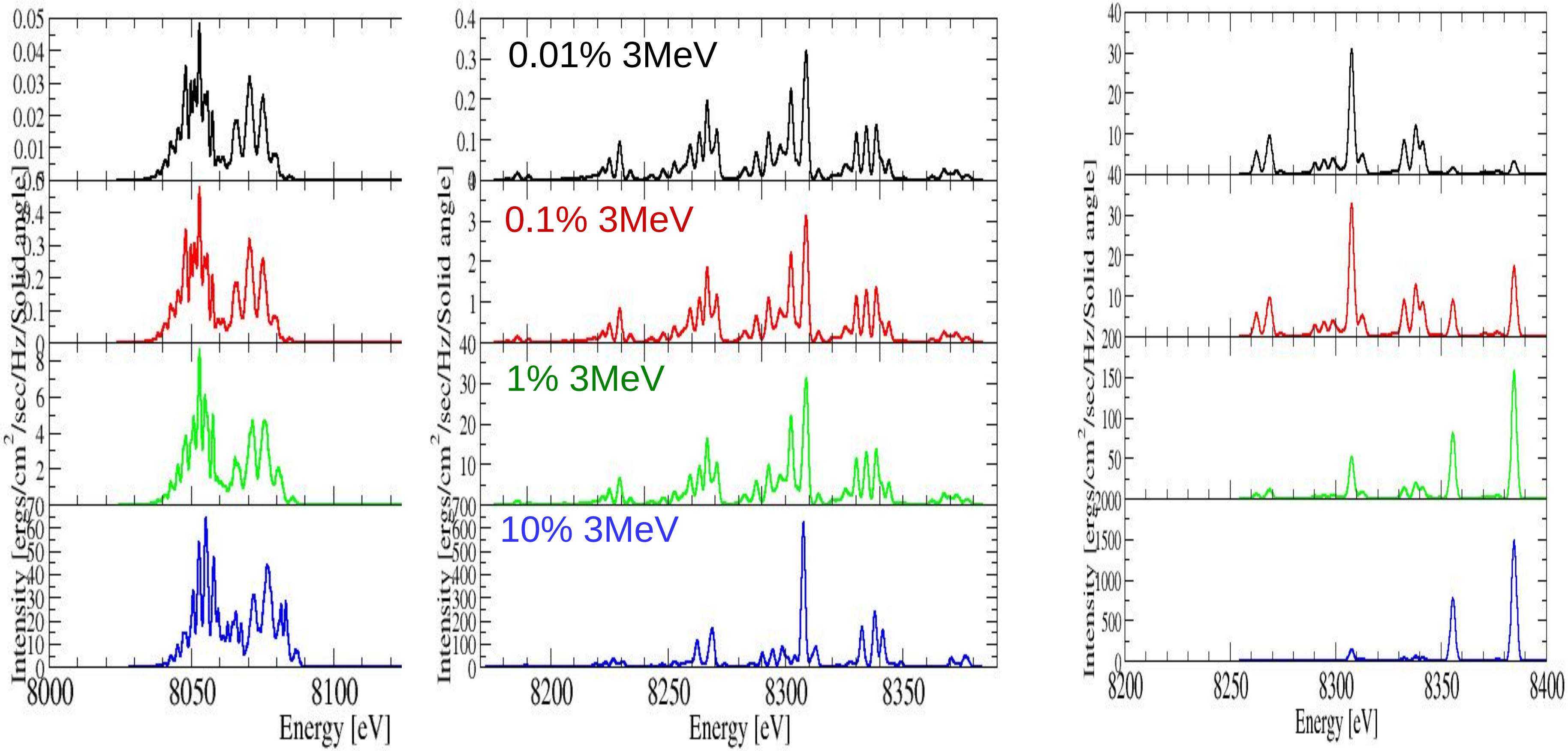

Investigation of K-α production: opacity effects and radiation trapping???

- **K-α lines become opacity-broadened with a plasma size of 1 – 100 μ.**
- **The self-absorption becomes non-negligible in population/CSD distributions.**

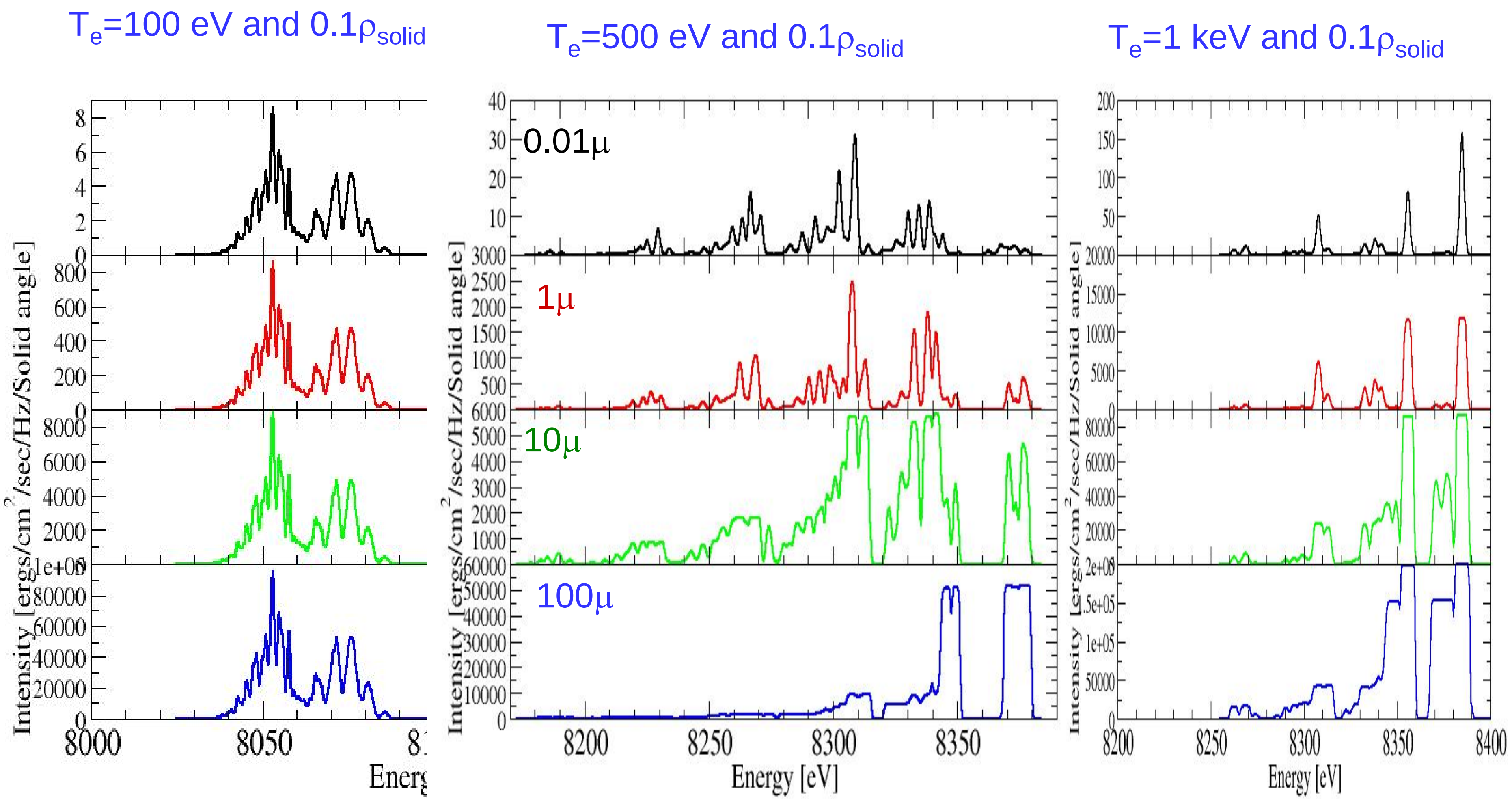

Investigation of K-α production: opacity effects and radiation trapping???

- **K-α lines become optically thick with a plasma size of 1 – 100 μ.**
- **When ions are in M-shell, the K-α optical depths are much smaller than L- or K-shell ions by orders of magnitude.**

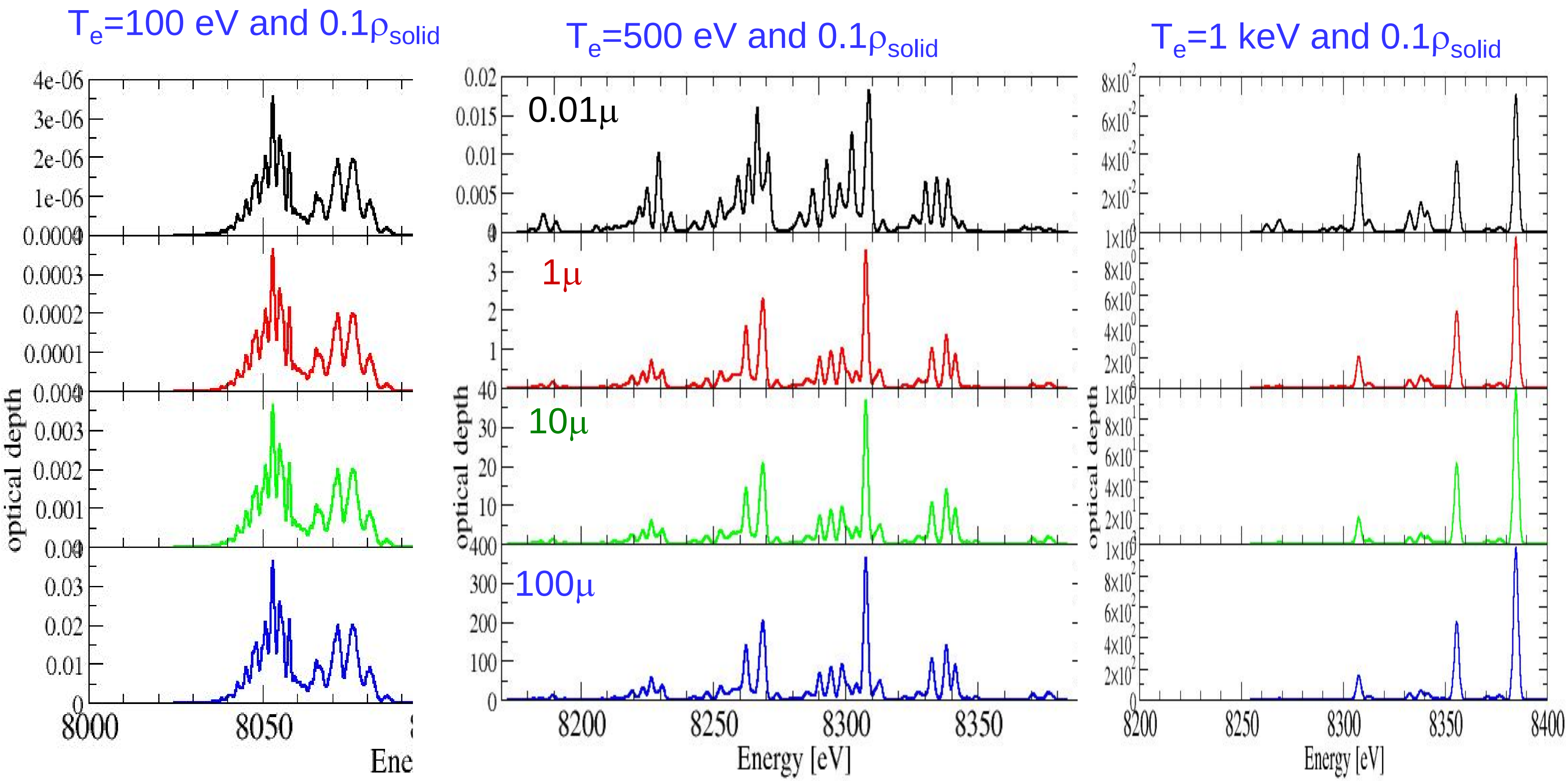

Ionization processes of ultra-short-pulse laser-produced plasmas

1) USP lasers with a fs pulse length will be operational in the near future.

2) Initially electrons are expected to be highly transient and highly non-equilibrium as well as population distributions.

3) Both electron and ion population distributions need to be solved self-consistently taking an account of all the elastic and inelastic collisions in the plasmas.

4) This approach will provide a tool to study the relaxation processes of non-equilibrium electron and ion population distributions

Ct27: Non-LTE kinetics code integrated with Boltzmann Eqn. Solver

a new capability for highly non-equilibrium fs timescale sources

$$\frac{\partial n_e(\varepsilon)}{\partial t} = \left[\frac{\partial n_e(\varepsilon)}{\partial t}\right]_{Elastic} + \left[\frac{\partial n_e(\varepsilon)}{\partial t}\right]_{\substack{Inelastic \\ \& Superelastic}} + \left[\frac{\partial n_e(\varepsilon)}{\partial t}\right]_{Sources} - \left[\frac{\partial n_e(\varepsilon)}{\partial t}\right]_{Sinks} + \left[\frac{\partial n_e(\varepsilon)}{\partial t}\right]_{\substack{Electron- \\ Electron}}$$

$$n_e(\varepsilon) = N_e \varepsilon^{1/2} f(\varepsilon) \quad \text{and} \quad \int d\varepsilon f(\varepsilon) \varepsilon^{1/2} = 1$$

- **Elastic losses to phonon (deformation potential) scattering**
- **Excitation and de-excitation of bound states**
- **Sources such as photo- and Auger electrons**
- **Sinks such as 3-body, dielectronic, and radiative recombination**
- **Electron thermalization due to collisions with other electrons**

Ct27 tested for transients generated by short-pulse source

XFEL test problem

Ionization distributions

Electron energy distributions

Relaxation time scales

200 eV-200 fs pulse with ΔE/E~0.003

10^{12} photons on solid Al 40μ spot

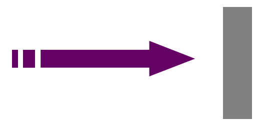

Assumptions

1) No initial solid-state structure

2) No plasma motion

1. Interaction of the high-energy photons with the initially solid density matter proceeds predominantly by the creation of inner shell ionization and photoelectrons will be produced at 105 eV.

2. This is followed by Auger decay and then by interaction of lower energy electrons with the atoms.

3. Electrons thermalize in a few fs due to *inelastic* e^--ion collisions

At 5 attoseconds: $N_e \sim 10^{16} cm^{-3}$ --- $T_e \sim 65$ eV --- $N_i \sim 6 \times 10^{22} cm^{-3}$

e-e elastic ν_{ee} : Coulomb $\sim 1.4 \times 10^9\ s^{-1}$

e-i inelastic ν_{ei} : excitation $\sim 5 \times 10^{16}\ s^{-1}$ --- ionization $\sim 2 \times 10^{16}\ s^{-1}$

Ct27 : Relaxation of initially generated photo-electrons can be studied

- The electron energy distribution function quickly establishes Maxwellian.
- T_e initially drops and increases to the equilibrium value

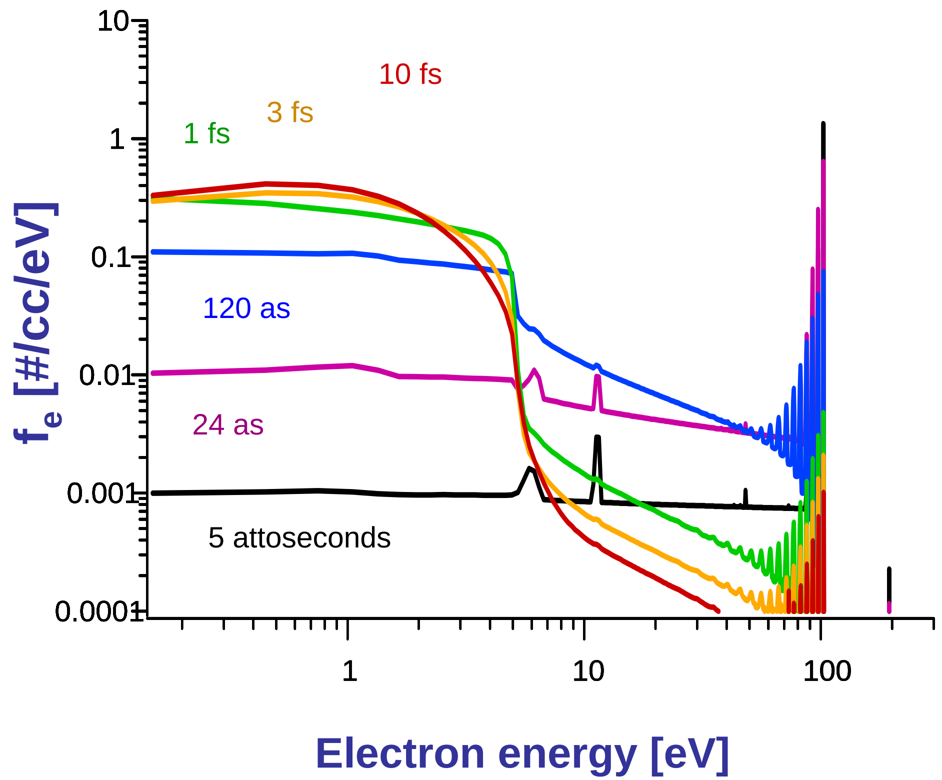

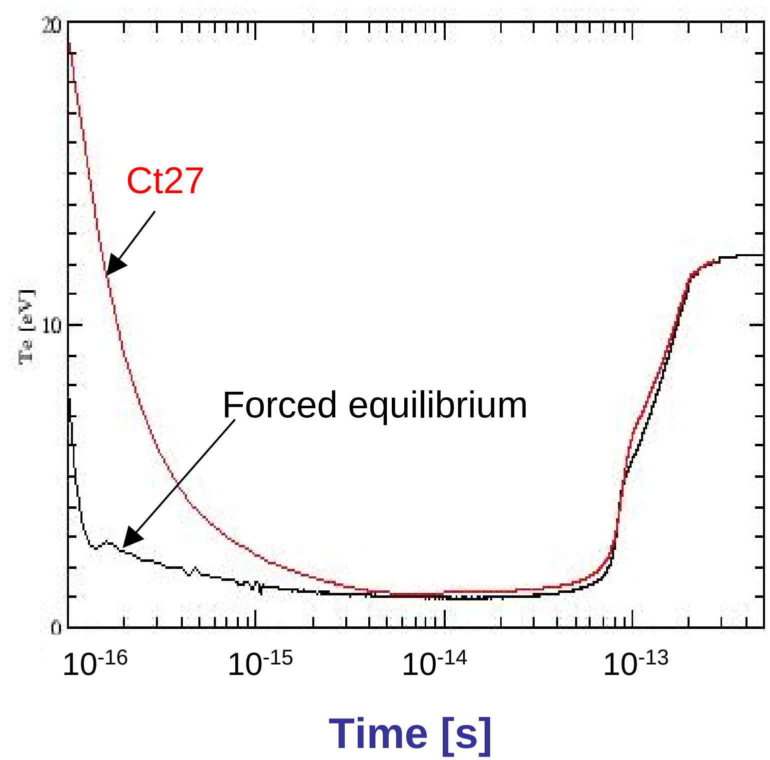

Spectral modeling of short-pulse laser-produced plasmas

1) Spectral modeling of laser-produced plasmas requires a comprehensive understanding of ionization processes

2) While a complete set of atomic data is essential to build a physically realistic population kinetics model, reasonably accurate atomic data is required for spectral analysis of observed spectra.

3) Combining FLYCHK population distribution and HULLAC atomic data, one can construct a realistic spectral model for data analysis.

4) When the radiation transport is important for inhomogeneous plasmas, the HULLAC–based model can be transported to a 3-D radiation transport code CRETIN

HULK: Detailed kinetics models consistent from low to high density created

- **HULLAC** (Hebrew University Lawrence Livermore Atomic Code) **can be used to generate a complete set of detailed atomic data**
  - **Developed by A. Bar-Shalom, M. Klapisch, J. Oreg, W. Goldstein**

- **HULK constructs a single kinetics model valid from very low density (coronal limit) to high density (fully collisional)**
  - **Low density plasmas**
    - Dielectronic Recombination and Excitation Autoionization
    - High-lying Rydberg states
  - **High density plasmas**
    - Approach to equilibrium : detailed balance
    - Continuum lowering

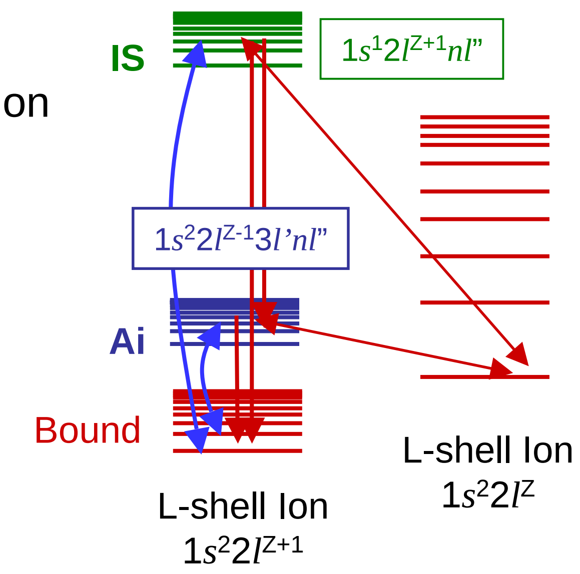

HULK: Ne-like lines and their satellites for 75 < Te < 150 eV expected for RAL Cu Can experiments (R. Shepherd)

Spectral calculation at Te=100 eV and Ne=10^{21}cm^{-3} shows that the measured spectra can be explained by Na-like and Mg-like satellites as well as Ne-like resonance lines

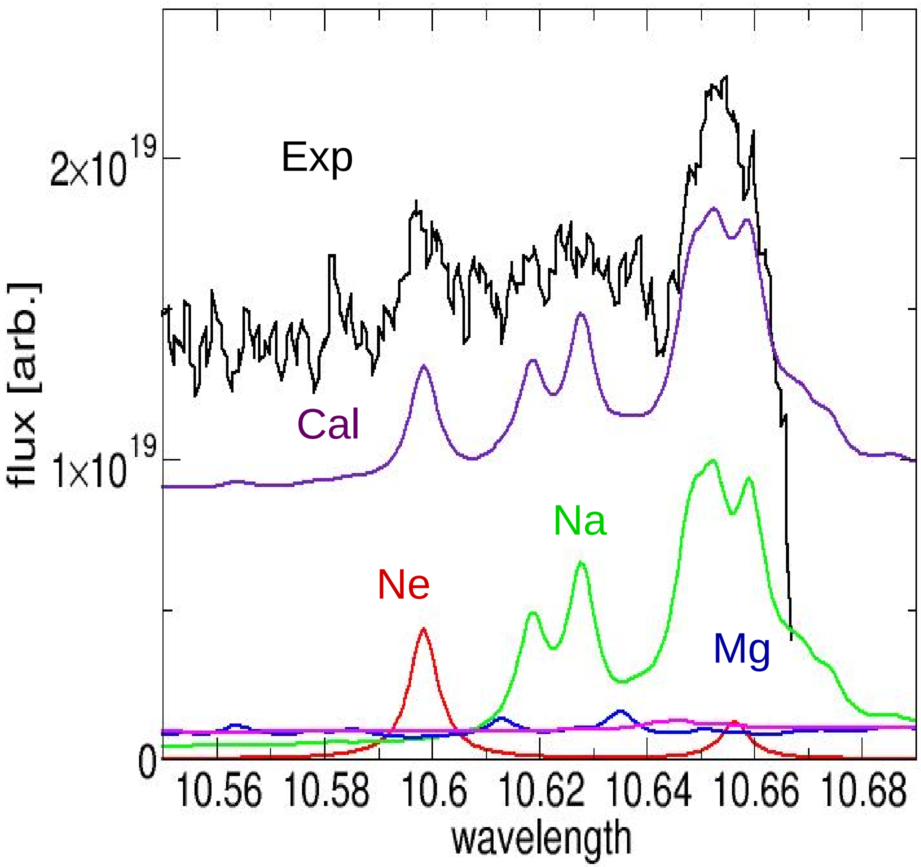

FLYCHK calculations

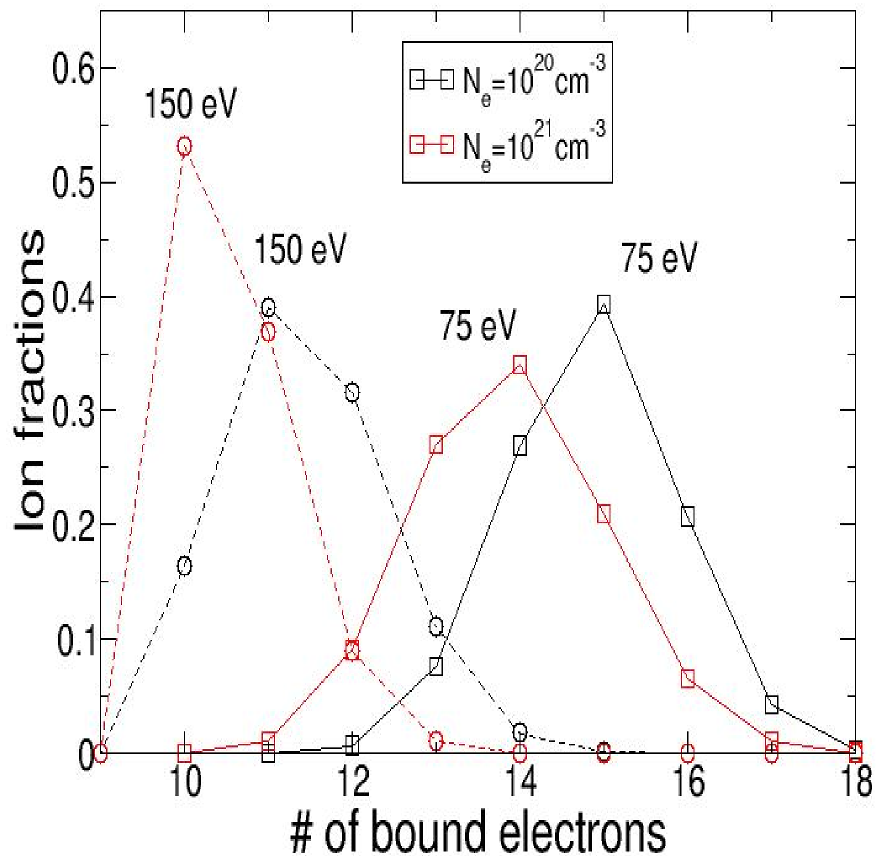

CRETIN: A 3-D radiative transport code can be used to understand inhomogeneous plasmas

Spectral calculation at Te=962.5 eV and Ne=10^{23}cm^{-3}
Ar-filled D2 Spherical target of 200 μm radius

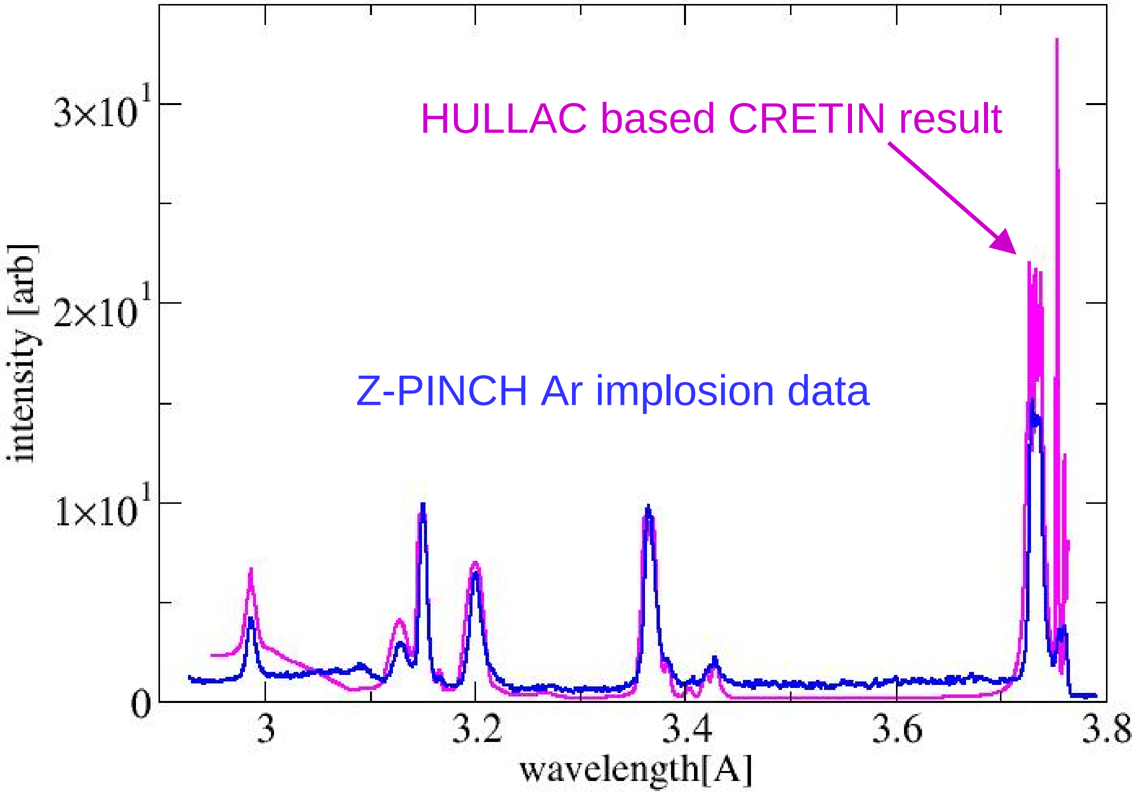

Summary: the next generation of population kinetics modeling tools will be available for SPL research

FLYCHK: **New simplified ionization balance model that is fast, accurate and easy-to-use for experimental planning with an option of detailed K-shell model**

Ct27: **New model to self-consistently treat populations and velocity distributions**

HULK: **Revised detailed kinetics and spectral modeling tool**

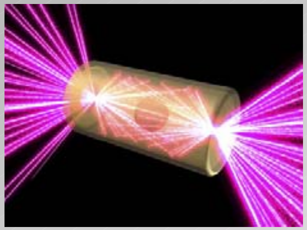

LSP SIMULATION OF COLLISIONLESS FAST ELECTRON STOPPING POWER

Cliff Thomas, Stanford University — **Mentor: Max Tabak, AX Division**

contact: saber@stanford.edu — **Lawrence Livermore National Laboratory**

Abstract: The possibility of easing the strict demands on indirect drive fusion by fast ignition has made a greater understanding of relativistic beam / plasma interactions imperative. As an approach to studying this phenomena, the suitability of LSP for modeling atomic-scale electron transport was investigated, and LSP was validated for calculating the plasma stopping power of a single electron. Current studies are considering the stopping power of multi-electron clusters – and enhanced stopping power is observed.

Outline

- Theoretical plasma stopping power for a single electron
  - The Fermi approach allows for a multi-body approximation to stopping power
  - The semi-classical solution (Bethe (1930)) is found through a simplification of Fermi solution
  - Multi-electron theory
- LSP's advantages over theory
- Of LSP, a single electron, and energy conservation
  - Energy conservation issues in LSP, self-loss common to PIC EM codes
  - 3 Games for ameliorating anomalous energy loss
- Validation of theory using LSP
  - Examples of LSP calculations versus theory
- Preliminary multi-electron results
  - Enhanced plasma stopping power

[1]

Theoretical Plasma Stopping Power

- Fermi approach includes multi-body approximation through a fluid formulation
  - Dielectric constant of form: $\varepsilon(w) = 1 - \frac{w_p^2}{w(w + i\upsilon_{coll})}$
  - Reduces to semi-classical solution at β→0 (same solution as Rutherford scattering + Bethe QM (1930))
  - Significant effects (multi-body coherency) at β→1 – this is important to dE/dx scaling at high β
  - At β→1 (see Jackson, 3rd edition, Ch13):

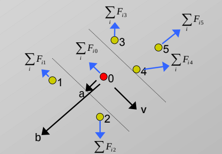

$$w_p^2 = \frac{4\pi N (Ze)^2}{m_e}$$

$$\left(\frac{dE}{dx}\right)_{b>a} = \frac{(ze)^2 w_p^2}{c^2} \ln\left(\frac{1.123c}{a w_p}\right)$$

- Extends to multi-electron clusters (Deutsch et al, etc.)
- Can't resolve r<a, can't accommodate plasma inhomogeneities, and can't capture beam instabilities, etc.
- Doesn't include dynamical effects (it is a steady-state solution).

[2]

LSP's Advantages

- Full multi-body approach (scattering treated for all impact parameters)
  - No floating constants (consider the consequences of 'a' in Fermi theoretical approach)
  - Reference frame approximations dropped
  - Trivial to extend to particle clusters and beams
- Dynamic acceleration treated naturally
- Easy to interrogate energy transfers to plasma, modes of energy transfer, instabilities, and more…

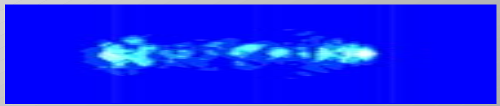

FIG [1] - |E| wake behind 1MeV electron in n = 10^{27} cm^{-3} plasma. Fundamental electric charge = 10e.

[3]

Of LSP, a single electron, and the problem of energy conservation

- Poor individual energy conservation (particles self-communicate in single Δt despite constant velocity)
  - Energy conservation = $f(\beta, \hat{v}, \Delta x, \Delta t)$
  - Two competing requirements on Δx, |self-effect|~Δx^{-2} and resolution~Δx
- 3 Games for improving energy conservation
  - (1) Minimize required resolution (usually means Δx << λ_D), or alter plasma parameters so the stopping power overwhelms the self-effect
  - (2) Choose optimum Δt

If $E_{electron}$ ~ 1MeV, Δx < λ_D,
Δt = Δt_{STAB} , T_e=5000eV, n_e=10^{26} cm^{-3}…
self-effect >> plasma stopping power !!!

If Eelectron ~ 1MeV, Δx < λ_D,
Δt = Δt_{OPT} , T_e=5000eV, n_e=10^{26} cm^{-3}…
self-effect < plasma stopping power !!!

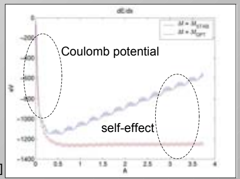

FIG [2]

  - (3) Subtract instantaneous self-fields to first order (there shouldn't be any instantaneous self-effect)
    - Run 2 tests, 1 in vacuum and 1 in plasma with the initial position and velocity duplicated
    - Only run the tests over a time period where the 2 trajectories nearly match
    - Take the difference. The result is the proper field causing deceleration + error estimation terms

Field on ballistic electron — Self-effect field — Stopping power contribution — Position and velocity Δ

[i] $$\vec{E}^q_{plasma+particle}(\vec{x}^q) = \sum_i^{time} \vec{f}(\vec{x}^q, \vec{x}_i^q, \vec{v}_i^q) + \sum_i^{time}\sum_j^{particle} \vec{f}(\vec{x}^q, \vec{x}_i^j, \vec{v}_i^j)$$

[ii] $$\vec{E}^q_{vacuum+particle}(\vec{y}^q) = \sum_i^{time} \vec{f}(\vec{y}^q, \vec{y}_i^q, \vec{w}_i^q) \longleftarrow \quad \vec{y}_i^q = \vec{x}_i^q + \Delta\vec{x}_i^q \quad \vec{w}_i^q = \vec{v}_i^q + \Delta\vec{v}_i^q$$

[iii] $$\vec{E}^q_{vacuum+particle}(\vec{y}^q) = \sum_i^{time} \vec{f}(\vec{x}^q, \vec{x}_i^q, \vec{v}_i^q) + \nabla_x \vec{f}\cdot\Delta\vec{x}^q + \nabla_x \vec{f}\cdot\Delta\vec{x}_i^q + \nabla_v \vec{f}\cdot\Delta\vec{v}_i^q + O(2) + \ldots$$

[iv] $$\vec{E}^q_{plasma+particle}(\vec{x}^q) - \vec{E}^q_{vacuum+particle}(\vec{y}^q) = \sum_i^{time}\sum_j^{particle} \vec{f}(\vec{x}^q, \vec{x}_i^j, \vec{v}_i^j) + O(1) + \ldots$$

[4]

Results for single electron tests (COLD PLASMA)

EX[1] $E_{electron}$ = 1MeV, Δx = 5x10^{-12} m, Δt = 9.5x10^{-21} s, ne = 10^{33} m^{-3}, Z_p = 1 — Error = +25%

dE/dx_N = -3.74x10^{-8} J/m = -233.43 keV/μm
dE/dx_T = -3.00x10^{-8} J/m = -187.25 keV/μm

EX[2] $E_{electron}$ = 1MeV, Δx = 5x10^{-12} m, Δt = 9.5x10^{-21} s, ne = 10^{32} m^{-3}, Z_p = 10 — Error = +14.3%

dE/dxN = -2.32x10^{-7} J/m = -1448.03 keV/μm
dE/dxT = -2.03x10^{-7} J/m = -1267.03 keV/μm

EX[3] $E_{electron}$ = 1MeV, Δx = 5x10^{-12} m, Δt = 9.5x10^{-21} s, n_e = 10^{32} m^{-3}, Z_p = 1 — Error = +2%

dE/dx_N = -3.85x10^{-9} J/m = -24.03 keV/μm
dE/dx_T = -3.91x10^{-9} J/m = -24.40 keV/μm

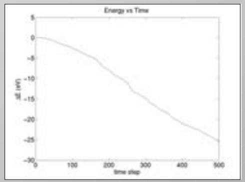

FIG [3] – Energy for EX[3].

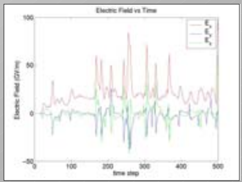

FIG [4] – Fields for EX[3].

[5]

A preliminary multi-electron test (COLD PLASMA)

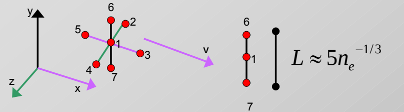

$$L \approx 5 n_e^{-1/3}$$

E^{1-7} = 1MeV, Δx = 5x10^{-12} m
Δt = 9.5x10^{-21} s, n_e = 10^{32} m^{-3}

- Expectation 1 (if particle spacing is > correlation length) $\left(\frac{dE}{dx}\right) \cong \sum_j^{particles} \left(\frac{dE}{dx}\right)^j_{b>a}$
  dE/dx1= -2.74x10^{-8} J/m = -170.83 keV/μm
- Expectation 2 (if particle spacing is < correlation length) $\left(\frac{dE}{dx}\right) \propto \left(\frac{dE}{dx}\right)_{b>a} \left(q = \sum_j q_j, m = \sum_j m_j\right)$
  dE/dx_2= -1.53x10^{-7} J/m = -954.95 keV/μm

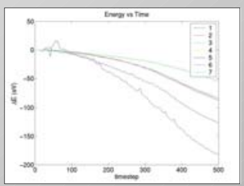

FIG [5]

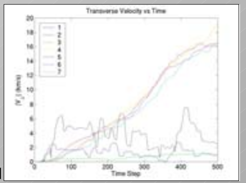

FIG [6]

- dE/dx_N= -1.33x10^{-7} J/m = -839.47 keV/μm (In the middle of the 2 expectations!)
- The plasma wake works to disrupt the organization of the cluster, and self-fields and plasma fields on the cluster tend to pull it apart. Should continue until inter-cluster distance > correlation length.
- Demonstrates potential to calculate dE/dx and rms deviation of particle in beam

[6]

Some Interesting Parameter Studies Using the LSP Code for Short-Pulse Applications

Presented to:

Short-Pulse Laser Matter Computational Workshop

Larissa Cottrill

August 25-27, 2004

This work was performed under the auspices of the U.S. Department of Energy by the University of California Lawrence Livermore National Laboratory under Contract No. W-7405-Eng-48.

Lawrence Livermore National Laboratory, P.O. Box 808, Livermore, CA 94551-0808

UCRL-POST-206307

Given LSP's wide range of uses as a modeling tool, we are exploring some of its less understood parameters

- LSP is currently being used for a number of short-pulse applications, such as
  - Effects of the initial electron distribution for fast ignition relevant experiments
  - Kα optimization for 1-D and 2-D x-ray backlighting
- Given the expanded role LSP is expected to have as a modeling tool for laser-plasma interactions in the future, a full understanding of the code's parameters is critical
- Over the course of its use, we have observed several interesting phenomena by varying a number of LSP parameters:
  - "fluid-streaming factor"
  - "discrete numbers" (particles per cell)

The "fluid-streaming factor" is a parameter within LSP whose attributes are not well understood

- The LSP manual defines the "fluid streaming factor" as a diffusion parameter used in the electron fluid model for a dense plasma such that
  - "small values (of order 0.1) reduce numerical diffusion of momentum"
  - "larger values have a stabilizing effect"
- For most of the simulations that have been performed using LSP, the fluid streaming factor has been set to a default value of 0.001 for closest agreement with experimental observations
- However, the effects of this parameter are not well understood and should be investigated further

We have modeled a generic Al target using various fluid streaming factors

- At early times in the simulation, variations in the fluid streaming factor appear to have little effect
- This can be seen by plotting the hot electron beam density at approximately 0.25 ps into the simulation

FSF=0.001 FSF=0.01 FSF=0.1

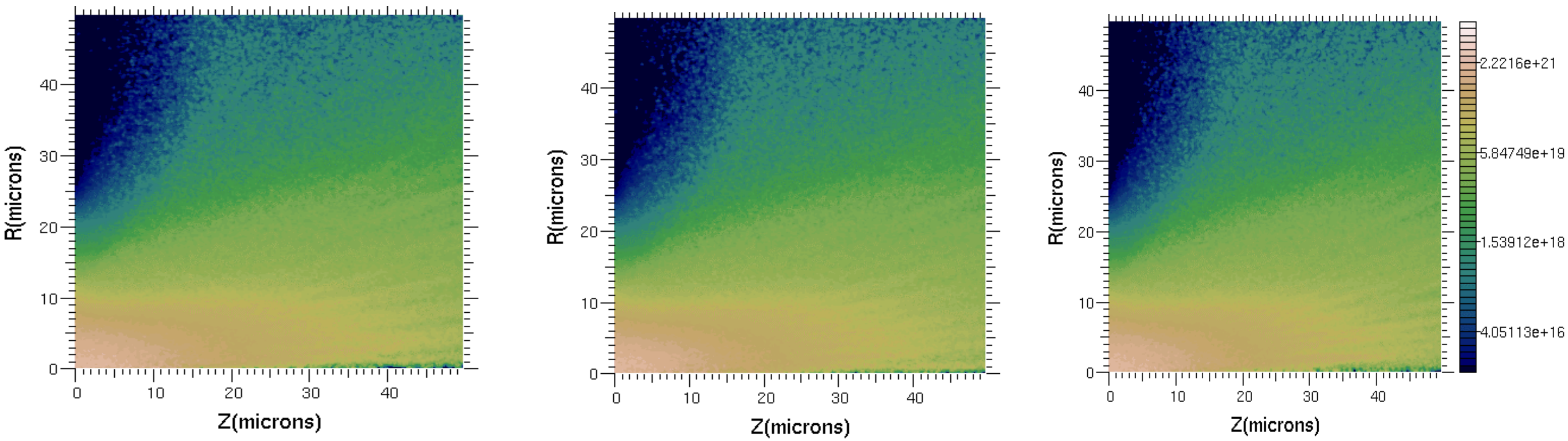

UCRL-POST-206307-4

Later times in the simulation reveal an interesting structure within the hot electron beam

- At later times, the hot electron beam appears to become more filamented as you increase the fluid streaming factor
- This can be seen by plotting the hot electron beam density at approximately 0.50 ps into the simulation

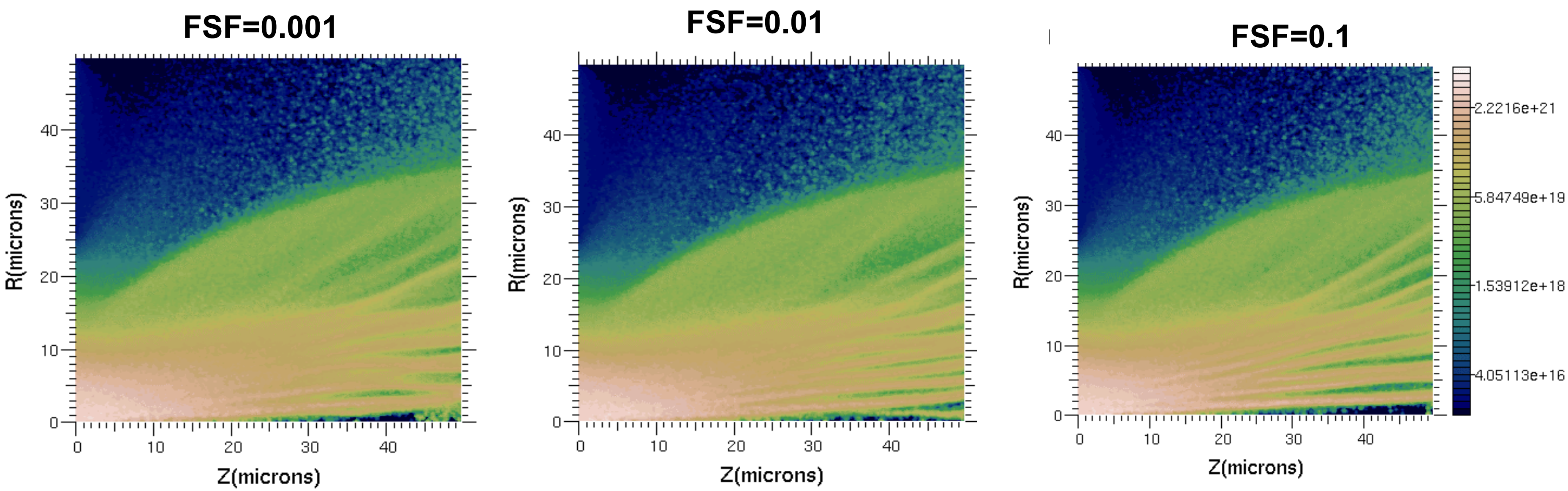

A more quantitative comparison can be seen from line-outs within the filamentation region

- By taking a radial average of the hot electron beam density between the 38-42μm region, the filamentation region can be better characterized
- The line-outs also confirm increased filamentation for later times

t=0.25ps

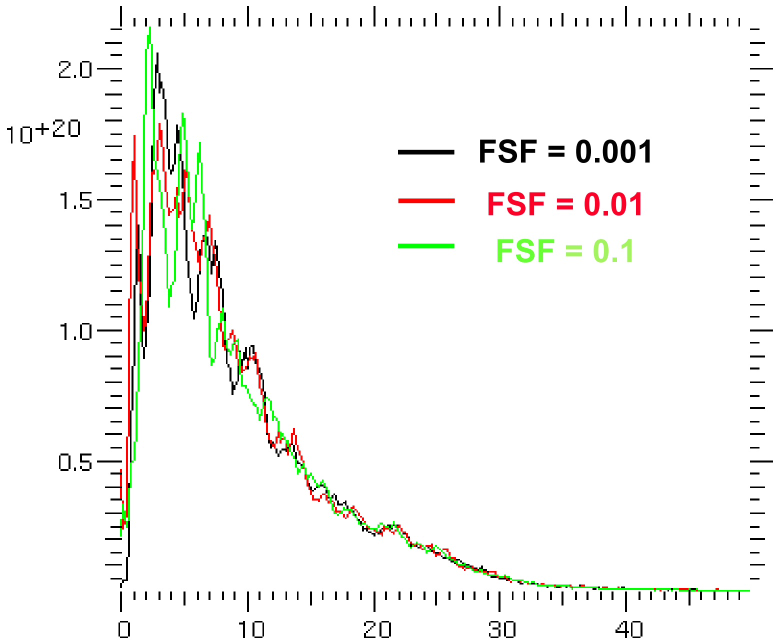

t=0.50ps

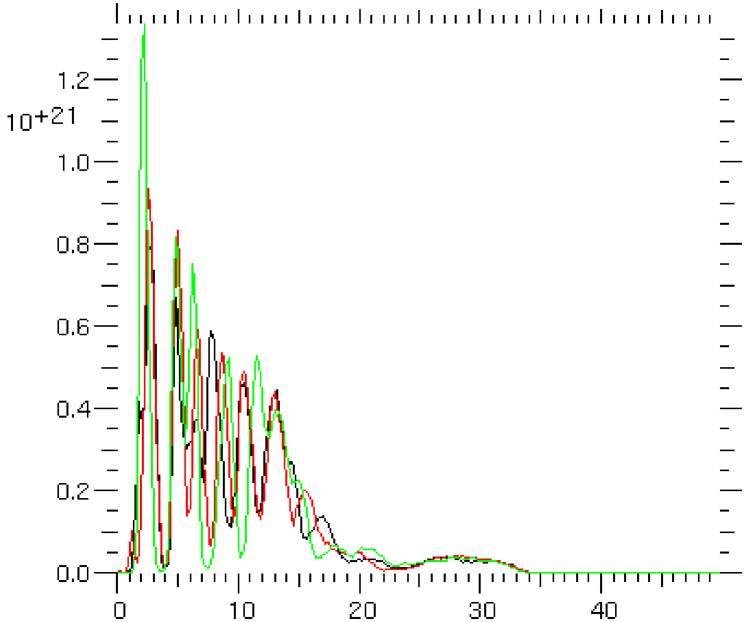

UCRL-POST-206307-6

The effects of the "discrete number" parameter are also not well understood

- The LSP manual allows the user to specify a discrete number, or number of particles per cell, for each direction of injection
- We have performed simulations in which the number of particles per cell is varied in the radial direction for 2-D geometries
- By increasing the number of particles per cell in the radial direction, the hot electron beam appears to become more filamented and the filaments begin to spread radially

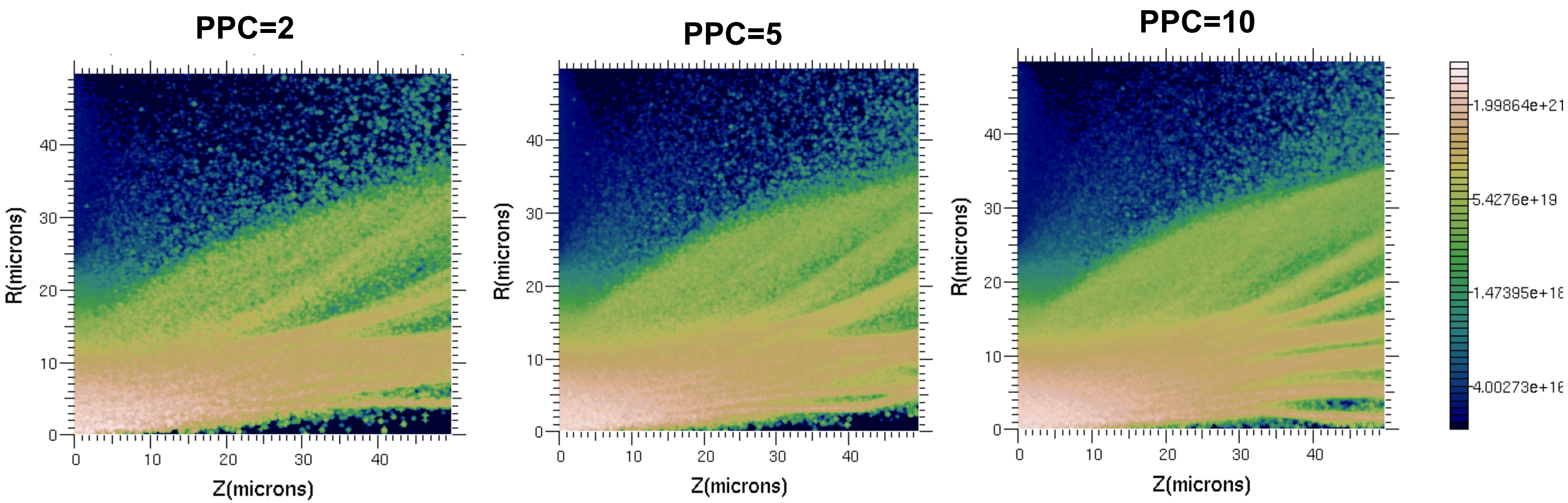

UCRL-POST-206307-7

Optimization of Kα Emission Yields for Short-Pulse High Intensity Laser-Solid Interactions

Presented to

Short Pulse Laser Matter Computational Workshop

L. A. Cottrill, M. H. Key, B. F. Lasinski, H. S. Park, B. A. Remington, R. A. Snavely, M. Tabak, R. P. J. Town
LLNL
J. F. Myatt
LLE
D. R. Welch
Mission Research Corp.

This work was performed under the auspices of the U.S. Department of Energy by the University of California Lawrence Livermore National Laboratory under Contract No. W-7405-Eng-48.

Lawrence Livermore National Laboratory, P.O. Box 808, Livermore, CA 94551-0808

UCRL-PRES-206093

Summary

The LSP and ITS codes have been used to model recent Kα backlighting experiments

- X-ray radiography will be an important diagnostic for NIF and one of the first uses of its short-pulse capability will be for backlighting
- Maximizing the production efficiency of Kα photons is essential for backlighting NIF targets
- 1-D and 2-D Kα backlighting geometries have been modeled
  - 40 keV edge on Sm foil (1-D)
  - 8 keV Au cone/Cu fiber target (2-D)
- Kα emission yields were compared using LSP and ITS to study the effects of how each code handles electromagnetic fields
  - ITS ignores the effects of fields on particles
  - LSP self-consistently calculates the field interactions

X-ray backlighting is a standard technique used for diagnosing the evolution of laser-driven experiments

- Backlighting, or "radiography," is an effective way to image the transient nature of hydrodynamic phenomena in high-density material interactions (i.e., x-ray or laser ablation)
- "Point projection" backlighting is a technique currently being explored in both 1D and 2D spatial resolution
- This technique consists of a backlighter "source" designed to provide a sufficient number and energy spectrum of x-ray photons to produce a high-quality image
- Previous backlighter sources have been "thermal," producing x-rays of only a few keV that cast a shadow of the sample on the detector

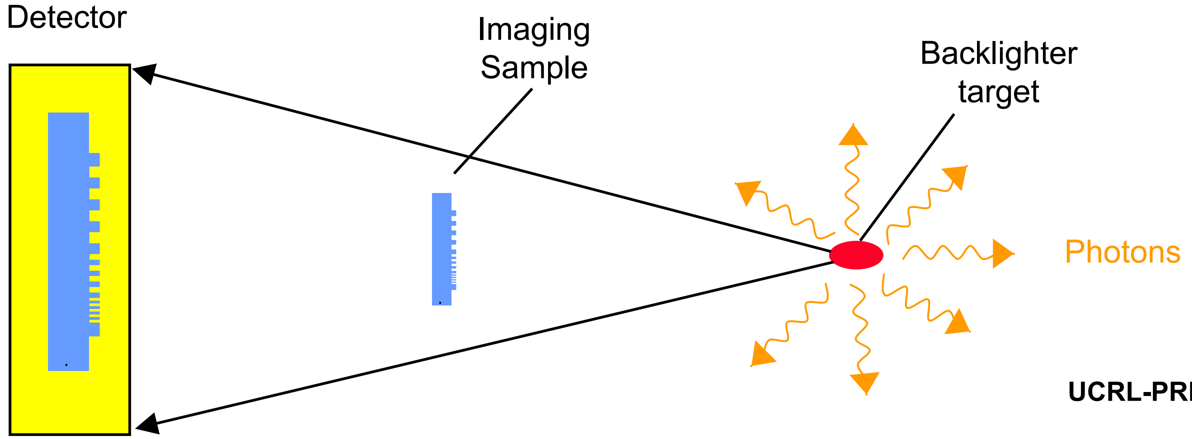

NIF experiments will require higher energy backlighter sources than thermal sources can provide

- Previous experiments using low-Z, low-mass targets allowed the use of low-energy (a few keV), thermal backlighters
- Experiments on NIF will use high-Z, relatively high-mass targets, requiring high energy photons for sufficient brightness

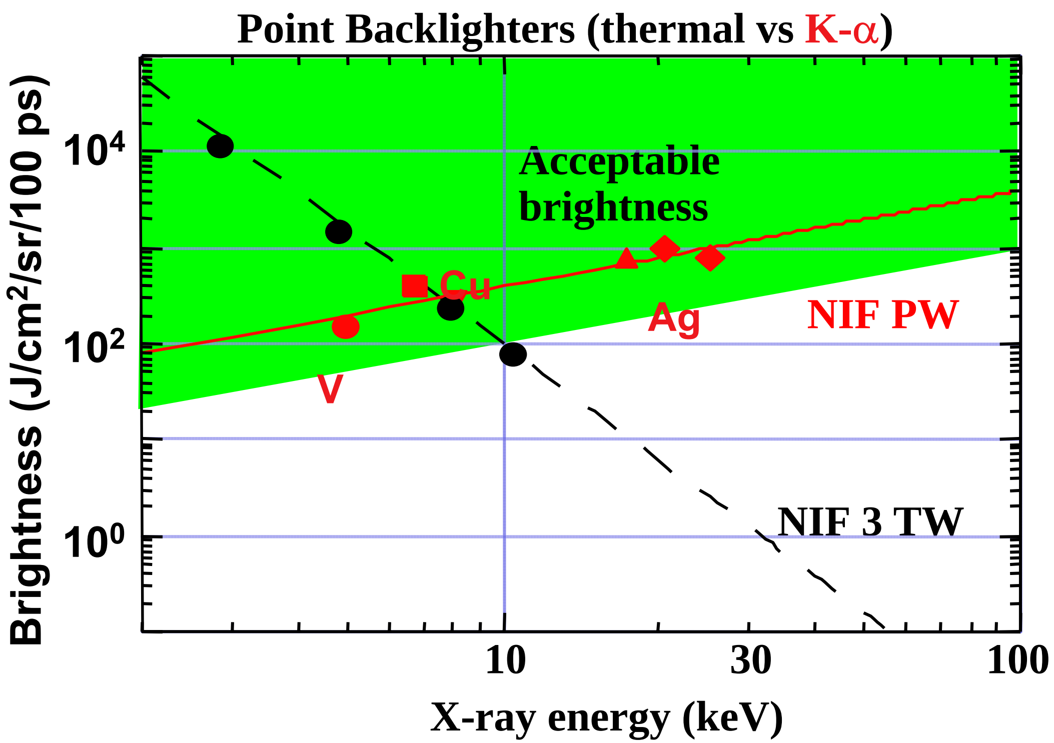

Remington, B.A.

The Solution: Use K-alpha x-ray sources driven by short-pulse, high intensity lasers to produce 20-100 keV x-ray sources

Concepts have been developed to produce suitable Kα backlighting sources

1-D Radiography

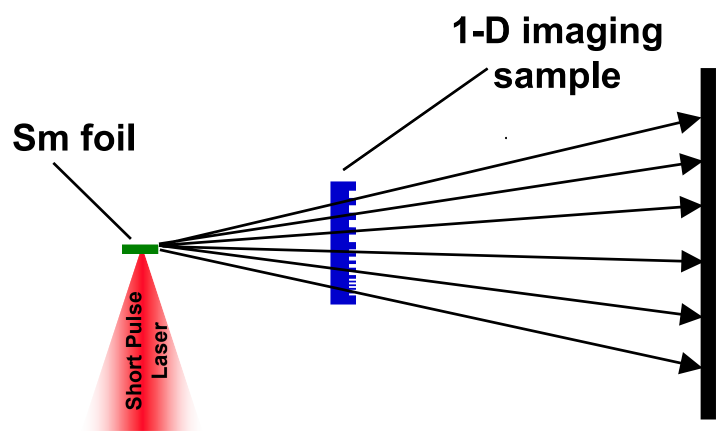

2-D Radiography

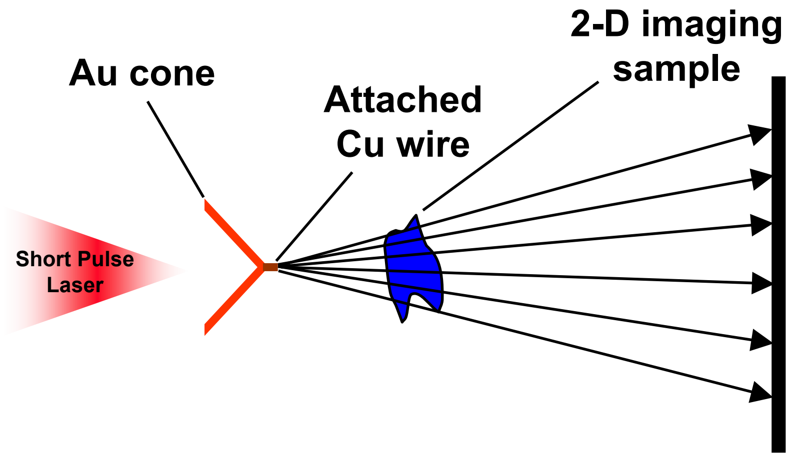

- Backlighter source consists of a disk positioned edge on
- Edge-on geometry has produced reasonably good radiography images at 40keV for samarium disk backlighters

- Backlighter source consists of a cone coupled to a fiber
- Cone-fiber geometry may increase laser-coupling and reduce divergence, allowing for small, bright point sources

We have performed ITS and LSP calculations of several proposed Kα radiography experiments

- The primary objective was to model experimental targets in LSP to characterize the Kα production efficiency and energy spectrum

- The ITS code has been the primary modeling tool for validating the experimental Kα conversion efficiencies to date; however, ITS
  - Ignores the effect of electromagnetic fields on the particles, and
  - Injects an ad-hoc electron beam into the target

- The LSP code self-consistently calculates the effect of the electromagnetic fields on the electrons, but still requires an electron beam source to be specified

ITS calculations were performed to model a recent Vulcan experiment

- The target geometry modeled was based on a 1-D radiography experiment using a Sm foil backlighter

Laser Parameters:

300J, 8μm spot size, 1ps pulse

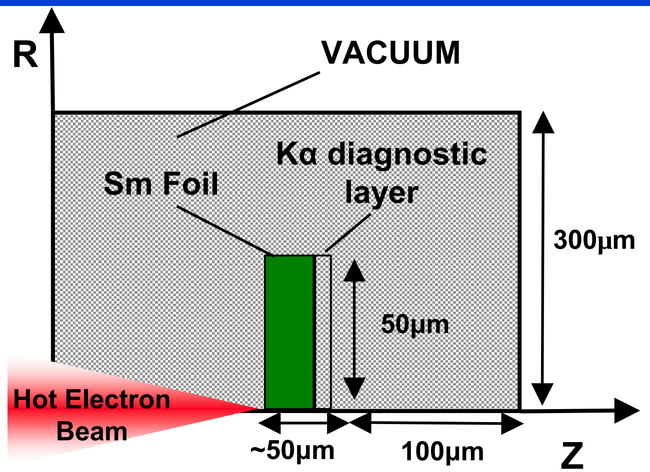

- In order to capture the electron refluxing within the target, we imposed external radial and axial electric fields within the code

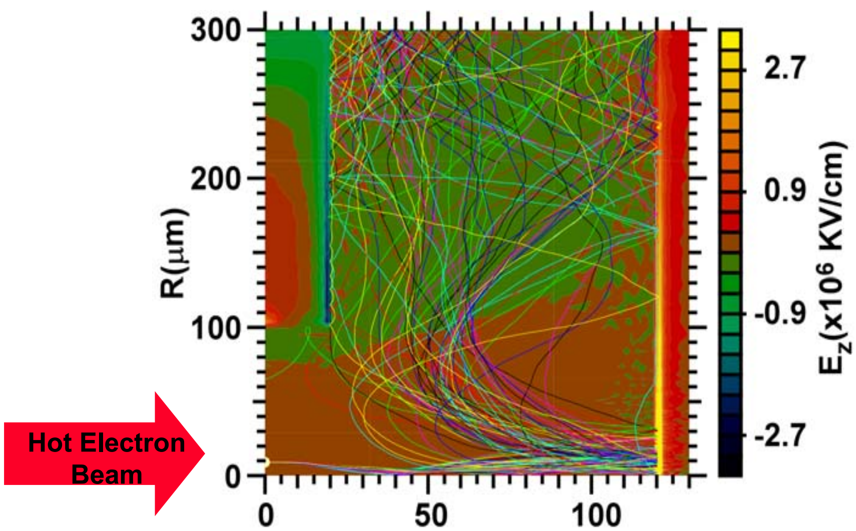

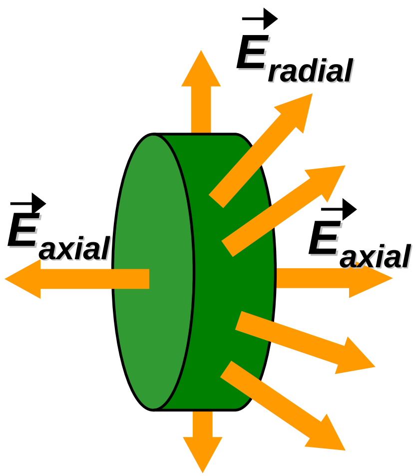

To better understand the effects of the fields, Kα yields were calculated for a range of target sizes

- **Simulations were performed for two cases:**
  - **radial and axial electric fields included within the vacuum region**
  - **axial fields only within the vacuum region**
- **Our results show that including the radial fields increases the Kα yield due to the trapping of the electrons**
- **Larger targets give an increased Kα yield**

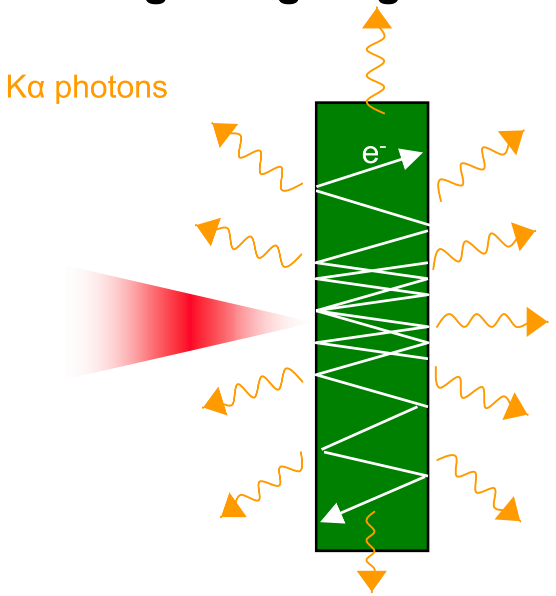

Electrons reflect from the target edges due to the imposed E fields

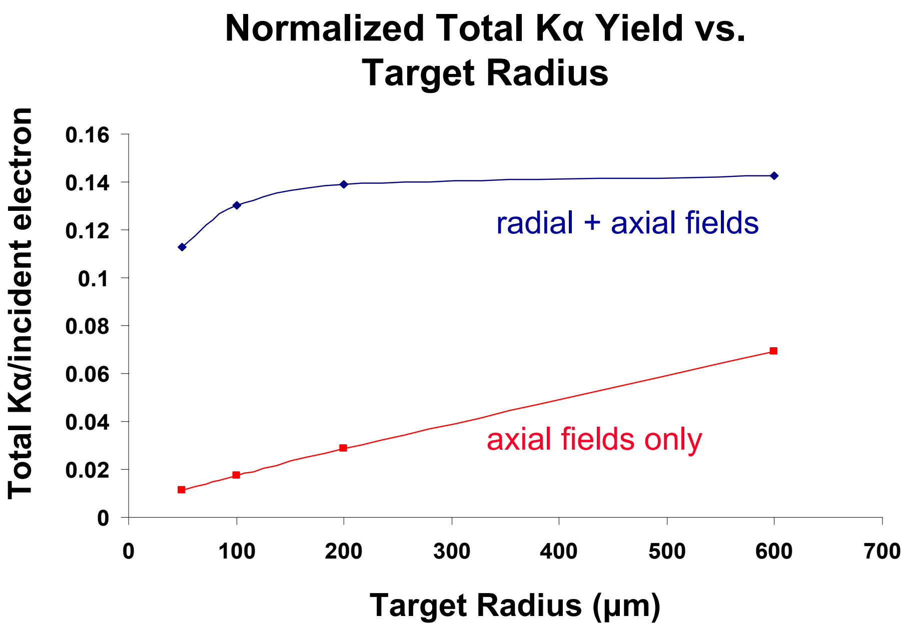

LSP[1] is a hybrid particle code used extensively in the ion beam community

- Simulations can be performed using:
  - 2-D in cylindrical geometry; and
  - 3-D in cartesian geometry.
- Employs a “direct implicit” energy conserving electromagnetic algorithm.
- Hybrid fluid-kinetic descriptions for electrons with dynamic reallocation.
- Scattering between the beam and background plasma included.
- Xgen cross-sections for Kα photon generation will be included
- Beam created by two methods:
  - Injection at target boundary;
  - Promotion from the background plasma.

[1] D. R. Welch, et al, Nucl. Inst. Meth. Phys. Res. A 242, 134 (2001).

The source of electrons is based on experimental data and scaling laws

Hot electron conversion efficiency

The efficiency at a particular intensity is based on experimental data

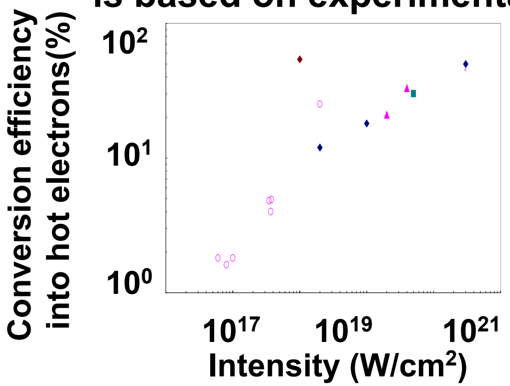

Hot electron temperature

The temperature of the hot electrons is based on Beg's experimental scaling[1]

$$T_{hot}\,(\text{keV}) = 100\,(I\lambda^2)^{1/3}$$

[1] A. R. Bell, J. R. Davies & S. M. Guerin, Phys. Rev. E 58, 2471 (1998).

Intensity Distribution

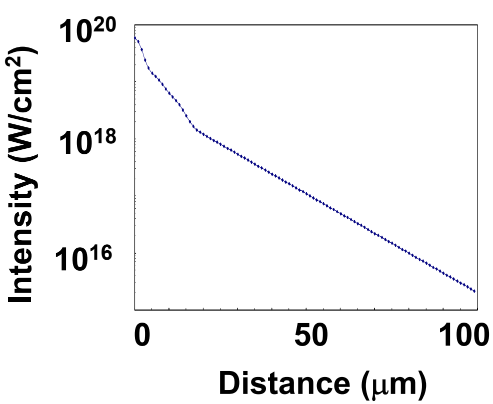

Apply Scalings

Hot electron input

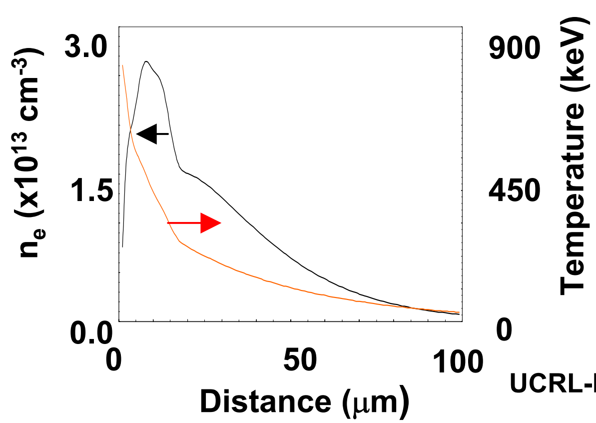

Until recently, an object had to be placed in the plasma to generate photons

- Objects are a way of representing material structures, they are:
  - Perfect conductors.
  - Electrons can pass through the object; ions cannot.
  - Electrons are not affected by fields in the object.
- Plasmas are the usual way to represent the target. Unlike objects, the plasma representation:
  - Allows electrons and ions to pass through.
  - Electrons are affected by fields.
  - Uses Spitzer conductivity.
- The code has been modified such that an object can be placed in the target without effecting the particle transport

Early modeling efforts showed that the conducting object modifies the hot electron beam propagation

- **Previously, we modeled targets based on experiments performed on the LULI and Vulcan lasers, but were constrained to use a conducting Cu fluor layer**
- **The presence of the conducting object causes a significant reduction in beam density in the rear layer of Al**

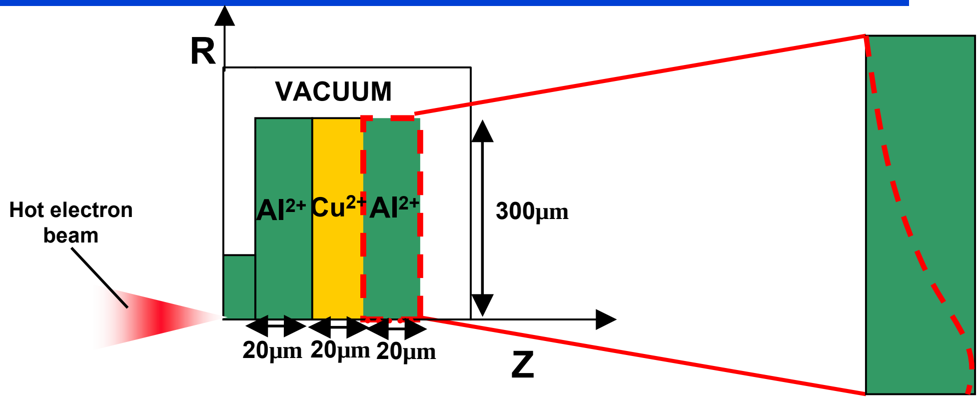

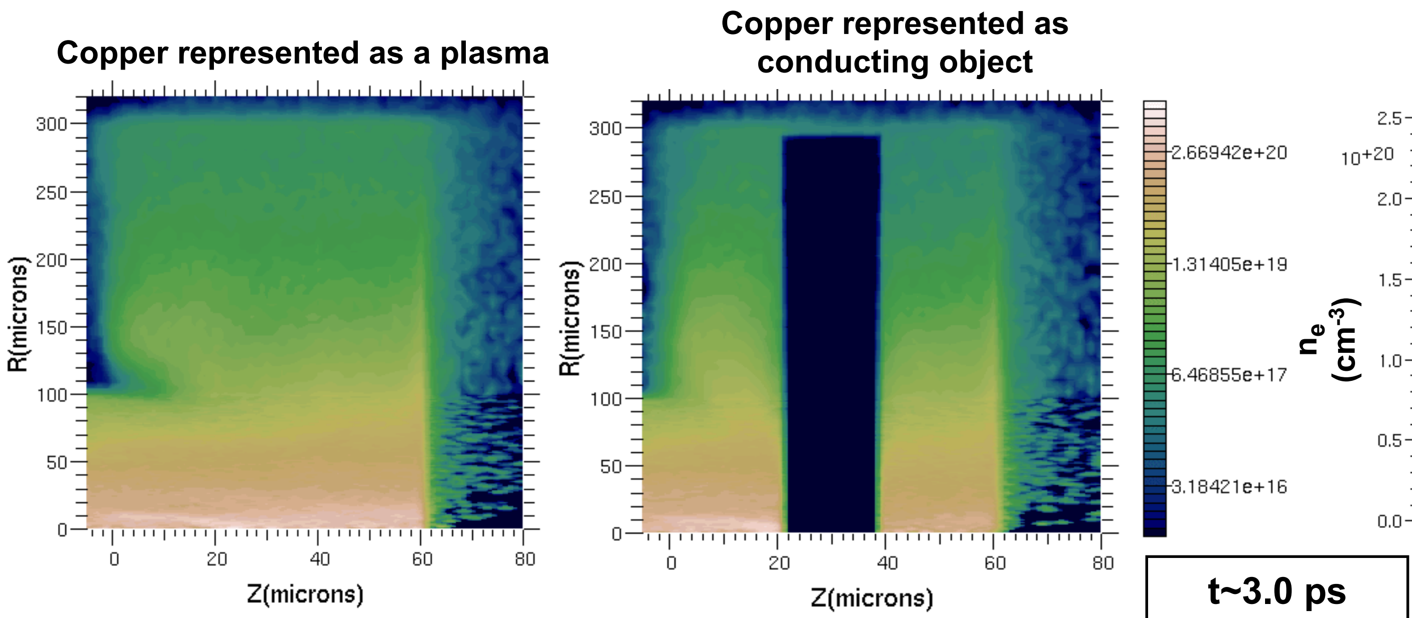

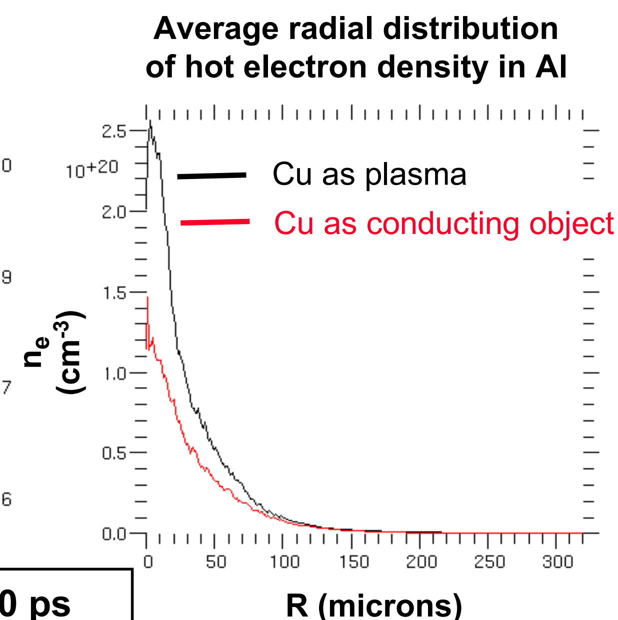

LSP was recently modified to remove the constraint of conducting object for photon production

- **Although the fluor layer must still be represented as an object, the conducting option can now be turned off such that the object is non-invasive**
- **Simulations of the multi-layer Al/Cu/Al target were redone using a non-conducting Cu object and do not appear to affect the electron transport**

Copper represented as a plasma

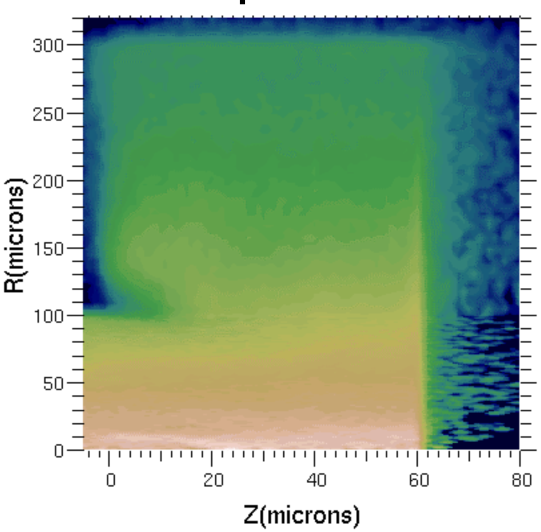

Copper represented as non-conducting object

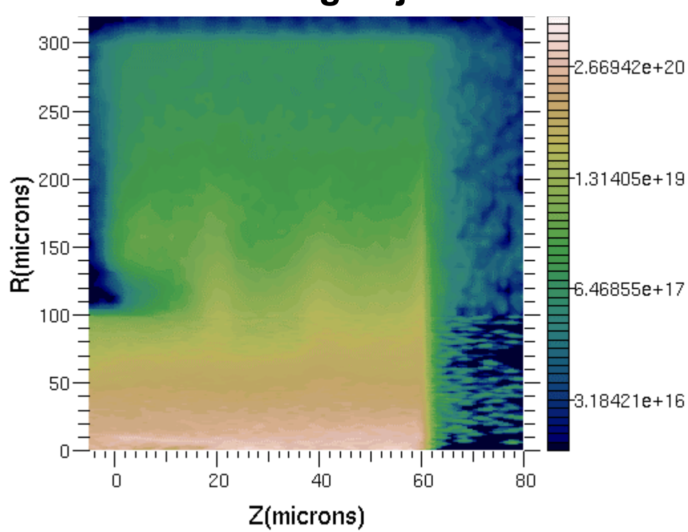

Average radial distribution of hot electron density

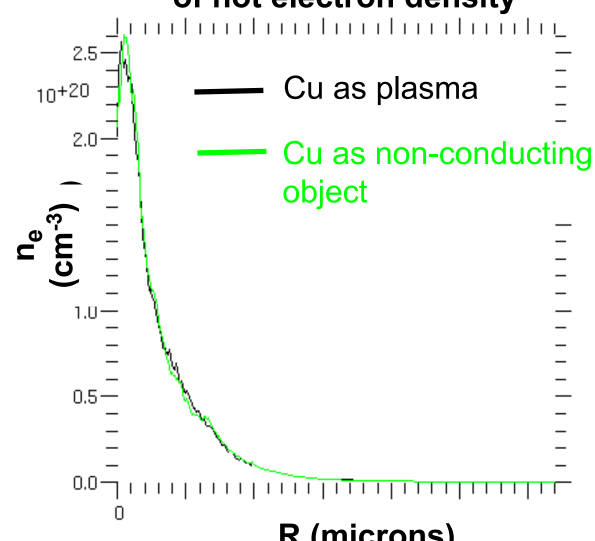

The Sm backlighter 1-D radiography experiment was also modeled in LSP to compare with ITS

- LSP self-consistently calculates the electric fields which are responsible for the refluxing, or "trapping," of the electrons

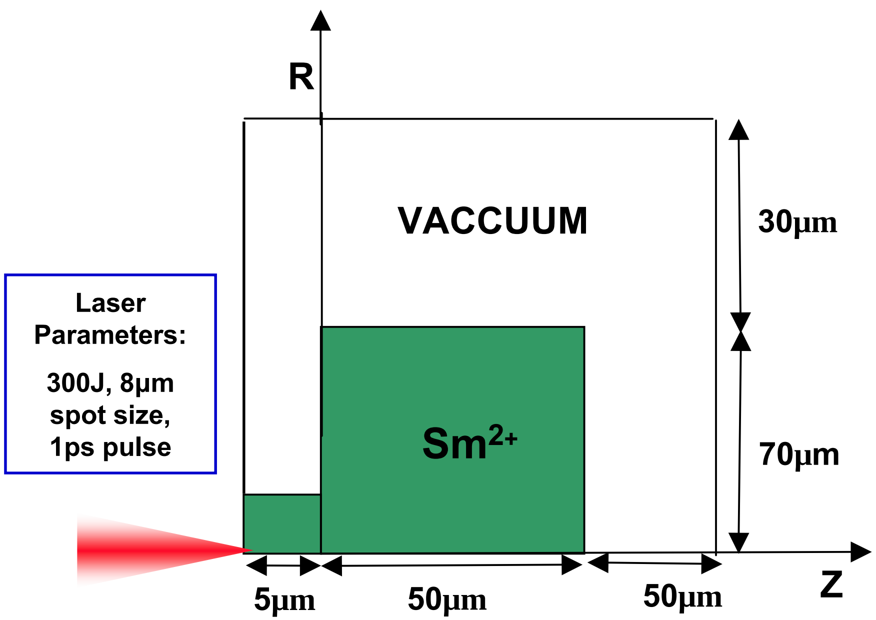

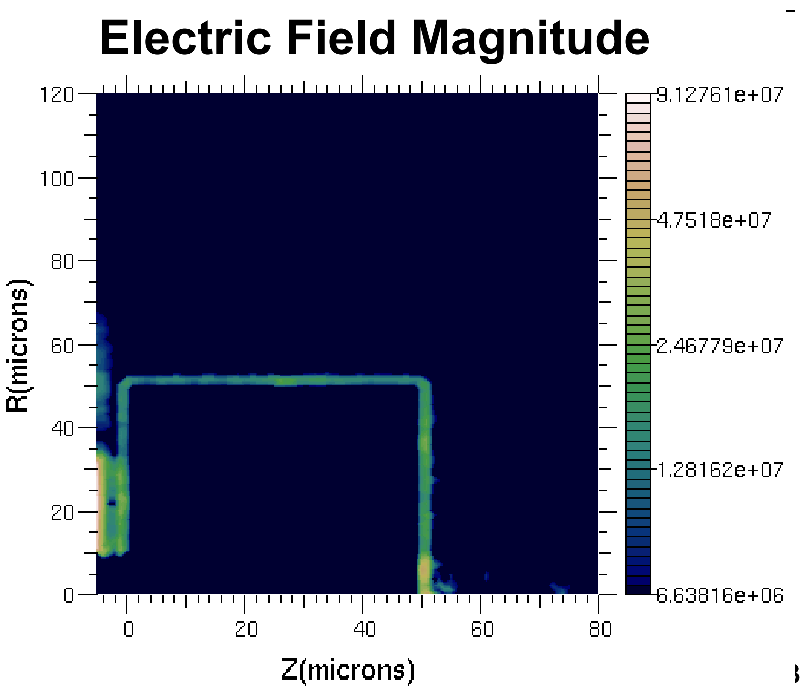

Kα images were generated at various times throughout the simulations

- Using LSP, we were able to calculate the birth positions of the photons
- A line-out was also extracted from each image to obtain a more quantitative comparison at each point in time
- A significant asymmetry was detected when taking similar line-outs in the horizontal direction, but it is currently under investigation

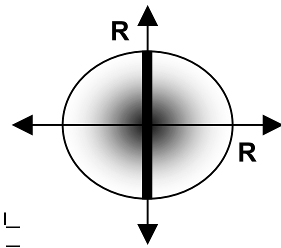

Normalized contour of photons created t ≤ 1 ps

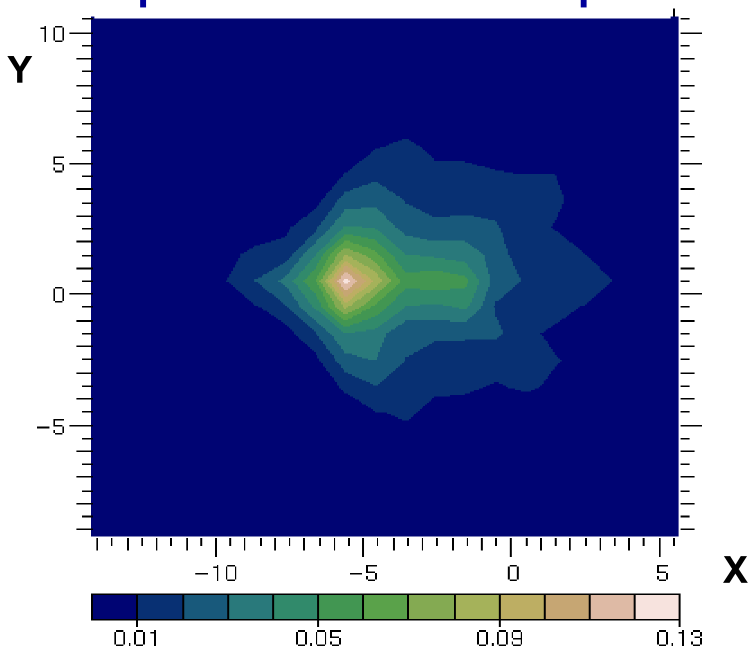

Time history of vertical line-outs of photon birth positions

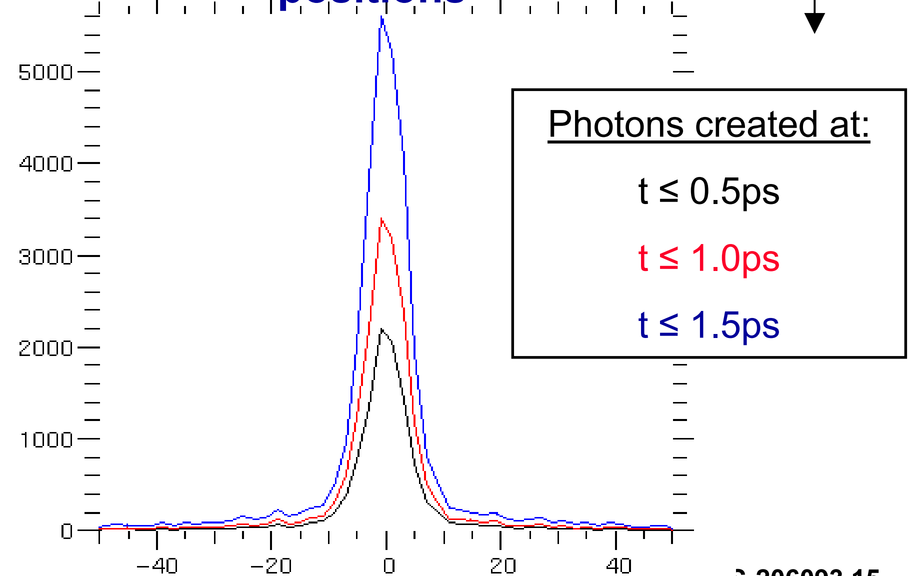

A cone-fiber target based on a recent Vulcan 2-D radiography experiment is being modeled in LSP

- Hot electrons were created by an "excitation" mechanism in LSP in which fluid electrons were promoted from the background plasma
- A time history of the hot electron number density shows the expected transit of electrons down the cone

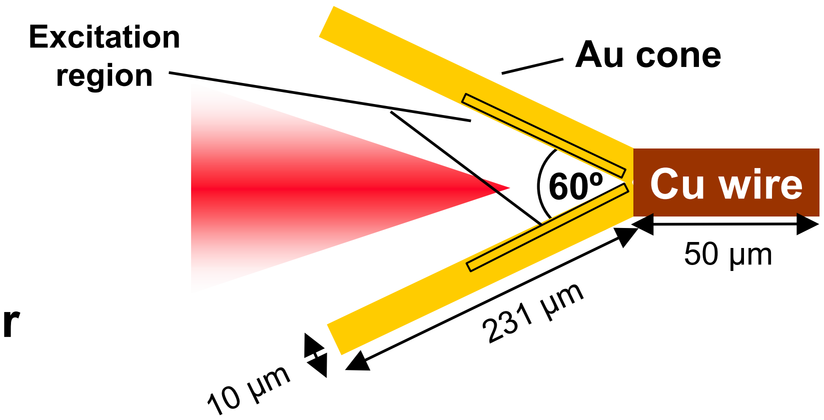

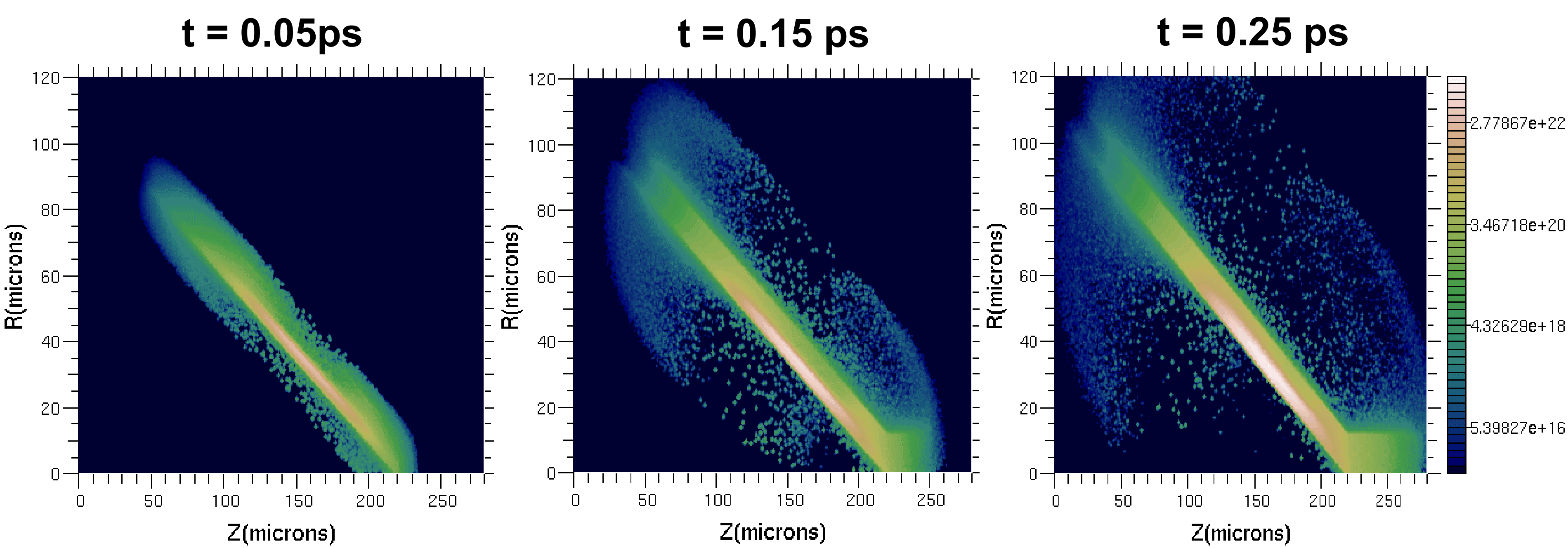

Several different cone materials are also being explored

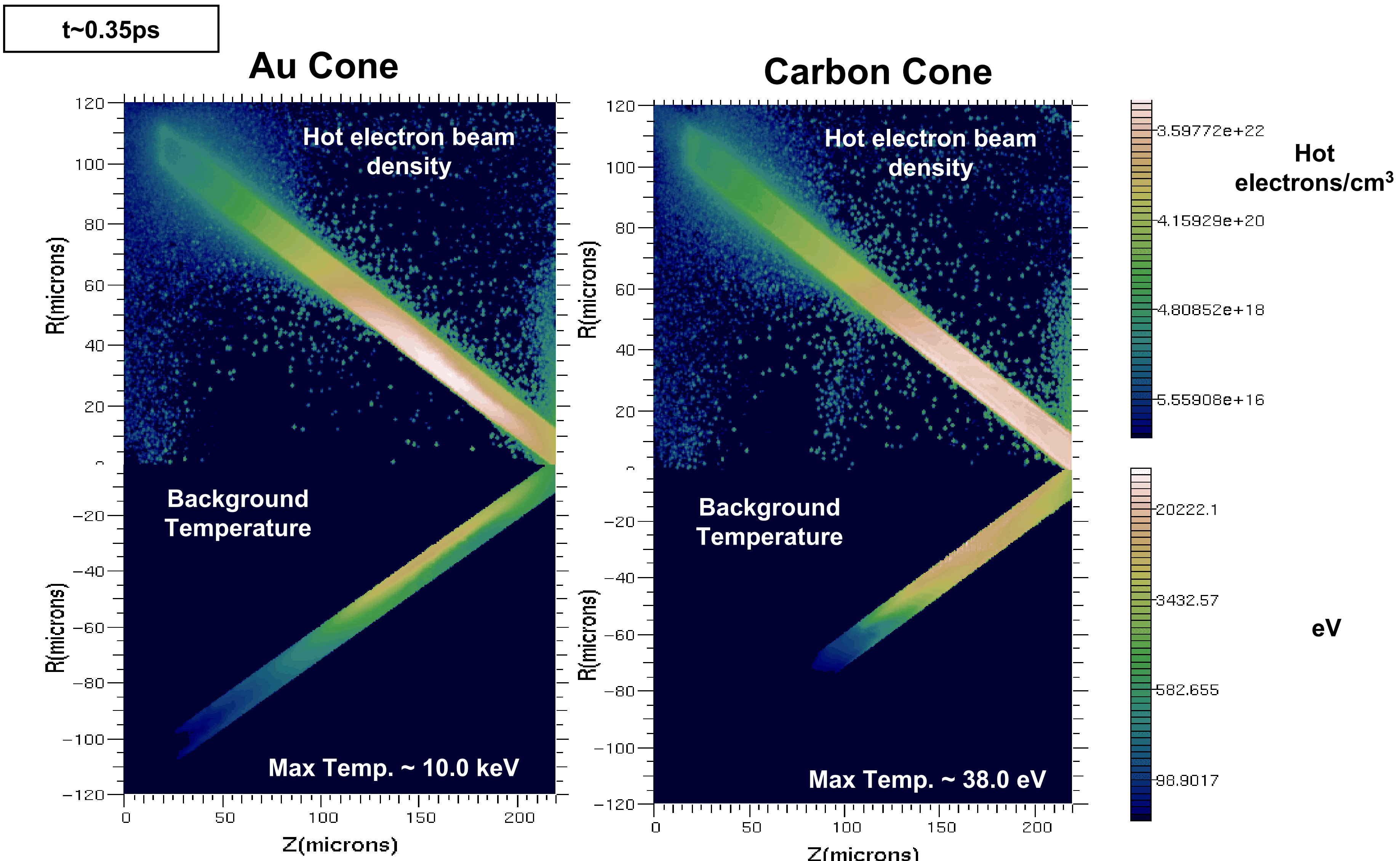

LSP has shown promising results for 1-D and 2-D Kα radiography modeling

- Maximizing the production efficiency of Kα photons is essential for backlighting NIF targets
- 1-D and 2-D backlighting geometries have been modeled in both LSP and ITS
  - 40 keV edge on Sm foil (1-D)
  - 8 keV Au cone/Cu fiber target (2-D)
- LSP has proven to be a more accurate tool for capturing the effects of electron refluxing than ITS
- Further calculations of the cone-fiber geometry are currently in progress
  - Analysis of the coupling efficiency of the laser light to Cu wire
  - Alternative laser/hot electron beam orientations

Electron and Proton Stopping Powers for FIS

Claude Deutsch

LPGP UParis XI Orsay,France

Short Pulse Laser-Matter Computational Workshop

Pleasanton,CA, August 25/27 2004 2004

« Atomic-scale » : Electron and proton stopping powers

- Relativistic electron stopping in partially degenerate targets. Intrabeam correlations. Multiple scattering contribution to REB depth penetration
- Collective (instabilities) VS. Collisional stopping triggering of instabilities
- Non relativistic proton and ion stopping. Inflight binary correlation effects. Multiple scattering in Hohlraum design

REB STOPPING IN ICF TARGET

REB PARAMETERS

- 3 kJ $\qquad \beta = 0.94 \qquad \gamma = 2.99$
- 10^{-11} sec peak laser illumination
- Cylinder radius $a = \frac{\sigma}{4}$, σ = core radius
- 1 MeV
- 3×10^8 A
- $\frac{I}{\pi a^2} = 6.1\times10^{13}\,A/cm^2$ $\qquad \sigma = 50\ \mu m$
- $n_p(r) = n_p(0)e^{-\frac{r^2}{\sigma^2}}$, $\qquad$ core density
- $n_b \quad = 6.63\times10^7 \times \frac{I}{\pi a^2} \times \beta^{-1} cm^{-3}$
- $\sim 1.3\times10^{22}\,cm^{-3}$

PRECOMPRESSED DT

300 g/cc *5 keV*

$\lambda_D \quad >> \quad \lambda\!\!\!^{-}_e \quad >> \quad \lambda_L$

$5.25 \times 10^{-9}\ cm \quad 3.9 \times 10^{-10}\ cm \quad 2.88 \times 10^{-11}\ cm$

$$a_{ee} = \left(\frac{4\pi}{3} n_e (cm^{-3})\right)^{1/3} = 1.34 \times 10^{-9}\ cm$$

$r_S = 0.25$ at $T = 0$

$$\Lambda = \frac{e^2}{k_B T \lambda_D} = 0.0055 \qquad \frac{\lambda\!\!\!^{-}_e}{\lambda_D} = 0.074$$

$$\alpha = \frac{k_B T}{\varepsilon_F} = 6.4$$

DENSE ELECTRON PLASMA
MOSTLY CLASSICAL

TARGET DIELECTRIC FUNCTION

- $$\varepsilon(\omega) = 1 - \frac{\omega_p^2}{\omega(\omega + i\nu_{coll})} \quad ,$$

Drude suitable for high velocity REB

$$\nu_{coll} = \frac{3.8 \times 10^{-6} n_e (cm^{-3})}{T_e (eV)^{3/2}} \ell n \ \Lambda$$

$$\ell n \Lambda = \ell n [9 n_e \lambda_D^3] = 6.305 \qquad \text{for}$$

T = 5 keV and $n_e = 10^{26}$ e-cm^{-3}

- $$\int_0^\infty d\omega \, \omega \, \mathrm{Im} \frac{1}{\varepsilon(\omega)} = -\frac{\pi}{2} \omega_p^2$$

$$N_{efold} = \delta_{max} T_{stop}$$

$$T_{stop} = \frac{1}{c} \int_{E_b^{min}}^{E_b^{max}} \frac{1 + \dfrac{E_b}{m_e c^2}}{\left[\left(\dfrac{E_b}{m_e c^2}\right)\left(\dfrac{E_b}{m_e c^2 + 2}\right)\right]^{1/2}} \times \frac{dE_b}{\dfrac{dE_b}{dx}}$$

$$\cong \frac{100}{4} \times 10^{-4} \text{ cm} \times \frac{1}{\beta_b c \text{ cm/sec}}$$

$$\cong 10^{-13} \text{ sec for 1 MeV REB}$$

BASIC MECHANISMS

❑MØLLER formula adapted to a classical plasma

$$-\frac{dE}{dx} = \frac{2\pi n_p e^4}{m_e \beta_b^2 c^2} \times \left[\ell n \frac{1}{2\tau_{min}} + \frac{1}{8} \times \left(\frac{\tau}{\tau+1} \right) - \frac{(2\tau+1)}{(\tau+1)^2} \ell n 2 + 1 - \ell n 2 \right]$$

$$\frac{\lambda_e}{\lambda_D} \uparrow \qquad \gamma - 1 \uparrow$$

cf. E. Nardi-Zinamon, Phys. Rev. A18, 1246 (1978)
and V.V. Val'chuck et al, Plasma Phys. Rpts **21**, 159 (1995)

❑Langmuir modes

$$-\frac{dE}{dx} = \frac{2\pi n_p e^4}{m_e \beta_b^2 c^2} \times \ell n \left[\frac{V_b}{w_p \lambda_D \left(\frac{3}{2} \right)^{1/2}} \right]^2$$

cf. D. Bohm, D. Pines , Phys. Rev. 85, 338 (1952)

Electron Stopping in Dense Plasma

- Non rectilinear trajectories
- Multiple and Quasi-Elastic Scattering
- 50% of projectile kinetic energy may be transfered in one collision to a target electron
- Bethe formula turned relativistic with

$$2\, m_e V^2 \rightarrow m_e V^2 \text{ and } V = c$$

- For 1 MeV electron projectiles, pair production and bremsstrahlung are negligible

$$E_b = \frac{800\,\text{MeV}}{Z+1.2}\text{, here } Z=1\text{, Brems \# stopping}$$

- Mutiple Diffusion worked out in a Gaussian approximation (small deflection angles)
- Excitation of collective Langmuir mode ($\omega = \omega_p$)

RANGE CALCULATION

Now, we consider the effective range

$$R = \int_{E_{max}=E_0=\ 1MeV}^{E_{min}=E_0/10=0.1MeV} \frac{dE}{dE/dx}, \qquad (1)$$

which is not an *a priori* rectilinear quantity (β=v/c).

The stopping power is then taken as the <u>sum</u> of

$$-\frac{dE}{dx}=\frac{2\pi n_p e^4}{me\beta^2c^2}\times\left[\ell n\frac{1}{2\tau_{min}}+\frac{1}{8}\left(\frac{\tau}{\tau+1}\right)-\left(\frac{2\tau+1}{\tau+1}\right)\ell n2+1-\ell n2\right]$$

where $\tau_{min} = \frac{\hbar(\text{projectile})}{m_e v}/\lambda_D$ **(target electrons)**

$\tau = \gamma - 1$, **and**

$$-\frac{dE}{dx}=\frac{2\pi n_p e^4}{me\beta^2c^2}\,\ell n\left(\frac{V}{\omega_p\lambda_D\left(\frac{3}{2}\right)^{1/2}}\right)^2$$

Eq. (1) thus becomes ($V = \beta^2$) with $E = (\gamma - 1)\, mec^2$,

$$R=\frac{(mec^2)^2}{4\pi n_p e^4}\times\int_{0.3025}^{0.8836}\frac{dvv}{(1-v)^{3/2}}\times\frac{1}{D(v)}=35\mu m$$

with

$$D(v)=\ell n(68.53v)+\ell n(68.026v^{1/2})+$$

$$+\ \frac{(1-\sqrt{1-v})^2}{8}-(2v+v-1)+1-\ell n2$$

ANGULAR DEFLECTIONS

Now, we look for an "effective slab thickness" featuring along the initial REB axis, the region where the range R is mostly located in. For that purpose, we equate R to a wiggly but continuously deflected electron projectile trajectory given as

$$R = \ell_o + \frac{1}{2}\ell_o \frac{\ell_o}{\lambda} + \frac{1}{2}\frac{\ell_o^{\,3}}{\lambda^2}$$

in terms of

λ^{-1} = Mean value of square average deflection per path length (in cm^{-1})

$$= 8\pi\left(\frac{e^2}{m_e c^2}\right)^2 \times \frac{Z(Z+1)}{A\beta^4} \times \left(1-\beta^2\right)\left[\ell n\left(\frac{137\beta}{Z^{1/3}\left(1-\beta^2\right)^{1/2}}\right) + \ell n(1.76) - \left(1+\frac{\beta^1}{4}\right)\right] n_p \left(cm^{-3}\right)$$

see : cf : R.H. Ritchie et al, Phys. Rev. **135**, A759 (1964) and B.P. Nigam et al, Phys. Rev. **115**, 491 (1959)

Nonrelativistic expression

$$\lambda^{-1} = \theta_{AV}^2 = \frac{4\pi_e^4 n_p x}{m_e^2 V^2 V^2} \times \ell n \frac{\theta_{max}}{\theta_{min}}$$

Coulomb logarithm^{-1} $\frac{1}{\Lambda} \sim 3$ or 5

Relativistic

$$\frac{\theta_{AV}^2}{N} = 8\Pi\left(\frac{e^2}{m_e c^2}\right)^2 \frac{Z(Z+1)\left(1-\beta^2\right)}{A\,\beta^4} \times I$$

Ion scatterers density (N)

$$I = \ell n \frac{137\beta}{Z^{1/3}\left(1-\beta^2\right)^{1/2}} + \ell n 1.76 - \left(1 + \frac{\beta^2}{4}\right)$$

Cf : R.H. Ritchie et al, Phys. Rev. **135**, A759 (1964) and B.P. Nigam et al, Phys. Rev. **115**, 491 (1959)

C. Deutsch et al P. R. L 77, 2483 (1996)

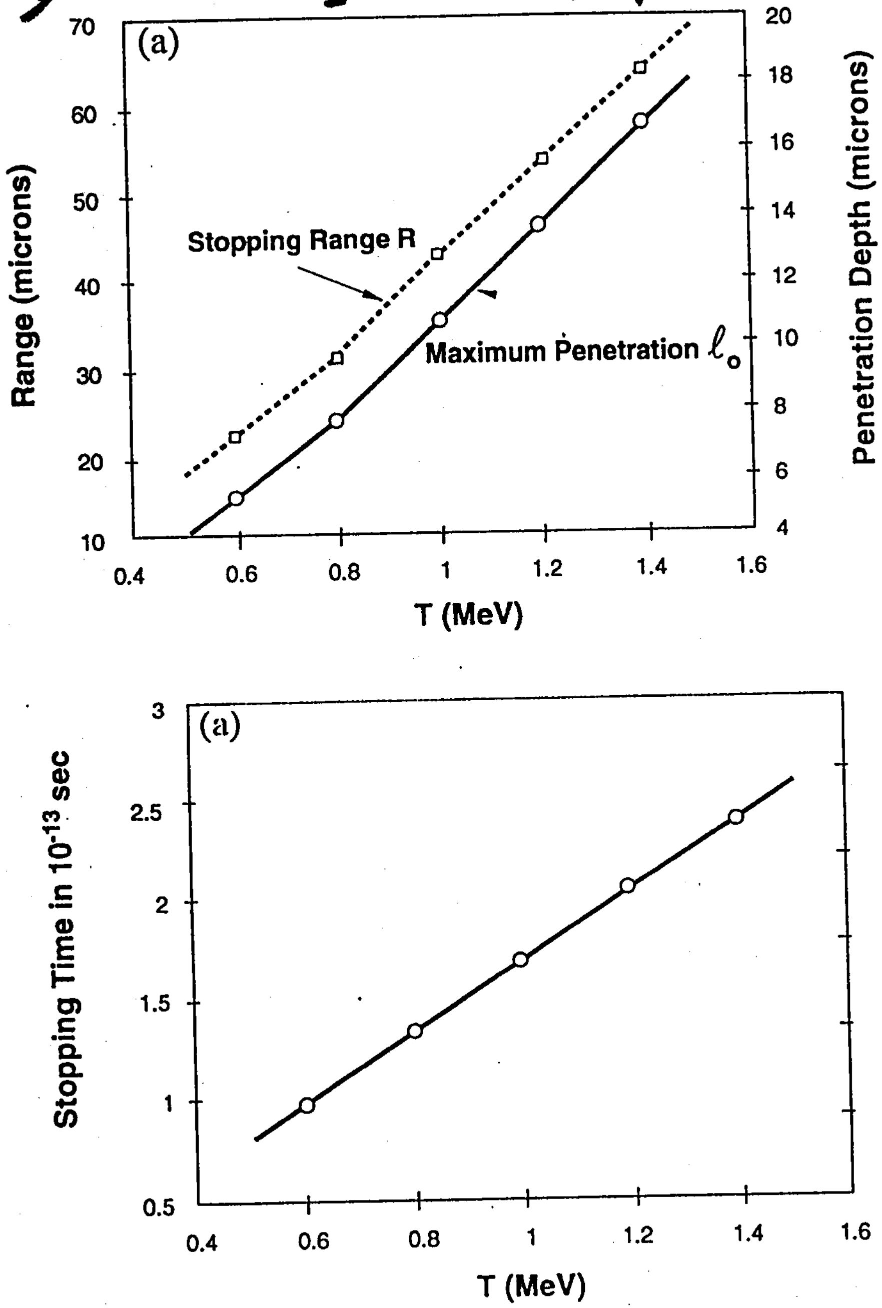

FIG. 1. (a) REB range R (μm) and maximum penetration depth ℓ_0 (cm) in a 300 g/cm³ DT target at 5 keV and $0.5 \leq T \leq 1.5$ MeV. (b) Corresponding stopping time t_{stop}.

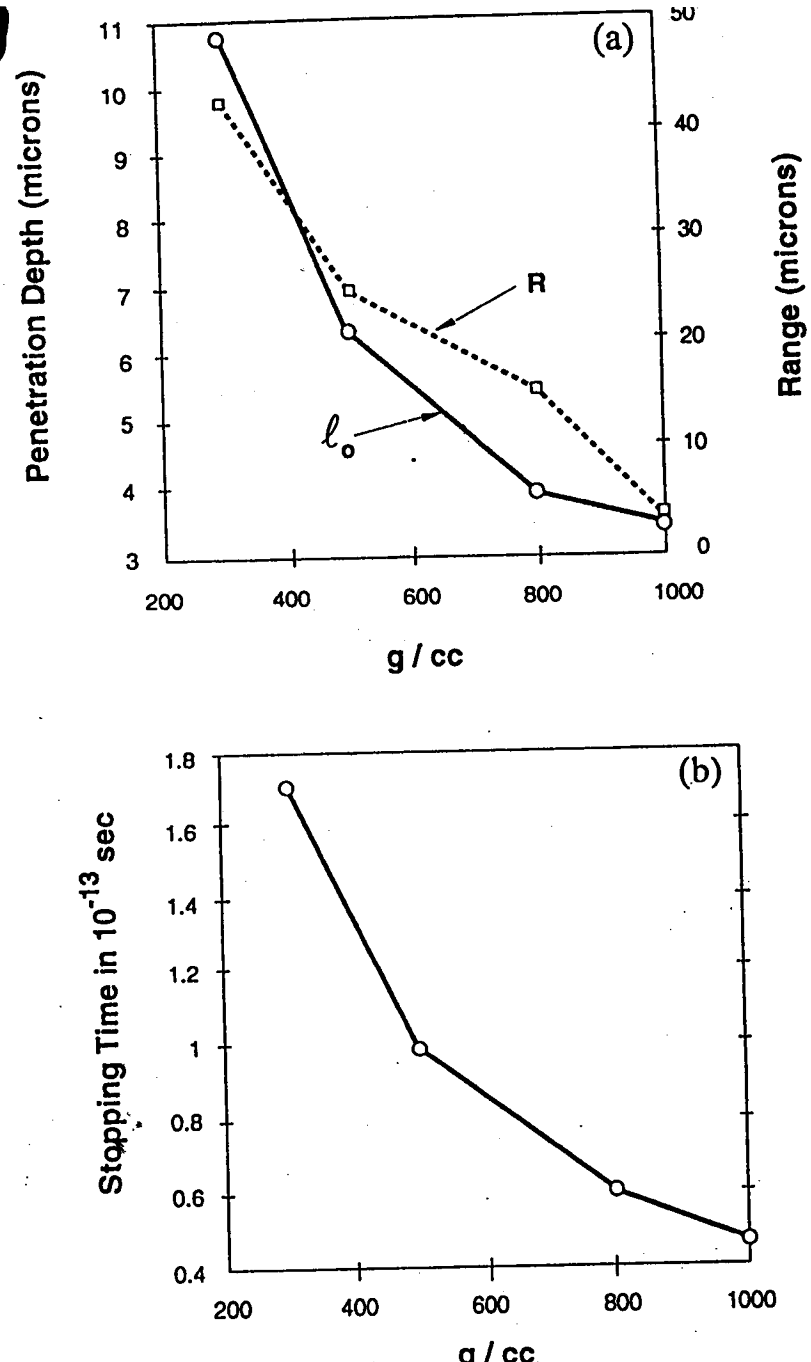

FIG. 2. (a) R and ℓ_0 for $T = 1$ MeV, and target density ranging from 300 up to 1000 g/cm³, with 5 keV temperature. (b) Corresponding stopping time t_{stop}.

REEB Stopping in Partially Degenerate Electron Fluid

So, we consider first the standard Fermi expression for the relativistic stopping of a single electron projectile ($x = \omega/\omega_p$)

$$\frac{dE_b^S}{dz} = \frac{2}{\pi} \cdot \frac{e^2 \omega_p^2}{v_b^2} \cdot \int_0^\infty dx\, x\, \mathrm{Im}\left[K_0(\lambda)\left(\frac{1}{\varepsilon} - \beta^2\right) \right] ,$$

with $\beta = \frac{v_b}{c}$, $\lambda = \frac{x \omega_p \lambda_D}{V_b} (1 - \beta^2 \varepsilon)^{1/2}$ evaluated through a Drudelike dielectric expression

$$\varepsilon(\omega) = 1 - \frac{\omega_p^2}{\omega(\omega + i v_{coll})} ,$$

CLASSICAL

suitable for high-velocity REBs with a collision frequency

$$v_{coll} = \frac{3.8 \times 10^{-6} \left[n_e (cm^{-3}) \right]}{\left[T_e (eV) \right]^{3/2}} \ell n \Lambda ,$$

Relativistic electron beam stopping

General expression for the stopping power in relativistic case (according to Landau)

$$-\frac{dE}{dx} = \frac{e^2}{\pi v_o^2}\int_0^\infty dkk\int_{-kv_o}^{+kv_o} d\omega\omega \mathrm{Im}\frac{1-\frac{v_o^2}{c^2}\varepsilon(k,\omega)}{\varepsilon(k,\omega)\left(k^2-\frac{\omega^2}{c^2}\varepsilon(k,\omega)\right)},$$

Quantum dielectric function

$$\varepsilon(Q,z) =$$

$$1+\frac{\alpha r_s}{4\pi Q^3}\left(\phi\left(\frac{z}{Q}+Q\right)-\phi\left(\frac{z}{Q}-Q\right)\right)+$$

$$i\frac{\alpha r_s\theta}{8Q^3}\ln\left(\frac{1+\exp\left(\eta-\frac{1}{\theta}\left(\frac{z}{Q}-Q\right)^2\right)}{1+\exp\left(\eta-\frac{1}{\theta}\left(\frac{z}{Q}+Q\right)^2\right)}\right),$$

where $Q=k/2k_F$, $z=\hbar\omega/4E_F$, $\alpha=(4/9\pi)^{1/3}$ and

$$\phi(x) = \int_0^\infty dyy\ln\left|\frac{x-y}{x+y}\right|/\left(1+\exp\left(\frac{y^2}{\theta}-\eta\right)\right).$$

Asymptotic expression for stopping power of the ultrarelativistic particles (according to Fermi and Landau)

$$-\frac{dE}{dx} = \frac{e^2\omega_p^2}{2c^2}\ln\left(\frac{c^2k_{max}^2}{\omega_p^2}\right),$$

where $k_{max} = mv_o/\hbar$.

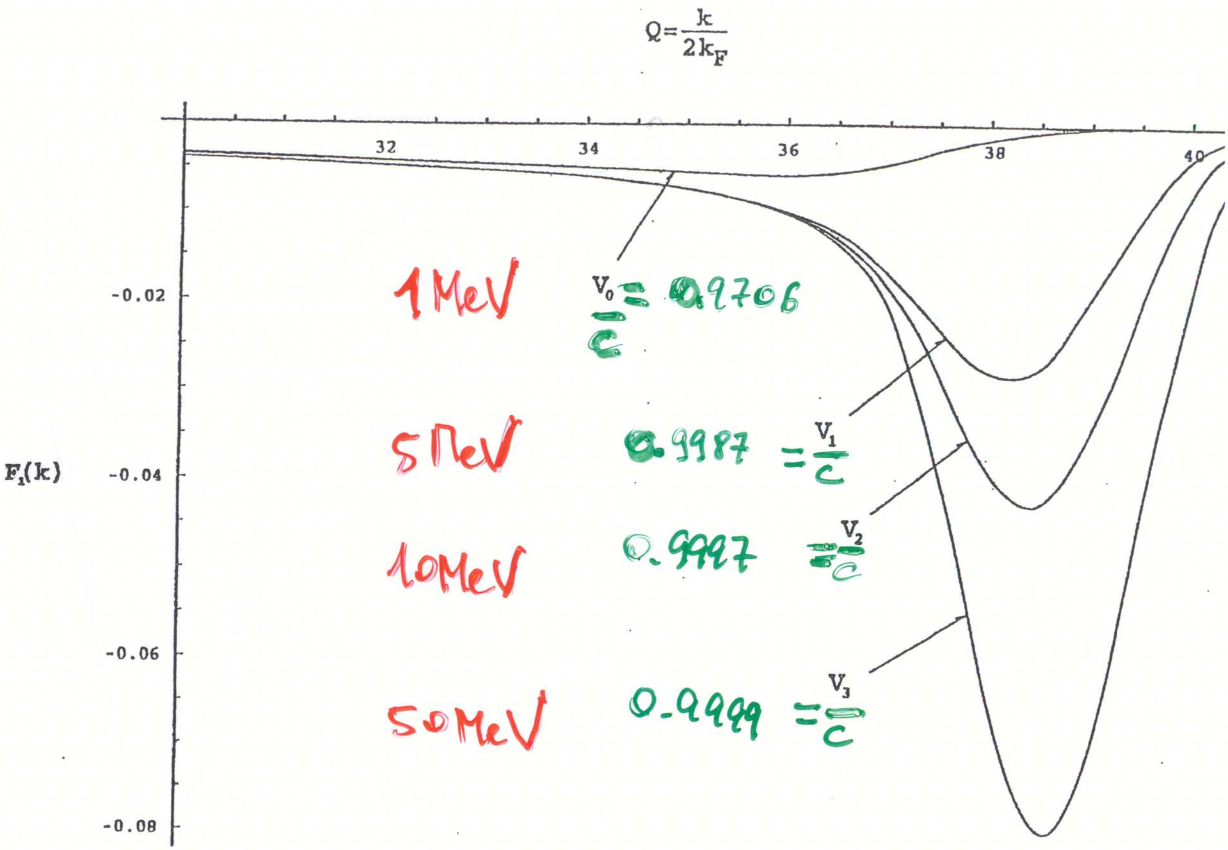

$$F_1(k) = -k \int_0^{kv} d\omega\, \omega \; \mathrm{Im} \frac{1 - \frac{v^2}{c^2}\varepsilon(k,\omega)}{\varepsilon(k,\omega)\left[k^2 - \frac{\omega^2}{c^2}\,\varepsilon(k,\omega)\right]}$$

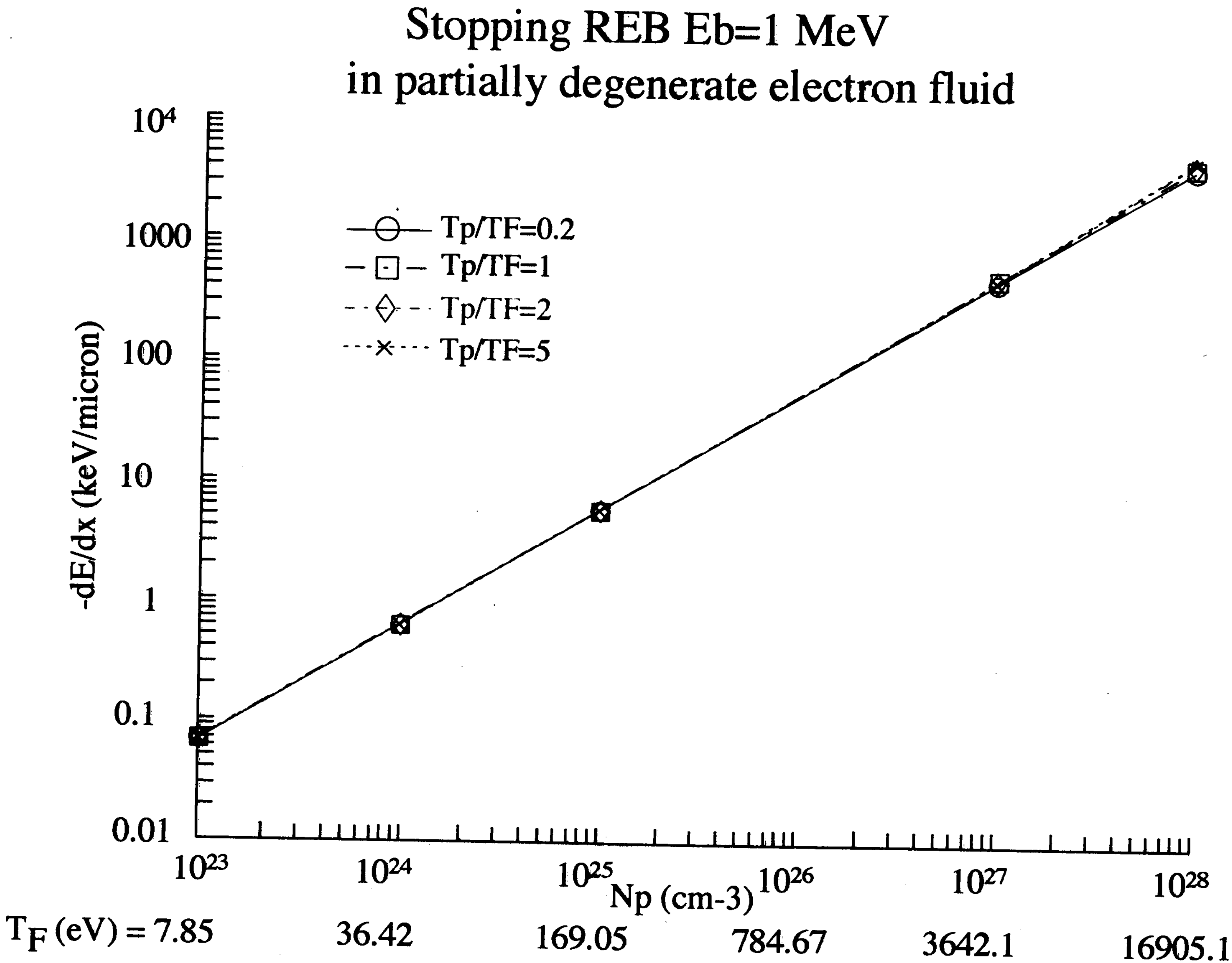

Stopping REB Eb=1 MeV
in partially degenerate electron fluid
-dE/dx (keV/micron)
10^4
1000
100
10
1
0.1
0.01
Tp/TF=0.2
Tp/TF=1
Tp/TF=2
Tp/TF=5
10^23
10^24
10^25
10^26
10^27
10^28
Np (cm-3)
T_F (eV) = 7.85
36.42
169.05
784.67
3642.1
16905.1

Stopping REB Eb=50 MeV in partially degenerate electron fluid

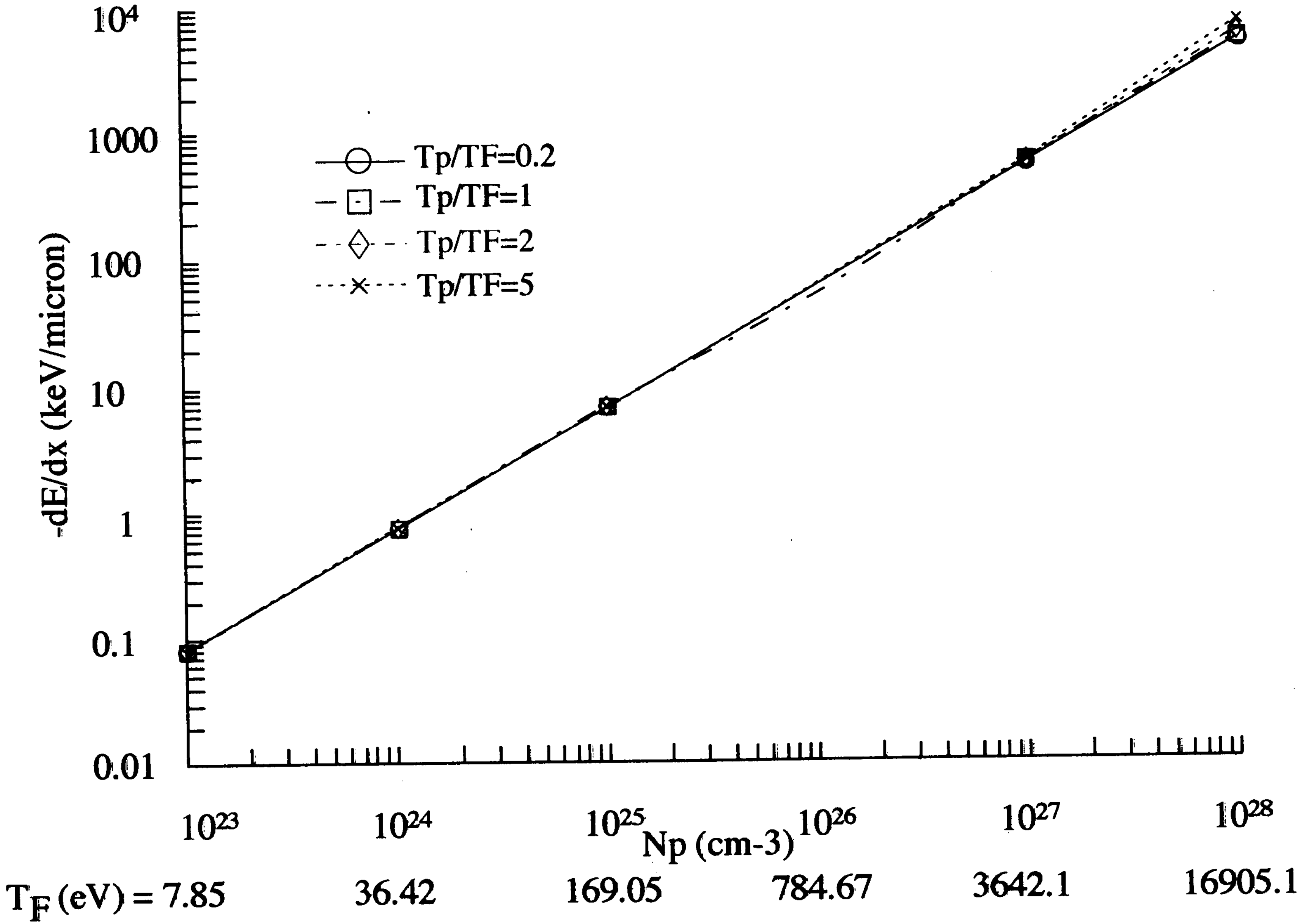

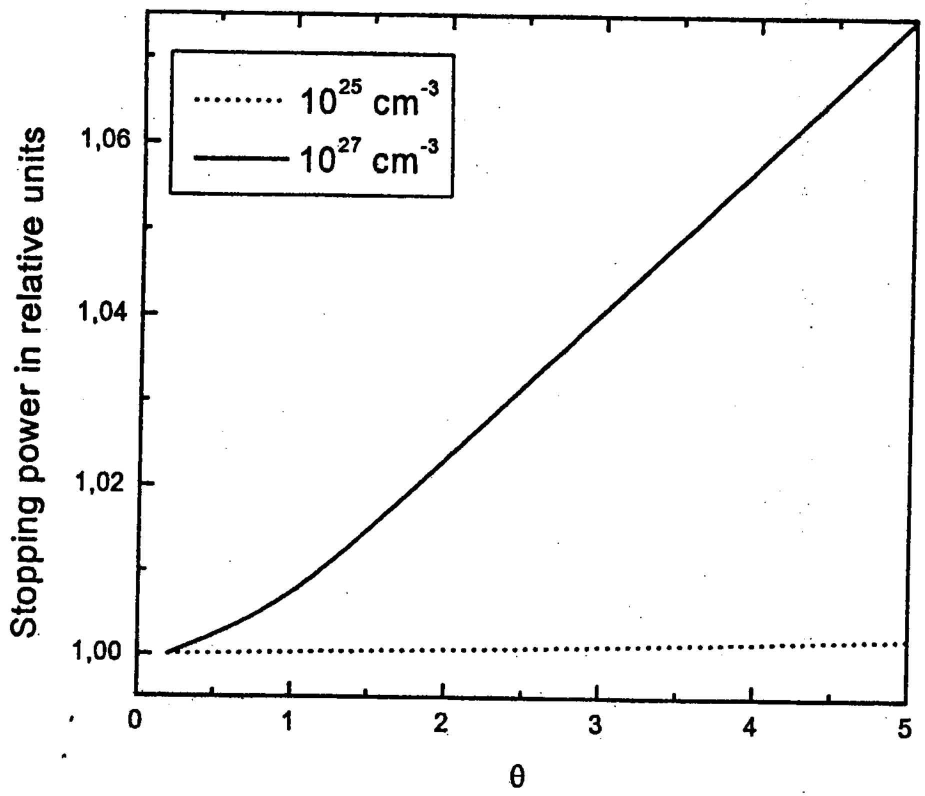

Stopping power of 1.61 MeV electron in quantum plasma.

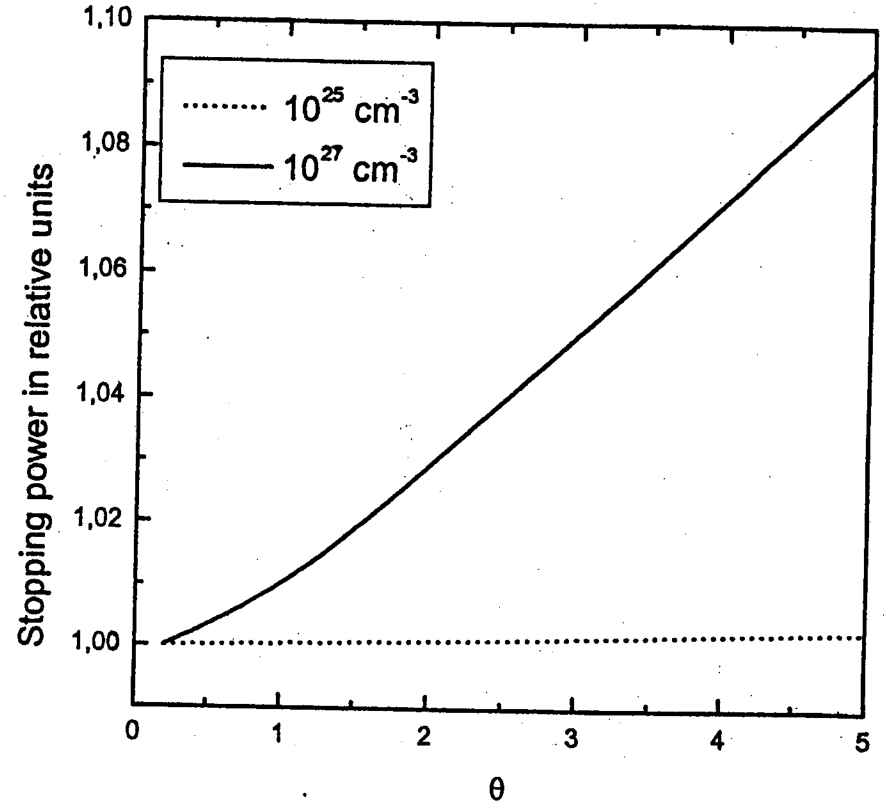

Stopping power of 39.5 MeV electron in quantum plasma.

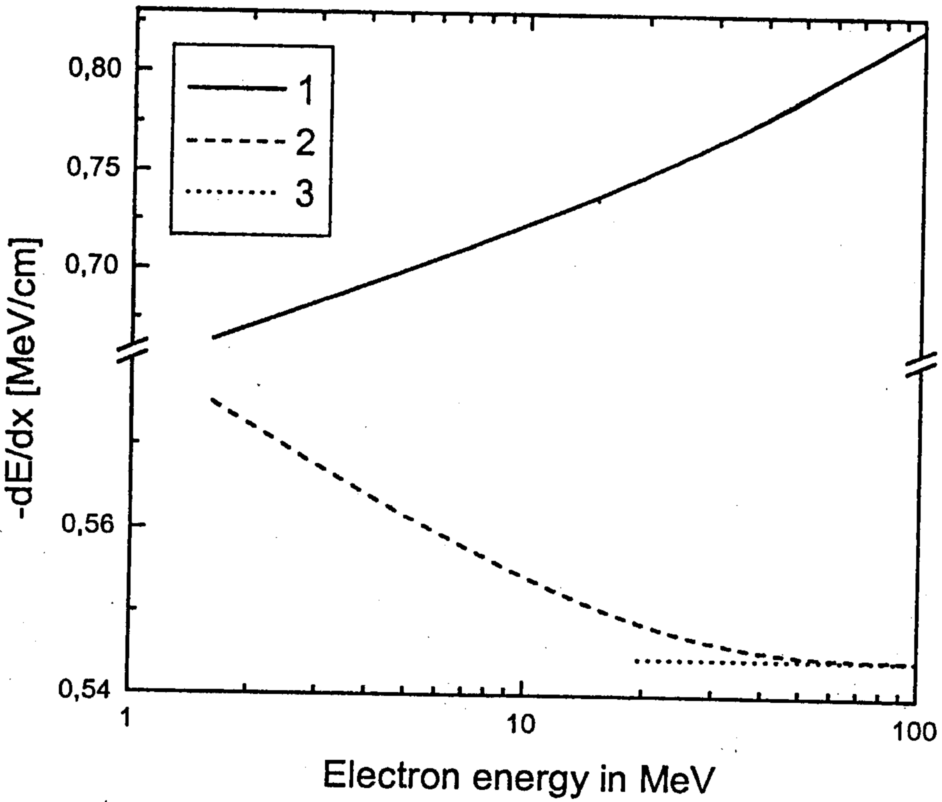

Stopping power of electron in plasma with =10^{23} cm^{-3} and θ=5.
· Numerical calculation with quantum dielectric function
· Numerical calculation with classical dielectric function
· Asymptotic formula

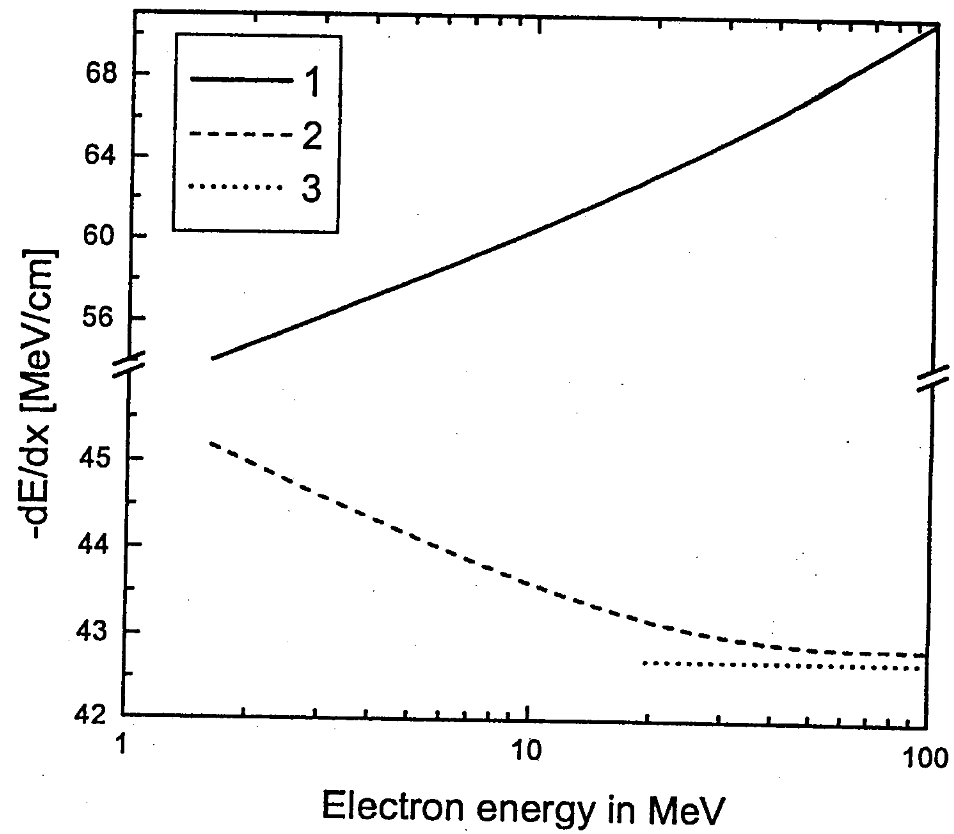

Stopping power of electron in plasma with n=10^{25} cm^{-3} and θ=5.

1. Numerical calculation with quantum dielectric function
2. Numerical calculation with classical dielectric function
3. Asymptotic formula

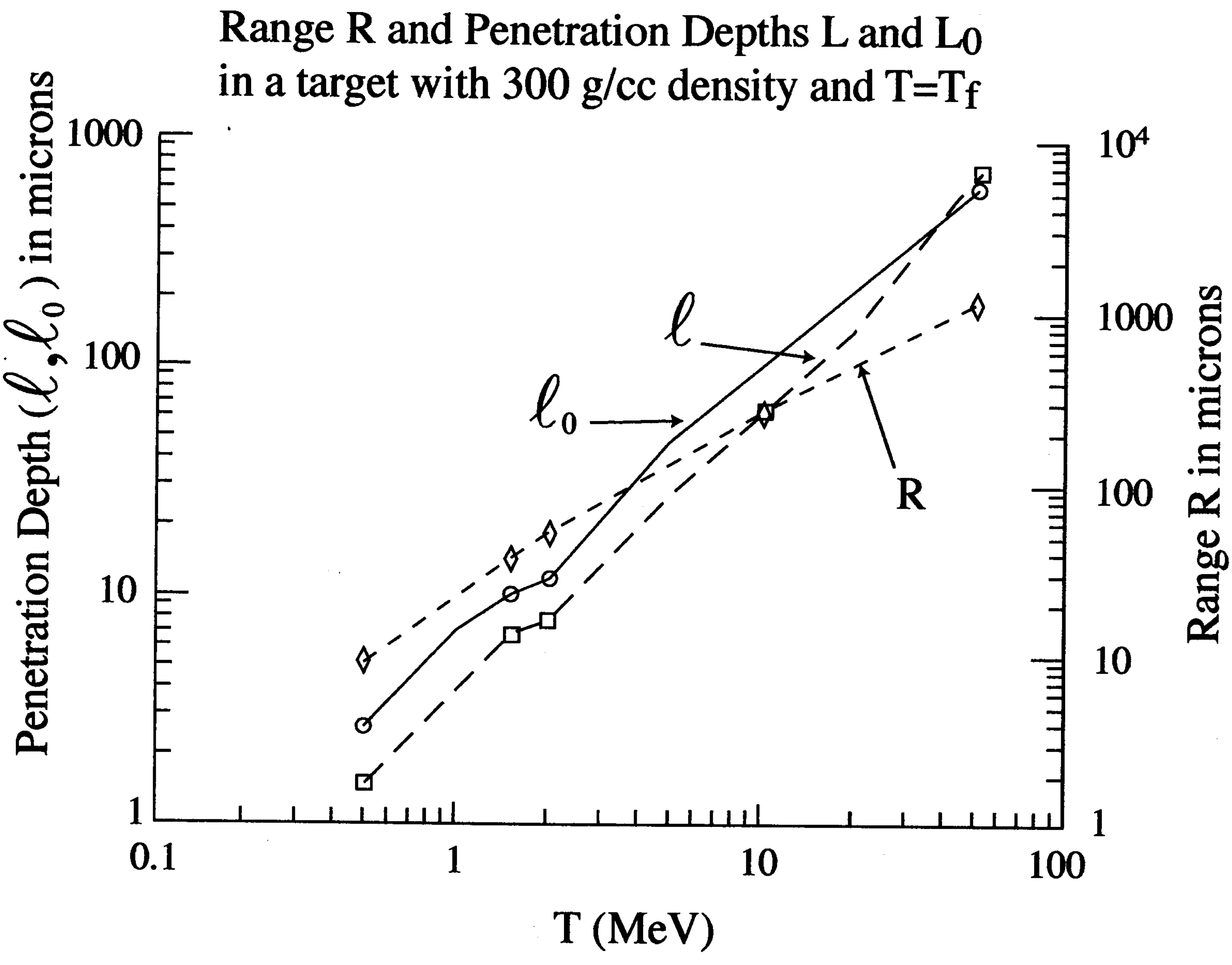

Range R and Penetration Depths L and L0
in a target with 300 g/cc density and T=Tf
Penetration Depth (ℓ, ℓ0) in microns
Range R in microns
T (MeV)
ℓ
ℓ0
R
1000
100
10
1
0.1
1
10
100
10^4
1000
100
10
1

NonRelativistic

Proton

Stopping

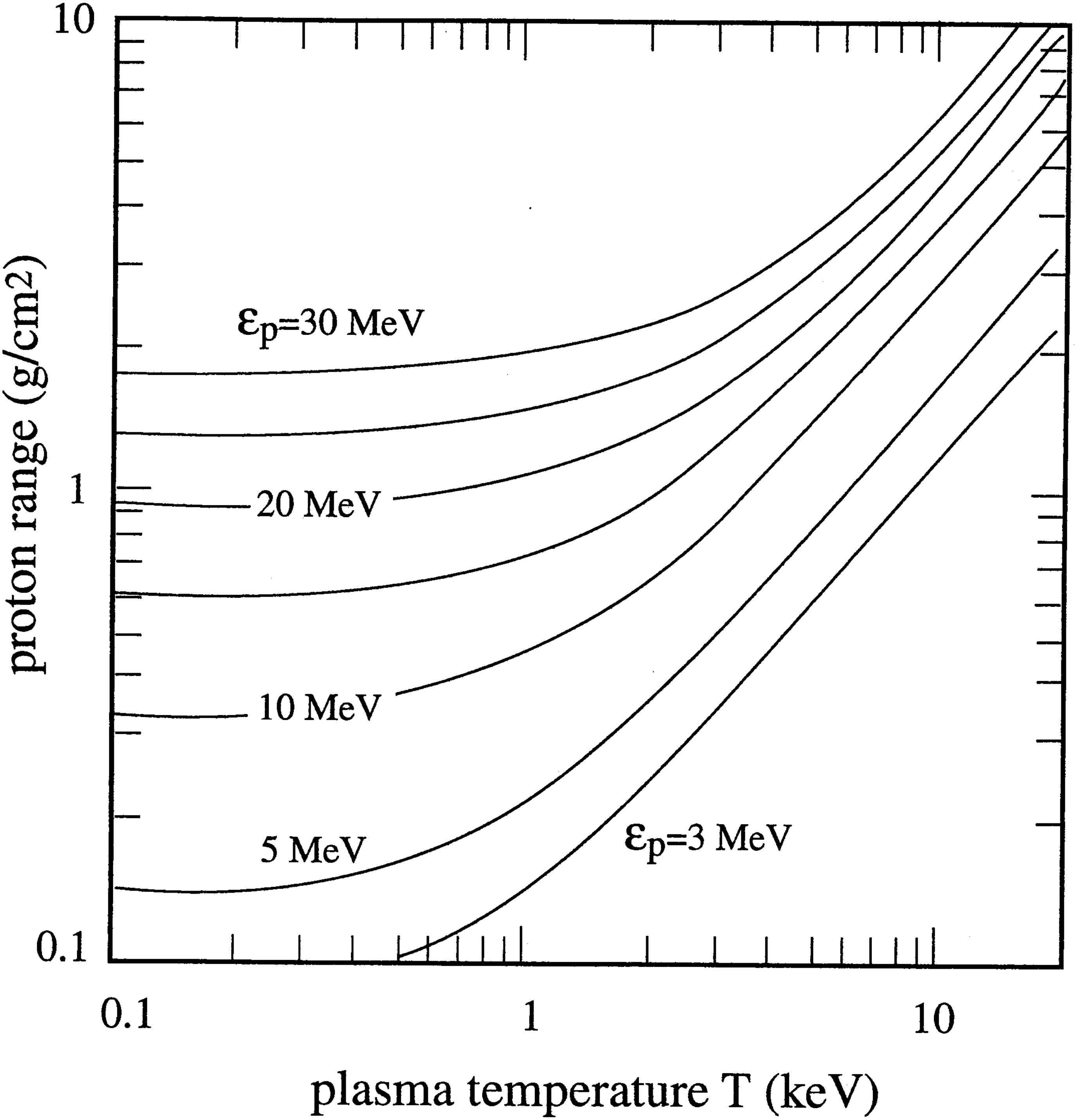

10
1
0.1
proton range (g/cm2)
εp=30 MeV
20 MeV
10 MeV
5 MeV
εp=3 MeV
0.1
1
10
plasma temperature T (keV)

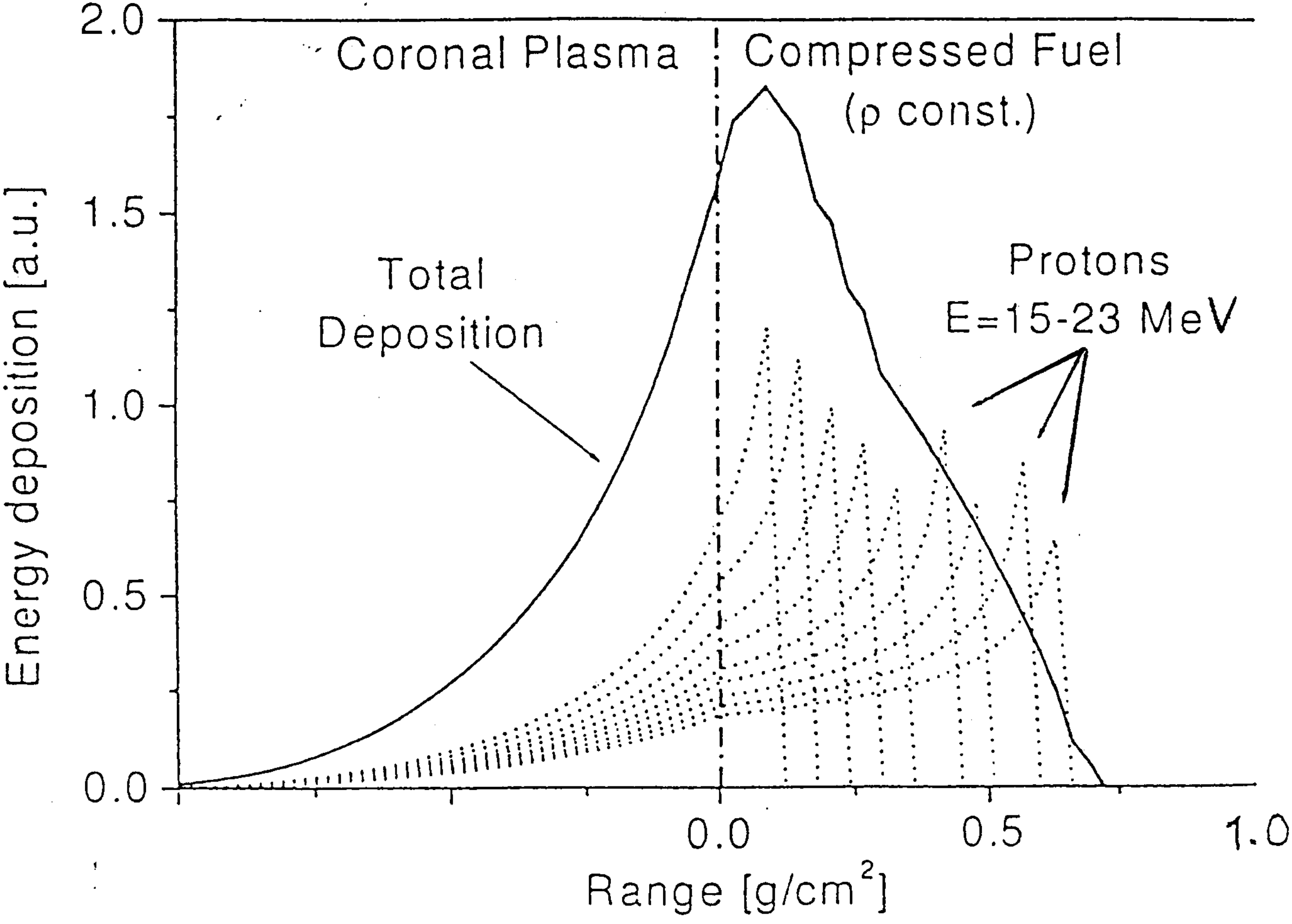

Coronal Plasma
Compressed Fuel
(ρ const.)
Total
Deposition
Protons
E=15-23 MeV
Energy deposition [a.u.]
2.0
1.5
1.0
0.5
0.0
0.0
0.5
1.0
Range [g/cm²]

REB STOPPING

2-Correlated projectiles

$$R = \frac{dE_c/dz}{2dE_s/dz}$$

$$\frac{dE_c}{dz} = \frac{2}{\pi} \cdot \frac{e^2 \omega_p^2}{c^2} \cdot \frac{L}{\beta_i \beta_y}$$

$$R_2 = \sum_{n=1}^{N-1} (N-n)\, L(n)$$

↑ longitudinal 2-correlated stopping number for $n\lambda_D$ interdistance

C. Deutsch and P. Fromy
phys. plasmas 6, 3587 (1999)
phys. Rev E 61, 4322 (2000)

Enhanced and Correlated stopping of femto produced Relativistic Electron Beams may significantly improves their penetration capabilities in the outer layers of the precompressed DT core with

$$n_p \sim 10\ n_b\ ,\ n_b \sim 10^{22}\ cm^{-3}$$

- **Two electron projectiles in close vicinity $\left(R \equiv R_{12} \leq \frac{V}{\omega_p}\right)$ of each other may combine their separate stopping through target polarization**
- **Output: mostly positively enhanced energy loss**
- **Extension to relativistic velocities of the low velocity enhanced correlated stopping**
- **N-clusters taken as linear superposition of 2-clusters dynamically correlated**

- **Stopping 2-cluster calculation for the excitation of langmuir modes (collective contribution)**

- **Bohr impact parameter approach for single particle stopping adaptated by D.W. Rule/M.H. Cha** *Phys. Rev.* A24, **55 (1981) to 2-cluster projectiles**

- **Supercompressed DT fuel mimiked by drude dielectric function**

- **2-cluster → N-cluster corrections to MeV R_{EB} stopping in dense DT**

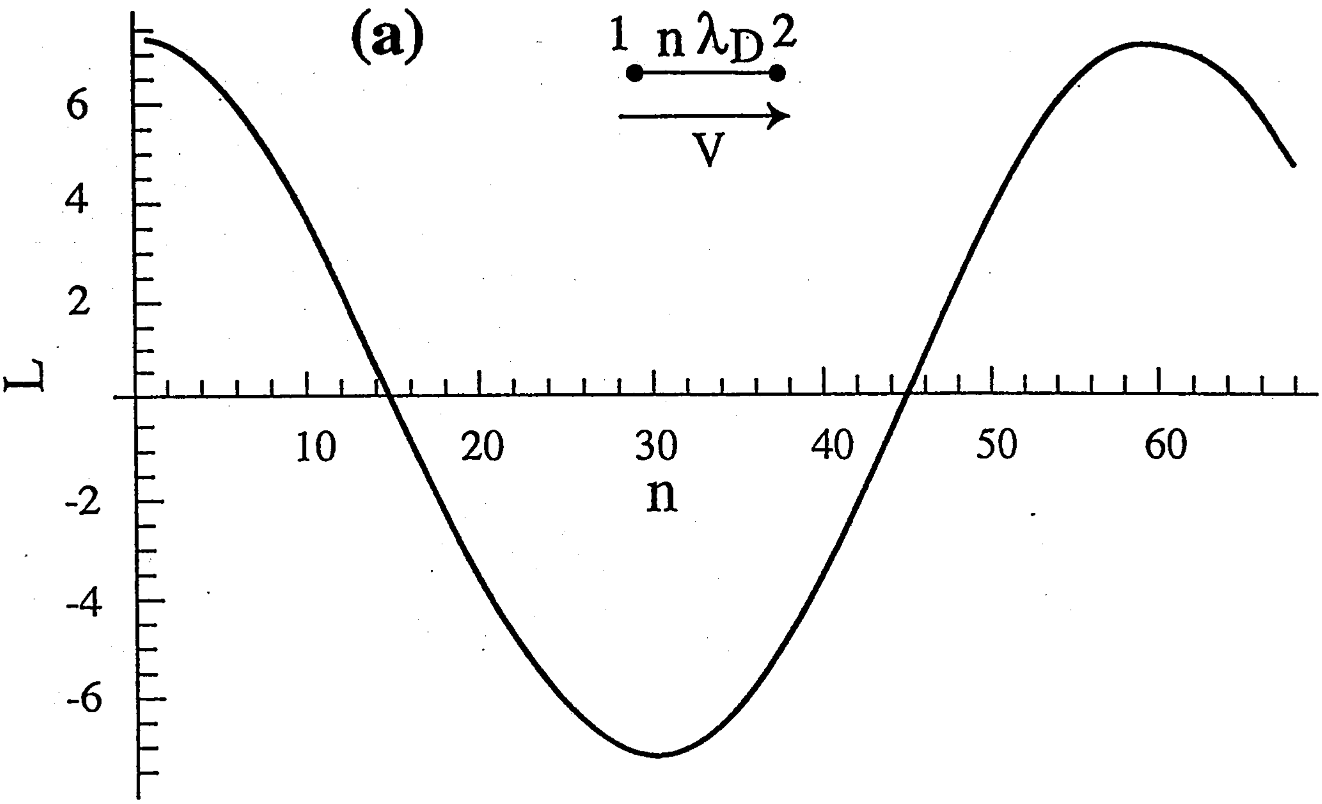
(a)
1 n λD 2
V
L
6
4
2
-2
-4
-6
10
20
30
40
50
60
n

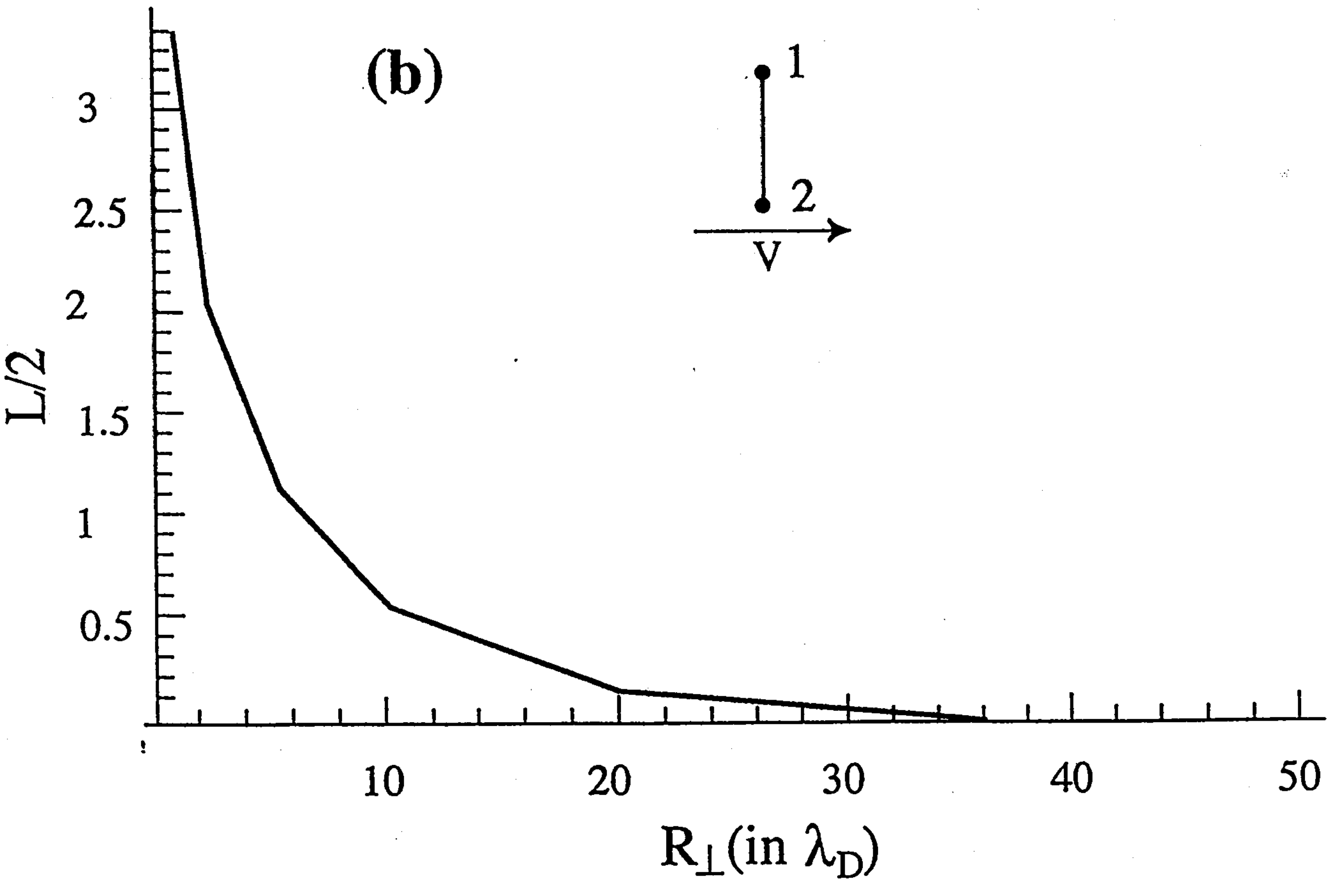
(b)
1
2
V
L/2
3
2.5
2
1.5
1
0.5
10
20
30
40
50
R⊥(in λD)

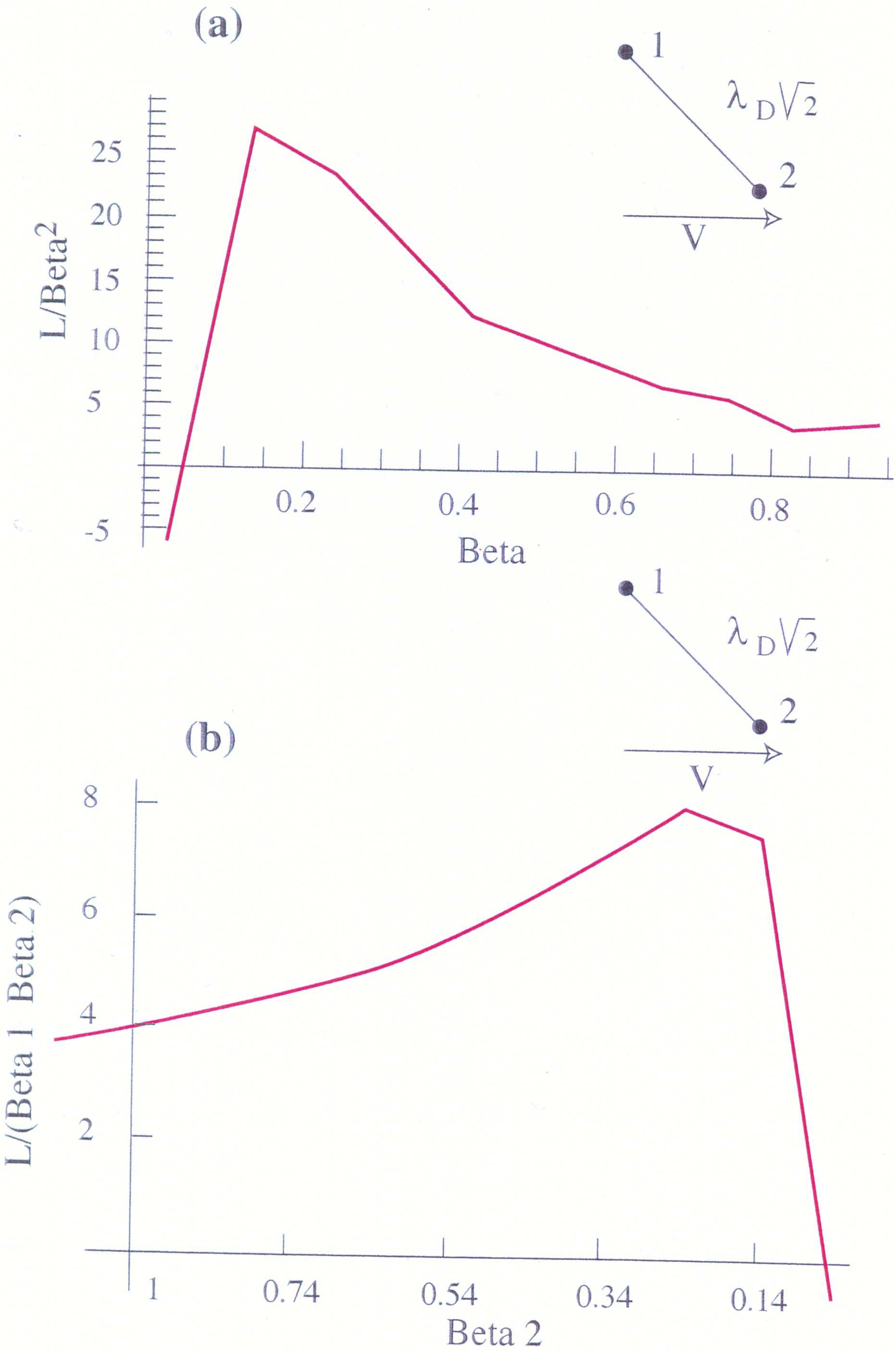
(a)
1
2
$\lambda_D\sqrt{2}$
V
L/Beta^2
25
20
15
10
5
-5
0.2
0.4
0.6
0.8
Beta
1
2
$\lambda_D\sqrt{2}$
V
(b)
L/(Beta 1 Beta 2)
8
6
4
2
1
0.74
0.54
0.34
0.14
Beta 2

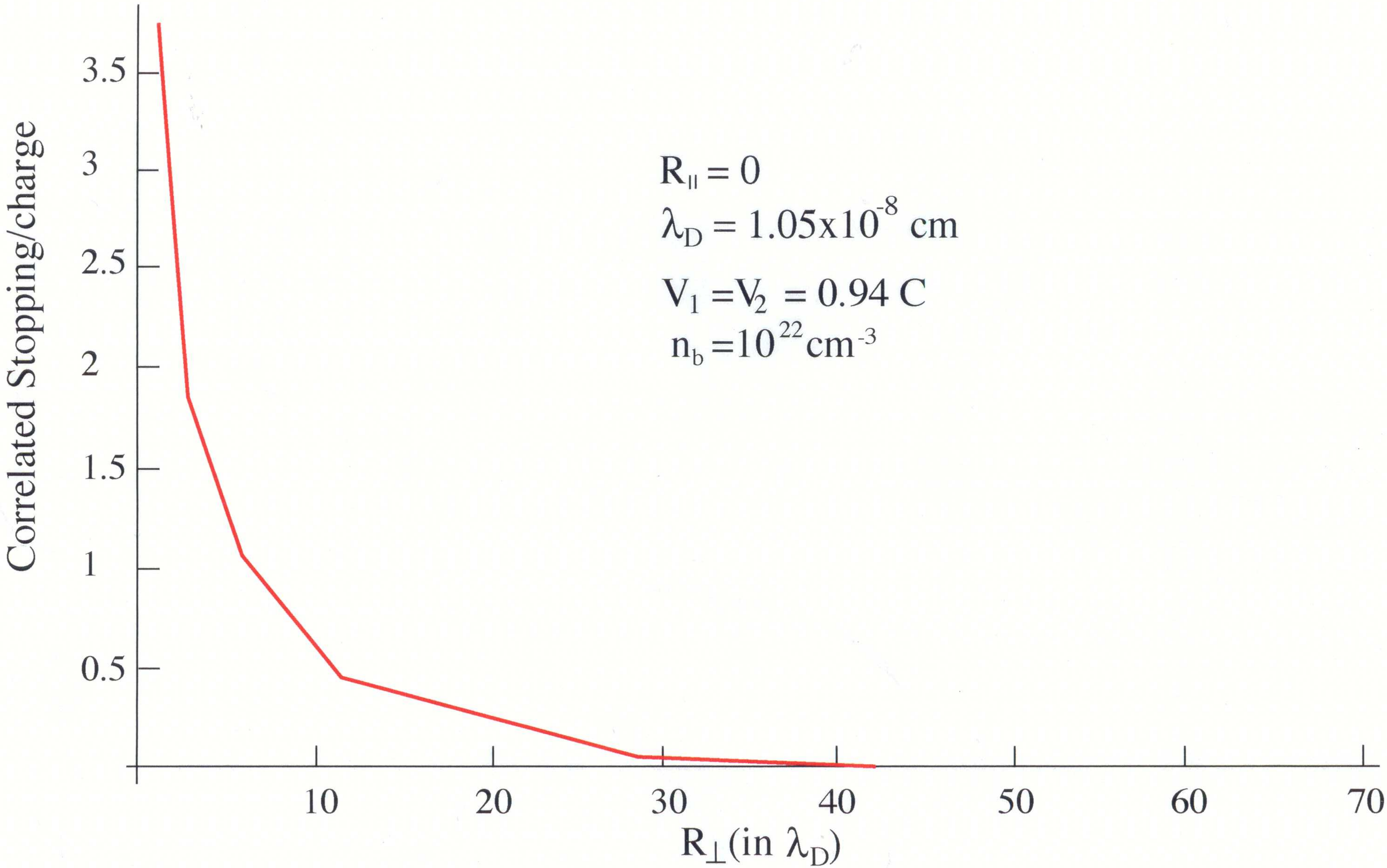
Correlated Stopping/charge
3.5
3
2.5
2
1.5
1
0.5
10
20
30
40
50
60
70
$R_\perp$(in λ_D)
$R_\parallel = 0$
$\lambda_D = 1.05\text{x}10^{-8}$ cm
$V_1 = V_2 = 0.94$ C
$n_b = 10^{22} \text{cm}^{-3}$

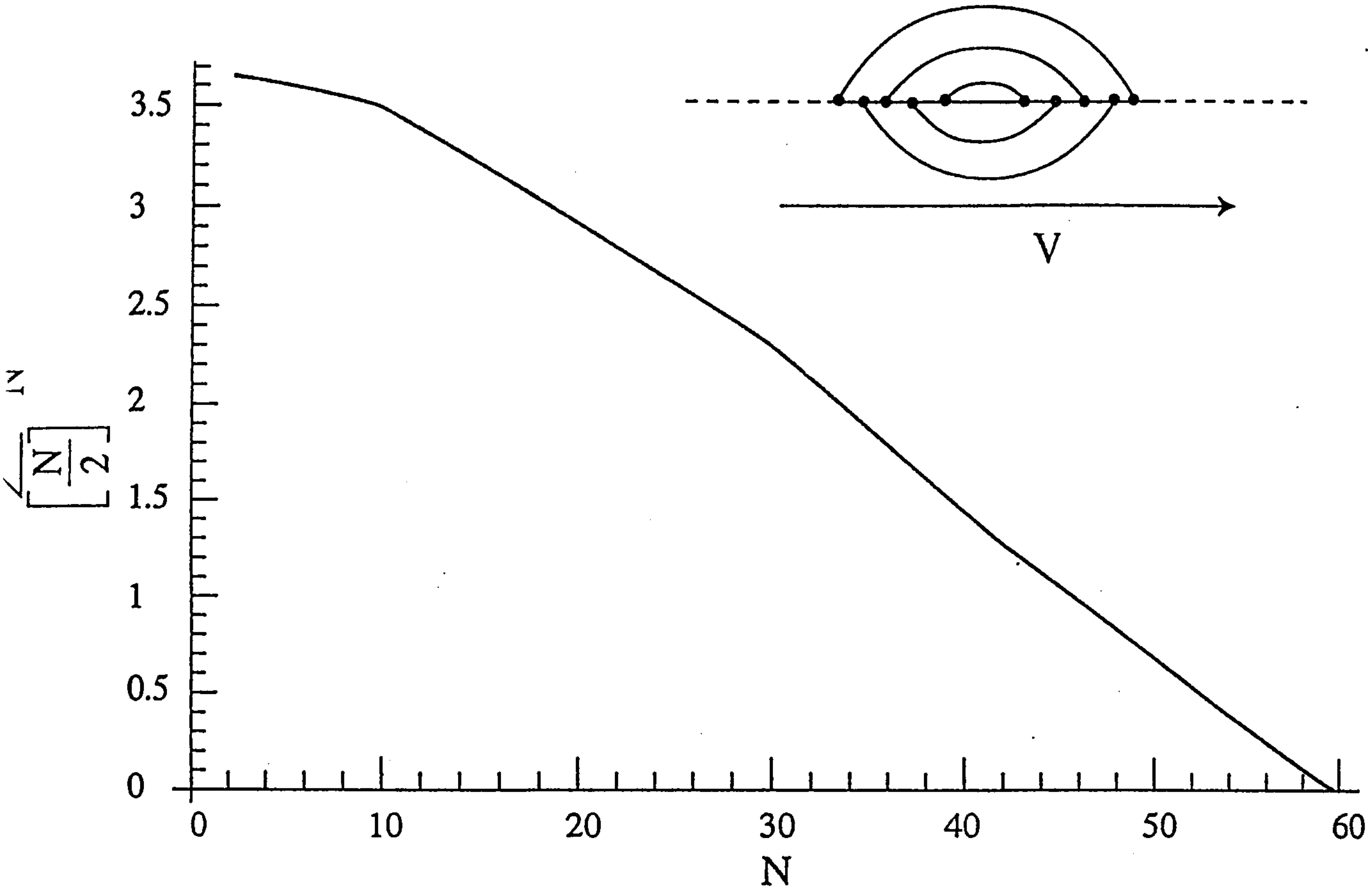

3.5
3
2.5
2
1.5
1
0.5
0
0
10
20
30
40
50
60
N
V

(b)

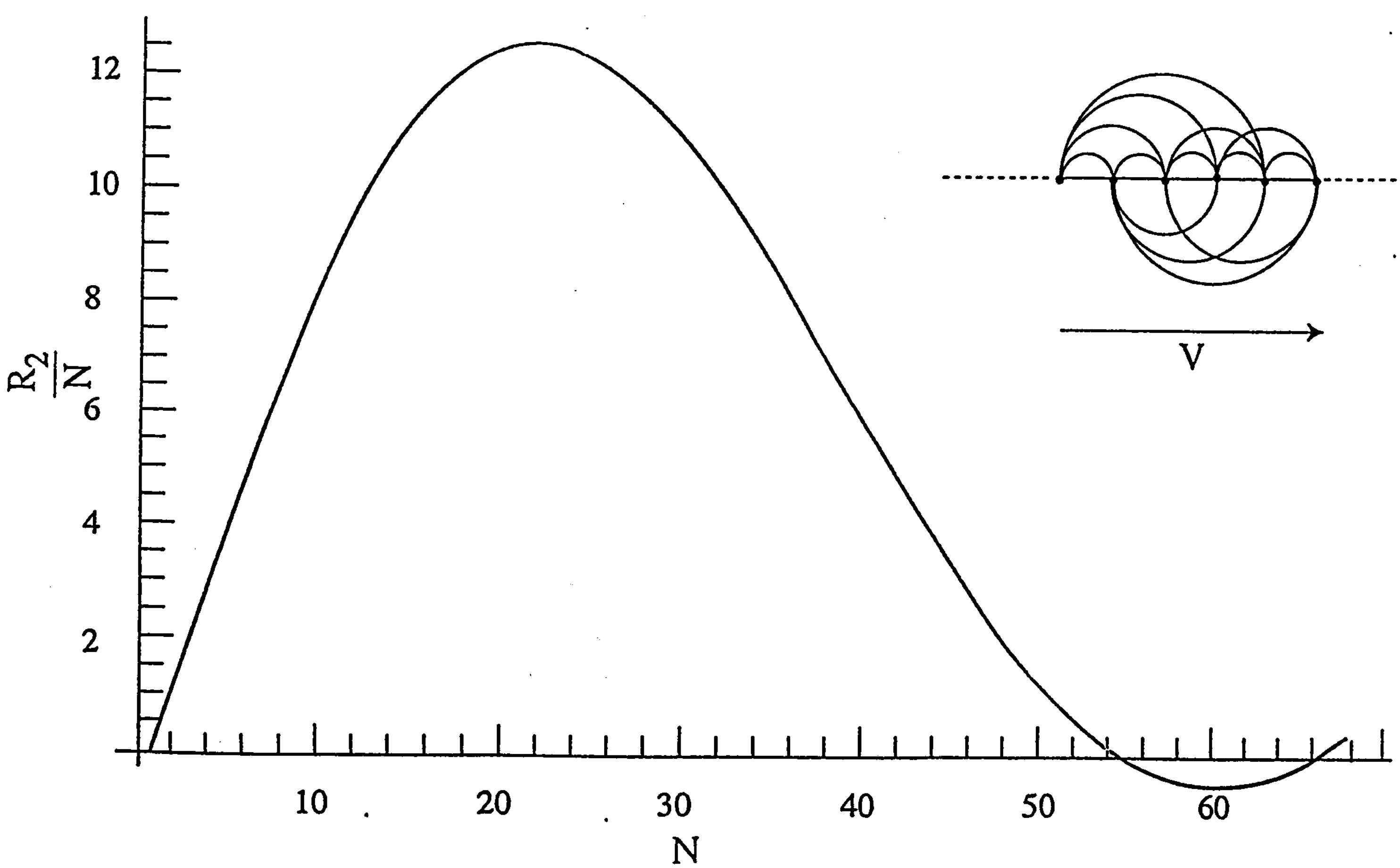

12
10
8
6
4
2
10
20
30
40
50
60
N
$\frac{R_2}{N}$
V

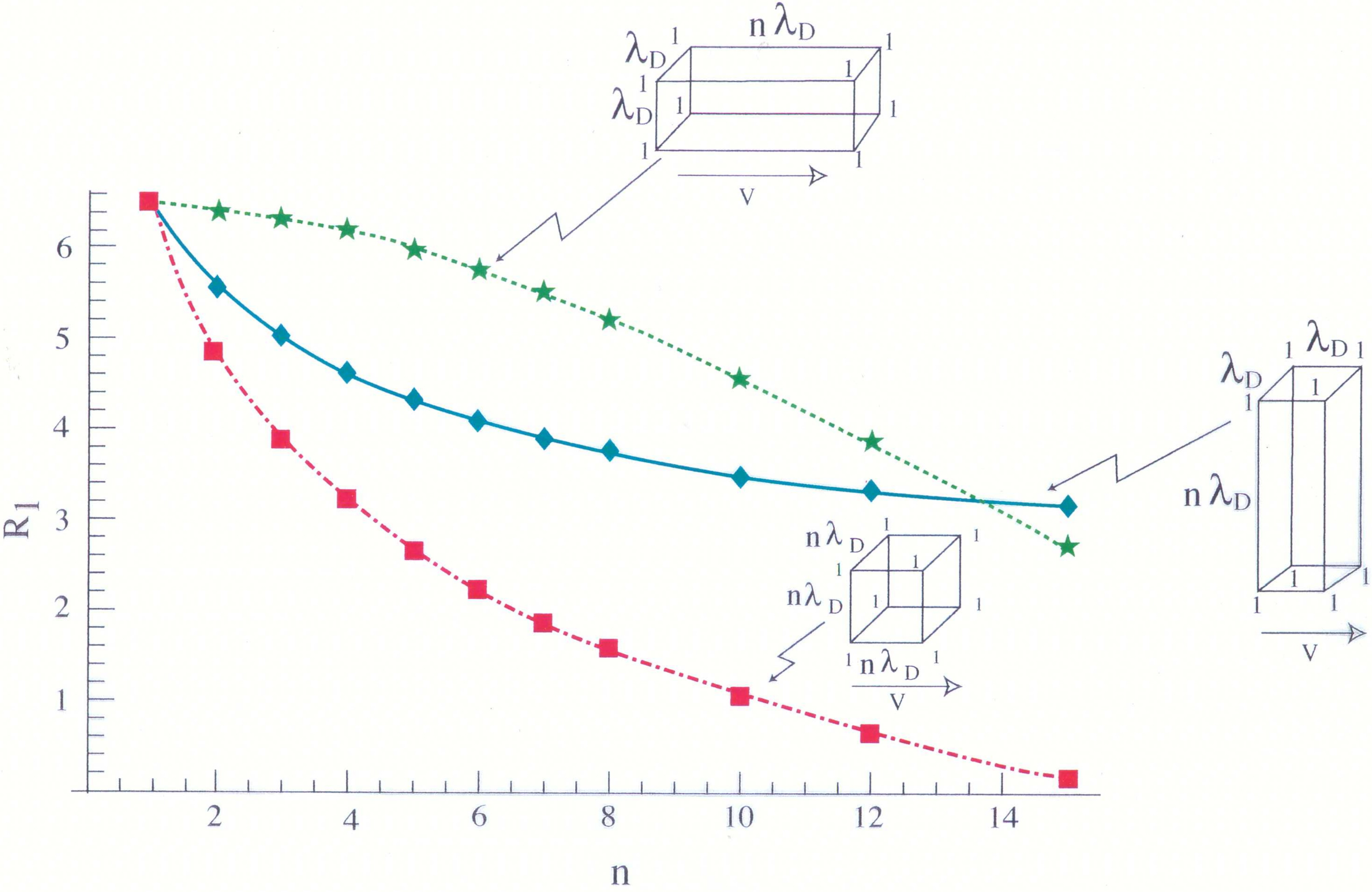

n λD
λD
λD
V
n λD
λD
λD
V
n λD
nλD
n λD
V
R1
n
1
2
3
4
5
6
2
4
6
8
10
12
14

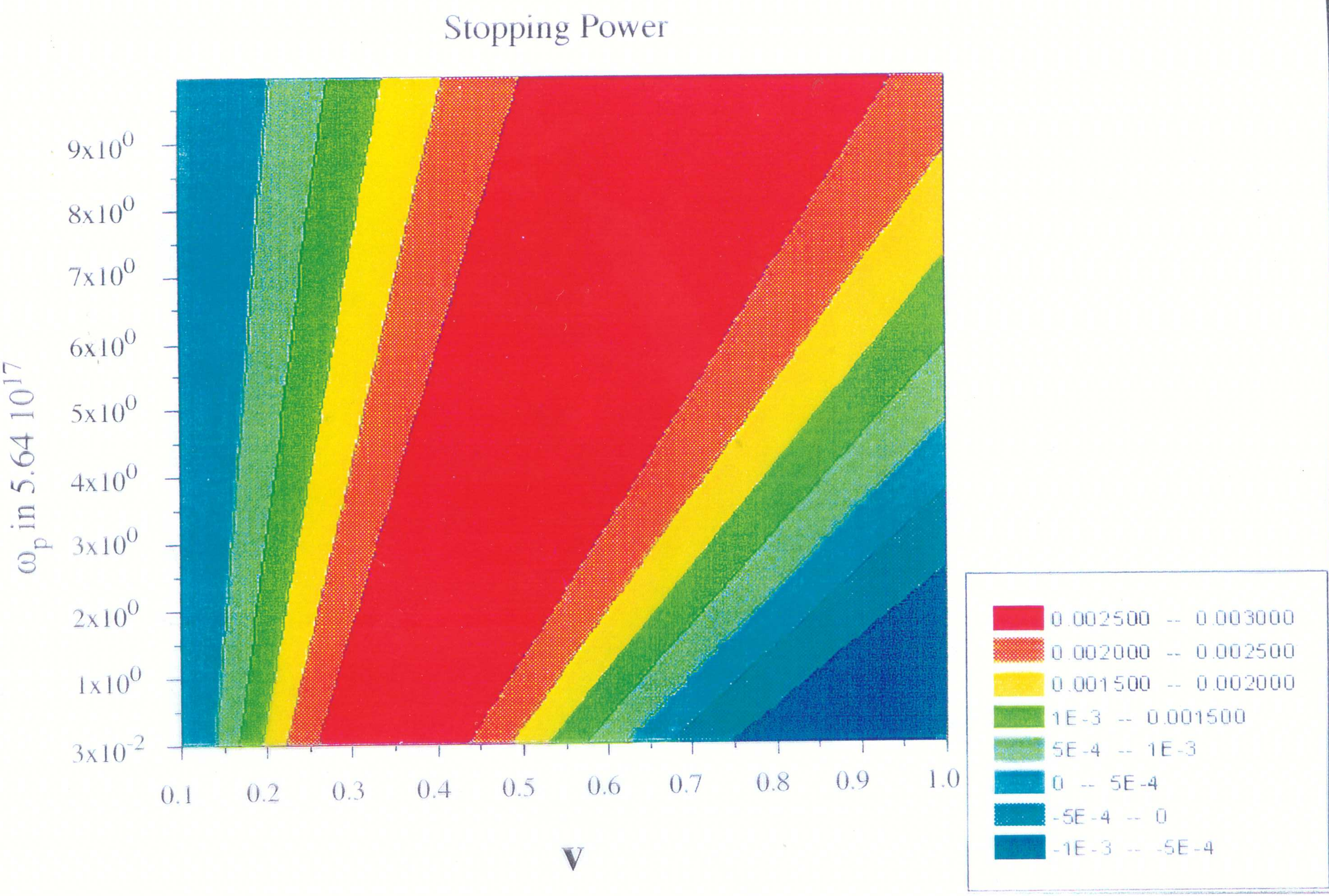

Stopping Power
ω_p in 5.64 10^17
9x10^0
8x10^0
7x10^0
6x10^0
5x10^0
4x10^0
3x10^0
2x10^0
1x10^0
3x10^-2
0.1
0.2
0.3
0.4
0.5
0.6
0.7
0.8
0.9
1.0
V
0.002500 -- 0.003000
0.002000 -- 0.002500
0.001500 -- 0.002000
1E-3 -- 0.001500
5E-4 -- 1E-3
0 -- 5E-4
-5E-4 -- 0
-1E-3 -- -5E-4

Proton beams may miss

the target through

multiple scattering

Even for a protecting foil close to the target, the dispersion is large, when considering a broad energy distribution

D=0.5 mm, 30 μm gold foil, energy distribution of present LULI source

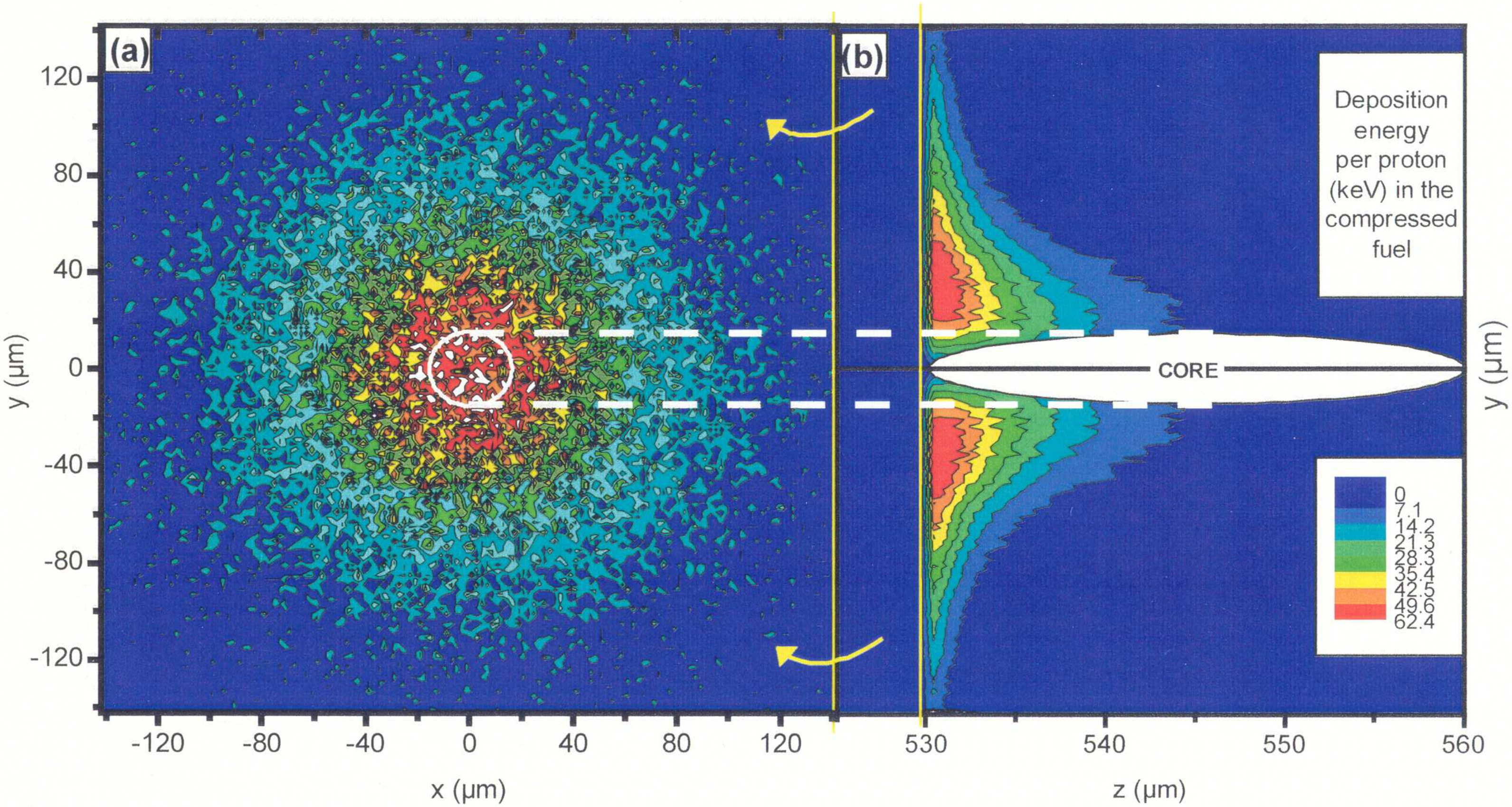

M. BARRIGA-CARRASCO, G. MAYNARD

The sensitivity on the shape of the energy distribution depends on the thickness of the protecting foil

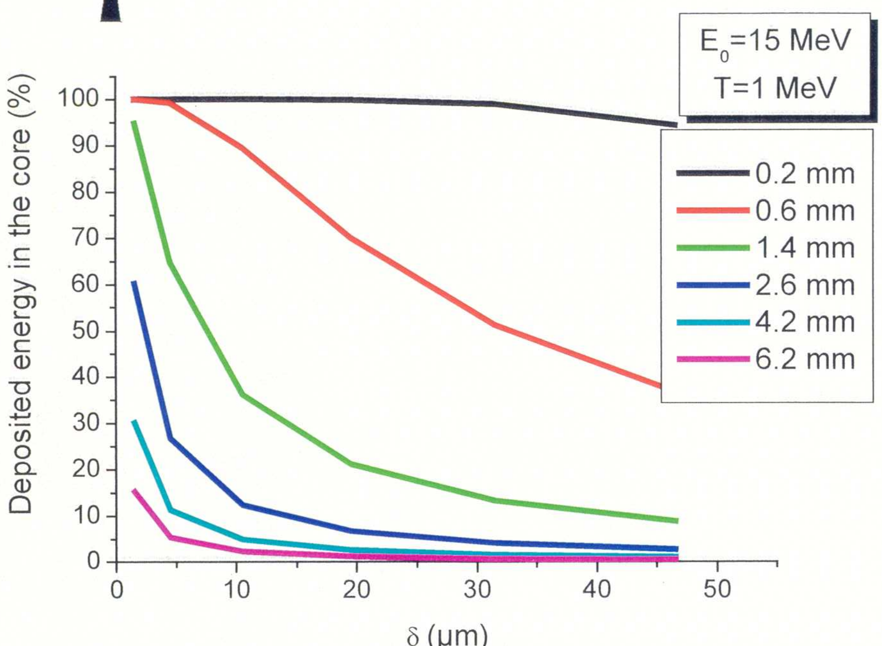

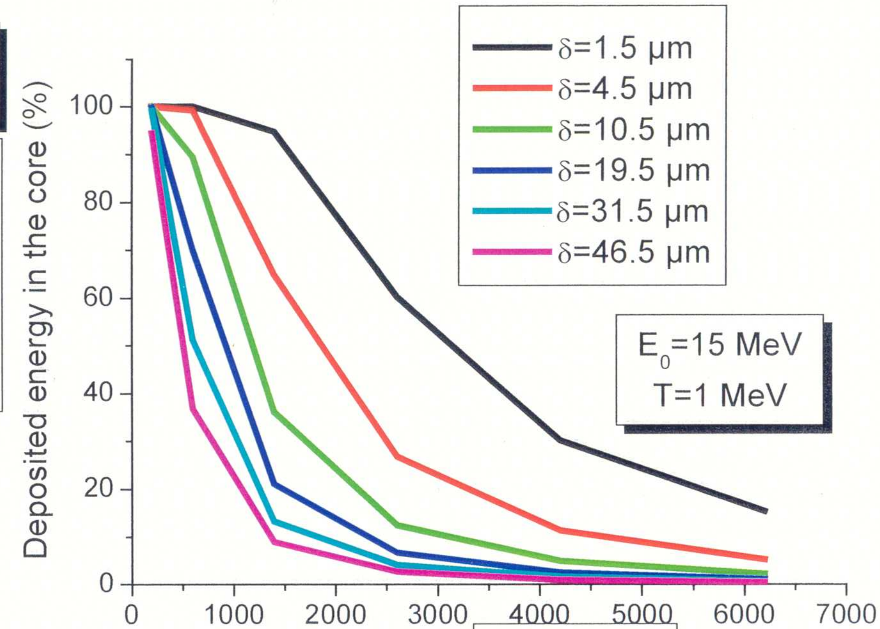

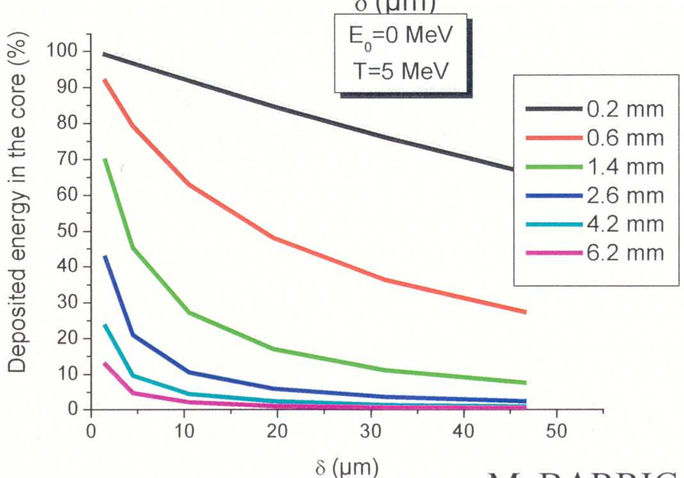

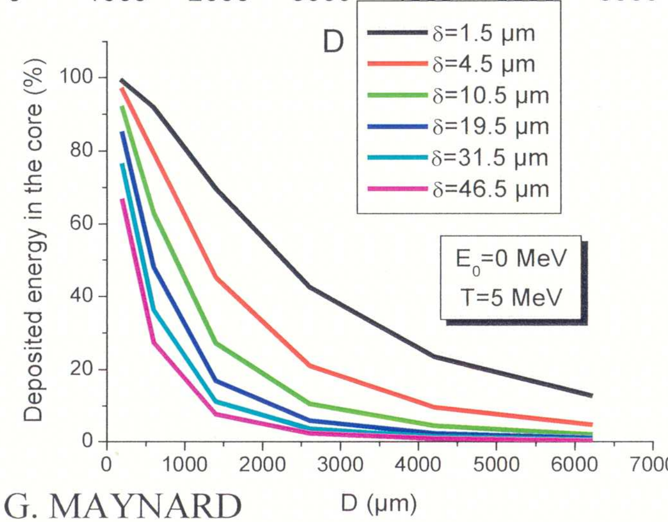

M. BARRIGA-CARRASCO, G. MAYNARD

Efficiency of energy deposition can be estimated through a simple formula for the width of the distribution in the transverse plane

$$\sigma(\mu m) = 0.07\frac{\sqrt{\delta(\mu m)}(D+\delta)(\mu m)}{E_p(MeV) - 0.15\delta(\mu m)/E_p(MeV)}$$

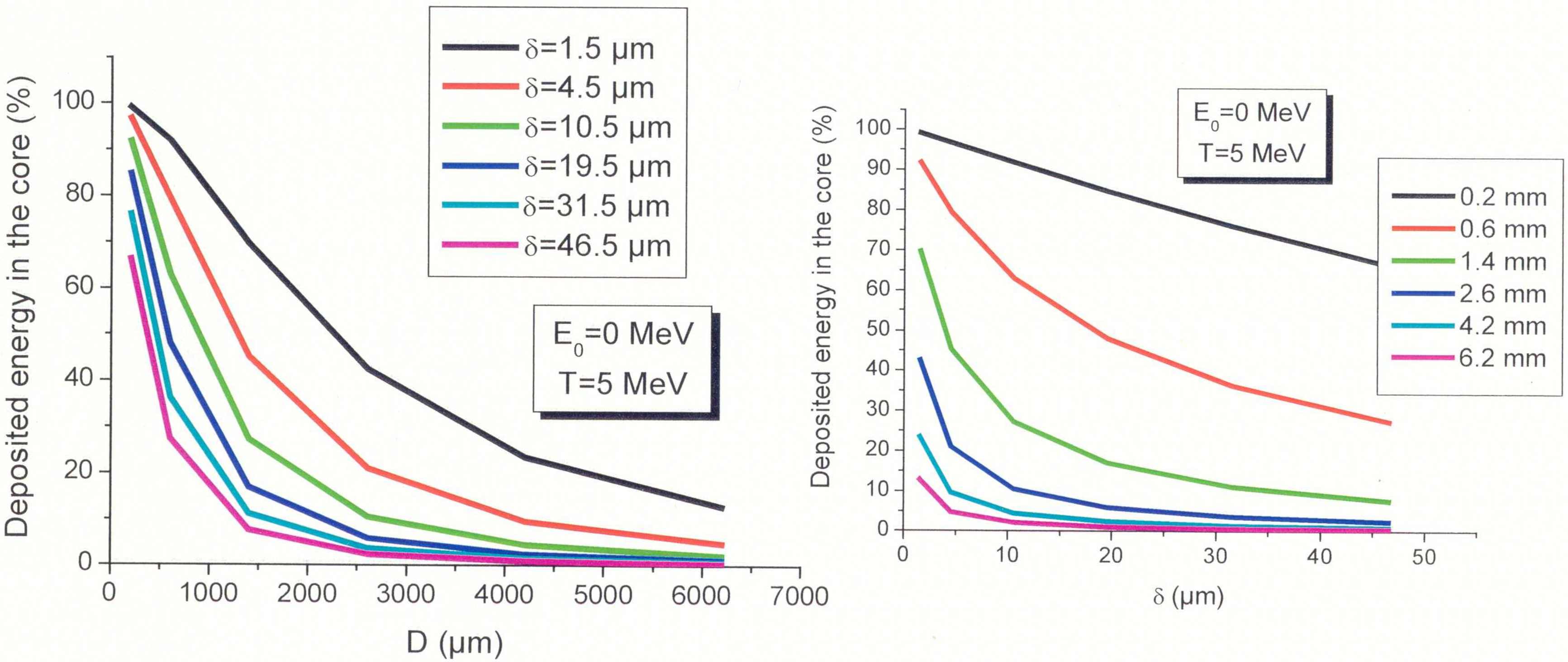

M. BARRIGA-CARRASCO, G. MAYNARD

An efficient protection of the LPS can require a substantial amount of heavy material on the path of the protons

MULTI2002, Rafael Ramis

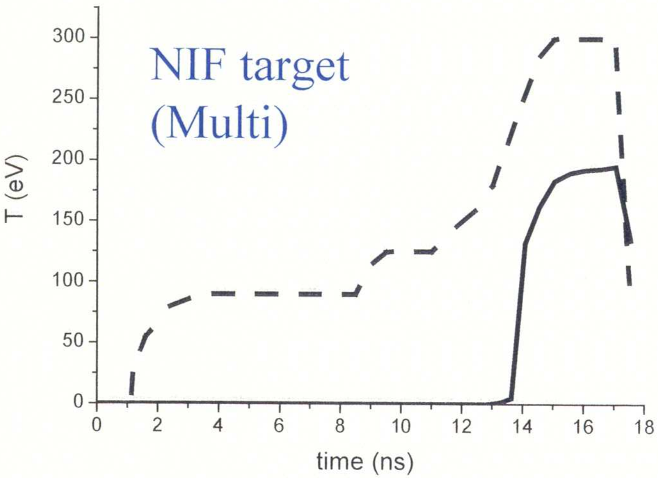

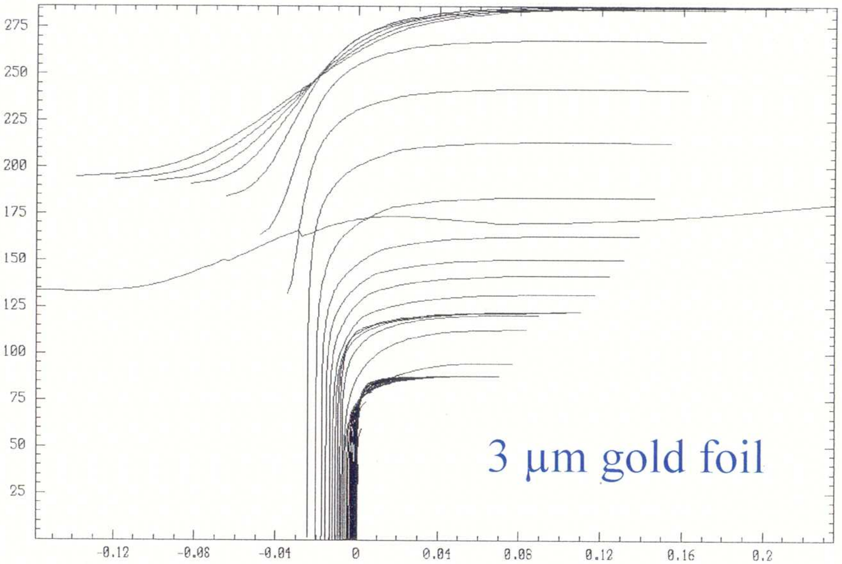

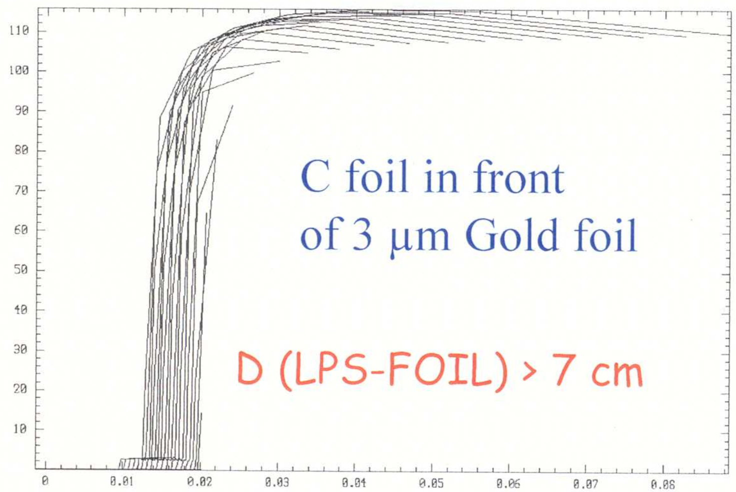

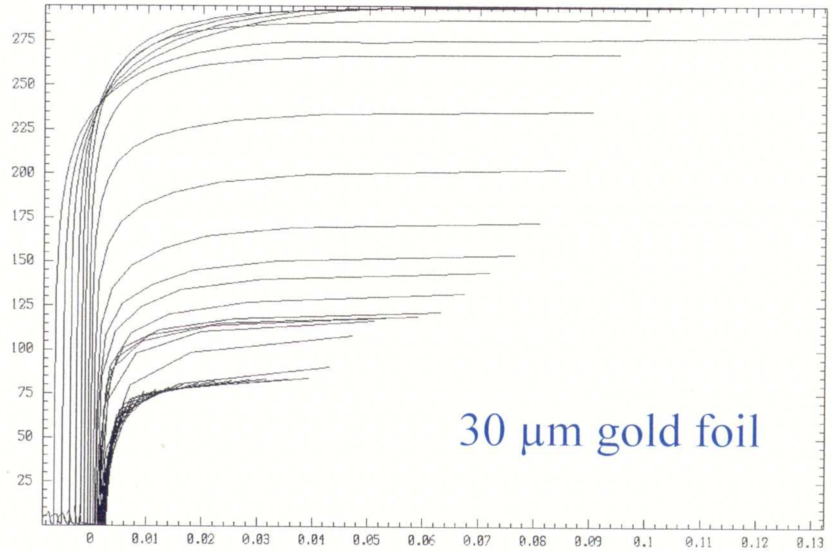

M. BARRIGA-CARRAS

Ignition Through Particles Stopping

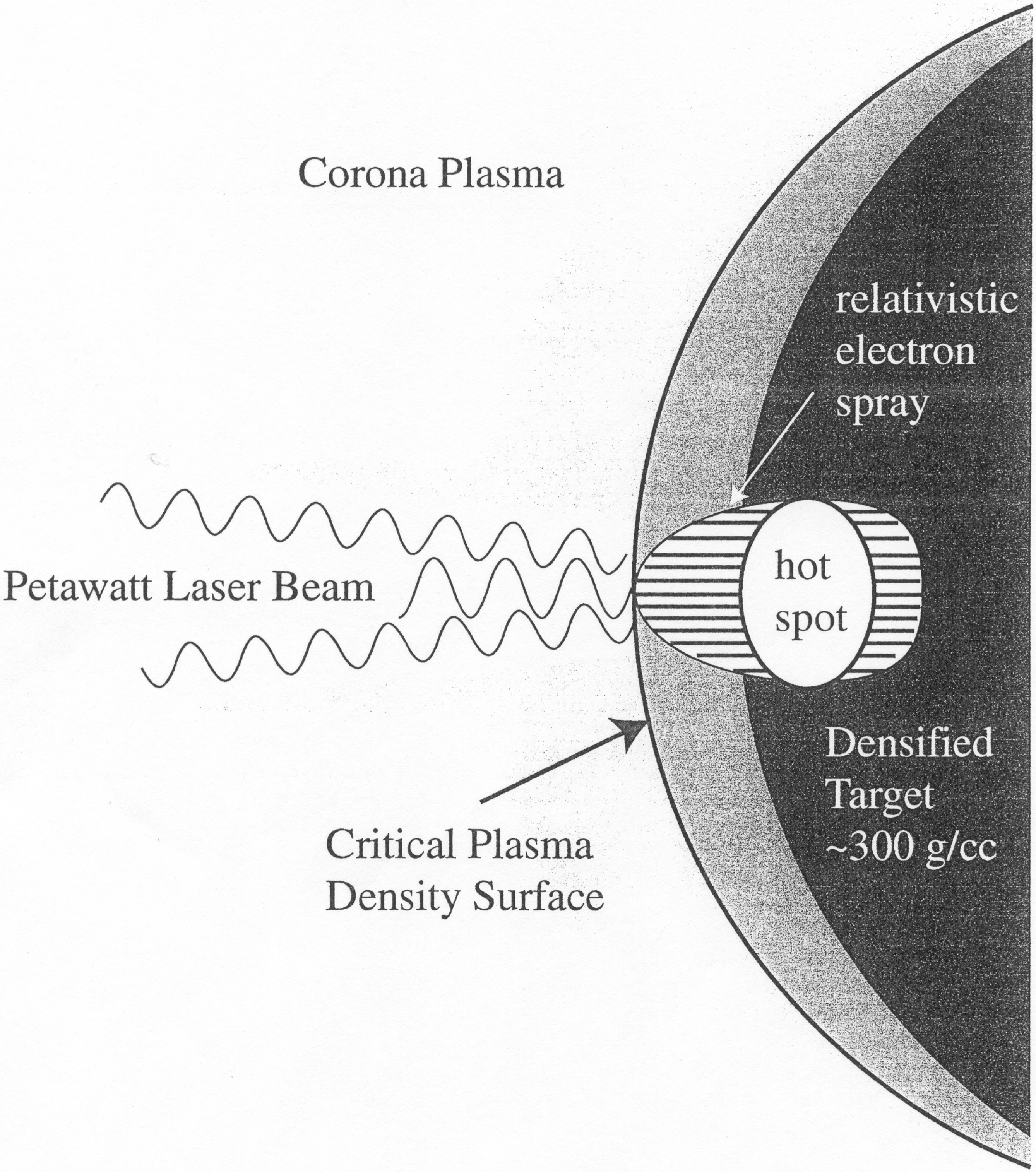
Corona Plasma
relativistic
electron
spray
Petawatt Laser Beam
hot
spot
Densified
Target
~300 g/cc
Critical Plasma
Density Surface

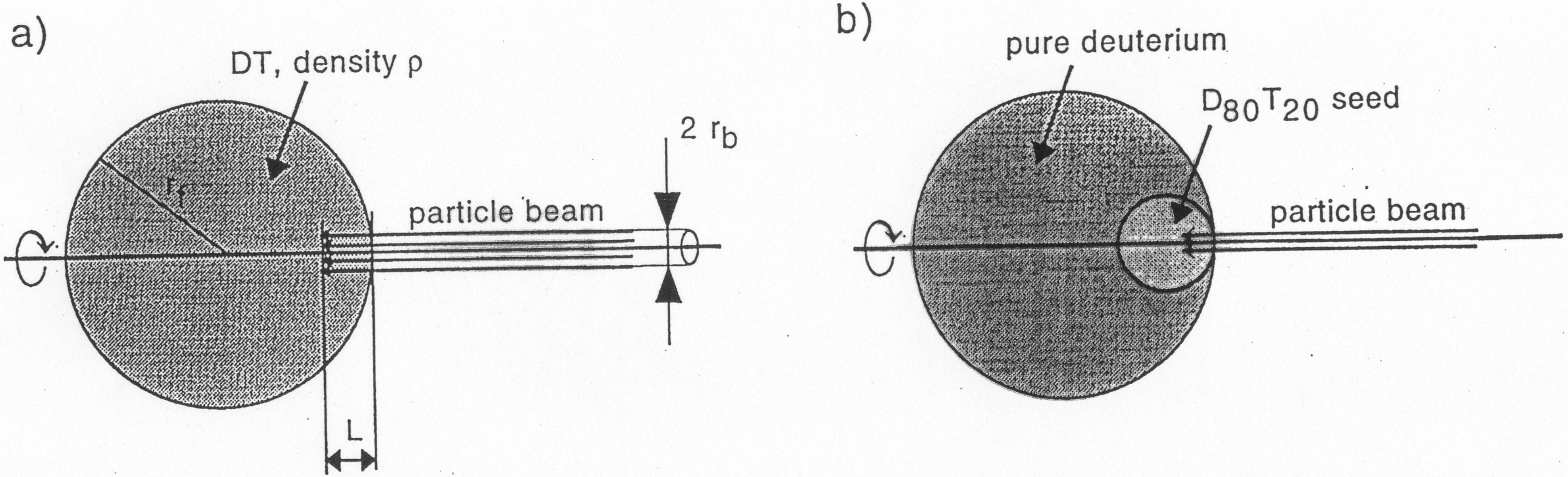

Figure 1. **DT (a), and DT-seeded deuterium target (b): initial conditions and irradiation scheme For uniform density, e.g. at t = 0, $L = R/\rho$.**

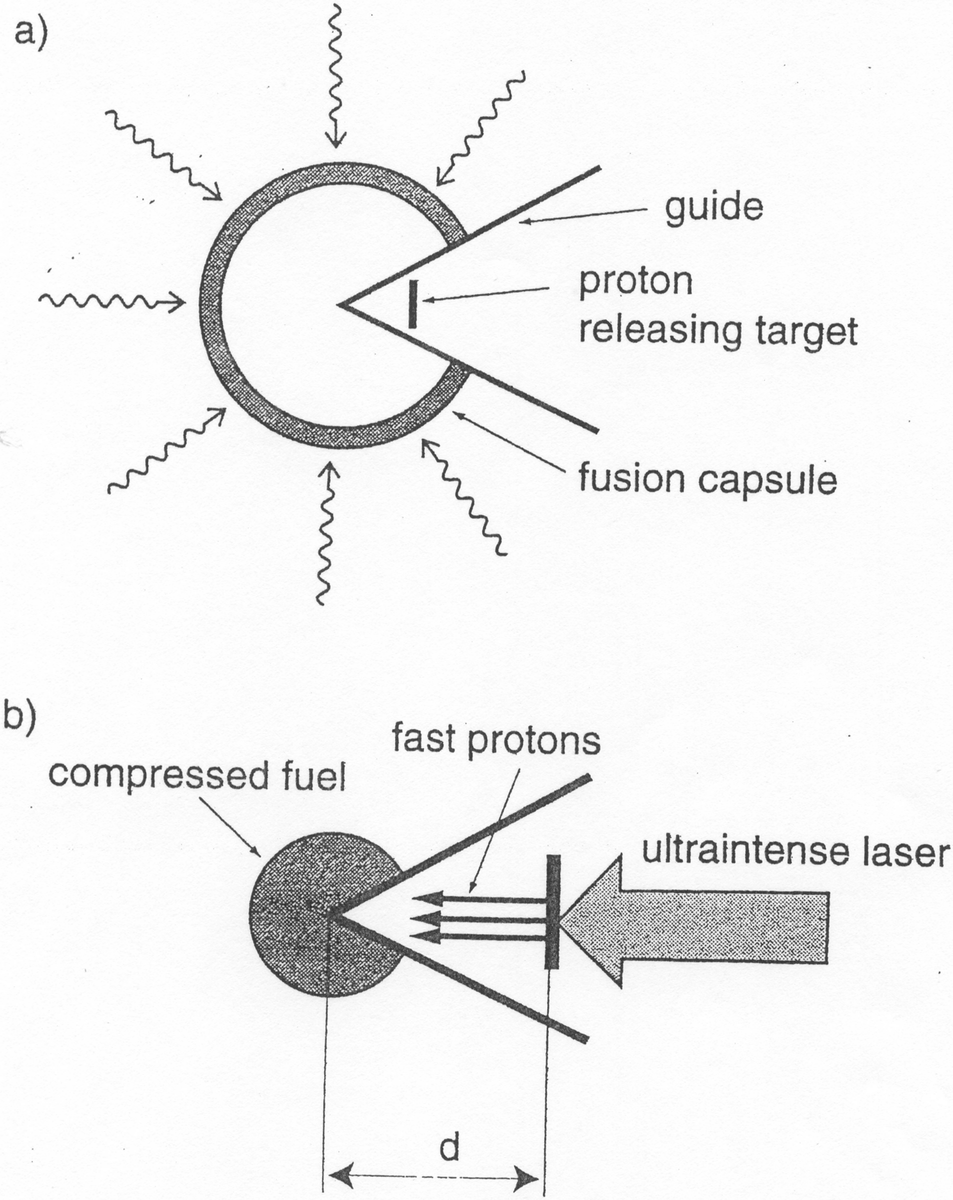
a)
guide
proton
releasing target
fusion capsule
b)
fast protons
compressed fuel
ultraintense laser
d

S. ATZENI, phys. plasmas Aug. 99

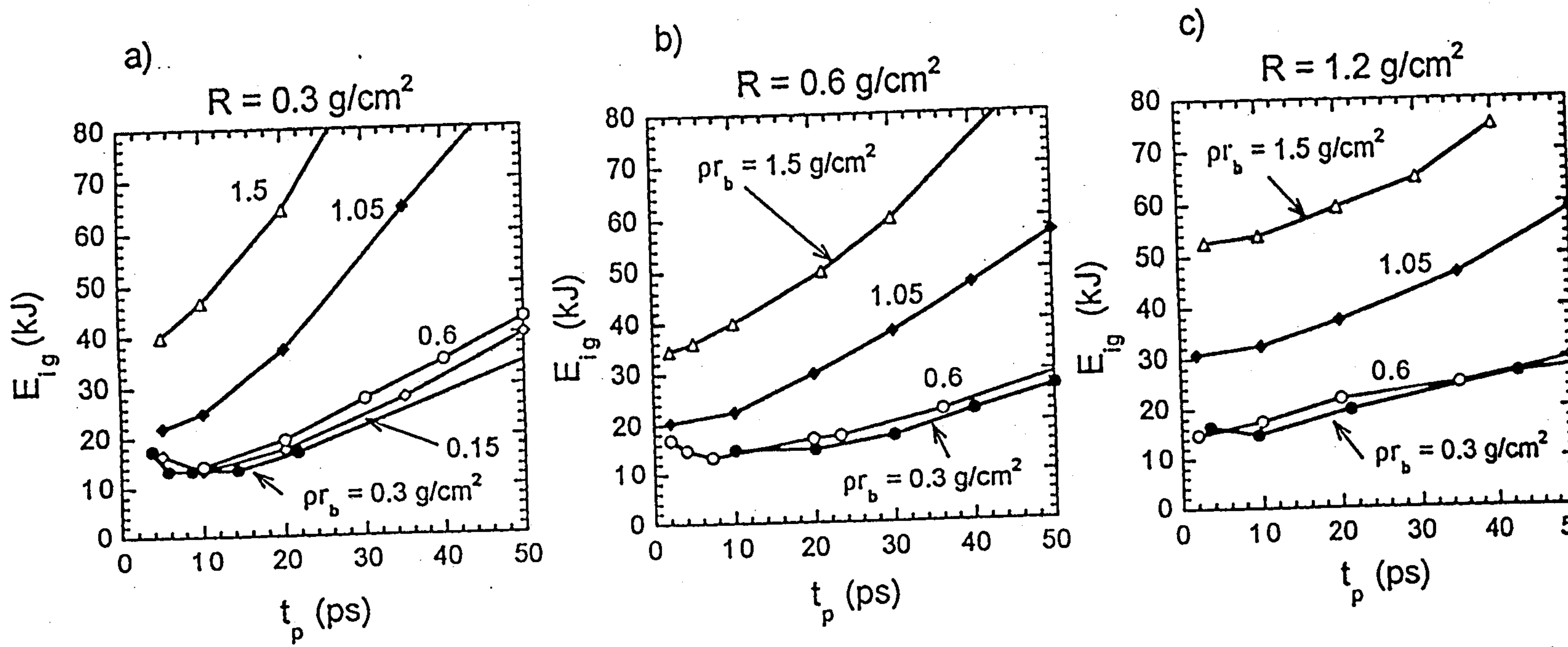

Minimum pulse energy for ignition, vs pulse duration, for DT fuel at $\rho = 300$ g/cm³ and different values of the beam radius r_b (see labels on the curves) and of the penetration depth R of the fast particles; a) $R = 0.3$ g/cm²; b) $R = 0.6$ g/cm²; c) $R = 1.2$ g/cm². Results for $R = 0.15$ g/cm² (not shown) and small focal spot are close to those for $R = 0.3$ g/cm².

$$E_{ig} = 140 \left(\frac{\rho}{100 \ \text{g/cm}^3} \right)^{-1.85} \text{kJ};$$

$$W_{ig} = 2.6 \times 10^{15} \left(\frac{\rho}{100 \ \text{g/cm}^3} \right)^{-1} \text{W};$$

$$I_{ig} = 2.4 \times 10^{19} \left(\frac{\rho}{100 \ \text{g/cm}^3} \right)^{0.95} \text{W/cm}^2.$$

CONCLUSION

- *HOT SPOT IGNITION SEEMS FEASIBLE*
- HIGHER TARGET DENSITIES (ρ=600-800 G/CC) LOOK PROMISING
- MORE STUDIES ARE NEEDED ON THE ELECTRONS-BEAM PLASMA INTERACTION NUMERICAL SIMULATION OF STOPPING AND MULTIPLE SCATTERING SHOULD BE HIGHLY RECOMMENDED
- REB STOPPING WITH AXIAL $\vec{B}$ COULD BE ALSO HELPFUL.

31st EPS Conference on Plasma Physics

Rapid Heating of Solid Density Material by the VULCAN Petawatt Laser*

R G Evans[1], E L Clark[1], R Clarke[2], R T Eagleton[1], A M Dunne[1], R D Edwards[1], W J Garbett[1], T J Goldsack[1], S James[1], D Neely[2], C Smith[1], B R Thomas[1], S J Rose[1,3]

1 AWE plc, Aldermaston, Reading RG7 4PR, UK
2 Central Laser Facility, CCLRC Rutherford Appleton Laboratory
3 Clarendon Laboratory, University of Oxford

** Experiment funded by the UK MoD*

Motivation

- Understand electron energy transport in high irradiance CPA experiments
- Prepare samples of hot dense material
- Relevant to fast ignitor physics

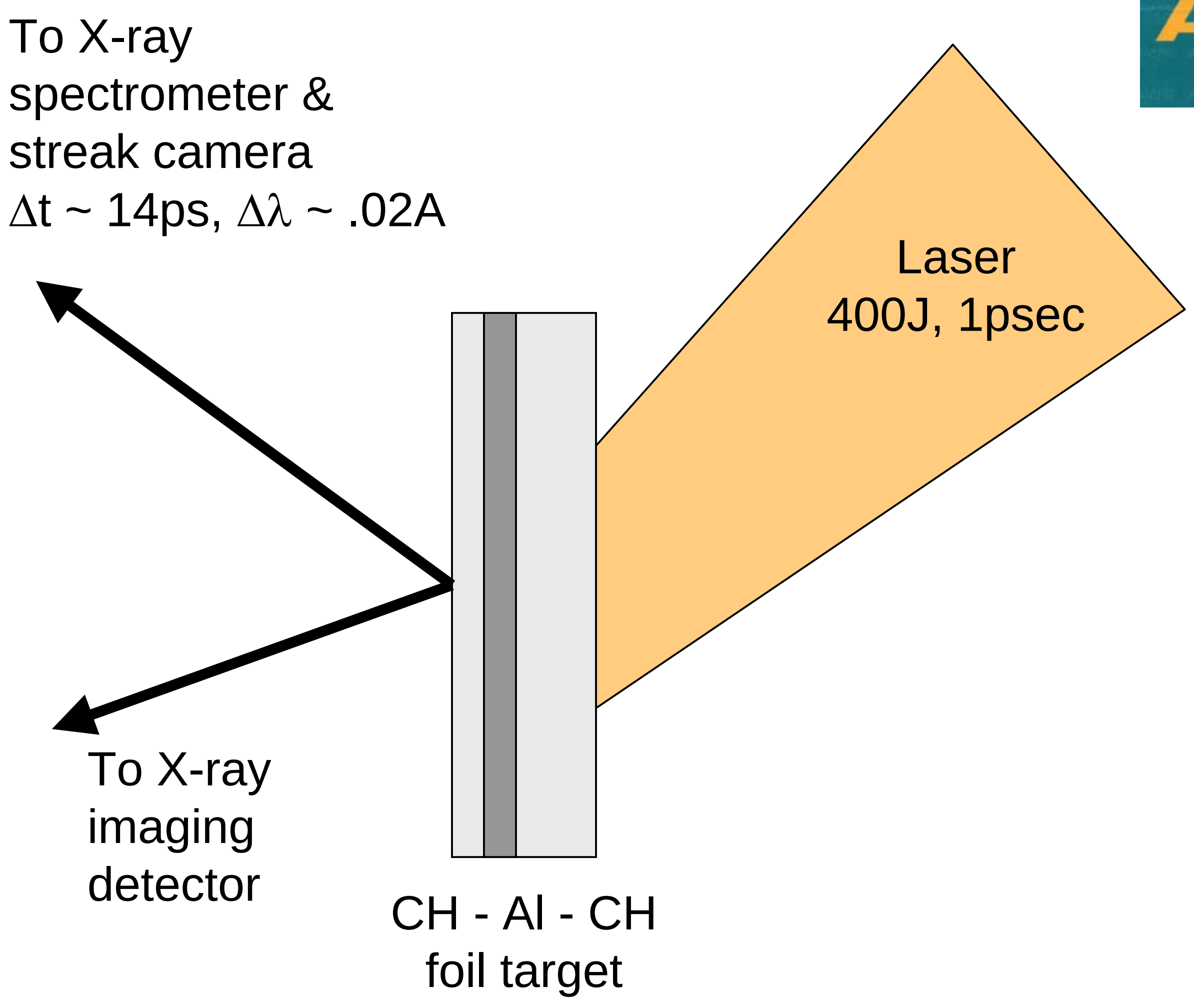

Buried layer heating experiment on VULCAN Petawatt

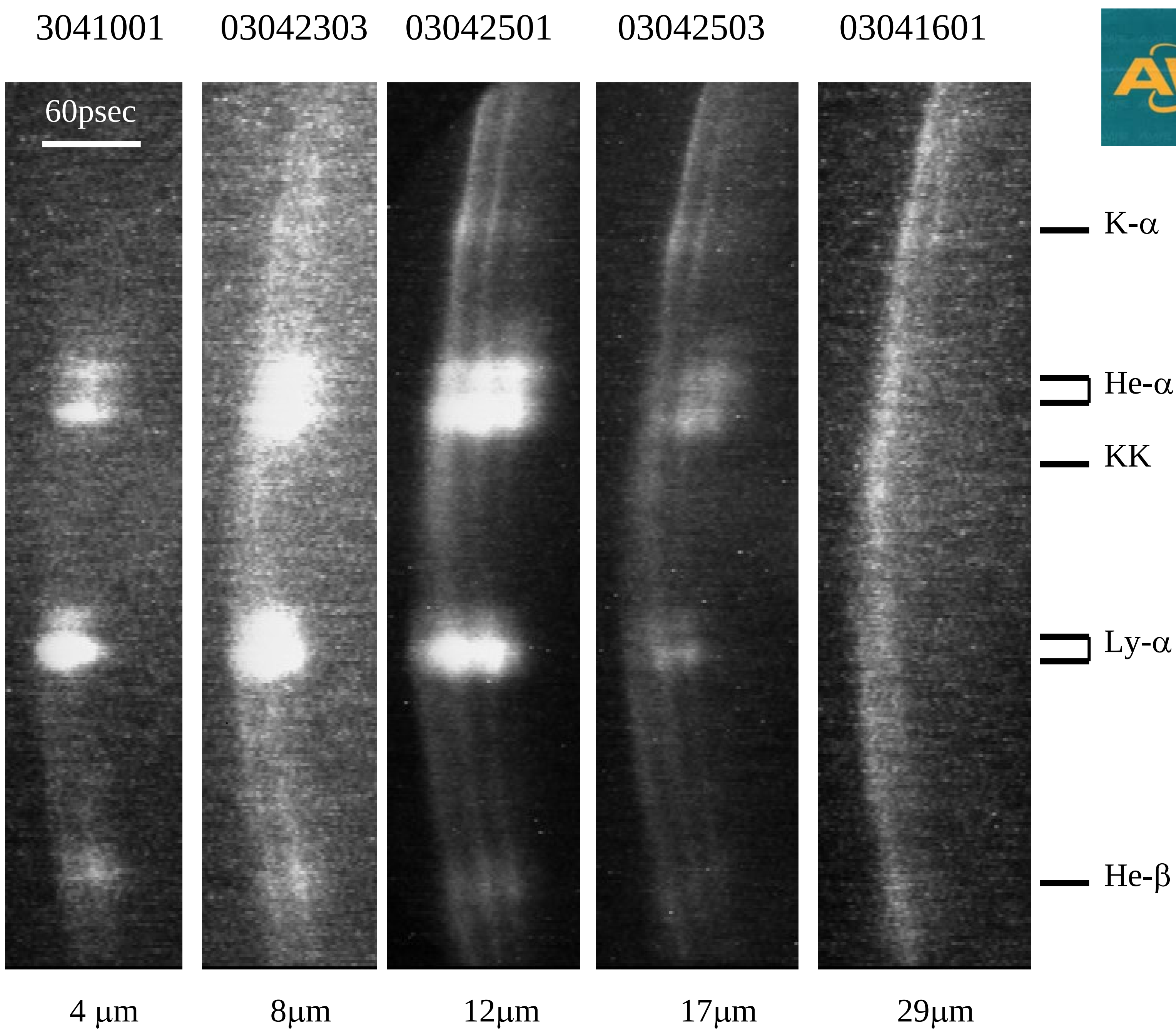

3041001
03042303
03042501
03042503
03041601
60psec
K-α
He-α
KK
Ly-α
He-β
4 μm
8μm
12μm
17μm
29μm

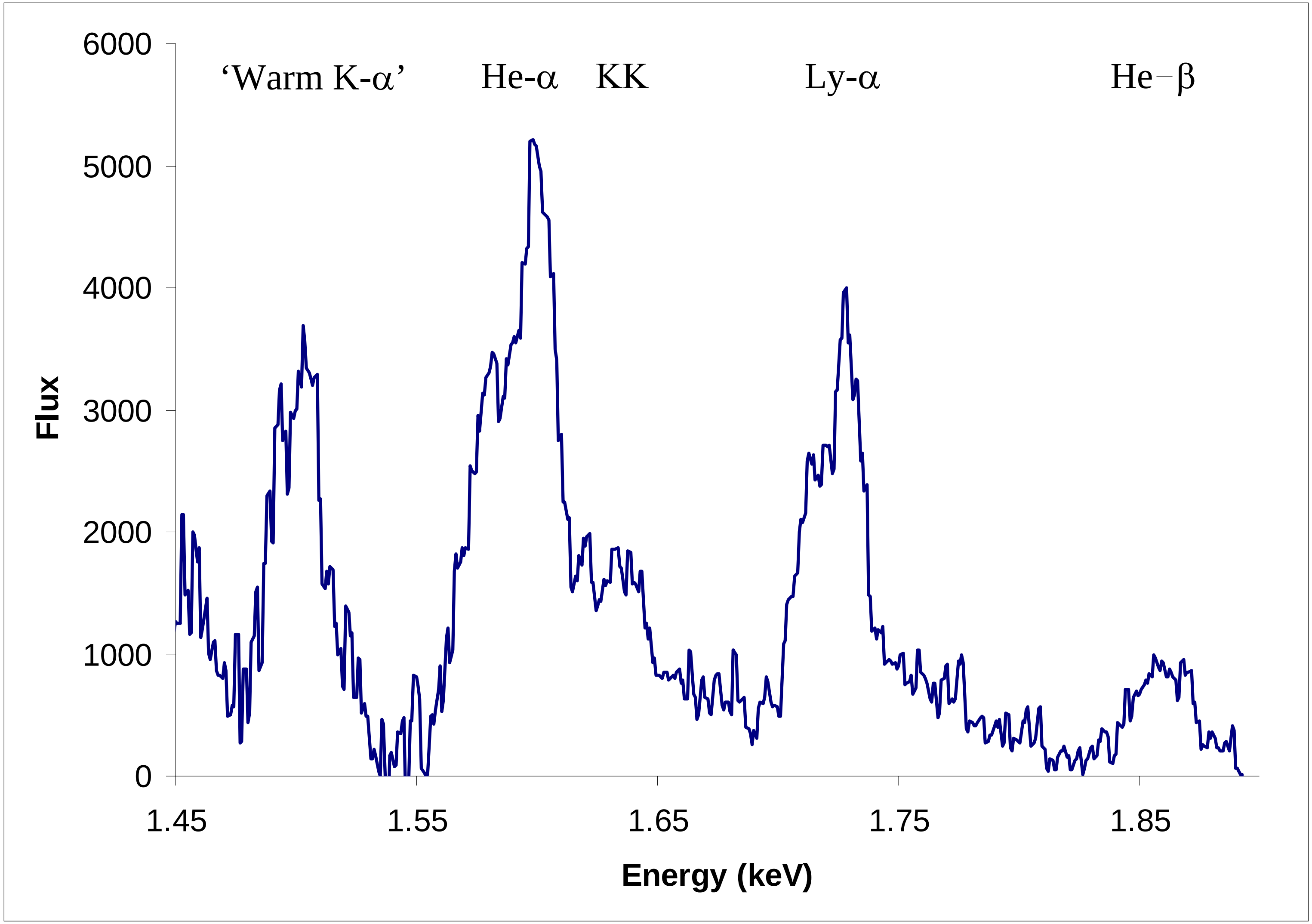

‘Warm K-α’
He-α
KK
Ly-α
He–β
Flux
0
1000
2000
3000
4000
5000
6000
1.45
1.55
1.65
1.75
1.85
Energy (keV)

The 'KK' spectral feature

Identified as a double K-shell vacancy ('hollow atom' transition) eg $2s^2 2p^2$ - $1s 2s^2 2p$ from Dirac-Fock calculations

Probably produced directly by the enormous flux of relativistic electrons - F ~ 3 x 10^{31} electrons cm^{-2} sec^{-1}

Potentially a diagnostic of the fast electron flux from the KK / K-α ratio

Shorter duration than thermal emission

Spectral Analysis Using FLY[1)]

FLY calculates atomic populations based on time dependent rate equations and opacity of a planar slab of material.

Includes many di-electronic satellite lines

Post process for observed spectrum including line shapes and opacity of homogeneous planar slab

Single material (aluminium)

Single temperature

Density and temperature allowed to vary in time

1) R W Lee and J T Larsen, Journal Quant Spect Rad Trans **56**, 535 (1996).

Spectral Analysis Using FLY

FLY shows that at solid density the populations are transient for < 1 psec

Experiment shows spectra are steady for 20-40 psec

Use FLY to deduce T_e after the laser pulse when most of the hot electrons have thermalised

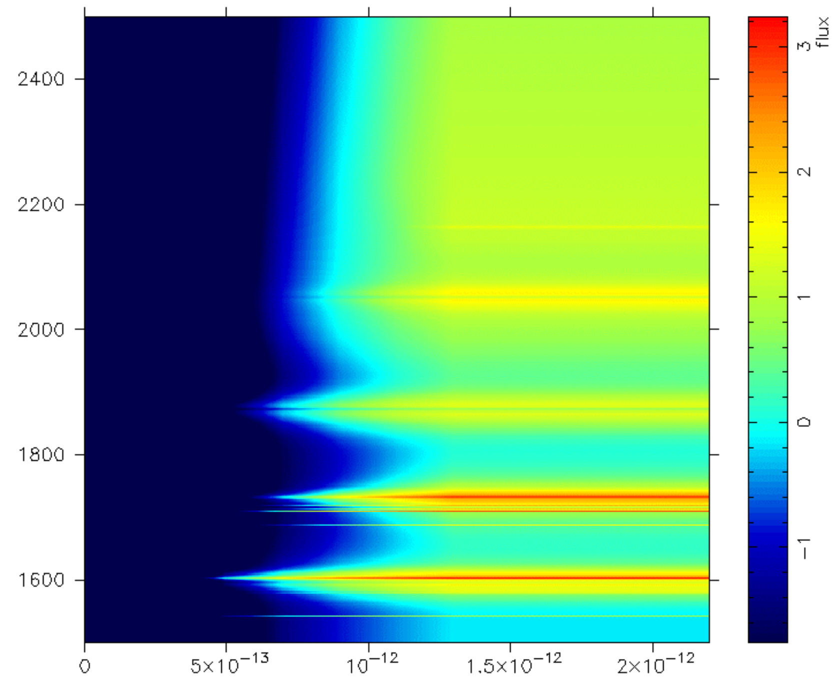

Density and Temperature from FLY

Simultaneously fit:

He-α and Ly-α shapes including satellite lines

Ly-α / He-α intensity; He-β width

Always consistent with $\rho \sim 0.5 - 3.0$ gm cm^{-3}

Not consistent with $\rho \sim 0.1$(decompressed) or $\rho \sim 8$ (shock compressed)

He-β always too weak by factor of 3 - 5. Implies hot core or residual effect of non-thermal tail

Depth (micron)	**Density(g cm^{-3})**	**Temp(eV)**	**Comment**
4	<1.0	> 600	Affected by laser pre-pulse ?
8.2	1.0 - 3.0	600 - 750	Over and under-exposed data, density from one, temperature from the other
12.1	1.0 - 3.0	450 - 550	He-α overexposed
17.1	1.0 - 3.0	400 - 550	Data from two shots
29	-	250	Estimated threshold of detectable emission

LSP[1)] Simulations of Electron beam heating

Implicit (D1) or Explicit PIC, PIC species may be collisional

Optional fluid species with perfect gas EOS and Spitzer transport coefficients

Laser generated hot electrons are PIC species, target electrons and ions are fluid species

Compile Options:

-DMULTI_PROCESS -DCAR_X_Y -DUNITS_MKS

-DMAX_SPECIES=4 -DCOLLISIONAL_PLASMA -DDIRECT_IMPLICIT

-DFLUID_PHYSICS -DFRICTIONAL_EFFECTS

Modify particle injection to mimic distribution of relativistic electrons from laser focus

1) D R Welch, D V Rose, B V Oliver, and R E Clark, Nucl. Instrum. Methods Phys. Res. A **464**, 134 (2001).

LSP Simulations - schematic

Electron Beam

2×10^{19} Wcm^{-2}

$T_{//}$2.5MeV
$T_{\wedge}$ 300keV

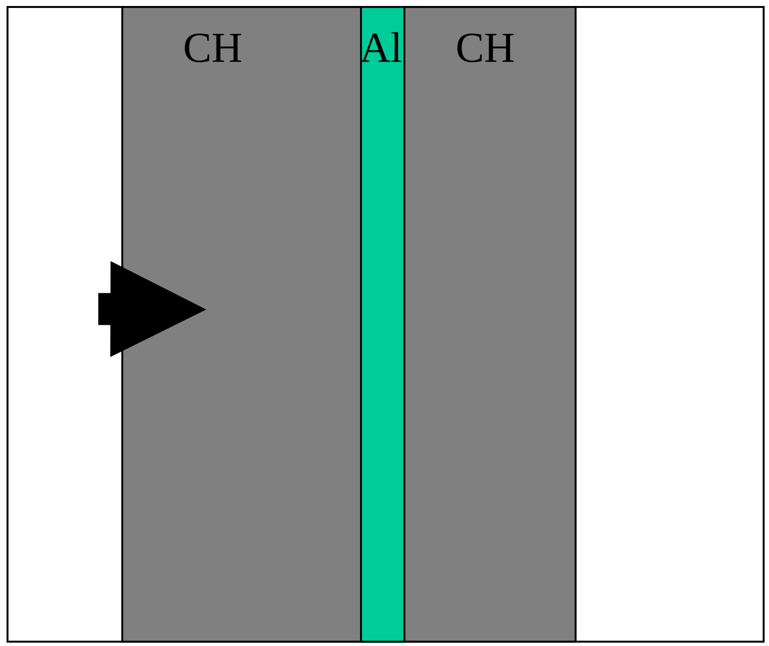

100μm x 100μm

800 x 800 cells

'Open' boundaries

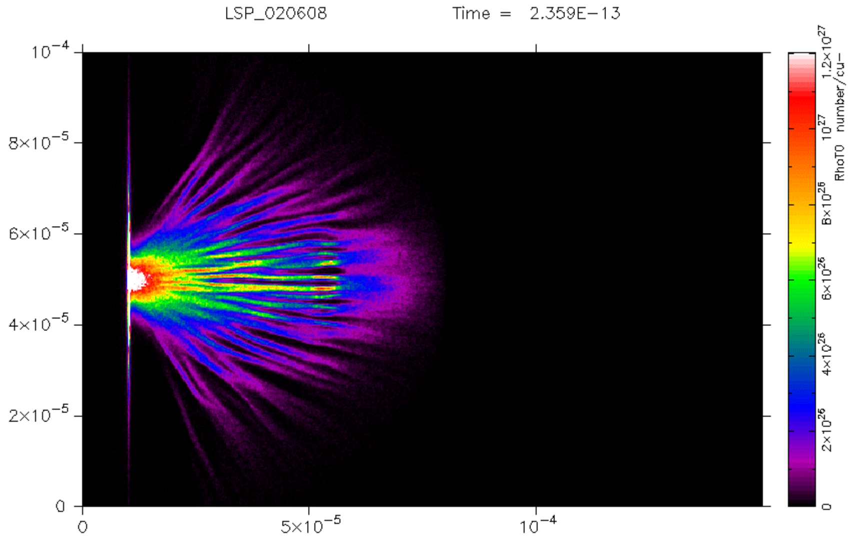
LSP_020608
Time = 2.359E-13
RhoT0 number/cu-

n_{HOT}

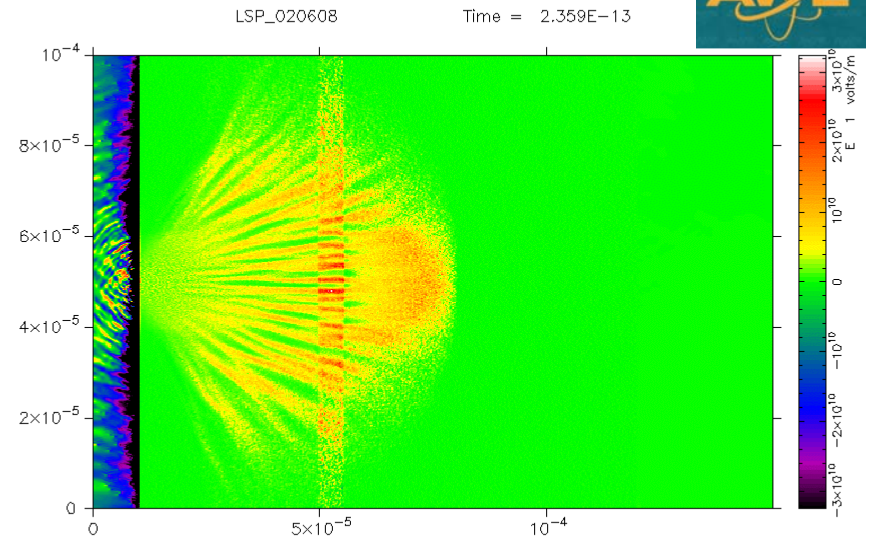
LSP_020608
Time = 2.359E-13
E 1 volts/m

E_x

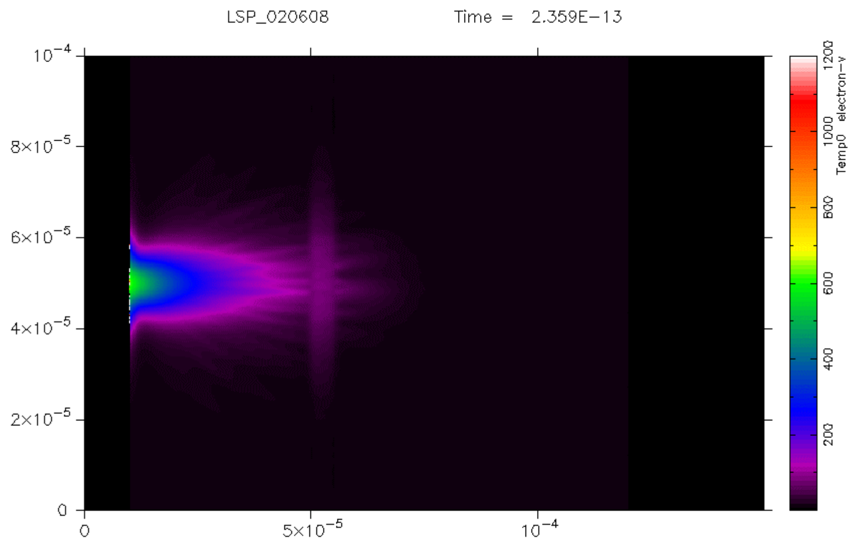
LSP_020608
Time = 2.359E-13
Temp0 electron-v

T_e

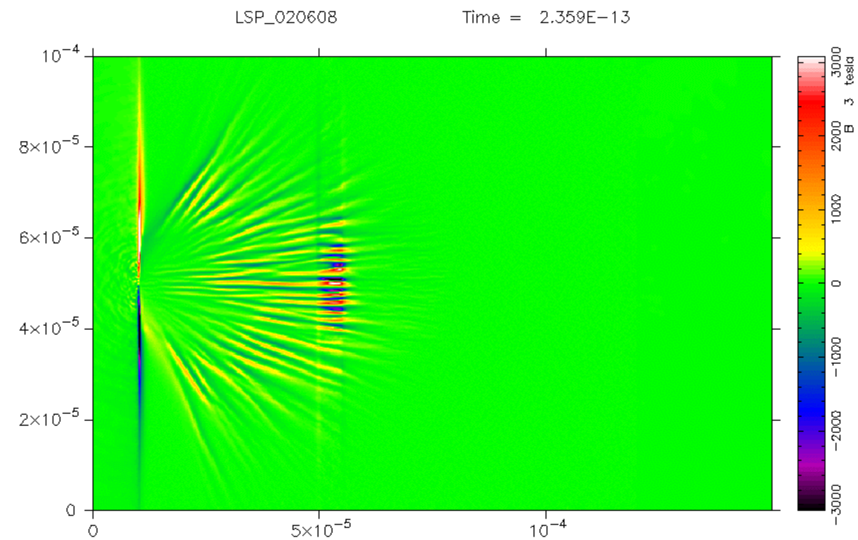
LSP_020608
Time = 2.359E-13
B 3 tesla

B_z

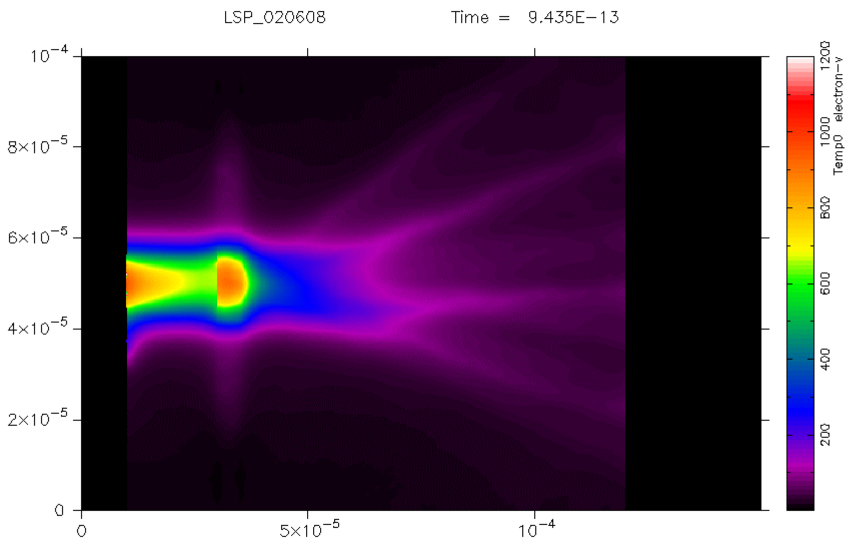

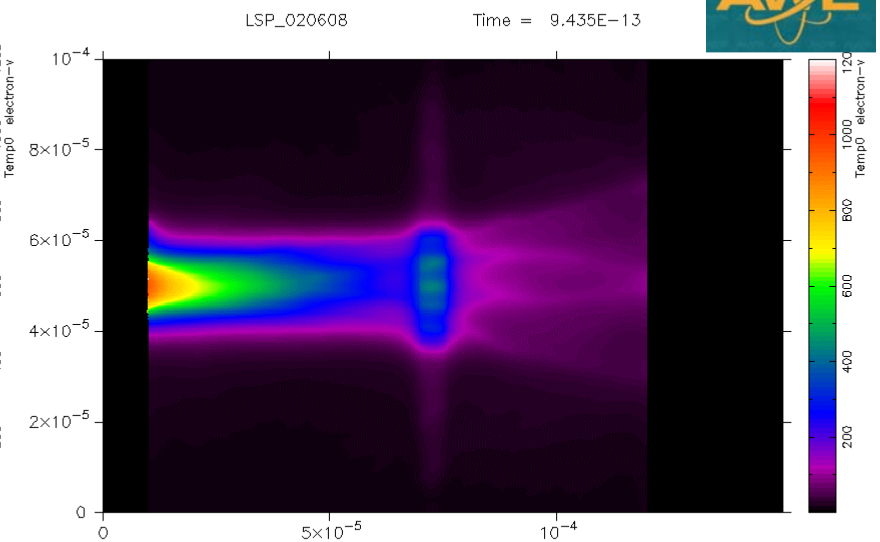

T_e with Al layer at various depths

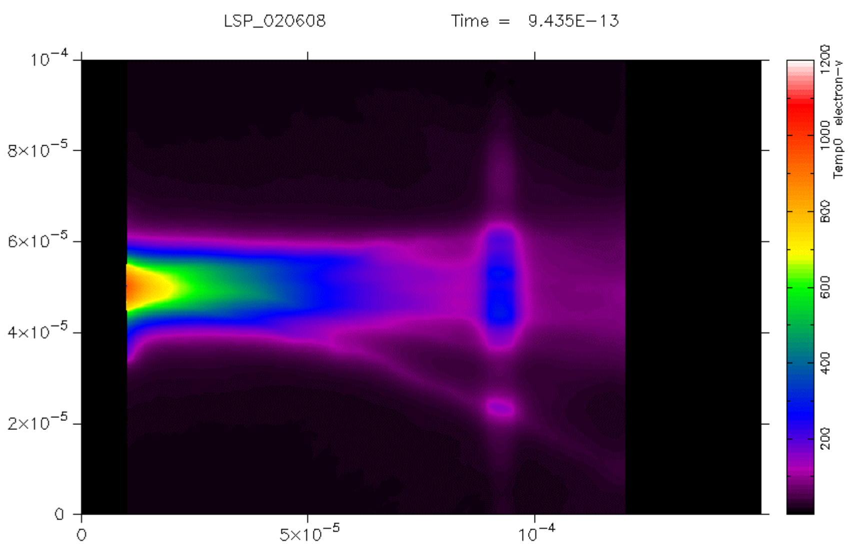

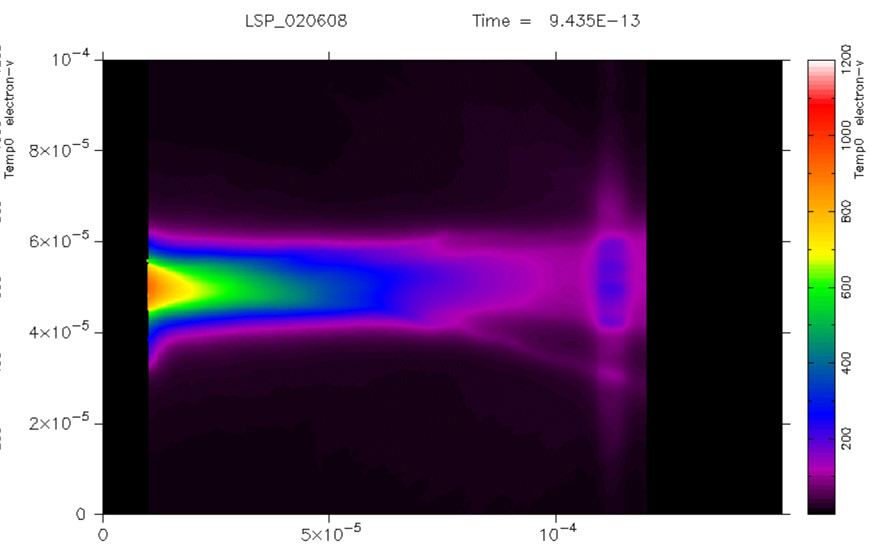

Electron Transport in thin tracer layer

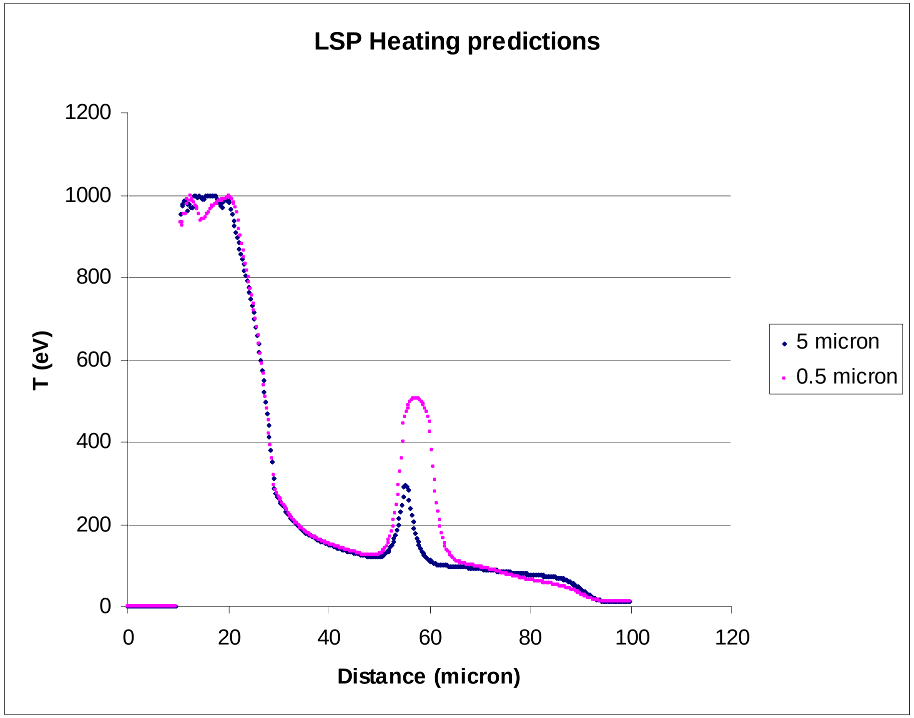

LSP uses flux-limited thermal conduction for fluid species

Full Fokker Planck treatment would be valuable

Electrons with E ~ 1.5 - 2.0keV have range equal to thickness of Al layer. Approximate equilibrium with CH substrate

Electron Inhibition due to pre-plasma

First described by Bond, Hares and Kilkenny[1)]

Spitzer resistivity η is approximately independent of ρ.

If material is expanded to lower density same current **j** produces same electric field **E** but over larger distance so larger potential drop

'Insulation' of lower energy hot electrons

D J Bond, J D Hares, and J D Kilkenny, Plasma Physics and Controlled Fusion **24**, 91 (1982).

Buried 5 μm Al layer: without prepulse and with prepulse

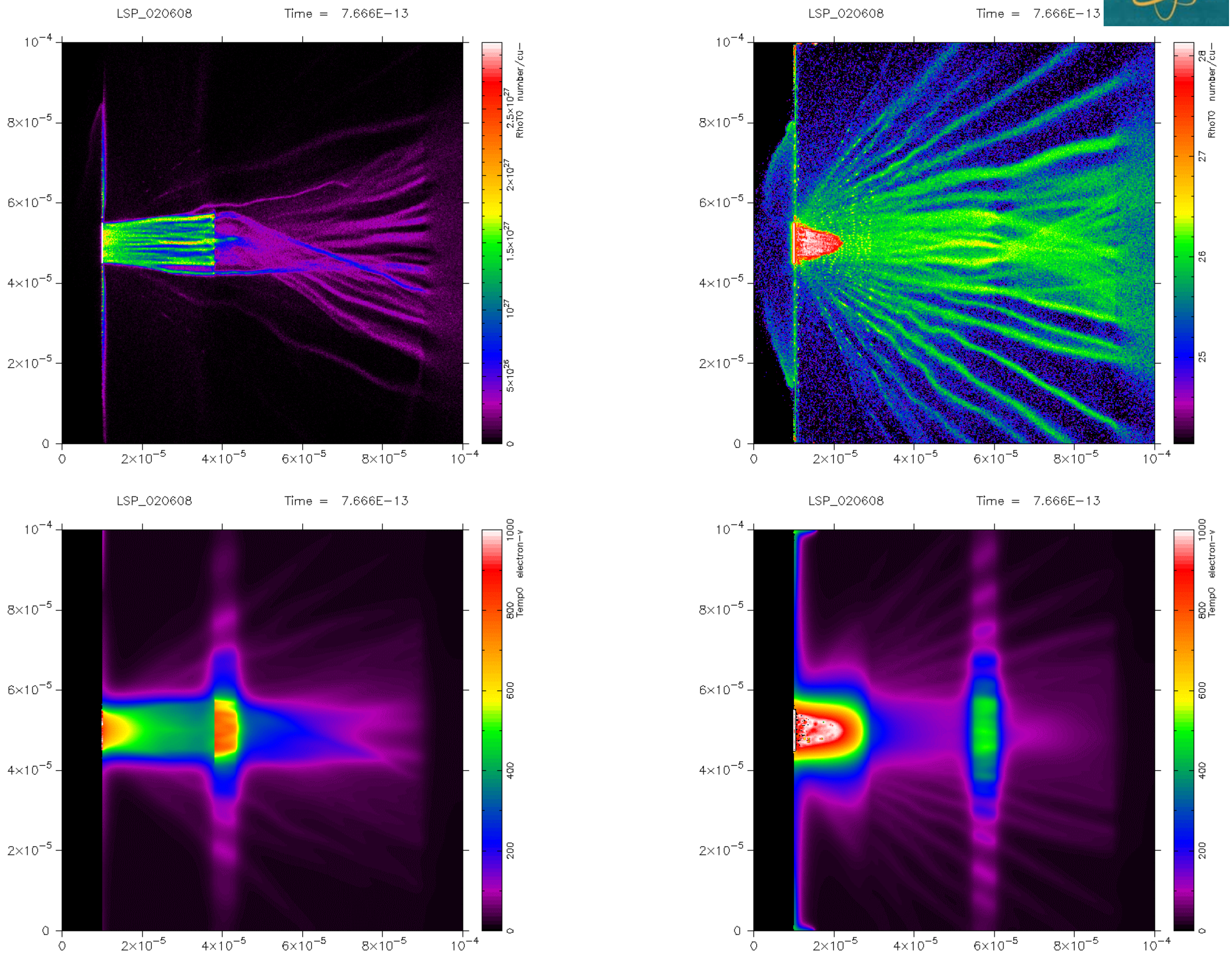

Best estimate of Pre-pulse effects

Laser pre-pulse level is estimated at 10^{-7}

pre-pulse irradiance 10^{13} Wcm^{-2}

2D hydro modelling shows equilibrium with critical density ~ 5 μm from ablation surface

In LSP add a 5 μm density ramp with electrons injected mid-way between n_c and solid.

Linear or two slope density ramp

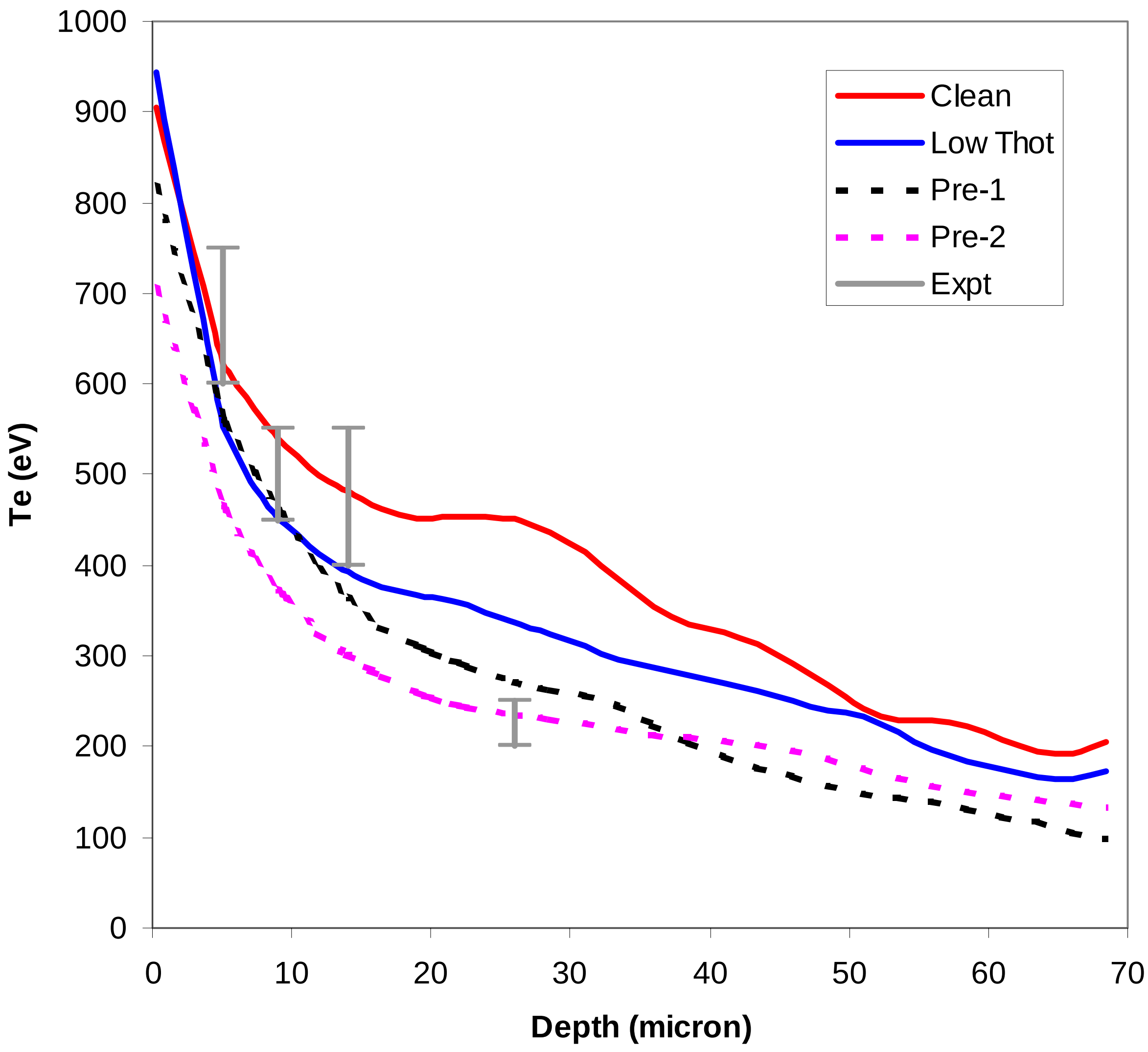

Te (eV)
1000
900
800
700
600
500
400
300
200
100
0
0
10
20
30
40
50
60
70
Depth (micron)
Clean
Low Thot
Pre-1
Pre-2
Expt

Density Effects in beam propagation

When resistive heating is dominant, E.j is largely independent of ρ but heat capacity is proportional to ρ.

Material heats more slowly and is resistive for longer

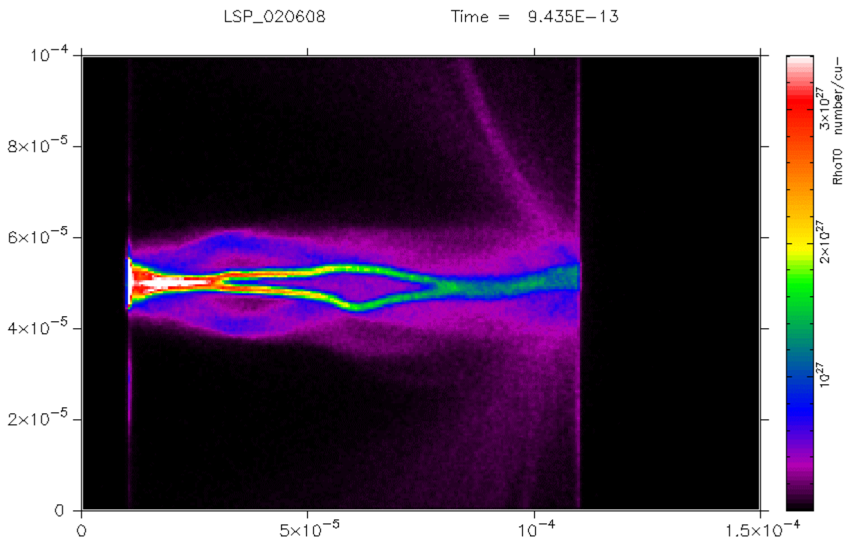

Beam density

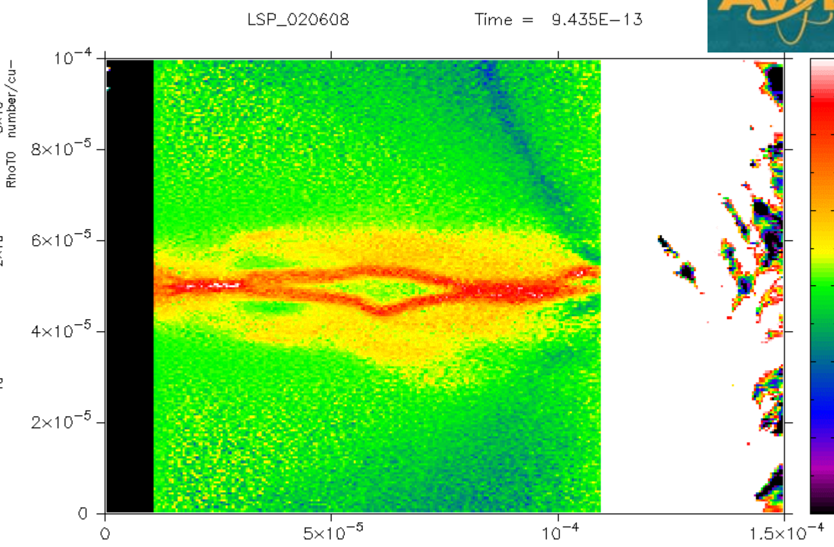

E_x

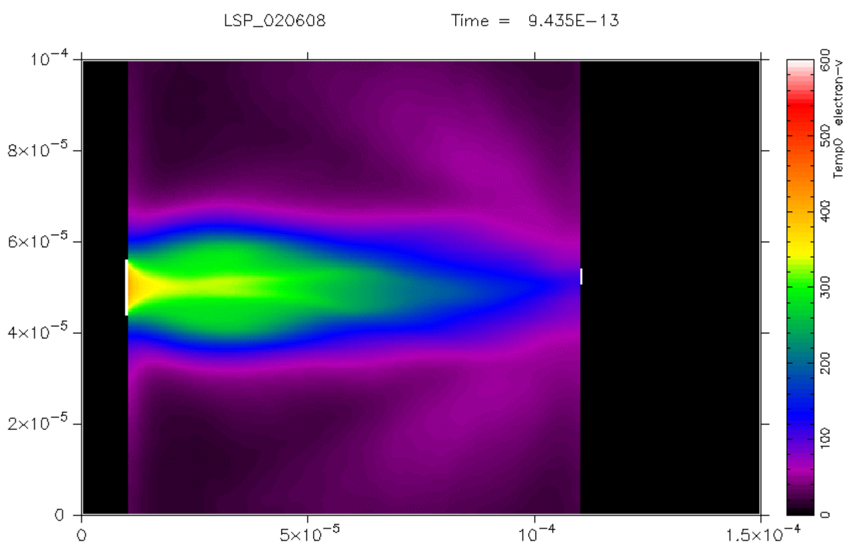

Electron temperature

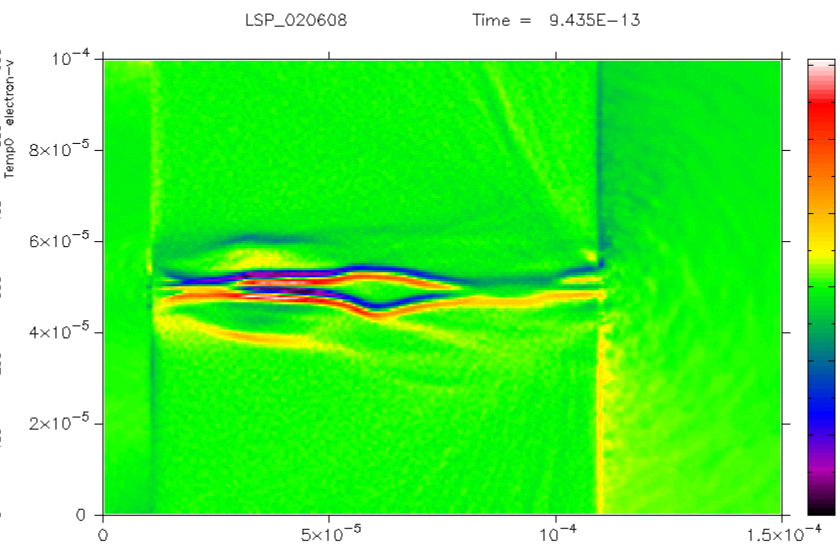

B_z

Change in behaviour depends only on background plasma density

Self-focussing at high density vs filamentation at lower density - agrees with Bell and Kingham PRL (2003)

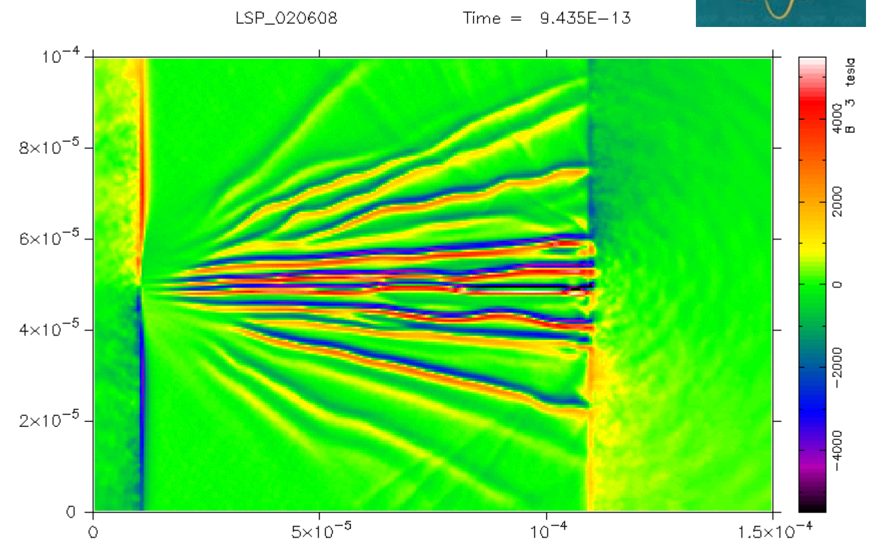

ρ = 1.0 gm cm^{-3}

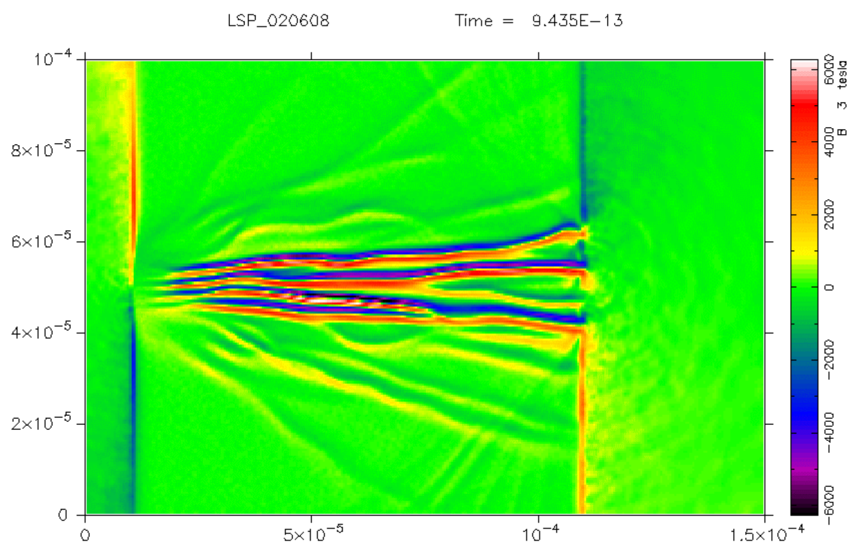

ρ = 2.0 gm cm^{-3}

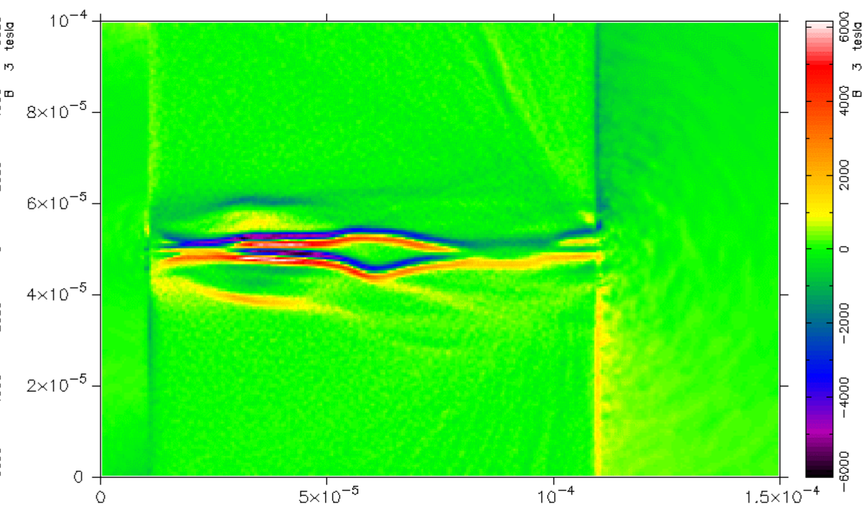

ρ = 4.0 gm cm^{-3}

Note reduced heating at higher densities (**E.j** independent of density but heat capacity µ density)

Difficult to resistively heat high density plasmas for fast ignition

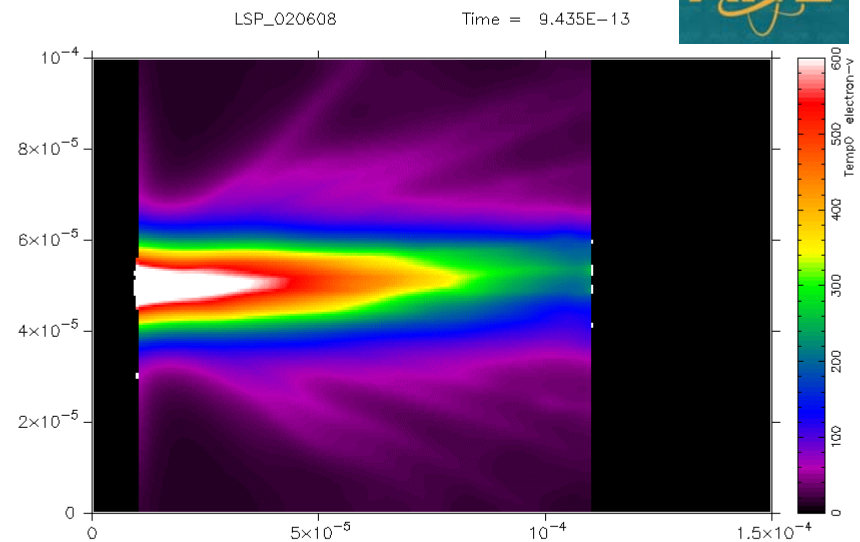

ρ = 1.0 gm cm^{-3}

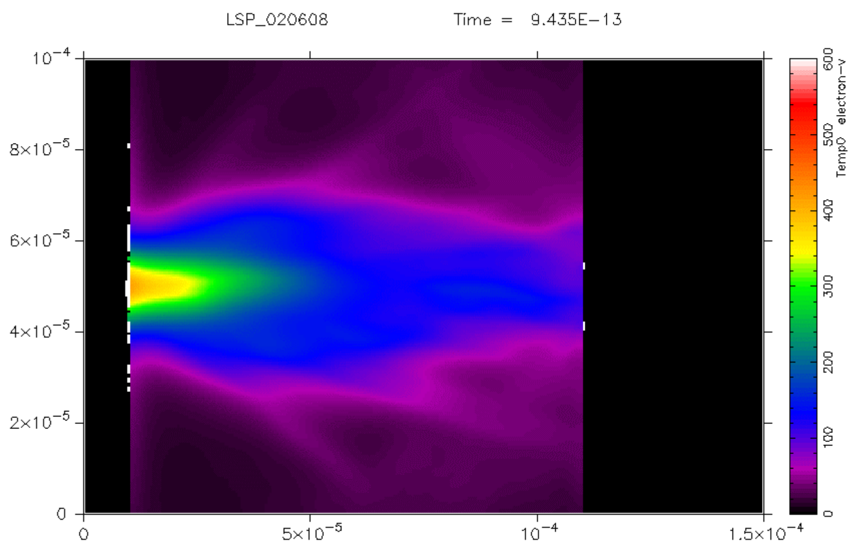

ρ = 2.0 gm cm^{-3}

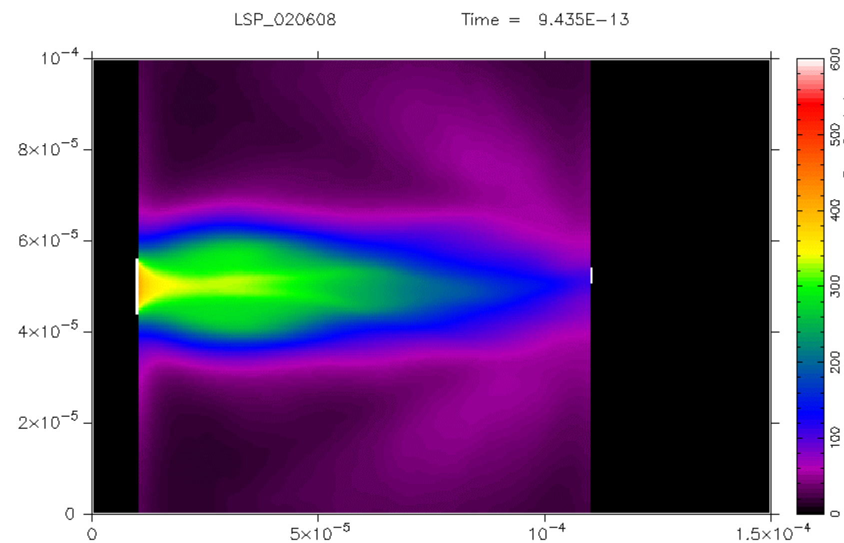

ρ = 4.0 gm cm^{-3}

Conclusions

Can heat material at solid density to > 500eV

uncertain influence of hot electrons on pressure

Electron energy transport is sensitive to laser pre-pulse

need hole boring to high density

LSP is a valuable modelling tool

can we tackle the whole CPA problem self-consistently?

Electron beam dynamics are density dependent via resistivity

probably need better resistivity models

propagation in (highly) compressed solids still an open issue

Grid size comparison - B3 field (‘Weibel’ mode)

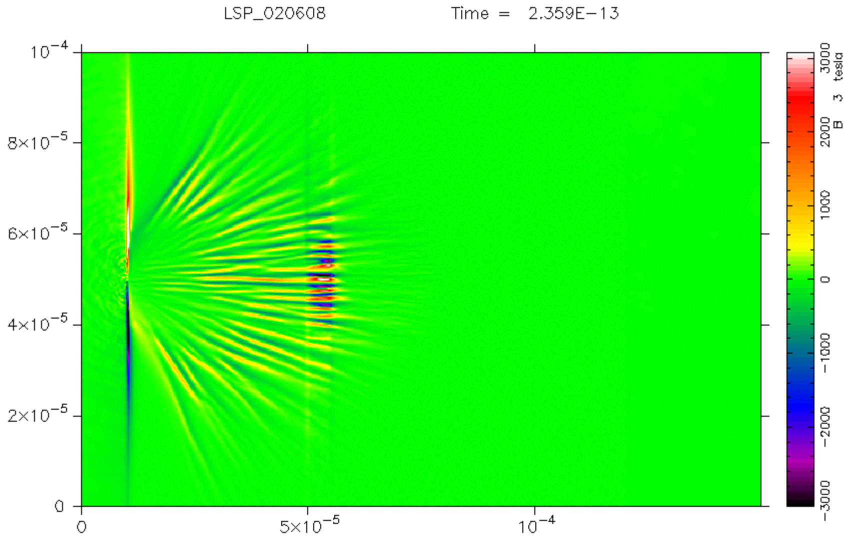

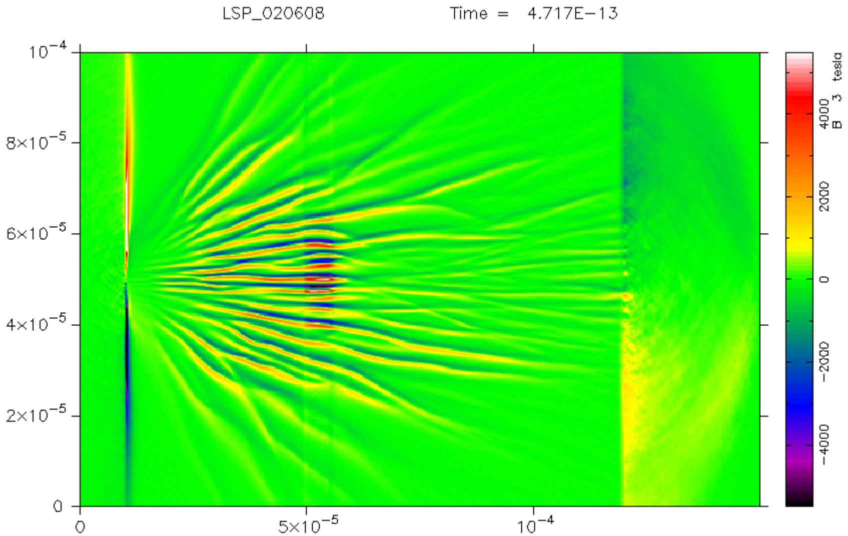

400 x 600 cells dx = 0.25 μm

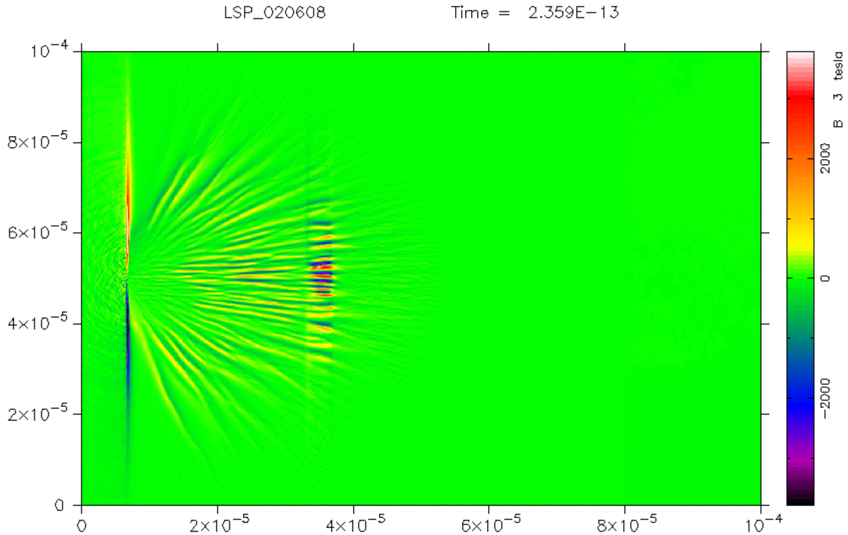

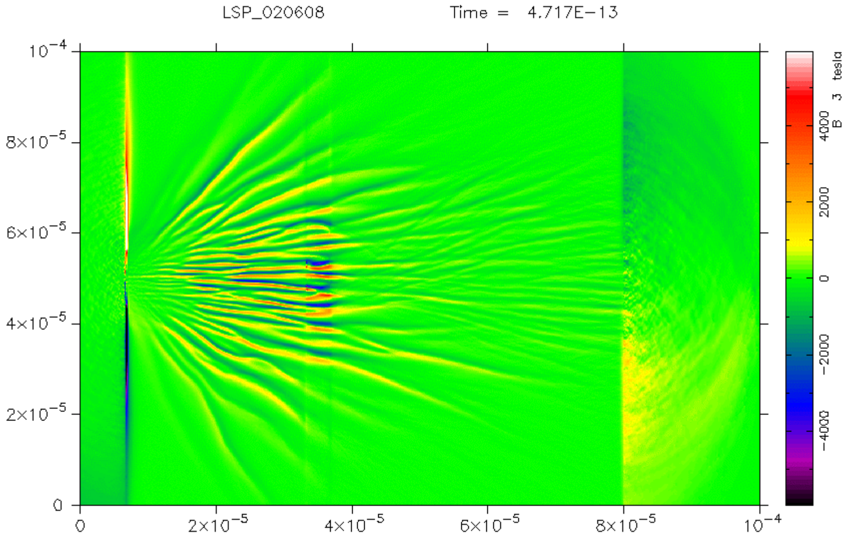

800 x 1200 cells dx = 0.125 μm

Grid size comparison - beam density and target T_e

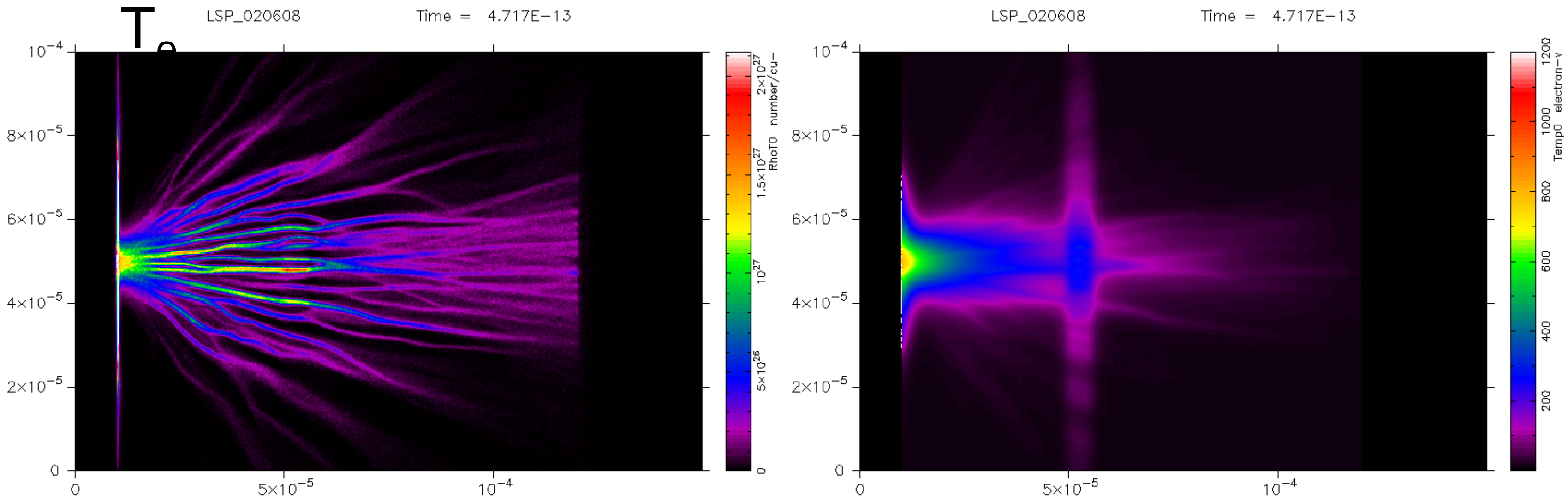

400 x 600 cells dx = 0.25 μm

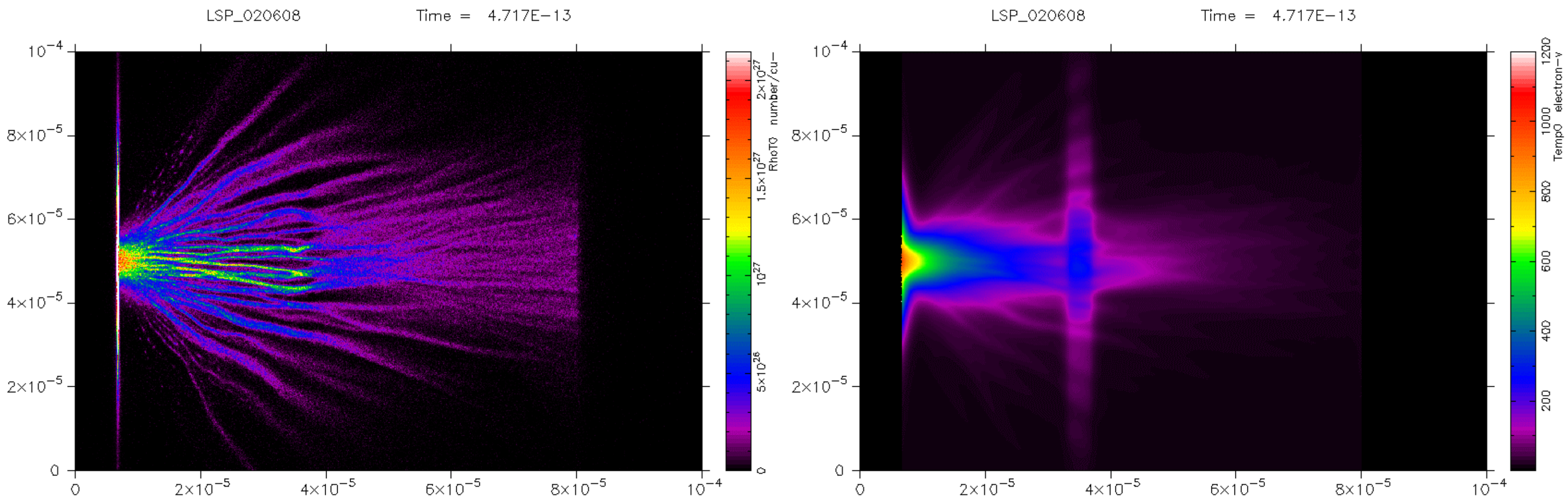

800 x 1200 cells dx = 0.125 μm

1eV 10eV 100eV

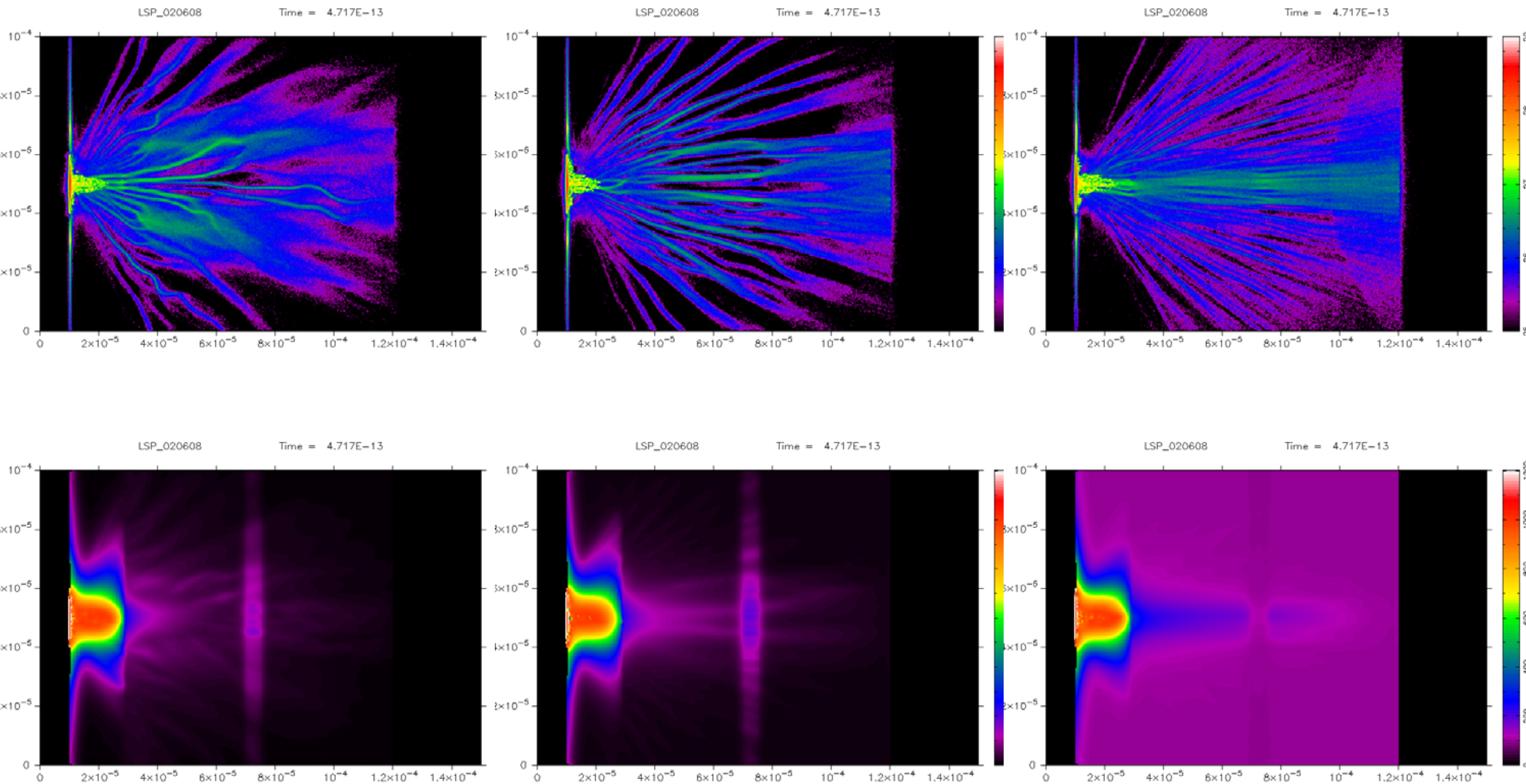

Vary initial T_e and T_i

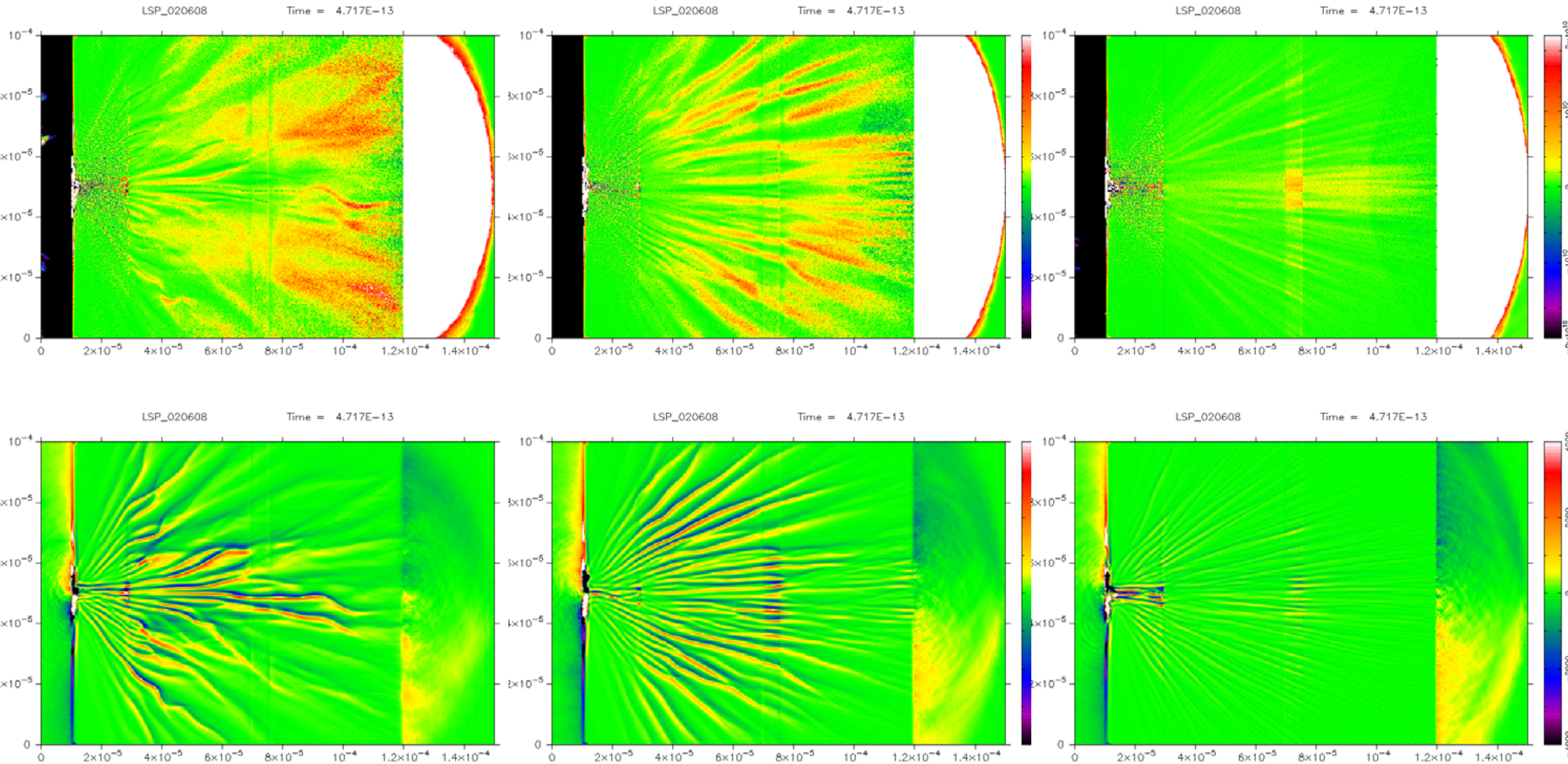
LSP_020608
Time = 4.717E-13
LSP_020608
Time = 4.717E-13
LSP_020608
Time = 4.717E-13
LSP_020608
Time = 4.717E-13
LSP_020608
Time = 4.717E-13
LSP_020608
Time = 4.717E-13
0
2×10⁻⁵
4×10⁻⁵
6×10⁻⁵
8×10⁻⁵
10⁻⁴
1.2×10⁻⁴
1.4×10⁻⁴

v6

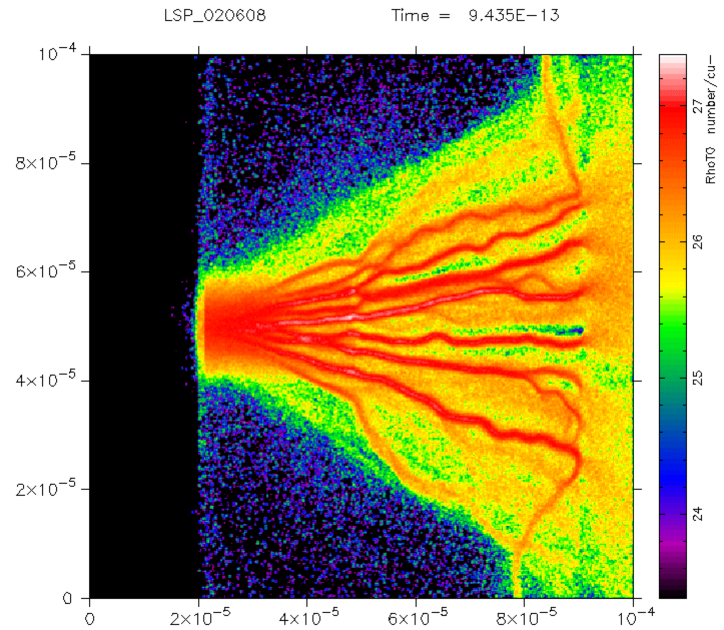

v7

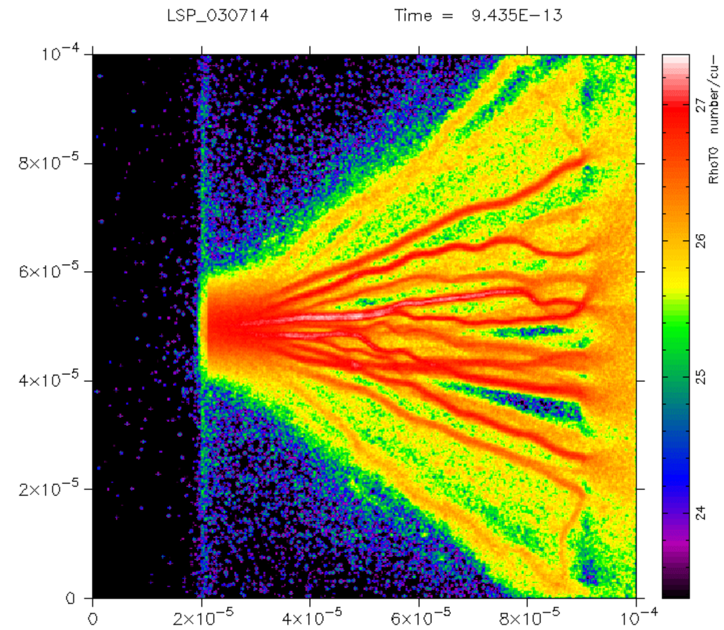

v8

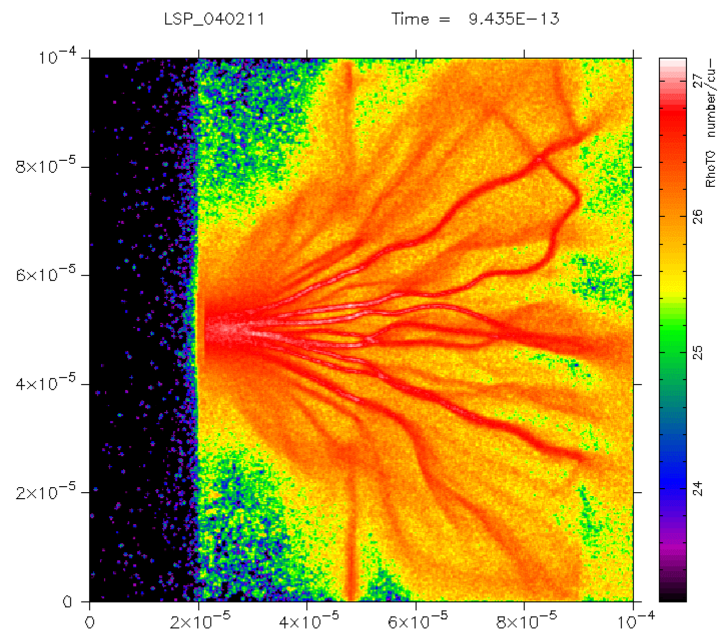

LSP version comparison

monoenergetic beam

v6

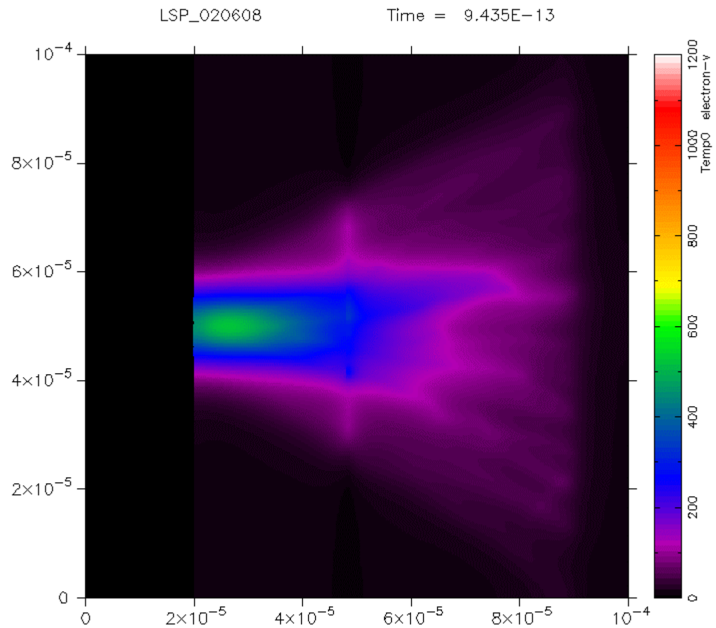

v7

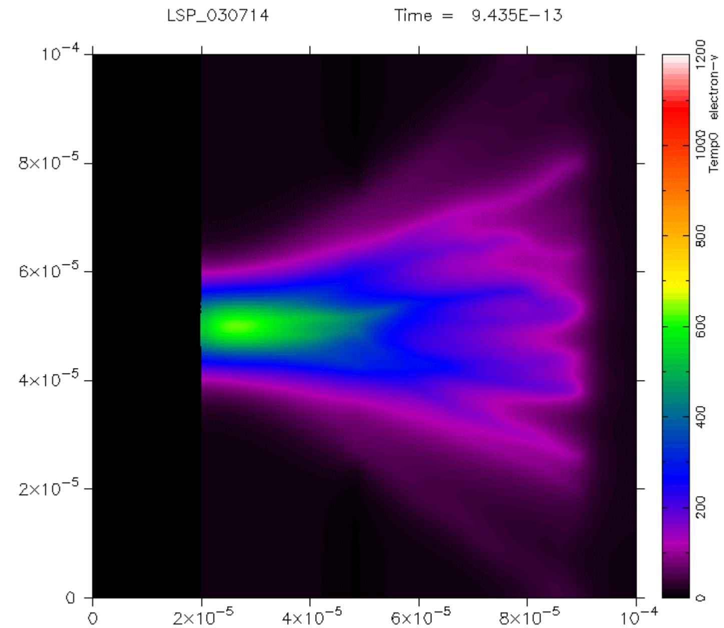

v8

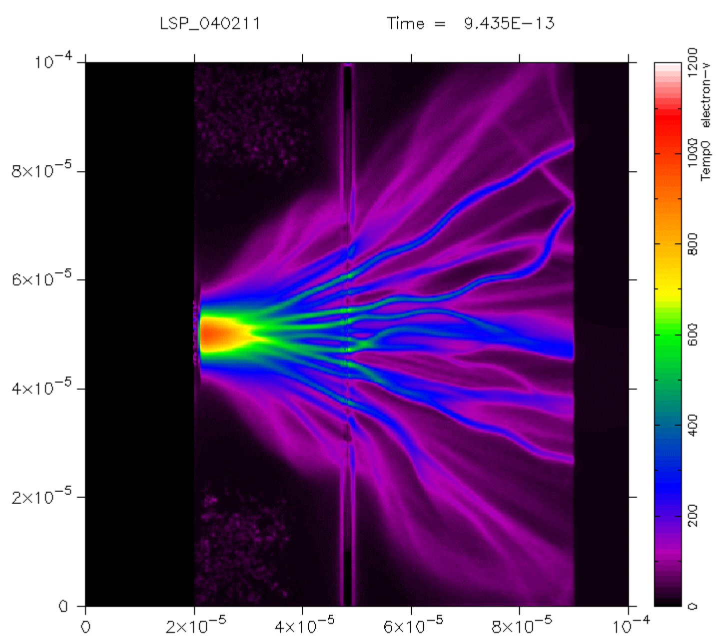

Note major difference in temperature structure in version 8

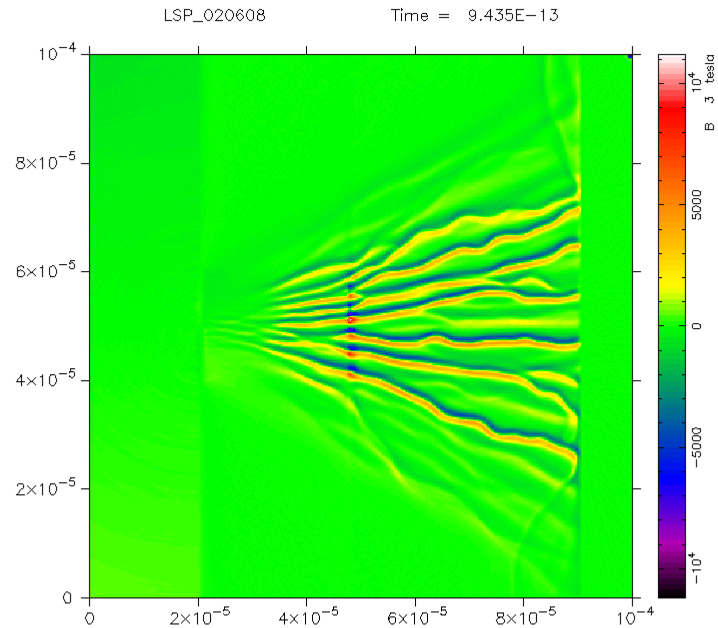
LSP_020608
Time = 9.435E-13
10^{-4}
8×10^{-5}
6×10^{-5}
4×10^{-5}
2×10^{-5}
0
2×10^{-5}
4×10^{-5}
6×10^{-5}
8×10^{-5}
10^{-4}
10^4
5000
0
−5000
-10^4
B 3 tesla

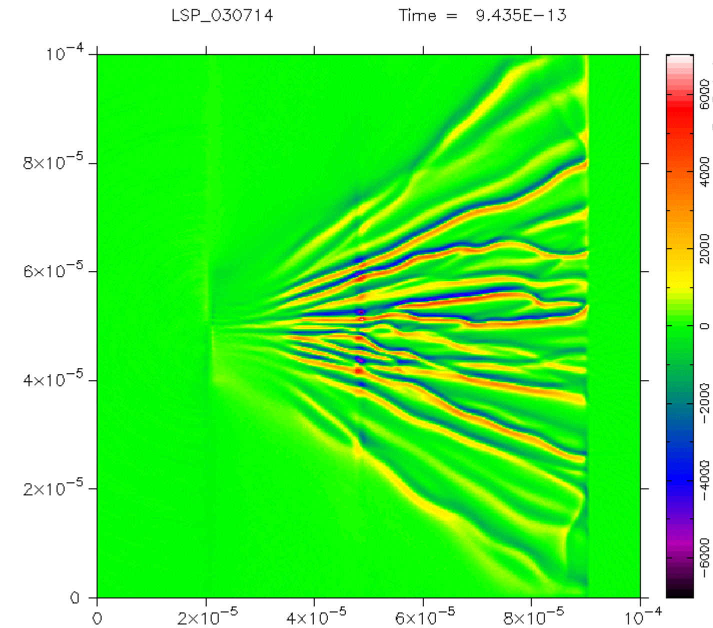
LSP_030714
Time = 9.435E-13
10^{-4}
8×10^{-5}
6×10^{-5}
4×10^{-5}
2×10^{-5}
0
2×10^{-5}
4×10^{-5}
6×10^{-5}
8×10^{-5}
10^{-4}
6000
4000
2000
0
−2000
−4000
−6000
B 3 tesla

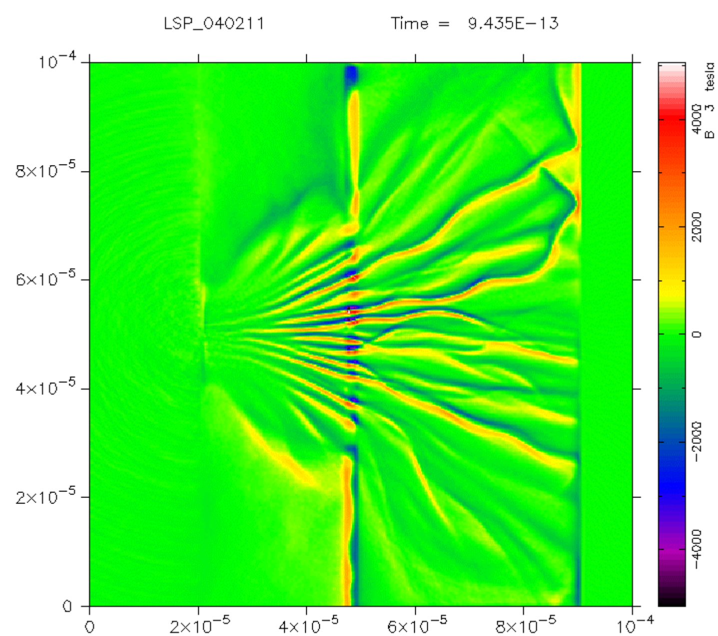
LSP_040211
Time = 9.435E-13
10^{-4}
8×10^{-5}
6×10^{-5}
4×10^{-5}
2×10^{-5}
0
2×10^{-5}
4×10^{-5}
6×10^{-5}
8×10^{-5}
10^{-4}
4000
2000
0
−2000
−4000
B 3 tesla

The way forward ??

- Hybrid is not very satisfactory
  - separate injection of electrons
  - poor description of return current near critical
  - parametrisation of resitivity
- Can implicit PIC (with collisions) do the whole problem ?
  - $\omega_{las}\Delta t << 1$ (resolve laser); $\omega_p \Delta t >> 1$ in solid (implicit required)
  - will need $\Delta x >> \lambda_D$ in solid - energy conservation ??
    - will strong collisions help ?
  - or can we reduce ω_p in solid but maintain ν_{coll} ?
- How can we validate any of this ?

PIC Simulations of the Weibel Instability

Roger G Evans

Plasma Physics Division AWE Aldermaston
and Imperial College

Work performed while William Penney Fellow
Physics Department, University of York

roger.evans@awe.co.uk or r.g.evans@physics.org

Osiris

2 1/2 D or full 3D PIC, multi-species

Momentum conserving

Strictly maintains div**E** = $4\pi\rho$

Periodic and Lindman boundary conditions

MPI parallel, running on small Linux cluster
(2 - 3 days per run)

Grateful thanks to Warren Mori et al at UCLA

Schematic of Weibel Growth

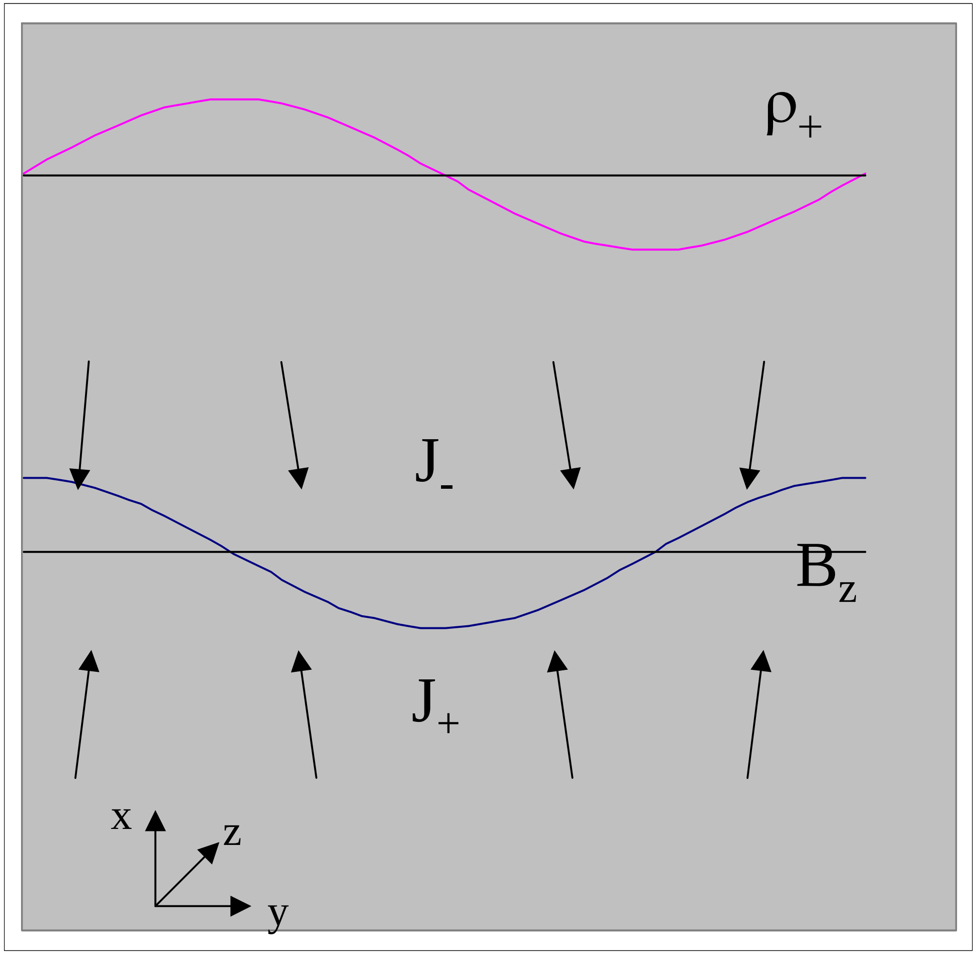

Initial uniform ρ_+ ρ_- j_+ j_-

perturb ρ_+ (and so j_+)

Induced B_z

Electron deflection in B_z accentuates ρ_+

ρ_- has opposite sign

j_+ j_- reinforce to enhance j

Previous work

PIC simulations from 1970 - first 2D e-m codes

Observed in PIC simulations of CPA interactions by Lasinski et al

Linear theory including transverse temperature and collisional damping, Califano et al, Pegoraro et al; Sentoku et al

detailed PIC simulations by Honda et al, Sentoku et al, Pukhov et al, Silva et al

Quick Summary

Linear growth rate ~ ω_{pb};

Wavenumber ~ c/ω_{pb}

Current filaments carrying ~ 1 Alfven current, surrounded by magnetic fields

Opposite polarity fields re-connect and filaments merge, k decreases

Magnetic field deflection and longitudinal momentum spread give rise to increased transverse momentum spread - stabilisation

Basic 2-1/2D Simulation

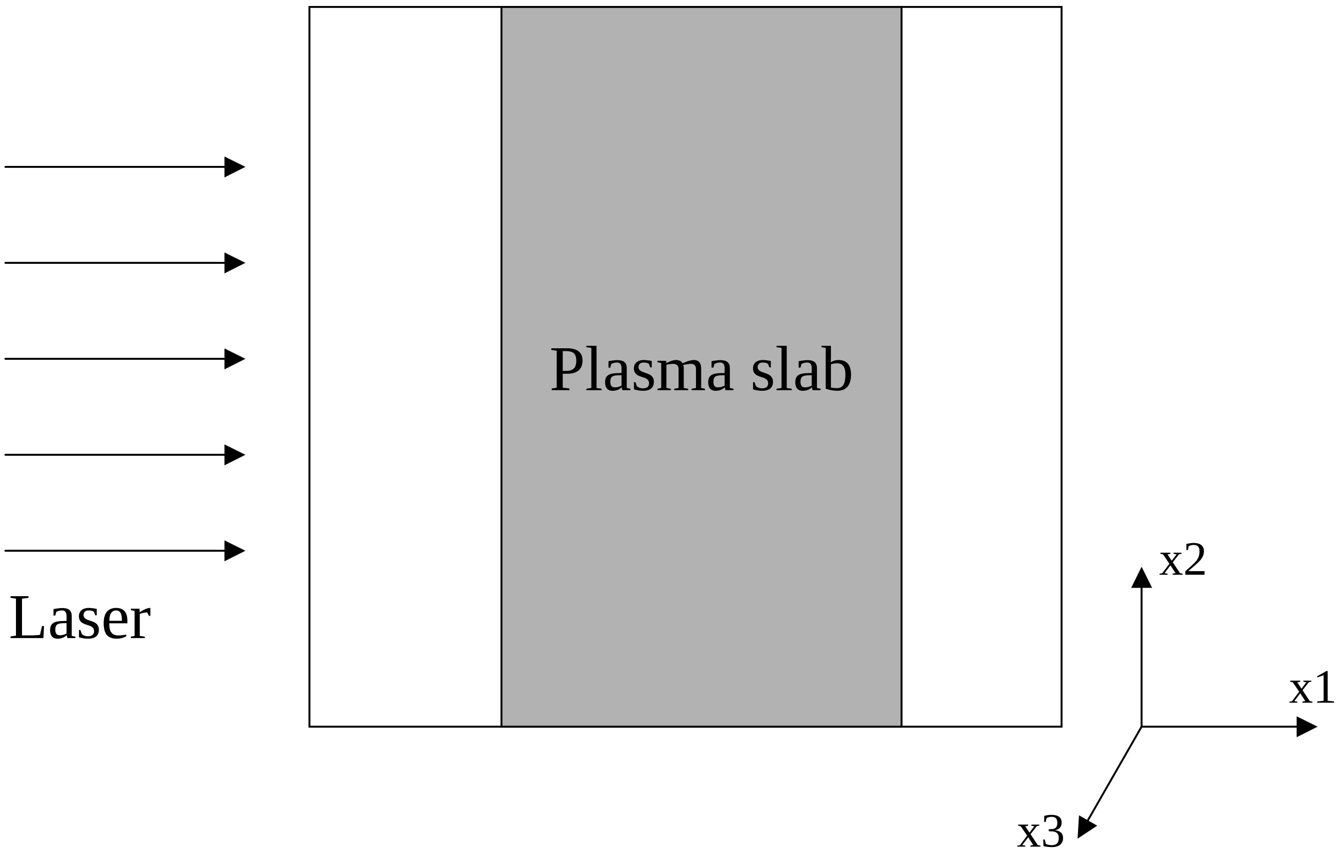

Baseline Simulation as Sentoku 1998

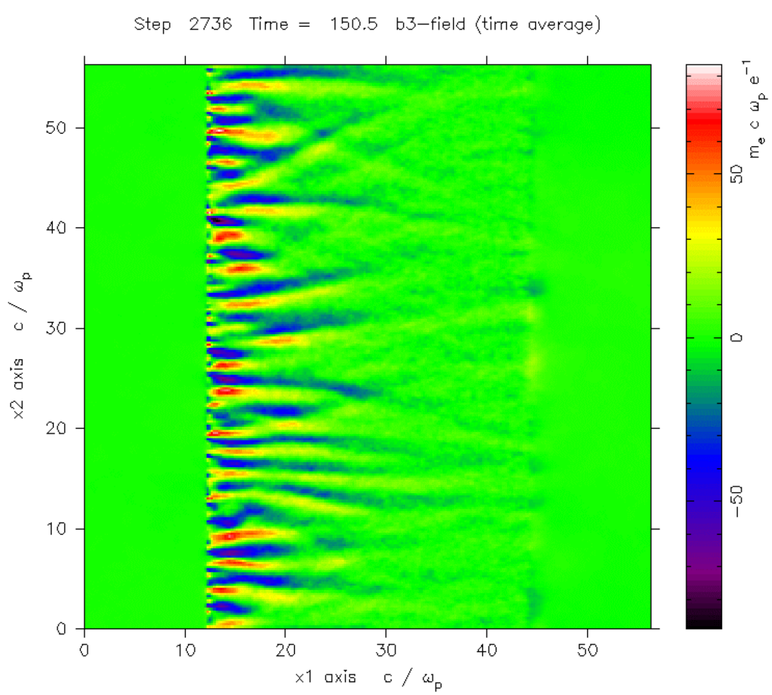

10^{19} W cm^{-2}

56 x 56 c/ω_p

512 x 512 cells

64 electrons (& ions) per cell

20 n_c slab

time average fields over 2 laser periods

Sensitive to number of simulation particles

25 electrons & ions / cell

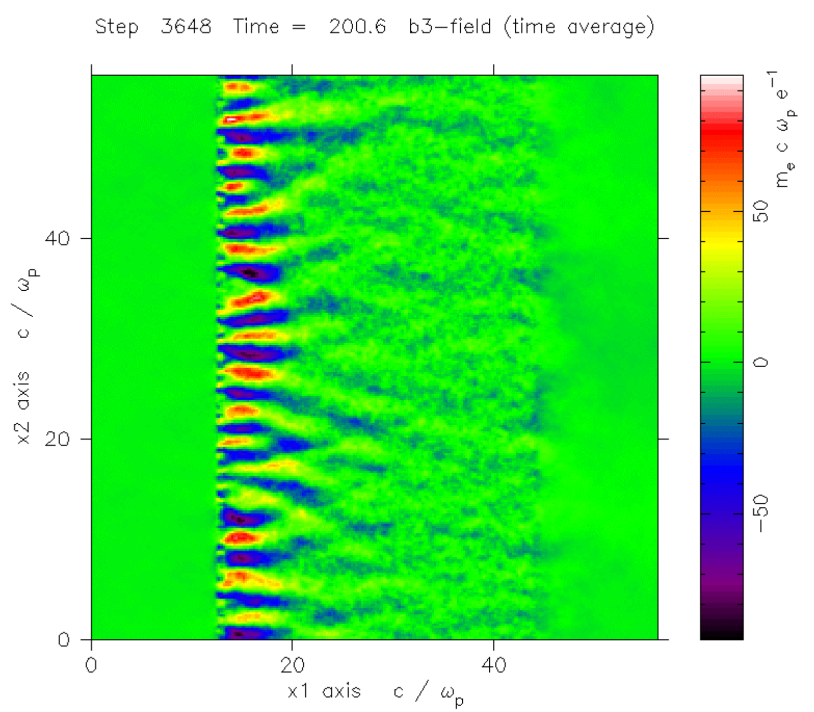

64 electrons & ions / cell

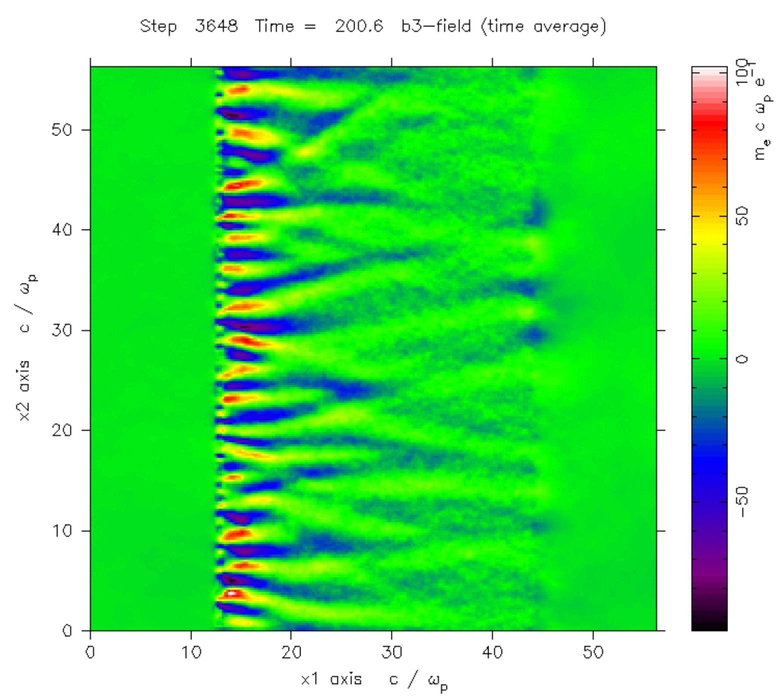

Temporal Development

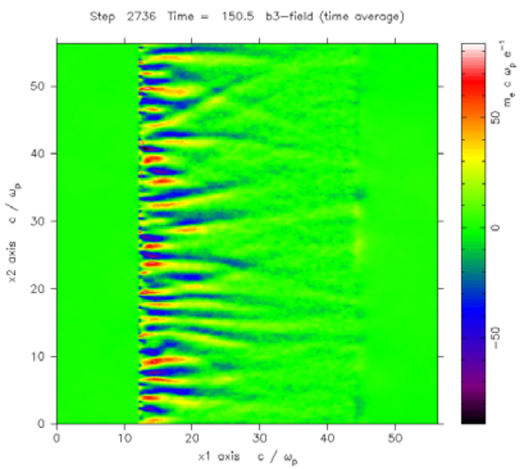

t = 24

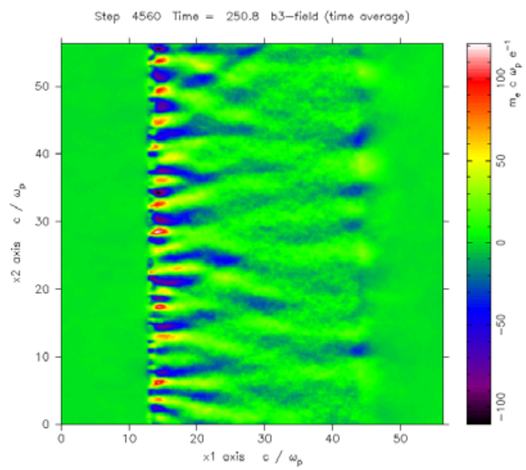

t = 40

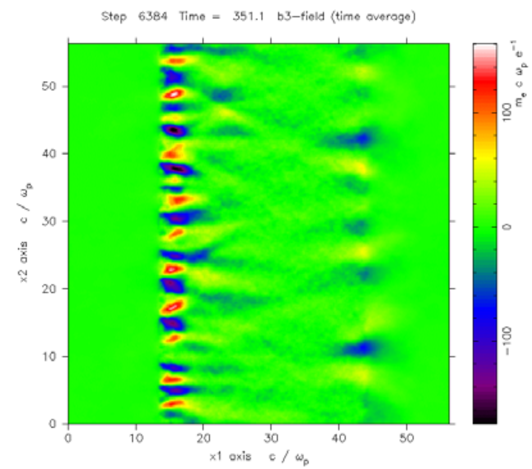

t = 56 τ_{laser}

OSIRIS

Weibel modes saturate due to the growth of transverse electron temperature $T_{\perp}$ as electrons of different $p_{//}$ are deflected in the magnetic field.

Stabilisation by the transverse pressure is described by Silva et al

Magnetic energy and increased $T_{\perp}$ are at the expense of $p_{//}$.

LSP

Physics is somewhat different - return current is resistive and described by fluid equations

Magnetic field grows to similar amplitude

Filaments are very persistent

Energy used to create magnetic field is significant

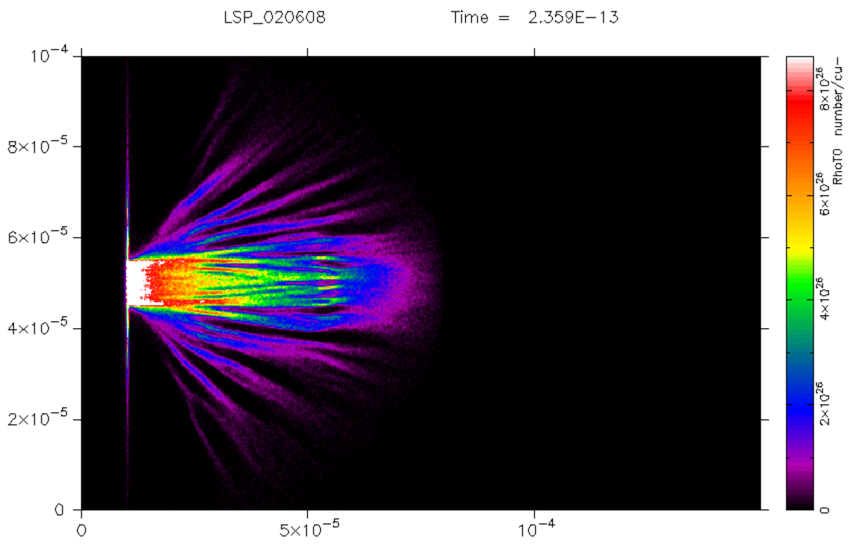
LSP_020608
Time = 2.359E-13
RhoT0 number/cu-

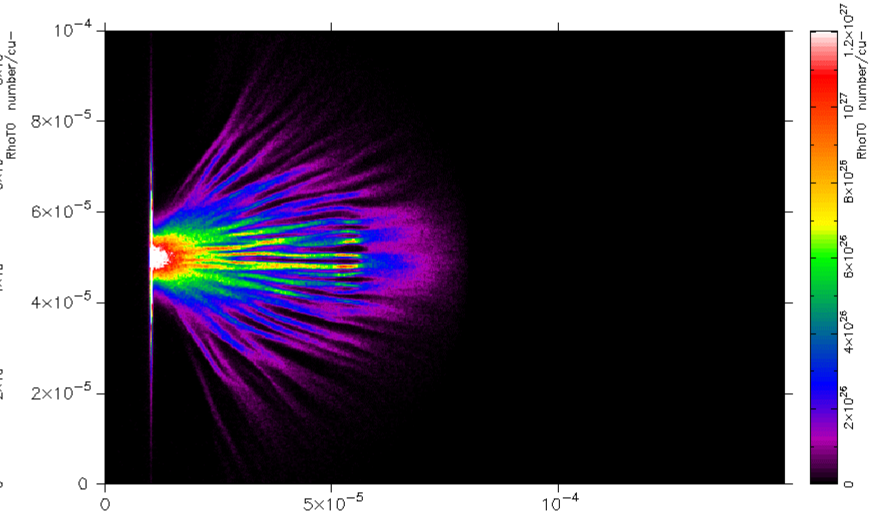
LSP_020608
Time = 2.359E-13
RhoT0 number/cu-

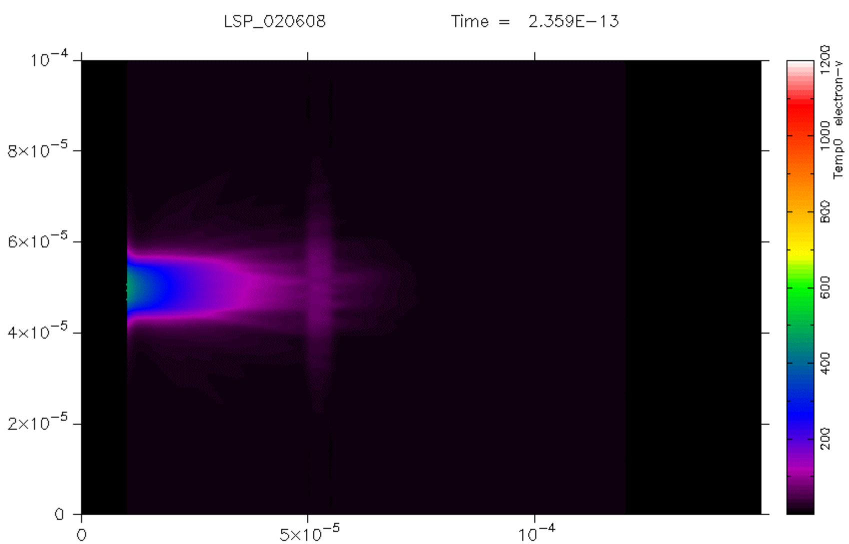
LSP_020608
Time = 2.359E-13
Temp0 electron-v

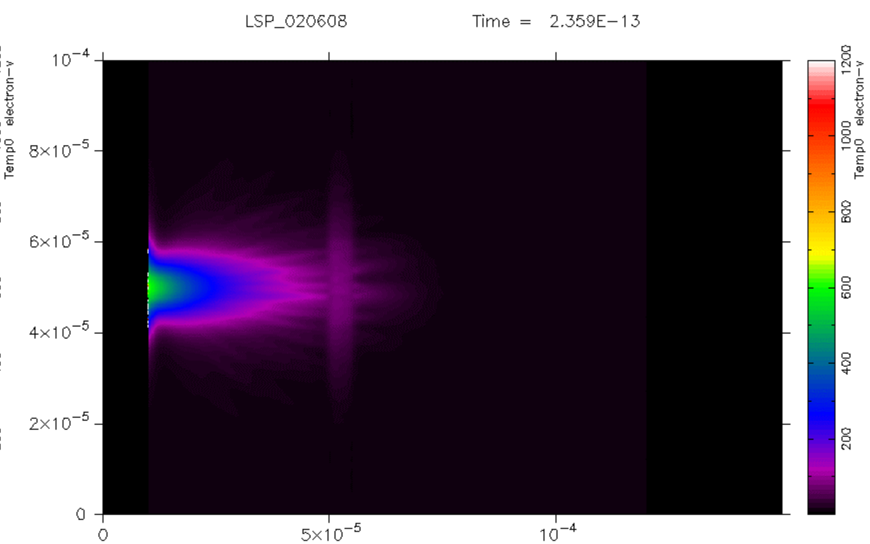
LSP_020608
Time = 2.359E-13
Temp0 electron-v

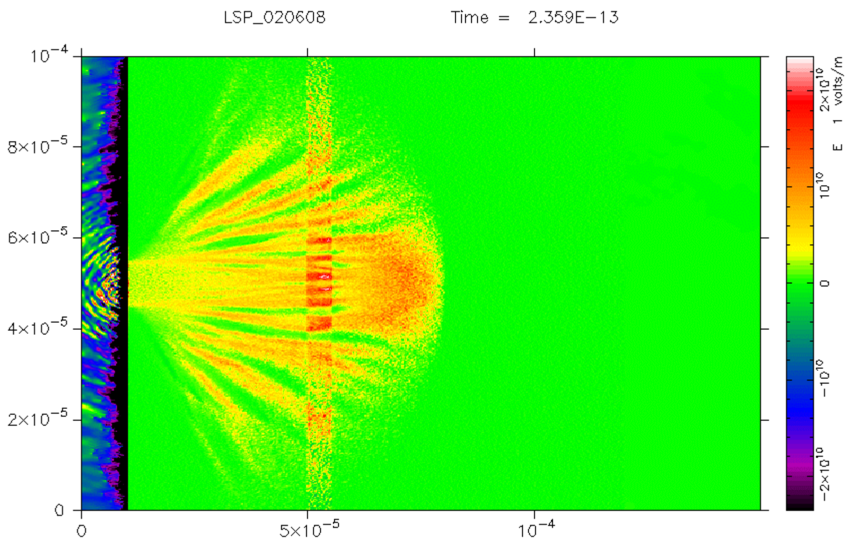
LSP_020608 Time = 2.359E-13
E 1 volts/m

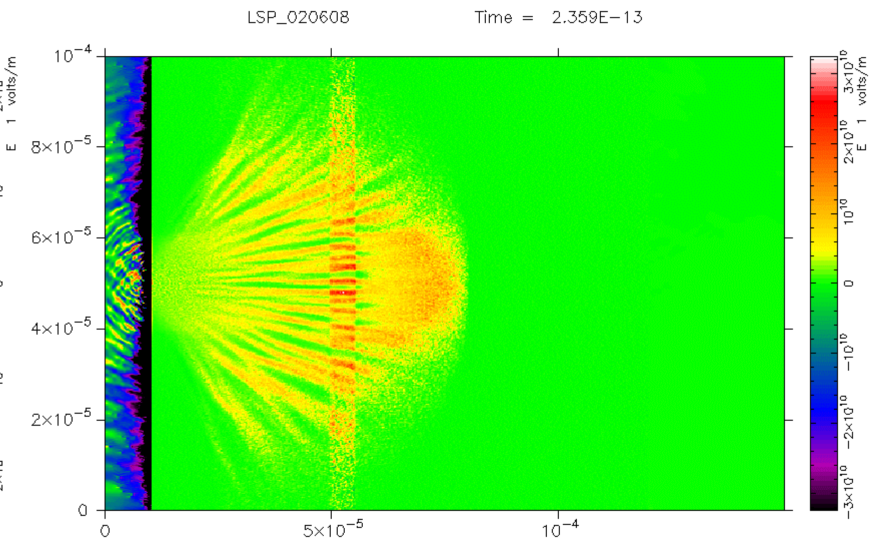
LSP_020608 Time = 2.359E-13
E 1 volts/m

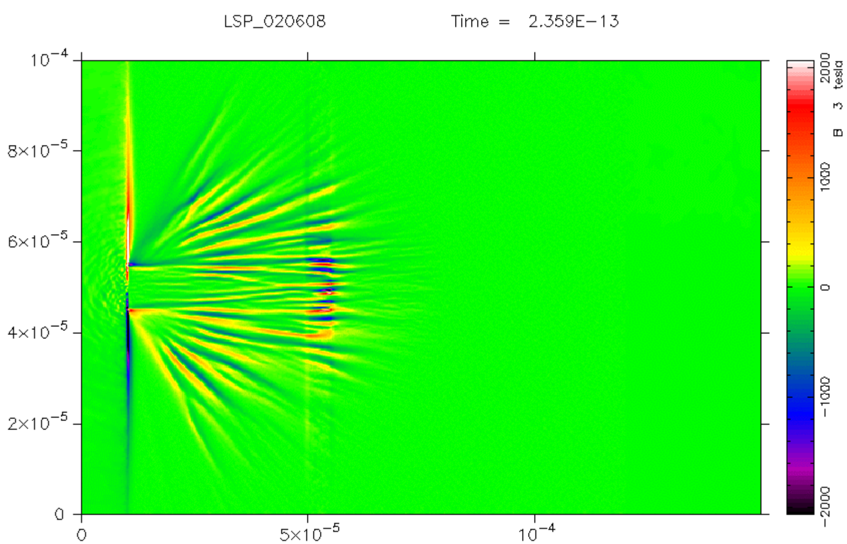
LSP_020608 Time = 2.359E-13
B 3 tesla

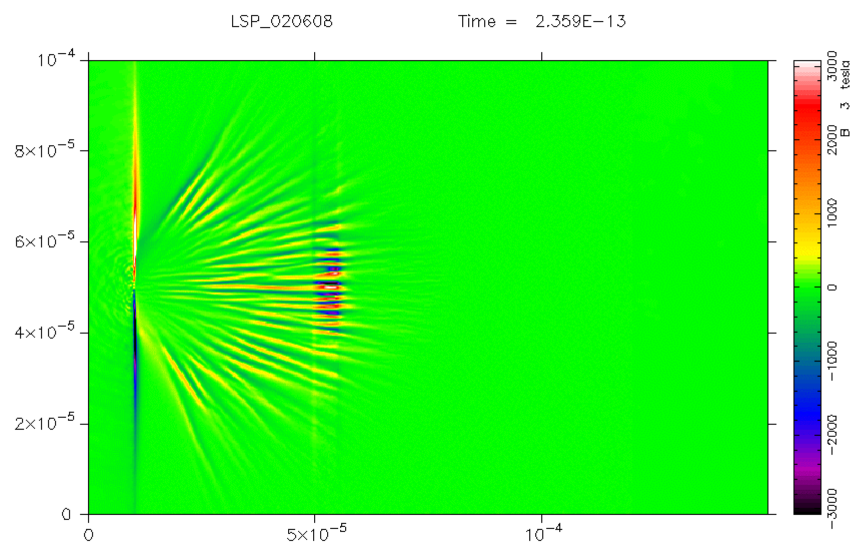
LSP_020608 Time = 2.359E-13
B 3 tesla

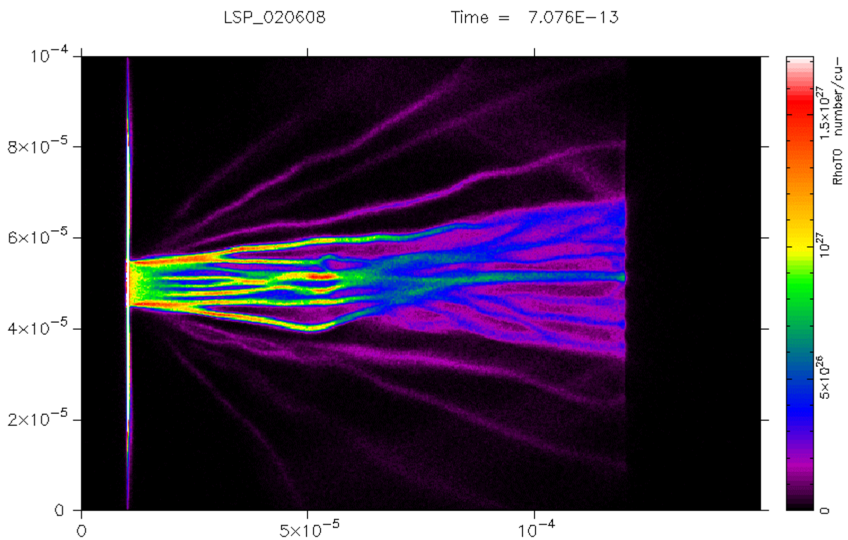
LSP_020608
Time = 7.076E-13
RhoT0 number/cu-
1.5×10^27
10^27
5×10^26
0
10^-4
8×10^-5
6×10^-5
4×10^-5
2×10^-5
0
5×10^-5
10^-4

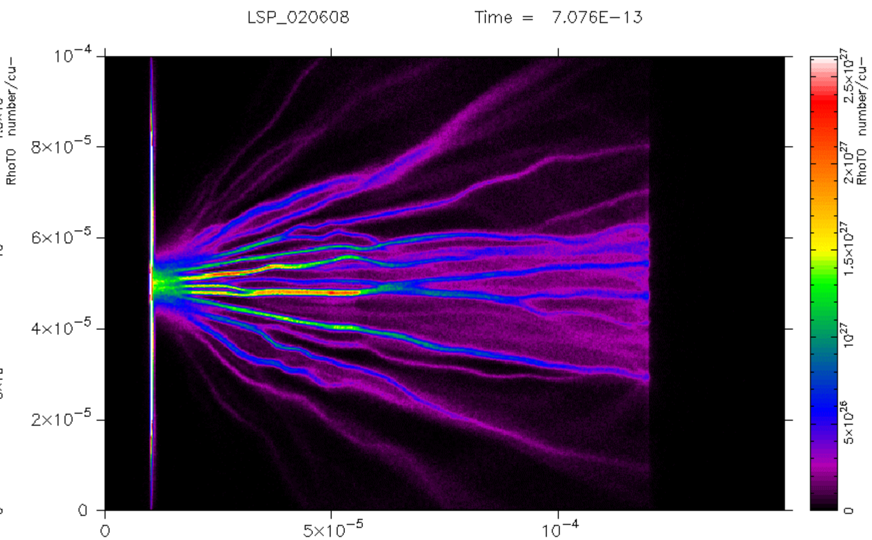
LSP_020608
Time = 7.076E-13
RhoT0 number/cu-
2.5×10^27
2×10^27
1.5×10^27
10^27
5×10^26
0
10^-4
8×10^-5
6×10^-5
4×10^-5
2×10^-5
0
5×10^-5
10^-4

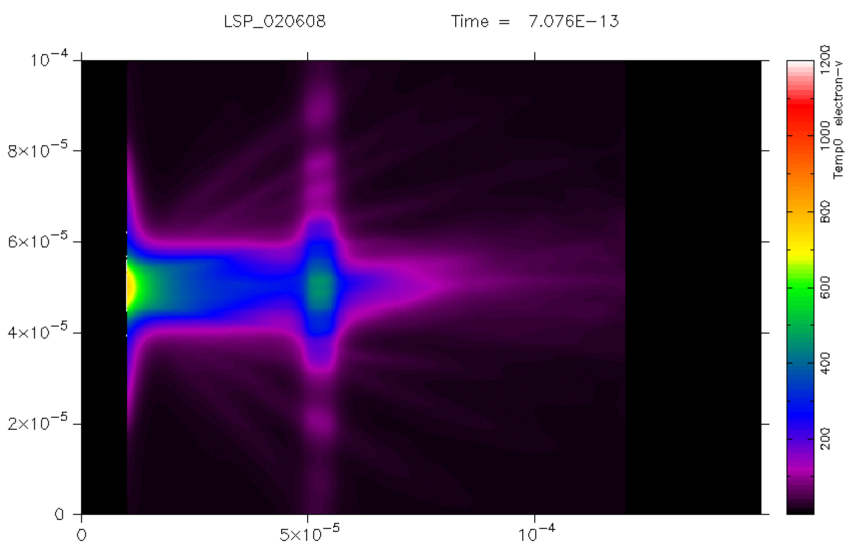
LSP_020608
Time = 7.076E-13
Temp0 electron-v
1200
1000
800
600
400
200
10^-4
8×10^-5
6×10^-5
4×10^-5
2×10^-5
0
5×10^-5
10^-4

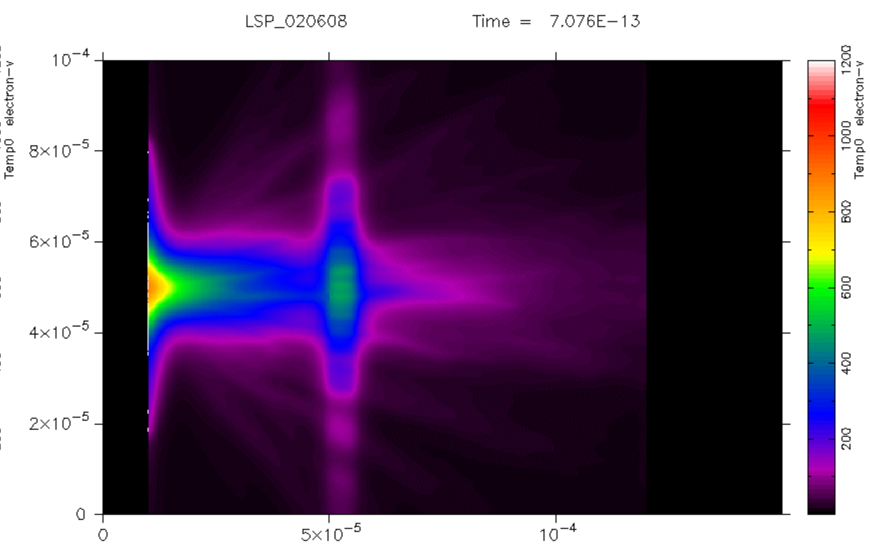
LSP_020608
Time = 7.076E-13
Temp0 electron-v
1200
1000
800
600
400
200
10^-4
8×10^-5
6×10^-5
4×10^-5
2×10^-5
0
5×10^-5
10^-4

Questions ...

- How do the two instabilities interact ?
  - low density seeds collisional mode
  - return current filamentation seeds collisionless mode
- What physics model will cover both ?
  - hybrid is inadequate near critical - return current drift ~c/4
  - PIC cannot (?) resolve λ_D in solid
  - can implicit or Darwin PIC be energy conserving for $\Delta x > \lambda_D$
  - can strong collisions in the solid hide lack of resolution ?
  - how to describe collisions in this limit ?

Modelling Collisions

- Do we need to keep n and ω_p in high density ?
  - eg scale ω_p as in some Fokker-Planck models
    - if we scale ω_p does anything else go wrong ?
      eg energy into small scale magnetic fields
- Can collisions be a sub-grid process
  - parametrise through n, T_e, T_i, v_{drift}, ...
    - how to generate the database
- How important are non-Coulomb collisions ?
  - $n\lambda_D^3 \sim 1$ in warm solid
- Consistency of particle and fluid collisions for hybrid models

High-Energy Kα Radiography with High-Intensity Short-Pulse Lasers

Short-Pulse Laser Matter
Computational Workshop
Aug. 25, 2004
UCRL-PRES-206222

Hye-Sook Park (LLNL)
on behalf of LLNL/NIF high energy radiography team

Introduction

- **Most of current Omega and planned NIF experiments utilizes 3-6 keV backlighters for imaging imploding objects**
- **NIF targets are bigger and made with denser material**
- **NIF is planning to install a Petawatt laser as an efficient source of high energy x-rays**
- **We want to develop hard Kα X-ray (20-100 keV) and broad-band Bremsstrahlung (MeV) sources as backlighters to image various stages of implosions and planar drive high Z materials**
- **Experiments to characterize Kα sources as function of laser parameters were performed using the LLNL's JanUSP and Vulan lasers**

O. L. Landen et al., RSI (2001)
D. K. Bradley et a., Opt. Lett (2002)

X-ray backlighting radiography is one of the most commonly used diagnostics for laser experiments

Imploding capsules

t = 5.7 ns, 4.7 keV, CH(Ge)

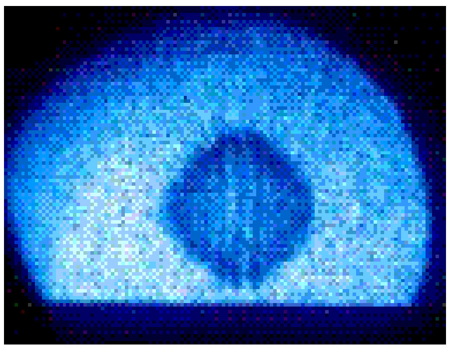

Glendinning *et al*., Phys. Plasmas 7, 2033 (2000)

Jets

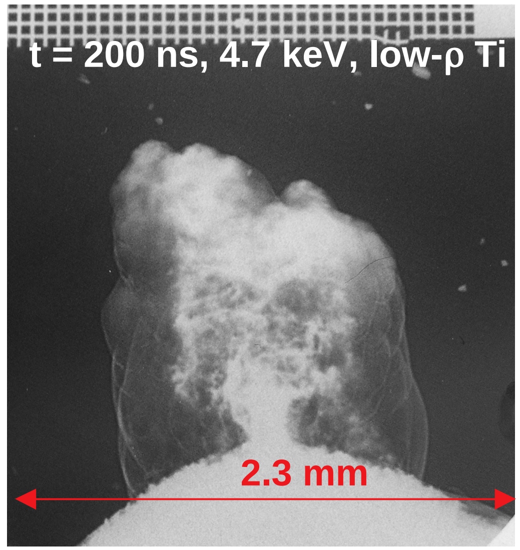

Foster, Rosen, Wilde, Perry, Blue, Frank, private commun. (2004)

Rippled foils

t = 21.5 ns, 4.3 KeV, Al

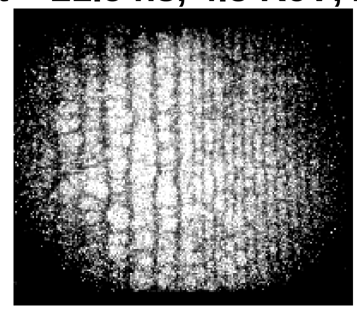

600 µm

Kalantar *et al*., Phys. Plasmas 7, 1999 (2000)

- **Until now this "conventional" radiography uses thermally driven x-rays at a few keV**
- **This method worked well for the low-Z and thin targets**

High energy backlighters allow us to diagnose a broader class of HED experiments

Current NIF limits

20 keV ⇒ 50-μm Fe samples
10-μm Au samples

NIF HEPW

70 keV ⇒ 3-mm Fe samples
0.3-mm Au samples

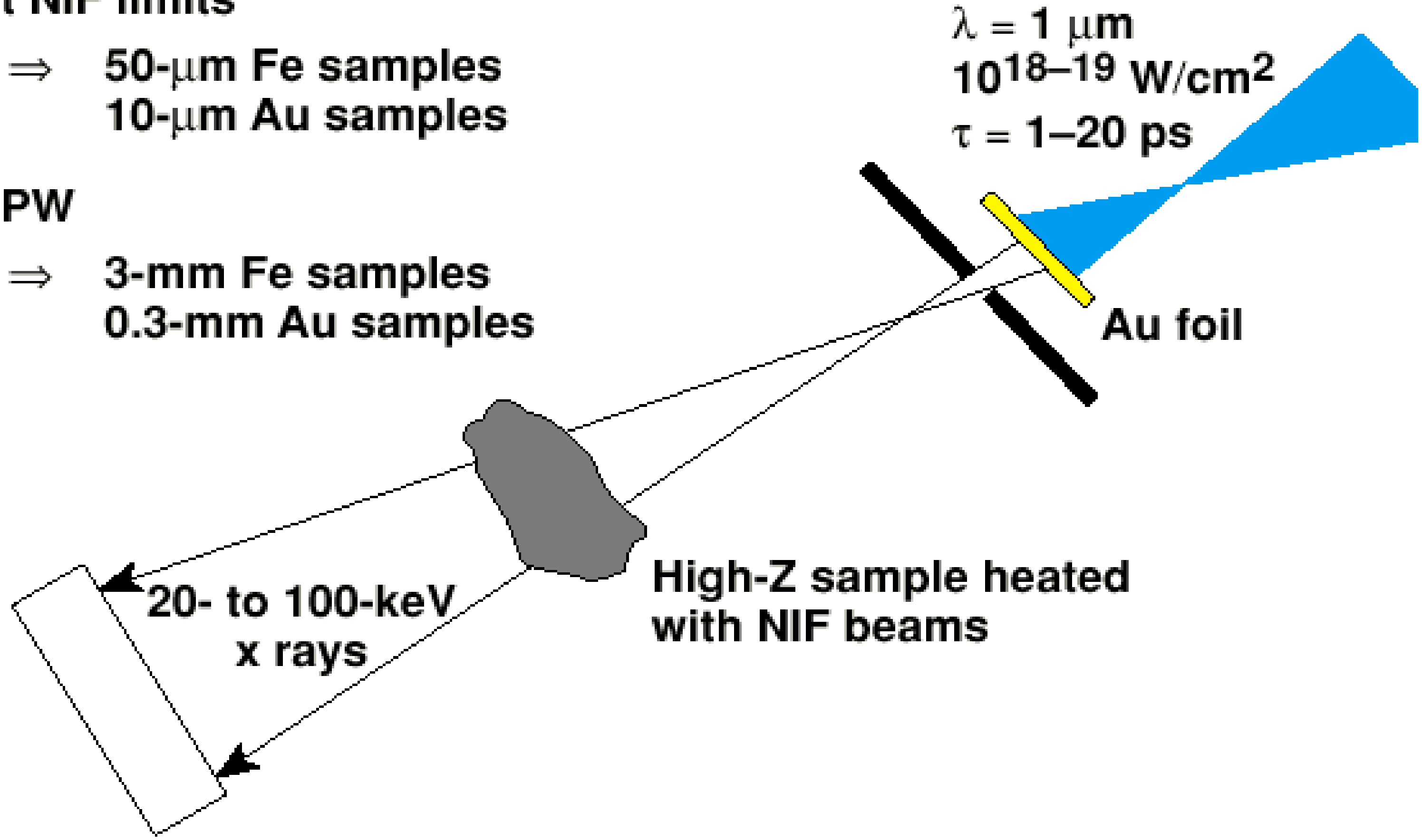

11272

Planned NIF/HEDES experiments require 1-D & 2-D radiography with <10 μm resolution at 20-100 keV

NIF
The National Ignition Facility

Material Strength

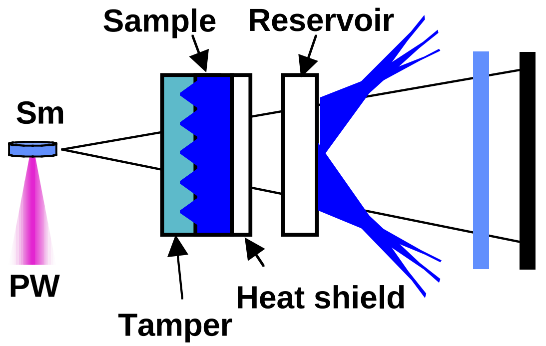

- Strength at high pressure
- NIF milestone in FY08 and FY10
- 40-100 keV, 10:1 S/N, 1 mm FOV

HED Implosion

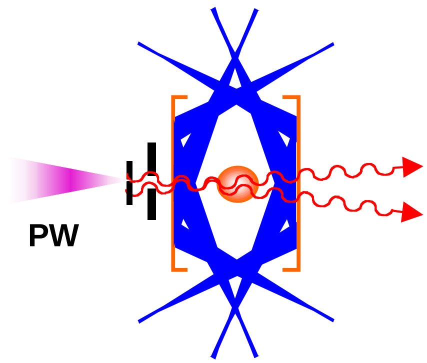

- Mid- to high-Z capsule
- NIF milestone in FY09
- 20-35 keV, 4 mm FOV
- Multi-view

Ignition Double Shell

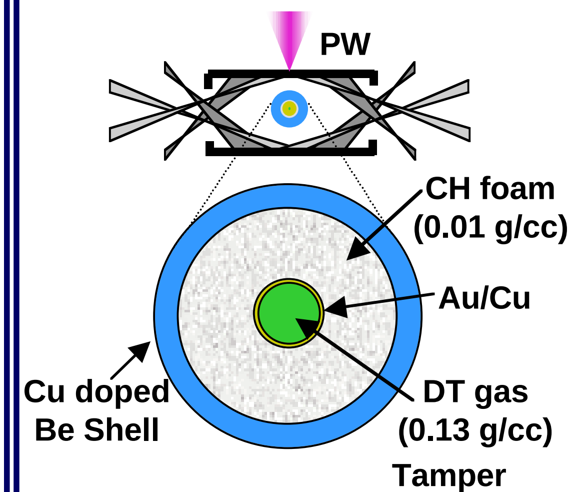

- Non-cryo ignition target
- Very high ρR during implosion phase
- 1 MeV broadband radiography, 1 mm FOV

The complete list, including EOS and Opacity experiments, has been compiled by the Petawatt Laser Users Group (PLUG)

Kα emission by high-intensity short-pulse lasers is very promising way to produce bright 20-100 keV sources

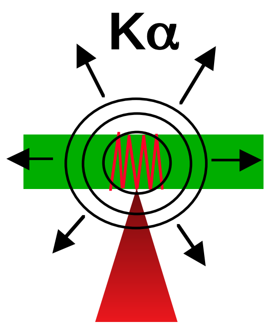

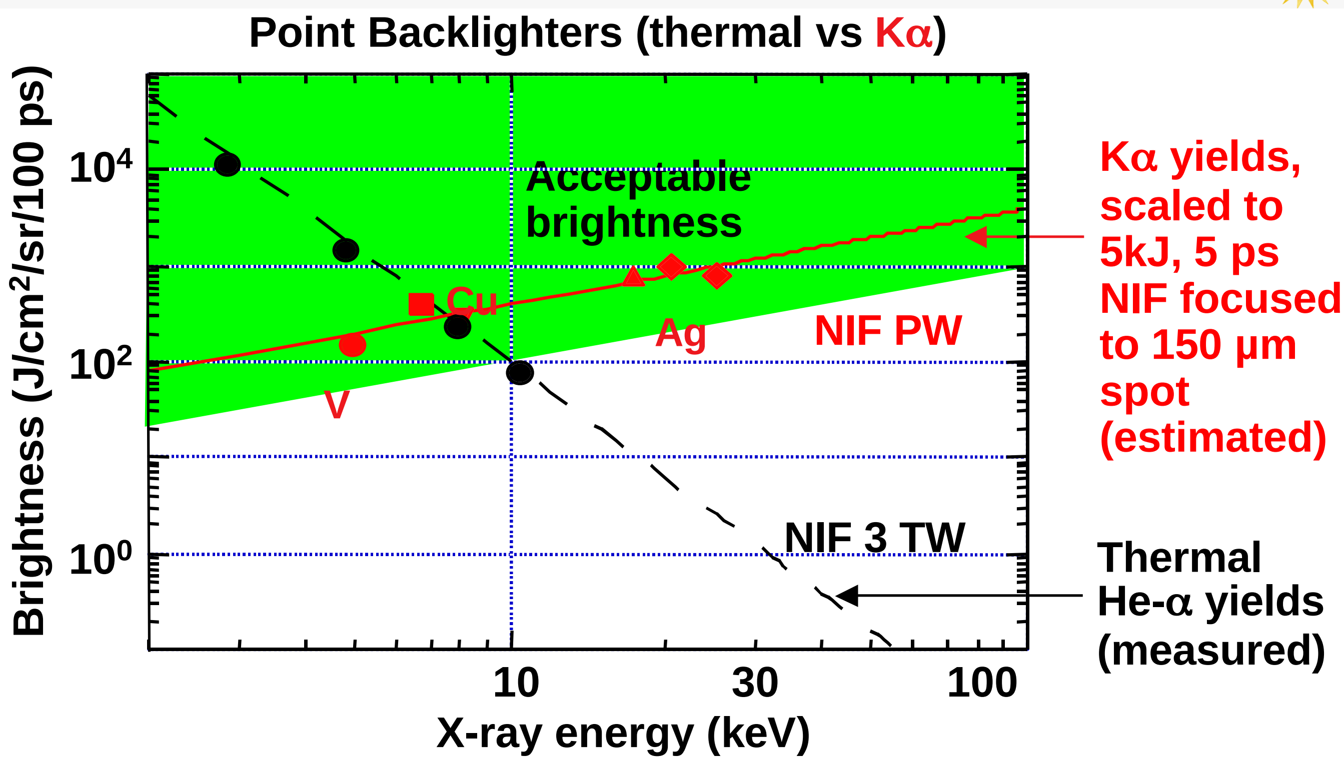

K-a references:

Jiang, Phys. Plas.2 (1995) 1702.
Rousse, PRE 50 (1994) 2200.
Wharton, PRL 81 (1998) 822.
Beg, Phys. Plas. 4 (1997) 447.
Guo, RSI 72 (2001) 41.
Stephens, PRE 69 (2004) 066414.

Thermal bkltrs:

Back, PRL 87, 275003 (2001); PoP 10, 2047 (2003).

Thermal backlighters cannot generate bright enough sources of 20-100 keV x-rays

We performed laser experiments to understand the characteristics of Kα sources

	JanUSP	Vulcan TAW	Vulcan PW	NIF ARC 1st deployment
E_{laser} @ TC	5 J	50-70J	100-300 J	800J
Spot size (FWHM)	4 μm	5-10 μm	10 μm	20-40 μm
Pulse duration	0.1 ps	1 ps	1 ps	10 ps
Max Intensity	10^{20} W/cm^2	10^{20} W/cm^2	10^{21} W/cm^2	10^{19} W/cm^2

We utilized JanUSP, Vulcan TAW, Vulcan PW to measure 22-40 KeV Kα source sizes, yields, dependence on laser parameters

JanUSP experiments utilize a single photon counting detector and a CsI/CCD imaging detector

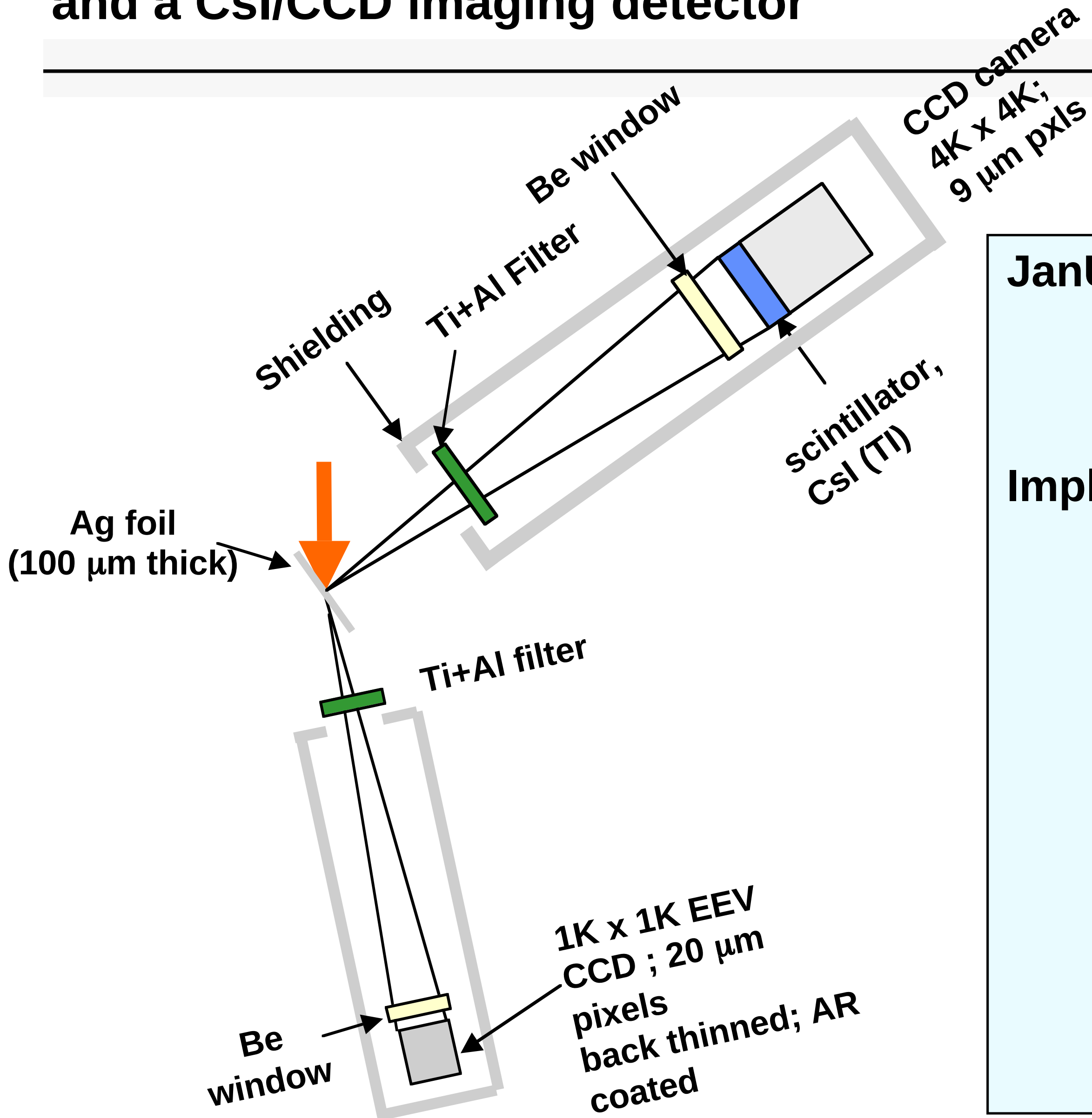

JanUSP Laser Parameters

- **E=5J; spot size=4 μm; pulse duration=100 fs; up to 3×10^{20} watt/cm^2**

Implemented 2 cameras

- **Hard X-ray Imaging camera with a CsI(Tl) scintillator fiber optic coupled to a 4096 x 4096 9 μm CCD**
- **Single photon counting camera with a back-thinned 1340 x 1300 20 μm pixel CCD to measure X-ray source spectrum**

Vulcan PW experiments utilized single photon counting detector and CsI imaging detector w/ pinhole array

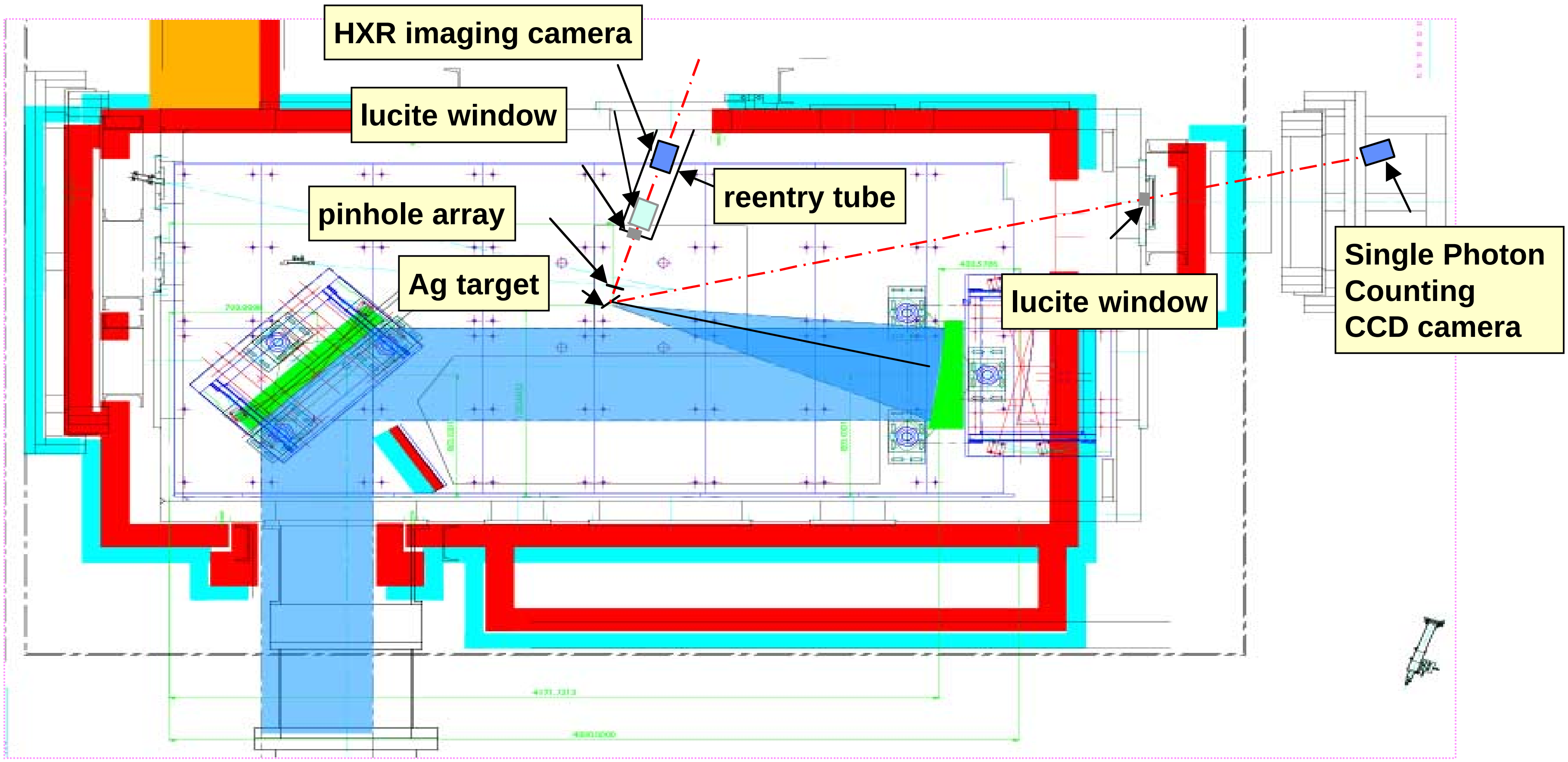

We measure Kα source size bigger than laser splot size

NIF
The National Ignition Facility

22 keV Kα+Brem Source Image
Vulcan PW (11/25/03)

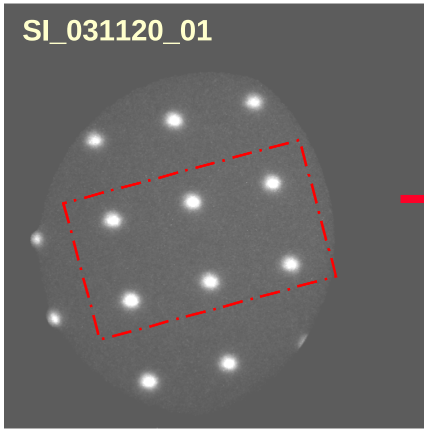

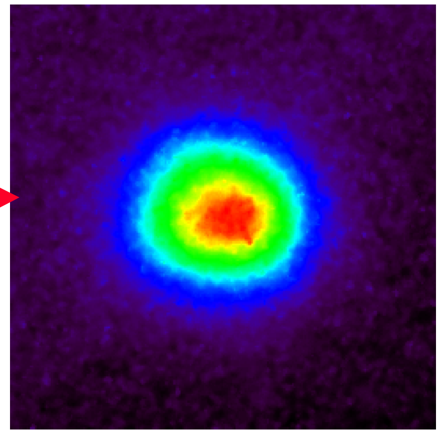

Horizontal lineout

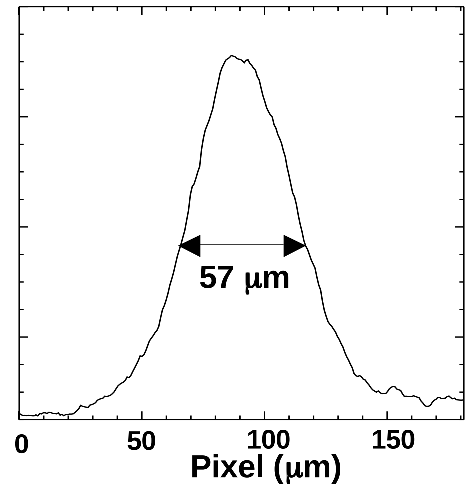

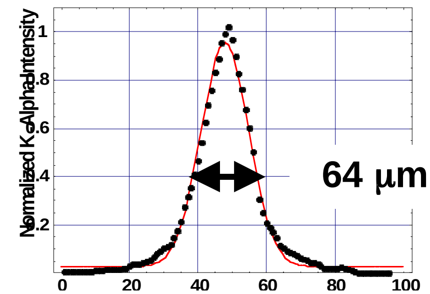

MPK model predicts
64 µm Kα size
(Snavely)

40 keV Kα+Brem Source Image
JanUSP (2/12/04)

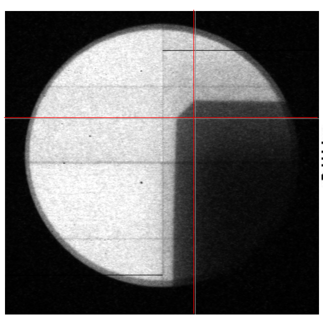

vertical lineout

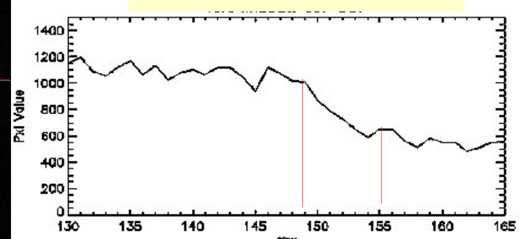

7 pxls= 60 µm

- We used RAL Vulcan petawatt lasers to characterize the high energy Kα sources
- The measured Kα source size is ~60 µm FWHM much larger than the laser spot sizes of 10 µm
- Electron transport effects determine the spot size for thin foil targets

Absolute 22 keV Ag Kα yield is measured using single photon Counting Camera

JanUSP Laser Shot

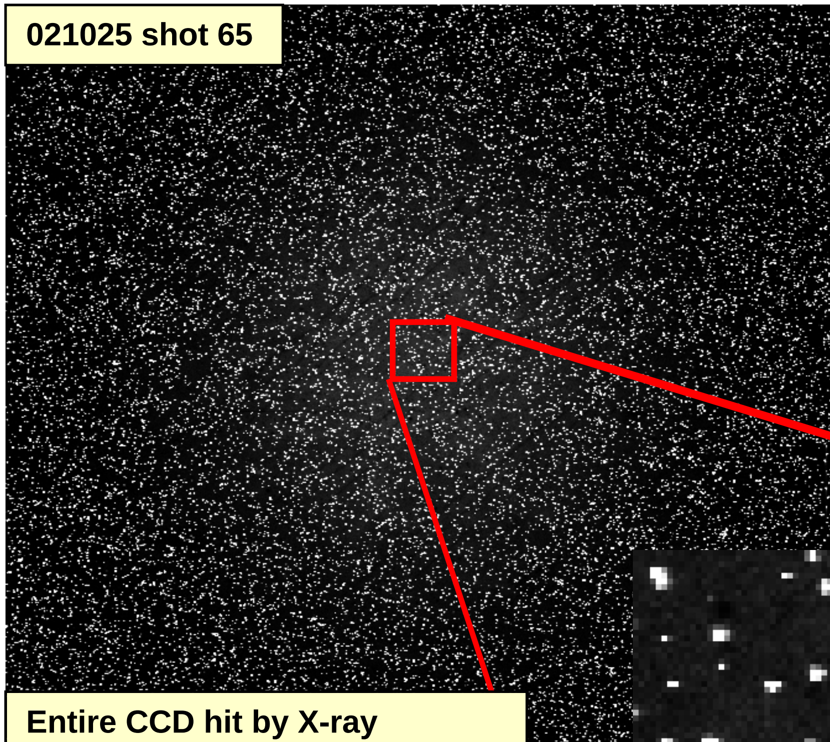

Entire CCD hit by X-ray photons

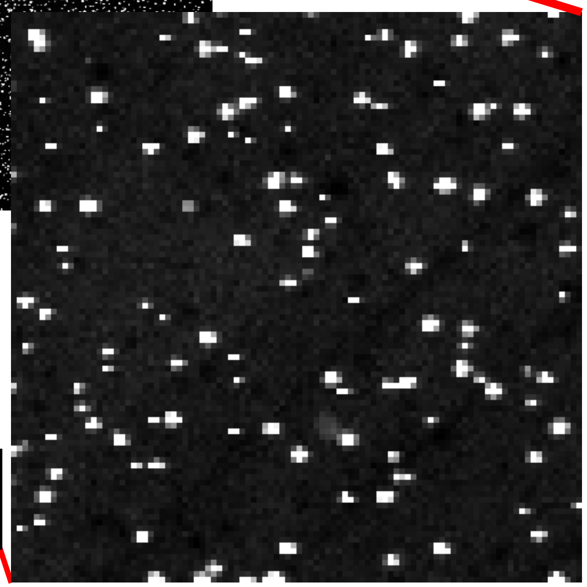

100x100 pxl zoomed view of central region

Laser parameters:
- E = 5.0 J,
- Spot size = defocused (8 μm dia FWHM)
- Pulse duration = 1 ps
- Pre-pulsed
- Intensity = 1.3×10^{19} W/cm^2

- Each hit is well separated to be counted as a single photon
- Special algorithm was needed to find 'blobs' and calculate sum counts for each blob

The absolute Kα conversion efficiency is 10^{-4}

- Absolute Kα photon yields have been measured using a single photon counting technique
- Error on measurement is large due to uncertainty in laser parameters and detector efficiencies
- Conversion efficiency of ~10^{-4} require higher energy laser to produce enough photons for high S/N experiment

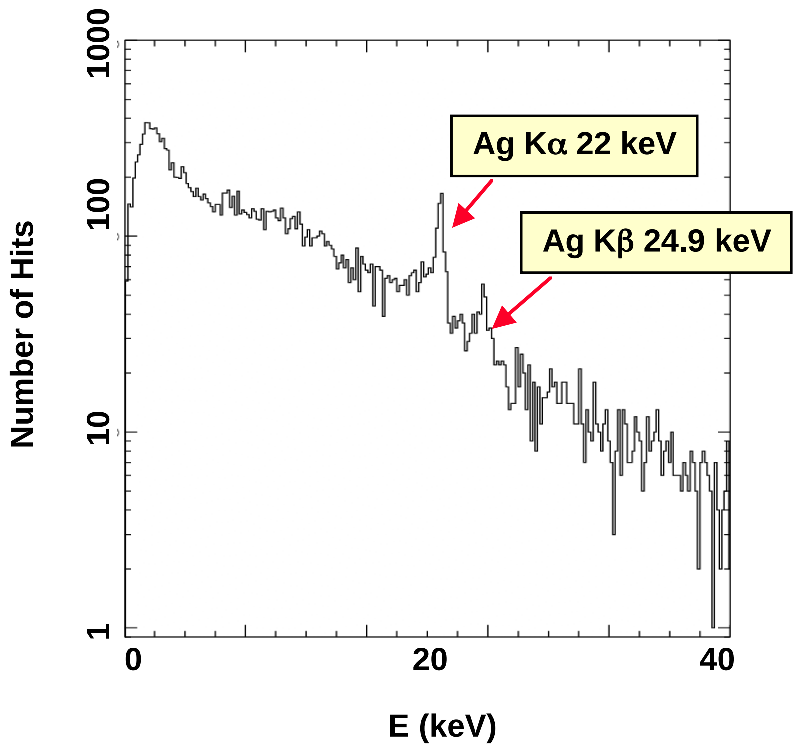

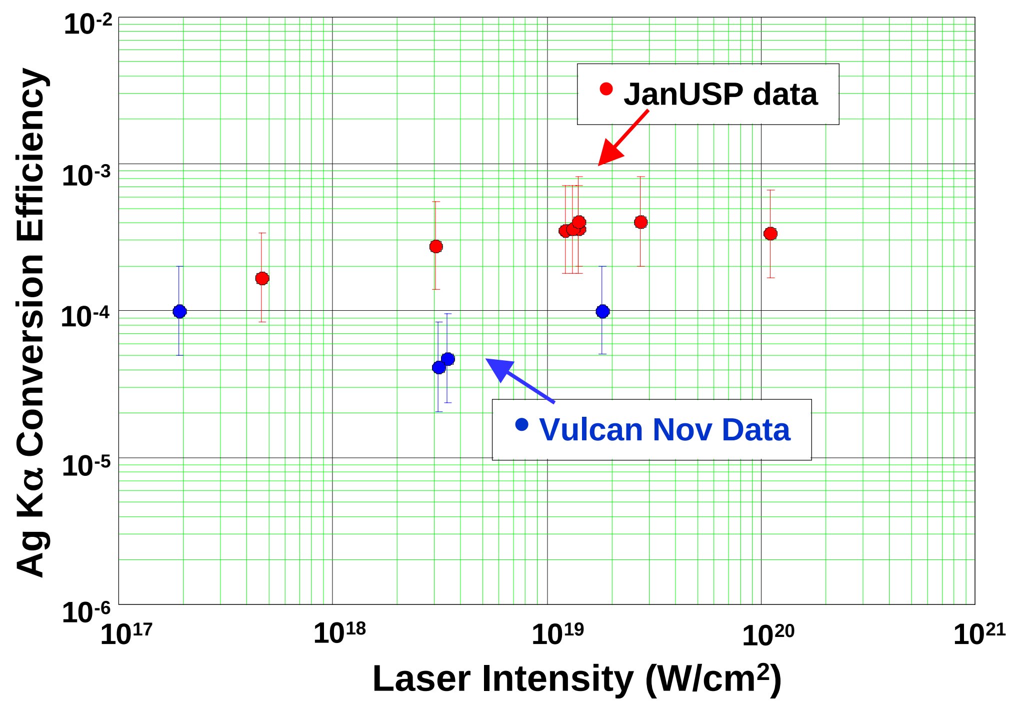

Optimization required to maximize source brightness but minimize background

22 keV Kα conversion efficiencies are nearly constant over a wide range of target thicknesses

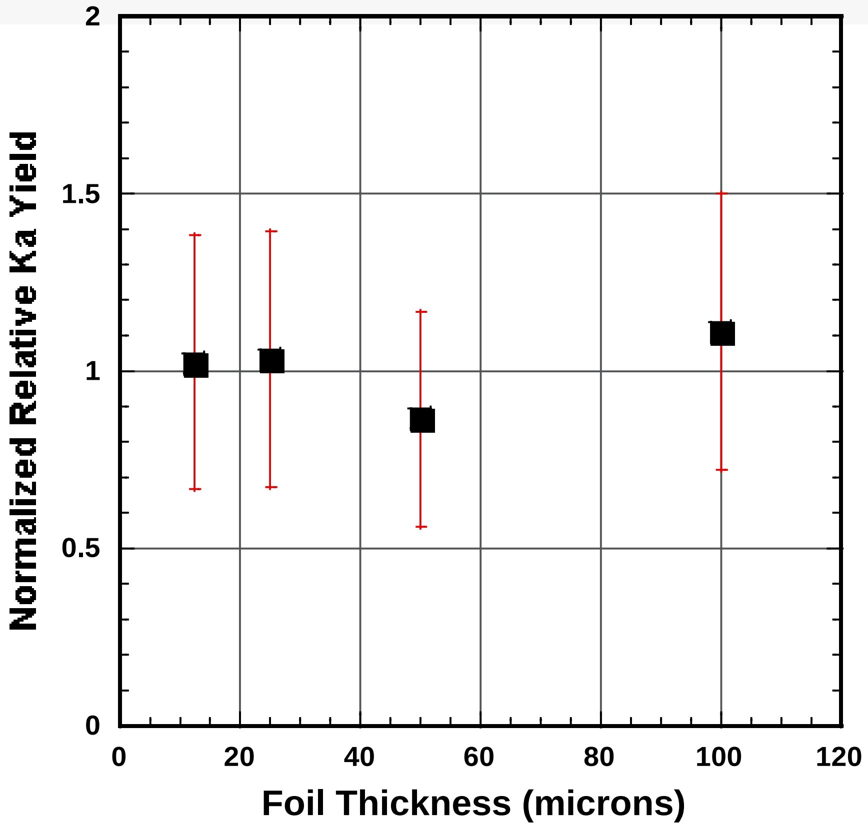

Electrons reflect from potential barriers at surfaces: Refluxing

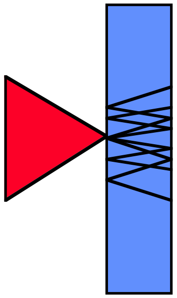

- Kα conversion efficiencies do not degrade for targets substantially thinner than the x-ray attenuation depth of ~ 70 µm
  - This may be due to reflux-enhancement model of Kα emission
  - This may be due to the hot electrons are generated only on the surface
  - When we use thinner target for the purpose of restricting source size, the x-ray photon yield will not be affected

Many ways to model Kα emission: a simple method is a combination of analytic assumptions and MC transport

Determine hot electron conversion efficiency dbased on laser intensity

$$\text{HoteEff}(I) := 10^{-1.01726} \cdot \left(\frac{I}{10^{18} \cdot \frac{W}{cm^2}} \right)^{0.287233}$$

Yasuike's [Rev. Sci. Instrum, 72, 1236 (2001)]

↓

Determine electron temperature (Thot) based on laser intensity

$$\text{LaserI}(\text{Thot}) := 10^{17} \cdot \left(\frac{\text{Thot}}{130 \cdot \text{keV}} \right)^2 \cdot \frac{W}{cm^2}$$

C. Reich [PRL 84, 4846 (2000)]

$$\text{Thot (keV)} = 100\,(I\lambda^2)^{1/3}$$

Bell [PRE, 58, 1998]

↓

Generate Boltzman electron distribution of temperature Thot

↓

ITS MC code for electron transport and Kα photon emission spectrum

(T. Phillips)

Source spectrum from ITS MC simulation for a 60 J, 1 ps laser interaction with a 12 μm thick Sm foil.

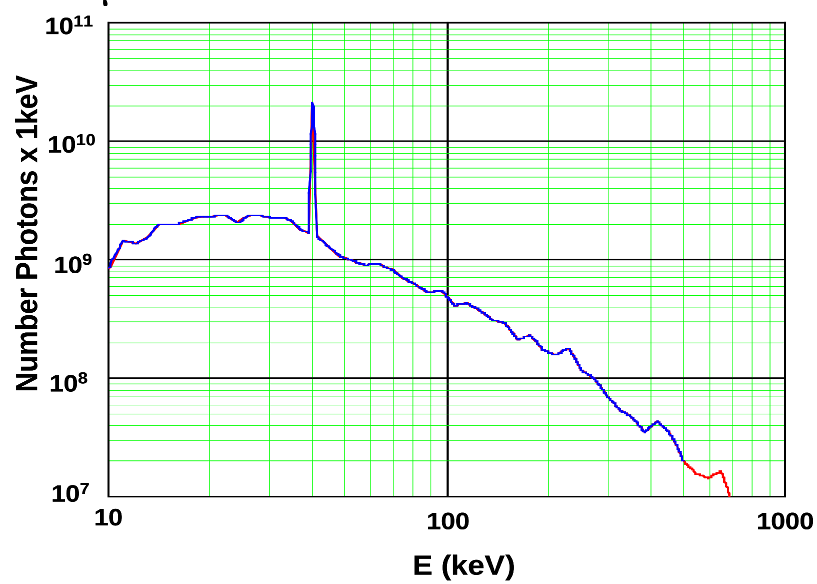

The ~40 keV Sm K-α source is being characterized for brightness and spectrum by radiographing an Au step wedge

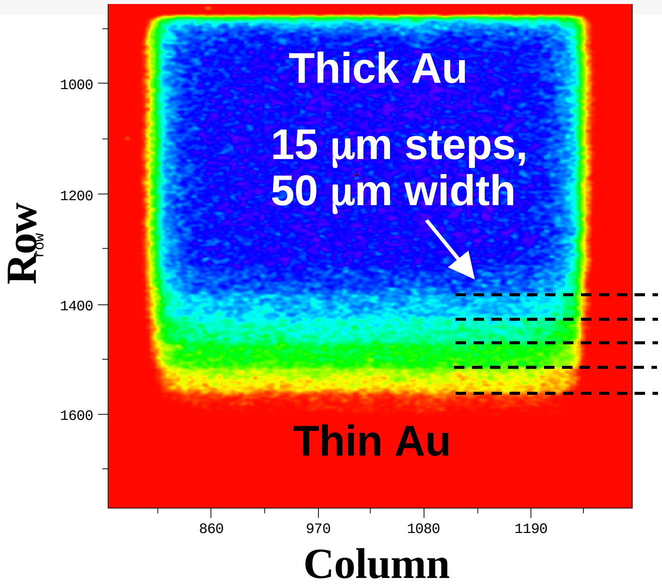

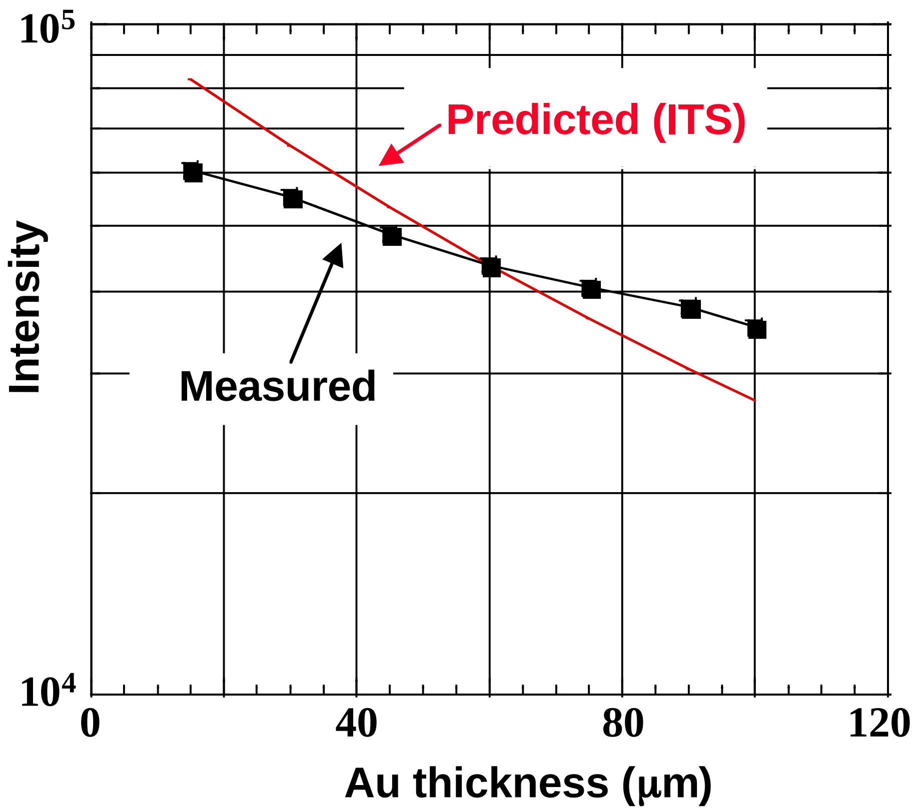

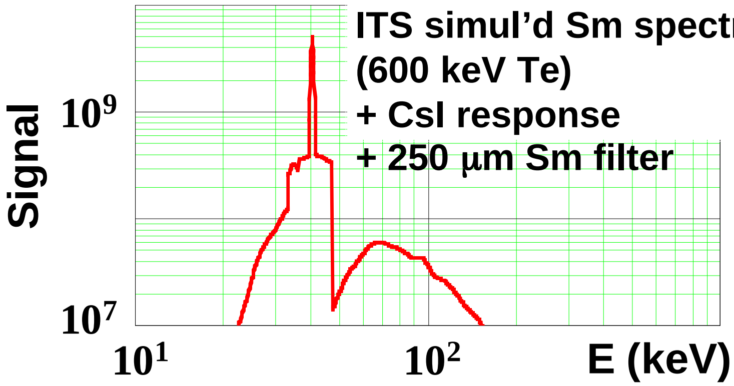

- This integral measurement suggests more high energy x-rays than predicted
- Spectrum for Sm K-α source at these conditions needs to be measured

Application to radiography: different Radiography techniques have different requirements for the x-ray source

Point Projection
Source has to be smaller than the desired spatial resolution

1-D: edge-on foil

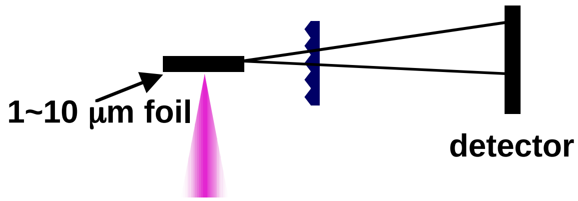

e.g. 40 keV photons/resolution element (10 µm) for strength expt is 10,000 photons

2-D with cone shape source

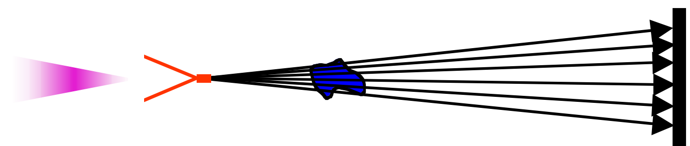

Physics issue whether we can ‘control’ hot electron spatial distribution

Area backlighter
Need hard X-ray imaging optics

Contact radiography

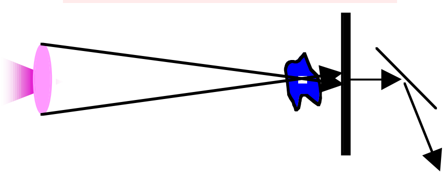

Can a close proximity imaging screen work on NIF?

2-D imaging w/ pinhole

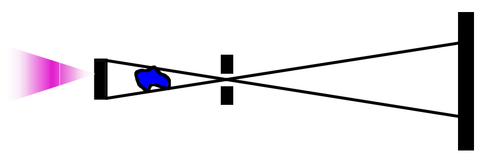

Not enough photons for required S/N imaging

2-D imaging w/ zone plates

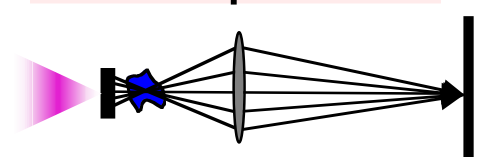

Large solid angle thru large aperture possible; difficulty in fabrication

We have developed a concept for 1D radiography at 40 keV

- We have attempted at Vulcan to demonstrate diagnosis of a NIF materials science radiography experiment
  - Edge-on Sm foil backlighter
  - "Rippled" Ta sample
  - Data taken onto CsI-CCD array

ITS output x CsI response x 250 μm Sm filter

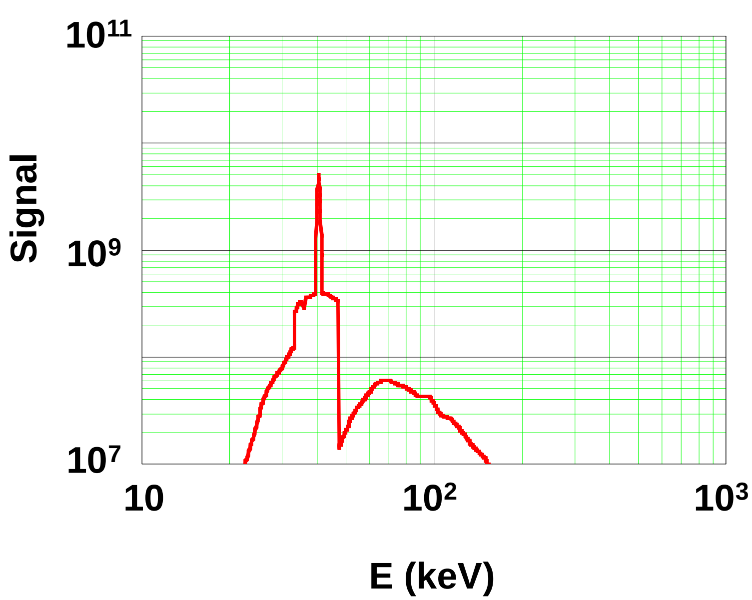

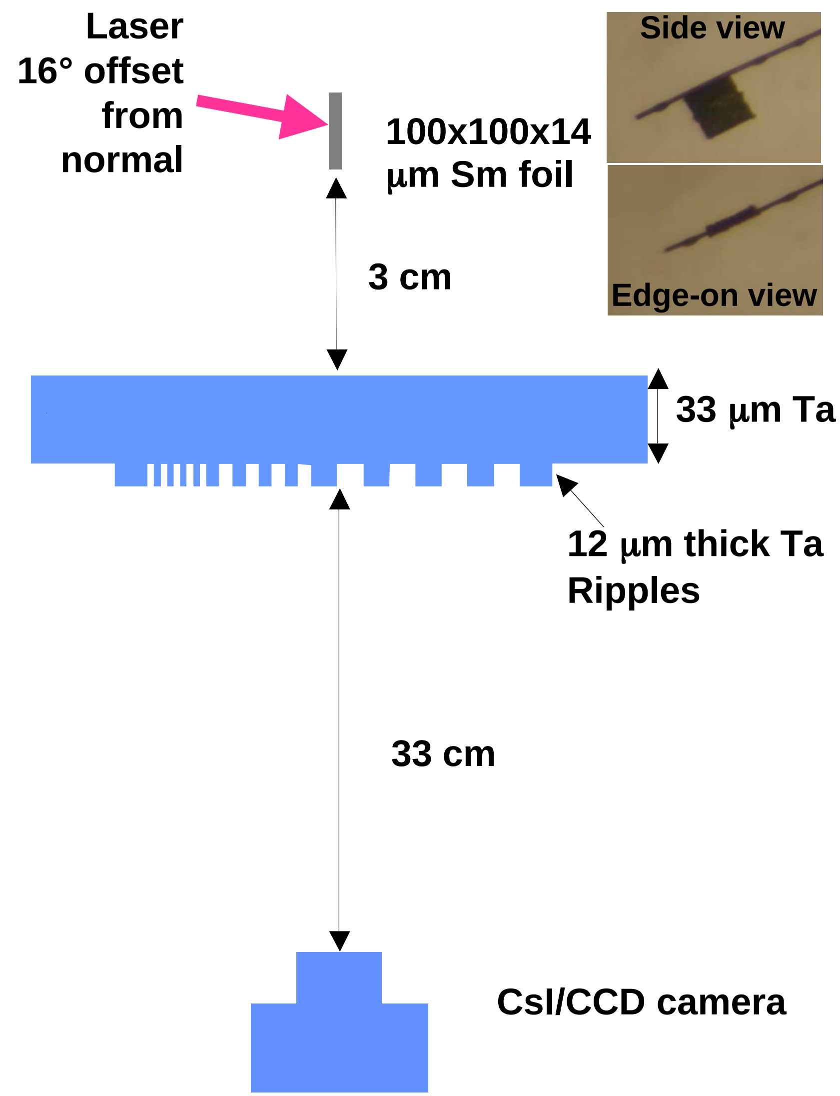

We have successfully demonstrated 1D radiography at 40 keV (6/04)

NIF
The National Ignition Facility

Target

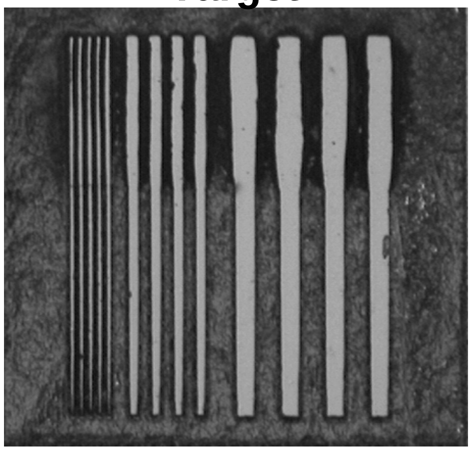

1D radiograph

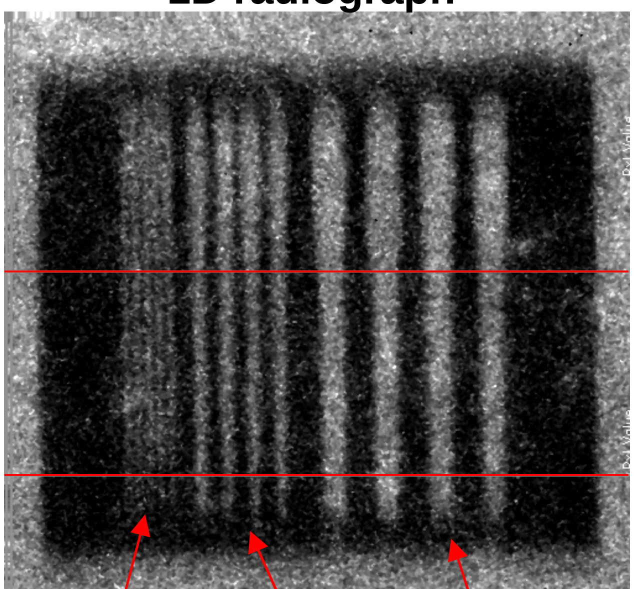

Using the Sm Kα backlighter at ~40 keV, we have shown on Vulcan (75J, 1.6 x 10^{18} W/cm^2) that reasonable radiography images through ~40µm of Ta are possible.

MTF = 0.1, 0.4, 0.5

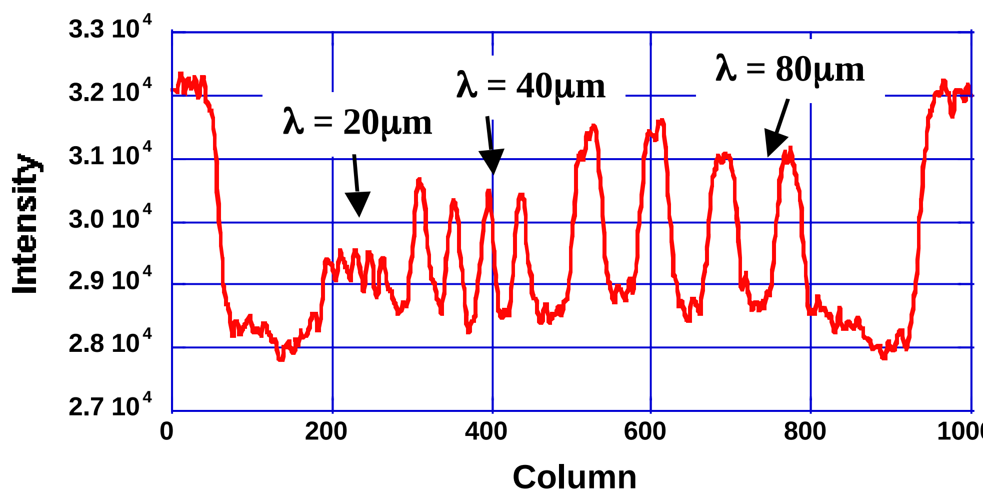

Better resolution is needed: MTF > 0.5 at 20 µm

Cone-fiber target may be a promising way to generate a localized bright source for 2-D radiography

NIF
The National Ignition Facility

We have tested an Au cone-fiber target at Vulcan

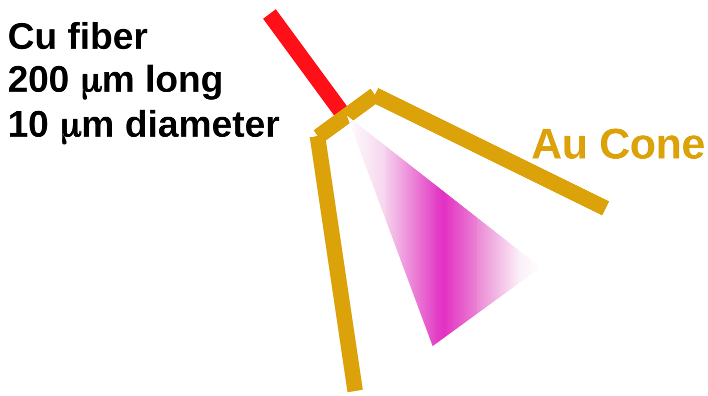

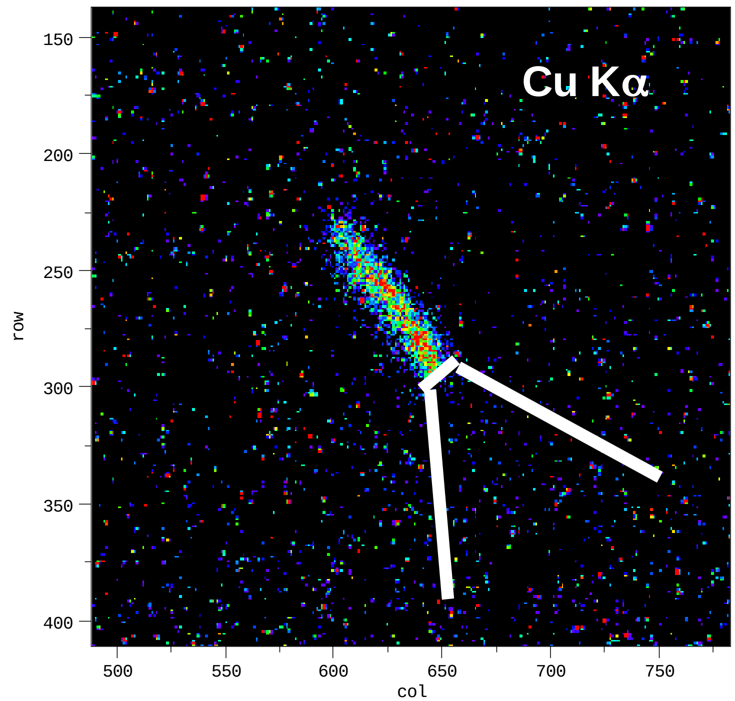

- XUV image of wire (200μmx10μm Cu) and yield of Kα both give estimates of the energy coupling efficiency and resulting isochoric heating
- Radiography source brightness is given by Kα yield (Data being analyzed)
- Do we understand laser coupling and electron guiding?

Contact radiography doesn't depend on small source size but require high resolution detector

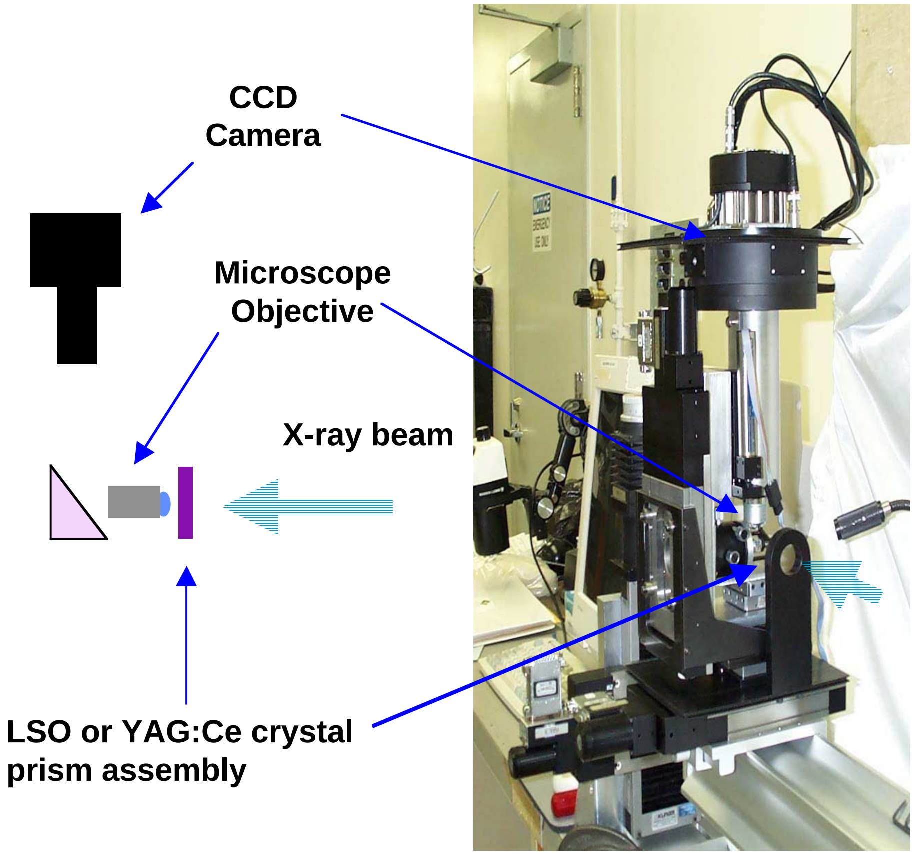

- **A similar system will be constructed as the main beam diagnostics for the LCLS FEL laser at SLAC (LLNL/PAT I-Div)**
- **We will evaluate this technology option for NIF experiments**

Modeling of K-α emission with a high-energy high-intensity short-pulse laser is new and challenging

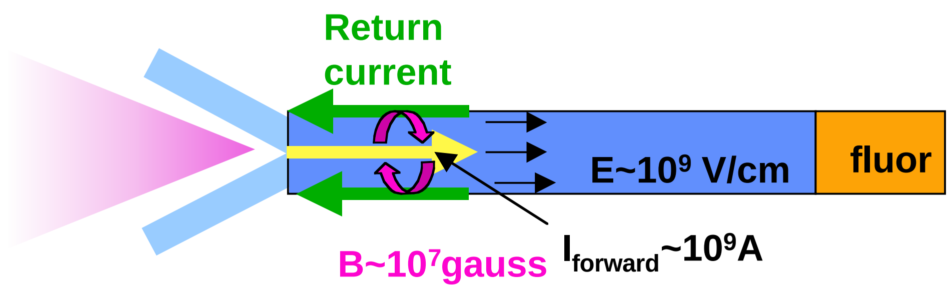

Suprathermal electron density

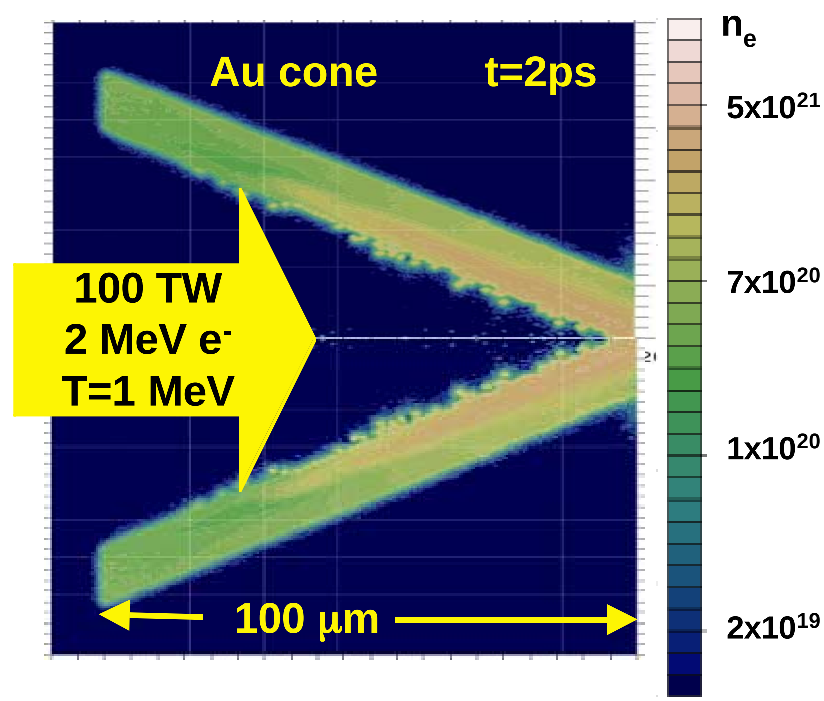

- Example LSP simulation

Laser-plasma interaction	Self consistent electron transport	Radiation physics
Prepulse Light scatter Hot electron generation		Bremsstrahlung K-α Line position Fluor efficiency Photon transport

Source confinement and radiation generation are determined by a complex set of physics phenomena

Simulation of real experiments will use LLNL’s state-of-the-art modeling capabilities

Input

Transport

output

LASNEX for prepulse calculations and raytrace

Design optimized collector geometry

ZOHAR-3D for laser plasma interactions

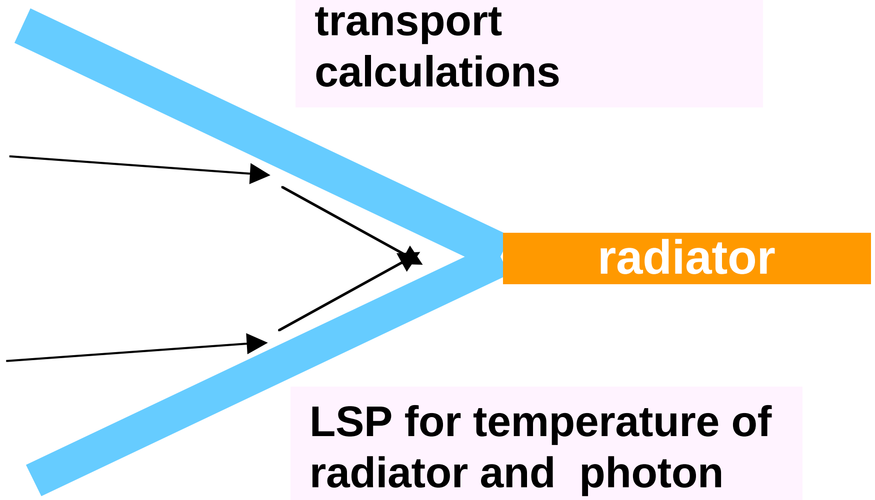

LSP for electron transport calculations

LSP for temperature of radiator and photon emission

DCHK for NLTE atomic physics

CRETIN for line transport

We will predict output intensity, direction and spectrum

MeV radiography was demonstrated on the Nova PW

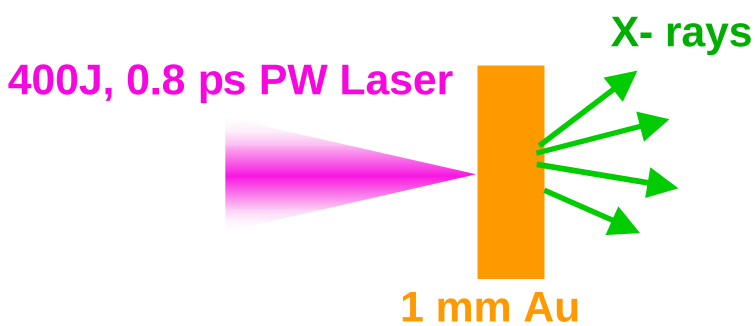

Measured Source Parameters

- 11 J of bremsstrahlung > 0.5 MeV
- Temperature: 5 MeV
- Source size: approx 500 μm
- Solid FWHM angle: 2 str

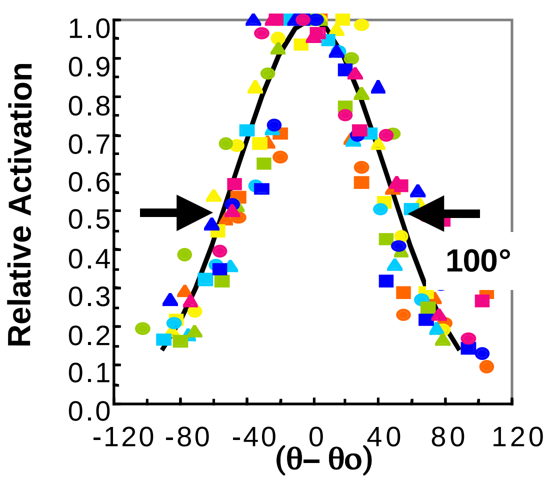

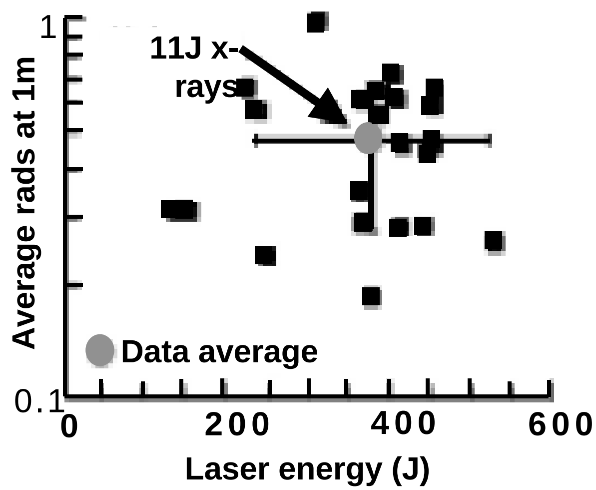

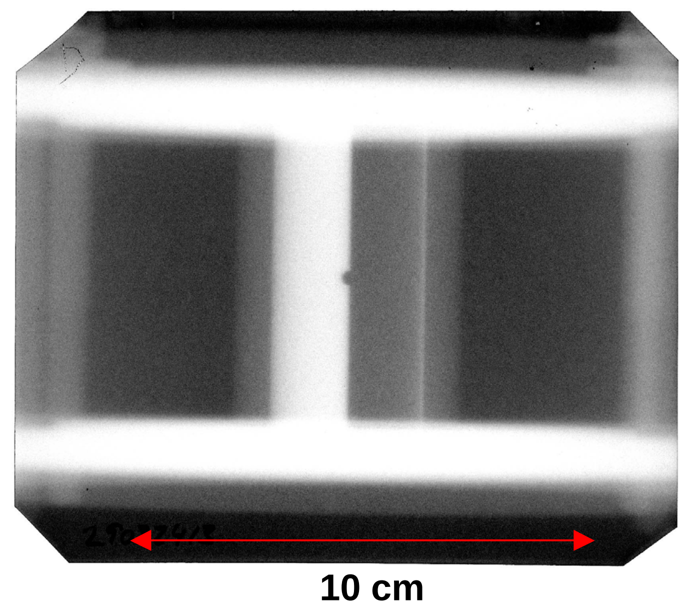

Angular pattern of MeV photons is broad

Sample radiograph of a massive W/Al/CH cylinder test object

Hatchett, PoP 7, 2076 (2000)

Some HED experiments require 2-D MeV radiography

We will develop an MeV cone-fiber target for point projection

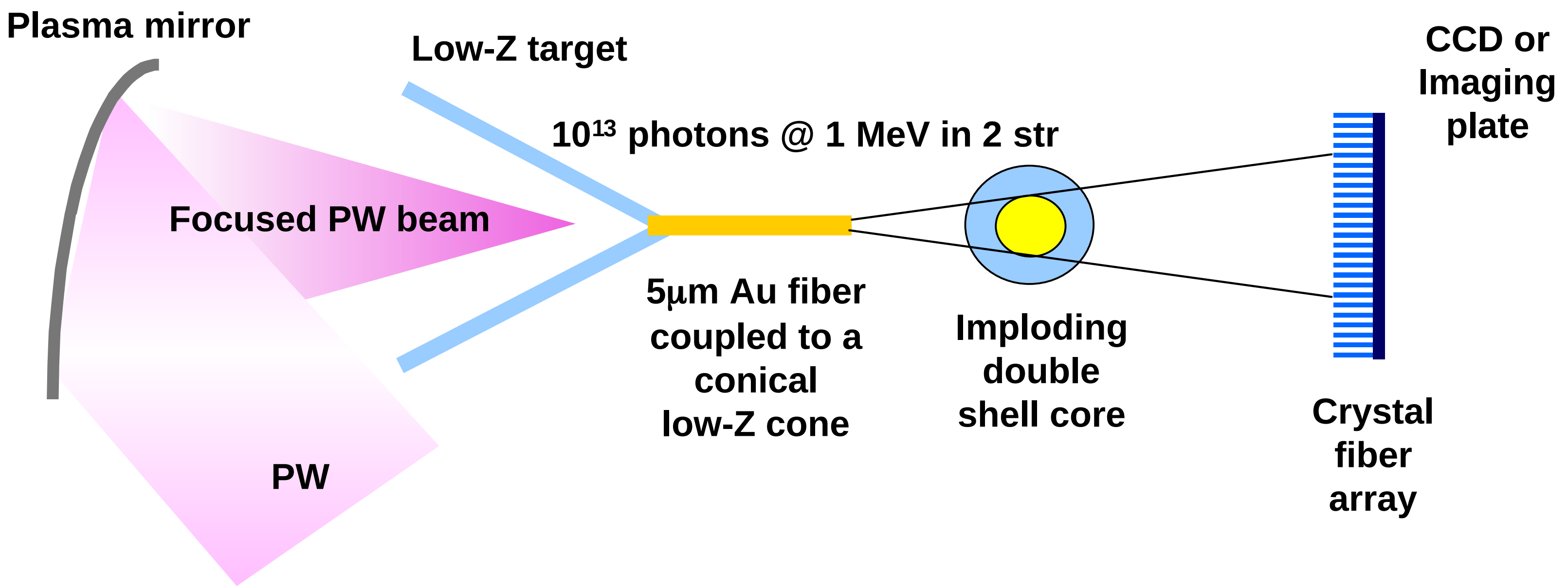

- **Initial estimate gives ~1000 detected photons/5 μm resolution element**
- **BUT this estimate is uncertain due to very complex physics**

An optimized imaging system will be developed for Kα radiography

CsI/ backthinned CCD

TEC +
Cooling Block

CsI(Tl)

Coolant

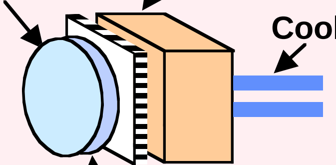

3 mm
fiber optic
faceplate

EEV42-40
Backthinned
CCD

Wickersham, RSI, 2004

CdTe camera

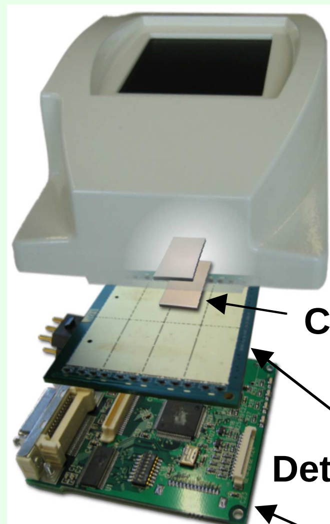

CdTe

Detector PCB

Interface PCB

Multilayer mirror for monochromator

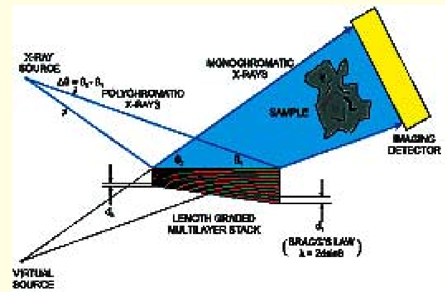

- Multilayer mirror can handle diverging beam
- W/SiC bilayers; d=2 nm
- >90% reflectivity

Schnopper, SPIE, 2001
Windt, JAP, 2000

Imaging plates

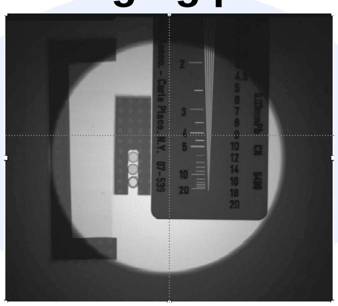

We require a camera with enhanced sensitivity, higher resolution, and reduced noise

Summary

NIF
The National Ignition Facility

- Kα radiography using the proposed NIF HEPW facility is a promising diagnostic for HEDS and ICF experiments
- Significant effort must be applied to characterizing and optimizing high-energy Kα sources
- Significant effort must be applied to development of imaging systems and detectors for high-energy Kα x-rays
- We measured the spectrum Kα and Kβ's from Ag foil hit by a short pulse JanUSP laser at LLNL and Vulcan Petawatt laser at RAL
- Measured Kα conversion efficiency was within a factor of 2 compared to the MC simulation
- More quantitative and qualitative modeling for Kα radiography is needed to optimize target geometry and to understand and reduce background

Analysis of Core Plasma Heating in Fast Ignition

T. Johzaki, H. Sakagami[A], H. Ruhl[B], H. Nagatomo, K. Mima, Y. Nakao[C]

ILE, Osaka Univ.,
Hyogo Univ.[A],
Univ. of Nevada, RENO [B],
Kyushu Univ.[C]

First Ignition Integrated Simulations

- **Introduction of FI^3 Project**
- **Imploded Core Plasma Profiles of Cone-Guided Targets**
- **Fast Electron Profiles Generated by Ultla-Intense Laser-Plasma Interactions**
- **Imploded Core Plasma Heating**
- **Summary**

ILE Osaka

FI^3 Project

Fast Ignition Integrated Interconnecting code Project

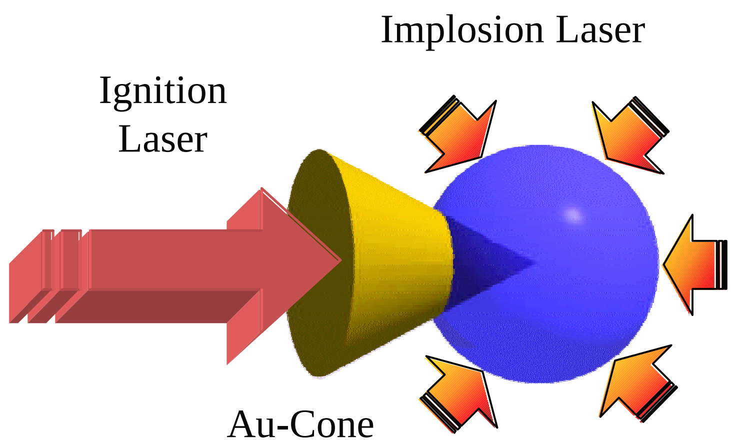

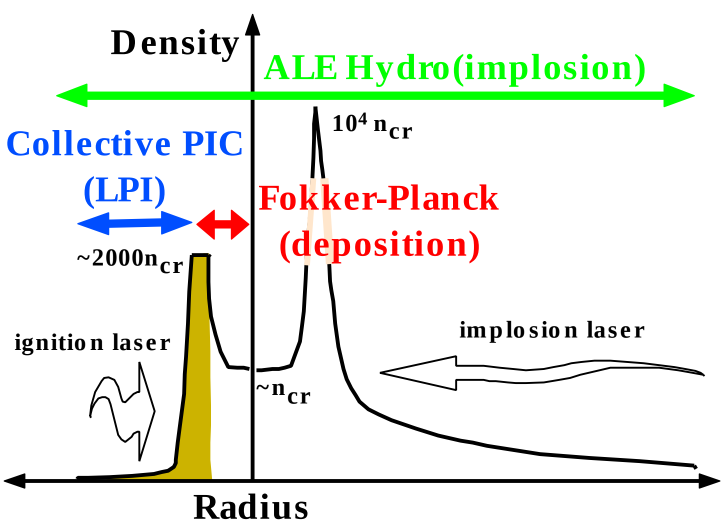

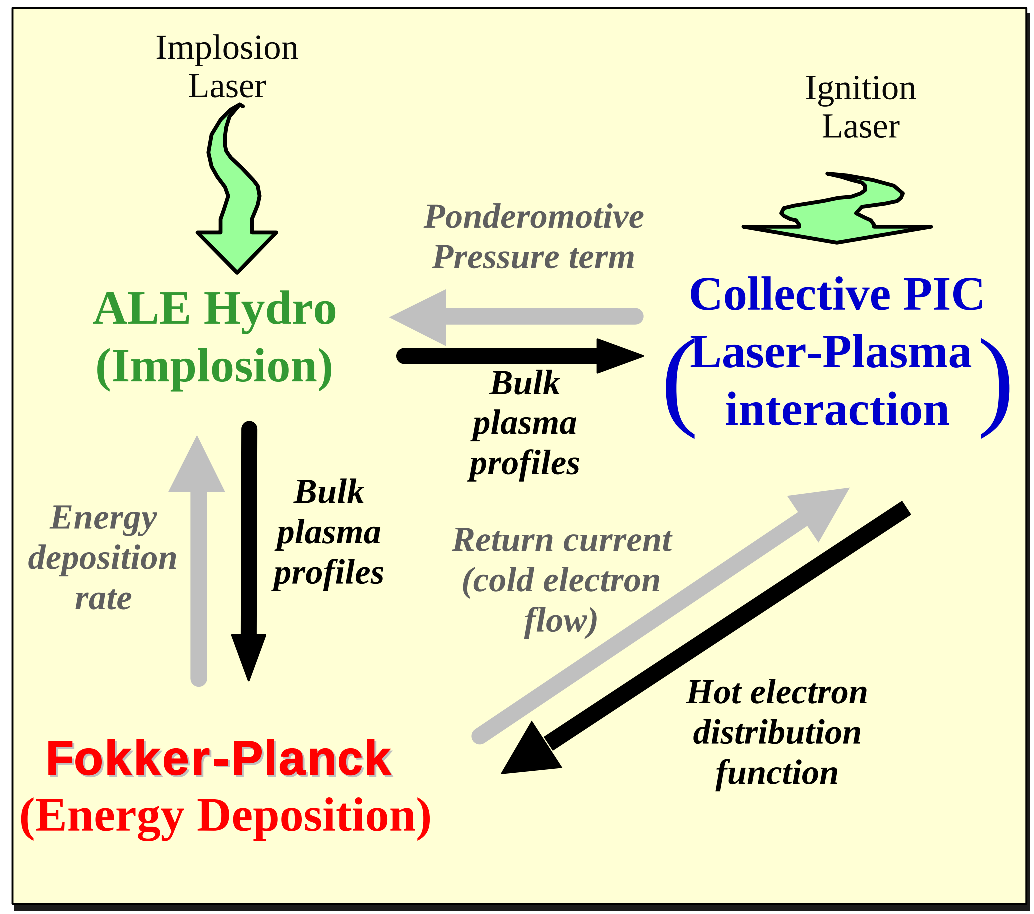

Implosion Simulation with "PINOCO"

ILE Osaka

(2D ALE-CIP Radiation-Hydro code, H. Nagatomo, ILE)

Implosion Laser condition

Wavelength :0.53mm

Energy (on target) : 3.5 kJ

Ray-trace : 1-D (radial direction)

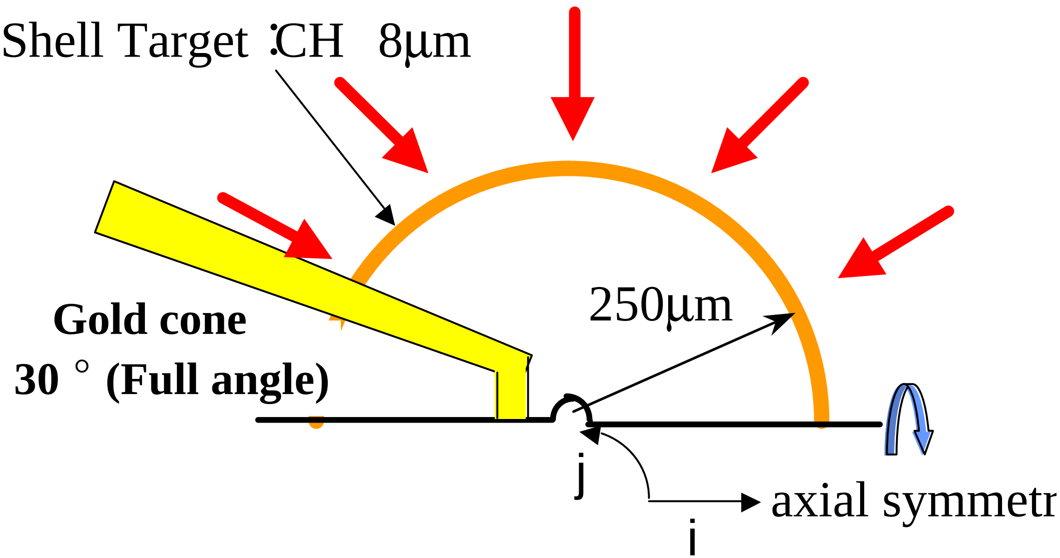

computational grids :280 (i- direction) x 280 (j - direction)

Compressed Core Porifle

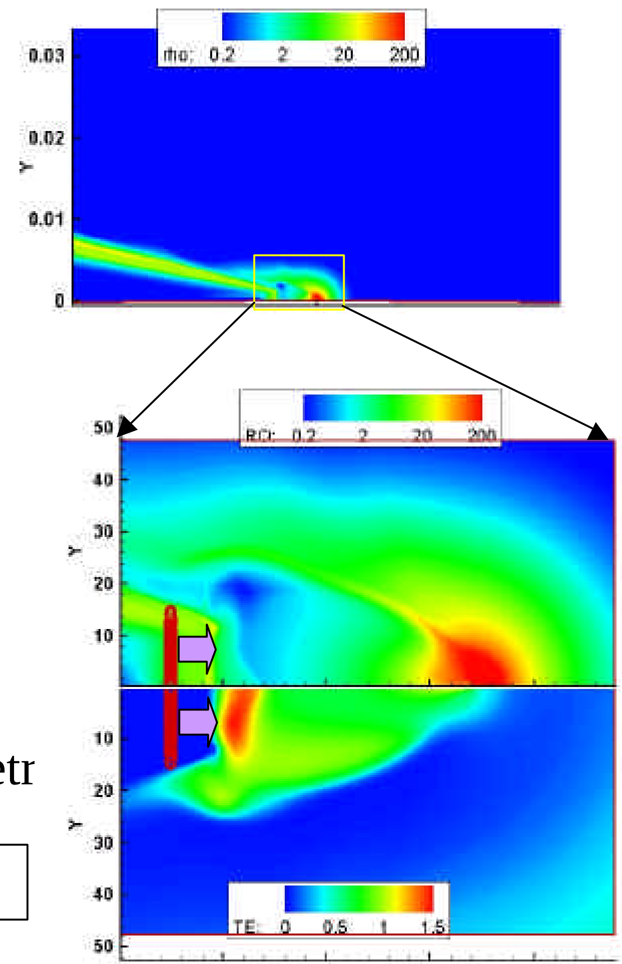

1-D Collective PIC Simulations

H. Sakagami, Hyogo Univ.
ILE Osaka

Simulation time: 1000 [fs]
  Dt = 0.0056 [fs] (0.0016w_L), ~ 177,000 steps
Spatial size: 308 [µm]
  Dz = 4.73e-3µm, (0.0045l_L), ~ 65,000 meshes
Total Number of Particle: ~ 3,574,000
  200 particles / mesh ($n > 2n_c$)
※ Ions: immobile

Laser Pulse

Gaussian Pulse,	t_{FWHM}	= 150fs
Wavelength,	l_L	= 1.06µm
Peak Intensity,	$I_{L,max}$	= 3 x 10^{19}
		or 1 x 10^{20} [W/cm^2]

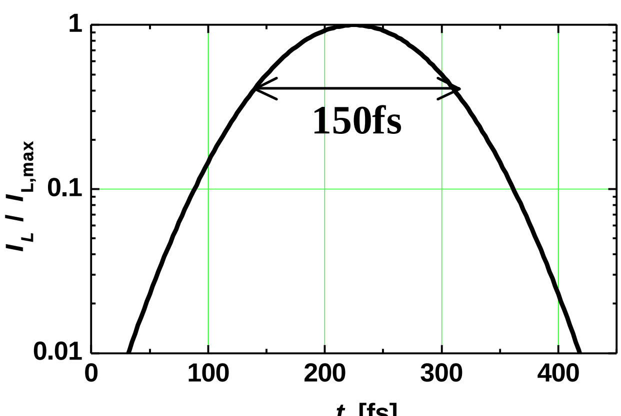

Initial plasma configuration

- Pre-plasma, scale length = 5 [µm]
- Peak density, $n_{e,peak}$ = 100n_c width = 10 [µm]
- Rear Plasma, $n_{e,rear}$ = 100n_c or 2n_c, width = 50 [µm]
- Vacuum region: front 153 [µm], rear 60 [µm]
  - ➢ ***Fast electrons are observed at 5* [mm] *behind of 100n_c region.***

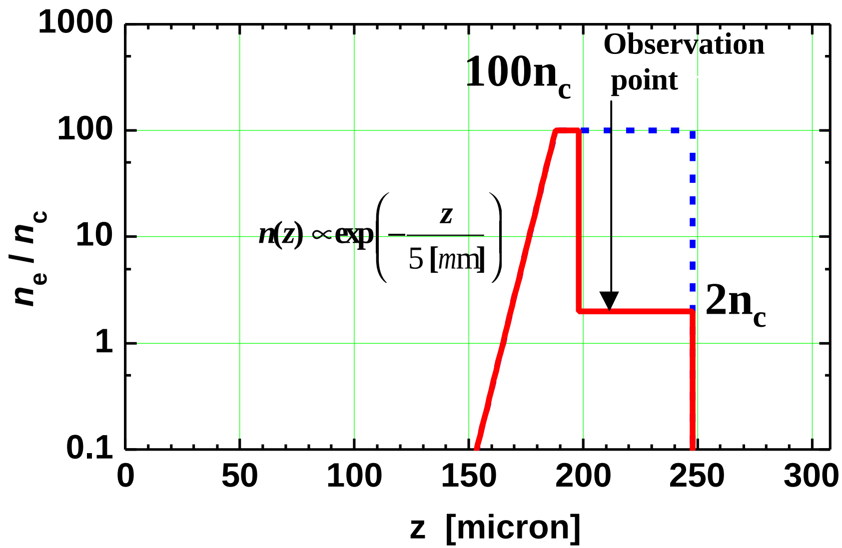

2-D Collisional PIC Simulation

ILE Osaka

H. Ruhl, University of Nevada, Reno

Number of particles：~128,000,000 (electrons)
Electrons & Ions (p(z=1) & Au(z=15)) : Mobile
Simulation time: 520fs (Dt = 0.04762fs)
Simulation box:100μm x 100μm(3000 x 3000grids, Dx = 0.033μm)

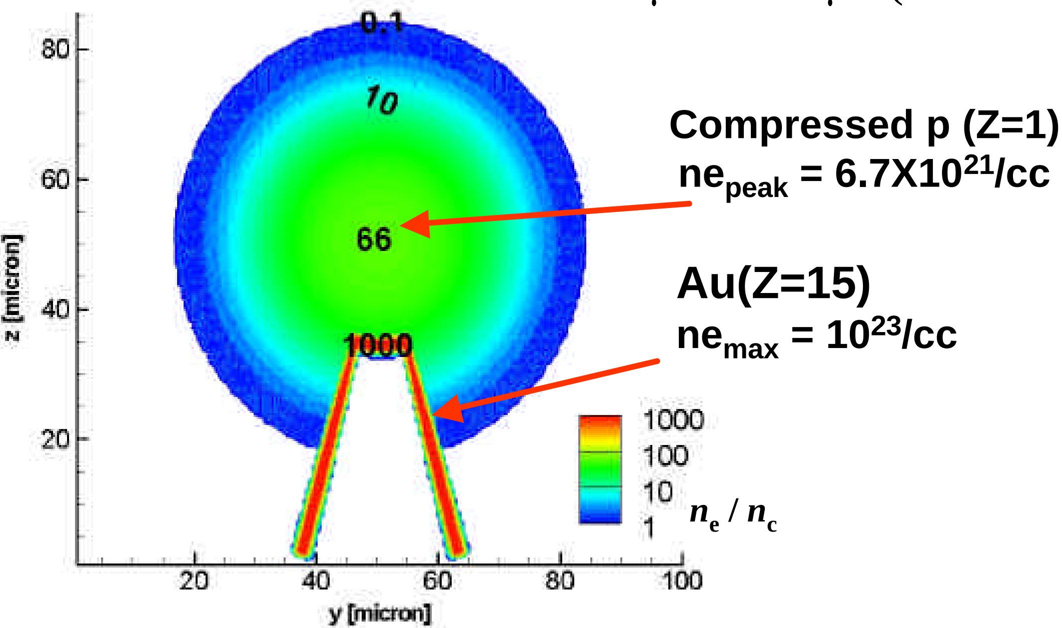

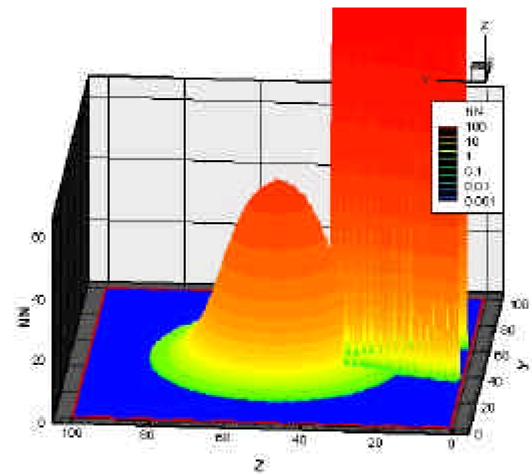

Laser: I_L = 10^{19}W/cm^2
Temporal profile: Flat after 2 l_L Gaussian ramping
Spatial profile: Gaussian (FWHM = 10μm)
l_L = 1μm

Estimation of Fast Electron Profiles Around the Cone Tip

ILE Osaka

Z-direction (Parallel to the laser)

-> divided into 3 zones

zone 1: Inside cone tip (z= 33 ~ 36mm)

zone 2: Ahead of cone tip (z= 36 ~ 40mm)

zone 3: Near dense core (z= 40 ~ 43mm)

Y- direction (Perpendicular to laser)

-> 1 region (45.5mm < *y* < 55.5mm)

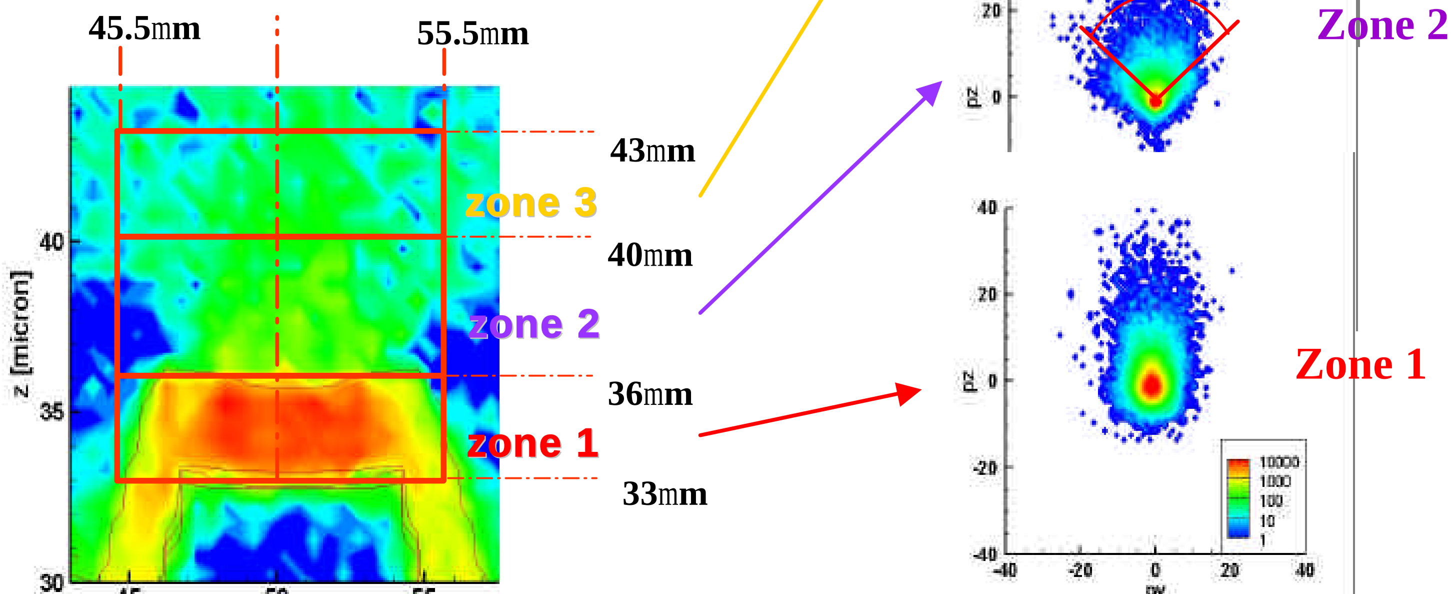

Angular distribution

Adjustment of Fast Electron Profiles

ILE Osaka

PIC sim.

Pulse length is shorter than PW condition (750fs).

Geometry effects (e.g. Cone-guiding for Laser and electrons) were not included (1D) or underestimated (2D).

1) Electron Beam Pulse Length was extended.

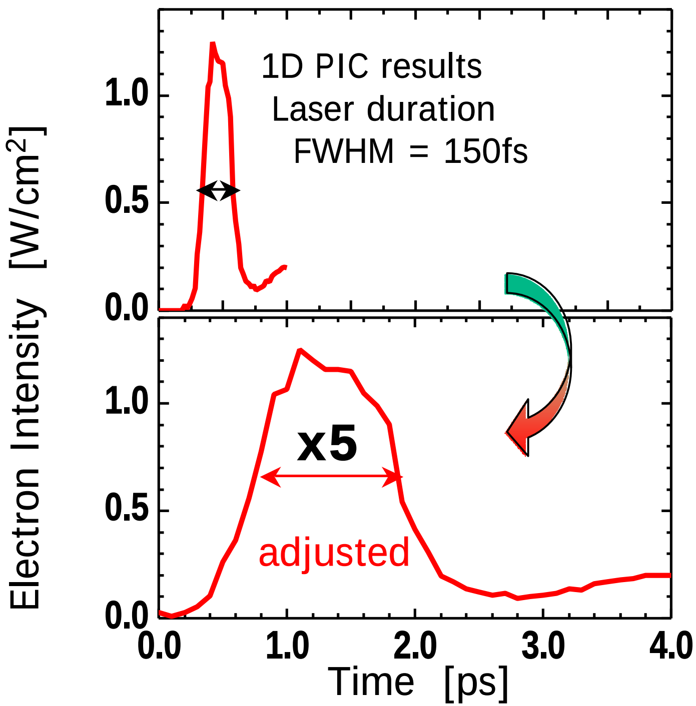

2) Intensity was adjusted so that the irradiated Laser energy is 300kJ.
⇒ (Cone-guiding effects)

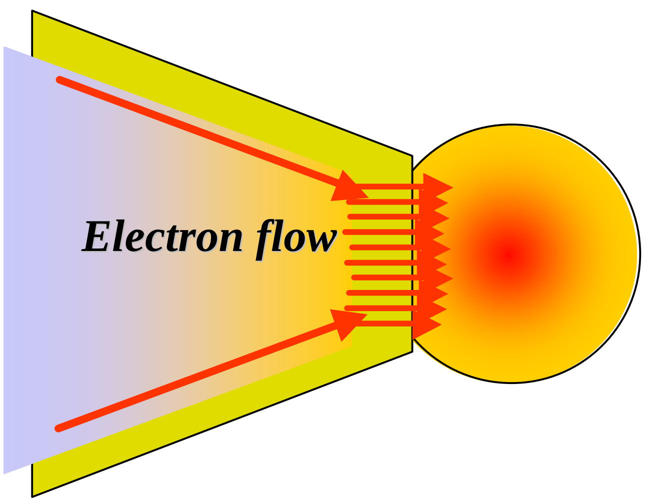

Adjustment of Fast Electron Profiles (Cont.)

ILE Osaka

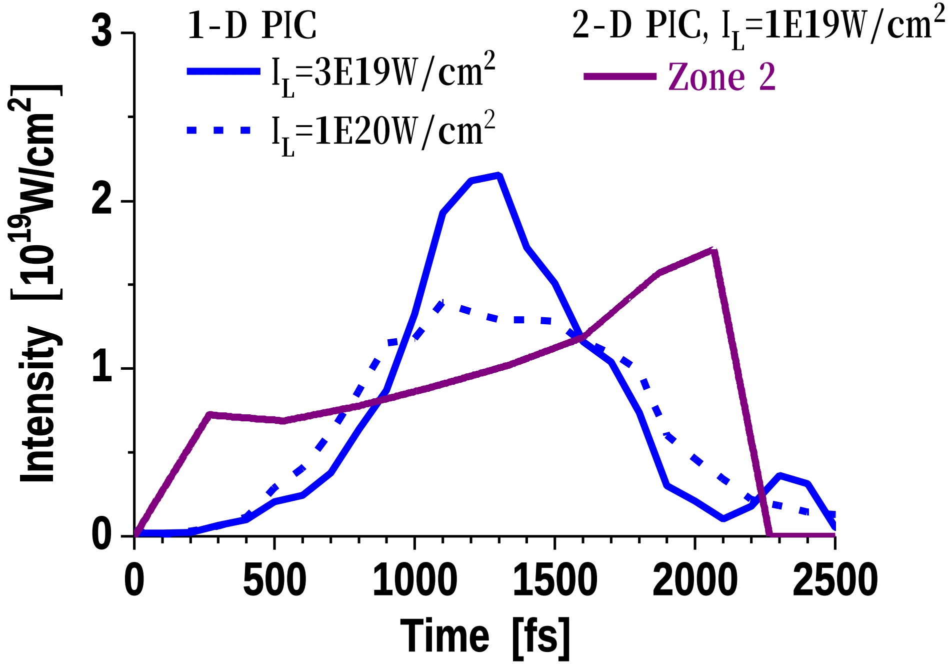

		REB Energy (After Adjust.)
1-D PIC	**I_L=3E19W/cm²**	**58.2 [J] ($h_{L,e}$ = 19.4%)**
	I_L=1E20W/cm²	**64.8 [J] ($h_{L,e}$ = 21.6%)**
2-D PIC	I_L=1E19W/cm²	
	zone 2	**81.7 [J] ($h_{L,e}$ = 27.1%)**

Electron Angular Distribution ($f(p_x,p_y)$)
~ Time-integrated ~

ILE Osaka

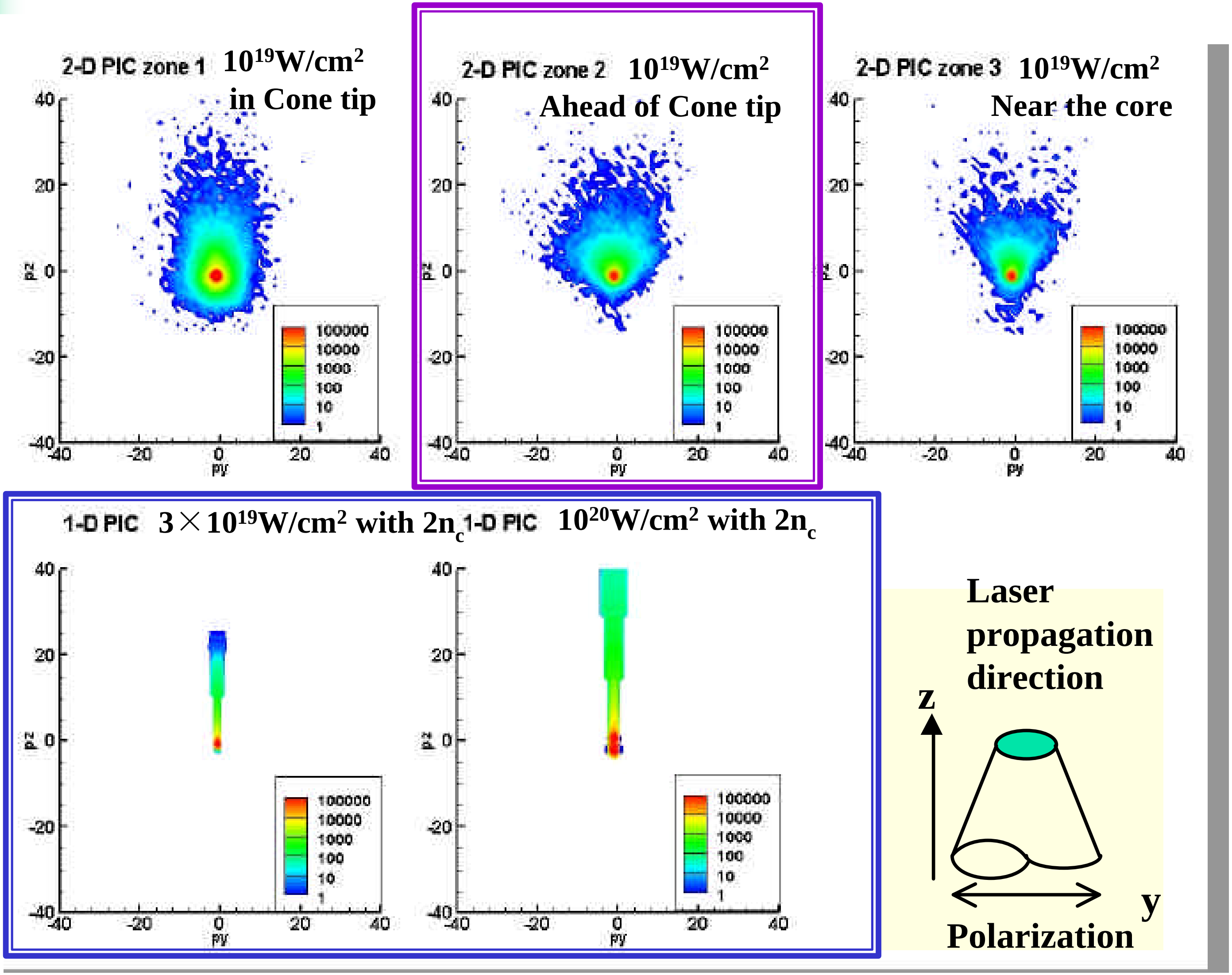

Fokker-Planck Simulation Model

ILE Osaka

Fast Electron Profiles
(PIC Code)

Fast electrons were injected at inner or outer surface of a gold cone.

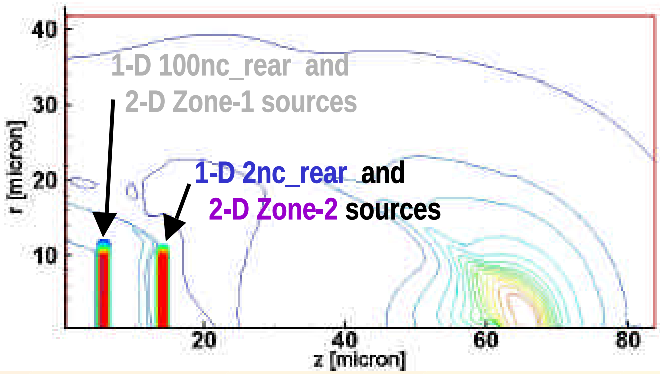

Imploded Core Profiles
(ALE Rad-Hydro Code)

Fast Electron Transport

Relativistic Fokker-Planck transport
Electromagnetic Fields

(x,y) – CIP (80x160 mesh)

(p) – Discontinuous Linear FEM (30 groups)

(m, f) – 2D Discrete Ordinate Sn method (144 directions)

r , *T*

Energy deposition rate

Radiation-Hydrodynamics

Bulk Plasma
- 1-fluid 2-temp. CIP code

Radiation
- Flux-limited diffusion

Electron Propagation and Heating rate

ILE Osaka

at t = 1300fs

1D PIC source (I_L=3x10^{19}W/cm^2 & $n_{e,rear}$ = 2n_c)

2D PIC source (I_L=1x10^{19}W/cm^2 & zone 2)

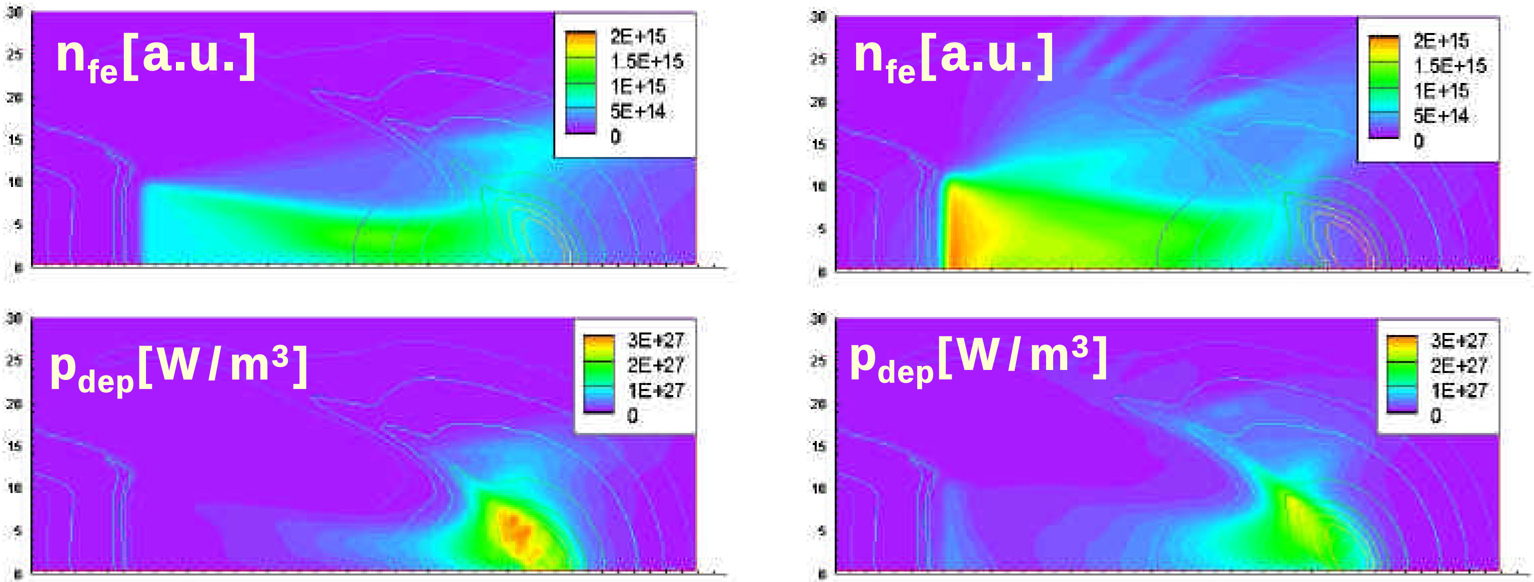

Temporal evolution of Core heating rate and ion temperature in dense-core region (ρ > 50g/cc)

ILE Osaka

(a) Core heating rate

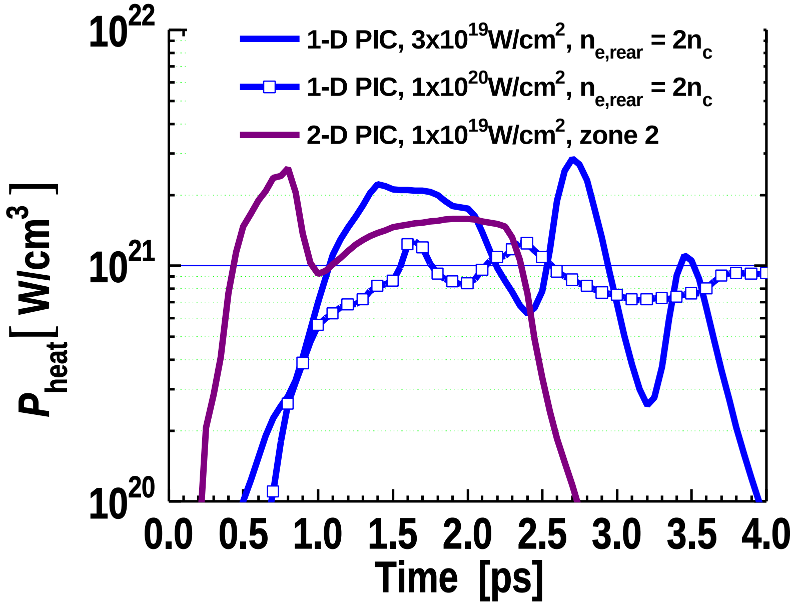

(b) Ion temperature

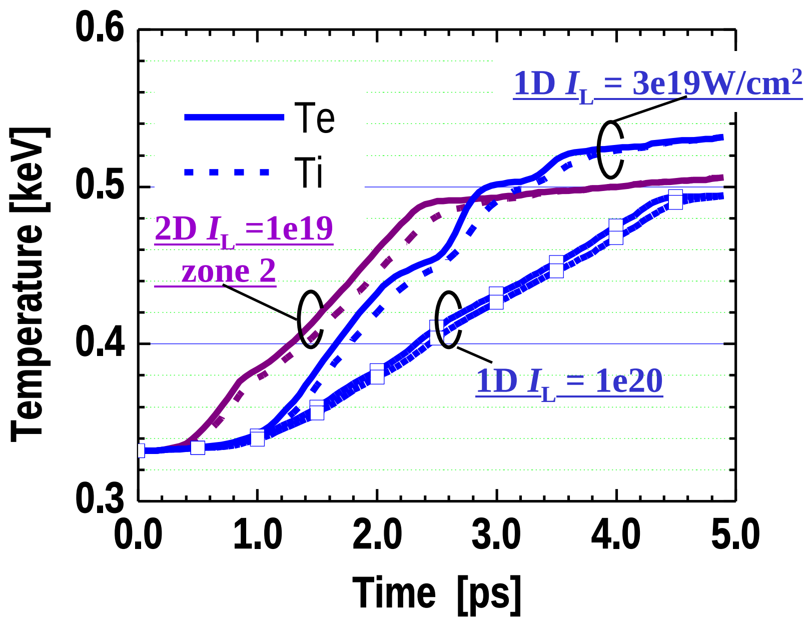

I_L [W/cm²]	ΔTe ~ ΔTi	Eheat/Esource	Eheat/E_L
1D PIC 3e19	0.20keV	31.7%	6.1%
1D PIC 1e20	0.17keV	25.0%	5.4%
2D PIC 1e19	0.18keV	20.0%	5.5%

ILE Osaka

Summary of Core Heating Analysis

The implosion and fast electron generation processes were considered.

Imploded core profiles <- ALE Rad.- Hydro. Code "PINOCO"

Fast electron profiles <- 1-D Collective PIC & 2-D Collisional PIC

※ ***Electron beam intensities were adjusted so that the total input energy corresponds to the PW experiments condition.***

Results

Fast electron profiles:

• **Energy coupling from Laser to Fast electrons**	**: 1-D PIC (~20%)**	**<**	**2-D PIC (27%)**
• **Averaged fast electron energy:**	**: 1-D PIC (~1 MeV)**	**~**	**2-D PIC(~1MeV)**
• **Angular spread of the fast electrons**	**: 1-D PIC (Beam)**	**<**	**2-D PIC(60~90deg.)**

Core heating properties:

• **Energy coupling from Fast electrons to Core**	**: 1-D PIC (25~30%)**	**>**	**2-D PIC (20%)**
-> Energy coupling from Laser to Core	**: 1-D PIC (~5%)**	**~**	**2-D PIC (~5%)**

The dense core is heated up to ~ 0.5keV, which is still lower than the reported PW experiment results (~0.8keV).

Multispecies Ion Acceleration off Short Pulse-Irradiated Targets

Andreas J. Kemp and H. Ruhl
University of Nevada, Reno, USA

In collaboration with
M.Schnürer, S. Ter-Avetisyan, P.V. Nickles
Max-Born-Institut, Berlin, EU

LLNL Computational Workshop, August 2004

We have investigated ion acceleration off water droplets that are irradiated with intense, ultra-short laser pulses

- Ion Acceleration via electrostatic field –
  Target Normal Sheath Acceleration (TNSA) Mechanism
- Most groups use microfabricated foil targets:
  - Accelerate surface deposits, ie CH, on metal targets
  - Plane or micro-machined surface with controllable structure
  - Typically ‚long‘ laser pulses, ~0.1 – 1ps
- Droplets versus foil targets:
  - Geometry: can treat droplet surface as plane as long as d<<R
  - Clean composition of target, no deposits on surface
  - Defined target volume
  - Charge-neutral: electrically insulated
- New: extremely short laser pulse ~40fs
- New: small volume, but larger than cluster (no explosive-type interaction)

Outline

- Experimental Setup and Conditions
- Isothermal Expansion of a Plasma with two Electron Temperatures into vacuum (TNSA-type model)
- Multispecies Plasma Expansion
  - Adiabatic vs. Isothermal Expansion
  - 1D and 2D Particle-in-Cell Simulations
- Beam Properties:
  - Laminarity
  - Symmetry
  - Ion Composition
- Towards a predictive model of multispecies ion accleration.

I. We study laser-ion acceleration experiments at Max-Born Institut Berlin with water droplets

- MBI Ti::Sapphire Laser: 800nm, 1019 W/cm2, 750mJ, 40fs pulse rep rate 10Hz, 10mu focus diameter
- Targets: Water droplets [H2O / D2O], 10mum radius, from nozzle
- Relevant diagnostic: MCP/CR39 + Thompson parabola to distinguish various charge/mass ratio ions
- Single-shot or time-integrated

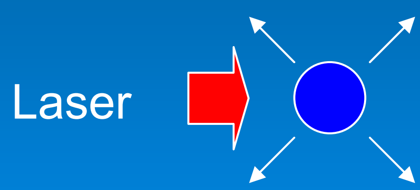

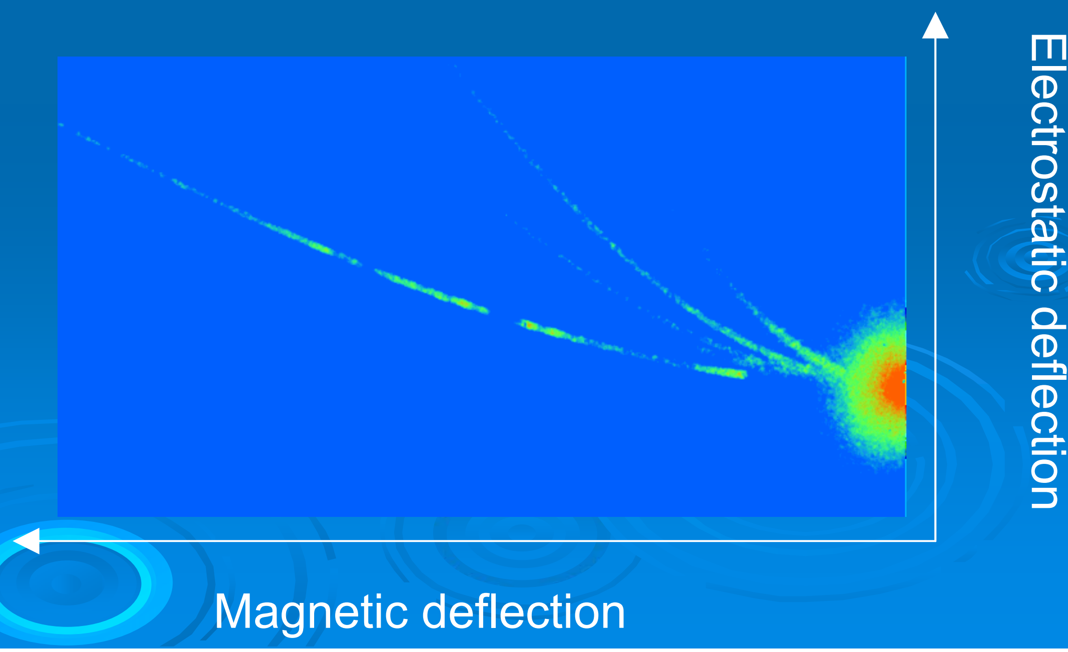

Proton spectra from short-pulse laser-irradiated water droplets show strong modulations

- Strong dip in 10-30% of all shots
- Position between 200-400 keV
- Weaker, but similar effect found in LLNL experiment at higher energy

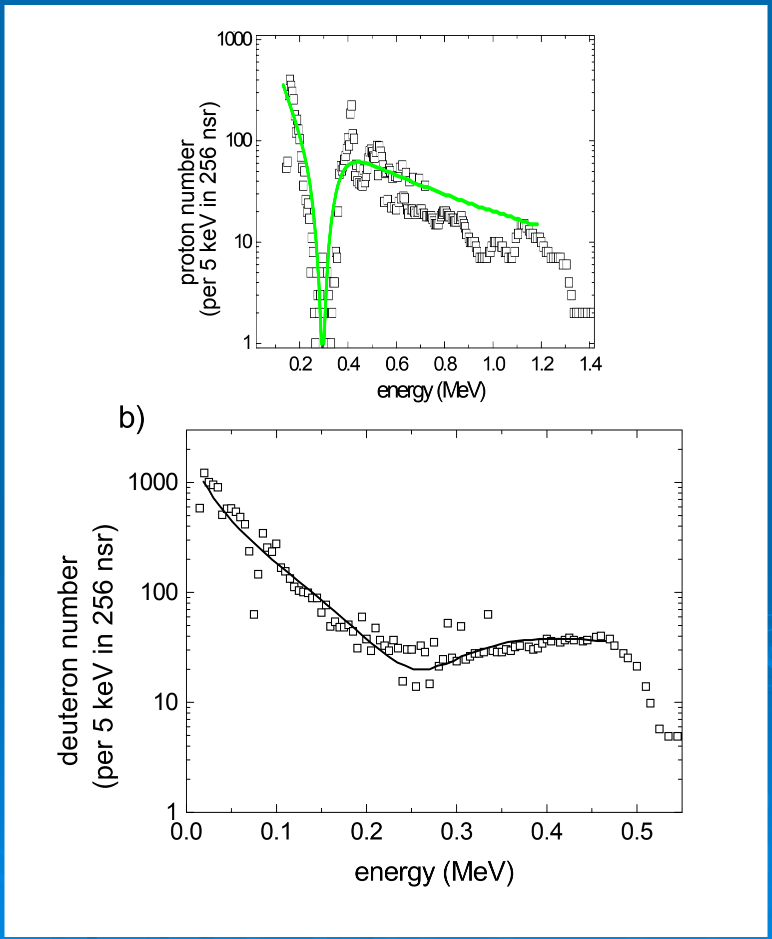

Allen et al, Phys. Plasmas (2003)

II. A classical isothermal 2T-plasma expansion model predicts dip in ion spectrum

- Two electron temperature Plasma
- Separation of ion populations leads to spatial/energy gap
- Gap determined by two parameters:
  - Hot-cold density ratio: position in Energy
  - Hot-cold temperature ratio > 9.9: depth
- Origin is x/t-dependence of ion sound velocity (in 1T model, sound velocity is constant)
- For Th/Tc>9.9, quasi-neutrality is violated locally, solution becomes triple-valued, ie. unphysical

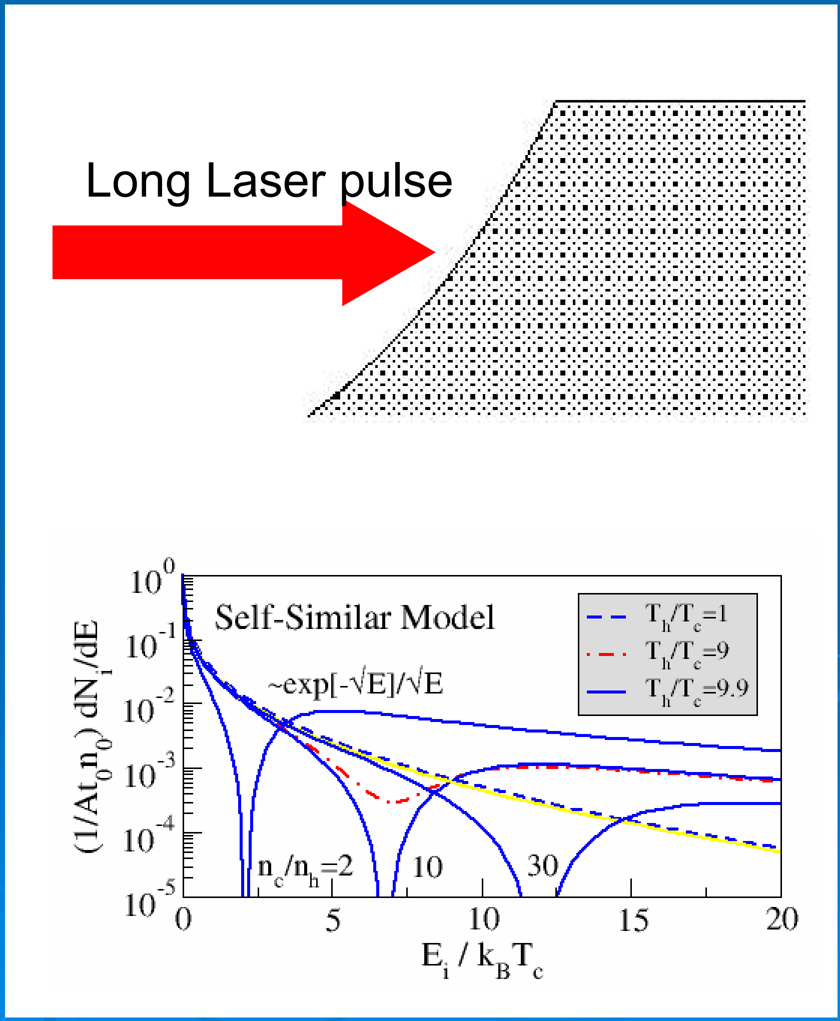

Wickens, Allen, Rumsby, PRL (1979)
Gurevich et al, JETP (1966)

We use 1d-PIC kinetic simulations to verify the self-similar 2T expansion model

- Particle-in-Cell simulation (LPIC) of 2Te-expanding plasma w/o laser:
  - NO laser
  - M(ion)=100 me, Tc=51.1eV,
  - Th/Tc=30, nc/nh=10.
  - Box and slab size sufficiently large
  - Use similarity variables for time, space
  - Resolve plasma Debye length, good statistics –1 Mio particles
- Expect at ion separation point:
  - large Ex-field
  - Jump in ion density
- Want to check physics response:
  - Electron temperature ratio
  - Shape of electron distribution

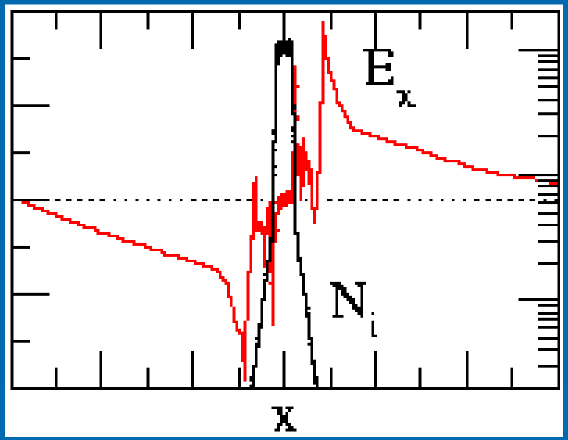

Schematic view of simulation

Our PIC results agree with self-similar 2T plasma expansion model – but only for unrealistic electron distributions

- Simulation reproduces WA model to reasonable degree:
  - Dip in ion spectrum
  - Position of gap in terms of x/t variable
  - More realistic electric field at gap
- Use smooth electron distribution ➡ dip and electric field vanish
- Interpretation of MBI experiment in terms of isothermal 2T plasma expansion model by Wickens+Allen is not justified

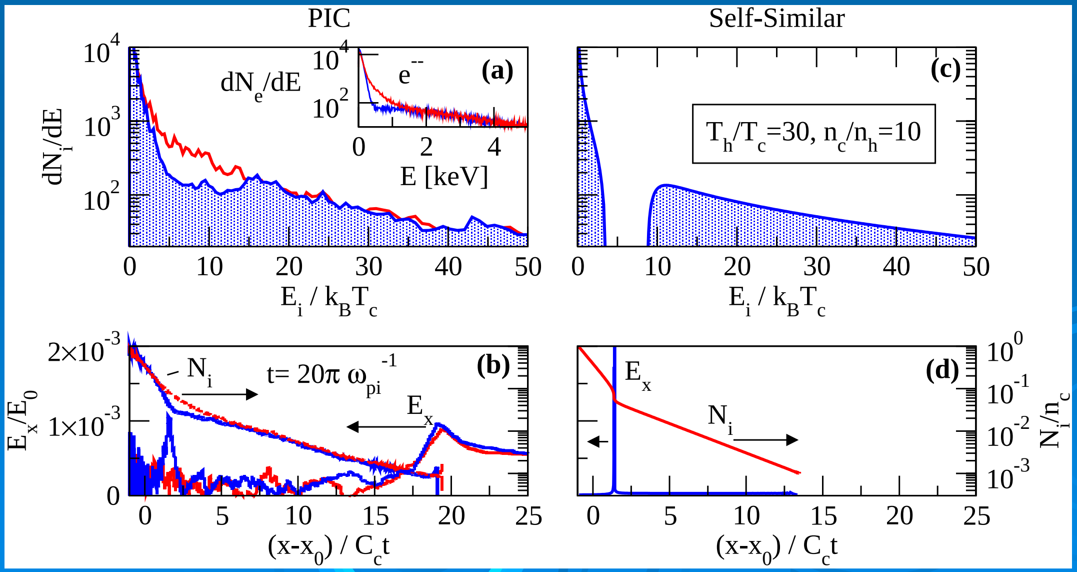

III. Laser-driven multi-species plasma expansion shows modulation in proton spectrum

- 1d Particle-in-Cell simulation of pre-ionized plasma slab, 1mu thick: deuterium and oxygen ions O+4
- Laser: 800nm, 1019W/cm2, 40fs sin2
- Spectrum and plasma behind target
  - dip in deuterium spectrum
  - cut-off in oxygen spectrum

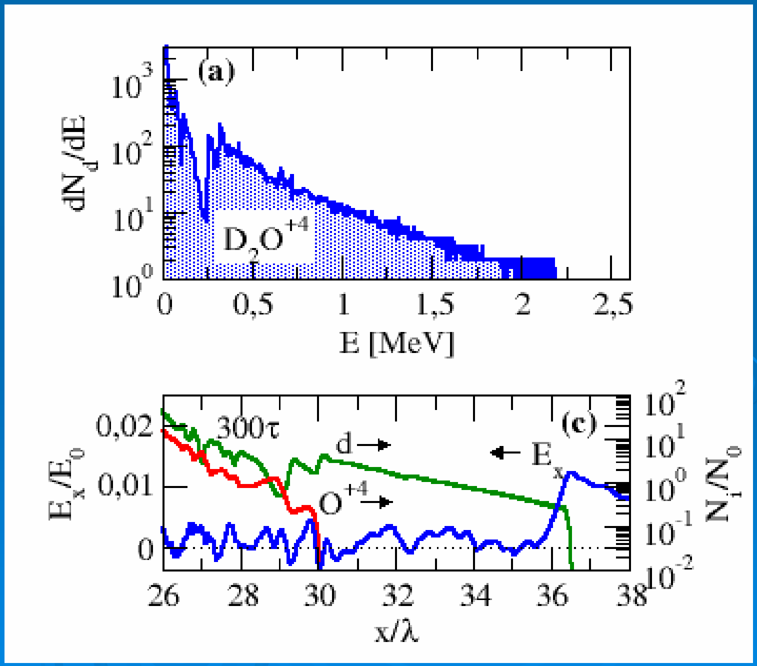

- Ion acceleration lasts much longer than 40fs laser pulse (ion kinetic energy):

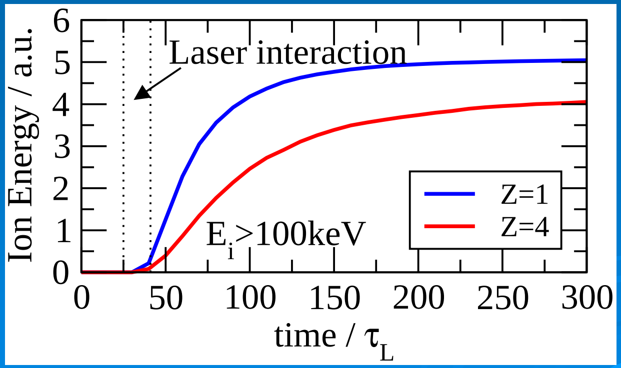

The spectral modulation is a multi-species effect: w/o oxygen ions, no dip in p-spectrum

- w/o oxygen ions:
  - no dip
  - larger maximum ion energy
- Evolution of electron distribution not isothermal !
- CW laser pulse:
  - Similar dip as for short pulse
  - much larger max. ion energies

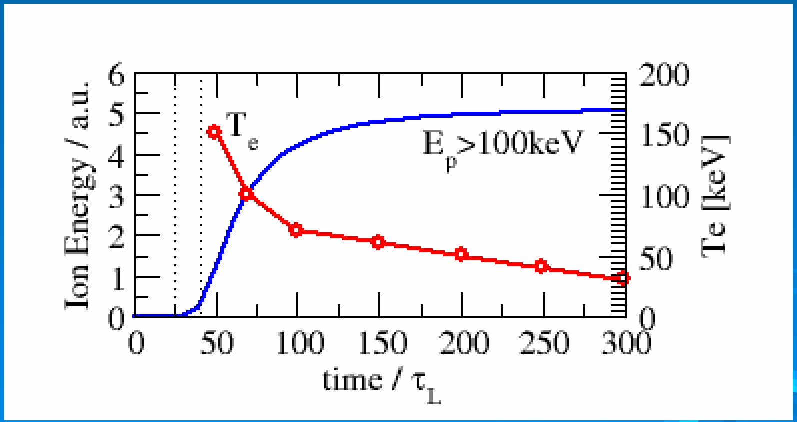

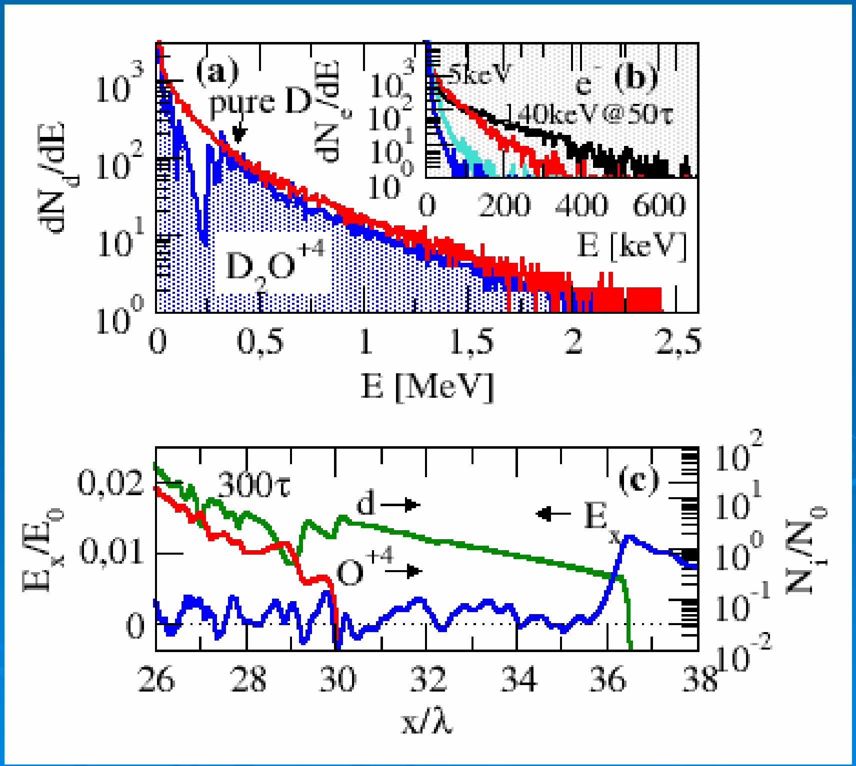

IV.a Beam properties: laser destroys isotropy on front side for protons, less for oxygen ions

- 2d PIC Simulation (PSC) of water droplet irradiated with 1019W/cm2, 40fs pulse with central irradiation
- Assume droplet to be ionized to protons and O+4
- Acceleration:
  - essentially 1D close to target surface, but:
  - Later in time beam the expands radially symmetric

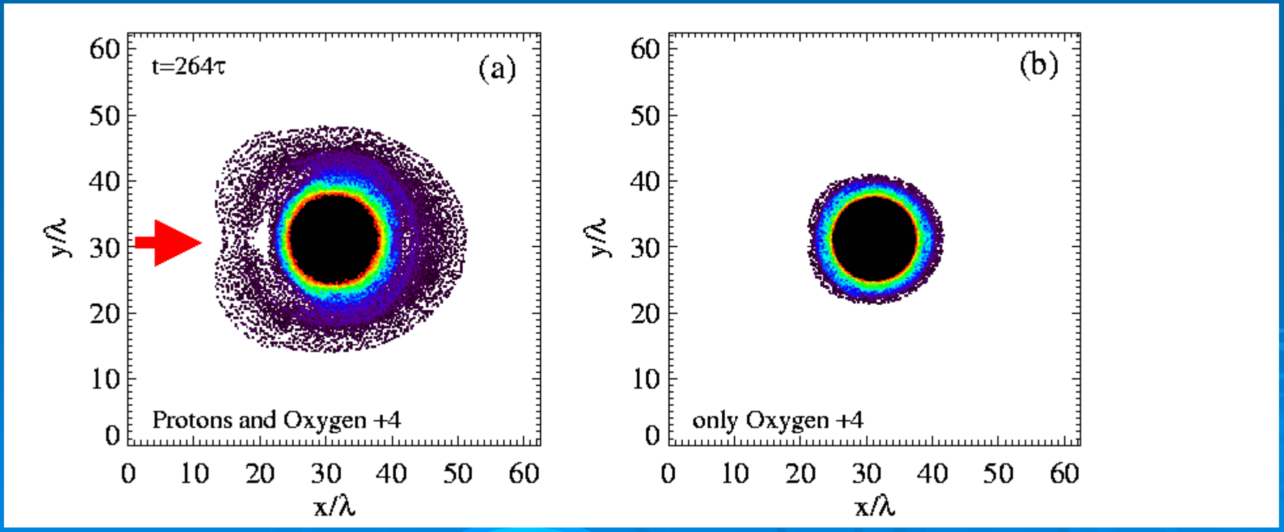

2d PIC simulations predict asymmetric beam expansion, but trends do not immediately agree with experiment

- Single-shot experiment predicts largest energy ions from 135 degrees
- Simulations of centrally irradiated targets:
  - predict paraxial ion fastest, 90deg slowest
  - Strong dip only in laser-irradiated side of target
  - Simulated energies larger than in experiment: charge states, ionization

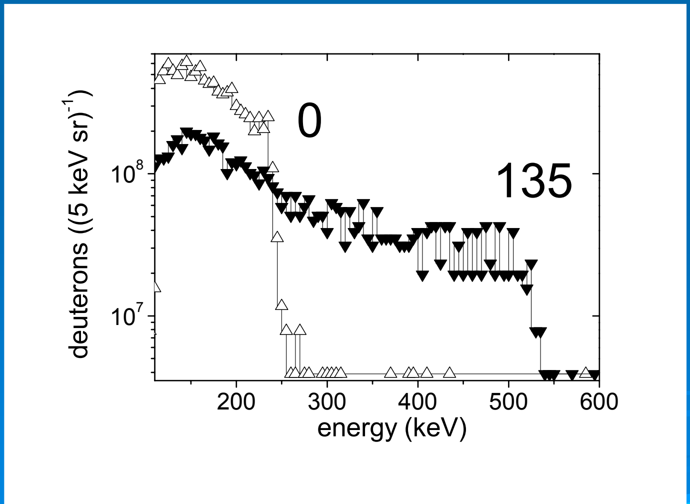

Exp: Single shot d-spectra, two-directional

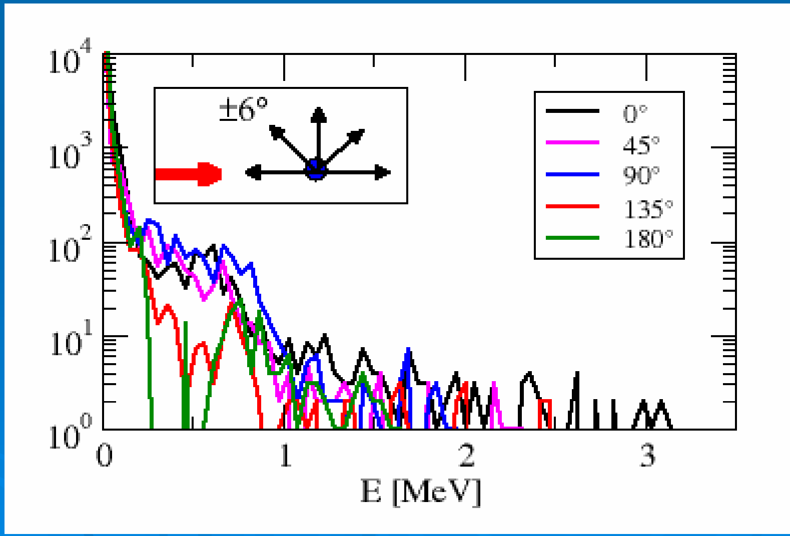

Sim: Directional p-spectra axial irraiation

135-asymmetry of ion acceleration can be explained with off-axial irradiation scenario

- Laser width similar to droplet diameter ➡ sensitive to exact position
- Simulation with non-central beam yields enhanced asymmetry
- Likely fluctuations in beam focus position during experiment can lead to observed asymmetry

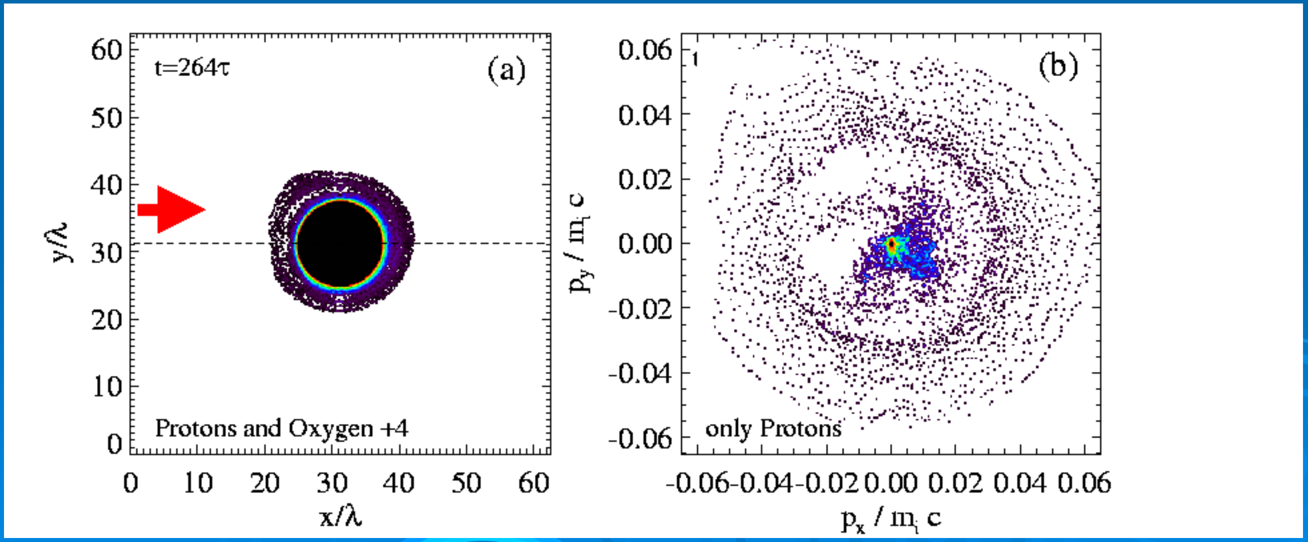

IV. b Laminarity of protons is destroyed by heavy ion species

- Longitudinal momentum space analysis in 2d PIC simulations: ‚loop‘ in proton trace [analogous to 1d results]
- Velocity at loop in proton spectrum coincides with oxygen front velocity
- Front-side gap is due to laser ponderomotive pressure

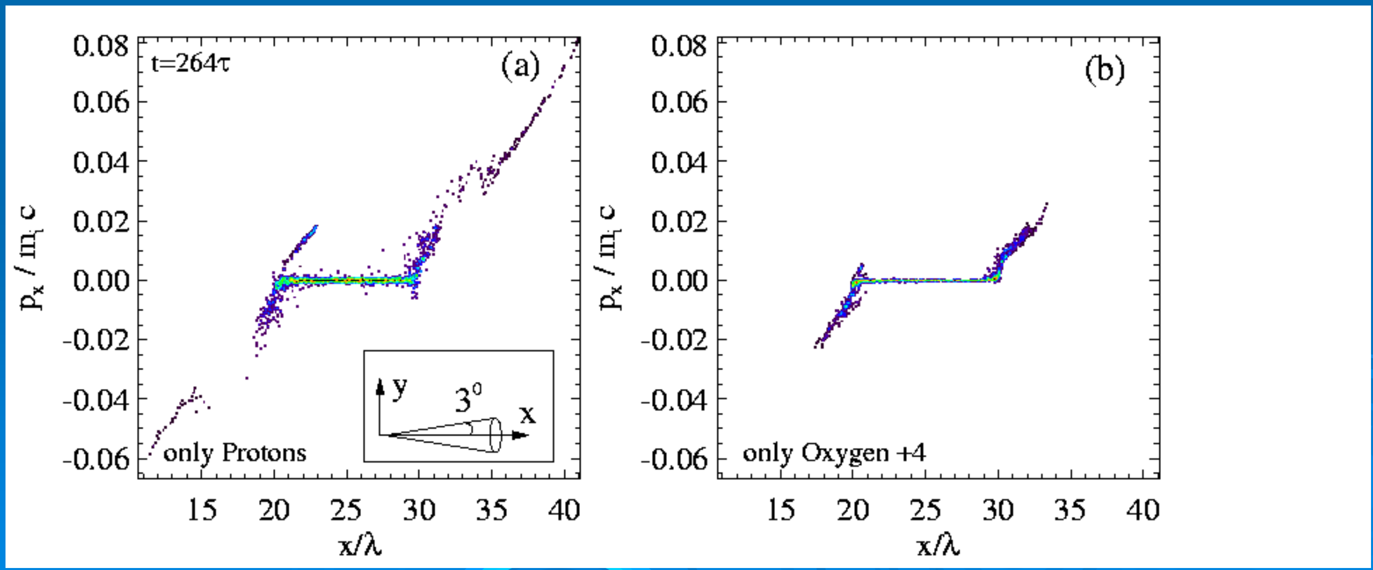

IV. c Ionization dynamics can be studied in PIC-MCC simulations with collisional and field ionization

- Field ionization via tunnel-process:
  - ADK, or Barrier Suppression Ionization
  - Electron born at rest
  - Ionization current j||E, such that jE=Ionization Energy

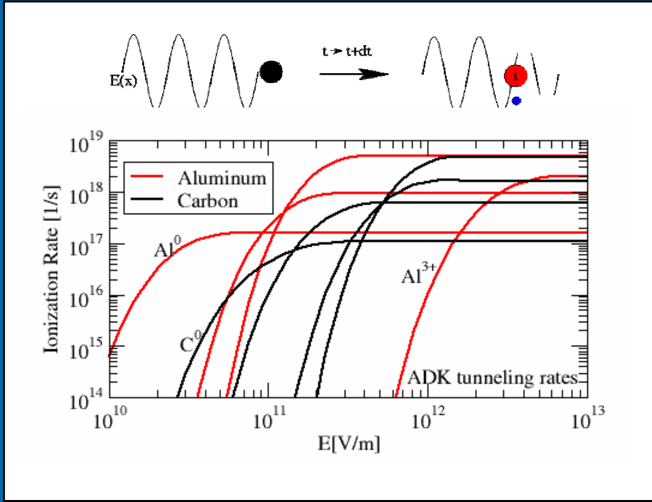

- Collisional Ionization:
  - Use tabulated x-sections or Lotz formula.
  - New electron born at rest
  - Ionization energy is taken from impact electron.
  - Work with maximum event rate, then distinguish processes randomly (“Null collision“ method)

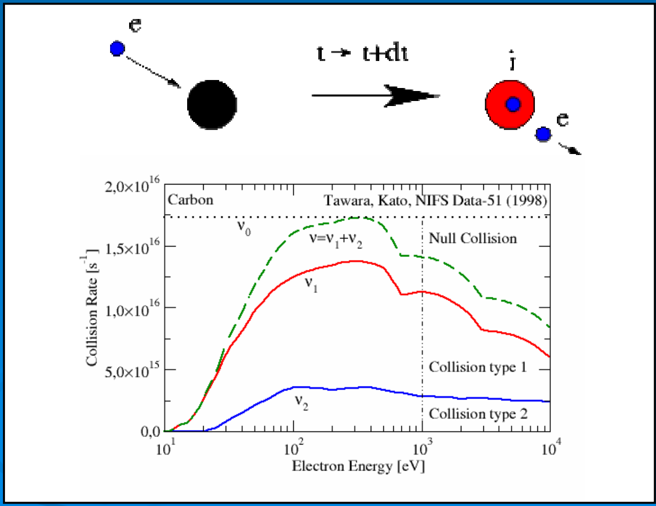

Ionization dynamics predicted by PIC-MCC agrees with max observed charge states found in experiment

- neutral D2O slab, 1mu thick
- Laser: 800nm, 1019W/cm2, 40fs
- full ionization dynamics:
  - field-,
  - collisional ionization,
  - binary collisions
- Dip in deuterium spectrum @ oxygen+6 expansion front
- O+6 on back by field ionization,
- Later collisional ionization in target
- Binary collisions do not matter

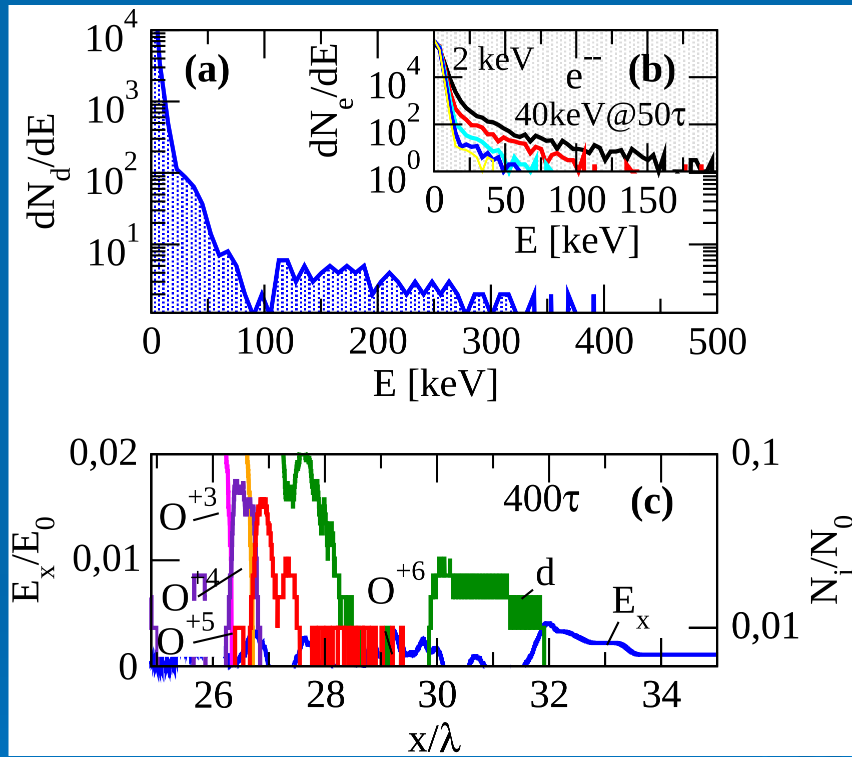

Summary / Outlook:

- Ultra-short pulse interaction with water droplets explained in terms of adiabatic multispecies expansion, in contrast to >300fs quasi-isothermal ion acceleration experiments
- Isothermal 2Te-model ruled out for ultra-short pulse ion acceleration, but useful for low-energy ions in long-pulse experiments
- Heavy ions leave imprint on proton spectra: laminarity, potential of protons as diagnostics [only small amount of heavy ions]
- Symmetry: in short pulses highest energy protons from 135deg
- High Charge states generation mechanism
- Droplets are clean and cheap targets for ion acceleration, but:
  - ultra-short pulses do not accelerate ions to maximum energies
  - Small targets, ASE large fluctuation in interaction conditions
- Requirements for predictive model:
  - precise understanding of field evolution for single-species
  - earlier models [Gurevich, Wickens+Allen] rely on isothermal condition

RADIATIVE EFFECT ON PARTICLE ACCELERATION VIA RELATIVISTIC ELECTROMAGNETIC EXPANSION

Koichi Noguchi, Rice University

Collaborators: E. Liang, Rice; K. Nishimura, LANL, S. Wilks, LLNL

- Introduction: γ-ray bursts and the acceleration mechanism
- Radiation Force
- Simulation Results: w/ or w/o Radiation
- Summary

UCRL-PRES-206187

Introduction: Gamma Ray Bursts

Temparature : Few keV~100 MeV
Duration : 2~200s
Frequency : 800>year

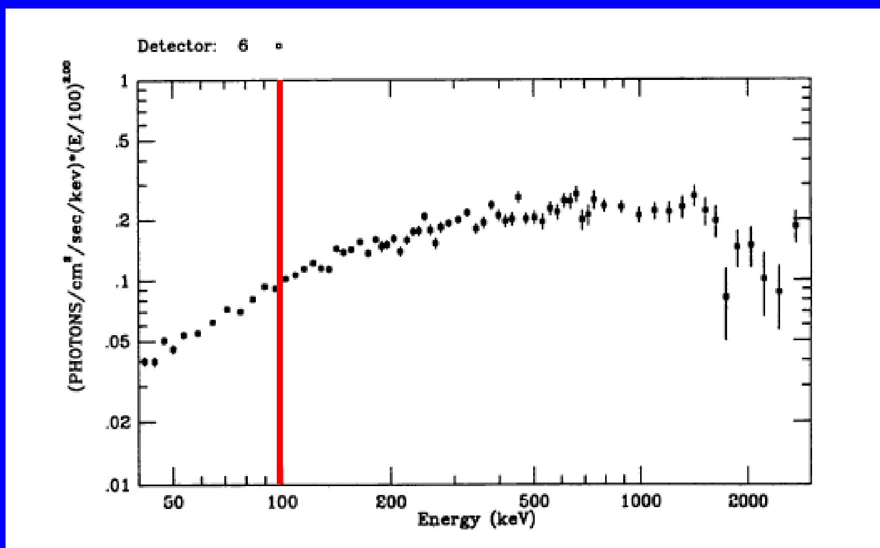

Schaefer et al., ApJS 92,285(1994)

Highly Non-Thermal
⇒PIC Simulation

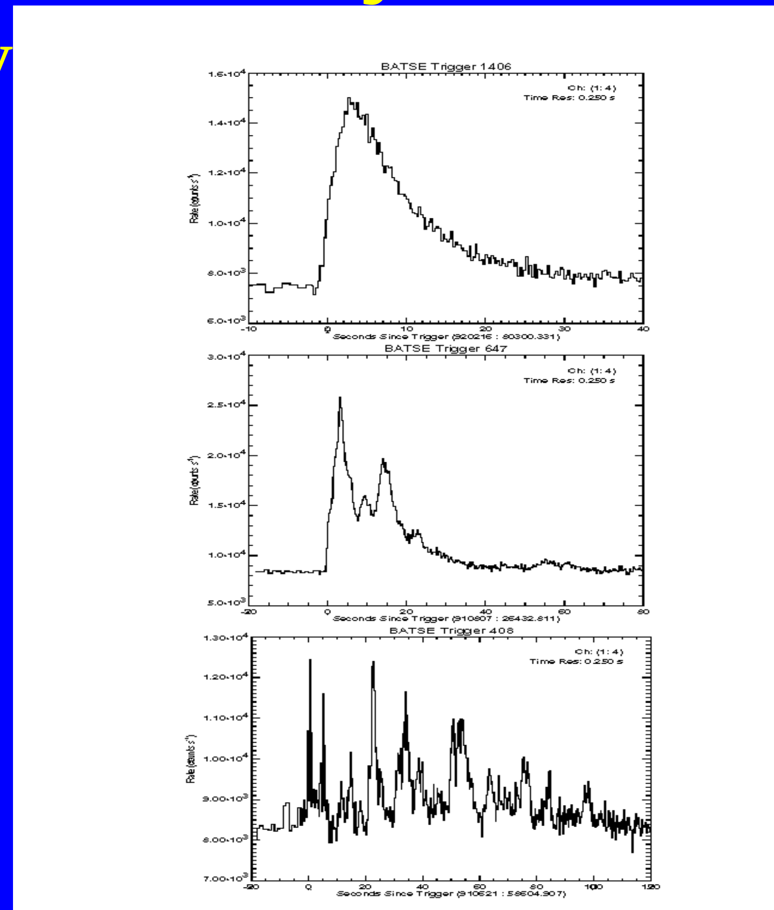

Sample BATSE GRB light curves

Extreme Time Profile Diversity

Our simulation regenerates unique signatures of GRBs including time profiles, spectra and spectral evolution

Introduction: Diamagnetic Relativistic Pulse Accelerator (DRPA)

DRPA may be relevant to prompt GRB emission and other impulsive high energy phenomena
DRPA may be testable in the laboratory with ultra-intense lasers

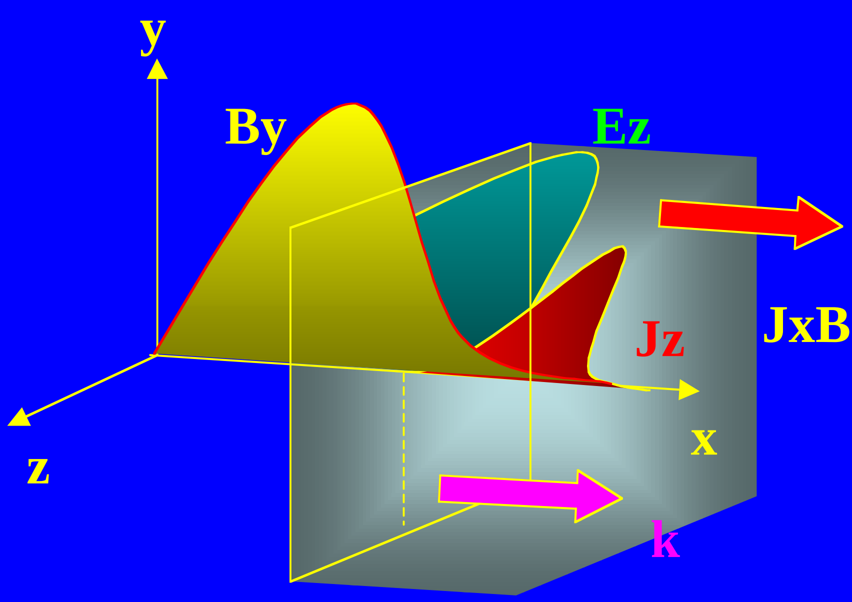

Ordinary Acceleration
$\gamma \sim (\Omega_e/\omega_{pe})^2$ **for e+e- plasma**

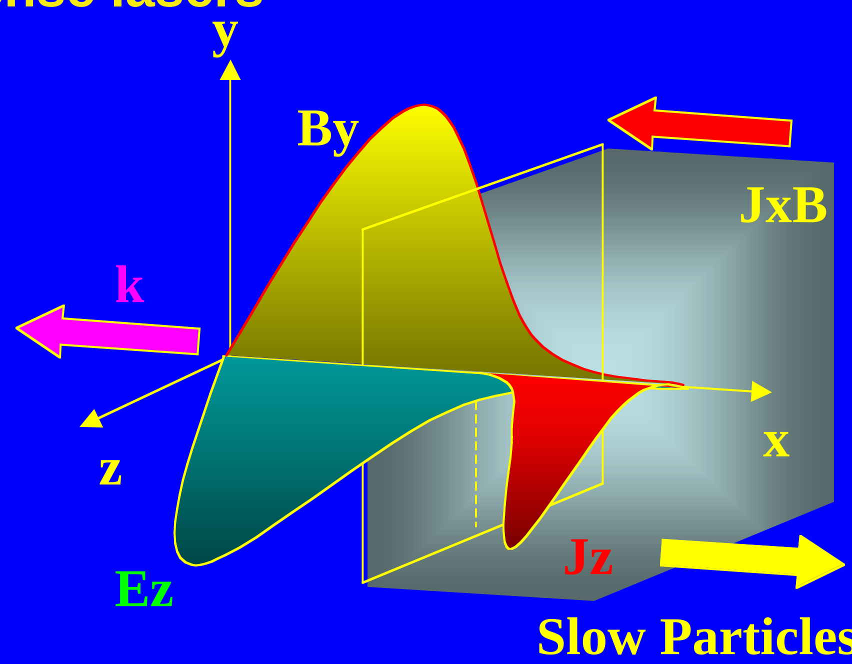

DPRA
$\gamma >> (\Omega_e/\omega_{pe})^2$ **for fast particles**

Non-radiative case I: Slab Geometry

Liang et al., Phys. Rev. L(2003)

Fireball, By,ρ= const.

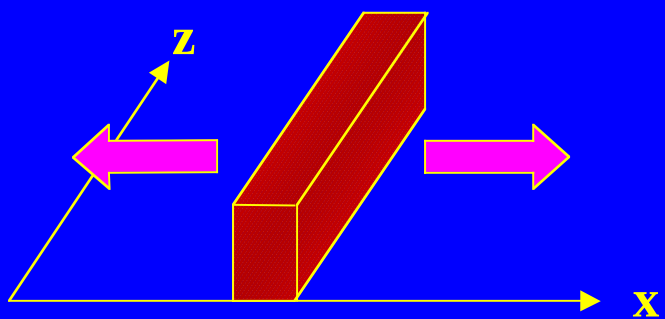

As the EM pulse pulls trailing plasma, it continues to shed slow tail particles and focus its acceleration on fewer and fewer fast particles.

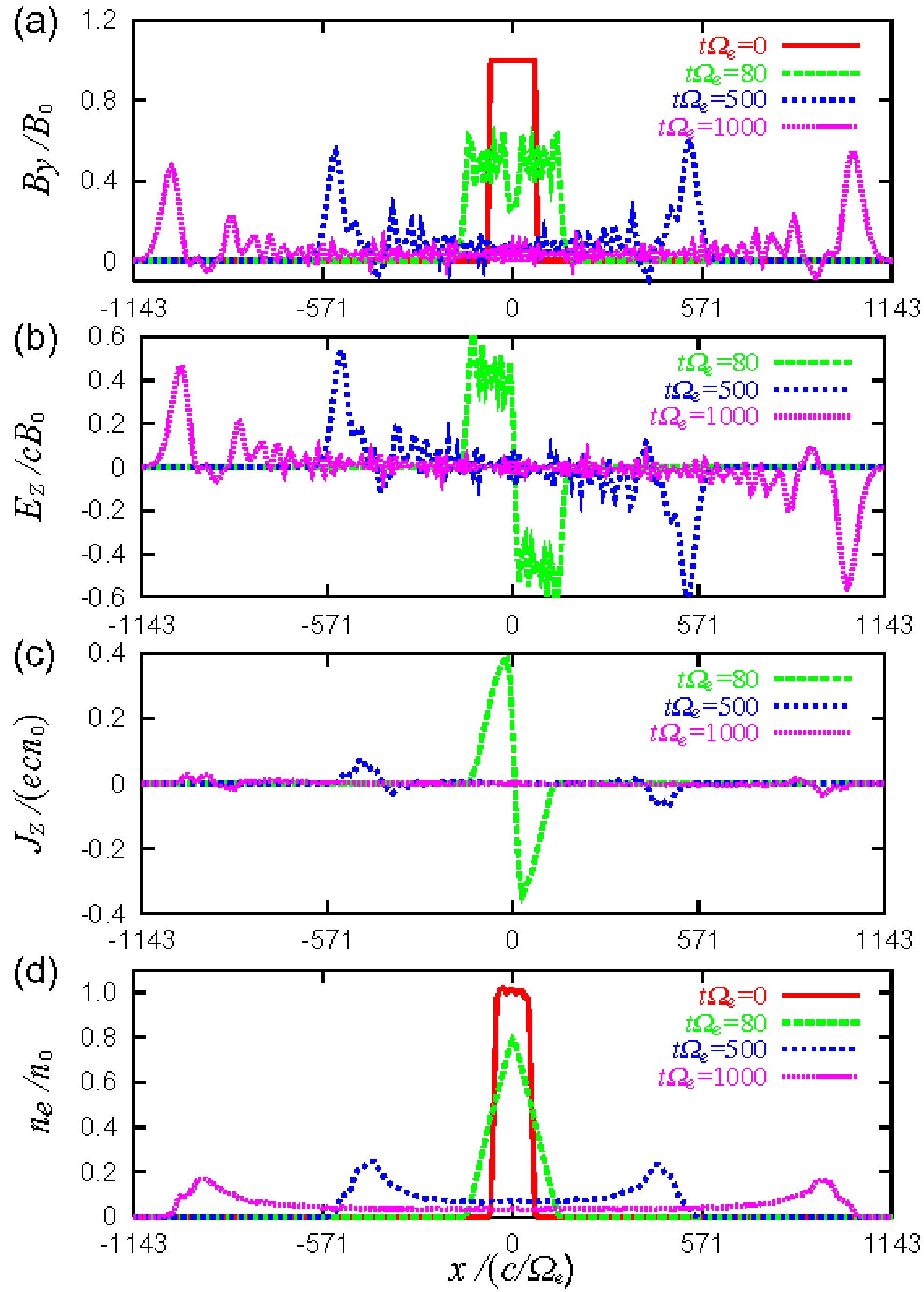

Radiation Force

Non-radiative Case : Energy is distributed only to field and particles

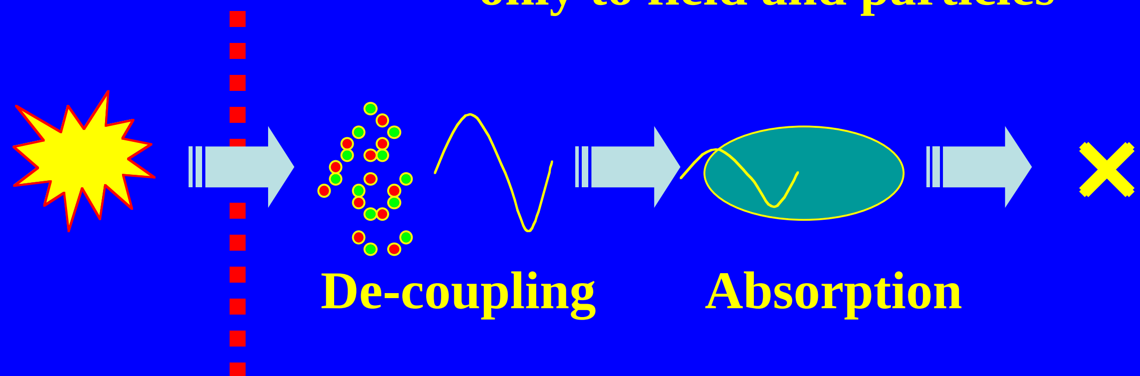

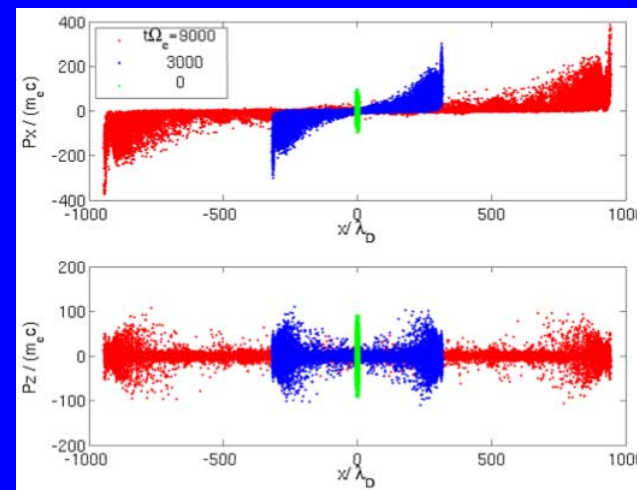

Radiative Case : Energy is transferred to field, particles and radiation

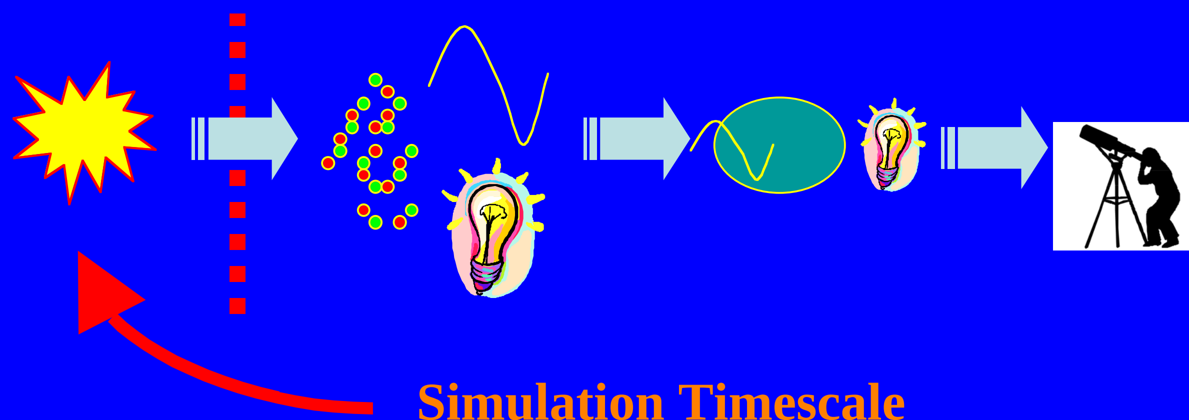

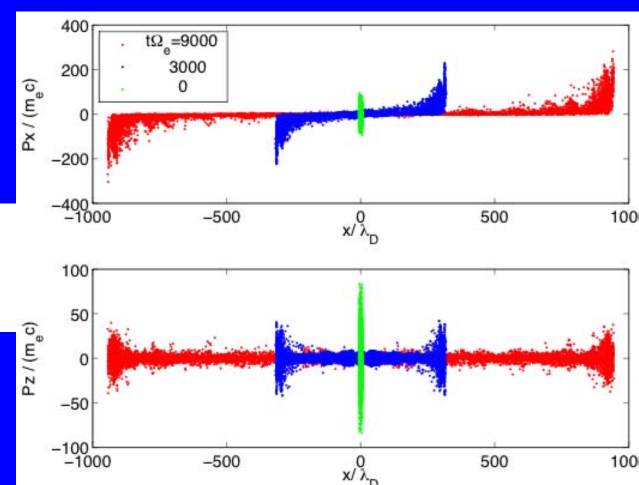

Simulation Timescale

Radiation Force(II)

(Landau & Lifshitz, P. 213)

Equation of Motion $$\frac{d\mathbf{p}}{dt} = \frac{e}{m}\left[\mathbf{E} + \frac{\mathbf{v}}{c}\times\mathbf{B} + \mathbf{f}\right]$$

Assumption: $$\mathbf{f} << \mathbf{E} + \mathbf{v}/c\times\mathbf{B}$$

where
$$\mathbf{f} = \frac{2}{3}\frac{e^3}{mc^3}\left[(1-\frac{v^2}{c^2})^{-1/2}\left\{\left(\frac{\partial}{\partial t} + \mathbf{v}\cdot\nabla\right)\mathbf{E} + \frac{\mathbf{v}}{c}\times\left(\frac{\partial}{\partial t} + \mathbf{v}\cdot\nabla\right)\mathbf{B}\right\}\right.$$

Ponderomotive Force Acceleration

$$+\frac{e}{mc}\left(\mathbf{E}\times\mathbf{B} + \frac{1}{c}\mathbf{B}\times(\mathbf{B}\times\mathbf{v}) + \frac{1}{c}\mathbf{E}(\mathbf{v}\cdot\mathbf{E})\right)$$

$$\left.-\frac{e}{mc^2}\frac{\mathbf{v}}{1-v^2/c^2}\left\{\left(\mathbf{E} + \frac{\mathbf{v}}{c}\times\mathbf{B}\right)^2 - \frac{1}{c^2}(\mathbf{E}\cdot\mathbf{v})^2\right\}\right]$$

Compton scattering

Normalization Constant for Overall Radiation

$$k = \frac{r_e\Omega_e}{c} = 1.64\times10^{-16}B[gauss]$$

We choose k=10^{-3} in simulations

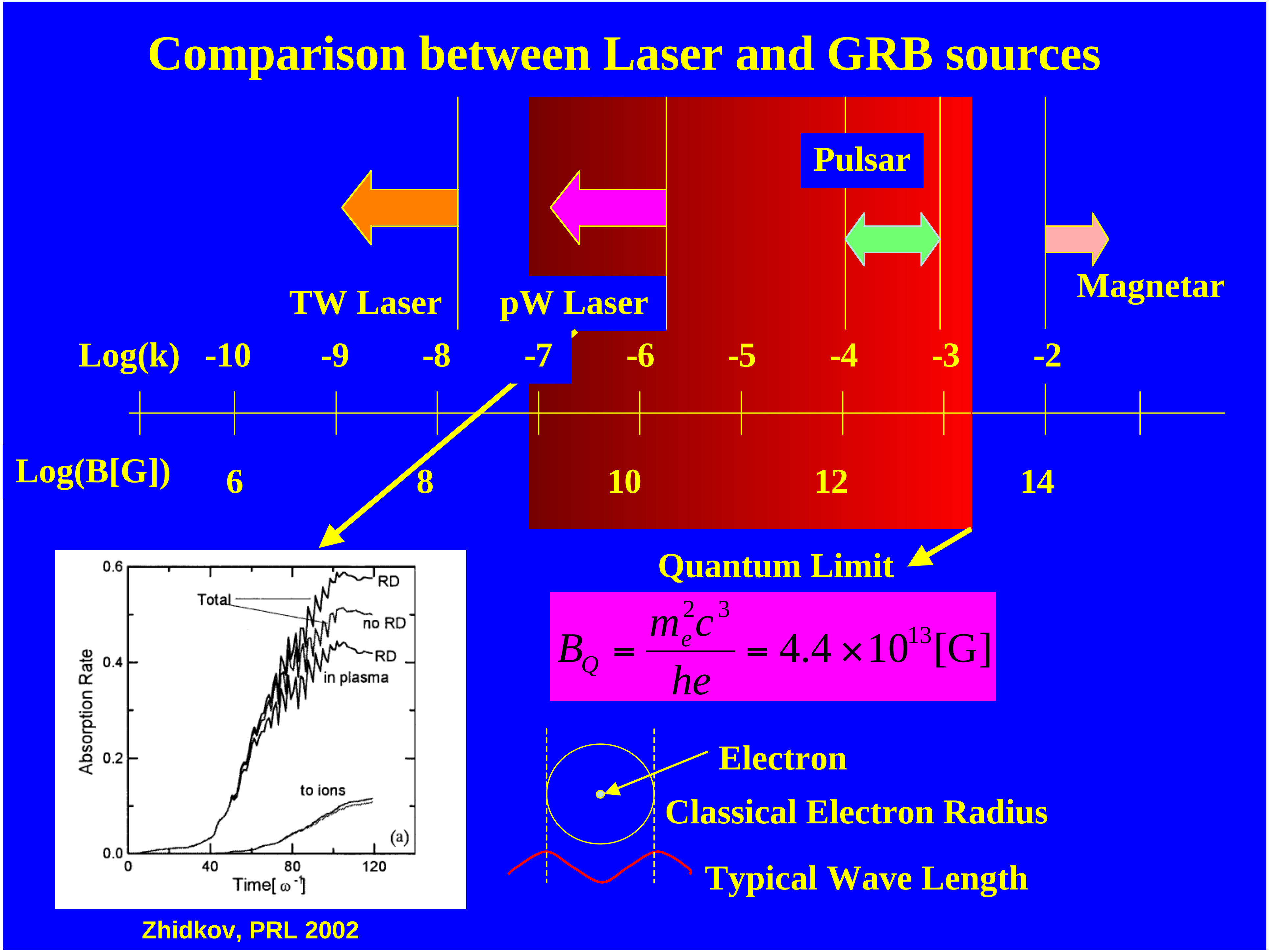
Comparison between Laser and GRB sources
Pulsar
TW Laser
pW Laser
Magnetar
Log(k) -10 -9 -8 -7 -6 -5 -4 -3 -2
Log(B[G]) 6 8 10 12 14
Quantum Limit
$B_Q = \frac{m_e^2 c^3}{he} = 4.4 \times 10^{13}[G]$
0.6
0.4
0.2
0.0
Absorption Rate
0 40 80 120
Time[ω⁻¹]
Total
RD
no RD
RD
in plasma
to ions
(a)
Electron
Classical Electron Radius
Typical Wave Length
Zhidkov, PRL 2002

Non-radiative case II: Cylindrical Geometry

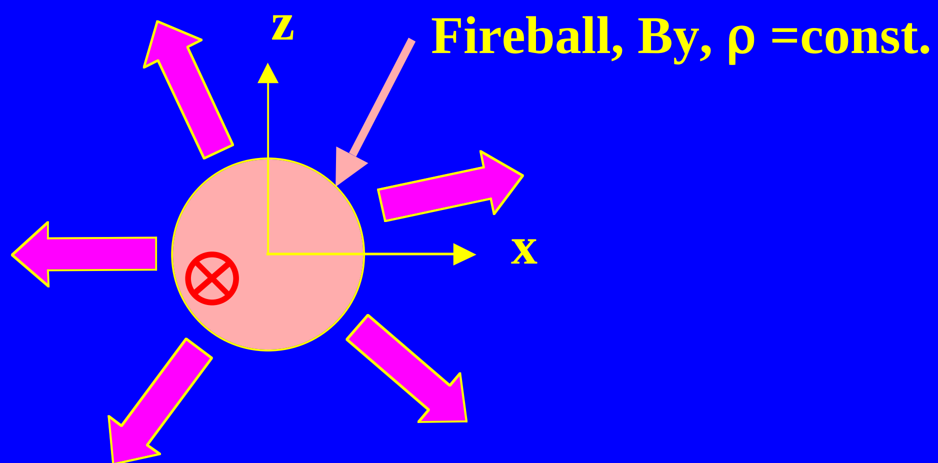

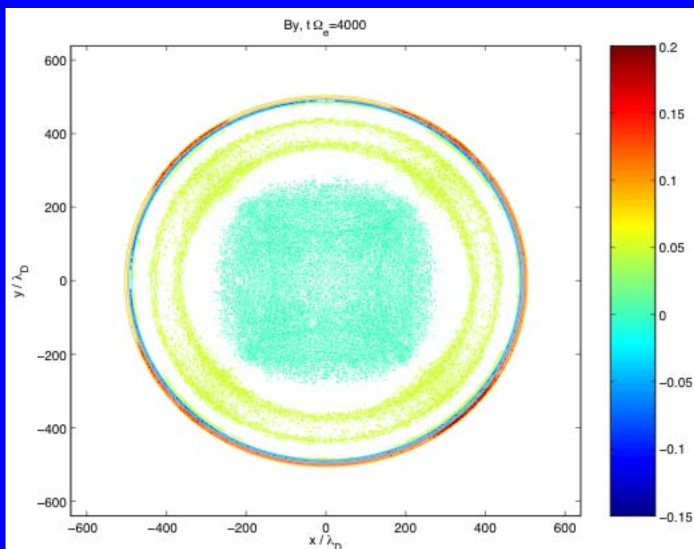

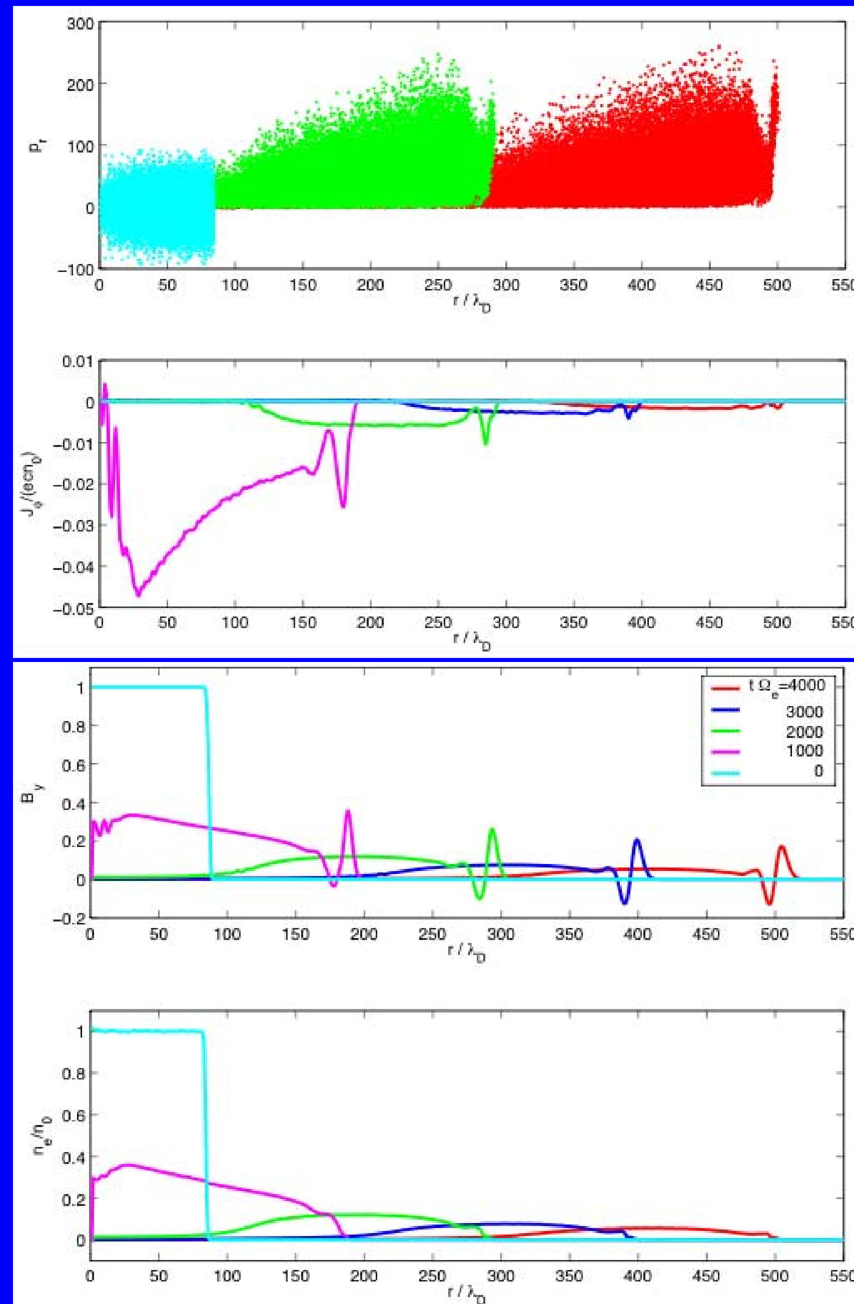

Radiative Case: Particle Acceleration

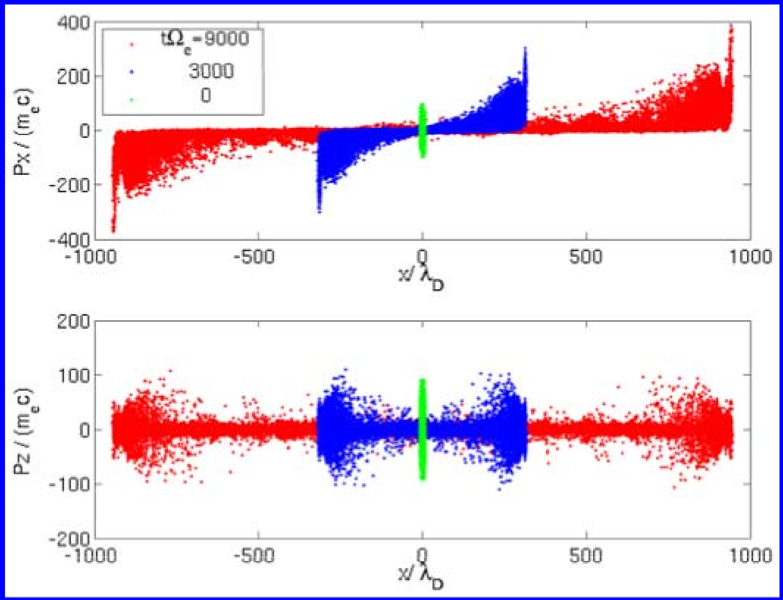

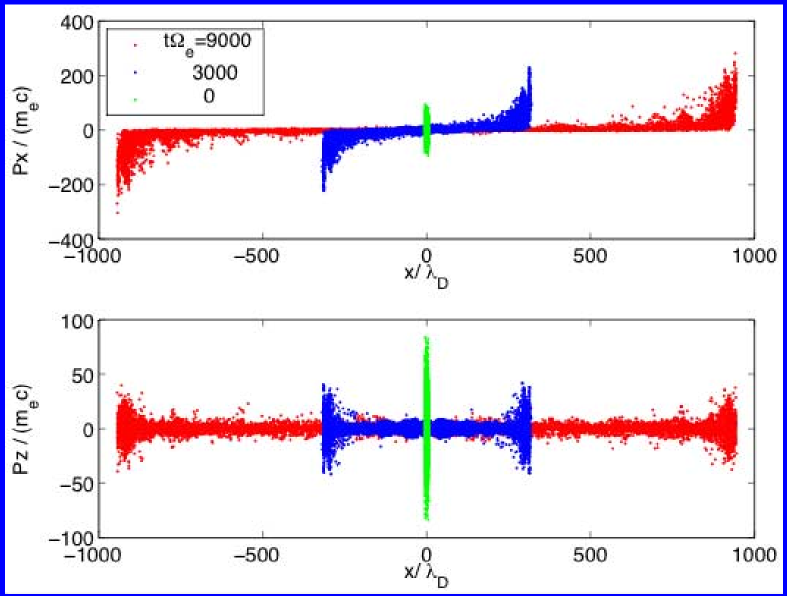

Non-radiative

Radiative

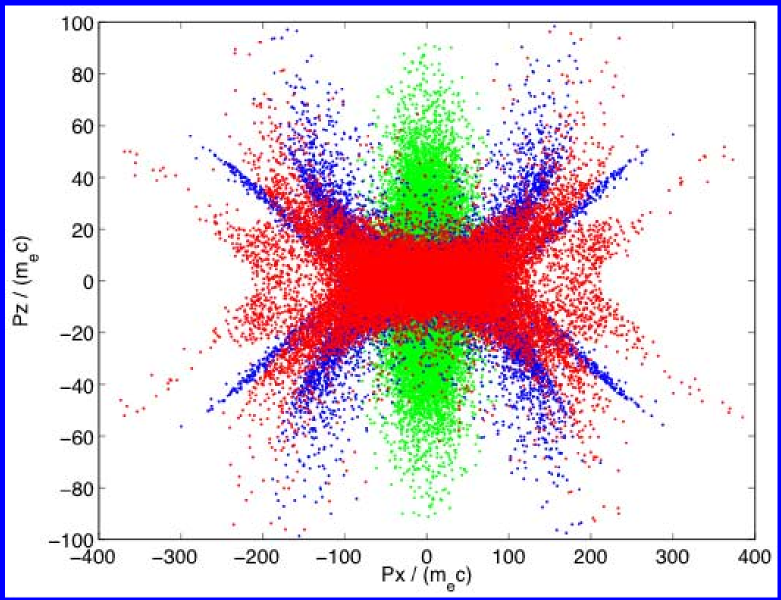

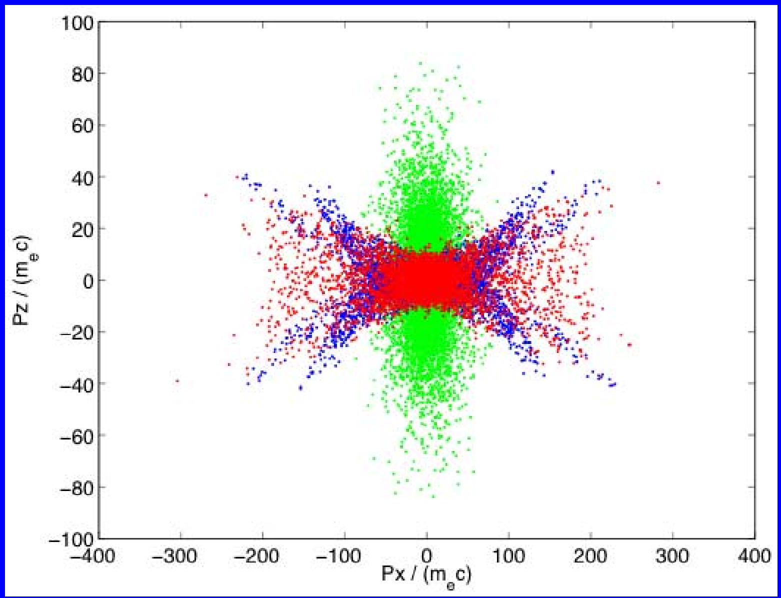

Radiative Case: Energy Conversion

Non-radiative: Dipole Formula

$$P_{DF} = \frac{2e^2}{3m^2c^3}\left(F_{//}^2 + \gamma^2 F_{\perp}^2\right)$$

Radiative: Landau-Lifshitz

$$P_{LL} = -\mathbf{v}\cdot\mathbf{f}_{rad}$$

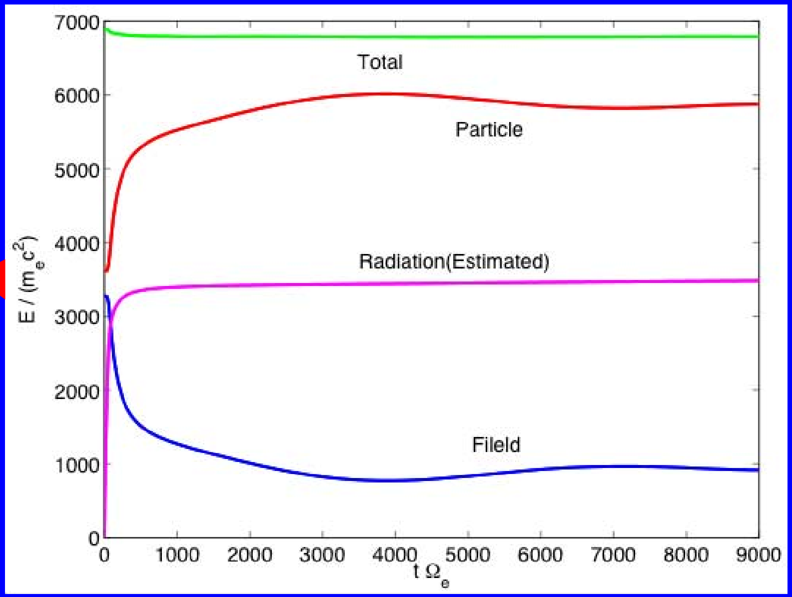

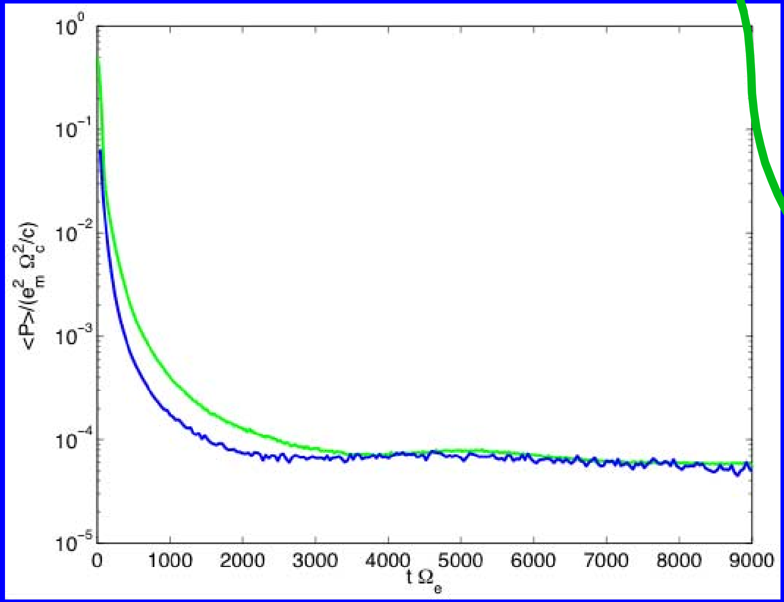

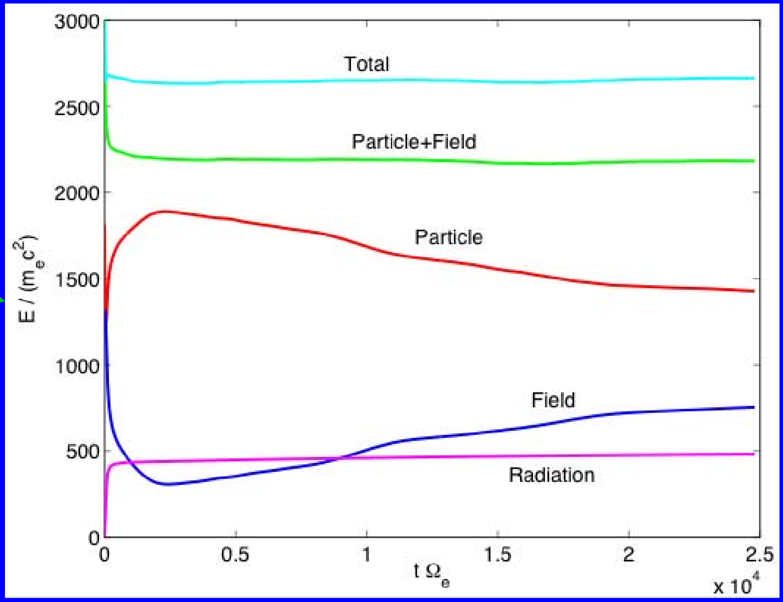

Summary

- The sudden expansion of magnetic-dominated e^+e^- plasmas leads to robust particle acceleration
- Radiation force is self-consistently solved, which irradiate most of energy in the direction perpendicular to the wave front.
- DRPA is still robust even with radiation.

Generation and Transport of Energetic Particles in Short-Pulse High-Intensity Laser Plasma Interactions.

Presented to:

34th Annual Anomalous Absorption Conference

B. F. Lasinski, C. H. Still, A. B. Langdon, R. P. J. Town, M. Tabak, D. E. Hinkel, and W. L. Kruer

AX Division, Lawrence Livermore National Laboratory

May 3 –7, 2004.

This work was preformed under the auspices of the U. S. Department of Energy by the University of California, Lawrence Livermore National Laboratory under contract No. W-7405-Eng-48.

Modeling with our MPP PIC code, Z3, provides electron source functions and contact with short-pulse experiments at high laser intensity.

- Current work centers on role of preformed plasma in simulations including both underdense and overdense plasma.
  - — Density profiles come from LASNEX simulations of the laser prepulse onto the target.
  - — One product of Z3 simulations is electron source functions for transport modeling with the implicit code LSP (D. R. Welch *et al*, Nucl. Inst. Meth. Phys. Res. A242, 134 (2001)). Closer linking of Z3 and LSP is in progress.
- Z3 simulations at oblique angles of incidence which more closely match experimental conditions are underway.
- New diagnostics for monitoring heated electrons and optical emissions are now in use.
- This plan requires 3D and large 2D simulations which are enabled by access to the most powerful MPP computers. (Z3 sometimes serves as a computer testbed).

In LSP simulations of generic electron transport experiments, hot electron beam parameters are the biggest uncertainty.

- This target is based on the experiments performed by Martinolli et al[1] on the LULI and Vulcan laser.

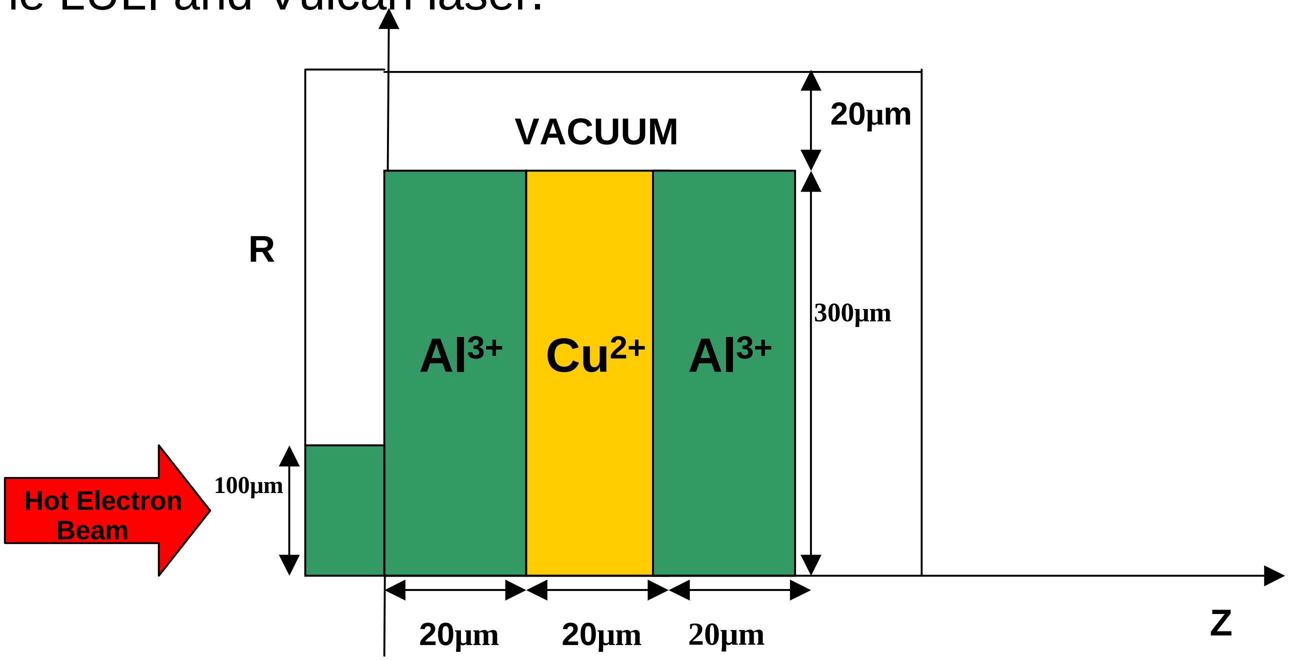

- 27J of hot electrons in a 1ps pulse with Beg scaling [T_{hot} (MeV) $=0.1(I\lambda^2/(10^{17}W/cm^2\mu m2))^{1/3}$] and a thermal spread of 300 keV injected into a 100µm Al^{3+} plasma.

[1]E. Martinolli, et al., Laser & Part. Beams 20, 171 (2002).

LSP modeling of generic electron transport experiments is successful.

- The temperature was obtained by post-processing the **LSP** energy data at the rear surface with a realistic equation of state.
- The **LSP** calculation matches the measured T_e pattern at the rear surface of the target.

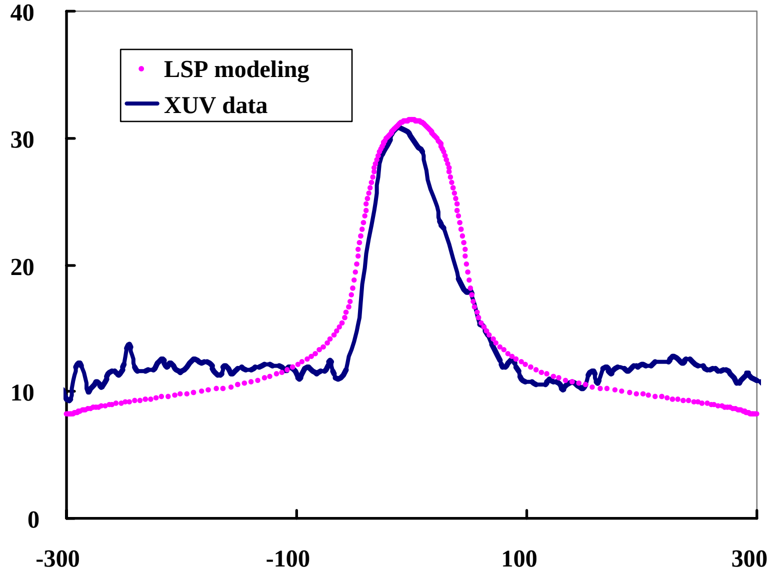

Linking of Z3 and LSP is underway to provide PIC based source functions for transport modeling.

Here report on 3 simulations using Z3 at incident intensity 10^{19} W/cm^2 for 1 μm light.

Z3 simulation geometry:

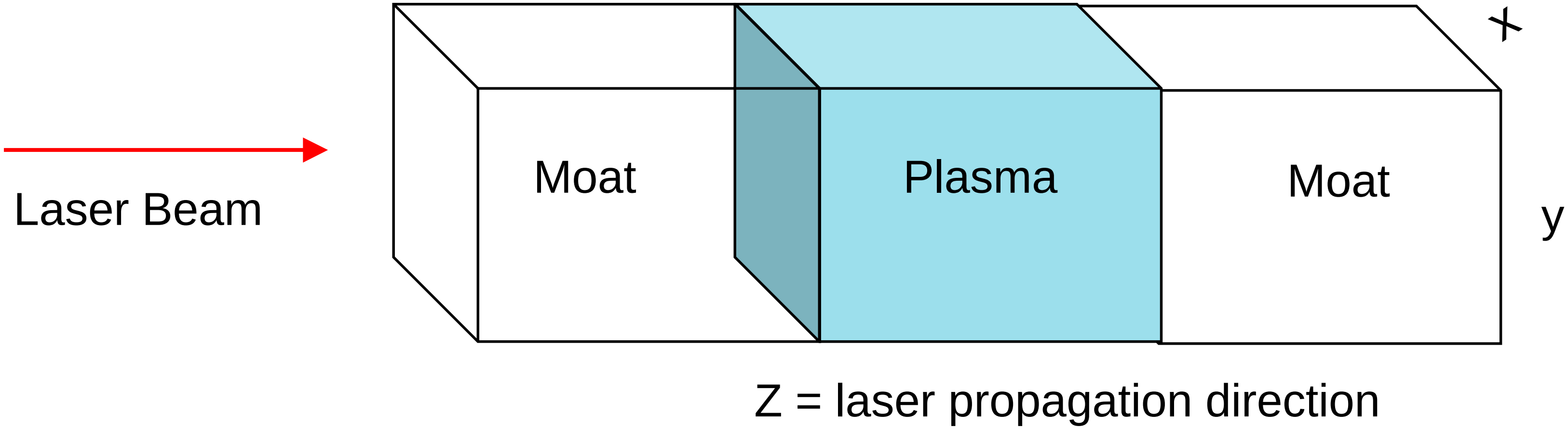

- Boundary conditions are "open" in z and periodic in the transverse dimensions.

- These simulations are 2D in the (x,z) plane. 3D simulations are presented in C. H. Still *et al*, "Modeling of Short Pulse High Intensity Laser-Plasma Interactions in 3D Simulations," this conference.

- Three cases: CH target, Au target, and oblique incidence onto an overdense plasma. All laser pulses have a 150 fs rise time and are linearly polarized in the simulation plane (E_x, B_y). Simulations have 2 species: electrons and ions.

Density profiles for Z3 simulations are obtained from LASNEX modeling of the prepulse onto the target.

Case 1: CH target

Density contours after 10 mJ absorbed by CH target:

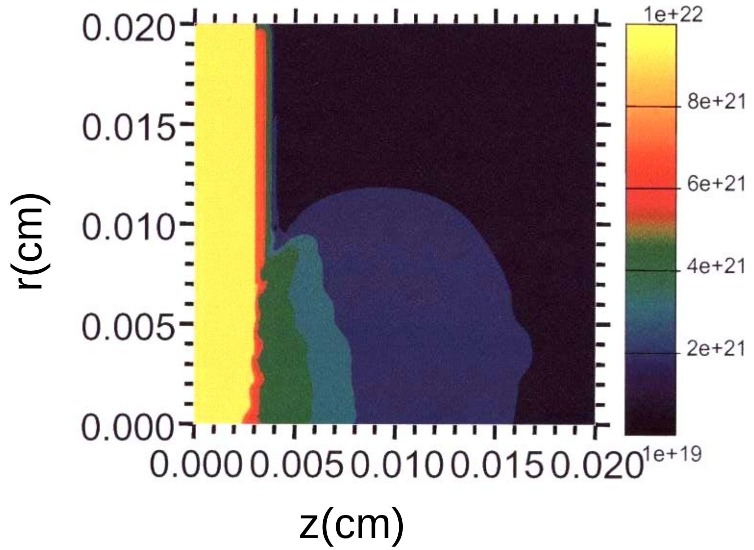

Lineout along the z axis provides density profile for **Z3**:

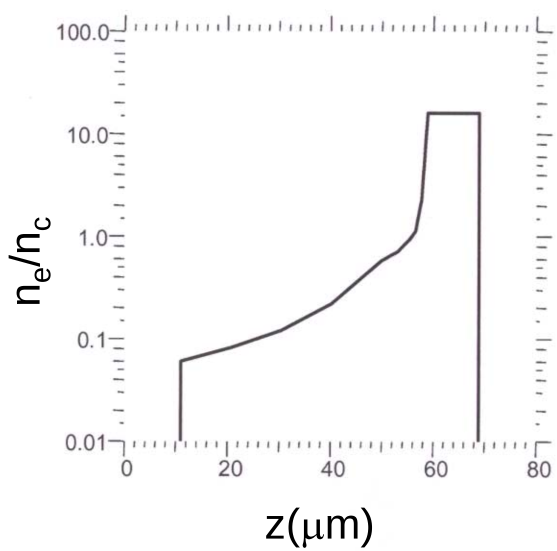

Simulation box is 768 × 2560 cells with 300 × 10^6 particles per species.

Beam focuses and undergoes deflection in the underdense plasma.

Case 1: CH target

As part of the Z3 diagnostics suite, we apply a low pass temporal filter to fields and fluxes to highlight the low frequency component. These filtered quantities have the subscript s. Here we plot the filtered Poynting flux.

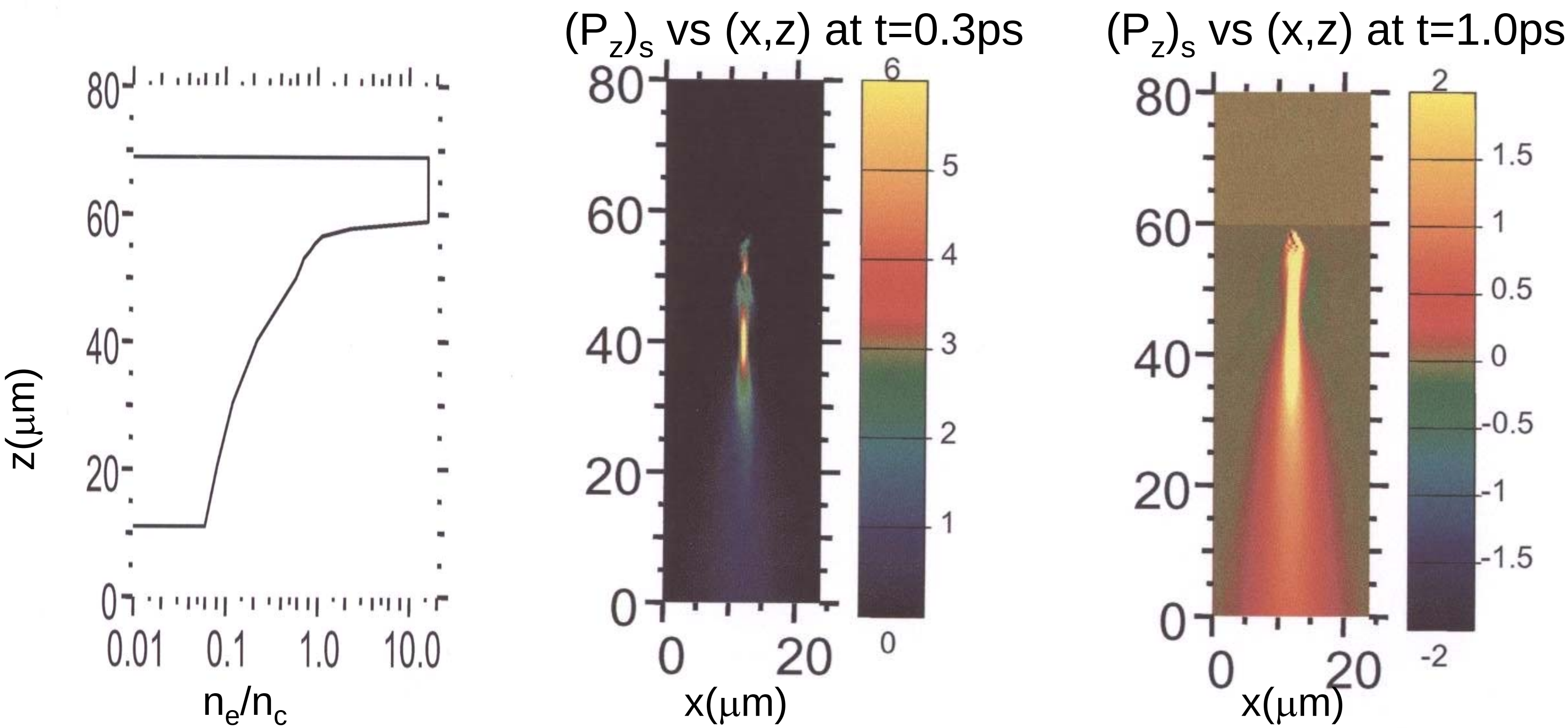

There is significant hot electron production in the underdense plasma

Case 1: CH target

Plot the (x,z) positions of electrons with $u_z > 0$ and energies > 10 MeV

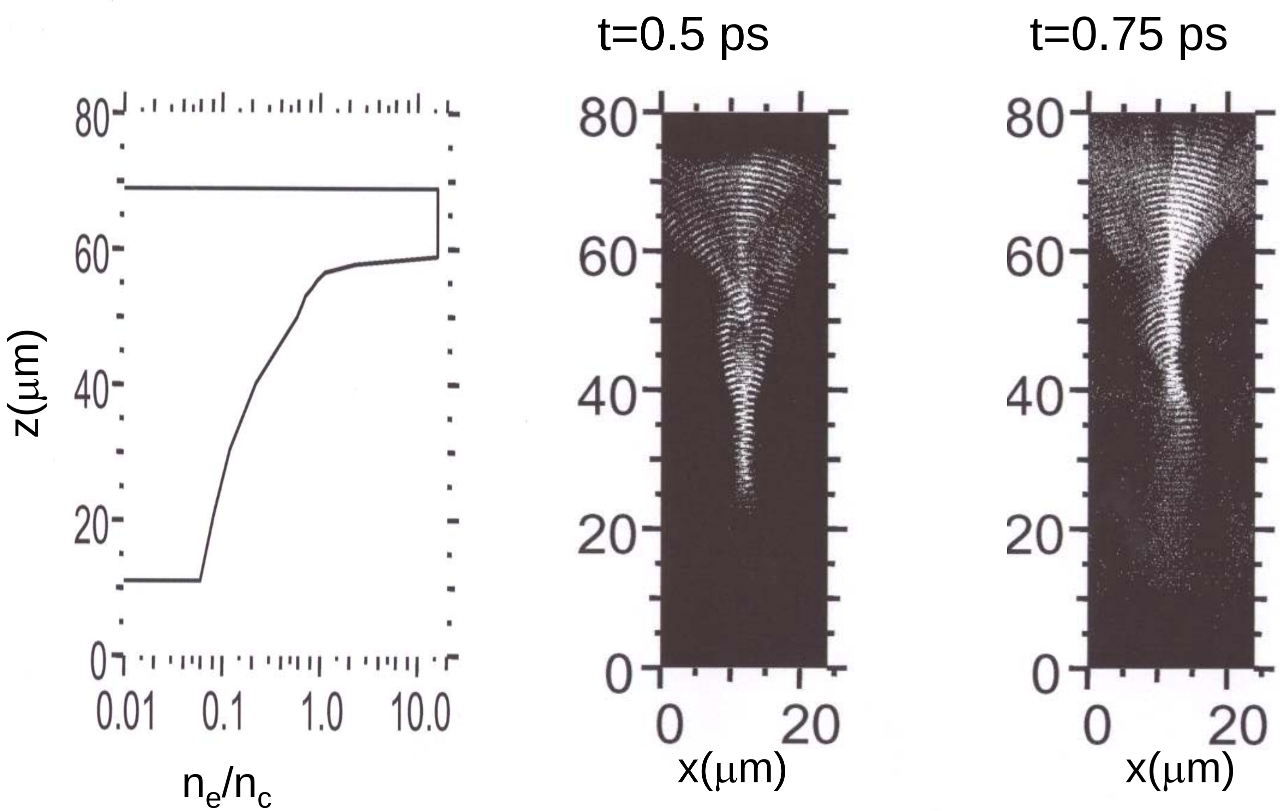

Electron bursts in the underdense region are once per plasma period.

Particle trajectories are consistent with the beam deflection.

As expected, there is less underdense plasma from a gold target.

Case 2: Au target

Density contours after 10 mJ absorbed by Au target:

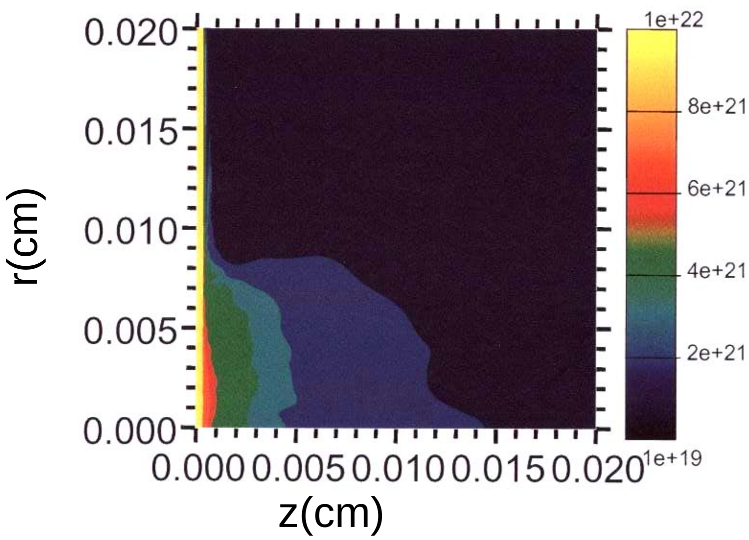

Z3 density profile is steeper than in CH case.

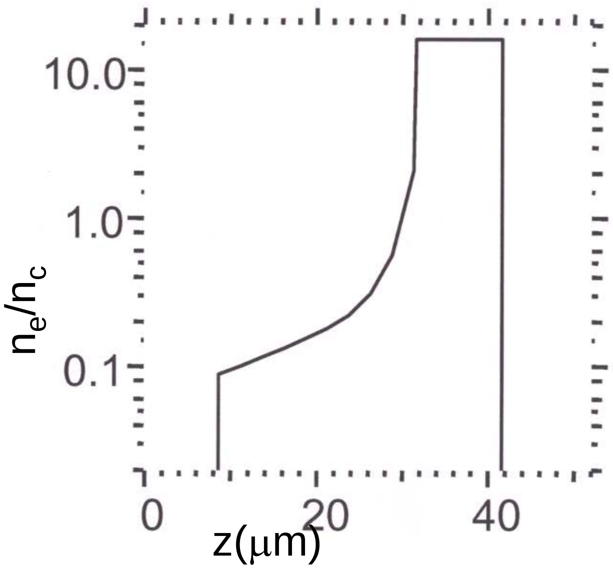

Simulation box is 768 ×1664 cells with 300 ×10^6 particles per species.

Again, beam focuses and undergoes deflection in this smaller underdense plasma.

Case 2: Au target

Plots of the filtered Poynting flux vs (x,z). Note the complicated interaction at the relativistic critical surface.

$(P_z)_s$ vs (x,z) at t=0.25ps

$(P_z)_s$ vs (x,z) at t=0.725ps

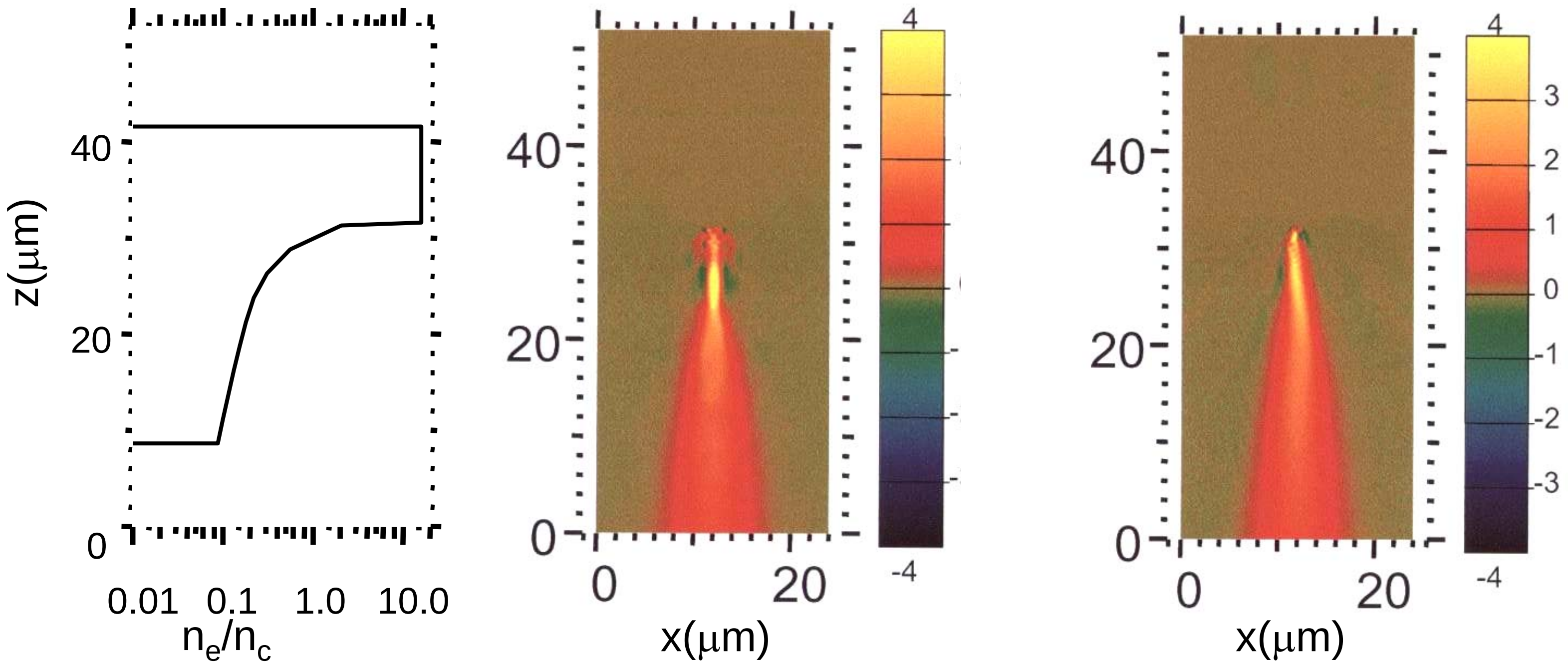

A channel forms in the underdense plasma.

Case 2: Au target

Plot of ion density (with maximum suppressed) vs (x,z) at t=0.250 ps

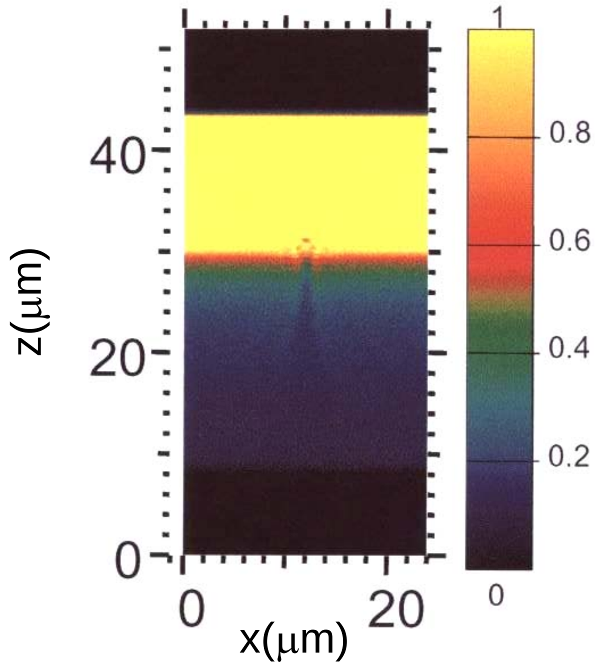

Plot of $(B_y)_s$ vs (x,z) at t=0.250 ps

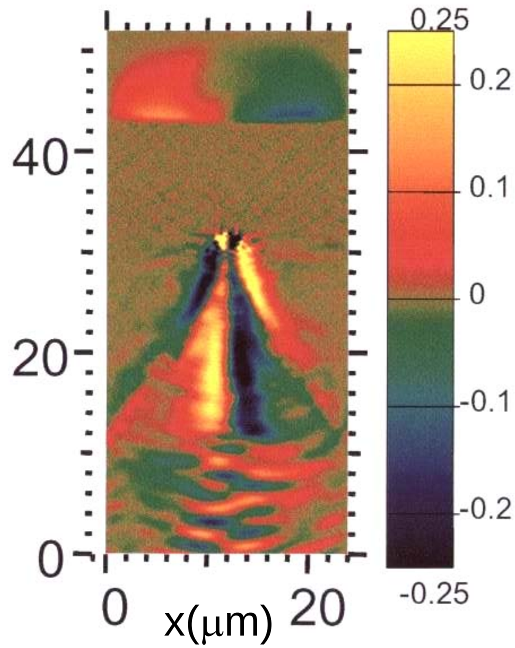

Electrons in the underdense plasma are going forward. Also find expected Weibel-like structure at the relativistic critical surface.

Energetic electron production is very complex.

Case 2: Au target

(x,z) positions of electrons with $u_z > 0$ and energy > 5 MeV at t = 0.25 ps

(x,z) positions of electrons with $u_z > 0$ and energy > 15 MeV at t = 0.4 ps

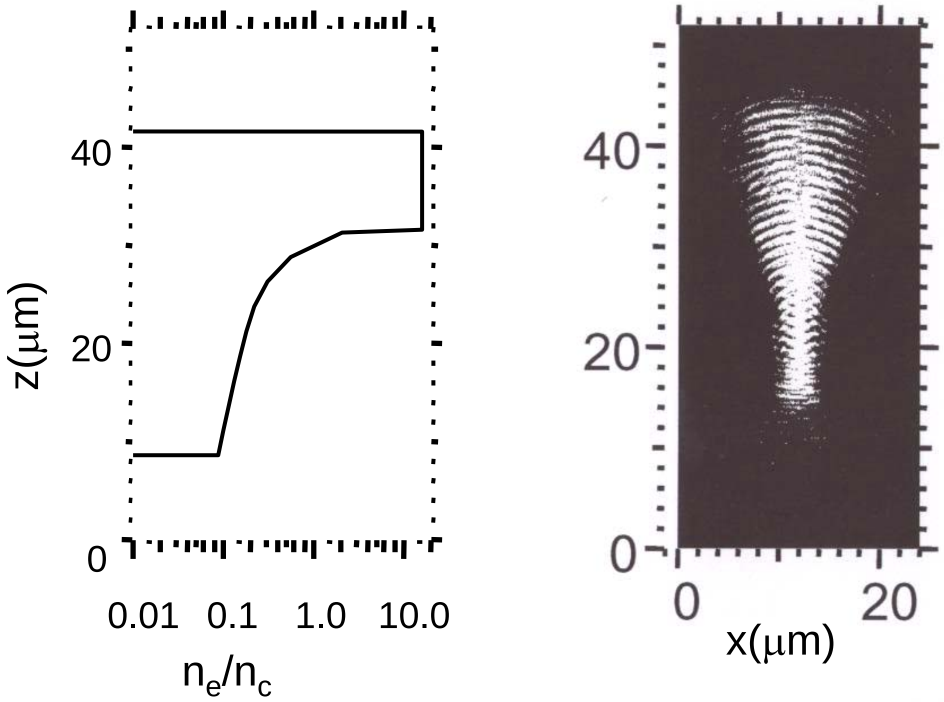

At oblique incidence, the reflected light distribution broadens in time.

Case 3: 30º angle of incidence

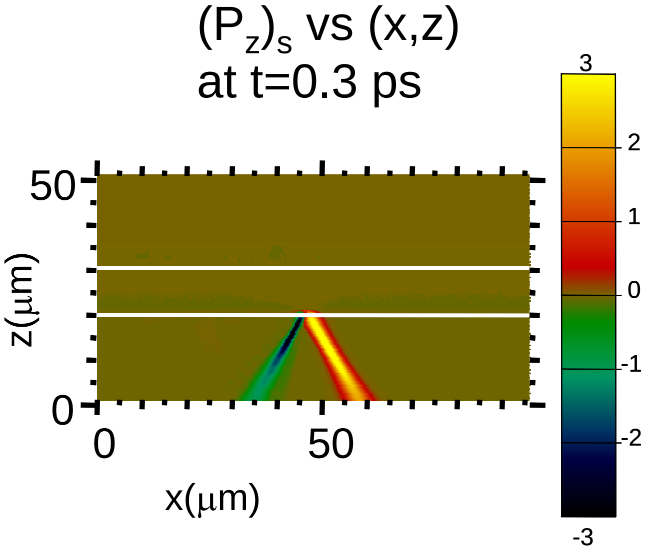

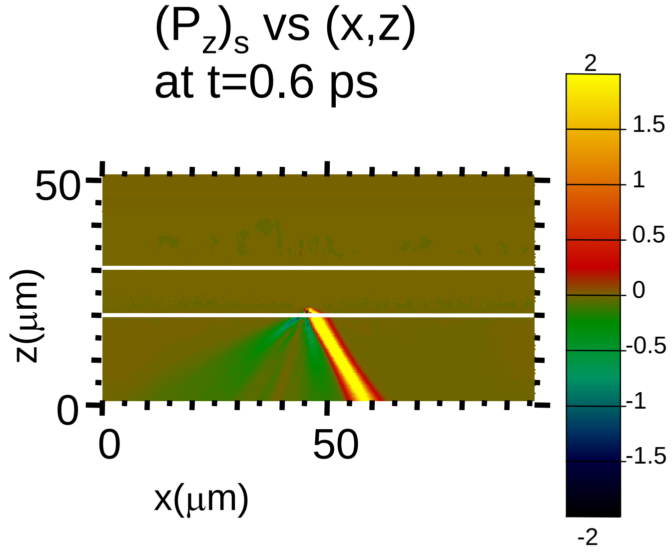

White lines indicate original position of 16 n_c plasma slab; there is no underdense plasma here.

Simulation box is 3072 ×1640 cells with 720 $\times 10^6$ particles per species.

Histories of outgoing light at probe positions in the incident plane illustrate the broadening of the reflected light distribution.

Case 3: 30º angle of incidence

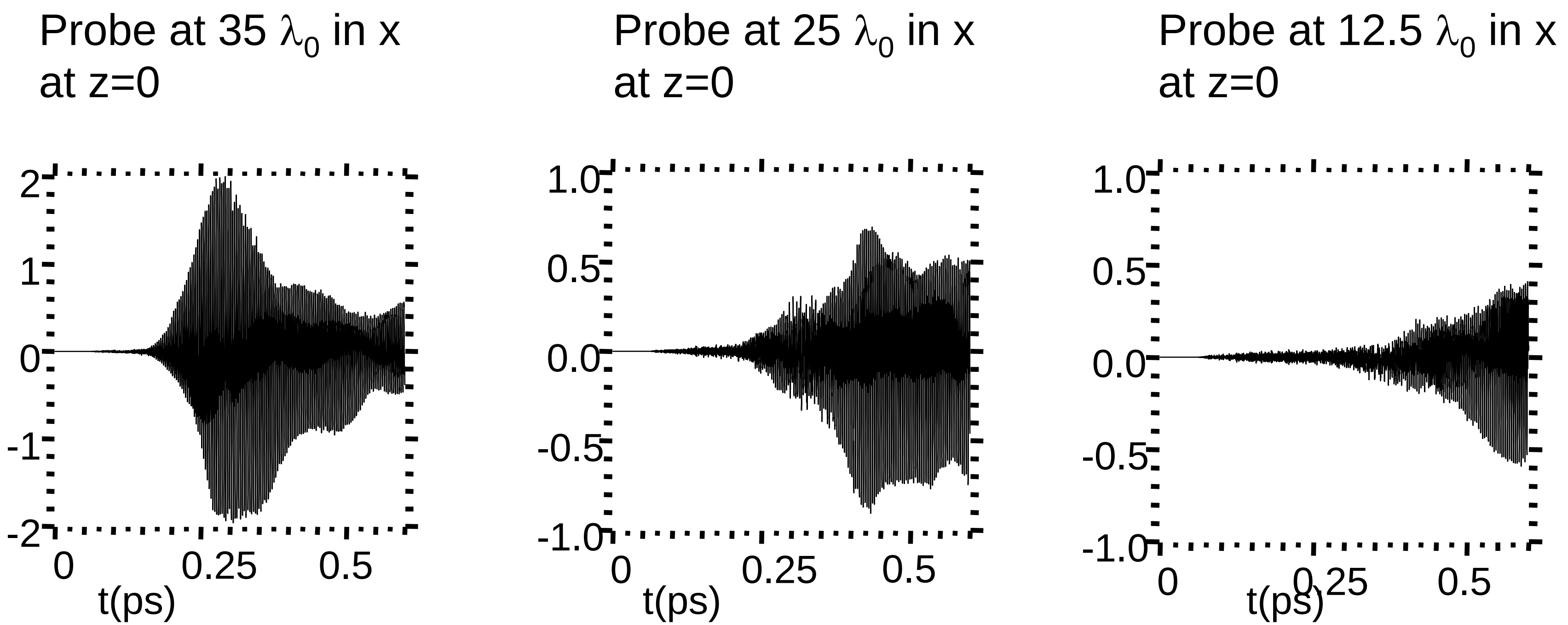

Spectral analysis of the reflected light is presented by A. B. Langdon *et al*, "Spectra of Scattered and Emitted Light in Modeling of High Intensity Laser Plasma Interactions," this conference.

Bursts of energetic electrons move away from the interaction region at very oblique angles

Case 3: 30º angle of incidence

(x,z) positions of electrons with $u_z > 0$ and energy > 5 MeV at t=0.3 ps.

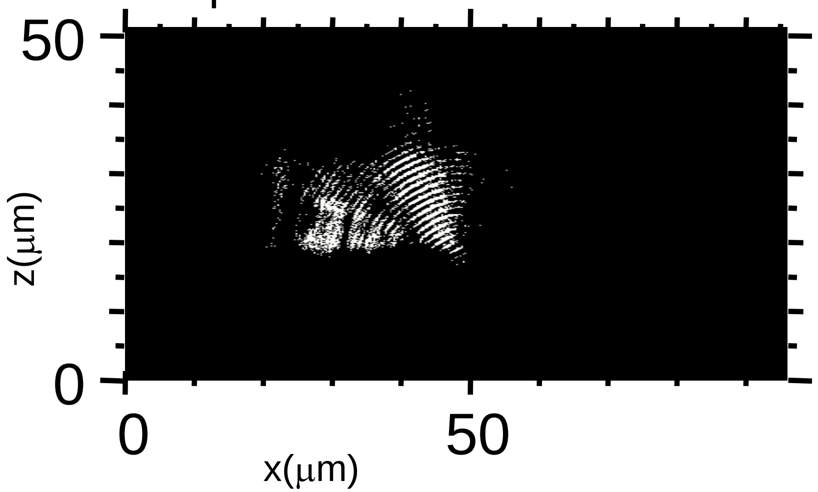

(x,z) positions of electrons with $u_z > 0$ and energy > 5 MeV at t=0.5 ps.

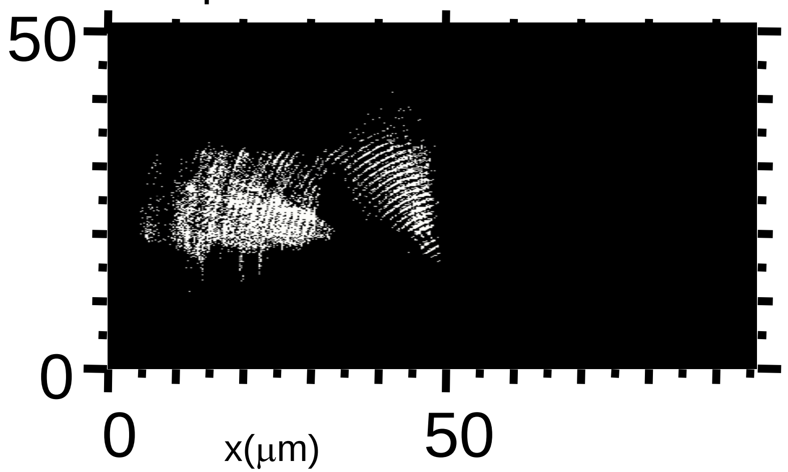

Our aim is to abstract the essential elements of hot electron production from Z3 simulations for input into LSP

Modeling with our MPP PIC code, Z3, provides electron source functions and contact with short-pulse experiments at high laser intensity.

- **Current work centers on role of preformed plasma in simulations including both underdense and overdense plasma.**
  - **Density profiles come from LASNEX simulations of the laser prepulse onto the target.**
  - **One product of Z3 modeling is electron source functions for transport modeling with the implicit code LSP (D. R. Welch et al, Nucl. Inst. Meth. Phys. Res. A242, 134 (2001)). Closer linking of Z3 and LSP is in progress.**
- **Z3 simulations at oblique angles of incidence which more closely match experimental conditions are underway.**
- **New diagnostics for monitoring heated electrons and optical emissions are now in use.**
- **This plan requires 3D and large 2D simulations which are enabled by access to the most powerful MPP computers. (Z3 sometimes serves as a computer testbed).**

Stopping of Directed Energetic Electrons in High-Temperature Hydrogenic Plasmas

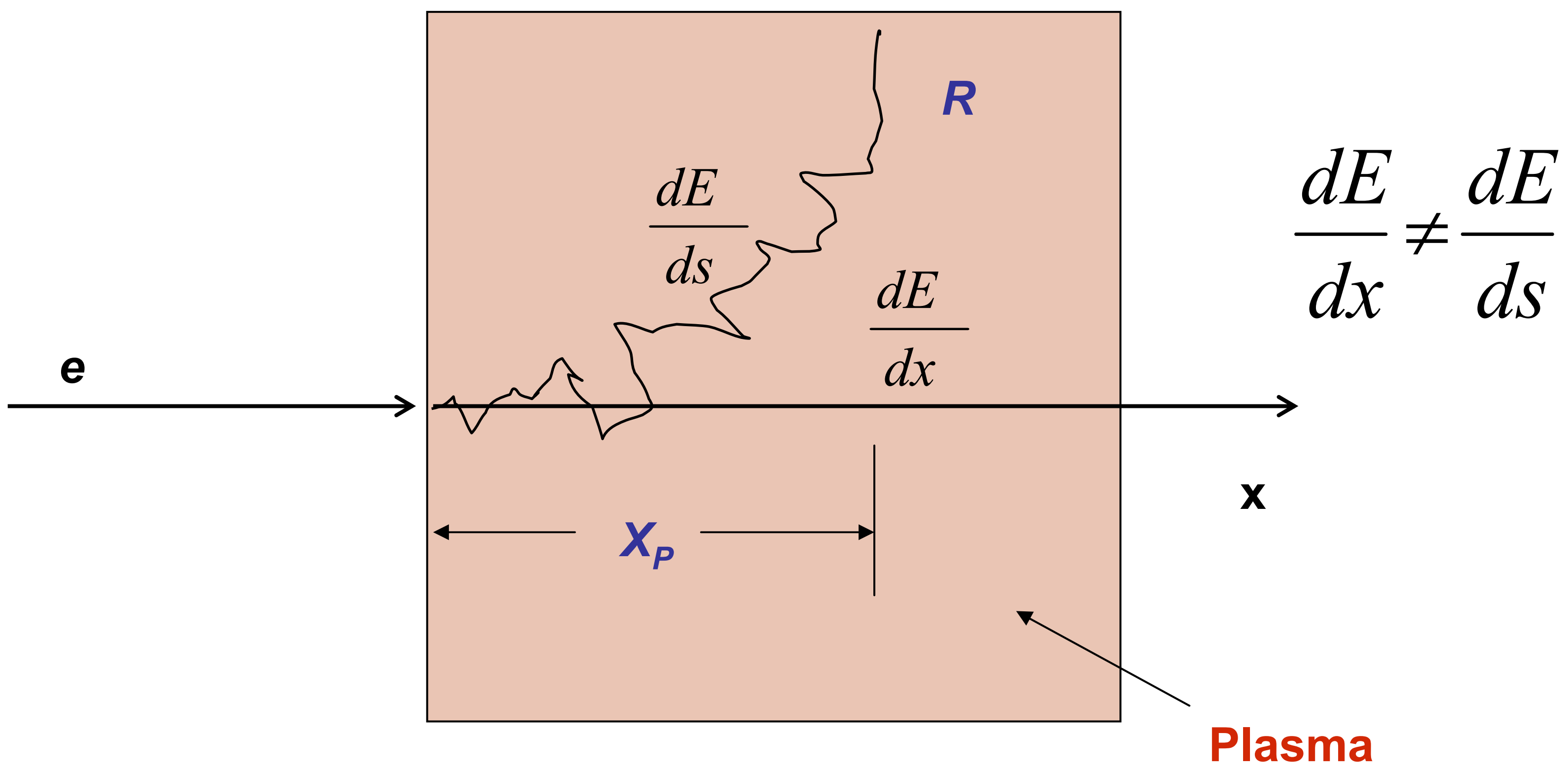

C. K. Li and R. D. Petrasso   MIT

Accepted and to be published in *Phys. Rev. E*

Linear-energy transfer is of relevance to the fast-ignition scheme in ICF

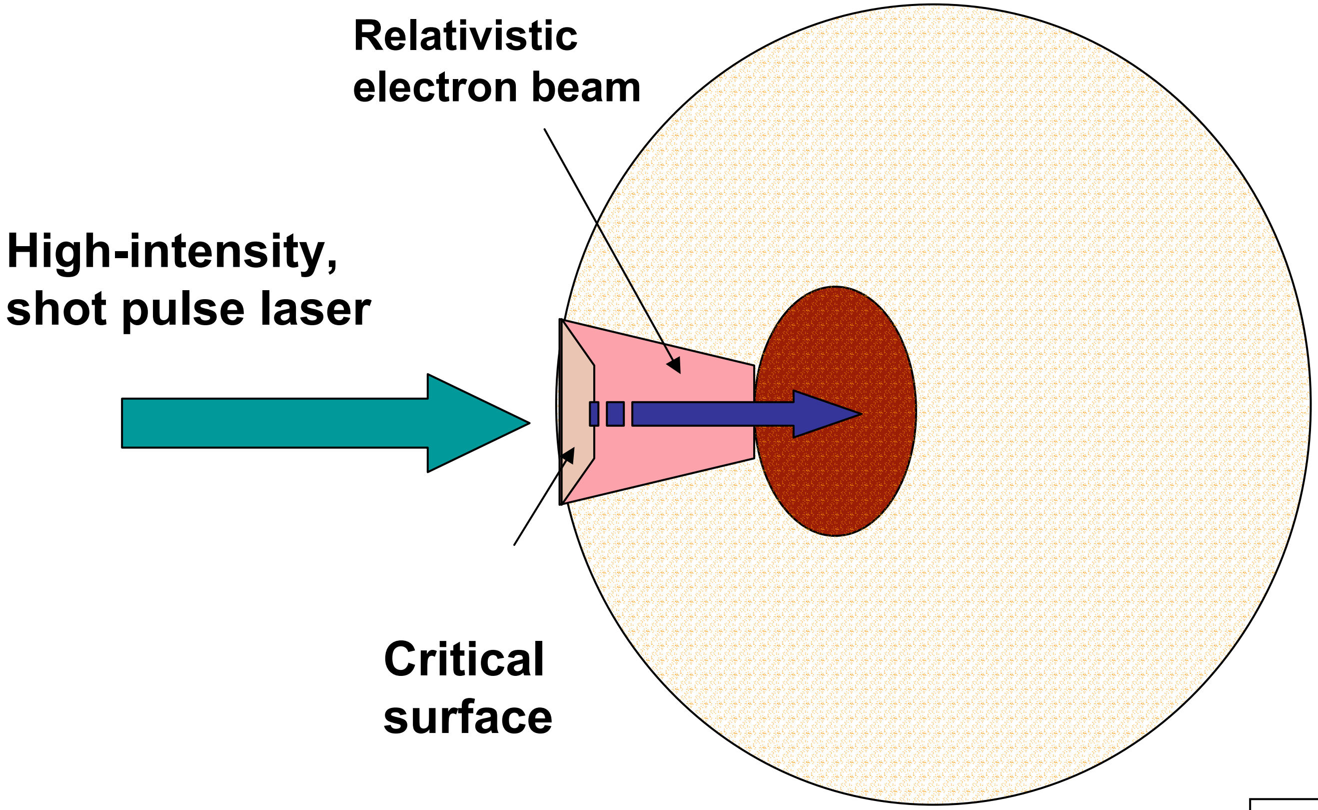

$n_b / n_e \sim 10^{-5}$

An analytical model is developed for relativistic electrons interacting with both plasma ions and electrons

- Electron-electron scattering is comparable to electron-ion scattering
- A simplified Møller (e->e) cross section is obtained for the analytic calculation
- Electron linear energy transfer in a plasma is enhanced by multiple scattering
- Electron penetration in a plasma is reduced by multiple scattering
- This theory will be tested by Monte Carlo calculation and by electron scattering experiments with H_2 (D_2) ice

Electron angular distribution due to multiple scattering is obtained by solving a diffusion equation

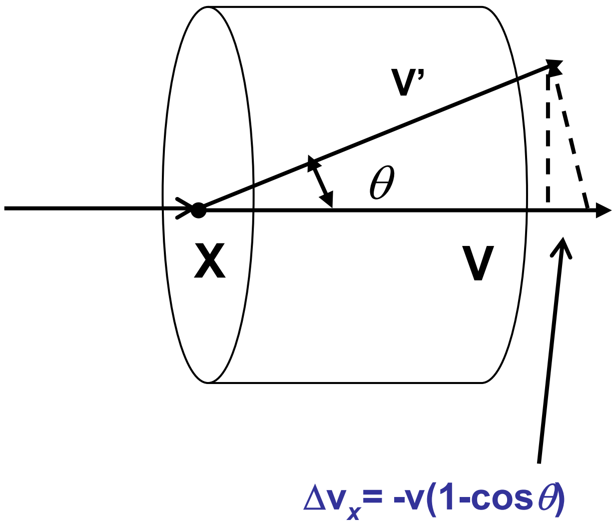

$$\frac{\partial f}{\partial s} + \mathbf{v}\cdot\nabla f = N\int\left[f(\mathbf{x},\mathbf{v}',s) - f(\mathbf{x},\mathbf{v},s)\right]\sigma\left(\left|\mathbf{v}-\mathbf{v}'\right|\right)d\mathbf{v}'$$

$$f(\theta,s) = \frac{1}{4\pi}\sum_{\ell=0}^{\infty}(2\ell+1)P_\ell(\cos\theta)\exp\left(-\int_0^s \sigma_\ell(s')\,ds'\right)$$

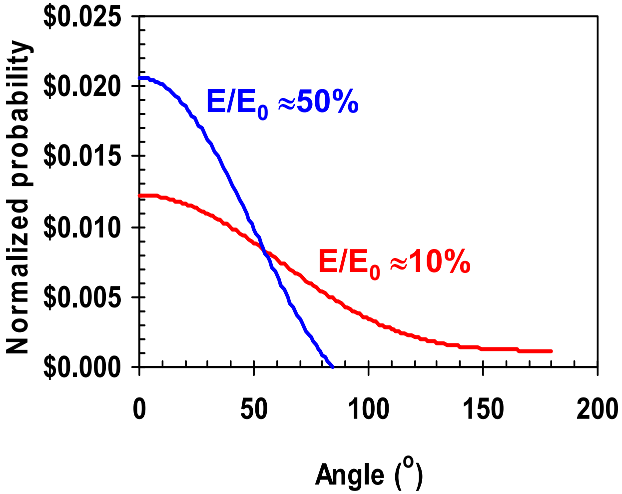

As a result of multiple scattering, a mean angular deflection <cosθ> is obtained:

MIT

$$< \cos\theta >= \int f(\theta, s) P_1(\cos\theta) d\Omega$$

$$= \exp\left(-\int_0^s \sigma_1(s') ds'\right) = \exp\left(-\int_{E_0}^{E} \sigma_1(E') \left(\frac{dE'}{ds}\right)^{-1} dE'\right)$$

Where the diffusion cross section (elastic scattering) and stopping power (inelastic scattering) are

$$\begin{cases} \sigma_1(E) = 2\pi N \int_0^{\pi} \left(\frac{d\sigma}{d\Omega}\right)(1-\cos\theta)\sin\theta d\theta \\ \frac{dE}{ds} = -\frac{2\pi r_0^2 m_0 c^2 n_i Z}{\beta^2}\left[2\ln\left(\frac{(\gamma-1)\lambda_D}{4r_0}\right) + 1 + \frac{1}{8}\left(\frac{\gamma-1}{\gamma}\right)^2 - \left(\frac{2\gamma-1}{\gamma}\right)\ln 2 + 2\ln\left(\frac{1.123\beta}{\sqrt{2kT_e/m_0c^2}}\right)\right] \end{cases}$$

For electron scattering off plasma electrons, Møller's cross section is simplified with a small-angle approximation

Møller's cross section in the CMC:

$$\frac{d\sigma(\theta^*)}{d\theta^*} = \frac{2\pi e^4 \sin\theta^* 2(\gamma+1)}{m^2\gamma^2 v^4}\left[\frac{4}{\sin^4\theta^*} - \frac{3}{\sin^2\theta^*} + \frac{(\gamma-1)^2}{4\gamma^2}\left(1+\frac{4}{\sin^2\theta^*}\right)\right]$$

Small-angle approximation, and transformed to Lab. Coordinates (LC):

$$\frac{d\sigma}{d\Omega} \approx \left(\frac{r_0}{\gamma\beta^2}\right)^2 \frac{(\gamma+1)^2}{\left(2^{\sqrt{(\gamma+1)/2}}\right)^4} \frac{1}{\sin^4\frac{\theta}{2}}$$

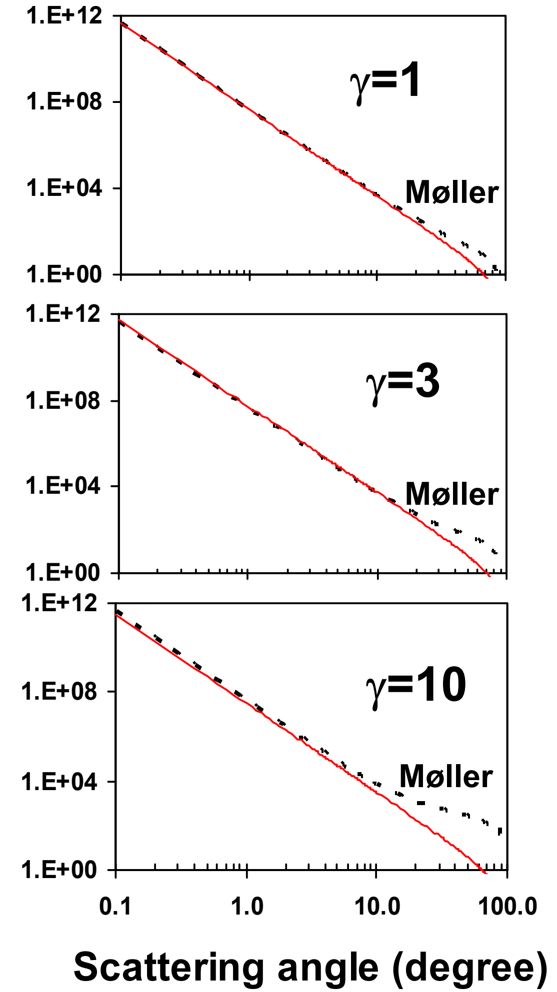

For hydrogenic plasmas when $\gamma \leq 10$, the electron scattering component is comparable to the ion component

$$R = \left(\frac{d\sigma}{d\Omega}\right)^{ee} \Big/ \left(\frac{d\sigma}{d\Omega}\right)^{ei}$$

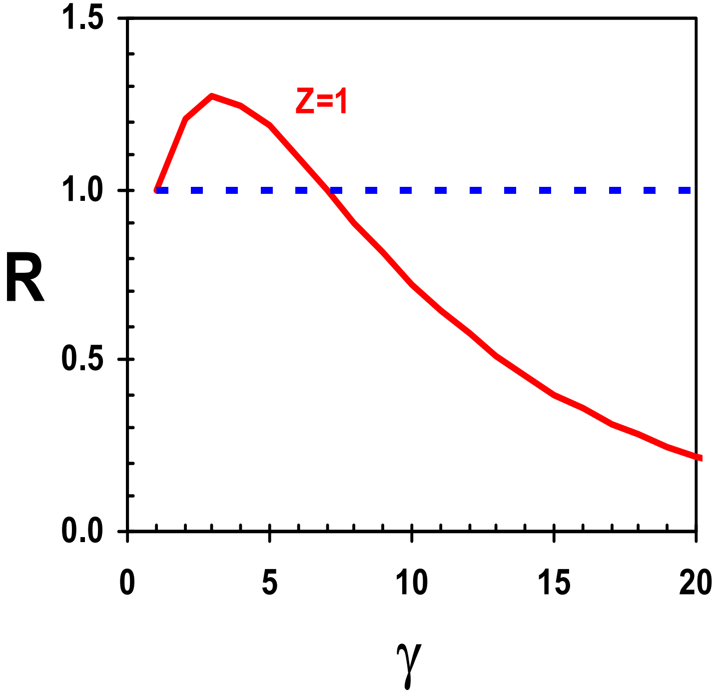

For hydrogenic plasmas when $\gamma \leq 10$, the electron scattering component is comparable to the ion component

$$R = \left(\frac{d\sigma}{d\Omega}\right)^{ee} \Big/ \left(\frac{d\sigma}{d\Omega}\right)^{ei}$$

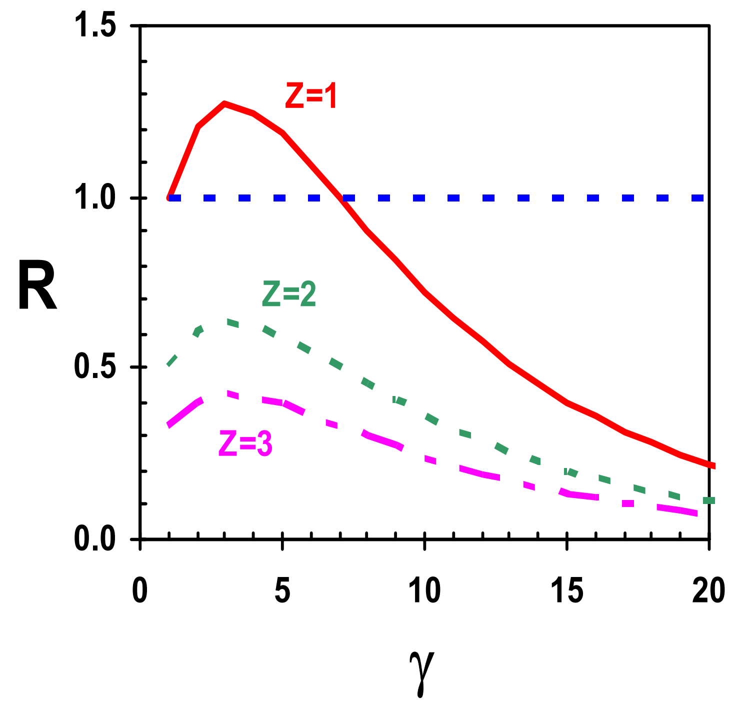

Multiple scattering enhances electron linear-energy transfer in plasmas

$$\frac{dE}{dx} = <\cos\theta>^{-1} \frac{dE}{ds}$$

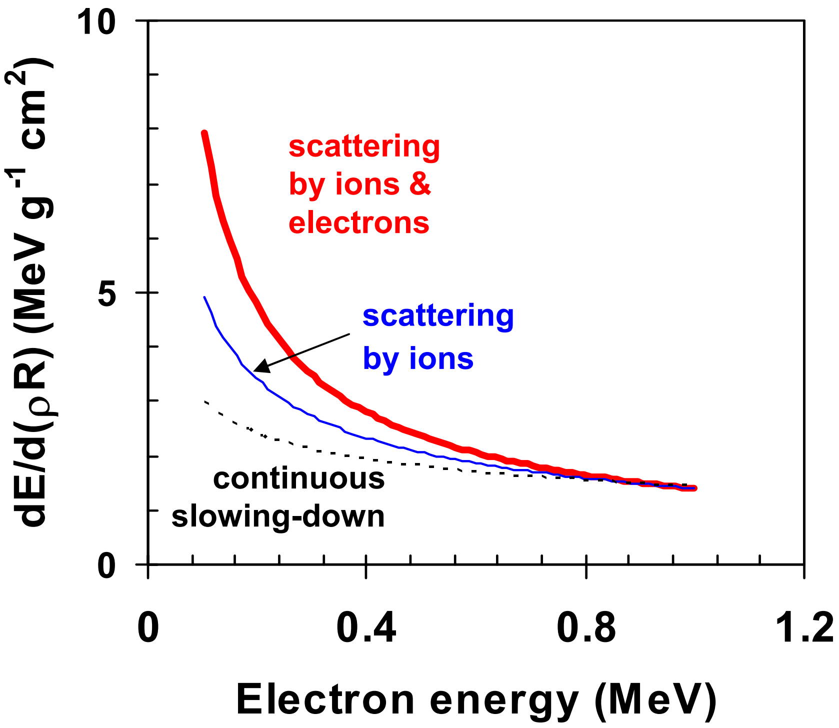

ρ = 300 g/cm^3; T_e = 5 keV

As a result of multiple scattering, the energy transfer increases notably near the end of the penetration, and the penetration is reduced

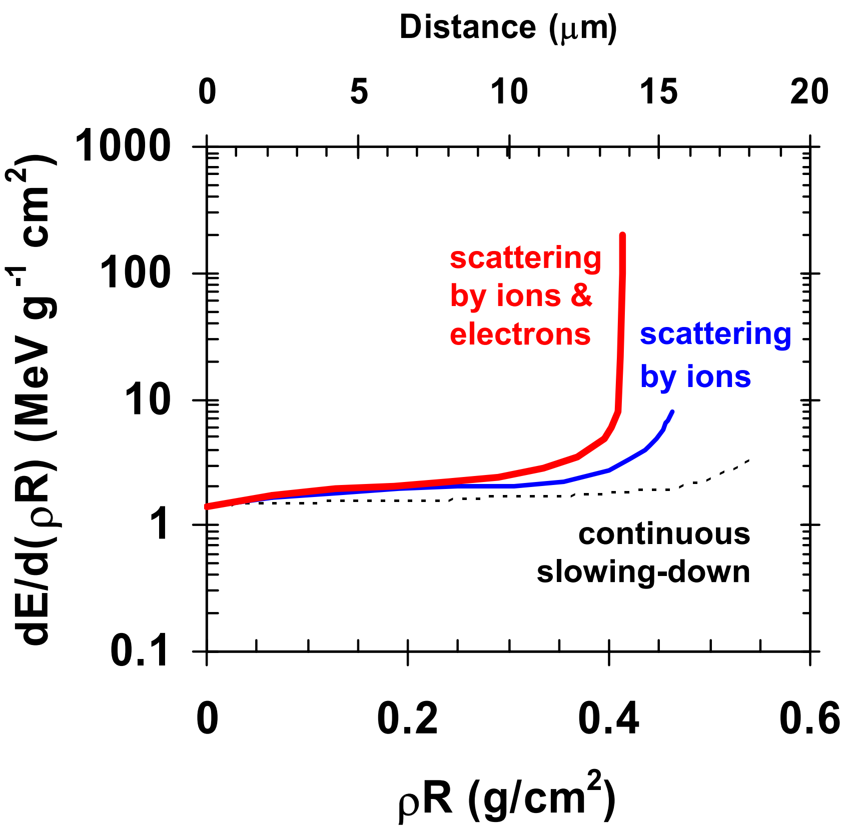

ρ = 300 g/cm^3; T_e = 5 keV

We plan to develop experiments at MIT for directly measuring electron stopping in cryogenic D_2

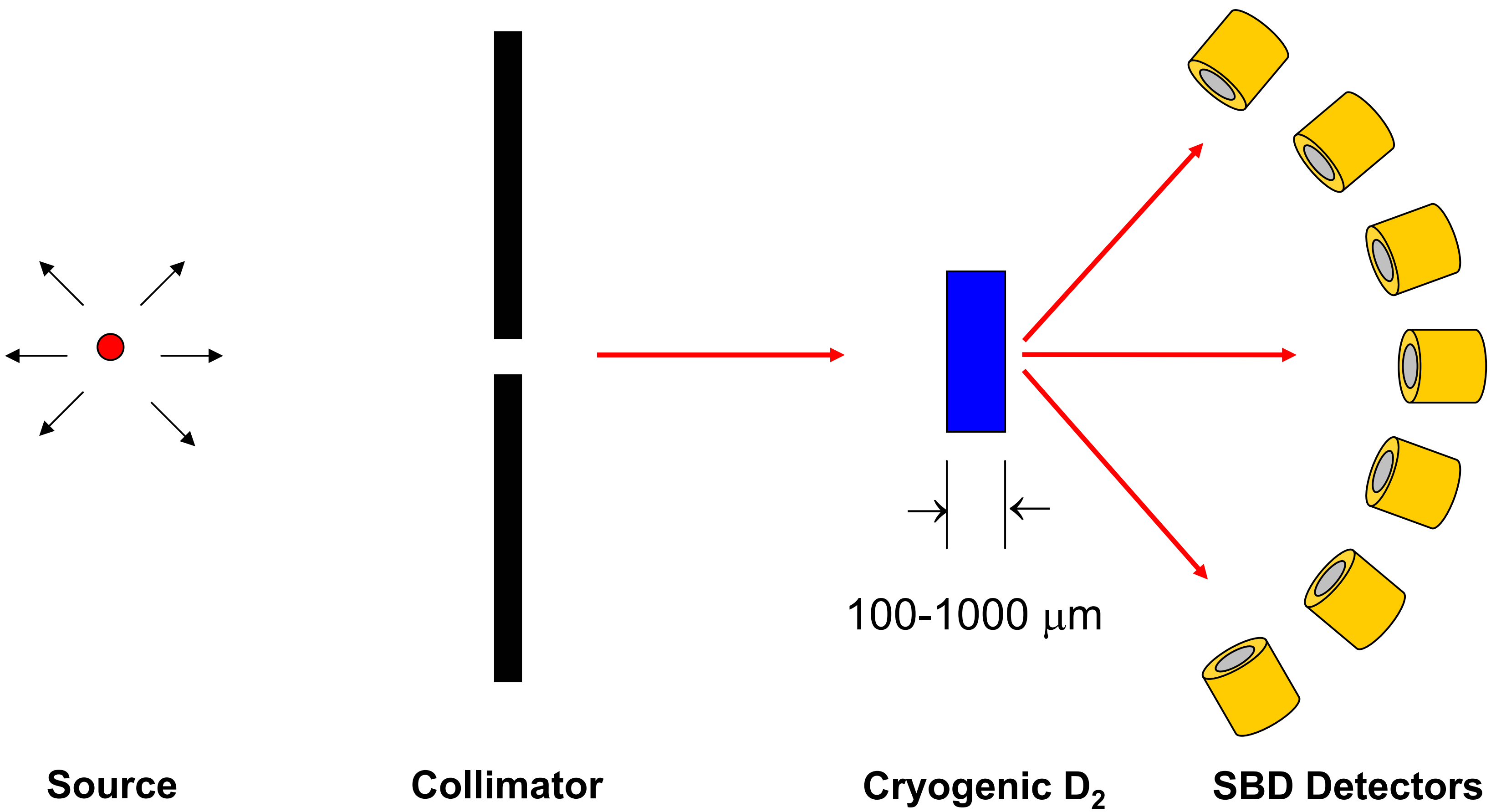

For these experiments we plan to use a Bi-207 source that produces electrons up to ~1MeV

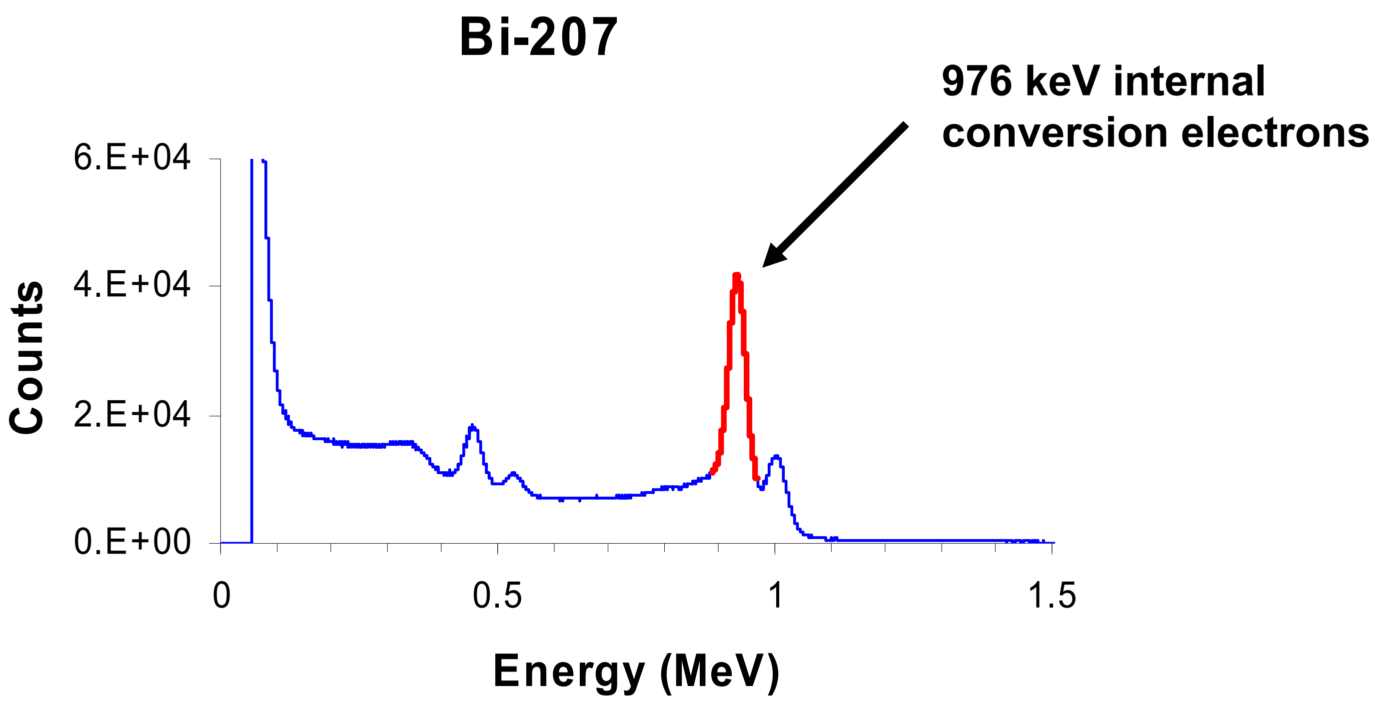

An analytical model is developed for relativistic electrons interacting with both plasma ions and electrons

- **Electron-electron scattering is comparable to electron-ion scattering**
- **A simplified Møller (e->e) cross section is obtained for the analytic calculation**
- **Electron linear energy transfer in a plasma is enhanced by multiple scattering**
- **Electron penetration in a plasma is reduced by multiple scattering**
- **This theory will be tested by Monte Carlo calculation and by electron scattering experiments with H_2 (D_2) ice**

Atomic Physics in Short Pulse Laser Experiments*

Short Pulse Laser Matter Computational Workshop

Pleasanton, California

August 25, 2004

Stephen B. Libby
Physics and Advanced Technologies
Lawrence Livermore National Laboratory
University of California

Atomic physics contributors: M. Chen, H.-K. Chung, M. E. Foord, R. W. Lee, S. Moon, J. Scofield, J. Albritton, R. M. More, M. Desjarlais, H. Yoneda

* UCRL-PRES-206280. Work Performed under the auspices of the US Department of Energy by LLNL under contract No. W-7405-ENG-48

Atomic Physics Issues Enter Short Pulse Experiments both as Microscopic Quantities and in Integrative Modeling

- **Outline (idiosyncratic selection from many possible topics):**
  - **K_α experiments serve both a fast electron velocity distribution diagnostic and for the development of petawatt driven hard x-ray backlighters. Interpretation of experiments highlight important atomic physics issues.**
    - **Detailed relativistic energy shifts and electron impact cross sections are required to get an accurate picture of the emission spectra and fluorescent yield.**
    - **The problem of the relaxation of a non-Maxwellian electron distribution in the presence of NLTE atomic physics is analogous to that of NLTE radiation transfer.**
    - **Radiation trapping?**
  - **The equation of state and electrical conductivity of cool plasmas requires consideration of negative ions and transport effects beyond an average atom, Drude picture.**

Integrated Simulations will Require Hydro, PIC/LSP, and NLTE Kinetics (M. Foord, H-K Chung, S. Moon)

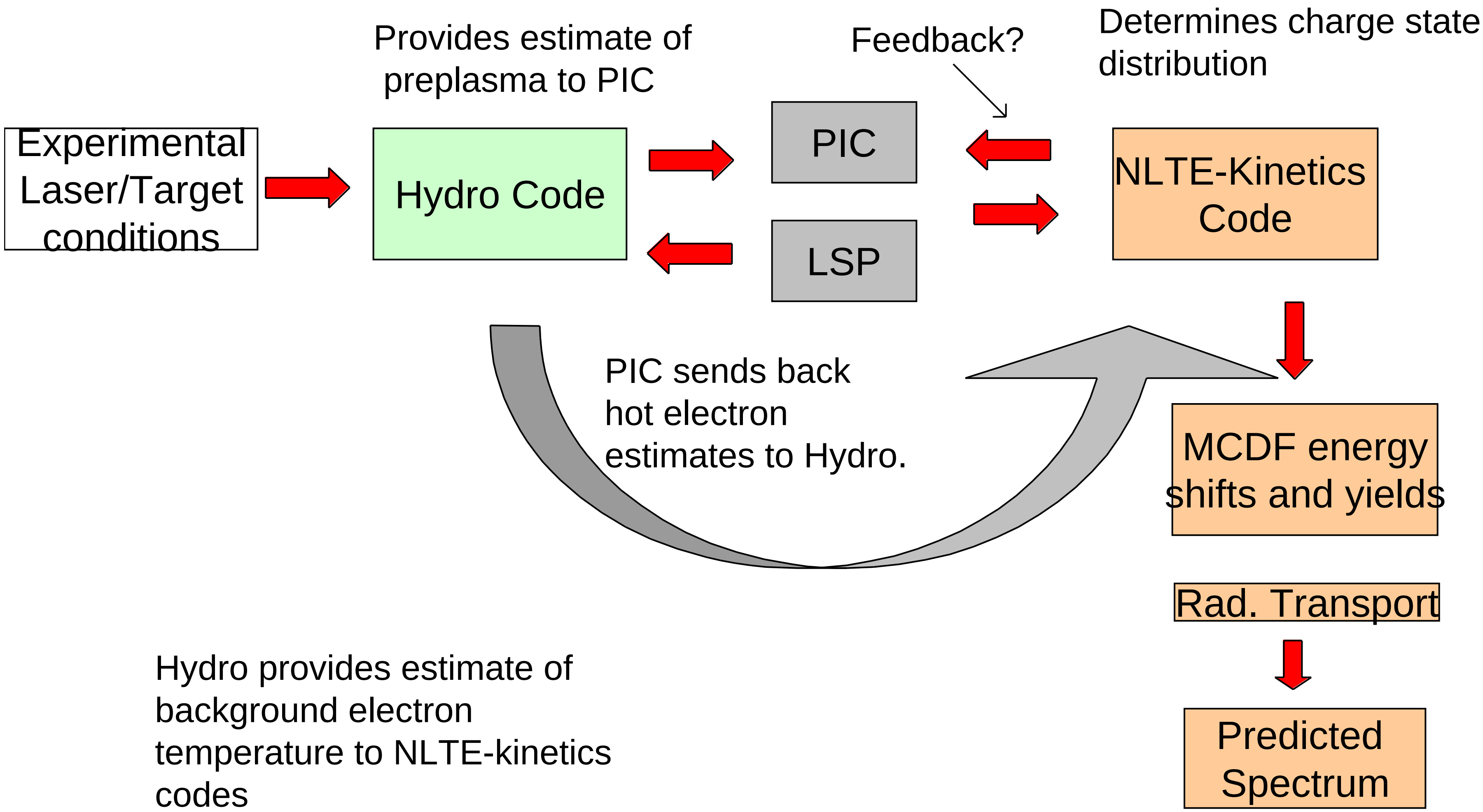

Physics & Advanced Technologies

Atomic Physics Considerations for Kα Emission

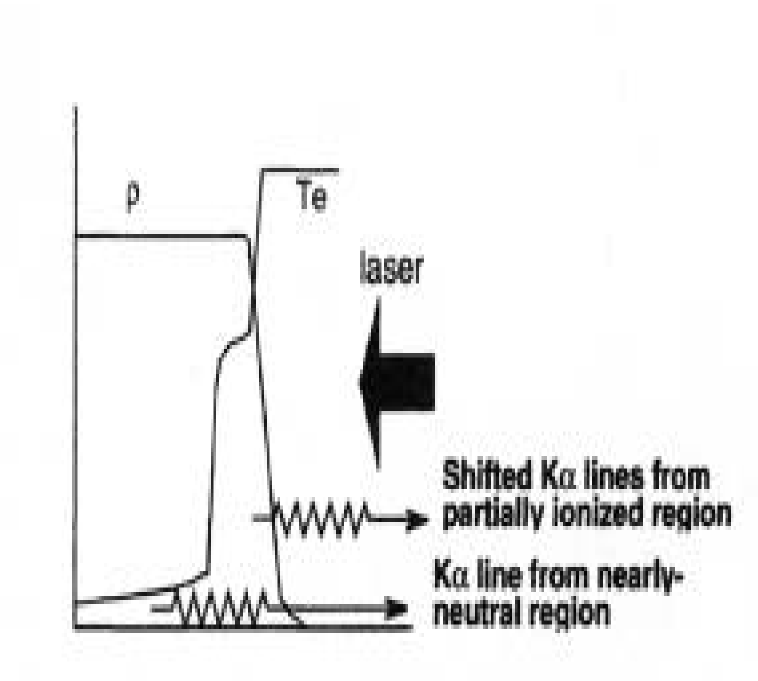

Kα emission depends on e- transport and atomic processes over a wide temperature range

Cl-CH 50 mJ 10^{17} W/cm^2 (Nichimura '02)

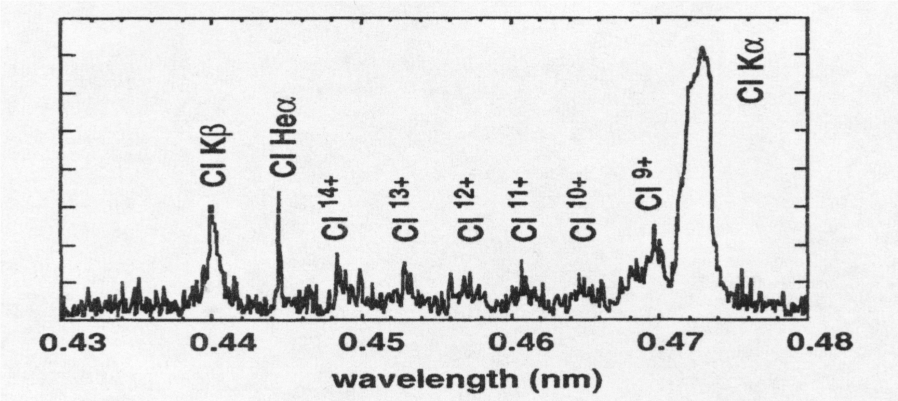

Ag 192 J Vulcan 2×10^{17} W/cm^2 (H-S Park '03)

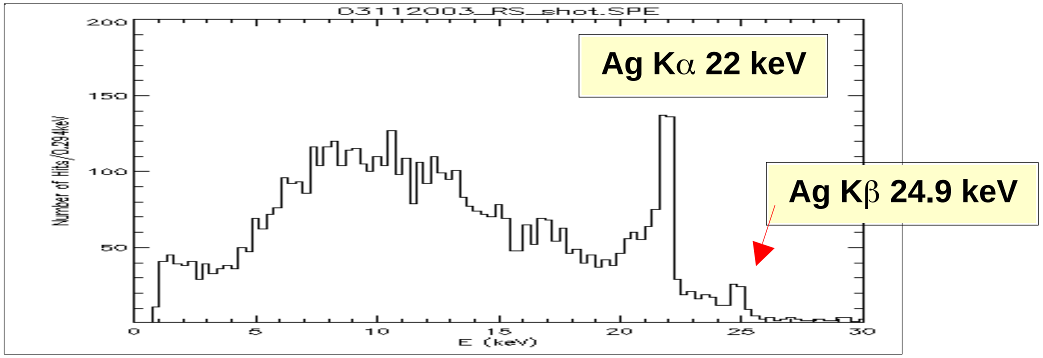

Physics & Advanced Technologies

Kα Energy Shifts are Calculated from the MCDF 'No-Pair' Relativistic Hamiltonian (M. Chen)

$$H_{\text{no-pair}} = \sum_{i=1}^{N} h_i + \Lambda_{++}(H_C + H_B)\Lambda_{++}$$

Atomic eigenstate function

$$\Psi(JM) = \sum_i c_i \phi_i(JM)$$

$$H\Psi = E\Psi$$

Variational MCDF equation

$$\sum_j (H_{ij} - \lambda\delta_{ij})c_j = 0$$

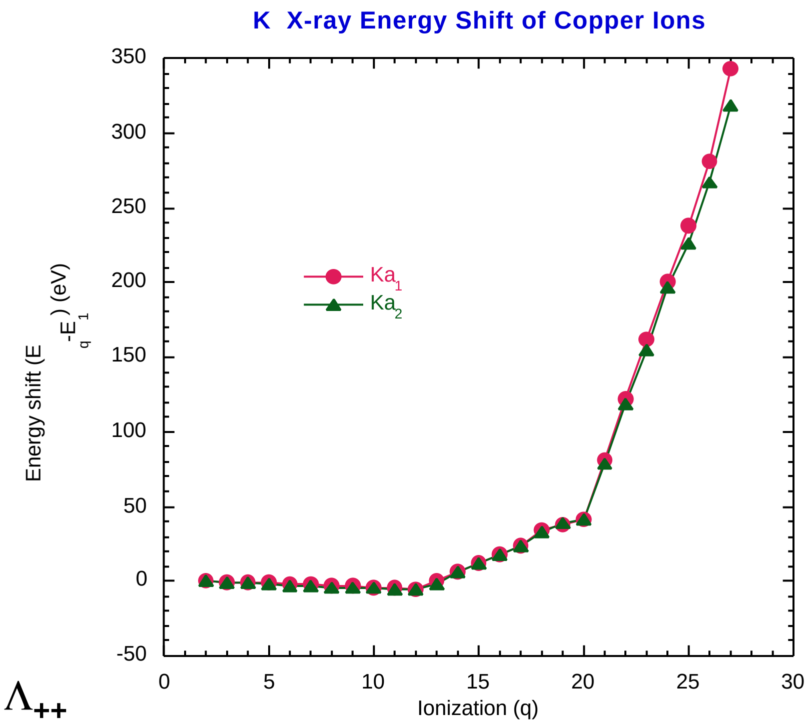

- **Positive-energy projection operators Λ_{++}**
- **Eigenenergy λ and eigenvector {ci} are obtained by diagonalizing the Hamiltonian matrix Hij**
- **Accuracy 1.5 eV out of a few keV - sufficient for shifted Kα emission of M-shell Cu ions (4eV).**

X-Ray fluorescence Yields Depend on Ionization and Must Correctly Include Selection Rules (M. Chen)

$$\overline{\omega} = \frac{\sum_{L,S}(2L+1)(2S+1)\omega(LS)}{\sum_{L,S}(2L+1)(2S+1)}$$

K-shell yield ω(K)=0.46
E(Kα1)=8047.4 eV)
E(Kα2)=8027.3 eV
Natural line width
G(Kα1)=2.1 eV
G(Kα2)=2.5 eV
Lifetimes
--K- hole =4.3x10^{-16} s
--L_3- hole =1.2x10^{-15} s

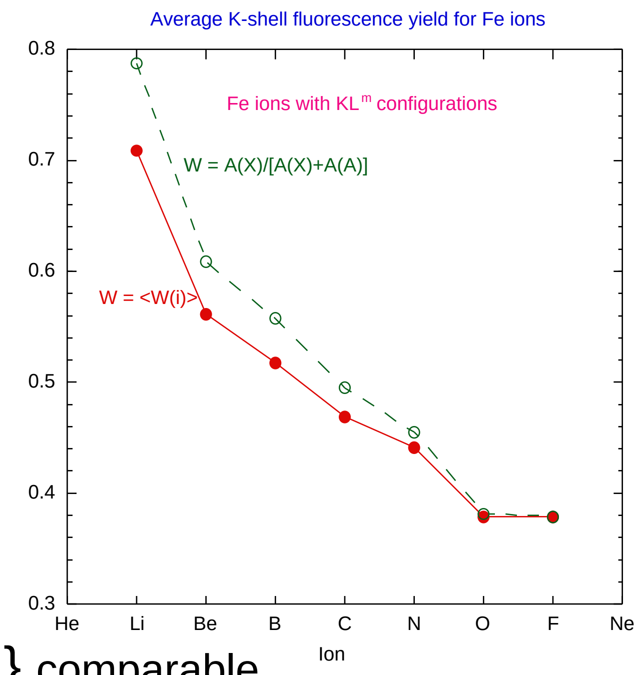

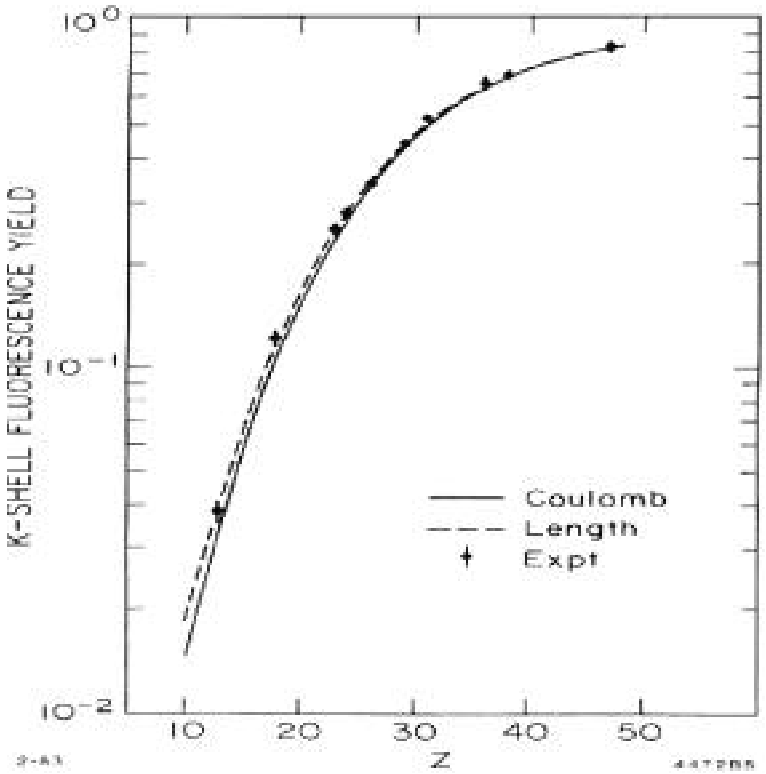

Competing processes:
Radiative decay
Auger decay } comparable
Collisional processes - 3B, DX smaller

Synthetic K Shell Spectra Including Ionization Effects (Shifts and Branching Ratios) (M. Chen)

Calculations assume thermal ion distribution and use 8 eV instrumental width

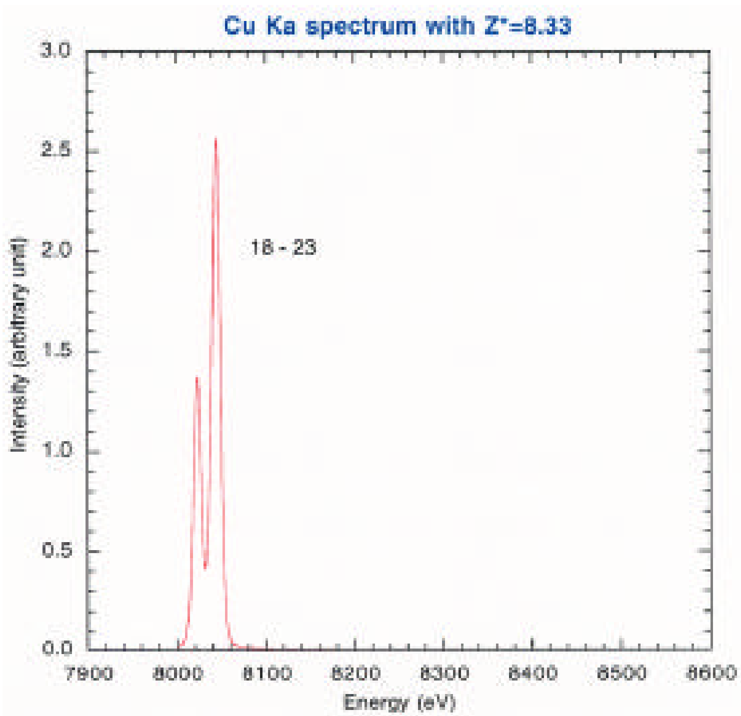

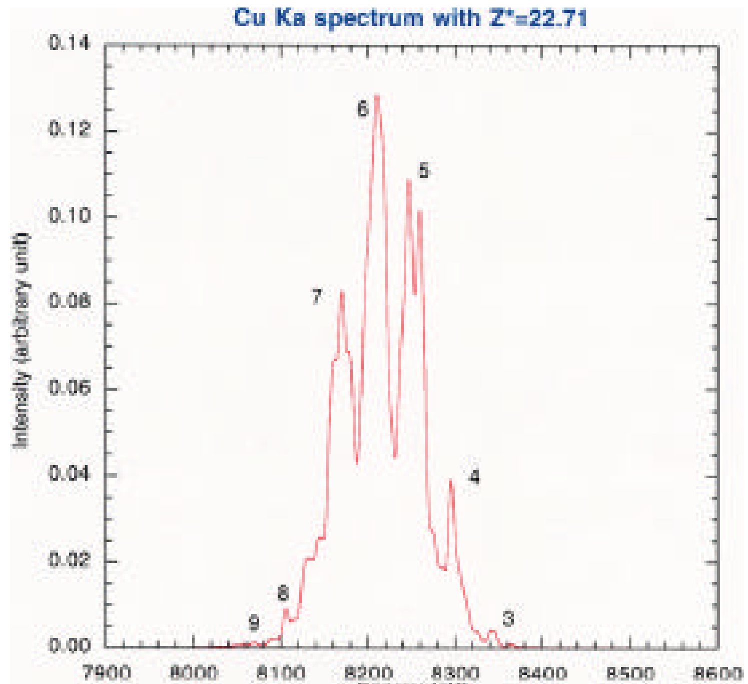

2p spin-orbit splitting dominates in M-shell

Multiplet splitting dominates in L-shell

Measuring L-shell shifts (~40 eV per charge state) should be feasible

Relativistic Electron IonizationCross Sections Scale Asymptotically like the Møller Cross Section (1)

- **Non-relativistic approximations include Thomson weak coupling and Lotz fit.**
  - **via angular analysis vs energy of Rutherford, cross section at energy ε, to transfer energy $\Delta\varepsilon$ is:**
    $d\sigma=(\pi e^4/\varepsilon)(d\,\Delta\varepsilon/(\Delta\varepsilon)^2)$
  - **The cross section for transfer exceeding ionization energy E is:**
    $\sigma=(\pi e^4/\varepsilon)(1/E - 1/\varepsilon)$

- **Relativistic cross sections (J. Scofield, Phys. Rev. A 18, 963, 1978)**
  - **Born Diagram (neglect exchange - should be good for disparate electron energies)**
  - **relativistic plane waves for incident and scattered high energy electron, distorted waves & relativistic Hartree-Slater for ejected electron**

L-shell ionization

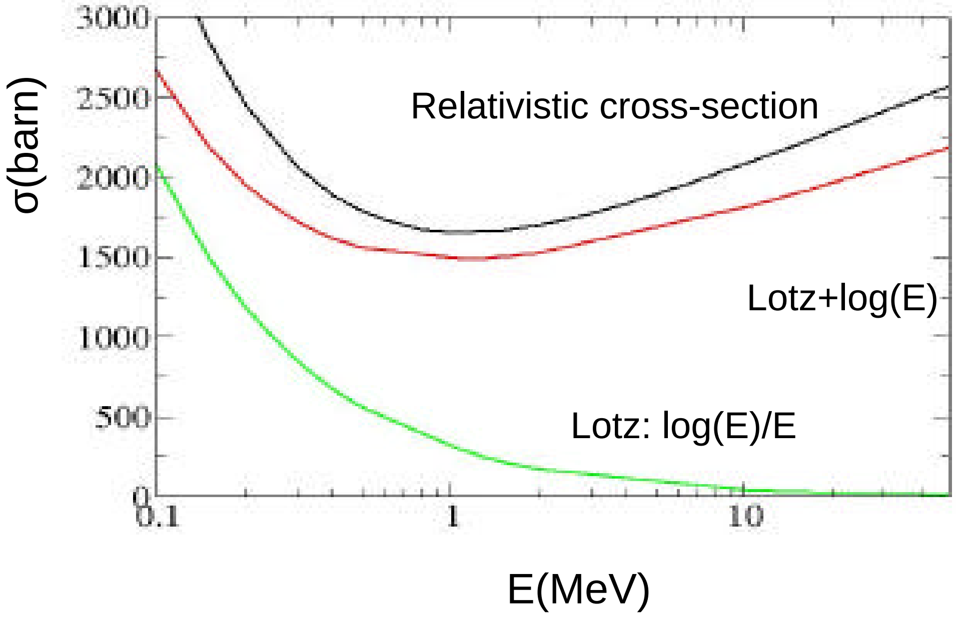

$$\sigma \quad \beta^{-2}\left[A\left[\ln\left(\beta^2/\left(1-\beta^2\right)\right)-\beta^2\right]+C\right]$$

Relativistic Electron IonizationCross Sections Scale Asymptotically like the Møller Cross Section (2)

• Møller (electron-electron) Scattering including exchange (Ahkiezer & Berestetskii, Quantum Electrodynamics):

$$d\sigma = \frac{r_0^2}{4v^4}\frac{[(2\frac{\varepsilon^2}{m^2})-1]^2}{\frac{\varepsilon^6}{m^6}}\{\frac{4}{\sin^4\vartheta}-\frac{3}{\sin^2\vartheta}+\frac{[(\frac{\varepsilon^2}{m^2})-1]^2}{[(2\frac{\varepsilon^2}{m^2})-1]^2}(1+\frac{4}{\sin^2\vartheta})\}d\Omega$$

• v, ε, and θ are respectively the incident velocity, energy and scattering angle in the cm system.

• Energy Loss is conveniently expressed in terms of $\Delta=(\varepsilon_1-\varepsilon_2)(/\varepsilon_1$-m) = 1/2 (1-cos($\theta$))

$$d\sigma = \frac{2\pi r_0^2}{v_1^2(x-1)}\frac{d\Delta}{\Delta^2(1-\Delta)^2}\{1-[3(\frac{x-1}{x})^2\Delta(1-\Delta)+(\frac{x-1}{x})\Delta^2(1-\Delta)^2\}$$

• Note log behavior as well as small Δ behavior (recovering Rutherford for for energy loss (x=ε_1/m)

NLTE Kinetics Code System with Boltzmann $f_e(E)$ Relaxation: FLYCHK/CT27 (H-K Chung, R.W. Lee, W. L. Morgan)

•***Built-in* atomic data sets** **(Hydrogenic model)**

•**Detailed population distributions considering collisional and radiative processes (Non-LTE solutions)**

•**Steady-state, time-dependent, and LTE solutions**

•**Arbitrary electron energy distribution functions with multiple Te option**

•**Atomic model includes the ground state, valence-shell excited levels, and inner shell levels for *all* ion stages from neutral through fully-stripped**

•**Easy and user-friendly interface**

(with an option of detailed K-shell modeling)

•**Accurate built-in atomic data for H, He and Li ions up to Z=26**

•**Spectral intensities and line shapes**

Steady State and Time Dependent Effects on Charge State Distribution for High Background Temperature (H-K Chung)

- For High T, CSD is most sensitive to LTE thermal effects: e.g. 1 keV is required for He-like ion production
- Hot electrons did not make substantial differences when temp high :
  - –Here relativistic cross-sections relevant to fluorescence.
- Time-dependent calculations show that the plasma will reach at its steady-state & LTE values within 1 ps ($N_e = 10^{23} cm^{-3}$)

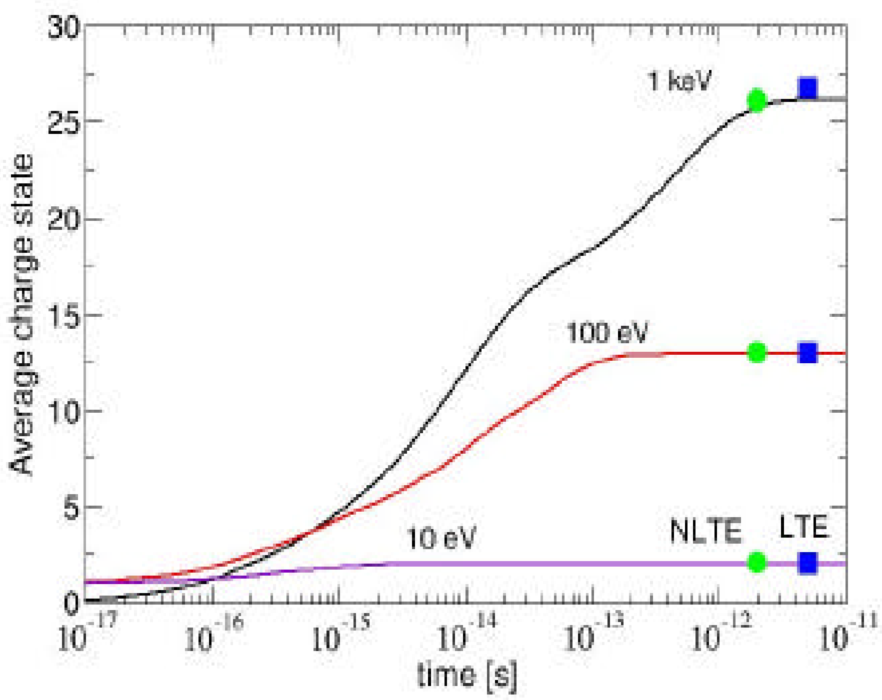

The Effect of Relativistic Cross Sections Depends on the Hot Electron Fraction and Background Temperature (H-K Chung)

Comparisons between non-relativistic (A) and relativistic (B) cases at N_e=10^{22} cm^{-3} for three different hot electron fractions at T_{hot}=3MeV

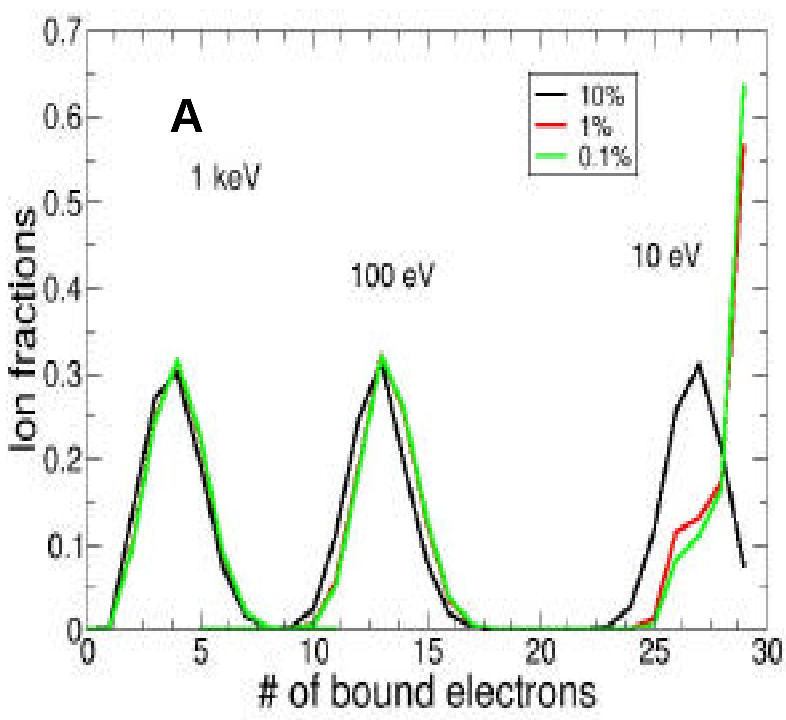

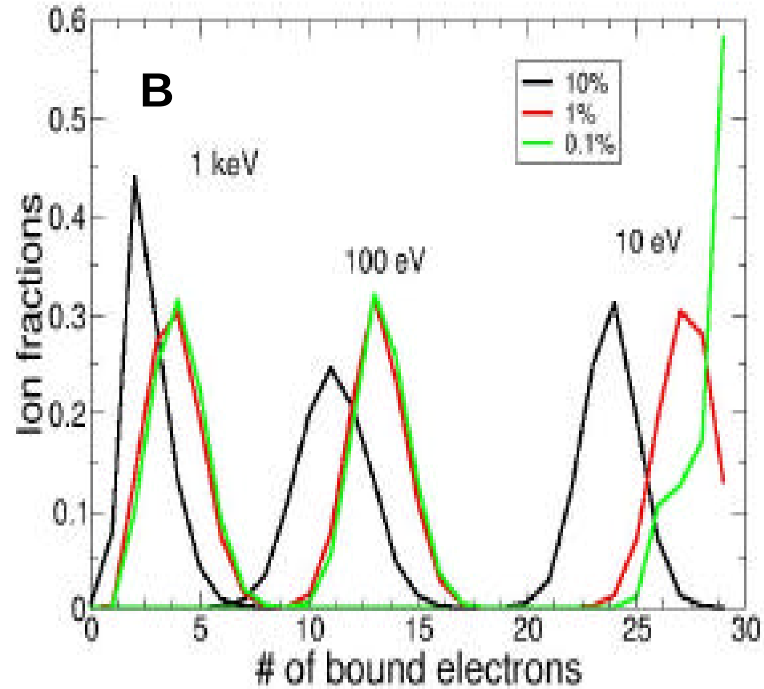

Low Temperature and Density Anomalous Effects in the Equation of State and Electrical Conductivity*

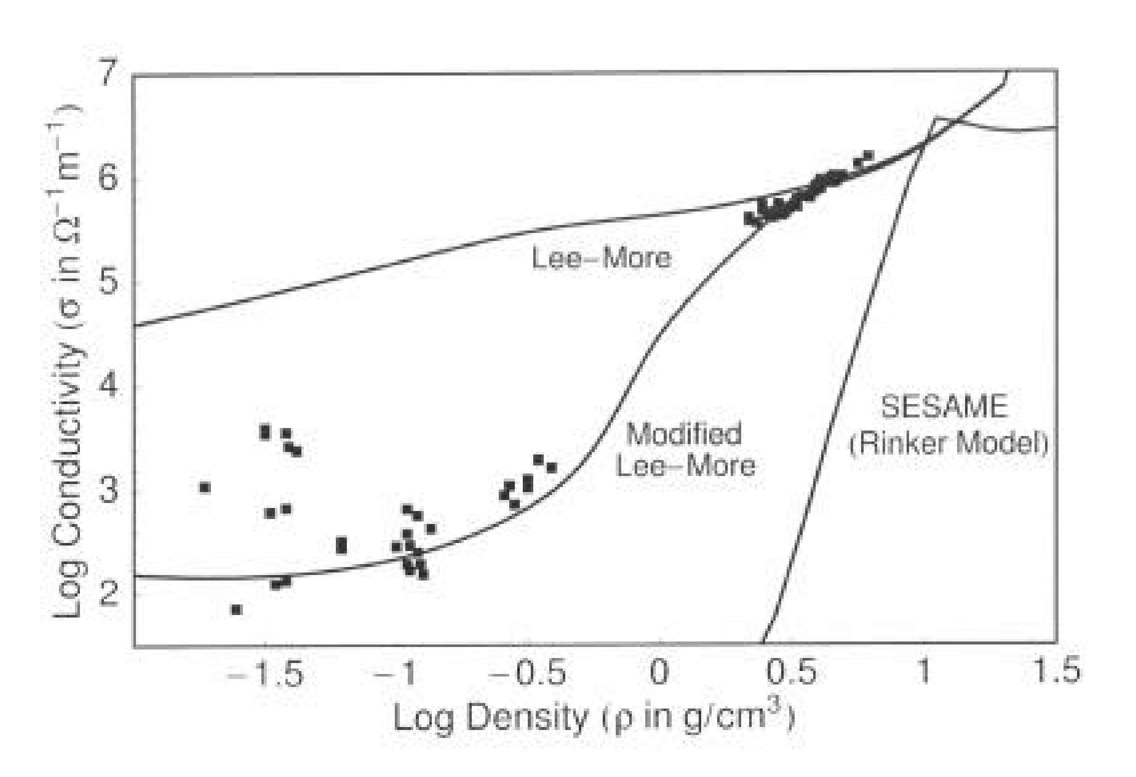

Lee-More model is a Drude type model with multiple mechanisms for n_e and τ in $\sigma = n_e e^2 \tau /m$ (including Mott minimum metallic conductivity).

Desjarlais's modified Lee-More model (blended Saha, pressure ionization, phenomenological e^- - neutral cross section - Contrib. Plasma Phys. 41, 2001, 267).

Need to add negative ions, as well as possible multi-center non average atom scattering.
***R. M. More, T. Kato, I. Murakami, M. Goto, H. Yoneda, G. Faussurier, M. Desjarlais, S. B. Libby to be published.**

Consequences of Au^- for ionization balance at low temperature and density - compensated semiconductor analog

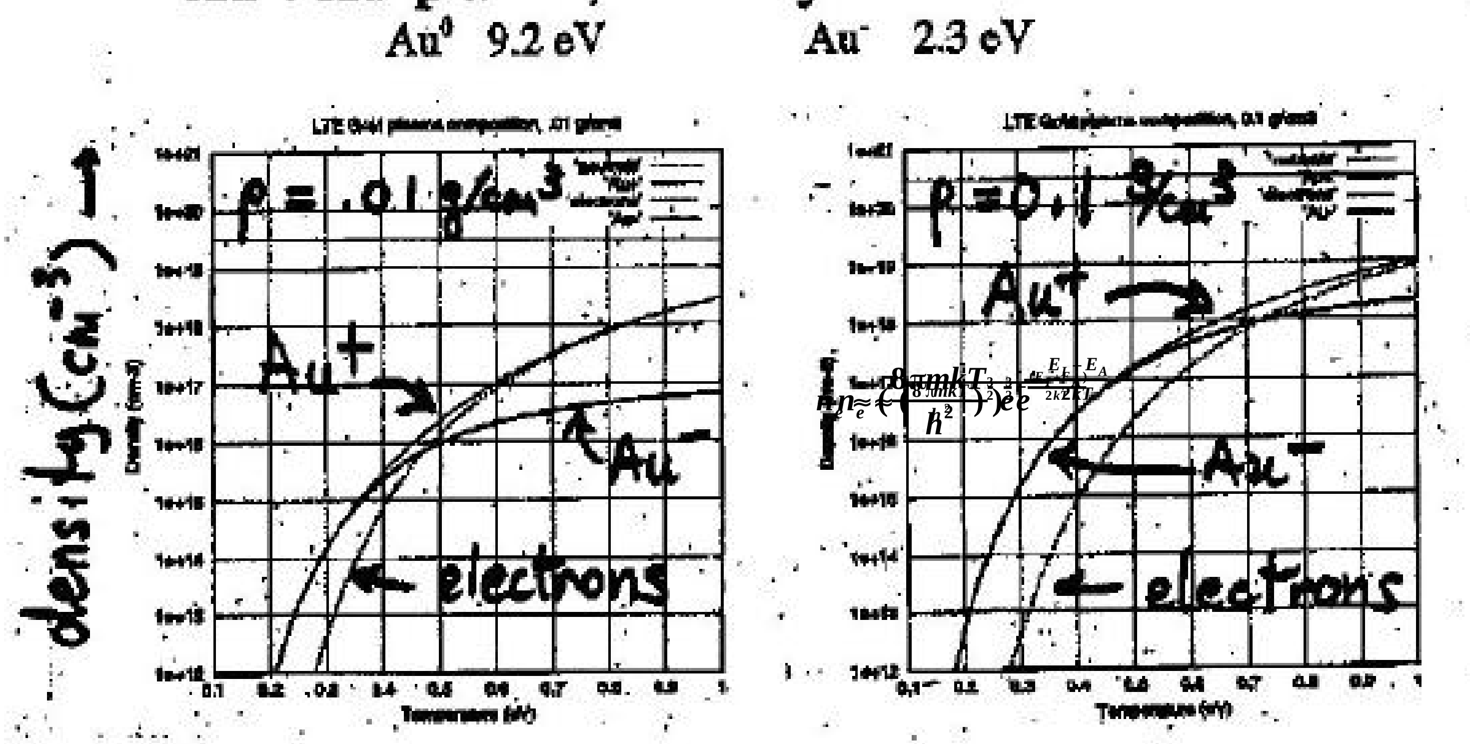

Simplified Saha argument

$$\frac{n_+ n_e}{G_1(T)} = n_0 e^{-\frac{E_I}{kT}}$$

$$\frac{n_0 n_e}{G_2(T)} = n_- e^{-\frac{E_A}{kT}}$$

$$n_- + n_e = n_+$$

$$n_e \approx \left(\frac{8\pi mkT}{h^2}\right)^{\frac{3}{2}} e^{-\frac{E_I + E_A}{2kT}}$$

Au, Au+, Au-, and e- ρ vs. T as predicted by the Saha equation (R. M. More) for densities of .01 and .1 gr/cc revealing the relative importance of the negative ion Au- vs. free electrons. σ will depend on degree of ‘compensation,’ neutral scattering cross section, and non-average atom effects. Analogous results for Cu (affinity ~ 1.23 eV and I ~ 7.73 eV).

Physics & Advanced Technologies

Enhanced implicit hybrid modeling of laser-matter interactions

R. J. Mason

E.S. Dodd and B.J. Albright

Los Alamos National Laboratory

Short-Pulse Laser Matter Computational Workshop

Pleasanton, CA

August 25-27, 2004

The Implicit Moment system is very straightforward (in 1-D, for B=0)

relativistic γ

$$\frac{\partial \vec{E}}{\partial t} = -4\pi e(Zn_i\vec{v}_i - n_e\vec{v}_e); \quad v_\alpha = u_\alpha/\gamma_\alpha; \quad n_e v_e = \sum n_\alpha v_\alpha; \quad \alpha = h, c$$

mass scaled momentum

n limited to ncrit

laser intensity

$$m_e \frac{\partial\, n_\alpha \vec{u}_\alpha}{\partial\, t} = -\nabla \bullet \overline{P}_\alpha - en_\alpha(\vec{E} + \frac{\vec{v}_\alpha\ x\ \vec{B}}{c}) - \frac{\omega_{p\alpha}^2}{2c\omega^2\gamma_\alpha}\frac{[n_r, n_{crit0}]_{\min}}{n_r}\nabla I - C_a\gamma_\alpha m_e n_\alpha(\vec{v}_\alpha - \vec{v}_i)$$

weighted particles

$$\overline{P}_h = \sum_j w_j u_j v_j; \quad v_j = u_j/\gamma_j; \quad \gamma_j = [1 + (u_{jx}^2 + u_{jtr}^2)/c^2]^{1/2}$$

$$u_h = \sum_j w_j u_j; \quad n_h = \sum_j w_j$$

hot e⁻: particles with weights w_j

cold e⁻: a fluid

ions : fluids or particles

The implicit differencing suppresses plasma wave instability at high densities

Heuristic for the B=0 limit

neglecting collisions

$$E^{(m+1)} = E^{(m)} + 4\pi e(n_h v_h^{(m+1)} + n_c v_c^{(m+1)} - Z n_i v_i^{(m+1)})\Delta t$$

*** includes ponderomotive acceleration**

$$v_h^{(m+1)} = \frac{1}{\gamma_h^{(m+1)}}(u_h^{(m)*} - \frac{1}{m_e n_h}\nabla \bullet \overline{P}_h \Delta t - \frac{e}{m_e} E^{(m+1)}\Delta t);$$

v_c and v_i from fluids or particles

$$E^{(m+1)} = \frac{(E^{(m)} - 4\pi \sum_\alpha \frac{q_\alpha n_\alpha \Delta t}{\gamma_\alpha^{(\oplus)}}(u_\alpha^{(m)*} - \frac{1}{m_e n_\alpha}\nabla \bullet \overline{P}_\alpha \Delta t)}{[1 + \omega_p^2 (\Delta t)^2 / \gamma_\alpha^{(\oplus)}]}$$

level (m) suffices

$$E^{(m)} \Rightarrow -4\pi e[\int_0^x (n_h^{(m)} + n_c^{(m)} - Z n_i^{(m)})\Delta t]$$

← **provides a field correction**

for 2D: see JCP '87 ref.

Significant considerations

- **New time step controllers can help to keep accelerations small under action of the PMF**

$$\frac{\Delta u}{c} = \frac{(|eE| + |f_{pmf}|)\Delta t}{mc} \leq 0.3$$

- **Hot electrons are presently emitted in a relativistic Maxwellian by the Wilks' rule -**

$$\gamma_h = [1 + \frac{I(W/cm^2)\lambda(\mu m)^2}{1.37\times 10^{18} f_l}]^{1/2}, \qquad T_h = \frac{(\gamma_h{}^2 - 1)mc^2}{3\kappa\gamma_h}$$

(with f_l = *2.0* for linear and *1.0* for circularly polarized light -- if T_h is too low $n_h >> n_{crit}$)

- **Small spot emission can be "choked" by**
  -

$$n_h \times (source\ area) = n_h c(2\pi r)$$

To start: we consider a semi-infinite slab hit by a 3 μm FWHM 1.3 x 10^{19} W/cm^2 1.06 μm pulse

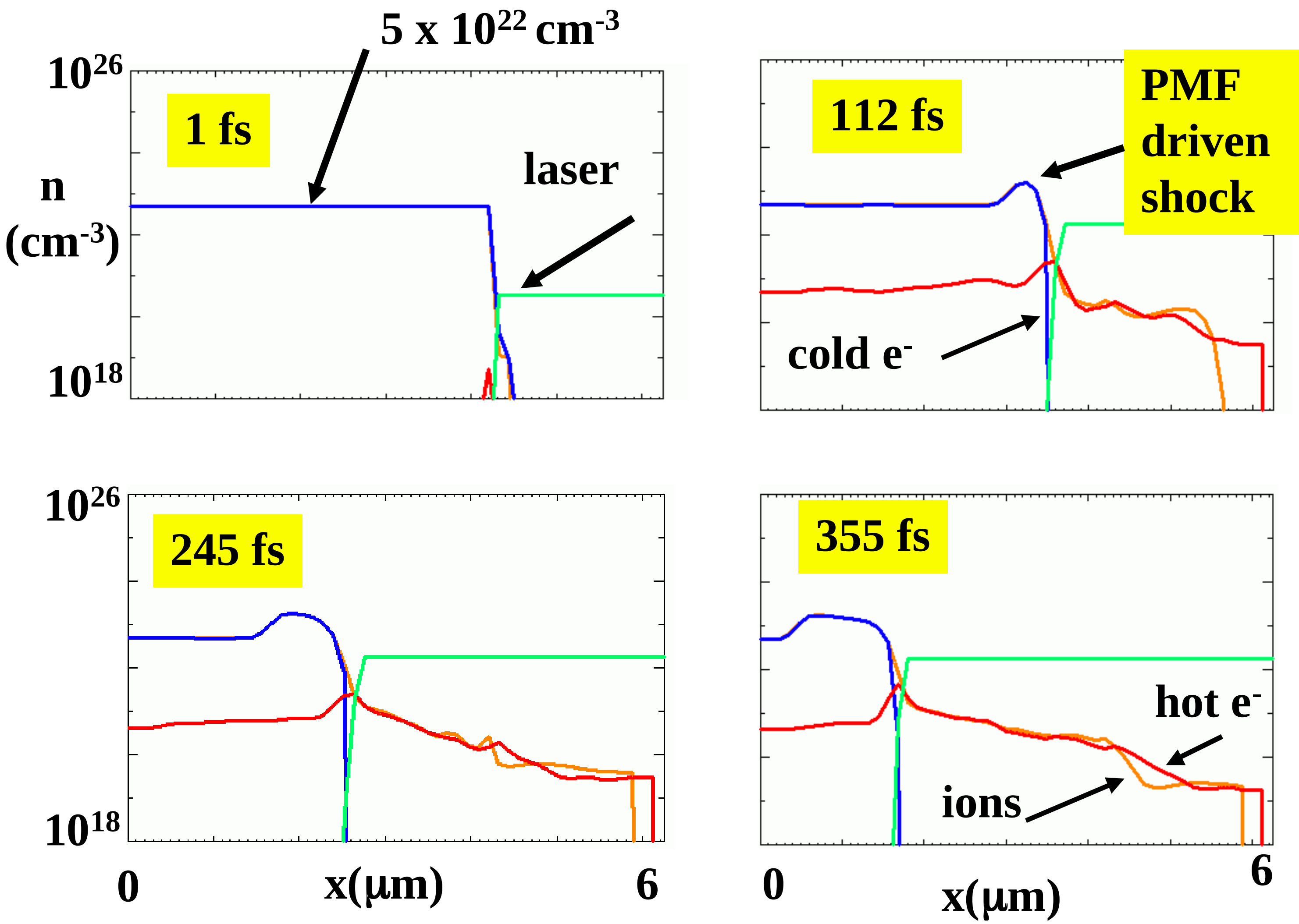

Note: Weibel instability on hot flow was seen in some early test runs, backside reflections can destroy this

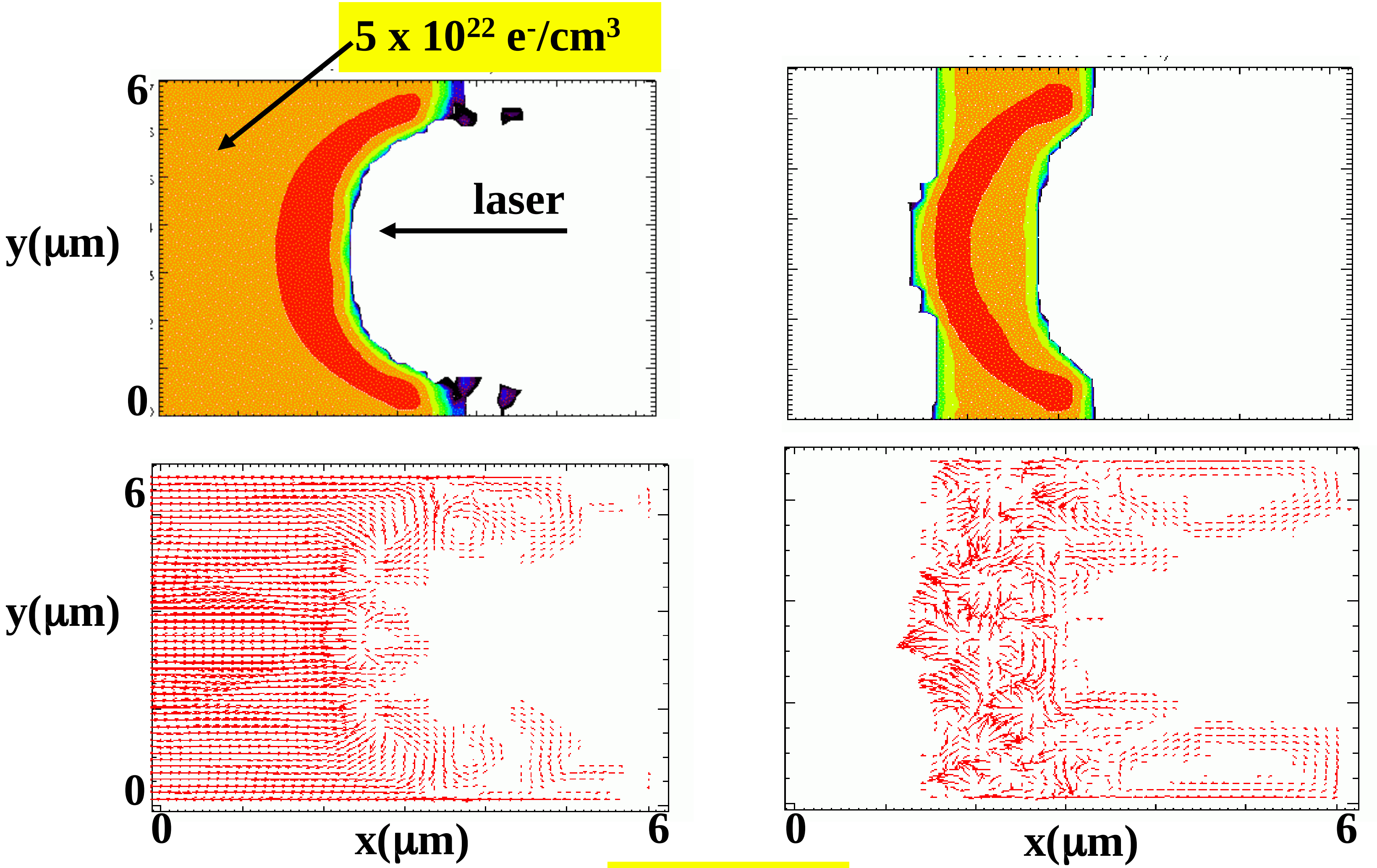

t=281 fs

Correspondingly, the hot electrons evolve to fill up the phase space in the foil region

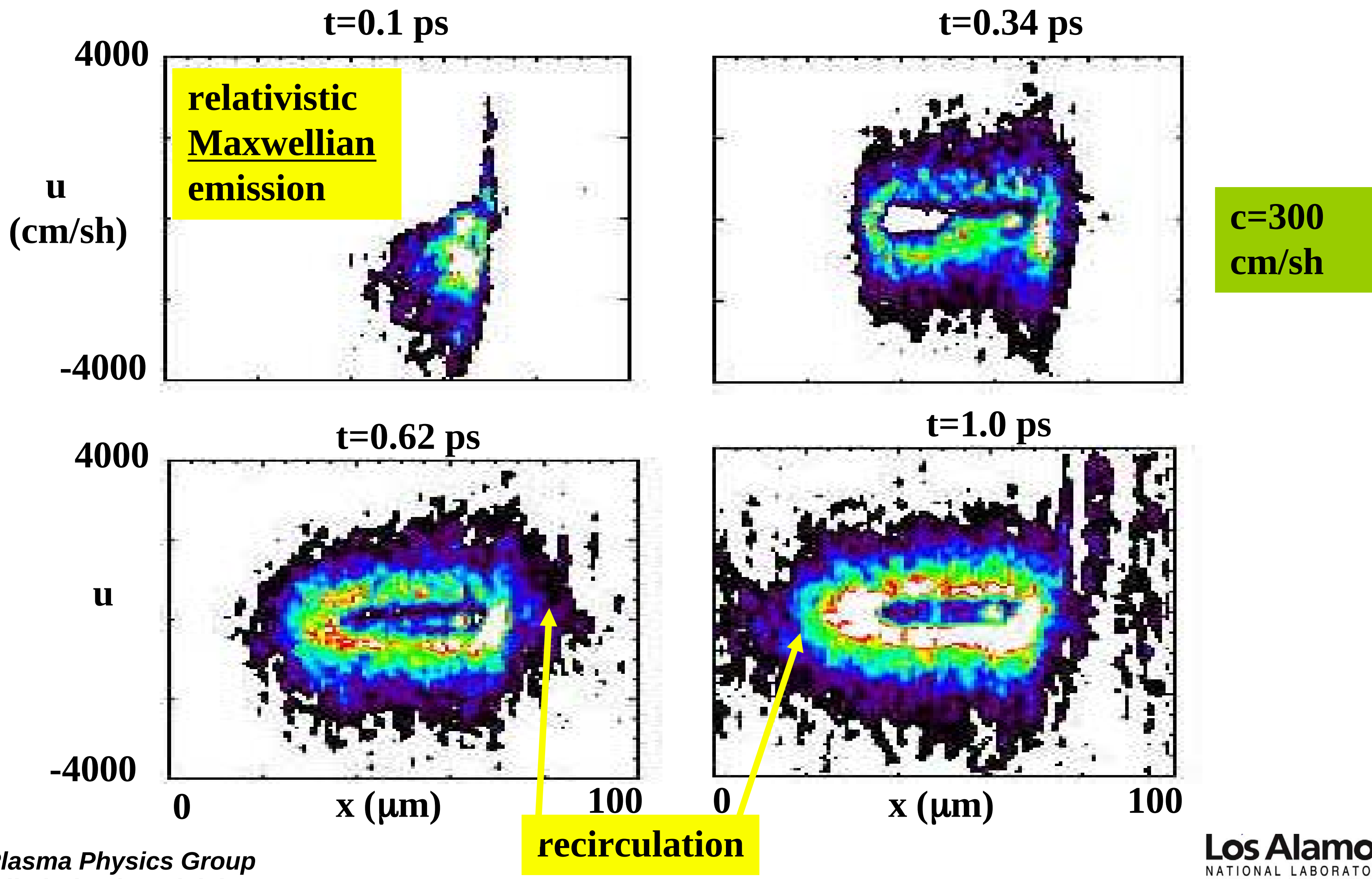

Artificial e⁻ emission from a central point shows the long time presence of a peak

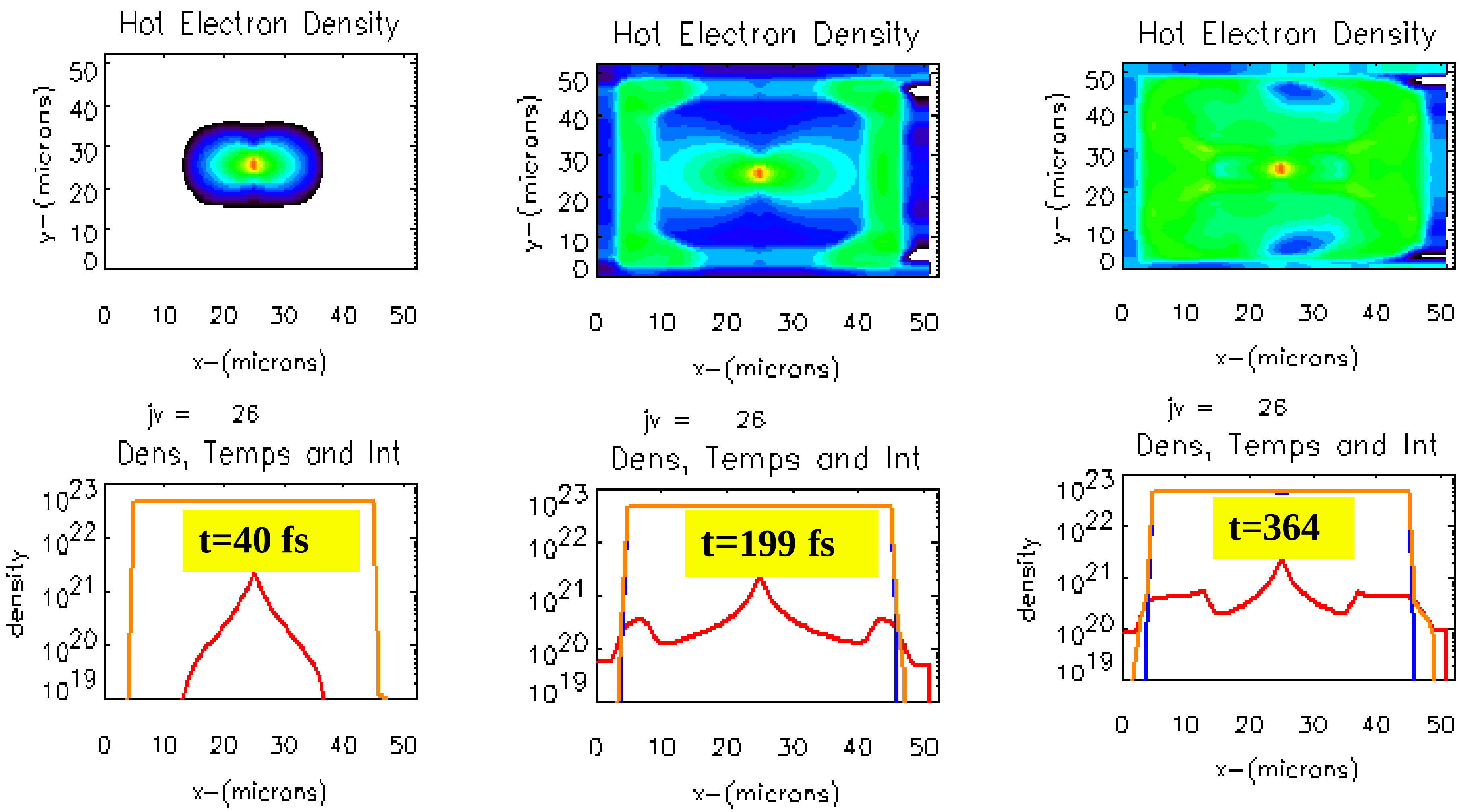

The same effect is evident with particle hot electrons, albeit more diffusive

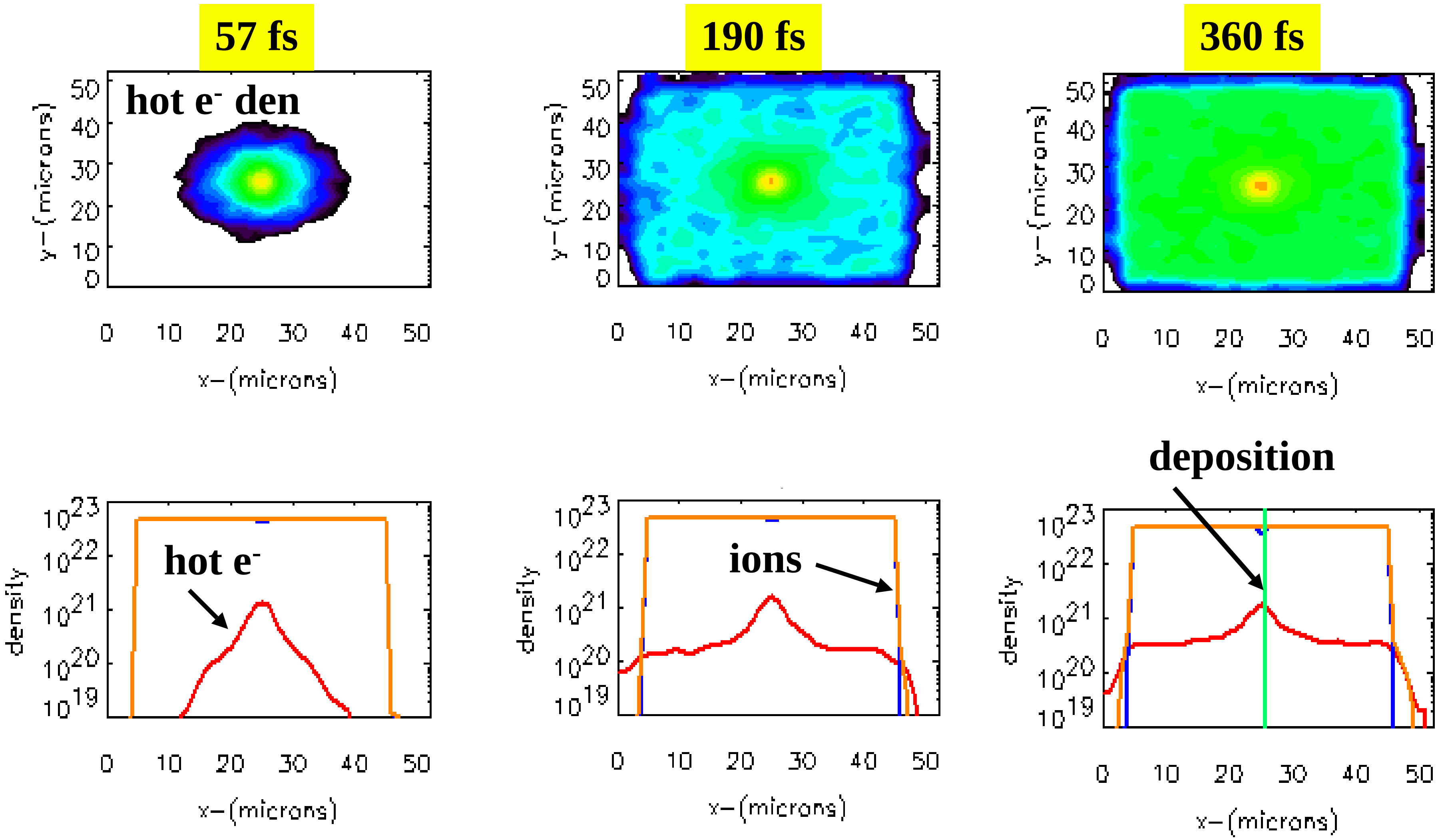

Small spots (~6 μm) geometrically retain high electron densities near their source

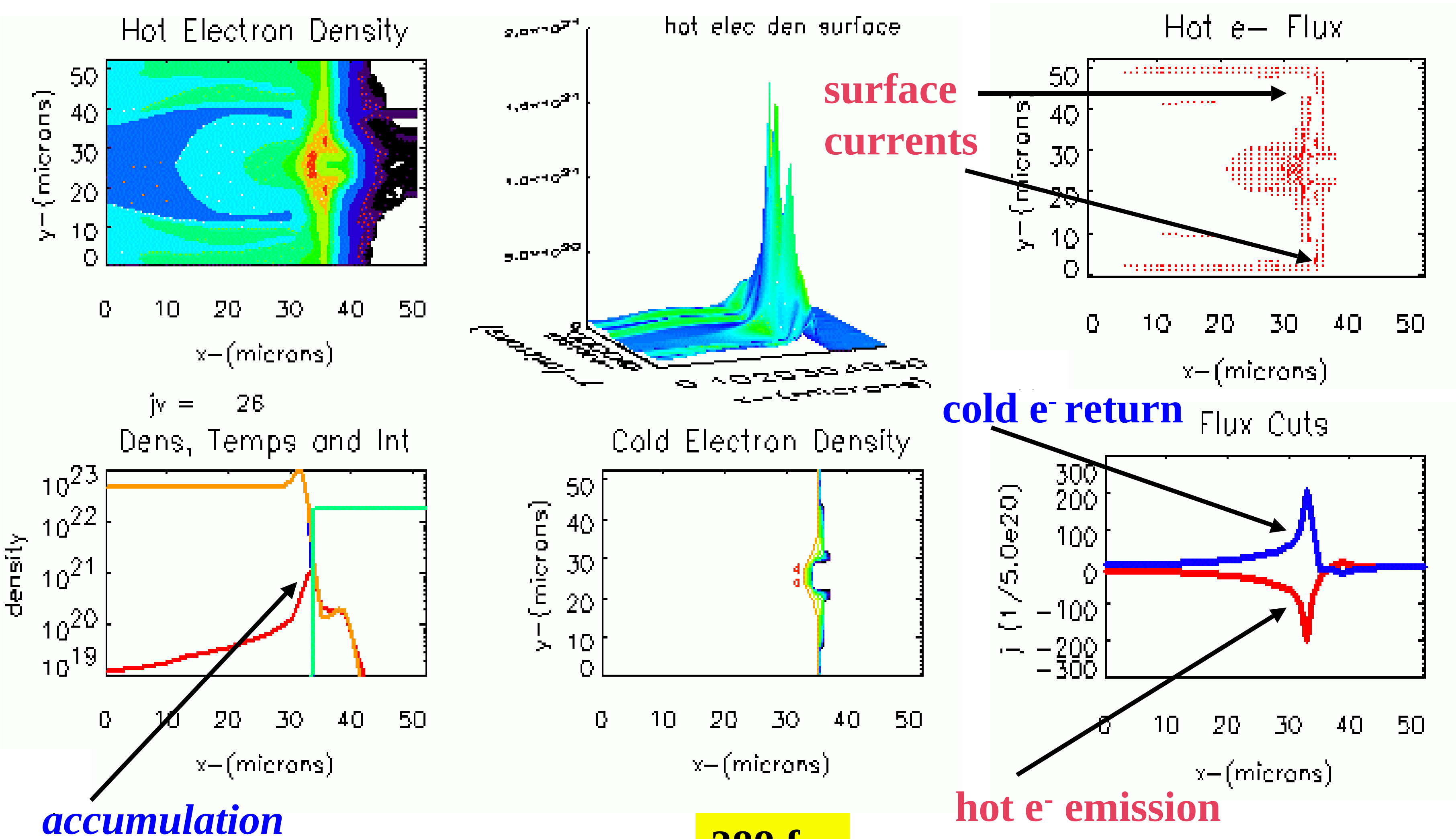

388 fs

Similar but more diffused results are obtained using particle hot electrons

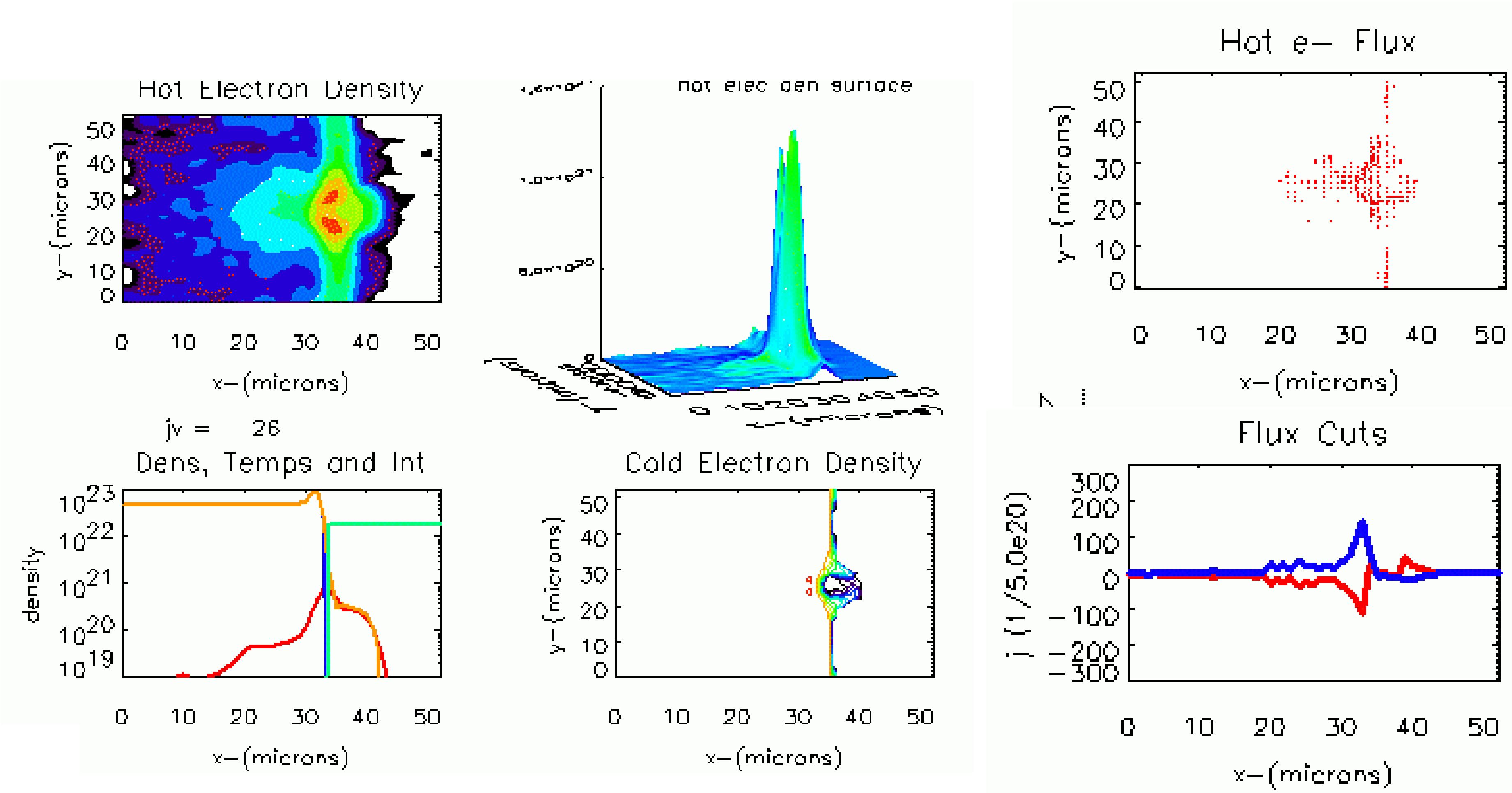

391 fs

Wide thin foils show spreading of the back-side blow-off, and e^- retention near spot

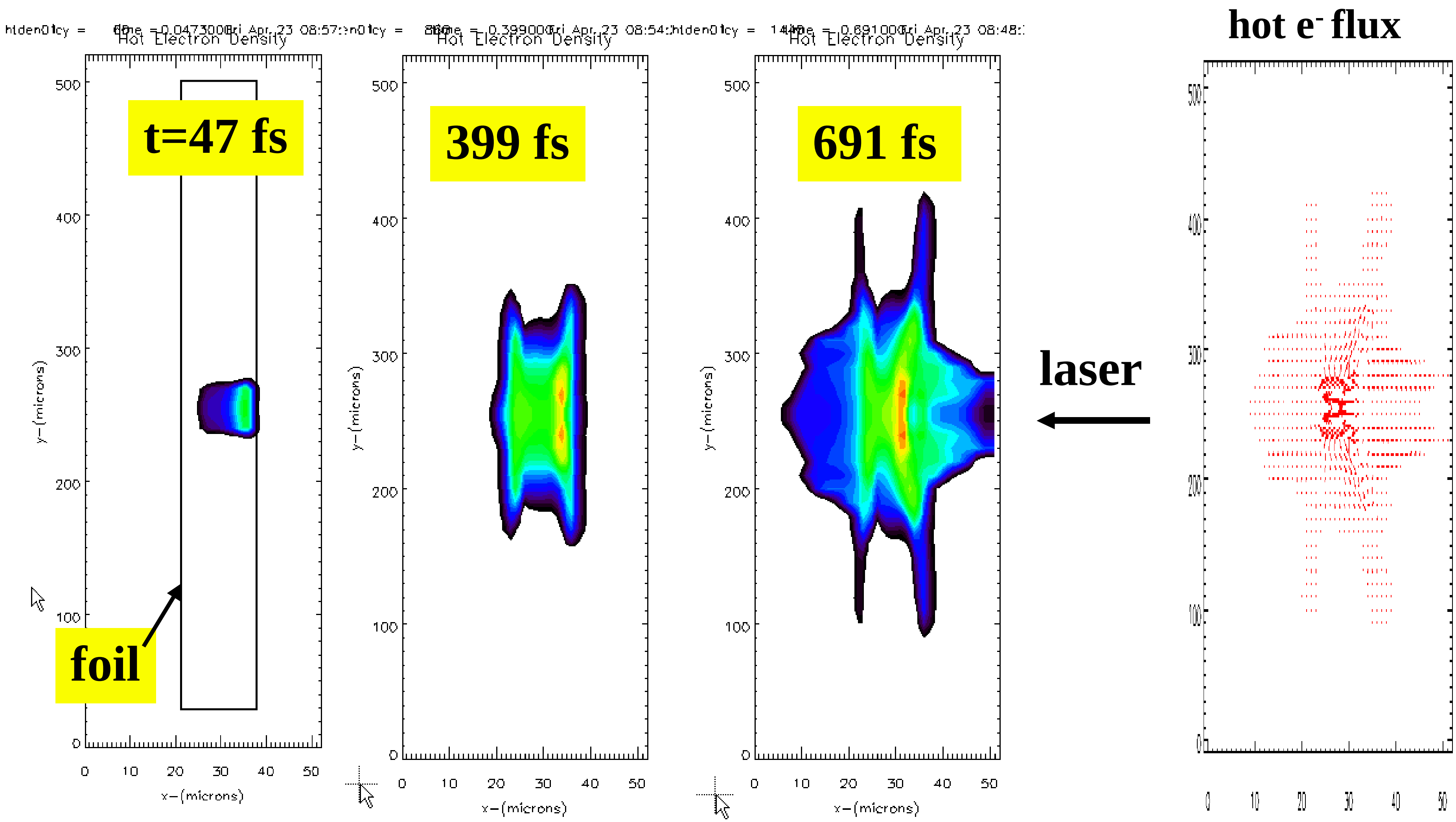

Plasma Physics Group
Applied Physics Division

$5 \times 10^{22}\ e^-/cm^3$

$I=1.3 \times 10^{19}\ W/cm^2$

Los Alamos
NATIONAL LABORATORY
Ideas That Change the World

Hot e^- and foil evolution: 100 x solid H_2 foil (5000 x critical) @ 2 $\times 10^{20}$ W/cm^2 illumination

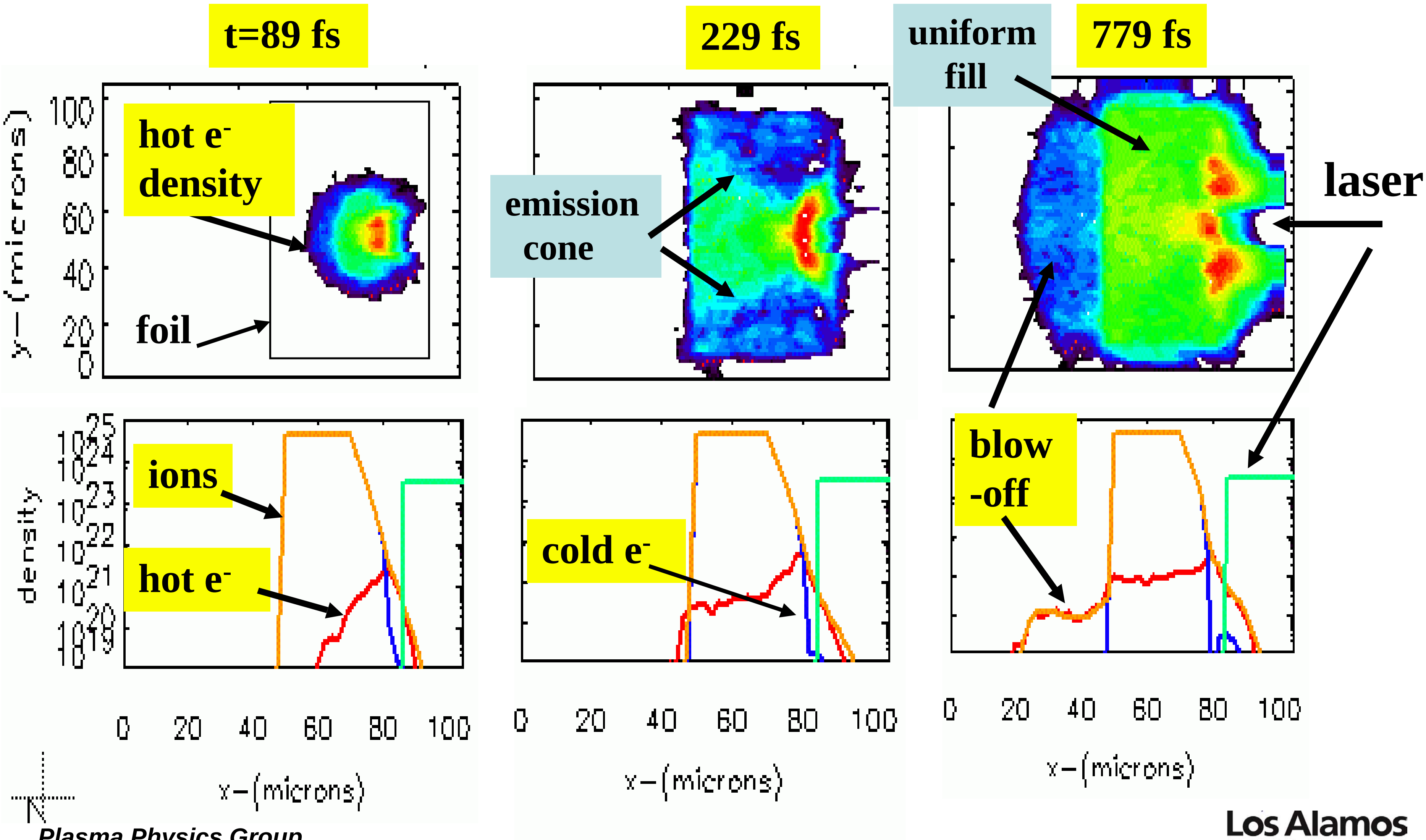

Corresponding E and B-field evolution

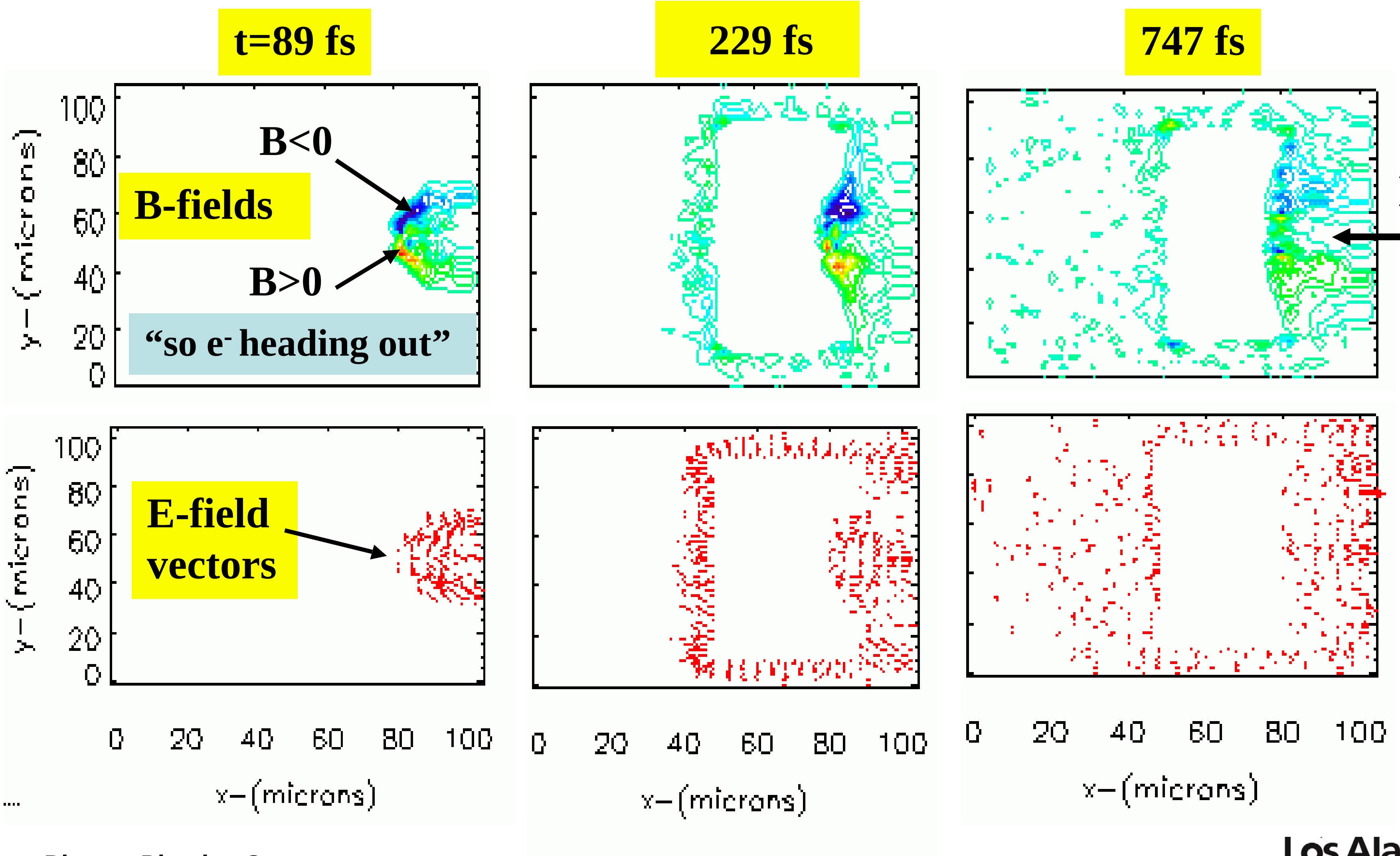

Plasma Physics Group
Applied Physics Division

Los Alamos
NATIONAL LABORATORY
Ideas That Change the World

The B-field amplitudes approach 200 MG and fluxes run at ~200 (μm/ps) x $10^{21} e^- /cm^3$

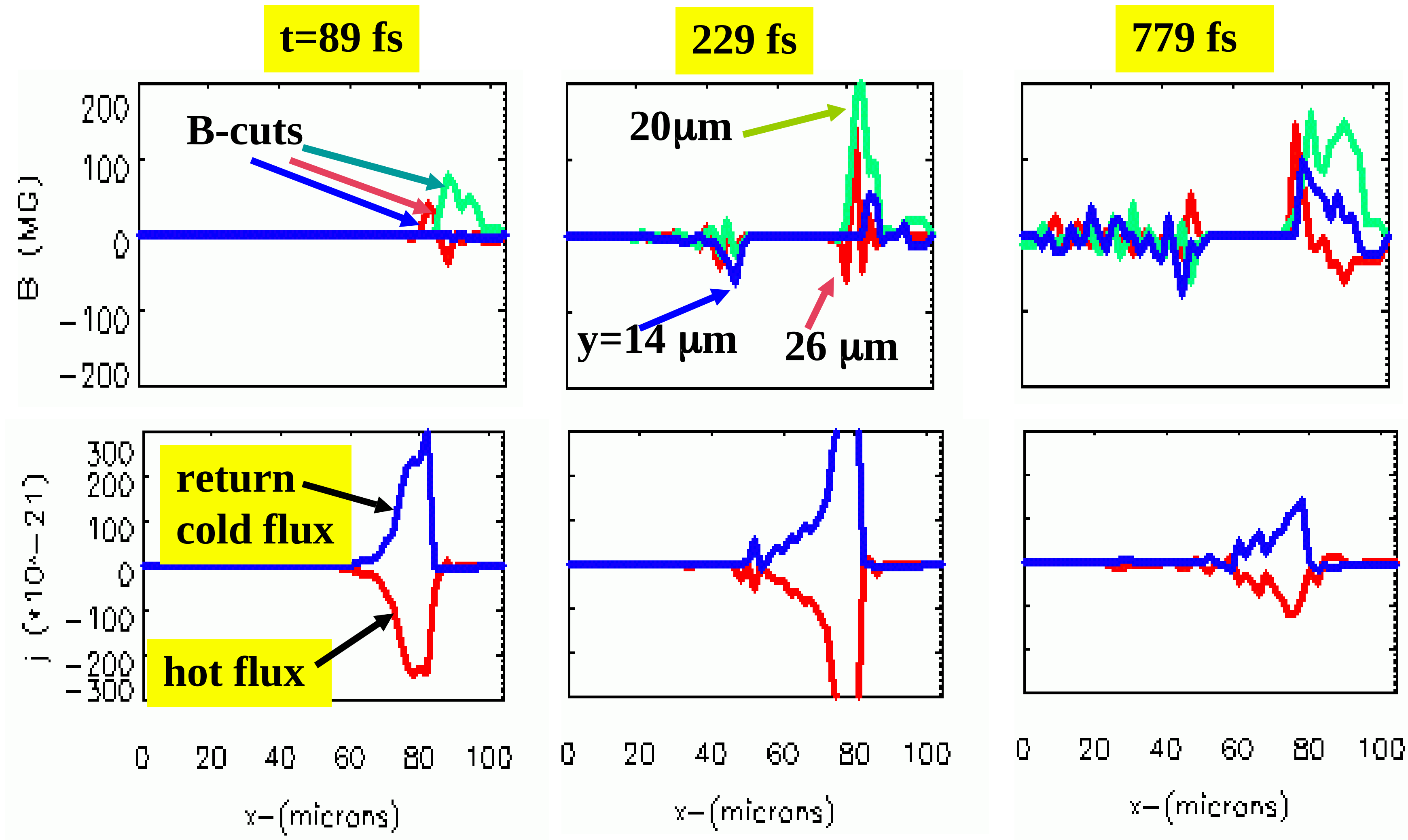

Plasma Physics Group
Applied Physics Division

Los Alamos NATIONAL LABORATORY
Ideas That Change the World

Component fluxes, laser beam, and hot electron phase space (at 779 fs)

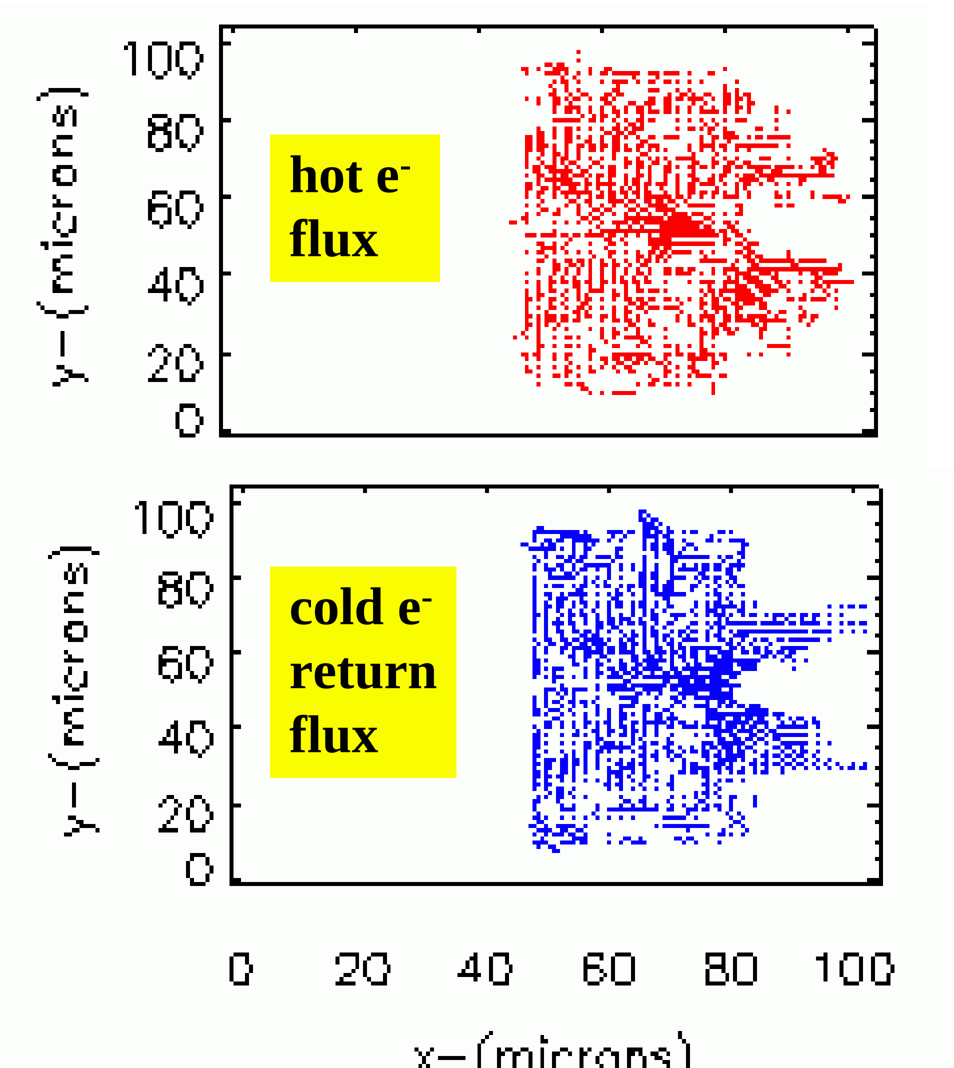

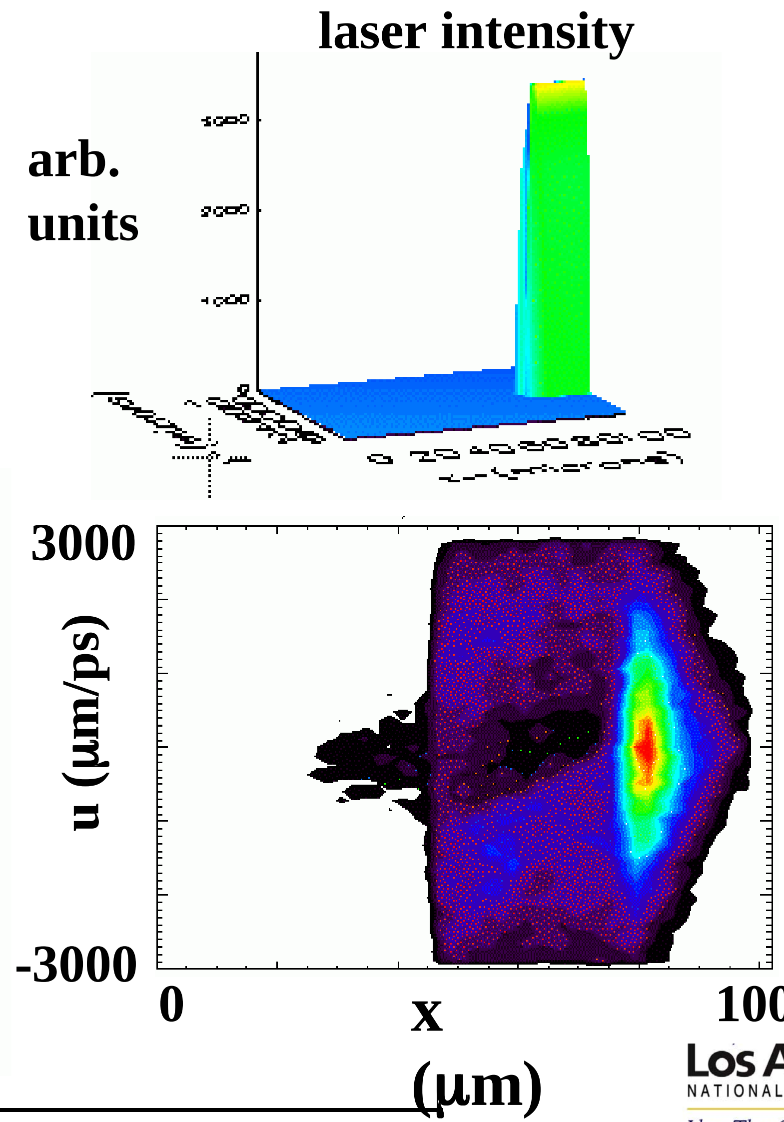

Higher resolution and hot e^- particles replicates PIC code Weibel instability

Full-PIC (Dodd)

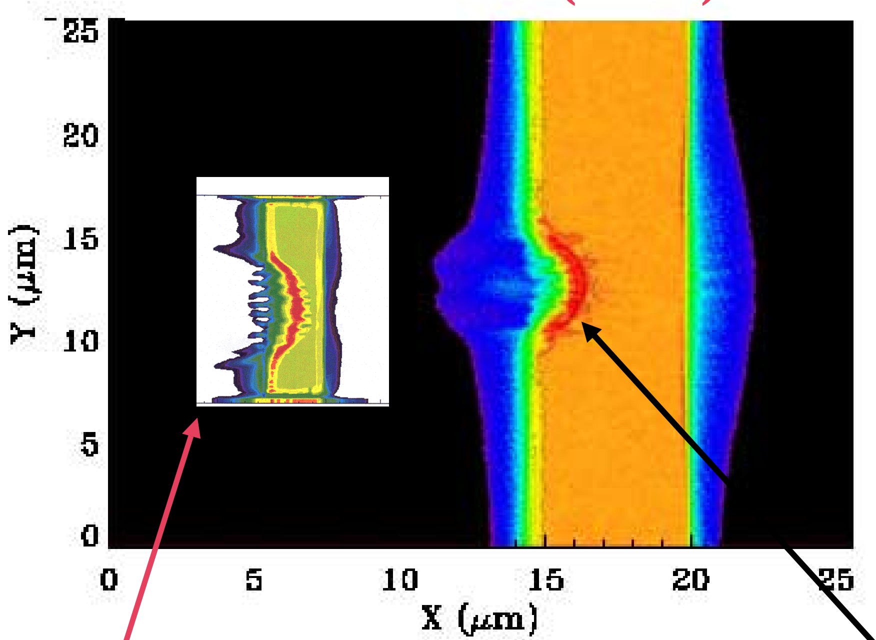

ANTHEM PIC/Hybrid

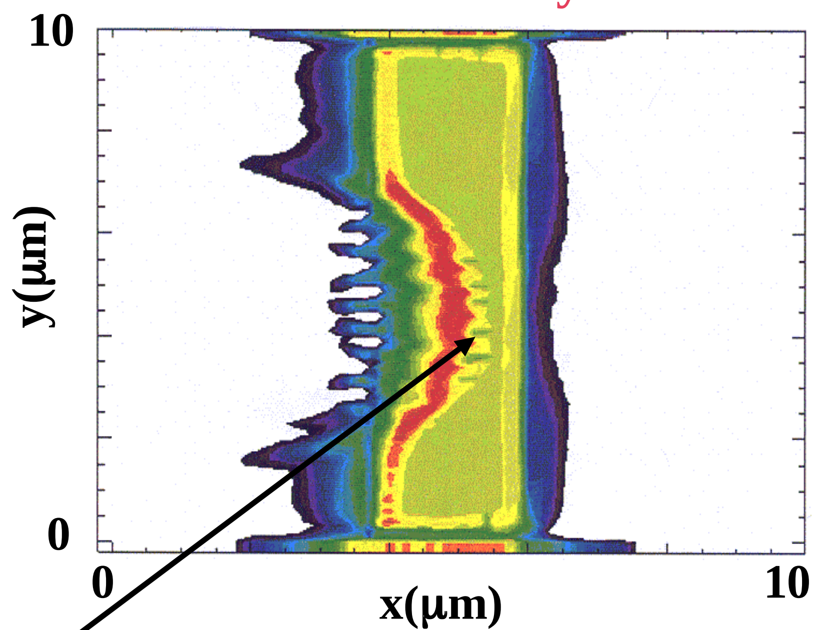

actual ANTHEM scale

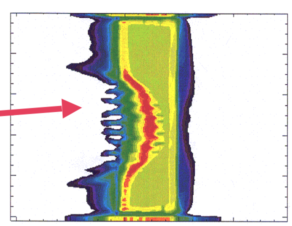

thinner foil

Weibel filaments

Wilks/Dodd ion emission study
$I = 2 \times 10^{20}$ W/cm^2 42 fs _ sine pulse

Observations

- **Our implicit approach requires mesh convergence studies and comparisons with more expensive explicit PIC runs**

- **For the future -- implicit calculation of the *E x B* light transport and absorption are feasible**

- **Relativistic fluid descriptions have been retained as options for both the hot and cold electron components**

- **Particle ions are available (although with less density dynamic range, *and no collisional shocks*) for fast ion blow-off studies**

Conclusions

- **Implicit models such as ANTHEM can provide new insights concerning short-pulse laser-matter interactions.**

- **Realistic, full-up short pulse laser target systems can be studied with limited computer resources**

- **The outgoing hot electron stream seems principally influenced by the source geometry plus vacuum reflections to maintain quasi-neutrality**

- **Ponderomotive influences strongly in evidence above 5 x 10^{19} W/cm^2**

- **No particular transport limitations evident from B-fields or instabilities**

- **In H_2 at 100-fold compression, no resistive effects appear significant**

- **The emission source needs careful study with traditional explicit PIC**

Ion Acceleration and THz Generation by Ultrashort Laser-Foil Interaction

Ion Effects

Peter Messmer[1],

David L. Bruhwiler[1], John R. Cary[2], Dimitre A. Dimitrov[1],

and the VORPAL Development Team

1. Tech-X Corporation
2. University of Colorado

Short-Pulse Laser Matter Workshop, August 25-27 2004

Acknowledgement

M.Tzoufras, F.S.Tsung, W.B.Mori

(UCLA)

S.Amorini, R.A.Fonseca, L.O.Silva

(IST, Portugal)

J.C.Adam , A.Heron

(École Polytechnique, France)

Outline

- Motivation
- VORPAL
- Model Setup
- Particle acceleration
- Low-frequency Waves
- Conclusion/Future work

Motivation

- Understand emission of THz from solids
  - Hamster et al (PRL, **71**, 17, 1993) via laser-plasma interaction at high densities
- Model (fluid based)
  - Explains emission at plasma frequency
  - Does not account for low frequency emission
- Only electrons included
  - Ions may be important (e.g. ion plasma frequency is 5-10THz)

=> Fully kinetic model required

VORPAL: Overview

- Plasma simulation code/framework
  - PIC, Fluid, hybrid model
- Original design: Wakefield acceleration
- Nieter & Cary, JCP, 2004, 196(2), p448, 2004

- Multi-Dimensional (N=1,2,3)
- Fully parallel
  - Scaling for > 4000 PEs
  - Flexible domain decomp
  - Dynamic load balancing
  - C++
- Output format: HDF5
- Postprocessing/Viz: IDL, OpenDX, GnuPlot

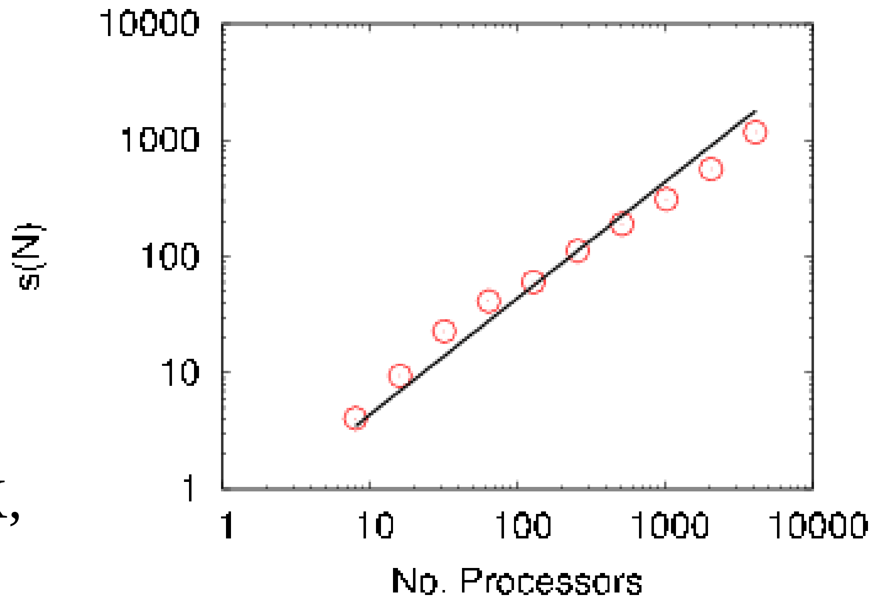

VORPAL speedup (C. Nieter)

http://www-beams.colorado.edu/vorpal/

VORPAL: Features

- Variety of particle emitters
  - Space Charge limited
- Parallel ES solver
  - Based on Aztec (Sandia)
  - Variety of solvers, preconditioners
    - Krylov solvers, alg. Multigrid
- DSMC
- Ionization
  - Field ionization
  - Impact ionization under development
- Direct Coulomb interaction
  - Hermite integrator

VORPAL: Applications

- Wakefield acceleration
- Electron cooling for RHIC
- High-power microwave breakdown
- Photonic bandgap structures

- Debris propagation in IFE chambers
- Dusty plasmas
- Gamma-ray bursts
- Magnetic reconnection

- … and Laser-Overdense interaction

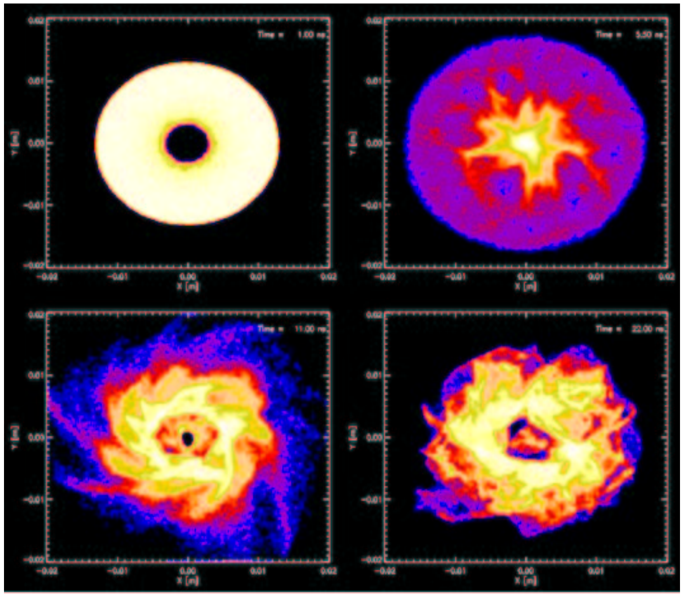

Figure : Time evolution of the ion density in a 2D VORPAL simulation, including debris ions, debris electrons, background ions and background electrons.

Original Setup

Oblique incidence

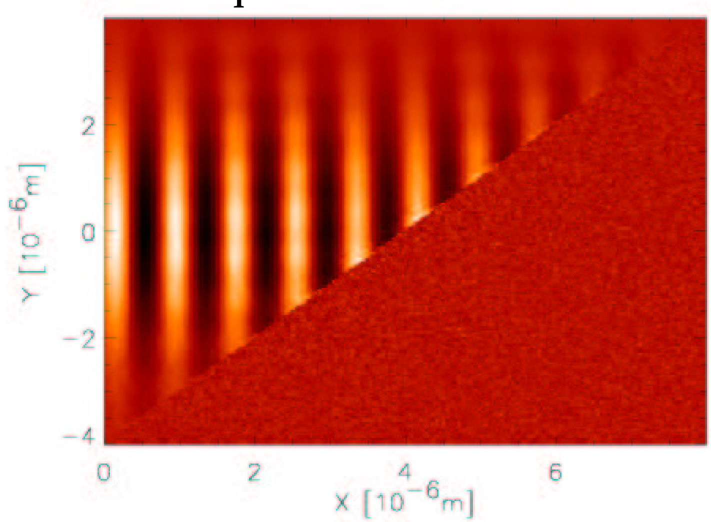

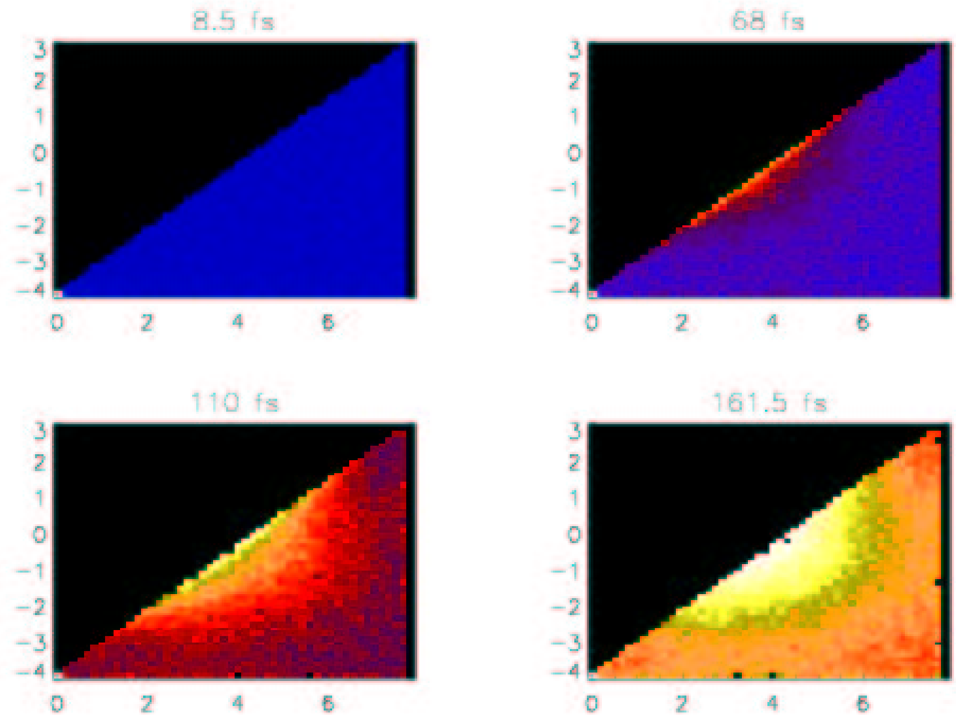

Electron temperature

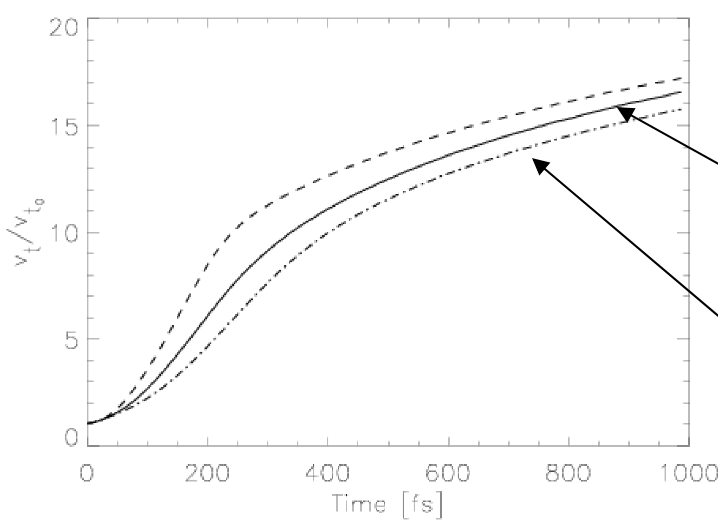

With pulse

Without pulse

Electron temperature

=> Strong num. heating

=> Look at smaller system

Model Setup (I)

Foil:

- He^+ ($6.68 \cdot 10^{-27}$kg), C^+ ($2 \cdot 10^{-26}$kg), pre-ionized
- Thickness: 1.5 μm
- Density: $\rho = 2.8 \cdot 10^{21}$ cm^{-3}

Laser:

- 800 nm (375 THz), 120fs, half-sine
- Normalized amplitude:
  - $a_0 = eE/mc\omega = 0.3 – 1.6$
  - Field 2.4 – 6.5 TV/m

Model Setup (II)

- High density challenging
  - Resolve Debye length -> dx = 10^{-9}m
  - Courant condition: dt < dx / c => dt = 10^{-18}s => 10^{6}-10^{7} timesteps

- Simulation setup:
  - Pseudo-1D, 2D, 1D
    - Want to see ion dyamics
  - Grid sizes: 3000x5 – 100’000x5, 4000x800
  - Transmission or reflection setup
  - Mainly interested in transmission setup

Overall Scenario

Laser pulse propagation

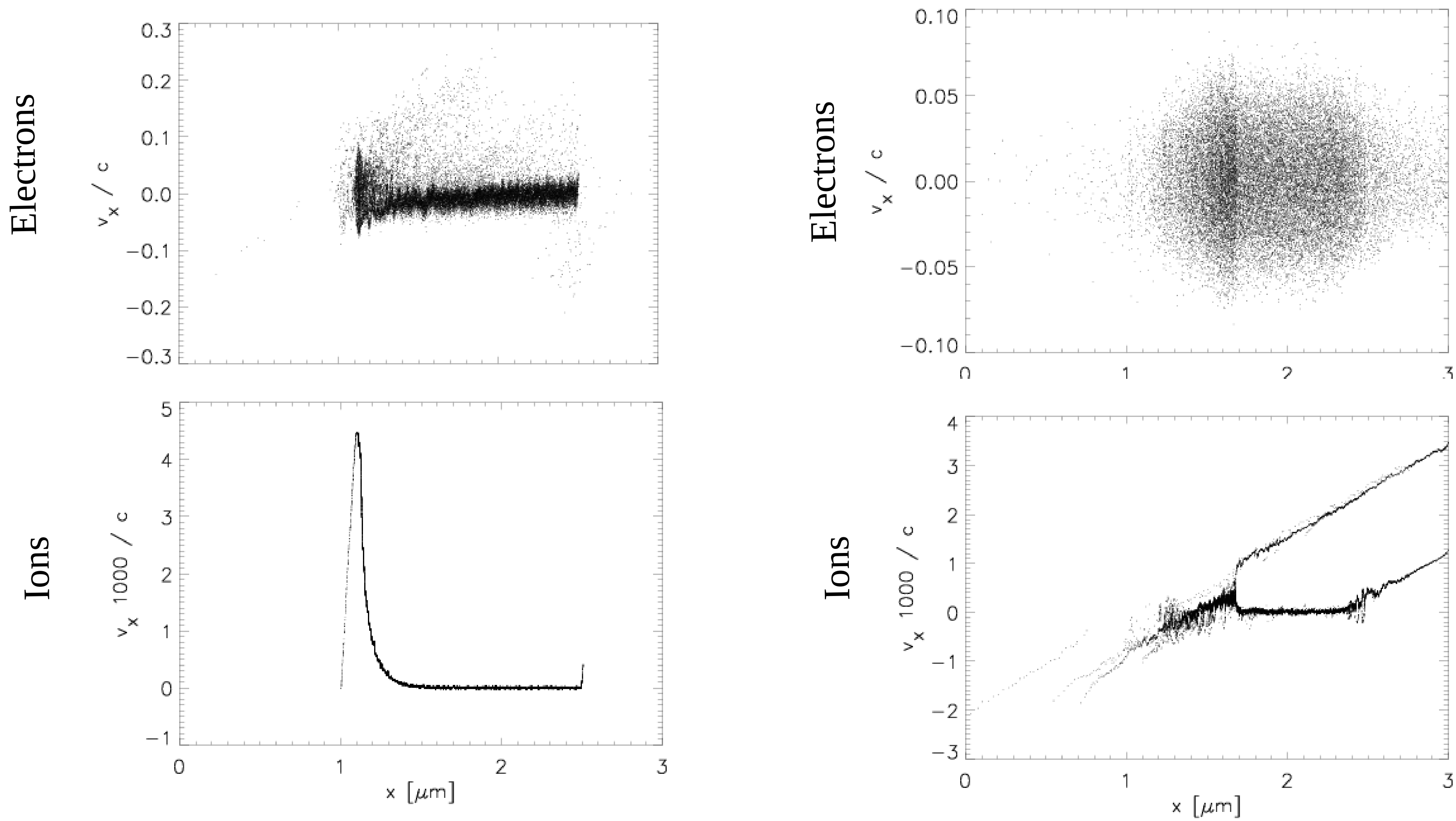

During Laser interaction (~100fs)

After laser turned off (~ 2ps)

Overview: Shock acceleration of Ions

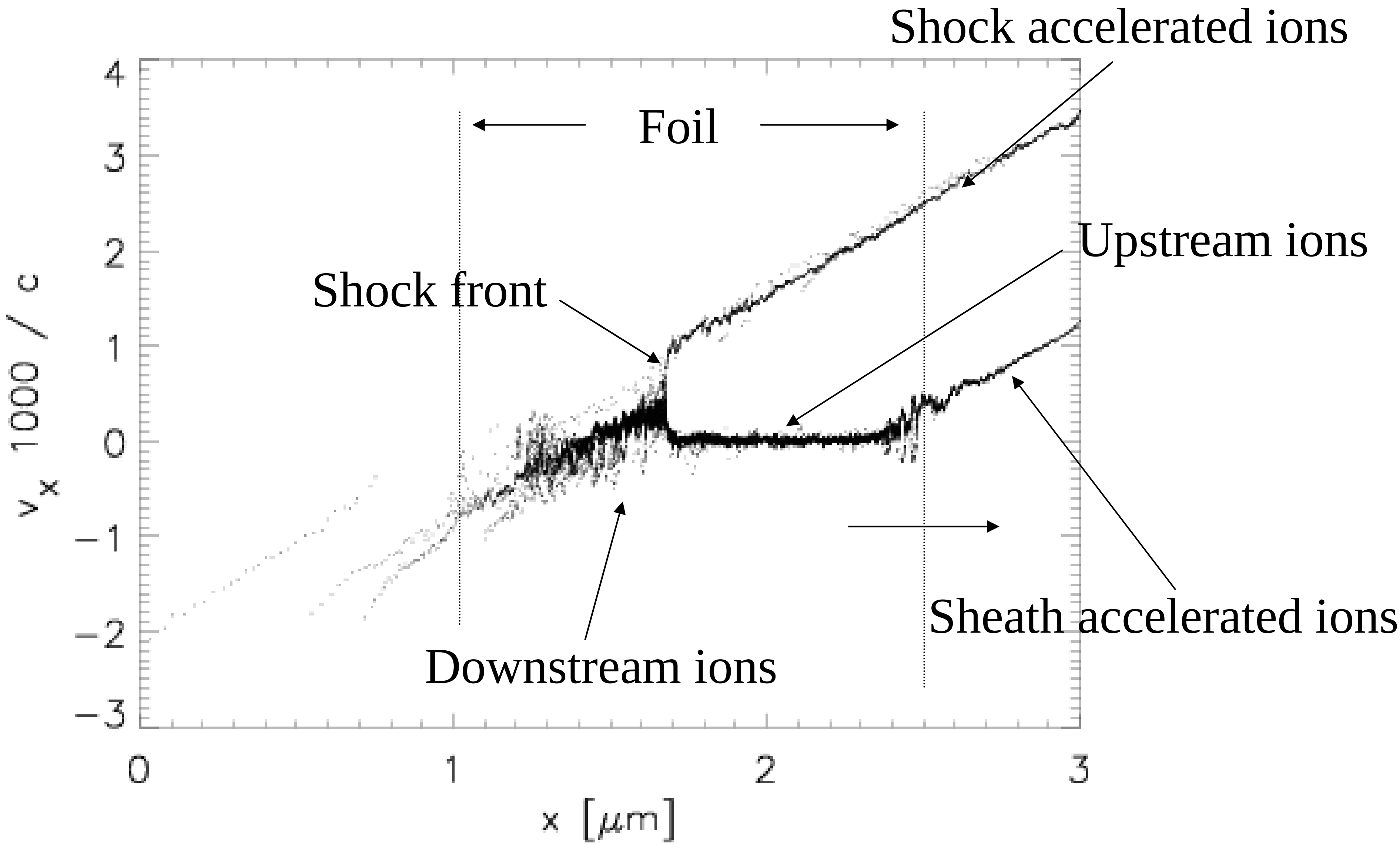

Phase Space structure indicates deceleration of shock!

Ion Acceleration inside the Foil

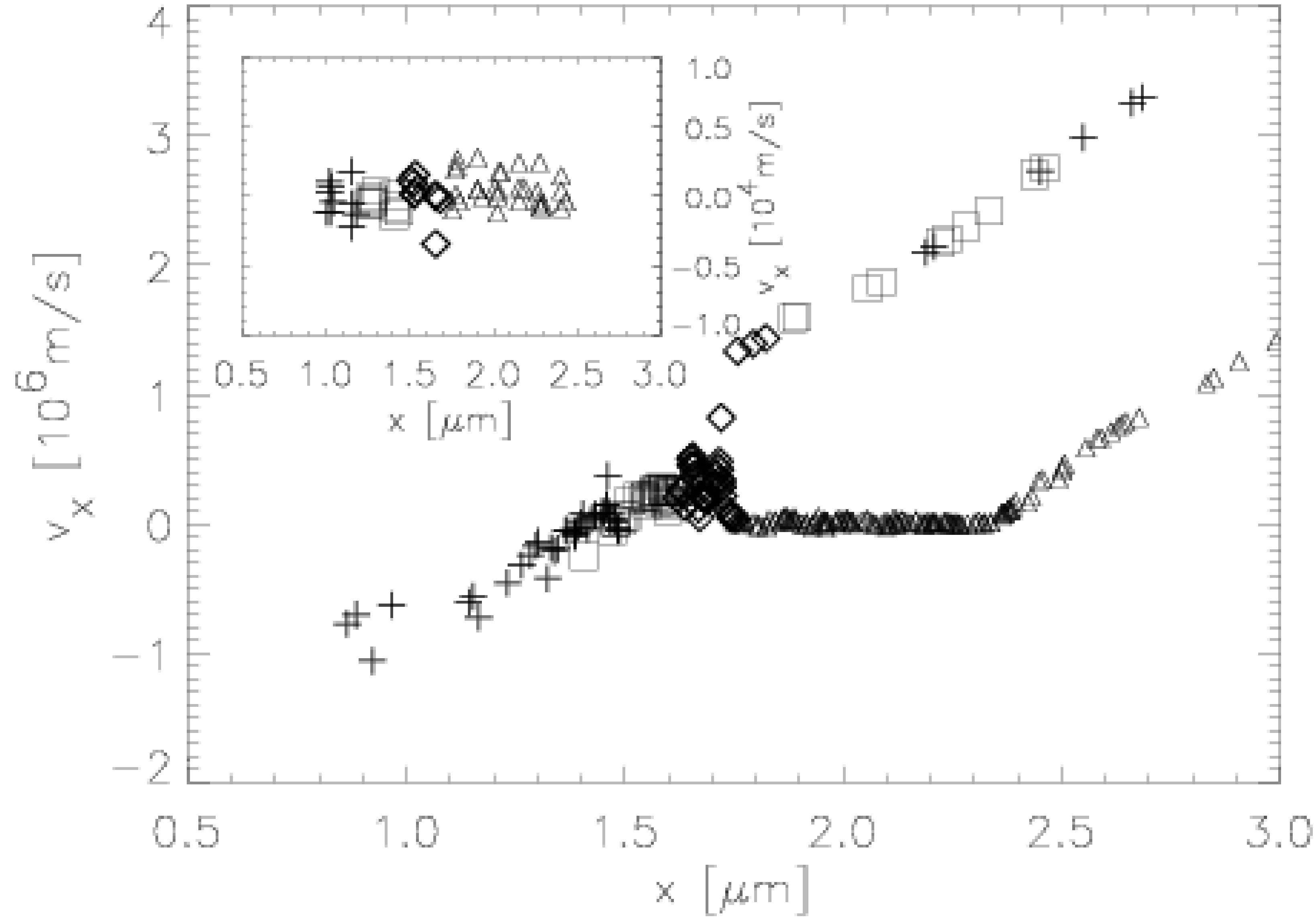

Detectable Particle Spectrum

- Place virtual detector behind foil
- Particle spectrum at different times
- Characteristic two-hump spectrum, sharp cut-offs

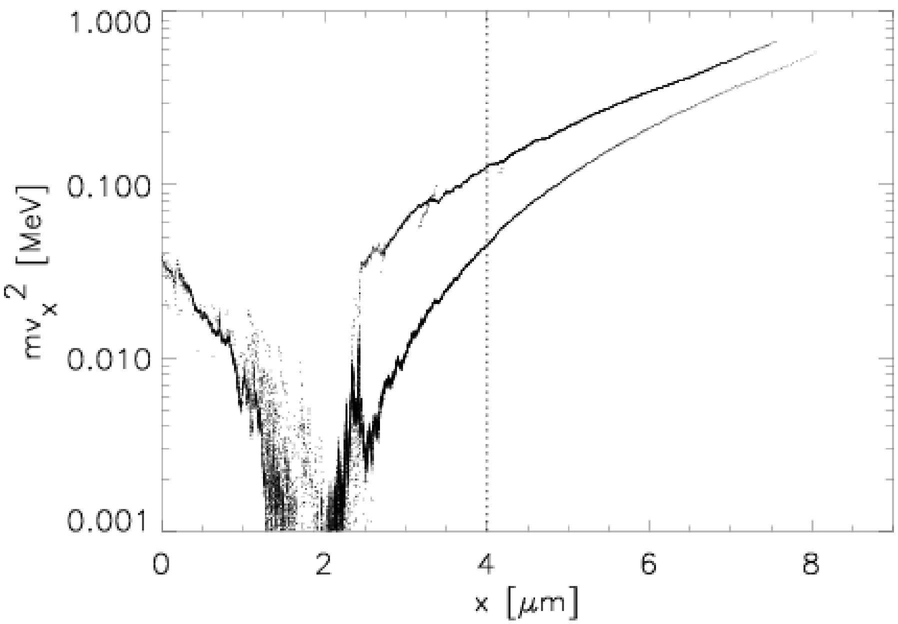

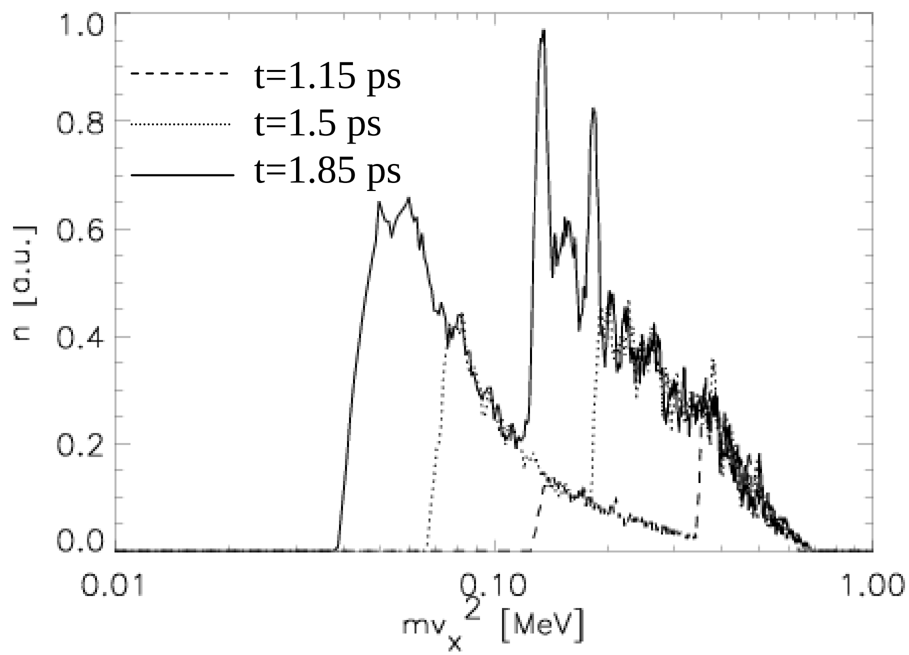

Shock propagation in 2D

t=0.65ps

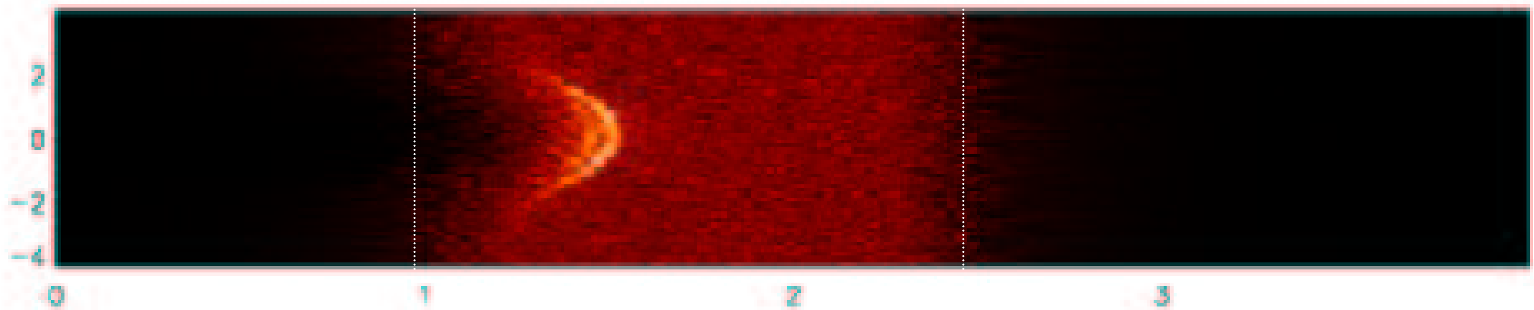

t=1.95ps

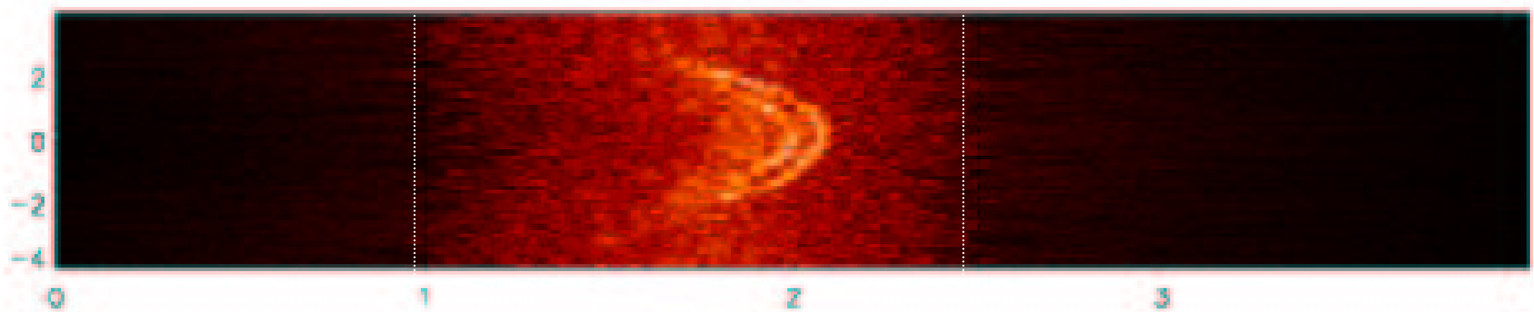

t=3.25ps

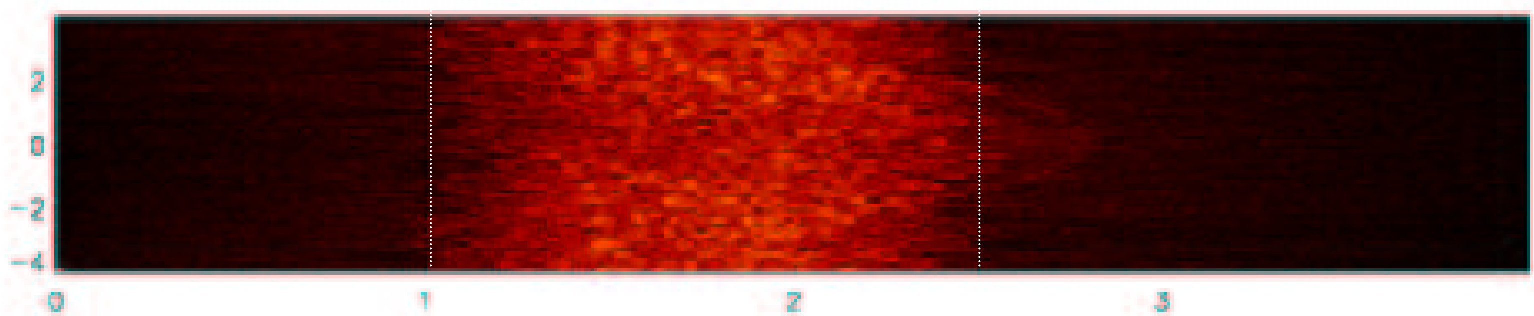

Shock decelerated in foil

- Strong deceleration of shock speed
- Also seen in ion phase space
- Determines ion energy

$E_{||}$ a_0=0.6

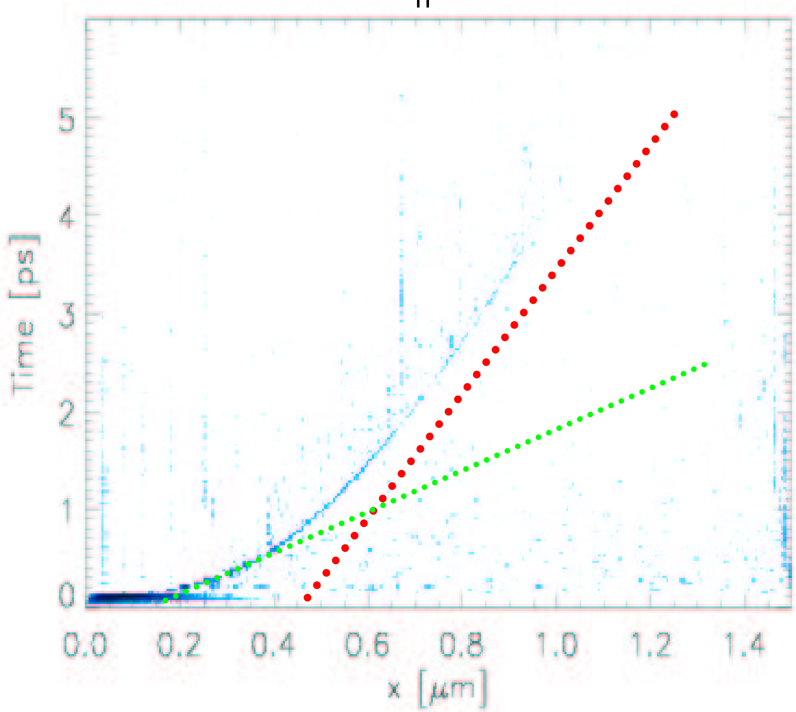

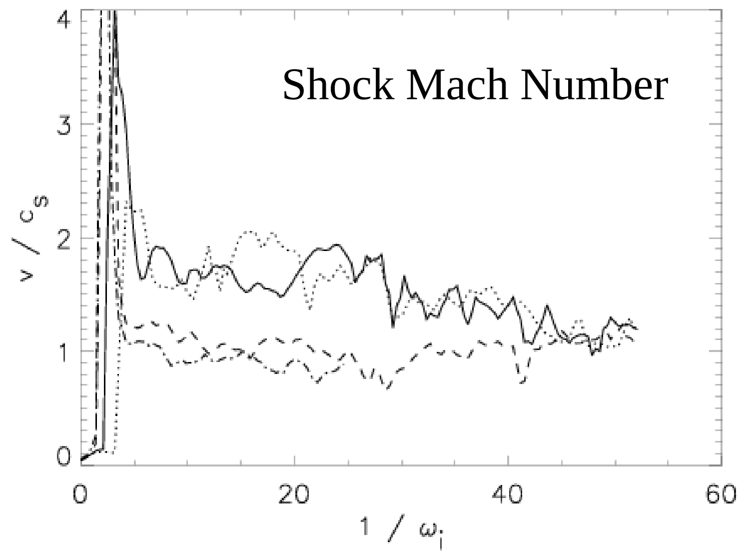

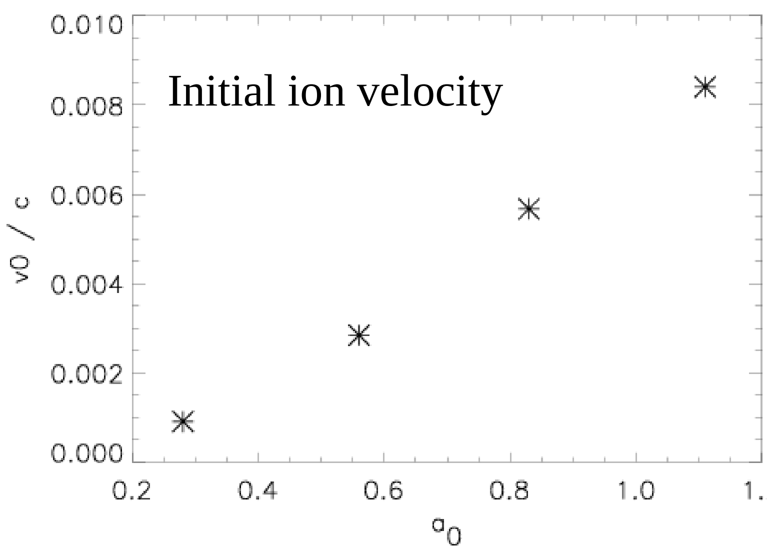

Longitudinal Waves in Foil

- Waves in front of shock:
  - Phase velocity consistent with sound velocity
  - cutoff at ion-plasma frequency
- => Ion-acoustic waves
- Waves in THz range
  - Candidates for emission
- Questions:
  - How do they radiate?

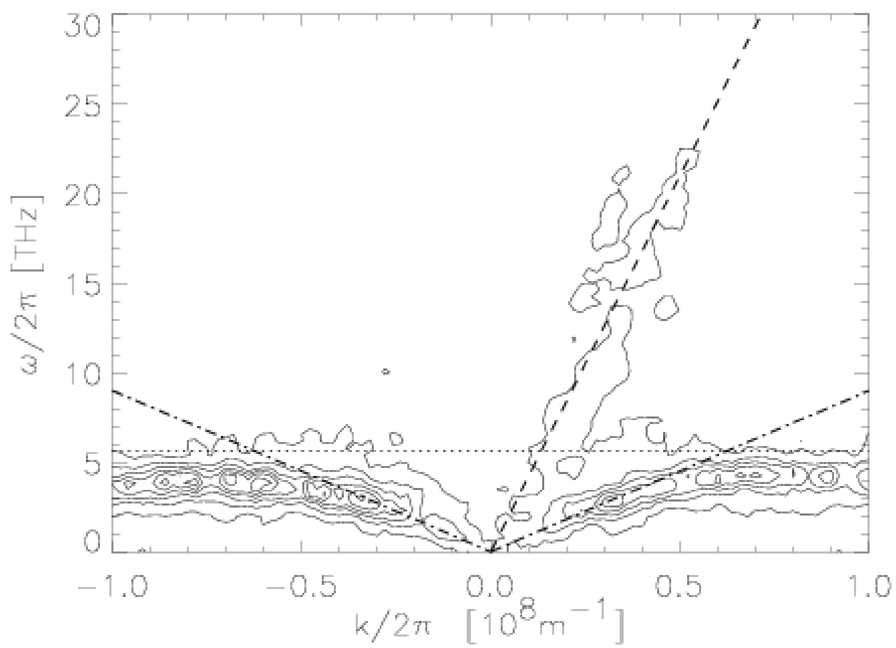

- Concentrate on shock accelerated ions

E-field Spectrum Inside Foil

- FFT in time at fixed location
- After laser pulse has left

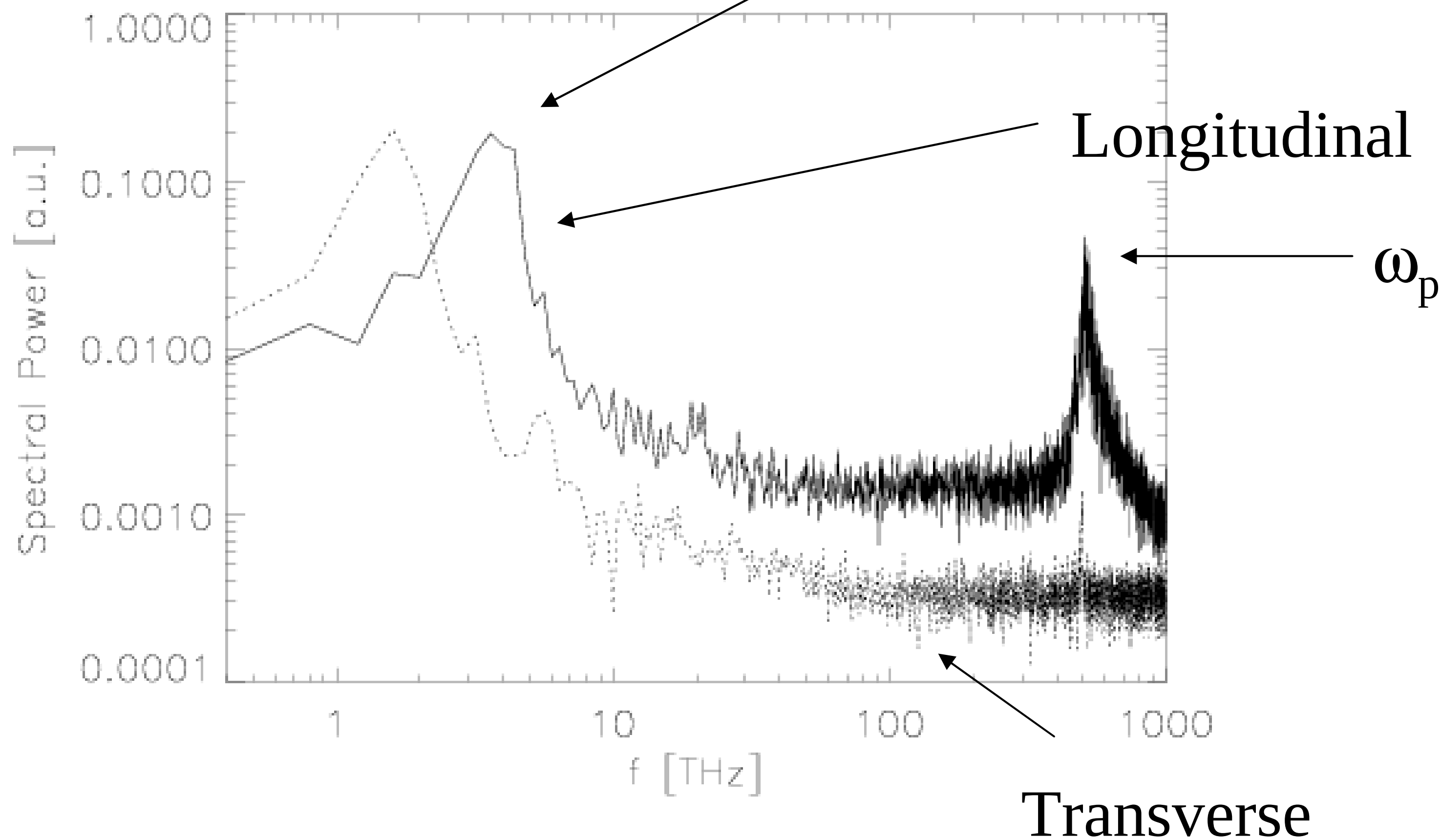

Transverse B Field Behind Foil

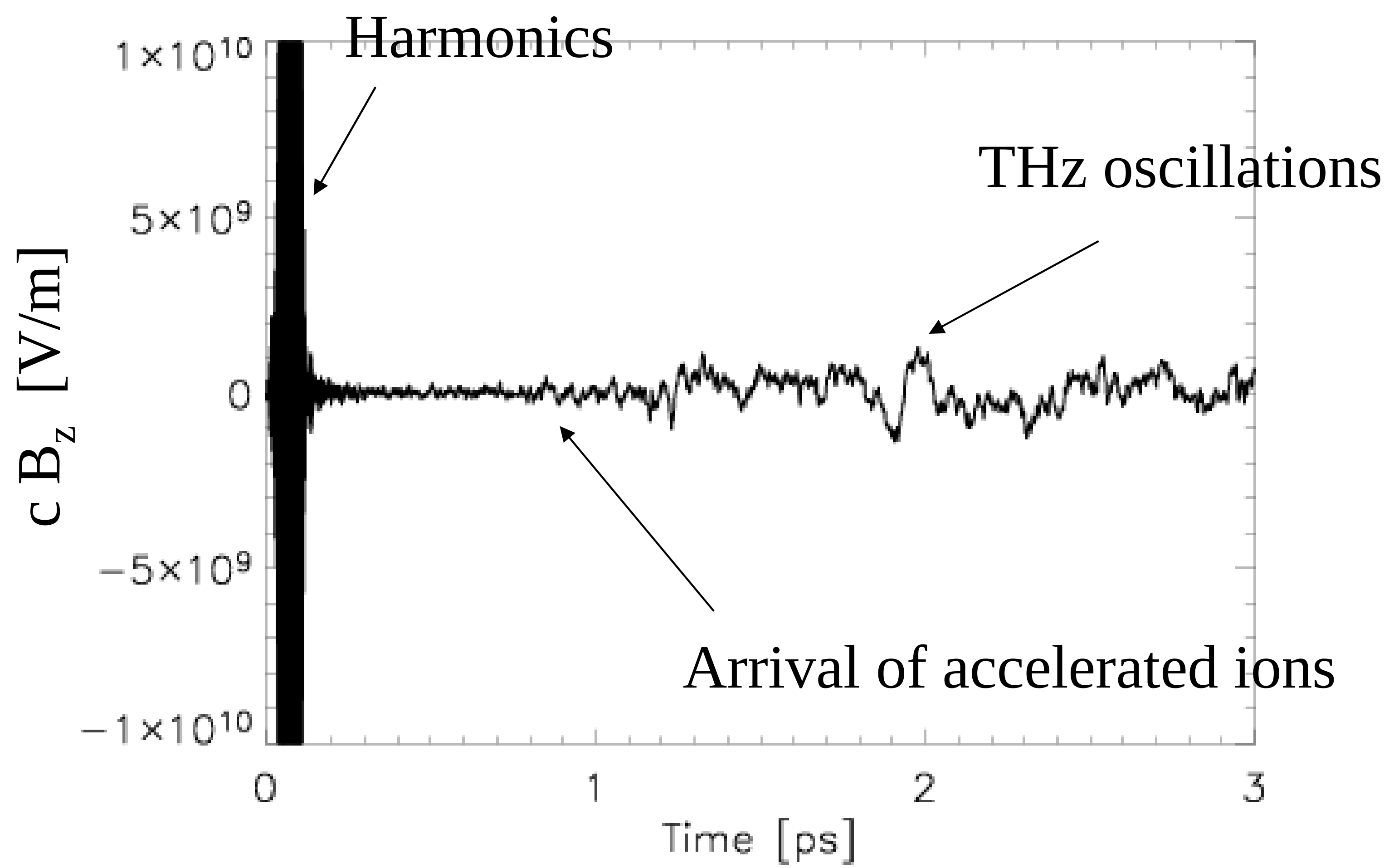

Low frequency waves

Dispersion relation behind foil

Shows two branches with different phase velocities

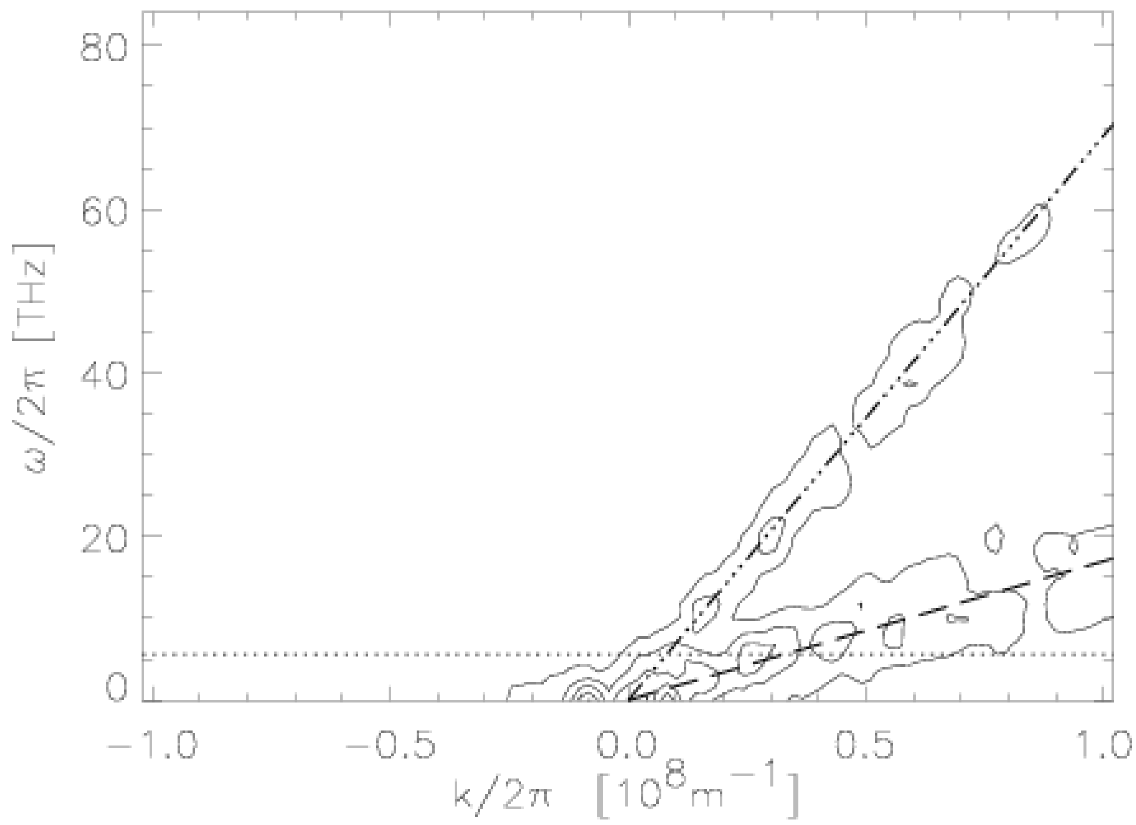

Intensity Dependence of Spectrum

k-integrated spectrum behind foil
Dependency of spectrum peak on intensity!

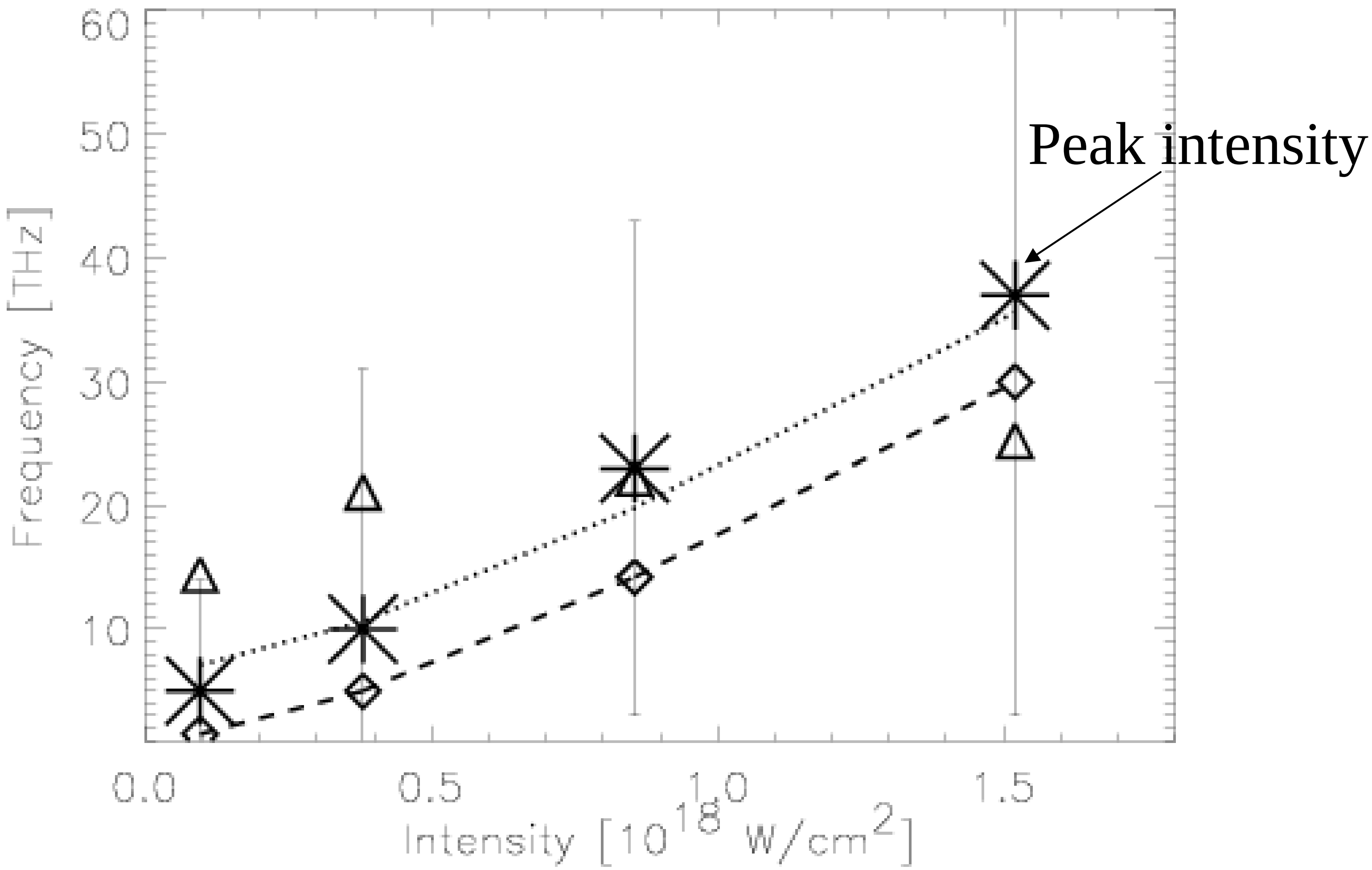

What causes transverse motion?

Transverse oscillations inside foil

Ions get transverse kick at shock

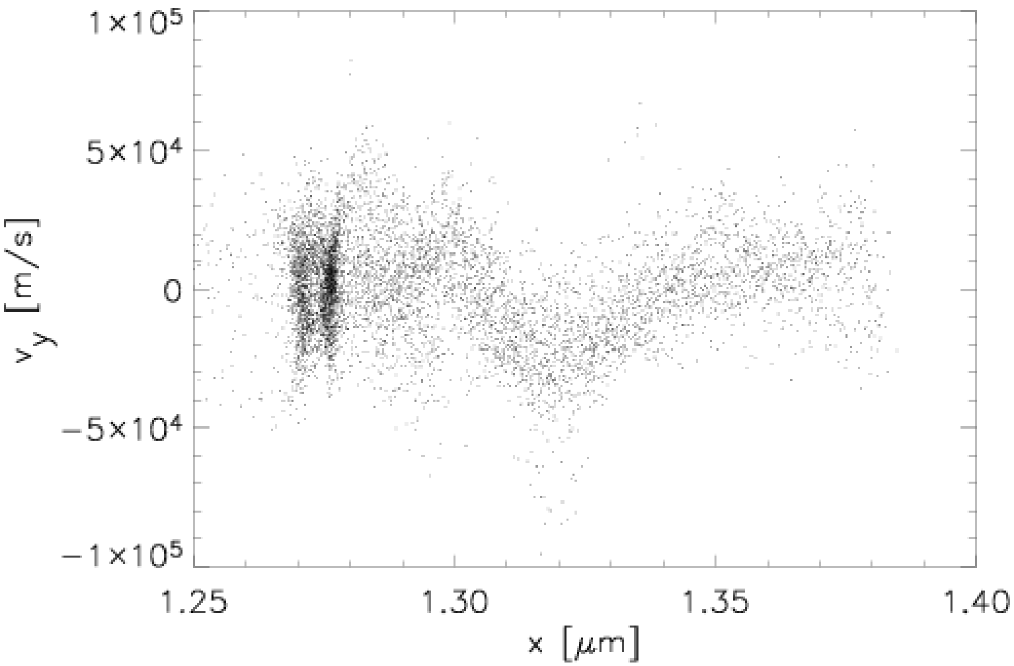

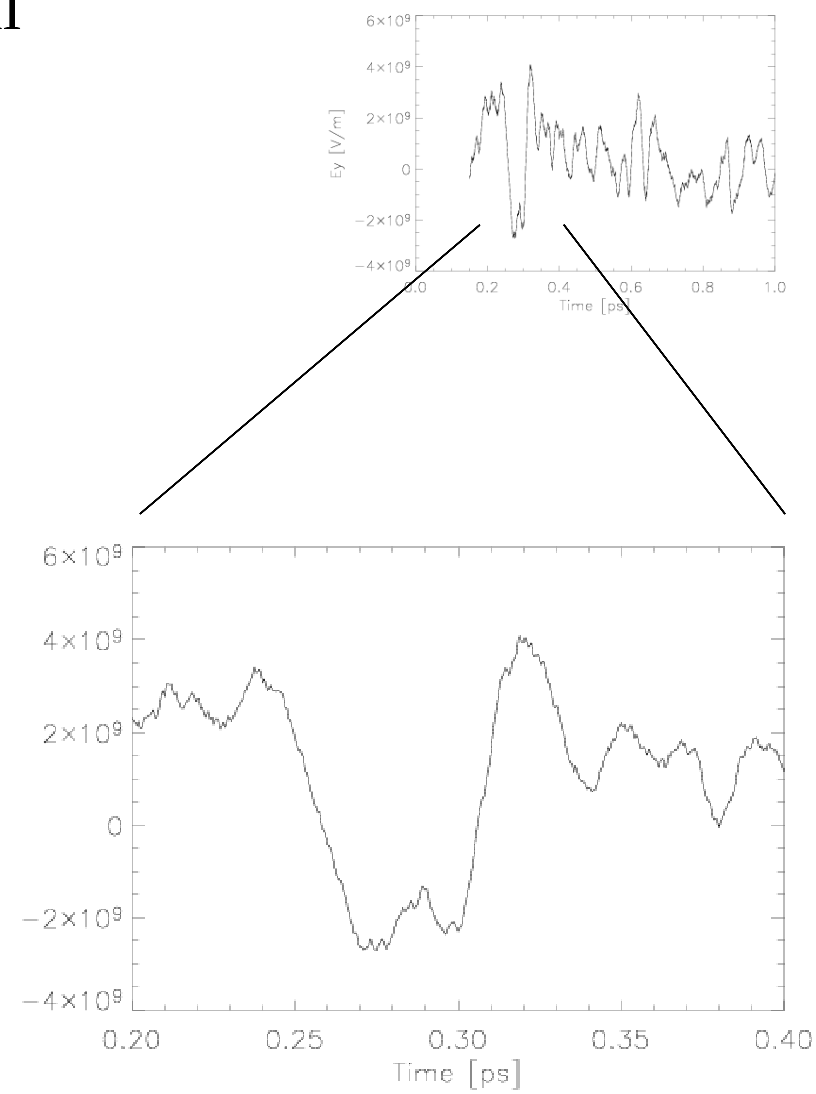

TECH

Conclusions

- See: Transverse THz oscillations behind foil
- Due to transverse ion velocities
  - Origin: Ions at shock front get transverse kick
- Other shock properties
  - Observable energy spectrum

- Future work:
  - Extended 2D region
  - See if other effects present
  - 3D (?)

Hybrid Particle-in-Cell Simulations of MeV Electron Transport in Fast-Ignition Targets

$$\eta = \eta_G \times \boxed{\eta_T} \times \eta_S$$

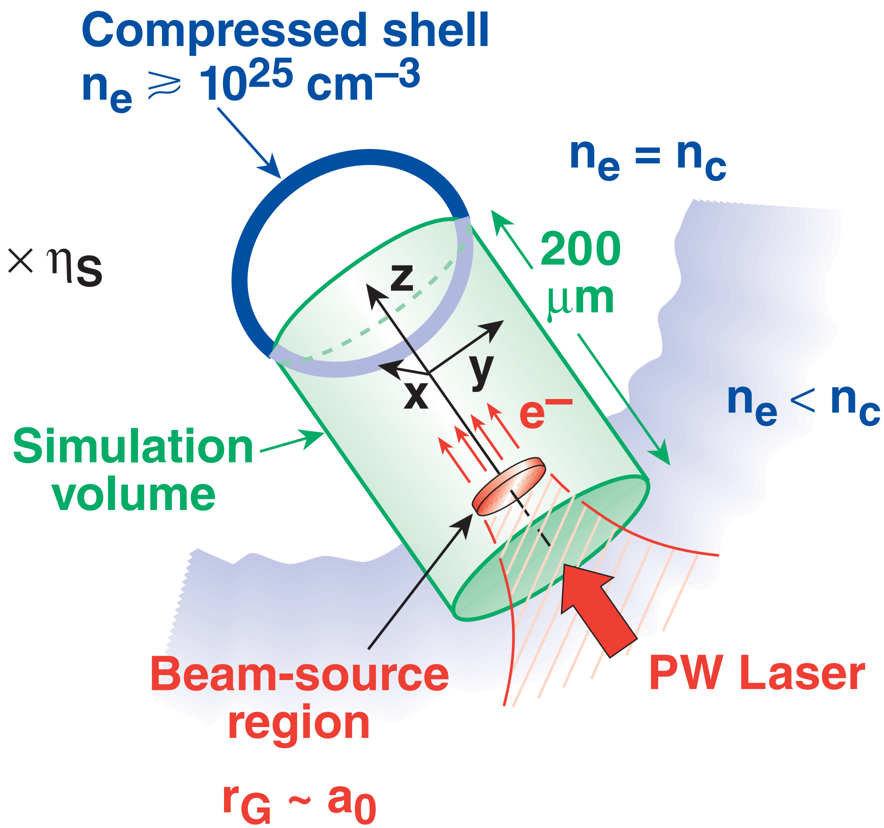

J. Myatt, A. V. Maximov, R. W. Short,
J. A. Delettrez, and C. Stoeckl
Laboratory for Laser Energetics
University of Rochester

Short-Pulse Laser–Matter
Computational Workshop
Pleasanton, CA
23–27 August 2004

Summary

Three-dimensional LSP[1] simulations of MeV electron transport predict a $\gtrsim$ 10% efficiency for a 20 μm radius core at a propagation distance of 40 μm

UR LLE

- The efficiency η_T = (energy reaching core/energy in fast electrons) and does not include stopping.
- From the beginning of fast ignition, it has been recognized that the transport distance needs to be made as small as possible leading to the concepts of hole boring and cone-focused implosions.
- Transport efficiency has been investigated using OMEGA profiles for two propagation distances.
- A standoff of 40 μm implies either hole boring or cone focused implosion.
- If electrons are generated near the critical surface the efficiency is reduced to ~ 1%.
- The efficiency is observed to be a weak function of the source temperature for the electrons.

[1]D. R. Welch *et al.*, Nucl. Instrum. Methods Phys. Res. A 464, 134 (2001).

The simulations take into account the self-generated EM fields and the charge/current neutralization by the background plasma

- MeV "beam" electrons are treated as kinetic particles.
  - generated by "promotion from background" in a prescribed source region for a duration of 10 ps.
  - The electron beam is given a directed momentum ~ 1 MeV/c and a thermal spread (beam temperature) that is varied (either 10 keV or 200 keV).
- Fluid response for the background plasma (both electrons and ions)
  - provides charge and magnetic neutralization (return current)
  - corresponds to OMEGA cryo implosion.
- Full Maxwell equations are solved.

The MeV electrons are either generated in the near critical density region or closer to the core as is appropriate for cone-focused ignition

$n_b \sim 10^{20}$ cm^{-3}, $I_b \sim 2$ MA, $r_G = 10$ μm

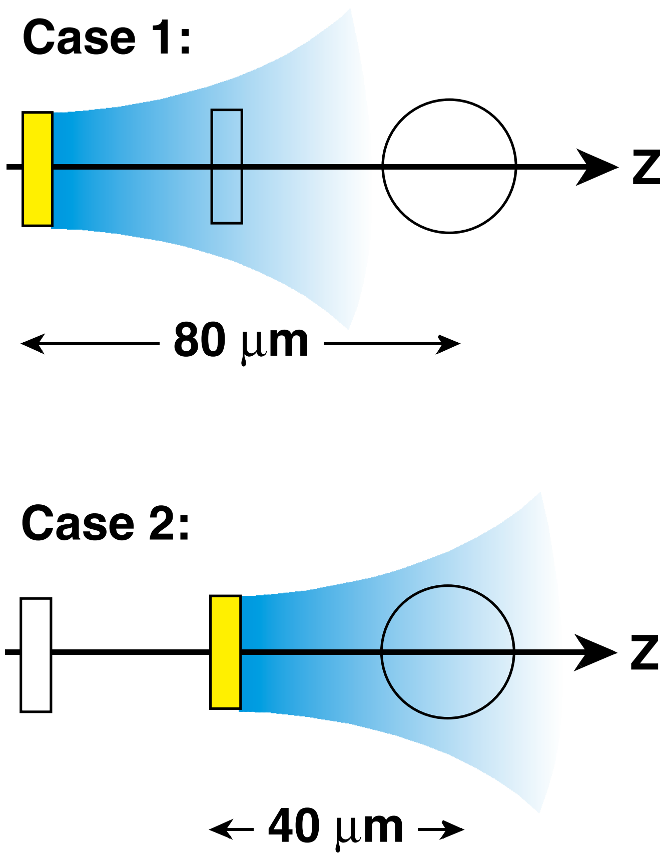

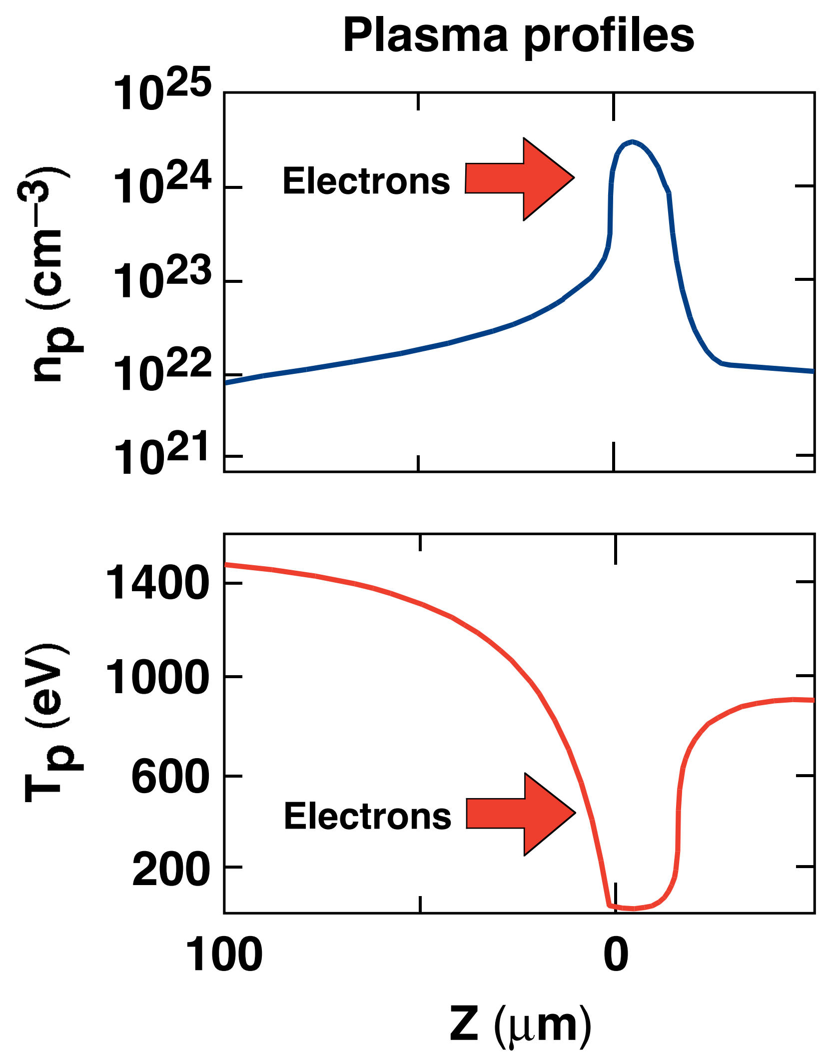

TC6509

The fractional energy flux through the core is investigated as a function of initial beam temperature for a fixed beam current

- From geometric considerations, a cold beam is better.
- Simulations show the opposite.

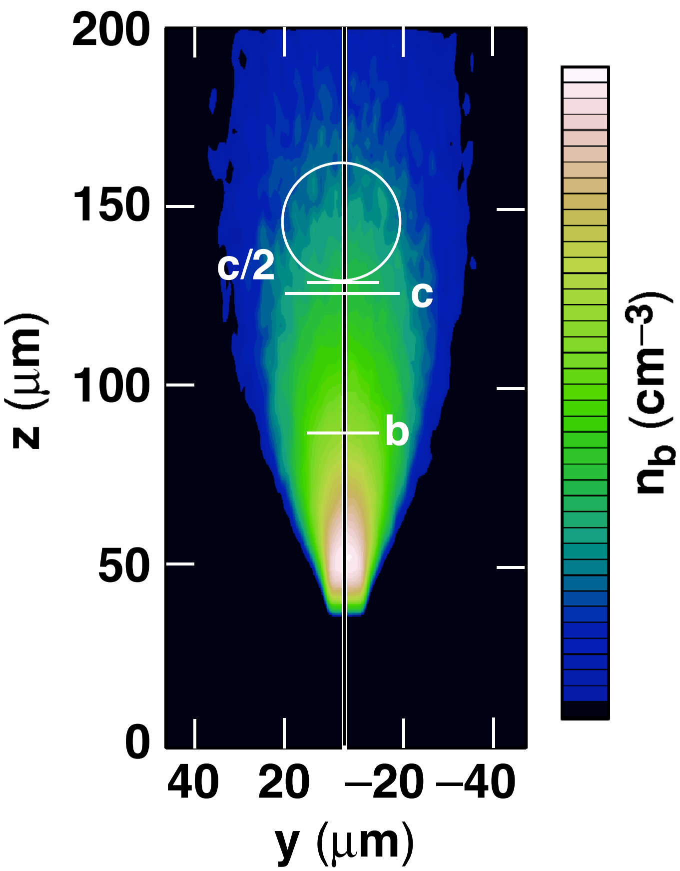

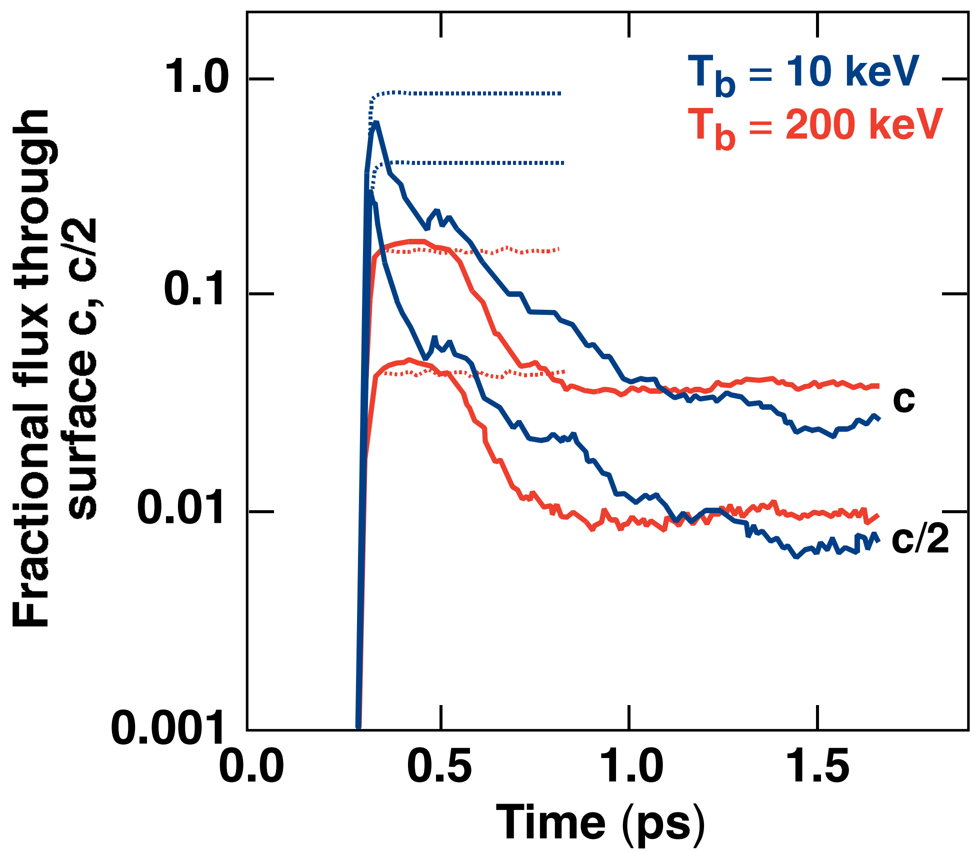

TC6510

Snapshots of the 10 keV beam show that the poor efficiency is due to the rapid onset of beam spraying

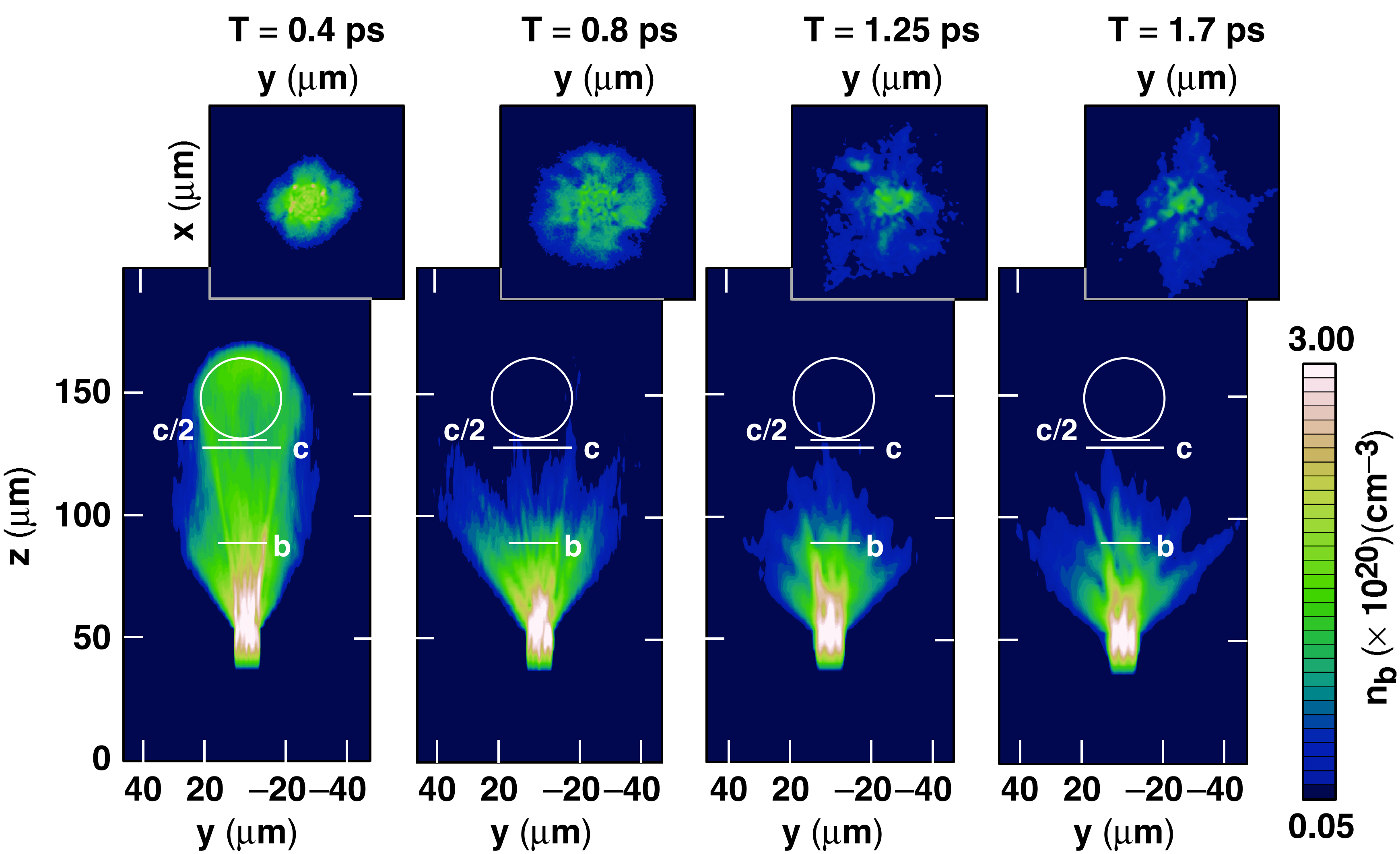

TC6511

Emittance growth is connected with the filamentation of current for the 10 keV beam and with beam focusing for the 200 keV case

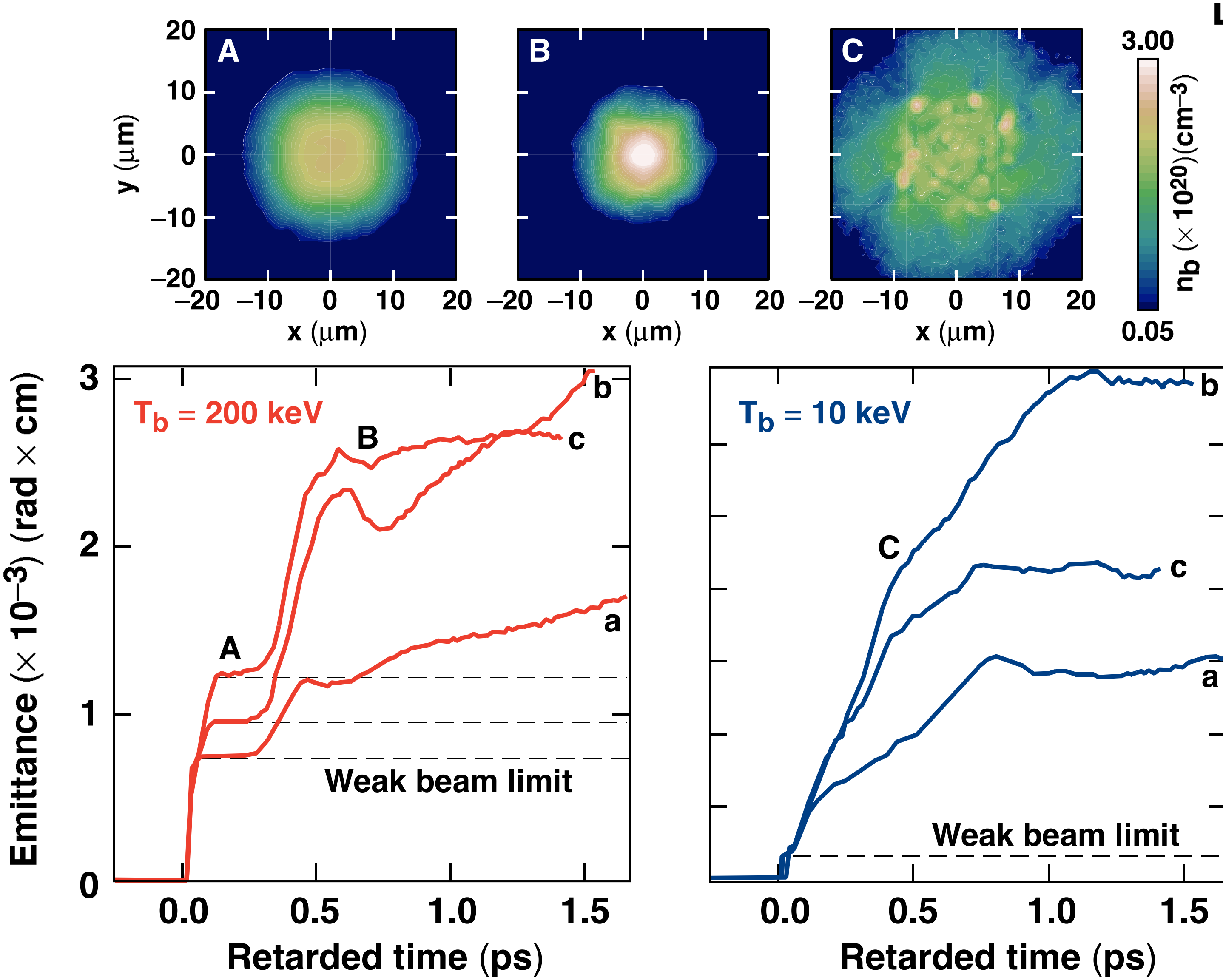

TC6512

Small scale filamentation is suppressed if the beam temperature is large enough

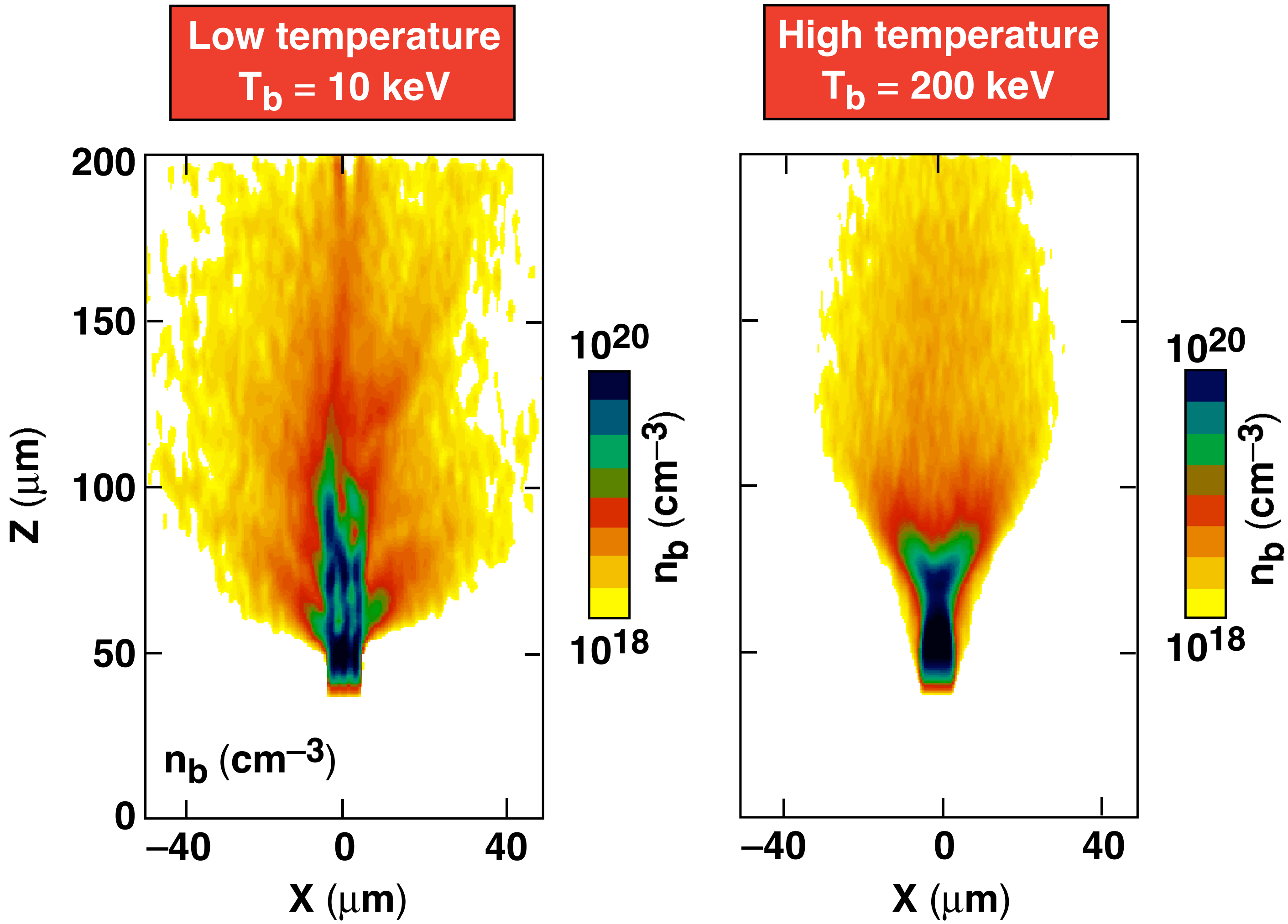

TC6457

Halving the propagation distance has a large impact on the transport efficiency

UR LLE

- The cold beam sees an order of magnitude improvement in efficiency.
- Geometric losses are smaller.
- The beam is weaker, (n_b/n_p) smaller.

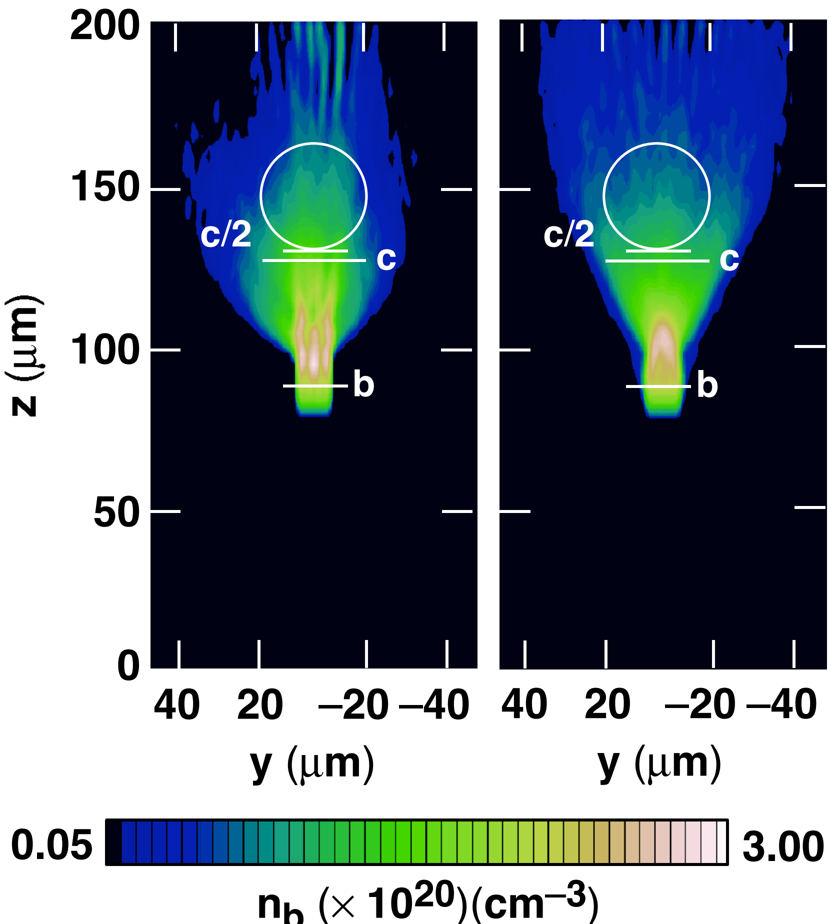

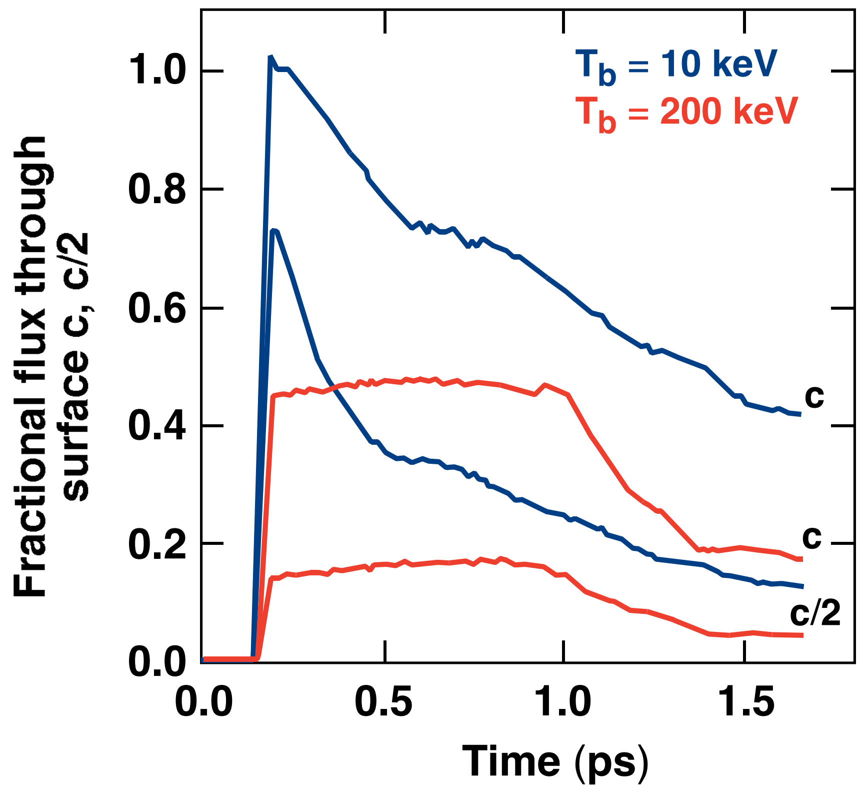

TC6513

Homogeneous simulations show that beam filamentation depends on the plasma density

UR LLE

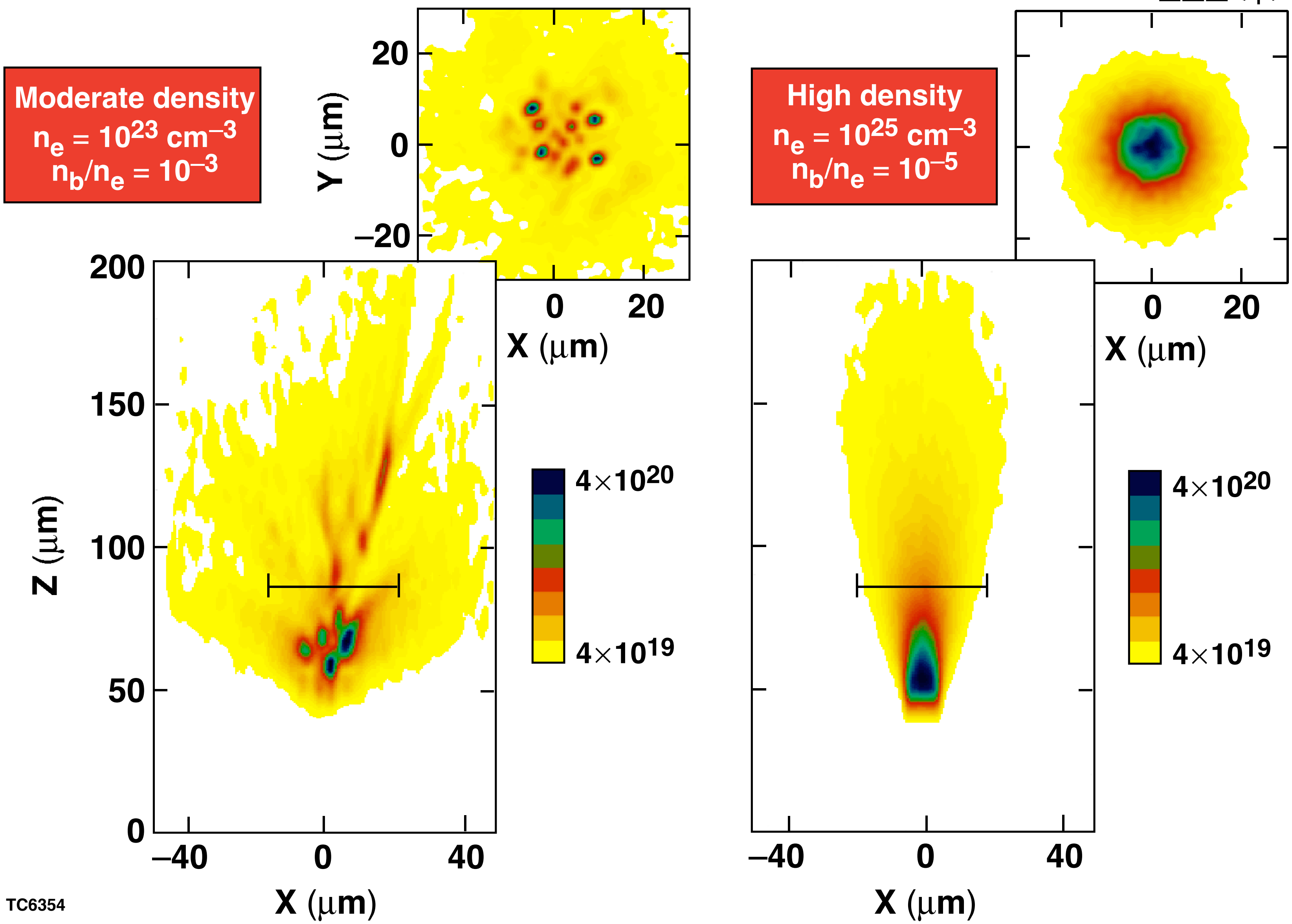

TC6354

Summary/Conclusions

Three-dimensional LSP[1] simulations of MeV electron transport predict a $\gtrsim$ 10% efficiency for a 20 μm radius core at a propagation distance of 40 μm

- The efficiency η_T = (energy reaching core/energy in fast electrons) and does not include stopping.
- From the beginning of fast ignition, it has been recognized that the transport distance needs to be made as small as possible leading to the concepts of hole boring and cone-focused implosions.
- Transport efficiency has been investigated using OMEGA profiles for two propagation distances.
- A standoff of 40 μm implies either hole boring or cone focused implosion.
- If electrons are generated near the critical surface the efficiency is reduced to ~ 1%.
- The efficiency is observed to be a weak function of the source temperature for the electrons.

[1] D. R. Welch *et al.*, Nucl. Instrum. Methods Phys. Res. A 464, 134 (2001).

TC6507a

PIC Simulation of Laser-Plasma Interaction in Fast Ignition

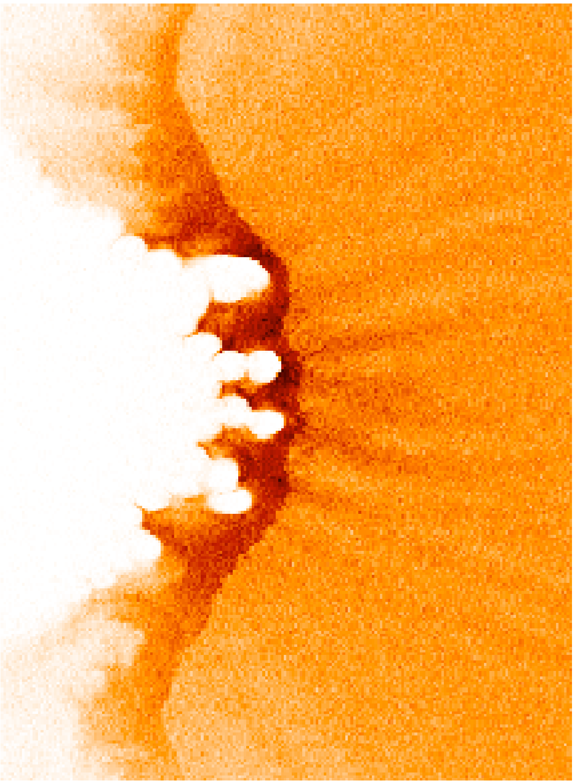

Chuang Ren

UCLA / University of Rochester

Outline

- Computational challenge in PIC modeling of FI target
- Collisions in PIC model
- Some recent PIC results for FI
  - Laser-plasma coupling
  - Fast electron characteristics
  - Current filament instability
- Summary

Model of compressed target in FI

- Model target: a plasma ball with a steeply rising density profile
  - Detail has to come from experiments & hydro simulations
  - The dense core region ($n \sim 10^{25\text{-}26}$/cc) may not be plasma

Compressed Pellet

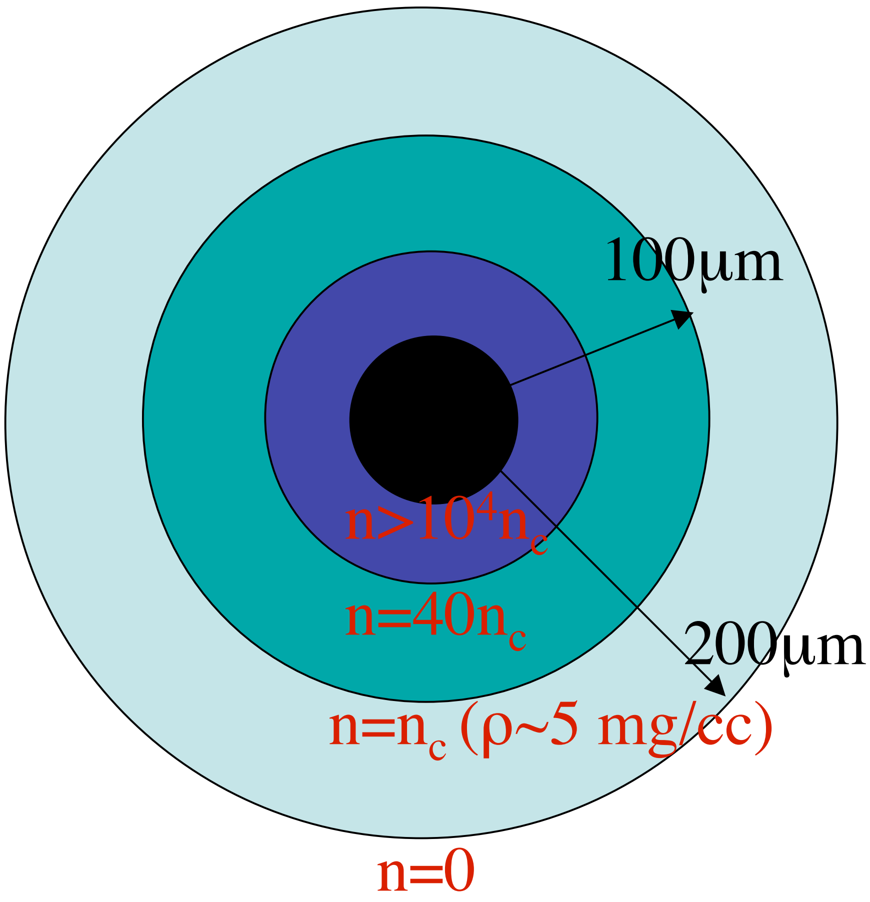

FI simulations requires tremendous computational resources

- For explicit PIC 3D simulations,
  - Total memory scales as $L^3 n^{3/2}$
  - Total particle-step scales as $L^3 T n^2$
- To simulate a $(50\mu m)^3$ plasma with $n=100n_c$ for 10ps requires ~6×10^2 TB memory (10^{13} particles) and 10^9 processor-hour (on Seaborg)
- State-of-art large PIC runs at Livermore used 7.2×10^9 particles
- Explicit PIC is to simulate model problems to understand the physics

Key issues in FI

- Energetic particle production (PIC simulation)
  - Laser-underdense plasma interaction
    - Channeling
    - Laser stability, e.g. hose/filament
  - Laser-plasma interface & vicinity ($n \leq 10^2\ n_c$)
    - Hole-boring
    - Fast e^- production
    - Fast e^- transport: current filament/magnetic field generation
  - Laser-solid material interaction
    - Energetic proton production/focusing
    - Laser-gold cone interaction for coned target
- Energetic particle transport/energy deposition in dense plasma (hybrid simulation)
  - Particle description for energetic components + fluid description for dense plasma ($n \sim 10^2\text{-}10^4\ n_c$)
  - Need to incorporate proper model for resistivity/collisionality

Particle-in-Cell Code Scheme

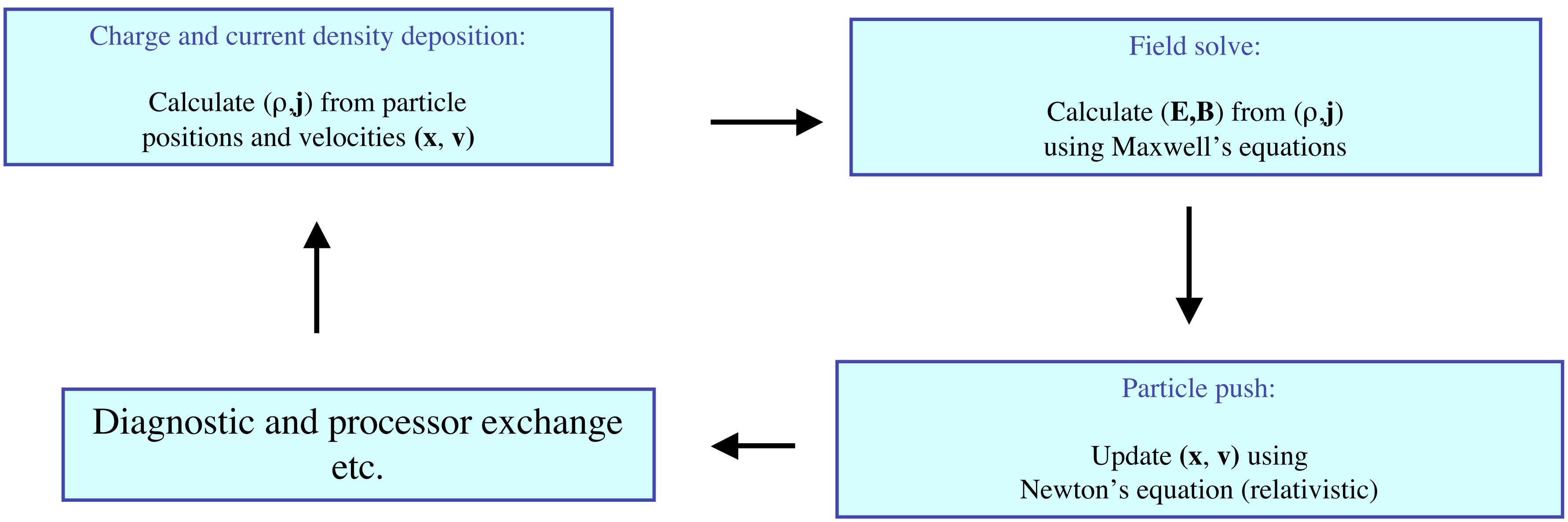

- best-understood model

Understanding collisions in PIC models and real plasmas is important

- Collisions are important to transport of energetic e^--beam
  - Resistivity and return current
- PIC models are not collisionless
  - Analysis & measurements have been done for electrostatic codes (e.g., Langdon, Dawson, Hockney)
- Difference between PIC models and real plasmas
  - Finite size particles: reducing collision rate
  - Less particles: increasing collision rate
  - Finite Δx and Δt

PIC simulation can match collisionality of real plasma in relevant range

- We can directly measure collisional effects in PIC simulations
- Results can be compared with theory (e.g. Krall & Trivelpiece)
  - $s=(1/2\pi)\ln\Lambda/(nu^2c/\omega_p{}^3)f(u/v_t)$
  - $s=7\text{x}10^{-6}$ (for $n=n_c$)
  - $s\sim n^{1/2}$
- We can match s by choosing simulation parameters

beam slow-down from OSIRIS

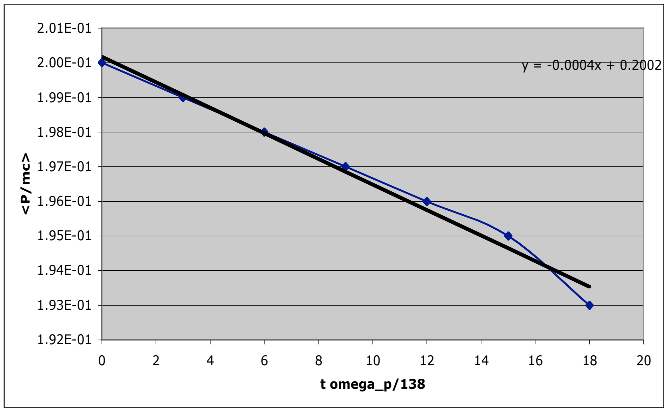

2D, T_e=7 keV, 400 ppc
Cold beam, $p_0/mc=0.2$
$s\equiv(dP/dt)/(mc\omega_p)=3\times10^{-6}$

An example of 2D PIC simulations

- 2D 1/4-size model
- Vacuum region between target and boundary to reduce boundary effects
- **12032×12032** grids
  - 2.4×10^8 particles and 6×10^4 steps
  - 256 nodes x 120 hr
  - 24 M particles' information saved
- **1μm**-laser, **I=$10^{20\text{-}21}$ w/cm^2**, spot size **7.5 μm, 1 ps** long, **s-&p-** polarized.

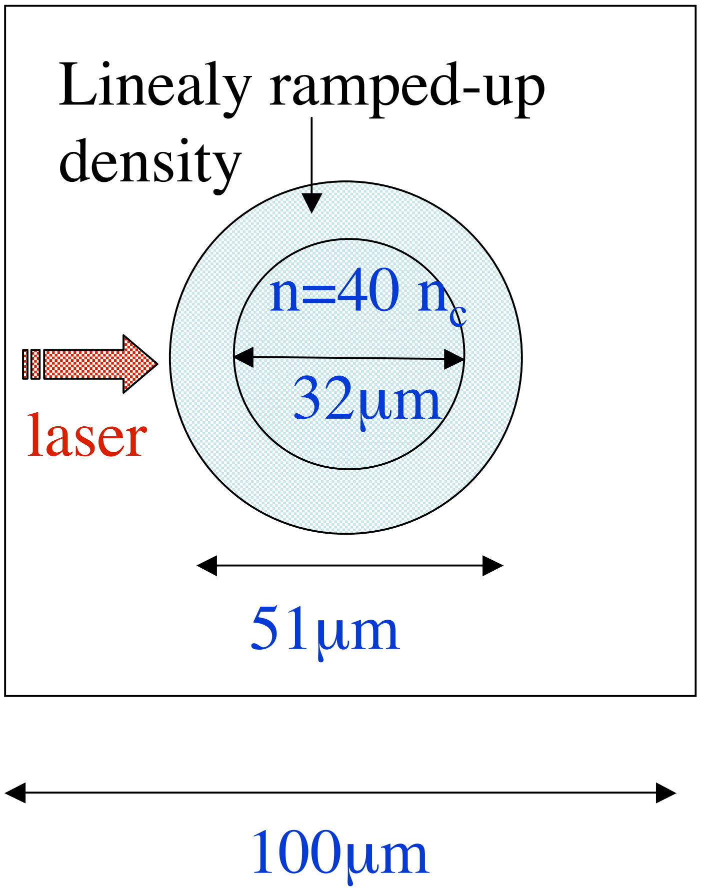

Electron Density Movie (S)

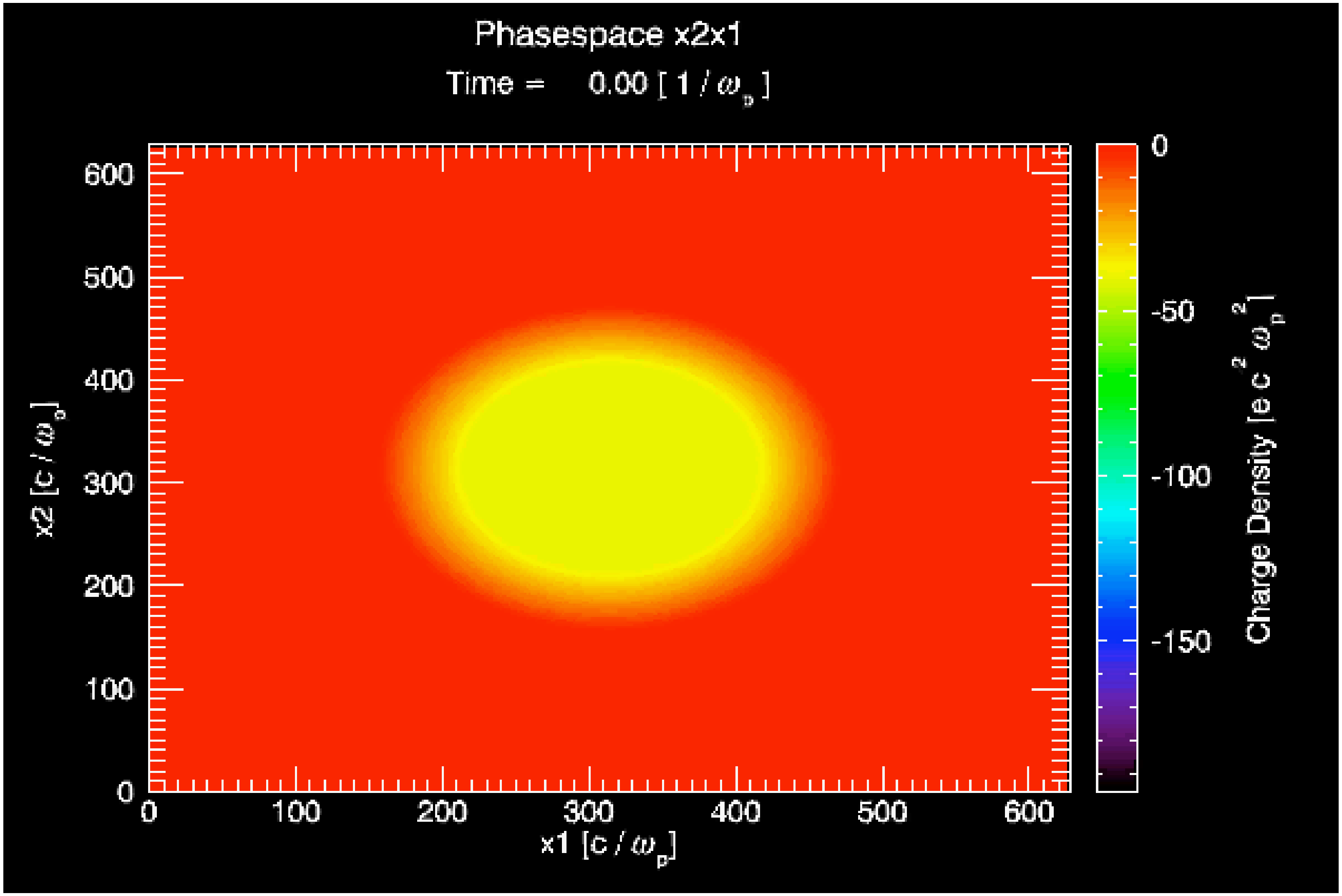

Laser-Plasma Interface Detail (S)

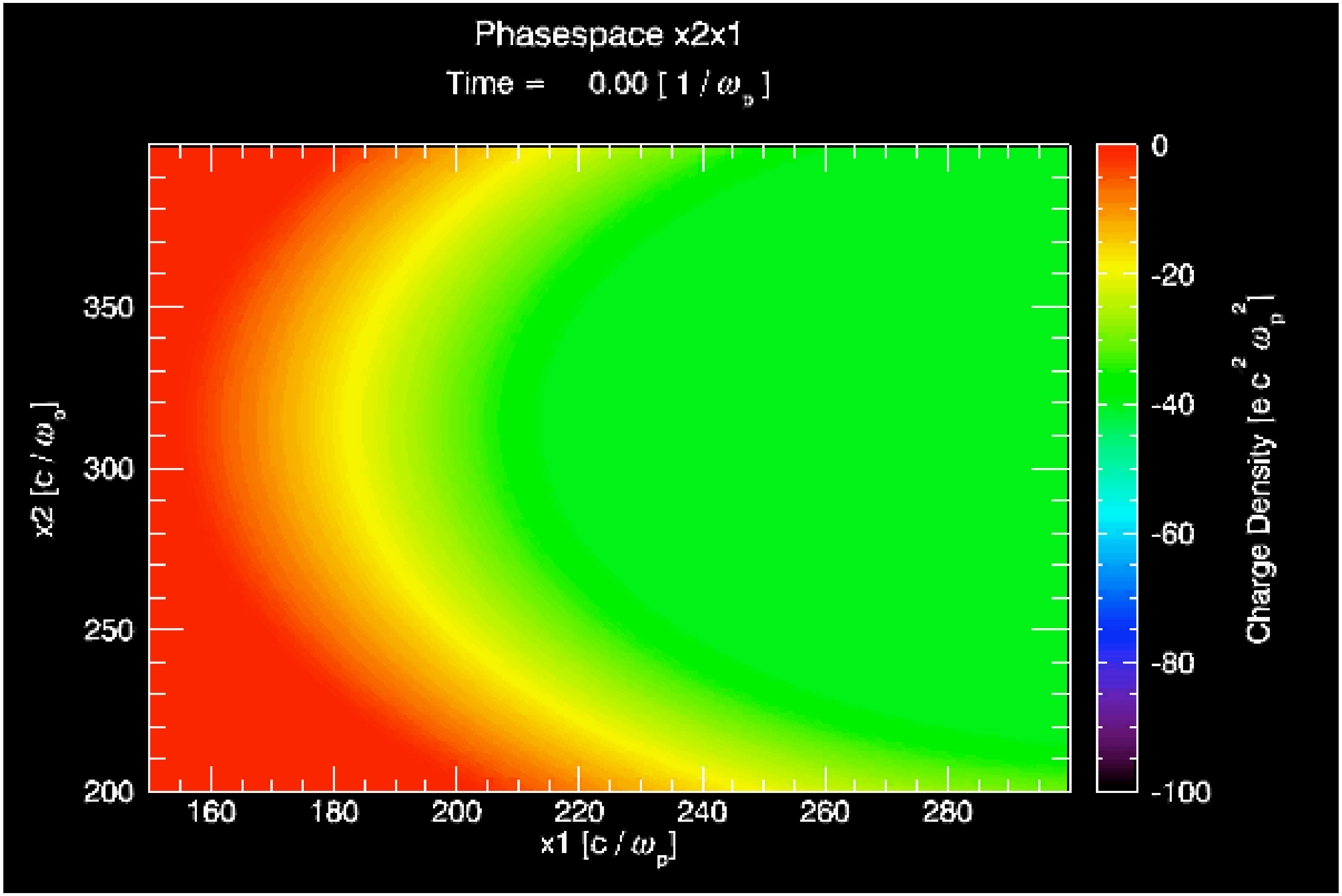

Laser-Plasma Interface Detail (P)

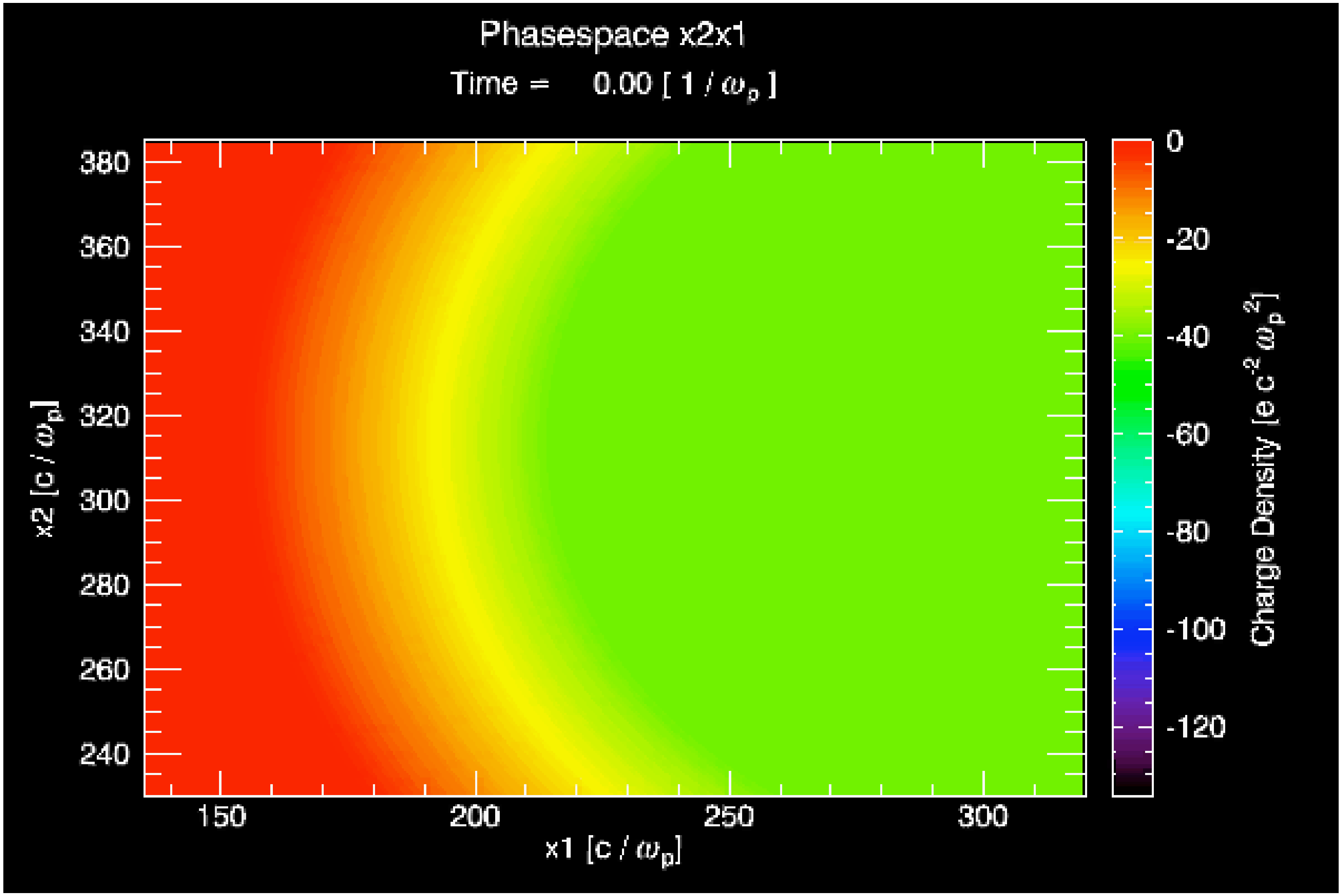

Density Ripples Caused By Laser Filaments

$|E_L|^2$ n_e

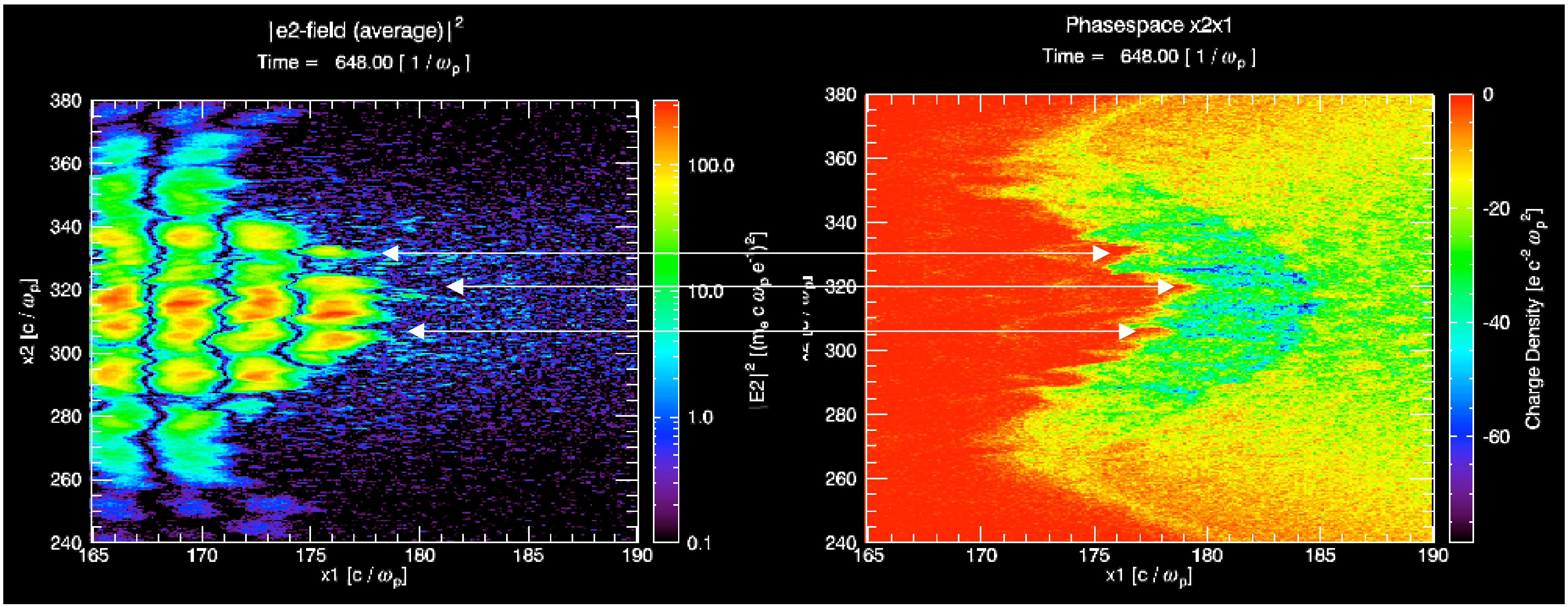

- Laser filament instability (Kaw et al., 1973)
- Seeding current filament

Laser absorption efficiency changes dynamically

- Absorption increases as critical surface ripples
- Absorption rate does not change significantly as intensity increases

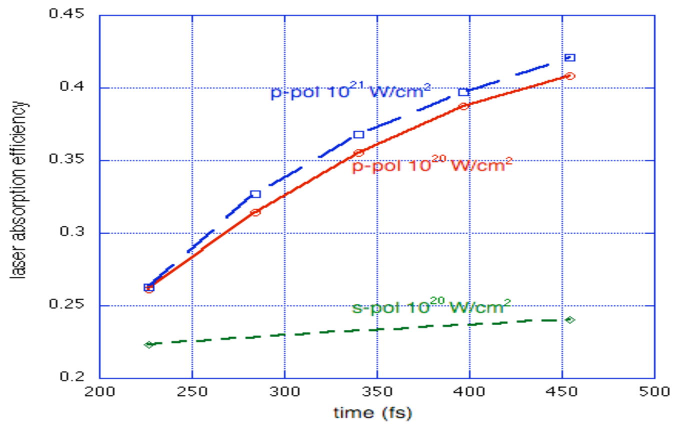

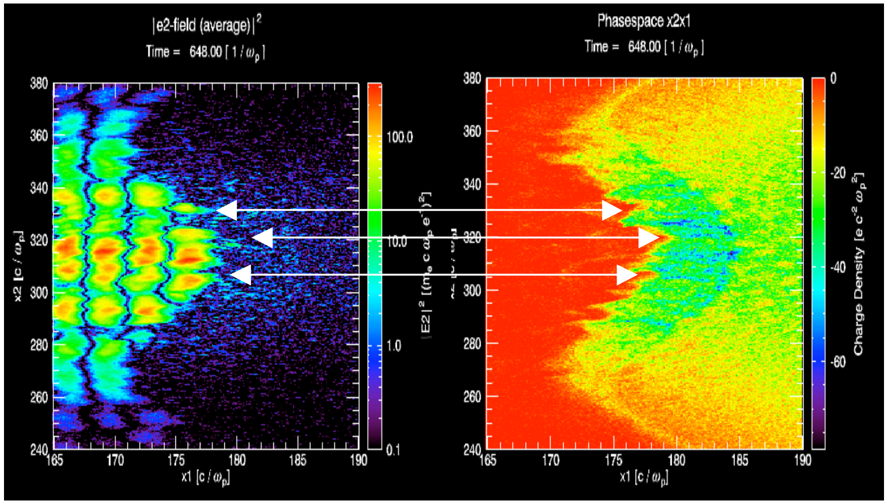

Higher laser intensity leads to higher fraction of super-hot electrons

- At 10^{20} W/cm^2, 45% of absorbed energy is carried by MeV electrons.

- MeV e- energy fraction is relatively independent of critical surface features.

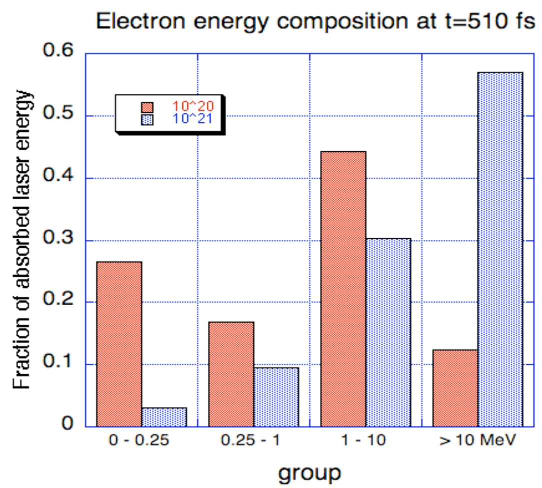

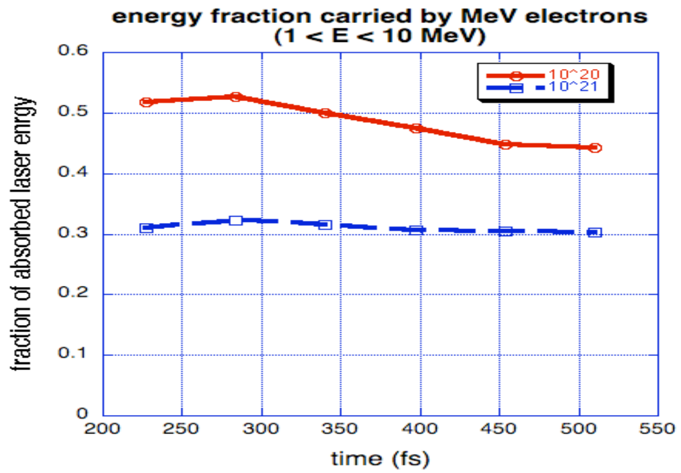

Current Filament Structure in Overdense Plasma

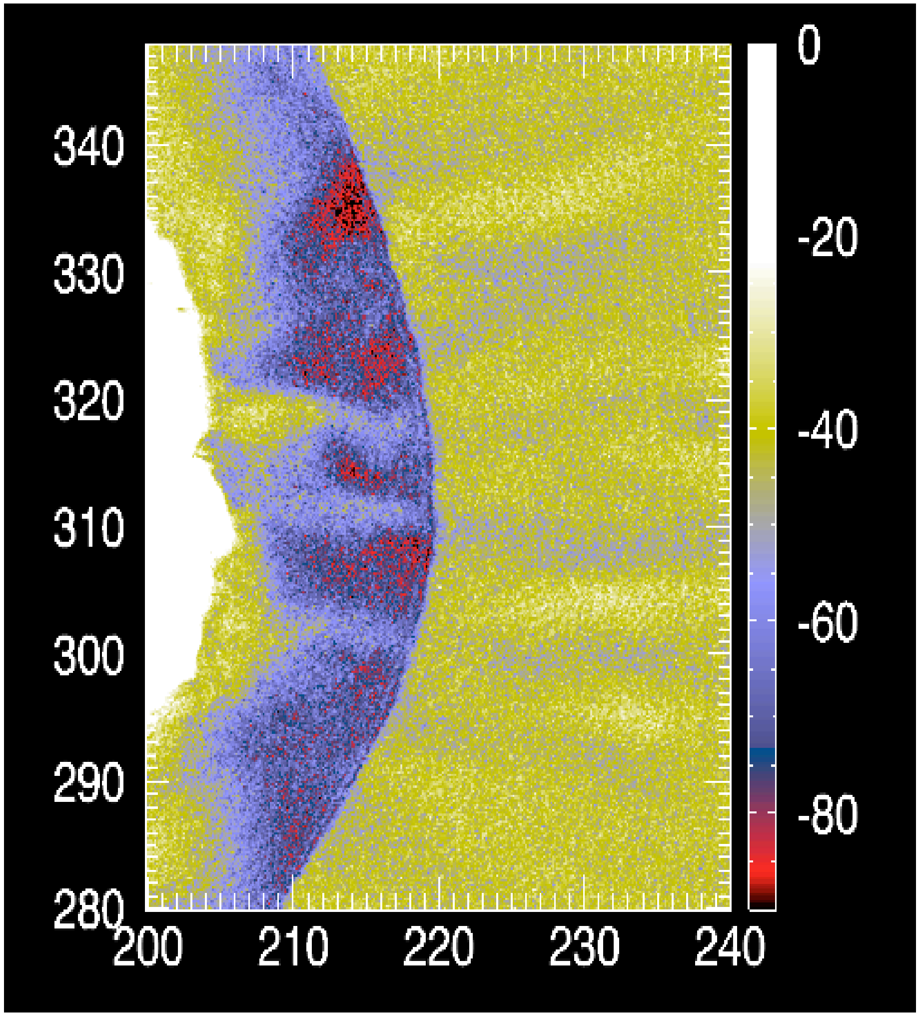

electron density (n_c)

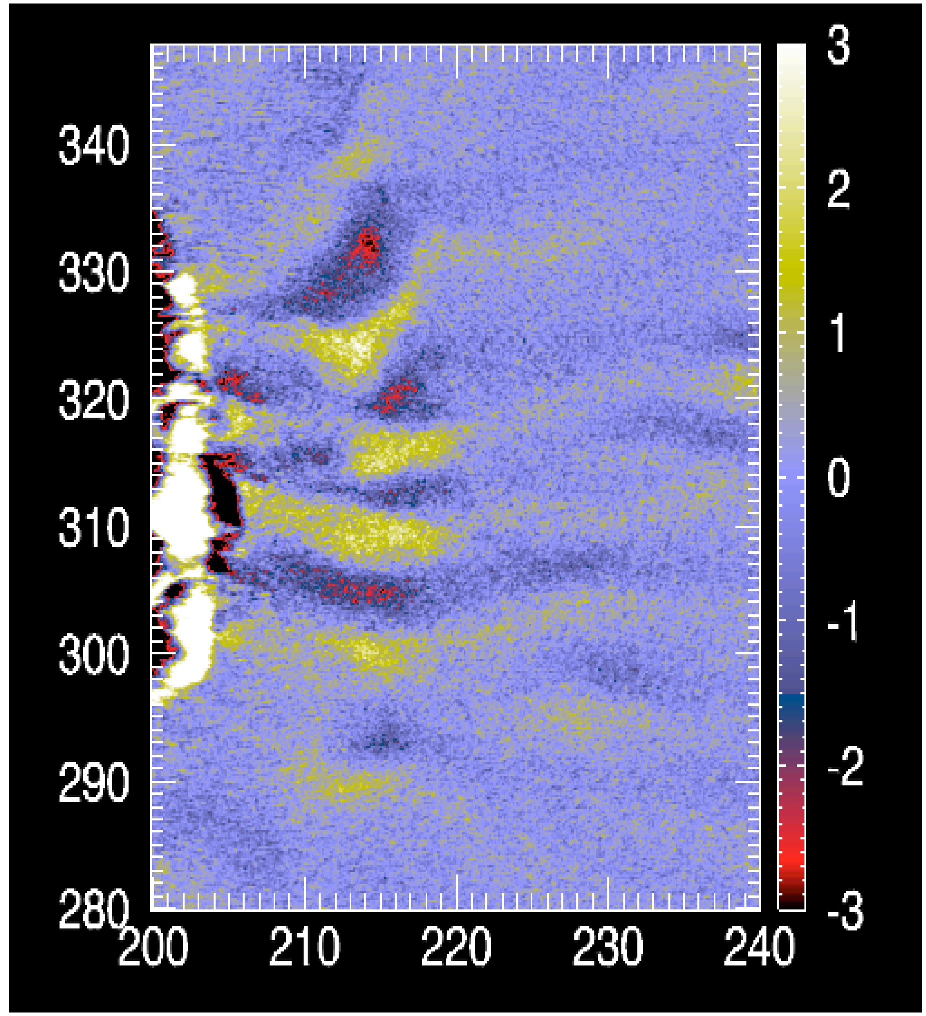

b3-field (100 MG)

Current Filament / Weibel Instability

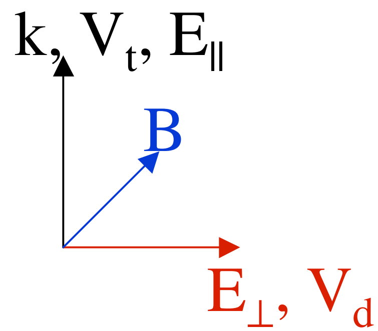

- I_f~ 30 MA >> Alfven current limit (100 kA)
  - Drives return current so that $I_f+I_r=0$
- Unstable to Weibel instability
  - Magnetic pinch > thermal pressure
  - Hot forward electrons vs cold return electrons
- Space charge effect

$$\sum \omega_{pj}^2 V_{dj}^2 / V_{tj}^2 > k^2 c^2 + \sum \omega_{pj}^2 \boxed{+\left(\sum \omega_{pj}^2 V_{dj} / k V_{tj}^2\right)^2}$$

- Ions play important role in neutralizing space charge
  - Instability grows on ion time scale in the shock region

Meshed forward/backward electrons

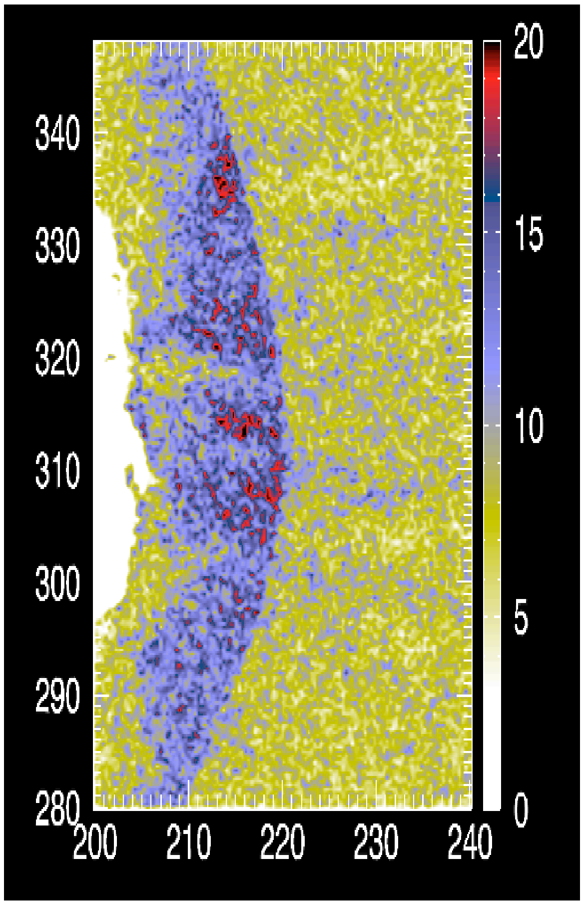

return current

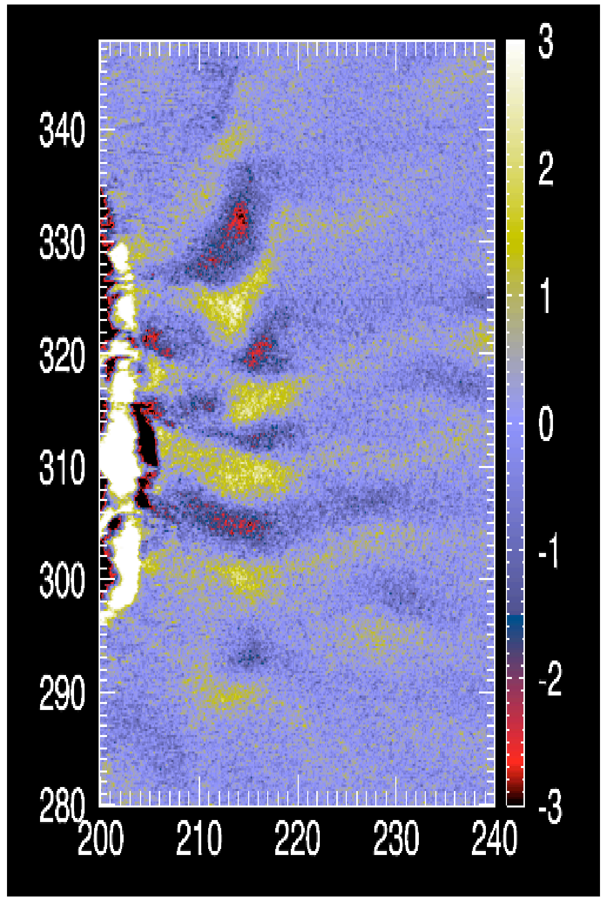

b3

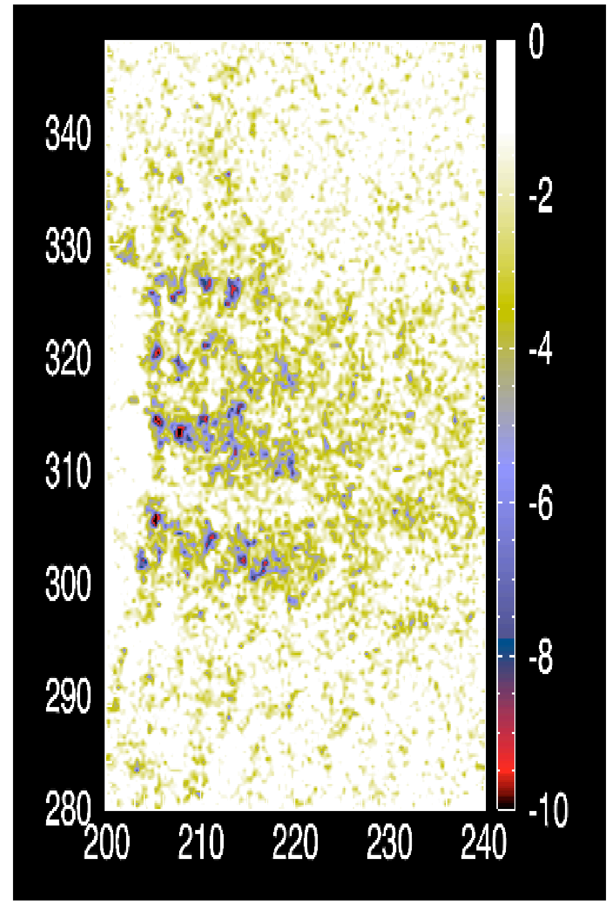

forward current
(>1MeV)

Ions Filament Too

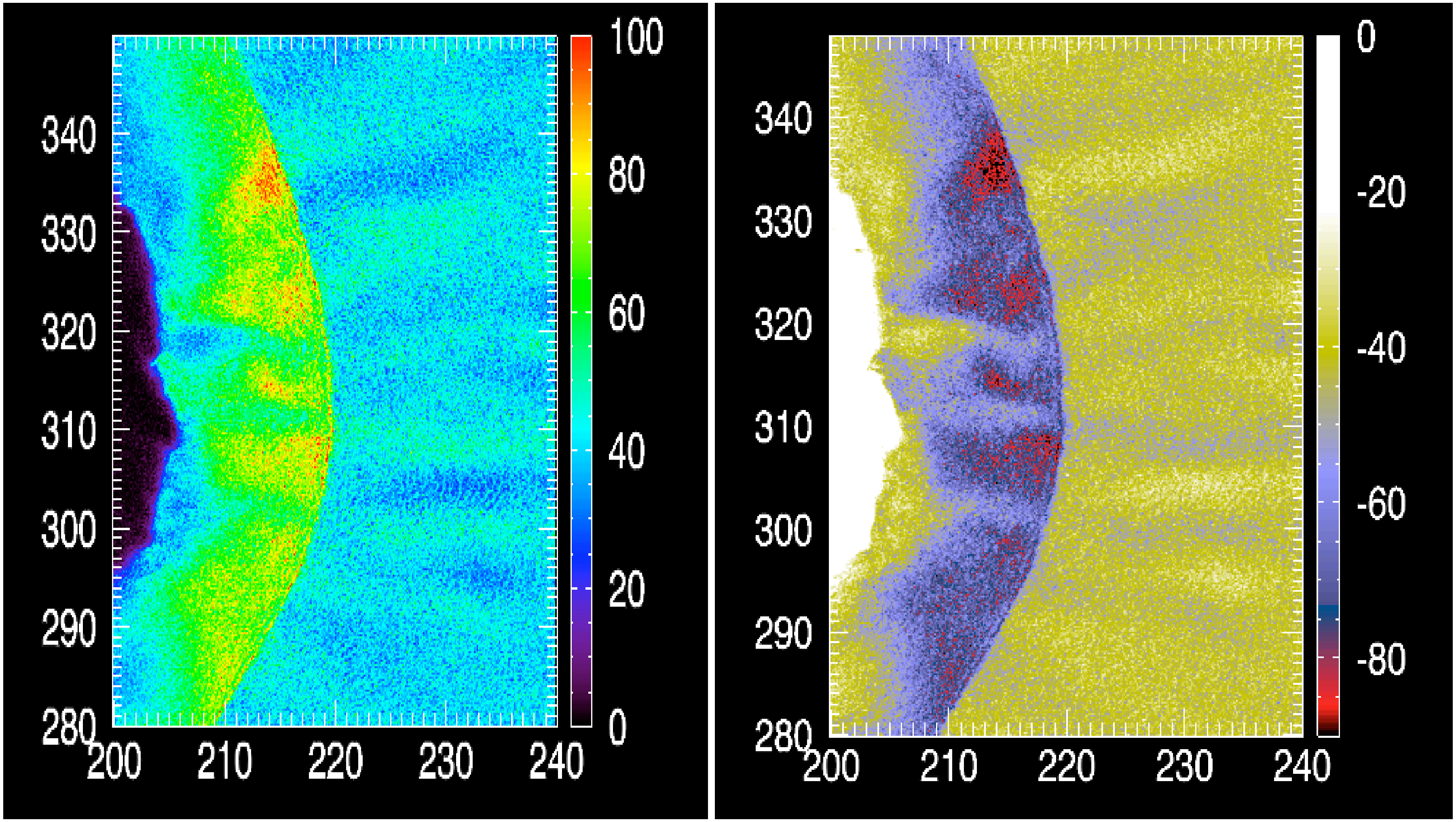

ion

electron

No Global Filaments Coalesce Seen with Large Simulation Box

B3 plots

t=330 fs

t=660 fs

Pukhov ‘97

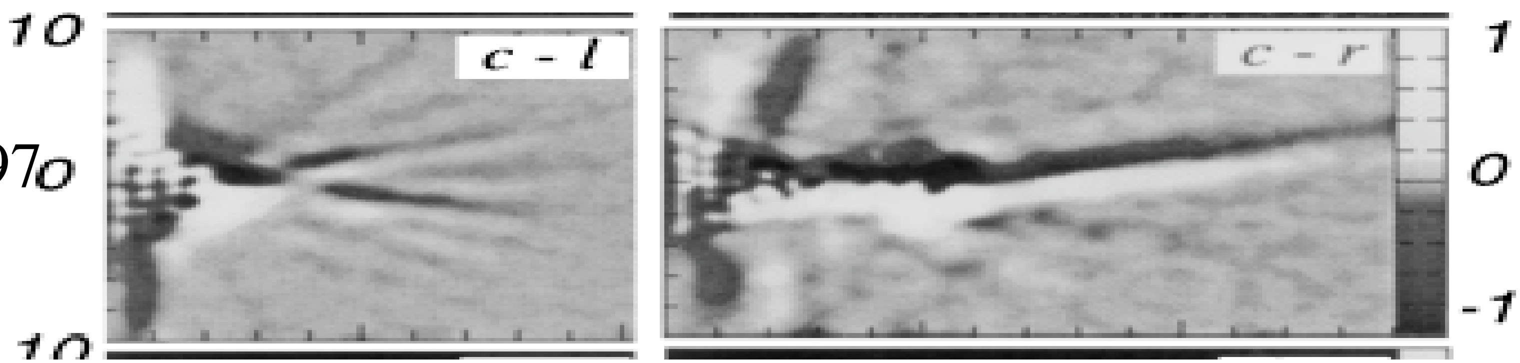

zoomed

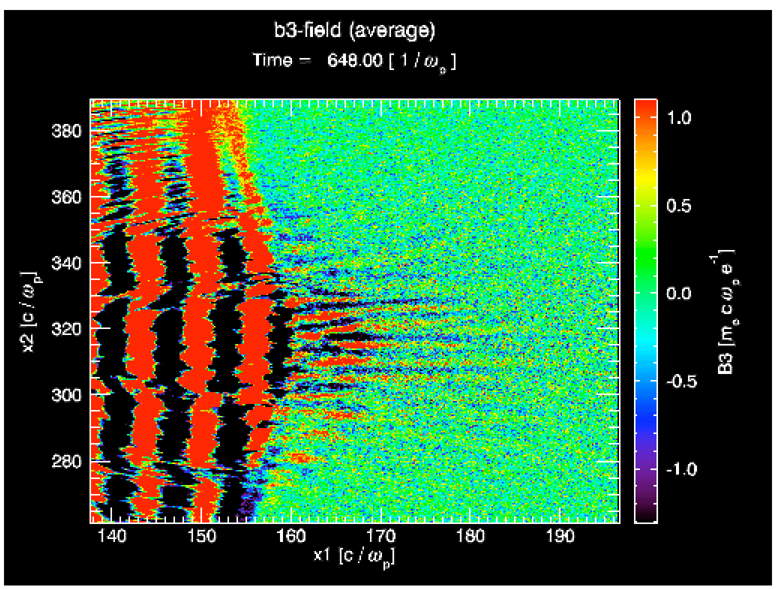

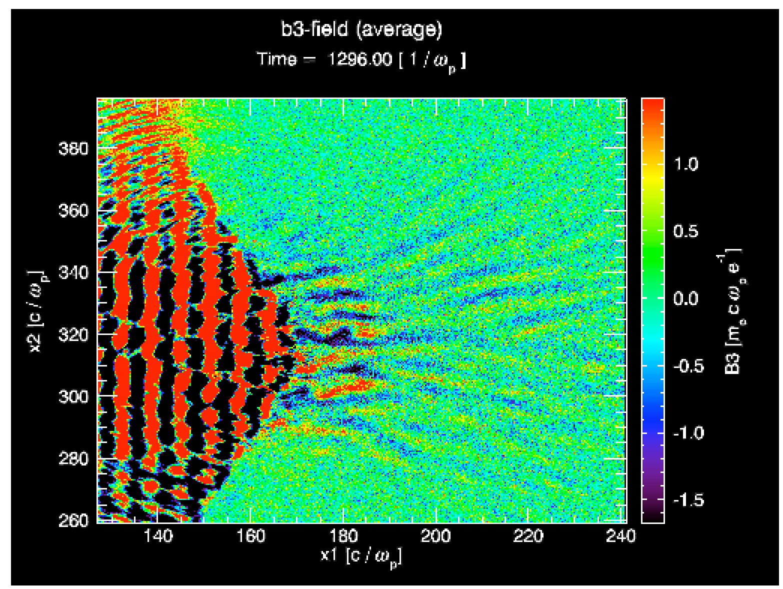

summary

- Full-size explicit PIC modeling for FI requires tremendous computational resources
- Interesting physics, including collisions, can be modeled in FI-relevant regime
  - PIC model is an important part of integrated simulations
- Effects of simulation limitations must be understood
  - dimensionality, size, and boundary conditions

Consensus from group discussion

- PIC model is a well-understood model. Different codes should give the 'same' answer to a problem with the same simulation parameters.
- Difficulties come when the full problem can not be simulated and scaled-down models must be used.
- We begin to address effects such as dimensionality, system size, boundary conditions, etc.
  - Need to use a realistic laser profile
- Experiments with preformed plasmas ($\leq 100\ n_c$) could provide clean comparison to PIC results.

Summary of presentations

- Fast electron distribution functions under various simulation conditions
  - Heating due to forward / return currents 2-stream instability in a discontinuous density profile (Sakagami, 1D PIC)
  - 2D vs. 3D; realistic pre-plasma profile (Lasinski and Still, in progress)
  - Effects of system size and boundary conditions (Ren, in progress)
  - *Kinetic electrostatic electron non-linear wave* observed in simulations and experiments (Afeyan)
- New numerical schemes for better and more efficient simulations
  - Split-wave scheme to improve numerical dispersion relation along grid lines (Sentoku)
  - Perfect-Matched-Layer boundary condition and Adaptive-Mesh-Refinement (Vay)
- Non-fast ignition applications
  - Atom cluster explosion driven by short pulse laser (Rose)
  - Pulse amplification by Raman back scattering (Charman)

Simulations of proton beams produced by the irradiation of thin foils with sub-picosecond laser pulses

H. Ruhl, T Cowan, J. Fuchs, and J. Fernandez
NTF, 5625 Fox Ave, Reno, NV 89506

Short Pulse Laser Matter Workshop
August 24 - 27, 2004

Outline

- Mechanisms of laser acceleration of ions
- The generation of markers in the beam
- RCF-stack detectors
- Experimental results of proton acceleration
- The PSC simulation code
- Direct simulations
- Effective simulations
- Conclusions

Mechanisms of laser-acceleration of ions

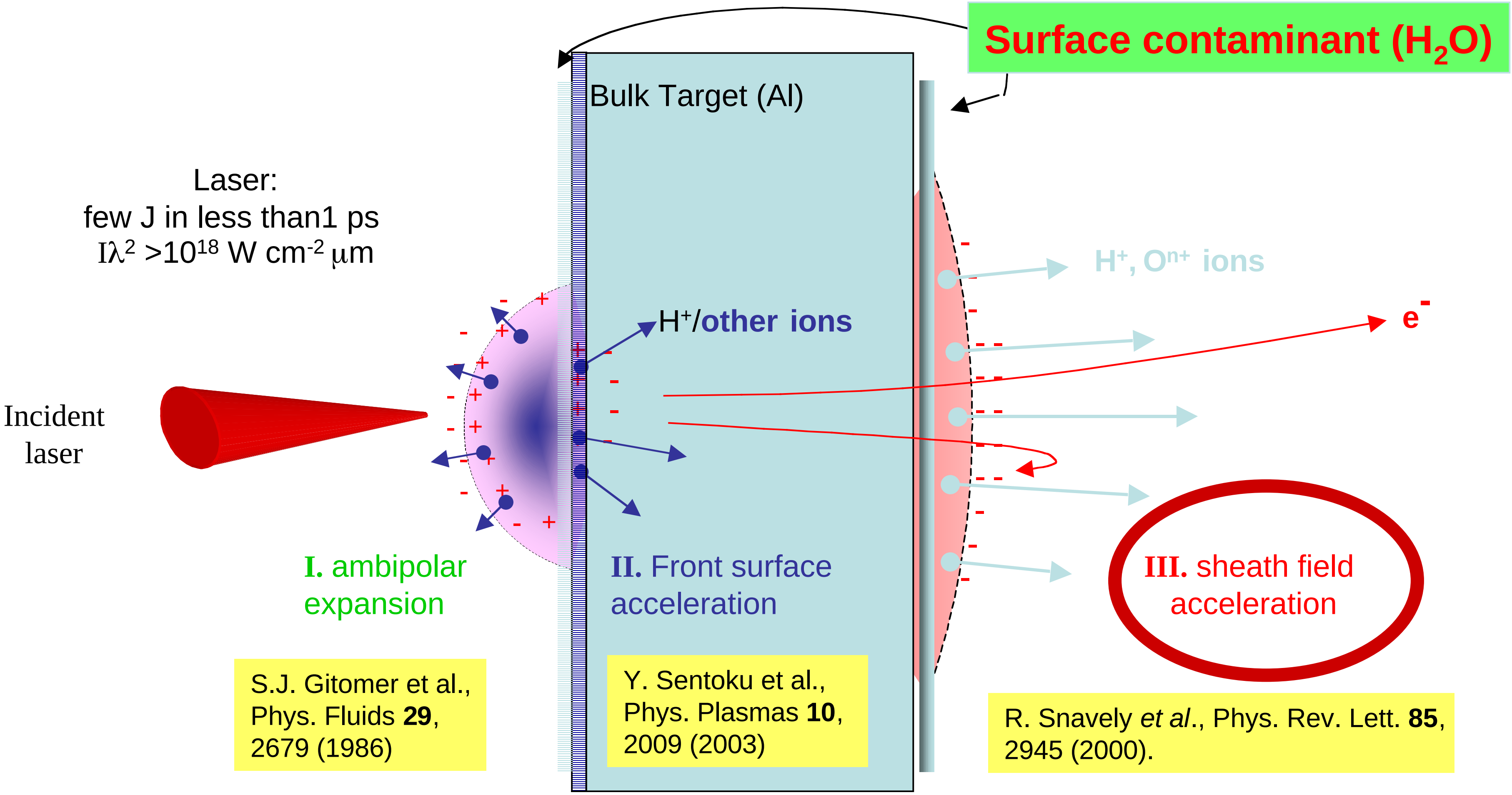

if target is heated ➔ efficient acceleration of heavy ions

M. Hegelich et al., Phys. Rev. Lett. **89**, 085002 (2002).

The generation of markers in the accelerated beam

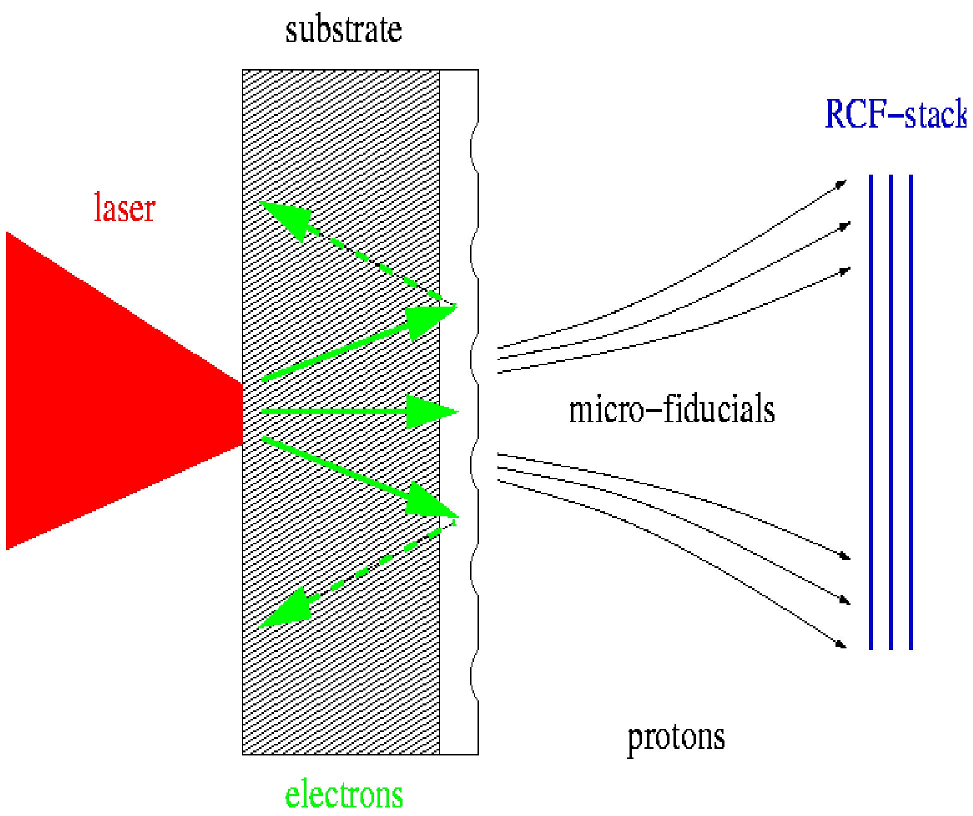

- Micro-grooves machined into the back surface produce fiducials in the accelerated beam as indicated in the figure.

- The fiducials can be used to measure the beam emittance and rear surface properties of the foil.

- RCF-stack detectors are frequently used in this context.

RCF-stack detectors

Experimental setup

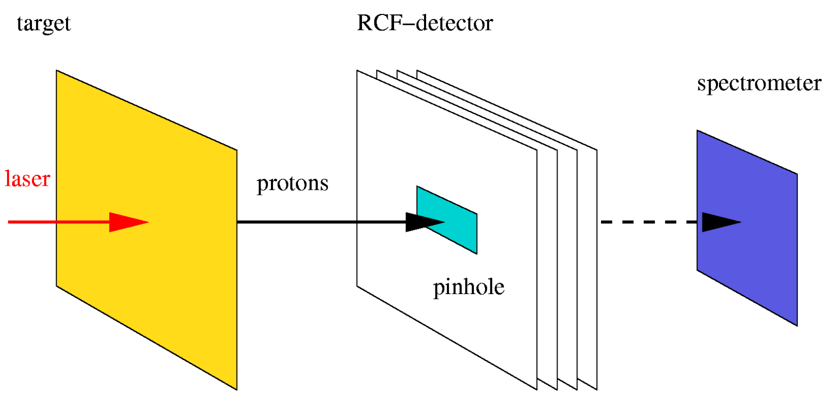

•Laser hits the target.
•Electrons are heated.
•Protons are accelerated.
•Divergence angles at a particular energy are recorded.
•The energy spectrum is recorded.

- Assumption of force free proton motion for $z_{\mathrm{RCF}} \gg z_{\mathrm{i}}(t_0)$.
- x_{RCF} and y_{RCF} represent location of protons at z_{RCF}.
- $\alpha_x \approx p_{\mathrm{x}}/p_{\mathrm{z}}$ and $\alpha_y \approx p_{\mathrm{y}}/p_{\mathrm{z}}$.
- RCF-stacks record the angle distibution of proton flow.

$$\begin{aligned} x_i(t_i) &= x_i(t_0) + v_{xi}(t_i - t_0) \\ y_i(t_i) &= y_i(t_0) + v_{yi}(t_i - t_0) \\ z_{RCF} &= z_i(t_0) + v_{zi}(t_i - t_0) \end{aligned}$$

$$\begin{aligned} x_{RCF} &= x_i(t_0) + \alpha_x z_{RCF} \\ y_{RCF} &= y_i(t_0) + \alpha_y z_{RCF} \end{aligned}$$

Experimental results

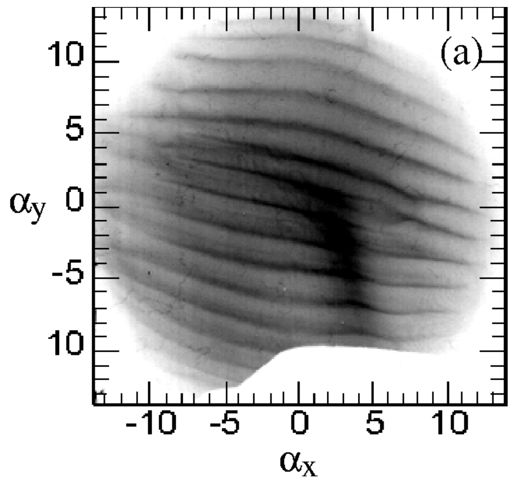

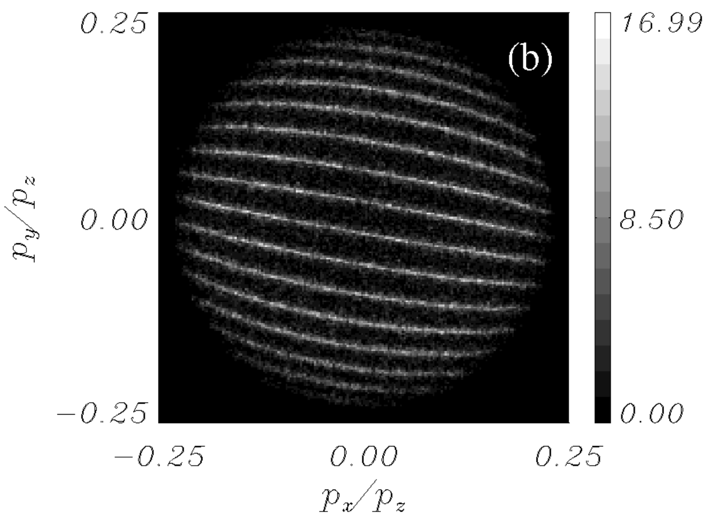

- Experimental RCF-radiograph is shown in plot (a).
- Effective simulation is shown in plot (b).
- Incident laser has Gaussian intensity distribution.
- Focal spot diameter at FWHM is $10.0\,\mu$m.
- Foil is Al with thickness $60.0\,\mu$m.
- Micro-grooves on target have $3.6\,\mu$m wavelength.
- α_x and α_y in degrees.
- Measured proton source size $\approx 56\,\mu$m for $E_p > 8\,$MeV.
- Projected proton source size $\approx 10\,\mu$m for $E_p > 8\,$MeV.
- Simulated proton source size $\approx 140\,\mu$m for $E_p > 3\,$MeV.

Experimental results

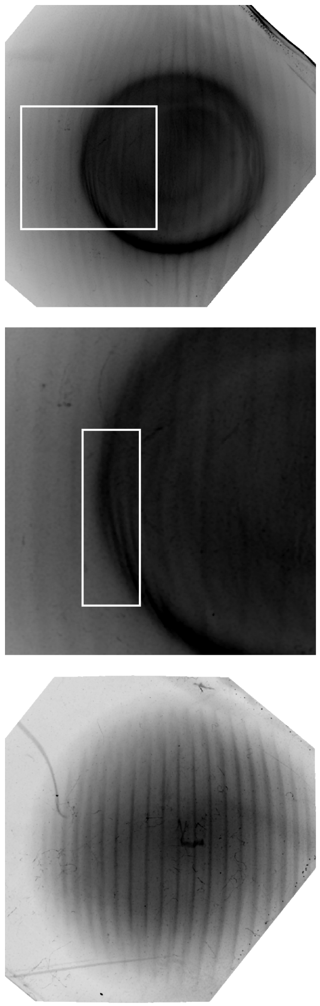

Experiment: T. Cowan, J. Fuchs, N. LeGaloudec
J. Fernandez et al.

There is a ring at 5MeV. Grooves become denser closer to the edge of the ring. The second picture from the top shows the magnified sector surrounded by a white rectangle in the top figure. The bottom figure shows an RCF-image at 8MeV.

Code topology, method and costs of a simulation

Plasma-Simulation-Code (PSC)

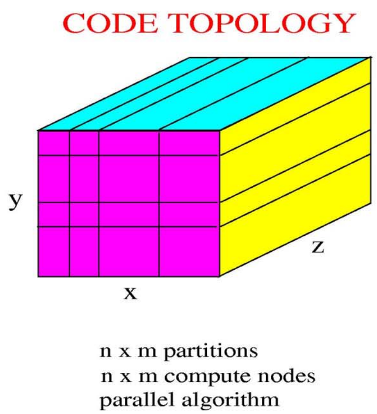

- code is cartesian and 3D
- laser irradiation along z
- beam injection along z
- open boundaries along z
- periodic boundaries along xy
- particle- and field exchange in xy
- dynamic load balancing
- code is portable with MPI, F90, C++
- code has field and impact ionization
- code has arbitrary binary collisions
- code has elementary nuclear reactions
- COMMERCIAL VERSION AVAILABLE

PSC is a Particle-In-Cell (PIC) code

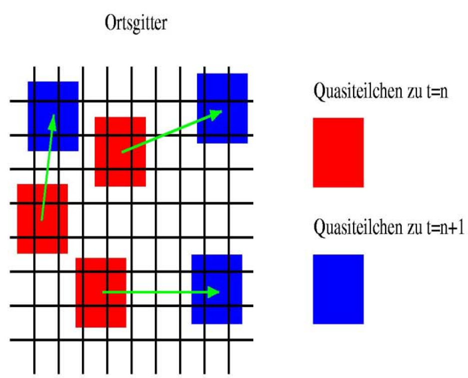

$$\left(\partial_t + \mathbf{v}\cdot\partial_{\mathbf{x}} + q\mathbf{E}\cdot\partial_{\mathbf{p}}\right) f = 0$$

$$f(\mathbf{x},\mathbf{p}) = \sum_l S(\mathbf{x},\mathbf{x}_l)\,\delta^3(\mathbf{p}-\mathbf{p}_l)$$

$$\frac{d\mathbf{x}_l}{dt} = \mathbf{v}_l$$
$$\frac{d\mathbf{p}_l}{dt} = q\,\mathbf{E}$$

- 3D space grid, no momentum grid

Details of focusing simulation

Step sizes

- time: min of $\Delta t \ll \frac{1}{\omega}$, $\Delta t \approx \frac{1}{\omega_p}$, $\Delta t \approx \frac{1}{\nu_{ei}}$
- space: min of $\Delta i \ll \lambda$, $\Delta i \approx \lambda_D$, where $i = x,y,z$
- condition: $\frac{1}{(c\Delta t)^2} > \frac{1}{(\Delta x)^2} + \frac{1}{(\Delta y)^2} + \frac{1}{(\Delta z)^2}$

Simulation parameters

- density: $n_0 = 1.0\cdot 10^{23}$ cm^{-3}
- temperature: $T_e = T_i = 100$ eV
- wavelength: $\lambda = 0.85\ \mu$m
- box: $0.1\mu\text{m} \times 100\mu\text{m} \times 100\mu\text{m}$
- duration: 2200 fs

Simulation costs

- platform: Intel P4 cluster
- time: $\Delta t = 5.0\cdot 10^{-17}$ s
- space: $\Delta x = \Delta y = \Delta_z = 3.0\cdot 10^{-8}$ m
- cells: $4\times 3000\times 3000 = 36000000$
- particles: 15000000
- RAM: 30.0 GByte
- nodes: 20
- duration: $200\times 20 = 2000$ CPU-hours
- data: 400.0 GByte

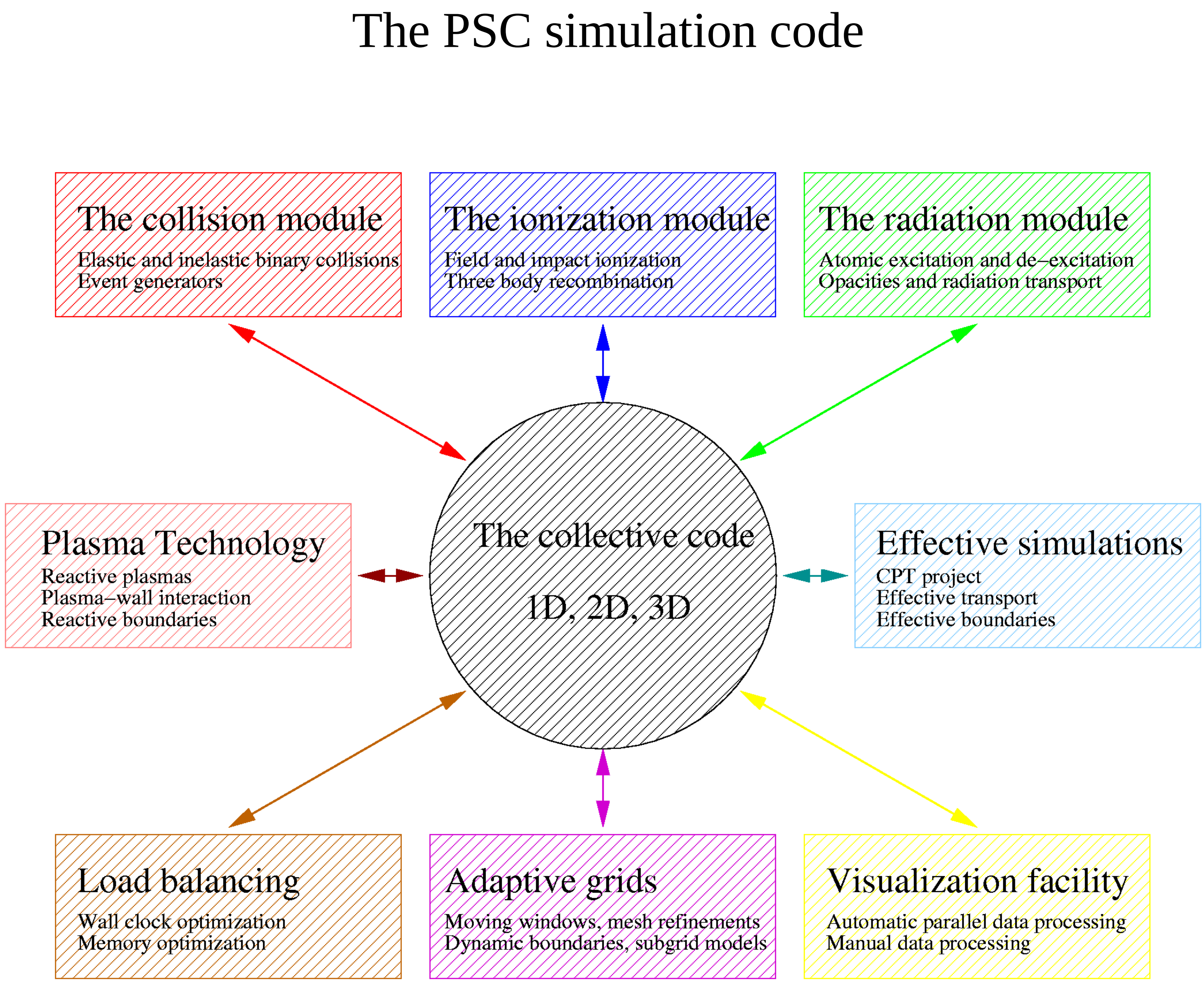
The PSC simulation code
The collision module
Elastic and inelastic binary collisions
Event generators
The ionization module
Field and impact ionization
Three body recombination
The radiation module
Atomic excitation and de−excitation
Opacities and radiation transport
Plasma Technology
Reactive plasmas
Plasma−wall interaction
Reactive boundaries
The collective code
1D, 2D, 3D
Effective simulations
CPT project
Effective transport
Effective boundaries
Load balancing
Wall clock optimization
Memory optimization
Adaptive grids
Moving windows, mesh refinements
Dynamic boundaries, subgrid models
Visualization facility
Automatic parallel data processing
Manual data processing

Equations solved in the Vlasov-Boltzmann part of the PSC code

$$\left(\partial_t + \vec{v}_k \partial_{\vec{x}} + q_k \left[\vec{E} + \vec{v}_k \times \vec{B}\right] \partial_{\vec{p}_k}\right) f_k$$
$$= \sum_{l=n,e,i} \int d^3 p_l \, v_{kl} \int d\Omega_\Psi \, \sigma \left(f_k' f_l' - f_k f_l\right)$$

Vlasov-Boltzmann equations

$$v_{kl} = \sqrt{(\vec{v}_k - \vec{v}_l)^2 - \frac{1}{c^2}(\vec{v}_k \times \vec{v}_l)^2}$$

$$\begin{aligned} \partial_t \vec{E} &= c^2 \vec{\nabla} \times \vec{B} - \vec{j}/\varepsilon_0 \\ \partial_t \vec{B} &= -\vec{\nabla} \times \vec{E} \\ \partial_t \rho &= -\vec{\nabla} \cdot \vec{j} \end{aligned}$$

Maxwell equations

$$\begin{aligned} \rho &= q_e \int d^3 p_e f_e + q_i \int d^3 p_i f_i \\ \vec{j} &= q_e \int d^3 p_e \vec{v}_e f_e + q_i \int d^3 p_i \vec{v}_i f_i \end{aligned}$$

Charge and current densities

Details of the collision operator

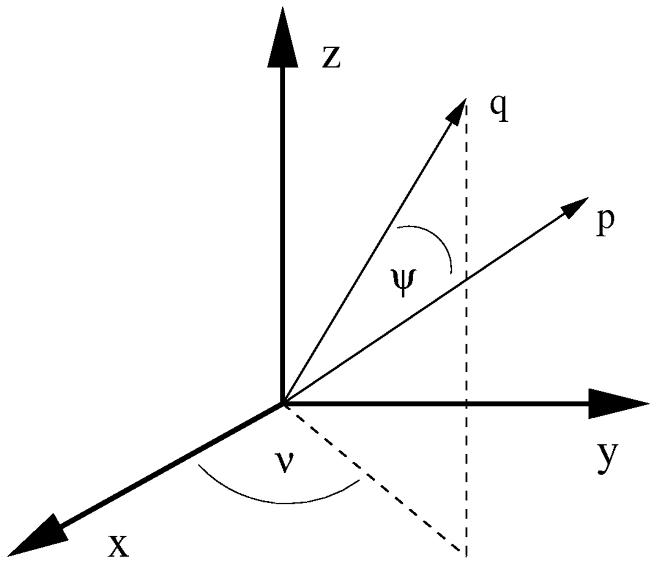

Two angles need to be generated to determine the post-collision vector q from the pre-collision vector p in the center of mass frame.

$$
\begin{aligned}
\mathbf{n} &= \frac{\mathbf{p}}{|\mathbf{p}|} \\
s &= (p_1 + p_2)^2 \\
|\mathbf{p}| &= \frac{1}{2\sqrt{s}} \left(\left[s - (m_1^2 + m_2^2)\, c^2 \right] - 4 m_1^2 m_2^2 \, c^4 \right)^{1/2} \\
|\mathbf{q}| &= \frac{1}{2\sqrt{s}} \left(\left[s - (m_3^2 + m_4^2)\, c^2 \right] - 4 m_3^2 m_4^2 \, c^4 \right)^{1/2} \\
\mathbf{q} &= q \cos\psi \, \mathbf{n} + q \sin\psi \sin\nu \, \frac{\mathbf{n} \times \mathbf{e}_z}{|\mathbf{n} \times \mathbf{e}_z|} + q \sin\psi \cos\nu \, \frac{(\mathbf{n} \times \mathbf{e}_z) \times \mathbf{n}}{|(\mathbf{n} \times \mathbf{e}_z) \times \mathbf{n}|}
\end{aligned}
$$

Details of the collision operator

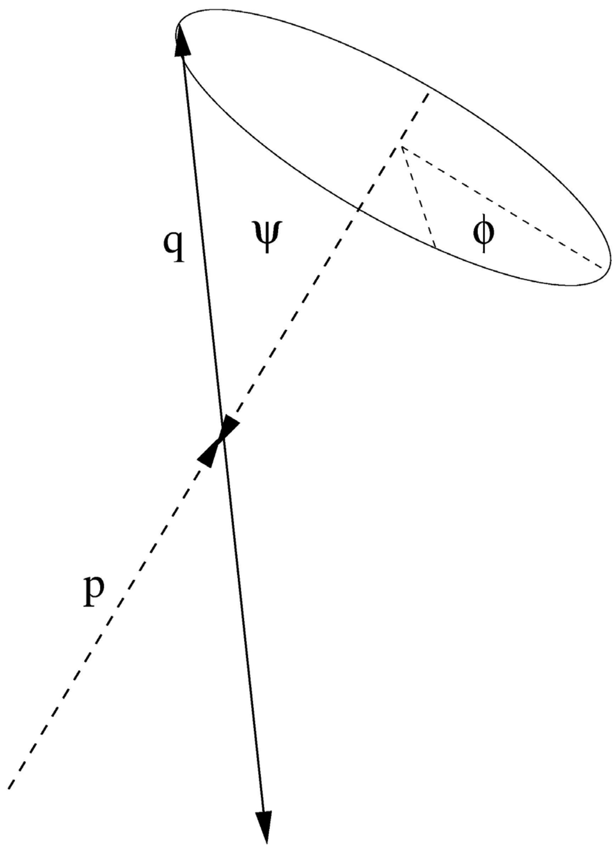

- Normal components of the scattered momenta are are assumed to have a Gaussian distribution.
- Uniform angle distribution assumed for large scattering angles.

$$\frac{1}{4\pi}\int_0^{2\pi} d\phi \int_0^{\psi} ds\, s \sin s = P(\psi)$$

$$\phi = 2\pi Q\,, \qquad \frac{1-\cos\psi}{2} = P\,, \qquad 0 \le P < 1\,, \qquad 0 \le Q < 1$$

$$\frac{1}{2\pi\nu dt}\int_0^{2\pi} d\phi \int_0^{\tan\frac{\psi}{2}} ds\, s\, e^{-\frac{s^2}{2\nu dt}} = P(\psi)$$

$$\phi = 2\pi Q\,, \qquad 1 - e^{-\frac{tan^2(\psi/2)}{2\nu dt}} = P\,, \qquad 0 \le P < 1\,, \qquad 0 \le Q < 1$$

$$\nu = \frac{q_i^2 q_j^2 n}{4\pi\varepsilon_0 m_R^2 v_R^3}\ln\Lambda\,, \qquad m_R = \frac{m_1 m_2}{m_1 + m_2}\,, \qquad v_R = |v_1 - v_2|$$

The NTF-cluster computer

- •96 compute nodes Ni with 2 GB RAM each.
- •23 TB hard drive capacity.
- •MPICH, PBS, C++, F90, IDL.
- •2 separate interconnects for file system (I) and computation (II).
- •Peak performance 0.2TFlop.

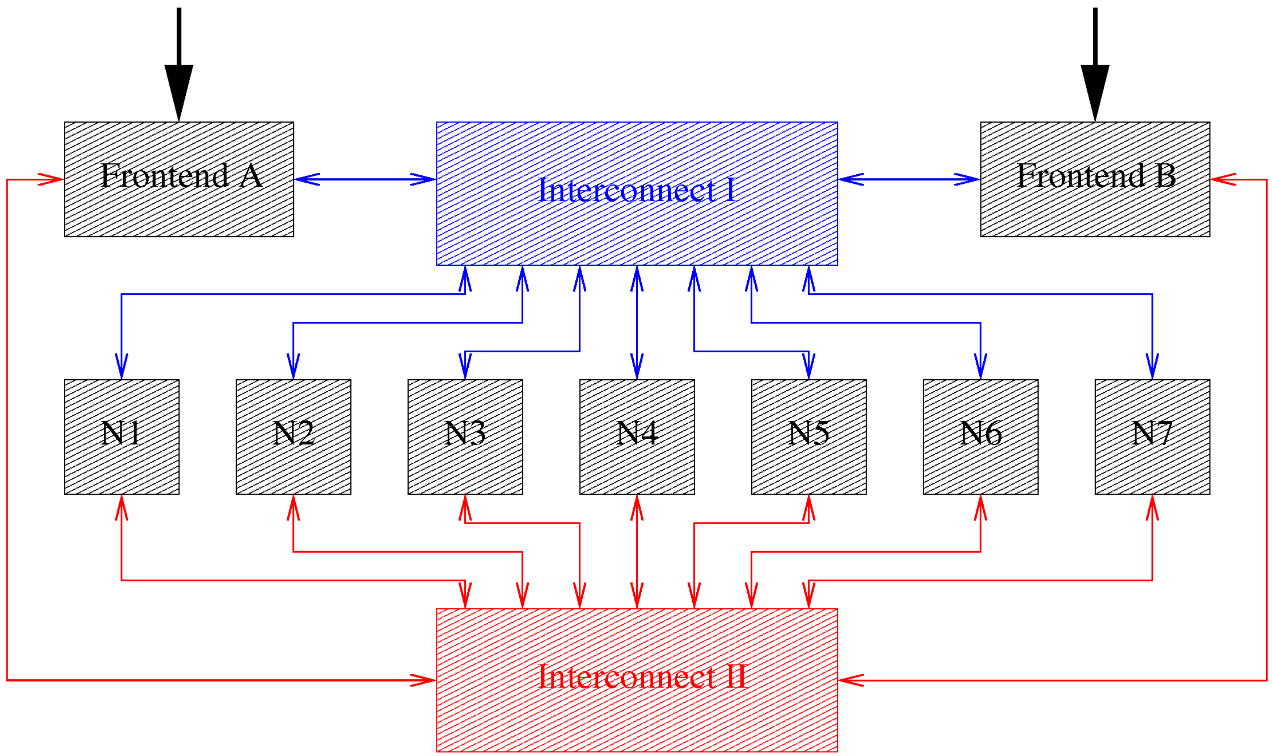

The setup of the simulation

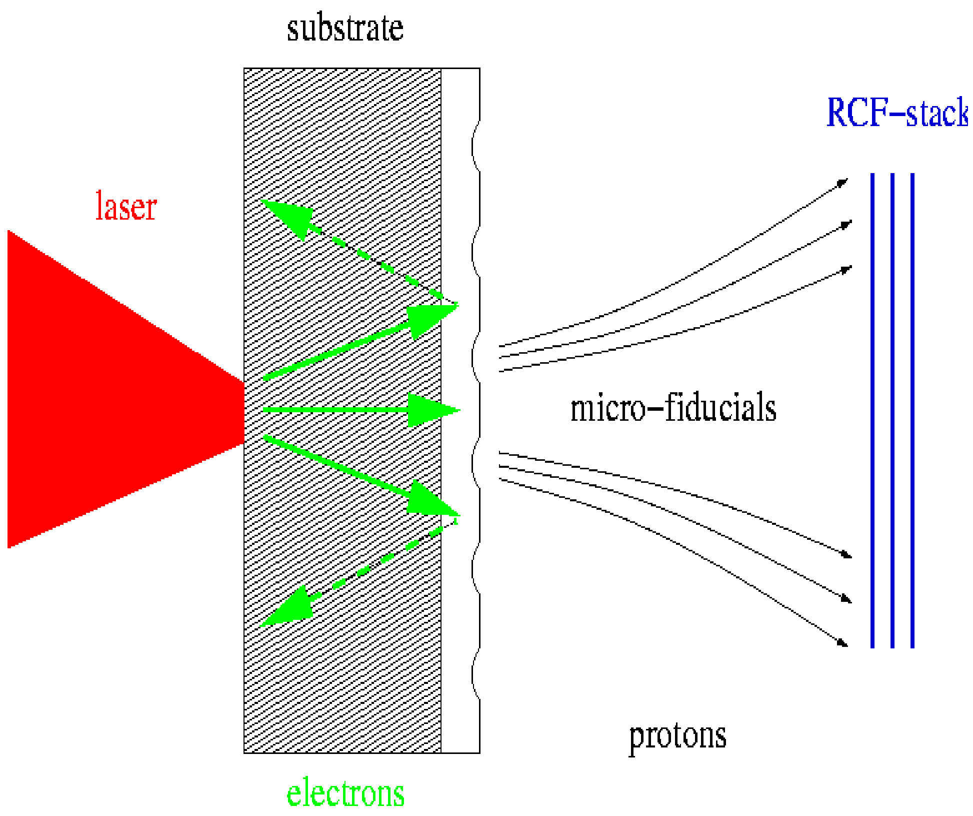

- 3000×3000 cells.
- $n_0 = 10^{23}\,\mathrm{cm}^{-3}$.
- $I_0 = 10^{19}\,\mathrm{Wcm}^{-2}$.
- 300 particles per cell.
- $T_e = 100\,\mathrm{eV}$.
- $T_i = 100\,\mathrm{eV}$.
- Substrate mass $m_s = 100\,m_p$.
- Film mass $m_f = m_p$.
- Film thickness $d_f = 0.1\,\mu\mathrm{m}$.
- Simulation is collisional.
- Simulation extends over $2\,\mathrm{ps}$.

Simulation results: phase space

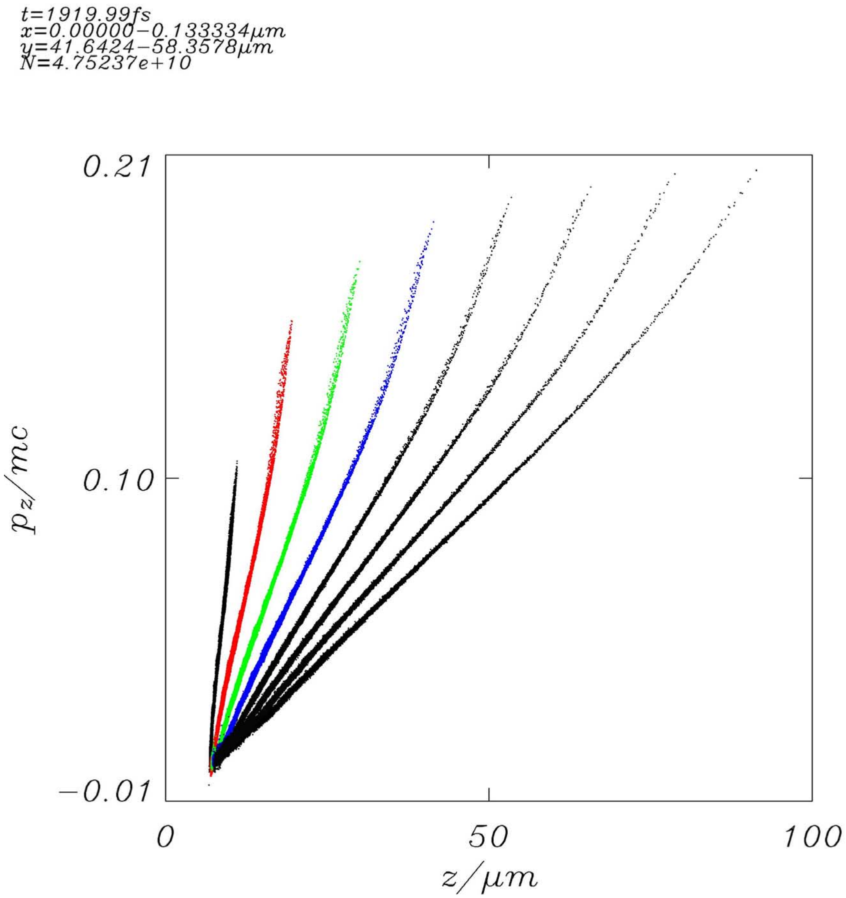

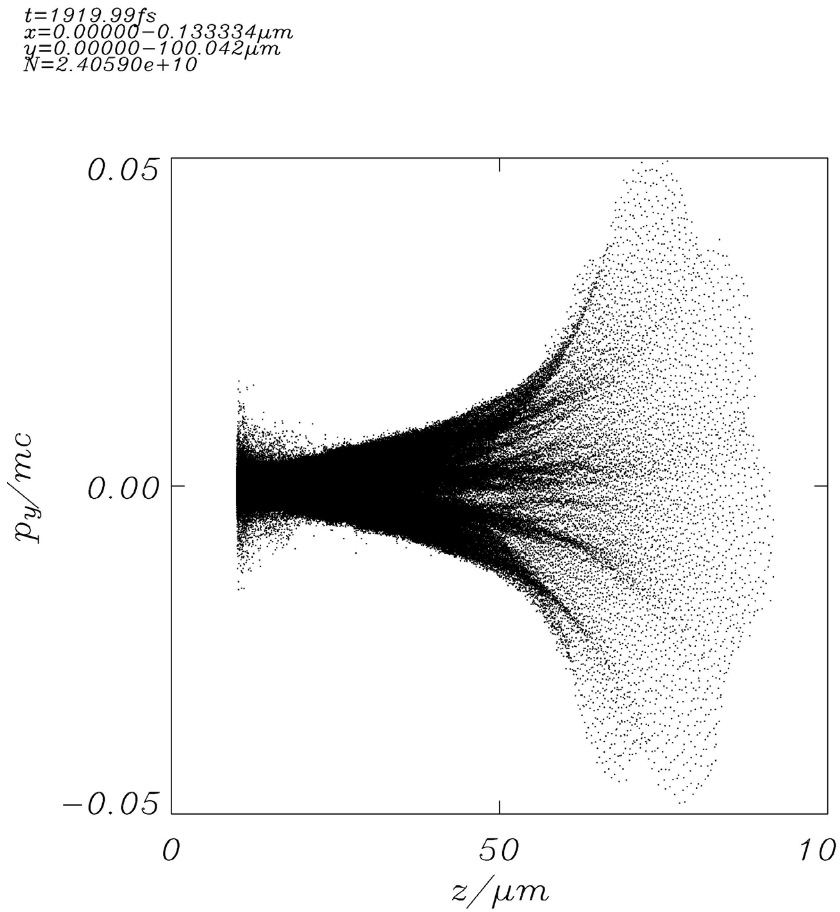

Simulation results: configuration space

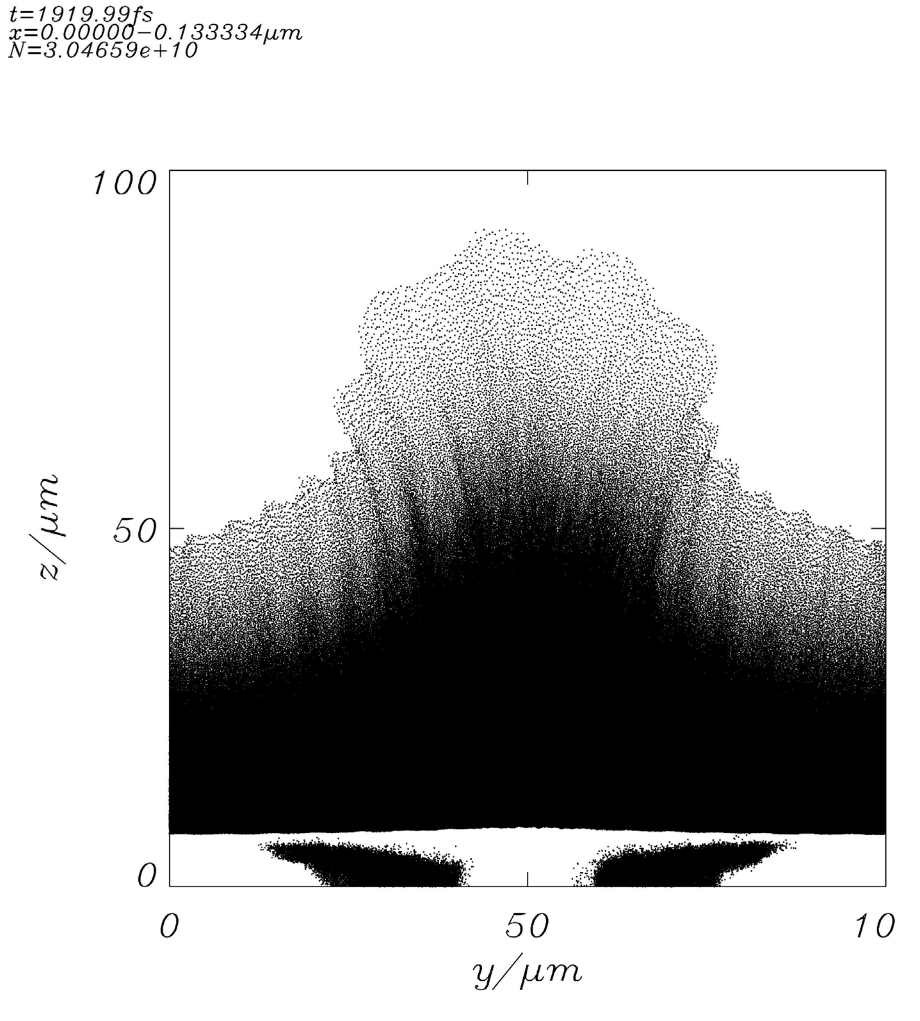

Initial momentum modulation embedded in flow expansion translates in proton dose modulation

direct imaging of the accelerating sheath

Phase I: virtual cathode

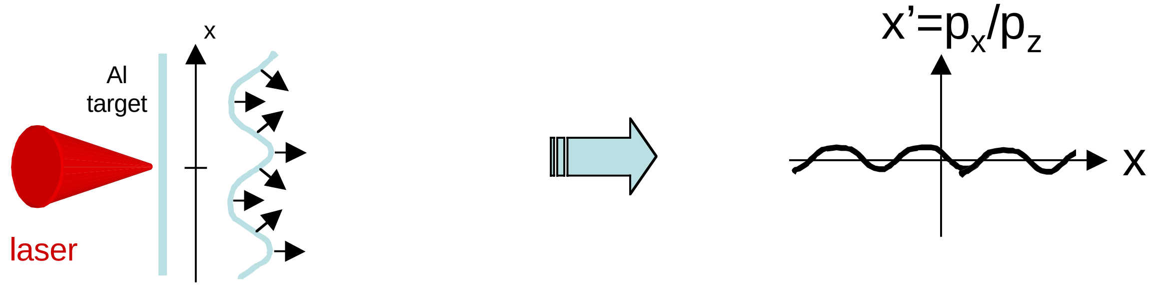

Phase II: sheath expansion

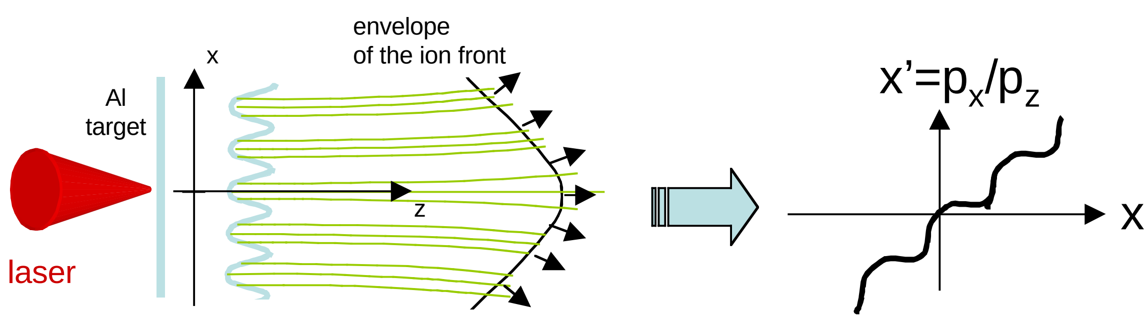

H. Ruhl, T. Cowan and J. Fuchs, Phys. Plasmas **11**, L17 (2004).

T. Cowan, J. Fuchs. H. Ruhl *et al*., Phys. Rev. Lett. **92**, 204801 (2004).

PSC simulation of flow envelope and image formation

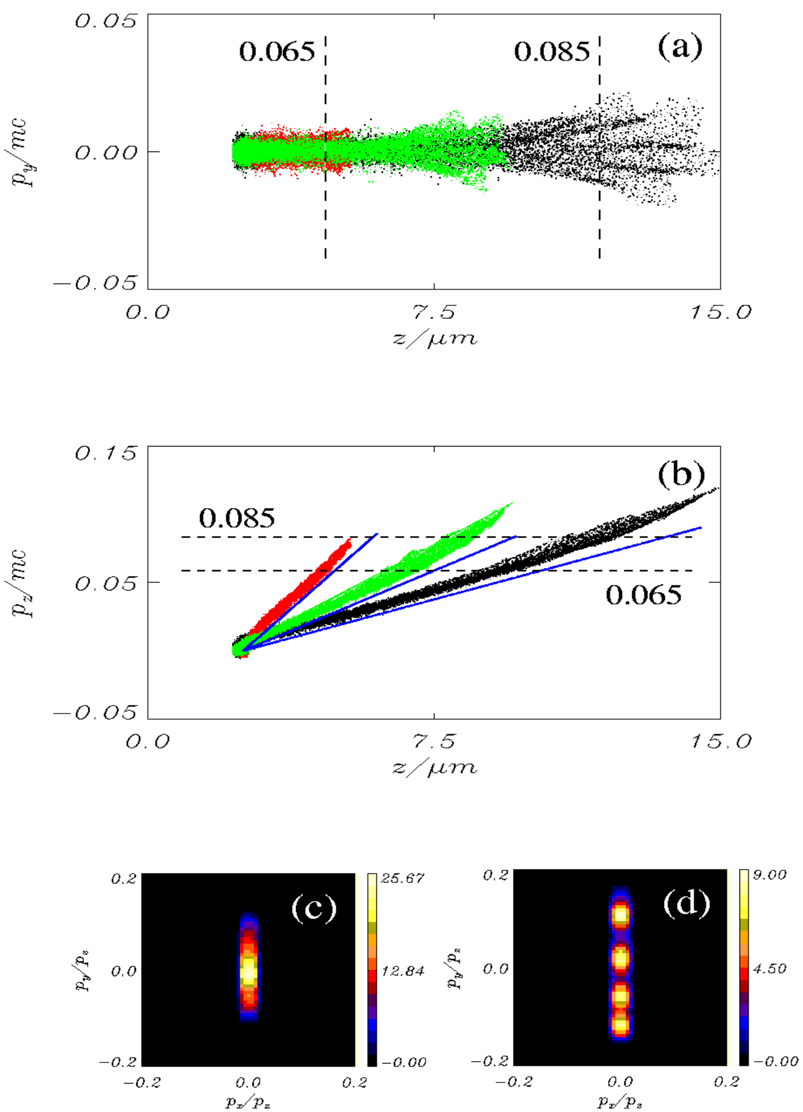

Plots (a,b) show the zp_y- and zp_z-planes of the proton phase space at $t = 300\,\mathrm{fs}$ (red), $t = 454\,\mathrm{fs}$ (green), and $t = 613\,\mathrm{fs}$ (black). Plot (a) shows micro-perturbations embedded into an expanding beam envelope due to the grooves at the rear target surface. The blue lines in plot (b) represent $p_z/m_pc = (z - z_0)/c\,(t - t_0)$ for the above times, where $z_0 = 2.5\,\mu\mathrm{m}$ and $t_0 = 170\,\mathrm{fs}$. The parameter z_0 is the location of the rear target surface and t_0 the time when the first protons accelerate. Plots (c,d) show the divergence angles α_x and α_y in color scales at 300 fs, where $0.06 \le p_z/m_pc \le 0.07$ and 613 fs, where $0.08 \le p_z/m_pc \le 0.09$. Both plots are generated by the same particles. Careful analysis shows that they follow a logarithmic flow envelope. For illustration the dashed lines in plots (a,b) indicate the proton populations between $p_z = 0.065\,m_pc$ and $p_z = 0.085\,m_pc$.

divergence angles

Effective simulations

$$p_y^0 = S_y\left(y^{-\frac{1}{2}} - y_0\right) + A_y \sin(k_y y) \;, \tag{1}$$

$$y^{n+\frac{1}{2}} = y^{n-\frac{1}{2}} + \Delta t \frac{p_y^n}{m_p} \;, \qquad p_y^{n+1} = p_y^n + C_y \Delta t \left(y^{n+\frac{1}{2}} - y_0\right) \;,$$

$$p_z^0 = S_z\left(z^{-\frac{1}{2}} - z_0\right) \;, \tag{2}$$

$$z^{n+\frac{1}{2}} = z^{n-\frac{1}{2}} + \Delta t \frac{p_z^n}{m_p} \;, \qquad p_z^{n+1} = p_z^n + C_z \Delta t \;.$$

From the simulation data we find for the parameters in the model $S_y \approx 6.5 \cdot 10^{-4} m_p c/\mu\text{m}$, $C_y \approx 5 \cdot 10^{-6} m_p c/\mu\text{m fs}$, $S_z \approx 2.5 \cdot 10^{-2} m_p c/\mu\text{m}$, $C_z \approx 4.2 \cdot 10^{-5} m_p c/\text{fs}$, $A_y \approx 0.003\, m_p c$, $y_0 = 20\,\mu\text{m}$, $z_0 = 2.5\,\mu\text{m}$, and $k_y = 2.51/\mu\text{m}$. The parameter y_0 is the location of the laser focus and z_0 of the rear target surface. We have $t^n = n\Delta t + t_s$, where $t_s = 300\,\text{fs}$ is the time when the effective particle simulation starts. We restrict the range of $z^{-1/2}$ such that we have $0.06 \le p_z/m_p c \le 0.07$ for all protons at 300 fs.

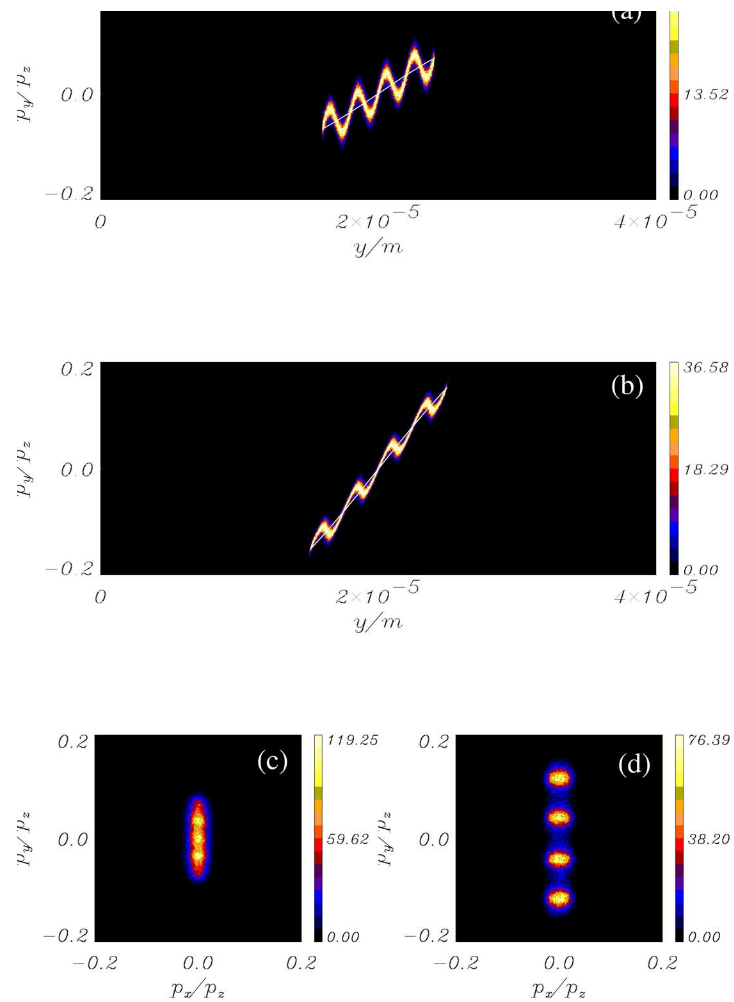

Effective simulations: more complexity

Distribution function for protons

$$\begin{aligned} f_p(\mathbf{x},\mathbf{p},0) &= N_p\, n_p(\mathbf{x}) \exp\left(-\frac{[\mathbf{p}-\mathbf{P}(\mathbf{x})]^2}{2m_p k_B T_p}\right) \\ n_p(\mathbf{x}) &= n_0 \exp\left\{-\frac{z-z_0}{L h(x,y)}\right\} \\ h(x,y) &= \exp\left\{-\frac{x^2+y^2}{r_0^2}\right\} \end{aligned}$$

$$z \leq z_0 + L h(x,y) \ln \frac{n_0}{n_p},$$

Initial perturbations

$$\begin{aligned} P_x &= A_x\, m_p c\, \sin(k_x x) \\ P_y &= A_y\, m_p c\, \sin(k_y y) \\ P_z &= A_z\, m_p c\, (z - z_0) \end{aligned}$$

Equations of motion

$$\begin{aligned} \mathbf{p}_i(t) &= \mathbf{g}[\mathbf{x}_i(t)] + \delta\mathbf{p}[\mathbf{x}_i(0)] \\ \mathbf{x}_i(t) &= \mathbf{x}_i(0) + \frac{1}{m_p}\int_0^t d\tau\, \mathbf{p}_i(\tau) \end{aligned}$$

$$\delta\mathbf{p}[\mathbf{x}_i(0)] = \mathbf{p}_i(0) - \mathbf{g}[\mathbf{x}_i(0)]$$

Transfer function

$$\begin{aligned} g_x &= C_r\, m_p c\, \frac{x(z-z_0)}{r_0^2} \exp\left\{-\frac{x^2+y^2}{r_0^2}\right\} \\ g_y &= C_r\, m_p c\, \frac{y(z-z_0)}{r_0^2} \exp\left\{-\frac{x^2+y^2}{r_0^2}\right\} \\ g_z &= C_z\, m_p c\, \frac{\ln \frac{z}{z_0}}{\ln \frac{z_1}{z_0}} \end{aligned}$$

Application of the method: Effective simulation

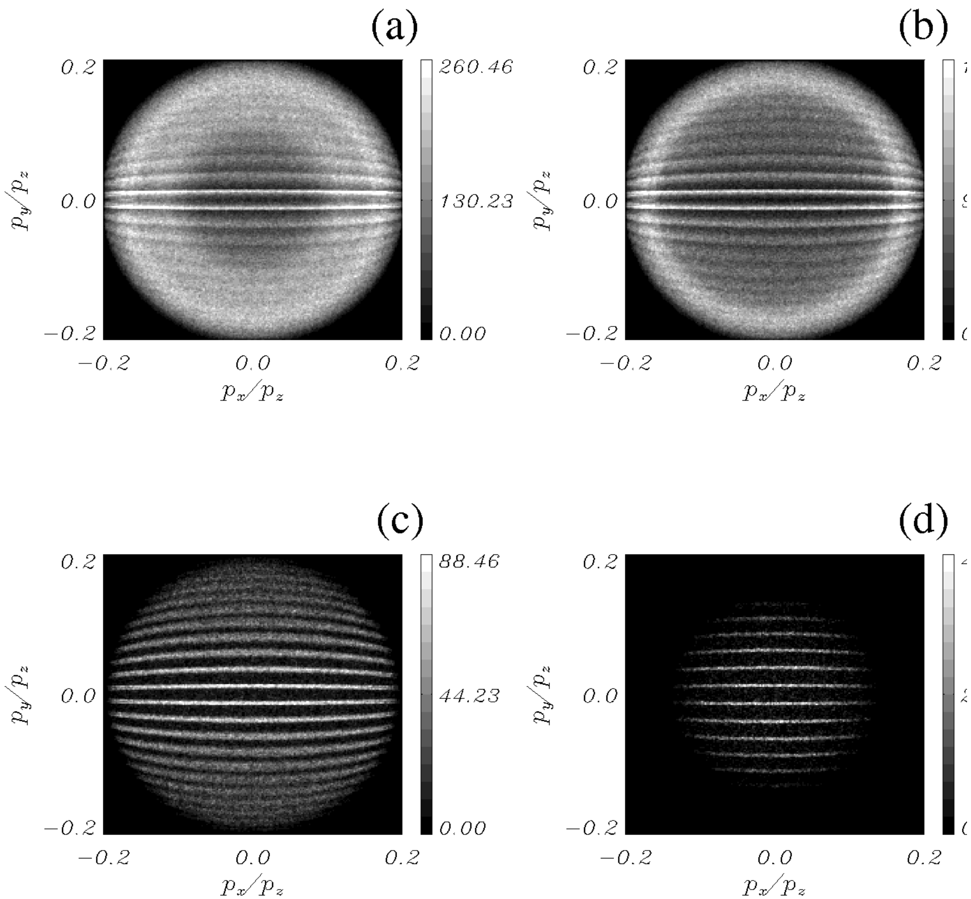

- Plot (a) shows rings at 2MeV.
- Plot (b) shows rings at 5MeV.
- Plot (c) shows grooves at 8MeV.
- Plot (d) shows grooves at 11MeV.

These results can now be used to predict the electro-magnetic fields in the flow via gx, gy, gz derived earlier!

r0=50μm
r1=140μm
cr=0.11
cz=0.12
L1=0.5μm
z0=3.0μm
z1=120μm
Ax=0.0
Ay=0.0006
Az=210000

Recent publications

•H. Ruhl, T. Cowan, and J. Fuchs, “Characterization of laser-accelerated proton flows with the help of surface images embedded into the flow”, Phys. Plasmas 11, L17 (2004).
•H. Ruhl et al.,”Ring structures in laser-accelerated proton flows: Their interpretation and Application”, submitted to PoP.
•T. Cowan et al., “Low emittance proton beams from laser irradiated metal foils”, Phys. Rev. Lett. 92, 204801 (2004).

Conclusions

•Ultra low emittance beams (< 0.002 mm mrad for E>5 MeV).
•Beam generated on sub-ps time scales.
•Electric field in the beam decays rapidly.
•Electrons co-propagate with the beam.
•Electrons can be removed without distorting the beam.
•10^12 protons per shot.

Fast Ignition Integrated Interconnecting Code Project for Cone-guided Targets

H. Sakagami, H. Nagatomo*, T. Johzaki* and K. Mima*

Comp. Eng., University of Hyogo

*ILE, Osaka University

Cone-Guided Target for Fast Ignition

- Ignition laser directly interacts with dense Au plasmas without propagating through underdense coronal plasmas.
- Generated hot electrons can easily reach a target core and deposit their energy.

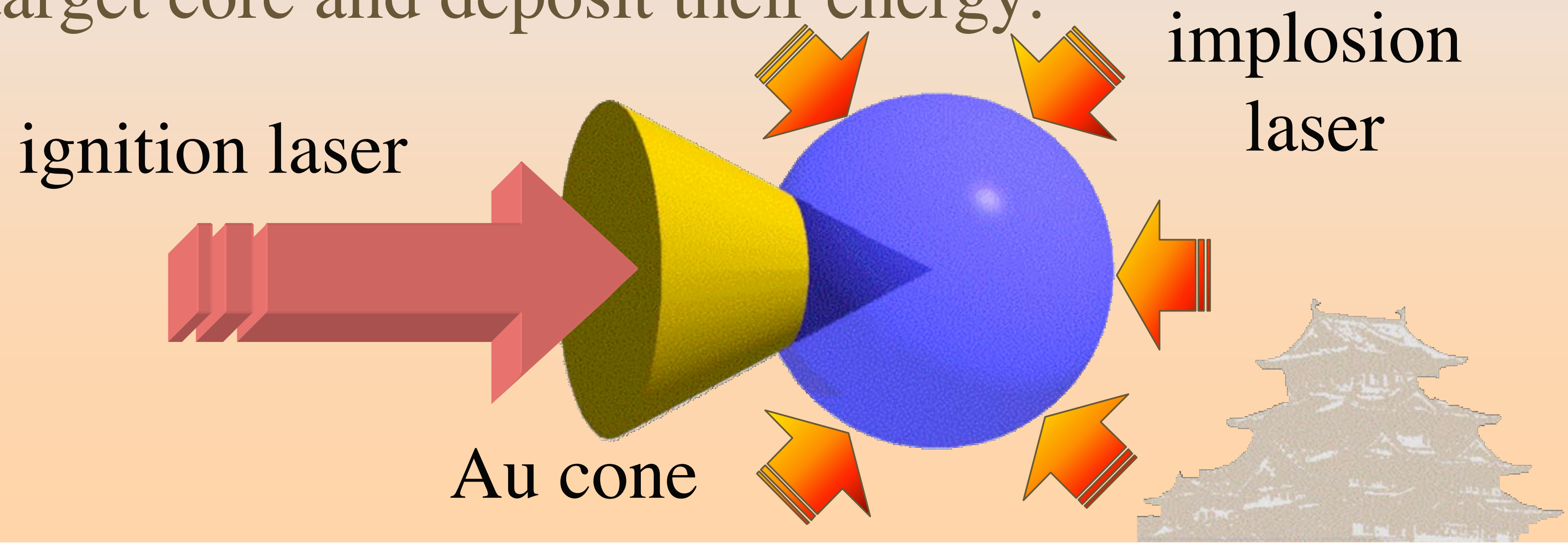

Difficulty and Discrepancy

- In Fast Ignition, physical quantities would vary in a very wide range and their time and space scales would be entirely different.
  - It is impossible to simulate the whole extent of Fast Ignition with a specific code.
- Simple conventional modeling for simulation could not describe experimental results.
  - Realistic modeling should be important.

FI^3 Project

- Fast Ignition Integrated Interconnecting code Project

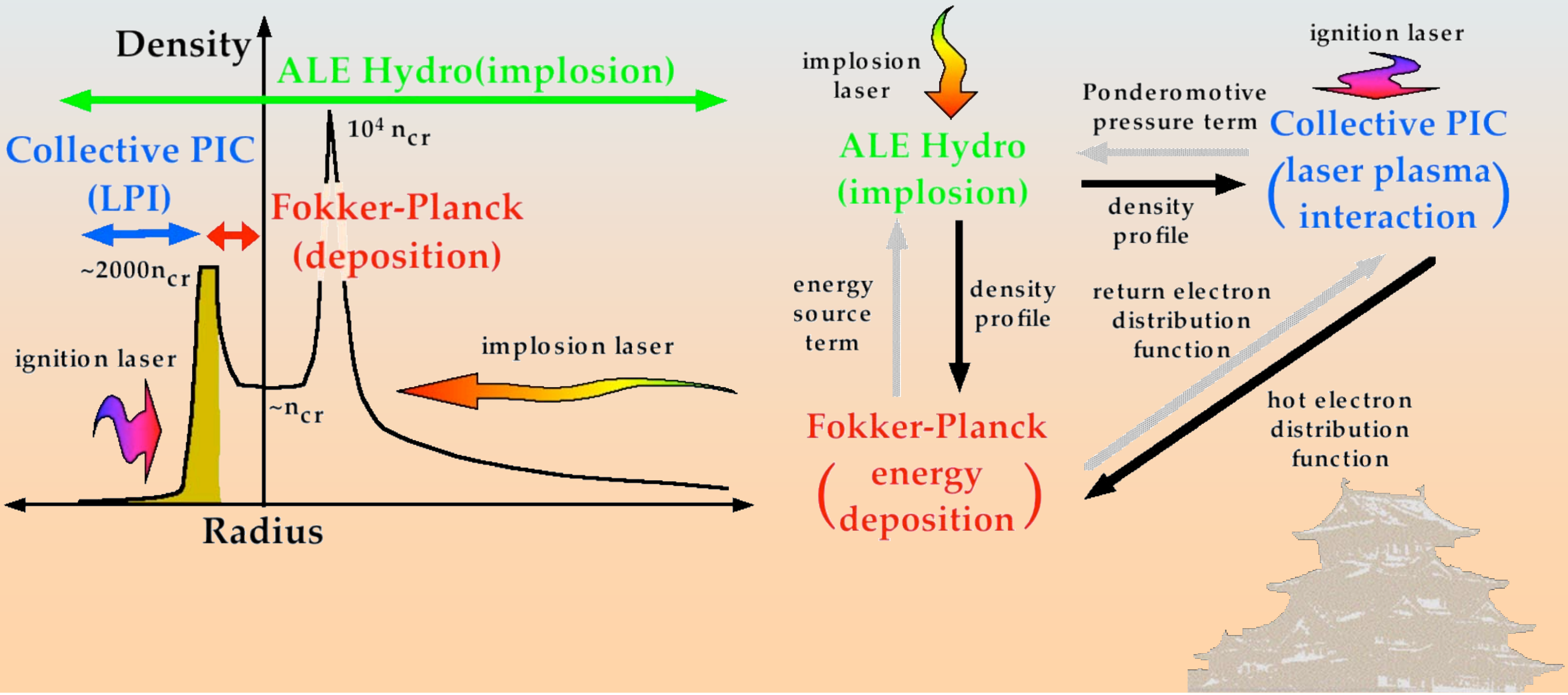

Integrated Simulation

Simulation Parameters of ALE

H. Nagatomo

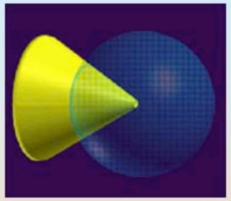

Laser condition

Wavelength : 0.53mm

Energy (on target) : 3.0kJ

Ray-trace : 1 - D (radial direction)

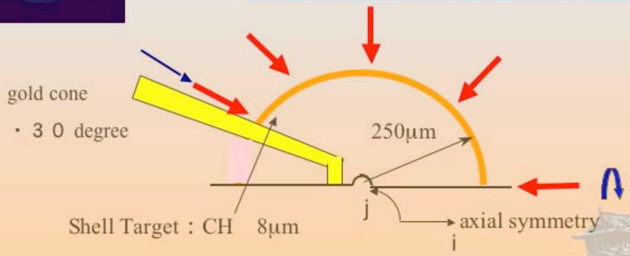

computational grids : 280 (i- direction) x 280 (j - direction)

Simulation Parameters of PIC

- ignition laser
  - Gaussian with FWHM = 90 [μm] (~ 750 [fsec])
  - $10^{\{19,20\}}$ [W/cm²-μm²],
- plasma
  - exponentially fitted ALE profile
    - length : 100 [μm], density : 0.1 ~ 100 n_{cr}
  - flat top plasma (50 [μm], 100 n_{cr})
  - 200 particles per mesh (n > 2 n_{cr})
- simulation time
  - 0 ~ 1500 [fsec], 250,000 time steps
  - 200 hours with AthlonXP 2200+

Simulation Parameters of FP

T. Johzaki

RFP Sim. Condition

space (x,y) – CIP (80×160 meshes)
momentum (p) – Discontinuous Linear FEM (30 groups)
Direction (μ, φ) – 2D Discrete Ordinate Sn method (144 directions)

Injected Beam profiles

(a) Two PIC sources (I_L = 10^{20} & 10^{19} [W/cm²])
(b) Three Mono-energy Beams (τ_{FWHM} = 300fs, I_{max}=3x10¹⁹ [W/cm²], E_0 = 1, 2 and 5 MeV)

Electron beam is injected at inner surface of a gold cone at maximum compression

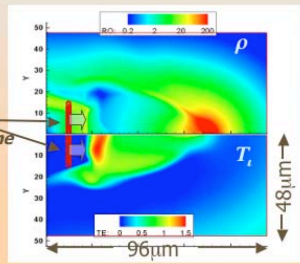

Heating Rate and Electron Temp. Profiles Comparing with Mono Temp. Electrons

T. Johzaki

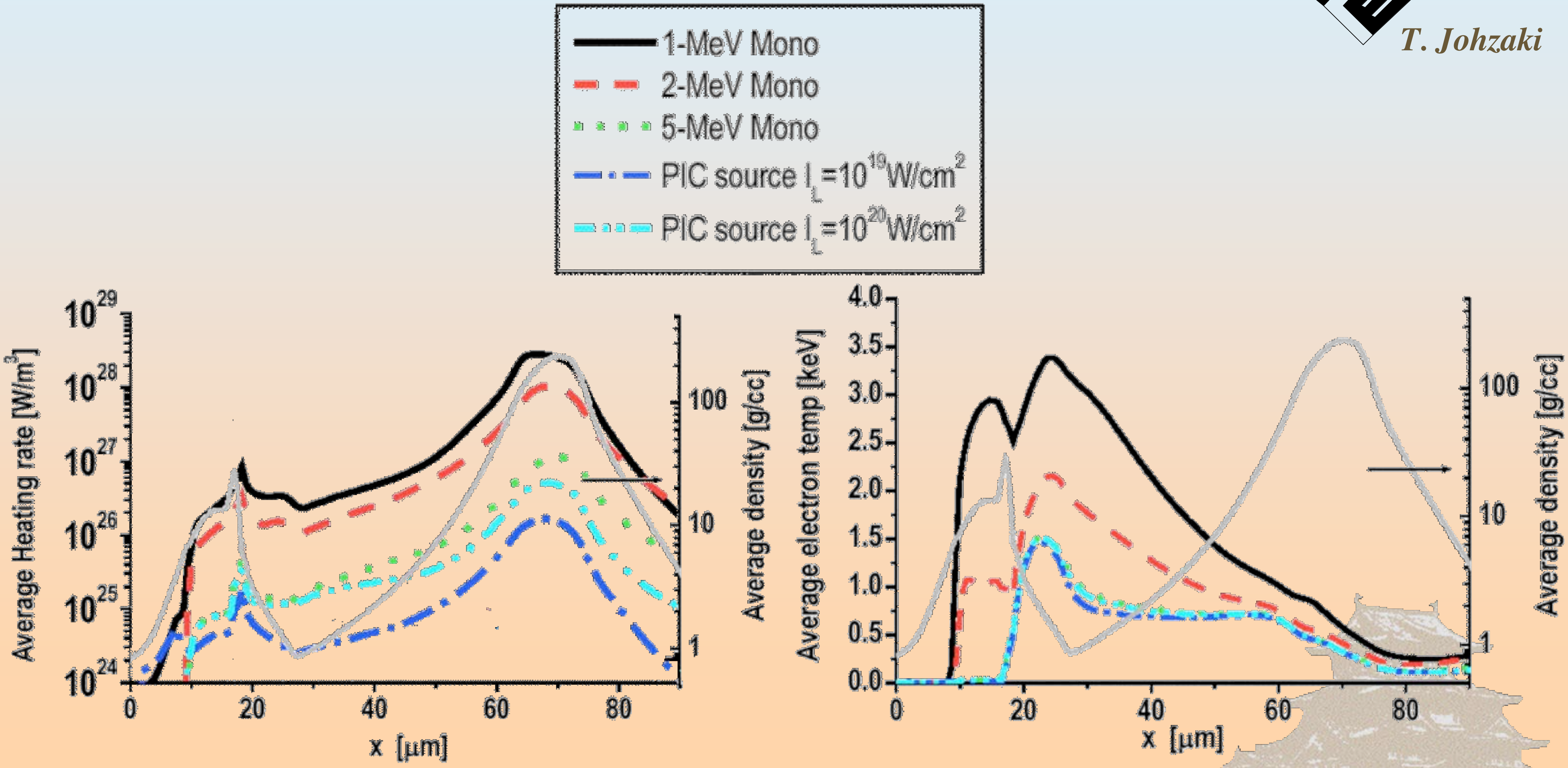

Core is NOT heated up!

- Main reason is that hot electrons are too hot!
- Multi dimensional effects with the cone ?
  - Large scale 2,3-D PIC simulations are needed.
- Hot electrons lose energy during transport ?
  - potential and/or instability ?
  - Prof. Taguchi has pointed out hot electron beam decay with his 3-D hybrid code simulations.
    - Coupling with PIC and Hybrid is needed.
- Recoiling is important ?
  - FP should treat recoiling.

1-D Collective PIC Simulations

Simulation time: 1000 [fs]
Δt = 0.0056 [fs] ($0.0016\omega_L$), ~ 177,000 steps
Spatial size: 308 [μm]
Δz = 4.73e-3μm, ($0.0045\lambda_L$), ~ 65,000 meshes
Total Number of Particle: ~ 3,574,000
200 particles / mesh ($n > 2n_c$)
※ Ions: immobile

Laser Pulse

Gaussian Pulse, τ_{FWHM} = 150fs
Wavelength, λ_L = 1.06μm
Peak Intensity, $I_{L,max}$ = 1×10^{20} [W/cm^2]

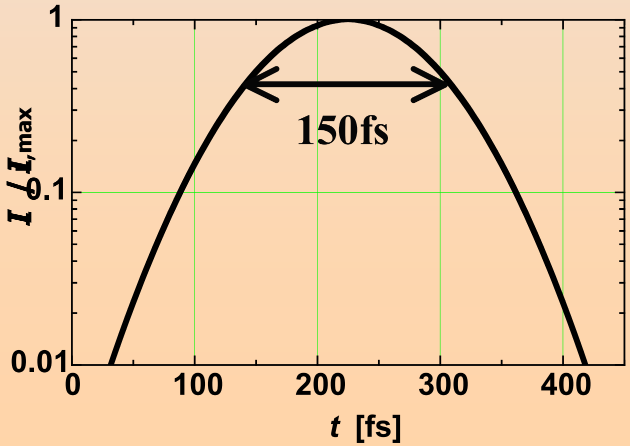

Initial plasma configuration

- Pre-plasma, scale length = 5 [μm]
- Peak density, $n_{e,peak} = 100n_c$ width = 10 [μm]
- Rear Plasma, $n_{e,rear} = 100n_c$ or $2n_c$, width = 50 [μm]
- Vacuum region: front 153 [μm], rear 60 [μm]
  - ➢ ***Fast electron profiles are observed at 5 [μm] behind of $100n_c$ region.***

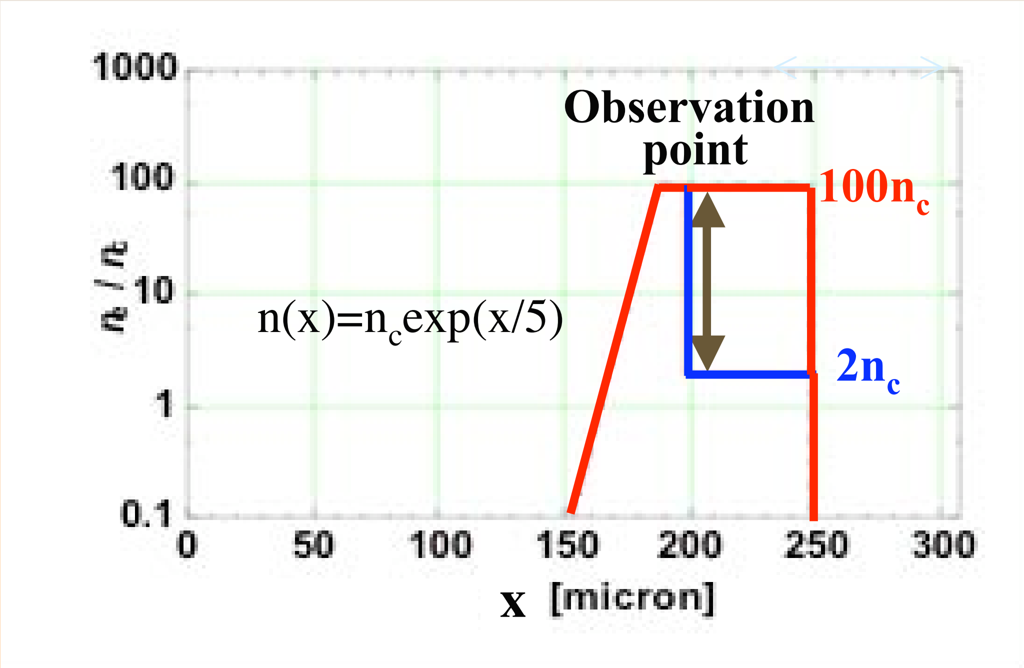

Energy Distribution of Fast Electrons

$I_{L,max} = 1\times10^{20}$W/cm^2

E > 0: Forward-directed electrons
E < 0: Backward-directed electrons

T. Johzaki

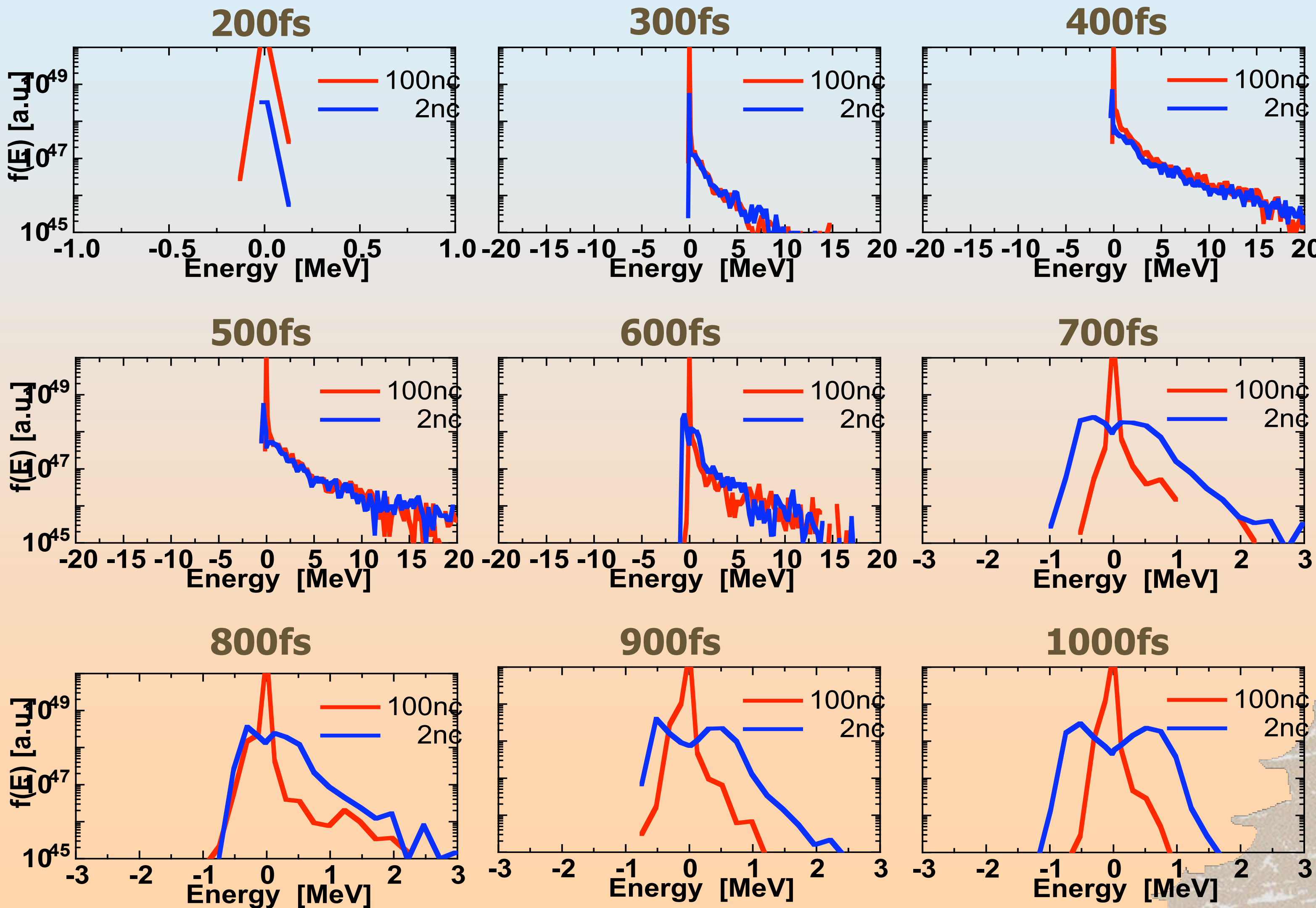

Contact Potential

- too small to stop hot electrons!

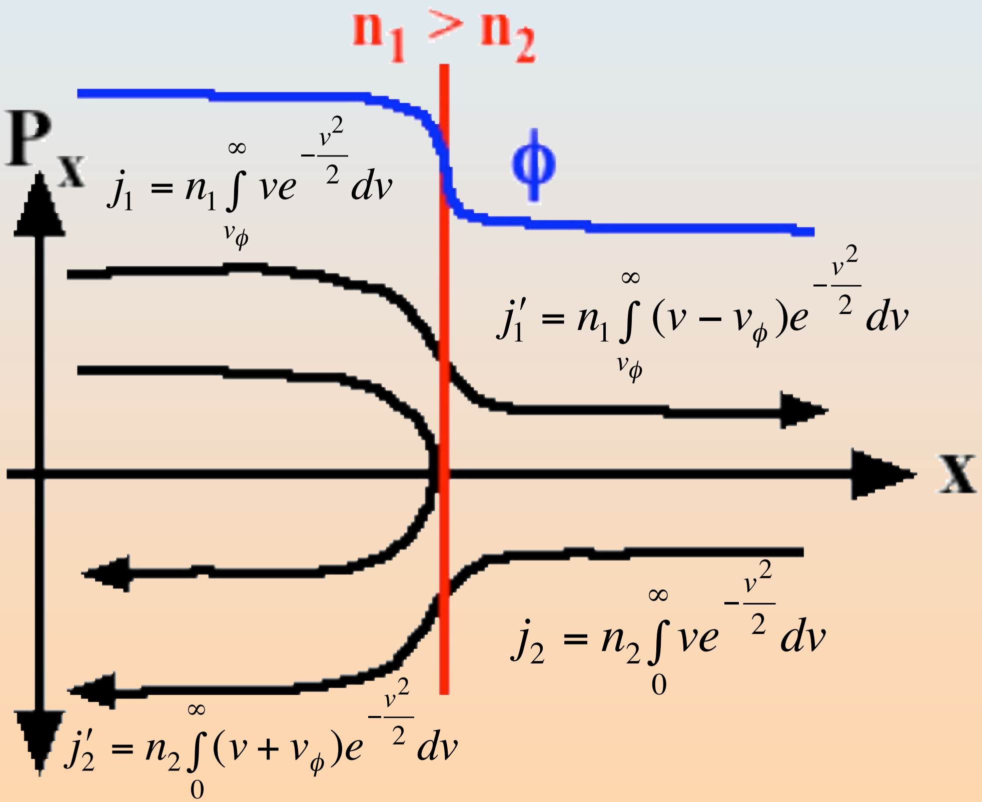

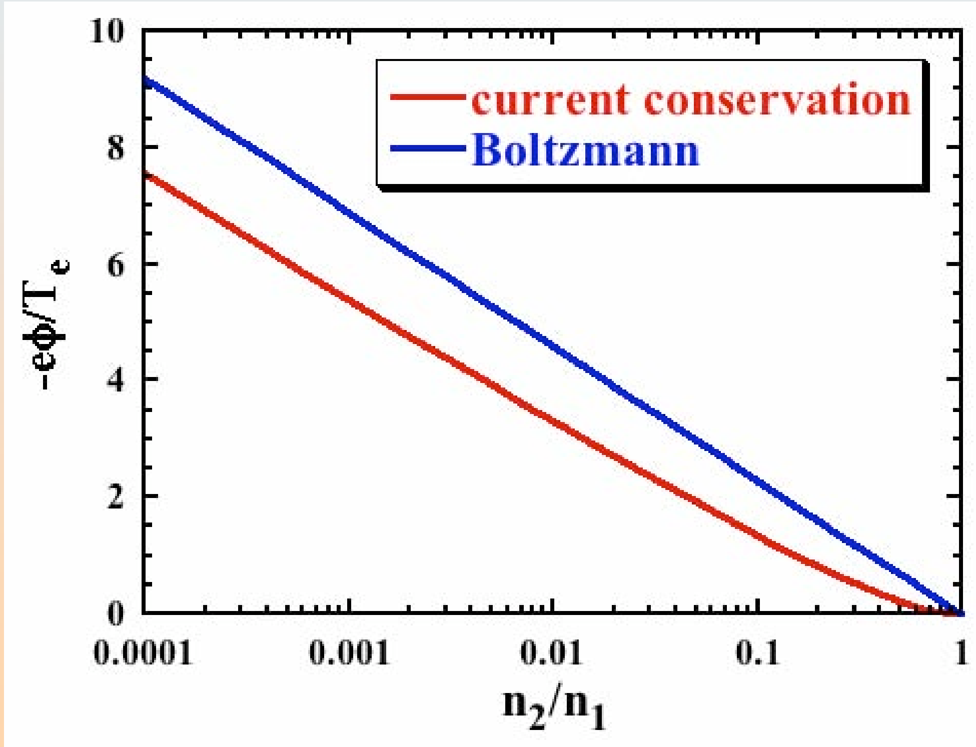

Bulk Return Currents

- All of bulk electrons must run to cancel hot electron current in case of $2n_c$.
  - $J_{hot} \sim 0.1(n_{max}v_{te}) \sim 5(2n_c v_{te})$

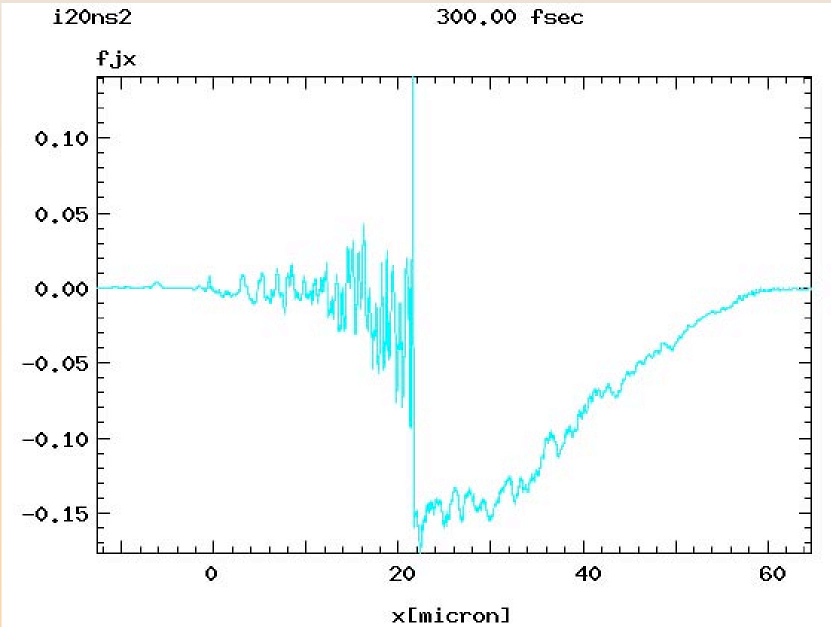

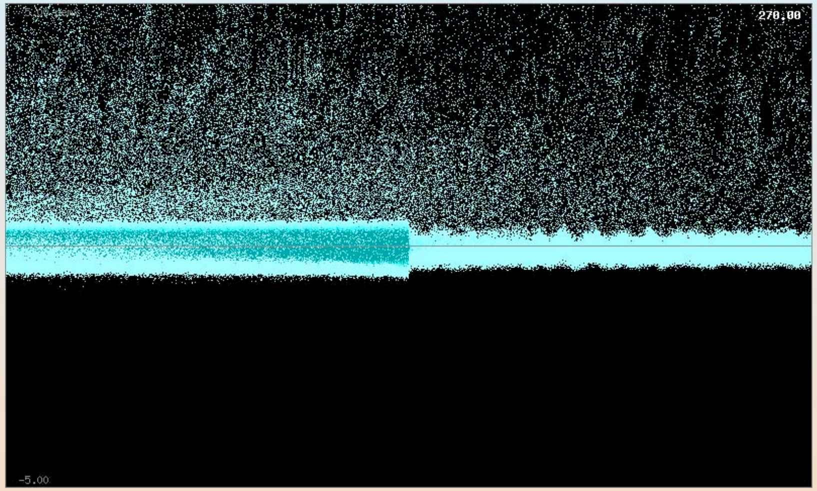

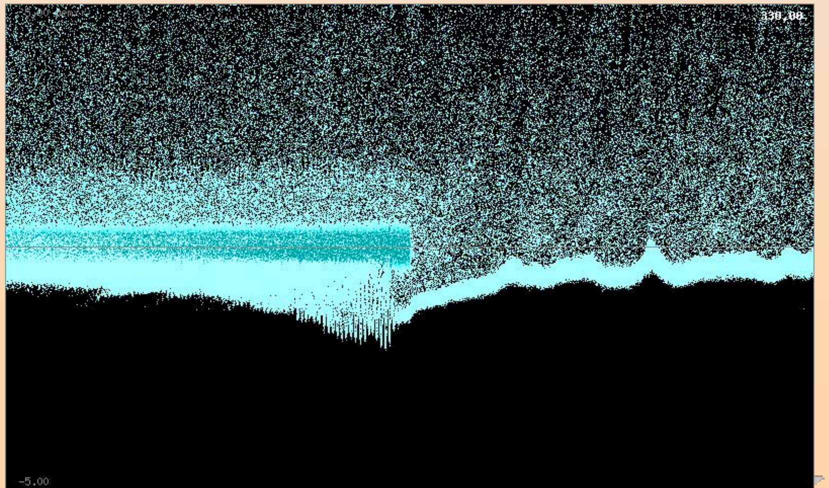

Two-stream Instability

- This return current causes the two-stream instability and bulk electrons are heated up.
  - In 2-,3-D, the Weibel instability instead

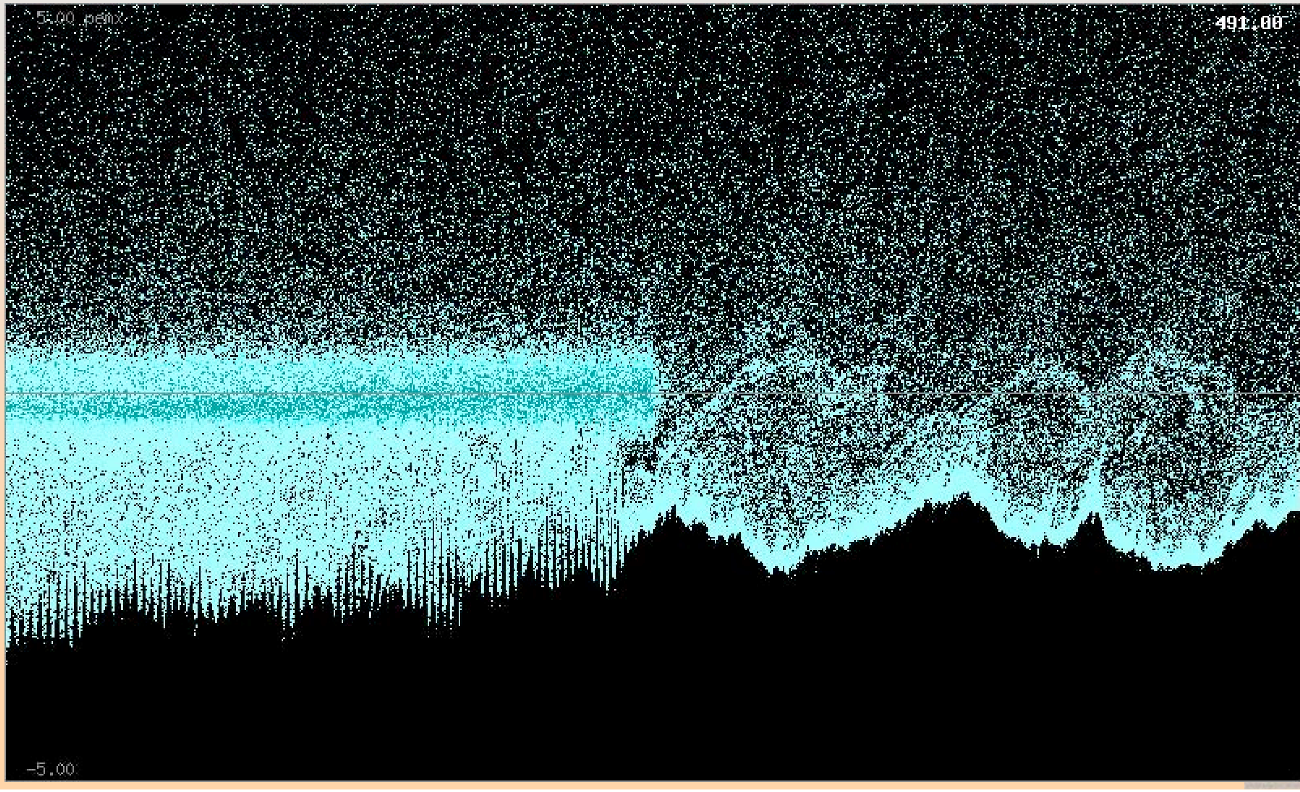

Sloshing Electrons

- If J_{hot} becames more than $2n_c c$, hot electrons are reflected at boundary by potential $e\phi/T_e$~100.
  - They are sloshing and continuously heating up bulk.

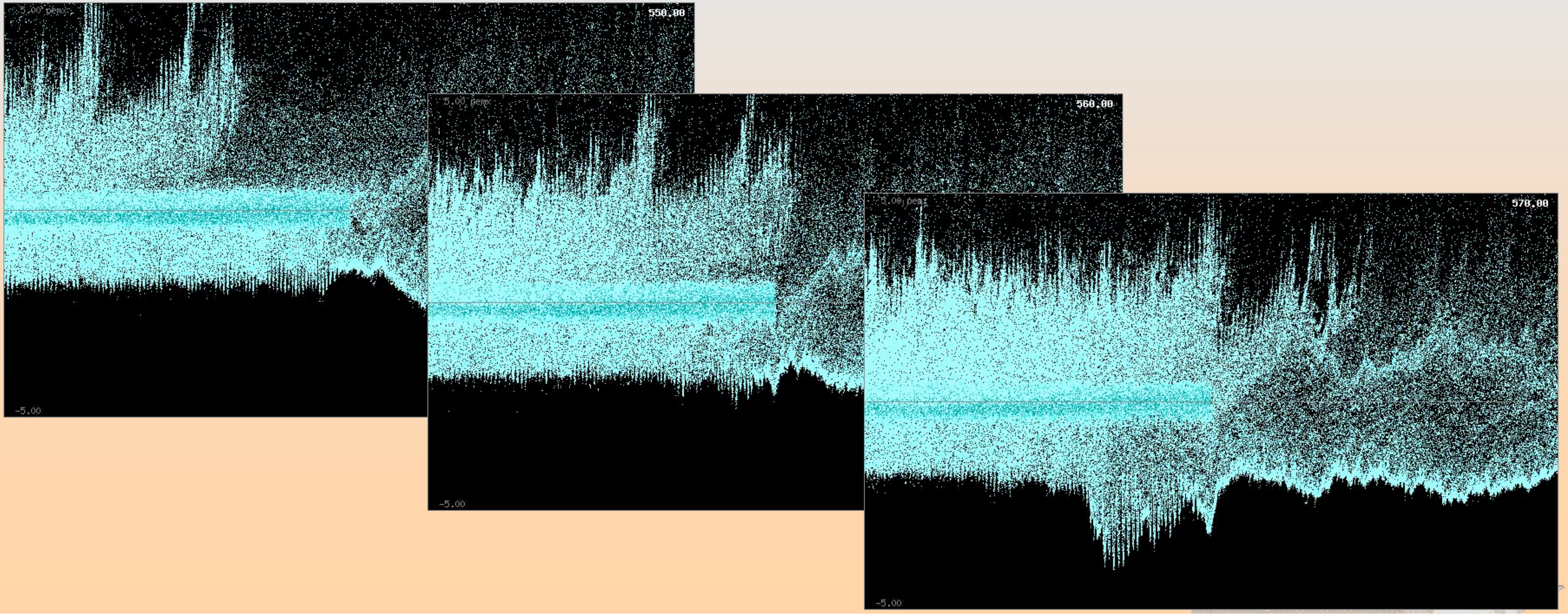

Fokker-Planck Simulation Model

Fast Electron Profiles
(PIC Code)

Fast electrons were injected at inner or outer surface of a gold cone.

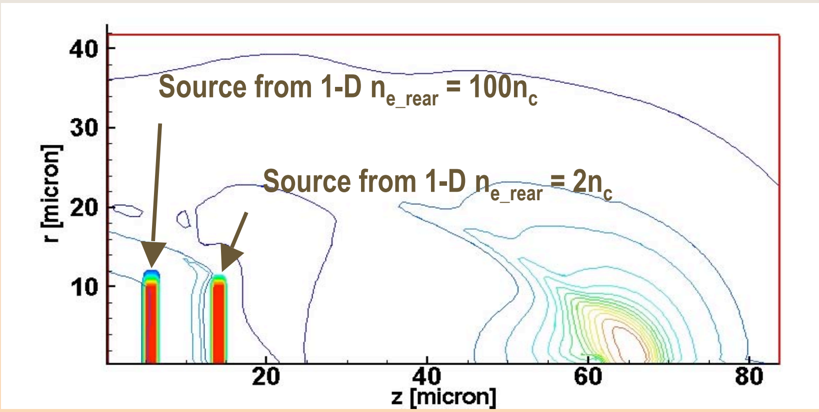

Imploded Core Profiles
(ALE Rad-Hydro Code)

Fast Electron Transport

Relativistic Fokker-Planck transport
Electromagnetic Fields

(x,y) – CIP (80×160 mesh)
(p) – Discontinuous Linear FEM (30 groups)
(μ, φ) – 2D Discrete Ordinate Sn method (144 directions)

ρ, T

Energy deposition rate

Radiation-Hydrodynamics

Bulk Plasma
- **1-fluid 2-temp. CIP code**

Radiation
- **Flux-limited diffusion**

Adjustment of Fast Electron Profiles for Nature Experiment

Pulse length (150fs FWHM) is shorter than PW condition (750fs).

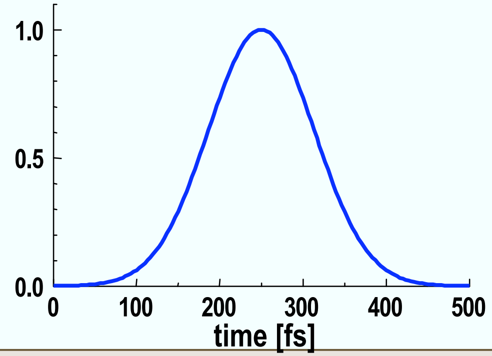

1D PIC sim.

2D effects (e.g. Cone-guiding for electrons) were not included.

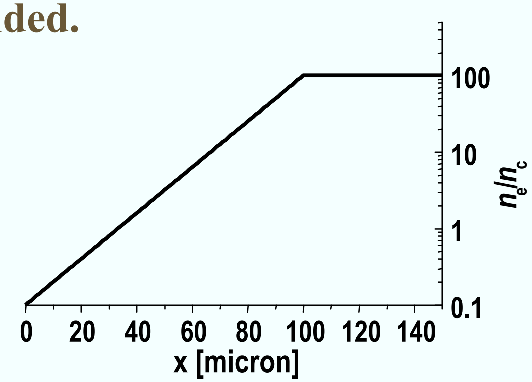

1） Electron Beam Pulse Length was extended.

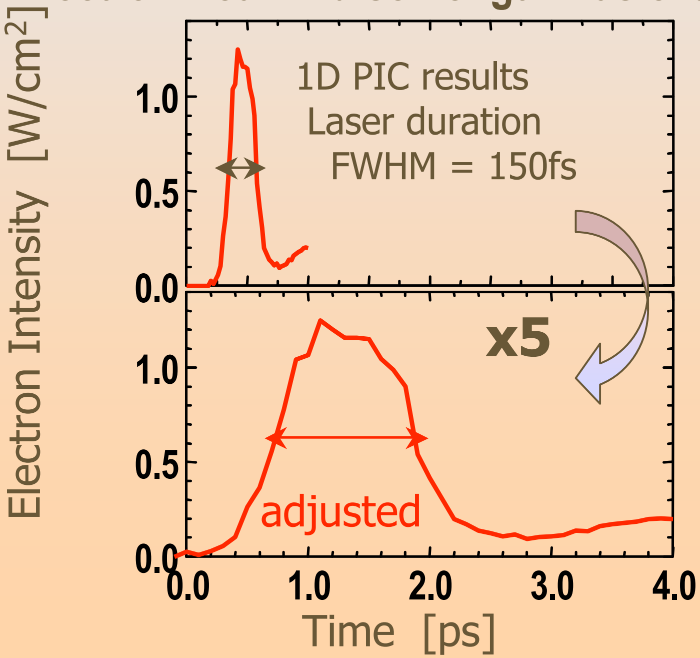

2） Intensity was adjusted so that the integrated electron beam energy is 100kJ.
(Cone-guiding effects)

E_{LPW}~500J

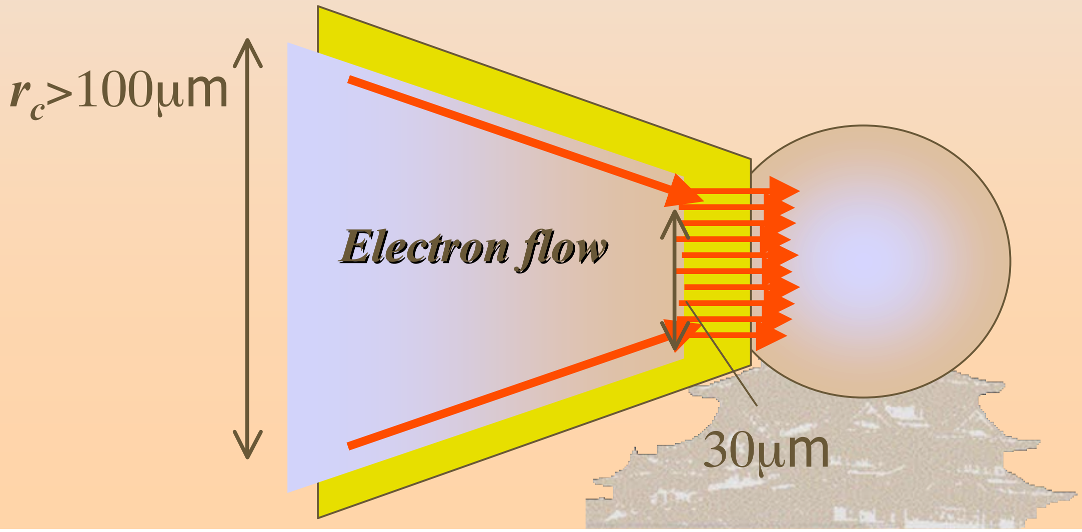

Temporal Evolution of Core Heating Rate and Electron, Ion Temperature

T. Johzaki

$I_{L,max} = 1\times10^{20}$W/cm^2

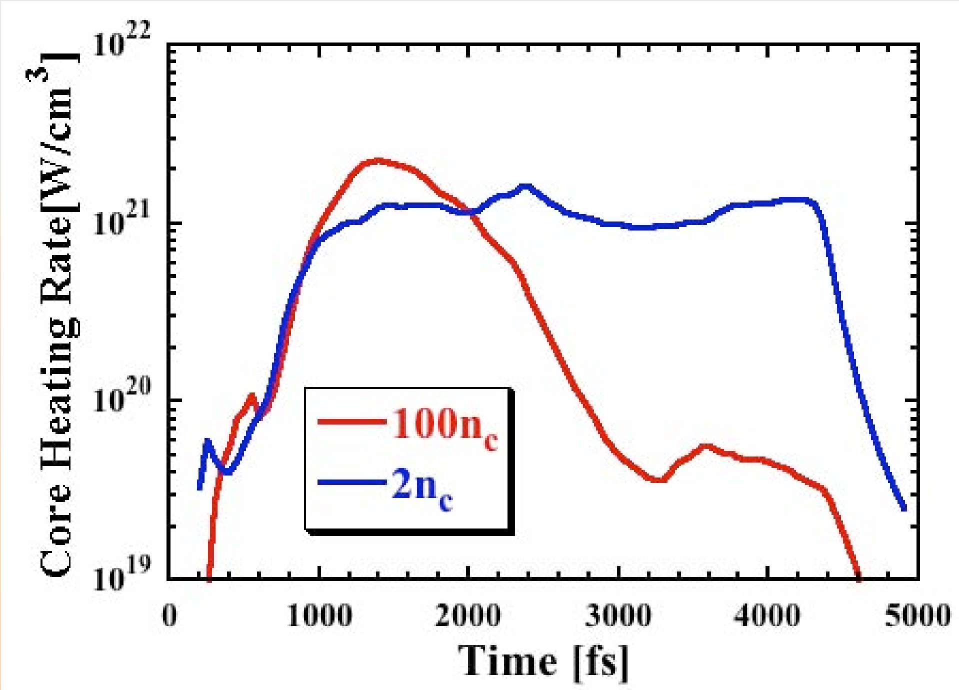

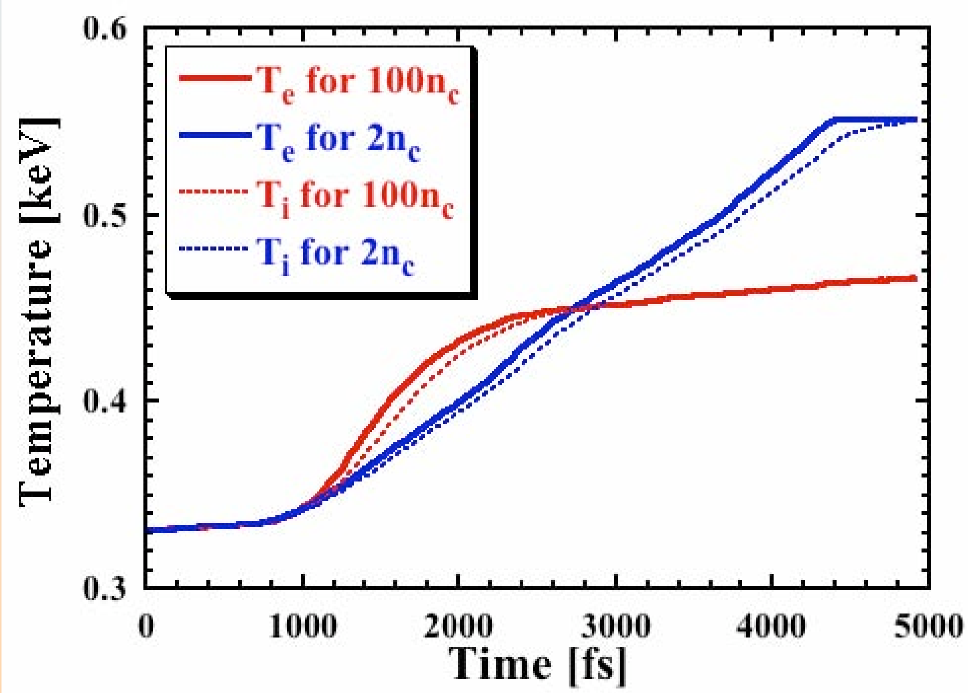

Core is heated up more than 20% with 2n_c!

Code Connection

- current method
  - save data into files.
  - transfer files between computers via FTP.
  - read data from files.
- We need more convenient and integrated way to exchange data. !
  - communicate data between codes.
  - use a specific protocol.

Interconnecting Protocol

- standard protocol is too heavy!
  - Globus, CORBA, SOAP
  - not easy to program
- TCP/IP based lightweight protocol
  - intra-site with LAN
  - inter-site with dedicated line and/or the Internet
- Distributed Computing Collaboration Protocol
  - simple and easy for computational scientists
  - procedure-free system

Design of DCCP

- Code (user's simulation program)
  - does not transfer data directly to another code
- Communicator
  - receive data from sender code
  - forward data between different sites
  - send data to receiver code
- Arbitrator
  - manage information of codes
  - control data communication

Implementation of DCCP

- dynamic negotiation for communication pair
  – Code can be invoked at an arbitrary computer.
- asynchronous communication
  – Data will be automatically saved/restored.

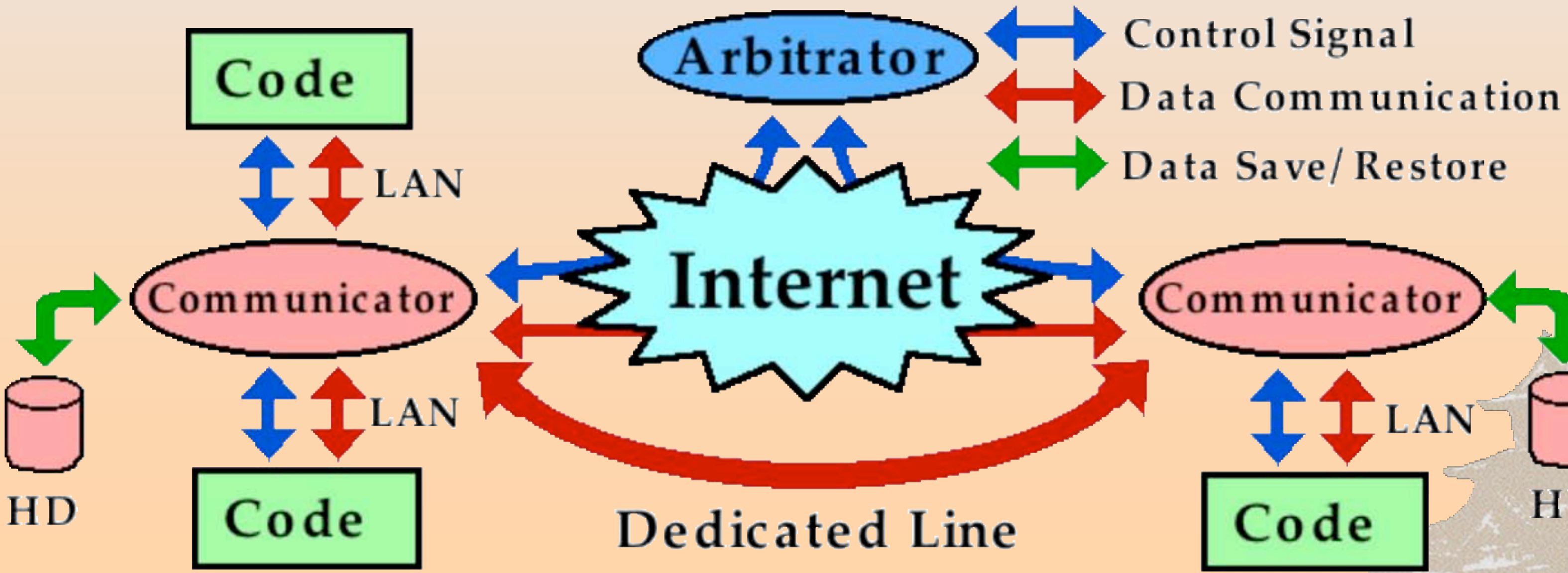

Implementation of Relay System

- relay DCCP communication packets which are prohibited by the firewall system
- Transponder
  - transparently implemented using NAPT technique

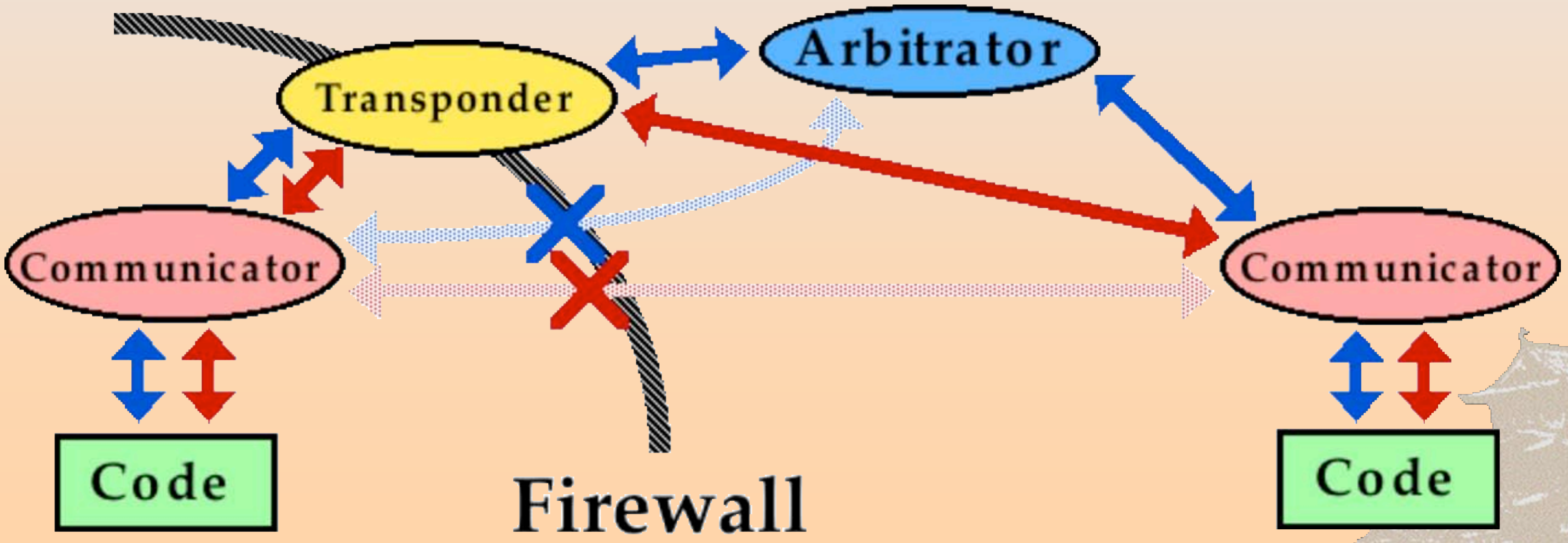

Configuration Files of DCCP

- config file for Code
  - IP address and port number of Communicator
- config file for Communicator
  - IP address and port number of Arbitrator
  - port number for listening
  - IP addresses for access allowed Codes/Communicators
- config file for Transponder
  - IP address and port number of Arbitrator
  - port number for listening
  - IP addresses of access allowed Communicators
- config file for Arbitrator
  - port number for listening
  - IP addresses of access allowed Communicators/Xponders

Fortran User Interface of DCCP

- Three level specification for transferred data
  - CodeName : unique identification of code
  - RunName : different simulation parameters
  - Tag : time dependent data

```
call DCCP_INITIALIZE ( CodeName, RunName, Cnd )
call DCCP_SEND ( DstCode, DstRun,
                                    N, Type, Data, Tag, Cnd )
call DCCP_UPLOAD ( Ndst, DstCodes, DstRuns,
                          N, Type, Data, Tag, Expire, Cnd )
call DCCP_RECEIVE ( SrcCode, SrcRun,
                          N, Type, Data, Tag, Timeout, Cnd )
call DCCP_FINALIZE ( Cnd )
```

Current Status of DCCP

- DCCP subroutines were installed into Pseudo-Hydro, RFP and PIC codes.
  - α version was released in Mar., 2004
  - β version was released in Jun, 2004
  - version 1.0 was released in Aug., 2004

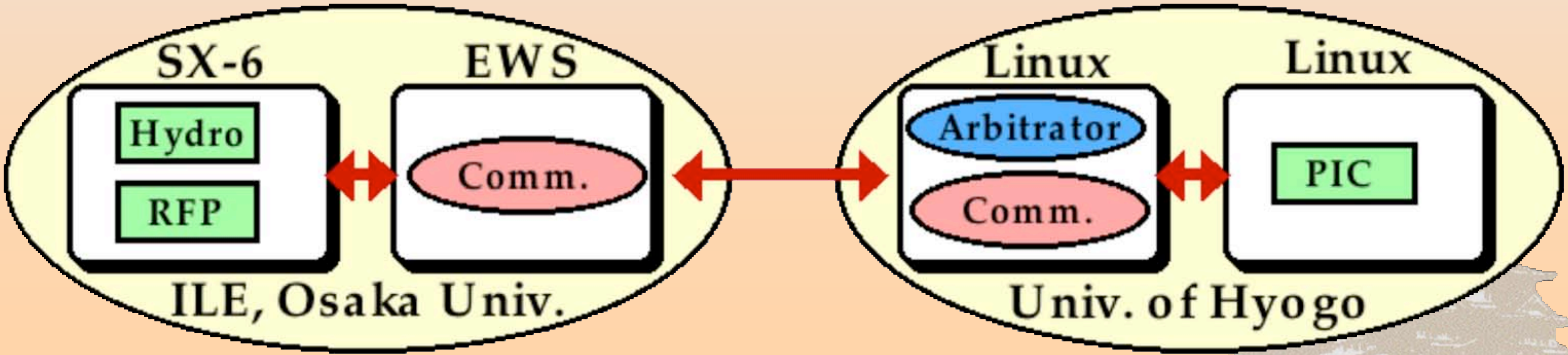

Pointing Device of Collimate High Density MeV Electrons

- 2D-PIC Simulation -

QuickTimeý Ç²
TIFFÅià èkÇ»ÇµÅj êLí£ÉvÉçÉOÉâÉÄ
Ç™Ç±ÇÃÉsÉNÉ`ÉÉÇ¾å©ÇÈÇžÇ½Ç…ÇÕïKóvÇ-Ç ÅB

Yasuhiko Sentoku
Nevada Terawatt Facility
University of Nevada, Reno

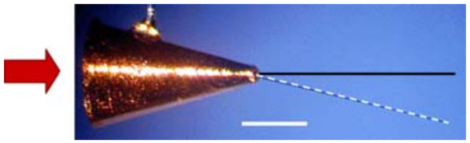

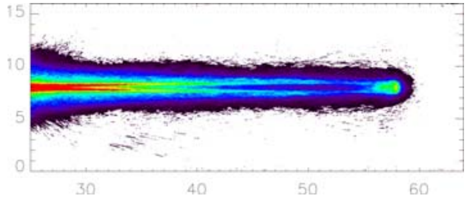

Co-authors

R. Kodama, Z. L. Chen, G. R. Kumar, Y. Toyama, Y. Izawa, K. Kondo, T. Matsuoka, H. Nakamura, M. Nakatsutsumi, T. Norimatsu, M. Tampo, K. A. Tanaka, T. Yabuuchi
Institute of Laser Engineering, Osaka University, Osaka, Japan

S. P. Hatchett, M. H. Key, R. A. Snavely
University of California, Lawrence Livermore National Laboratory, CA, USA

T. E. Cowan, J. Fuchs
University of Nevada, Department of Physics, Nevada Terawatt Facility, NV, USA

R. Freeman
University of California, Davis, Department of Applied Science, CA, USA

P. A. Noreys
Rutherford Appleton Laboratory, UK

R. B. Stephens
General Atomics, CA, USA

Introduction

Using shaped target like hollow-cone, the laser light can be focused into a micron-scale spot[1]. This will increase the laser intensity one-order magnitude higher and also improve the coupling of laser energy to the fast electrons. The accelerated electrons are guided along the cone-surface and concentrate around the tip of cone.

Recent experiment with a hollow cone attached a fine wire showed an extremely bright spot, which is also much narrower than that from a plane target.

The purpose of this work is to make the guiding mechanism along the wire clear and study the electron beam quality by 2d-PIC simulations.

[1] Y. Sentoku et al., Phys. Plasmas 11, 3083 (2004).

Demonstration of guiding and collimation of high-density MeV electrons

Laser: 300 TW, 180 J

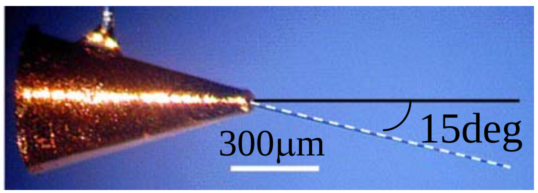

Cone: gold
angle=30 deg.
size of tip = 30µm

Wire: carbon
diameter = 5µm
length = 1mm

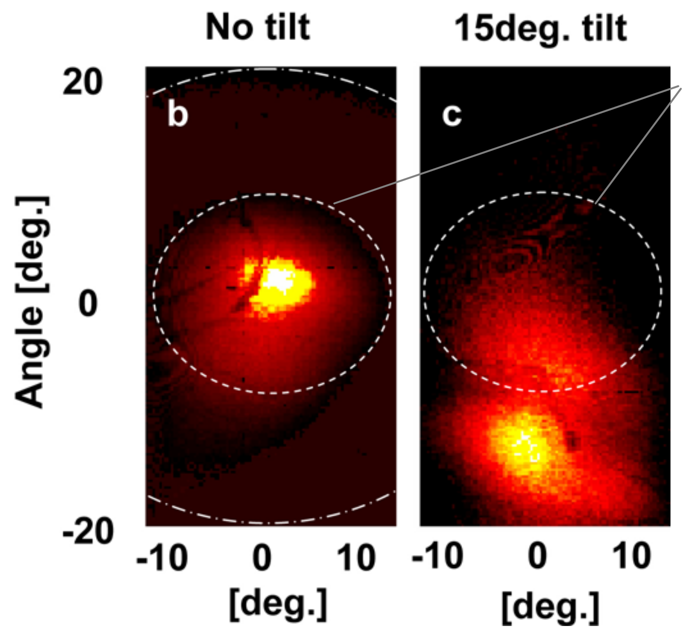

Spot size from a plane target

Spatial distribution of 3.5 MeV electrons with an imaging plate

Coupling from the laser to the MeV electrons by a factor 2 as compare with that in a simple plane target.

Summary of experiments

Divergence of electron beam

Cone+wire	**:**	**5 deg.**
Cone	**:**	**20-30 deg.**
Plane	**:**	**30-40 deg.**

The peak intensity of emission from the straight wire is enhanced by a factor 10 as compared to that without wire.

The relative energy flux of the electrons in the cone+wire cloud be significantly higher than that in a simple plane target by a factor 20 - 30.

2d-PIC simulation: cone+wire

Laser:
- **a = 3, 300 fs**
- **spot size = 20 μm**

Initial target structure

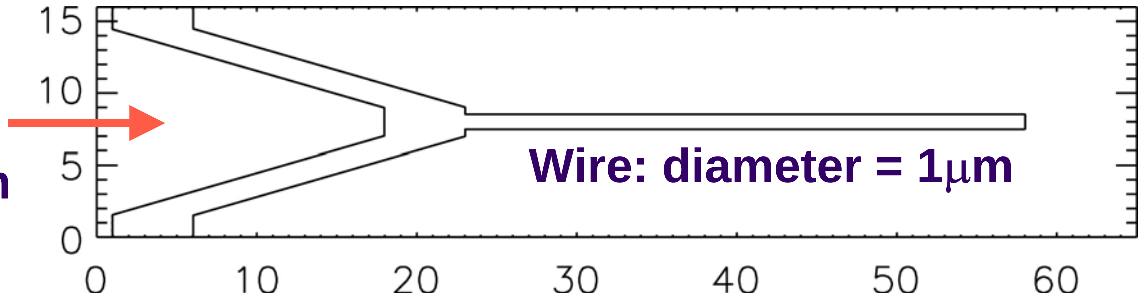

Wire: diameter = 1μm

Initially fully ionized deuteron, $n_e = 10^{22} cm^{-3}$

Magnetic field and radial electric field propagate along the wire

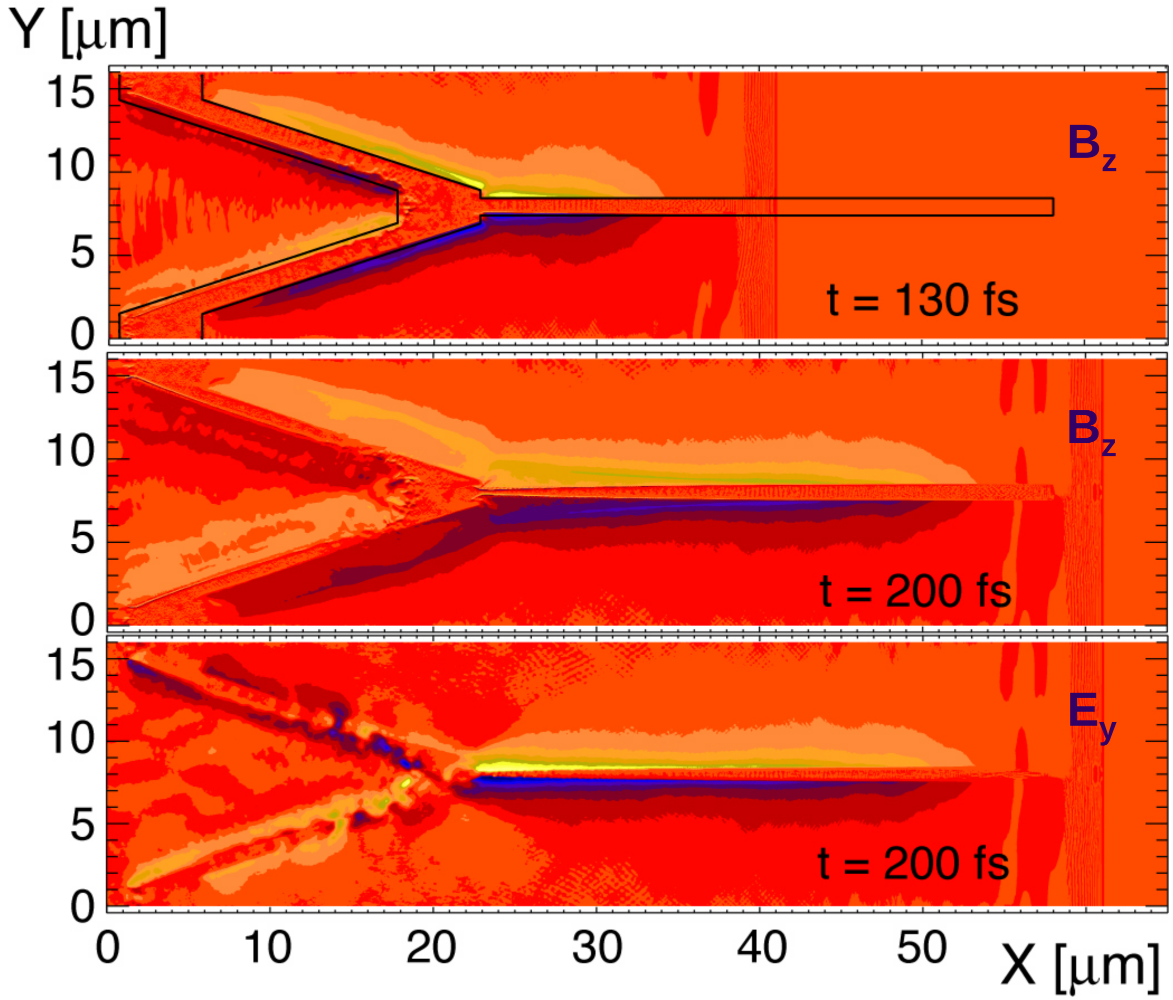

Levels:
$-0.6B_0 \sim 0.6B_0$
(B_0 = 320 MG)

Levels:
$-0.6E_0 \sim 0.6E_0$
($E_0 = 9.6\text{x}10^{12}$V/m)

MeV electrons guiding mechanism

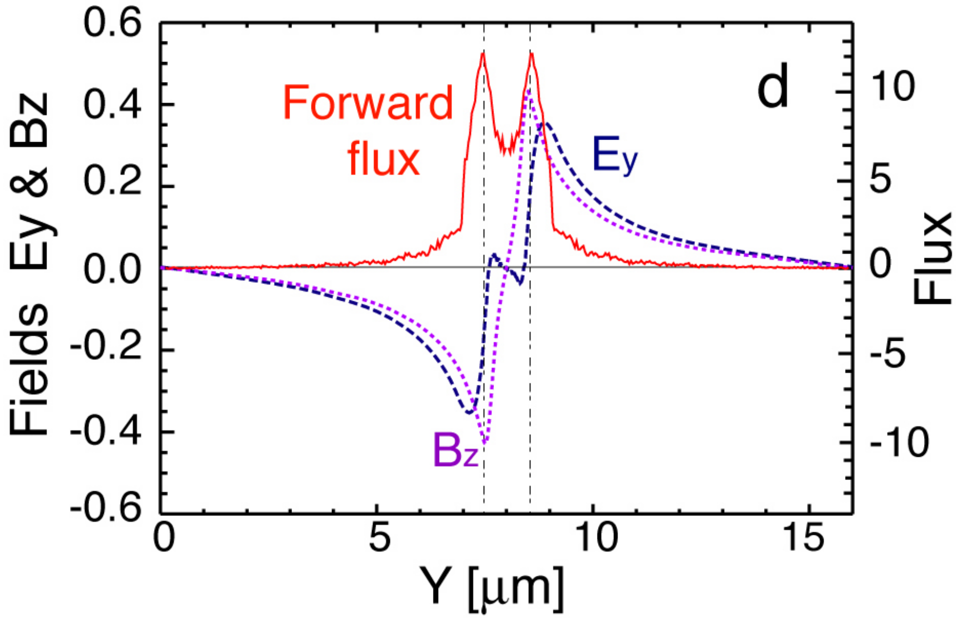

Fields profile at X=40μm

The fields are normalized by the incident laser (E_0=9.6x10^{12}V/m, B_0=320MG)

The peak E_y and B_z are given approximately by

$$E_y = 4\pi e N_e \,, \quad B_z = 4\pi e N_e (v_e / c)$$

N_e: number of e^- expanding outside the wire
v_e: the hot electrons' mean velocity

When v_e ~ c, two forces eE_y and $E(v_e/c)B_z$ ~ eB_z are balanced.

This fields balance results in the collimation and confinement of e^-.

Guiding and collimation of MeV electrons along the wire

QuickTimeý Ç²
TIFFÅìà èkÇ»ÇµÅj êLí£ÉvÉçÉOÉâÉÄ
Ç™Ç±ÇÃÉsÉNÉ`ÉÉÇ¾å©ÇÈÇΩÇ…ÇÕïKóvÇ-Ç ÅB

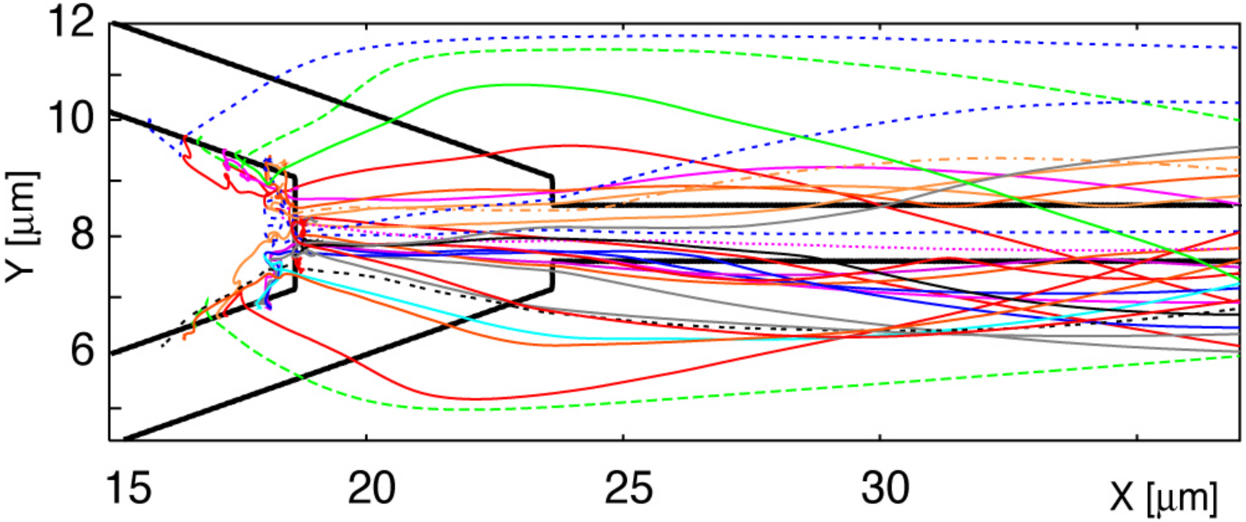

Trace of the particles which escape from the top of wire

MeV electrons are pushed outside by Bz and come back into wire by Ez

Return current in the wire are pinched by magnetic fields

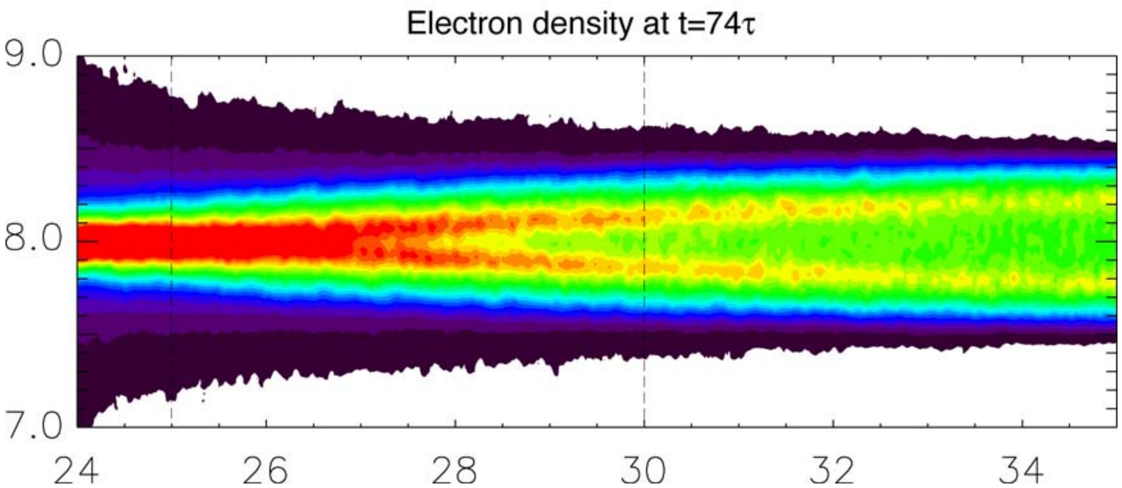

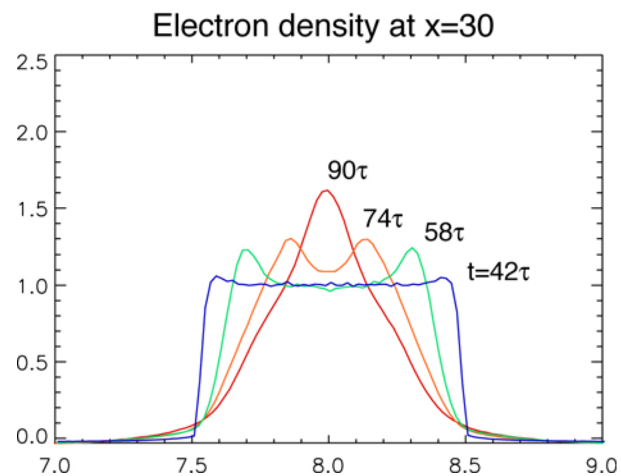

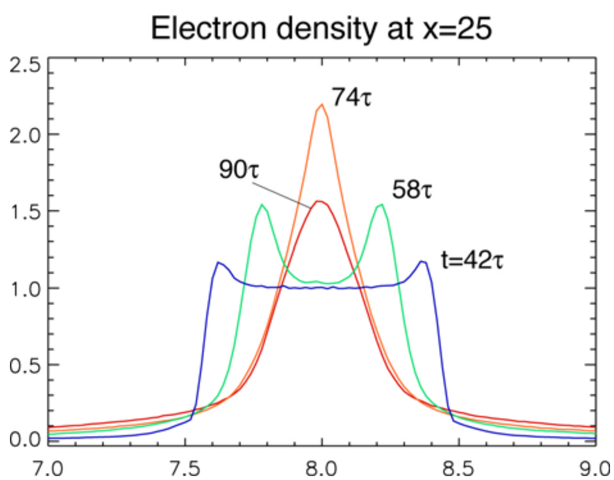

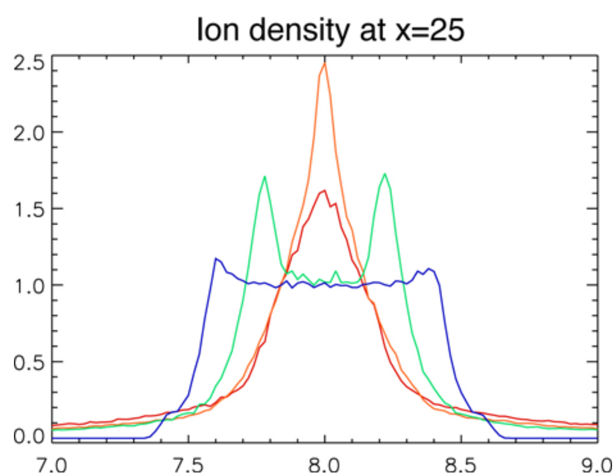

Cone+wire target generates one-order magnitude intense electron beam

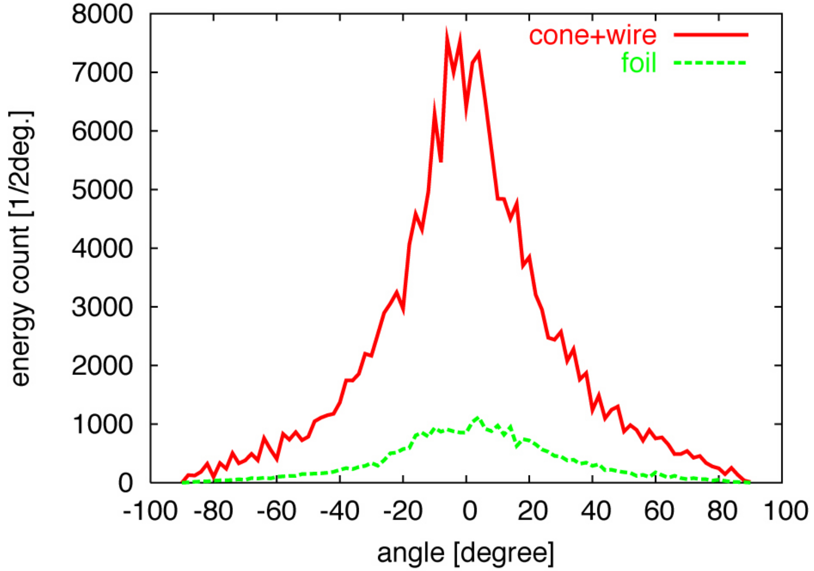

Foil: 5μm flat target

Angular distribution of forward escaping electrons from the target

Electron loses its transverse energy through propagation along wire

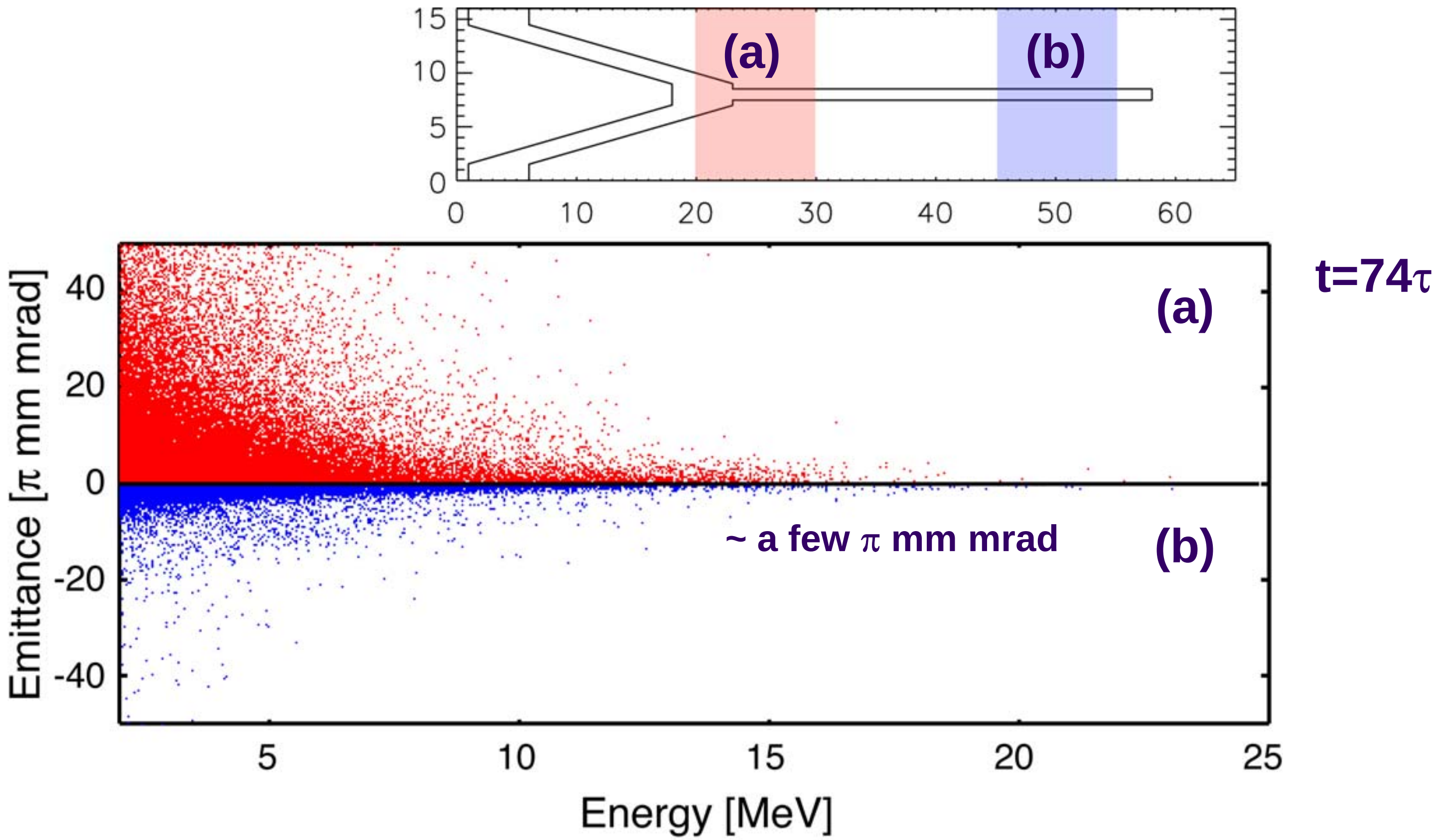

Beam emittance is improved through propagation along the wire.

Only the transverse energy drops

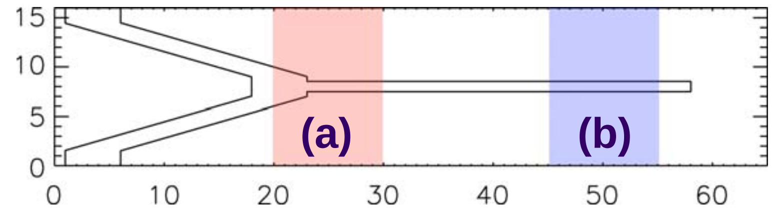

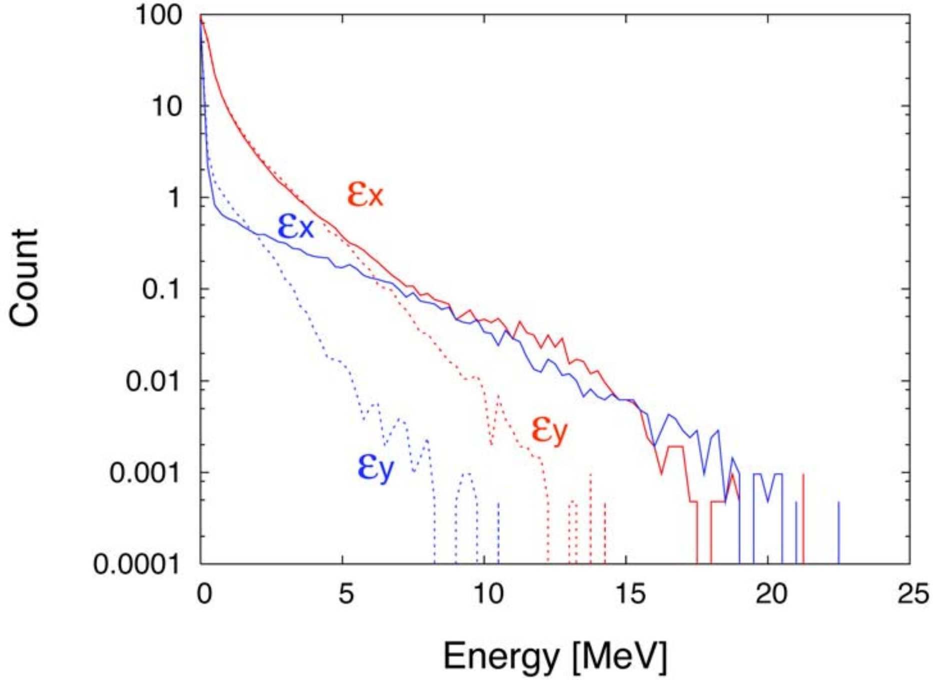

Energy spectra in x&y direction at two observation point

Total charge of MeV electrons is about nC from a few hundred fs pulse.

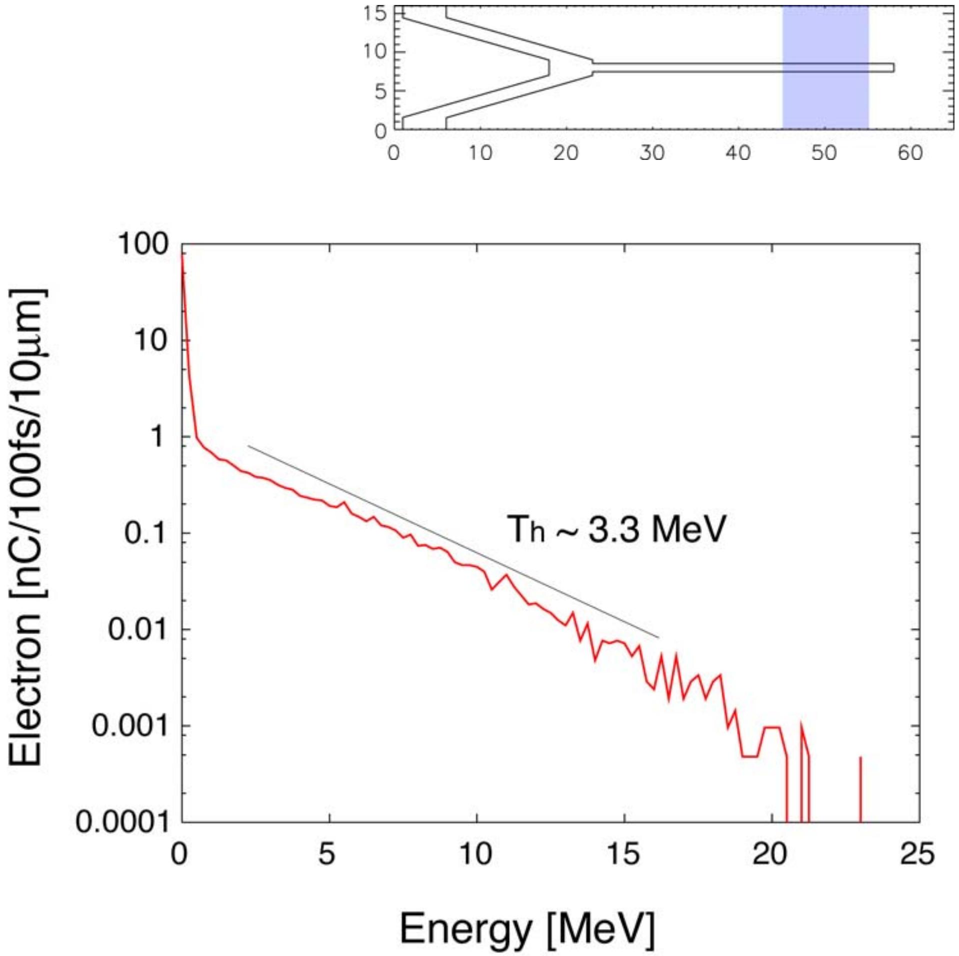

Shorter pulse laser can make bunched electron beam

Pulse length = 70 fs ~ 20 μm

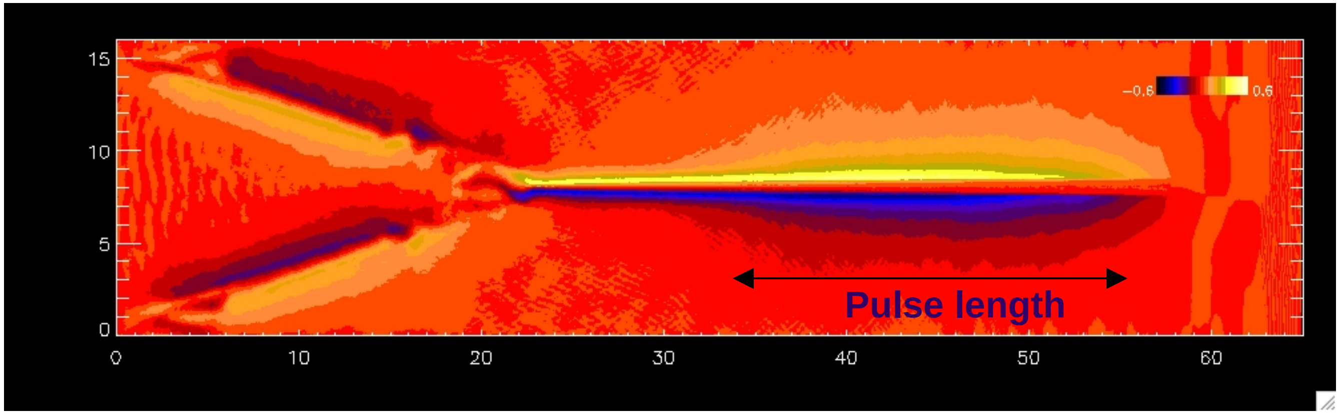

Summary

- Cone+wire target generates highly collimated dense MeV electron beam. This is demonstrated both by experiment and simulation.
- MeV electrons are guided by the field balance between the magnetic fields and the sheath fields.
- Since MeV electrons have transverse energy, they come out from the wire, as a result, they induce the electromagnetic fields. Through this process, background ions and electrons are pinched and heated up and then the MeV electrons lose their transverse energy. As a result, the beam emittance is improved.
- By changing the pulse length, number of MeV electrons and also the bunch length are tunable.

High Energy Ion Acceleration in Interaction of Short Laser Pulse with Dense Plasma Target

- to find optimal laser parameters of ion acceleration -

Y. Sentoku,

J. Fuchs, T. Cowan, A. Kemp, H. Ruhl

University of Nevada, Reno

Nevada Terawatt Facility (NTF)

QuickTimeý Ç²
TIFFÅià èkÇ»ÇµÅj êLí£ÉvÉçÉOÉâÉÄ
Ç™Ç±ÇÃÉsÉNÉ`ÉÉÇ¾å©ÇÈÇžÇ½Ç…ÇÕïKóvÇ-Ç ÅB

Motivation of This Study

High energy ion acceleration by ultra-short laser pulse has attracted people's attention, because of its possibility for various applications, e.g. compact neutron source, keV-100 MeV range ion source.
It is important to know the acceleration mechanism and the characteristic of high energy ions to design the applications, to increase the ion energy and/or the conversion efficiency.

Basic Questions

- Where do these ions comes from, front side of target or rear ?
- Which laser pulse length can produce more energetic ions, longer or shorter ? (using the same laser energy)
- How do we get more energetic and better conversion efficiency ?

Outline

There are two origins of
the forward accelerated ions.

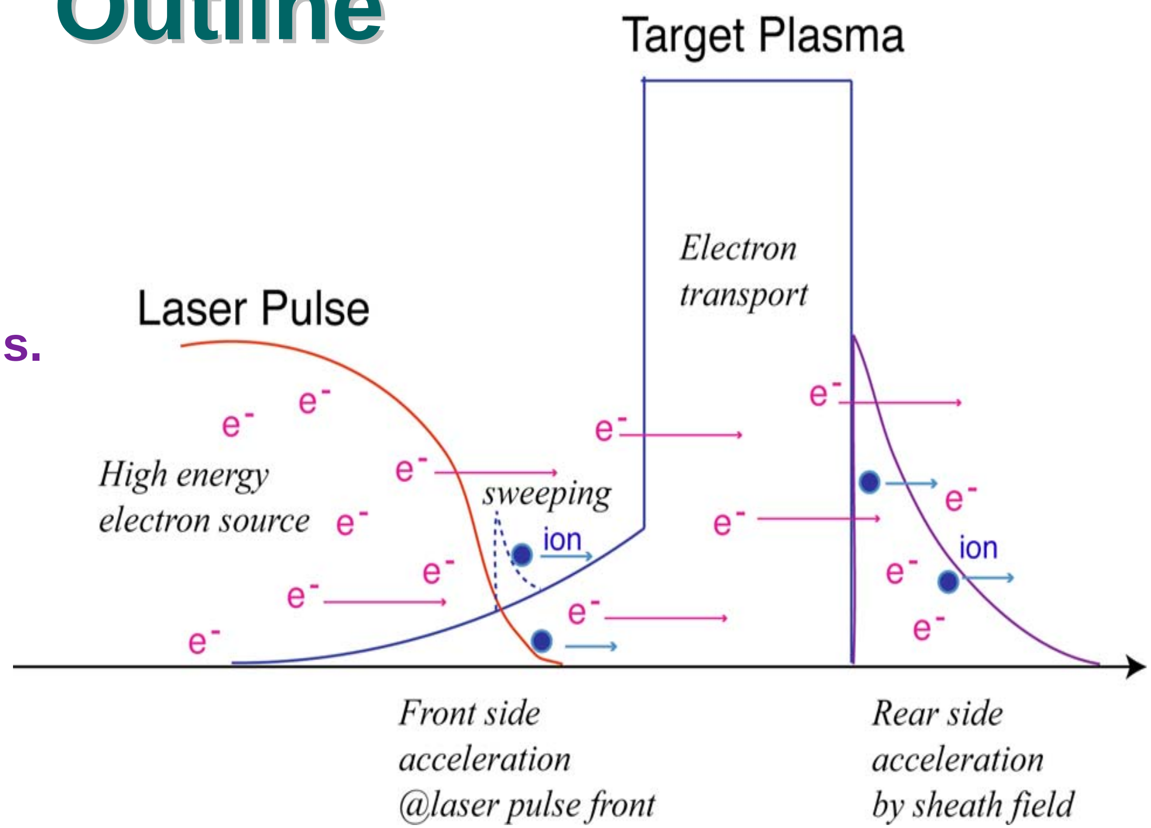

1. Characterize the front side acceleration by sweeping potential.
2. Characterize the rear side acceleration by sheath potential.
3. Systematic study of ion energy with various laser conditions, e.g. pulse length, intensity, to find an optimum laser parameters.
4. Summary

Front Side Acceleration

At the pulse front, the ponderomotive potential sweeps some electrons and piles them at the pulse front. At the equilibrium, the ponderomotive potential balances with the electrostatic potential, (sweeping potential).

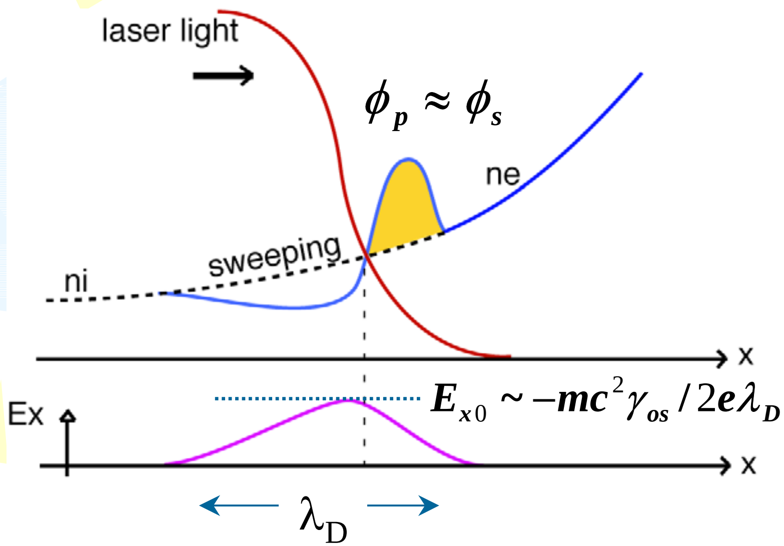

The sweeping length is the Debye length.

$$\lambda_D \sim \frac{2\pi c}{\omega_p} = \frac{2\pi c}{\omega_0}\sqrt{\frac{\gamma_{os} n_c}{n_e}} \cong \frac{2\pi c}{\omega_0}$$

where

$$\gamma_{os} = \sqrt{1 + 2\langle a^2 \rangle}$$

The sweeping potential ϕ_s is given by

$$\phi_s = mc^2(\gamma_{os} - 1)$$

Ponderomotive potential

From the ion's equation of motion in the sweeping potential, the acceleration time τ_{sw} is given by

$$\tau_{sw} = \int_0^{\lambda_D} \frac{dx}{v_i(x)} = \sqrt{\frac{2M\lambda_D}{eE_{x0}}} \sim \sqrt{\frac{M}{m\gamma_{os}}}\tau$$

And the maximum velocity

$$\frac{u_{sw}}{c} = \sqrt{\frac{2\phi_s}{M}} = \sqrt{\frac{2m}{M}\left[\left(1 + \frac{I\lambda^2}{1.37\times 10^{18}}\right)^{1/2} - 1\right]}$$

When the laser pulse τ_L is shorter than time τ_{sw}

$$v_x = \left(\frac{\tau_L}{\tau_{sw}}\right)\cdot u_{sw}$$

Coulomb Explosion Occurs at Overtake Point

When the faster ions overtake the slower ones, the ion density increases and has a very sharp peak.

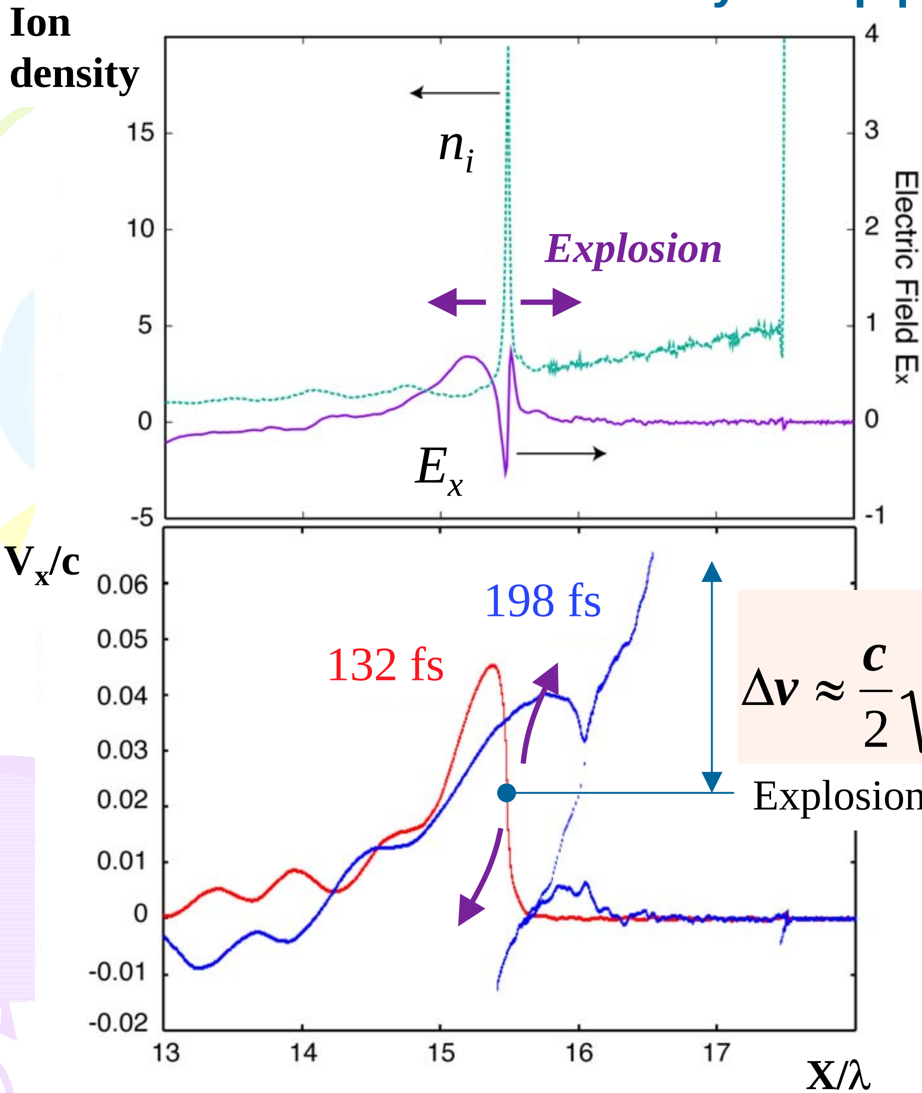

Unshielded potential (= Explosion Potential) ~ $T_e = mc^2(\gamma_{os}-1)^{1/2}$

This is the same amount of energy as the sweeping potential.

Different from the conventional shock acceleration.

$$\Delta v \approx \frac{c}{2}\sqrt{\frac{2\phi_p}{M}} = 0.5u_{sw}$$

$$V_{max} \approx 1.5u_{sw}$$

Deuteron Spectrum in Experiment is Consistent with 2D-PIC

Deuteron phase plot velocity X-V_x/c

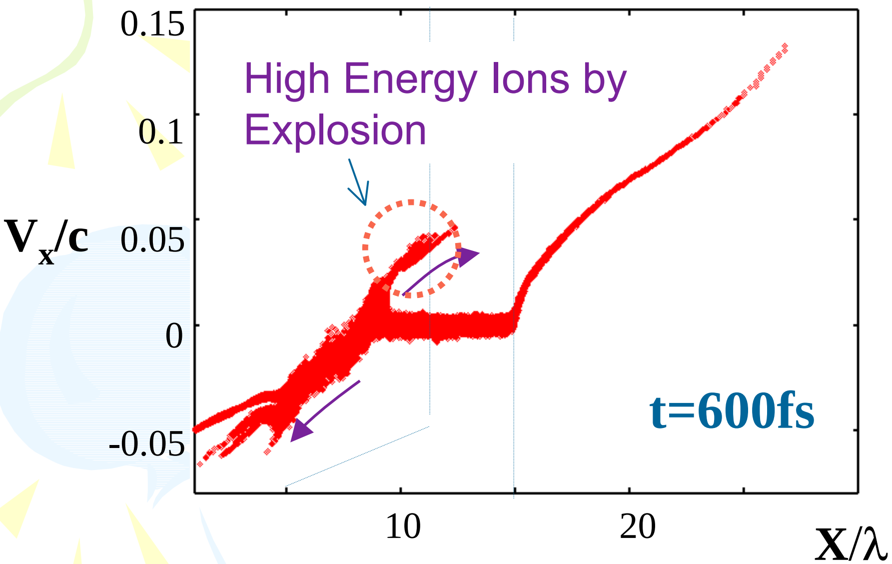

Experiment @ ILE, Osaka Univ.

500fs, 50J, 1054nm, 2×10^{19}W/cm^2

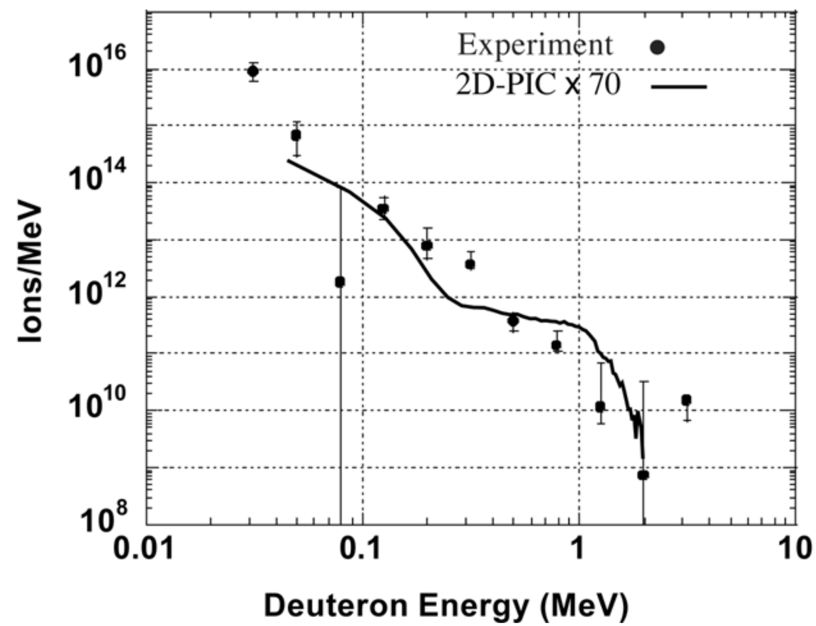

Fast deuteron spectra calculated from the neutron data.

Deuteron Density Profile

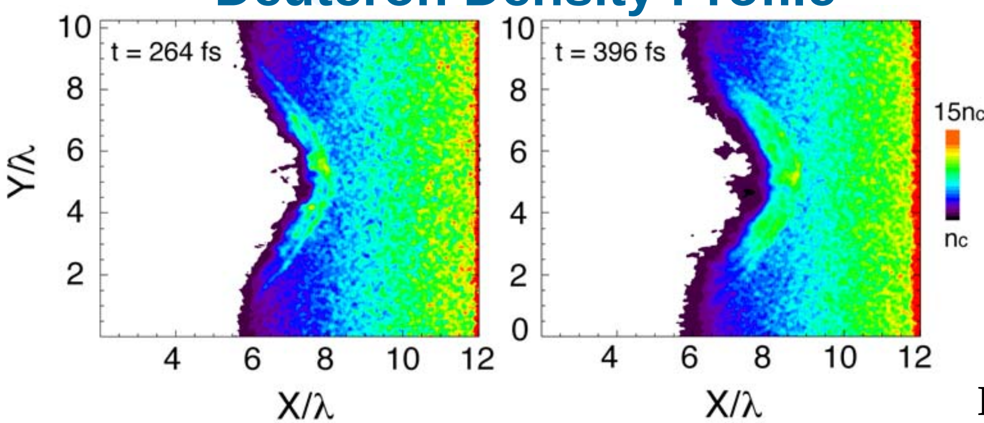

N. Izumi, Y. Sentoku et al., PRE, 65, 036413 (2002)

The Anisotropic Ion Acceleration in Preplasma

Hole-boring by 20 TW laser pulse - 3D-PIC -

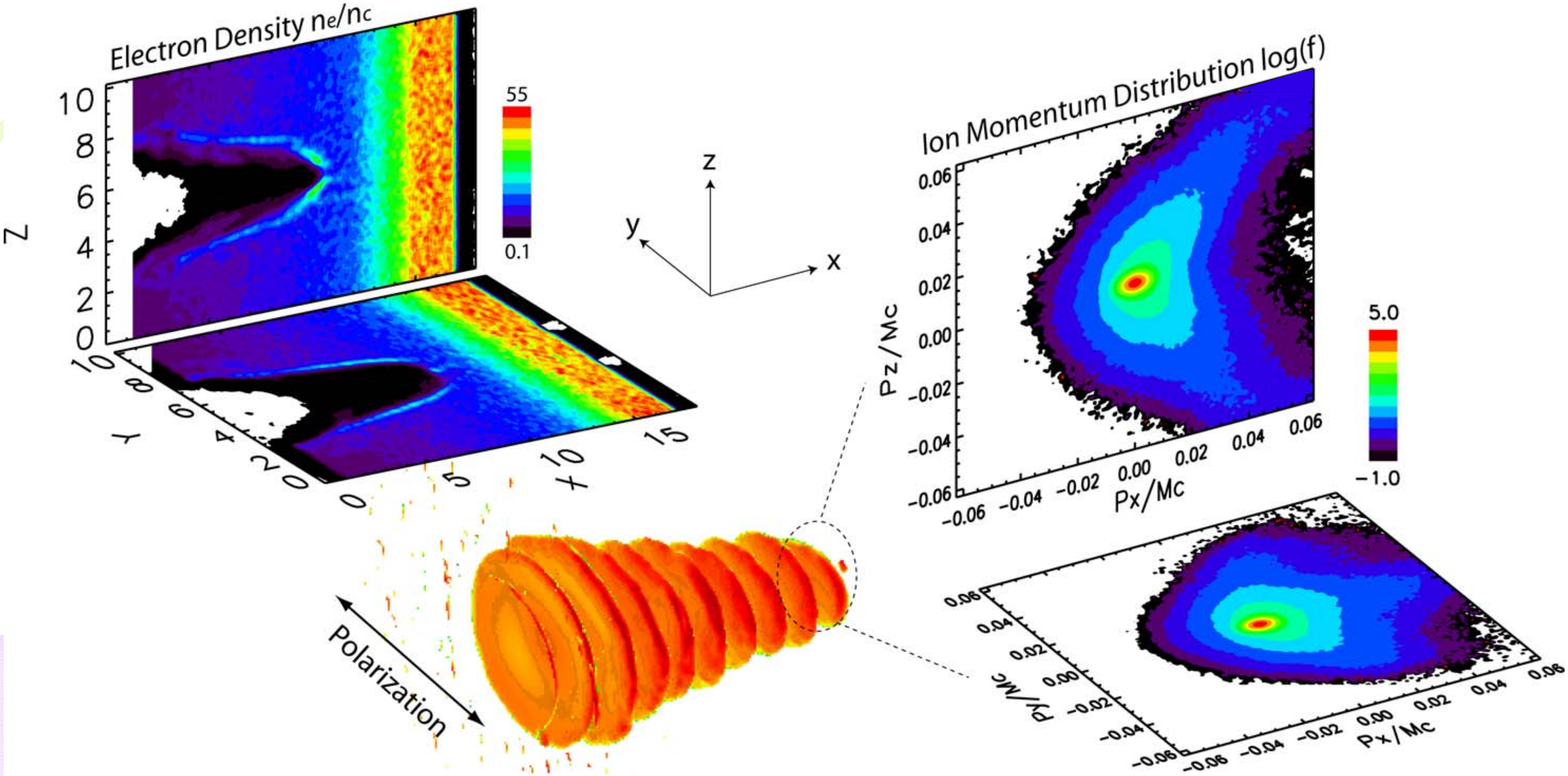

Iso-surface of Laser E-Field
E=0.1

Rear Side Acceleration

- Recirculation enhances the sheath potential -

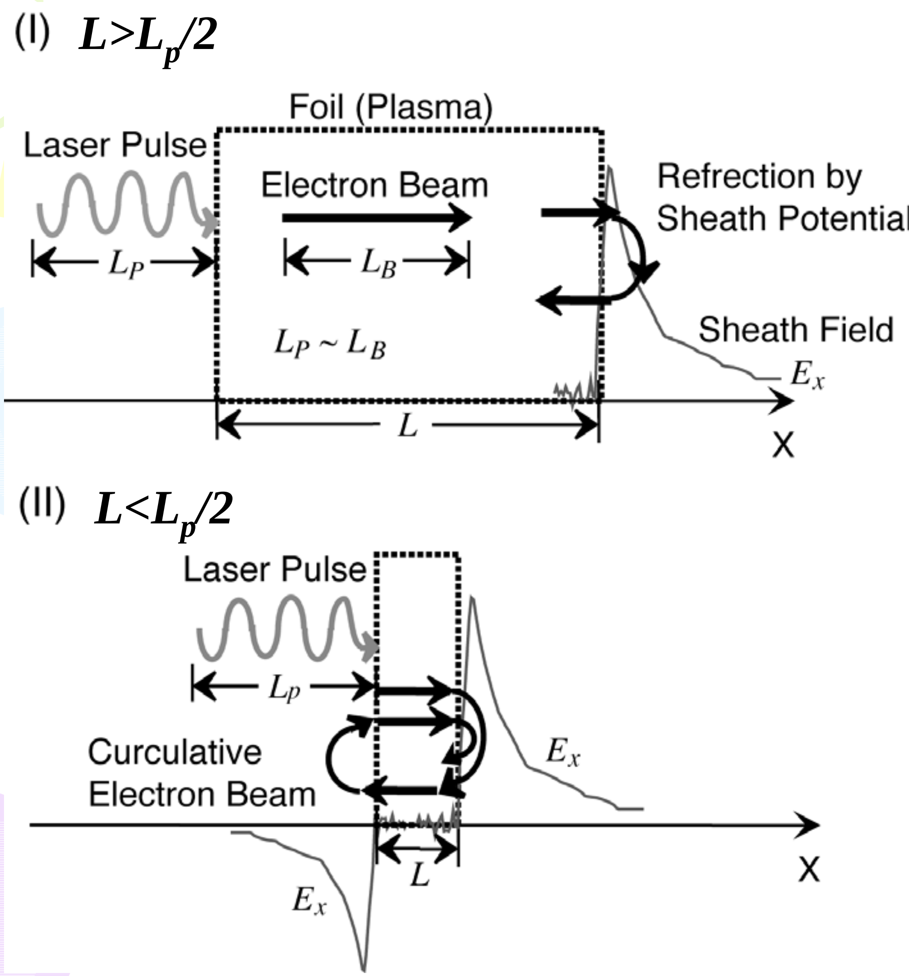

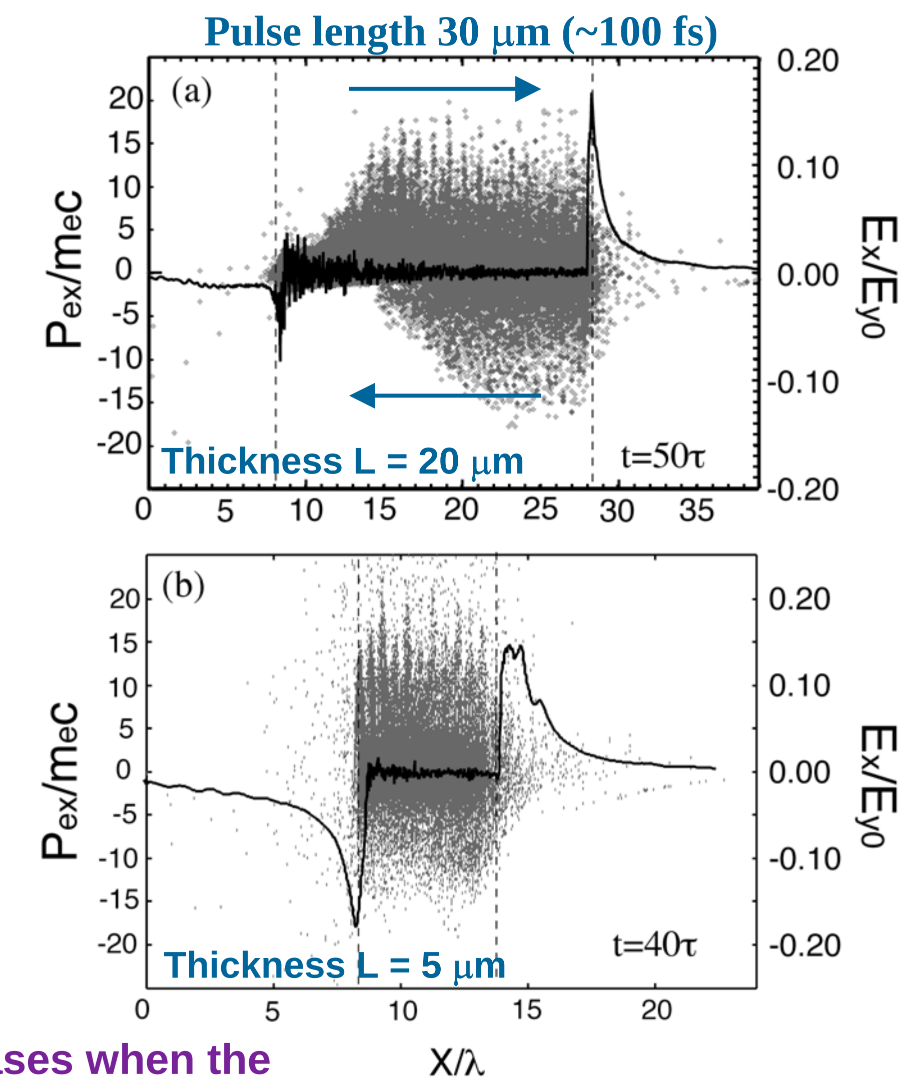

The hot electron density inside the target increases when the target thickness is less than half of pulse length. ($L<L_p/2$)

The Maximum Ion Energy Increases with $\alpha = L_c/L$
- test simulation by 1D-PIC -

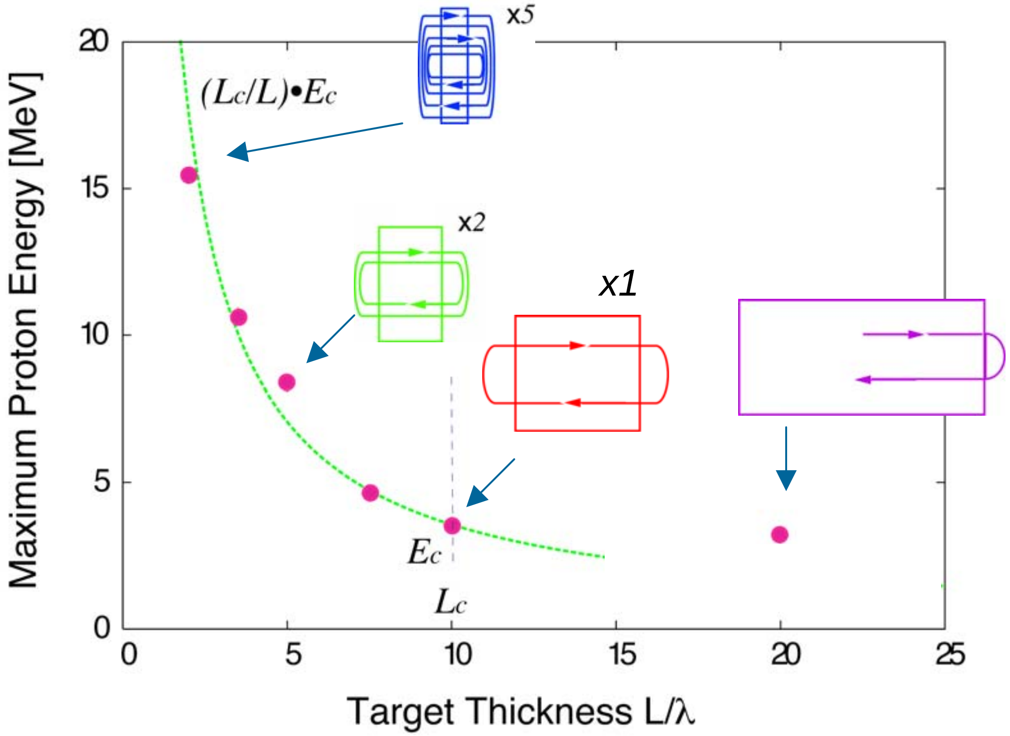

The final ion energy increases with a factor (L_c/L) due to the recirculation effect.

$$\varepsilon_{ion} = \frac{L_c}{L} E_c$$

Rear Side Ion Energy Increases by the Electron Recirculation

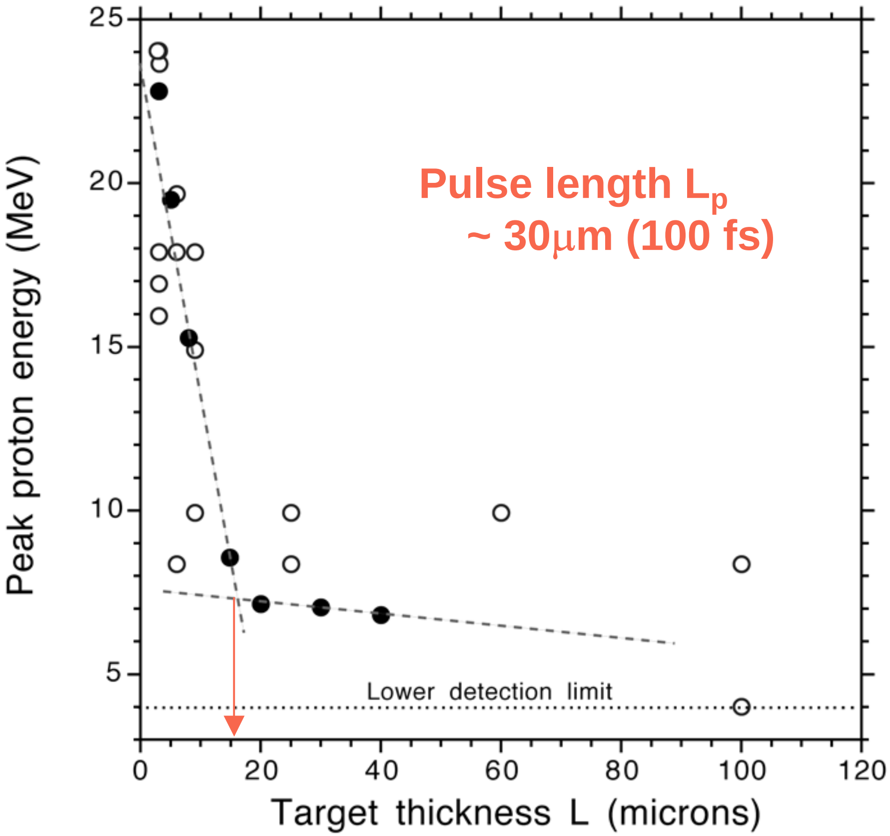

(Aluminum)

Experiment:

LLNL, 0.8μm, 100fs, 10^{20}W/cm^2

Simulation:

2D-PIC with slab target

There are two distinct slopes present in both the simulations and the experiment data.
The slope is changing at 15~20 μm by the hot electron recirculation.

A. J. Mackinnon, Y. Sentoku *et al.*, Phys. Rev. Lett. 88, 215006 (2002).

Parameter Study to Find Optimum Laser Pulse

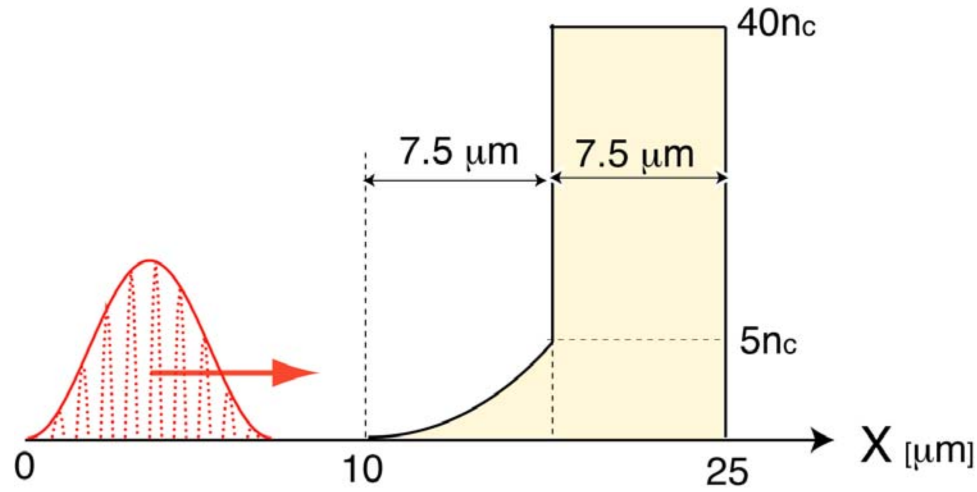

Laser Pulse

- **Length : 10 ~ 500 fs**
- **Intensity: 10^{17}~$5x10^{19}$ W/cm^2**
- **Pulse shape $\sin[\pi (t/\tau_L)]^2$ $(0<t<\tau_L)$**

Target Plasma

- **Full ionized hydrogen (M = 1840)**
- **Maximum density : 40n_c**
- **Thickness : 7.5 μm**
  + preplasma : 7.5 μm
  (exponential profile)

Pulse Length Dependence of Maximum Ion Energy

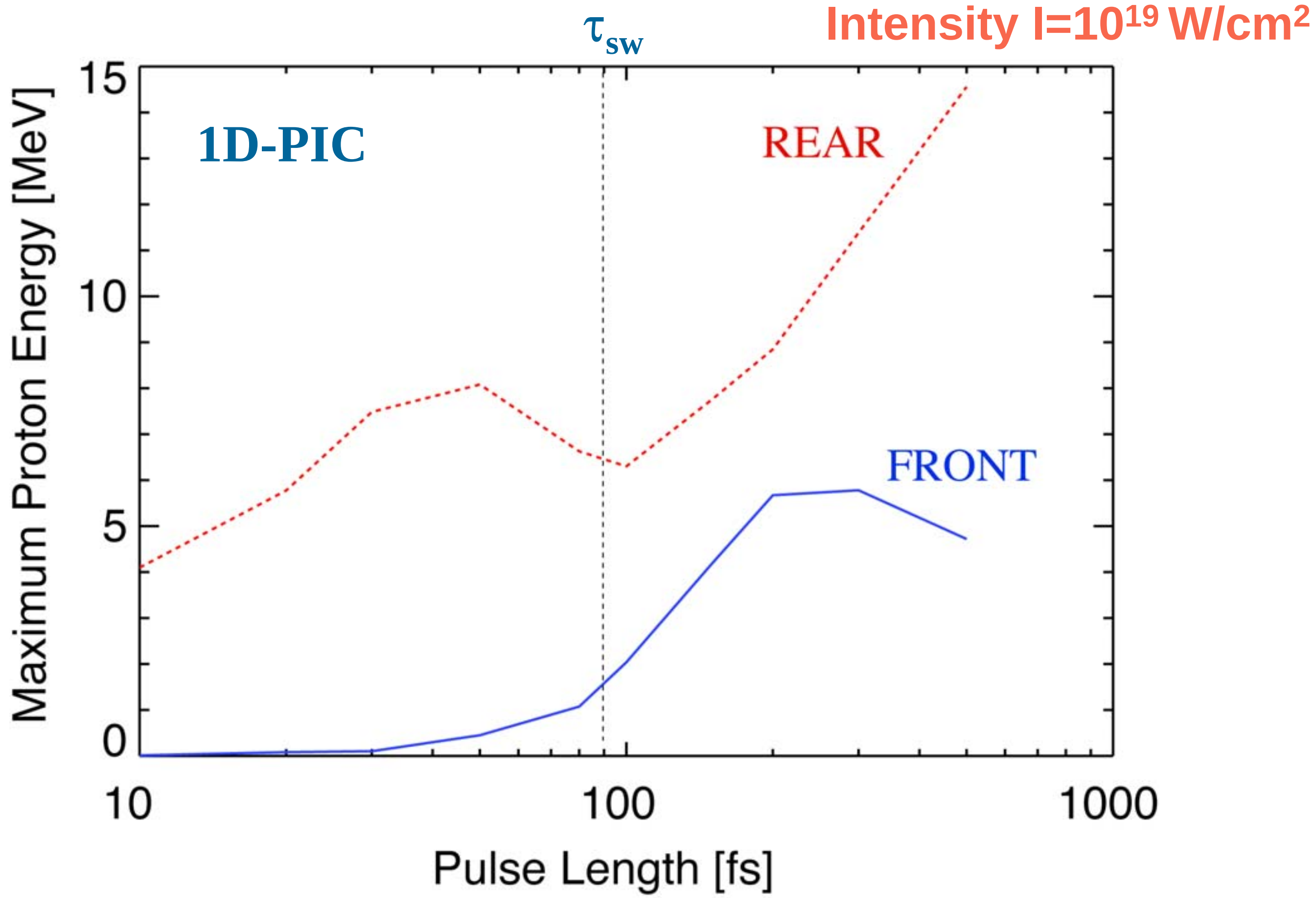

Sweeping time : $\tau_{sw} \sim \sqrt{\frac{M}{m\gamma_{os}}}\tau \cong 90\mathrm{fs}$

Front Side Field Prevents Hot Electrons Flowing into Target

Intensity $I=10^{19}\ W/cm^2$

Electron phase plot X-p_x/mc

(a) short pulse case ($\tau_L<\tau_{sw}$)

τ_L=50 fs

(b) long pulse case ($\tau_L>\tau_{sw}$)

τ_L=100 fs

Sweeping time scale :

$$\tau_{sw} \sim \sqrt{\frac{M}{m\gamma_{os}}}\tau \cong 90\mathbf{fs}$$

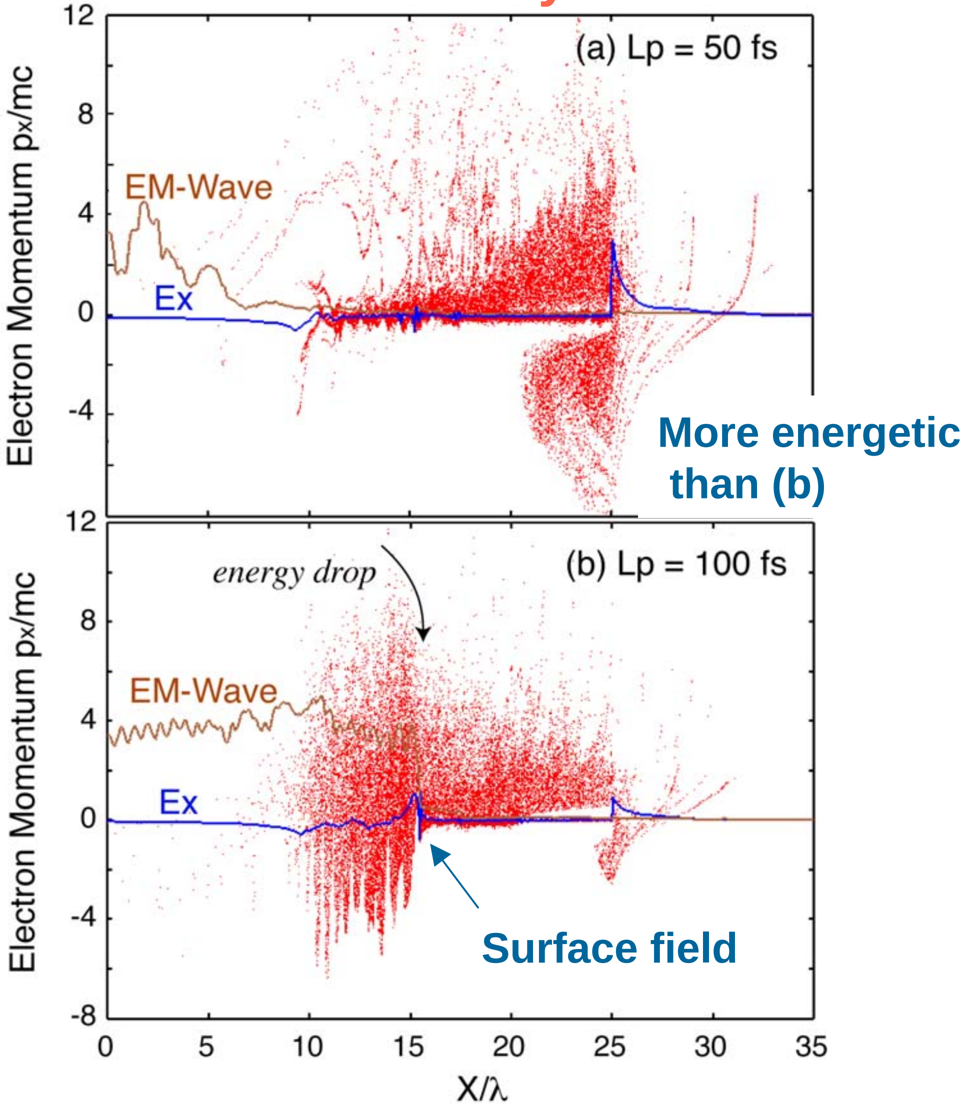

Pulse Length Dependence of Conversion Efficiency

Intensity I=10^{19} W/cm^2

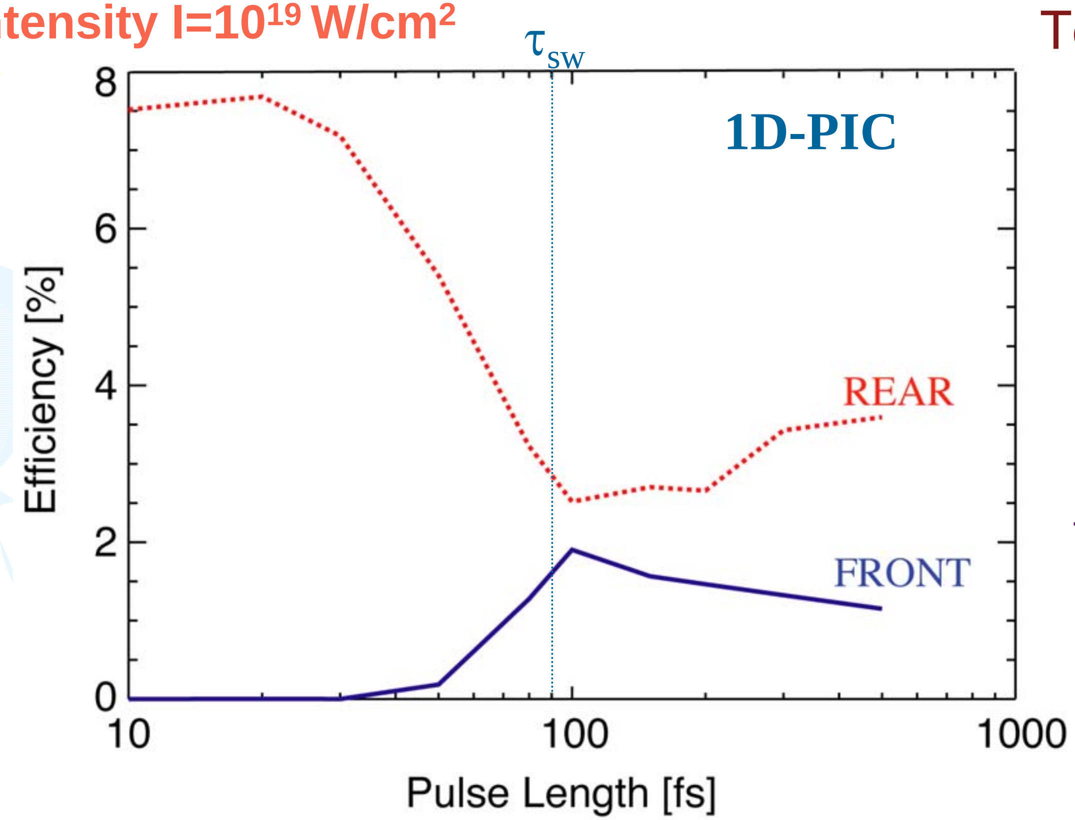

To achieve high efficiency

Rear side acceleration :
Short pulses ($\tau_L < \tau_{sw}$) has better conversion efficiency.

Front side acceleration :
Pulse must be sufficiently longer than the sweeping time scale ($\tau_L > \tau_{sw}$) .

The conversion efficiency of the laser energy to high energy protons (>100keV).

Sweeping time : $$\tau_{sw} \sim \sqrt{\frac{M}{m\gamma_{os}}}\tau \cong 90\mathbf{fs}$$

Intensity & Pulse Length Dependence

- Maximum Proton Energy from REAR side -

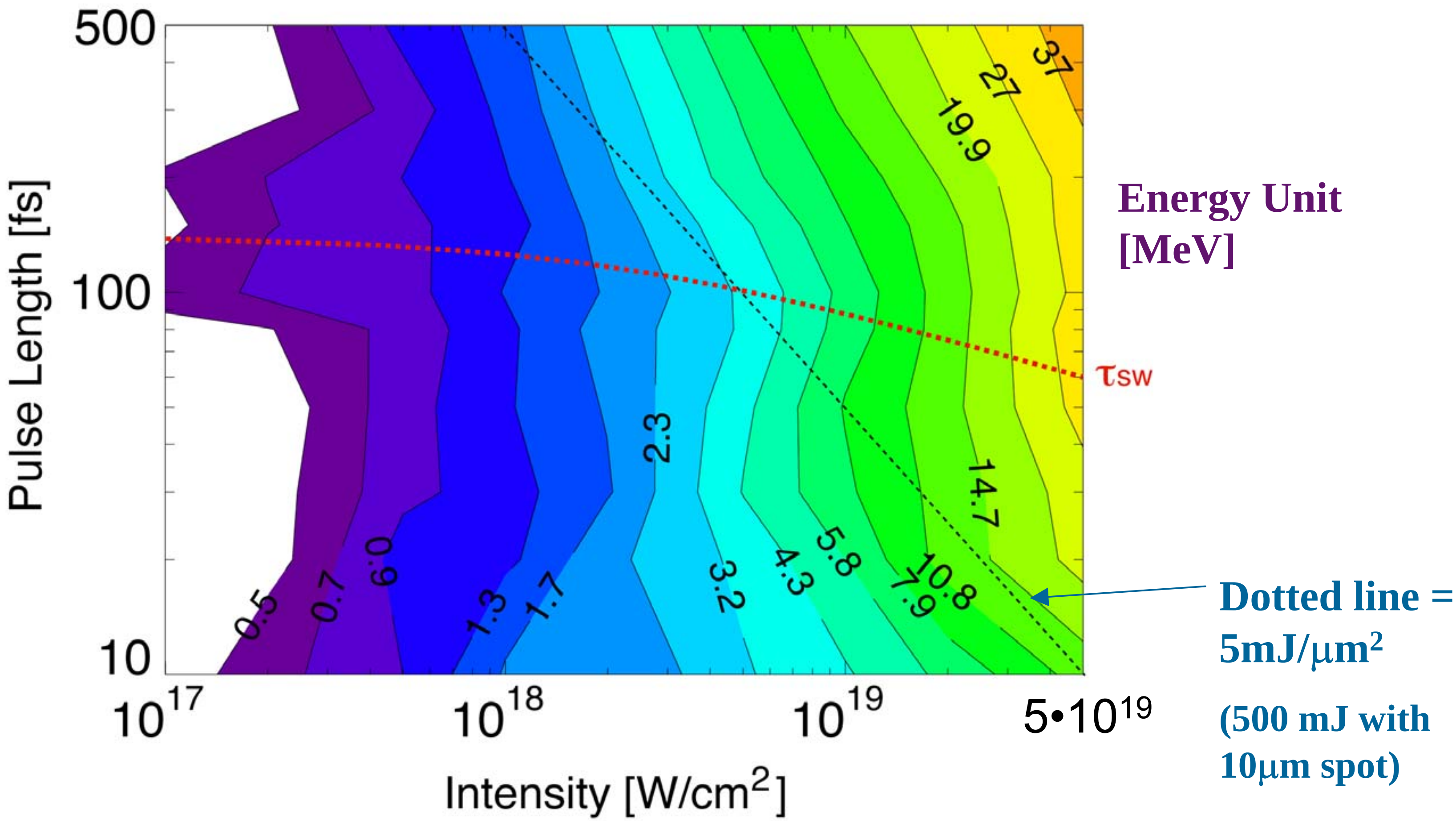

The short pulses, 10~20 fs, generate the highest energy in the same laser energy.

The Longitudinal Velocity Distribution and Angular Distribution

- 2D PIC -

P-pol laser, 10^{19} Wcm^2

Ions phase plot at 1ps (P-pol)

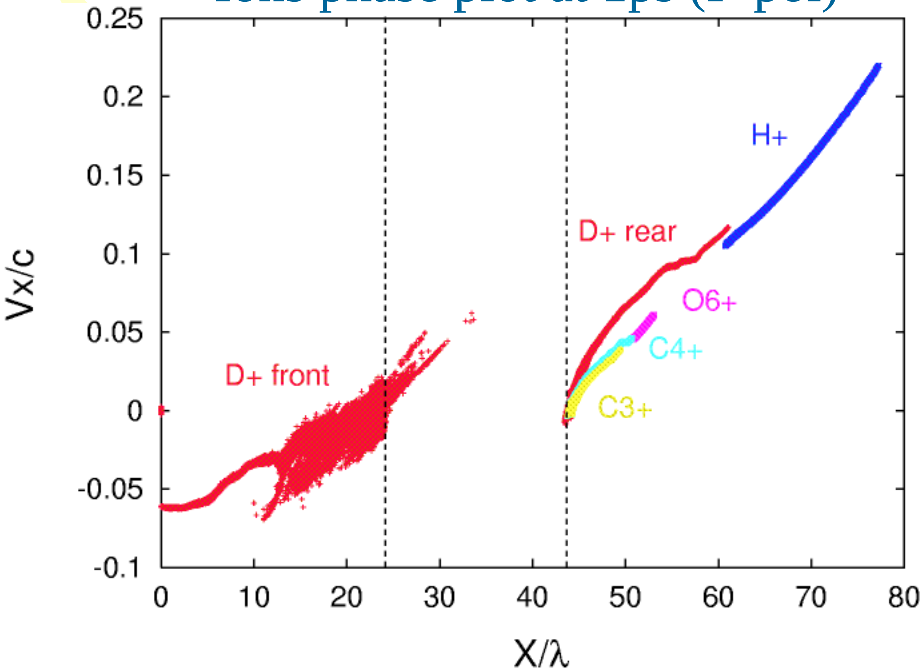

48.5 deg aperture of the catcher

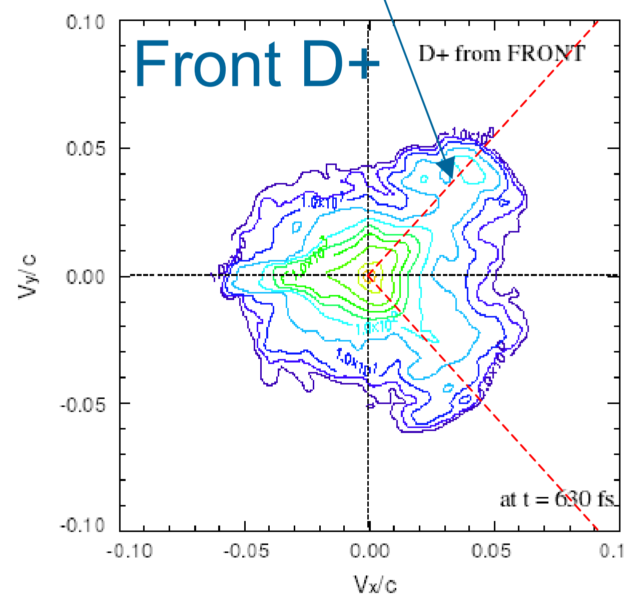

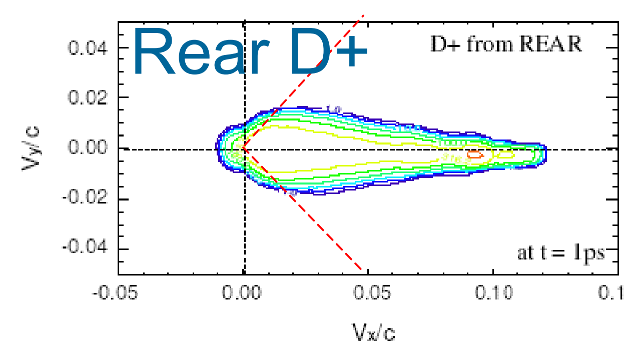

2D PIC simulation shows very different angular distribution for front- and rear-accelerated D+.

Experimental evidence : 2 proton beams

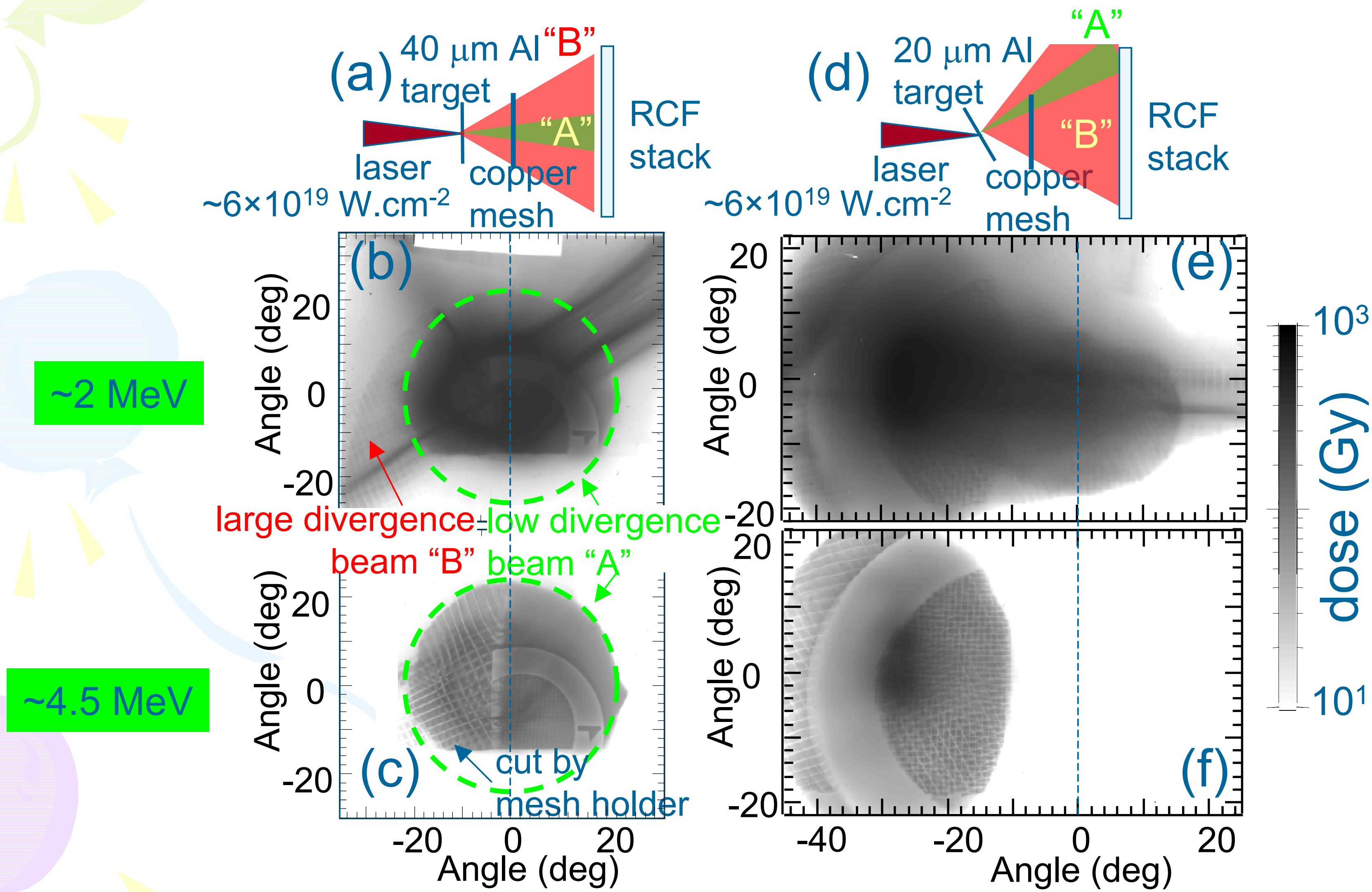

More energetic H^+ observed → rear ones

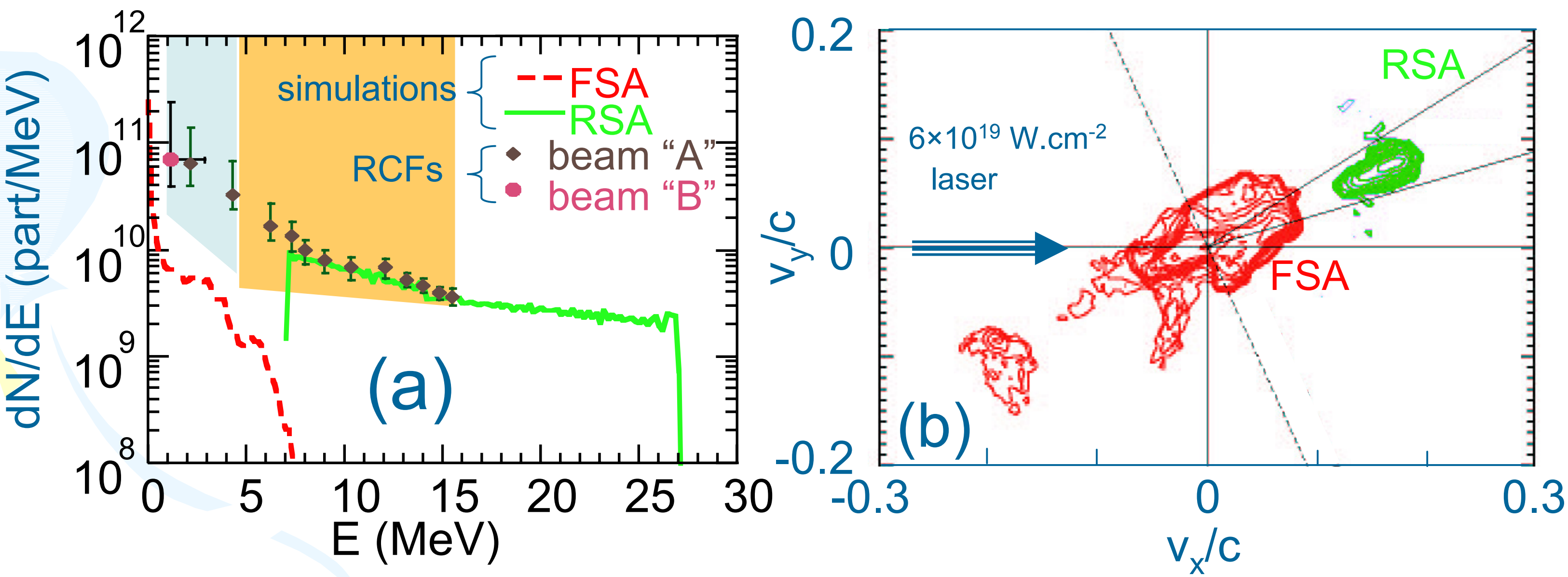

SUMMARY

1. Front side sweeping acceleration (FSA)
    - The sweeping acceleration time scale τ_{sw} is obtained.
    - The final ion velocity is given.
2. Rear side sheath acceleration (RSA)
    - The recirculation of the hot electrons is important in RSA.
    - The maximum ion energy is close to the maximum electron energy at the critical thickness, L_c. (when N_i << N_{eh})
    - When the target is thinner than the L_c, the peak ion energy is enhanced by a factor (L_c/L) in 1D world.
3. Pulse length dependence
    - The short pulse (10~20fs) has the highest conversion efficiency in the RSA. Using the thinner target, more higher efficiency can be achieved.
    - To make a application using FSA, like neutron source, the pulse length should be the a several times longer than τ_{sw}.

Long Pulse Pushes Surface and Shifts up the Final Velocity

Simulation with a long pulse (500 fs)

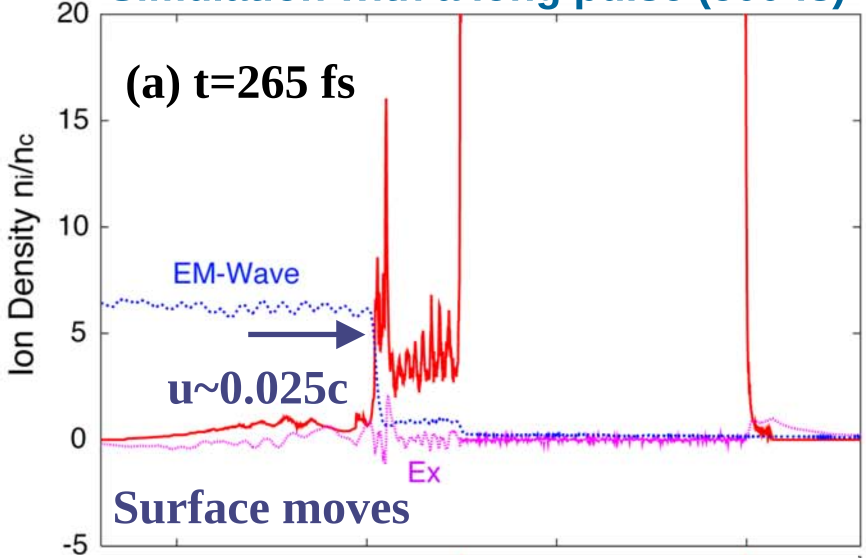

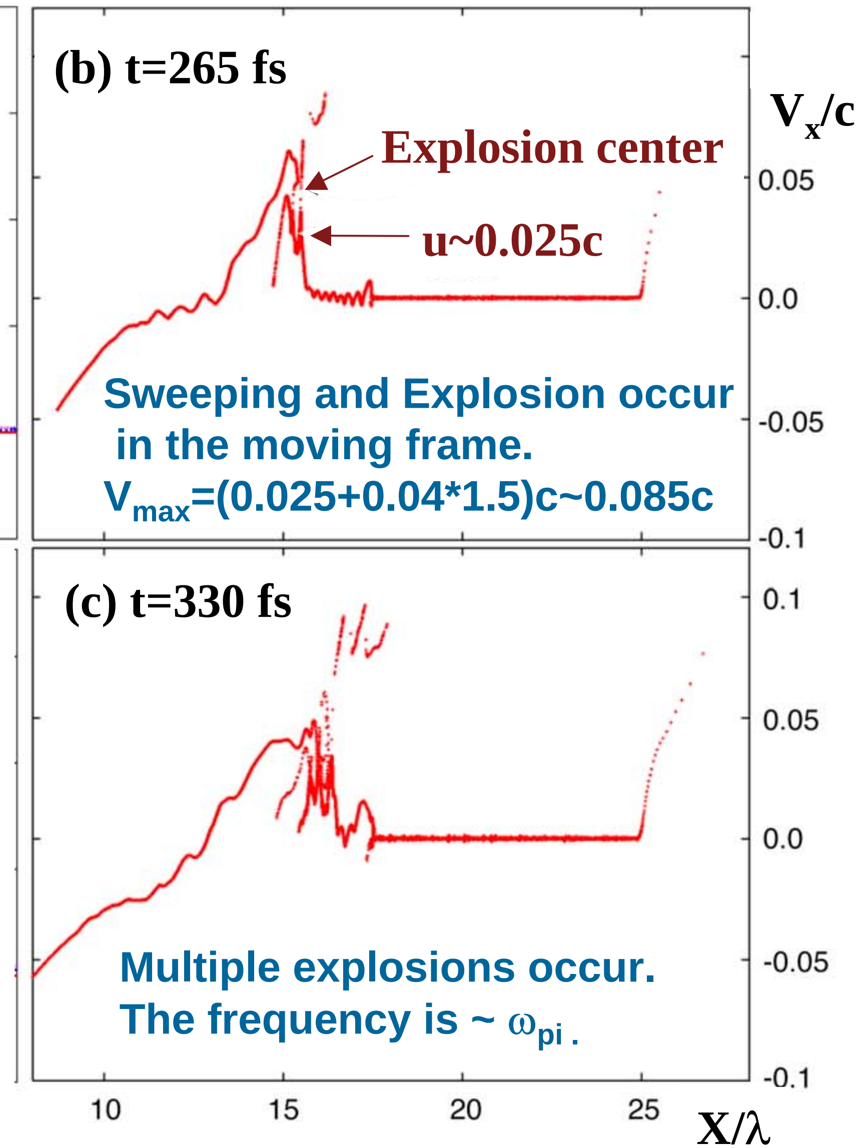

The final maximum velocity is

$$V_{max} \approx \underline{u} + 1.5u_{sw}$$

here $$\frac{u}{c} = \left(\frac{n_c}{2n_{pe}} \frac{Zm}{M} \frac{I\lambda^2}{1.37\times 10^{18}} \right)^{1/2}$$

Pulse Length Dependence of Maximum Energy

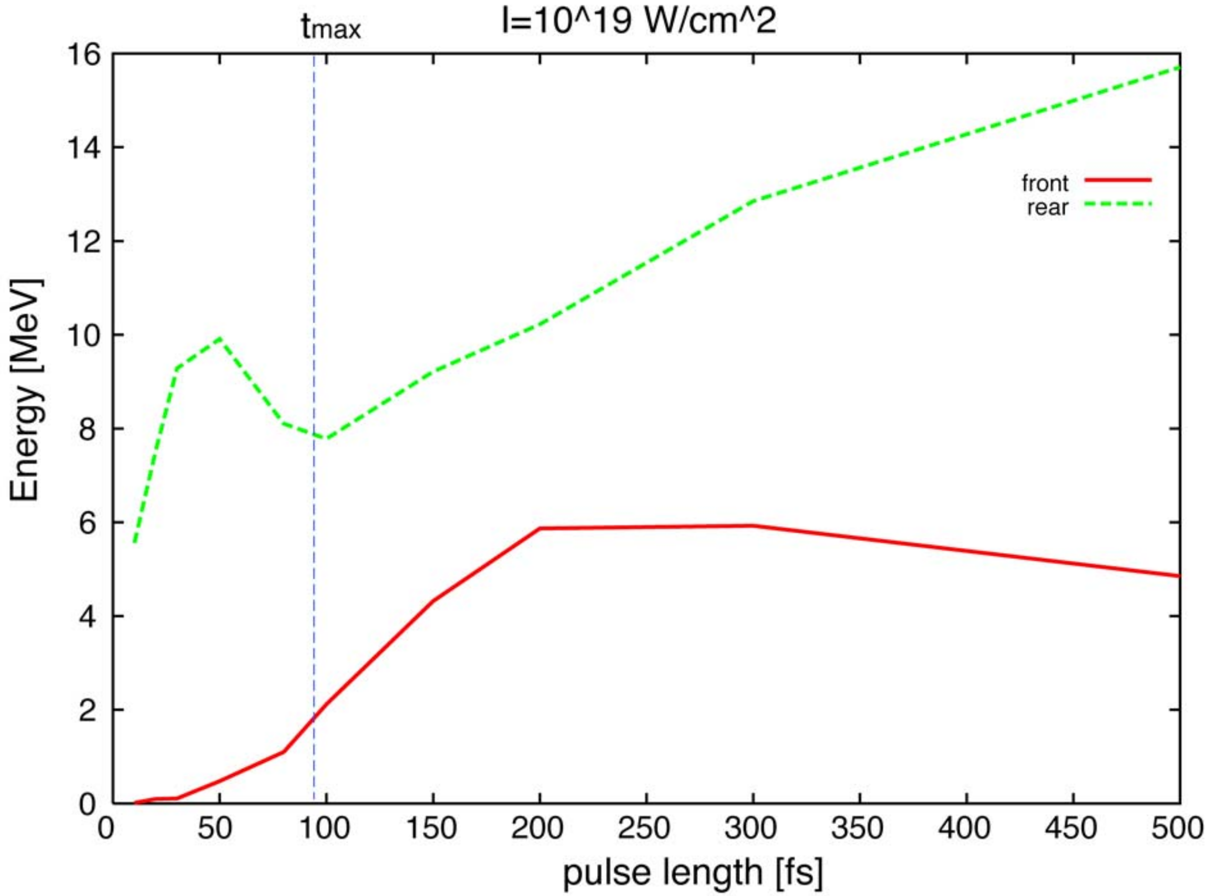

Numerical Dispersion Free Maxwell Solver for multi-dimensional PIC

Yasuhiko Sentoku
Nevada Terawatt Facility
University of Nevada, Reno

Motivation

To improve the PIC performance, e.g. more faster, more larger scale, more dense plasma, we want to reduce the number of grid per wavelength.

But don’t want to increase the numerical dispersion.

In this paper, the directional splitting scheme to integrate the Maxwell equations is first introduced to multi-dimensional PIC.

The performance of this scheme is studied and compared with the FDTD scheme.

Finite Differential Time Domain method (FDTD)

Maxwell equation

$$\frac{\partial \mathbf{B}}{\partial t} = -c\nabla \times \mathbf{E}$$

$$\frac{\partial \mathbf{E}}{\partial t} = c\nabla \times \mathbf{B} - 4\pi \mathbf{J}$$

Finite differential equations

$$\frac{\mathbf{E}^{n+1} - \mathbf{E}^{n}}{\Delta t} = c\nabla \times \mathbf{B}^{n+1/2} - 4\pi \mathbf{J}^{n+1/2}$$

$$\frac{\mathbf{B}^{n+1/2} - \mathbf{B}^{n-1/2}}{\Delta t} = -c\nabla \times \mathbf{E}^{n}$$

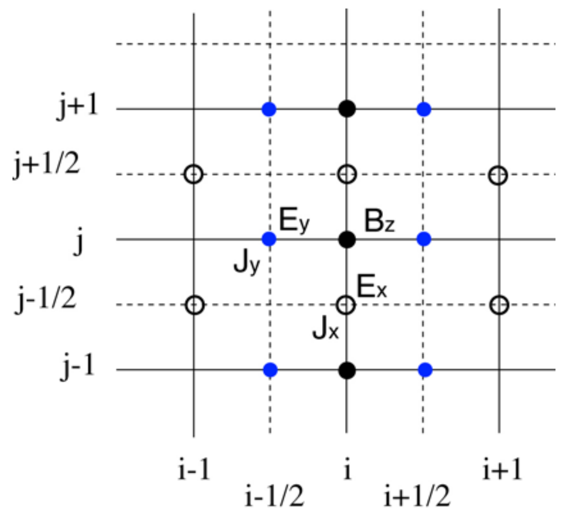

Definition of fields on grid

Both the space and time centered differences.

FDTD: Numerical dispersion

$$\left(\frac{\sin \omega \Delta t/2}{c\Delta t}\right)^2 = \left(\frac{\sin k_x \Delta x/2}{\Delta x}\right)^2 + \left(\frac{\sin k_y \Delta y/2}{\Delta y}\right)^2$$

Obviously ω is real when $c\Delta t < c\Delta t_c \equiv \sqrt{\dfrac{\Delta x \Delta y}{\Delta x^2 + \Delta y^2}}$

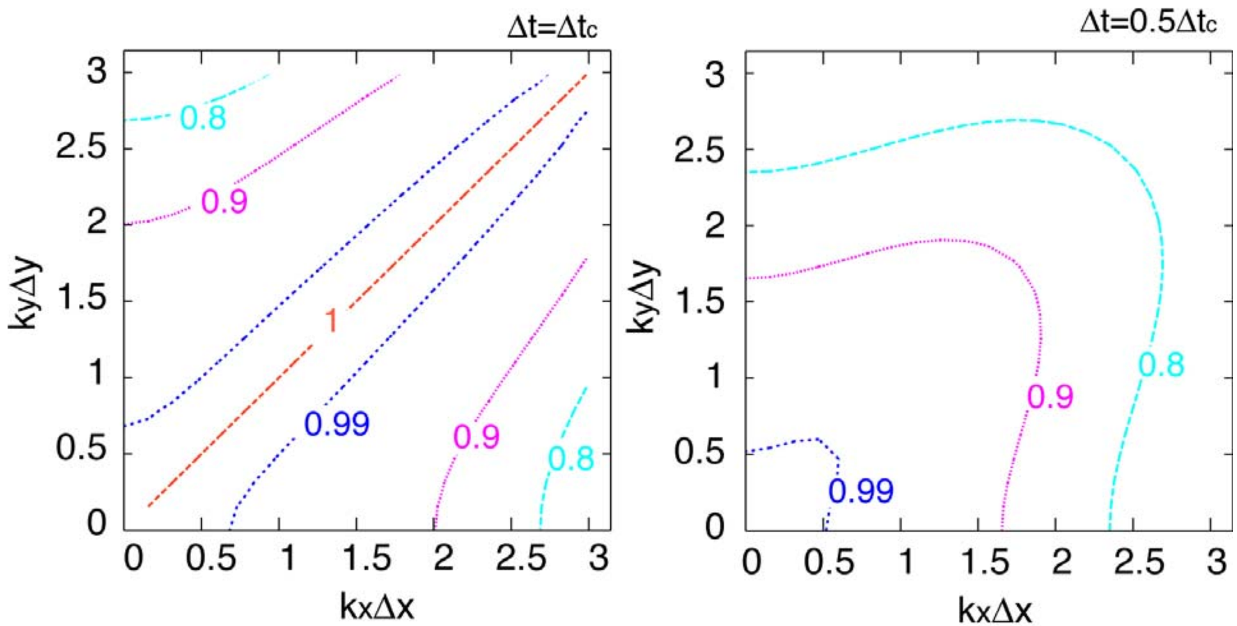

Map of phase velocity by FDTD

FDTD: Wave propagation

$\lambda/\Delta x=5,\ \Delta t=0.7\Delta t_c$

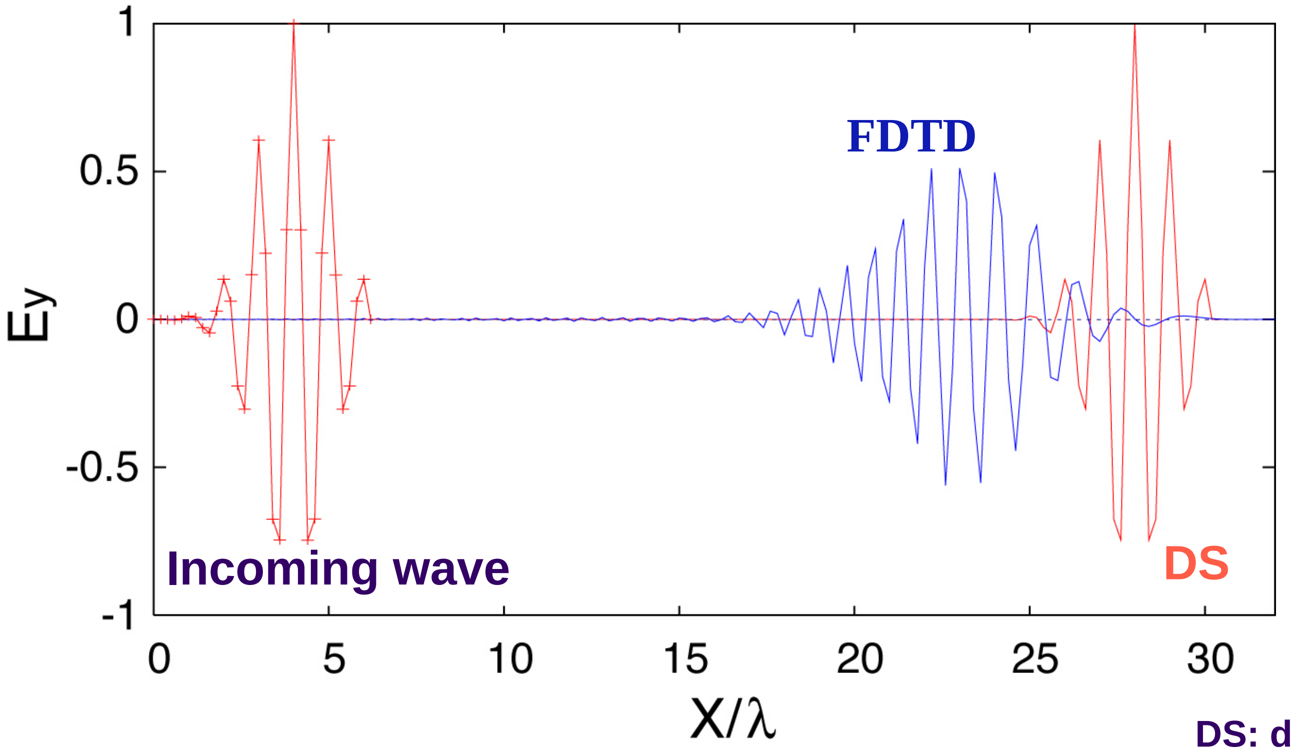

DS: directional splitting

High frequency waves delay by FDTD.

Equation of wave propagation

Equation of wave with constant velocity c (c>0)

$$\frac{\partial f}{\partial t} + c\frac{\partial f}{\partial x} = 0$$

Finite difference equation,

$$f(x_i + \Delta x, t_n + \Delta t) = f(x_i, t_n)$$

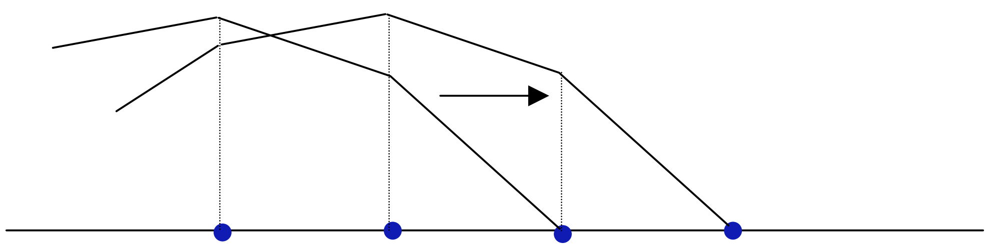

If Δx=cΔt, the numerical solution of this equation is very easy, just copy the grid value to the next grid.

Are the Maxwell equations rewritten as this form? YES!

Directional splitting (DS) method for PIC

Maxwell equation

$$\frac{\partial \mathbf{B}}{\partial t} = -c\nabla \times \mathbf{E}$$

$$\frac{\partial \mathbf{E}}{\partial t} = c\nabla \times \mathbf{B} - 4\pi \mathbf{J}$$

$$\frac{\partial}{\partial t}\begin{pmatrix} E_x \\ E_y \\ B_z \end{pmatrix} + \begin{pmatrix} 0 & 0 & 0 \\ 0 & 0 & c \\ 0 & -c & 0 \end{pmatrix} \frac{\partial}{\partial x}\begin{pmatrix} E_x \\ E_y \\ B_z \end{pmatrix} + \begin{pmatrix} 0 & 0 & c \\ 0 & 0 & 0 \\ c & 0 & 0 \end{pmatrix} \frac{\partial}{\partial y}\begin{pmatrix} E_x \\ E_y \\ B_z \end{pmatrix} = -\begin{pmatrix} J_x \\ J_y \\ 0 \end{pmatrix}$$

Step1: x-direction

$$E_y^{\pm} = B_z \pm E_y$$

$$\frac{\partial E_y^+}{\partial t} + c\frac{\partial E_y^+}{\partial x} = -\frac{1}{2} J_y$$

$$\frac{\partial E_y^-}{\partial t} - c\frac{\partial E_y^-}{\partial x} = +\frac{1}{2} J_y$$

$$\frac{\partial}{\partial t}\begin{pmatrix} E_x \\ E_y \\ B_z \end{pmatrix} + \begin{pmatrix} 0 & 0 & 0 \\ 0 & 0 & c \\ 0 & -c & 0 \end{pmatrix} \frac{\partial}{\partial x}\begin{pmatrix} E_x \\ E_y \\ B_z \end{pmatrix} + \begin{pmatrix} 0 & 0 & c \\ 0 & 0 & 0 \\ c & 0 & 0 \end{pmatrix} \frac{\partial}{\partial y}\begin{pmatrix} E_x \\ E_y \\ B_z \end{pmatrix} = -\begin{pmatrix} J_x \\ J_y \\ 0 \end{pmatrix}$$

Step2: y-direction

$$E_x^{\pm} = B_z \mp E_x$$

$$\frac{\partial E_x^+}{\partial t} + c\frac{\partial E_x^+}{\partial y} = +\frac{1}{2} J_x$$

$$\frac{\partial E_x^-}{\partial t} - c\frac{\partial E_x^-}{\partial y} = -\frac{1}{2} J_x$$

$$\frac{\partial}{\partial t}\begin{pmatrix} E_x \\ E_y \\ B_z \end{pmatrix} + \begin{pmatrix} 0 & 0 & 0 \\ 0 & 0 & c \\ 0 & -c & 0 \end{pmatrix} \frac{\partial}{\partial x}\begin{pmatrix} E_x \\ E_y \\ B_z \end{pmatrix} + \begin{pmatrix} 0 & 0 & c \\ 0 & 0 & 0 \\ c & 0 & 0 \end{pmatrix} \frac{\partial}{\partial y}\begin{pmatrix} E_x \\ E_y \\ B_z \end{pmatrix} = -\begin{pmatrix} J_x \\ J_y \\ 0 \end{pmatrix}$$

DS: Calculate the numerical dispersion

Step1: x-direction

$$E_y^{n+1} = E_{y0}\exp[k_x x_i + k_y y_j - \omega(t_n + \Delta t)]$$

$$= \frac{B_{z0}+E_{y0}}{2}\exp[k_x(x_i - \Delta x) + k_y y_j - \omega(t_n)] - \frac{1}{2}J_{y,i-1/2,j}$$

$$-\frac{B_{z0}-E_{y0}}{2}\exp[k_x(x_i + \Delta x) + k_y y_j - \omega(t_n)] - \frac{1}{2}J_{y,i+1/2,j}$$

$$B_z^{n*} = B_{z0}\exp[k_x x_i + k_y y_j - \omega(t_n^*)]$$

t_n*: medium time

$$= \frac{B_{z0}+E_{y0}}{2}\exp[k_x(x_i - \Delta x) + k_y y_j - \omega(t_n)] - \frac{1}{2}J_{y,i-1/2,j}$$

$$+\frac{B_{z0}+E_{y0}}{2}\exp[k_x(x_i + \Delta x) + k_y y_j - \omega(t_n)] + \frac{1}{2}J_{y,i+1/2,j}$$

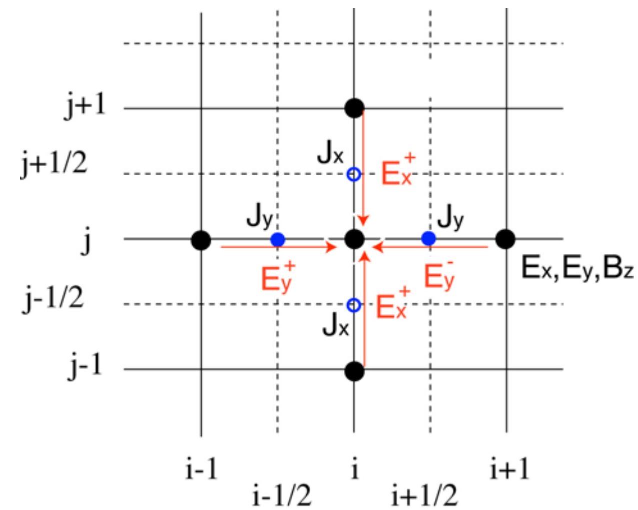

Step2: y-direction

$$E_x^{n+1} = E_{x0}\exp[k_x x_i + k_y y_j - \omega(t_n + \Delta t)]$$

$$= -\frac{B_{z0}}{2}\exp[k_x x_i + k_y(y_j - \Delta y) - \omega(t_n^*)] + \frac{E_{x0}}{2}\exp[k_x x_i + k_y(y_j - \Delta y) - \omega(t_n)] - \frac{1}{2}J_{x,i,j-1/2}$$

$$+\frac{B_{z0}}{2}\exp[k_x x_i + k_y(y_j + \Delta y) - \omega(t_n^*)] + \frac{E_{x0}}{2}\exp[k_x x_i + k_y(y_j + \Delta y) - \omega(t_n)] - \frac{1}{2}J_{y,i,j+1/2}$$

$$B_z^{n+1} = B_{z0}\exp[k_x x_i + k_y y_j - \omega(t_n + \Delta t)]$$

$$= \frac{B_{z0}}{2}\exp[k_x x_i + k_y(y_j - \Delta y) - \omega(t_n^*)] - \frac{E_{x0}}{2}\exp[k_x x_i + k_y(y_j - \Delta y) - \omega(t_n)] + \frac{1}{2}J_{x,i,j-1/2}$$

$$+\frac{B_{z0}}{2}\exp[k_x x_i + k_y(y_j + \Delta y) - \omega(t_n^*)] + \frac{E_{x0}}{2}\exp[k_x x_i + k_y(y_j + \Delta y) - \omega(t_n)] - \frac{1}{2}J_{y,i,j+1/2}$$

DS: Numerical dispersion

$$\cos\omega\Delta t = \frac{1}{2}\left(-1 + \cos k_x\Delta x \cos k_y\Delta y + \cos k_x\Delta x + \cos k_y\Delta y\right)$$

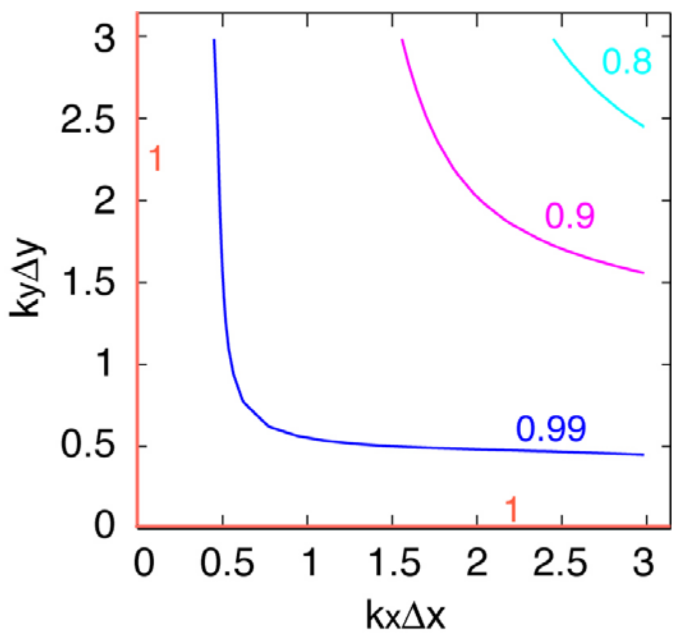

Map of phase velocity by DS

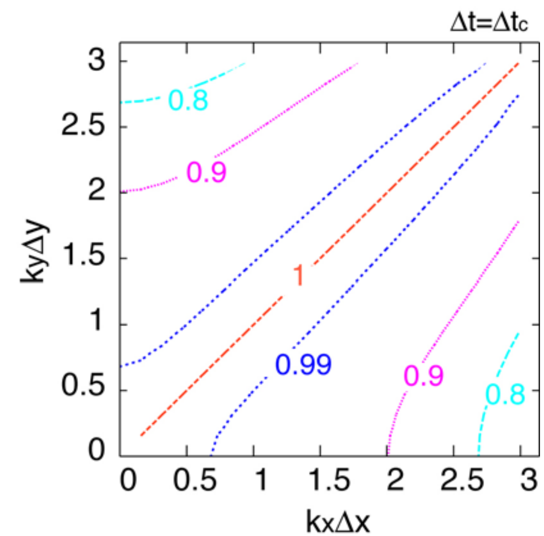

Map of phase velocity by FDTD

Test I: Single particle motion in a plane wave

Laser: a=1

In a plane wave, a particle orbit in the momentum space is described by $p_x = p_y^2/2$.

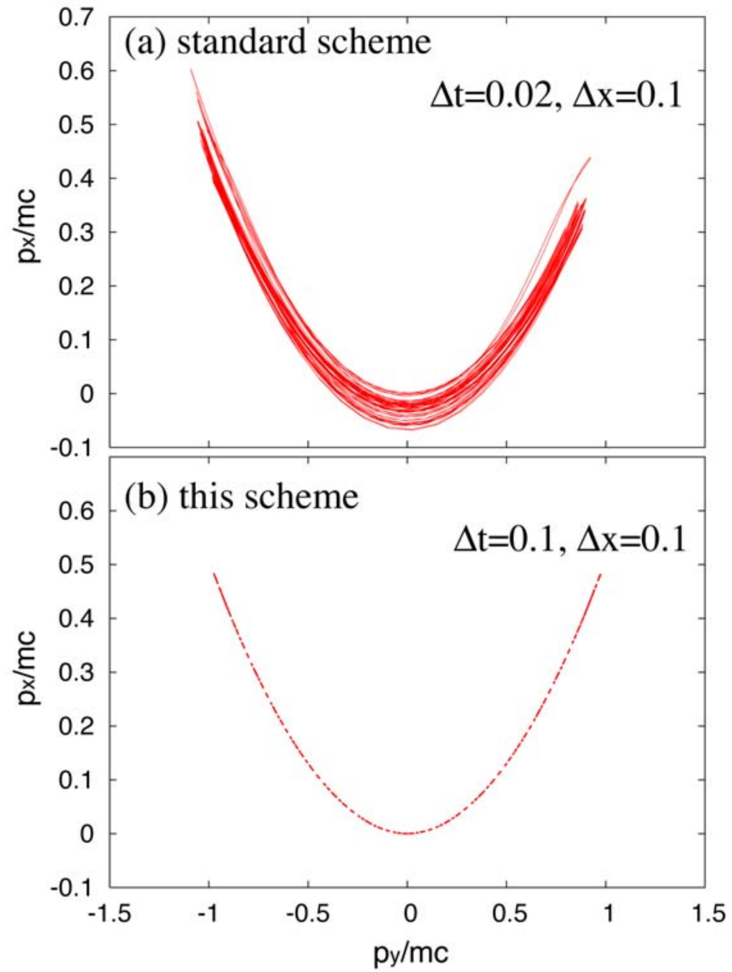

10 mesh/wavelength is enough to solve the particle motion with DS.

Test II: Wake fields

Laser: a = 1, pulse length = 5λ

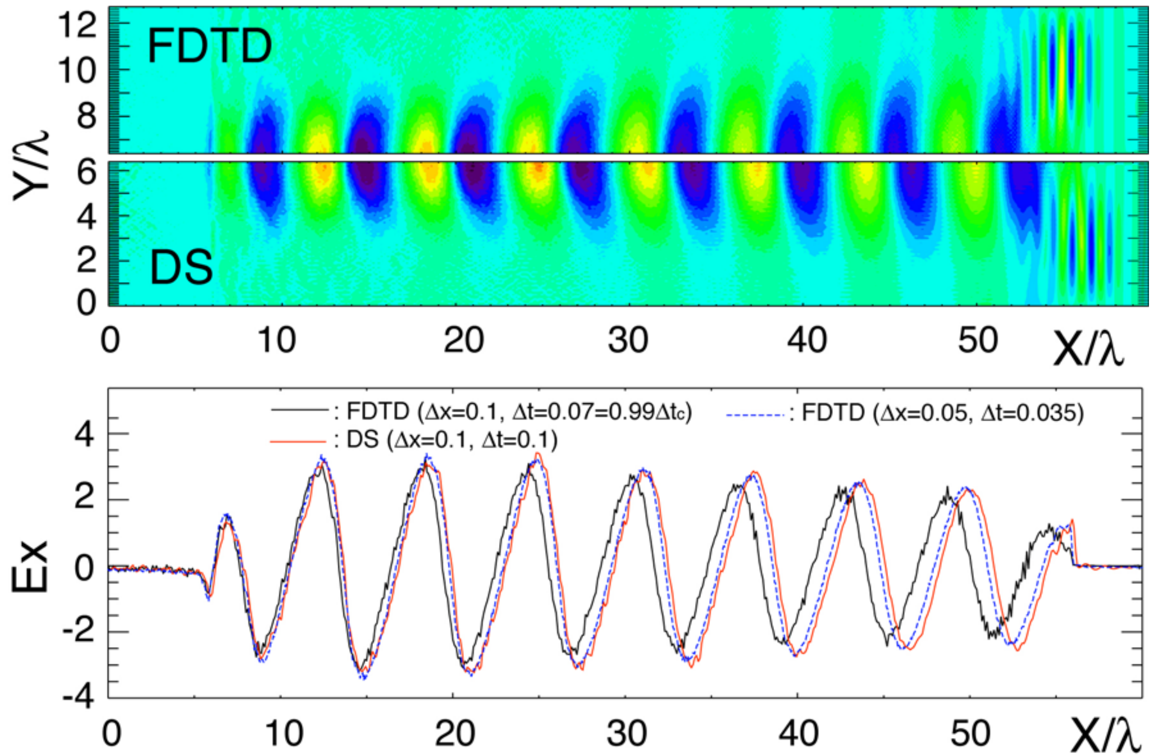

DS:
300x128 mesh

10 mesh is enough for one laser wavelength with the DS scheme.
The FDTD needs two times more meshes.

Merits of DS

- The DS has much less numerical dispersion than the FDTD along the grids.
- Simulation can do with less computational cost.
- Very easy to make the wave escaping boundary.
- The DS is a local solver, easily parallelized.
- Easy to extend to 3D configuration.

UCRL-PRES-203907

Modeling of short pulse high intensity laser-plasma interactions in 3D simulations

Presented to:

34th Annual Anomalous Absorption Conference

C. H. Still, B. F. Lasinski, and A. B. Langdon

AX-Division, LLNL

May 2004

This work was performed under the auspices of the U.S. Department of Energy by the University of California Lawrence Livermore National Laboratory under Contract No. W-7405-Eng-48.

Lawrence Livermore National Laboratory, P.O. Box 808, Livermore, CA 94551-0808

Short-pulse high-intensity laser plasma interaction modeling in 3D PIC codes

- **This presentation:**
  - **Z3 massively parallel PIC simulations**
  - **3-D simulations with laser normally and obliquely incident onto overdense plasma**
    - **characteristics of reflected light and electron generation**

- **Also see:**
  - ***Generation and Transport of Energetic Particles in Short-Pulse High-Intensity Laser Plasma Interactions*, Lasinski *et al*. [This session]**
  - ***Spectra of Scattered and Emitted Light in Modeling of High Intensity Laser Plasma Interactions*, Langdon *et al*. [Session 1p]**

Computer performance increases enable ever larger PIC simulations.

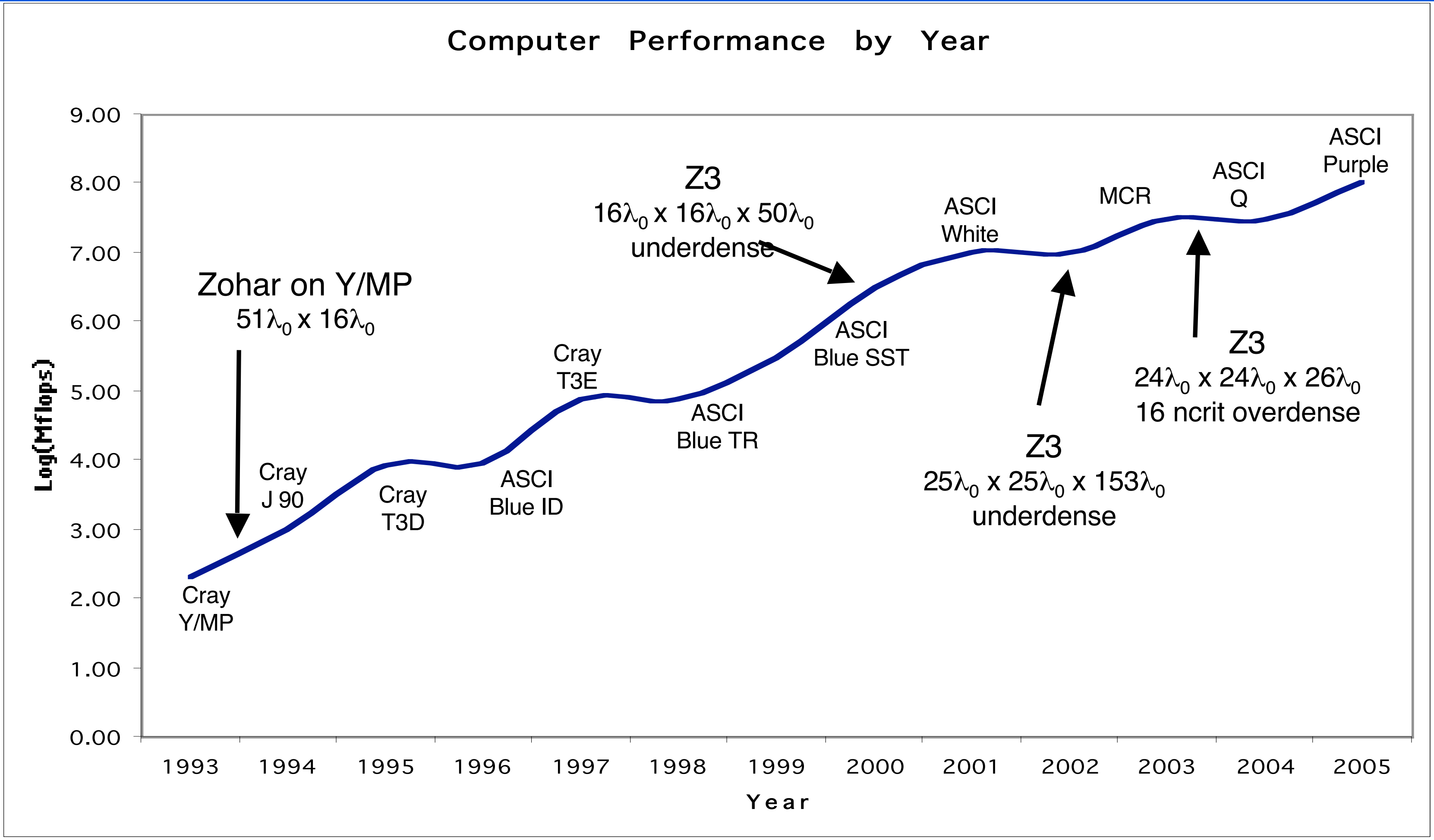

Projections from runs on ASCI Purple prototype fall on this curve.

Z3 is at the forefront of large, heroic, particle-in-cell (PIC) modeling.

- MPP code via explicit message passing using MPI
  – Domain decomposition onto 3-D processor grid provides flexibility.
- 3-D electromagnetic relativistic particle mover, field solve and Poisson solve are parallel and optimized for cache efficiency
- Many diagnostics for code validity and problem analysis. A parallel capability for interactive post-processing has been implemented.
- Enables 3-D simulations and large 2-D simulations
  – E.g. on $24\lambda_0 \times 24\lambda_0 \times 26\lambda_0$ grid with ion and electron species (3.6 G pt each) modeling short-pulse, high-intensity laser-plasma interactions in a 16 n_{crit} overdense plasma, could run 15000 steps in about 15 days (512 cpu of MCR, #7 on TOP500 list). For comparison, this corresponds to ~49 Cray Y/M-P years.

Particle mover has been designed to operate efficiently in parallel

- 3-space + 3-momenta relativistic electromagnetic particle mover
- Highly cache optimized by interleaving particles
- Particle load is distributed via spatial domain decomposition (3-D)
- The move/collect operation is efficient.
  - E.g. total time (*including communication*) to move 2 species with 3.6 G pt each on 768 × 768 × 840 cell grid using 512 cpus on MCR is ~53 sec (ie., 3.8 μsec for 512 pts on 512 cpu).
- Particle sorting is provided as a separate operation. (This further improves cache performance.)
  - Sort time for the above mentioned case is ~40 sec.

The **E**-**B** formulation of Maxwell's equations is solved in parallel.

- Solution is by finite differences with one layer of guard cells.
- Interleaving field components provides high cache efficiency.
- A 3-D domain decomposition provides scalability.
- 2nd order accuracy is maintained by staggering the field components.
- Boris' correction to **E** ensures flux conservation (div(**E**) = ρ).
  - Uses 2-D parallel FFT and parallel tridiagonal solve.
- Outgoing electromagnetic wave boundary conditions at z=0, z=L_z provide for the introduction of a laser electric field (typically, simulations use periodic boundary conditions in x,y).

Field components are staggered to maintain 2nd order accuracy and conservation.

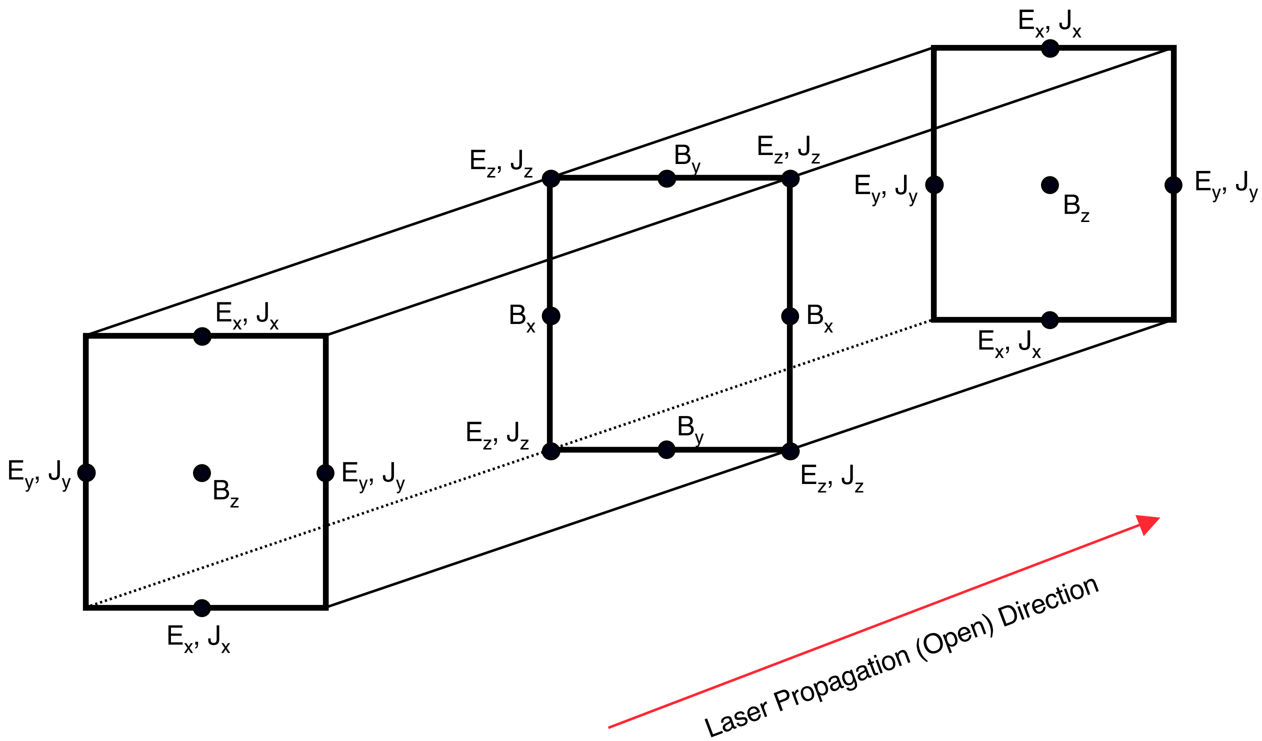

Z3 is built under the Yorick interpreter.

- **Allows coupling physics modules into "a code" for a specified application.**
- **Additional physics routines can be rapidly prototyped in interpreter code for evaluation, and then re-implemented in compiled code if additional speed is needed.**
- **Time loop is in interpreted code and is readily customized.**
- **Input decks are actually interpreted programs which call the compiled physics packages.**
- **Facilitates development of user-developed diagnostics, and aids in debugging.**
- **Provides dump/restart files, history files, and graphics.**
- **Leverages other efforts (pF3d, Lip, Zohar).**
- **See ftp://ftp-icf.llnl.gov/pub/Yorick/doc/index.html**

The 3-D simulations model a slab.

Simulation A: normal incidence

- $n_e = 16\ n_{crit}$ 10 λ_0 thick slab in a $24\lambda_0 \times 24\lambda_0 \times 26\lambda_0$ volume ($768^2 \times 840$ cells). 3.6 G ptcls each, ion & electron; T_e = 50 keV, $Z\ T_e/T_i$ = 10.
- $I = 10^{19}$ W/cm^2 red laser (polarized E_x) incident normal to the plasma in x,y.

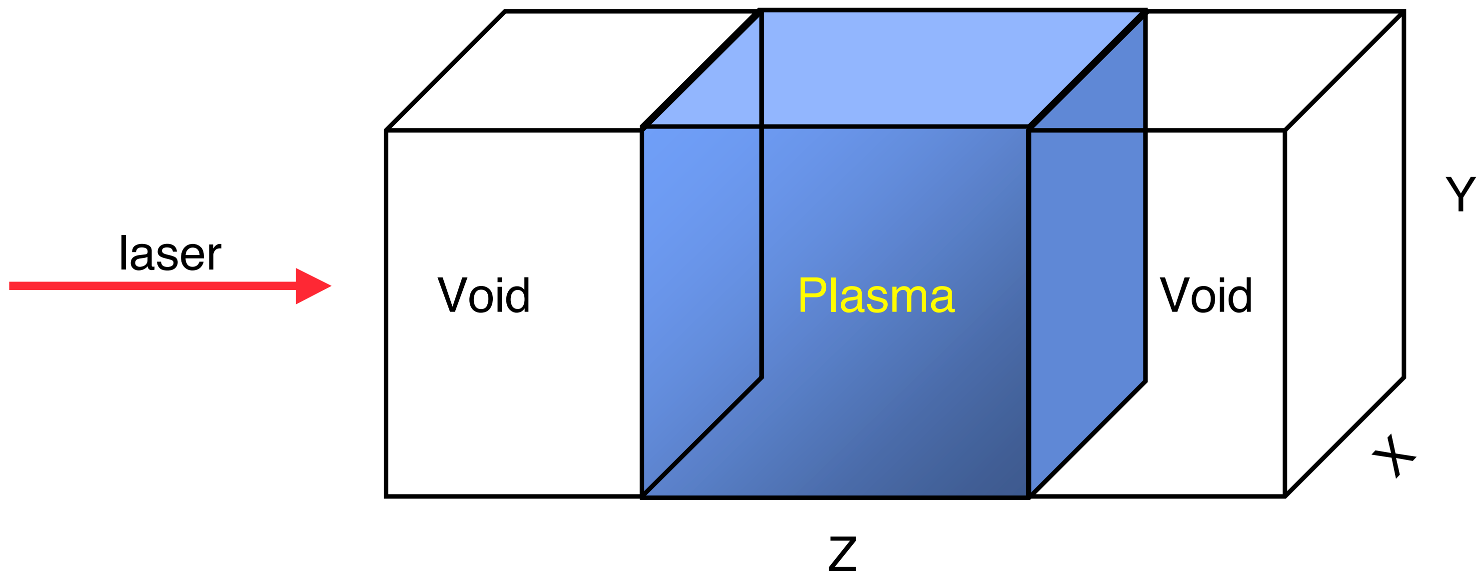

At early time, the light begins to reflect.

Simulation A: normal incidence

- **Slices of the Poynting vector P_z (scaled in [-2,2]) and current J_z are shown at time 0.3 ps.**

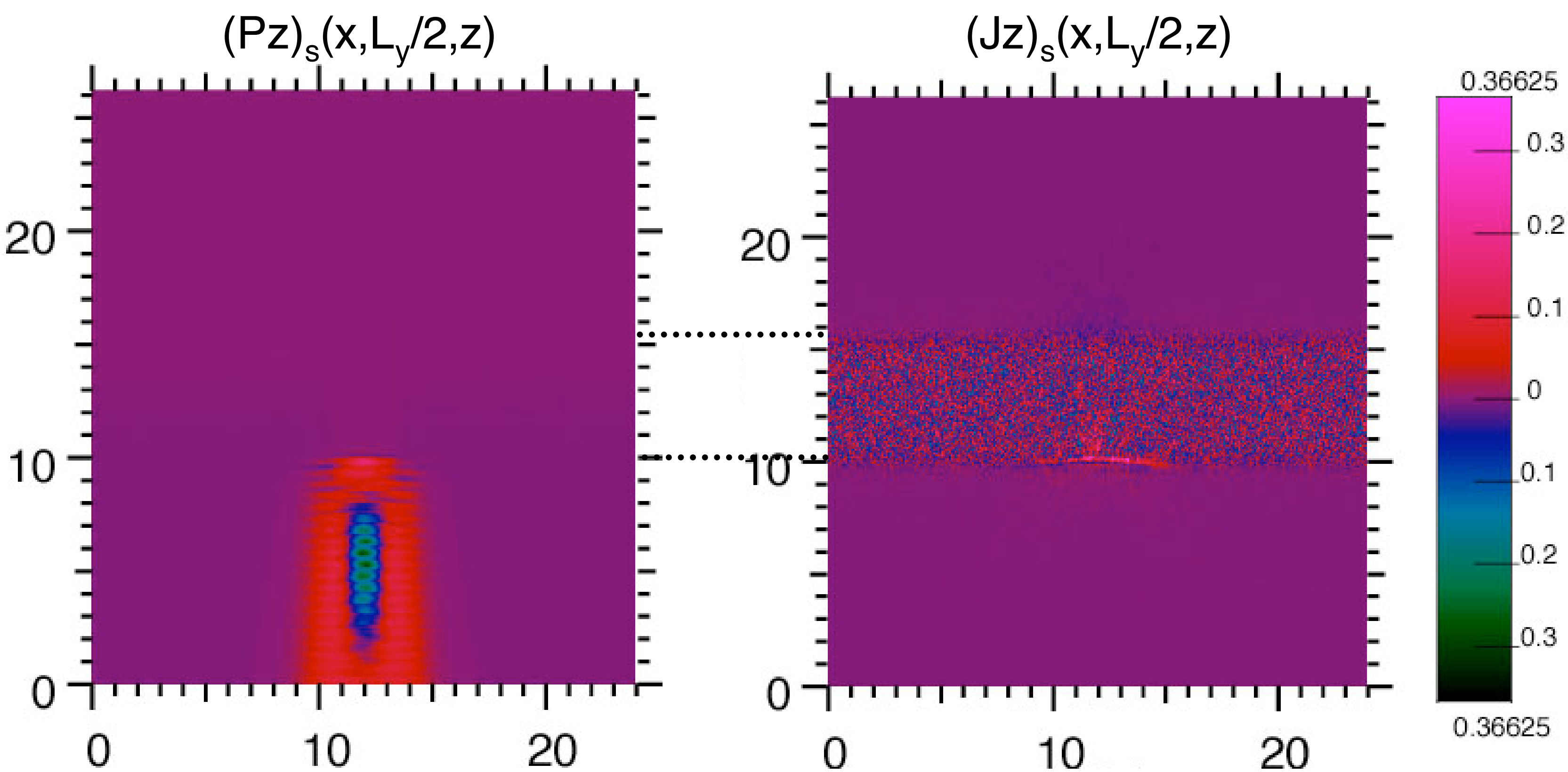

As time continues, the reflection increases, and electron "fingers" form in the plasma.

Simulation A: normal incidence

- **Slices of the Poynting vector Pz (scaled in [-2,2]) and current Jz are shown at time 0.5 ps.**

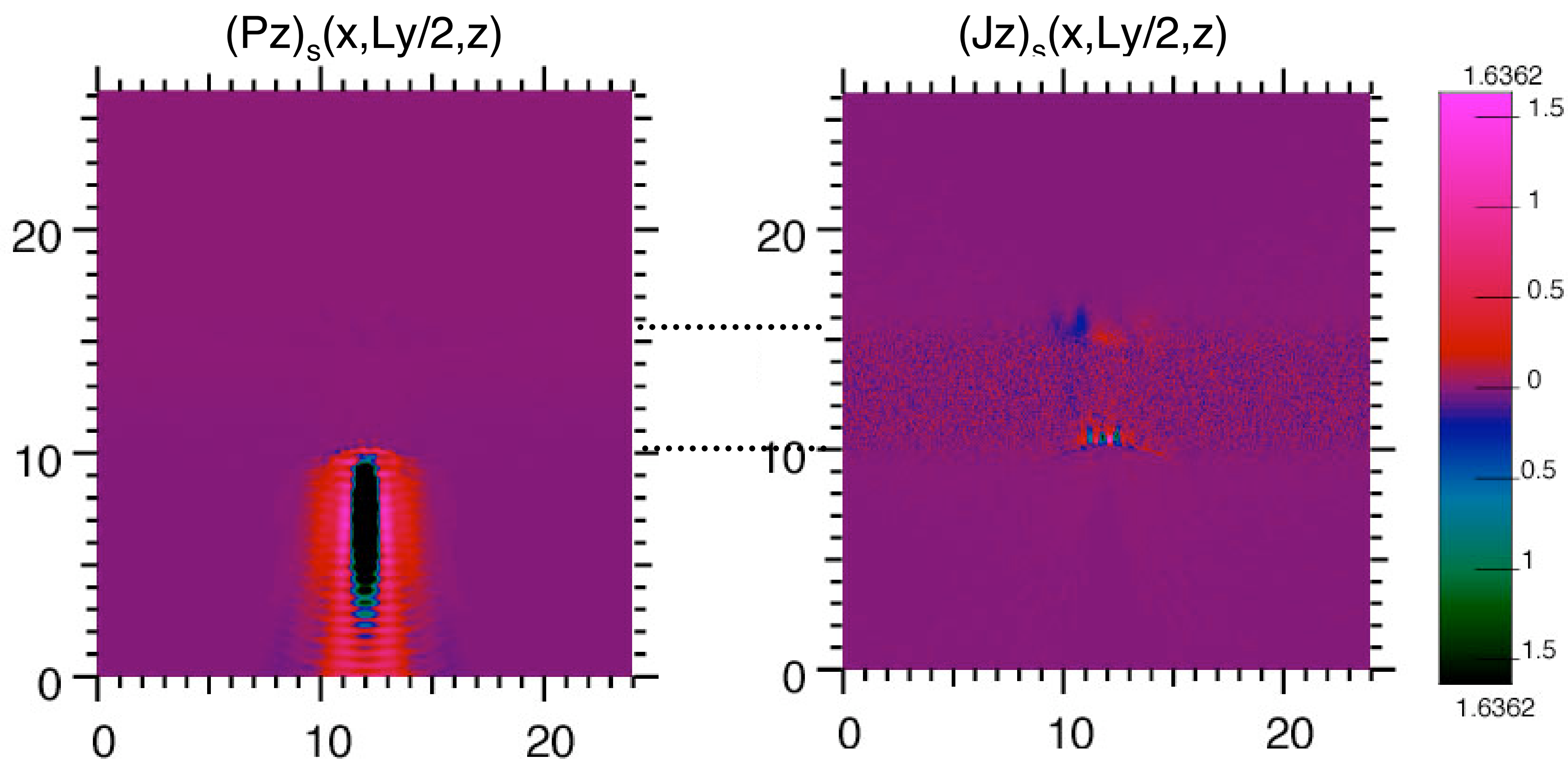

Later the light is bottled up: the reflected light spreads, and the fingers develop structure.

Simulation A: normal incidence

- **Slices of the Poynting vector Pz (scaled in [-2,2]) and current Jz are shown at time 0.7 ps.**

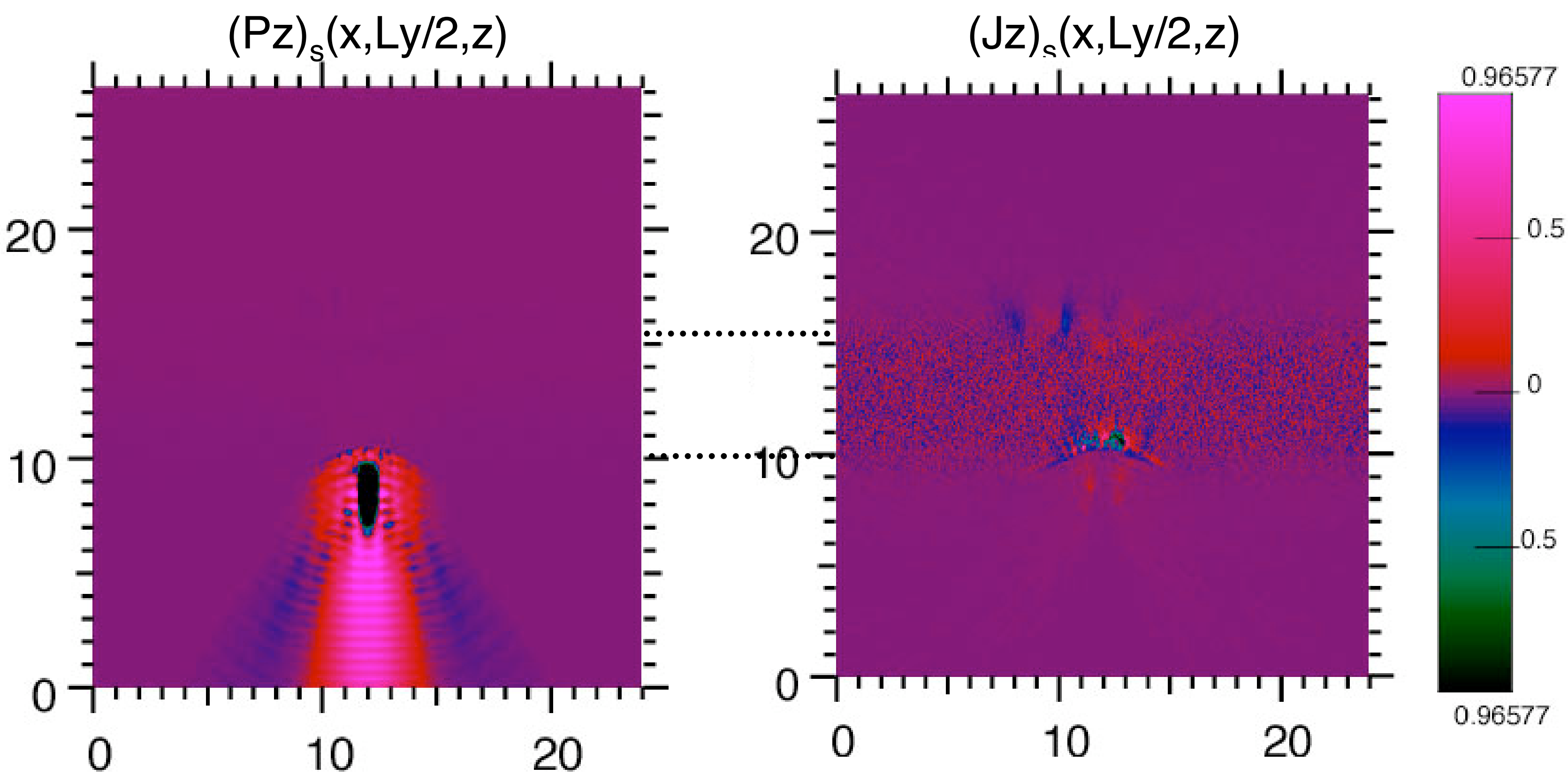

Energy plots confirm the light is “bottled” up between bursts.

Simulation A: normal incidence

- **Reflected light (black) is superimposed on the incident laser (cyan).**
- **There is a burst of reflected light around 0.125 ps and another around 0.7 ps, and not much in between.**

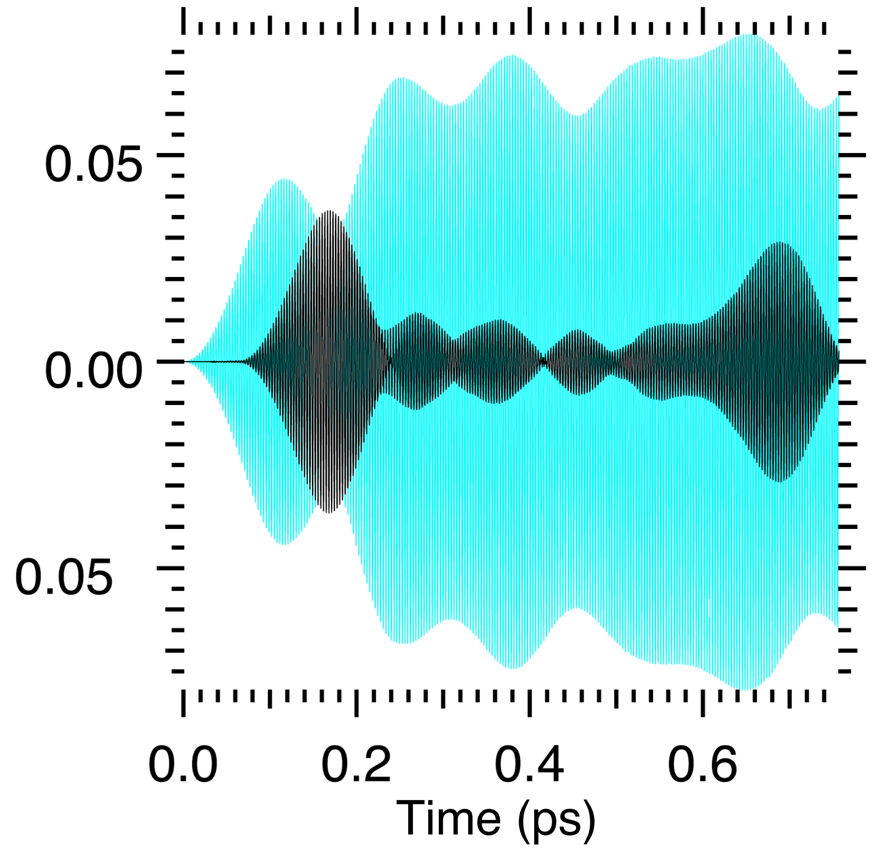

These images show the electrons above 2 MeV integrated through the Y-volume.

Simulation A: normal incidence

Particle plots with u_z>0.

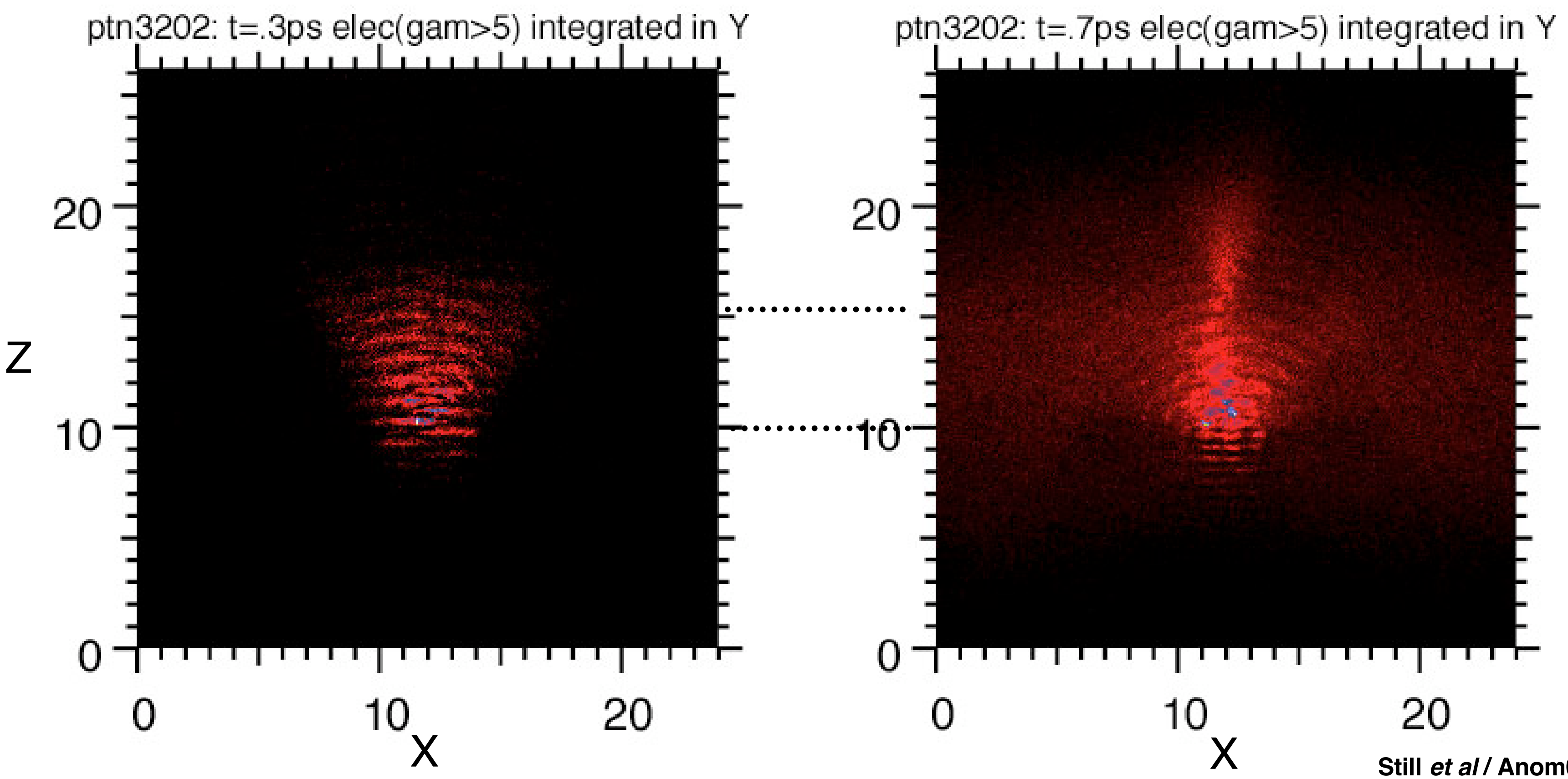

These images show the electrons above 2 MeV integrated through the X-volume.

Simulation A: normal incidence

Particle plots with u_z>0.

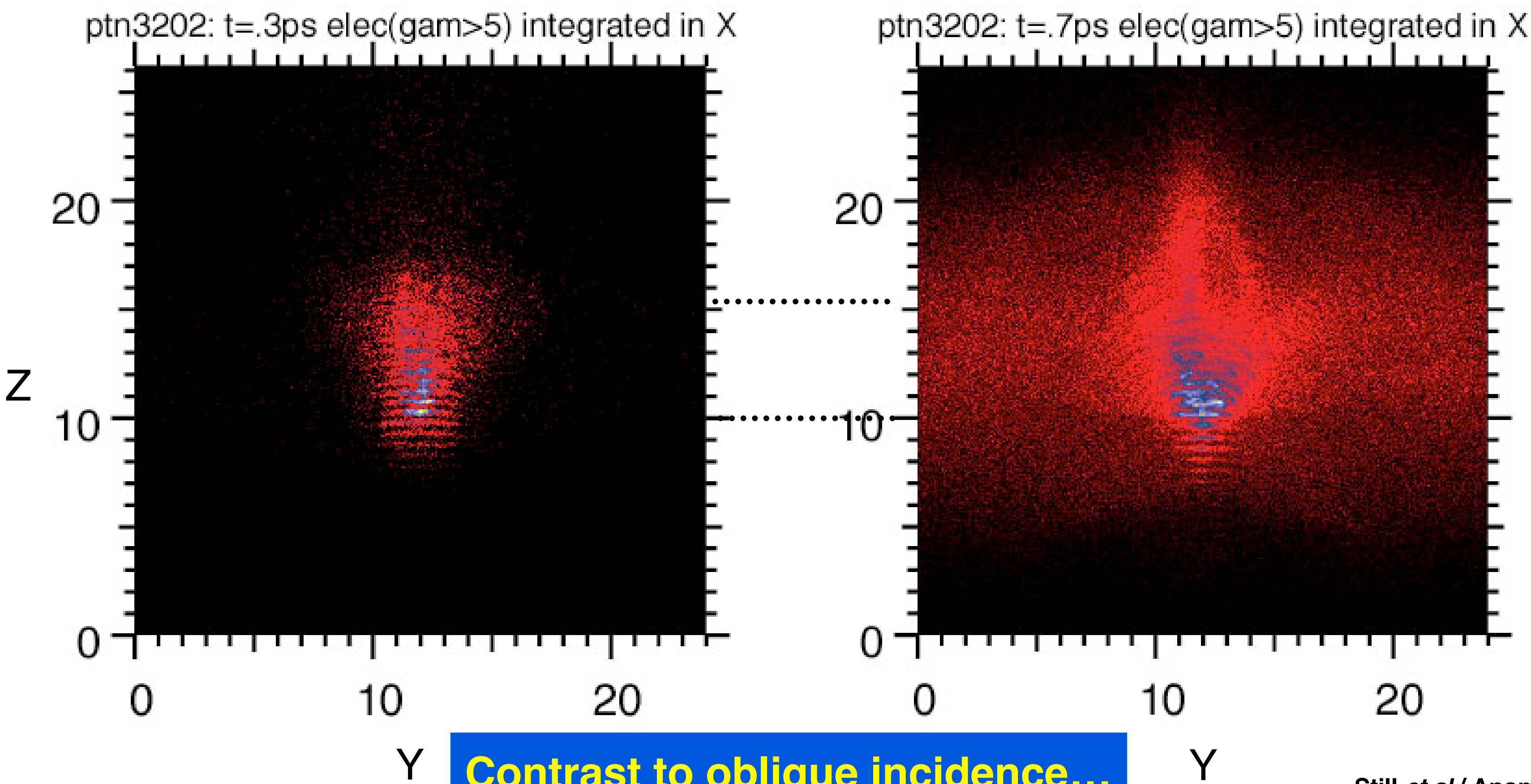

Contrast to oblique incidence…

The 3-D simulations model a slab in 3-D.

Simulation B: oblique incidence

- $n_e = 16\ n_{crit}$ $10\lambda_0$ thick slab in a $24\lambda_0 \times 24\lambda_0 \times 41\lambda_0$ volume ($768^2 \times 1312$ cells). 1.8 G ptcls each, ion & electron; $T_e = 50$ keV, $ZT_e/T_i = 10$.
- $I = 10^{19}$ W/cm^2 red laser (polarized E_x) incident at 30° to the plasma in x, and normal to the plasma in y.

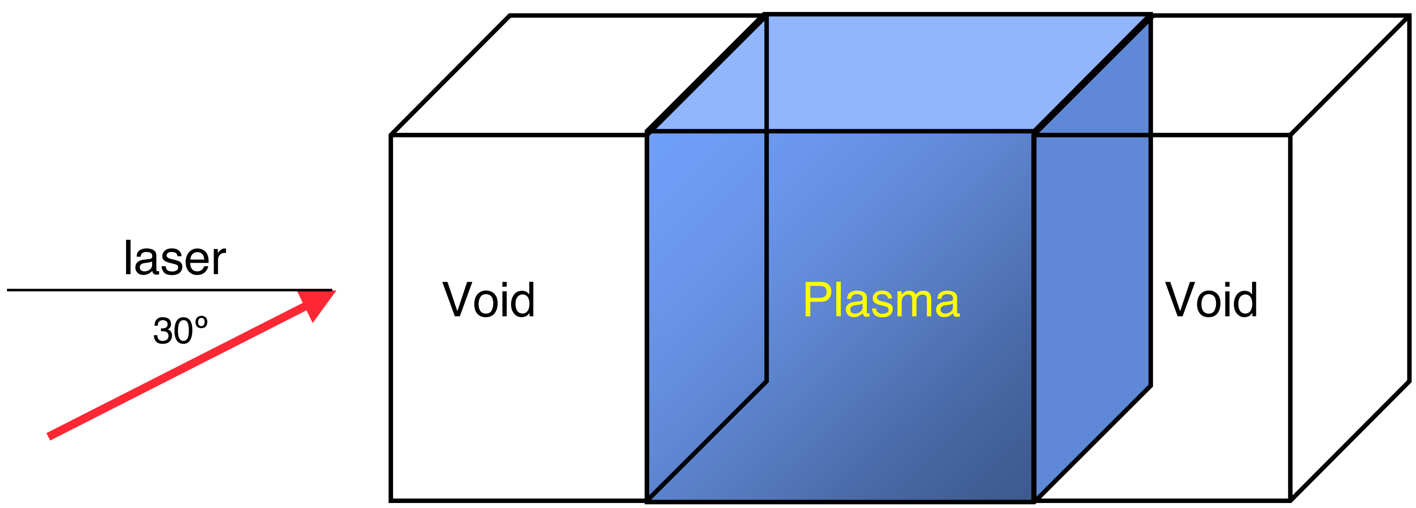

In the oblique direction, the reflected light spreads significantly.

Simulation B: oblique incidence

- **At early time, reflected light appears at the specular angle, and little spreading is evident**
- **At later time, the reflected light spreads so significantly that the light along the specular angle disappears.**
- **$(Pz)_s$ is plotted with range [-2,2].**

Poynting vector $(Pz)_s(x,Ly/2,z)$

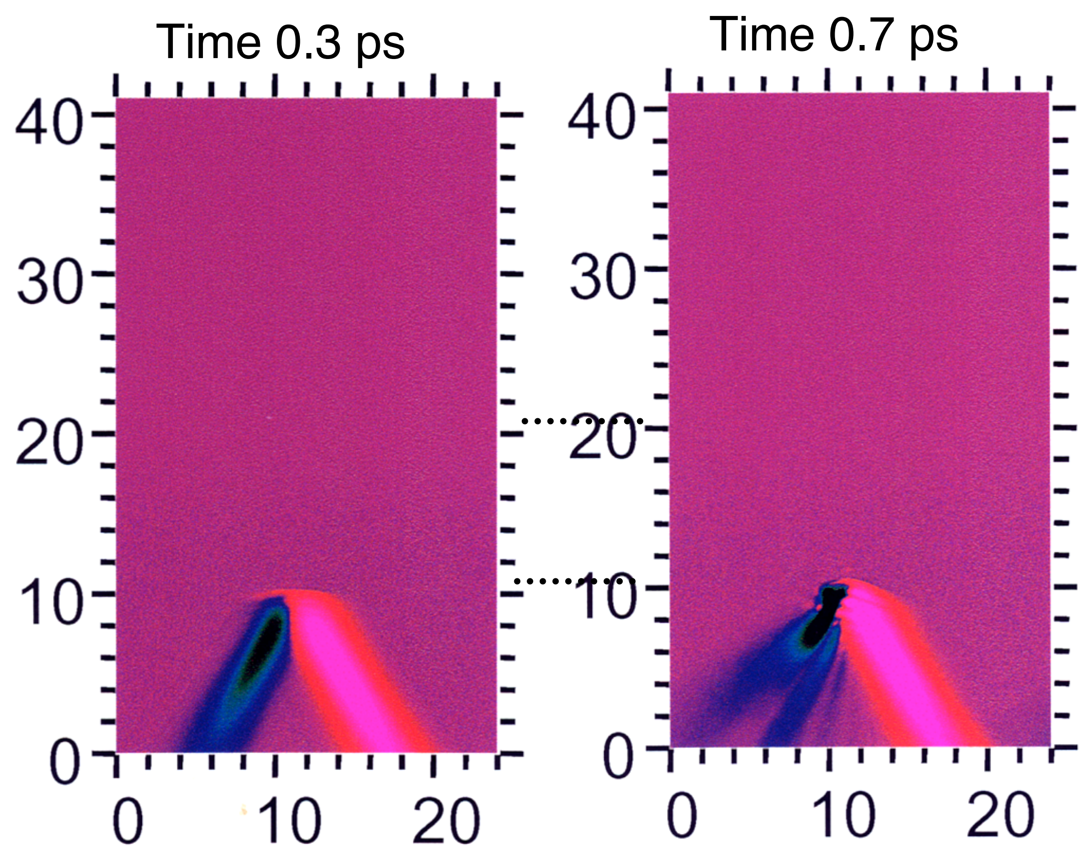

History plots at various probe positions in the reflected light confirm the spreading.

Simulation B: oblique incidence

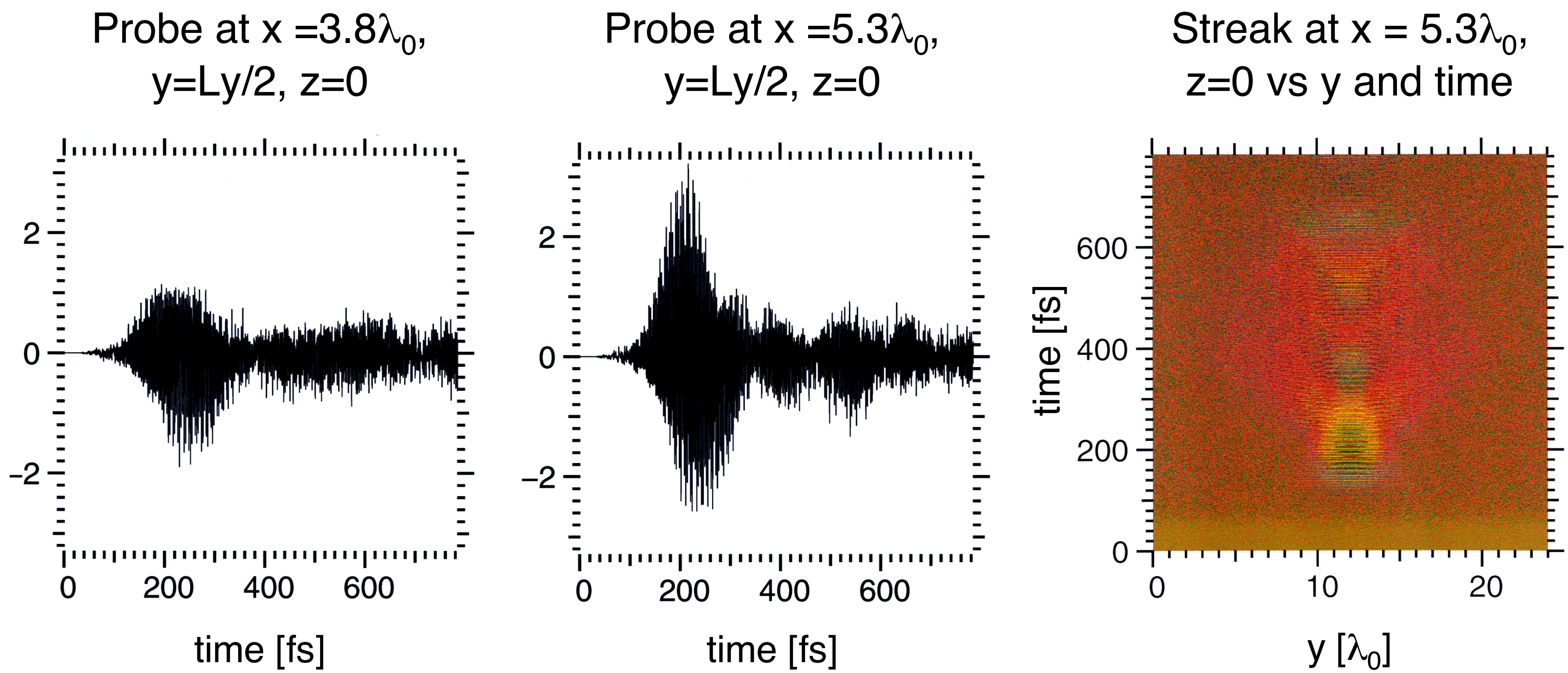

Oblique incidence gives rise to very different particle structure.

Simulation B: oblique incidence

- **Simulation B: oblique at 30° in X, and normal in Y, time .3 ps**
- **Particle positions with u_z>0, γ>5, integrated in the third dimension.**
- **Initially, electrons are pushed in the direction of laser propagation, and some spreading begins to develop.**

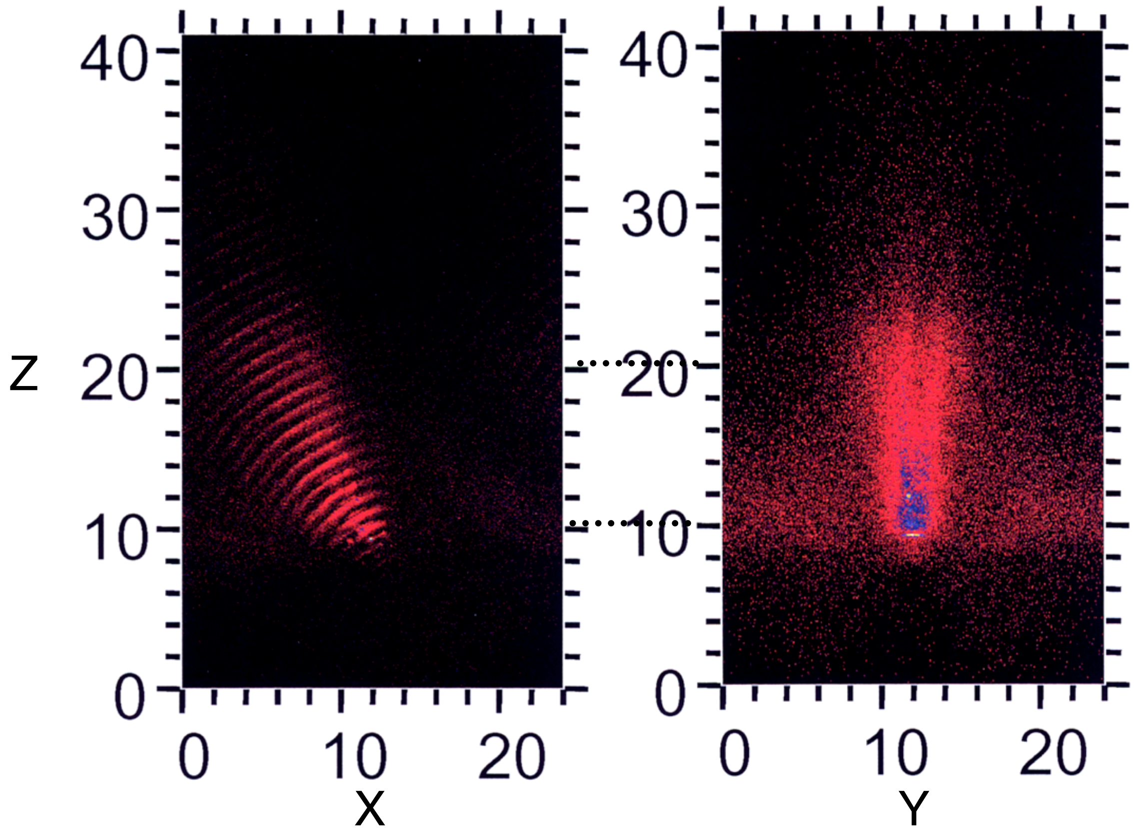

Later in time, few electrons are traveling in the laser propagation direction.

Simulation B: oblique incidence

- **Simulation B: oblique at 30° in X, and normal in Y, time .7 ps**
- **Particle positions with $u_z>0$, $\gamma>5$, integrated in the third dimension.**
- **Later, the electrons begin to spread into distinct jets.**

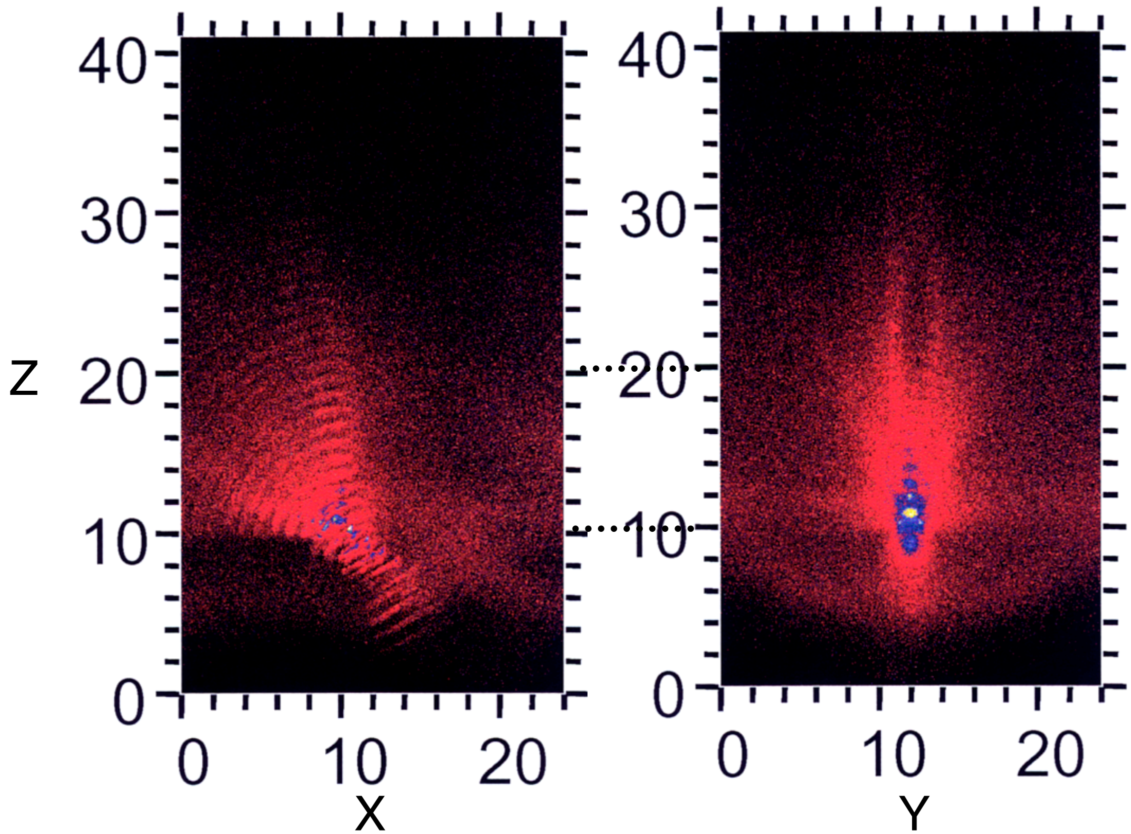

We are exploring 3-D visualization of the structure of energetic electron flows.

Simulation B: oblique incidence

- **Simulation B: oblique at 30° in x, and normal in y, time 1.0 ps**
- **(x, y, z) positions of electrons with $u_z>0$, $\gamma>9$ (4 MeV)**
- **Note the harmonic structure, even as the electron "jets" form.**
- **Particles are mapped into RGB true color by their velocities. [ux=red, uy=green, uz=blue]**
- **This plot was made with yorgl (Steve Langer's GL extensions to yorick).**

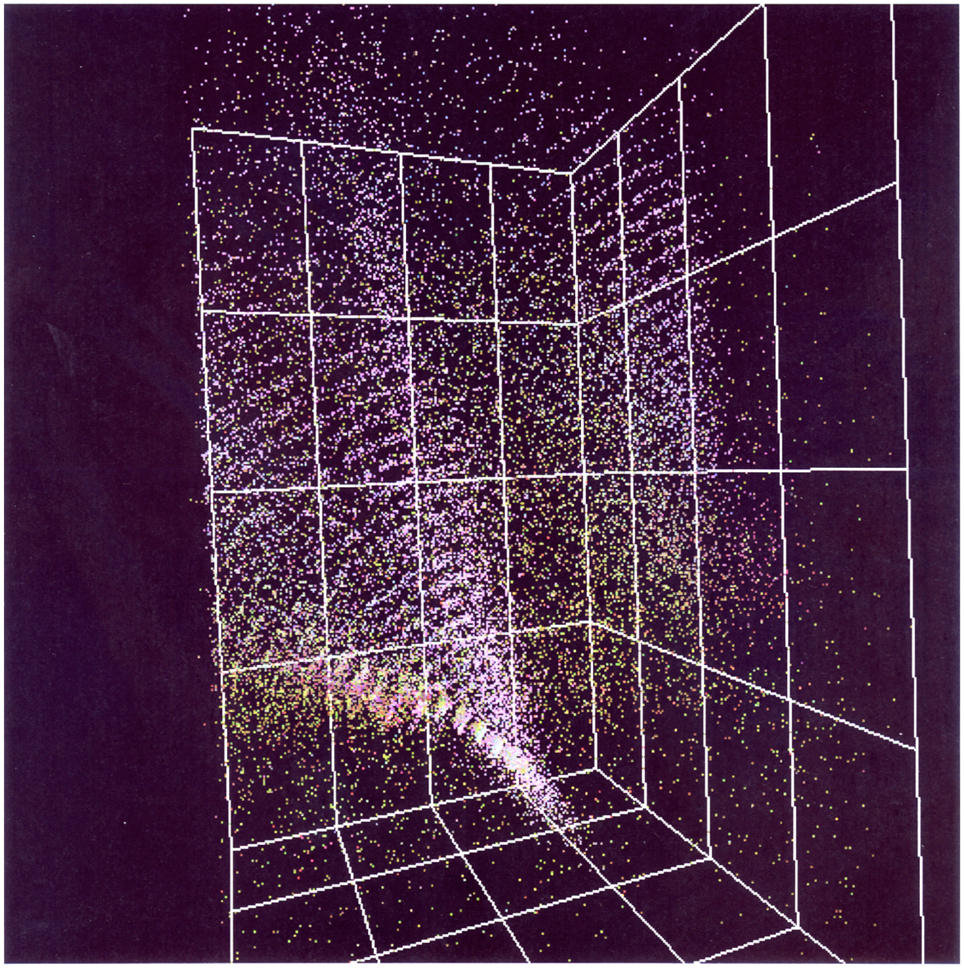

• Modeling Stopping and Scattering in Heavy Ion Accelerators •

Peter Stoltz
Tech-X Corp.

Ion stopping and scattering are important in heavy ion accelerators for fusion and HEDP applications

- Halo ions that strike the accelerator walls can scatter from the wall, generate unwanted electrons and generate neutral gas.
- The rate of scattering and rate of production of electrons and neutral gas depend on the stopping of the ions in the wall.
- SRIM is a standard code for modeling ion-solid interactions, but SRIM runs only on Windows and the source is difficult to modify
- Tech-X is working to develop a code with capabilities similar to SRIM but open source and cross platform.

Particles in a heavy-ion accelerator will interact with the wall

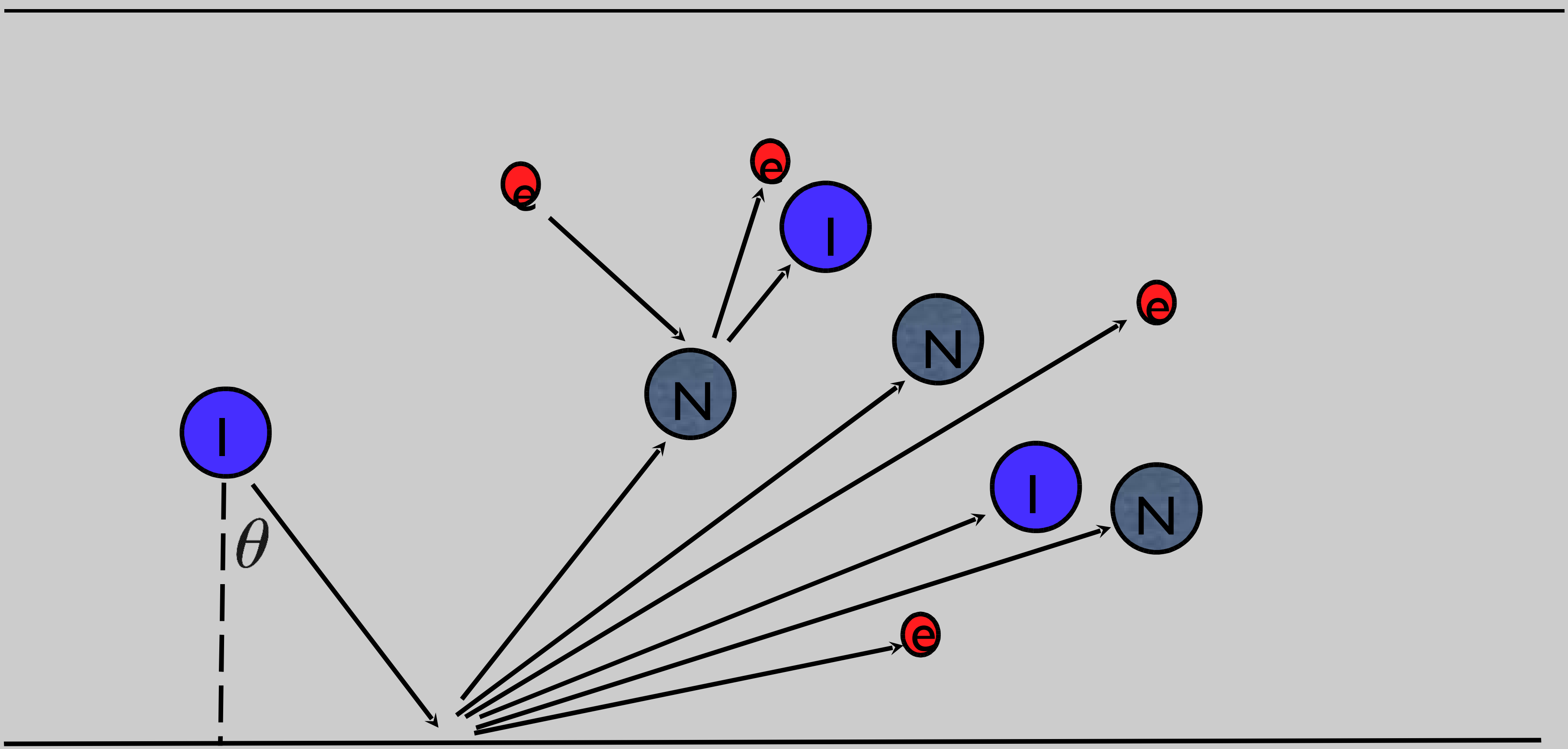

SRIM is one way to estimate ion scattering in these applications

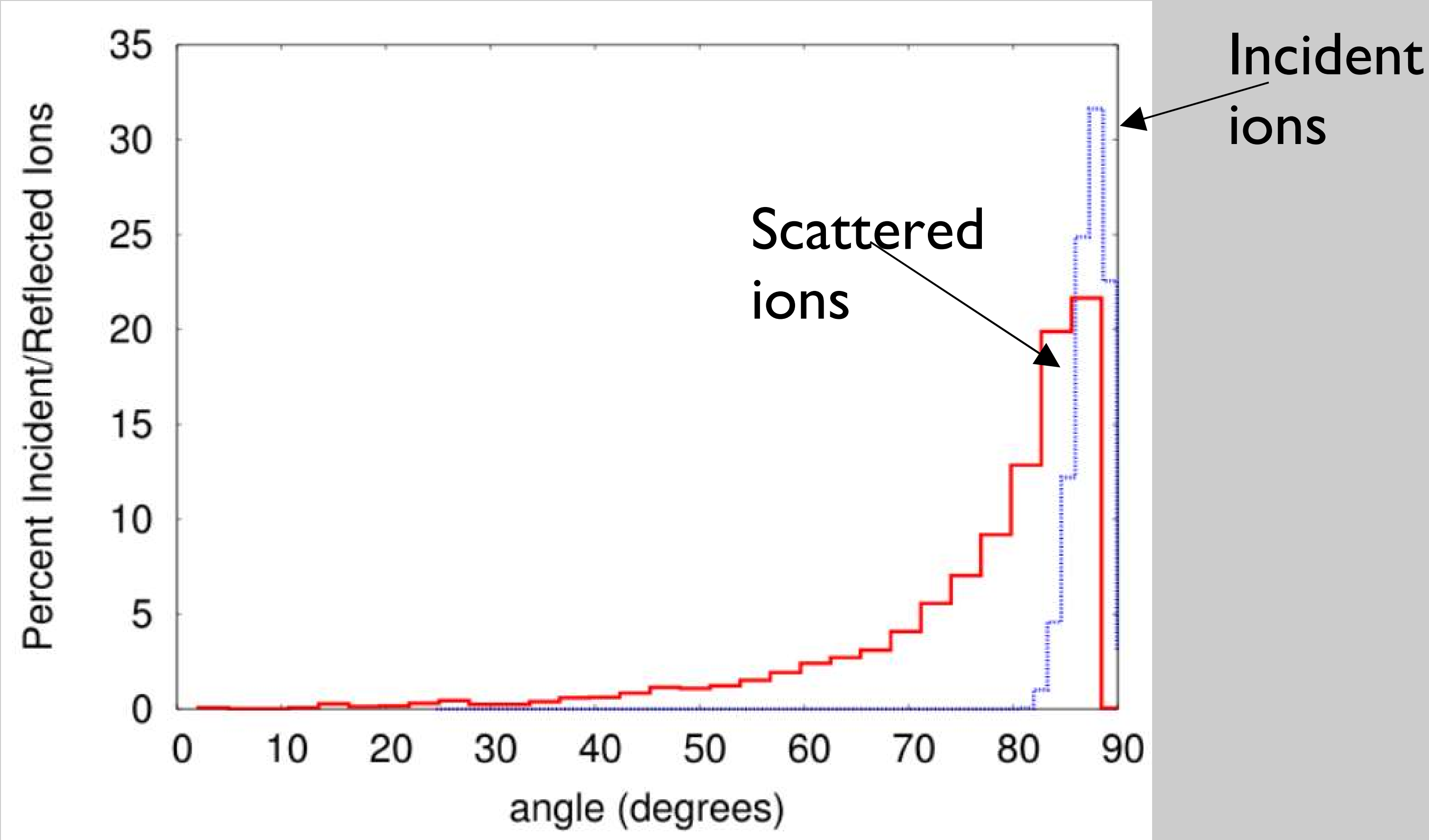

Ion scattering also may explain grazing electron yields

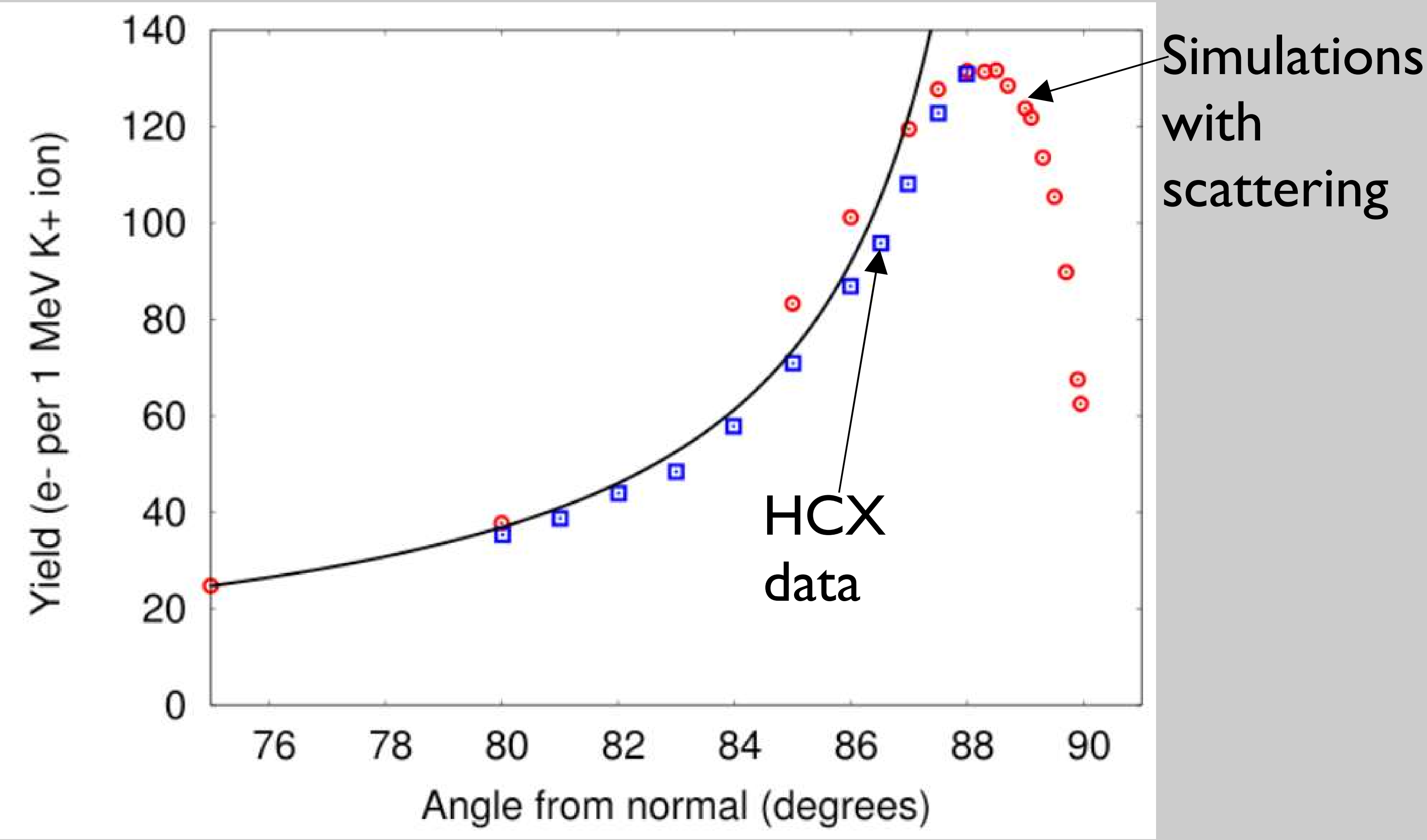

While SRIM is well known and well tested, it runs only on Windows and is extremely difficult to modify

- The SRIM source code (written in BASIC) is difficult to modify to add features or port to Unix/Linux or Mac OS.
- The CRANGE code from Berkeley has some of the same functionality, and the source code is openly available
- We have begun to modify CRANGE to include extra functionality and to benchmark CRANGE against SRIM

The CRANGE code compares well with SRIM in some regimes

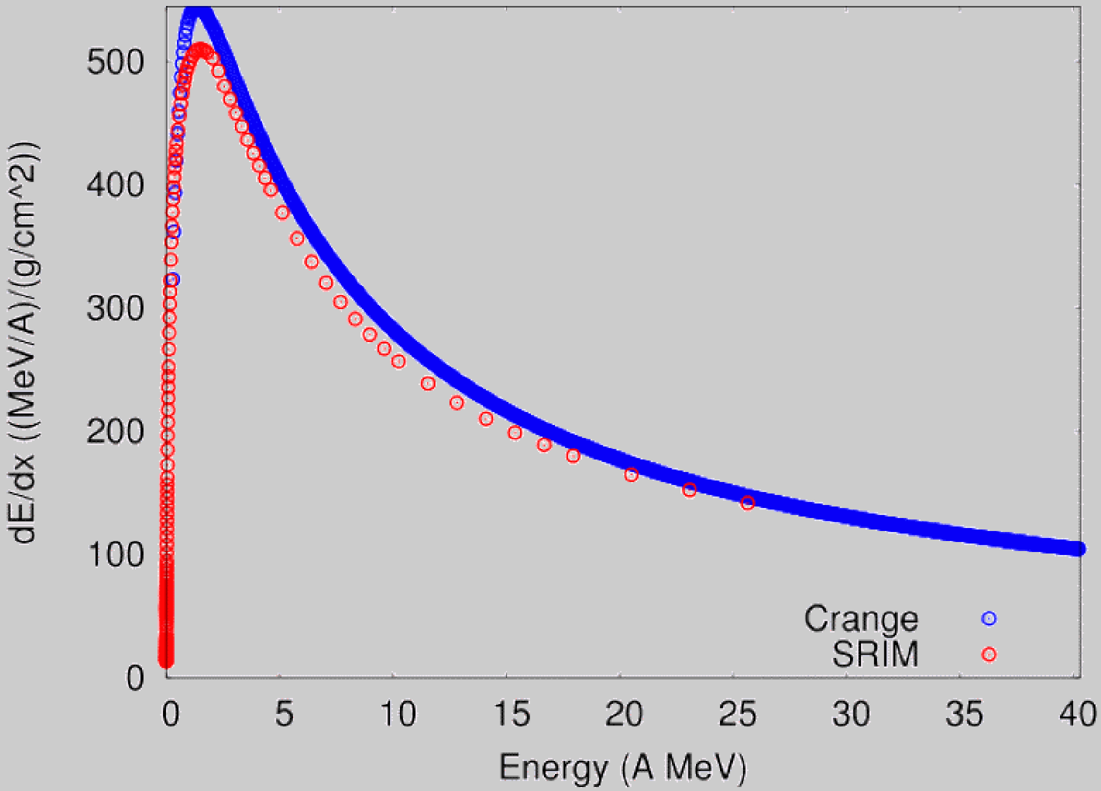

dE/dx v. E for 1.0 MeV K+ striking stainless steel

CRANGE provides dE/dx, range and an approximate ion-induced electron yield

Terminal — vim — 80x18

```
dipole.txcorp.com(3)% python
Python 2.2.3 (#2, Sep 10 2003, 14:42:34)
[GCC 3.2.3] on linux2
Type "help", "copyright", "credits" or "license" for more information.
>>> import crange
>>> z_p=1
>>> a_p=1
>>> ke_p=1.
>>> theta_p=88.
>>> print crange.SEY(ke_p,theta_p,z_p,a_p,target_name='Cu')
44
>>> z_p=19
>>> a_p=39
>>> ke_p=10.
>>> theta_p=0.
>>> print crange.SEY(ke_p,theta_p,z_p,a_p,target_name='SS-304')
33
```

SEY is based on model by Rothard, *et. al.*, and is proportional to dE/dx

Dramatic progress in fast ignition was made in a recent Japanese cone-focused experiment[1]

- A 500TW ignitor beam gave:
  - greater than 20% energy coupling (through electron transport) to the CD fuel; and
  - a 100-fold increase in DD neutron yield
  - The coupling efficiency may degrade in full-scale targets.

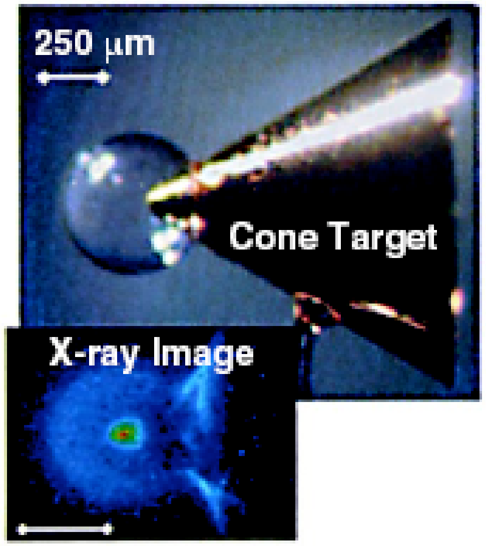

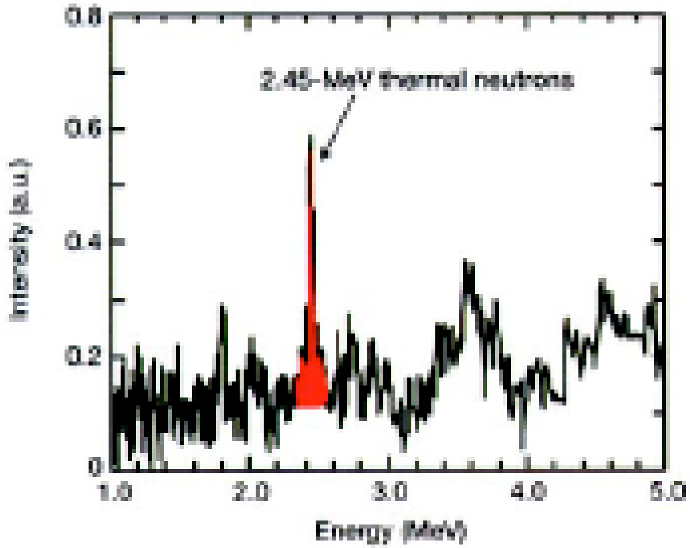

What is laser-electron coupling?

Does cone focus energy to fuel?

Do these results scale to ignition conditions?

[1]R. Kodama et al, Nature 418, P933 (2002).

Introduction to Fast Ignition

High Intensity Computational Physics Workshop

Pleasanton,CA

August 25,27

Max Tabak

Lawrence Livermore National Laboratory

This work was performed under the auspices of the U.S. Department of Energy by the University of California Lawrence Livermore National Laboratoryunder contract No. W-7405-Eng-48.

Technology advances had made innovative concepts possible: ultra-high brightness lasers may allow a fundamentally new method of igniting inertial fusion capsules

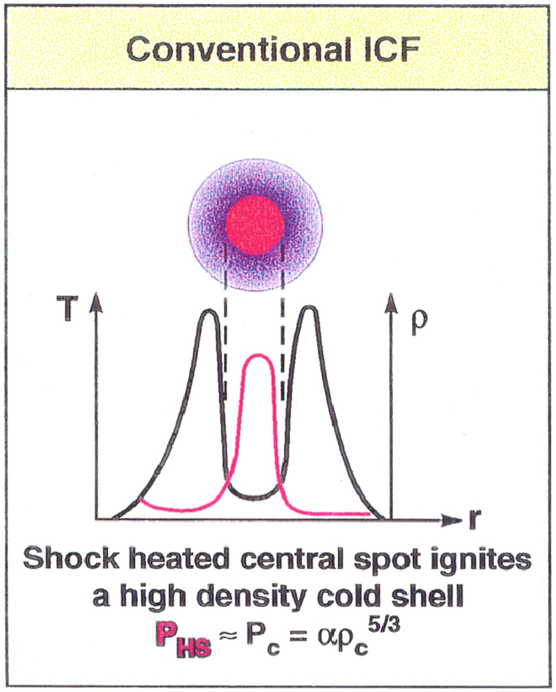

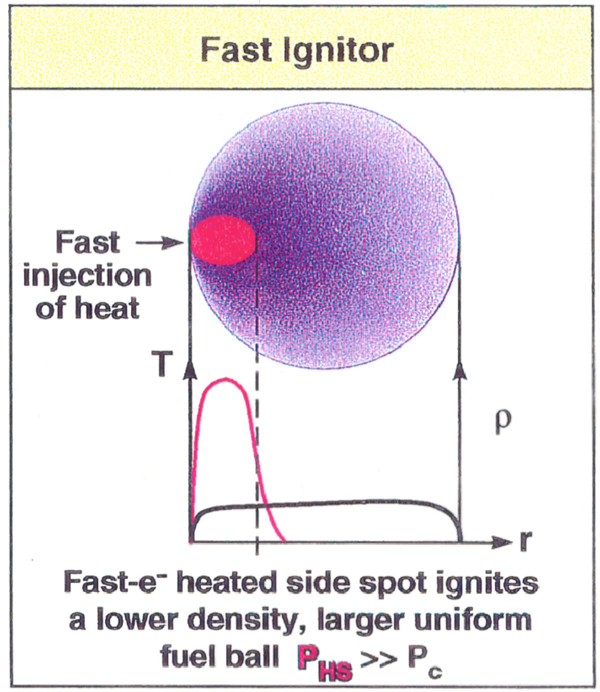

* Tabak, Hammer, Glinsky, Kruer, Wilks, Woodworth, Campbell, & Perry *Phys. Plasmas* **1**, 1626 (1994).
** H. Azechi et al., *Laser Part. Beams* **9**, 2 (1991).

Advantages of Fast Ignitor

- Fast Ignitor implosions are less stressing: (mix, convergence, ...)
- Lower $\rho \Rightarrow$ more mass to burn ($E_c \approx \alpha M_c \rho_c^{2/3}$) $\Rightarrow$ Higher Gain

Significant R&D is required to explore potential of this concept

Conflicting heating and compression requirements determine gain curves

Why is there a non-trivial energy requirement to achieve ignition and burn?

Little energy is required to assemble enough fuel to bootstrap and achieve high gain

E_{comp}µ M_c□$_c^{2/3}$
Vanishes for
□$_{c=}$ □$_{solid}$

Little energy is required to heat bootstrap region to ignition temperature

$E_{hotspot}$µ (□R)$_{HS}^{3}$ T/□$^{2}_{HS}$
Vanishes for □□>
for fixed □R

Want to maximize □M(/E_{tot}) including both energies
□ = □R /(□R +6)

What are possible relations between hotspot and mainfuel?

- Isochoric => uniform density(and huge pressure jump)
- Isobaric => uniform pressure(and low density hotspot)

What is effect of ignition dynamics on gain curves

- Is it legitimate to assume that both isochoric and isobaric models have the same ignition criteria? No!!

- Ignition means that hotspot reaches 30 keV where burn efficiency is calculated.
  - -Lower temp OK because □v becomes quite large
  - -But need "ignition time" to bootstrap to burn temperature
  - -Include power loss from hydro&electron conduction

	pressure	radius	Stagnation time
isobaric	Stagnation pressure	Main fuel radius	100's of ps
isochoric	Ignition pressure	Hotspot radius	~ 10 ps

- Atzeni has charted Fast Ignition requirements

Atzeni,et.al., have found ignition windows and gain curves including loss terms

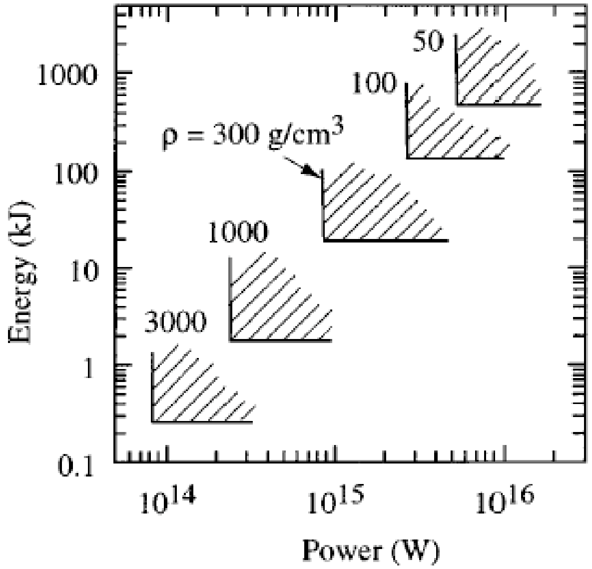

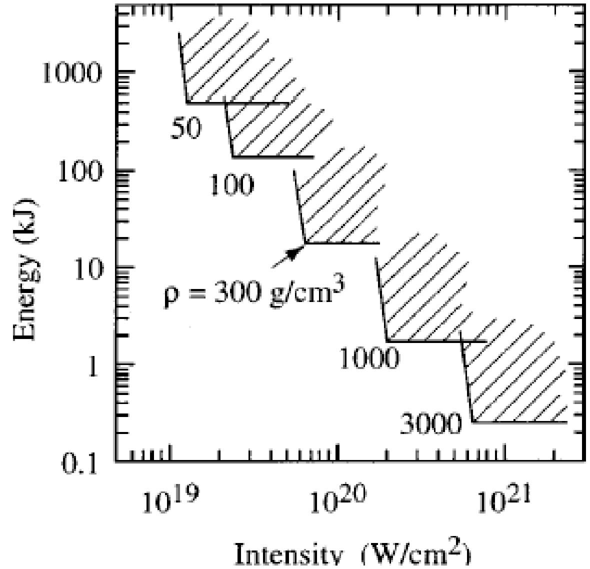

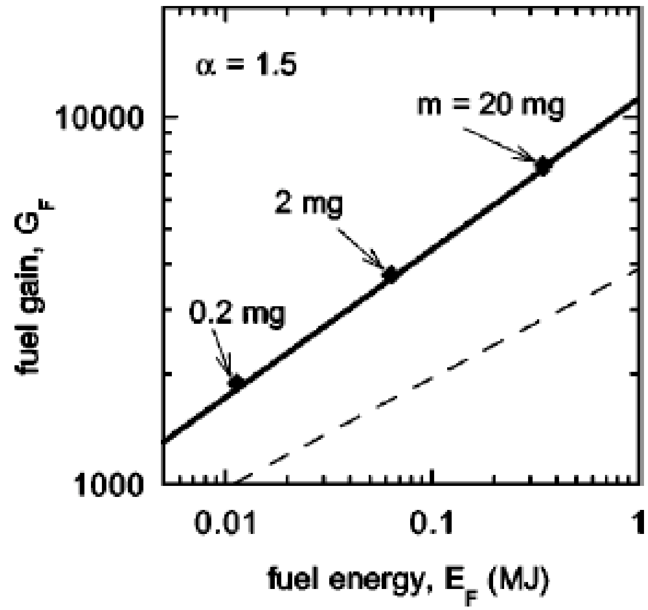

Ignition criteria:
T=12 keV, ρR=0.5 gm/cm^2
E_{ign}(kJ)=140(100 gm/cc/ρ)$^{1.85}$

How do the gain curves depend on the minimum radius of the ignition spot?

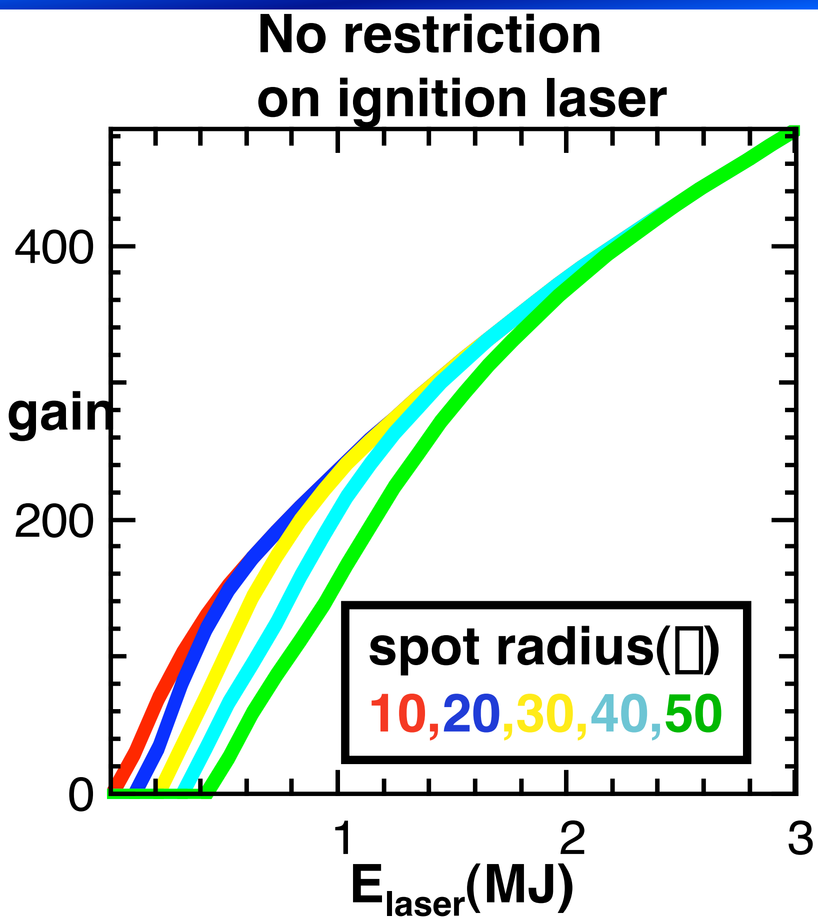

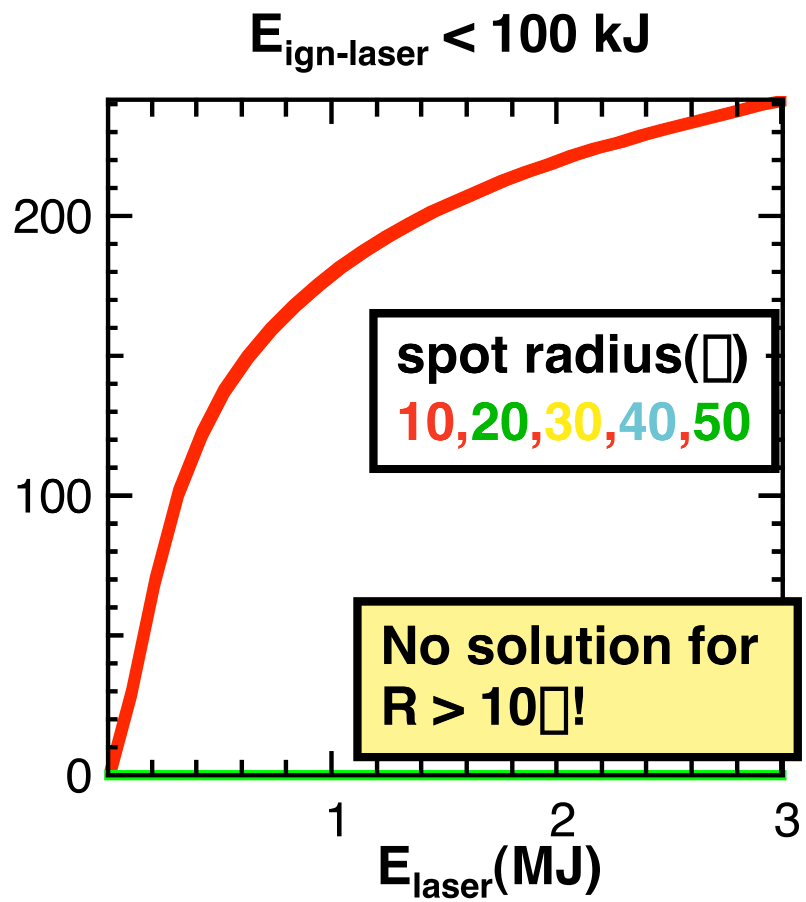

Current experiments show e⁻ spreading to 20□ spot from much smaller laser spot!

The system gain depends strongly coupling efficiency from laser to ignition region

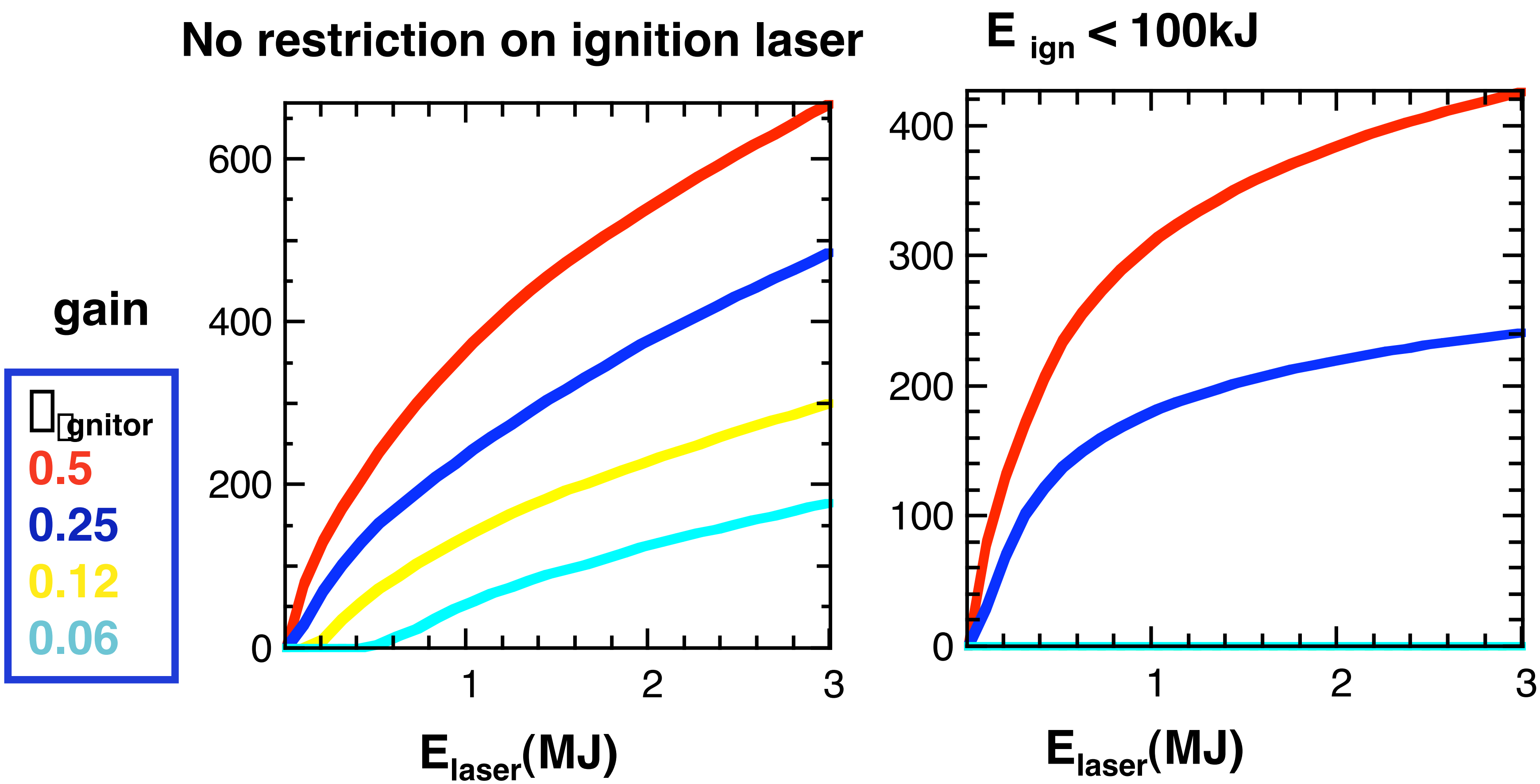

The system gain depends on the range of the relativistic electrons

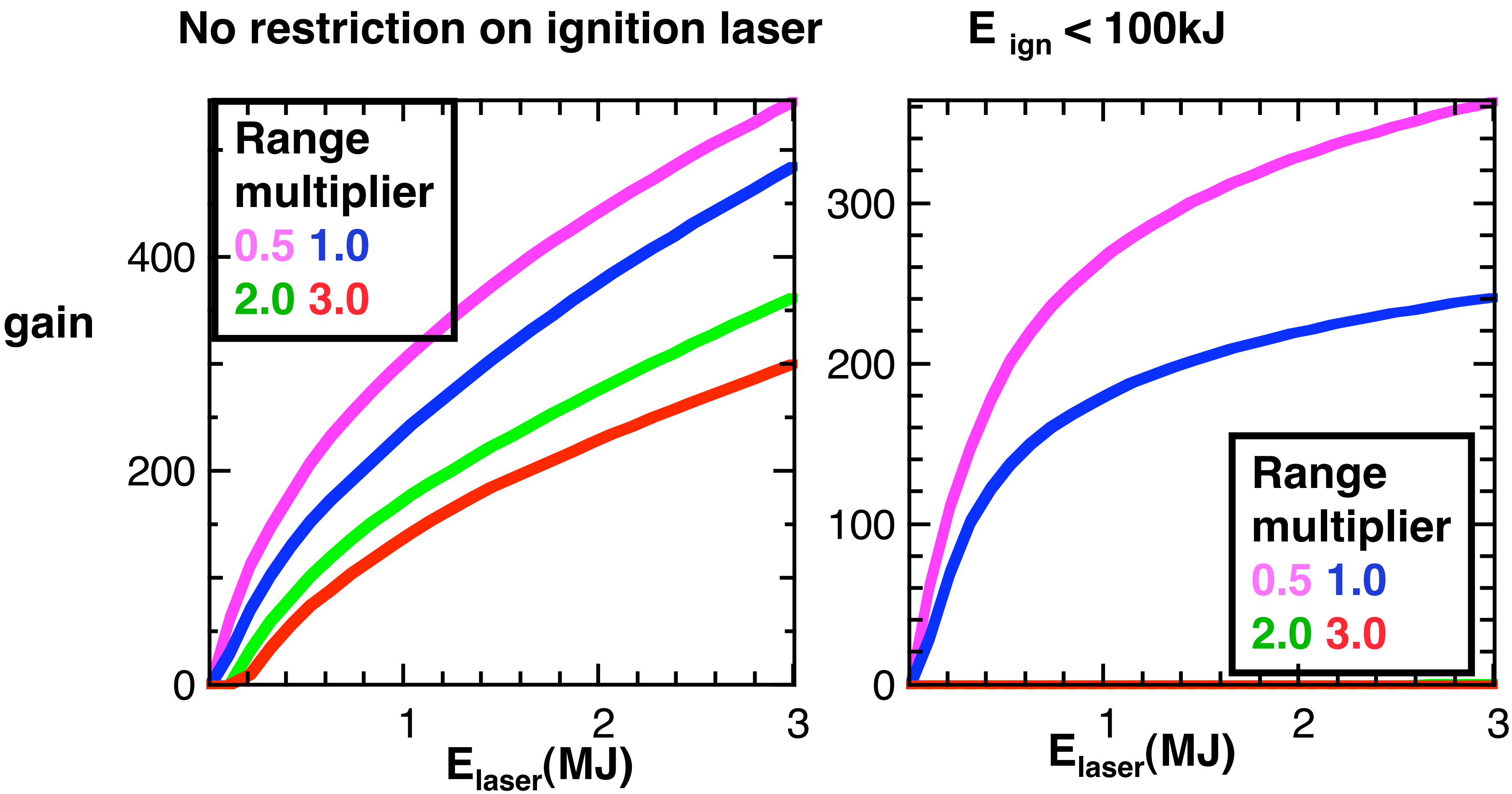

Nominal range(gm/cm²) = 0.6 T(MeV)
T=(I/1.2*10¹⁹W/cm²)^1/2

What design and physics issues will determine these gain curves?

•How to assemble fuel

-Efficiently produce high density fuel without low density center

•How to couple energy to fuel

-Laser transport(get energy close to fuel)

-Filamentation and hole boring(transport can spread and absorb laser energy

-Cone focus geometries

-Asymmetric implosions

-Other ideas

-Laser plasma interaction and coupling efficiency(make hot e^- with what phase space distribution)

-Electron transport(deliver energy from critical surface to fuel)

-Multiple scattering plasma instabilities

-Proton generation and transport(efficiency, brightness, shorting out, multiple scattering, long pulse behavior)

Several schemes to shorten distance between critical density and the ignition region were explored

The compressed fuel is produced by an implosion
The critical surface has radius ≈ initial radius ~ mm
How can we hit 30μm spot from this distance?

Ponderomotive holeboring ,relativistic transparency and/or cone focus geometry are possible routes to reduce this distance

P=2I/c for mirror

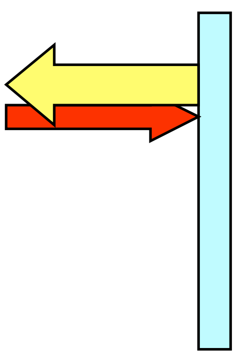

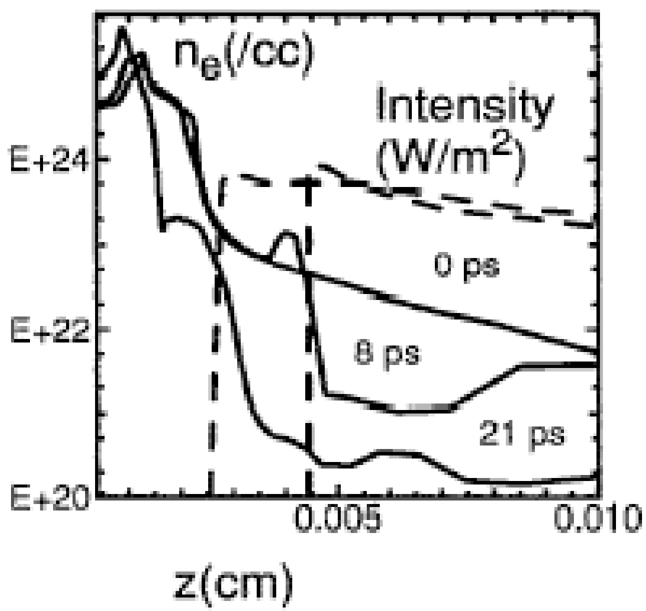

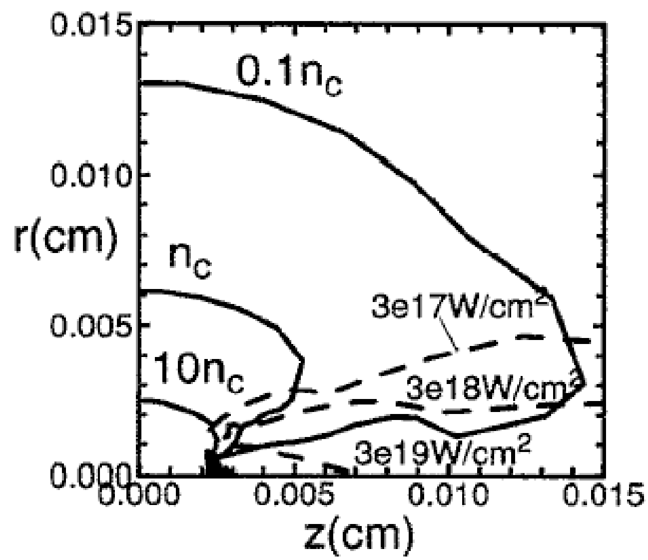

As the sole technique to reduce the distance between critical and high density, hole boring is probably insufficient

Aberrated beams likely to filament

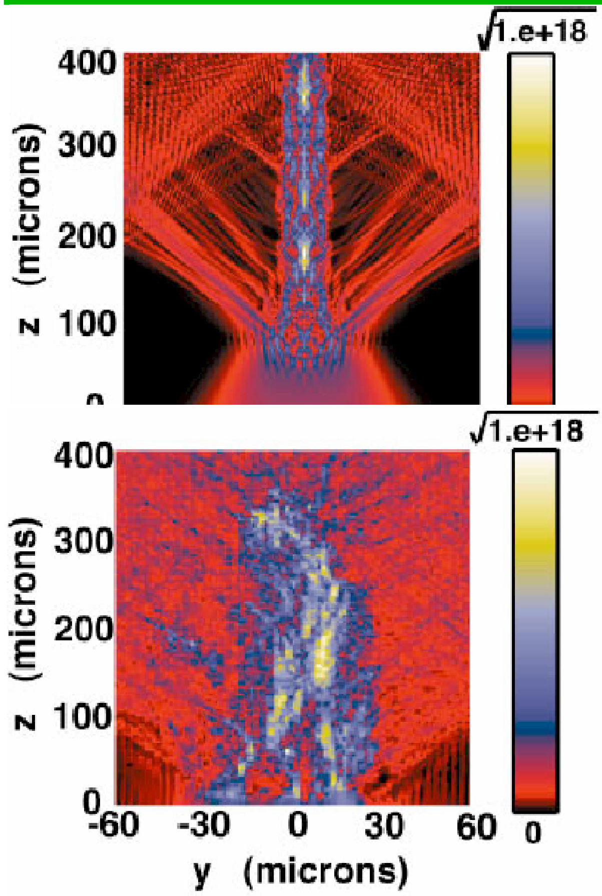

Large channel aspect ratio will lead to significant losses on walls

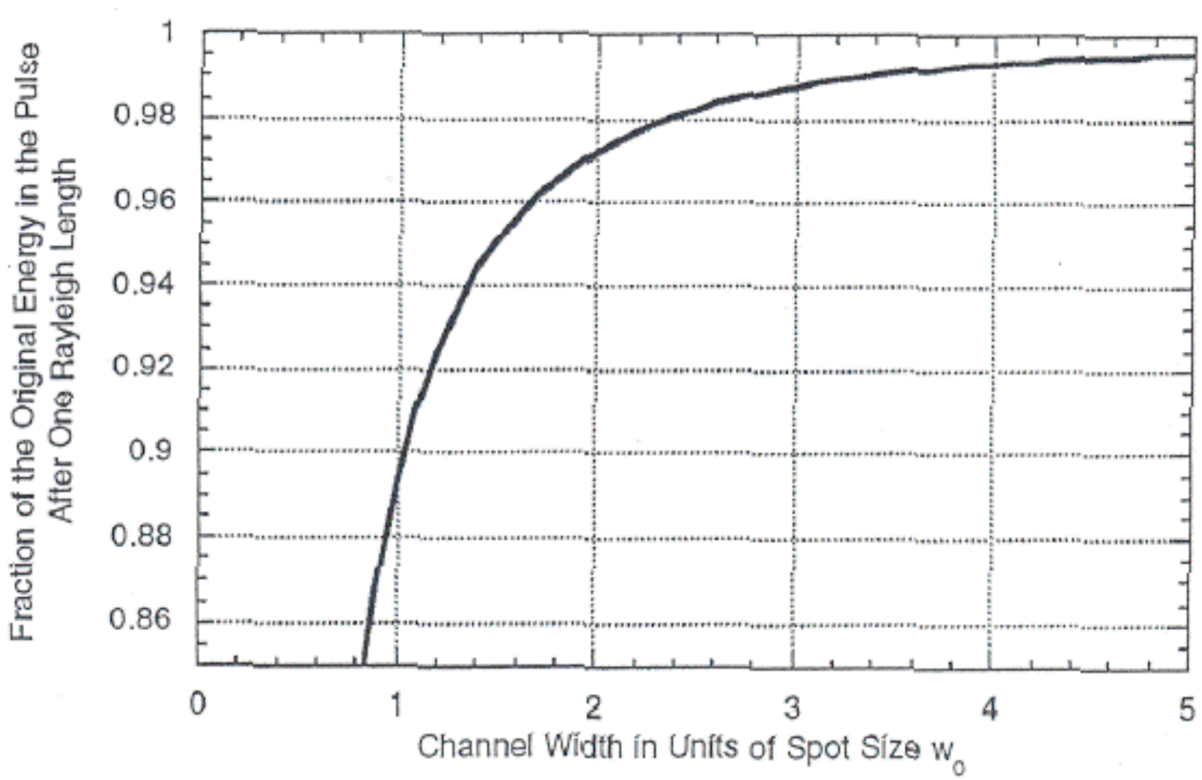

No experiment has demonstrated propagation through mm's of plasma with good efficiency. Still possible for smaller plasmas.

Energy spreads even in small prepulse plasmas when driven hard

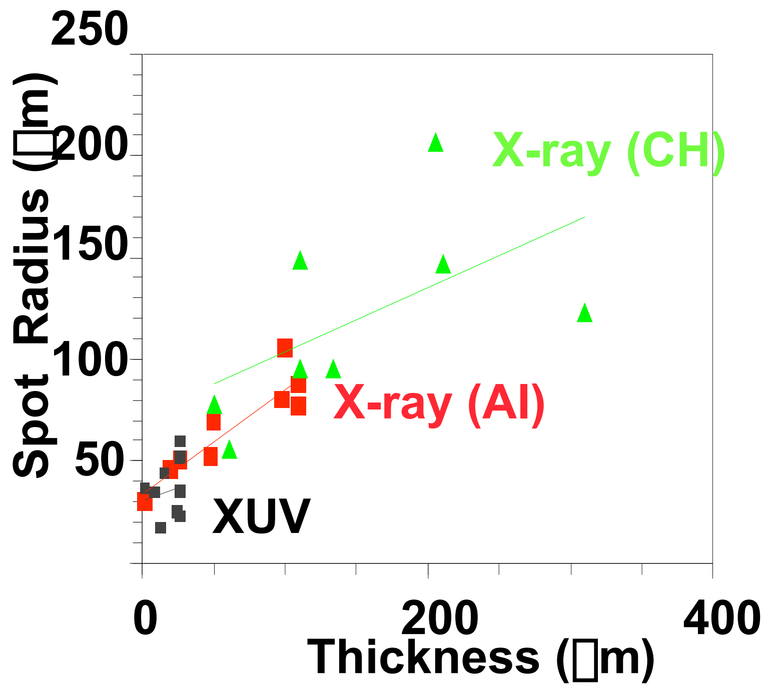

Laser spot is <10□
with broad wings

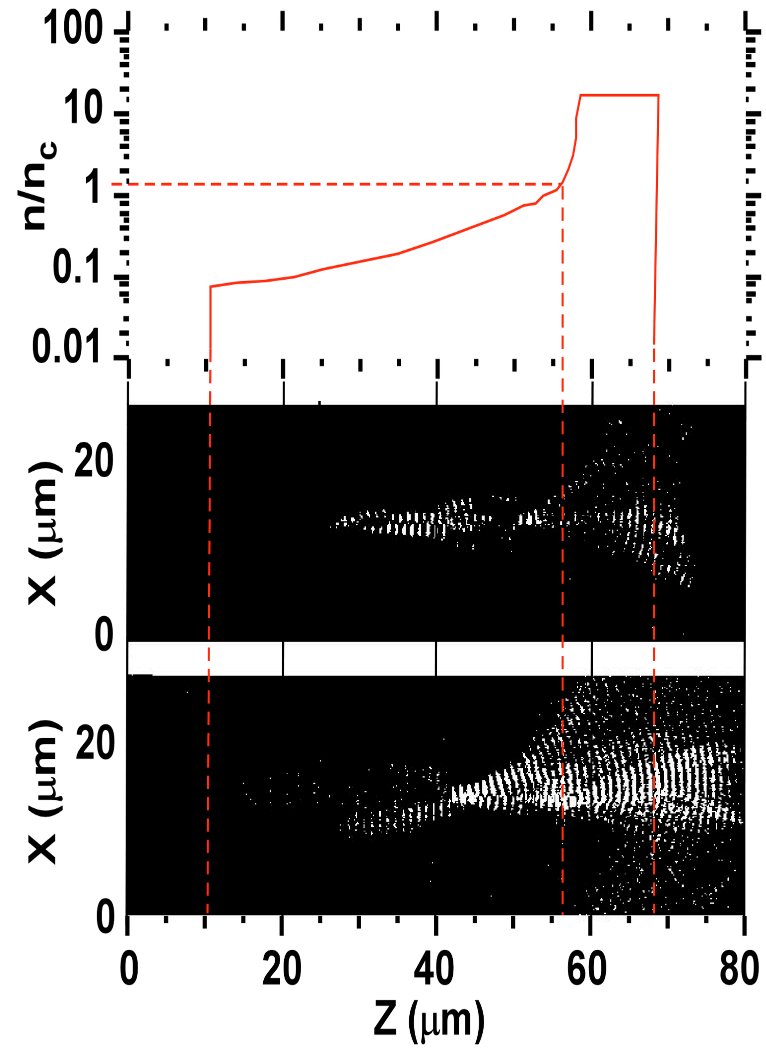

Cone focus designs provide access to assembled core

A NIF-like scheme

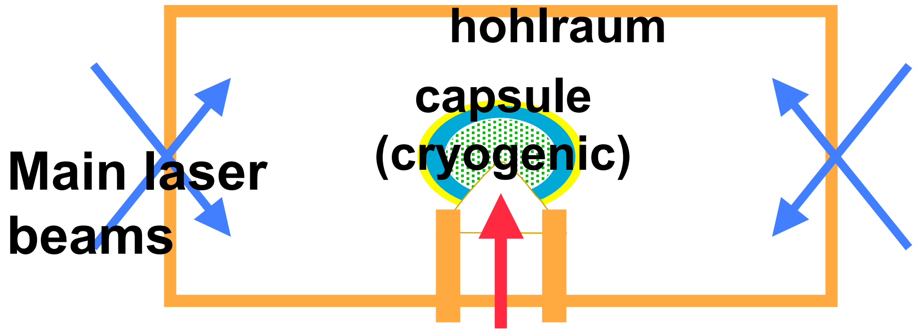

Ignitor beam(s)
(short pulse)

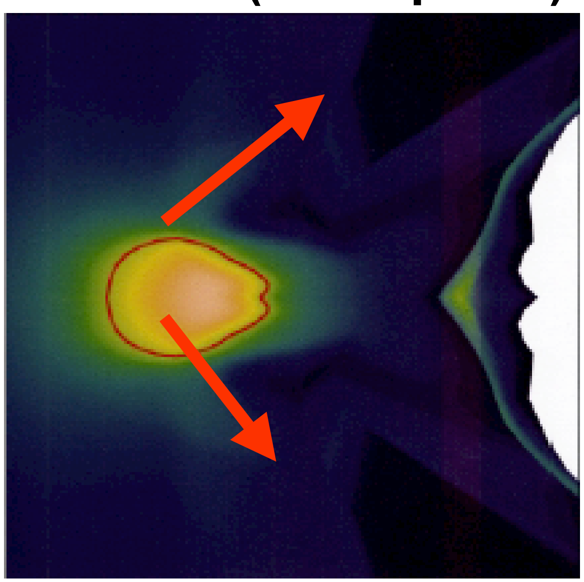

Hydro issues:
- Entrainment of cone material
- Produce imploded core without central void and good efficiency

Light coupling issues
- Collect and focus light from large area
- How does light scatter from cone?
- How will light scatter in prepulse plasma?
- What is nature of hot electrons produced?

Z3 shows scattered electron and photon distributions

- 2D simulations have experiment scale size and duration
- A 10^{19} W/cm^2 laser incident on a 16 n_c plasma (shown by white lines) at a 30° angle of incidence.
- Reflected light will be used in more complex geometries
- (z,x) phase space plot of electrons with energies > 5 MeV.

What is behavior over 10's of ps?

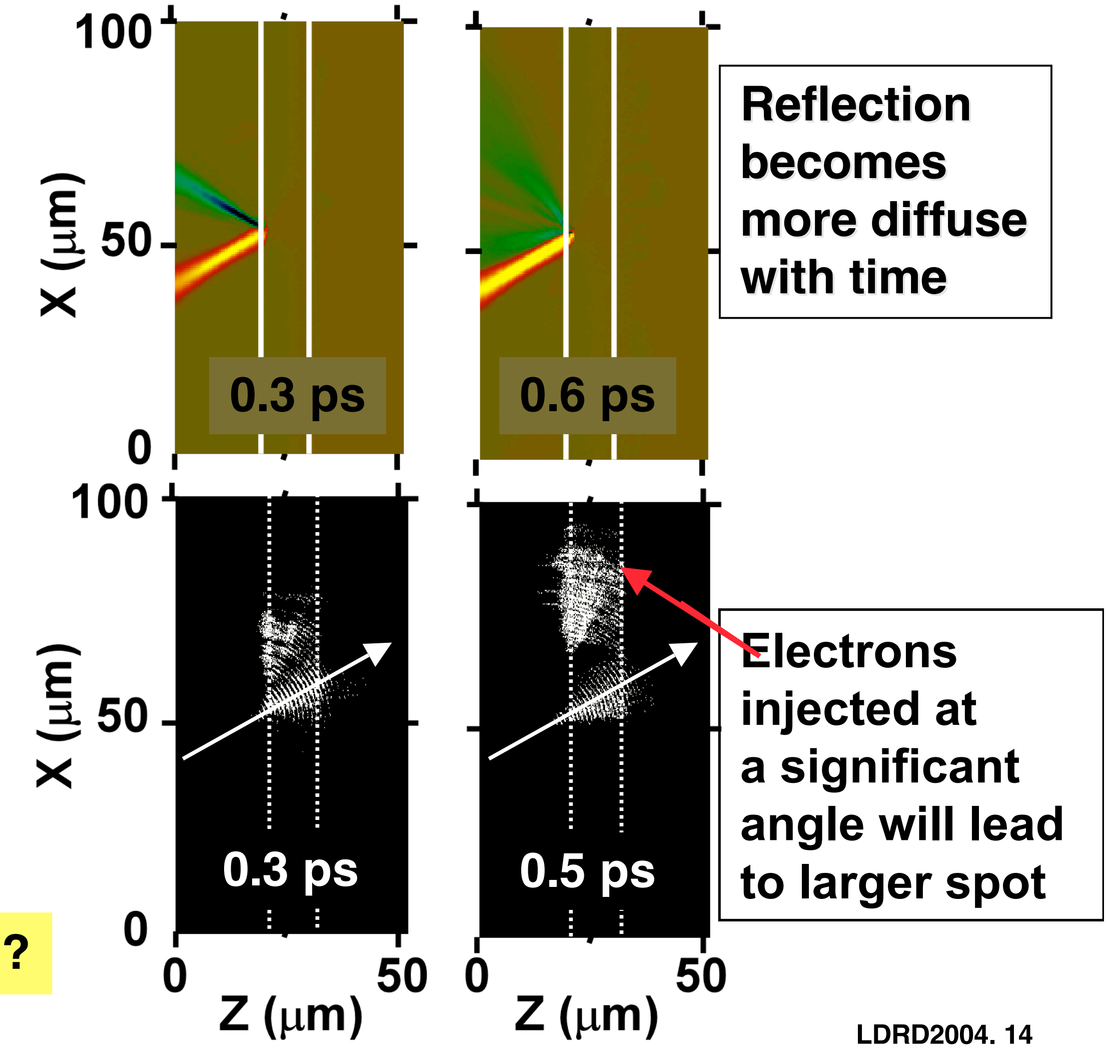

High intensity light can couple efficiently to dense matter via collisionless mechanisms

Two mechanisms:

If E points into plasma,

- oscillatory excursion > plasma scale height
- Electron doesn't feel decelerating field
- 'Not-so-resonant resonant absorption"

If large E parallel to plasma

- B field will rotate motion into plasma
- Electron in vacuum would have figure 8
- Absorption increases with intensity
- "J x B heating"

Rippling of surface increases absorption

PIC simulations see absorption 40-50%

- Sometimes 90% with holeboring at high I

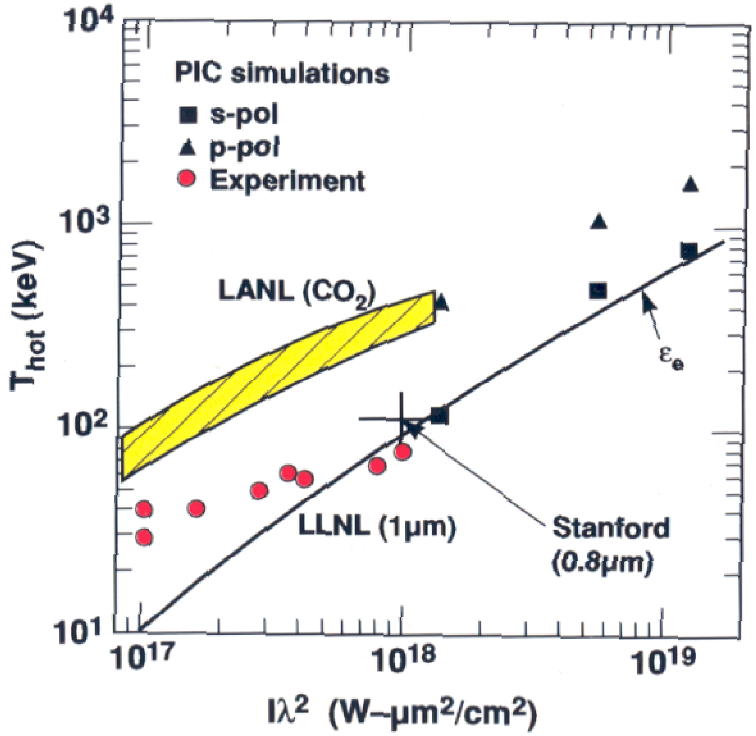

Integrated results from ILE,Osaka are encouraging

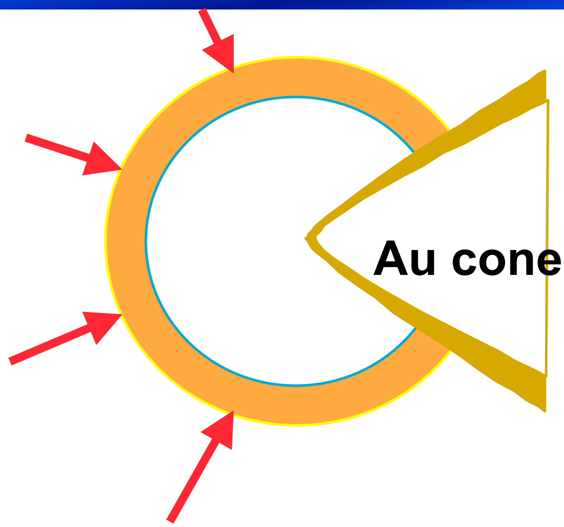

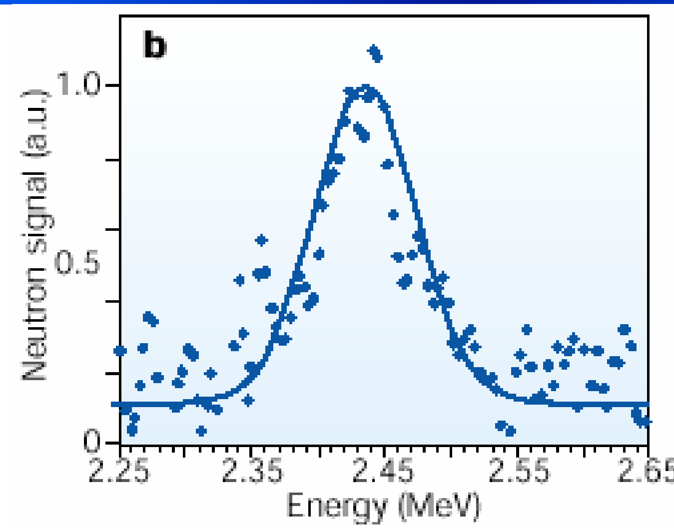

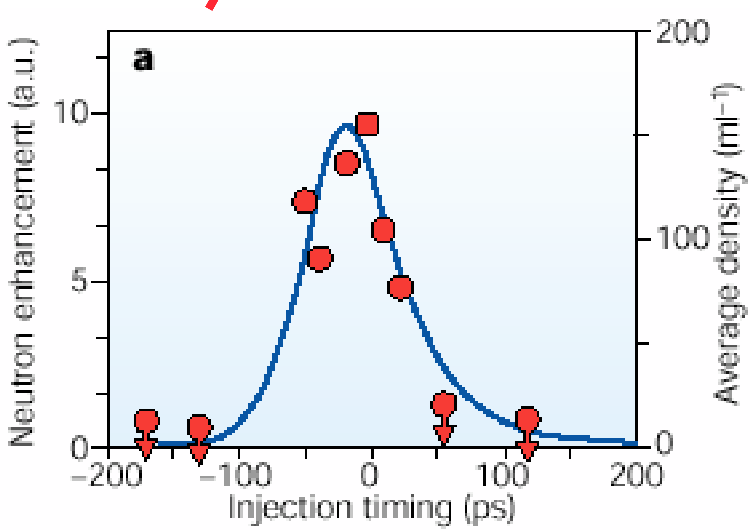

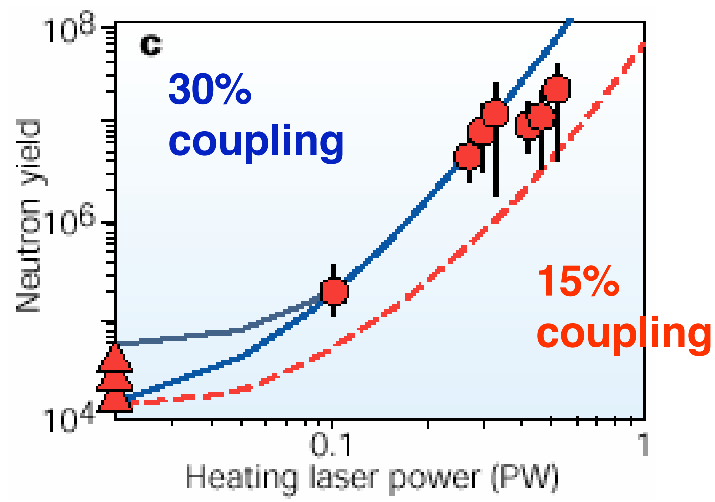

Infer 15-25% coupling efficiency from laser to compressed fuel!

Can cones concentrate short pulse energy for Fast Ignition and radiography applications ?

Suprathermal electron density

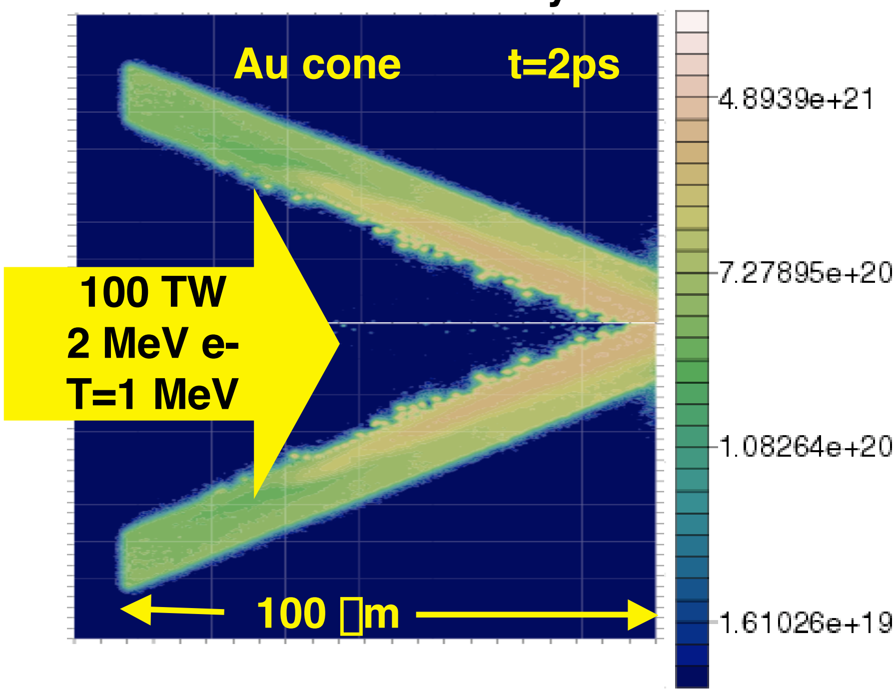

- Transport calculation in dense collisional plasma

- By concentrating electrons from a large area, we can break the correlation between electron intensity and particle range

- Need to include LPI,prepulse, laser transport, effect of plasma instabilities, and self consistent charge state(EOS, conductivity and scattering)

- This calculation only transports ~10% of electron energy to end
  - Why is experiment so much better?

The transport of electrons is controlled by multiple scattering, effects of macroscopic E&B fields and possibly by microinstabilities

Scattering affects range and angular distribution

dE/dx ~ Z_{eff}^2 n_e/□^{2} *Log □ => for relativistic e^- □(□x) ~ E

Deutsch has suggested $Z_{eff} \neq 1$

Hots are so dense and fast that multiple electrons can scatter before shielding electrons move

<□^{2}> ~ Z_{eff}^2 □(□x) /$L_{rad}p^2$

Charges and currents produced by the laser are so large that nothing can move without significant neutralization

Power = I V or 10^{15}W = 1 MV * 10^9A (Alfven current ~ 5*10^4A)

Curl B = j*□$_0$ => B=I □$_0$ /(2□r) or for r=30microns B=6.7 10^{10} gauss

Energy=QV or 10^5J = 1 MV * 0.1 Coulombs

Div E=□/□$_0$ => E= Q/(□$_0$2□r^2) or for r=30microns E= 9 10^{16} V/m

In some simulations microinstabilities(filamentation,2 stream) show stopping Power ~10^4 classical, possibly not seen in normal density experiments

Protons can be accelerated directly with ponderomotive pressure or via a virtual cathode at the rear surface

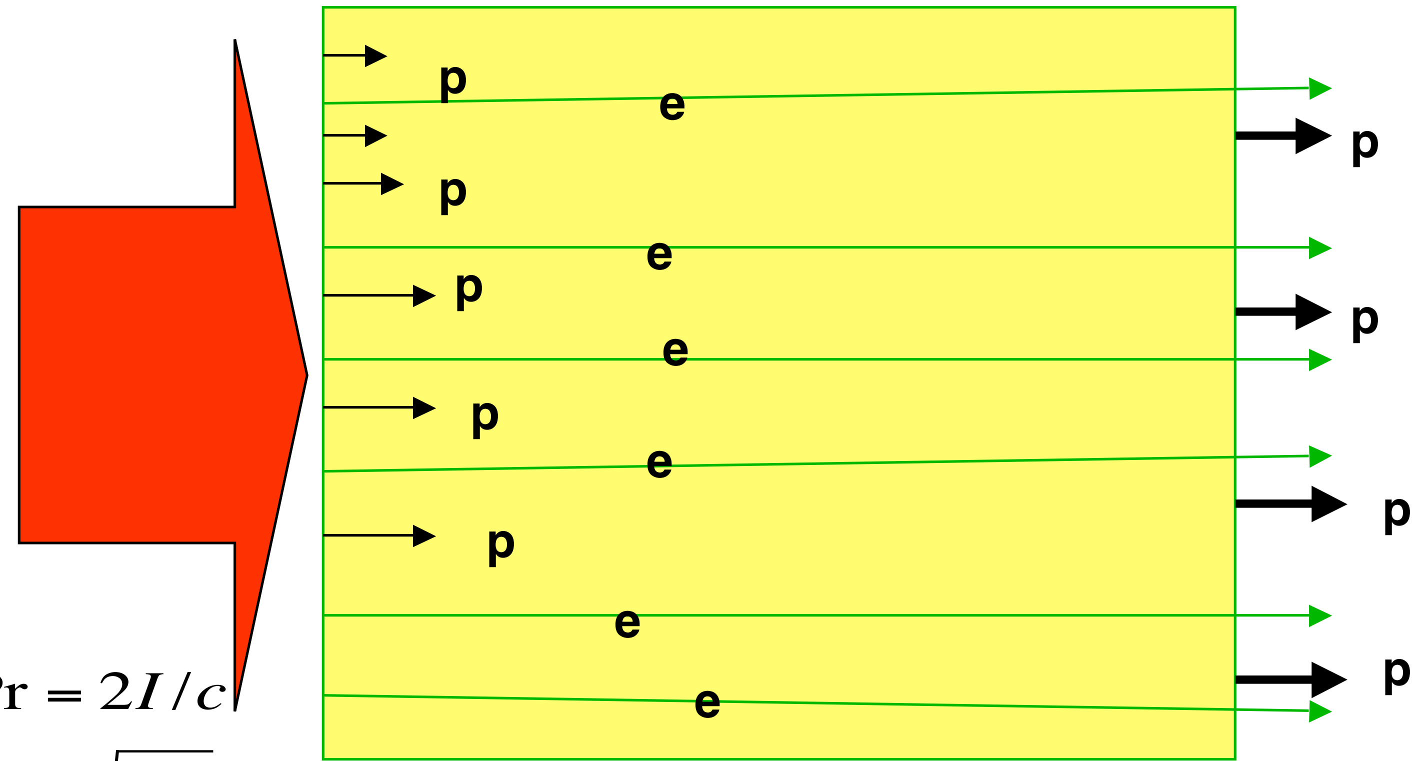

Isothermal expansion driven by hot electrons

□ □1-25%
Maybe 50% in old CO_2 exp

$$\Pr = 2I/c$$

$$u = \sqrt{\frac{\Pr}{2\rho}}$$

$$\eta = \frac{u\Pr}{I}$$

< 3% @10^{19}W/cm^2

Amazingly bright source

Because protons are more massive than electrons, ballistic focusing schemes are considered

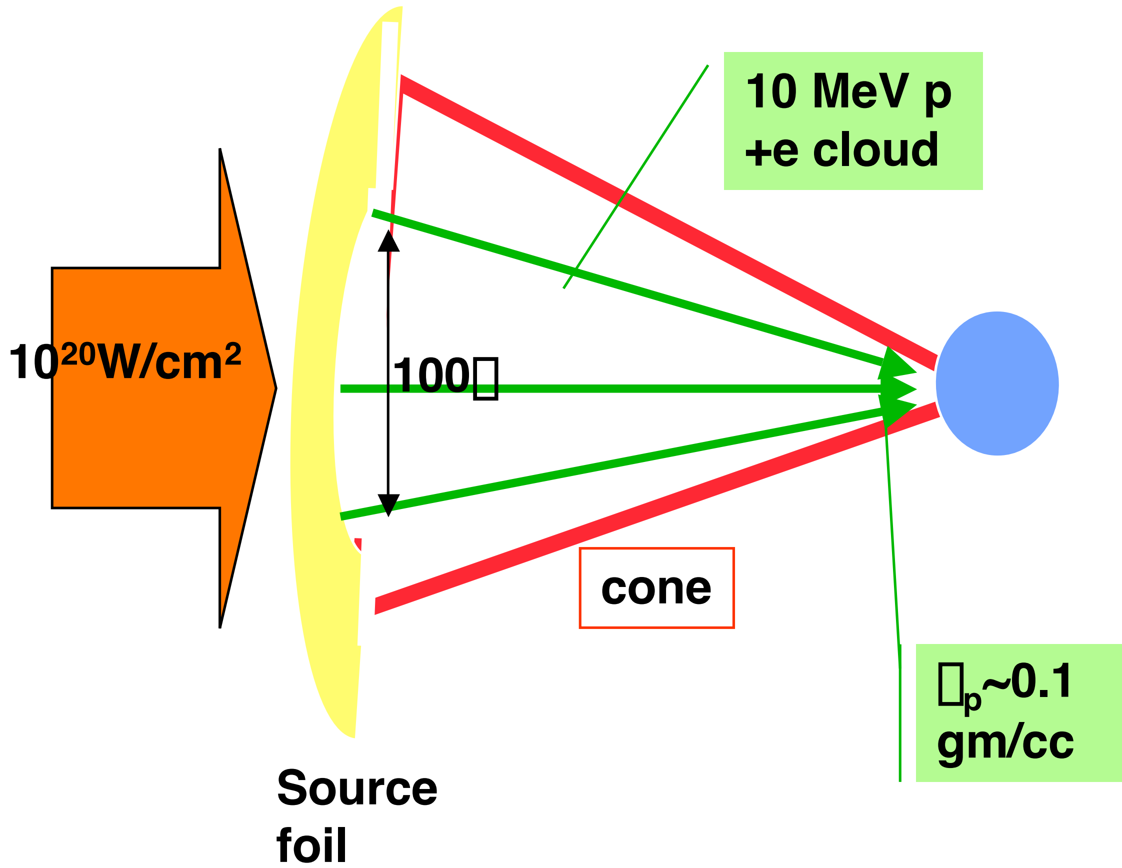

Issues:

Focusing when high beam pressure

Efficiency

Compression leakage shorts out foil?

Foil quality in long pulse

Anomalous stopping due to micro-instabilities has been investigated with PIC codes

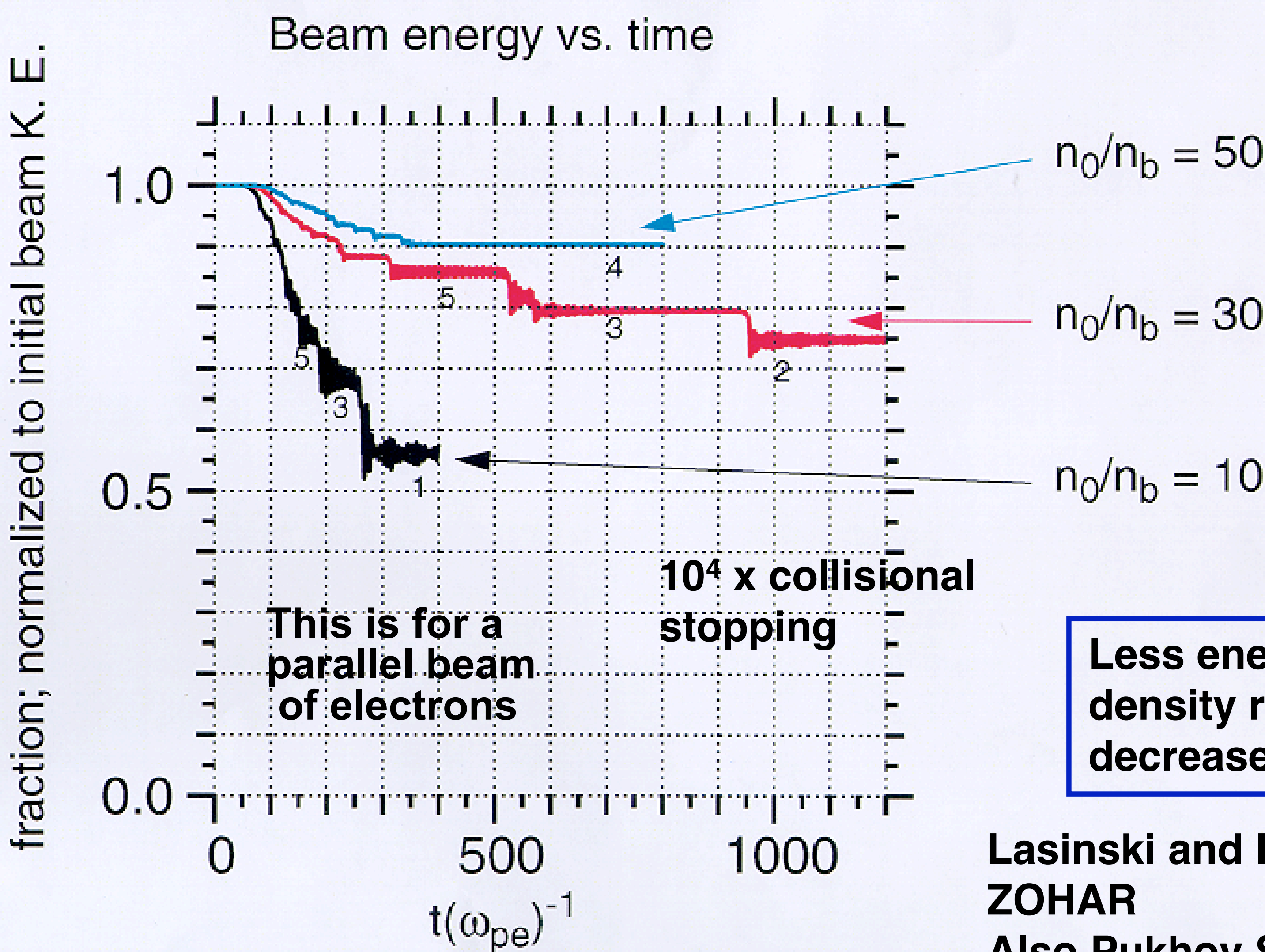

Less energy is lost as density ratio decreases

Lasinski and Langdon
ZOHAR
Also Pukhov,Sentoku…

Analytic models show that microinstabilities are suppressed by beam temperature and large n_e/n_b(but by different amounts)

Weibel instability threshold

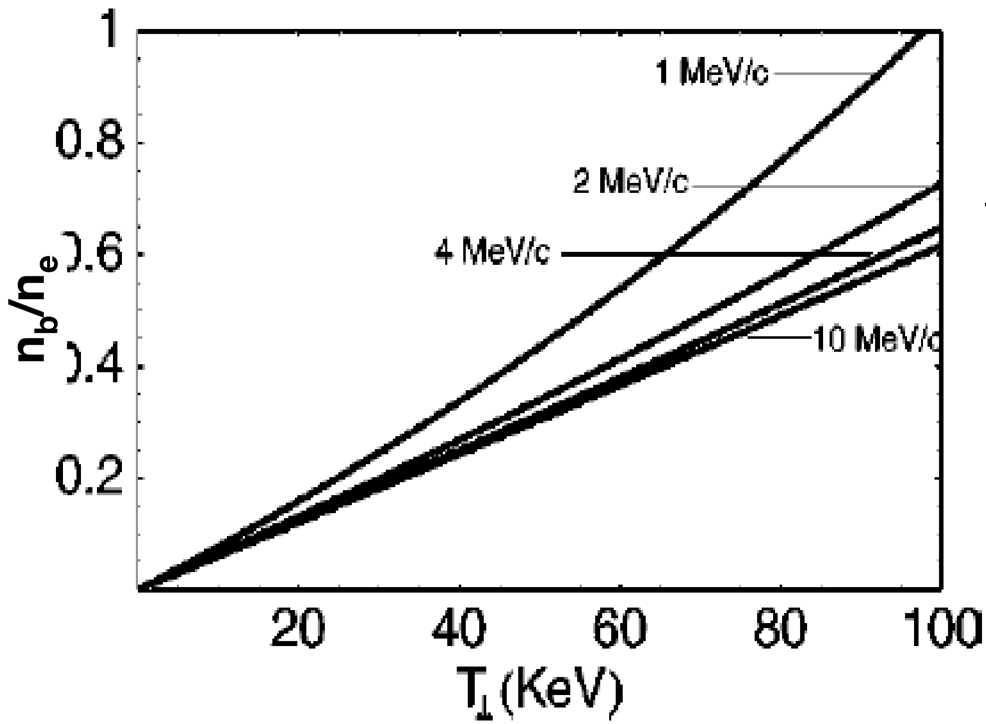

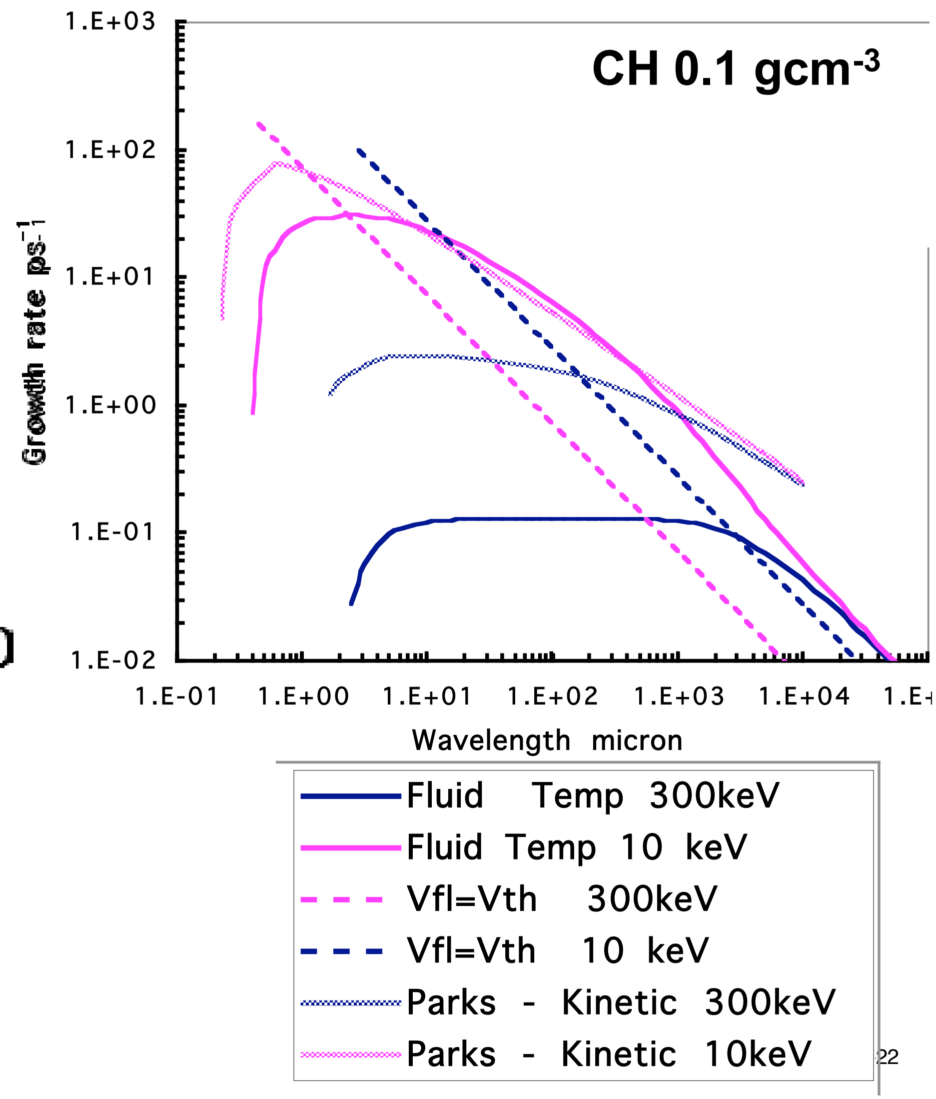

Uses waterbag distribution:
Fixed longitudinal momentum with tophat transverse distribution

Silva,et.al.

Ion acceleration by sudden creation of hot electrons has higher field and greater power in steeper initial gradients.

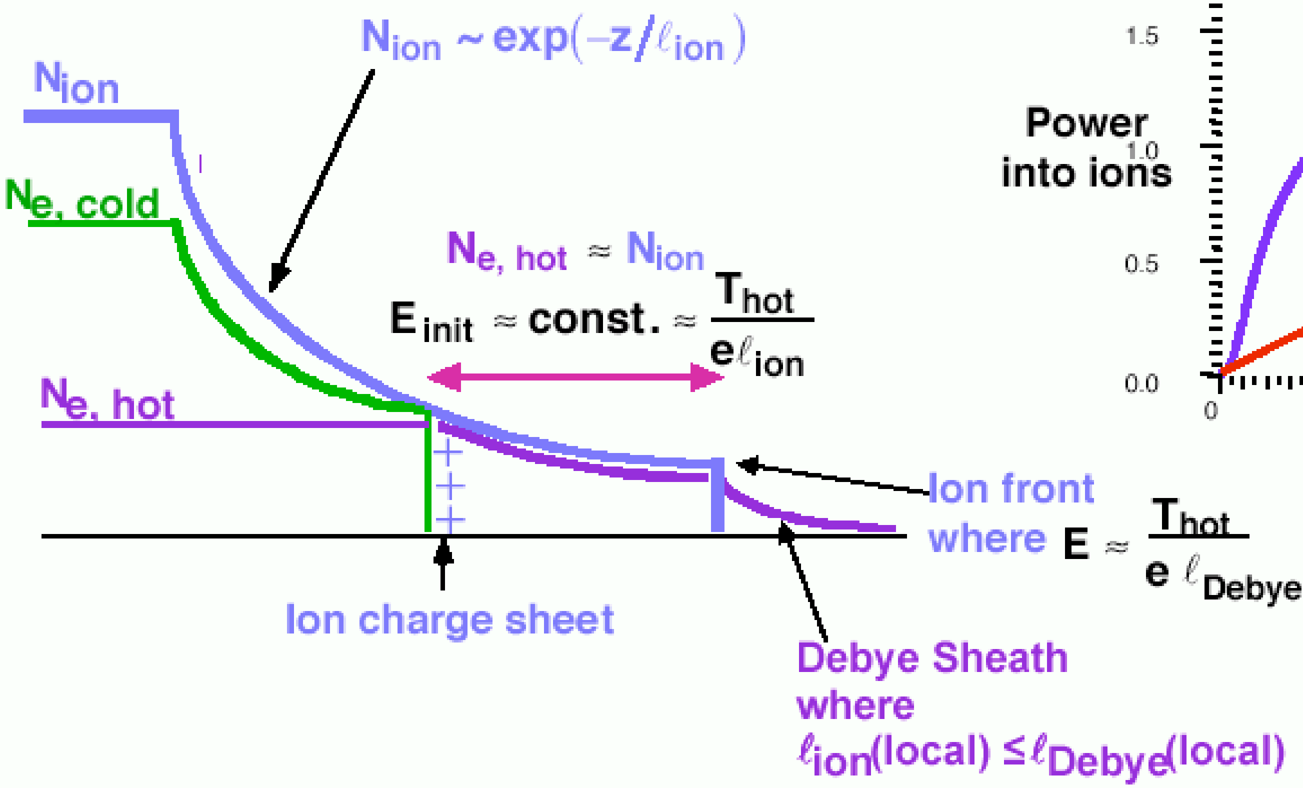

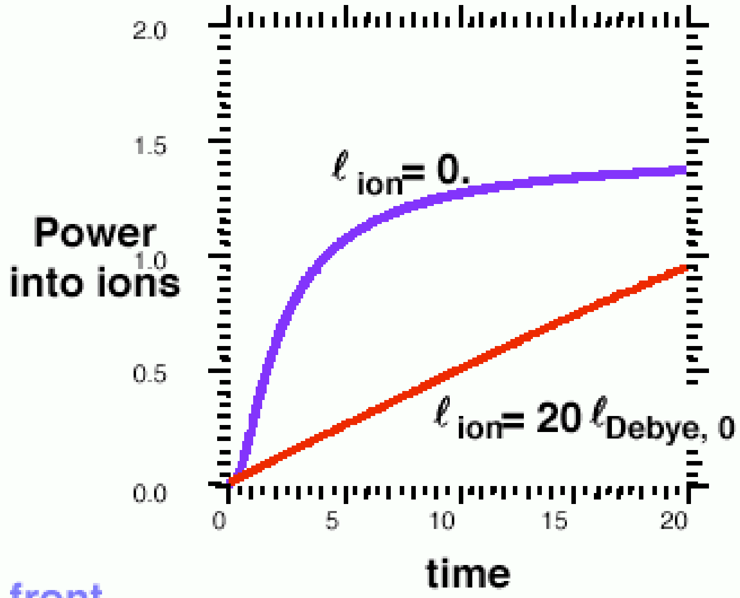

Ion acceleration continues until hots are energetically depleted — by dE/dx or by accelerating ions — in a few ps.

sph_APS99_ionschem

The energy and density of the hot electrons set the scales of things in the physics.

1. Length: Debye length of hots

$$\ell_0 \approx \sqrt{\frac{T_{hot}}{4\pi e^2 N_{hot}}} = 2.4\,\mu\text{m} \left(\frac{T_{hot}}{1\text{MeV}}\right)^{1/2} \left(\frac{N_{hot}}{10^{19}}\right)^{-1/2}$$

2. Velocity: ("sound" speed)

$$c_s \approx \sqrt{\frac{T_{hot}}{m_{ion}}} = 9.8\ \mu\text{m ps}^{-1} \left(\frac{T_{hot}}{1\text{MeV}}\right)^{1/2} \left(\frac{m_{ion}}{m_p}\right)^{1/2}$$

3. Time:

$$\tau \approx \sqrt{\frac{\ell_0^2 m_{ion}}{T_{hot}}} = 0.24\ \text{ps} \left(\frac{N_{hot}}{10^{19}}\right)^{-1/2}$$

4. Sheath Electric field:

$$E \sim \frac{T_{hot}}{e\ell_0} = \frac{\text{MegaVolts}}{\text{microns}}$$

Ion acceleration mechanism is a new variation on an old theme: sheath field from hot electrons.

1. Laser <u>suddenly</u> creates large number of hot electrons:

$$\langle E_e \rangle \sim T_{hot} \sim U_{ponderomotive} \sim \text{few MeV} \quad \text{at } I\lambda^2 \sim 10^{20}\ \text{W cm}^{-2}\ \mu\text{m}^2$$

$$\#\ \text{hots} \sim \frac{\eta E_{laser}}{\langle E_e \rangle} \sim \frac{200\ \text{J}}{\text{few MeV}} \sim \text{several} \leftrightarrow 10^{14}$$

2. Hots <u>fly through</u> "thin" (~1mm x 1mm x 100 μm) targets; a small fraction escape, charging target to $eV_{target} > \langle E_e \rangle$

3. Hots circulate in and near target, set up sheath and sheath electrostatic field (>> charge-up field): ie Colds sag inward isolating a + surface charge of ions whose field contains the sheath of hots.

$$N_{e,\ hot} \sim \frac{\text{several } 10^{14}}{10^{-4}\ \text{cm}^3} \sim \text{several } 10^{18}\ \text{cm}^{-3}$$

4. Sheath field accelerates the ions.

After 10 years, there are still no showstoppers apparent for Fast Ignition

- Coupling efficiency appears adequate at 15-25%

- Lots of challenges remain

    - Improved implosion and ignition schemes
        - Reduce distance between critical high density
        - Improve efficiency of producing compressed core
        - Optimal energy deposition profile for short pulse

    - Develop detailed understanding of electron transport

    - Focus ion beams to high intensity and produce them with good efficiency

    - Understand scaling to high energy and long pulses

    - Need reactor scenario utilizing Fast Ignition

Early experiments showed that moderate intensity beams could penetrate 100’s of of n_c plasma with thermal filamentation

I_{peak}=5 10^{15}W/cm^2
gaussian pulse

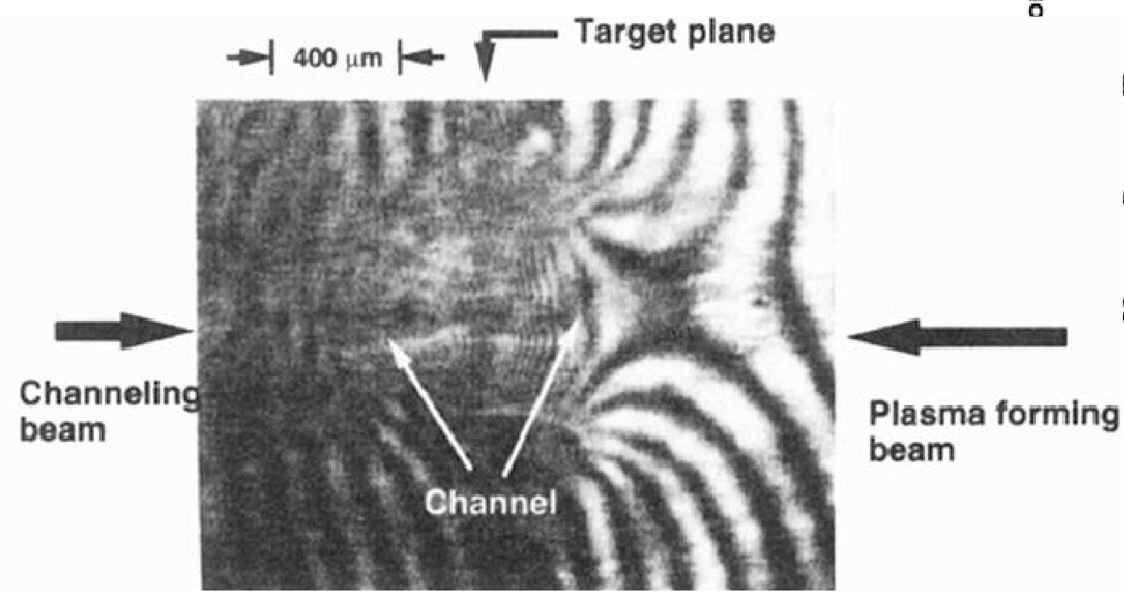

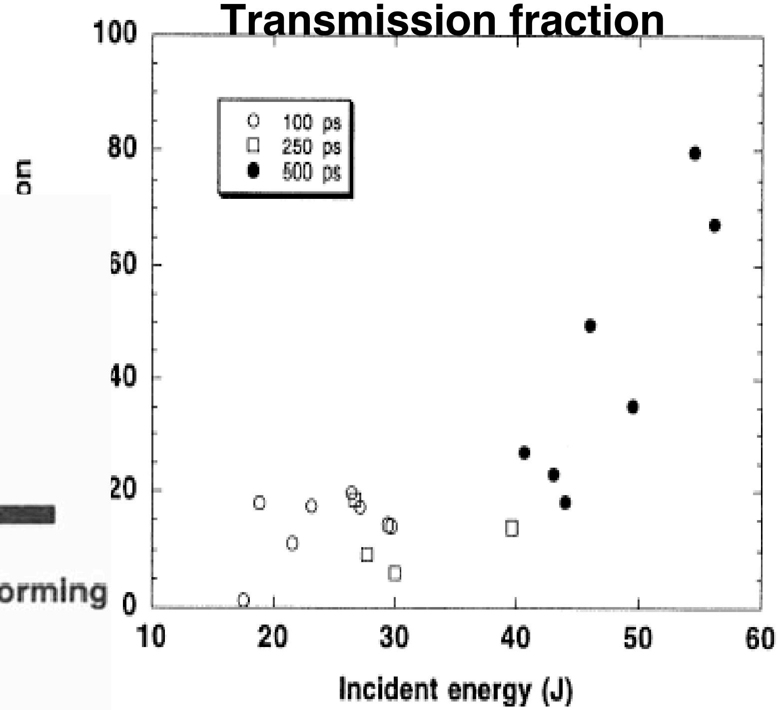

n_e(peak)=0.3n_c

Young,et.al.

But, coronal plasmas are have mm extent
Holeboring pulse took 100’s of ps even for 500 plasma
Transmitted pulse may be filamented

Are there any ideas to reduce the central low density region in implosion?

Low density region halves □R

□ □ down 30% and ignition more difficult

Reduce central entropy by allowing mass to escape through aneurysm

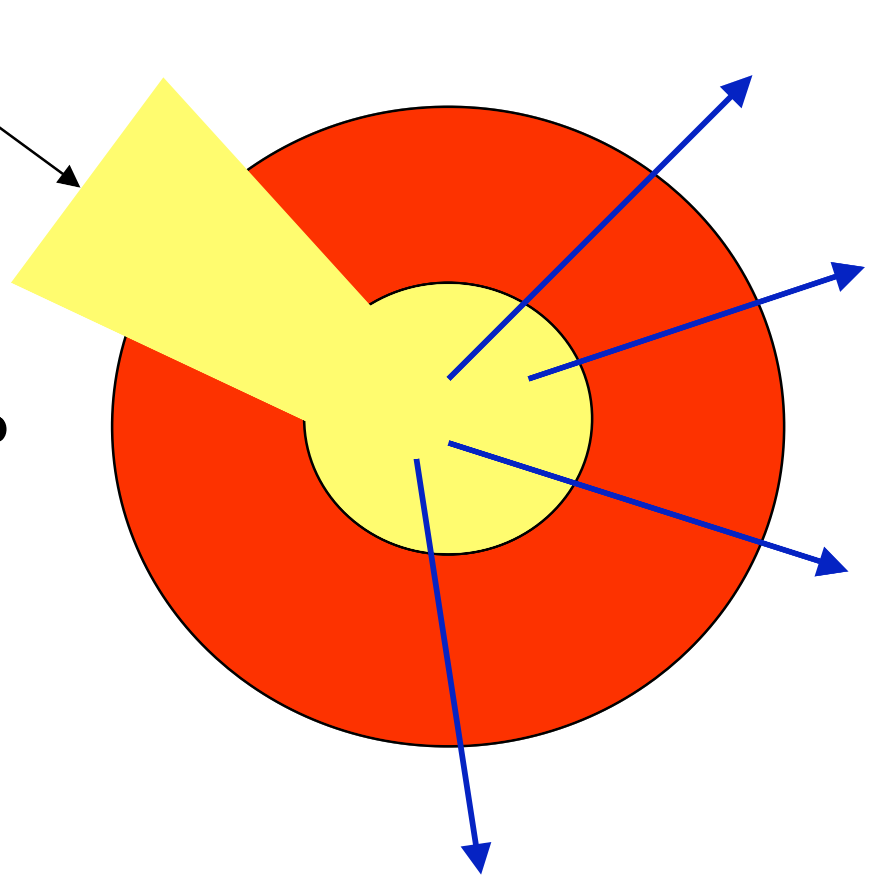

Poison center to produce radiative collapse

Mass escape should be early so minimum work is done on hotspot

Omega capsules were roughly 1/5 ignition scale; all CH.

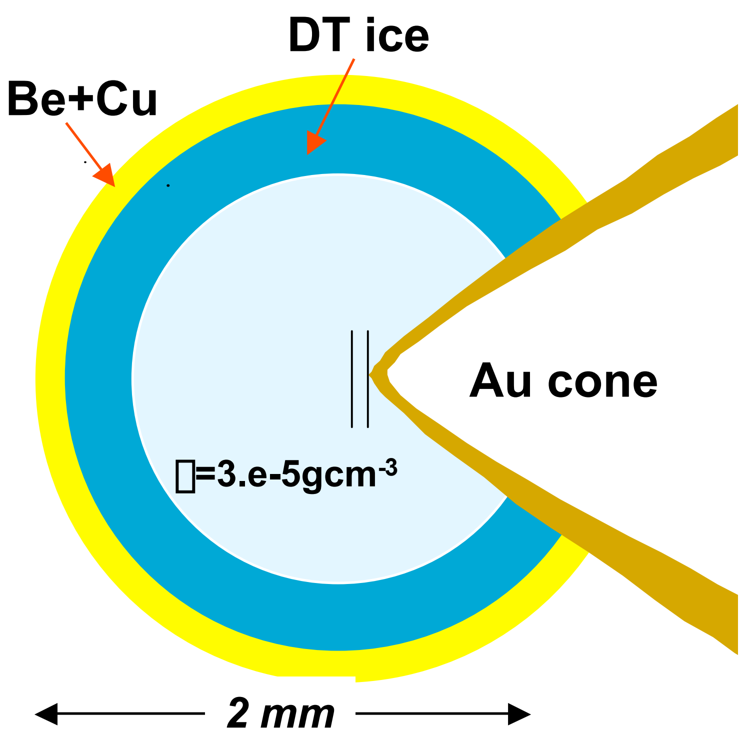

Ignition scale

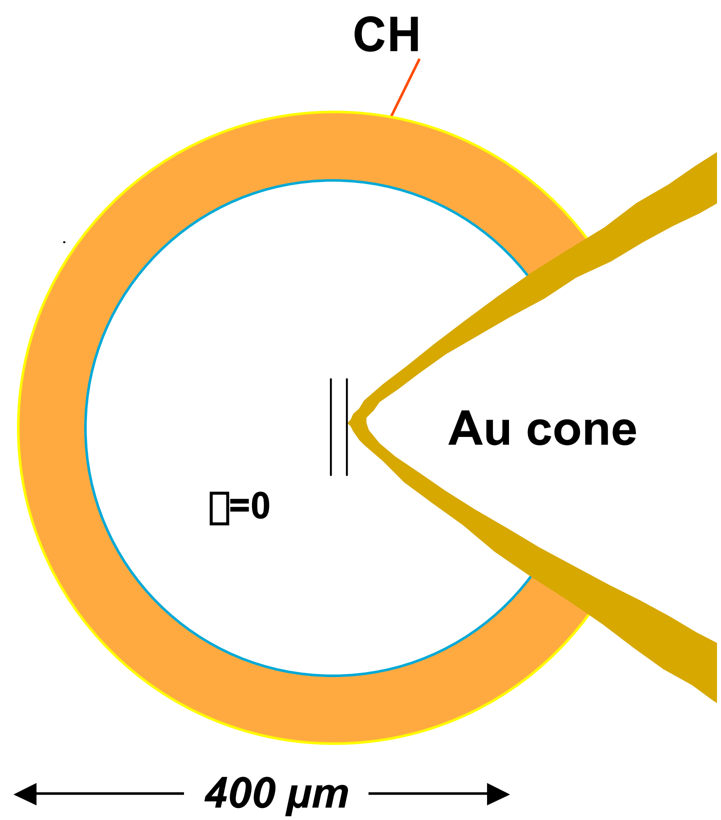

Omega scale

Backlit images (@8 keV) show convergence of cone-focussed targets was very similar to prediction — with perhaps a small time offset.

Experiment

225 µm

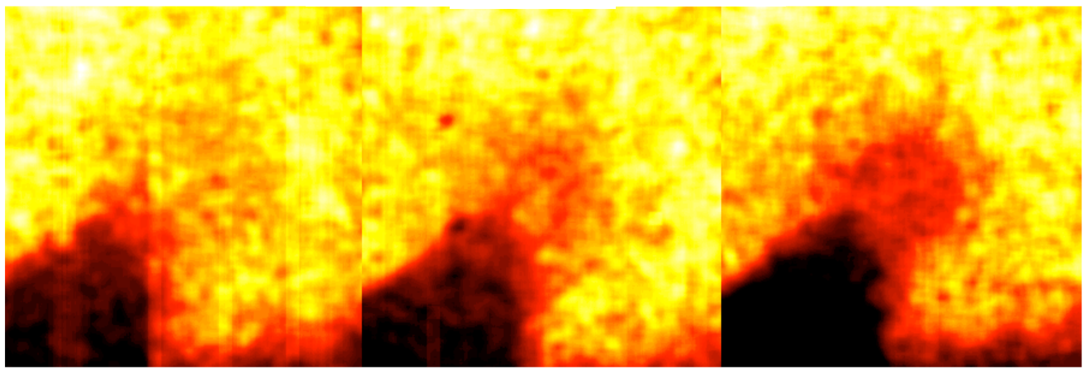

t = 3.0 ns 3.1 ns 3.2 ns

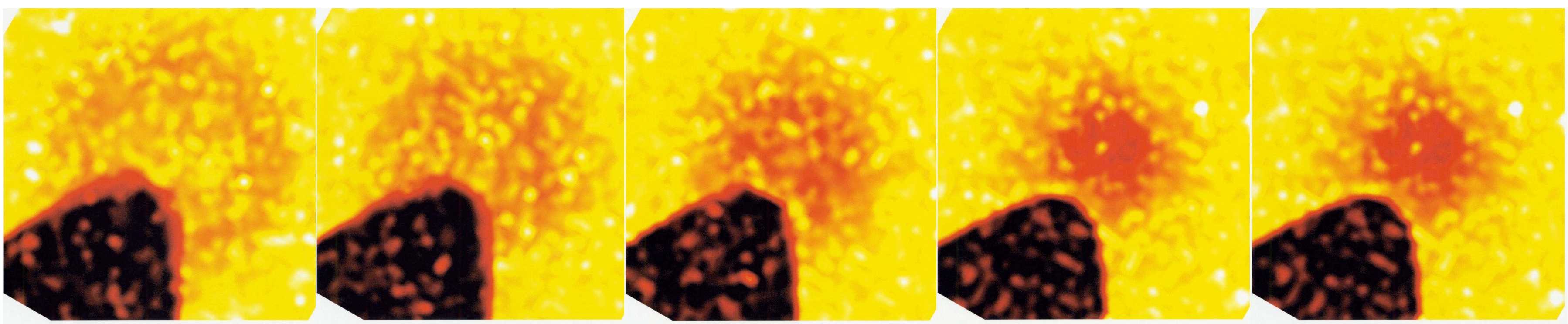

t = 3.0 ns 3.1 ns 3.2 ns 3.3 ns 3.4 ns

Prediction (with pixelation, noise, and smoothing like exp. images)

Comparison shows some exp. evidence for gold entrainment near tip of cone.

Apparent experimental convergence of cone-focussed targets is probably much less than their true convergence.

Prediction for 8 keV backlit images

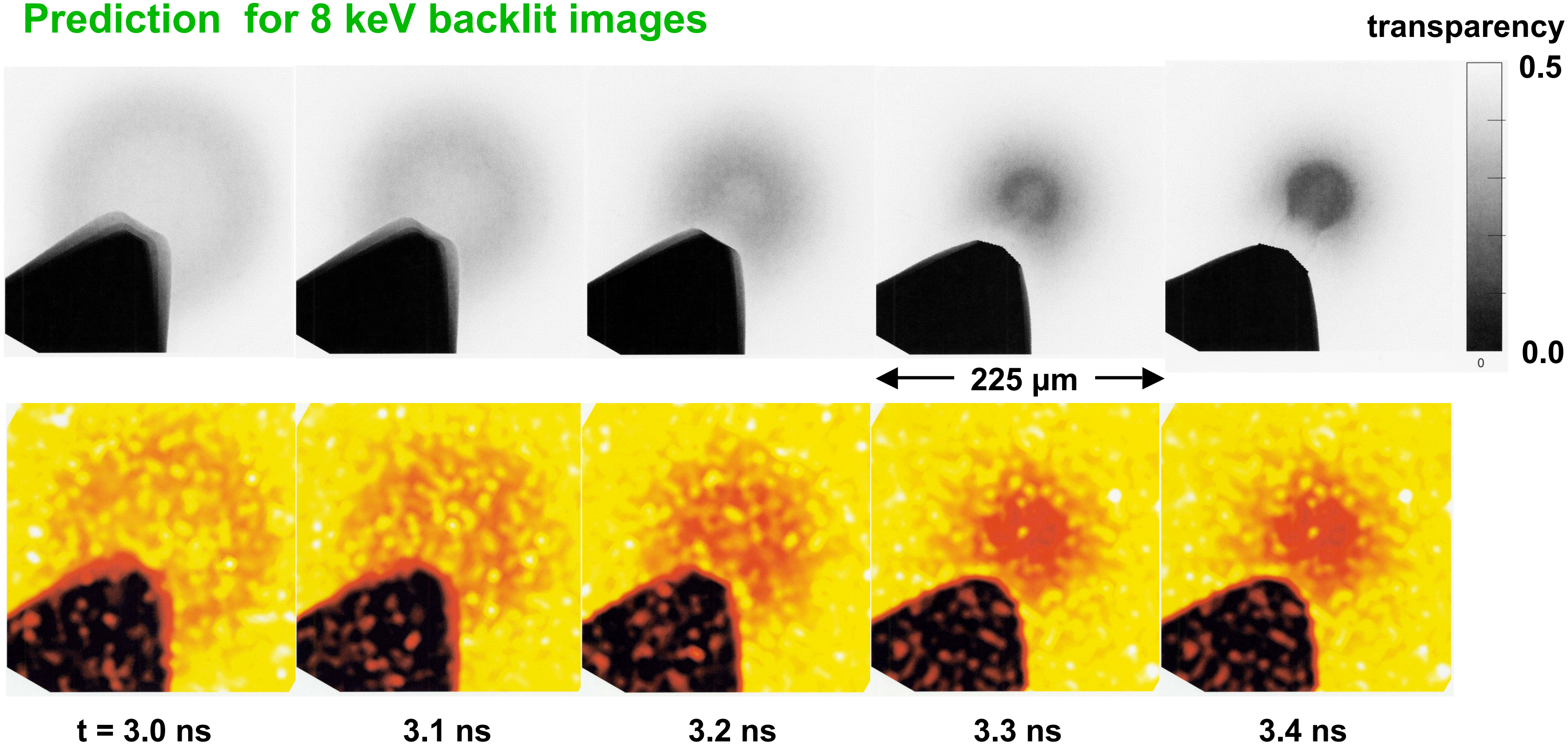

Prediction — with pixelation, noise, and smoothing like exp. images.

MHD models(Jim Hammer,Tony Bell) and hybrid code calculations predict fields in 5-30MG range and particles propagating as warm beams

MHD models treat hot and cold electrons as two fluids with stationary ion background

Fluids characterized by:

- $n_{H,C}$ **particle densities**
- $T_{H,C}$ **fluid temperature**
- $P_{H,C}$ **fluid pressures**
- $v_{H,C}$ **fluid drift velocities**
- ν_{HC} **drag coefficient between hots and colds**

Newton's law for two species:

$$n_H m_H \frac{d\vec{v}_H}{dt} = -\nabla P_H - e n_H \left(\vec{E} + \frac{\vec{v}_H}{c} \times \vec{B} \right) - n_H m_H \nu_{HC} \left(\vec{v}_H - \vec{v}_C \right)$$

Assume hots are collisionless; net force on hots much less than individual terms; there is a steady state

$$-\frac{\nabla P_H}{e n_H} + \vec{E} + \frac{\vec{v}_H}{c} \times \vec{B} \approx 0$$

MHD models II

Colds are also in steady state:

$$\vec{E} + \frac{\vec{v}_C}{c} \times \vec{B} = \eta_C J_{cold}$$

Scattering of colds from ions only

Currents must approximately cancel or magnetic and electric fields get crazy

$$J_{cold} \approx -J_{hot}$$

Magnetic force on colds << force on hots and maybe electric force on colds

$$\vec{E} = -\eta_C J_{hot}$$

Hot force law becomes:

$$\Rightarrow \quad \frac{\nabla P_H}{e n_H} \approx -\eta J_H + \frac{\vec{v}_H}{c} \times \vec{B} \approx 0$$

MHD models III

Remaining hot equations:

$$\dot{n}_H + \nabla \cdot n_H \vec{v}_H = 0$$

Current conservation

$$\dot{\vec{B}} = -c\nabla \times \vec{E} = c\nabla \times \left(\eta J_H\right)$$

Faraday's law

Limiting cases:
Electric force on hots << magnetic force

$$-\frac{\nabla P_H}{e n_H} + \frac{\vec{v}_H}{c} \times \vec{B} \approx 0$$

Bennett pinch condition but driven by Faraday's law, not $\nabla \times \nabla \times \vec{B} = 4\pi J / c$

In cylindrical geometry

$$v_{H_z} = \frac{cT_H}{e n_H B} \frac{\partial n_H}{\partial r}$$

$$\dot{B} = c\frac{\partial E_z}{\partial r} = \frac{\partial}{\partial r} \frac{\eta c^2 T_H}{B} \frac{\partial n}{\partial r}$$

MHD models IV

An ansatz for a solution

$$n_H = n_0 \exp\left(-\frac{r^2}{2r_0^2}\right)$$

$$B = B_0 \frac{r}{r_0} \exp\left(-\frac{r^2}{4r_0^2}\right)$$

$$B_0 = \sqrt{\frac{\square T_H c^2 n_0 t}{r_0^2}}$$

Warm beam of constant radius composed of a magnetized plasma

Magnetic field grows as forward and currents diffusively separate

Drift velocity decreases as B increases
Effectively reduces practical range

Quiet about divergent flows

More detailed descriptions are provided by code calculations

Hybrid calculations are used to model kinetic particles traversing dense collisional plasmas

Hybrid codes have been used to model electron transport relevant to Fast Ignition

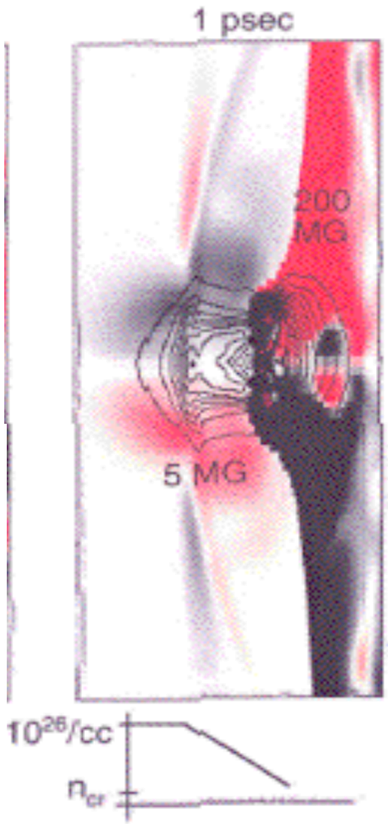

ANTHEM showed propagation as warm beam up gradient to 10^{26}

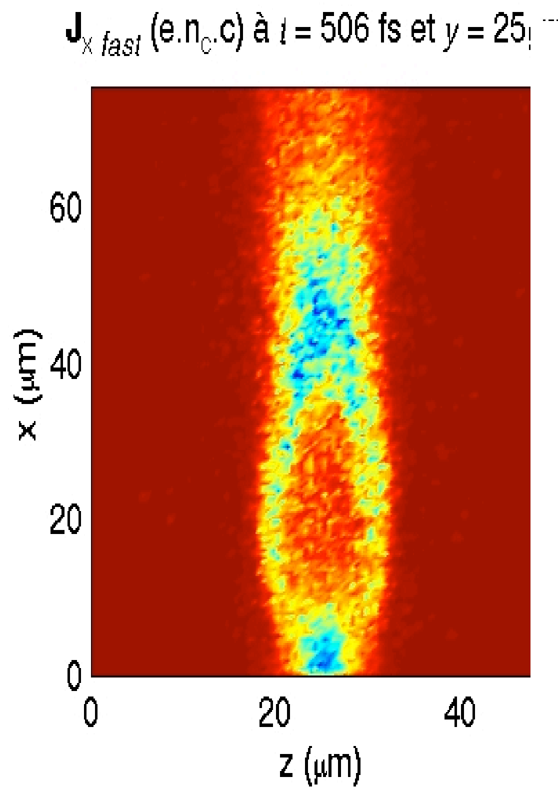

PARIS showed magnetic guiding, the filamentation Instability and annular current

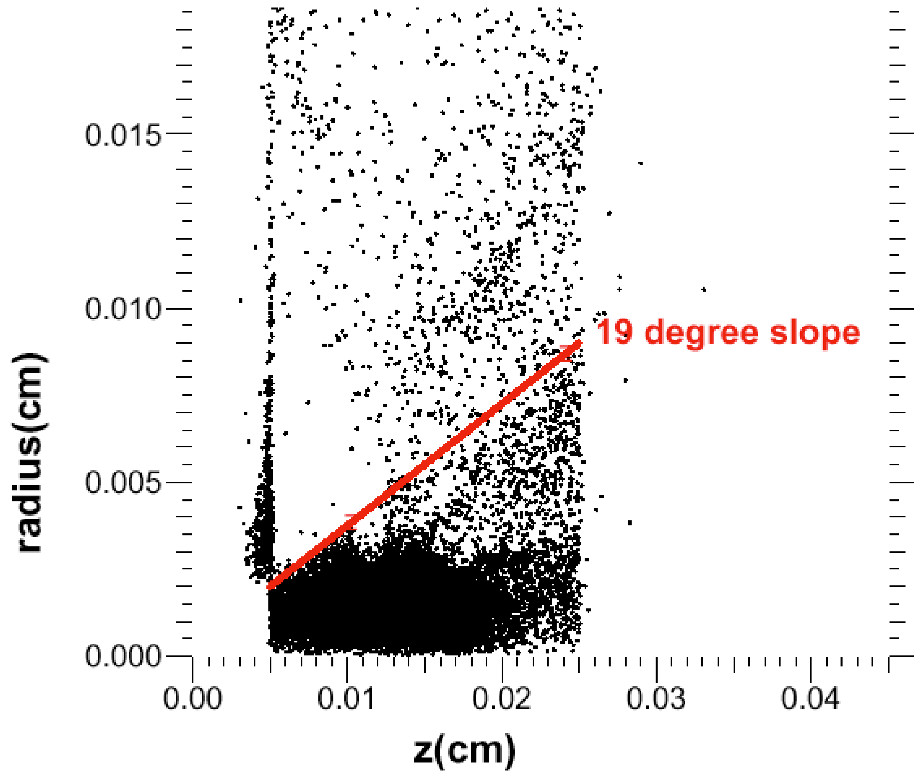

LSP showed beam divergence and magnetic breakup near jumps in Conductivity. 3D code

Dramatic progress in fast ignition was made in a recent Japanese cone-focused experiment[1]

- A 500TW ignitor beam gave:
  - greater than 20% energy coupling (through electron transport) to the CD fuel; and
  - a 100-fold increase in DD neutron yield
  - The coupling efficiency may degrade in full-scale targets.

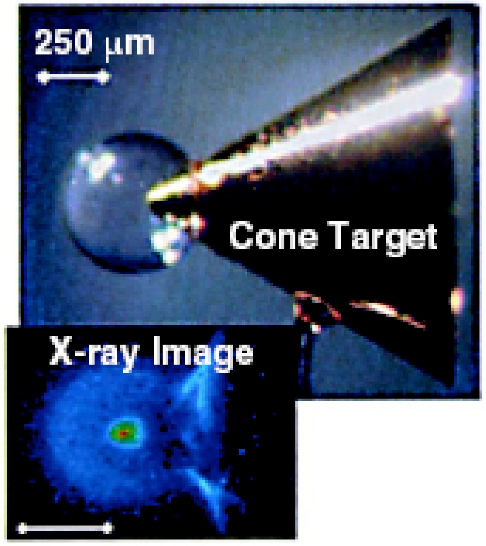

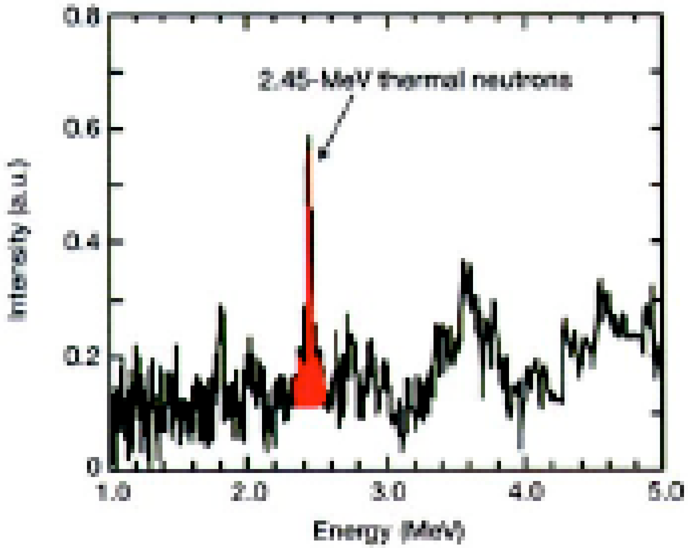

What is laser-electron coupling?

Does cone focus energy to fuel?

Do these results scale to ignition conditions?

[1]R. Kodama et al, Nature 418, P933 (2002).

Stopping power calculations

Presented to:

Workshop on computational physics of short pulse laser interactions

Max Tabak

Lawrence Livermore National Laboratory

8/25-04-8/27/04

This work was performed under the auspices of the U.S. Department of Energy by the University of California Lawrence Livermore National Laboratory under Contract No. W-7405-Eng-48.

Lawrence Livermore National Laboratory, P.O. Box 808, Livermore, CA 94551-0808

De/dx specific deposition;few energies

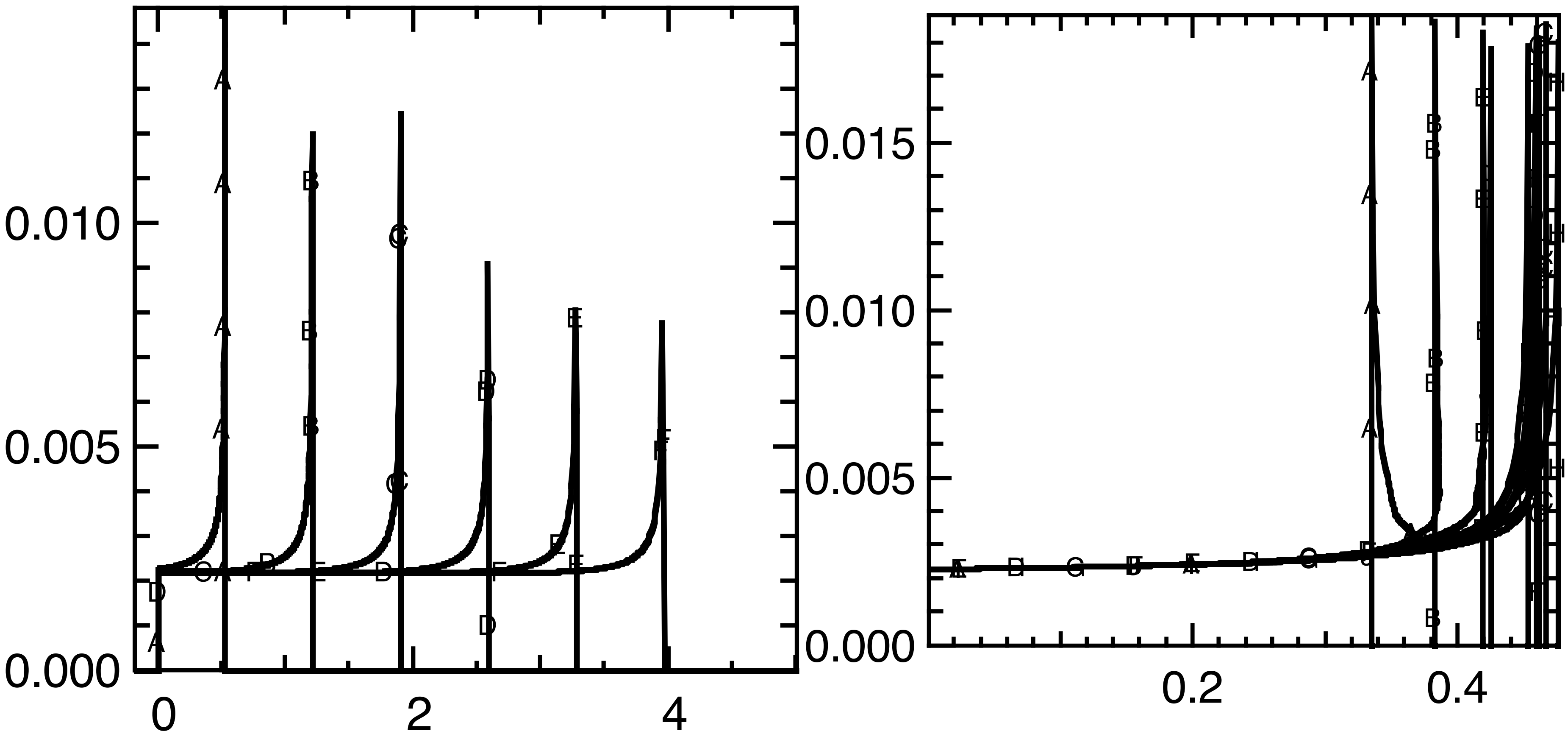

Identifying Marker. 2

Fractional deposition,initially forward;6 energies

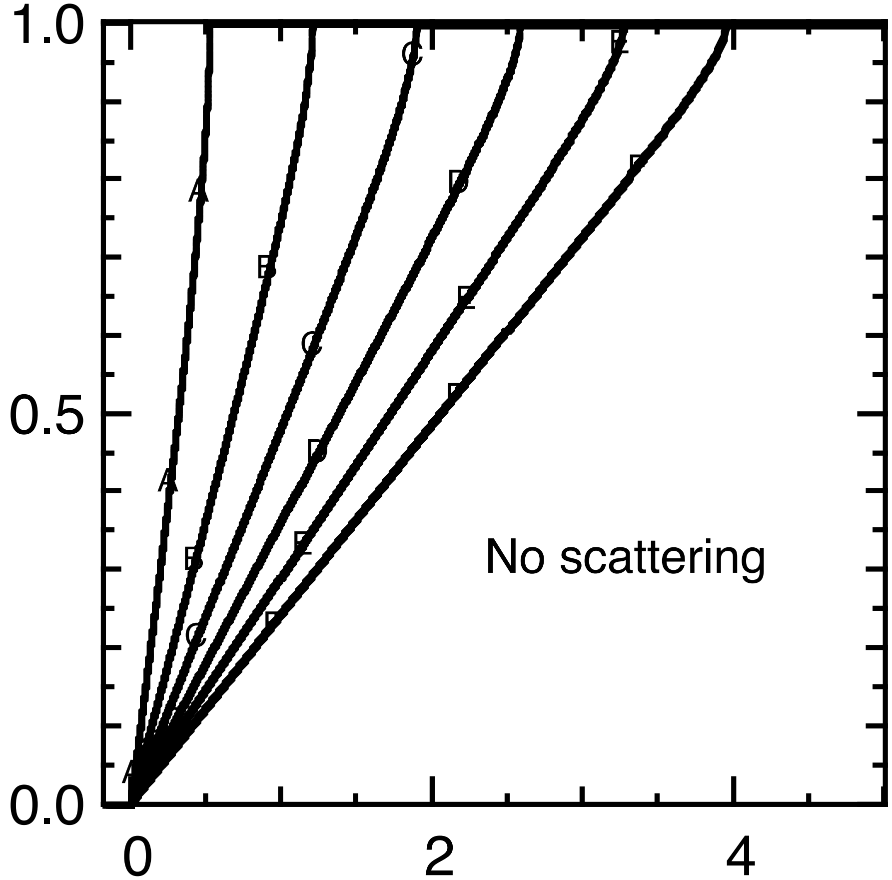

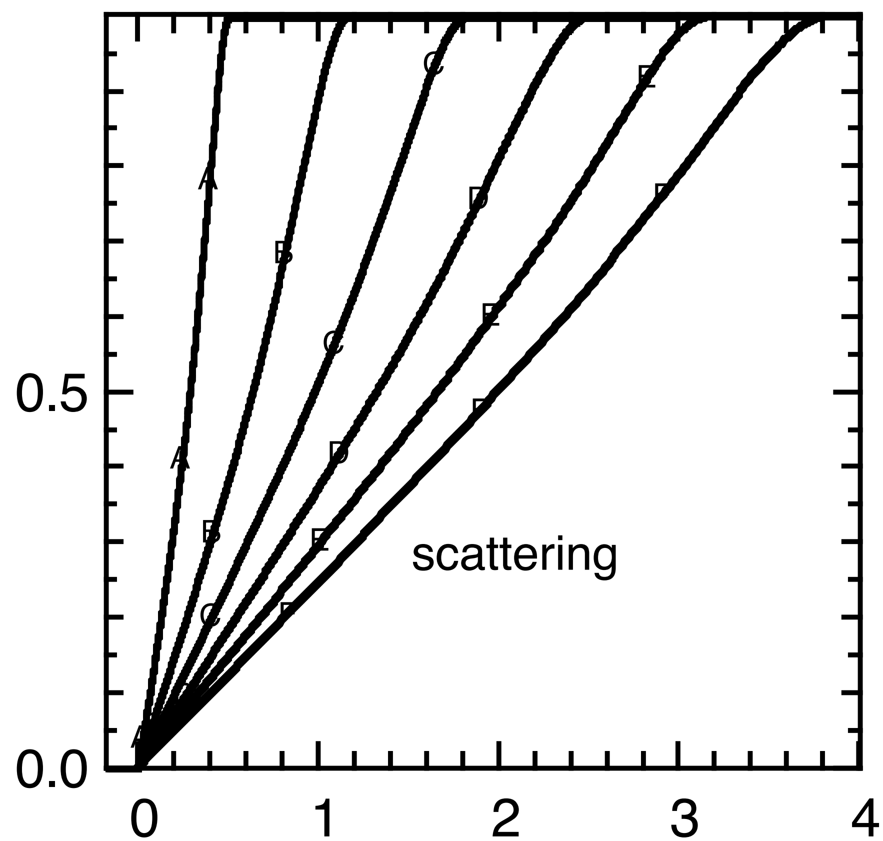

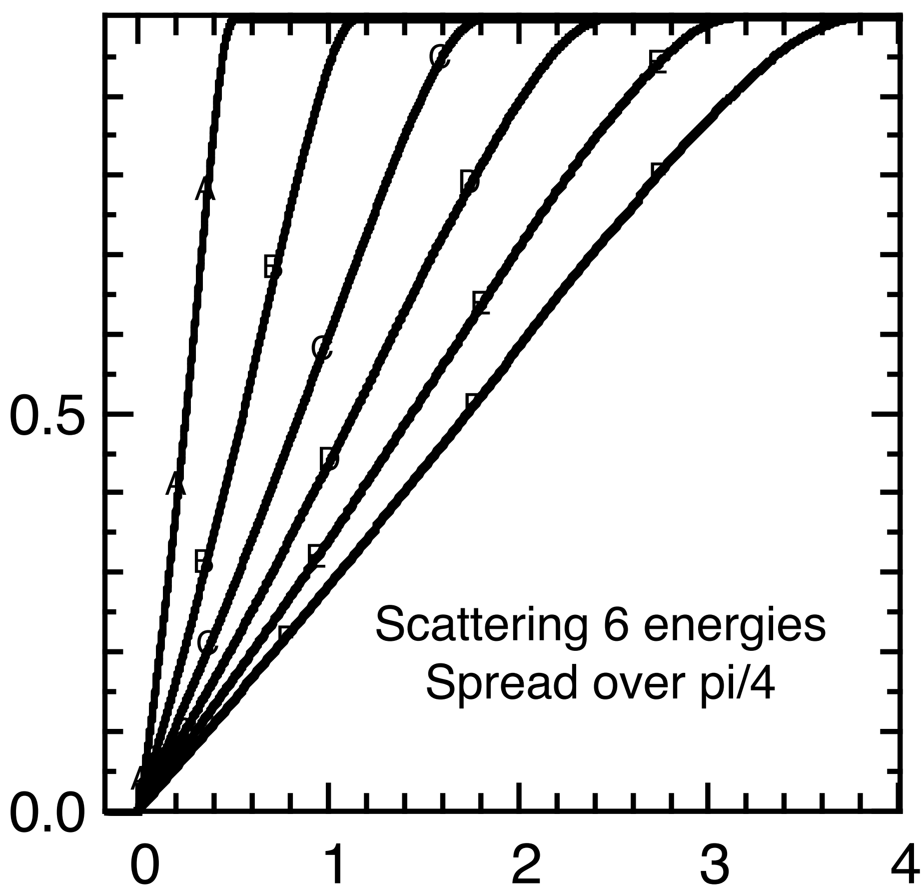
0.5
0.0
0
1
2
3
4
Scattering 6 energies
Spread over pi/4

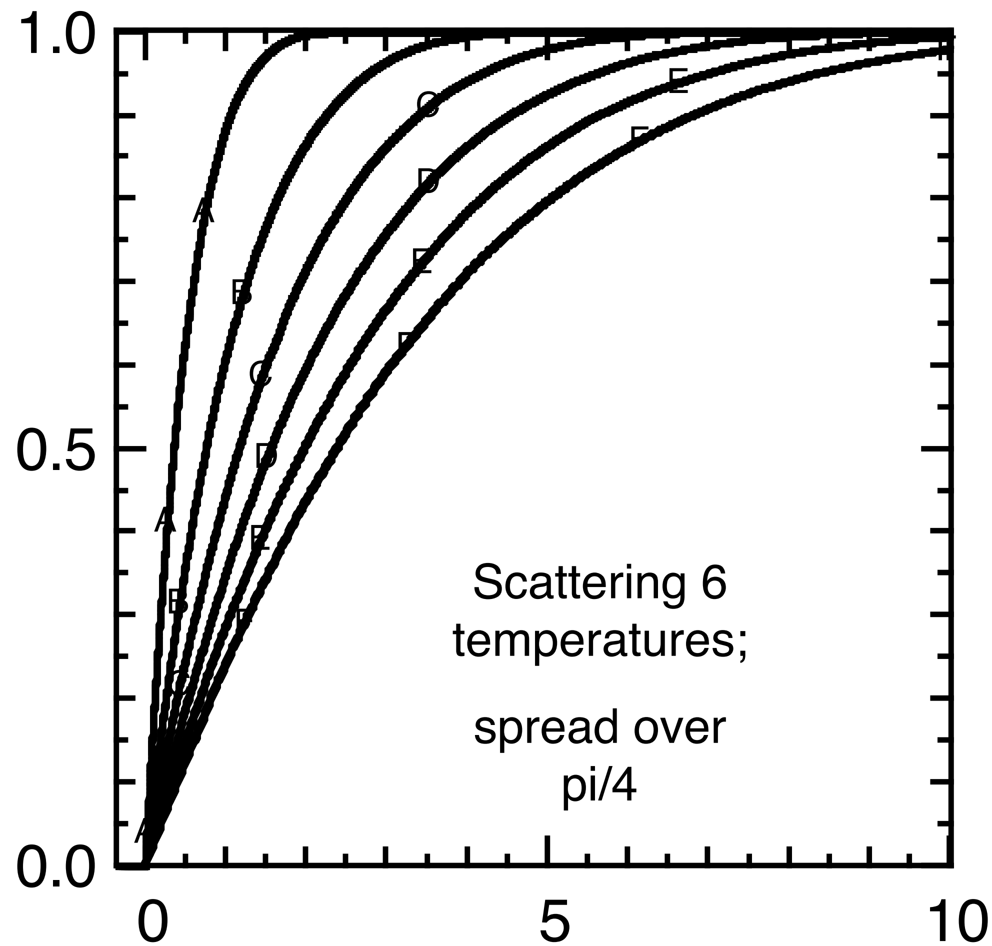
1.0
0.5
0.0
0
5
10
Scattering 6
temperatures;
spread over
pi/4

Simulations of Electron Transport Experiments for Fast Ignition using LSP

Presented to:
Short-Pulse Laser Matter Computational Workshop
Pleasanton, CA

Richard P. J. Town
AX-Division
Lawrence Livermore National Laboratory
August 25, 2004

This work was performed under the auspices of the U.S. Department of Energy by the University of California Lawrence Livermore National Laboratory under Contract No. W-7405-Eng-48.

Lawrence Livermore National Laboratory, P.O. Box 808, Livermore, CA 94551-0808

UCRL-PRES-204413

The LSP code has been used to study fast ignition relevant transport experiments

- A critical issue for Fast Ignition is understanding the transport of the ignitor electrons to the fuel.
- Experiments have shown a rapid increase in beam width followed by reasonable collimation with a 20° half angle.
- We have used the LSP code to:
  - generate simulated Kα images;
  - model XUV images; and
  - model cone focus experiments.
- The LSP code has been used to study the effect on beam transport of:
  - non-Spitzer conductivity; and
  - the initial beam divergence.

The XUV image can be used to estimate the temperature of the rear surface

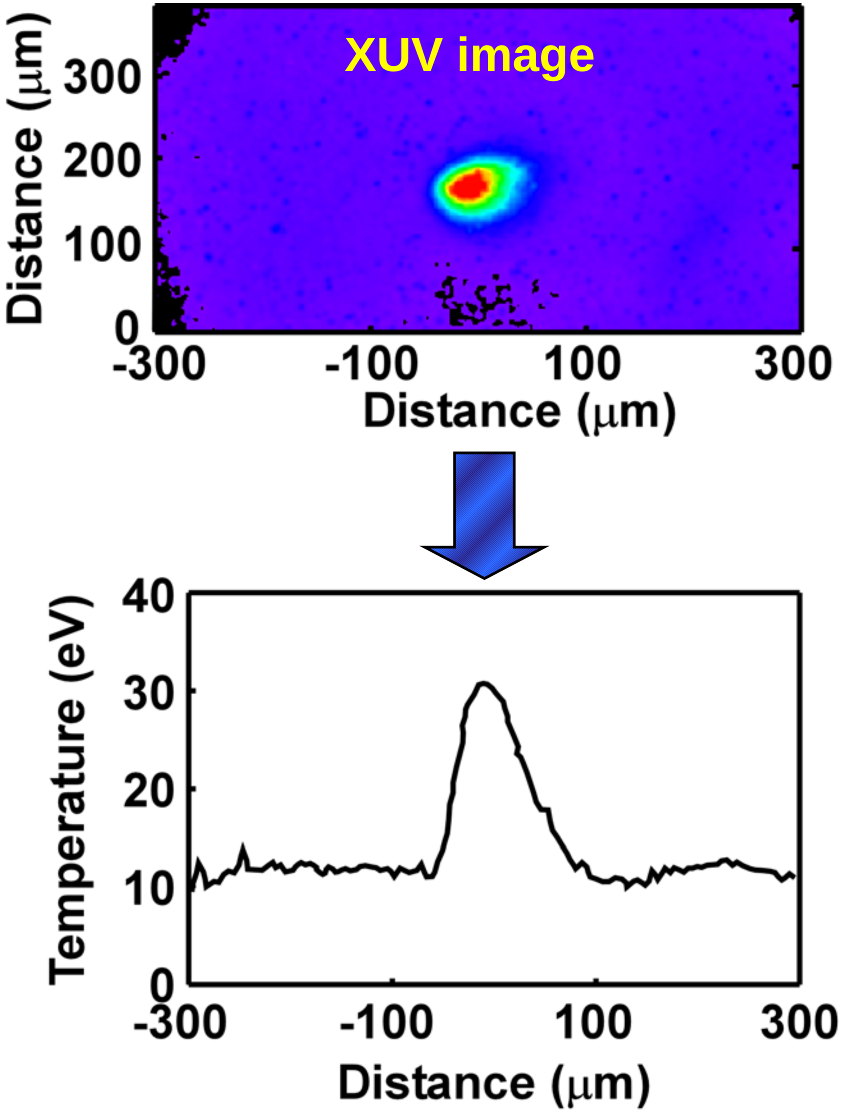

- A series of *LASNEX* calculations of isochorically heated Al targets establishes the relationship between temperature and intensity.

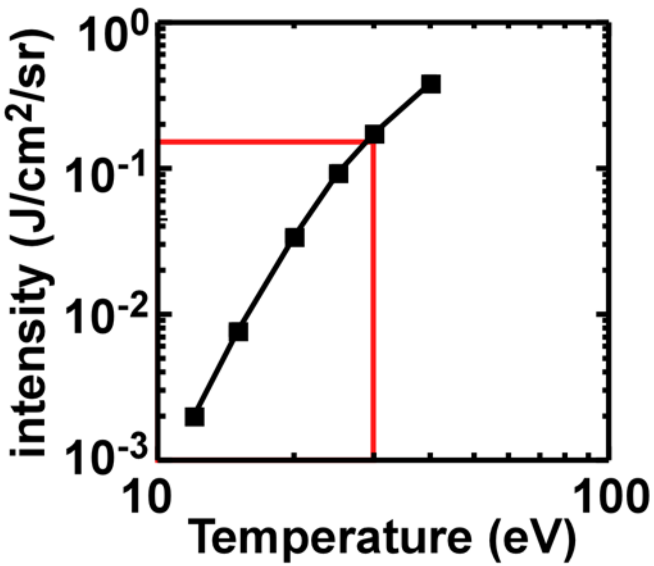

Experiments on MeV electron transport have been performed by researchers around the world

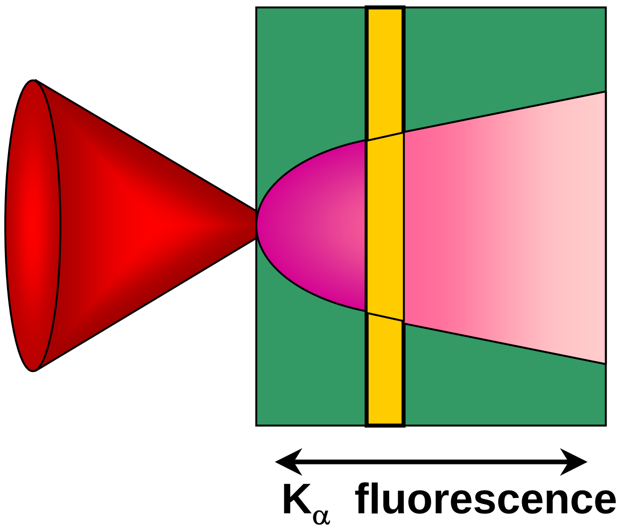

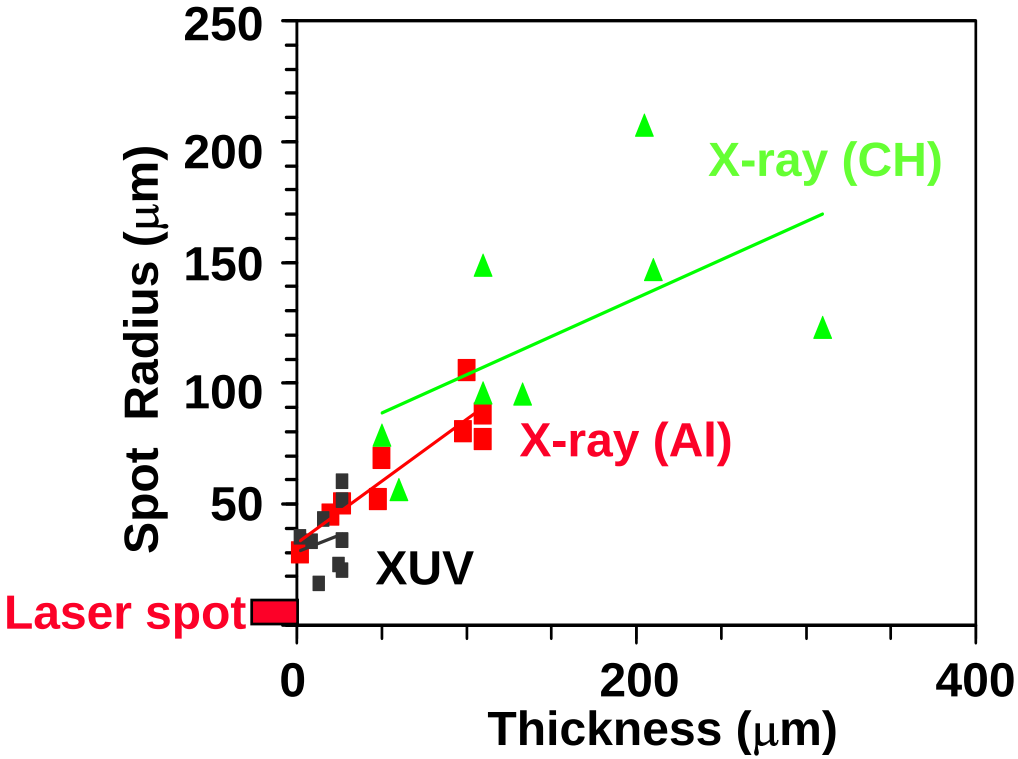

- Experimental data[1] show:
  - a rapid increase in beam size in the first few microns; and
  - a fairly collimated (20° half angle) beam in the bulk of the material.

[1]M. H. Key, et al, 5th Workshop on Fast Ignition of Fusion Targets (2001).

We have performed simulations of generic electron transport experiments

- The targets are based on the experiments performed by Martinolli et al[1] on the LULI and Vulcan laser.
- The big uncertainty is the initial hot electron beam parameters.

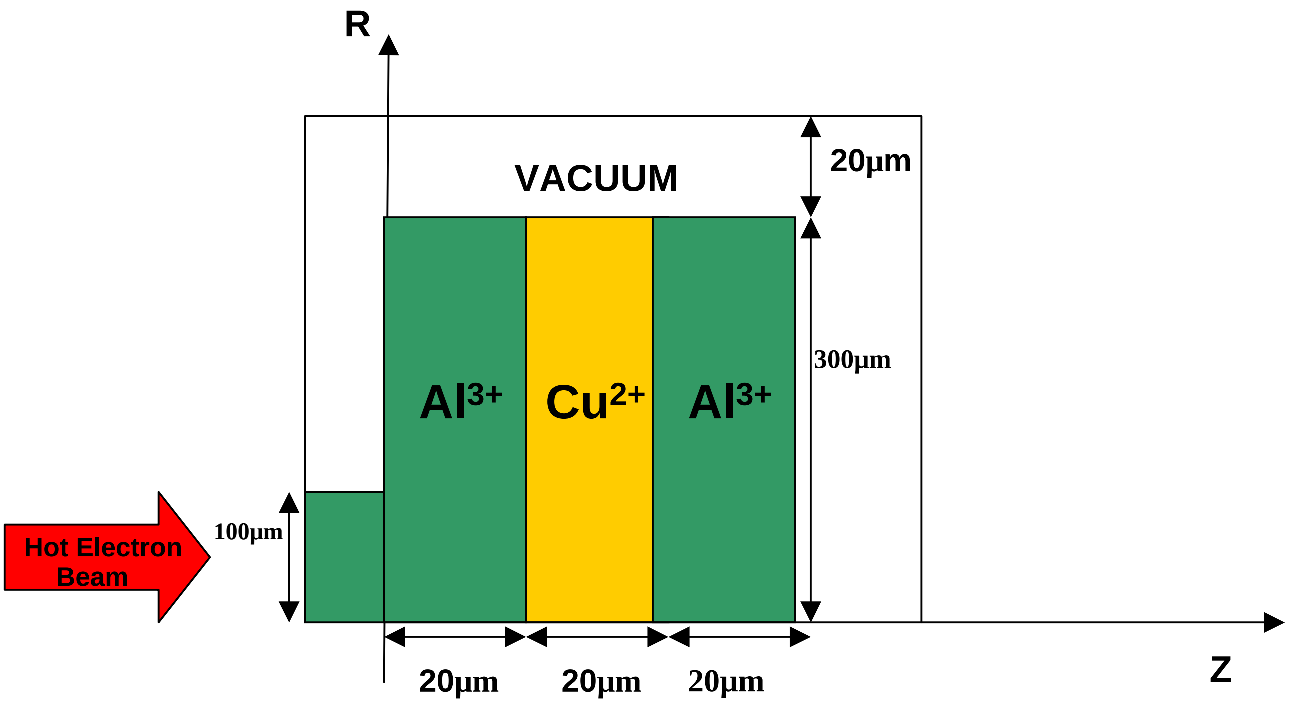

[1]E. Martinolli, et al., Laser & Part. Beams 20, 171 (2002).

A significant "halo" surrounds the short-pulse high intensity spot

- Typical data from Nova Petawatt laser shows about 30 to 40% of the laser energy in the central spot.

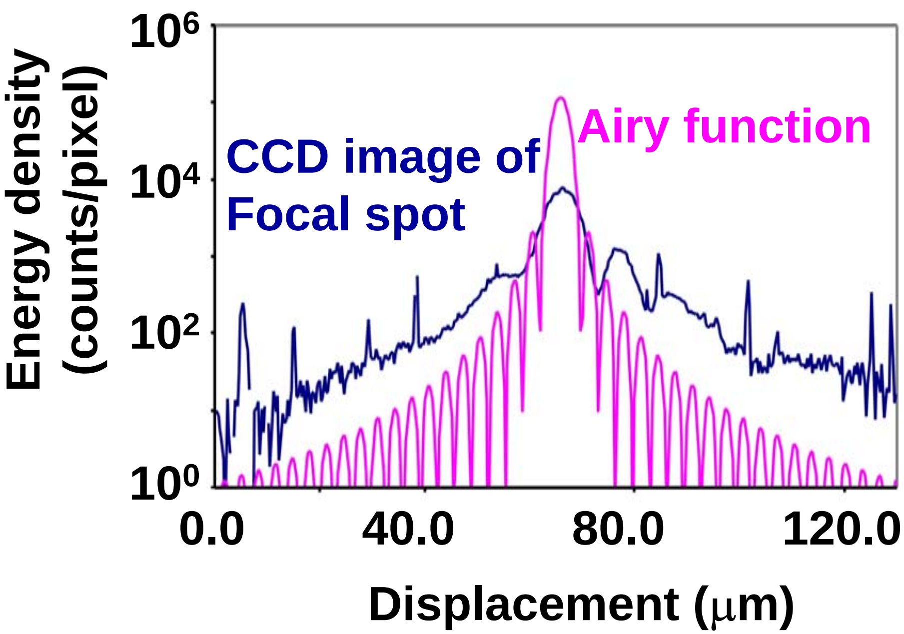

- We have approximated the laser intensity pattern as two Gaussians.

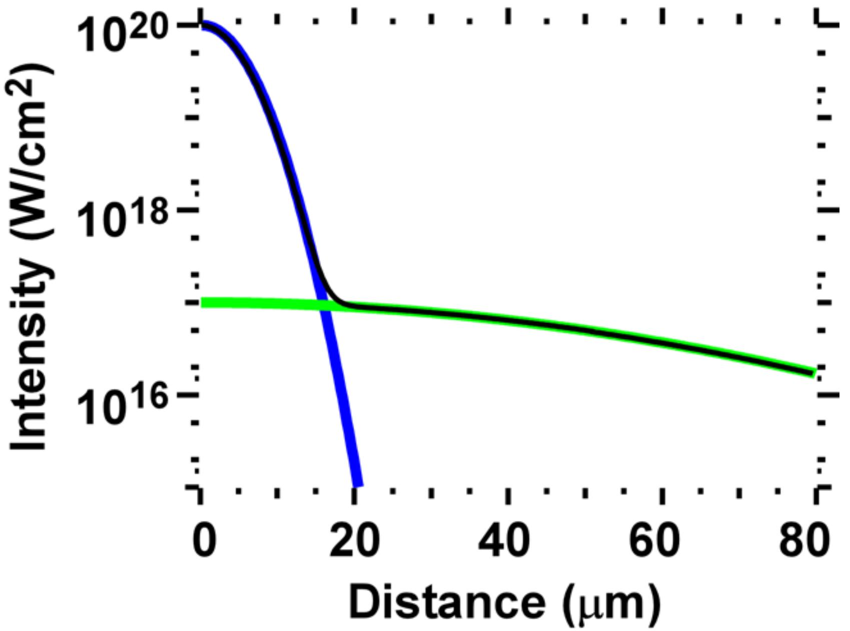

Determining the input electron distribution is based on experimental measurements

- **The conversion efficiency into hot electrons has been measured by many experimentalists over a wide range of intensities:**

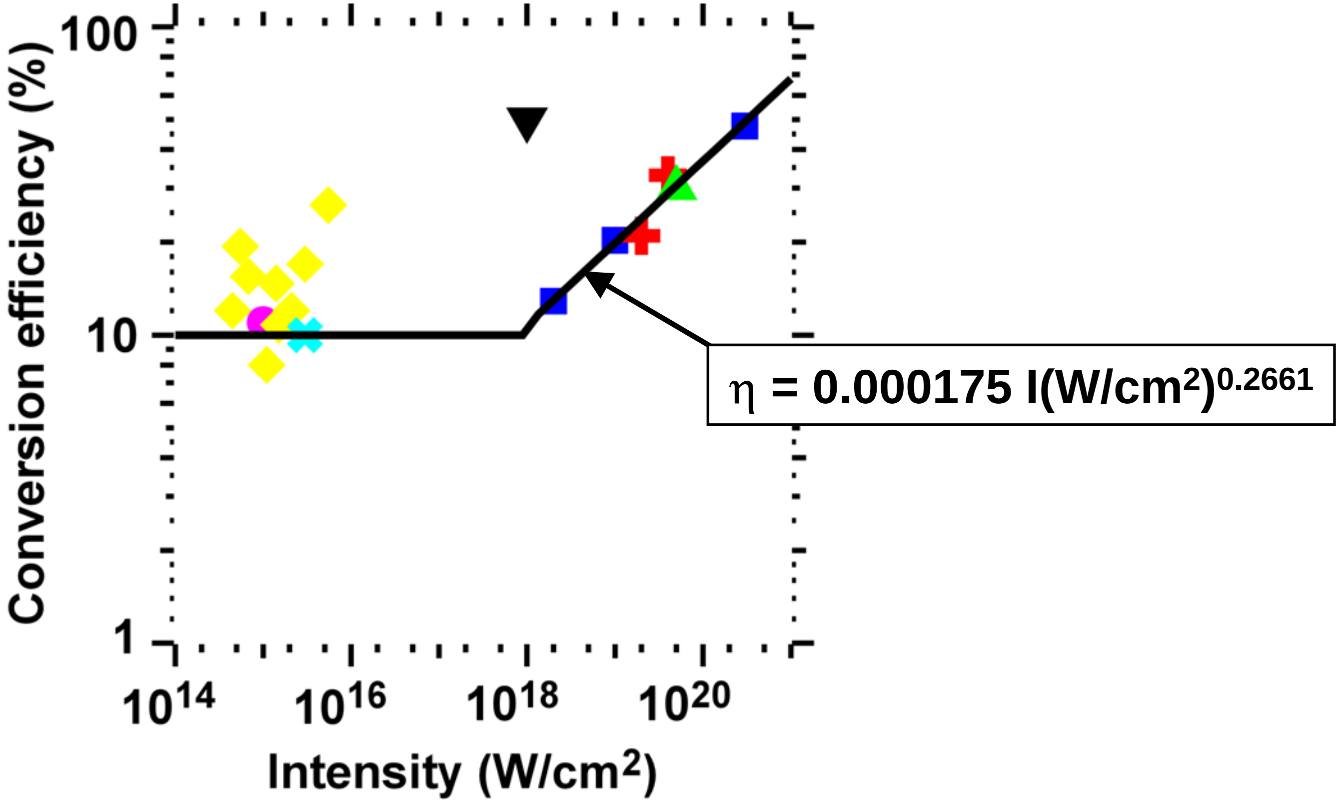

There are two well-known scaling laws for hot electron temperature which we have used

- **Pondermotive scaling:**

$$T_{hot}(MeV) = (I\lambda^2/(10^{19} W/cm^2 \mu m^2))^{1/2}$$

- **Beg scaling:**

$$T_{hot}(MeV) = 0.1(I\lambda^2/(10^{17} W/cm^2 \mu m^2))^{1/3}$$

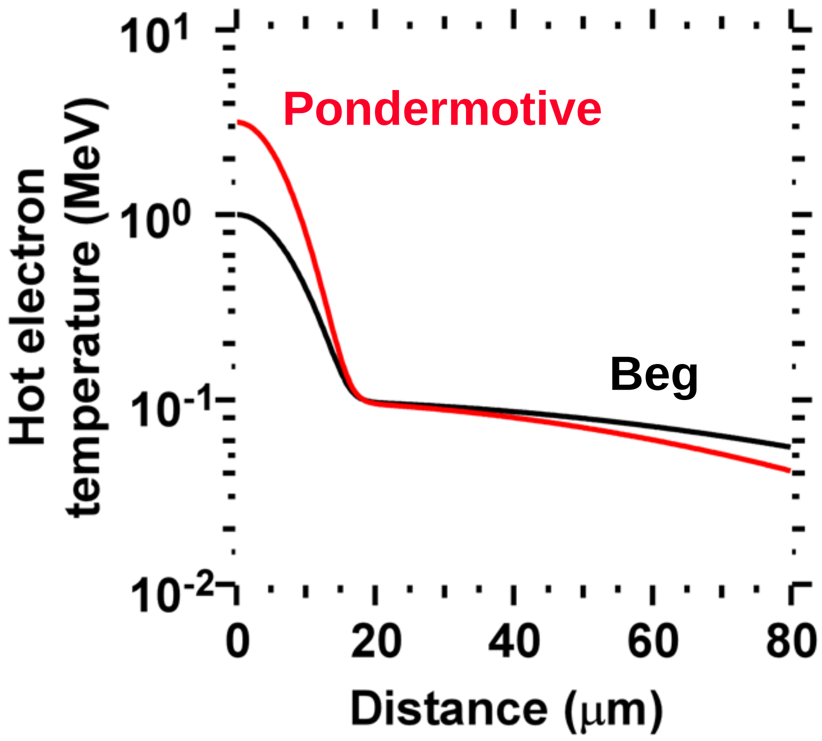

The current density and energy distribution can now be defined in terms of laser intensity

- Using the new Python front end to LSP the injected beam energy and current density can be calculated from:
  - conversion efficiency; and
  - hot temperature scaling law.
- A thermal spread is also added.

```
rold = 0.0
for i in range(400):
   r = (i+0.5)*0.00002
   intensity = Gaussian(r, 1.0e-3, 1.0e20, 0.0, 1.0e12)
               +Gaussian(r, 1.0e-2, 1.0e17, 0.0, 1.0e12)
   if intensity > 0.0:
      thot = BegScaling( intensity )
      ehot = 1.6022e-16*thot
      area = pi*(r**2-rold**2)
      lpower = intensity*area
      epower = lpower*conversionEfficiency(intensity)
      Density =1.6022e-19*epower/(area*ehot)
   rold = r
```

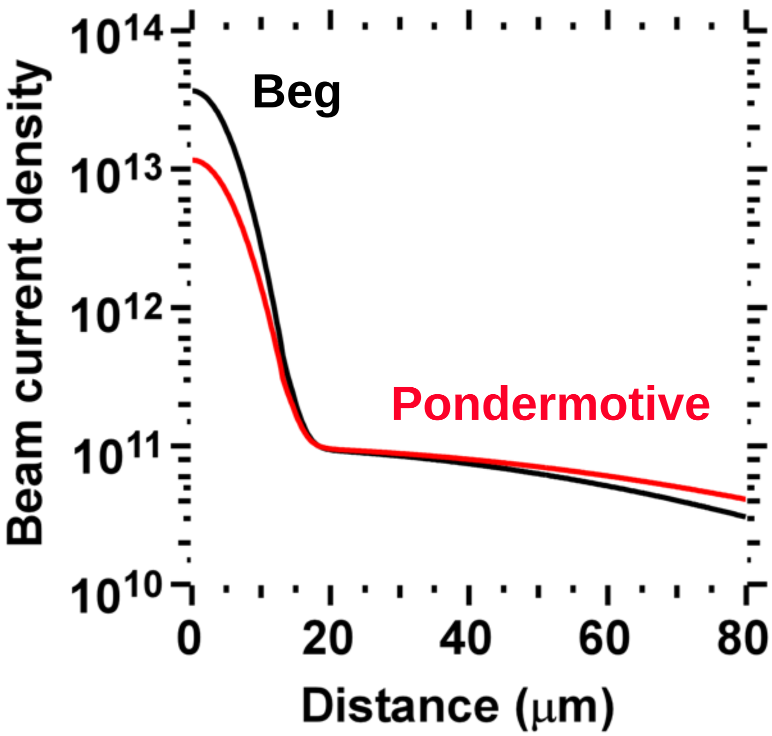

The LSP calculation matches the measured temperature pattern at the rear surface of the target

- 27J of hot electrons, in a 1-ps pulse, with Beg scaling and a thermal spread of 300keV injected into a 100μm Al^{3+} plasma.
- The temperature was obtained by post-processing the LSP energy data at the rear surface with a realistic equation of state.

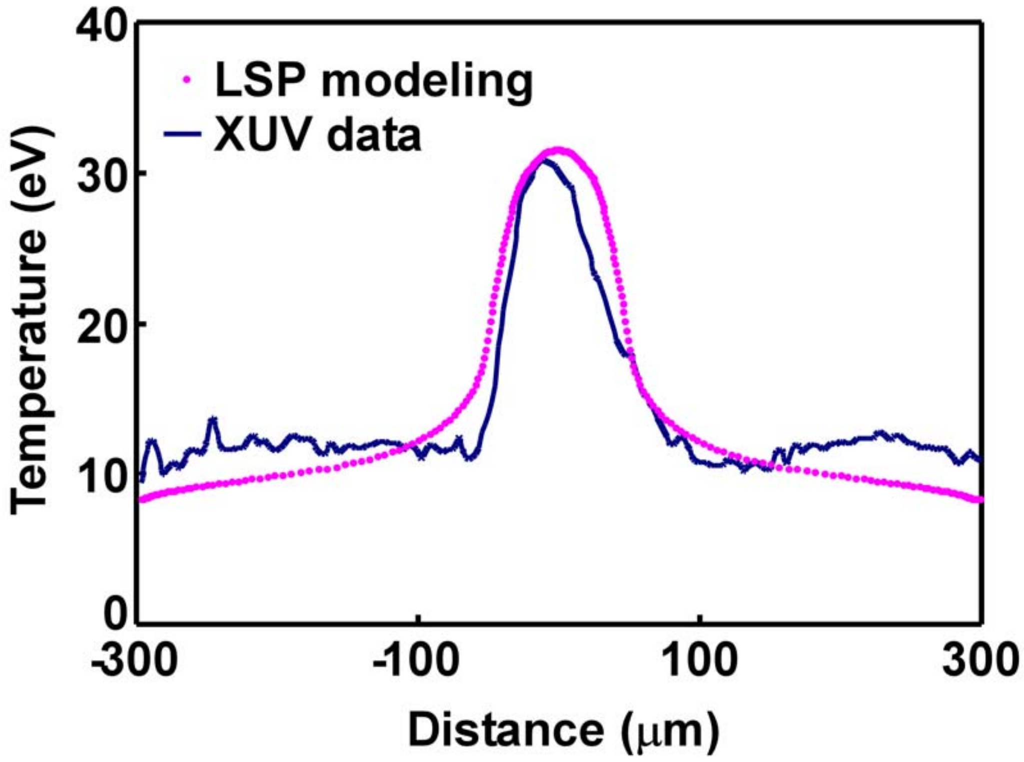

Collaborators:

- C. Chen, L. A. Cottrill, M. H. Key, W. L. Kruer, A. B. Langdon, B. F. Lasinski, B. C. McCandless, R. A. Snavely, C. H. Still, M. Tabak, S. C. Wilks,
  LLNL, Livermore, CA, USA.

- D. R. Welch,
  MRC, *Albuquerque, NM, USA.*

Proton Radiography of Electric and Magnetic Fields

Presented to:
Short-pulse Laser Matter Computational Workshop
Pleasanton, CA

Richard P. J. Town
AX-Division
Lawrence Livermore National Laboratory
August 25, 2004

This work was performed under the auspices of the U.S. Department of Energy by the University of California Lawrence Livermore National Laboratory under Contract No. W-7405-Eng-48.

Lawrence Livermore National Laboratory, P.O. Box 808, Livermore, CA 94551-0808

UCRL-PRES-203599

LSP has been used to postprocess LASNEX output to model proton deflectometry of electromagnetic fields

- LASNEX predicts the existence of large magnetic fields in NIF ignition hohlraums.
- Proton deflectometry has been proposed as a means of measuring these magnetic fields.
- Recent experiments have demonstrated proton deflectometry in laser-solid interactions.
- The LSP code has been used to post-process the electric and magnetic fields calculated by LASNEX in these experiments.

LASNEX predicts the generation of large magnetic fields in NIF ignition hohlraums

- **The magnetic field is generated at the hohlraum walls and then convected into the gas fill.**

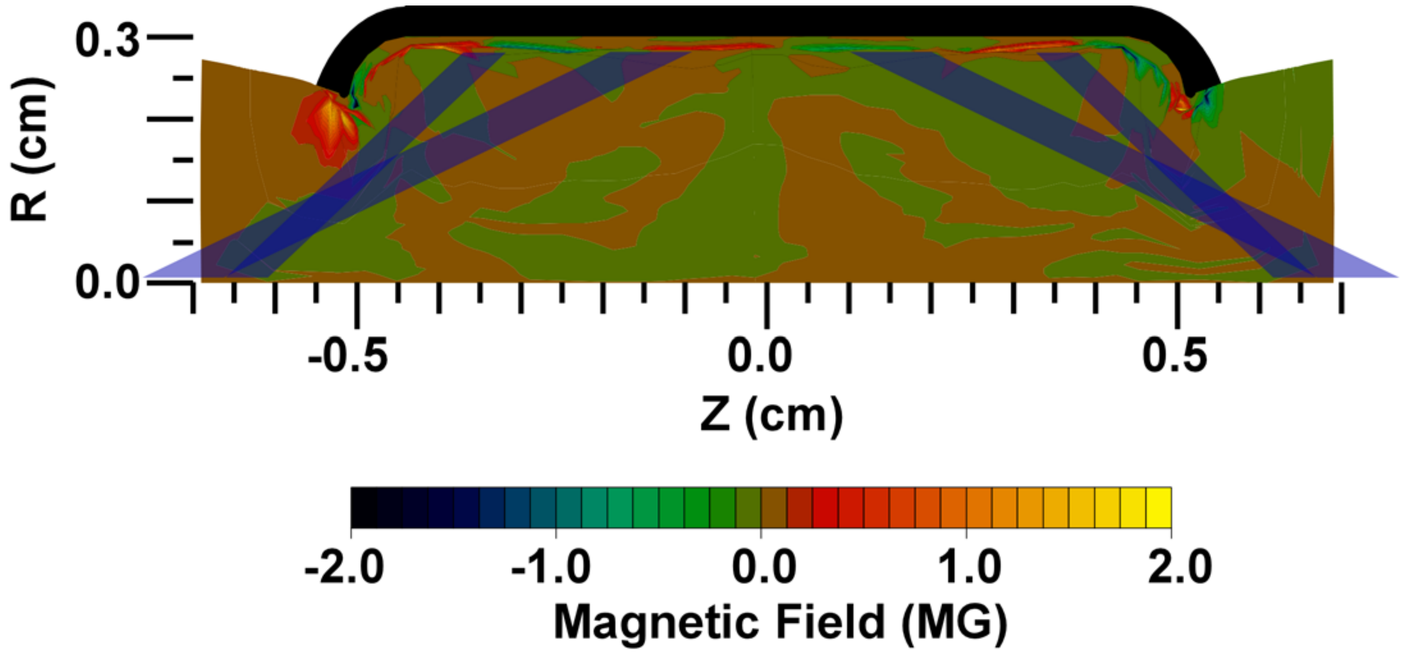

We are developing the experimental technique and the theoretical understanding to use proton deflectometry to measure these fields

Transient E and B fields have been probed experimentally using proton deflectometry[1]

- Recent experiments at LULI have generated proton deflectometry images.

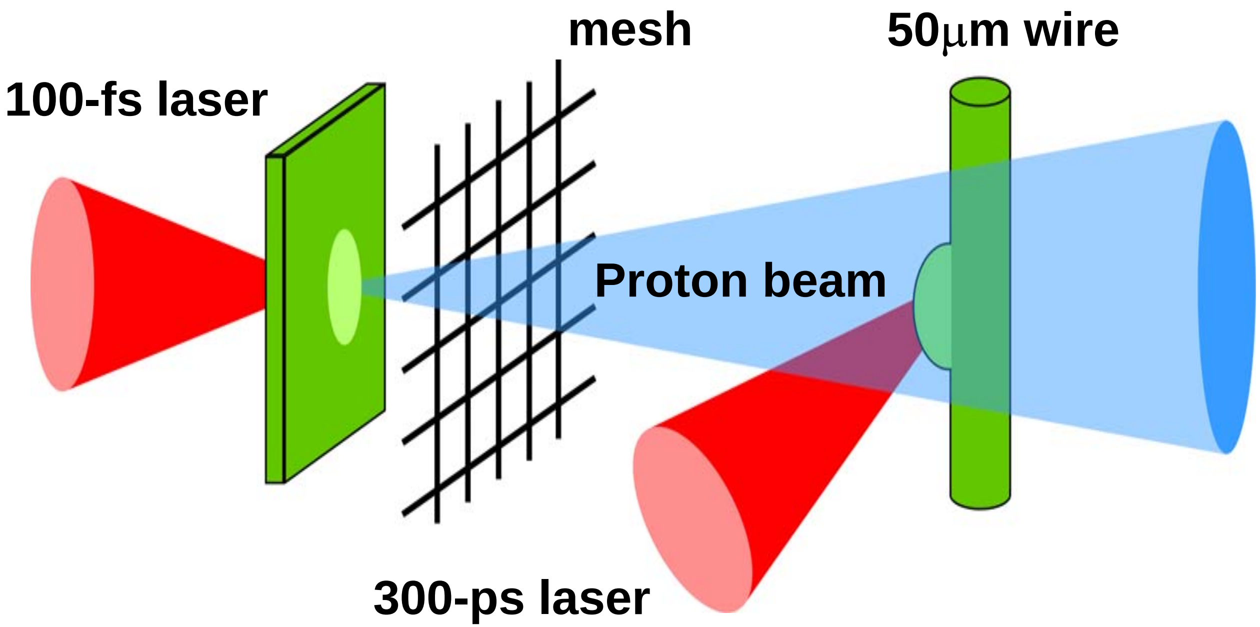

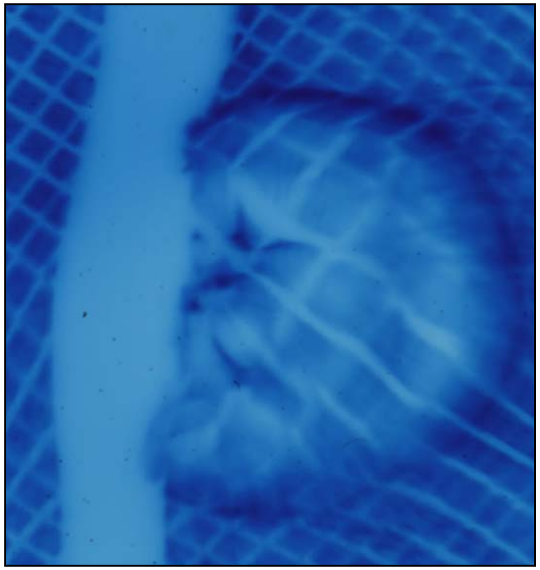

[1]A. J. Mackinnon et al, MO-1, IFSA-03 conference.

Protons are tracked in 3D through the LASNEX fields and then ballistically followed to the detector

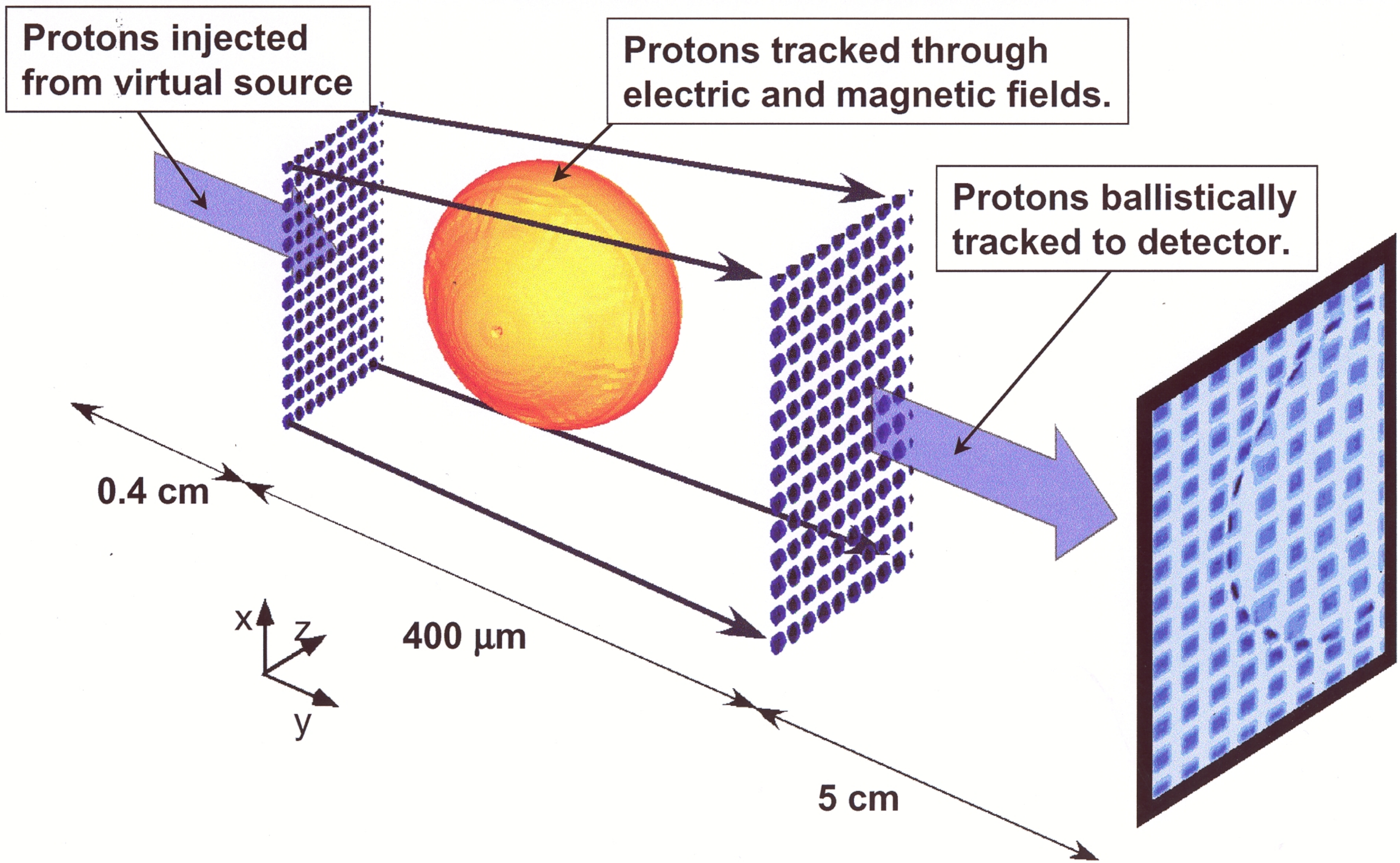

The magnitude and shape of the proton deflection is changed by the different electric fields

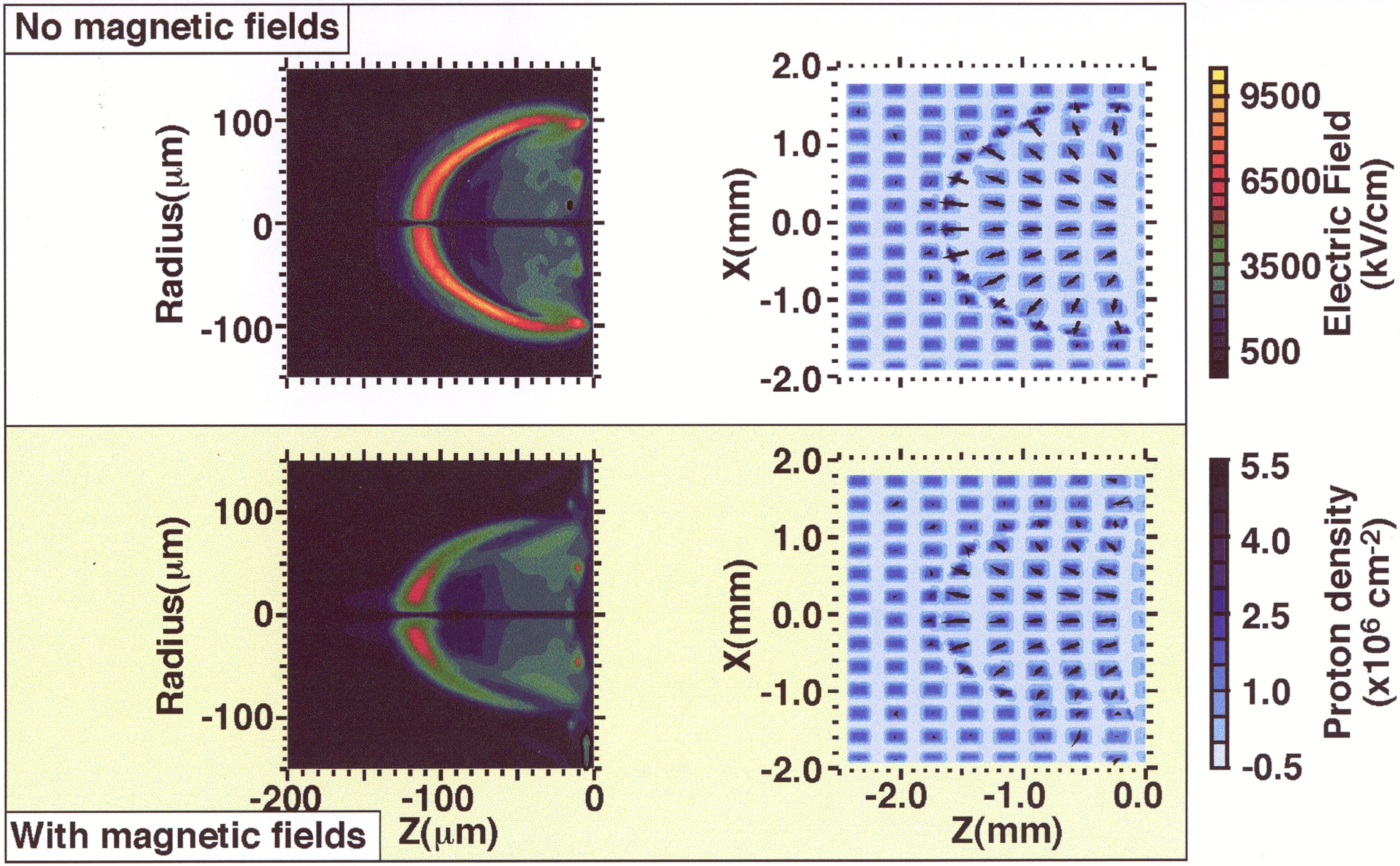

The electric field imparts additional transverse momentum to the protons

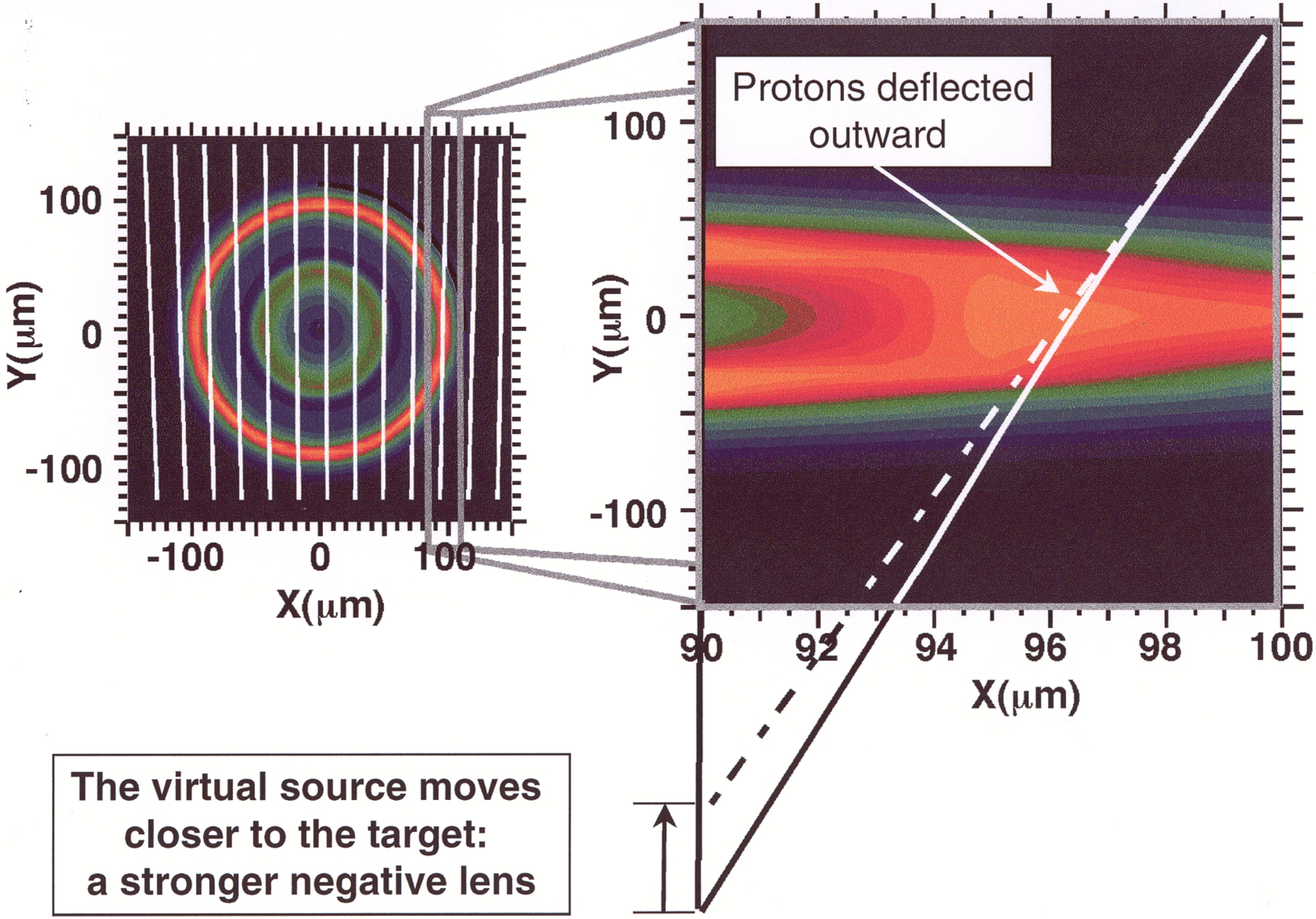

The virtual source moves closer to the target: a stronger negative lens

Magnetic fields of the order of 1MG have little effect on side-on proton deflectometry

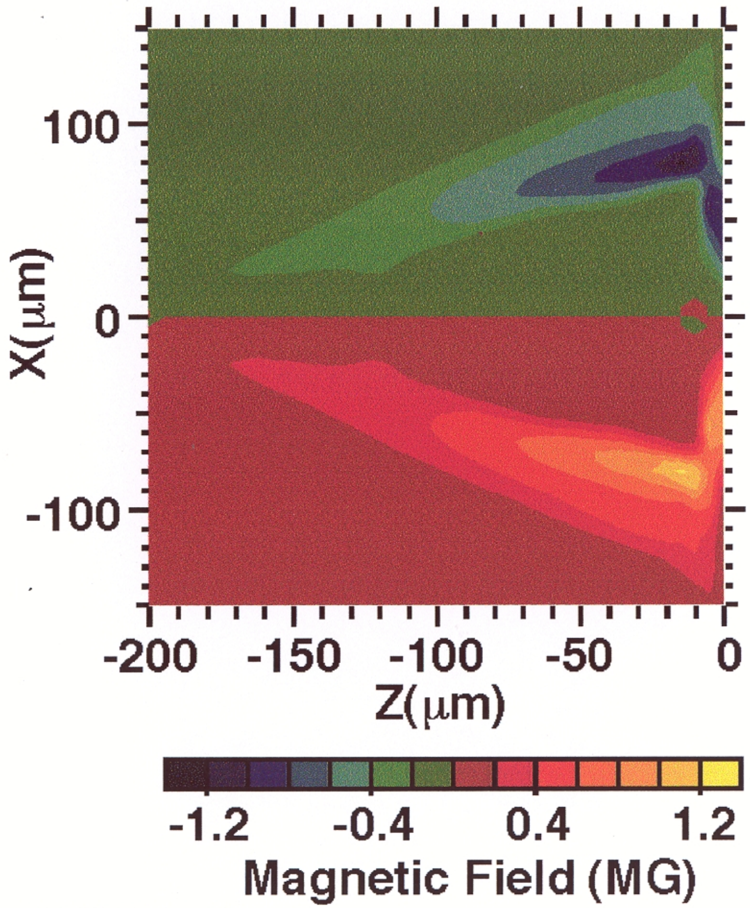

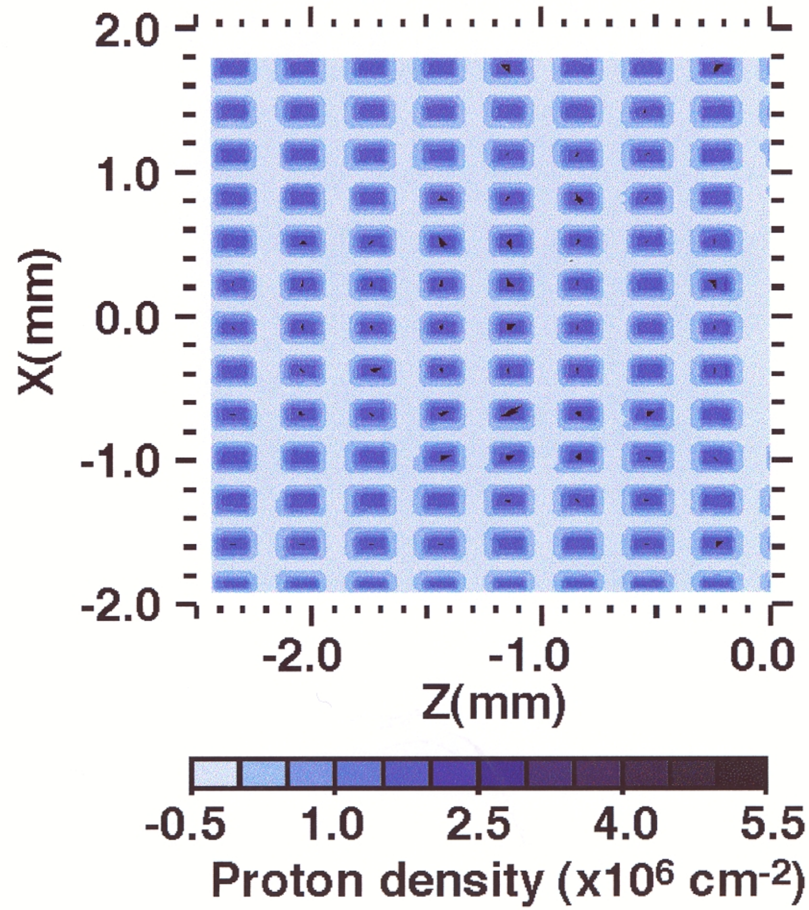

Run: mag182 pla4

Side-on deflectometry is not sensitive to the torroidal magnetic fields

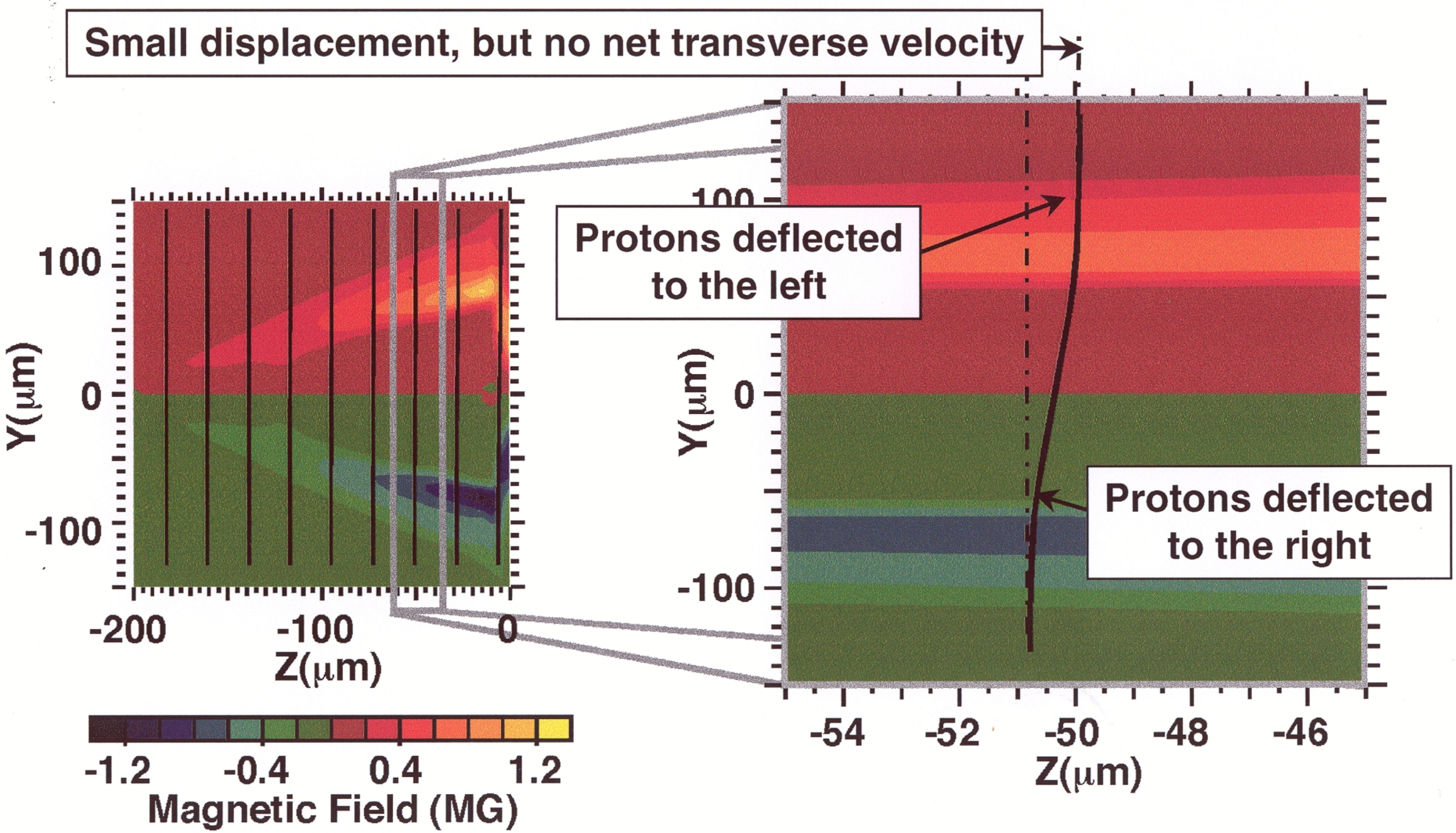

Face-on deflectometry is sensitive to the torroidal magnetic field

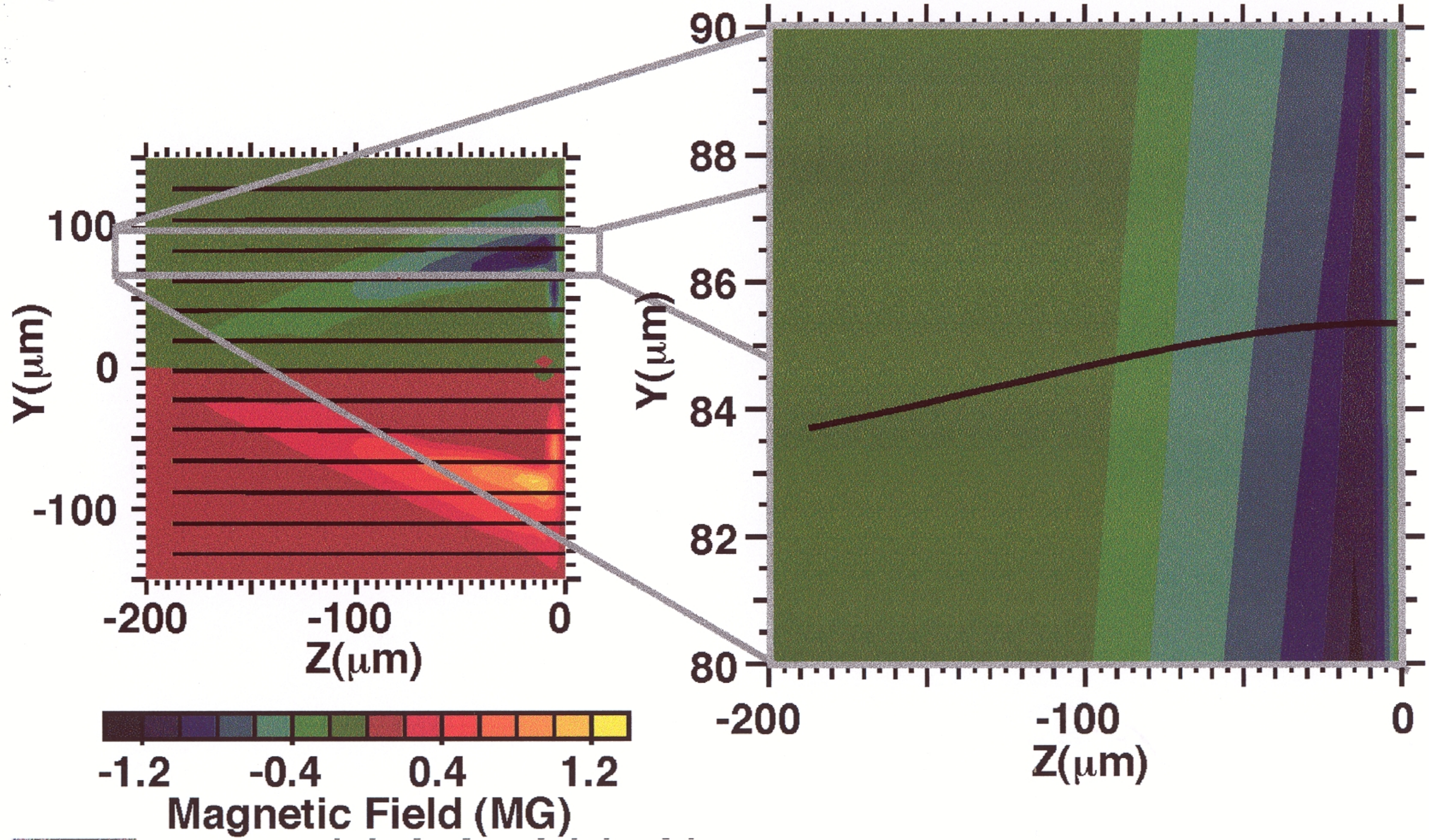

The lowest energy protons yield the largest deflections through electric and magnetic fields

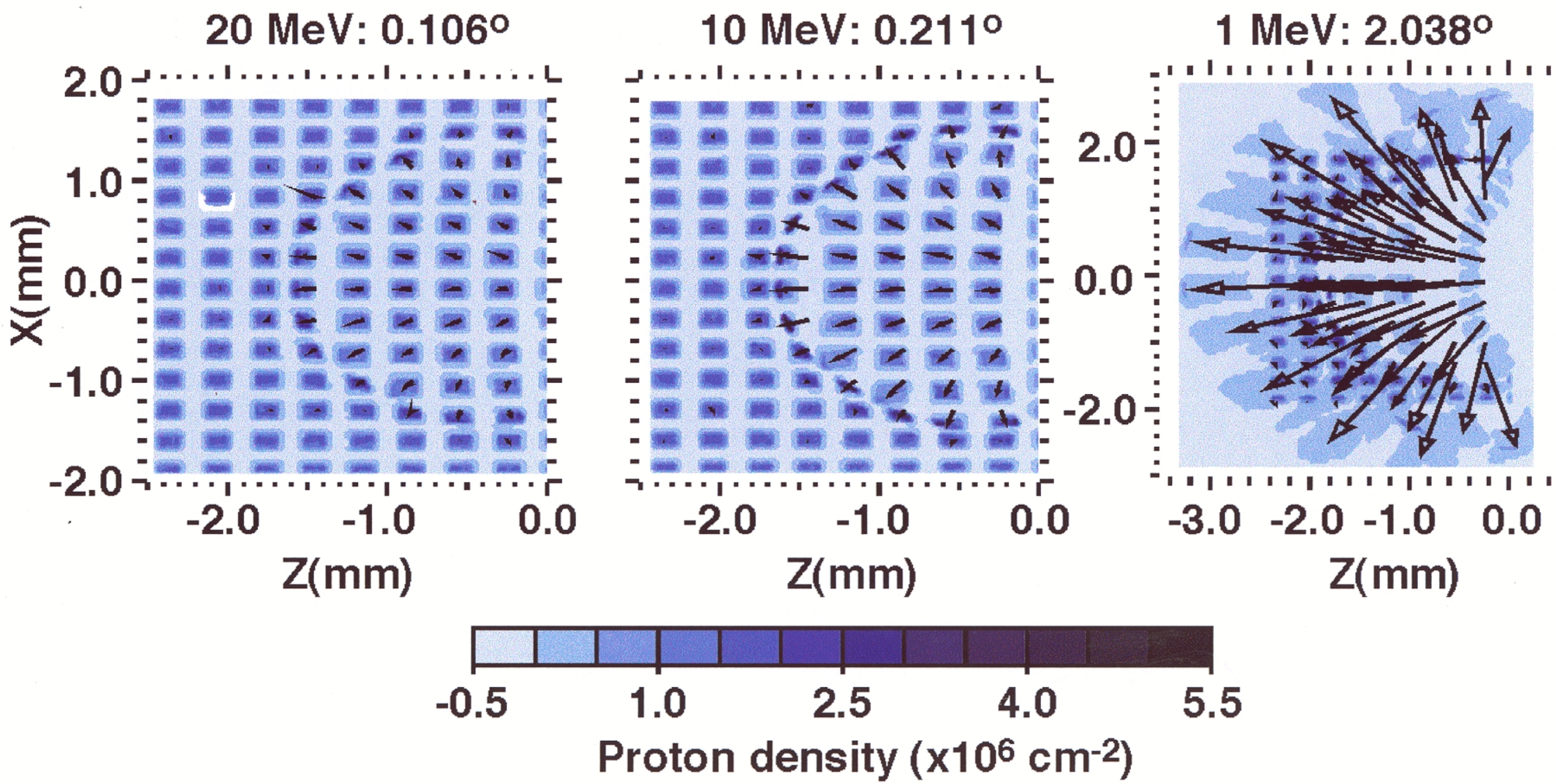

Run: pla2p

The deflection scales differently with proton energy with electric and magnetic fields

- For a constant electric field the deflection scales as v^{-2}.
- For a constant magnetic field the deflection scales as v^{-1}.

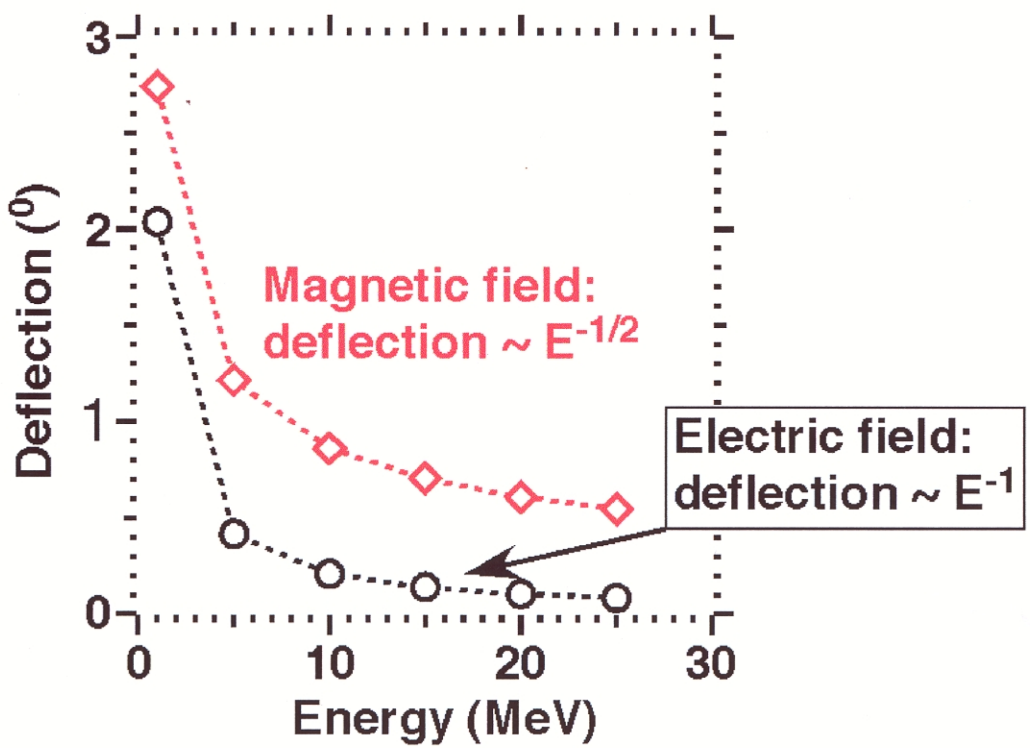

Collaborators:

- **M. J. Edwards, W. L. Kruer, A. B. Langdon, B. F. Lasinski, A. J. Mackinnon, P. K. Patel, M. Tabak, *LLNL, Livermore, CA, USA.***
- **M. Borghesi, L. Romagnani, *The Queen's University of Belfast, Belfast, UK.***
- **G. Pretzler, T. Toncian, O. Willi, *Heinrich-Heine Universtät, Düsseldorf, Germany.***
- **J.C. Gauthier, P. Audebert*, LULI, Ecole Polytechnique, France.***
- **D. R. Welch, MRC, *Albuquerque, NM, USA.***

Some numerical techniques developed in the Heavy-Ion Fusion program

J.-L. Vay - Lawrence Berkeley National Laboratory

Collaborators:

- **A. Friedman, D.P. Grote - Lawrence Livermore National Laboratory**
- **J.-C. Adam, A. Héron - CPHT, Ecole Polytechnique, France**
- **P. Colella, P. McCorquodale, D. Serafini - Lawrence Berkeley National Laboratory**

The Heavy-Ion Fusion program has developed, and continues to work on, numerical techniques that have broad applicability:

- **Absorbing Boundary Conditions (ABC)**
- **Adaptive Mesh Refinement (AMR) for Particle-In-Cell (PIC)**
- **Advanced Vlasov methods (moving grid,AMR)**
- **Cut-cell boundaries**

Short-Pulse Laser Matter Computational Workshop
Pleasanton, California - August 25-27, 2004

Absorbing Boundary Condition: Extended PML

Extended Perfectly Matched Layer

Maxwell

$$\varepsilon_0 \frac{\partial E_x}{\partial t} = \frac{\partial H_z}{\partial y}$$

$$\varepsilon_0 \frac{\partial E_y}{\partial t} = -\frac{\partial H_z}{\partial x}$$

$$\mu_0 \frac{\partial H_z}{\partial t} = -\frac{\partial E_y}{\partial x} + \frac{\partial E_x}{\partial y}$$

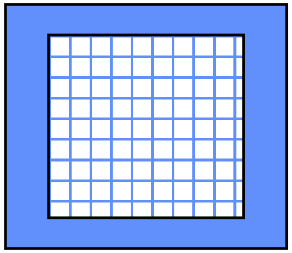

Principles of PML:

- Field vanishes in layer surrounding domain.
- Layer medium impedance Z matches vacuum's Z_0

Split Maxwell

$$\varepsilon_0 \frac{\partial E_x}{\partial t} = \frac{\partial H_z}{\partial y}$$

$$\varepsilon_0 \frac{\partial E_y}{\partial t} = -\frac{\partial H_z}{\partial x}$$

$$\mu_0 \frac{\partial H_{zx}}{\partial t} = -\frac{\partial E_y}{\partial x}$$

$$\mu_0 \frac{\partial H_{zy}}{\partial t} = \frac{\partial E_x}{\partial y}$$

Berenger PML

$$\sigma_y E_x + \varepsilon_0 \frac{\partial E_x}{\partial t} = \frac{\partial H_z}{\partial y}$$

$$\sigma_x E_y + \varepsilon_0 \frac{\partial E_y}{\partial t} = -\frac{\partial H_z}{\partial x}$$

$$\sigma_x^* H_{zx} + \mu_0 \frac{\partial H_{zx}}{\partial t} = -\frac{\partial E_y}{\partial x}$$

$$\sigma_y^* H_{zy} + \mu_0 \frac{\partial H_{zy}}{\partial t} = \frac{\partial E_x}{\partial y}$$

If $\frac{\sigma_u}{\varepsilon_0} = \frac{\sigma_u^*}{\mu_0}$ with u=(x,y)

=> $Z=Z_0$: no reflection.

Extended PML

$$\sigma_y E_x + \varepsilon_0 \frac{\partial E_x}{\partial t} = \frac{\partial H_z}{\partial y} \frac{c_y}{c} + \bar{\sigma}_y H_z$$

$$\sigma_x E_y + \varepsilon_0 \frac{\partial E_y}{\partial t} = -\frac{\partial H_z}{\partial x} \frac{c_x}{c} + \bar{\sigma}_x H_z$$

$$\sigma_x^* H_{zx} + \mu_0 \frac{\partial H_{zx}}{\partial t} = -\frac{\partial E_y}{\partial x} \frac{c_x^*}{c} + \bar{\sigma}_x^* E_y$$

$$\sigma_y^* H_{zy} + \mu_0 \frac{\partial H_{zy}}{\partial t} = \frac{\partial E_x}{\partial y} \frac{c_y^*}{c} + \bar{\sigma}_y^* E_x$$

If $\frac{\sigma_u}{\varepsilon_0} = \frac{\sigma_u^*}{\mu_0}, \frac{\bar{\sigma}_u}{\varepsilon_0} = \frac{\bar{\sigma}_u^*}{\mu_0}$ and $c_u = c_u^*$

=> $Z=Z_0$: no reflection.

Plane wave analysis of PML and Extended PML

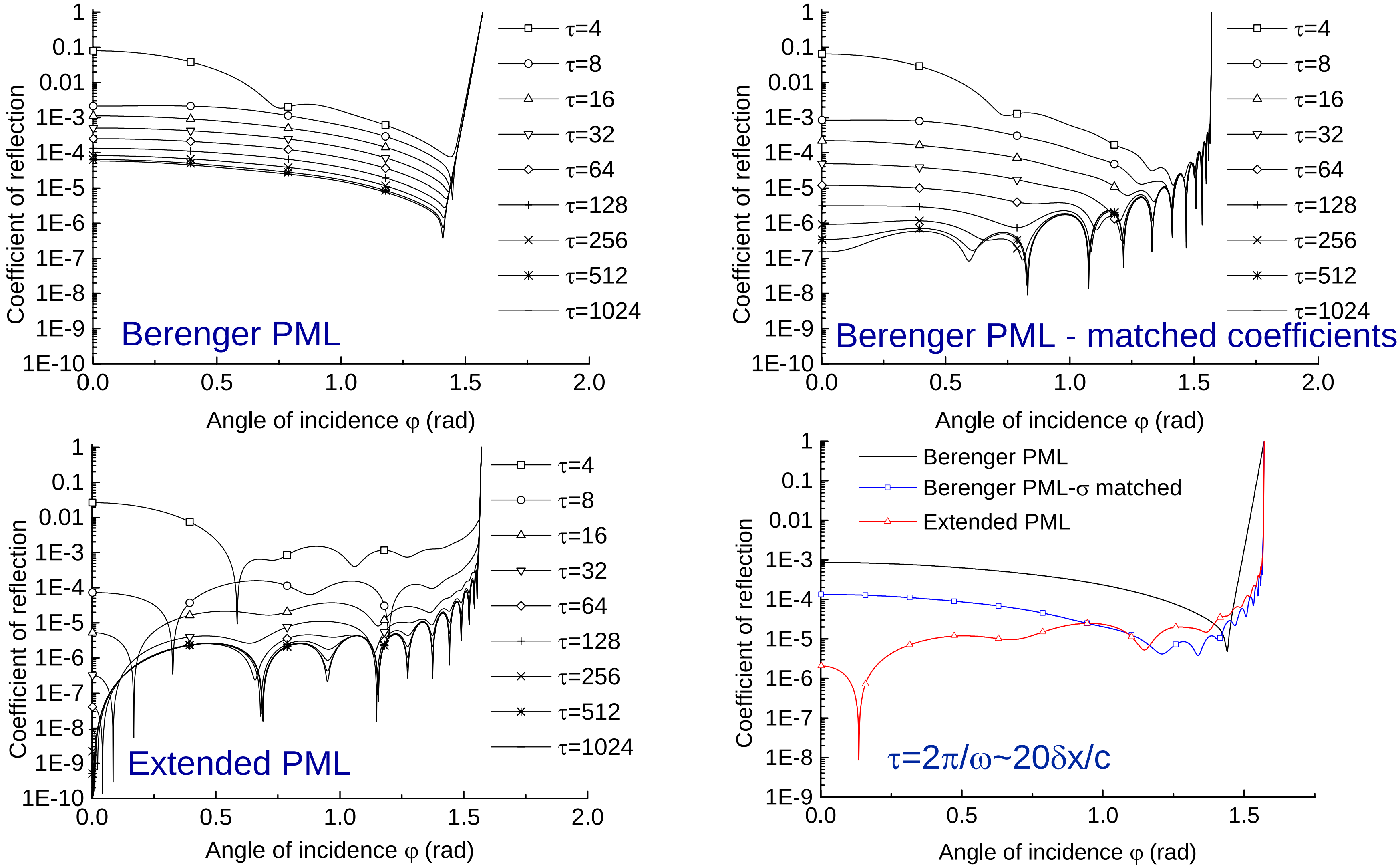

- **matching condition on coefficients in PML layer improves absorption**
- **Extended PML another overall improvement**

Extended PML implemented in EM PIC code Emi2d

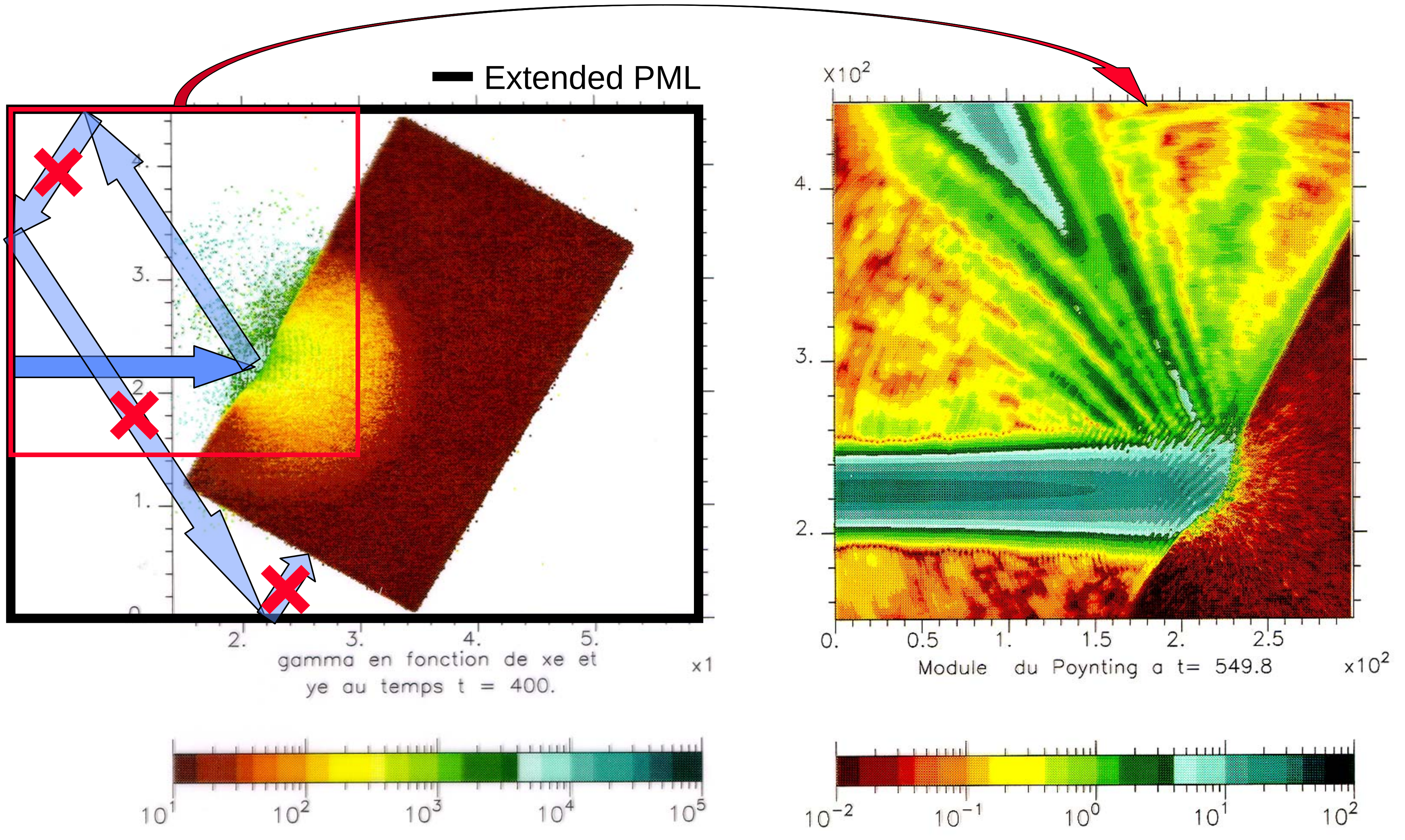

Adaptive Mesh Refinement for Particle-In-Cell

End-to-end modeling of a Heavy Ion Fusion driver

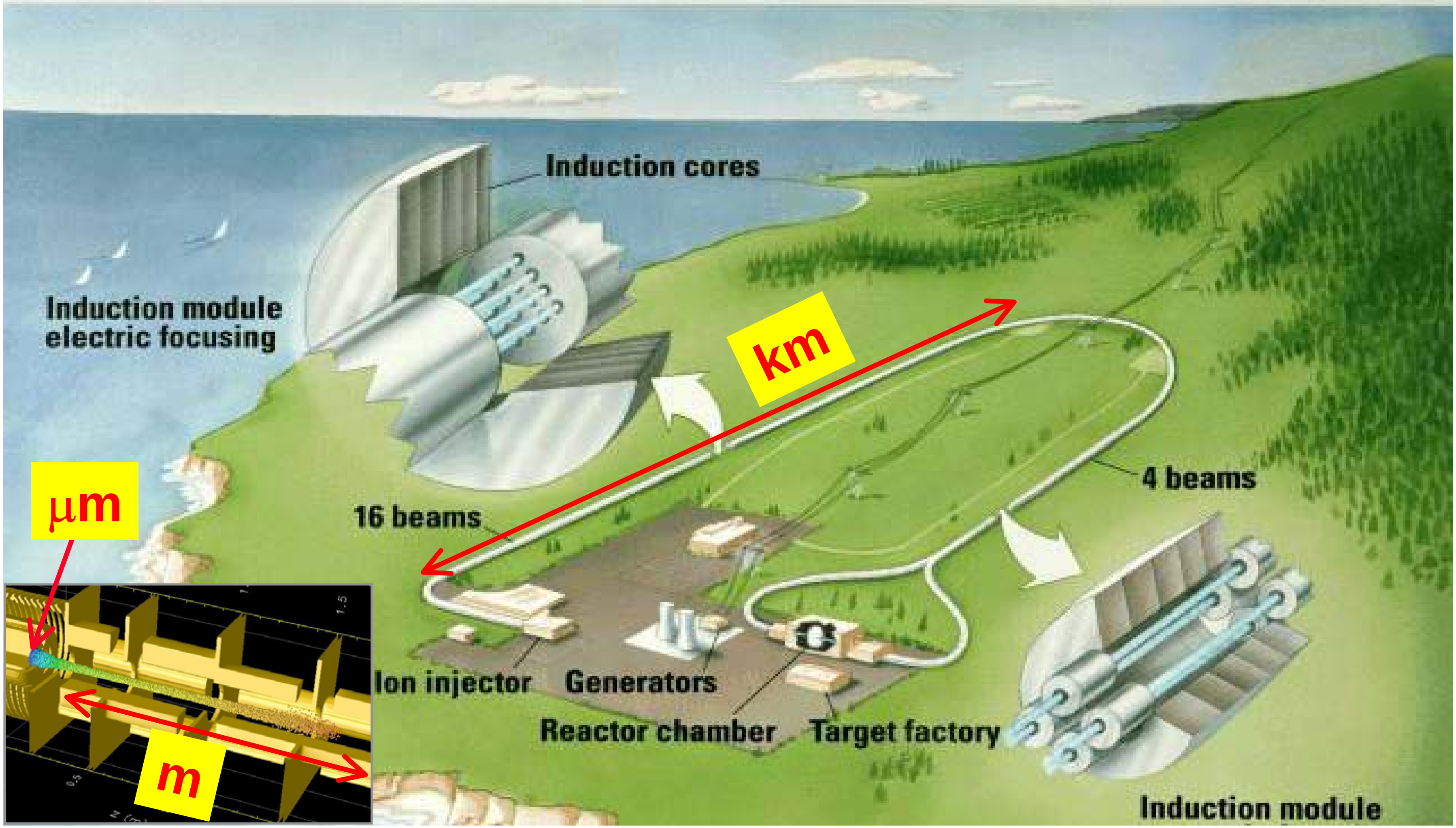

challenging because length scales span a wide range: μm to km(s)

The Adaptive-Mesh-Refinement (AMR) method

- **addresses the issue of wide range of space scales**
- **well established method in fluid calculations**

3D AMR simulation of an explosion (microseconds after ignition)

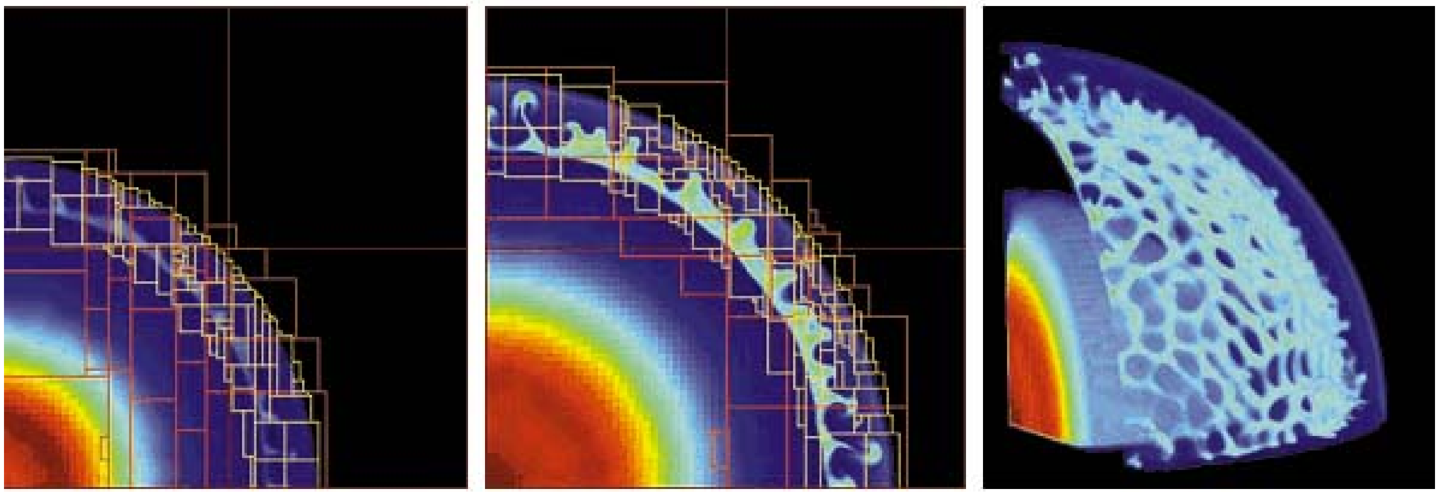

AMR concentrates the resolution around the edge which contains the most interesting scientific features.

- **potential issues with PIC at interface**
  – **spurious self-force on macro-particles**
  – **violation of Gauss' Law**
  – **spurious reflection of short wavelengths with amplification**

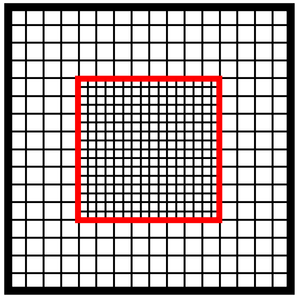

3D WARP simulation of High-Current Experiment (HCX)

Modeling of source is critical since it determines initial shape of beam

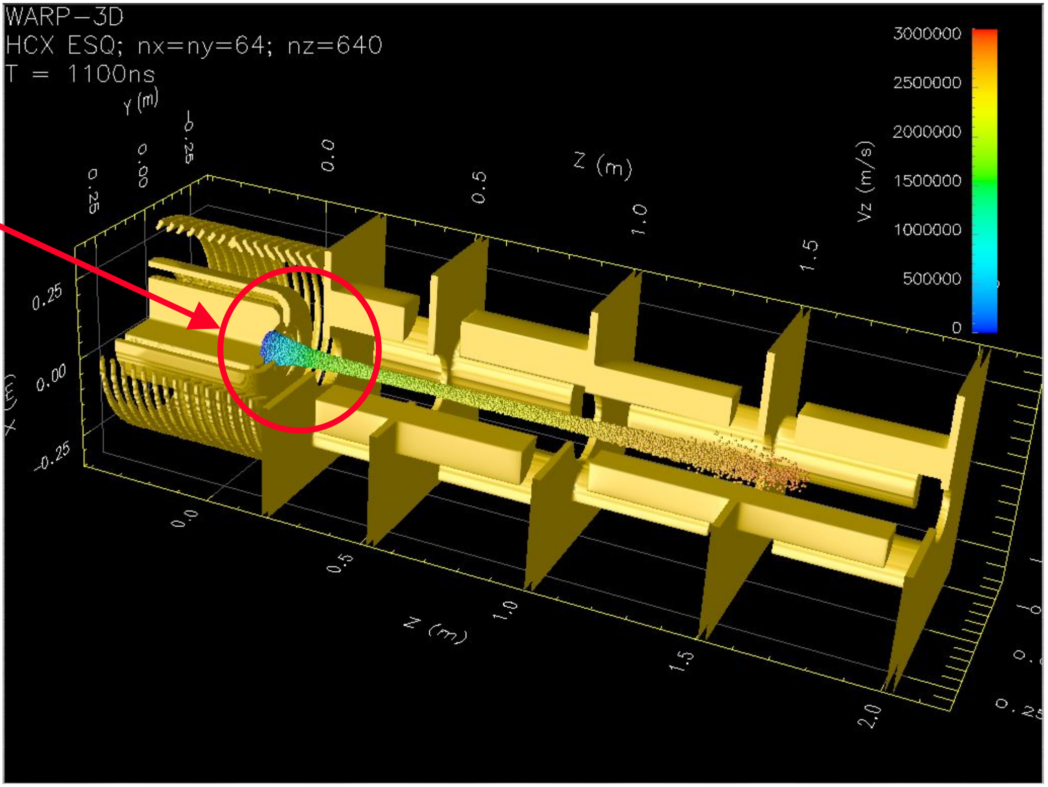

WARP simulations show that a fairly high resolution is needed to reach convergence

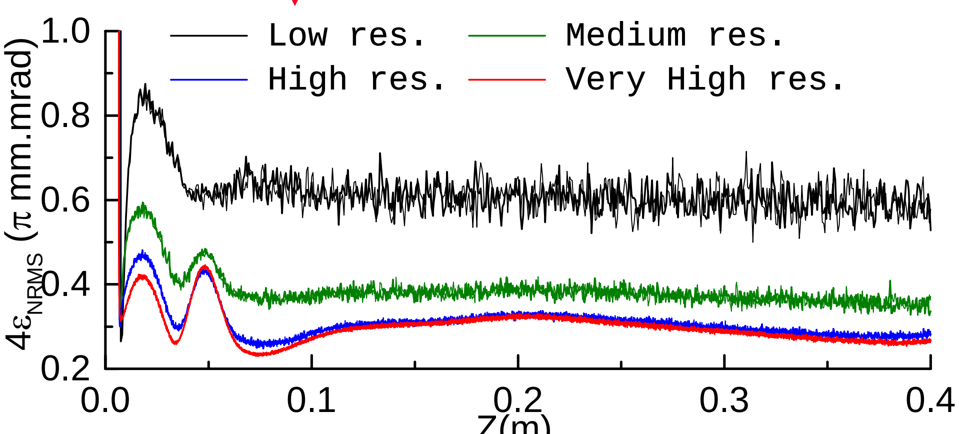

Run	Grid size	Nb particles
Low res.	56x640	~1M
Medium res.	112x1280	~4M
High res.	224x2560	~16M
Very High res.	448x5120	~64M

Example of AMR calculation with WARPrz: speedup ~10.5

Run	Grid size	Nb particles
Low res.	56x640	~1M
Medium res.	112x1280	~4M
High res.	224x2560	~16M
Low res. + AMR	56x640	~1M

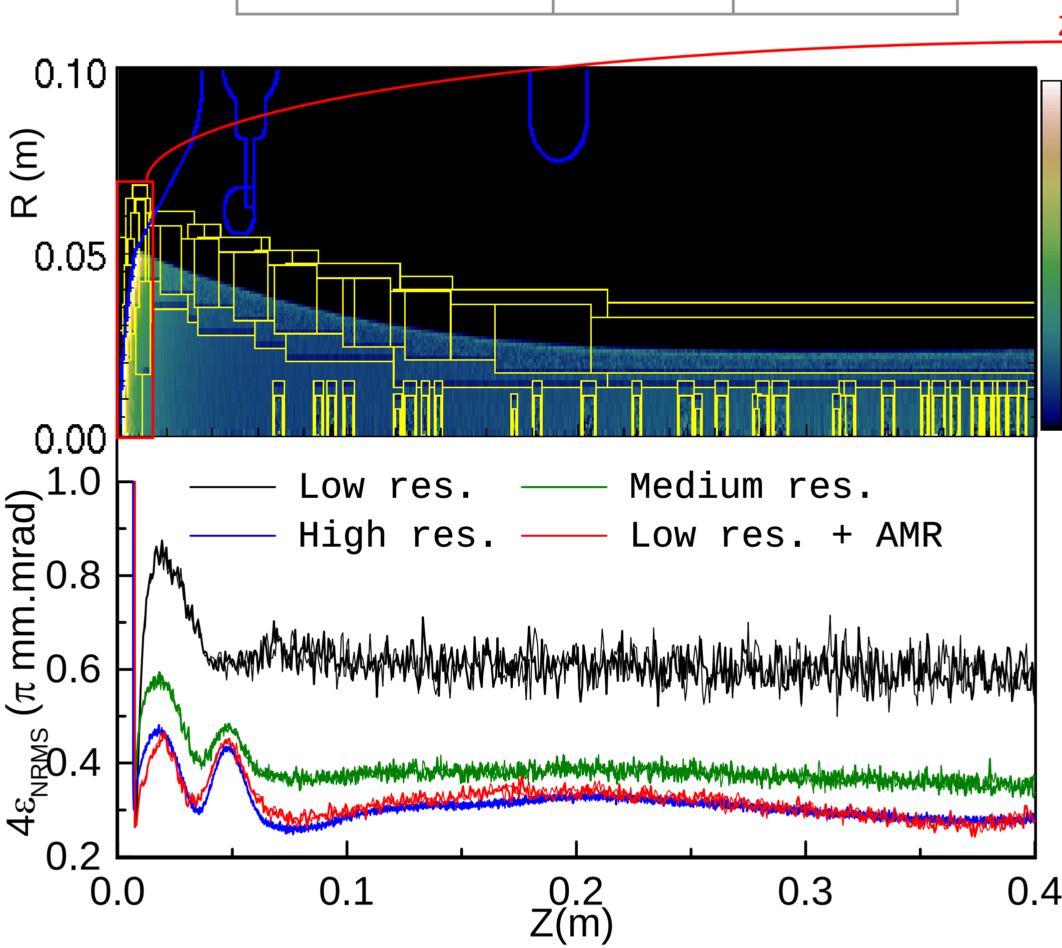

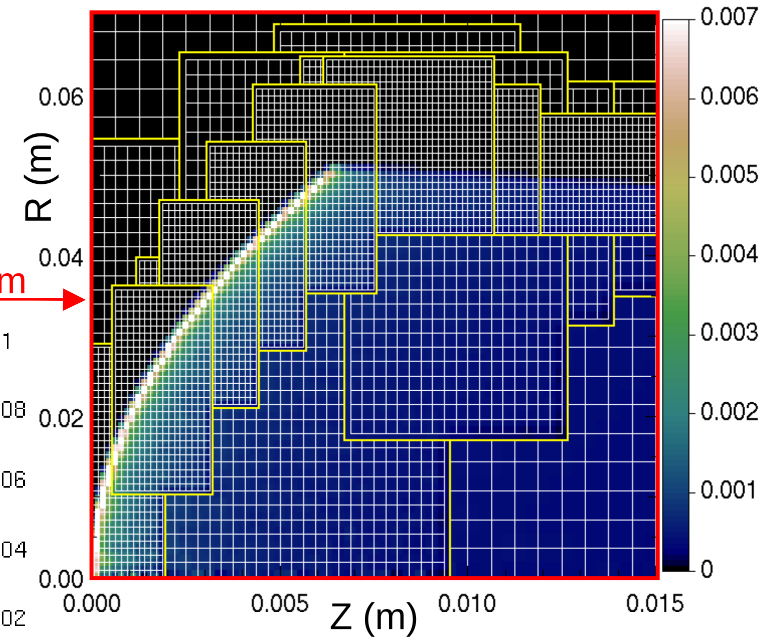

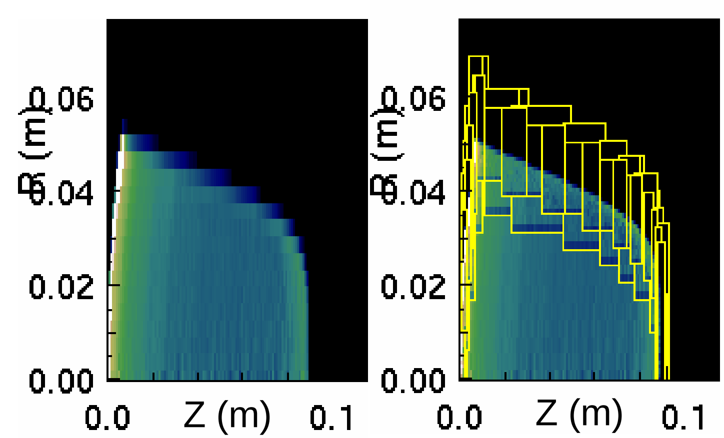

Refinement of gradients: emitting area, beam edge and front.

3D WARP simulation of HCX shows beam head scrapping

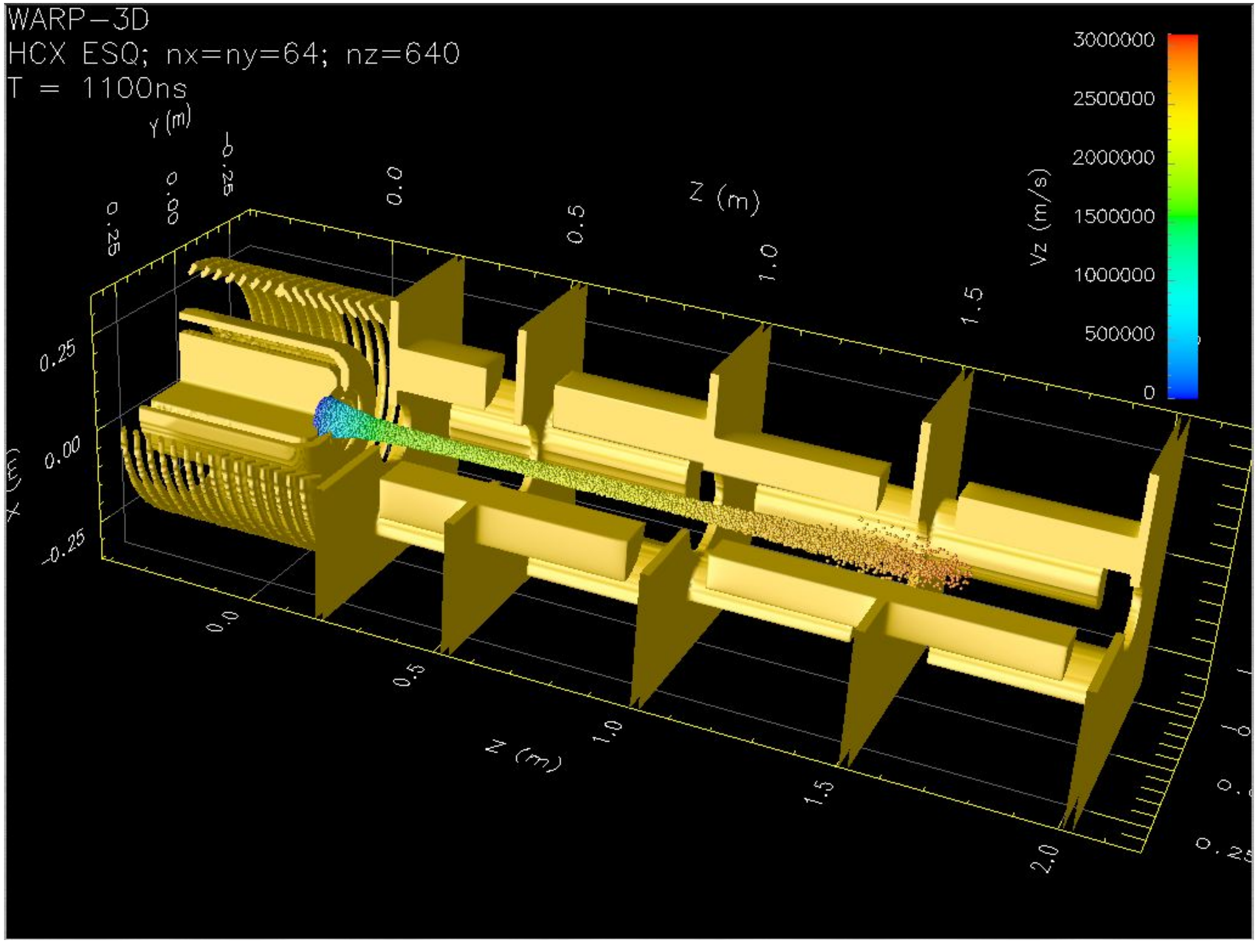

Rise-time τ = 800 ns
beam head particle loss < 0.1%

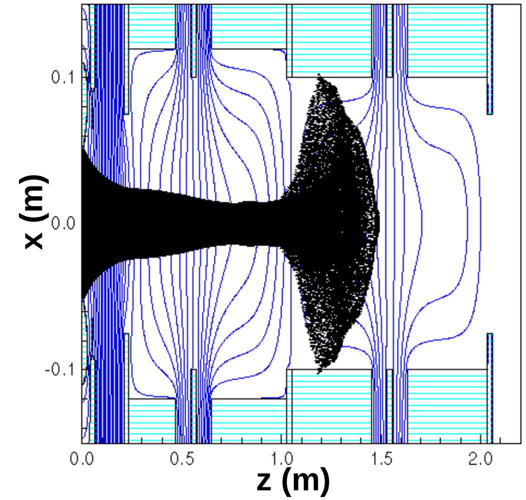

Rise-time τ = 400 ns
zero beam head particle loss

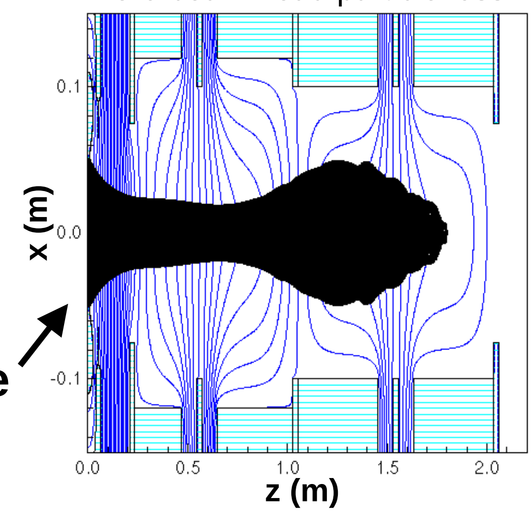

- **Simulations show: head cleaner with shorter rise-time**
- **Question: what is the optimal rise-time?**

1D time-dependent modeling of ion diode

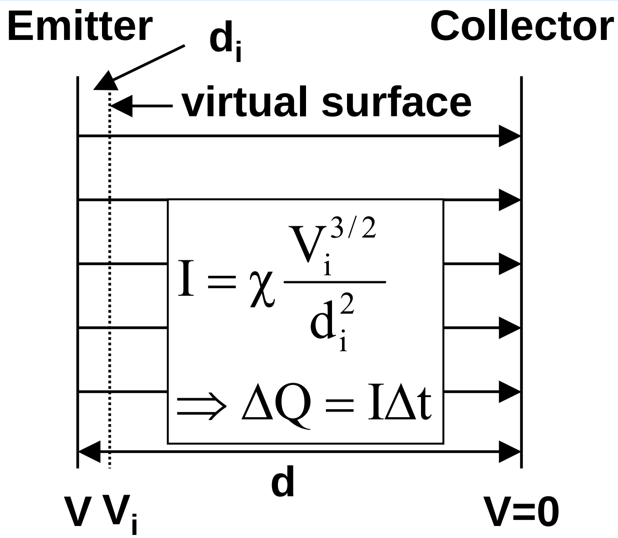

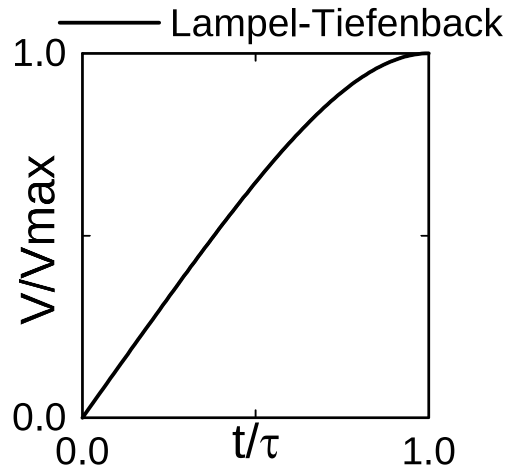

$$\frac{V(t)}{V_{max}} = \frac{t}{3\tau}\left[4 - \left(\frac{t}{\tau}\right)^3\right]$$

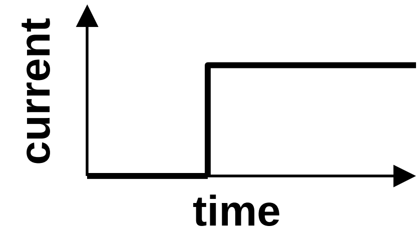

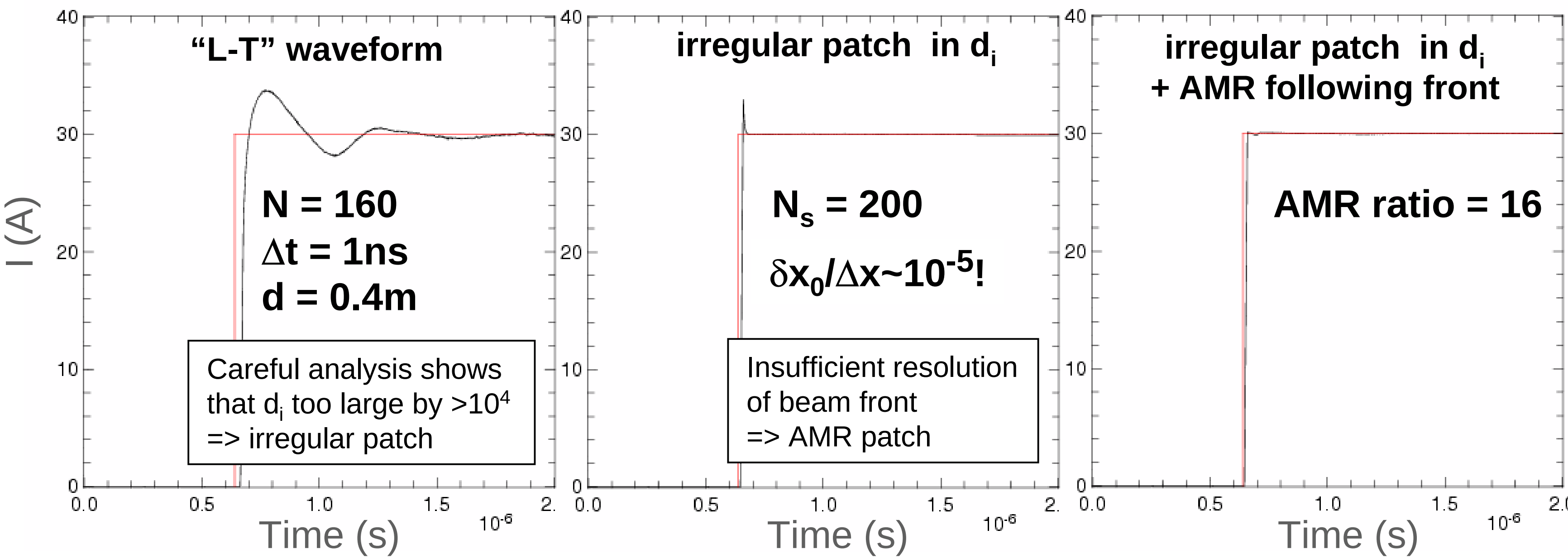

MR patch suppresses long wavelength oscillation - AMR patch suppresses front peak

Application to three dimensions

- Specialized 1-D patch implemented in 3-D injection routine (2-D array)
- Extension Lampel-Tiefenback technique to 3-D implemented in WARP
  - predicts a voltage waveform which extracts a nearly flat current at emitter

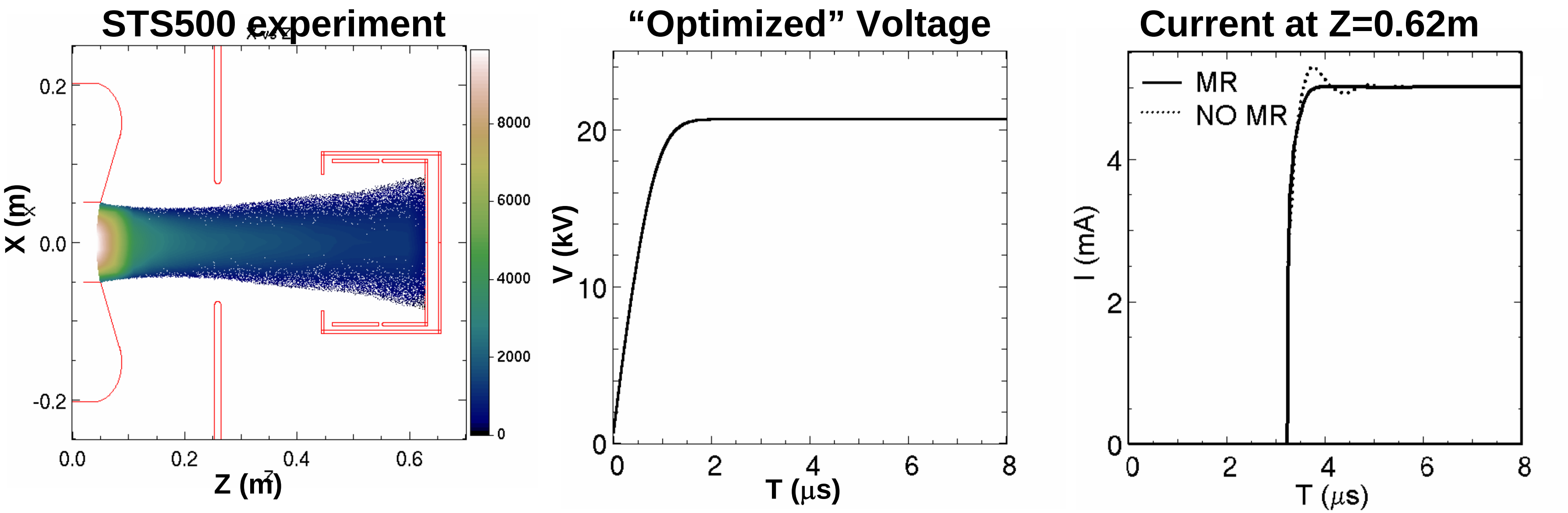

- Run with MR predicts very sharp risetime (not square due to erosion)
- Without MR, WARP predicts overshoot

MR patch key in simulation of STS500 Experiment

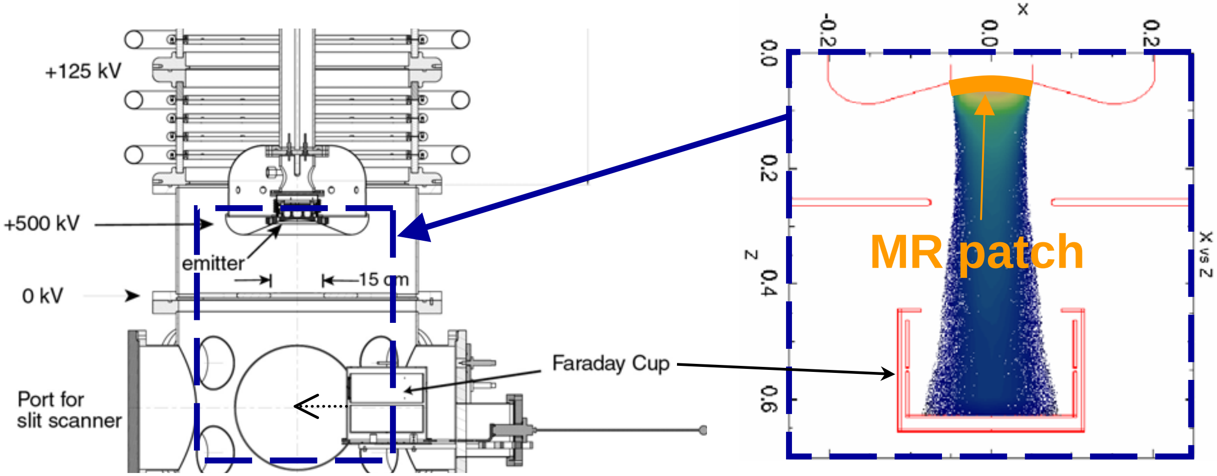

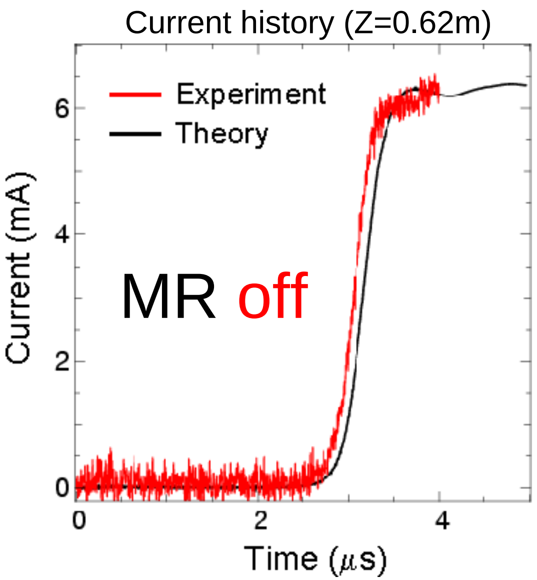

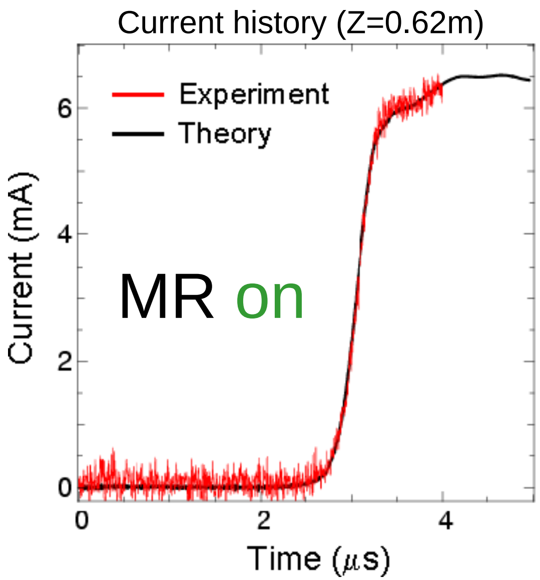

- Mesh Refinement essential to recover experimental results
- Ratio of smaller mesh to main grid mesh ~ 1/1000

New MR method implemented in EM PIC code Emi2d

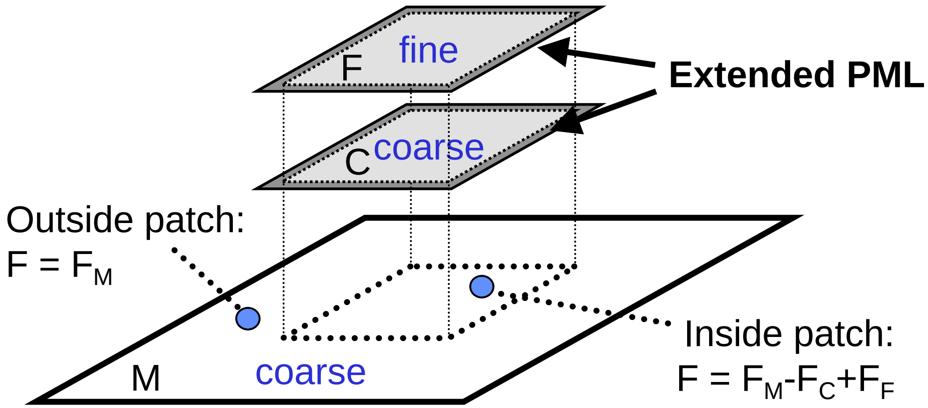

Mesh refinement by substitution

Applied to Laser-plasma interaction in the context of fast ignition

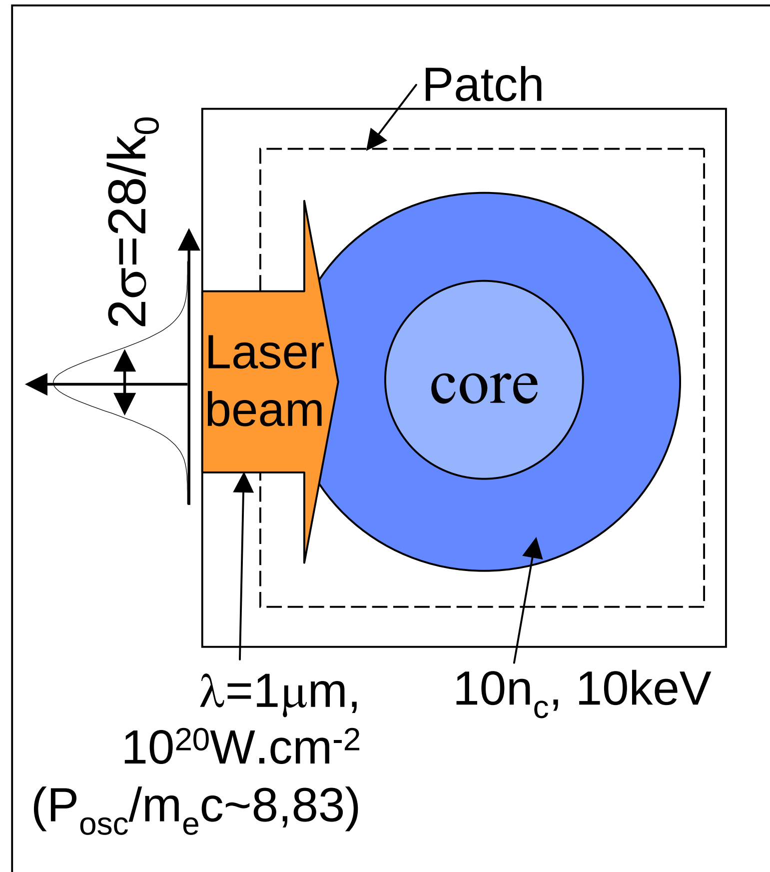

Illustration of instability in 1-D EM tests

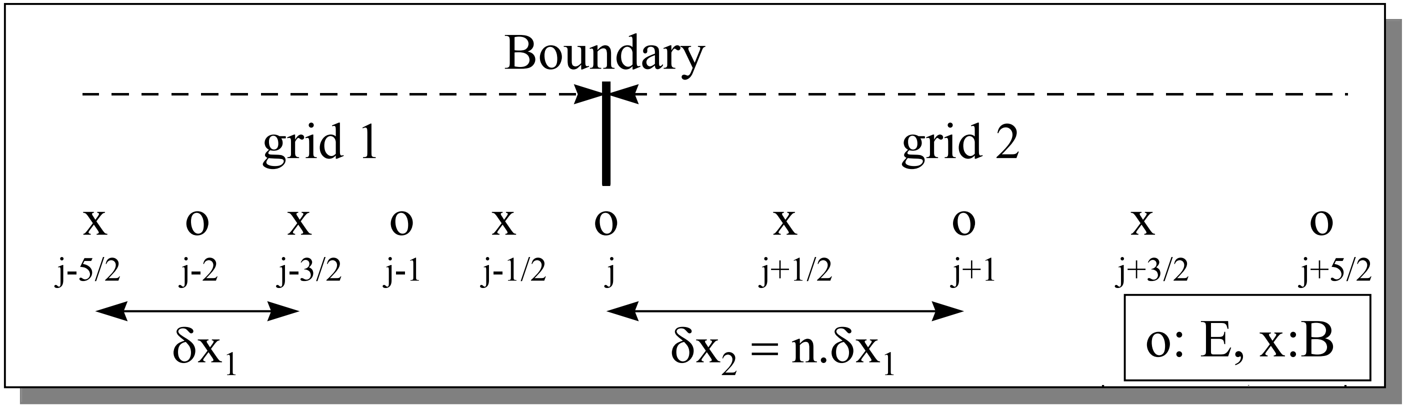

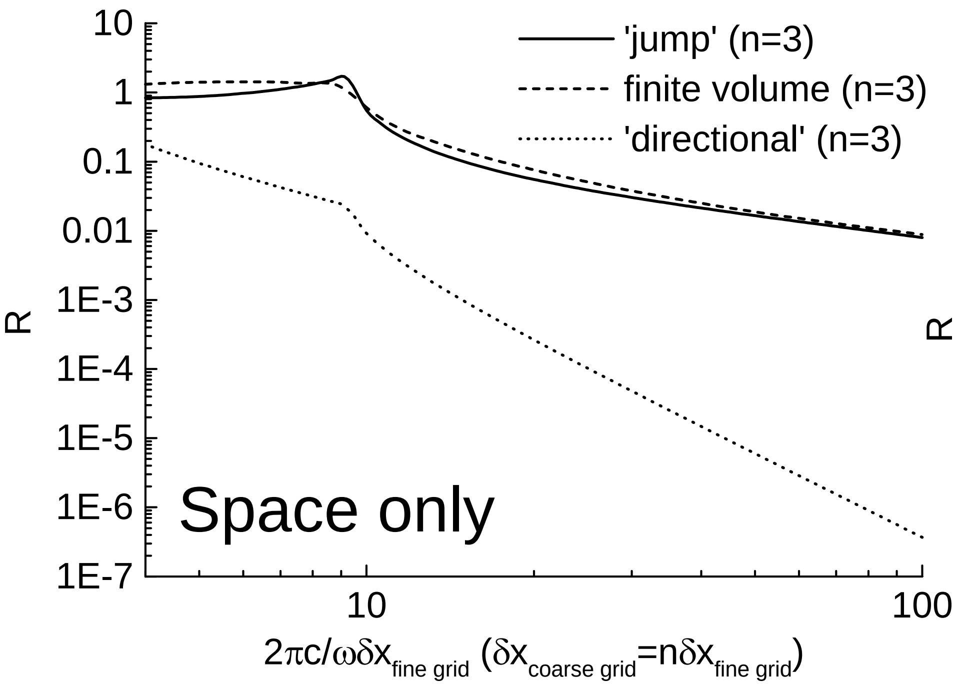

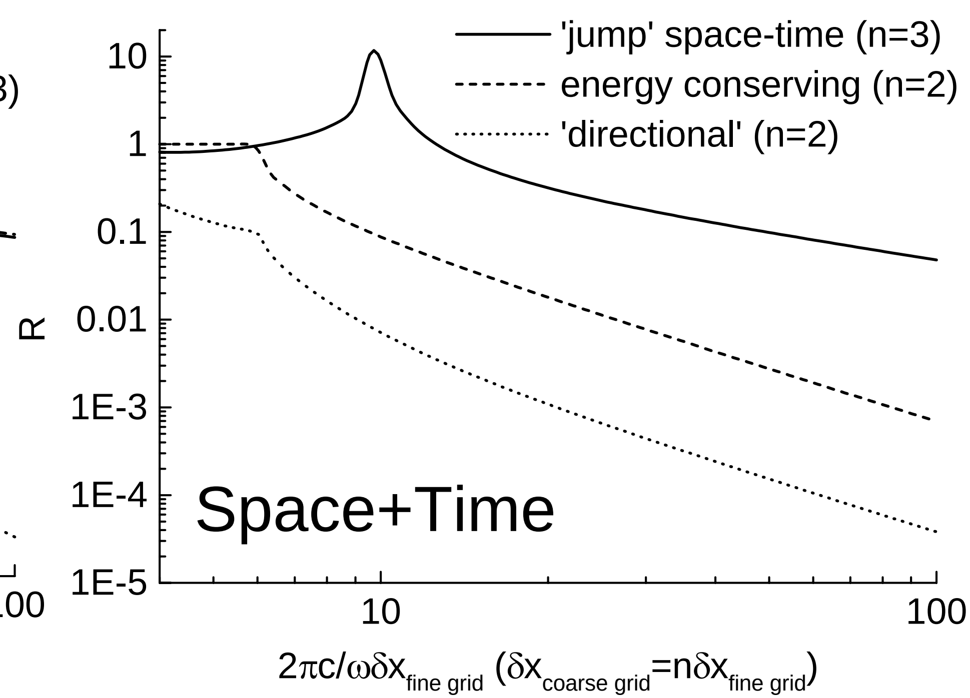

Most MR schemes relying on interpolations are potentially unstable.

Comparison patch on/off very encouraging

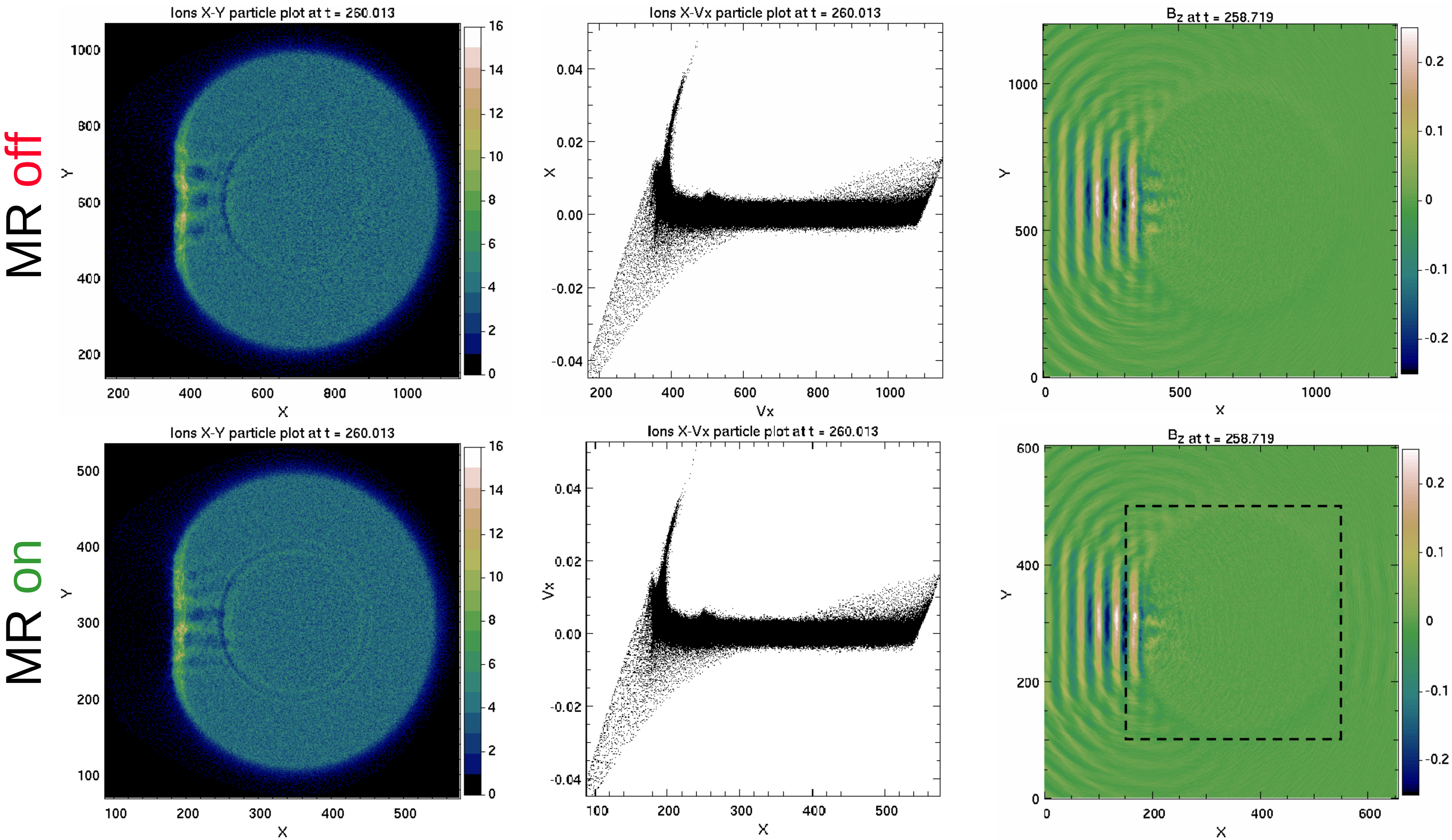

- same results except for small residual incident laser outside region of interest
- no instability nor spurious wave reflection observed at patch border

Effort to develop AMR library for PIC at LBNL

- **Researchers from AFRD (PIC) and ANAG (AMR-Phil Colella's group) collaborate to provide a library of tools that will give AMR capability to existing PIC codes (on serial and parallel computers)**
- **The base is the existing ANAG's AMR library Chombo**
- **The way it works**

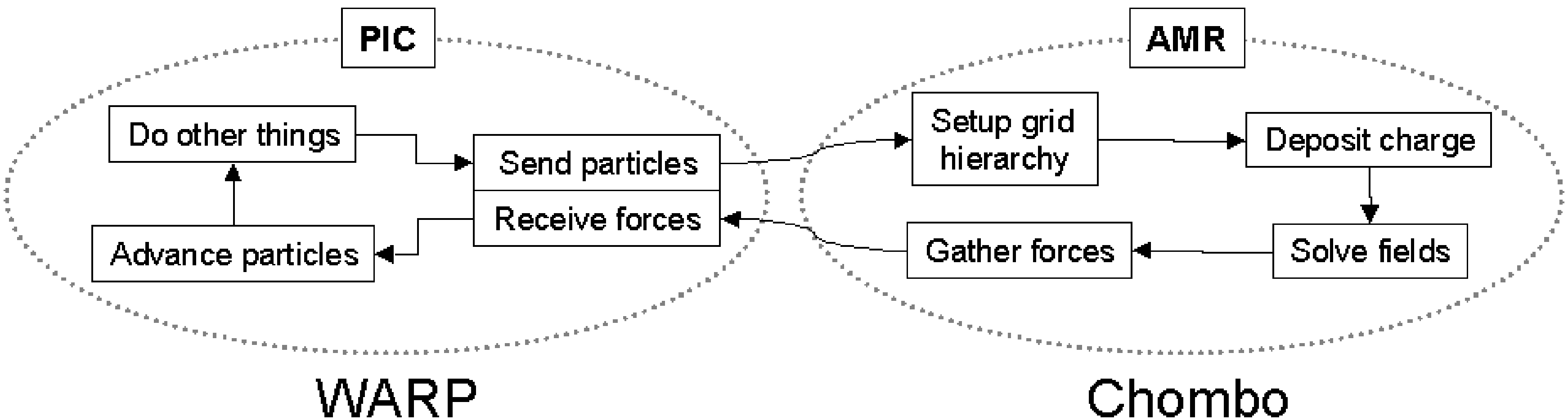

- **WARP is test PIC code but library will be usable by any PIC code**

Example of WARP-Chombo injector field calculation

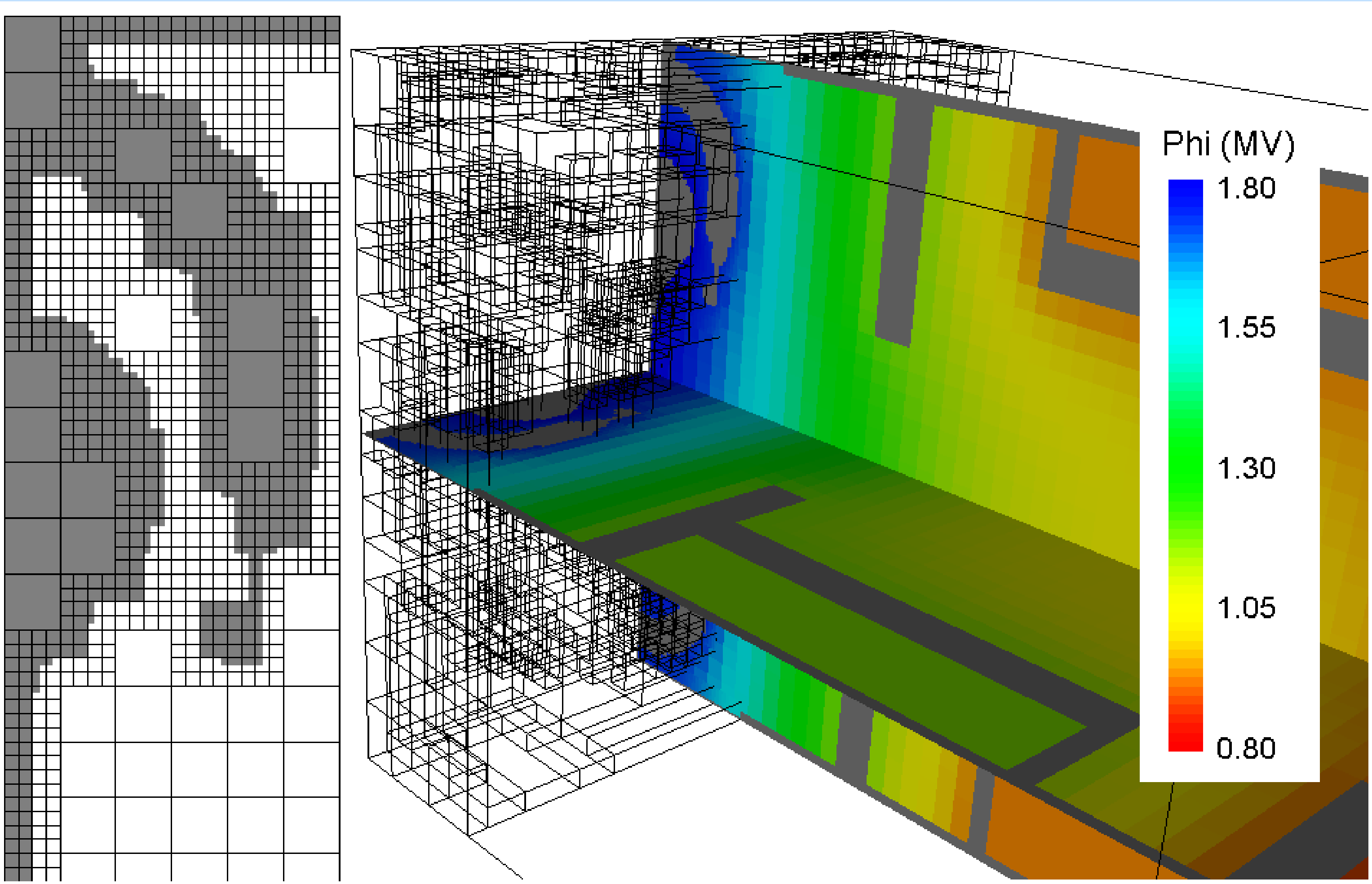

- Chombo can handle very complex grid hierarchy
- Electrostatic solver implemented, electromagnetic solver planned

References

Extended PML

J.-L. Vay, “Asymmetric Perfectly Matched Layer for the Absorption of Waves”, *J. Comp. Physics* **183**, 367-399 (2002)

AMR-PIC

Vay JL., Colella P., Kwan JW., McCorquodale P., Serafini DB., Friedman A., Grote DP., Westenskow G., Adam JC. ,Heron A., Haber I., “Application of adaptive mesh refinement to particle-in-cell simulations of plasmas and beams”, *Physics of Plasmas,* **11(5)**, 2928-2934, 2004

Some numerical techniques developed in the Heavy-Ion Fusion program

J.-L. Vay - Lawrence Berkeley National Laboratory

Collaborators:

- A. Friedman, D.P. Grote - Lawrence Livermore National Laboratory
- J.-C. Adam, A. Héron - CPHT, Ecole Polytechnique, France
- P. Colella, P. McCorquodale, D. Serafini - Lawrence Berkeley National Laboratory

The Heavy-Ion Fusion program has developed, and continues to work on, numerical techniques that have broad applicability:

- Absorbing Boundary Conditions (ABC)
- Adaptive Mesh Refinement (AMR) for Particle-In-Cell (PIC)
- Advanced Vlasov methods (moving grid,AMR)
- Cut-cell boundaries

Short-Pulse Laser Matter Computational Workshop
Pleasanton, California - August 25-27, 2004

Extended Perfectly Matched Layer

Principles of PML

- field vanishes in layer surrounding domain,
- layer medium impedance Z matches vacuum's Z_0.

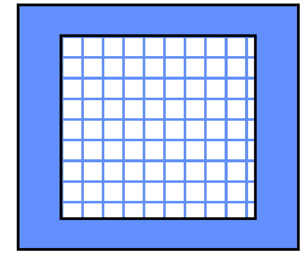

Berenger PML => Extended PML

$$
\begin{aligned}
\sigma_y E_x + \varepsilon_0 \frac{\partial E_x}{\partial t} &= \frac{\partial H_z}{\partial y} \frac{c_y}{c} + \bar{\sigma}_y H_z \\
\sigma_x E_y + \varepsilon_0 \frac{\partial E_y}{\partial t} &= -\frac{\partial H_z}{\partial x} \frac{c_x}{c} + \bar{\sigma}_x H_z \\
\sigma_x^* H_{zx} + \mu_0 \frac{\partial H_{zx}}{\partial t} &= -\frac{\partial E_y}{\partial x} \frac{c_x^*}{c} + \bar{\sigma}_x^* E_y \\
\sigma_y^* H_{zy} + \mu_0 \frac{\partial H_{zy}}{\partial t} &= \frac{\partial E_x}{\partial y} \frac{c_y^*}{c} + \bar{\sigma}_y^* E_x
\end{aligned}
$$

If $\frac{\sigma_u}{\varepsilon_0} = \frac{\sigma_u^*}{\mu_0}, \frac{\bar{\sigma}_u}{\varepsilon_0} = \frac{\bar{\sigma}_u^*}{\mu_0}$ and $c_u = c_u^*$ with u=(x,y), $Z=Z_0$ => no reflection.

Extended PML implemented in EM PIC code Emi2d

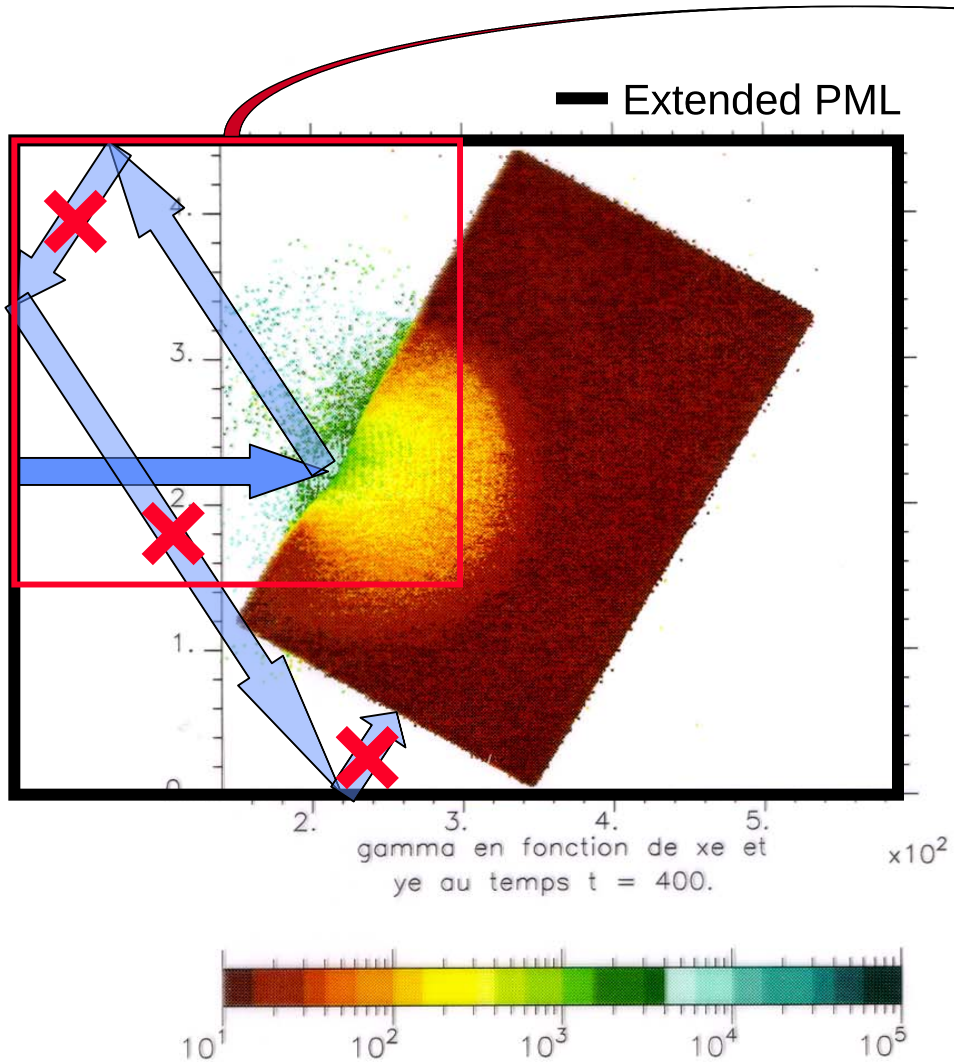

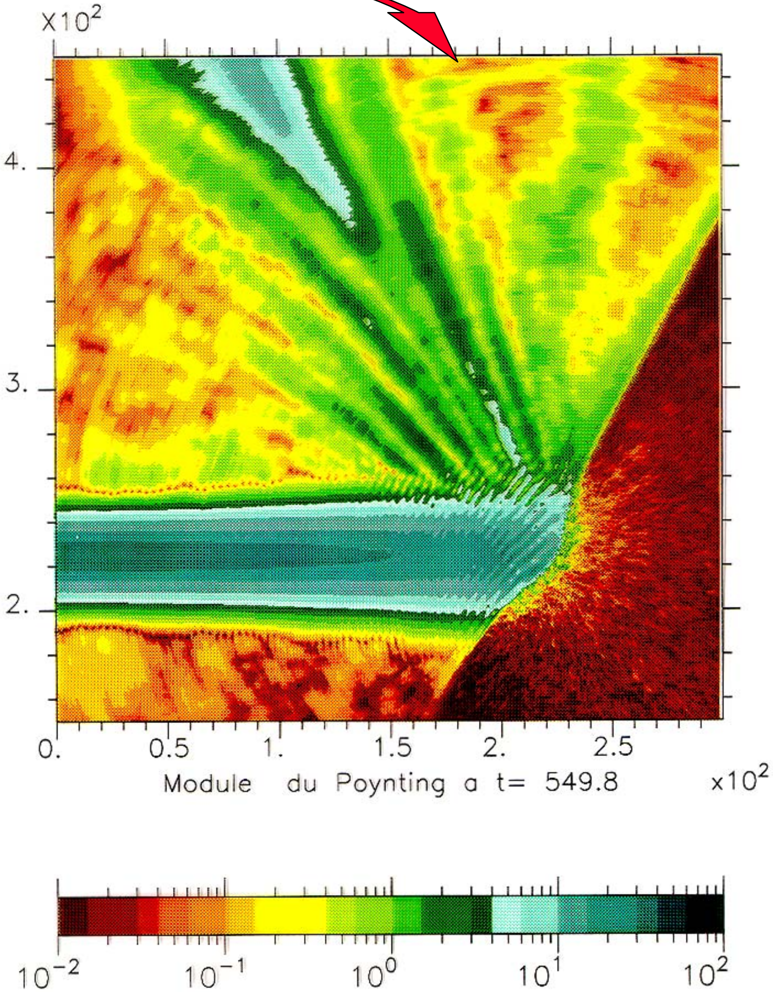

The Adaptive-Mesh-Refinement (AMR) method

- **addresses the issue of wide range of space scales**
- **well established method in fluid calculations**

3D AMR simulation of an explosion (microseconds after ignition)

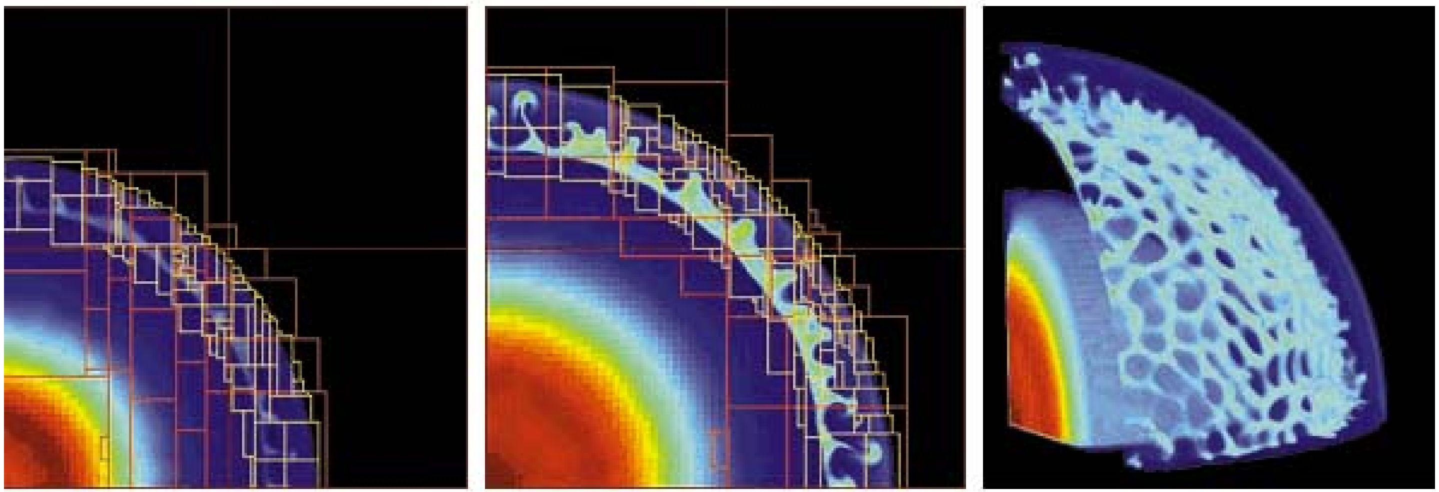

AMR concentrates the resolution around the edge which contains the most interesting scientific features.

- **potential issues with PIC at interface**
  - **spurious self-force on macro-particles**
  - **violation of Gauss' Law**
  - **spurious reflection of short wavelengths with amplification**

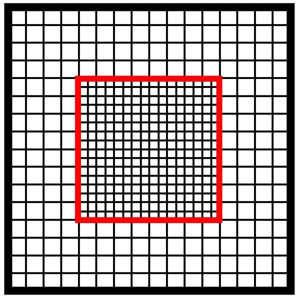

3D WARP simulation of High-Current Experiment (HCX)

Modeling of source is critical since it determines initial shape of beam

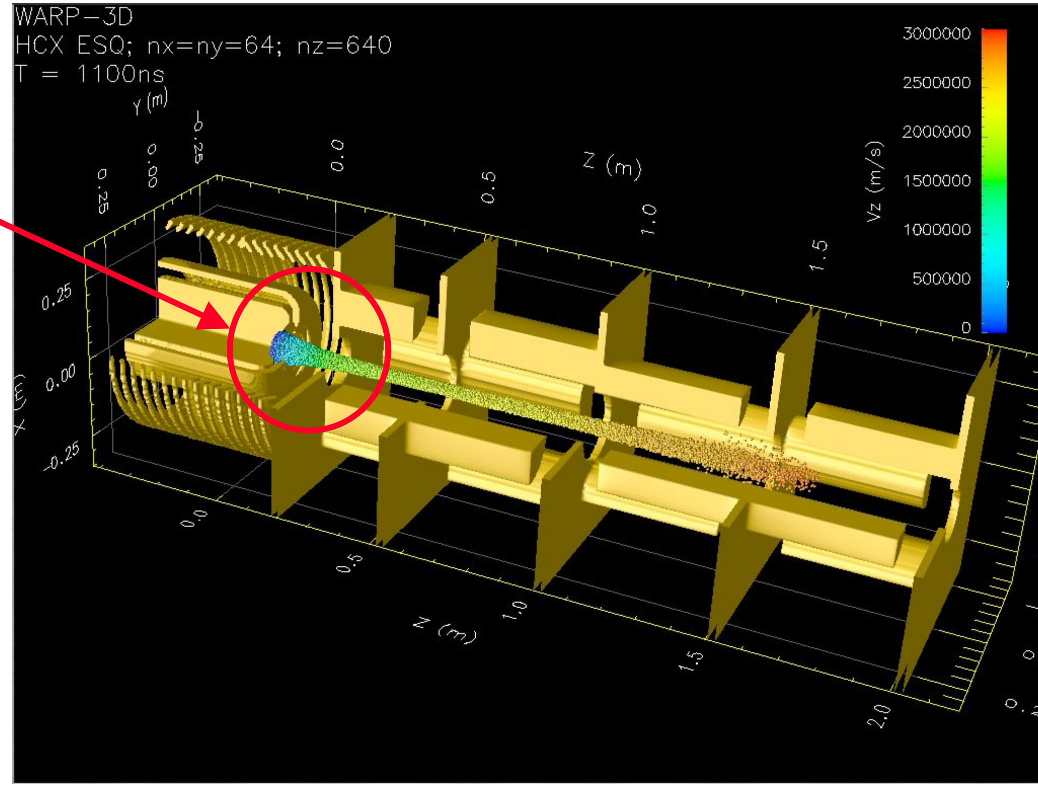

WARP simulations show that a fairly high resolution is needed to reach convergence

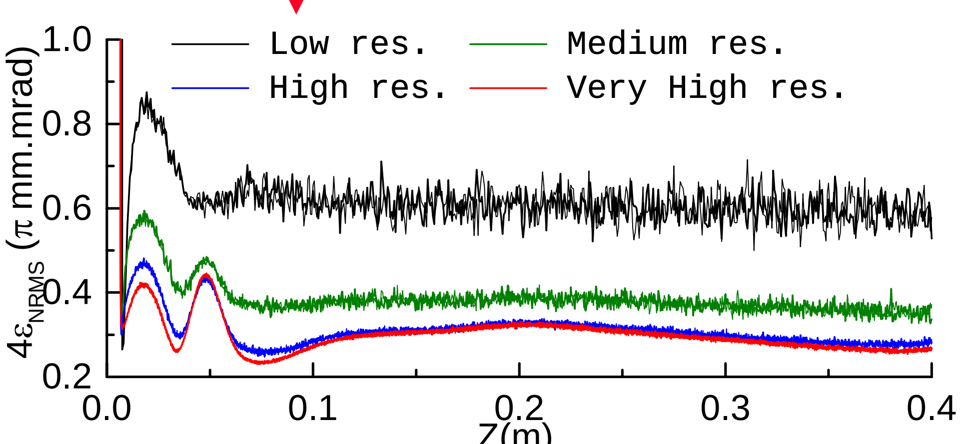

Run	Grid size	Nb particles
Low res.	56x640	~1M
Medium res.	112x1280	~4M
High res.	224x2560	~16M
Very High res.	448x5120	~64M

Example of AMR calculation with WARPrz: speedup ~10.5

Run	Grid size	Nb particles
Low res.	56x640	~1M
Medium res.	112x1280	~4M
High res.	224x2560	~16M
Low res. + AMR	56x640	~1M

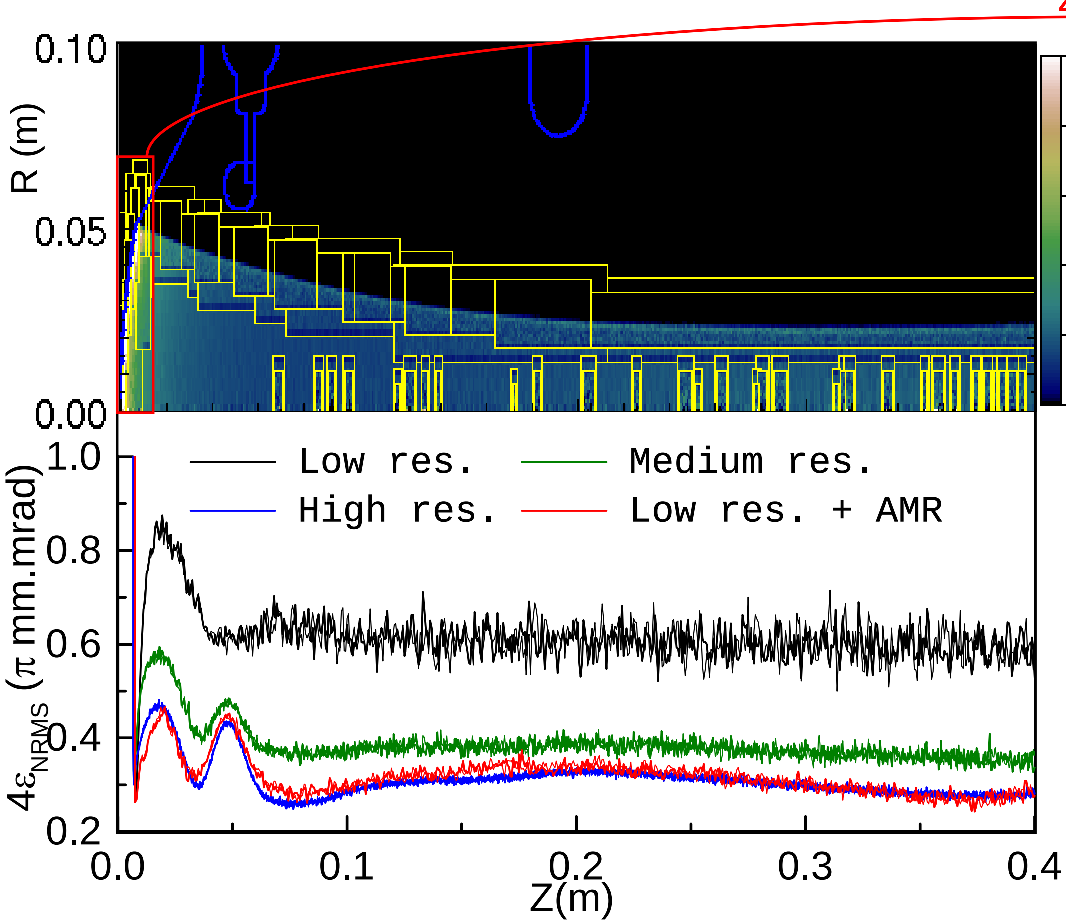

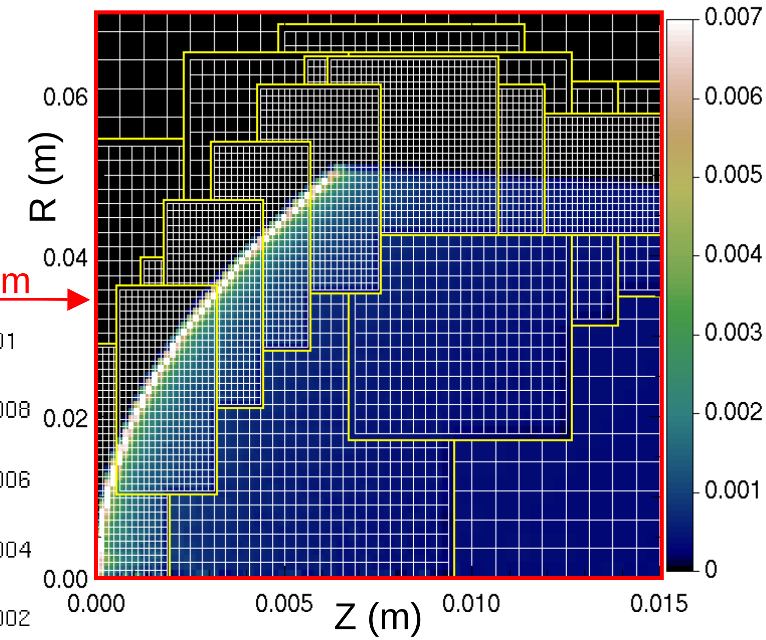

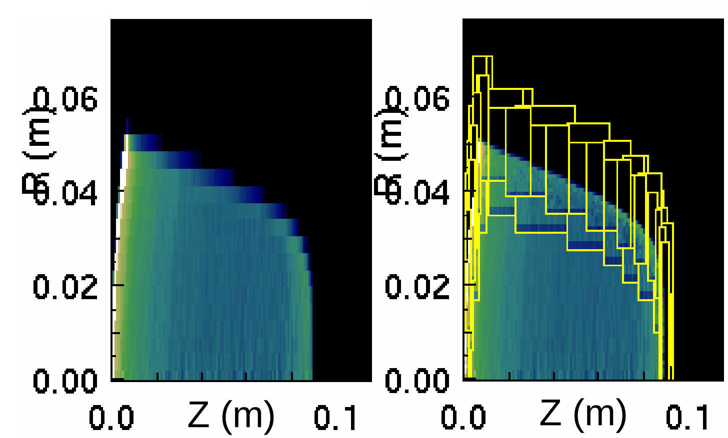

Refinement of gradients: emitting area, beam edge and front.

MR patch key in simulation of STS500 Experiment

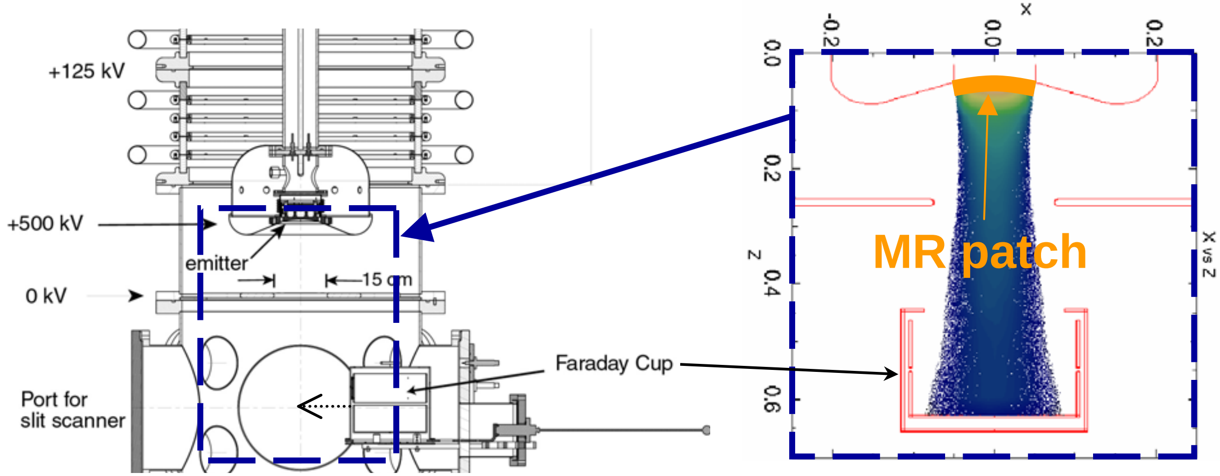

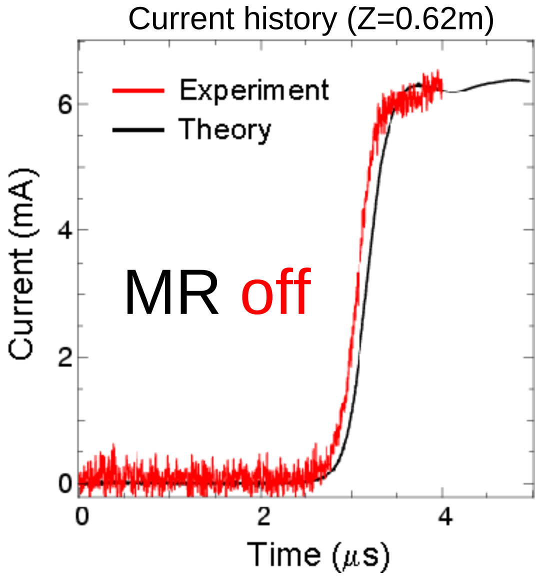

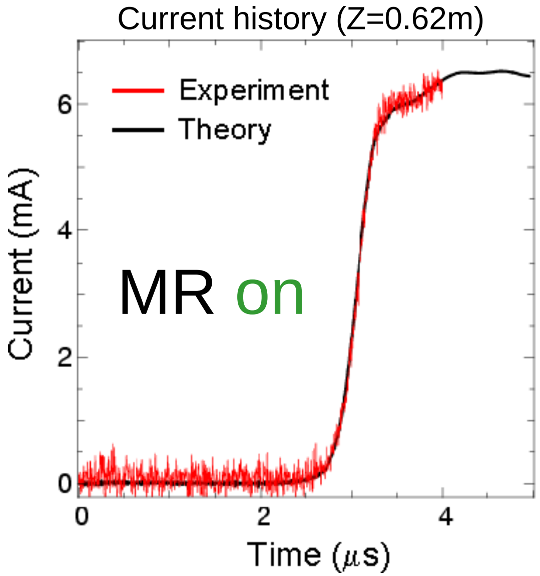

- Mesh Refinement essential to recover experimental results
- Ratio of smaller mesh to main grid mesh ~ 1/1000

New MR method implemented in EM PIC code Emi2d

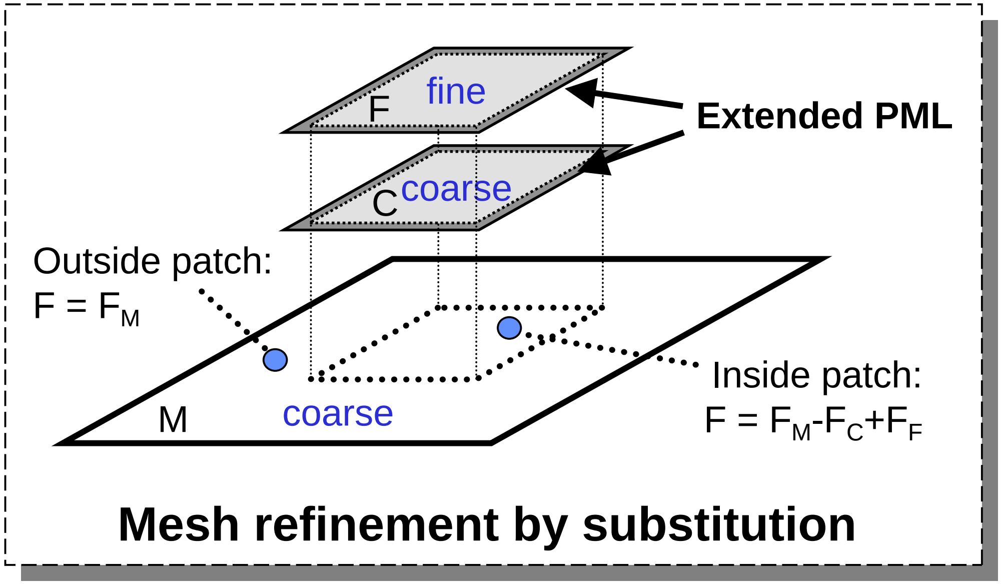

Applied to Laser-plasma interaction in the context of fast ignition

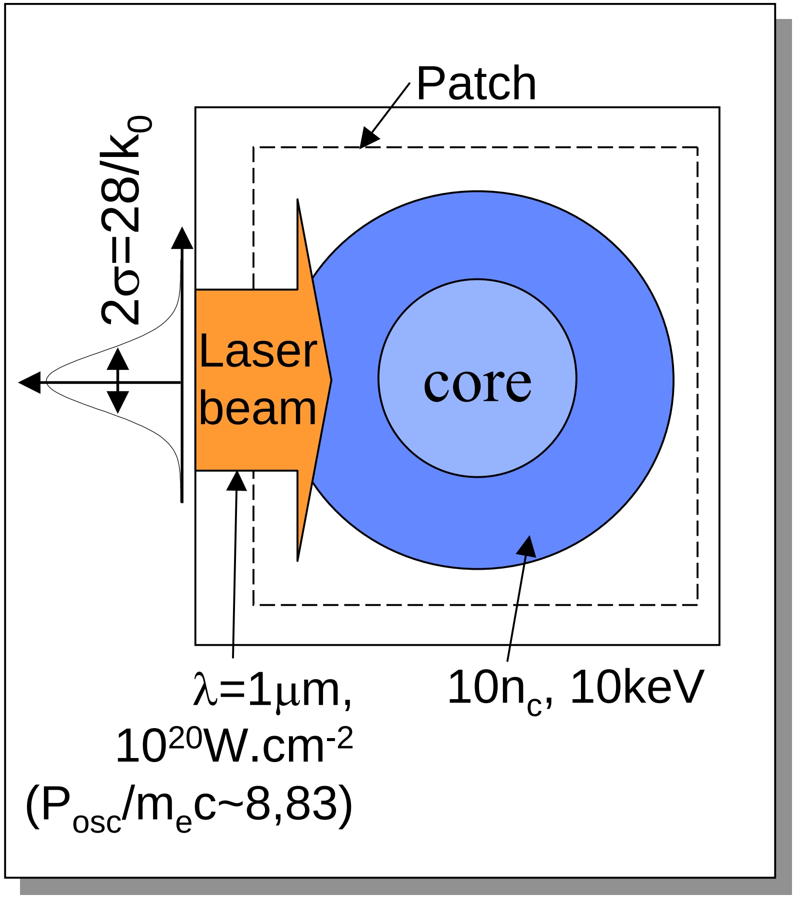

Comparison patch on/off very encouraging

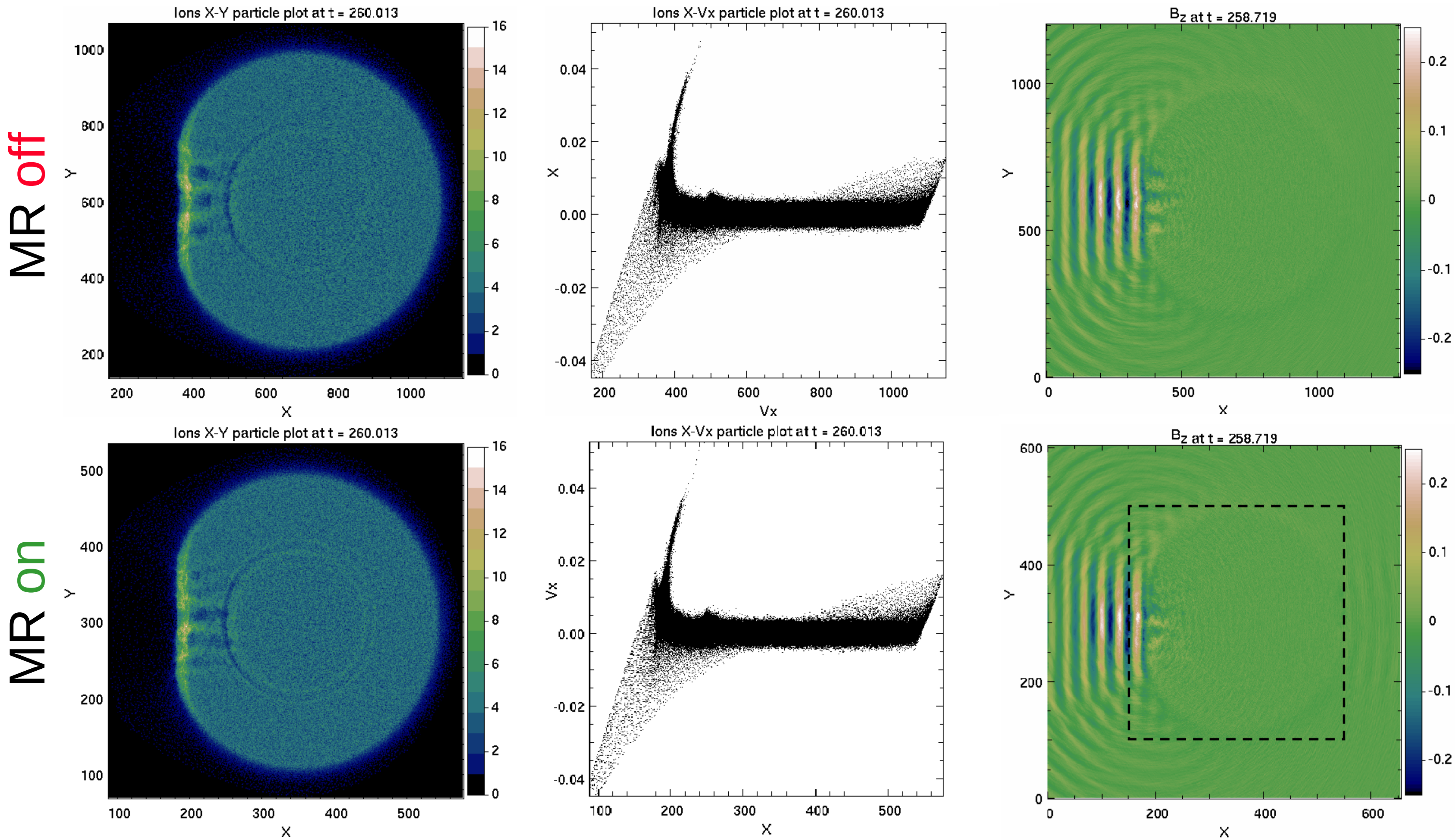

- same results except for small residual incident laser outside region of interest
- no instability nor spurious wave reflection observed at patch border

Backup slides

Goal: end-to-end modeling of a Heavy Ion Fusion driver

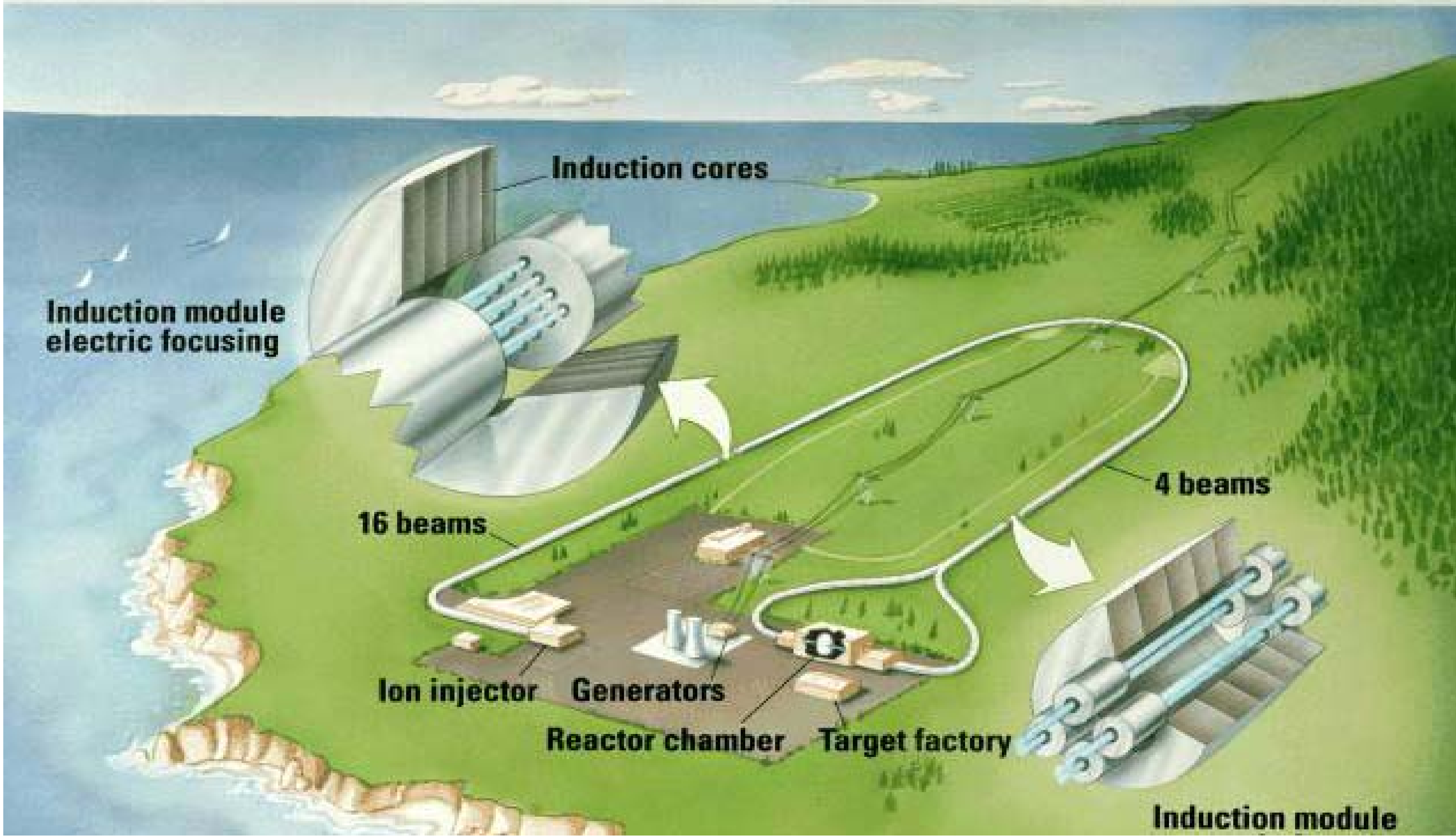

challenging because length scales span a wide range: μm to km(s)

Time and length scales in driver and chamber span a wide range

Time scales:

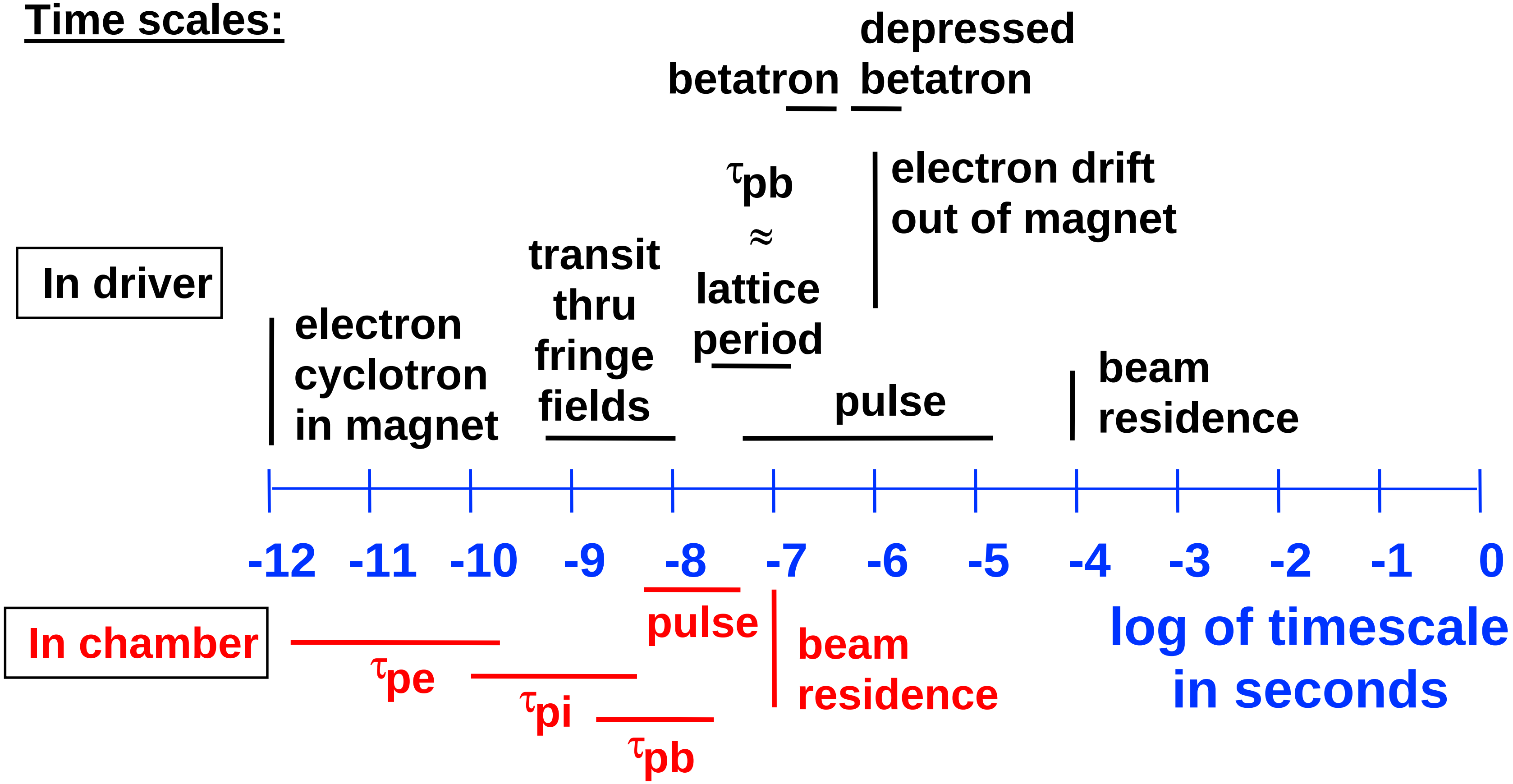

Length scales:

- electron gyroradius in magnet ~10 μm
- $\lambda_{D,beam}$ ~ 1 mm
- beam radius ~ cm
- machine length ~ km' s

Illustration of instability in 1-D EM tests

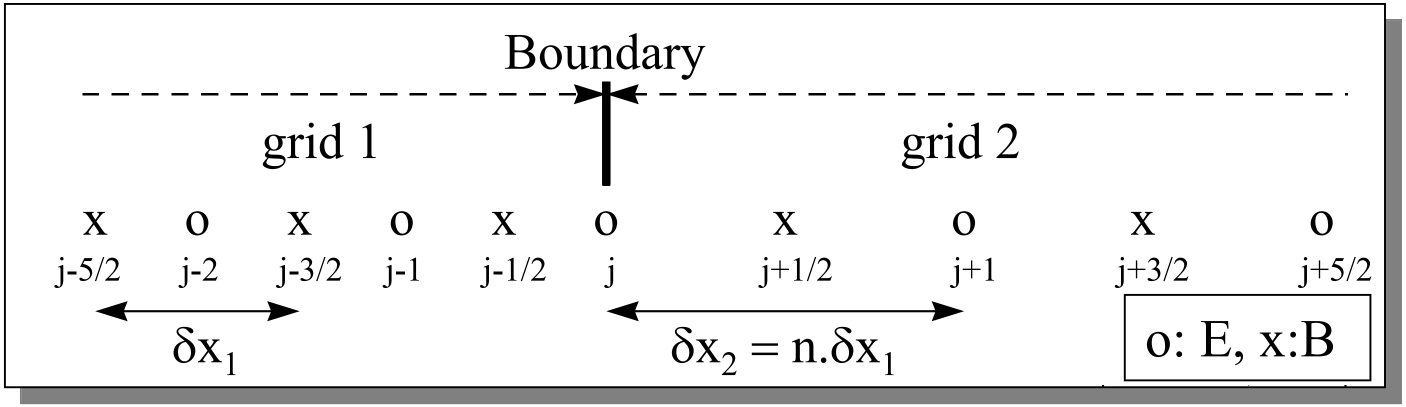

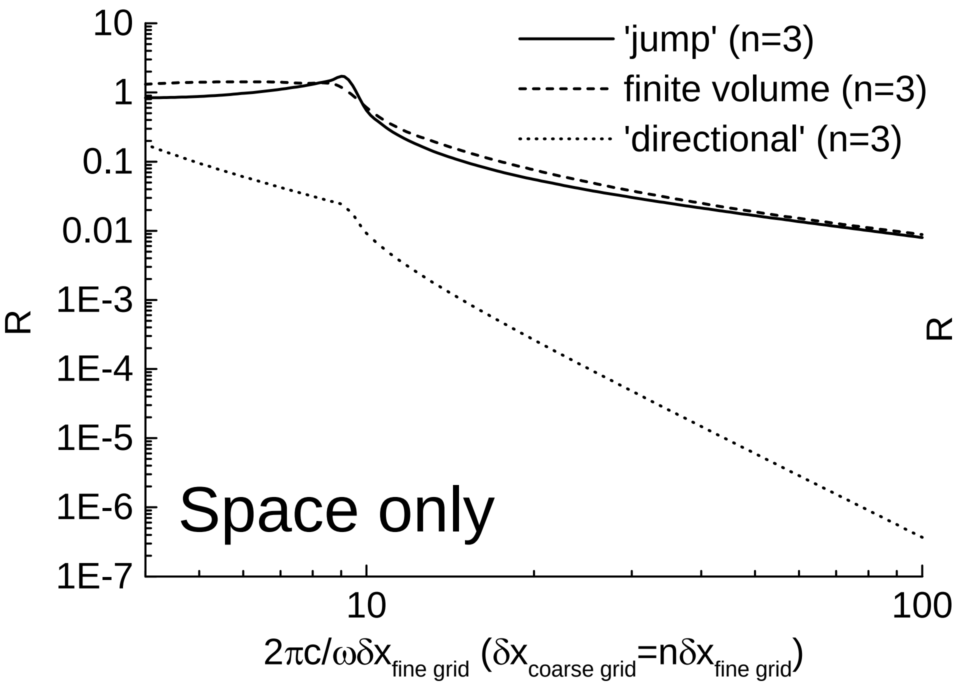

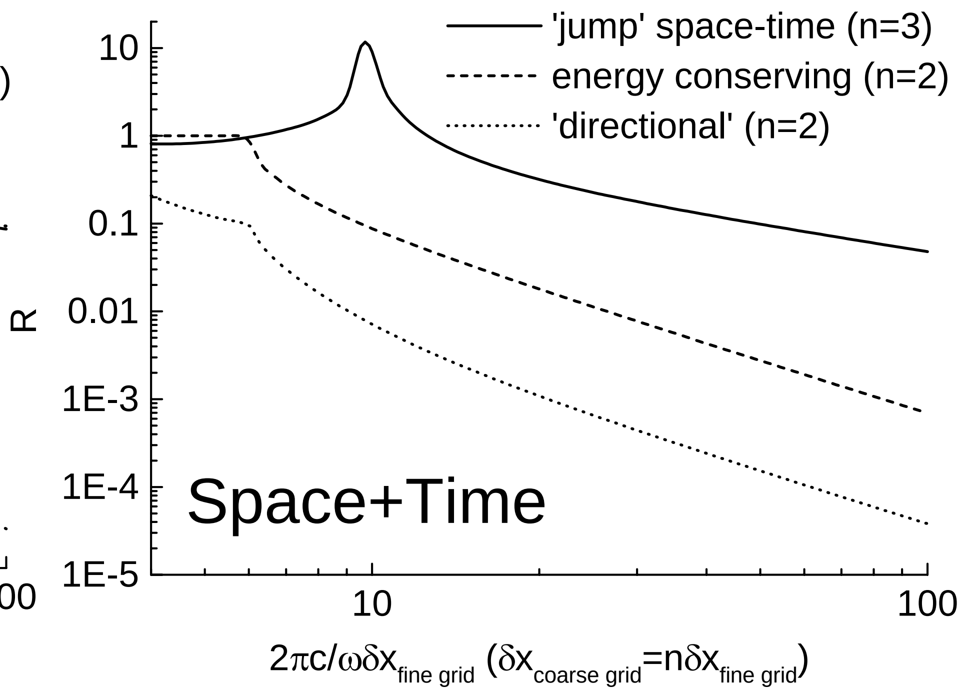

Most schemes relying on interpolations are potentially unstable.

3D WARP simulation of HCX shows beam head scrapping

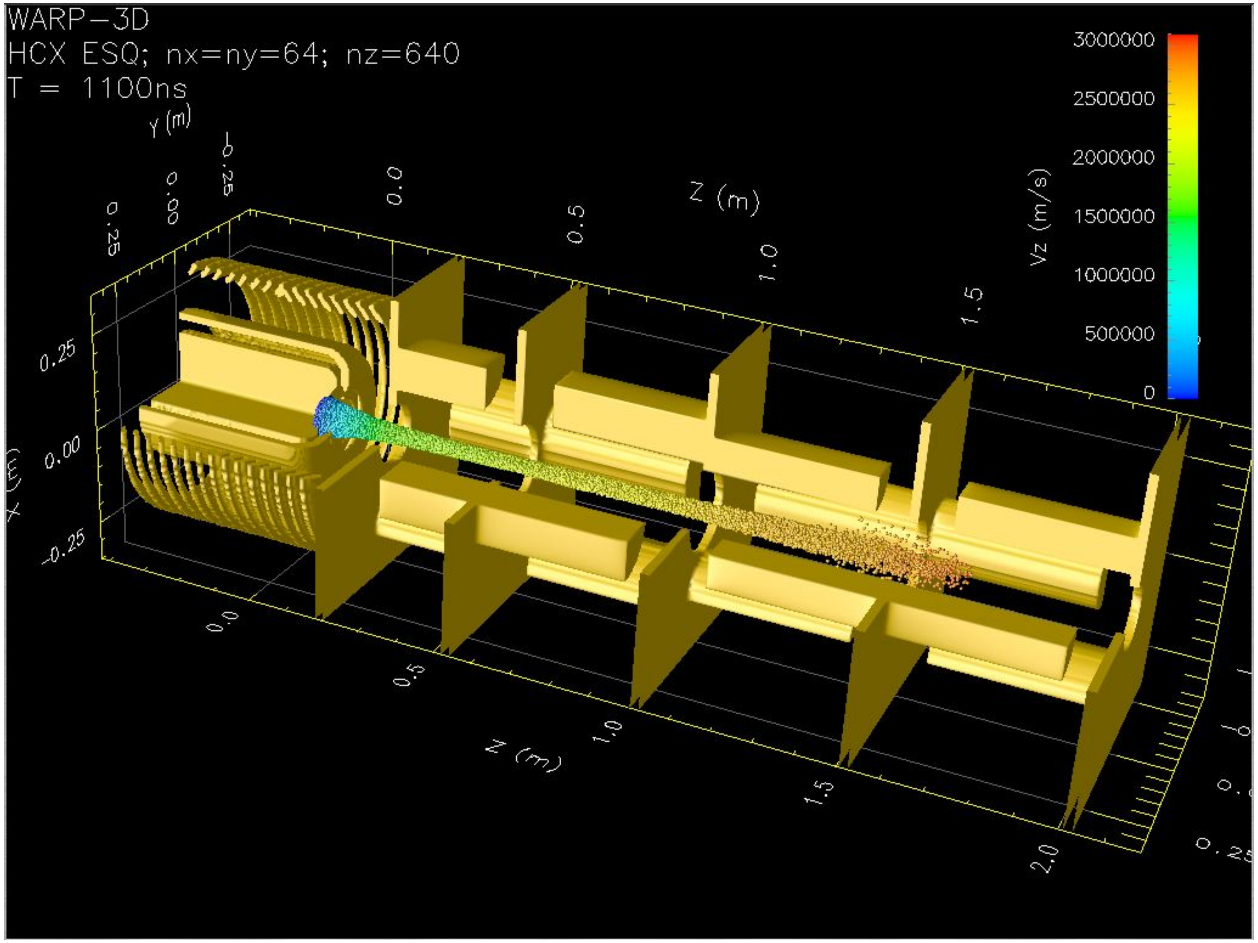

Rise-time τ = 800 ns
beam head particle loss < 0.1%

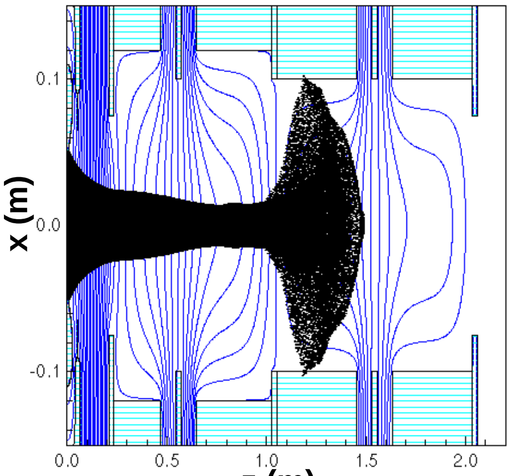

Rise-time τ = 400 ns
zero beam head particle loss

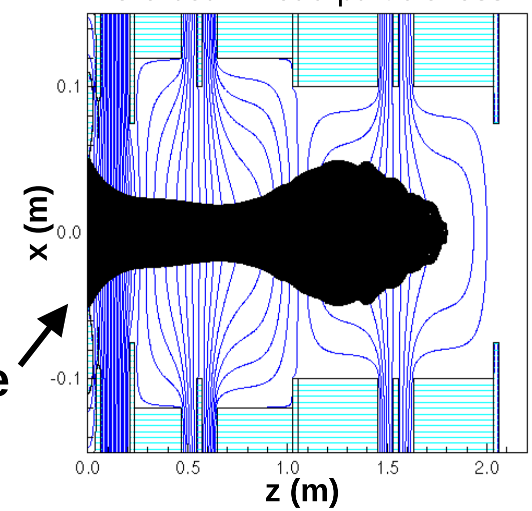

- **Simulations show: head cleaner with shorter rise-time**
- **Question: what is the optimal rise-time?**

1D time-dependent modeling of ion diode

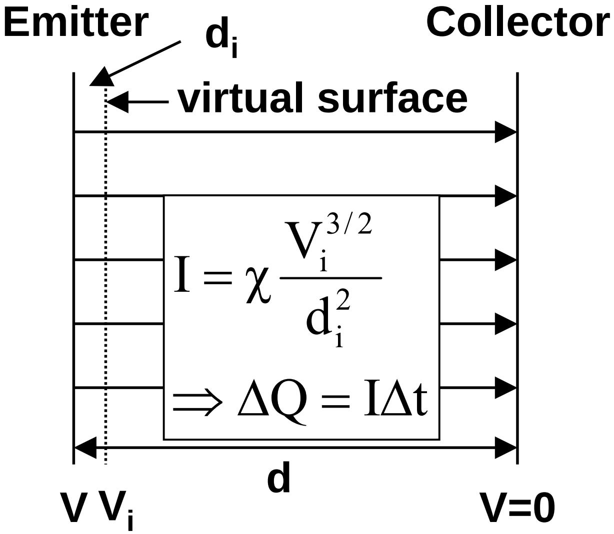

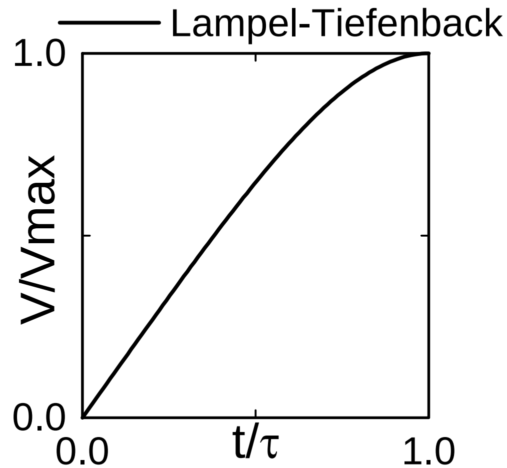

$$\frac{V(t)}{V_{max}} = \frac{t}{3\tau}\left[4 - \left(\frac{t}{\tau}\right)^3\right]$$

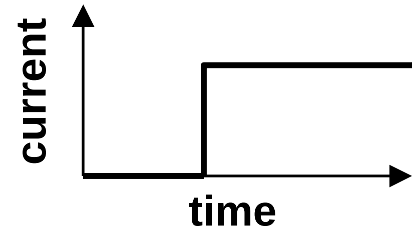

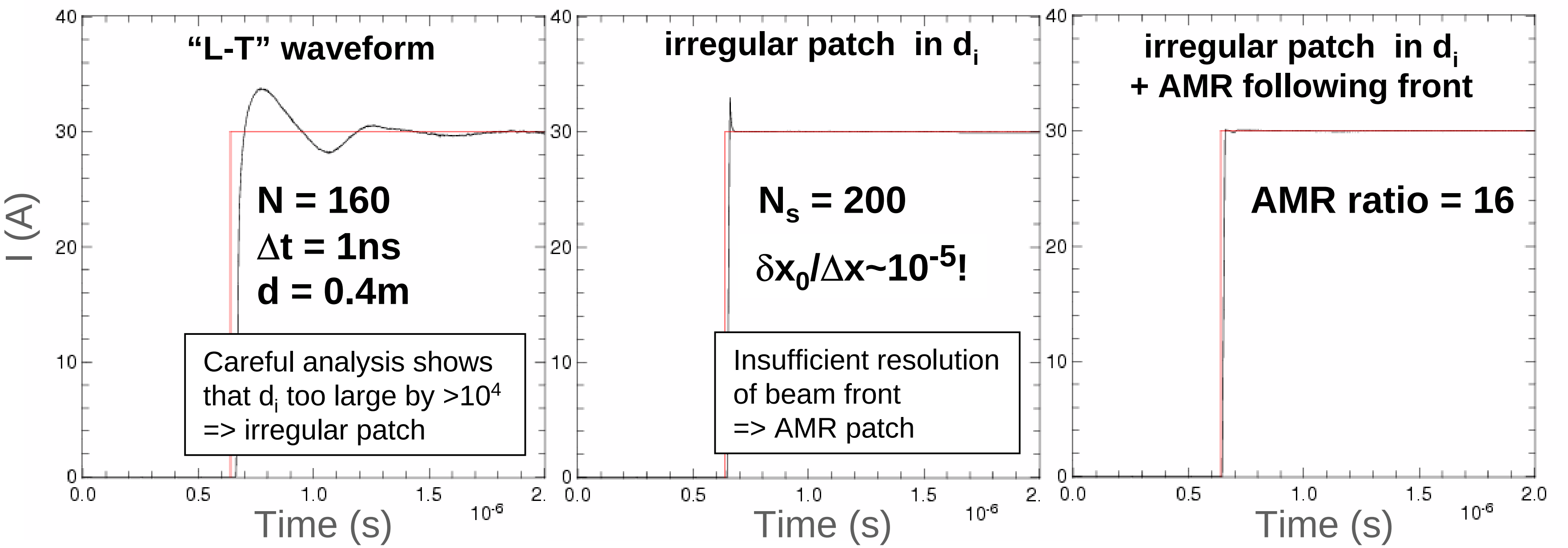

MR patch suppresses long wavelength oscillation

Adaptive MR patch suppresses front peak

Application to three dimensions

- Specialized 1-D patch implemented in 3-D injection routine (2-D array)
- Extension Lampel-Tiefenback technique to 3-D implemented in WARP
  - ➢ predicts a voltage waveform which extracts a nearly flat current at emitter

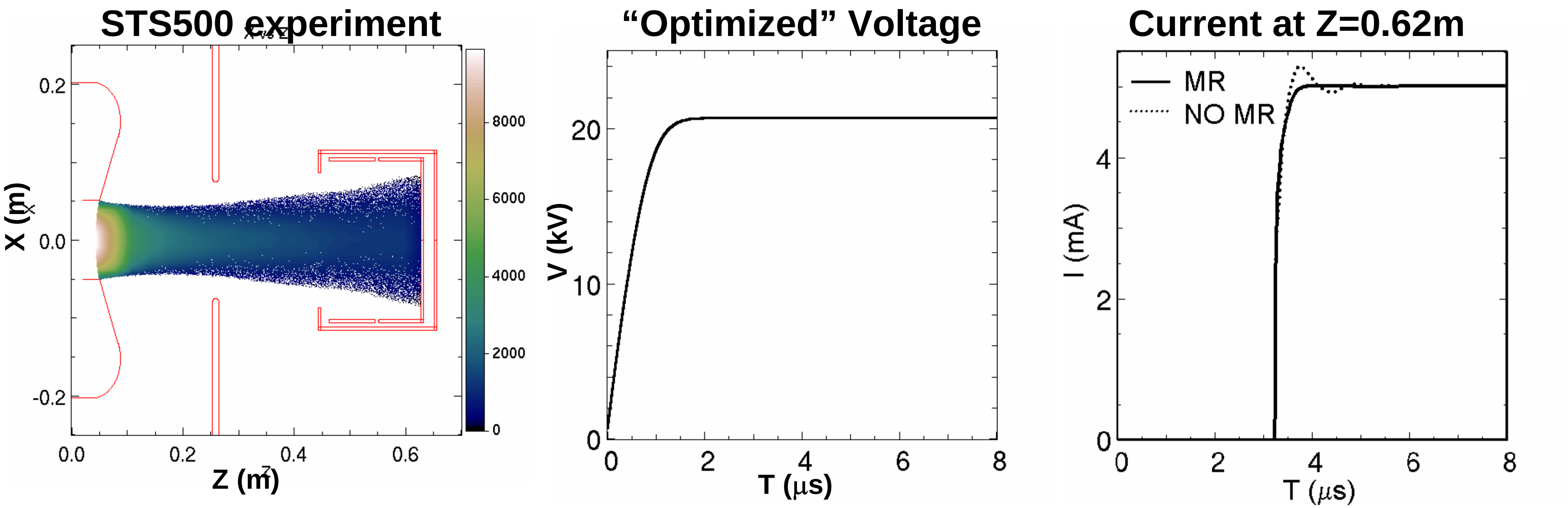

- Run with MR predicts very sharp risetime (not square due to erosion)
- Without MR, WARP predicts overshoot

Effort to develop AMR library for PIC at LBNL

- Researchers from AFRD (PIC) and ANAG (AMR-Phil Colella's group) collaborate to provide a library of tools that will give AMR capability to existing PIC codes (on serial and parallel computers)
- The base is the existing ANAG's AMR library Chombo
- The way it works

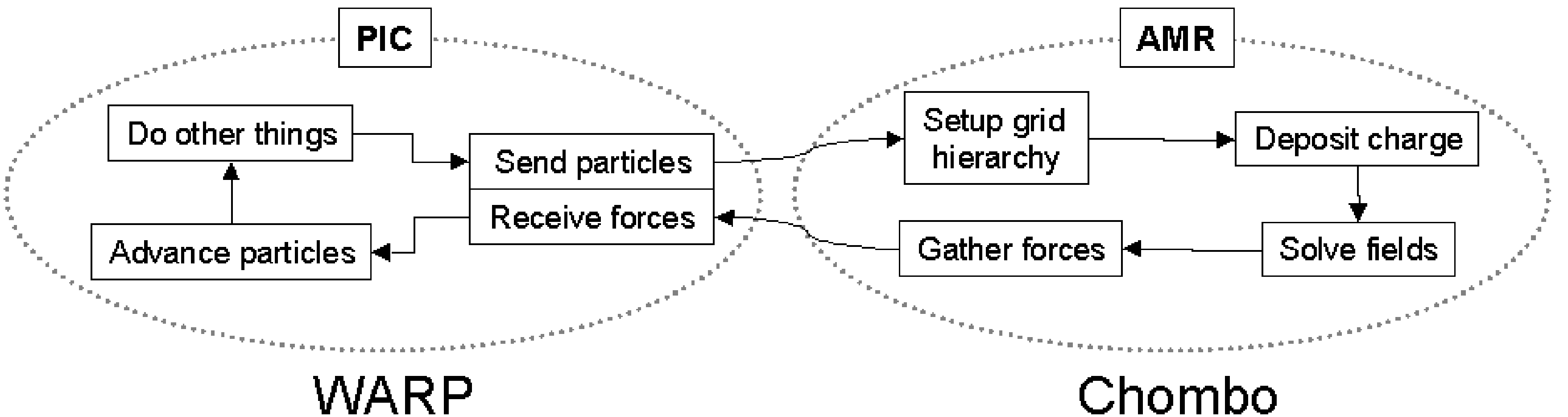

- WARP is test PIC code but library will be usable by any PIC code

Example of WARP-Chombo injector field calculation

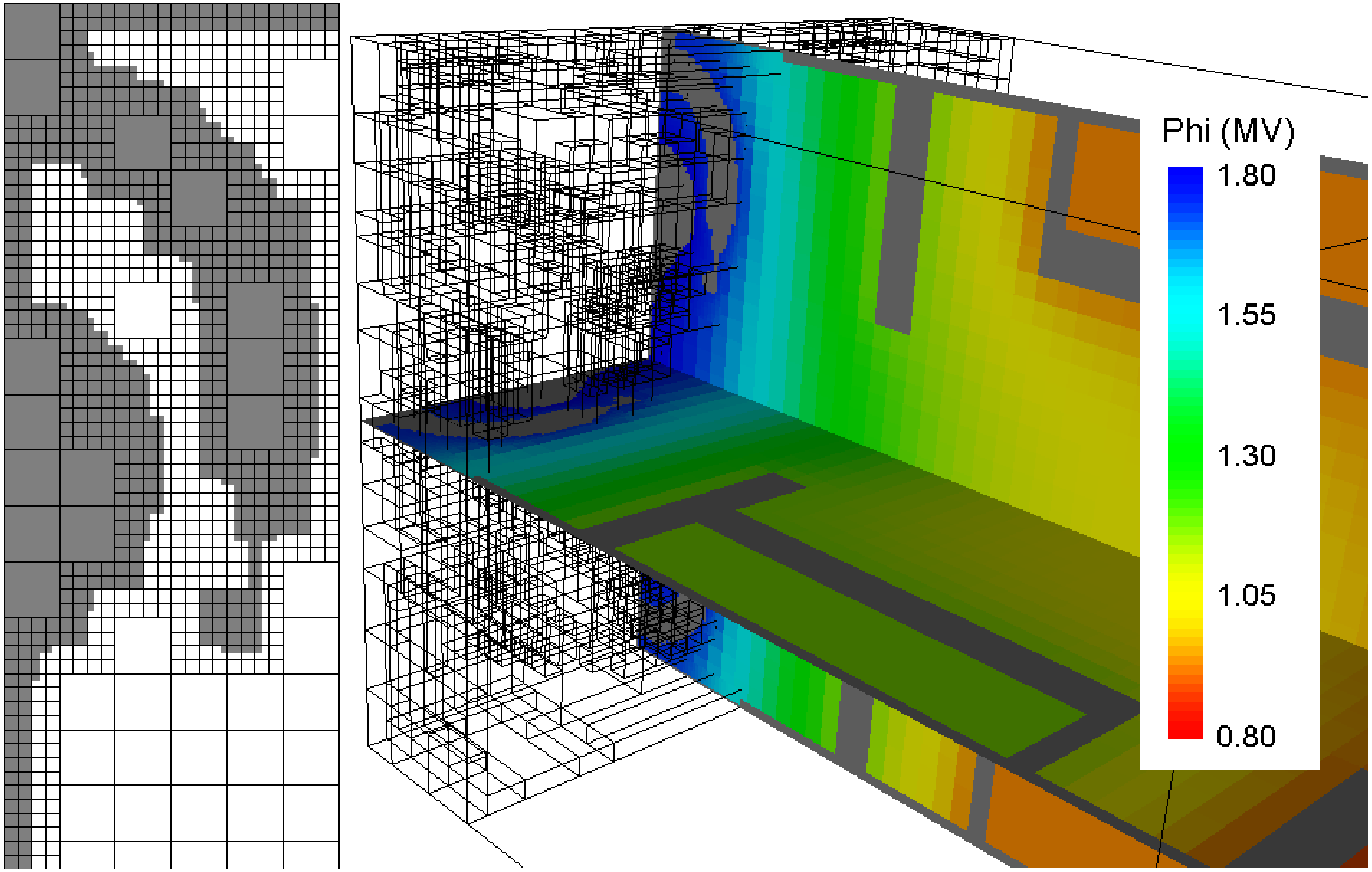

- Chombo can handle very complex grid hierarchy

Extended Perfectly Matched Layer

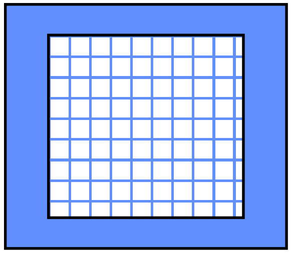

Principle of PML:
Field vanishes in layer surrounding domain.
Layer medium impedance Z matches vacuum's Z_0

Maxwell

$$\varepsilon_0 \frac{\partial E_x}{\partial t} = \frac{\partial H_z}{\partial y}$$
$$\varepsilon_0 \frac{\partial E_y}{\partial t} = -\frac{\partial H_z}{\partial x}$$
$$\mu_0 \frac{\partial H_z}{\partial t} = -\frac{\partial E_y}{\partial x} + \frac{\partial E_x}{\partial y}$$

Split Maxwell

$$\varepsilon_0 \frac{\partial E_x}{\partial t} = \frac{\partial H_z}{\partial y}$$
$$\varepsilon_0 \frac{\partial E_y}{\partial t} = -\frac{\partial H_z}{\partial x}$$
$$\mu_0 \frac{\partial H_{zx}}{\partial t} = -\frac{\partial E_y}{\partial x}$$
$$\mu_0 \frac{\partial H_{zy}}{\partial t} = \frac{\partial E_x}{\partial y}$$

Berenger PML

$$\sigma_y E_x + \varepsilon_0 \frac{\partial E_x}{\partial t} = \frac{\partial H_z}{\partial y}$$
$$\sigma_x E_y + \varepsilon_0 \frac{\partial E_y}{\partial t} = -\frac{\partial H_z}{\partial x}$$
$$\sigma_x^* H_{zx} + \mu_0 \frac{\partial H_{zx}}{\partial t} = -\frac{\partial E_y}{\partial x}$$
$$\sigma_y^* H_{zy} + \mu_0 \frac{\partial H_{zy}}{\partial t} = \frac{\partial E_x}{\partial y}$$

If $\frac{\sigma_u}{\varepsilon_0} = \frac{\sigma_u^*}{\mu_0}$ with u=(x,y)

=> $Z=Z_0$: no reflection.

Extended PML

$$\sigma_y E_x + \varepsilon_0 \frac{\partial E_x}{\partial t} = \frac{\partial H_z}{\partial y}\frac{c_y}{c} + \bar{\sigma}_y H_z$$
$$\sigma_x E_y + \varepsilon_0 \frac{\partial E_y}{\partial t} = -\frac{\partial H_z}{\partial x}\frac{c_x}{c} + \bar{\sigma}_x H_z$$
$$\sigma_x^* H_{zx} + \mu_0 \frac{\partial H_{zx}}{\partial t} = -\frac{\partial E_y}{\partial x}\frac{c_x^*}{c} + \bar{\sigma}_x^* E_y$$
$$\sigma_y^* H_{zy} + \mu_0 \frac{\partial H_{zy}}{\partial t} = \frac{\partial E_x}{\partial y}\frac{c_y^*}{c} + \bar{\sigma}_y^* E_x$$

If $\frac{\sigma_u}{\varepsilon_0} = \frac{\sigma_u^*}{\mu_0}, \frac{\bar{\sigma}_u}{\varepsilon_0} = \frac{\bar{\sigma}_u^*}{\mu_0}$ and $c_u = c_u^*$

=> $Z=Z_0$: no reflection.

Hybrid Particle-In-Cell Simulation

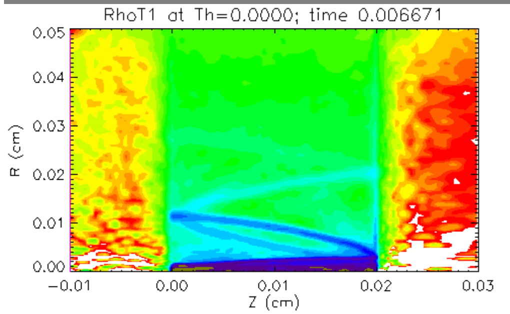

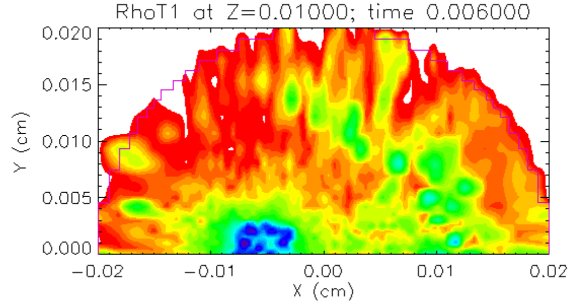

D. R. Welch (drwelch@mrcabq.com), T. P. Hughes, R. E. Clark,
D. V. Rose, B. V. Oliver, and C. Mostrom
ATK Mission Research
Albuquerque, NM 87110

August 25, 2004
Short-Pulse Laser-Matter Computational Workshop
Pleasanton, CA

What the heck is hybrid?

- Hybrid can mean many things to many people - there is no wrong answer
- Traditionally means plasma species are treated with different equations of motion
  - Kinetic, gyro-kinetic, fluid with and without inertia
  - Implicit schemes to study low-frequency phenomena
- Usually involves the inclusion of collisions

Why hybrid? Standard explicit PIC is limited by several constraints

- Resolution of Debye length
  - Results in plasma heating until $\Delta x \approx \lambda_D$
- Resolution of electron plasma (ω_p) and cyclotron (ω_c) frequency
  - Results in plasma phase space growth
- Electromagnetic Courant Limit
  - Results in exponential energy growth
- Cell Aspect Ratio < 4
  - Phase space distortion

Hybrid codes can overcome many of these constraints while neglecting or damping high frequency waves

- Implicit field, Darwin solvers can relax Courant, aspect ratio limits
- Energy conserving schemes can remove Debye length instability
- Implicit PIC, inertial and noninertial fluid schemes integrate over particle orbits and relax ω_p, ω_c constraints
- Energy conservation can be better accounted for with hybrid fluid models, EOS

There have been three hybrid approaches relevant to LPI

- Inertialess electron model – tensor conductivity for electron EOM (Paris, IPROP, SOLENS, ICEPIC)
- Implicit Fluid Moment model (ANTHEM, DYNADE)
- Direct-Implicit fully-kinetic PIC descriptions (AVANTI, LSP)

Each has advantages and disadvantages

D. W. Hewett, J. Comp. Phys. **38**, 378 (1980)
L. Gremillet, et al, Phys. Plasmas, **9**, 941 (2002).

R. J. Mason, J. Comp. Phys. **41**, 233 (1981)
J. Denavit, J. Comp. Phys. **342**, 337 (1981)
J. R. Davies, Phys. Rev. E **68**, 056404 (2003)

D. W. Hewett and A. B. Langdon, J. of Comp. Phys. 72, 121 (1987)
D. R. Welch, et al, *Nucl. Instrum. Meth. Phys. Res.* A **464**, 134 (2001).

Inertialess Electron Model

- Make use of Ohm's Law for electron EOM

Plasma electron current term

$$\frac{\partial \boldsymbol{E}}{\partial t} = \frac{1}{\varepsilon}\left(\nabla \times \frac{\boldsymbol{B}}{\mu}\right) - \boldsymbol{J} - \sigma \cdot \left(\mathbf{E} + \mathbf{v} \times \mathbf{B}\right)$$

$$\frac{\partial B}{\partial t} = -\nabla \times E$$

- Full fields, Darwin (no EM waves) or MHD (no displacement current)
- Energetic beam particles, ions can be followed as PIC particles

Ohm’s model used successfully for transport in collisional matter

- Solutions do not have to be implicit and are thus fast
- Net current, resistive instabilities well modeled
  - Plasma dielectric function can introduce inertial effects
- LPI, sheath, collisionless physics are not adequately modeled
  - difficult to conserve charge

The Implicit Fluid Moment System*

$$\frac{\partial \vec{E}}{\partial t} = -4\pi e(Zn_i\vec{v}_i - n_e\vec{v}_e); \quad v_\alpha = u_\alpha / \gamma_\alpha; \quad n_e v_e = \sum n_\alpha v_\alpha; \quad \alpha = h, c$$

$$m_e \frac{\partial n_\alpha u_\alpha}{\partial t} = -\nabla \bullet \overline{P}_\alpha - en_\alpha \vec{E} - \frac{[\omega_{p\alpha}^2]_{\lim}}{2c\omega^2\gamma_\alpha}\nabla I - \nu_{\alpha i}\gamma_\alpha m_e n_\alpha (v_\alpha - v_i),$$

$$\overline{P}_h = \sum_j w_j u_j v_j; \quad v_j = u_j / \gamma_j; \quad \gamma_j = [1 + (u_{jx}^2 + u_{jtr}^2)/c^2]^{1/2}$$

$$u_h = \sum_j w_j u_j; \quad n_h = \sum_j w_j$$

*Thanks to Rod Mason for slides

System is solved implicitly

neglecting collisions

$$E^{n+1} = E^{n} + 4\pi e(n_h v_h^{n+1} + n_c v_c^{n+1} - Z n_i v_i^{n+1})\Delta t$$

*** includes ponderomotive acceleration**

$$v_h^{n+1} = \frac{1}{\gamma_h^{n+1}}(u_h^{n*} - \frac{1}{m_e n_h}\nabla \bullet \bar{P}_h \Delta t - \frac{e}{m_e}E^{n+1}\Delta t);$$

v_c and v_i from fluids or particles

$$E^{n+1} = \frac{(E^{n} - 4\pi \sum_{\alpha} \frac{q_\alpha n_\alpha \Delta t}{\gamma_\alpha^{(\oplus)}}(u_\alpha^{n*} - \frac{1}{m_e n_\alpha}\nabla \bullet \bar{P}_\alpha \Delta t)}{[1 + \omega_p^2 (\Delta t)^2 / \gamma_\alpha^{(\oplus)}]}$$

level (m) suffices

Implicit noise reduction from denominator

$$E^{n} \Rightarrow -4\pi e[\int_0^x (n_h^n + n_c^n - Z n_i^n)\Delta t]$$

Poisson correction

Fluid Moment Method can be fast

- Eulerian fluid treatment requires less computation than particle, large density variation much easier
- Hydro Courant Limit remains – similar to particle limit
- Charge is not conserved requiring correction – can be noisy, time consuming
- Solution with B fields and multiple dimensions can be complicated, requiring multiple iterations
- Higher order moments can be important, unless fast particles treated with particles

Example of ANTHEM electron transport

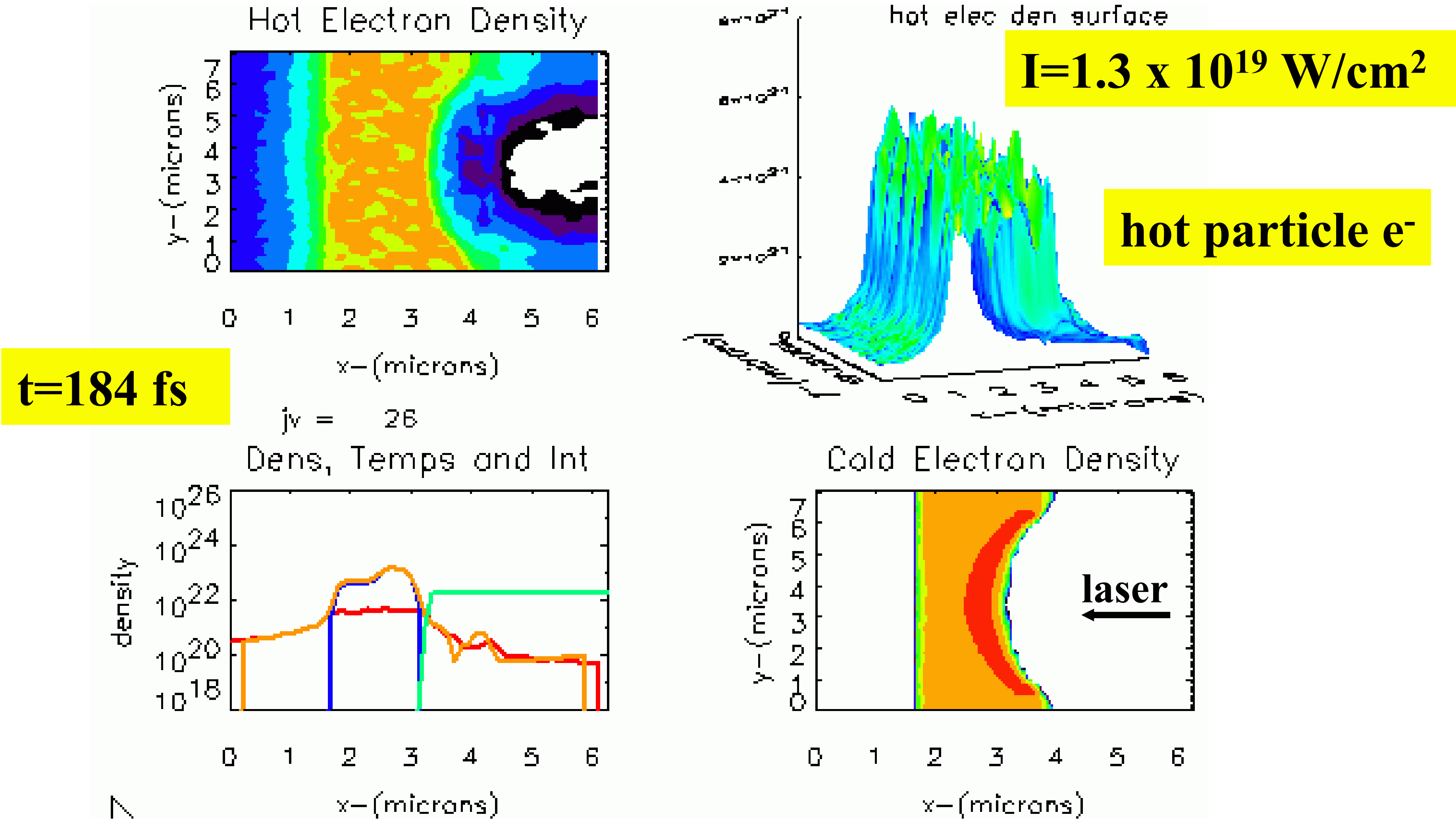

EM Direct Implicit PIC uses linear response of current to predict new fields

Explicit algorithm uses a leap frog method for momentum and position advance with
$\mathbf{a}^n = q/m\ \mathbf{E}^n(\mathbf{x}^n)$

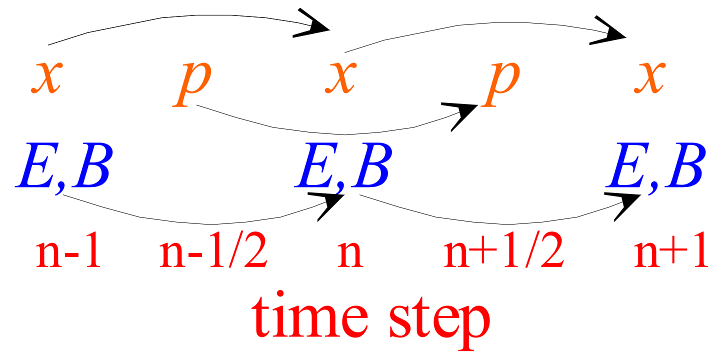

$$\boldsymbol{p}^{n+1/2} = \boldsymbol{p}^{n-1/2} + \Delta t \left[a^n + \left(\boldsymbol{p}^{n-1/2} + \boldsymbol{p}^{n+1/2} \right) / \left(2\gamma^n \right) \times q\boldsymbol{B}^n(\boldsymbol{x}^n)/mc \right],$$

- Implicit algorithm pushes particle momentum $\boldsymbol{p}$ using half of the old electric field and new $\mathbf{a}^n = ½(\mathbf{a}^{n\text{-}1} + q/m\ \mathbf{E}^{n+1}(\mathbf{x}^{n+1}))$

- Need to know **E** at new position and time

Particles must be pushed twice

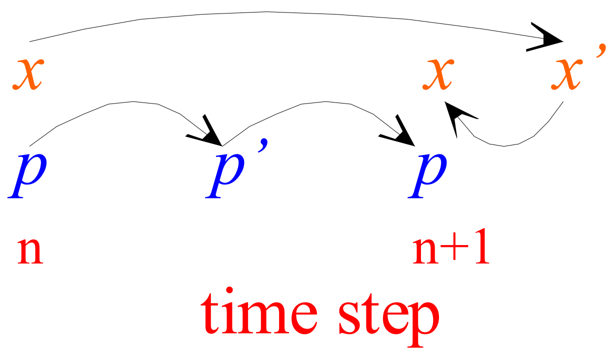

$$\frac{\partial \boldsymbol{E}}{\partial t} = \frac{1}{\varepsilon}\left(\nabla \times \frac{\boldsymbol{B}}{\mu}\right) - \boldsymbol{J} - \delta \boldsymbol{J},$$

- First, push particle with $\mathbf{E}^{n+1}(\mathbf{x}^{n+1}) = 0$
- The EM fields are then pushed using linear correction terms to predict the effect of $\mathbf{E}^{n+1}(\mathbf{x}^{n+1})$ on the perturbed current $\delta \mathbf{J} = \langle \mathbf{S} \rangle \bullet \mathbf{E}^{n+1}(\mathbf{x}^{n+1})$ ($\langle \mathbf{S} \rangle$ is the susceptibility)
- Momentum and position are then corrected in final push

See D. W. Hewitt and A. B. Langdon, J. Comp. Phys. **72**, 121-155 (1987).

Modified Field Equations

- Particle <S> summed on grid

$$\langle \boldsymbol{S} \rangle = \frac{\rho \Delta t q}{2\gamma^{n+1/2} m} \left(\langle \boldsymbol{T} \rangle - \mathbf{v}^{n+1/2} \mathbf{v}^{n+1/2} \right).$$

- <T> is the magnetic rotation tensor, $\Omega = \Delta t\, q\, \mathbf{B}^n / (2\gamma mc)$

$$\langle \mathbf{T} \rangle = \frac{1}{1+\Omega^2} \begin{bmatrix} 1+\Omega_1^2 & \Omega_1\Omega_2 + \Omega_3 & \Omega_1\Omega_3 - \Omega_2 \\ \Omega_1\Omega_2 - \Omega_3 & 1+\Omega_2^2 & \Omega_2\Omega_3 + \Omega_1 \\ \Omega_1\Omega_3 + \Omega_2 & \Omega_2\Omega_3 - \Omega_1 & 1+\Omega_3^2 \end{bmatrix},$$

- Field equations are modified to account for perturbed current and centered at the n+1/2 step

$$\frac{\boldsymbol{E}^{n+1} - \boldsymbol{E}^n}{\Delta t} = \frac{1}{\varepsilon} \left(\nabla \times \frac{\boldsymbol{B}}{\mu} \right)^{n+1/2} - \boldsymbol{J}^{n+1/2} - \langle \boldsymbol{S} \rangle \cdot \mathbf{E}^{n+1},$$

As in Fluid Moment System, <***S***> term reduces charge fluctuations by $1+(\omega_p \Delta t)^2$

Direct Implicit retains most physics, but most complex to solve

- Implicit field solution can be slow --- 2 step ADI method is not iterative*
- More processor communication --- unavoidable
- More difficult to include collisions --- especially in highly collisional regime
- Momentum conserving algorithms do not conserve energy

*Zheng, IEEE Trans. Micro. Theory and Tech., **48**, 1550, (2000)
Welch, in Comp. Phys. Comm. (2004)

Reasonable energy conservation possible with refinements

- Calculation of currents from particle motion satisfies Gauss's Law exactly, conserving charge
- Currents calculated from susceptibilities and advance of particle energy are first-order accurate
- Particles obtain energy advance consistent with change in potential energy
- Energy conserving results in non-zero particle self forces
  - Cloud-in-Cell reduces effect somewhat
- Variable numerical damping*

$$\boldsymbol{a}_n = .5\left[\theta \boldsymbol{E}_{n+1}\frac{q}{m} + (2-\theta)\boldsymbol{b}_{n-1}\right]$$

$$\boldsymbol{b}_n = .5\left[(2-\theta)\boldsymbol{E}_{n+1}\frac{q}{m} + \theta \boldsymbol{b}_{n-1}\right]$$

θ = 0 undamped C0

θ = 1 full D1 damping

*Friedman, J. of Comp. Phys., **90**, 292-312 , 1990.

Implicit PIC can conserve energy over a wide range of parameters

eg. Expanding 2.8×10^{13}-cm^{-3} plasma blob in a 50-cm radius, 100- cm long tube

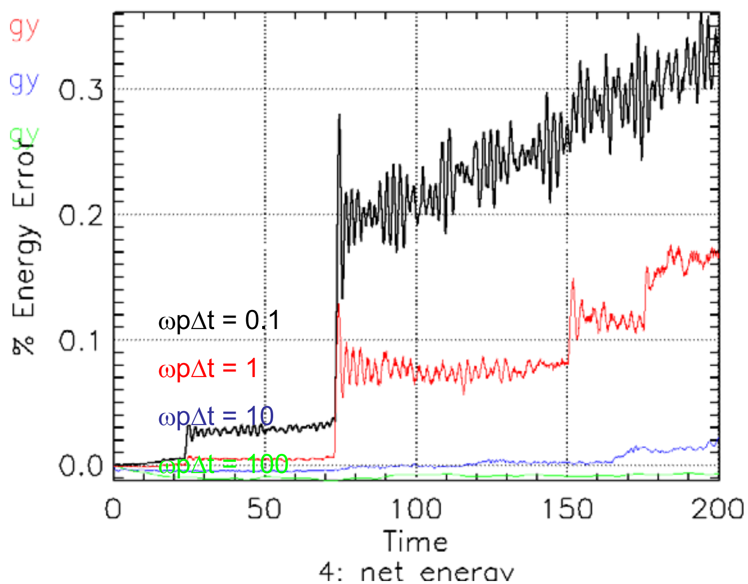

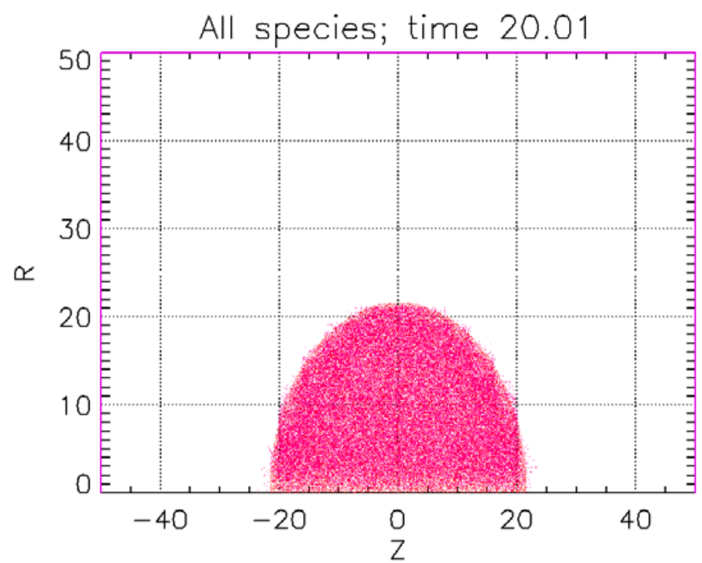

Errors are small even for highly implicit time steps

Approach permits both fluid and kinetic PIC particles

- Due to statistics, for very long, collisional simulations energy conservation can be compromised with kinetic particles
- LSP mitigates this problem using a **PIC fluid** electron description. Particles are pushed with ensemble velocity and a pressure gradient term is added to the equation of motion. The fluid electron has an internal energy

$$\frac{3}{2} n_e \frac{dT_e}{dt} = -n_e T_e \nabla \cdot \mathbf{v}_e + \sum_j \frac{2 m_e n_e}{m_j \tau_{je}} \left(T_j - T_e \right) + \nabla \cdot \kappa \nabla T_e + Q_e - n_e \frac{dE_{ie}}{dt},$$

pdV thermalization conduction ohmic inelastic losses

$$m_e n_e \frac{du_e}{dt} = -\nabla p_e - \nu_{ei} \gamma_e m_e n_e (v_e - v_i),$$

If both fluid and kinetic particles are PIC, a transition conserves momentum

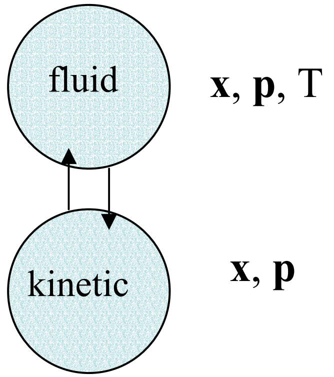

- Need a criterion for transition
  - Runaway rate
  - Phase space
- In LSP
  - Fluid electrons *transition* to kinetic if $m\,v^2 > 3F\,T$
  - Kinetic electrons *transition* to fluid if $m\,v^2 < 3T$ and $\omega_p\,\Delta t > 1$
  - The transition conserves momentum exactly, energy to within roughly 10% depending on F (typically 0.1)
  - The scheme usually results in hot, low-density electrons residing in the kinetic component and thermal, dense electrons in the fluid

Solid density matter requires a model for particle interaction

- Typically Monte Carlo techniques are used assuming Spitzer, LM (Lee & More, Phys. Fluids **27**, 1273 (1984)) or LMD (Desjarlais, et al, Phys. Rev. E **66**, 025401 (2002))
  - particle by particle within a cell (DSMC)
  - moments summed on grid (drifting Maxwellian)
- Atomic physics can be handled in several ways
  - EOS
  - Collisional Radiative Equilibrium or rate equations (very expensive in multiple D)
  - Post-process detailed CR using code such as SPECT-3D (J. MacFarlane, Prism)
- Easy to incorporate into fluid solutions
- Corrections (applied fields and <S>) must be made for PIC in highly collisional ($\nu\Delta t > 1$) regime
  - Momentum push can be separate from fields
  - Can be noisy or require many particles

3D cyl LPI and proton generation simulation

- 10-μ Au foil shows electron transport to back surface, tight proton beam
- Fluid electrons from 0-10 μ, kinetic in LPI region

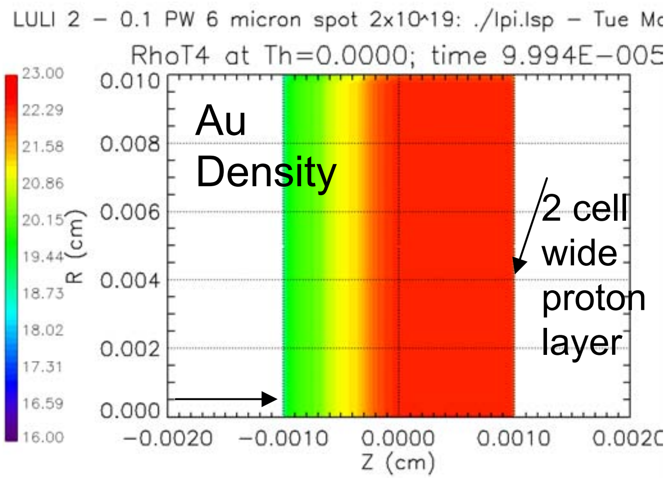

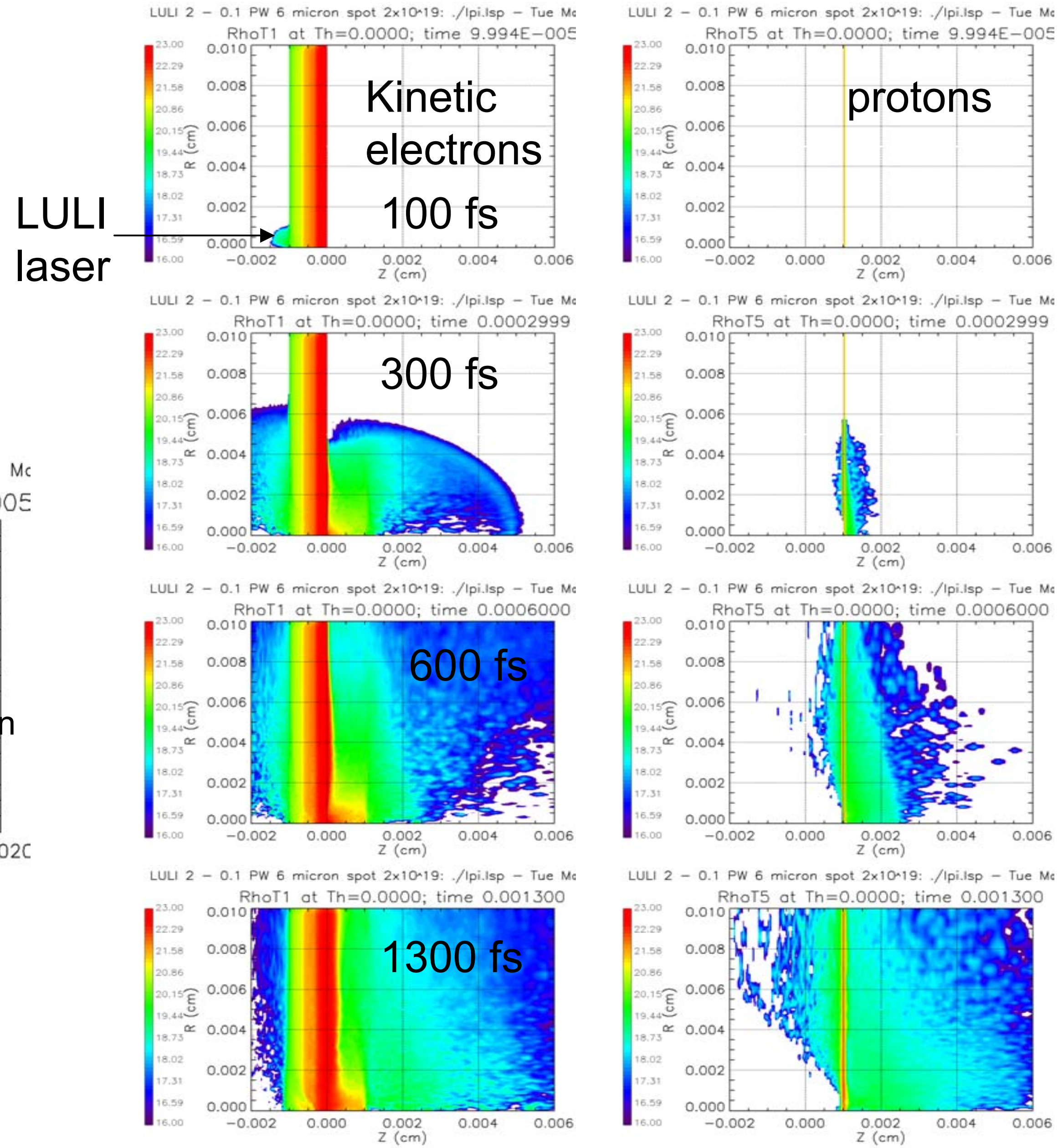

Hybrid simulation can provide insight for larger/longer problems

Issues

- Parallel iterative field solvers are improving
- Algorithm may be stable, but
  - numerical issues remain
  - P vs E conservation
  - PIC vs CIC
  - key physics may not resolved
- Particle management
  - How many particles do we need?
  - Algorithms for splitting and combining
- Implementation of atomic physics – How much detail?
  - EOS vs time-dependent CR
- Retaining all hybrid approaches (fluid and PIC) can allow for simulations of LPI and fast particle transport from vacuum to solid – *goal is to have all approaches available in toolkit*

Limitations/advantages of models

Plasma model	Debye instability	$\omega_p \Delta t$ constraint	$\omega_c \Delta t$ constraint	c Δt constraint	Use/Comments
Explicit momentum conserving	yes!	yes!	yes!	yes	Micro simulations of LPI, sheath physics
Explicit energy conserving	no	yes	yes	yes	Cell size relaxed Lower T, n plasma
Direct Implicit wtih vxB in <S>	no	not if 1< $\omega_c \Delta t$	not if 1<$\omega_p \Delta t$	relaxed	Iterative solvers Slowest, ideal for magnetized plasma
Direct implicit, no vxB in <S>	no	no	yes	no	Unconditionally stable Medium fast, high density plasma
Ohmic with EM, Darwin, MHD	no	no	relaxed	Solver dependent	Highly collsional plasma, gas breakdown

Supporting Slides

Gaussian Laser Beams in 3-D and 2-D Slab Geometries*

$$E_x(r,z,t) = E_o \frac{w_o}{w(z)} Exp\left(-\frac{r^2}{w(z)^2}\right)\cos\left[kz - \omega t - \eta(z) + \frac{kr^2}{2R(z)}\right]$$

3-D geometry with azimuthal symmetry

$$E_x(x,z,t) = E_o \sqrt{\frac{w_o}{w(z)}} Exp\left(-\frac{x^2}{w(z)^2}\right)\cos\left[kz - \omega t - \frac{\eta(z)}{2} + \frac{kx^2}{2R(z)}\right]$$

2-D slab geometry

$\partial / \partial y = 0$

$$z_o = \frac{\pi w_o^2 n}{\lambda}$$

Rayleigh length

$$w(z)^2 = w_0^2\left(1 + \frac{z^2}{z_0^2}\right)$$

Beam waist (minimum at z = 0)

$$R(z) = z\left(1 + \frac{z_o^2}{z^2}\right)$$

Radius of curvature

$$\eta(z) = \tan^{-1}\left(\frac{z}{z_0}\right)$$

Phase angle

Expressions valid in paraxial approximation:

$\lambda / z_o << 1$

$B_y = n\, E_x + O(\lambda / z_o)^2$

All other field components $O(\lambda / z_o)^2$

Assumes linear polarization. Some minor modifications necessary to accommodate circular polarization in 3D case.

Input: specify E_0, λ, and the laser spot w_0 at a 'z' location

* See e.g. R. Guenther, "Modern Optics", John Wiley & Sons, 1990

Two-sided illumination of plasma

- 4-cm wavelength light from left and right focused to 2 cm mid-cube (20x20x20cm)
- Plasma density just above critical, 6×10^{12} cm^{-3}

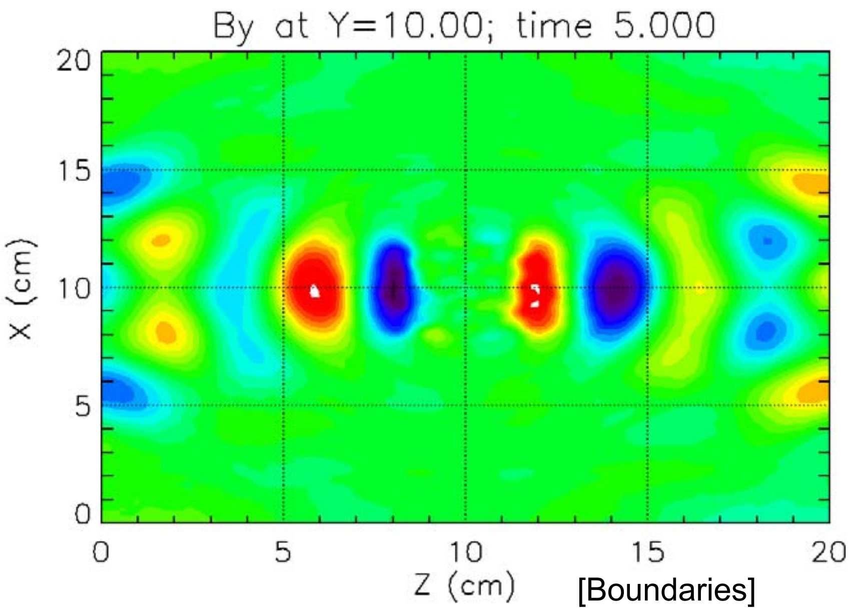

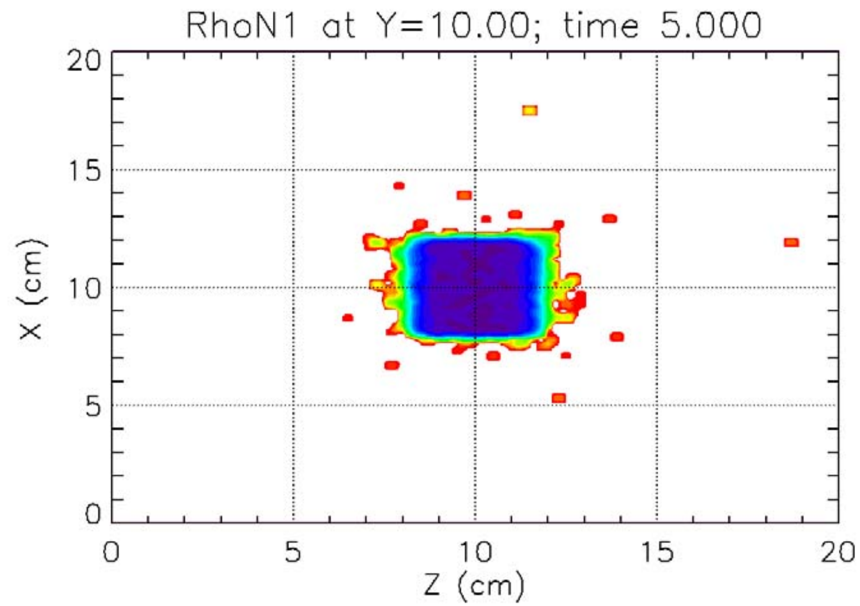

Implicit field solvers best handle large angle incidence of waves at boundaries

```
[Boundaries]
outlet ; z = 0 plane
from 0.0  0.0 0.0
to  20.0 20.0 0.0
phase_velocity 1
drive_model LASER
reference_point 10.0 10.0 10.0  ;
focal spot position
components 1 0 0
phases 0 0 0
temporal_function 1
analytic_function 2
```

```
function2
type 19
coefficients
 4.0 ; wave-length
 2.0 ; spot_size
;
```

Modeling of the LULI proton beam neutralization experiment

Dale R. Welch (drwelch@mrcabq.com)
ATK Mission Research
Michael Cuneo, Robert Campbell, Thomas Mehlhorn
Sandia National Laboratories

August 25-27, 2004
Short-Pulse Laser-Matter Computational Workshop
Pleasanton, CA

Work supported by SNL

3D Luli Simulation

- 10-micron gold foil with very thin hydrogen layer
- 100-1000 monolayers of protons on surface

- 25 J of 1-μm laser energy focused on a 6-μm FWHM spot
  - 10^{21} cm^{-3} critical density
  - 2×10^{19} W/cm^2 intensity
  - 350 fs duration
- Laser propagated into a 3-eV Au^{+2} plasma with **fixed** ion charge state
  - 100 μm radius, 10-μm Au
  - 10-micron blowoff Au plasma 10^{19}-3×10^{22} cm^{-3}
- Implicit cylindirical simulation
  - Spatial resolution 0.1 μm at slab edges, cΔt = 0.04 μm
  - 4 azimuthal spokes
  - Kinetic electrons used in blowoff plasma, fluid in slab

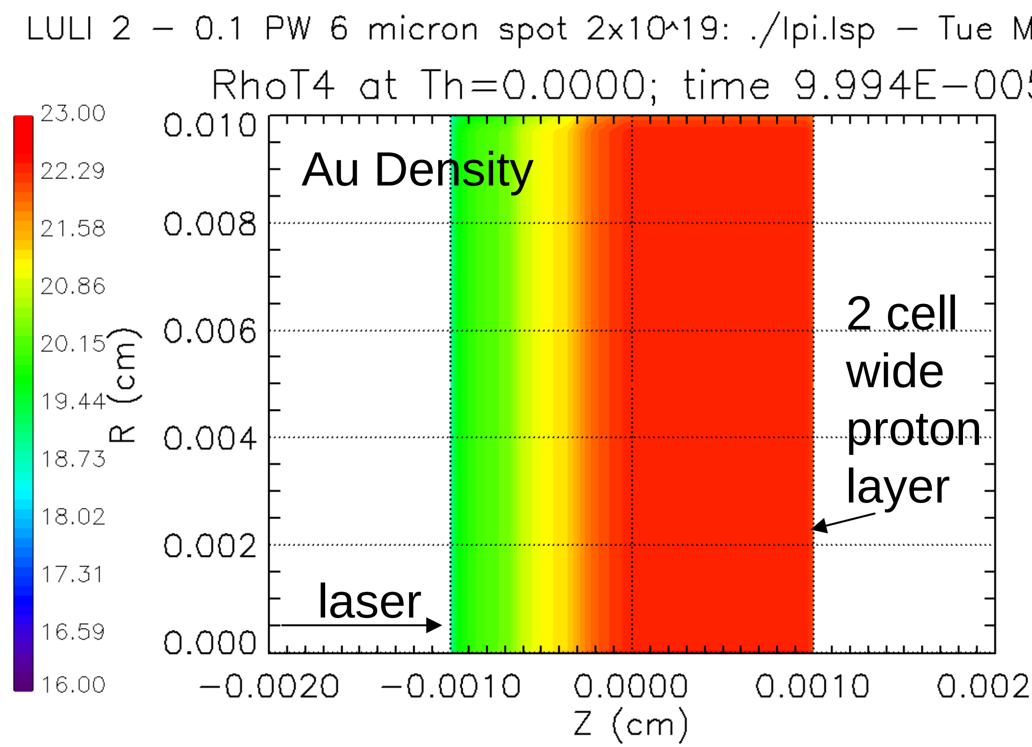

Laser penetrates blowoff plasma

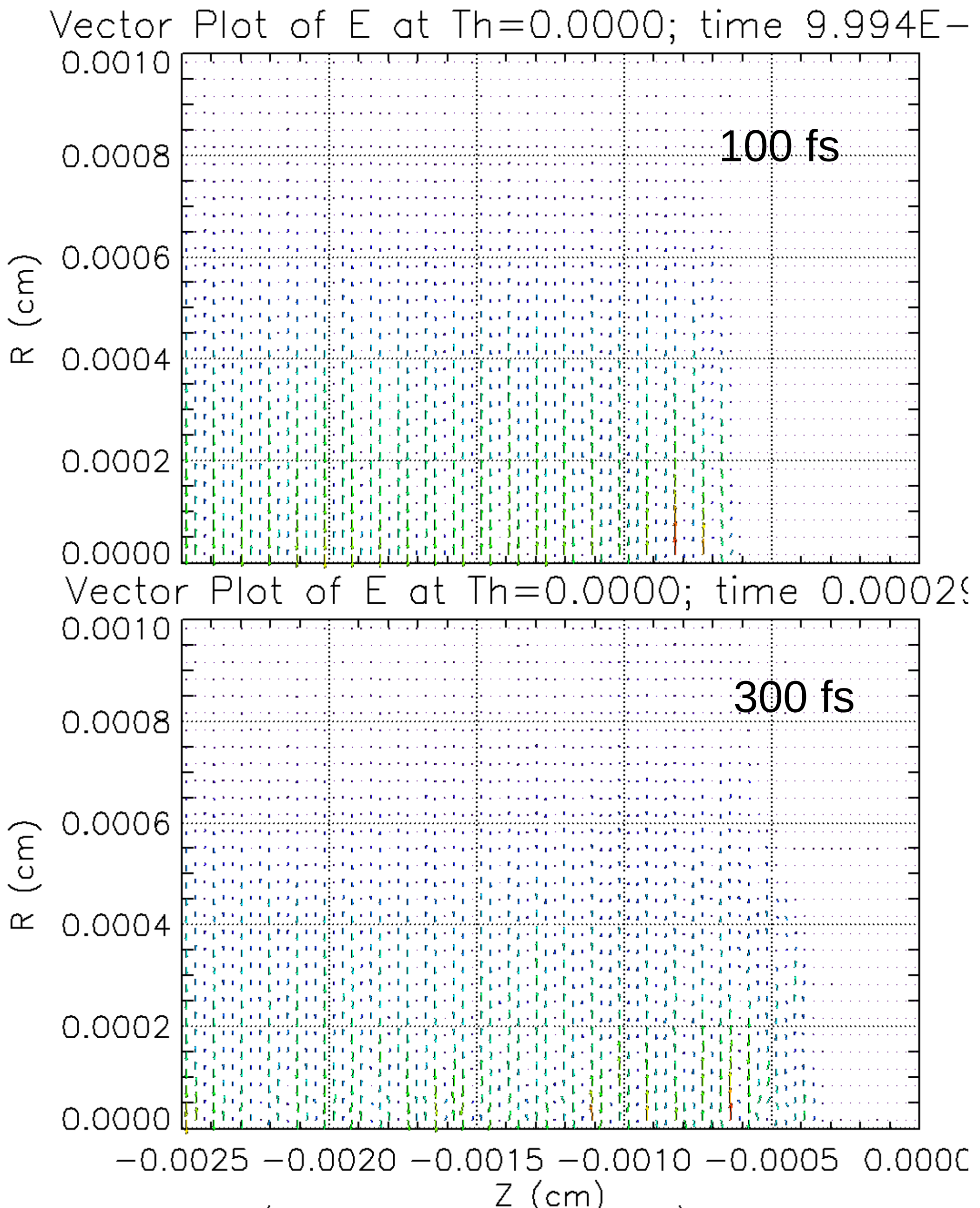

Fast electron, proton density evolution

- 10-micron Au foil
- electron transport to back surface
- proton beam from back surface

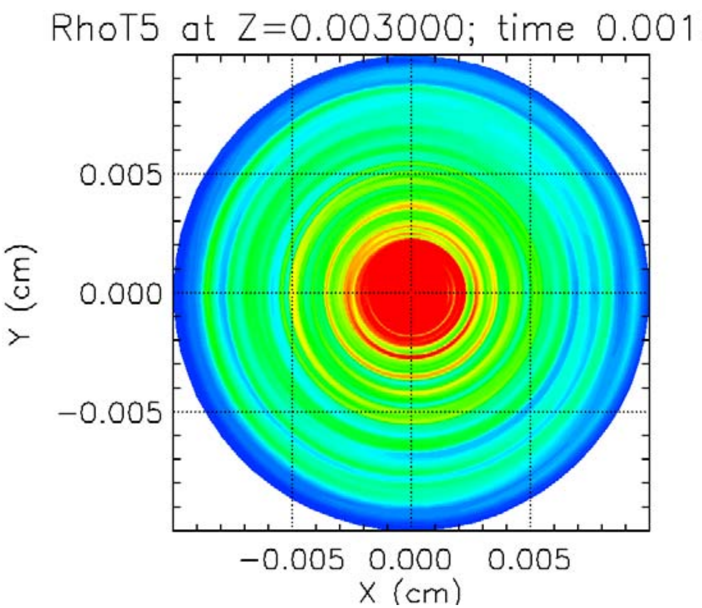

p⁺ at z=30μm, 1300fs

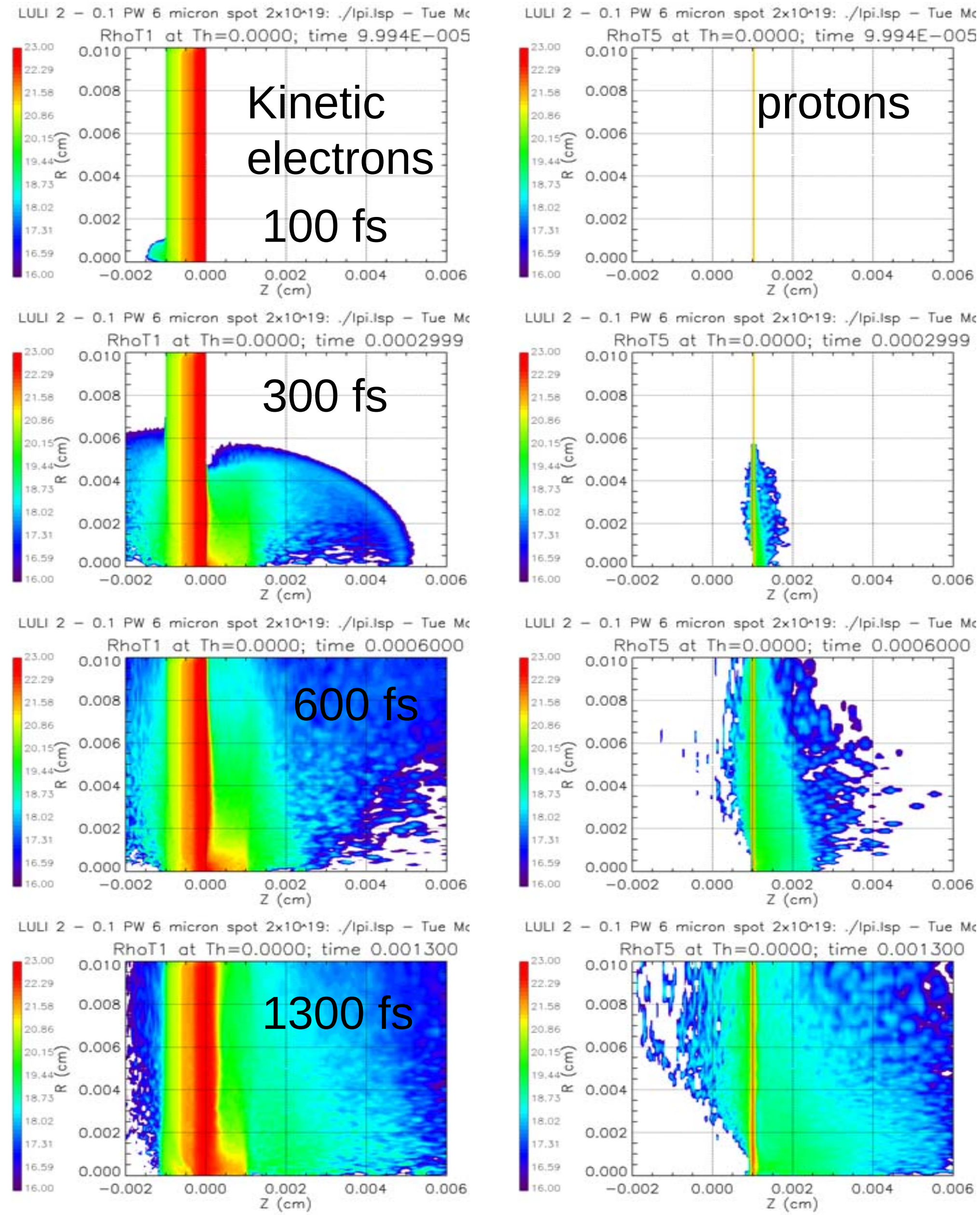

Energetic Proton beam accelerated from vacuum interface

- Roughly 0.2-2-pi-mm-mrad normalized emittance --- too hot?
- Roughly 15% conversion efficiency of laser to proton energy

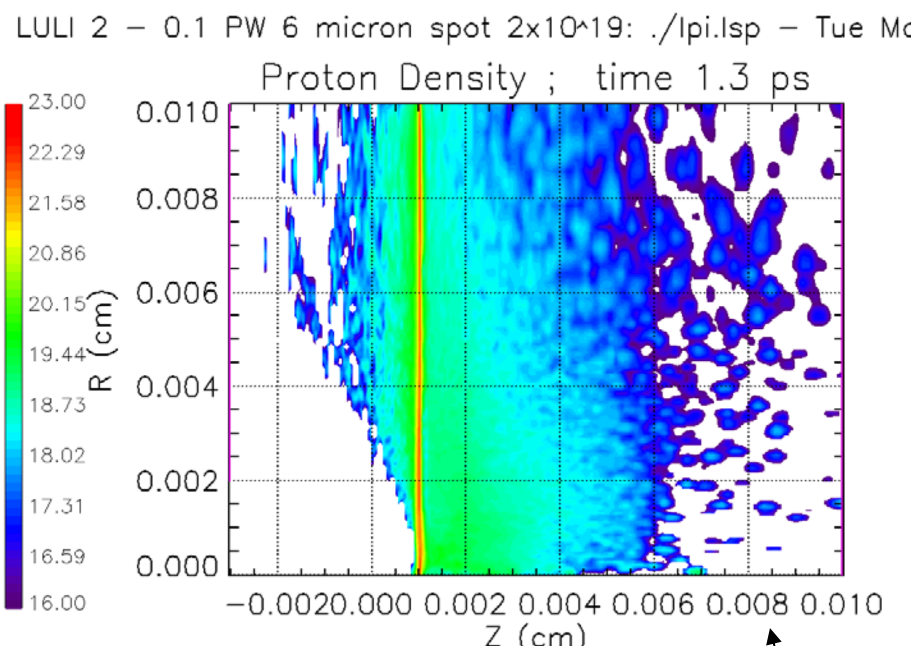

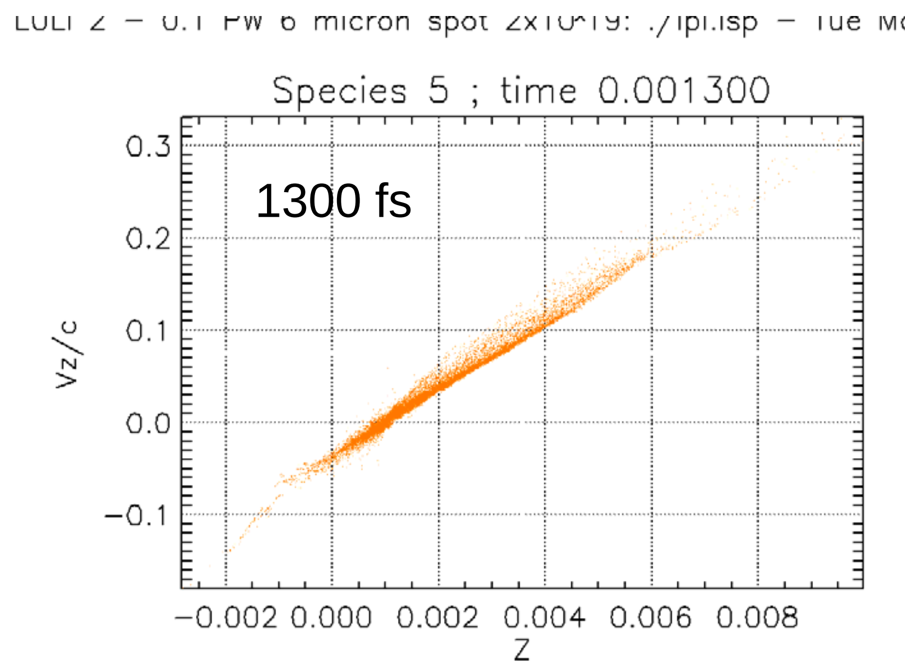

Attempting to capture electrons and protons at .0085 cm for reinjection into longer simulation

Transport simulation to 4 cm

- Electrons and protons striking z = 0.0085 cm plane are stored and injected into a 2nd longer simulation box
- The new simulation is 2d and has a 1.5-cm outer radius and a 4-cm extent
- Assumption in simulation is that the plasma is injected through a 0 potential surface that can emit electrons – this avoids having to run LPI simulation even longer to accumulate electrons
- Particle statistics are getting stretched thin but still ok at this distance

Density plots of species

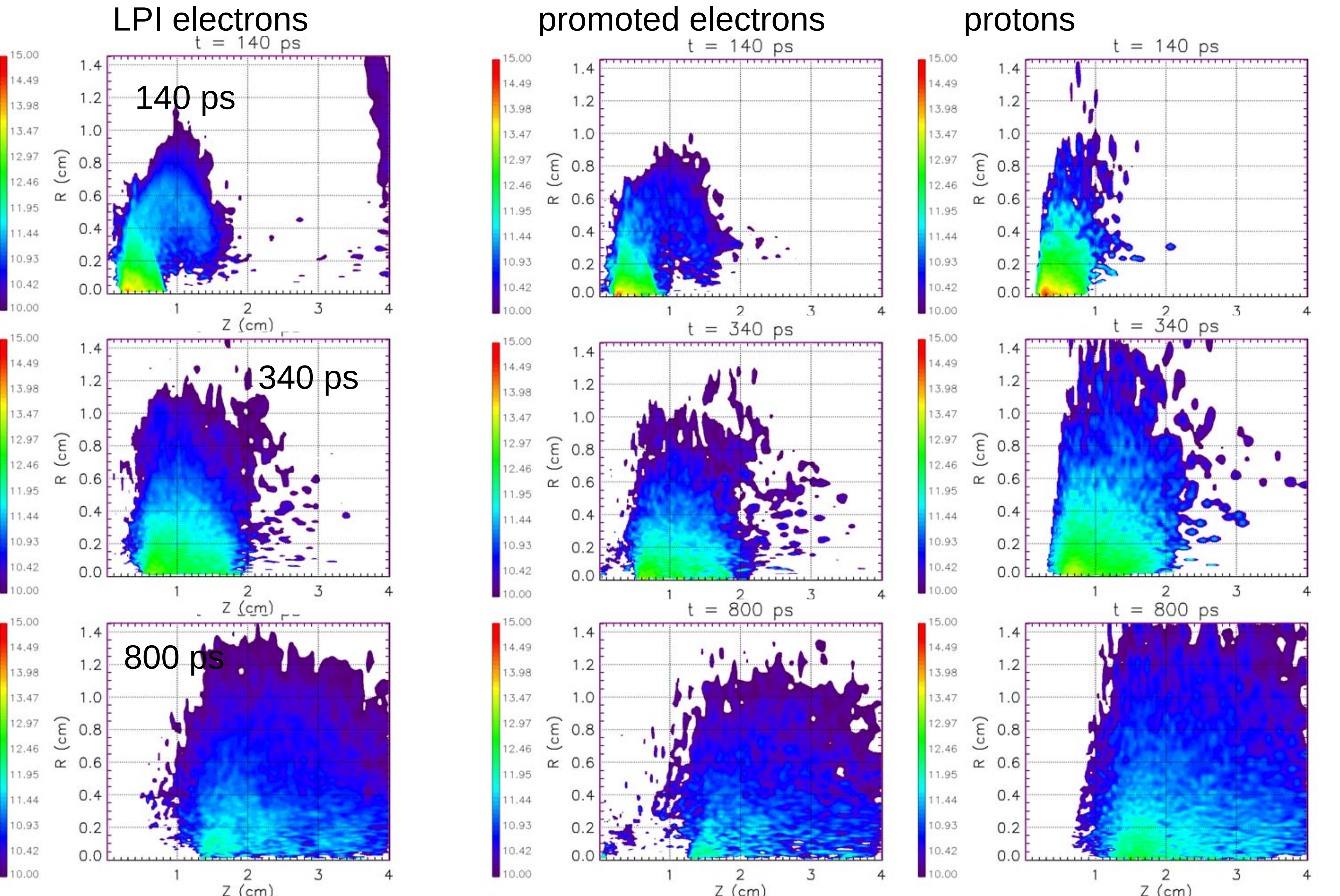

Electron energies cool to 3000 eV

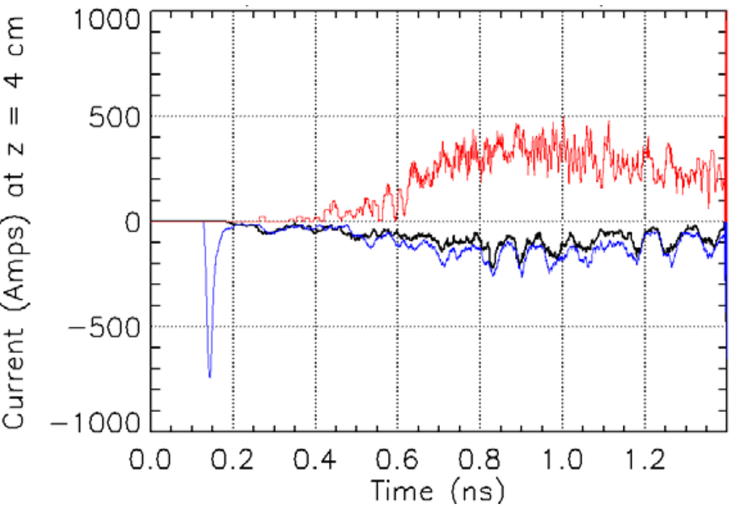

LPI electrons
plas electrons
protons

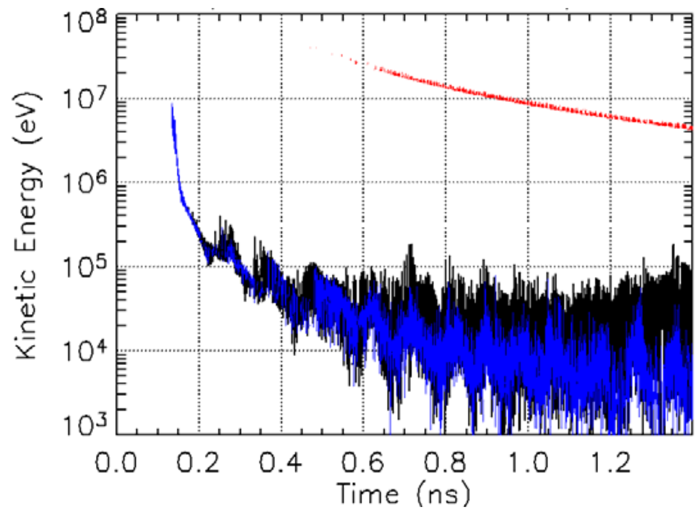

LPI electrons at 4 cm fall to < 10 keV energy

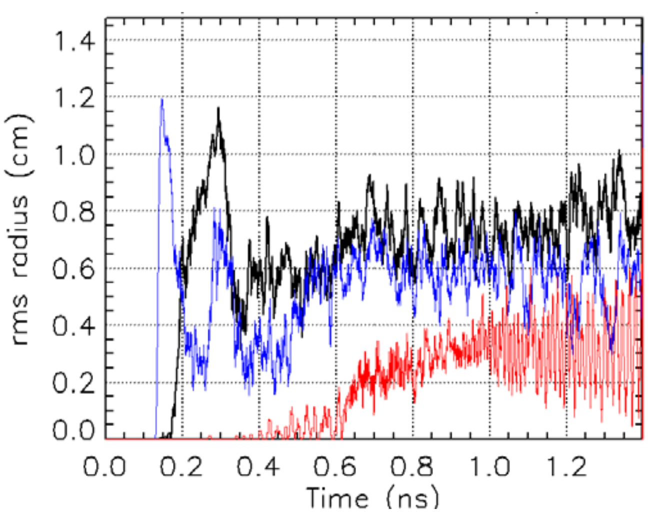

Particle statistics are insufficient for emittance

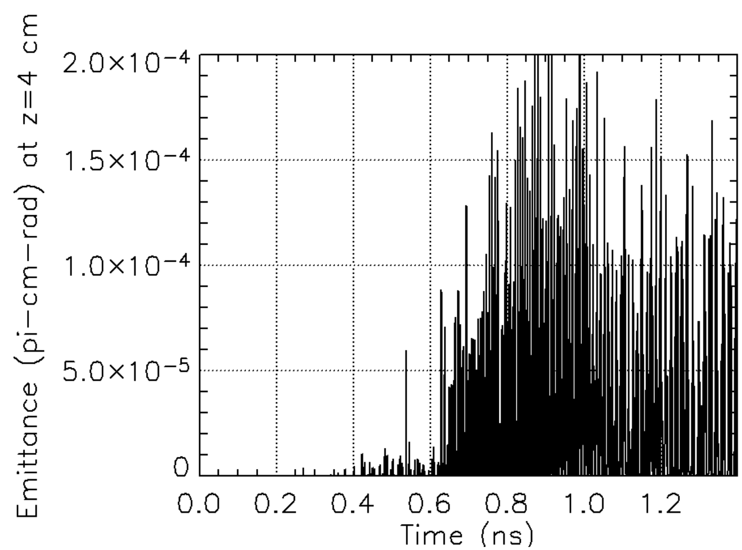

Temperatures cool to 100-300 eV

LPI electrons promoted electrons protons

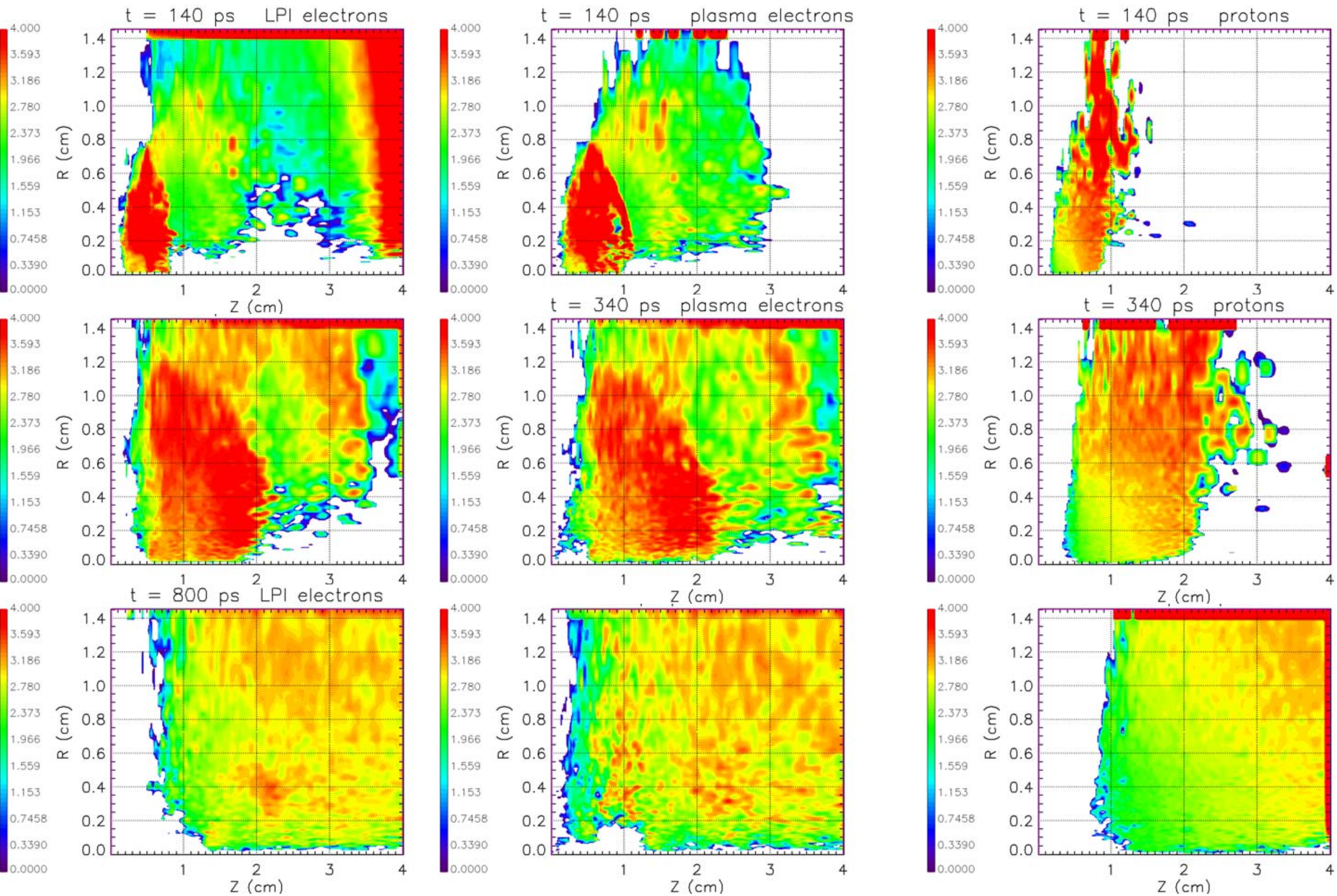

Conclusions

- Integrated simulation of LPI and beam transport in slab and vacuum are possible given 3D cylindrical coordinates and blow-off plasma.
- With roughly the observed current and divergence, a low emittance proton beam with a tail-to-head energy ramp is produced

Review of Ion Acceleration Portion of Computational Short Pulse Workshop

S. C. Wilks

LLNL

UCRL-PRES-206186

Ion beam generation, transport, and focusing

1. Tony Bell Imperial College
2. Andreas Kemp University of Nevada, Reno
3. Peter Messmer Tech-X
4. Koichi Noguchi Rice University
5. Hartmut Ruhl University of Nevada
6. Scott Wilks LLNL

1.	Bedros	Afeyan	Polymath Research
2.	Jean-Luc	Cambier	Air Force Research Laboratory
3.	Eric	Esarey	LBNL
4.	Roger	Evans	AWE / Imperial College
5.	Richard	Freeman	The Ohio State University
6.	Alex	Friedman	LLNL / HIF-VNL
7.	David	Grote	LLNL/LBNL
8.	Steve	Hatchett	LLNL
9.	Tomoyuki	Johzaki	Osaka University
10.	Barbara	Lasinski	LLNL
11.	Stephen	Libby	LLNL
12.	John	Lindl	LLNL
13.	Steven	Lund	LLNL
14.	Rodney	Mason	Los Alamos
15.	Brian	McCandless	LLNL
16.	Jose	Milovich	LLNL
17.	Warren	Mori	UCLA
18.	Bryan	Oliver	Mission Research
19.	Chuang	Ren	University of Rocheste
20.	rAdam	Sefkow	PPPL
21.	Bert	Still	LLNL
22.	Peter	Stoltz	Tech-X Corp.
23.	John	Tonge	UCLA
24.	Richard	Town	LLNL
25.	Jean-Luc	Vay	LBNL
26.	Jonathan	Wurtele	UC Berkeley and LBNL

The Questions we attempted to answer.

- Coordinator: *Scott Wilks (LLNL)*
- What are the proton generation mechanism efficiencies?
- How sensitive to resolution are the answers?
- Can hybrid PIC be used?
- How does electron flow affect proton generation?
- How can we control the generation and focusing of the protons?
- What is the optimum proton energy for radiography?
- What are the qualities that set ions using these mechanisms apart from “standard” ion beams?
- What governs ion flux?
- What is the optimal distance of “proton lens” from target?

Progress we made on these questions…

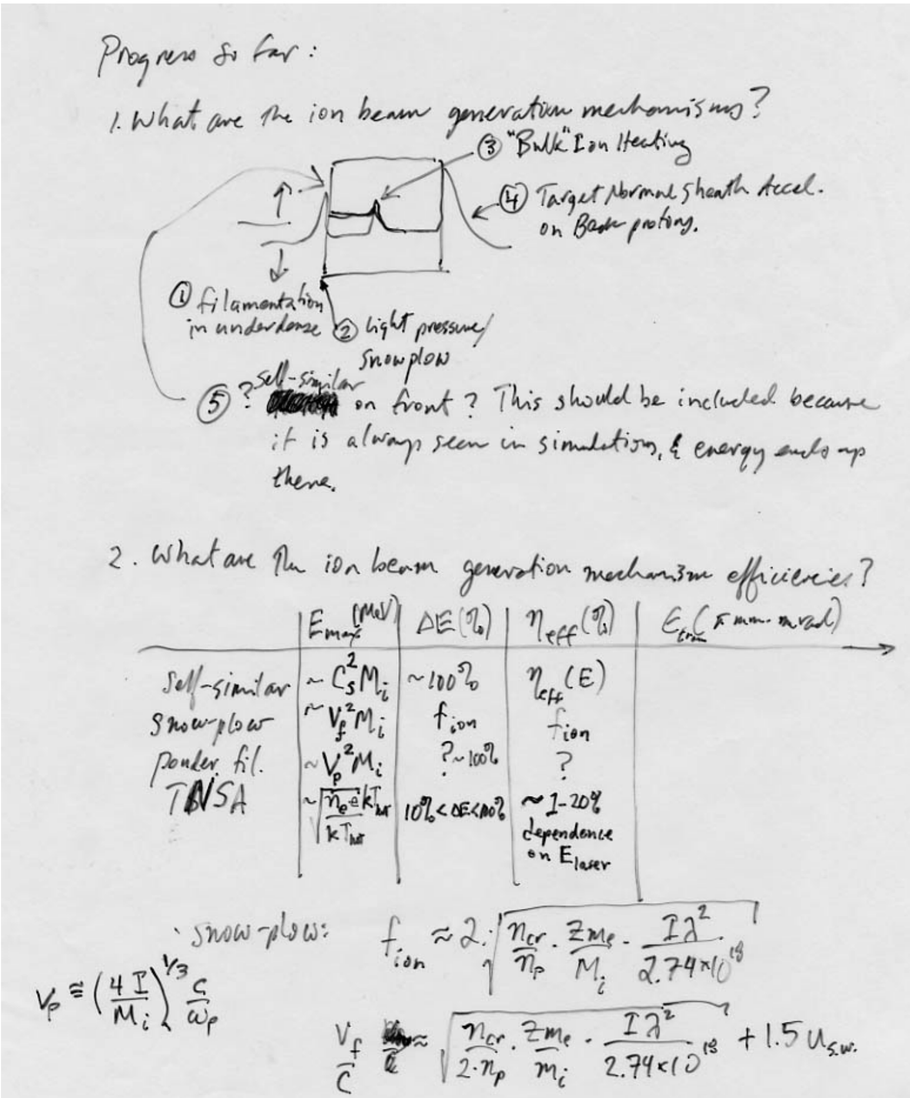

Progress so far:

1. What are the ion beam generation mechanisms?

⑤ ? self-similar on front ? This should be included because it is always seen in simulation, & energy ends up there.

2. What are the ion beam generation mechanism efficiencies?

	E_{max} (MeV)	ΔE (%)	η_{eff} (%)	ϵ_{trn} (π mm-mrad)
Self-similar	$\sim C_s^2 M_i$	~100%	$\eta_{eff}(E)$	
snow-plow	$\sim V_f^2 M_i$	f_{ion}	f_{ion}	
ponder. fil.	$\sim V_p^2 M_i$	? ~100%	?	
TNSA	$\sim \sqrt{\frac{n_e e k T_{hot}}{k T_{hot}}}$	10% < ΔE < 100%	~1-20% dependence on E_{laser}	

snow-plow: $f_{ion} \approx 2 \cdot \sqrt{\frac{n_{cr}}{n_p} \cdot \frac{Z m_e}{M_i} \cdot \frac{I \lambda^2}{2.74 \times 10^{18}}}$

$V_p \cong \left(\frac{4 I}{M_i}\right)^{1/3} \frac{c}{\omega_p}$

$\frac{V_f}{c} \approx \sqrt{\frac{n_{cr}}{2 \cdot n_p} \cdot \frac{Z m_e}{m_i} \cdot \frac{I \lambda^2}{2.74 \times 10^{18}}} + 1.5 u_{s.w.}$

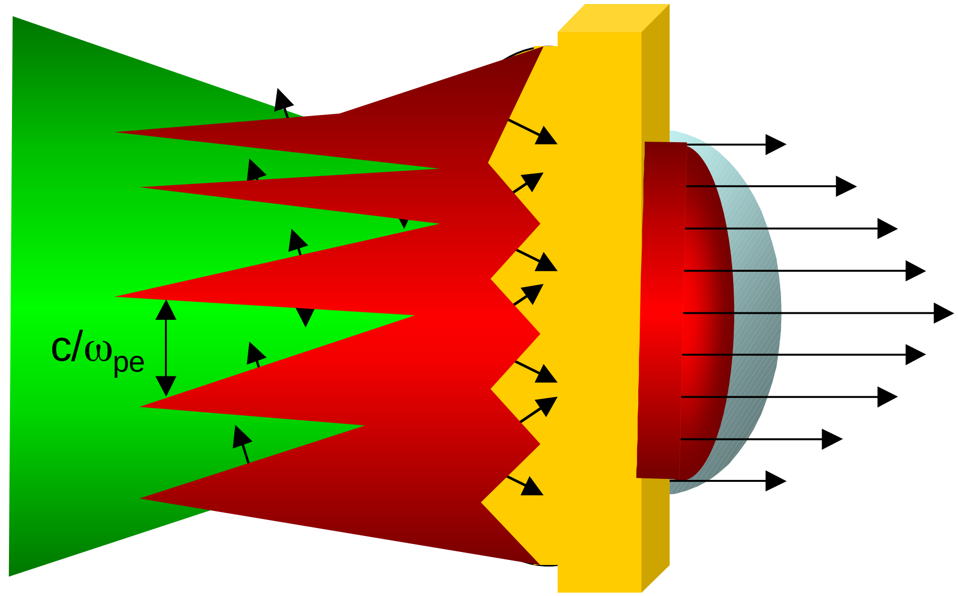

$t < t_{crit}$

Where e^- generated from Prepulse or ASE cannot disrupt back surface.

Ion Acceleration Group:

Review of yesterday: (Aug. 25)

1.) We added the following questions to this list:

1. Fast Ignitor related:
   1. What is optimal hemi-sphere/f-number/distance from target for maximum energy deposition into compressed cone?
   2. How to shield from x-rays?
   3. How fast/important is Gap Closure?

2. Is there an easy way to make the proton beam have less energy spread in longitudinal direction?

3. How small an area can the proton "focus" from a proton lens be?

4. What governs ion flux? (S. Hatchett will speak to this.)

2. Comments:

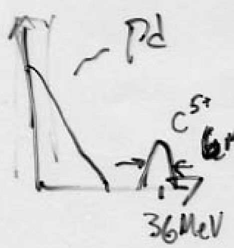

1. Get PBFA people involved ~ lessons learned.
2. Possible application: Study of ~~fission~~ transport through fusion target chamber?
3. Efficiency seems to scale with laser energy (M. Key)
   Y. Sentoku showed simulation results on this.
4.

3. Presentations:
   1. Y. Sentoku : Explicit PIC results & Recirculation effect on proton E_{max}, η_{eff}
   2. T. Bell : FP/Vlasov results.

Review of Thursday Aug 26

1. S. Hatchett - theory of TNSA
2. D. Welch - LSP study of TNSA (rear-surface protons.)
3. M. Hegelich - Exp't : multi-species ions.
4. P. Messmer - VORPAL (PIC code): "bulk" ion acceleration.
5. M. Key - Exp't. results of proton heating.
6. A. Kemp - Water droplet proton acceleration: dip in ion spectra.
7. H. Ruhl - Transfer function approach (proton transport.)

* Refined some of the questions / Important open issues for further investigations.

1. Optimization of proton lens configuration for F.I.
   1. Size of final focus: "parabolic" (achromatic proton lens...)
   2. Distance from implosion?
   3. X-ray / particle shielding needed?
2. Why does $\eta_{eff} \propto E_{laser}$?
3. How does acceleration scale with pulse length? (i.e. is 1 pSec maximum pulse length for acceleration?)
4. How good is the quasi-neutrality assumption in the rear side proton sheath? (Unacceptable, or just minor effect?)
5. What is the best way to make relatively mono-energetic ions? Answer: Multispecies : Question: How efficient? Possible to maximize it?

An attempt to classify which type of codes can study what types of physics.

Codes possible to study protons:

Acceleration mechanisms	PIC	Fluid	Hybrid fluid e⁻/particle ions	Reduced Description	Fokker-Plank	Vlasov	Fokker-Plank + Vlasov
self-similar	✓	✓	✓	?			
snow-plow	✓ ½		✓ ½	×			
ponder motive fil.	✓		✓	×			
TNSA	✓	✓	✓	?			
Bulk Ion	×	✓		×			
proton transport	✓			✓			
proton heating	×	×		✓			

α= can use that code
X = can't use that code
? = not obvious

Hybrid seemed a likely choice. What has been done to date?

Some notes concerning some recent hybrid PIC simulations.

Hybrid: protons off the back.

① Mora (2003): (only 1 species)

$$n_e = n_{e0}\, e^{e\Phi/kT_e} \qquad (1)$$

$$\frac{dE}{dx} = 4\pi e\,(n_e - Z n_i) \qquad (2)$$

② Bychenkov (2004): 2 species of electrons:

$$n_h = n_{h0}\, e^{e\Phi/kT_h}$$

$$n_c = n_{c0}\, e^{e\Phi/kT_c} \qquad (1)$$

$$\frac{dE}{dx} = 4\pi e\left(\sum_{\beta=c,h} n_{\beta 0}\, e^{e\Phi/kT_\beta} - \sum_\alpha Z_\alpha n_\alpha\right) \qquad (2)$$

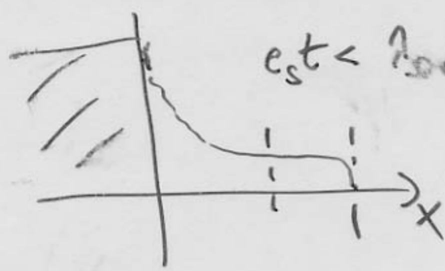

$$c_s t < \lambda_{De} \Rightarrow E_x$$

$$T\,\frac{\partial_x n}{n} \sim E_x$$

The following few viewgraphs are a small subset of experimental results on ion acceleration we used as starting points for discussions of how to benchmark codes to experiment. Also, they pointed to what type of code development needs to be done in the future to model these experiments.

Ion Acceleration from M. Hegelich.

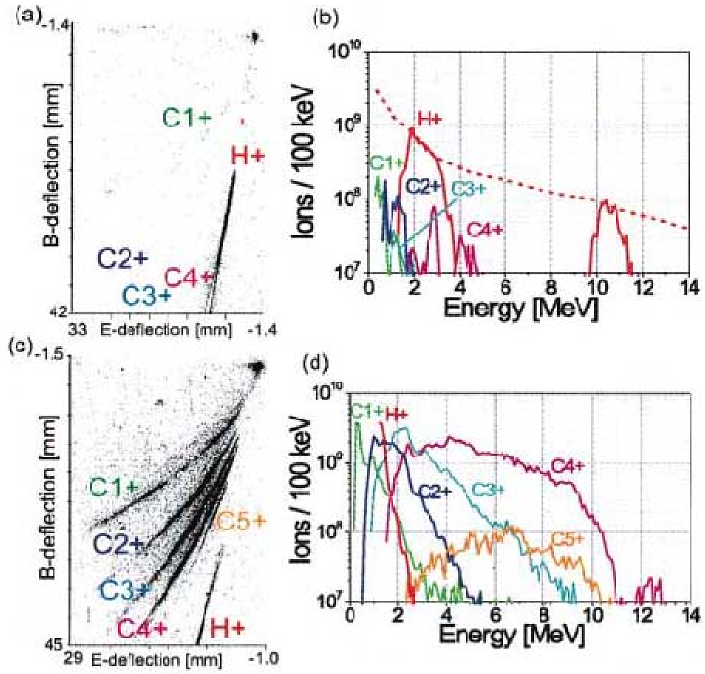

FIG. 1 (color). (a) Ion traces (on CR39) from an unheated Al | C target and (b) corresponding spectra. The gap in the proton signal is due to the CR-39 detector which is optimized for heavier particles. The dotted line illustrates the H^+ spectra as obtained with the proton spectrometer. (c) Ion traces from a heated Al | C target and (d) corresponding spectra. The ion signals are strongly enhanced. The spot in the upper right corner of (a),(c) is the pinhole image formed by neutral atoms.

M. Hegelich, S. Karsch, G. Pretzler, D. Habs, K. Witte, W. Guenther, M. Allen, A. Blazevic, J. Fuchs, J. C. Gauthier, M. Geissel, P. Audebert, T.Cowan, and M. Roth, Phys. Rev. Lett. **89**, 085002 (2002).

Prav Patel proton experiments December 2003 Science & Technology Review.

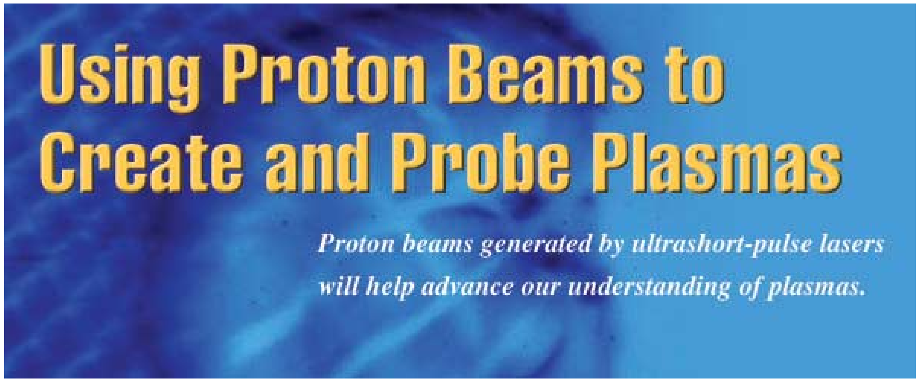

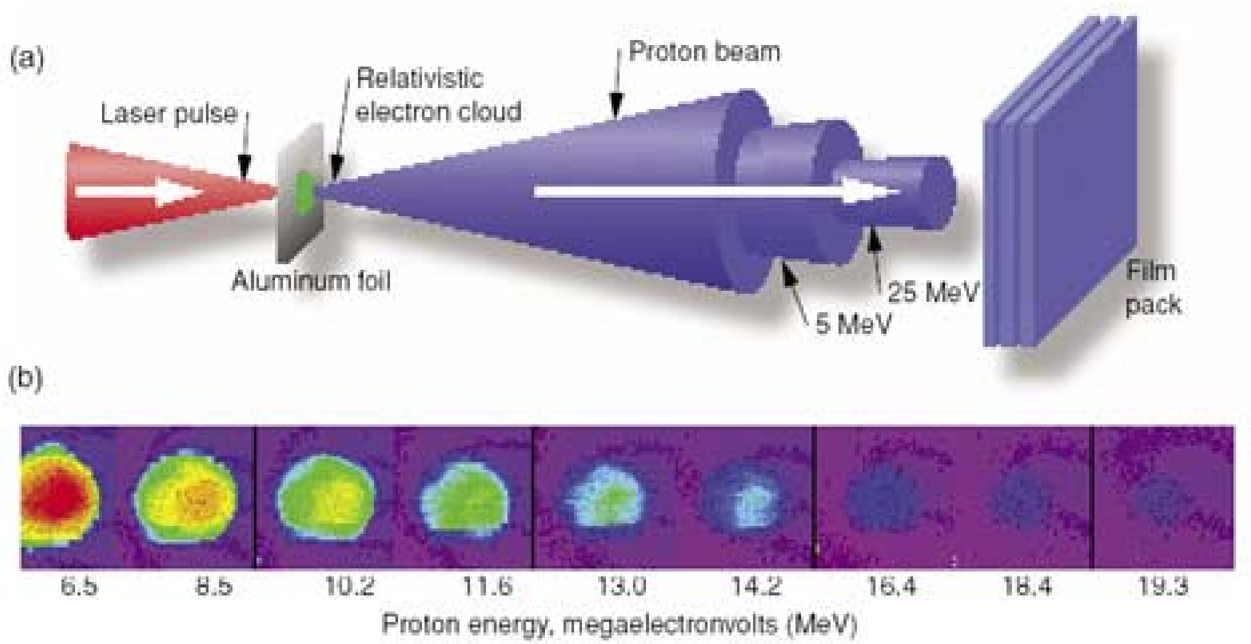

Proton source experiments have revealed the effect of recirculating electrons on proton acceleration.

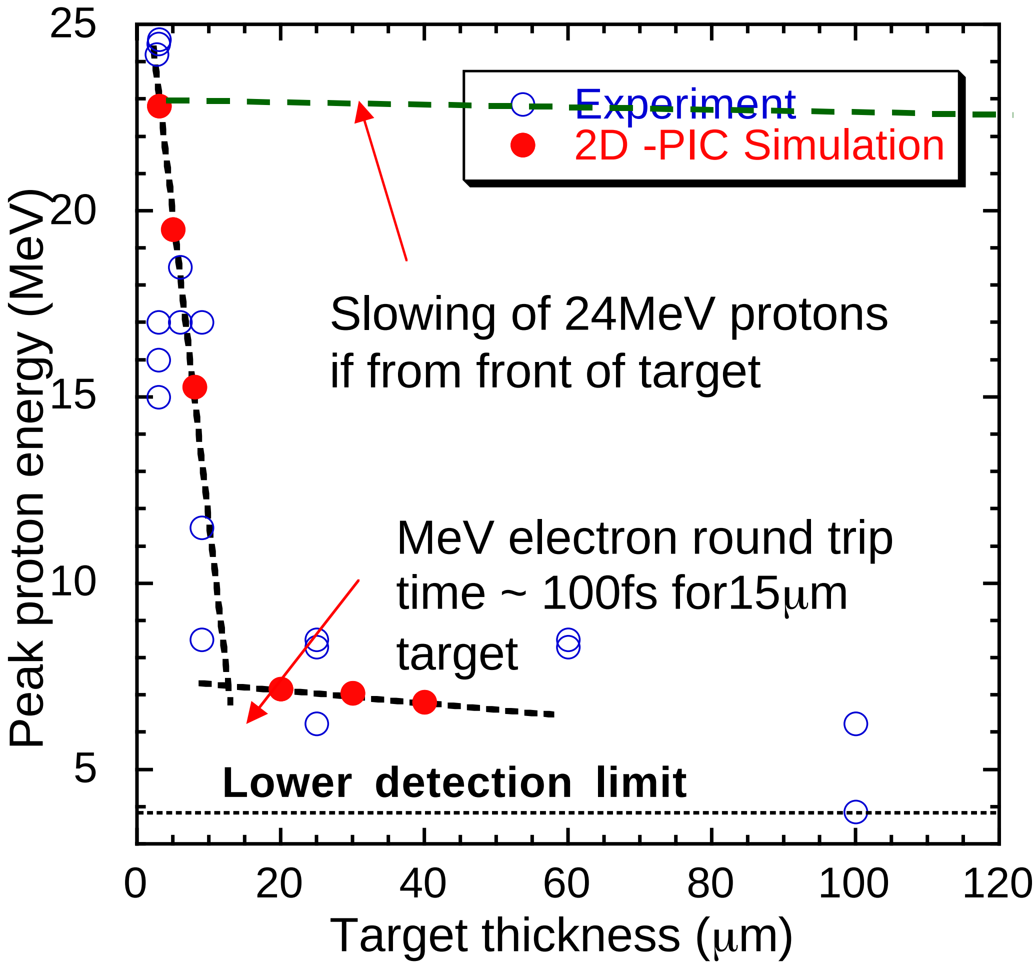

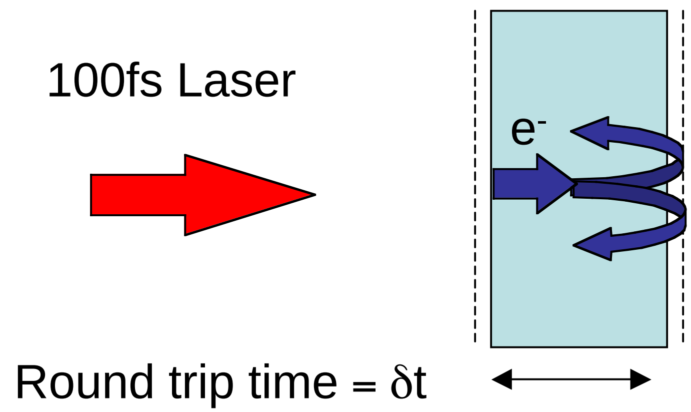

- MeV electrons highly relativistic: For 5μm target δt ~ 34fs
- Electrons re-circulate ~3 times before end of pulse
- Possible route to scaling to higher proton energies on large laser systems

A.J.Mackinnon et al., Physical Review Letters 88, 215006-1

Kaluza, Schreiber, Santala, Tsakiris, Eidmann, MTV & Witte proton experiments.

VOLUME 93, NUMBER 4 PHYSICAL REVIEW LETTERS week ending 23 JULY 2004

Influence of the Laser Prepulse on Proton Acceleration in Thin-Foil Experiments

M. Kaluza, J. Schreiber, M. I. K. Santala, G. D. Tsakiris, K. Eidmann, J. Meyer-ter-Vehn, and K. J. Witte
Max-Planck-Institut für Quantenoptik, Hans-Kopfermann-Straße 1, D-85748 Garching, Germany
(Received 8 December 2003; published 20 July 2004)

We investigate the influence of the laser prepulse due to amplified spontaneous emission on the acceleration of protons in thin-foil experiments. We show that changing the prepulse duration has a profound effect on the maximum proton energy. We find an optimal value for the target thickness, which strongly depends on the prepulse duration. At this optimal thickness, the rear side acceleration process leads to the highest proton energies, while this mechanism is rendered ineffective for thinner targets due to a prepulse-induced plasma formation at the rear side. In this case, the protons are primarily accelerated by the front side mechanism leading to lower cutoff energies.

DOI: 10.1103/PhysRevLett.93.045003 PACS numbers: 52.38.Kd, 29.30.Ep, 41.75.Jv

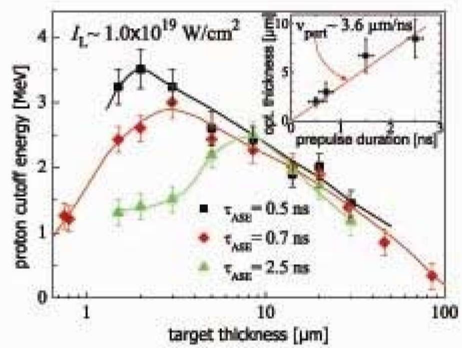

FIG. 1 (color). Proton cutoff energies for differently thick targets and prepulse durations, τ_{ASE}, of 0.5, 0.7, and 2.5 ns, respectively, at $I_L = 1.0 \times 10^{19}$ W/cm^2. For longer τ_{ASE}, the maximum proton energies are achieved with thicker foils. The inset gives the optimal thickness, depending on τ_{ASE}.

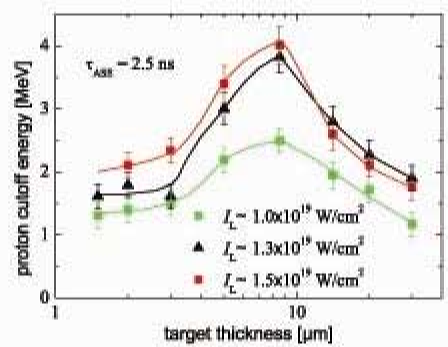

FIG. 2 (color). Proton cutoff energies for differently thick targets and different laser intensities for a prepulse duration of $\tau_{ASE} = 2.5$ ns. The cutoff energies vary with the laser intensity, but the optimal target thickness depends on τ_{ASE} only (cf. Fig. 1).

Selected experiments: Matt Allen Front and Back acceleration.

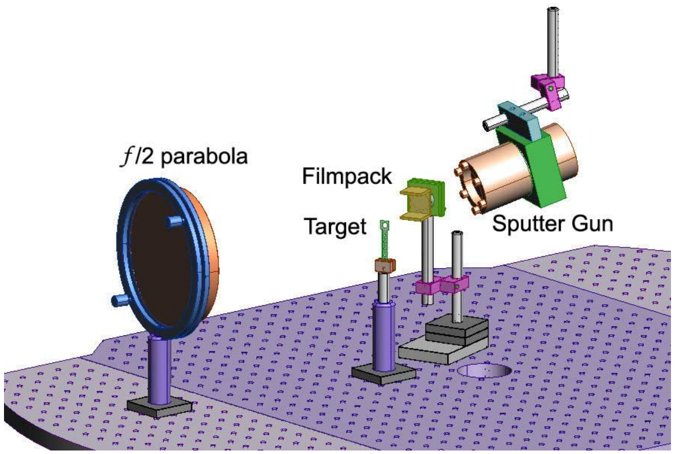

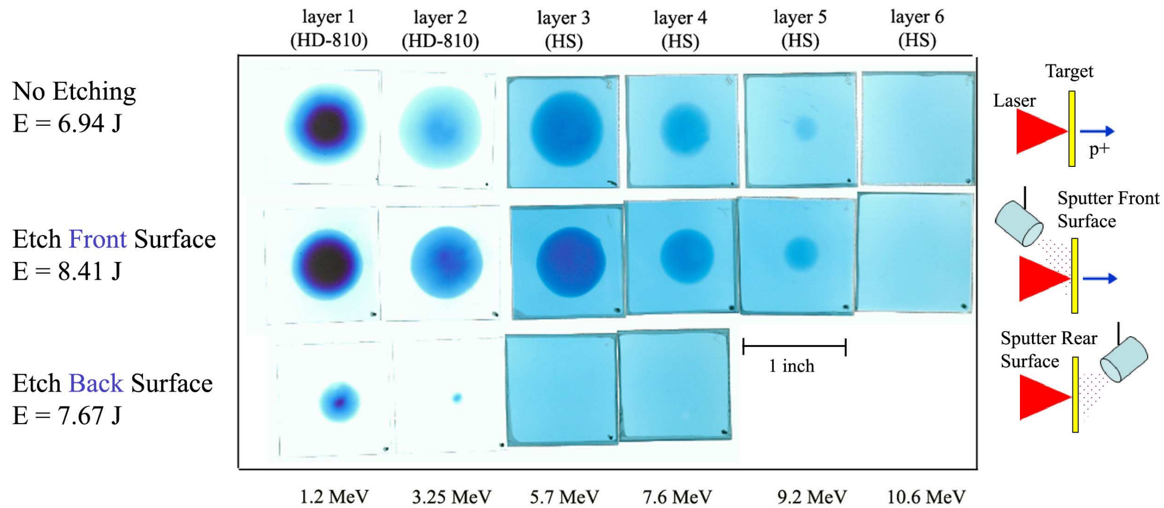

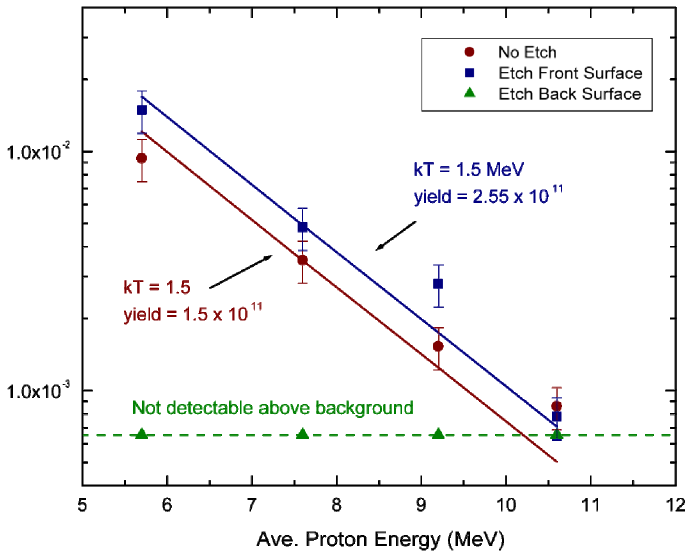

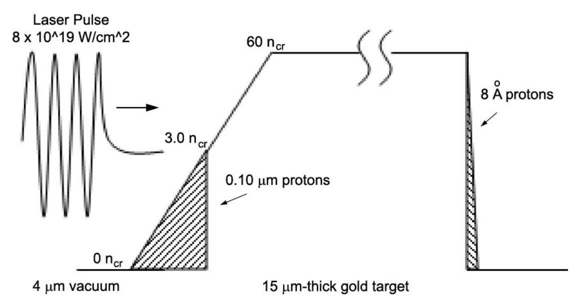

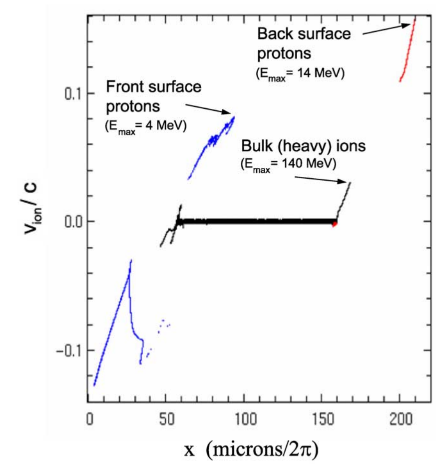

Matthew Allen, Pravesh K. Patel, Andrew Mackinnon, Dwight Price, Scott C. Wilks, and Edward Morse, “Experimental evidence of back-surface ion acceleration from laser irradiated foils”, submitted to PRL (2004).

Laboratory Astrophysics

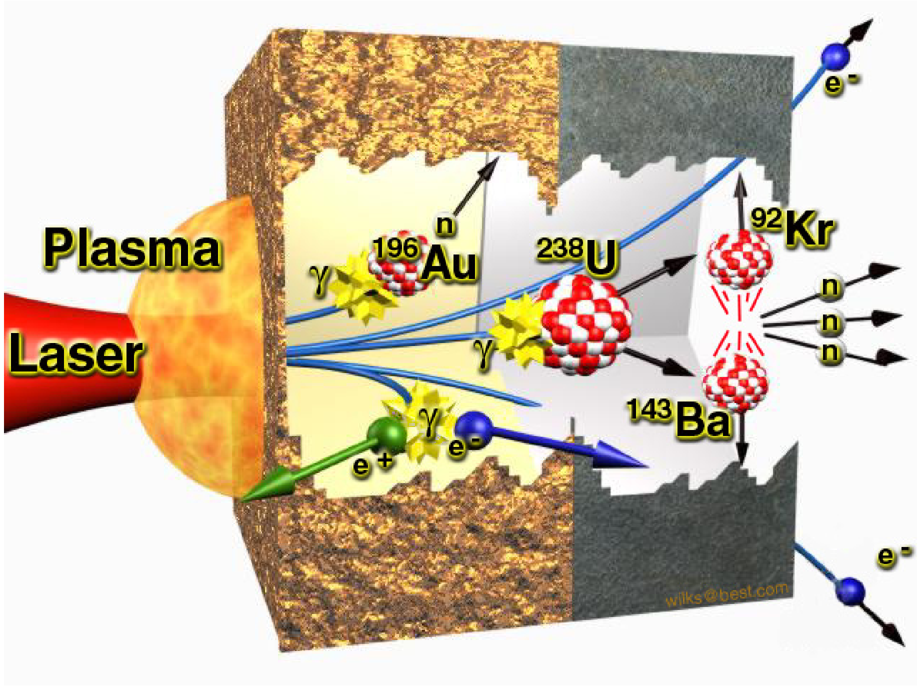

S. C. Wilks

R. Klein, B. Remington, S. Moon, P. Patel, A. Mackinnon, D. Ryutov, H. Chen, H.-K Chung, W. Kruer, M. Key, M. Tabak, R. Town, R. Shepherd, M. Allen, A. B. Langdon, and T. Cowan

Lawrence Livermore National Laboratory

E. Liang, K. Noguchi, K. Nishimura, D. Kocevski

Rice University

This project is supported by LLNL Laboratory-Directed Research and Development and ILSA.

ILSA's Short Pulse Laser Matter Computational Workshop
Pleasanton, CA
August 23, 2004

UCRL-PRES-206188

This work was performed under the auspices of the U.S. Department of Energy by the University of California, Lawrence Livermore National Laboratory under Contract No. W-7405-ENG-48.

Outline

1. Neutron Stars, Photon Bubbles, & Petawatt Lasers

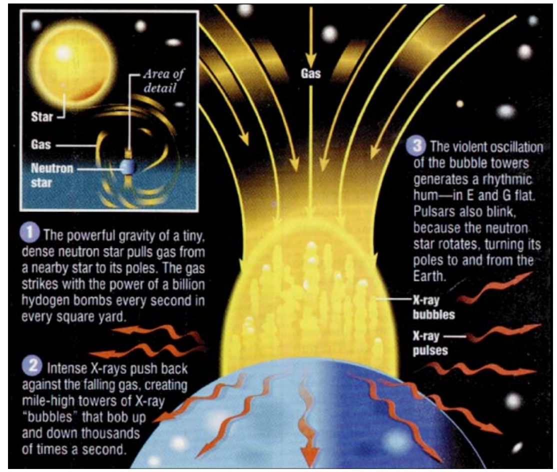

2. Gamma Ray Bursts & Electron Positron Plasmas

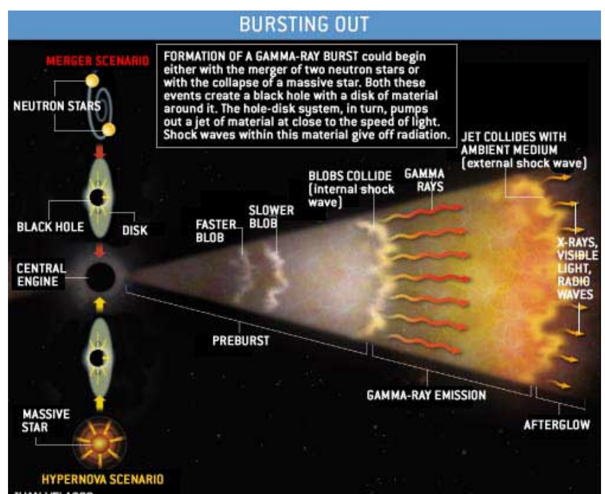

Ultra-intense lasers can reach energies and densities of some interesting astrophysical objects.

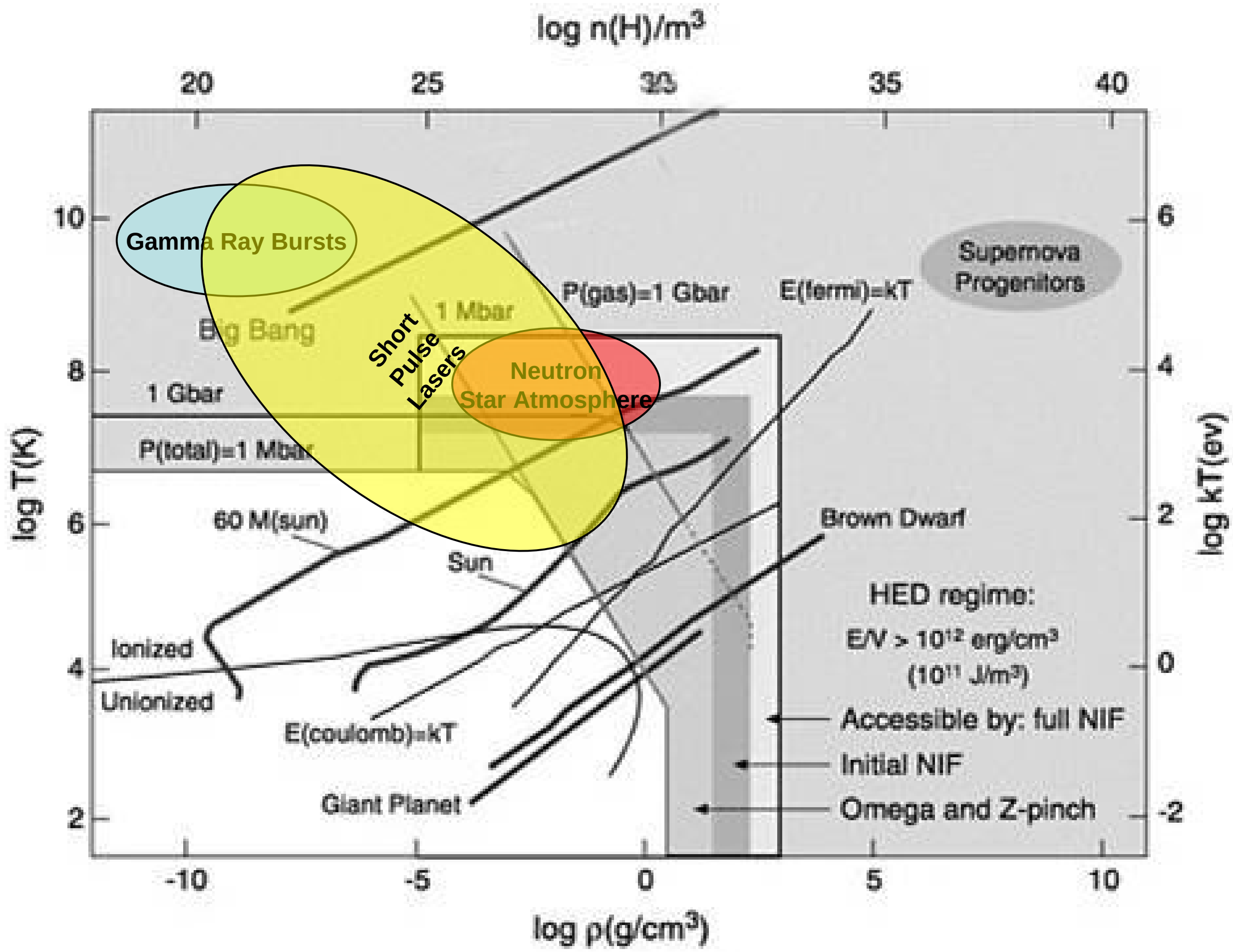

Can we design laboratory experiments that create these extreme conditions?
This would allow us to shed light on phenomena happening light years away

From: “Frontiers in High Energy Density Physics: The X-Games of Contemporary Science” National Research Council of the National Academies.

The environment of an accreting x-ray pulsar involves extreme physical conditions; generates photon bubbles.

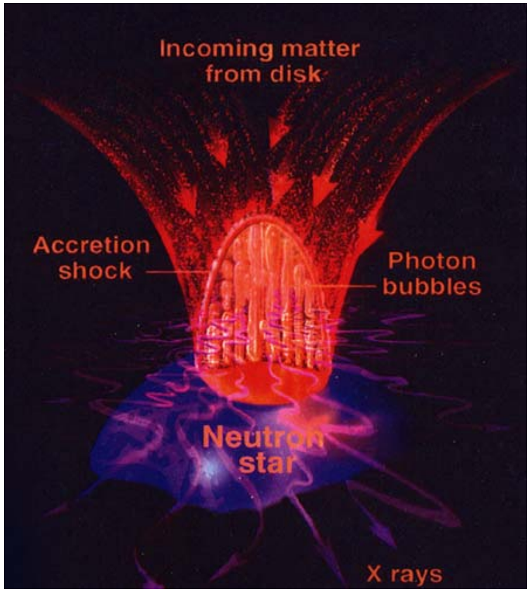

Simulation of photon bubbles*

Velocity of matter in an acretion column

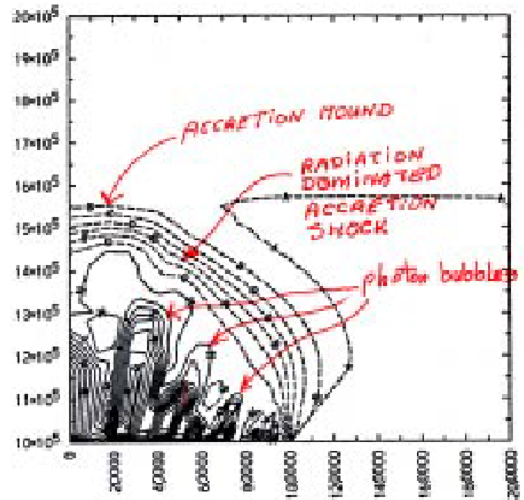

Rossi X-ray Timing Explorer, RXTE

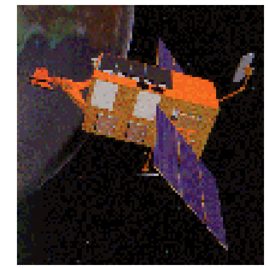

Real Satellite data

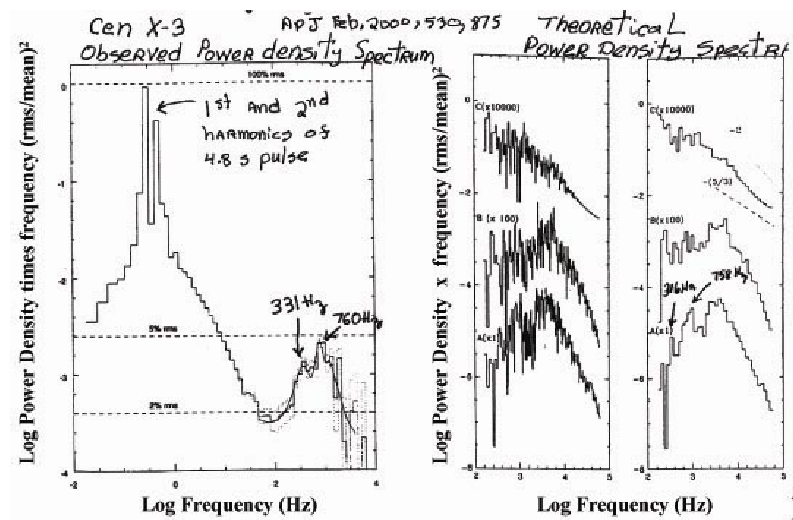

Properties of Accretion Column

$L_{cap} \geq 10^{36}$ erg/s

$A_{cap} \sim 1$ km²

$T \sim 10$ keV

$\rho_{ff} \sim 10^{-3}$ g/cm³

$P_{e} \sim P_{ion} \sim 10^{14}$

$P_{rad} \sim 10^{18}$

$P_{B\text{-field}} \sim 10^{22.5} \gg P_{rad} \gg P_{e,ion}$

$\rho_{eff} \sim 10^{14}$

$B_{surface} \sim 1($ $\quad B_{sun} \sim 10^{2}$ G $\quad B_{ISM} \sim 10^{-6}$ G

$F_x \simeq 300,00($ ... Watts / m² - sec

*R. I. Klein , J. G. Jernigan , J. Arons , E. H. Morgan , and W. Zhang, “GRO J1744 28 and Scorpious X-1: First Evidence for Photon Bubble Oscillations and Turbulence,” **The Astrophysical Journal Letters, v469:L119, 1996 October.**

Neutron Star atmospheric conditions possible in the lab?

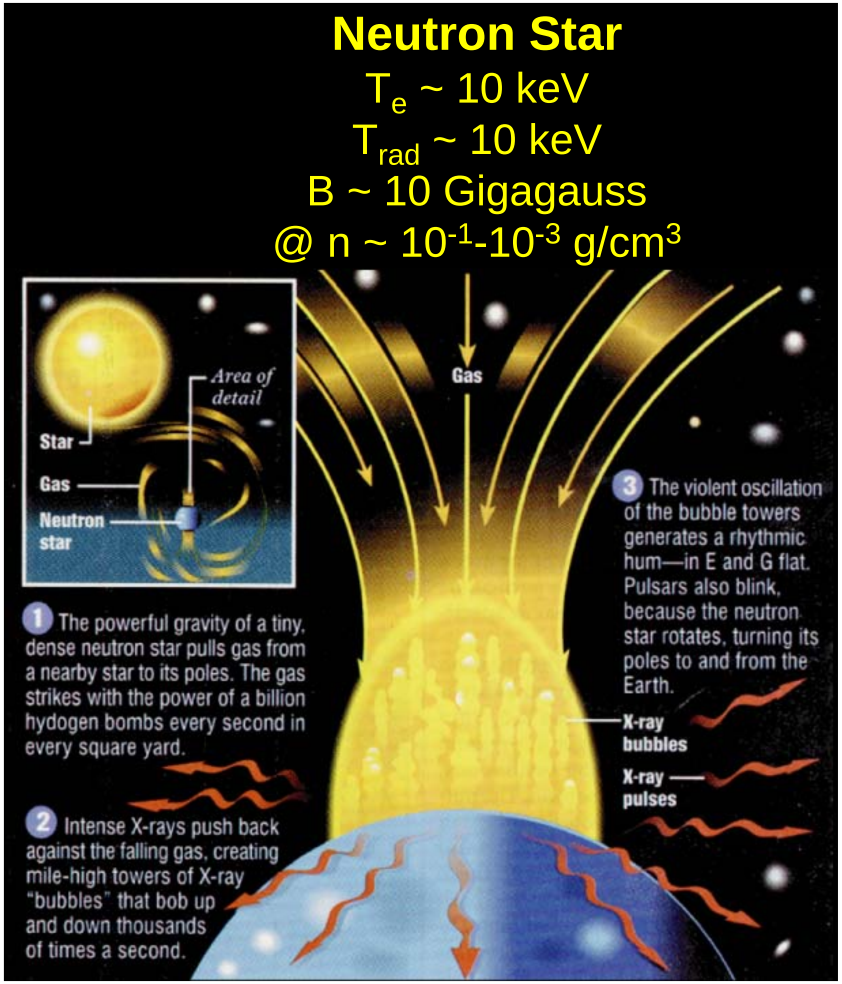

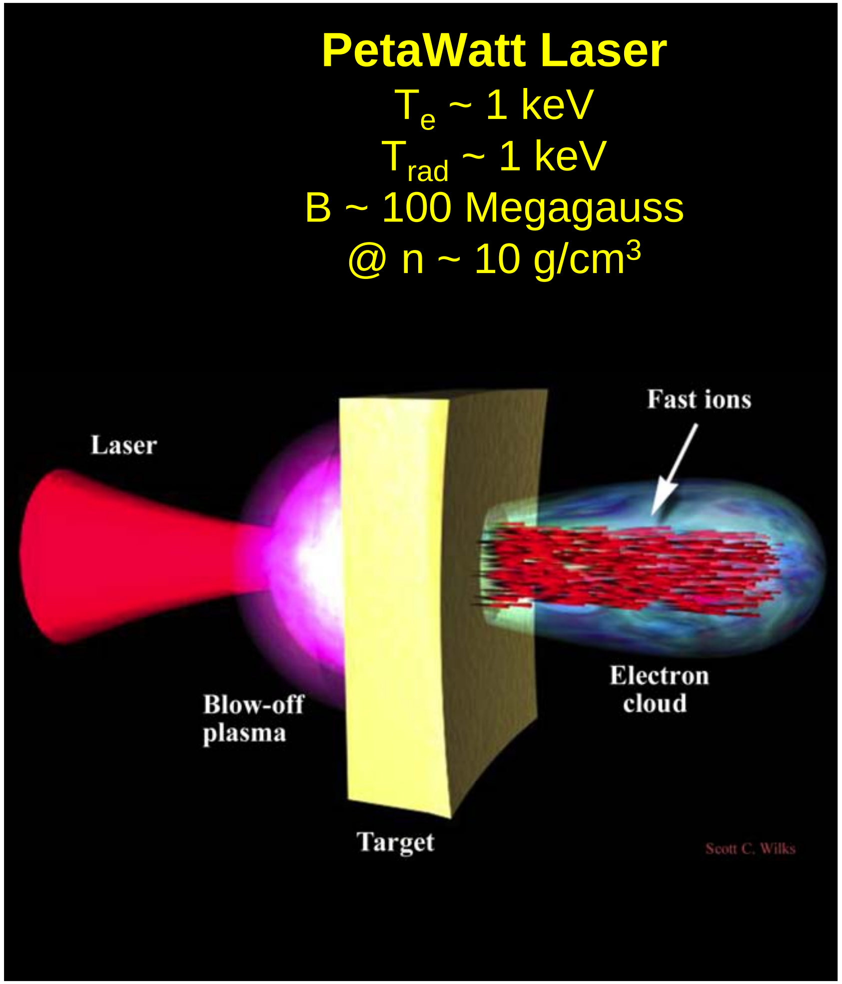

The minimal requirements for photon-bubble instability are difficult: B-field requirement suggests investigating possibility of PetaWatt laser experiments.

S. Moon, S. Wilks, R. Klein, B. Remington, D. Ryutov, H. Chen, J. Kuba, A. Mackinnon, P. Patel, R. Shepherd, A. Spitkovsky, R. Town, and R. Heeter "A Neutron Star Atmosphere in the Laboratory with Petawatt Lasers", accepted for publication in *Astrophysical and Space Sciences*, (2004)

Long predicted to exist in USP exp't's, large (GigaGauss) B fields have only recently been measured at RAL.

1992 PIC predicted large B-field near surface*

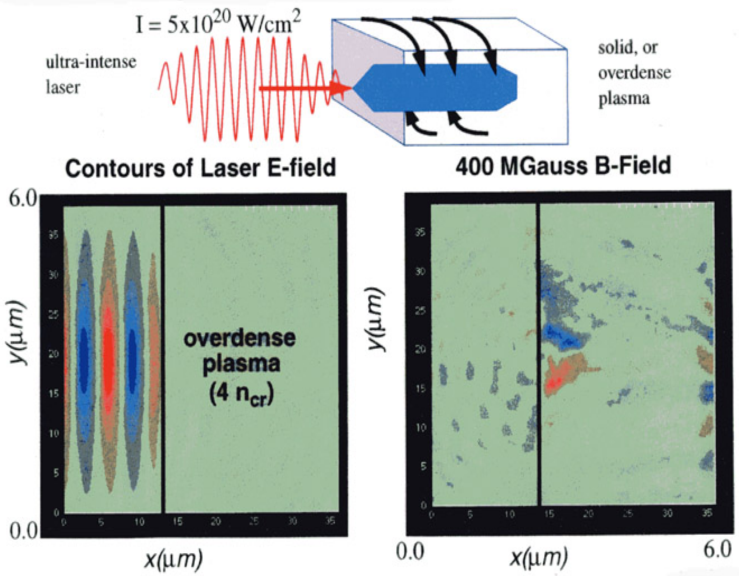

* S. C. Wilks, W. L. Kruer, et.al. "Absorption of ultrashort, ultra-intense laser light", PRL, 33 1992.

New methods of modeling needed for B-fields in solids

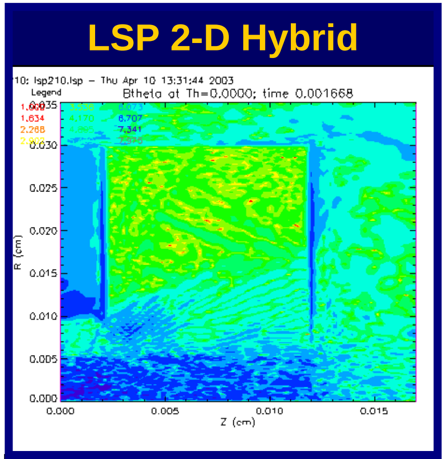

B_θ (magnetic field) in space (x and y)(single-sided illum.)

…seen experimentally at RAL in 2002⁺

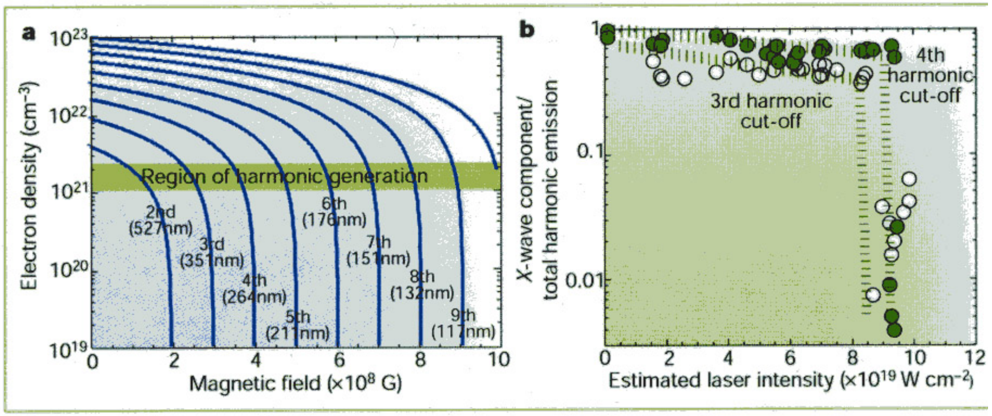

Figure 1 Laboratory measurement of magnetic fields greater than 340 megagauss. **a,** Plot of *x*-wave cut-offs for various harmonic (second, third, and so on) of 1.054-µm radiation in terms of plasma electron density and magnetic field. **b,** *X*-wave/total harmoni emission of third harmonic (hollow circles) and fourth harmonic (filled circles) for a series of laser shots.

+ M TATARAKIS, I WATTS, F N BEG, E L CLARK, A E DANGOR, A GOPAL, M G HAINES, P A NORREYS, U WAGNER, M -S WEI, M ZEPF & K KRUSHELNICK " Measuring huge magnetic fields", Nature 2002.

Experiments on Petawatt at RAL in the UK probe.

LLNL Experiment Set-Up on RAL (P.K. Patel)

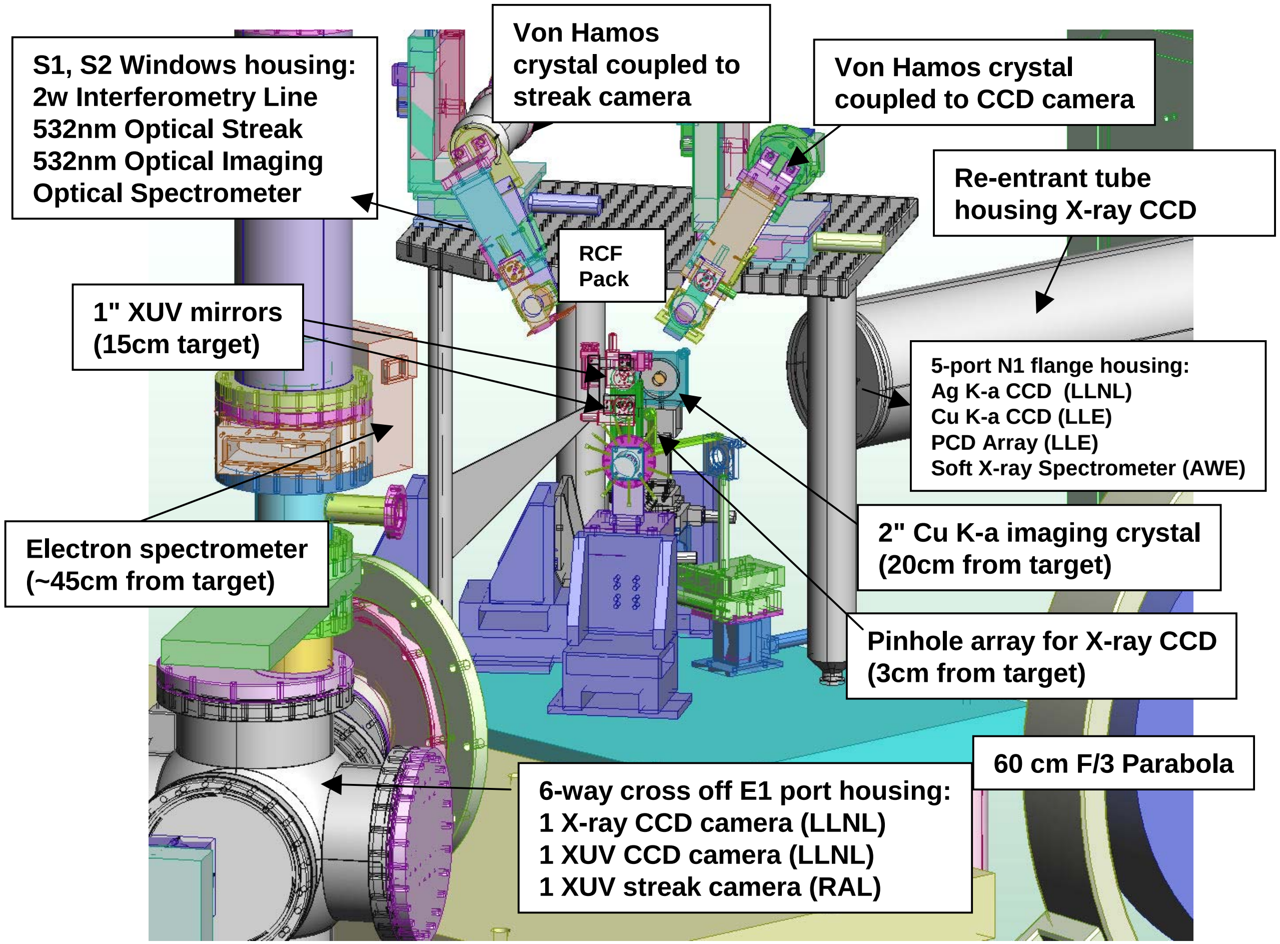

PK Patel et. al., “Overview of the LLNL experimental campaign on the Vulcan Petawatt laser, Rutherford Report (2004)

Laser Parameters:	Target:
E = 300 J	
τ_{pulse} = 1 pS	Copper foil
D_{spot} = 6 μm	10 μm thick

RAL Petawatt Experiment Crew - 2003

Prav Patel, Mike Key, Andy Mackinnon, Rich Snavely, Hye-Sook Park, Jeff Koch, Ronnie Shepherd, Hui Chen, Mark May, Jaroslav Kuba, Nobuhiko Izumi, Scott Wilks, Roger Van Maren
Lawrence Livermore National Laboratory

Jim King, Bingbing Zhang, Kramer Akli, Rick Freeman
UC Davis, CA

Richard Eagleton
AWE, Aldermaston, U.K.

Satya Kar, Lorenzo Romagnani, Marco Borghesi
Queen's University, Belfast, U.K.

Christian Stoeckl, Wolfgang Theobald
LLE, University of Rochester, NY

Rich Stephens
General Atomics, San Deigo, CA

Rob Clarke, Rob Heathcote, David Neely, Darren Neville, Pete Brummitt, Martin Tolley, Steve Hawkes, Christina Henandez-Gomez, Colin Danson
Rutherford Appleton Laboratory, U.K.

Modeling provides input to experiment design (i.e., targets) and post-experiment analysis. What is the electron energy distribution to expect?

Fiber Array Compact Electron Spectrometer (FACES) built by Hui Chen can look at energetic electrons.

Spectrometer energy coverage:
- 10 keV -500 keV (100 Gauss)
- 100 keV - 60 MeV (1000 Gauss)

Detectors:
Scintillating fiber coupled to a CCD camera

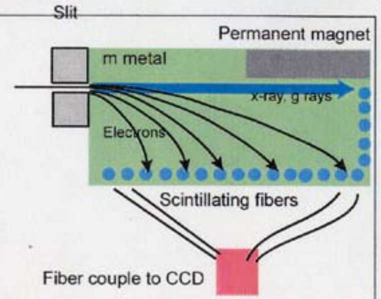

Fiber-CCD interface

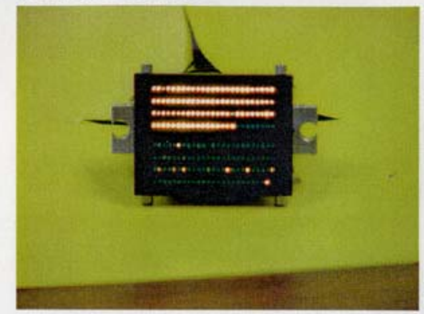

The FACES assembly

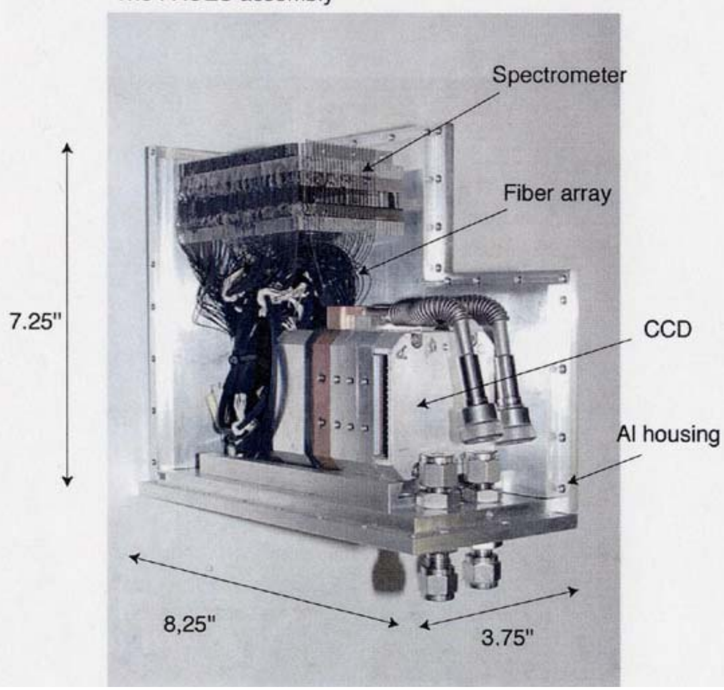

Sample e- spectra from JanUSP

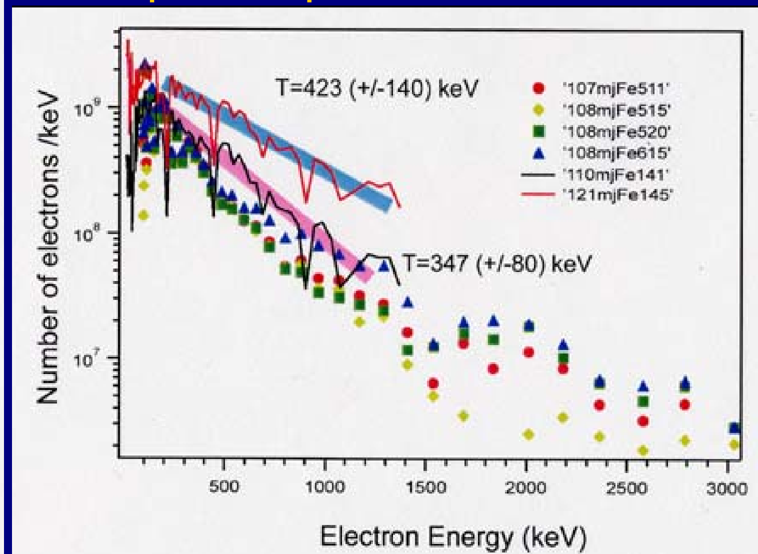

T_e of escaping e- measured: 0.01-60 MeV.

1. "A Compact Electron Spectrometer for hot electron measurement in pulsed laser solid interaction", **Hui Chen**, P. K. Patel, D. F. Price, B. K. Young, P. T. Springer, R. Berry, R. Booth, C. Bruns, and D. Nelson, Review of Scientific Instruments, 74, 1551 (2003).

For now, we must run codes in “serial” to interpret & design experiments at these extreme temperatures and densities.

Interferogram of Cu Foil

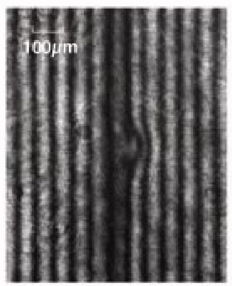

Figure 4. Interferogram of a 20μm thick Cu foil taken 100 ps before the main pulse. The PW beam is incident from the right.

RAL laser transverse spot

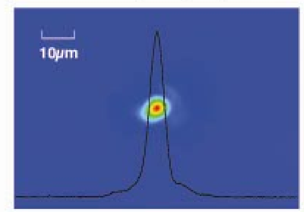

Figure 3. Vacuum focal spot measurement of CW beam with microscope objective and 8-bit CCD camera.

PIC electron phase space

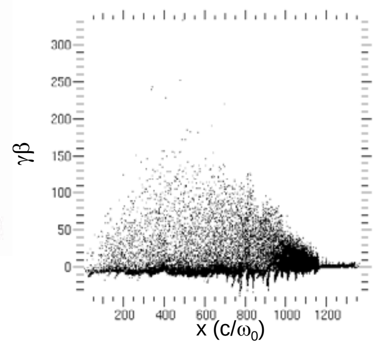

Cu L-shell x-ray streak camera raw and line out

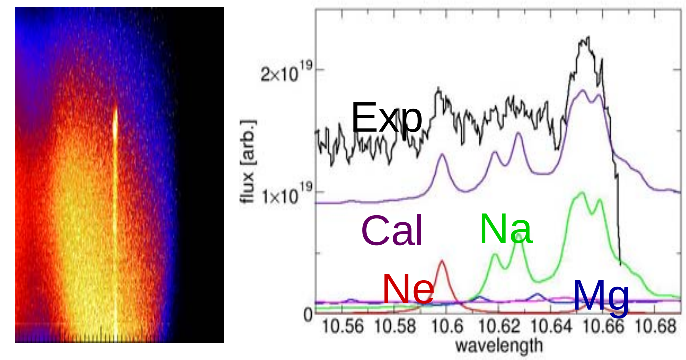

Experimental Measurement of pre-plasma & spot sizes → Hydro Code → LSP / PIC → Atomic Physics Codes

1. Tries to match experimentally measured preplasma.

2. Provides estimate of pre-plasma to PIC

3. PIC sends back hot electron estimates to Hydro.

4. Hydro provides estimate of background electron temperature to APC’s.

5. Provides estimate of Hot electrons to APC’s.

6. Compare to experiment and theory.

1st step: S. Moon runs prepulse with hydro code to get estimate of preformed plasma to be used in PIC codes.

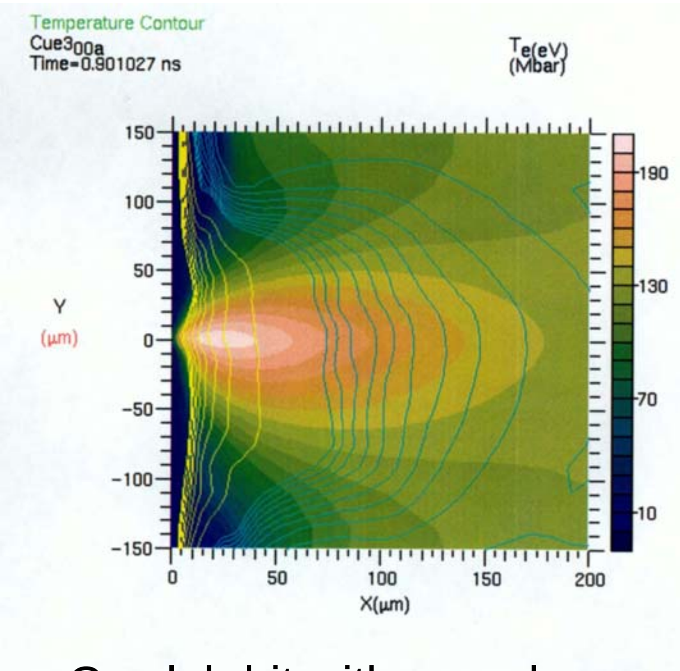

Cu slab hit with prepulse:
$I = 4\times10^{12}$ W/cm^2
12 μm FWHM Gaussian on
a 40 μm FWHM Gaussian
$\tau \sim 1$ nsec

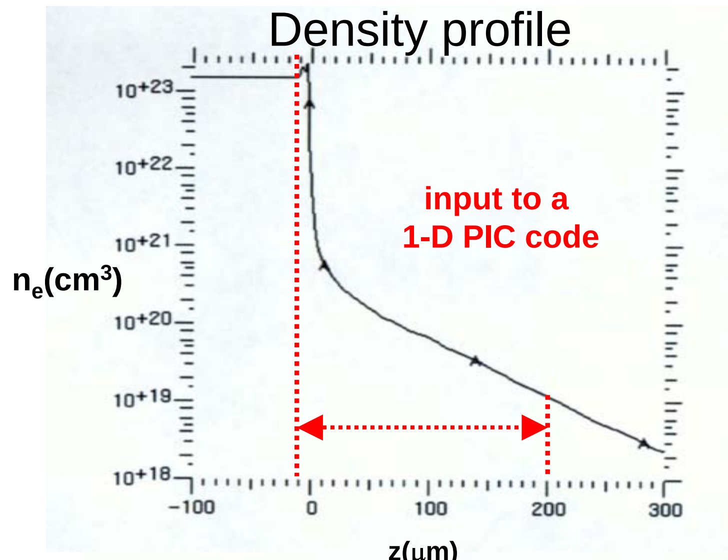

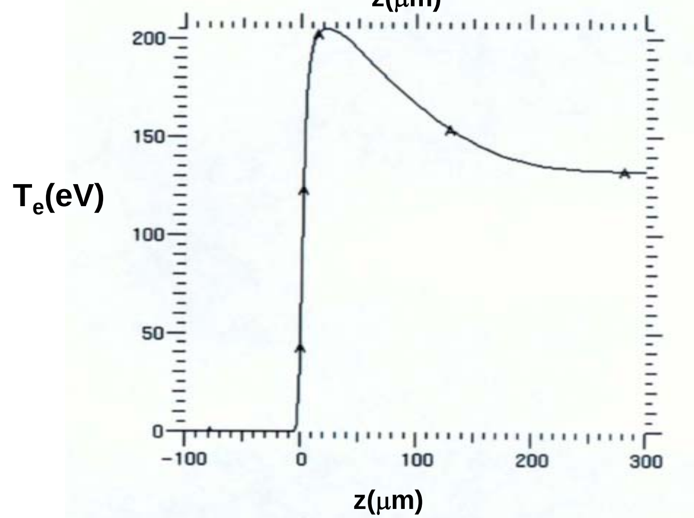

We take this density profile, and input it into a 1-D PIC code. We then run the ultra-intense laser ($I = 5\times10^{20}$ W/cm^2) into it, as the EM coupling (which PIC does so well) is dominant when $I \gg 1\times10^{18}$ W/cm^2.

2^{nd} Step: PIC simulations using hydro density profile: we find 2 hot electron temperatures, in this case.

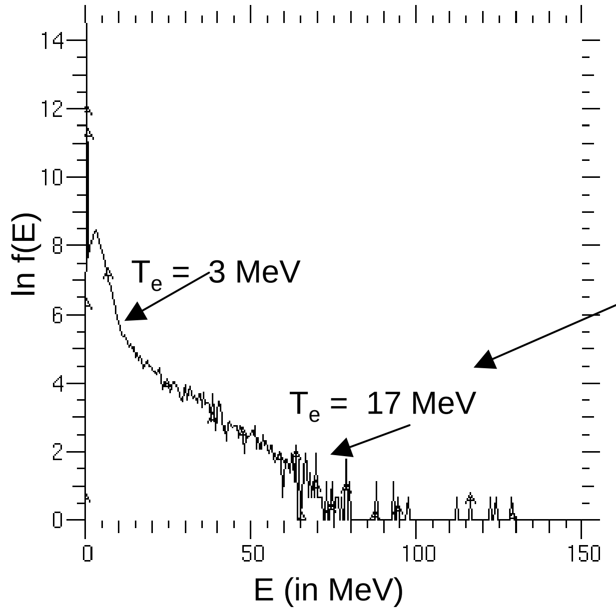

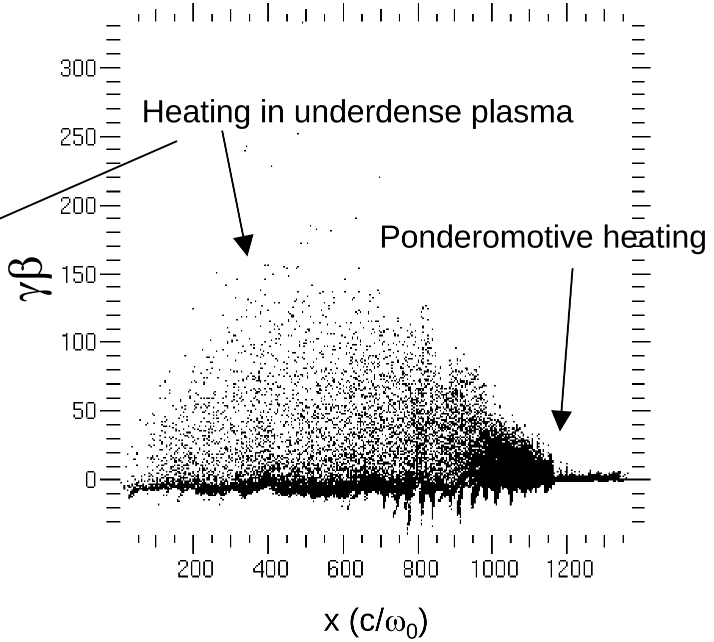

Low Energy Component consistent with Ponderomotive Heating*

$$kT_{hot} = \left[\sqrt{\left(1+\frac{I\lambda^2}{2.8\times10^{18}}\right)}-1\right]\times511keV \sim 2.9MeV$$

*kT_{hot} scaling from S. C. Wilks, W. L. Kruer, et.al. “Absorption of ultrashort, ultra-intense laser light”, PRL., **33** 1992.)

Simulation predictions compared favorably to electron spectra taken by Hui Chen, Nov. 2003.

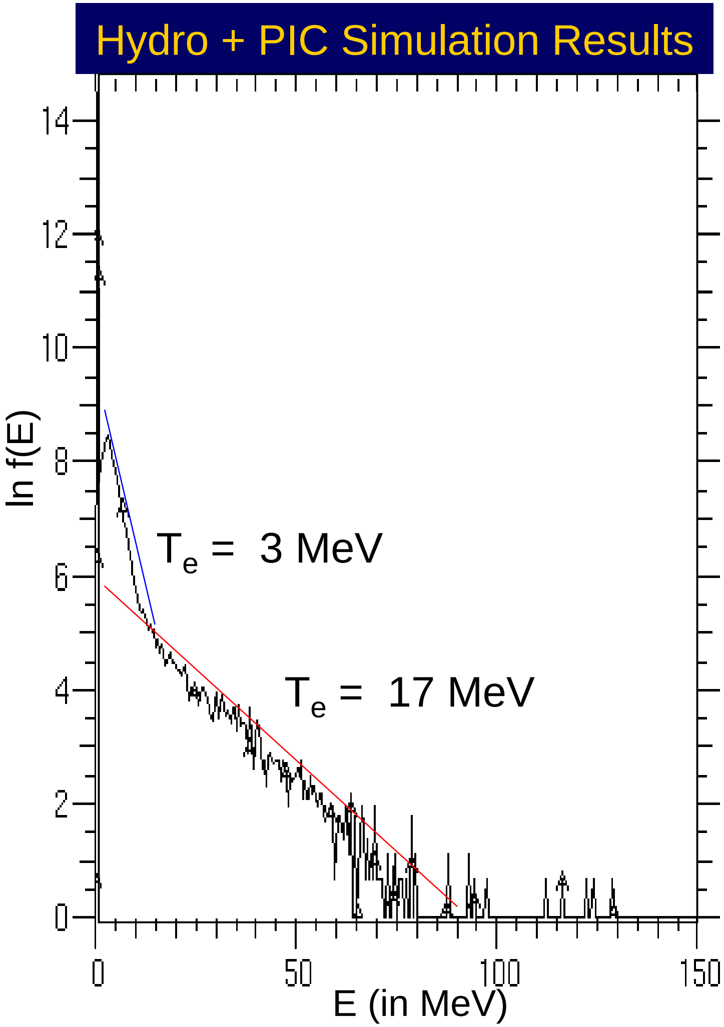

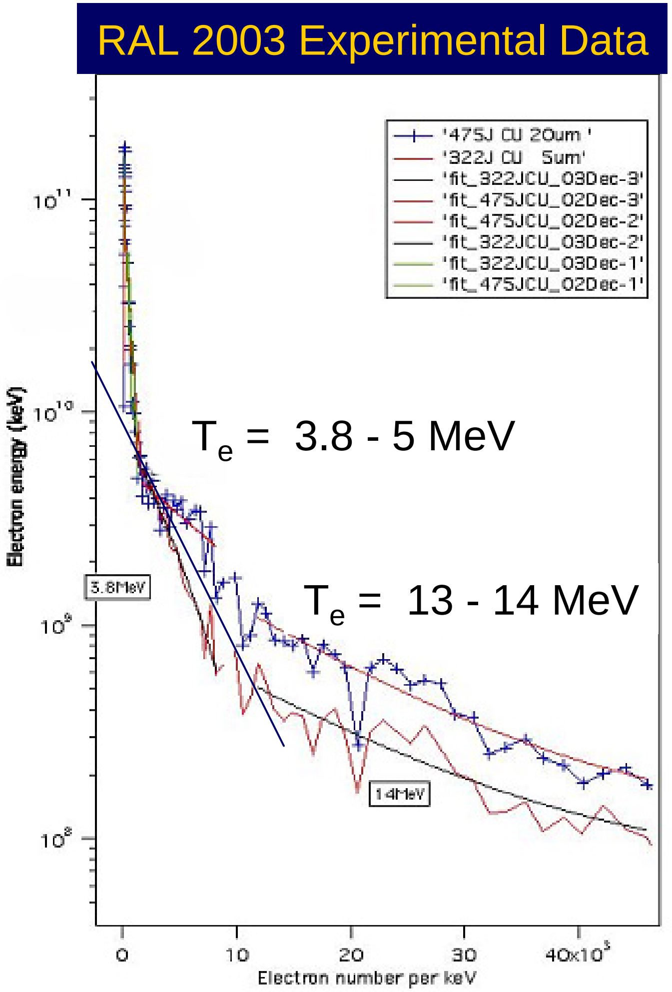

H. Chen, S. C. Wilks, S. Moon, H. Chun, P. Patel, R. Shepard, et. al. “Experimental Observation of Enhanced Electron Heating in Laser-Solid Interactions”, UCRL-JRNL-203377 (2004).

3rd Step: Hyun-Kyung Chung now inputs these simulation predictions into atomic physics codes. (T_e and e- spectra)

Put T_{hot}'s in hydro code:

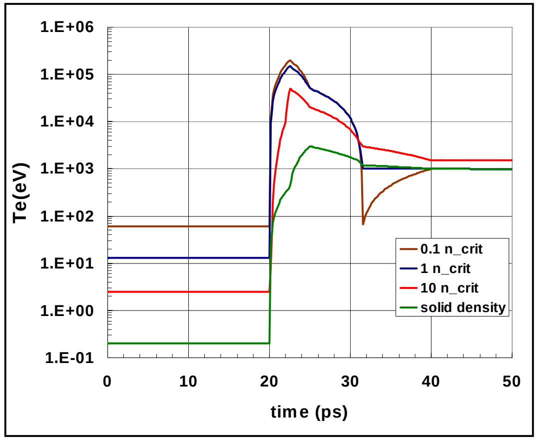

Ionization balance for Cu, Te = 1keV, T_{hot} = 3 MeV

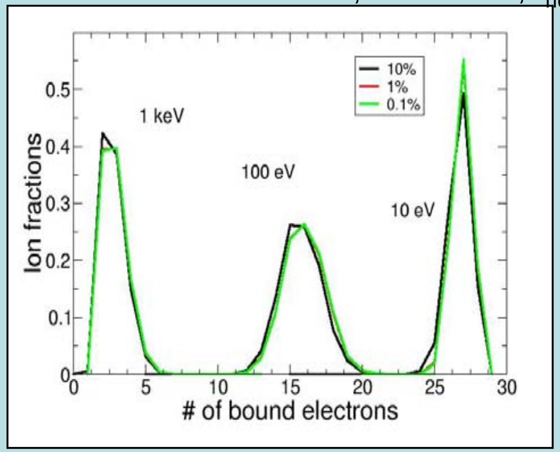

Hot electrons have little effect on <Z>

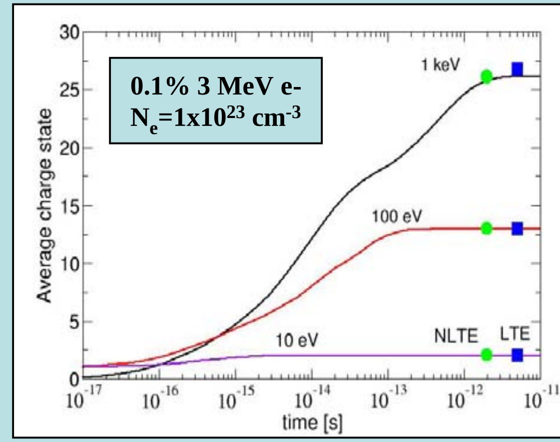

Ionization equilibration time t = 1 ps at 1 keV , t = 0.1 ps at 100 eV

Started with:

~120 J of hot electrons (~ 10^{20} cm^3) with energy distribution matching PIC (T_e ~ 3 MeV), inside 100 μm^3 volume of Copper target with various background temperatures 1,10, 100, 1000 eV.

Copper at 150 eV

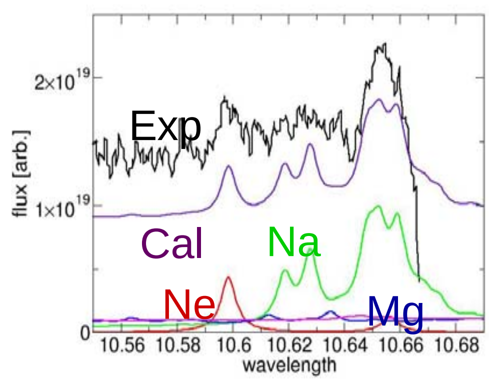

Ionization balance for Cu

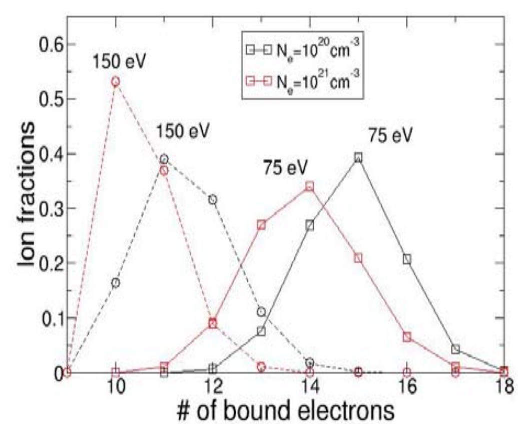

Ultimately, we will end up with spectra from Cu at various T_e and compare with experiment.

Switch Gears: This time, experimental results suggest astrophysical application: Electron Positron Plasmas.

LLNL Petawatt experiments first to see positrons for laser-plasma interactions

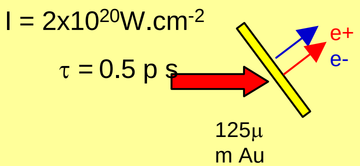

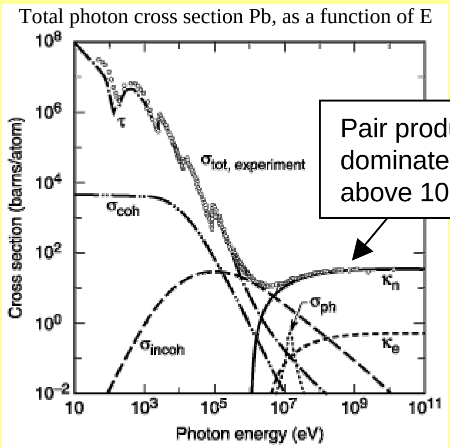

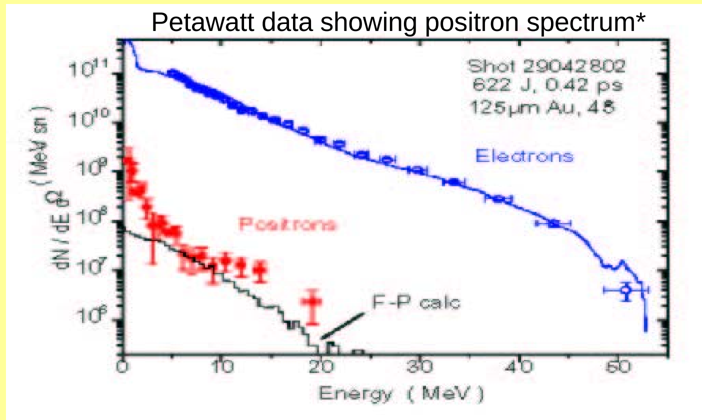

*T. E.Cowan, A. W. Hunt, M. D. Perry, W. Patterson, D. Pennington, C. Brown, S. C. Wilks, S. Hatchett, T. W. Phillips, Y. Takahashi, W. Faountain, T. Parnell. J. Johnson, “High Energy Electrons and Laser-assisted Nuclear in PW Laser-Solid Interactions”, Proceedings of INt’l Conf. On Lasers 1997, New Prleans (1997.)

Astrophysical applications experiment proposals quickly followed…

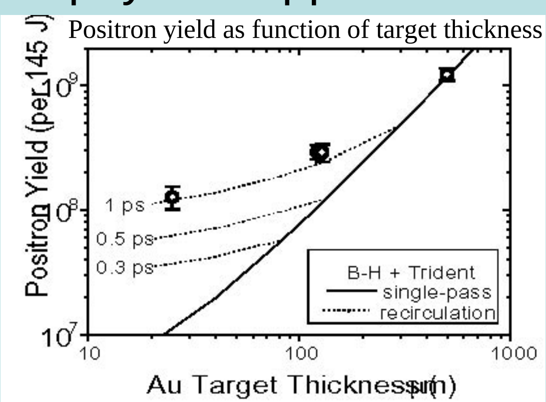

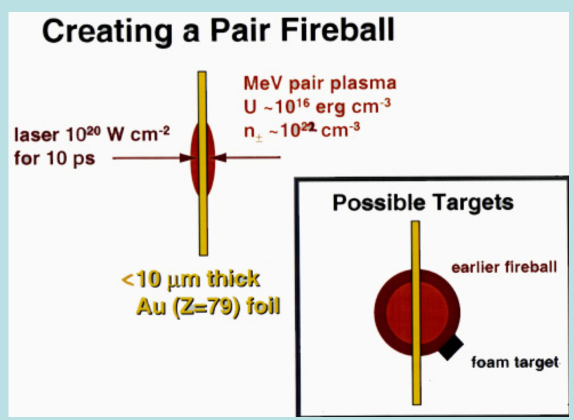

“Pair Production by Ultraintense Lasers”, Edison P. Liang, Scott C. Wilks, and Max Tabak, PRL **81**, 4887 (1998).

“Electron-Positron Plasmas Created by Ultra-Intense Laser Pulses Interacting with Solid Targets”, S. C. Wilks, H. Chen, E. Liang, P. Patel, D. Price, B. Remington, R. Shepherd, M. Tabak, W. Kruer, to be published, *Astrophysics and Space Sciences*, (2004).

How many pairs can we expect to produce with ultra-intense laser-solid interactions?

The characteristic kinetic energy of electrons generated by an ultra-intense laser interacting with a foil is roughly[1]

$$kT_{hot} \sim m_e c^2 \left[\sqrt{1 + \frac{I\lambda^2}{2.8 \times 10^{18}}} - 1 \right]$$

$$I = E/(A^*\tau_p)$$

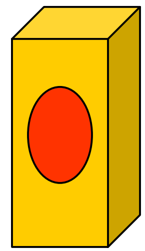

In the limit of low annihilation rates, pair density grows as

$$\frac{dn_+}{dt} \cong \frac{dn_{ei}}{dt} + \frac{dn_{\gamma i}}{dt}$$

Putting in the proper cross sections and integrating

$$n_+ = Zn_i\left[\exp(\Gamma t) - 1\right]/2$$

where the pair growth rate[2] is given by:

$$\Gamma = 2n_i c \int d\gamma \sigma_{ei} f (1 - \gamma^{-2})^{1/2}$$

So higher T_{hot} (~ f) means more electrons → more pairs

Temp. vs. Laser Intensity

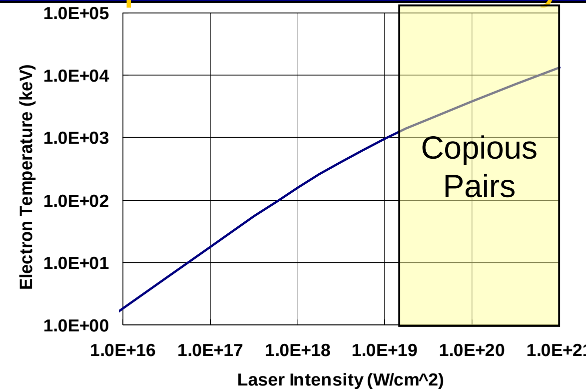

Are there enough positrons?

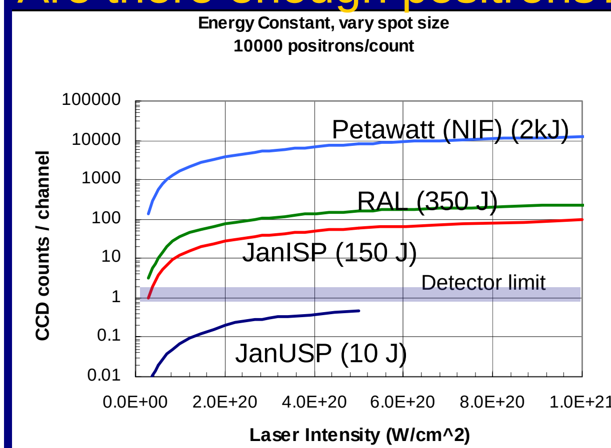

High energy lasers produce plenty

Hotter electron temperatures mean *MORE* positrons! → More energy, intensity…

1. "Absorption of Ultraintense Laser Pulses", S. C. Wilks, W. Kruer, M. Tabak, A. B. Langdon, PRL **69**, 1383 (1992).
2. "Pair Production by Ultraintense Lasers", Edison P. Liang, Scott C. Wilks, and Max Tabak, PRL **81**, 4887 (1998).

Electron-Positron (Pair) Plasmas are thought to play a key role in Gamma Ray Bursts, the most energetic objects in the Universe..

Gamma Ray Bursts (GRB's)

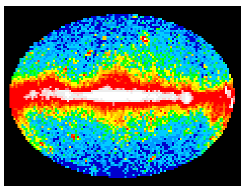

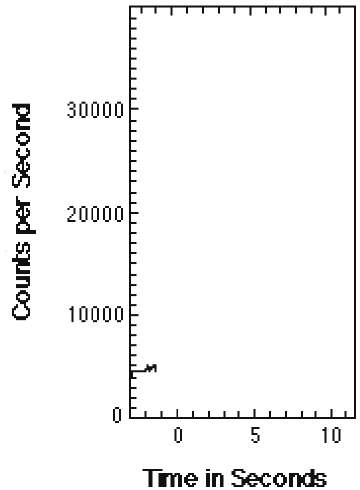

First detected 1967
10^{52} erg s^{-1} seen (1 per day)
Gravitational wave source
Many competing theories

Gamma Ray Burst Model

84, Number 17 PHYSICAL REVIEW LETTERS 24 Apr

Electron-Positron Outflow from Black Holes

Maurice H. P. M. van Putten
Massachusetts Institute of Technology, Cambridge, Massachusetts 02139
(Received 26 August 1999)

Cosmological gamma-ray bursts (GRBs) appear as the brightest transient phenomena in the Universe. The nature of their central engine is a missing link in the theory of fireballs to stellar mass progenitors, and may be associated with low mass black holes. In contact with an external magnetic field B, black hole spin produces a gravitational potential on the wave function of charged particles. We show that a rapidly rotating black hole of mass M produces outflow from initially electrostatic equilibrium with normalized isotropic emission $\sim 10^{48}(B/B_c)^2(M/7M_\odot)^2 \sin^2\theta$ erg/s, where $B_c = 4.4 \times 10^{13}$ G. The half-opening angle satisfies $\theta \geq \sqrt{B_c/3B}$. The outflow proposed as input to GRB fireball models.

PACS numbers: 97.60.Lf, 04.70.Dy

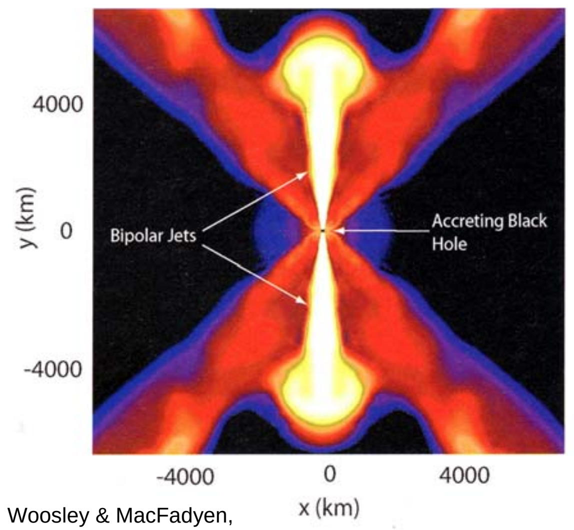

Woosley & MacFadyen,
A&A. Suppl. 138, 499 (1999)

Creating this exotic plasma would shed light on physics of GRB's.

If it is possible to create and characterize "mini-fireballs" of pure pairs, we can start to examine the physics behind GRB's.

If it is possible to create and characterize "mini-fireballs" of pure pairs, we can start to examine the physics behind GRB's.

Big Question is: How are the e+e- accelerated and how do they radiate?

Competing GRB Models: B or not B?

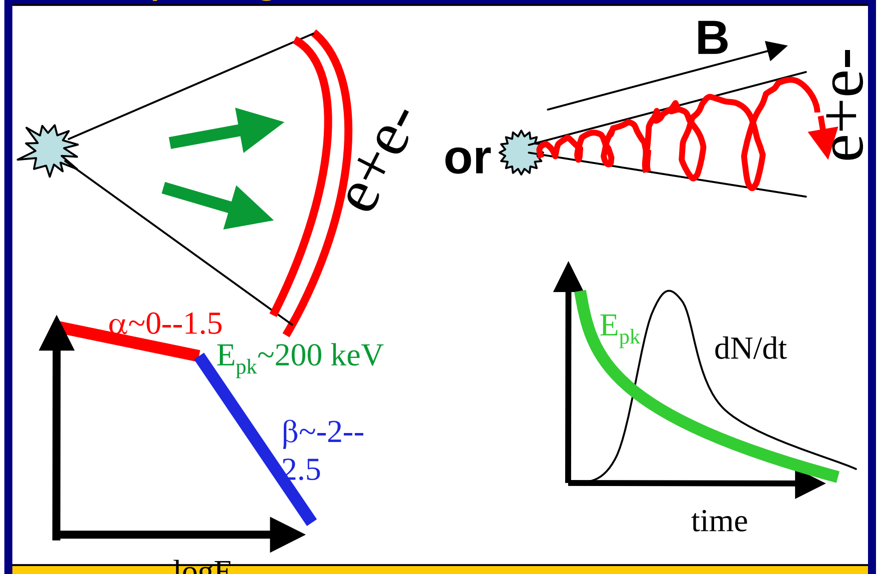

GRB spectra resemble smoothly broken power law with spectral break energy E_{pk} ~ few hundred keV. E_{pk} decays before intensity.

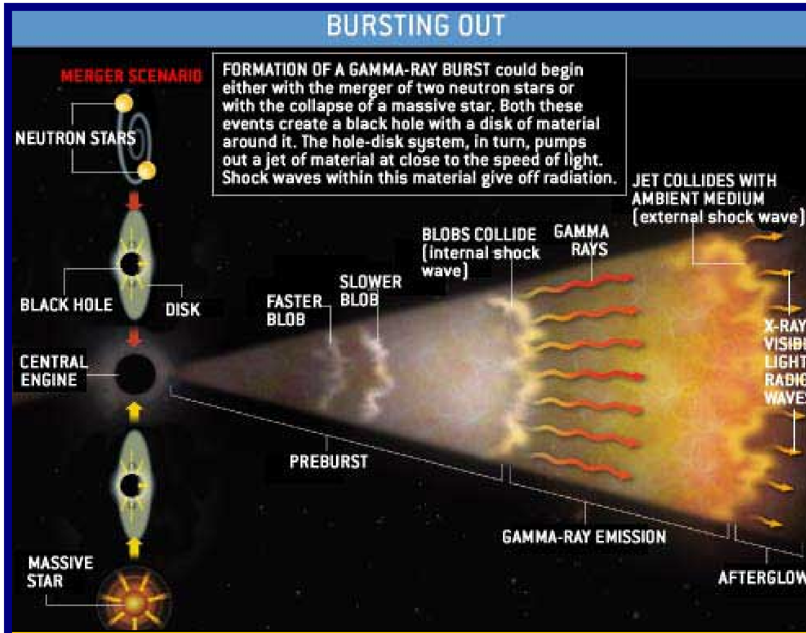

Internal shocks:Hydrodynamic energy*

Colliding with another pair fireball can mimic the internal shock model of GRB's, allowing us to study how expansion energy of the jet can be converted into gamma rays.

Colliding with another pair fireball can mimic the internal shock model of GRB's, allowing us to study how expansion energy of the jet can be converted into gamma rays.

*A. Bruce Langdon, Jonathan Arons, and Claire E. Max, "Structure of Relativistic Magnetosonic Shocks in Electron-Positron Plasmas",PRL **61**, 779 (1988).

Sample BATSE GRB light curves show extreme diversity: from single smooth FRED pulse to complex, chaotic, multiple peaks.

The CGRO Mission

(1991 - 2000)

The Compton Gamma Ray Observatory was the second of NASA's Great Observatories. Compton, at 17 tons, was the heaviest astrophysical payload ever flown at the time of its launch on April 5, 1991 aboard the space shuttle Atlantis. Compton was safely de-orbited and re-entered the Earth's atmosphere on June 4, 2000.

Compton had four instruments that covered an unprecedented six decades of the electromagnetic spectrum, from 30 keV to 30 GeV. In order of increasing spectral energy coverage, these instruments were the **Burst And Transient Source Experiment** (**BATSE**), the Oriented Scintillation Spectrometer Experiment (OSSE), the Imaging Compton Telescope (COMPTEL), and the Energetic Gamma Ray Experiment Telescope (EGRET). For each of the instruments, an improvement in sensitivity of better than a factor of ten was realized over previous missions.

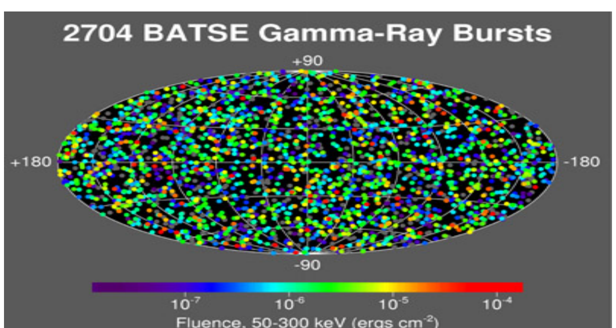

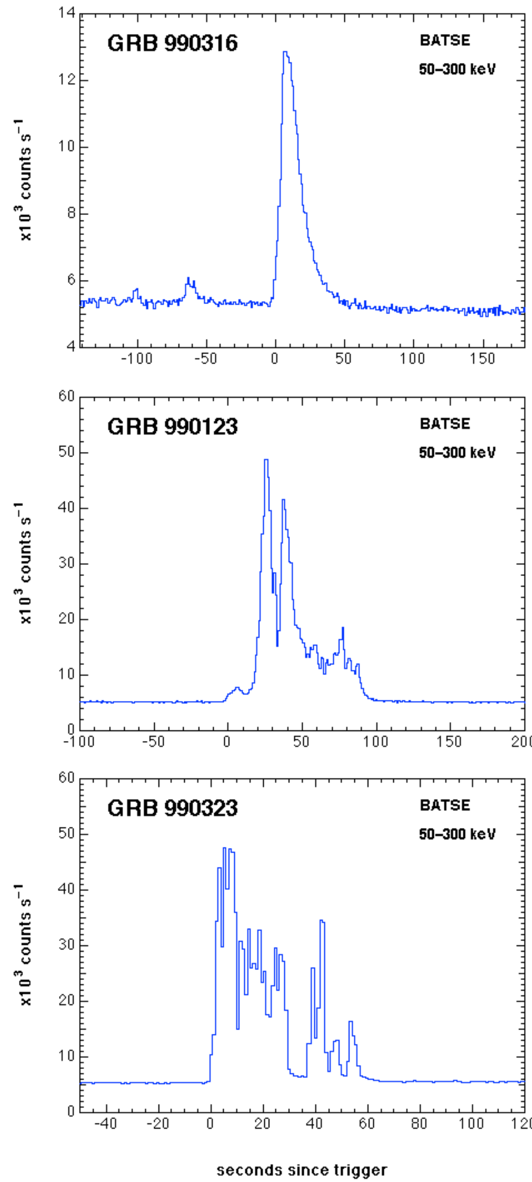

Example of attempting to simulate the actual conditions in e^+-e^- outflow of a GRB. (E. Liang and K. Nishimura)

PIC simulations of strongly magnetized electron-positron plasma expansion

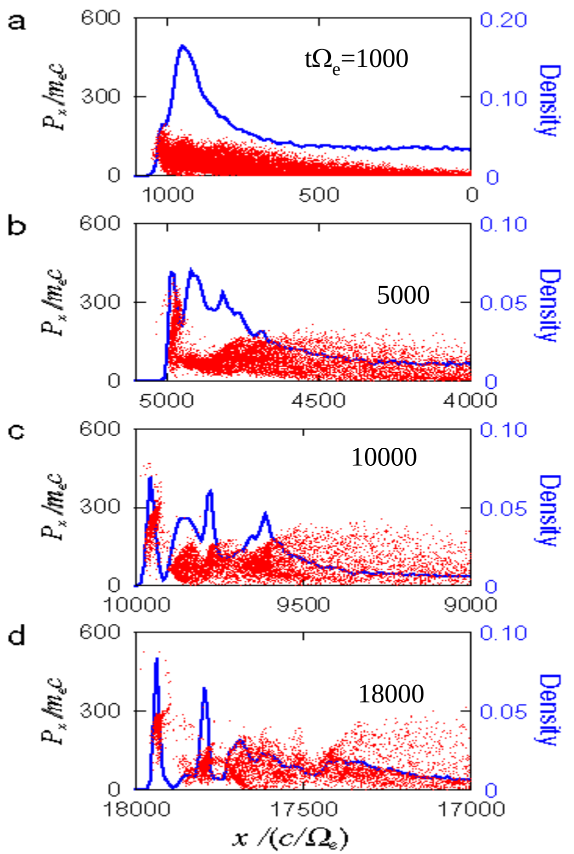

Computer simulated pulse profile of strongly magnetized electron-positron plasma expansion (left, from Liang & Nishimura PRL 92, 175005 (2004)) compares favorably with gamma-ray burst light curves from the BATSE catalog. Such e+e- expansion may be studied with ultra-intense laser experiments.

Assume $I_{x\text{-rays}} \sim n_{e+e-}$

Next step: Justify the jump from density to x-rays
(D. Kocevski, Rice University)

Measured X-ray energy time Histories measured by BATSE

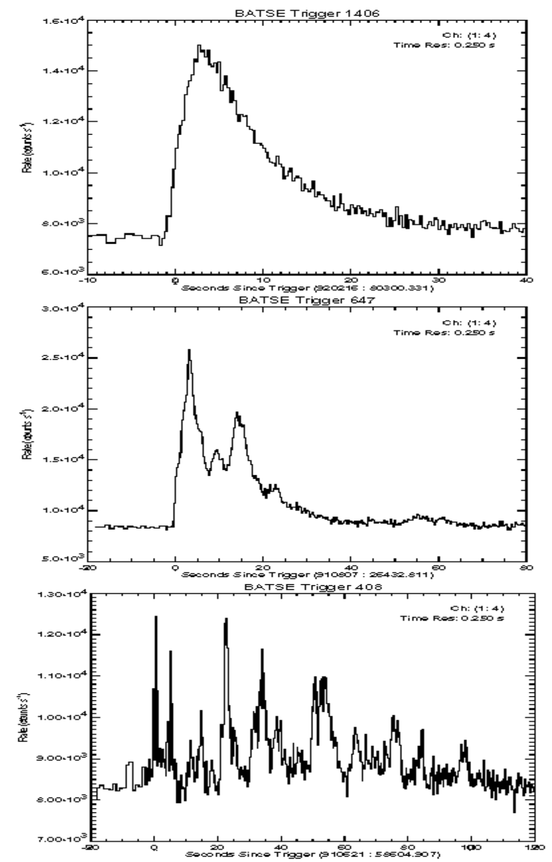

More simulations results show " characteristic fall-off at shock front.

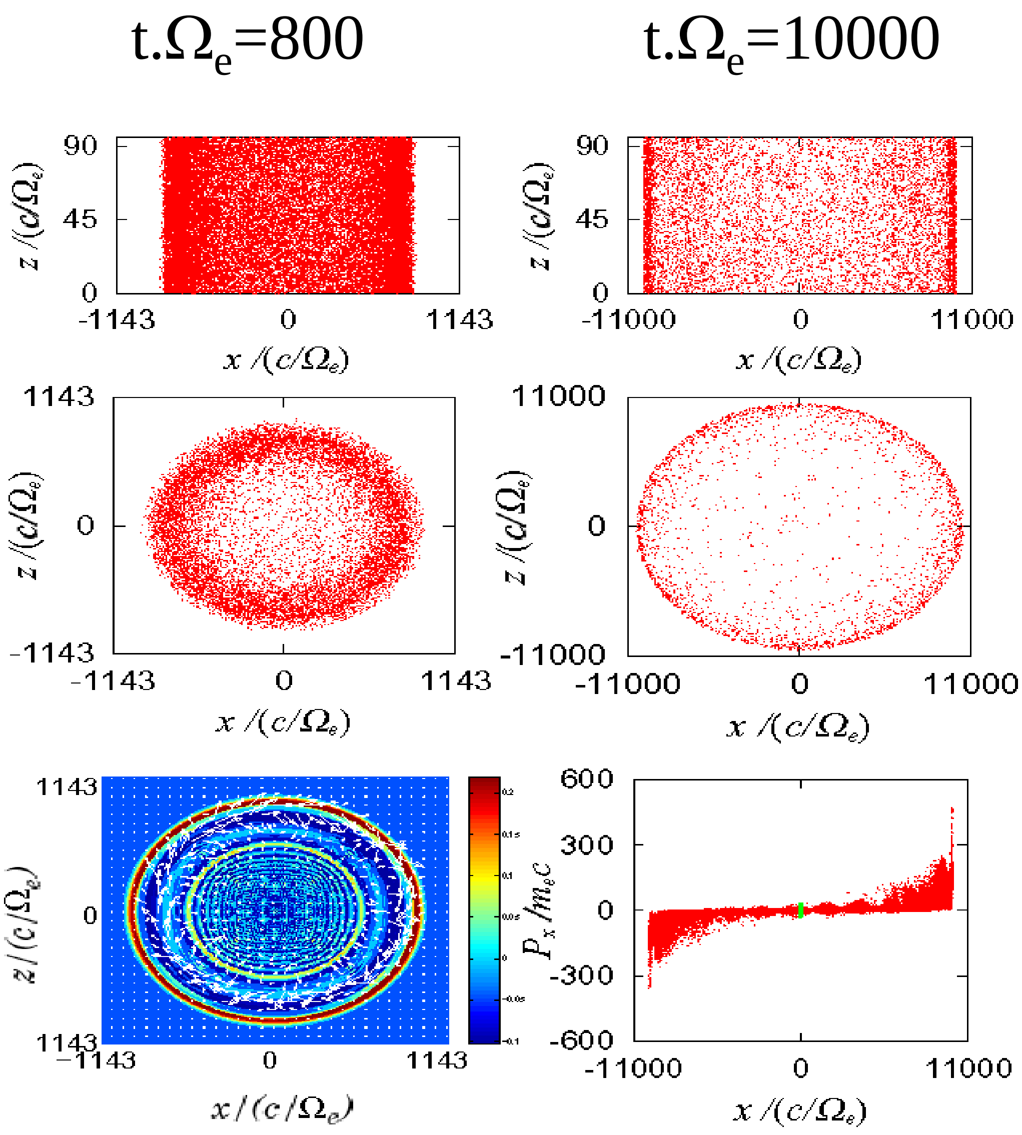

Simulations by Anatoly Spitkovsky (Stanford University) show interesting electron-positron interactions.

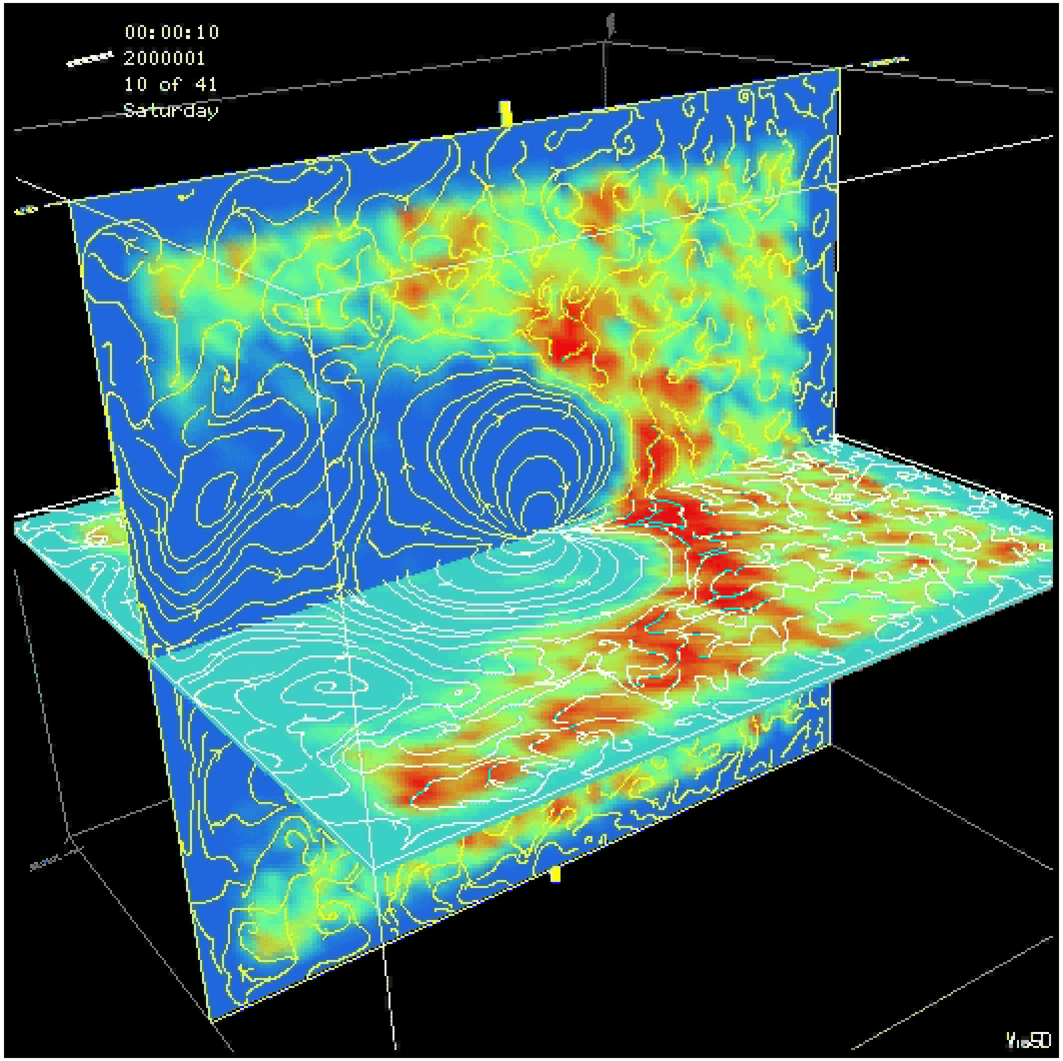

A. Spitkovsky and J. Arons, ApJ, 2004

Conclusions

Simulations can bridge the gap between laboratory and astrophysics.

Strong interplay between experiment and simulation strengthens both.

With Prav Patel: Can we use proton beams?

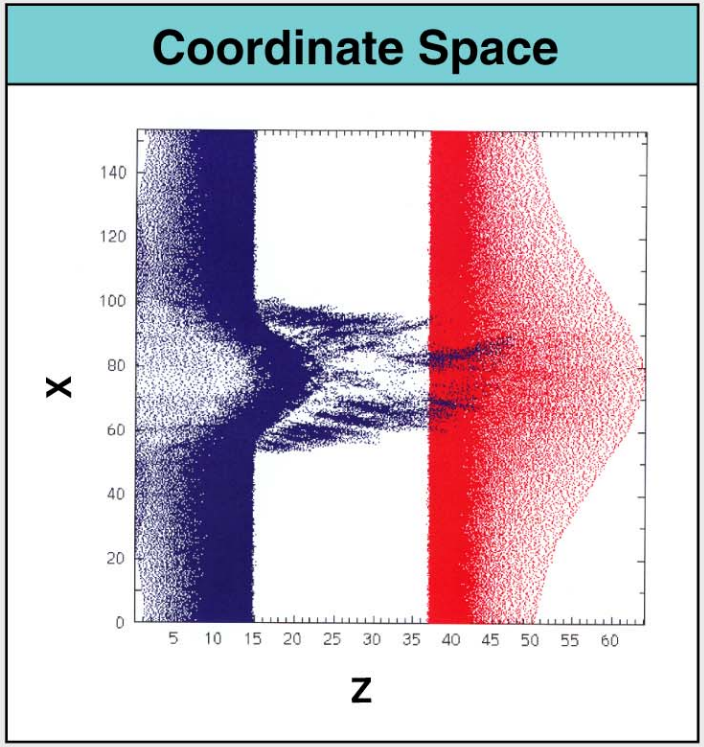

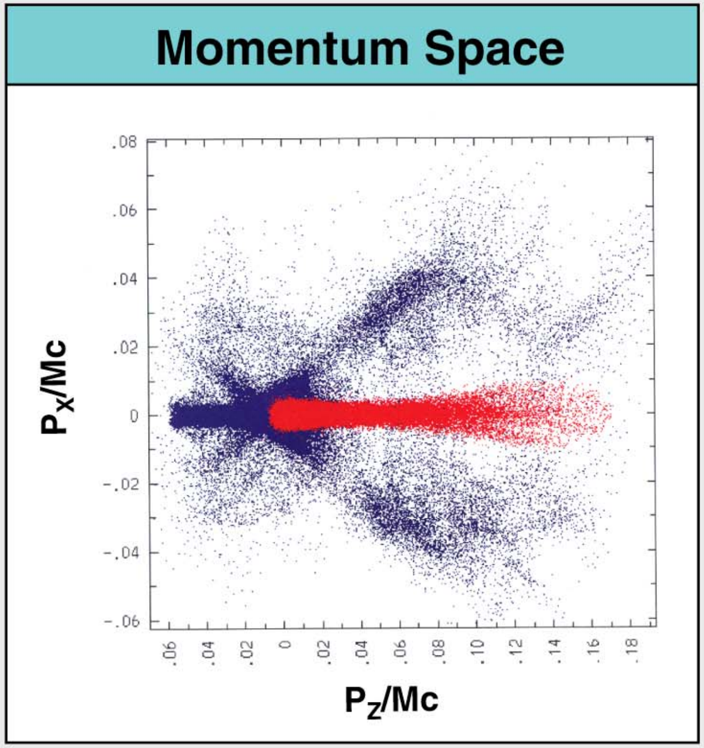

PIC Simulations of laser-target interaction predict different properties for ions accelerated from front and rear surfaces of a thin foil target

Can we use lasers to make hot electrons that interact with dense material to create pairs?

Ionization-Acceleration-Bremsstrahlung

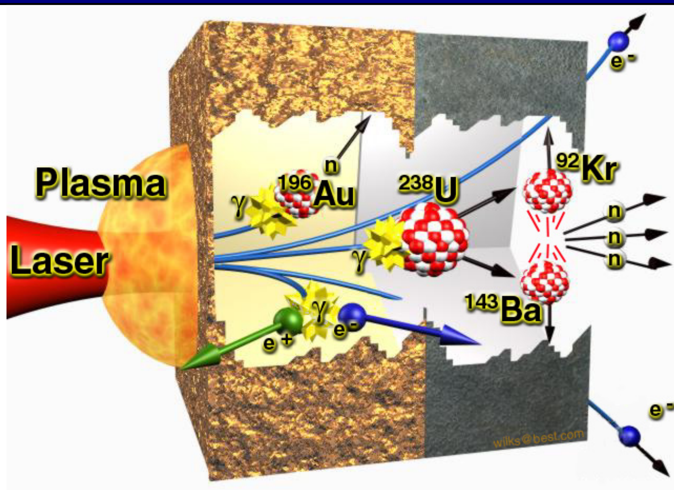

Laser generates hot e- which create photons.

Pair Production

Total photon cross section in lead, as a function of energy.

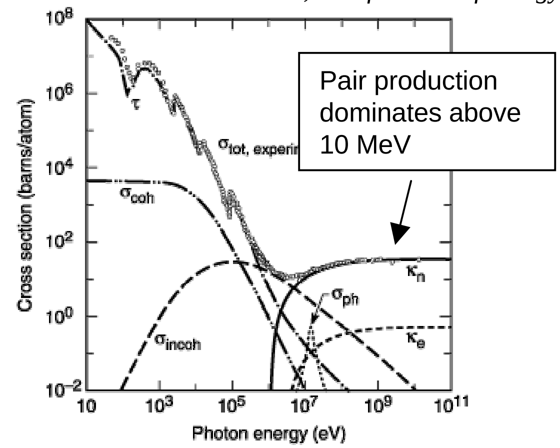

Electrons and photons create pairs.

Pairs and electrons rush out, creating a mini "pair fireball"

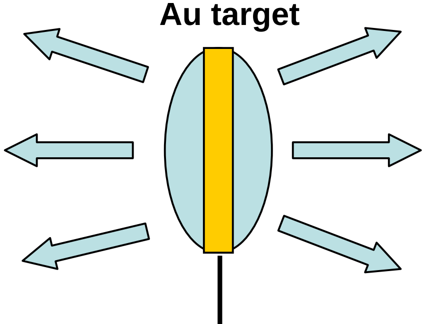

Gold ions 1000's of times heavier than e+ and e-. Pairs rush out ahead at relativistic speeds.

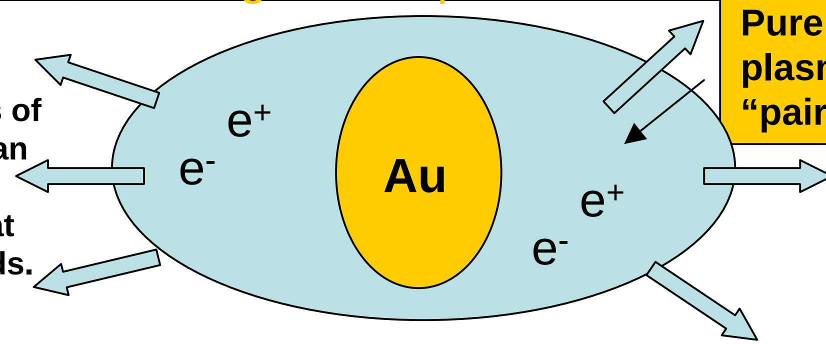

Pure pair plasma or "pair fireball"

Early time (~ 100 fsec)

Late time (> 100 psec)

Summary of diagnostics

- ***Cu K-α Single Hit CCD***

  Absolute yield of Cu K-α for variety of targets and laser irradiation conditions (focal spot size and pulselength scans)

- ***XUV Imaging CCD***

  Measured electron heating at rear surface of Cu foils

- ***XUV Streak Camera***

  As above but time-resolved data (distinguishes prompt heating vs. shock heating)

- ***Transimission Grating Spectrometer***

  Good time-resolved soft x-ray spectra from front of Cu foils and Hohlraums - should give temperature/ionisation information

- ***PCD Array***

  Absolute time-resolved radiation temperature for Cu foils and Hohlraums around 1 keV region

- ***Electron Spectrometer***

  MeV electron spectra obtained on all shots

- ***Cu L-shell X-ray Spectrometer***

  Cu L-shell spectra obtained on some shots

3-D PIC simulations of Weibel in electron-positron plasmas by UCLA team.

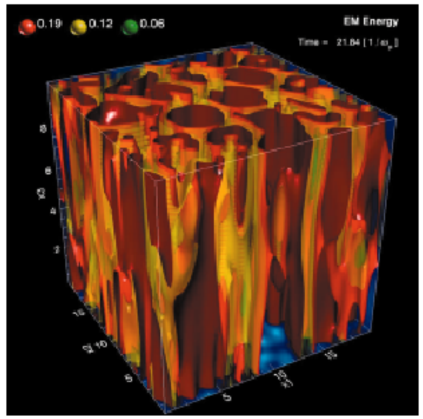

Fig. 1. Electromagnetic energy density at $t = 21.84\omega_{pe0}^{-1}$ for three isosurfaces, in the collision of an electron cloud, moving up in the box, and a positron cloud, moving in the opposite direction, showing inner regions of higher electromagnetic energy density.

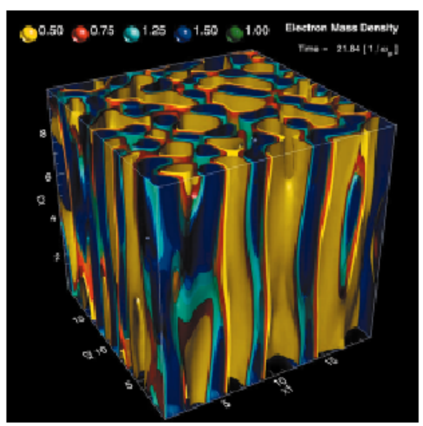

Fig. 2. Electron/positron mass density at $t = 21.84\omega_{pe0}^{-1}$: the mass density is normalized to the background density.

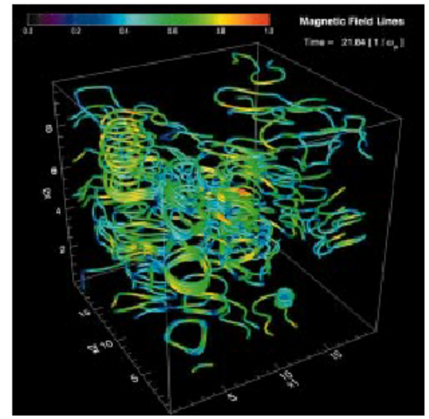

Fig. 3. Magnetic field lines for the conditions of Figs. 1 and 2: the local strength of the magnetic field is given by the color code.

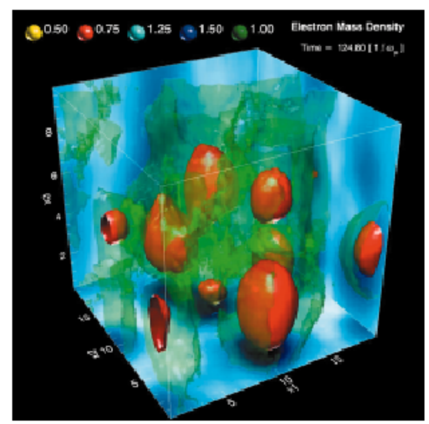

Fig. 4. Electron mass density at a later stage of the instability: electron/positron mass density holes are evident in the red isosurface ($n_{e-RED} = 0.75n_{e0}$).

[3] R. L. Morse and C. W. Nielson, "Numerical simulation of the Weibel

Diagnostics Fielded in Experiment

1.	Cu K-α imaging CCD	8keV K-α x-ray emission, 2D (time-int)
2.	XUV imaging CCD	68eV XUV emission, rear surf, 2D (time-int)
3.	XUV streak camera	68eV XUV emission, rear surf (time-res)
4.	Cu L-shell x-ray spectrometer	9-10Å x-ray spectra, front surf (time-int)
5.	Cu L-shell x-ray streak camera	9-10Å x-ray spectra, front surf (time-res)
6.	Electron spectrometer	Electrons
7.	Optical spectrometer	Specular laser light spectrum
8.	Radiochromic Film Pack	Protons
9.	Ag/Au K-α single photon	22keV K-α x-ray flux (time-int)
10.	Cu K-α single photon CCD	8keV K-α x-ray flux (time-int)
11.	Ag/Au K-α imaging CCD	22keV K-α x-rays imaged (time-int)
12.	2ω interferometer	Pre-plasma scalelength (time-res)
13.	2ω self-emission imaging	2eV optical emission, rear surf
14.	2ω self-emission streaked	2eV optical emission, rear surf (time-res)
15.	X-ray Pinhole camera	>1keV x-ray emission, front surf (time-int)
16.	Transmission grating spec	20-100Å soft x-rays, front surf (time-res)
17.	Neutron detectors	Neutrons
18.	PCD array	Abs. radiation field, front surf (time-res)
19.	RF coils	EMP from target interaction

Electron CDSA Range

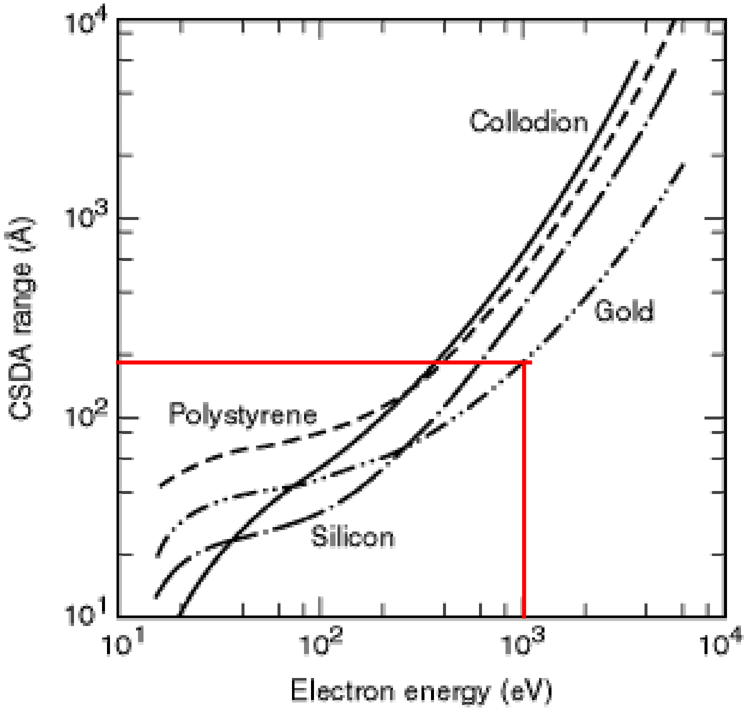

Fig. 3-3. *Plot of the CSDA range, as a function of energy, for gold and silicon and for polystyrene,* $(C_8H_8)_n$*, with a density of 1.05 g/cm*^{3}*. The measured electron range in collodion with a density of 1 g/cm*^{3} *is also plotted.*

Rossi XTE Satellite Details

The Rossi X-ray Timing Explorer, RXTE, was launched on December 30, 1995. RXTE is designed to facilitate the study of time variability in the emission of X-ray sources with moderate spectral resolution. Time scales from microseconds to months are covered in a broad spectral range from 2 to 250 keV. It is designed for a required lifetime of two years, with a goal of five years.

Mission Characteristics

- Lifetime : 30 December 1995 to the present
- Energy Range : 2 - 250 keV
- Special Features : Very large collecting area and all-sky monitoring of bright sources
- Payload :

  •Proportional Counter Array (PCA)
  2-60 keV energy range, 6500 sq cm, time resolution 1 microsec
  •High Energy X-ray Timing Experiment (HEXTE)
  15-250 keV energy range, 2 X 800 sq cm
  •All-Sky Monitor (ASM)
  2-10 keV energy range, 30 mCrab sensitivity

  - Science Highlight:

    •Discovery of kilohertz QPO's
    •Discovery of spin periods in LMXRB
    •Detection of X-ray afterglows from Gamma Ray Bursts
    •Extensive observations of the soft state transition of Cyg X-1
    •Observations of the Bursting Pulsar over a broad range of luminosities, providing stringent test of accretion theories.

Details of photon bubble instability (abstract from R. Klein, et. al. 1996 ApJ article

We discuss our recent Rossi X-Ray Timing Explorer (RXTE) observations of GRO J1744-28, which discovered quasi-periodic oscillations (QPOs) of the intensities in the energy band 3--12 keV during observations starting on 1996 January 18.77 UT. We have found that the power spectrum in the frequency band 5--1000 Hz consists of two red-noise components that can be characterized by two power laws, each with an index of -5/3 and a QPO peak centered at 40 Hz. We suggest that *the power peak is due to a newly discovered form of turbulence in the accretion column of super-Eddington accretion-powered pulsars driven by photon bubble instabilities*. These instabilities give rise to strong power peaks at frequencies characteristic of photon diffusion and bubble coalescence in the highly nonlaminar accretion column resulting in photon bubble oscillations (PBOs). The relationship between the rms amplitude of the PBOs and the intensity is in qualitative agreement with observations. Our calculations also suggest that the observed high-frequency red-noise component with a -5/3 power-law index from 40 to 600 Hz is the first evidence of photon bubble turbulence in the accretion column of an X-ray pulsar. Recent RXTE observations of Sco X-1 have found high-frequency QPOs at 1100 and 830 Hz. We show that PBOs at these frequencies are a natural consequence of photon bubble instabilities. We also show that the rms amplitudes of the calculated PBOs at these frequencies are consistent with the observations. We predict that further RXTE observations of Sco X-1 should reveal additional PBOs at 2000 and 2600 Hz as well as a broadband continuum spectrum with a -5/3 power law, extending from 3000 to several times 104 Hz.

Ion Acceleration UCRL-PRES-206186

Acceleration Mechanisms
- Front – Simple Scaling Law
- Back – Simple Scaling Law
- Dependence on electrons T_e/transport

Recent Experiments
- Matt Allen – Front vs. Back
- Hegelich – Heavy Ions
- RAL –

Possible Applications
- Fast Ignition / EOS (Prav)
- Radiography (Andy)
- Medical Accelerators (Hartmut)

Future Directions
- Reduced Descriptions (Hartmut)
- Modeling Experiments (EOS) (Prav)

Proton generation, transport, and focusing

- Coordinator: *Scott Wilks (LLNL)?*
- What are the proton generation mechanism efficiencies?
- How sensitive to resolution are the answers?
- Can hybrid PIC be used?
- How does electron flow affect proton generation?
- How can we control the generation and focusing of the protons?
- What is the optimum proton energy for radiography?
- What are the qualities that set ions using these mechanisms apart from “standard” ion beams?

Full view of Ion Acceleration

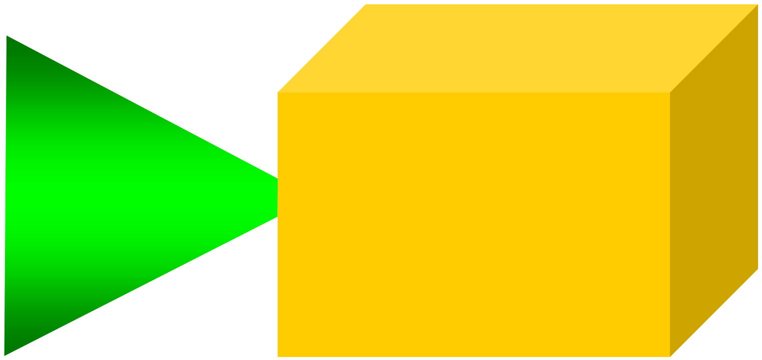

$$\frac{v_f}{c} = \sqrt{\frac{n_{cr}}{n}\frac{Zm_e}{m_i}\frac{I\lambda^2}{2.8\times10^{18}}}$$

$$U_b = \frac{T_e}{eL_n} l_{acc}$$

Acceleration on back of target

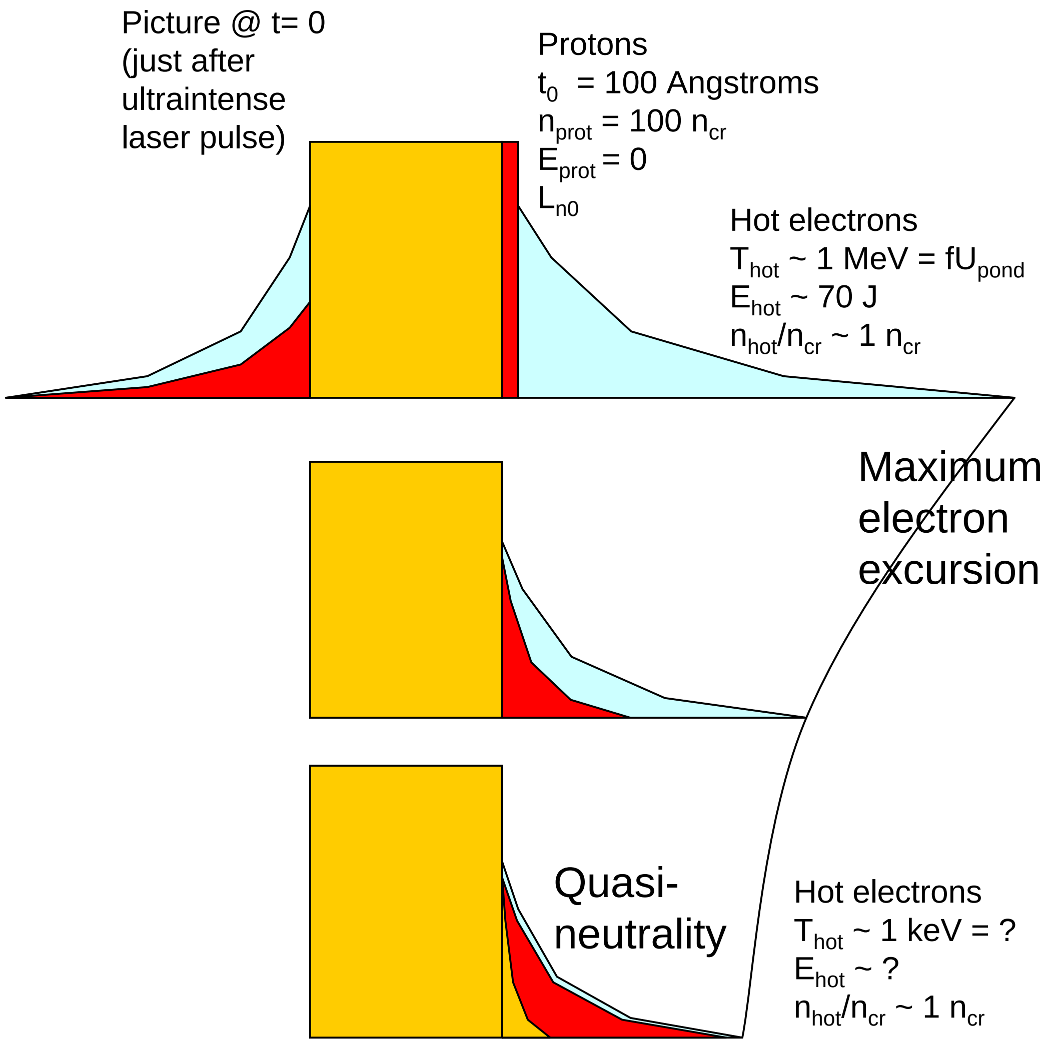

Hot electrons lose energy by:

1. Ionization ν ~ 1 fsec
2. Collisions ν ~ 10 fsec
3. Radiation ν ~ 10 fsec
4. Ions ν ~ 100 fsec

Assume that the interaction
Is over in 10 pSec.

1 psec * 3×10^{10} cm/sec = 300 μm

Directionality of Ion Beams

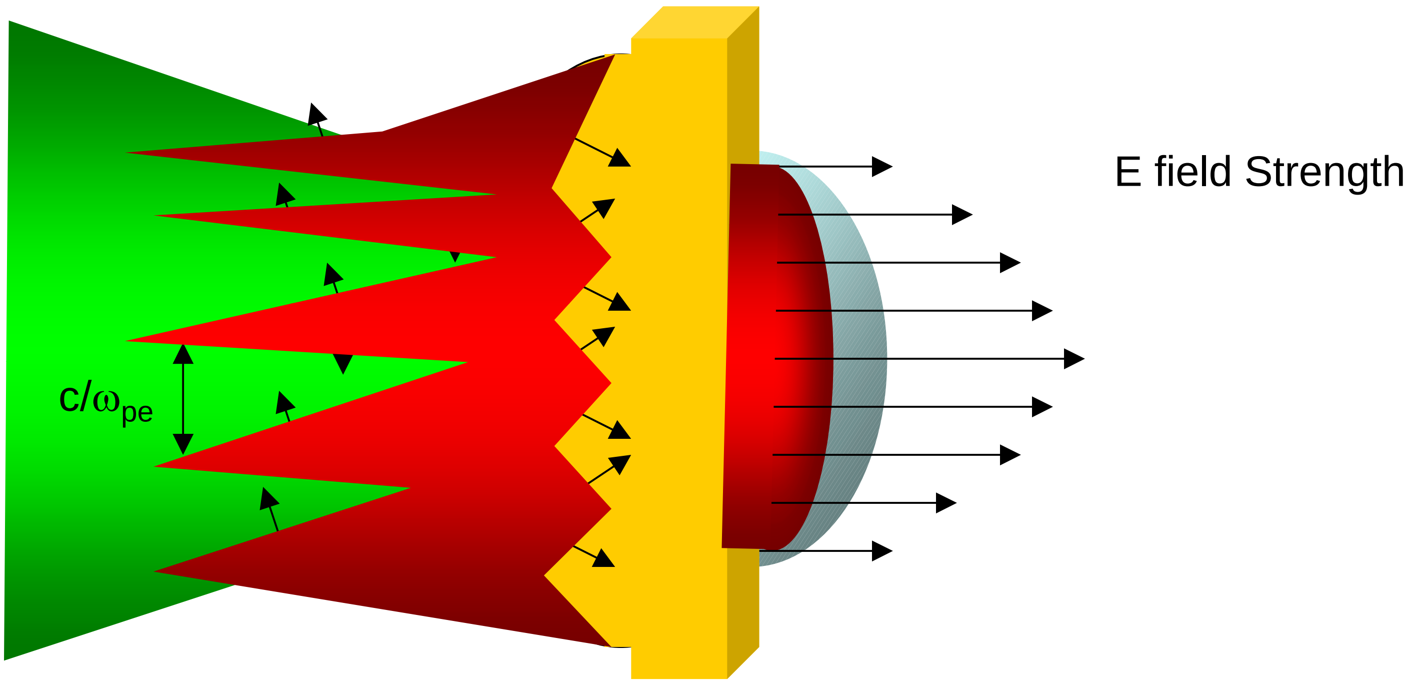

$t < t_{crit}$

Where e^- generated from Prepulse or ASE cannot disrupt back surface.

Illustration of front vs. back acceleration showing proton directionality.

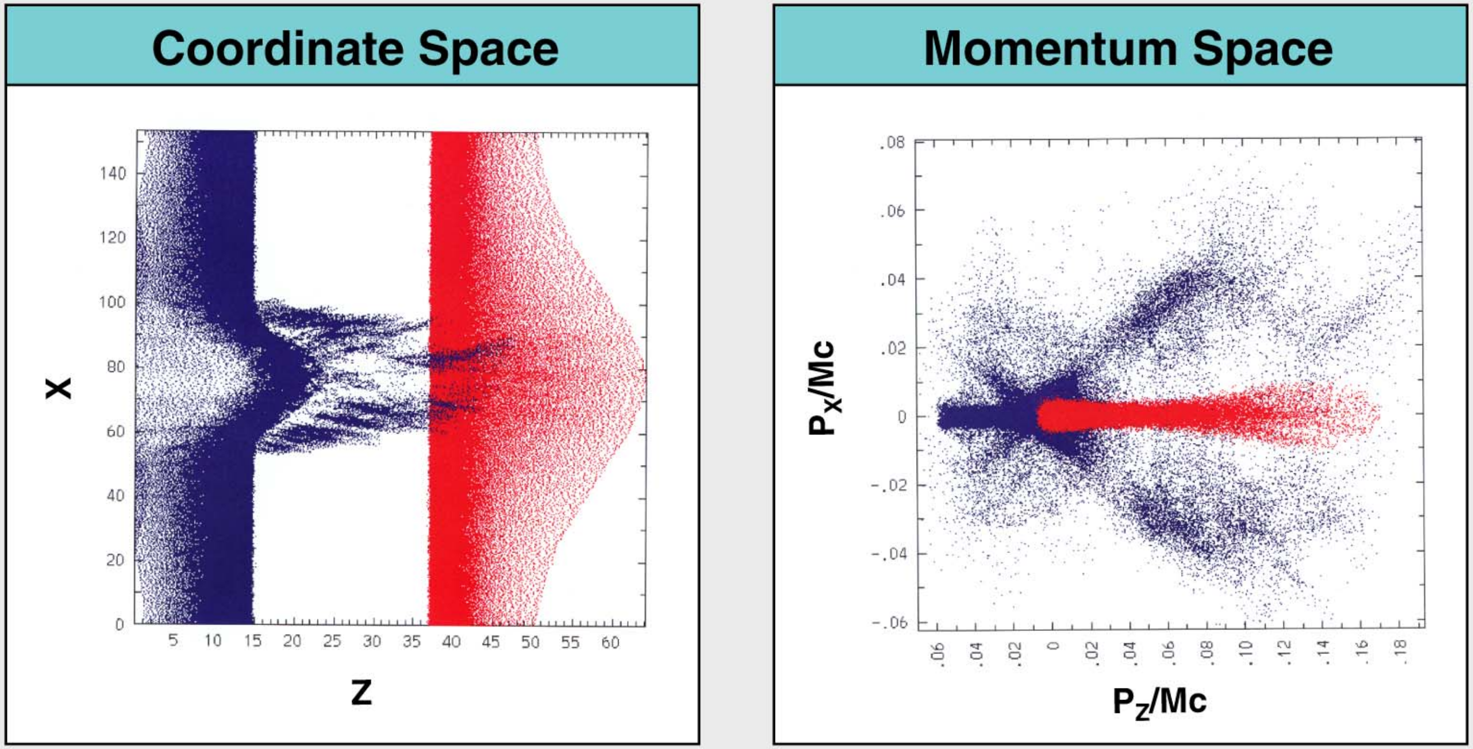

PIC Simulations of laser-target interaction predict different properties for ions accelerated from front and rear surfaces of a thin foil target

P01637-tec-u-015

Monoenergetic protons from two electron-temperature, multi-ion species plasma expansion is seen in PIC simulations

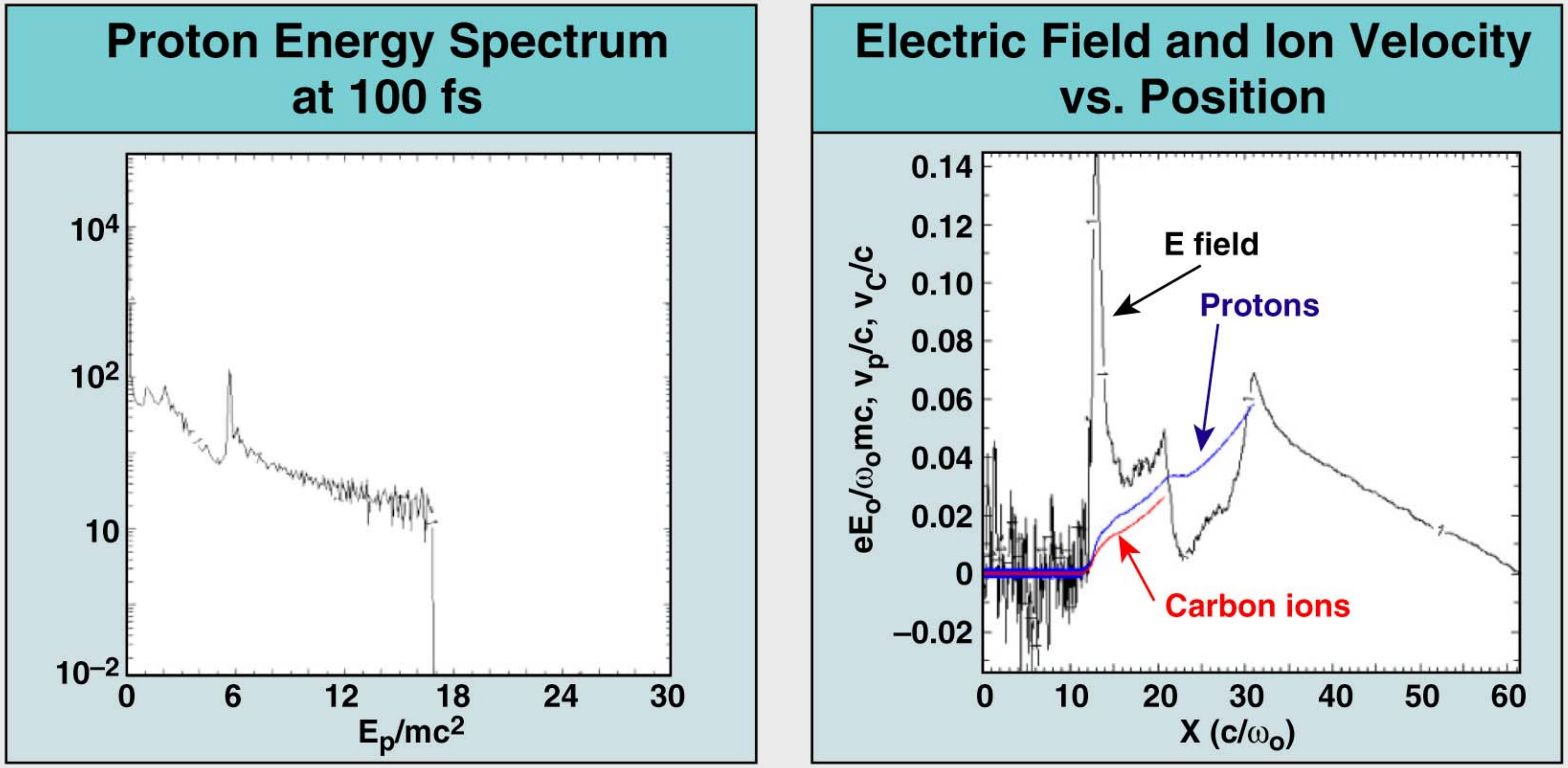

Recent progress on understanding detailed multi-species effects was only possible with the close interplay between experiment and theory

P01637-tec-u-010

Original plasma lens simulation: how small can you really focus? What are the limiting factors?

With initially uniform electron and ion density distributions, plasma expansion from curved target foil exhibits ion focusing

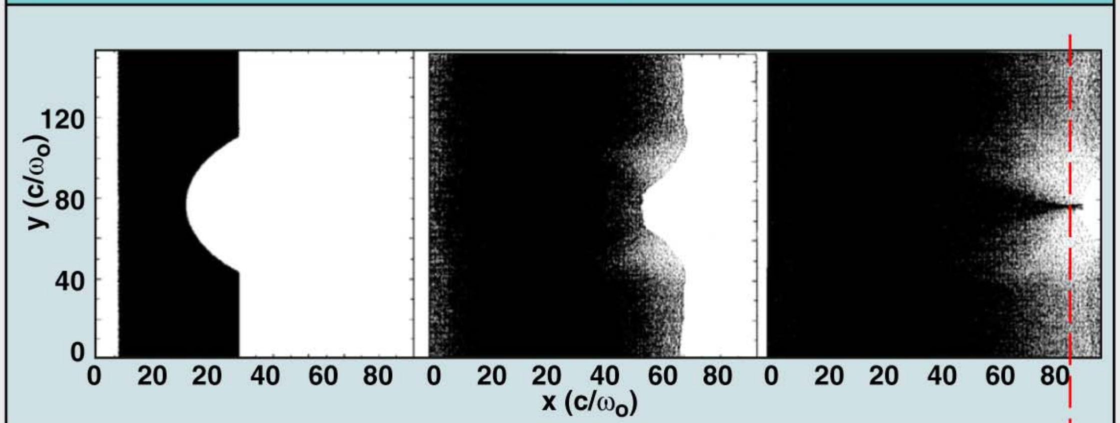

Larger scale simulations are required to assess feasibility of ion focusing for potential applications

- ion injector for accelerator
- plasma jet source for lab astrophysics
- high energy density source for ion- matter interaction experiments

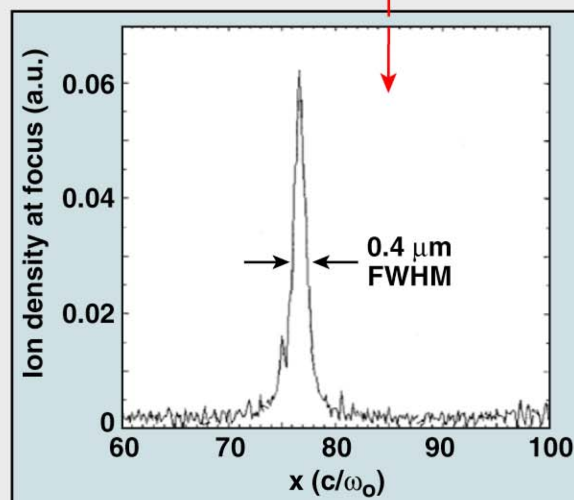

P01637-tec-u-016

Ion Acceleration

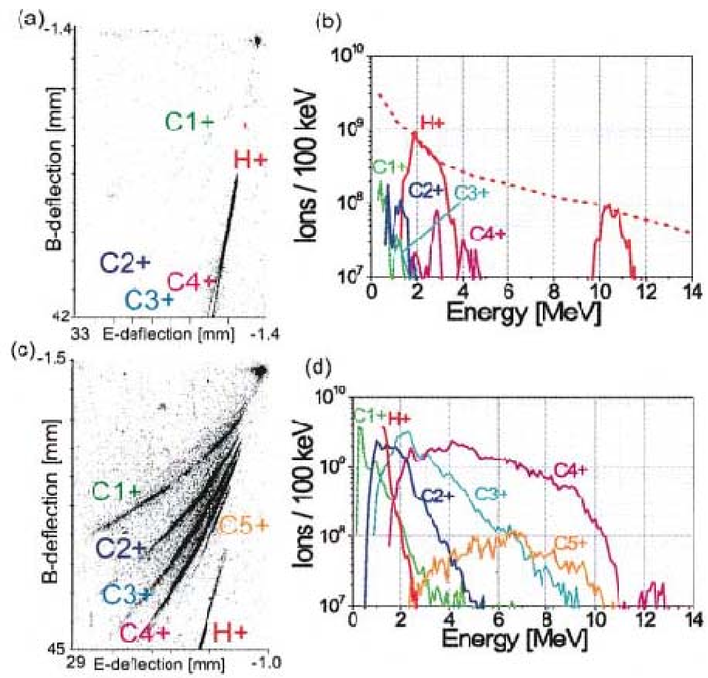

FIG. 1 (color). (a) Ion traces (on CR39) from an unheated Al | C target and (b) corresponding spectra. The gap in the proton signal is due to the CR-39 detector which is optimized for heavier particles. The dotted line illustrates the H^+ spectra as obtained with the proton spectrometer. (c) Ion traces from a heated Al | C target and (d) corresponding spectra. The ion signals are strongly enhanced. The spot in the upper right corner of (a),(c) is the pinhole image formed by neutral atoms.

M. Hegelich, S. Karsch, G. Pretzler, D. Habs, K. Witte, W. Guenther, M. Allen, A. Blazevic, J. Fuchs, J. C. Gauthier, M. Geissel, P. Audebert, T.Cowan, and M. Roth, Phys. Rev. Lett. **89**, 085002 (2002).

Experimental procedure for separating the front from the back protons:Sputter Gun Experiment (Matt Allen)

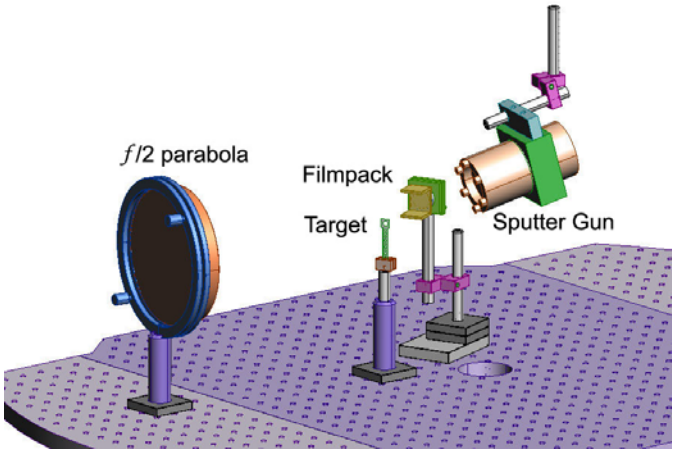

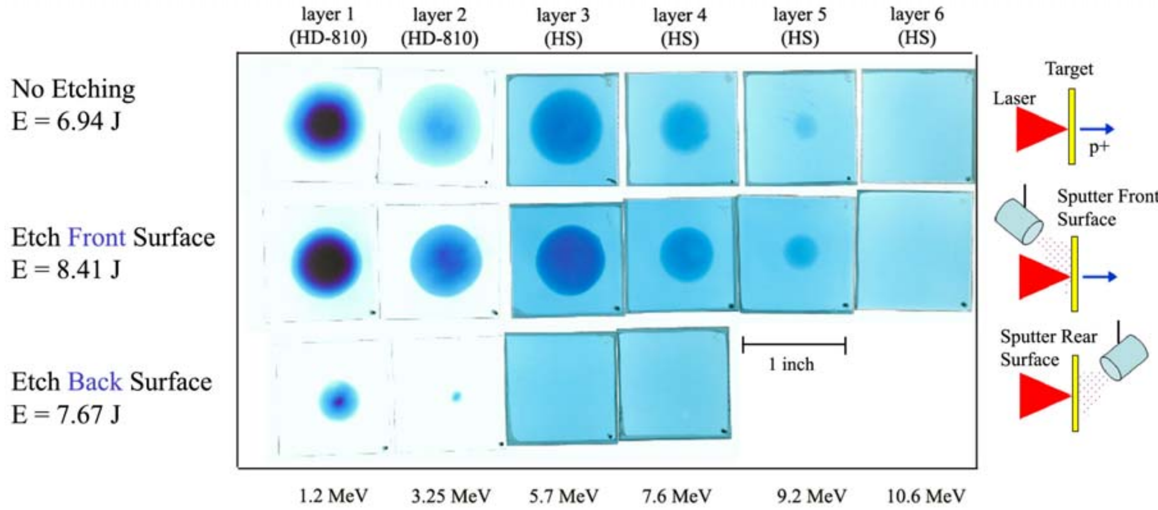

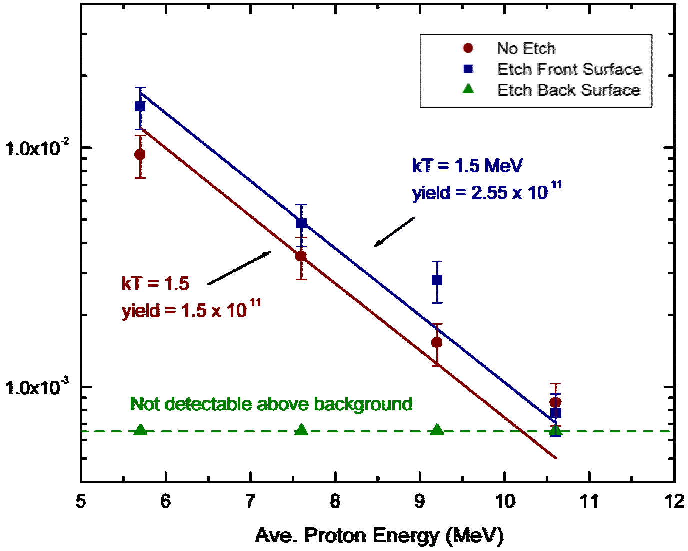

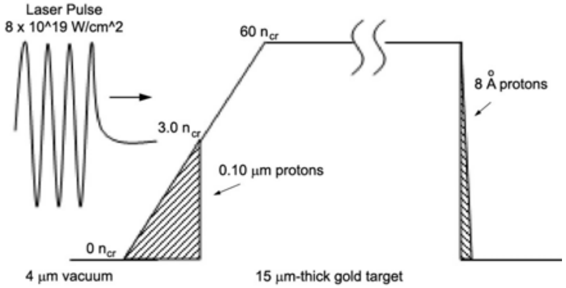

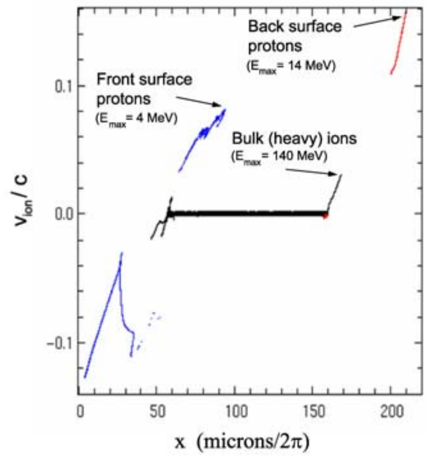

Matthew Allen, Pravesh K. Patel, Andrew Mackinnon, Dwight Price, Scott C. Wilks, and Edward Morse, “Experimental evidence of back-surface ion acceleration from laser irradiated foils”, submitted to PRL (2004).

Proton source experiments have revealed the effect of recirculating electrons on proton acceleration

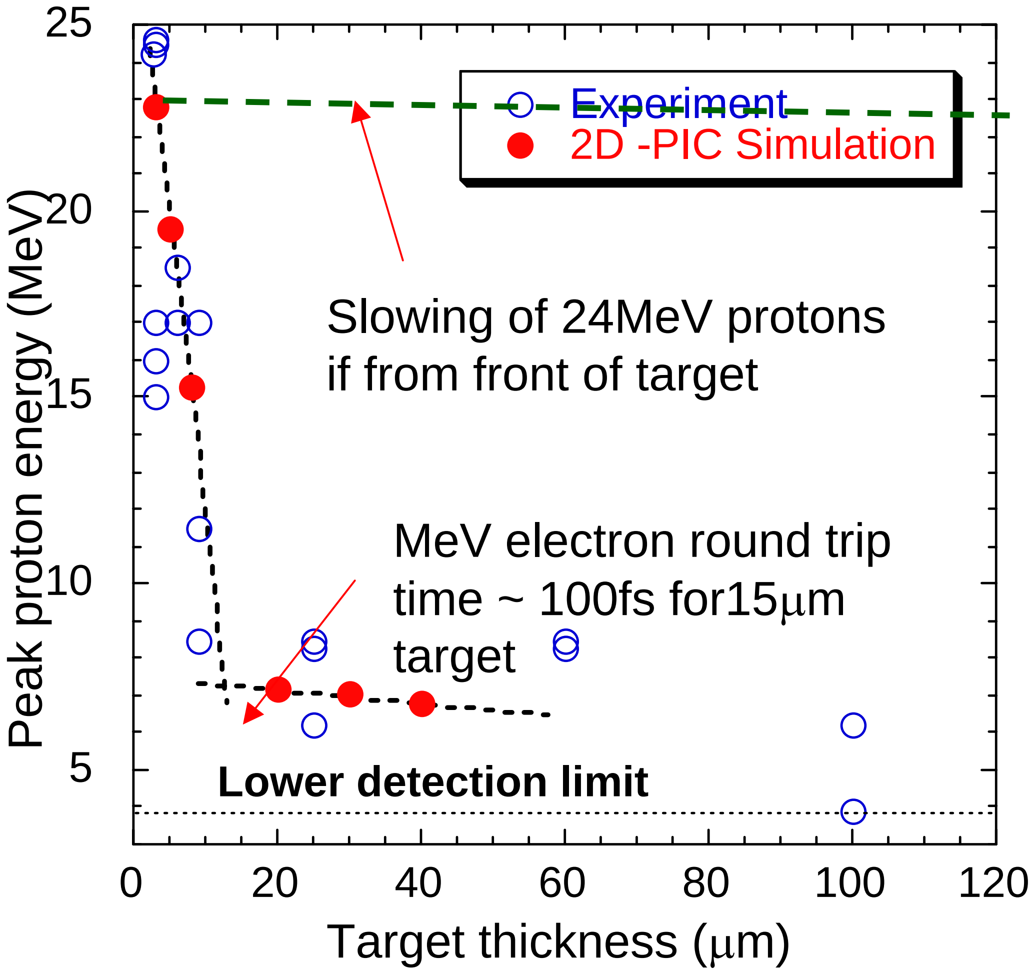

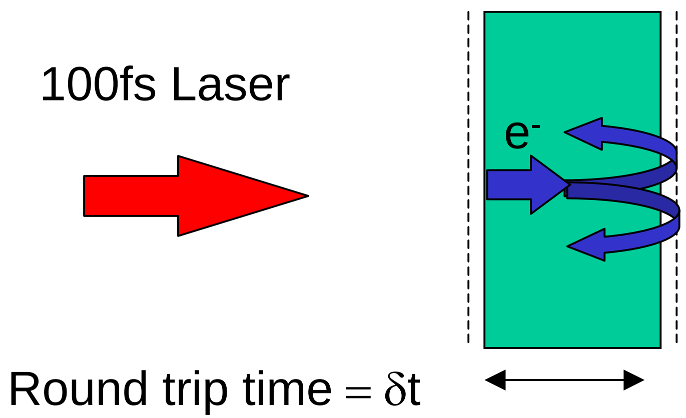

- MeV electrons highly relativistic: For 5μm target δt ~ 34fs
- Electrons re-circulate ~3 times before end of pulse
- Possible route to scaling to higher proton energies on large laser systems

A.J.Mackinnon et al., Physical Review Letters 88, 215006-1

In essence - for thin targets, larger fields accelerate protons for longer times, resulting in higher peak energies

Temporal evolution of E field

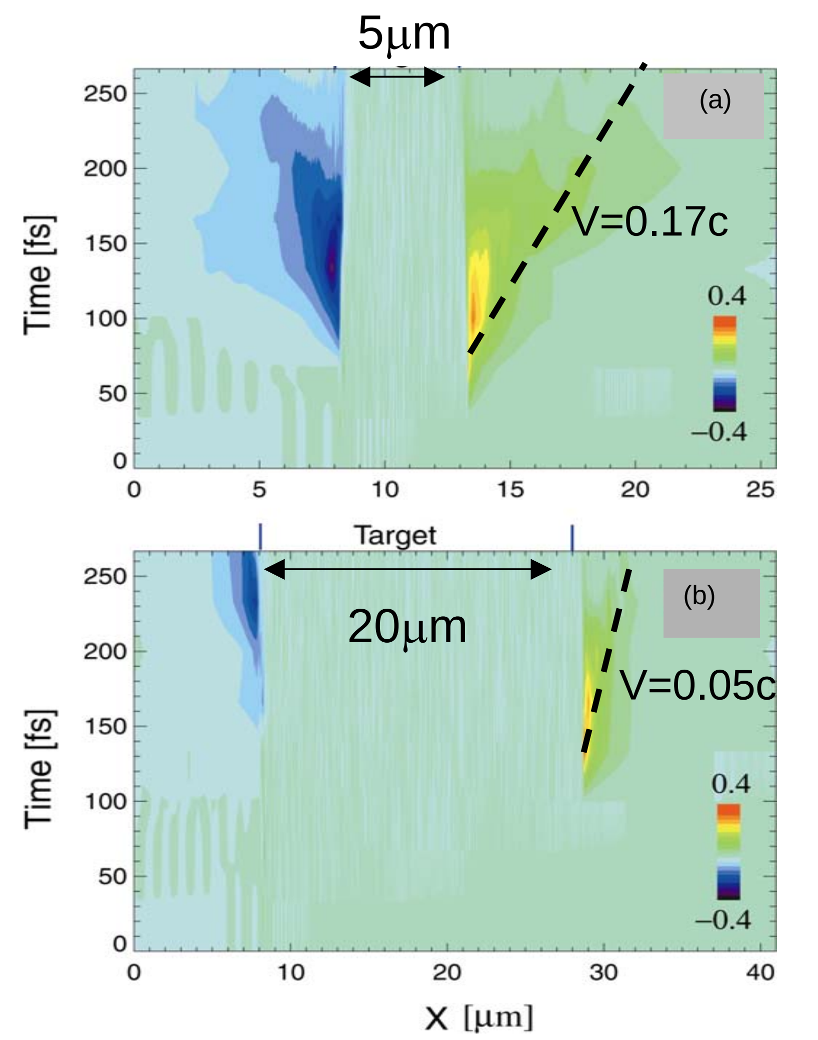

Proton energy vs time

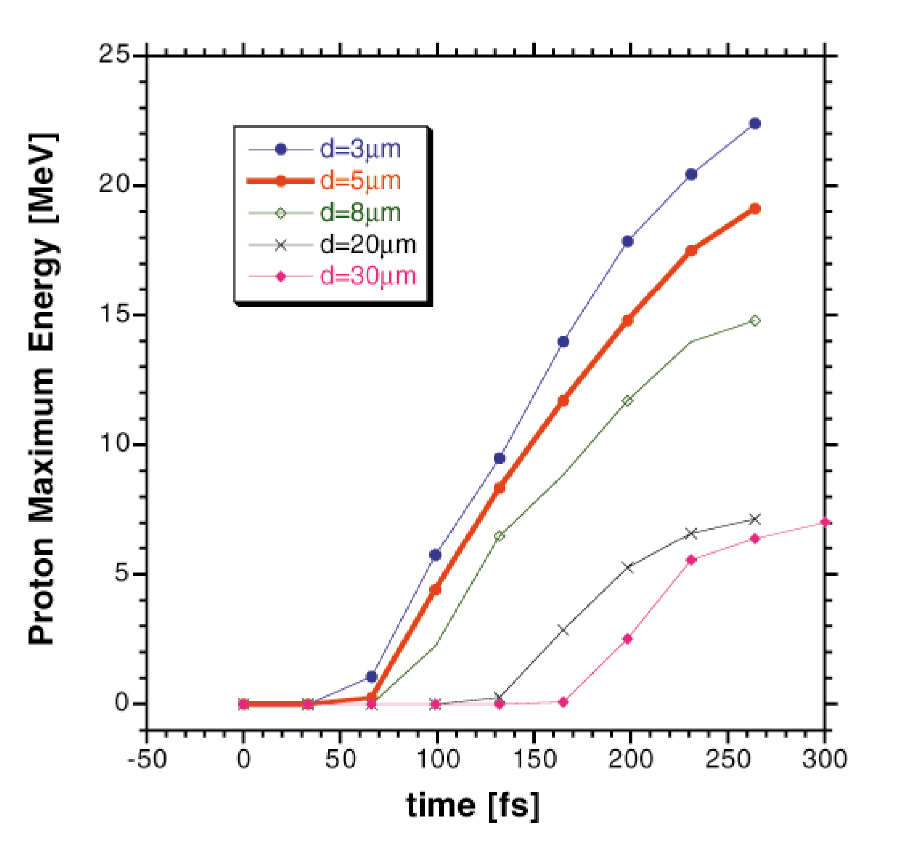

For targets thicker than a single round trip - acceleration begins only after the laser pulse turns off - giving the plateau region in the peak proton energy

 A.J.Mackinnon et al., Physical Review Letters 88, 215006-1

Andy Mackinnon "wish list"

Areas where we need simulations include realistic simulations of proton focusing in real targets.

1) For proton fast ignition do we need things like protector foils to make sure plasma,x-rays or scattered light do not perturb the proton foil. Can we simulate the sort of environment that that proton foil will be in.

2) What do we know about the space integrated lower energy part of the proton spectrum - from 5MeV down. This is difficult to measure and so we typically extrapolate down to ~1MeV by assume the slope does not change from a Boltzmann or maxellian at energies below 5MeV. This is maybe not a good assumption in all cases. Can simulations help here? (this is important for fast ignition)

Simple model of protons through grid, then through B field.

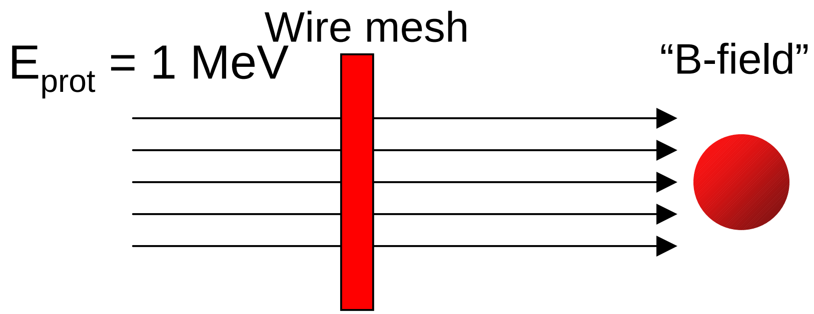

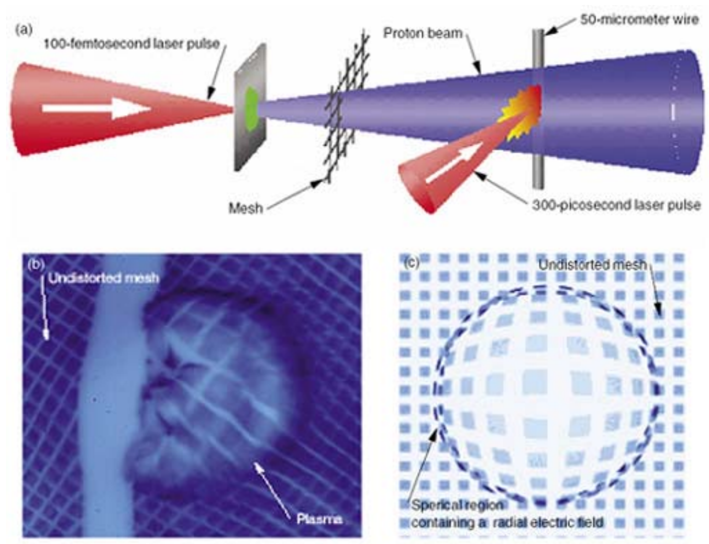

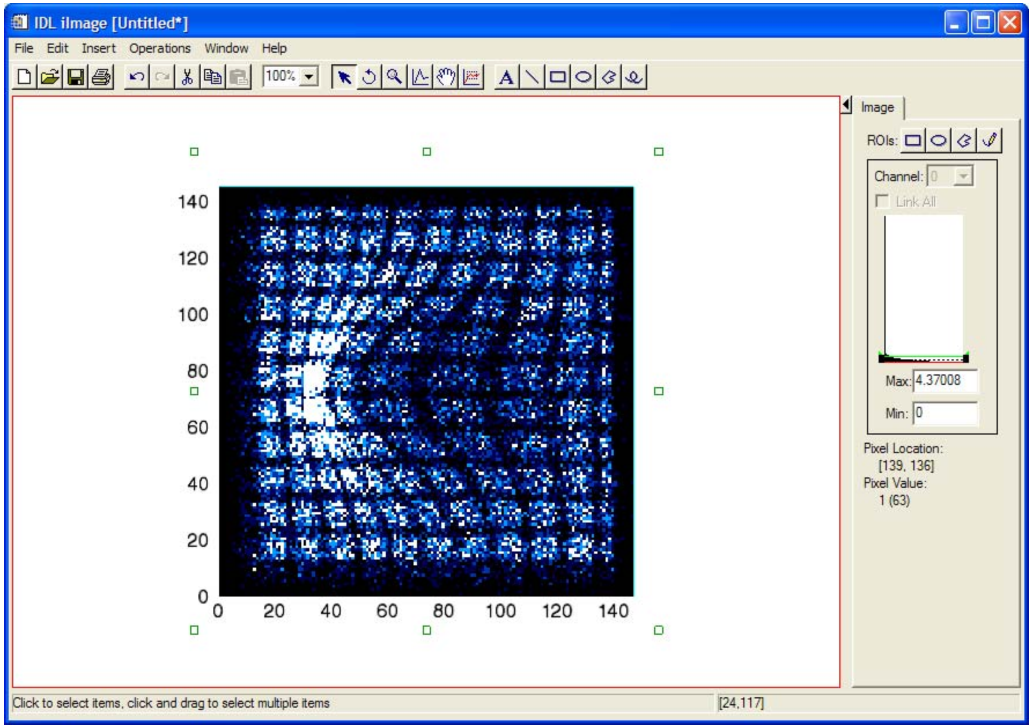

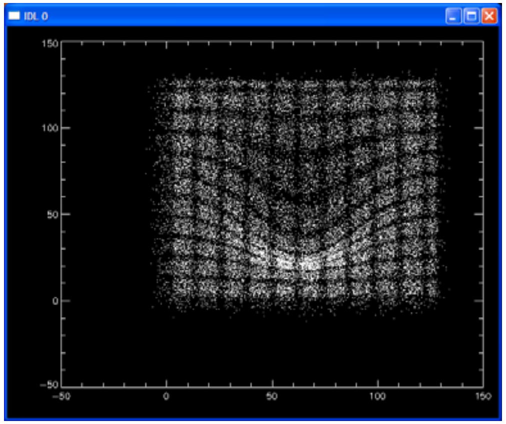

Kaluza, Schreiber, Santala, Tsakiris, Eidmann, MTV & Witte proton experiments.

VOLUME 93, NUMBER 4 PHYSICAL REVIEW LETTERS week ending 23 JULY 2004

Influence of the Laser Prepulse on Proton Acceleration in Thin-Foil Experiments

M. Kaluza, J. Schreiber, M. I. K. Santala, G. D. Tsakiris, K. Eidmann, J. Meyer-ter-Vehn, and K. J. Witte
Max-Planck-Institut für Quantenoptik, Hans-Kopfermann-Straße 1, D-85748 Garching, Germany
(Received 8 December 2003; published 20 July 2004)

We investigate the influence of the laser prepulse due to amplified spontaneous emission on the acceleration of protons in thin-foil experiments. We show that changing the prepulse duration has a profound effect on the maximum proton energy. We find an optimal value for the target thickness, which strongly depends on the prepulse duration. At this optimal thickness, the rear side acceleration process leads to the highest proton energies, while this mechanism is rendered ineffective for thinner targets due to a prepulse-induced plasma formation at the rear side. In this case, the protons are primarily accelerated by the front side mechanism leading to lower cutoff energies.

DOI: 10.1103/PhysRevLett.93.045003 PACS numbers: 52.38.Kd, 29.30.Ep, 41.75.Jv

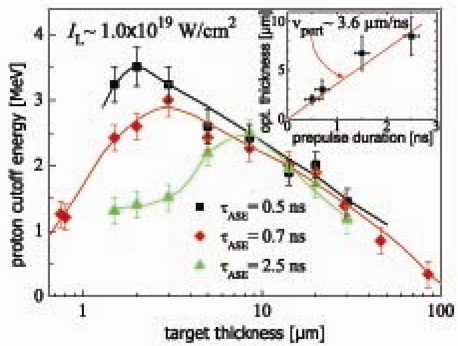

FIG. 1 (color). Proton cutoff energies for differently thick targets and prepulse durations, τ_{ASE}, of 0.5, 0.7, and 2.5 ns, respectively, at $I_L = 1.0 \times 10^{19}$ W/cm^2. For longer τ_{ASE}, the maximum proton energies are achieved with thicker foils. The inset gives the optimal thickness, depending on τ_{ASE}.

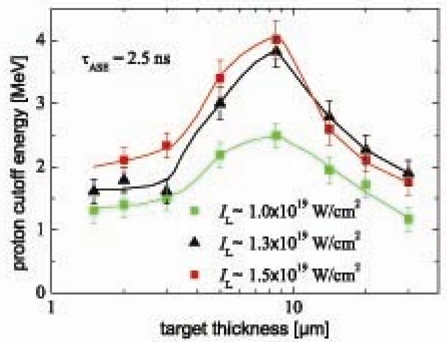

FIG. 2 (color). Proton cutoff energies for differently thick targets and different laser intensities for a prepulse duration of $\tau_{ASE} = 2.5$ ns. The cutoff energies vary with the laser intensity, but the optimal target thickness depends on τ_{ASE} only (cf. Fig. 1).

scw 8/30/2004

Prav experiments of proton focusing

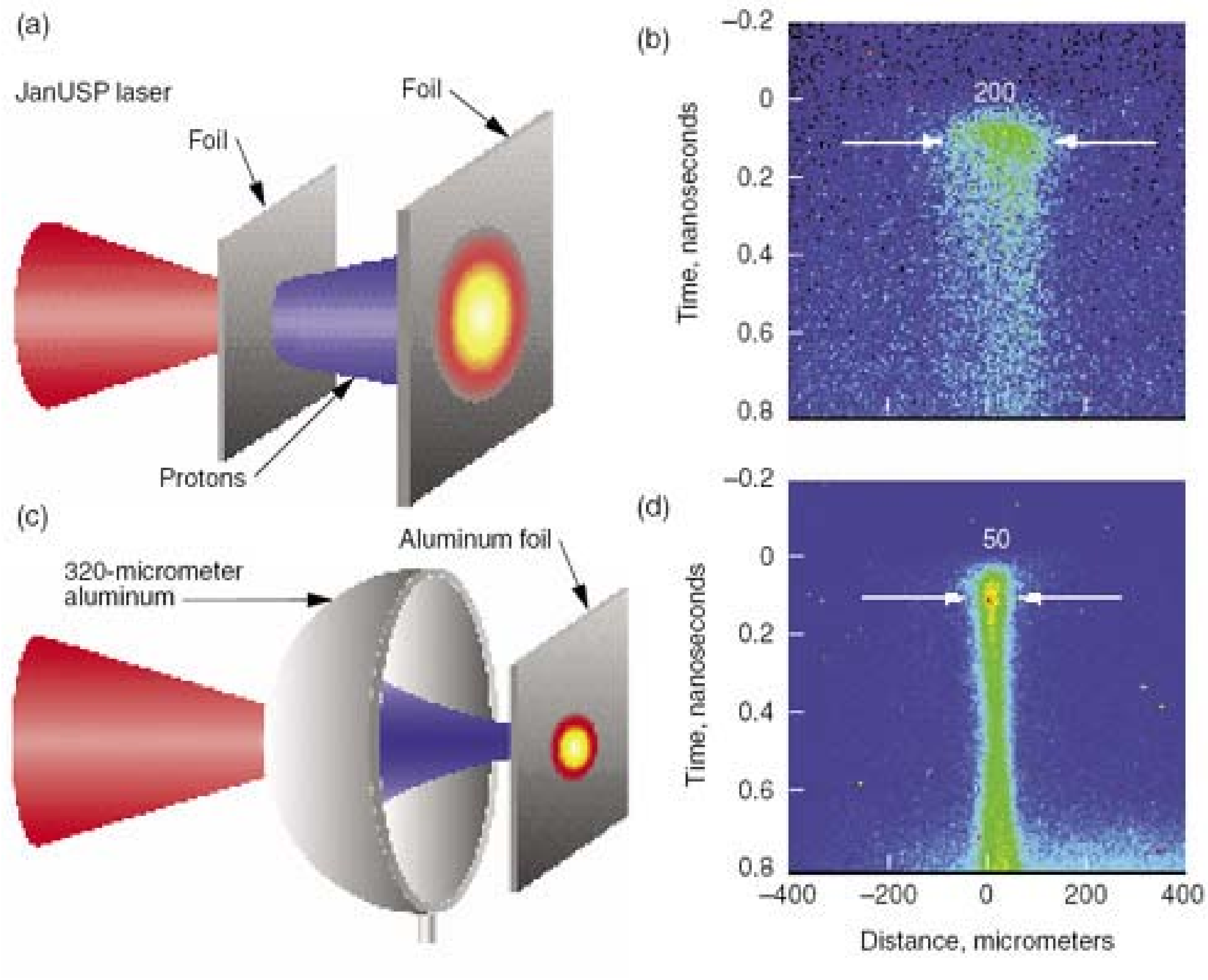

Prav Patel proton experiments December 2003 Science & Technology Review.

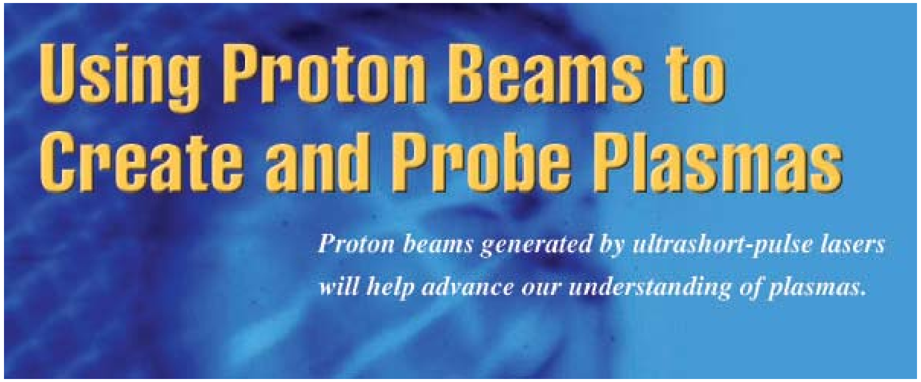

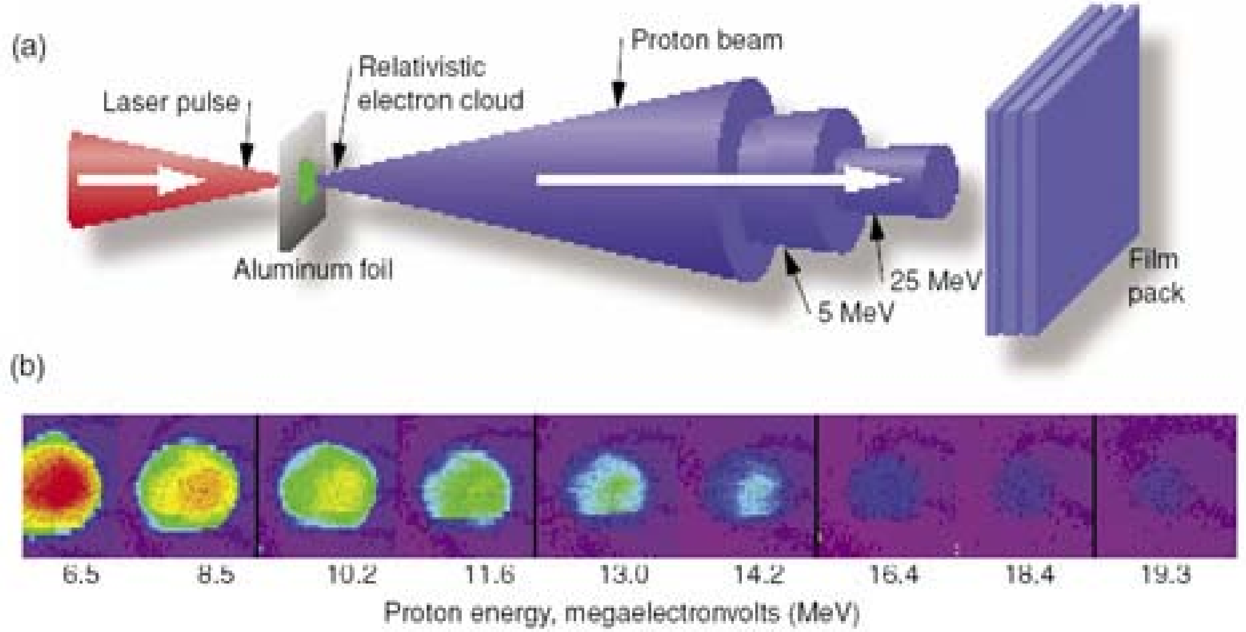

Another example: Proton experiments for Matt Allen.

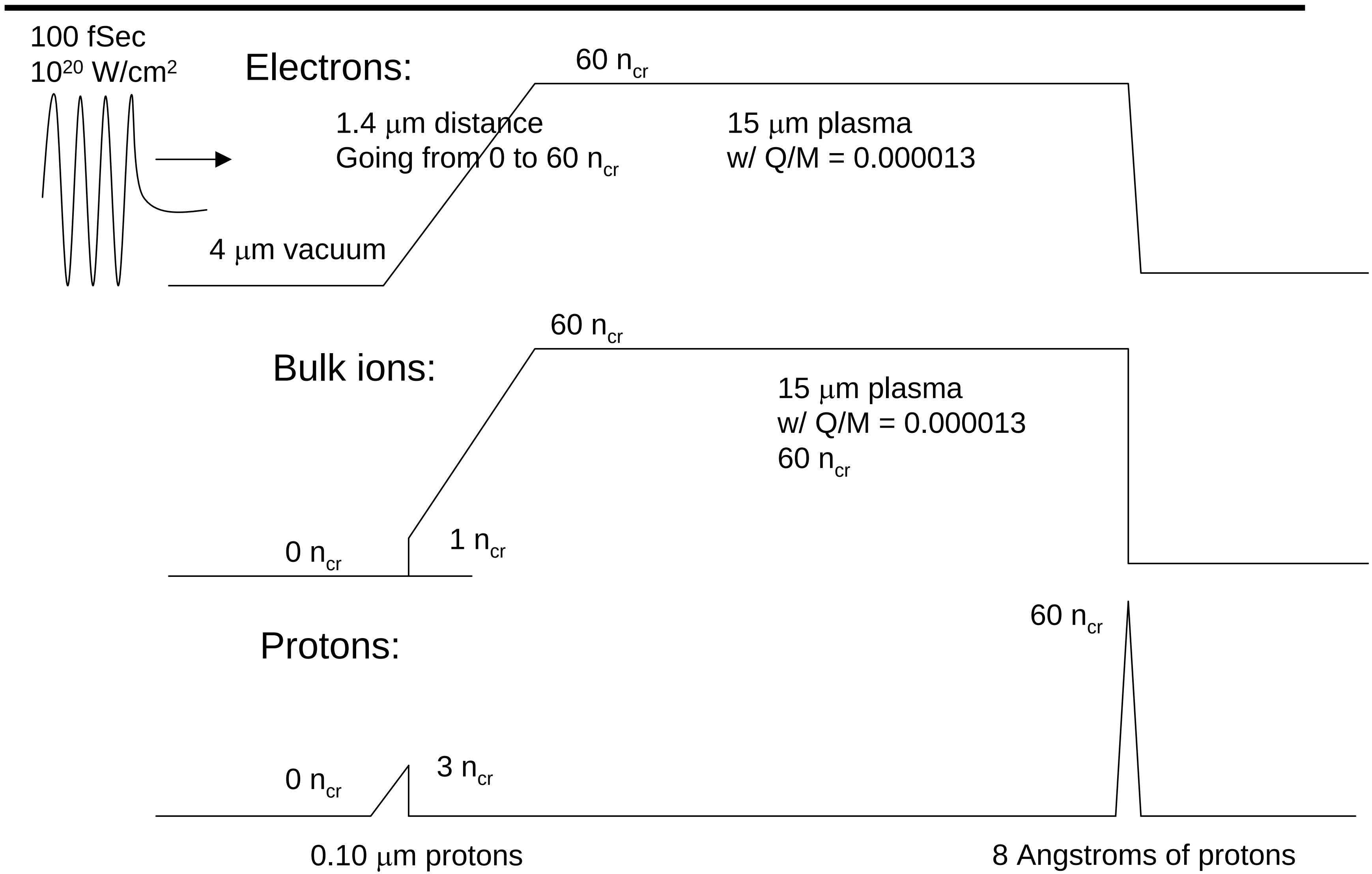

scw 8/30/2004

Nx = 500, dt = 0.05

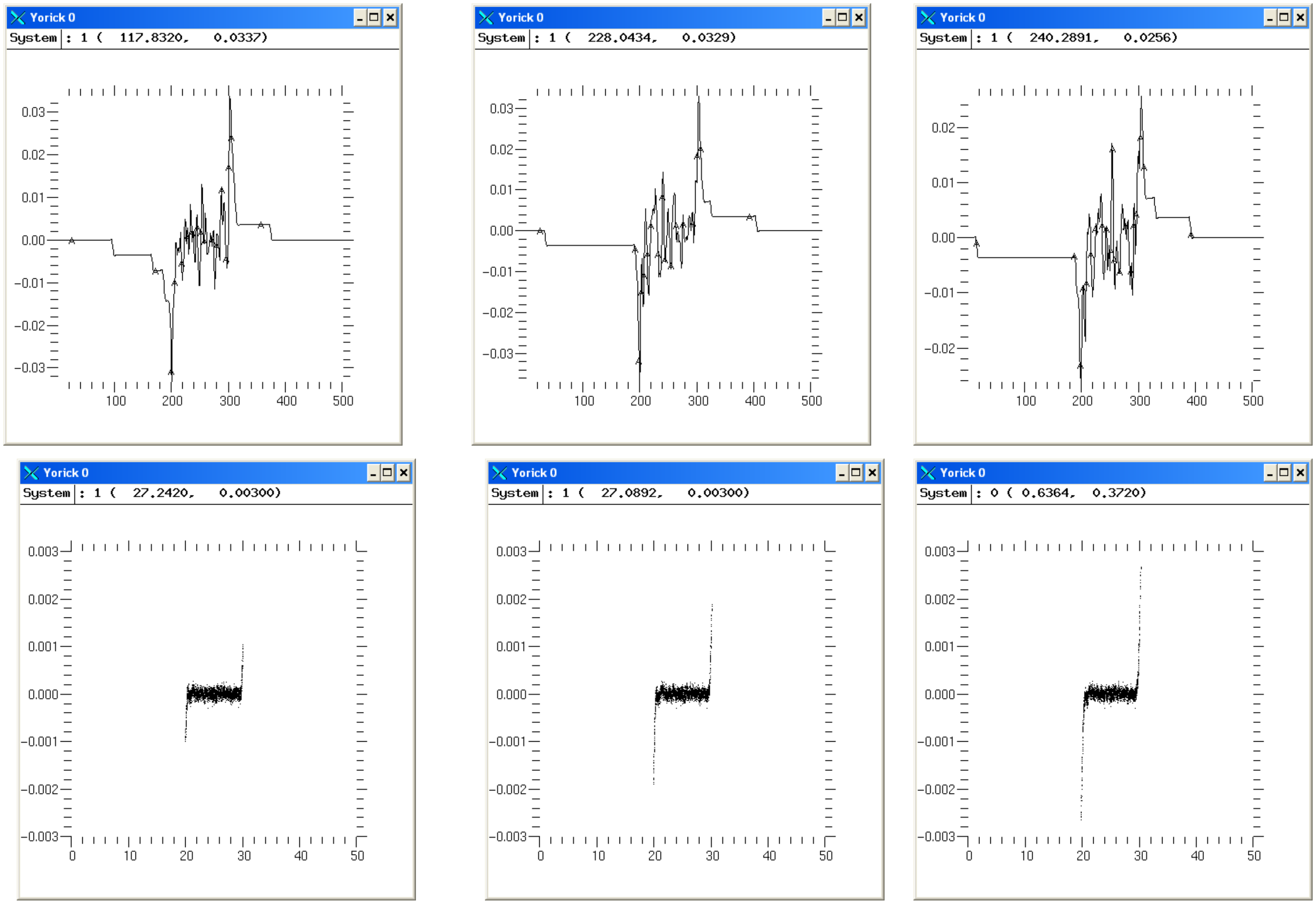
Yorick 0
System : 1 (117.8320, 0.0337)
0.03
0.02
0.01
0.00
−0.01
−0.02
−0.03
100
200
300
400
500
Yorick 0
System : 1 (228.0434, 0.0329)
0.03
0.02
0.01
0.00
−0.01
−0.02
−0.03
100
200
300
400
500
Yorick 0
System : 1 (240.2891, 0.0256)
0.02
0.01
0.00
−0.01
−0.02
100
200
300
400
500
Yorick 0
System : 1 (27.2420, 0.00300)
0.003
0.002
0.001
0.000
−0.001
−0.002
−0.003
0
10
20
30
40
50
Yorick 0
System : 1 (27.0892, 0.00300)
0.003
0.002
0.001
0.000
−0.001
−0.002
−0.003
0
10
20
30
40
50
Yorick 0
System : 0 (0.6364, 0.3720)
0.003
0.002
0.001
0.000
−0.001
−0.002
−0.003
0
10
20
30
40
50

Nx = 1000, dt = 0.04

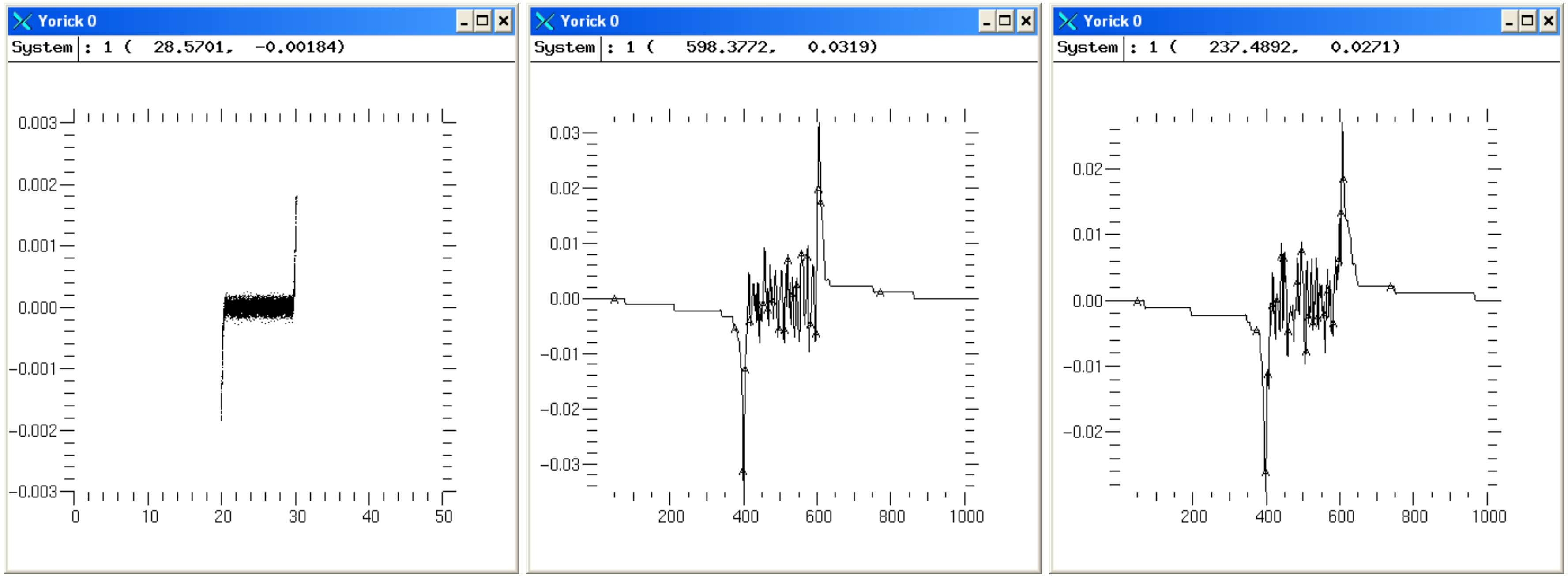

Compare with 2 different mass ratios for heavy ions (Au).

qm = 0.0000138

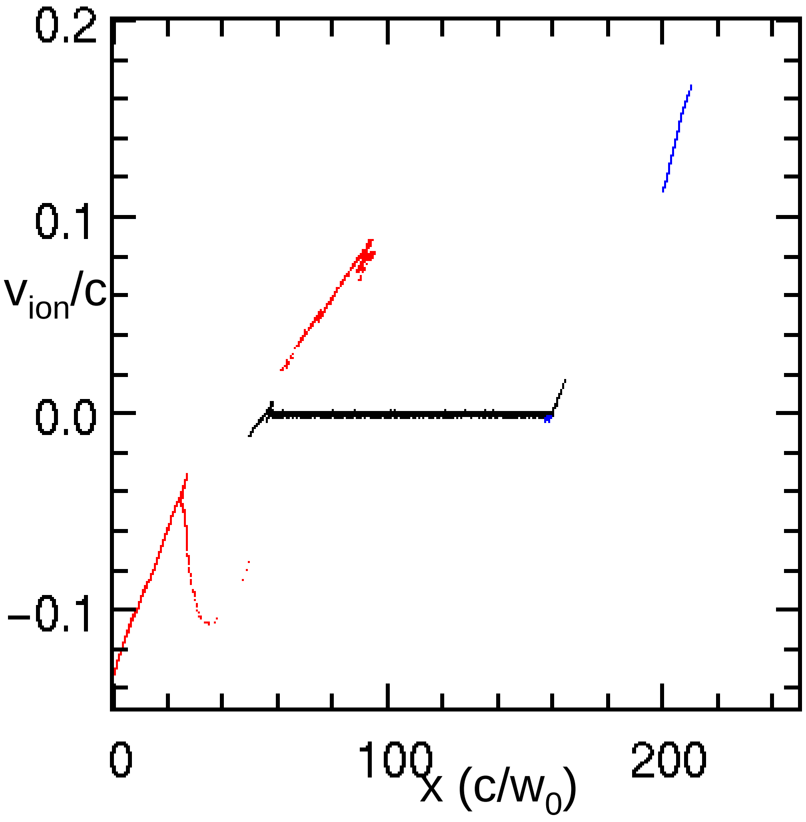

qm = 0.000038

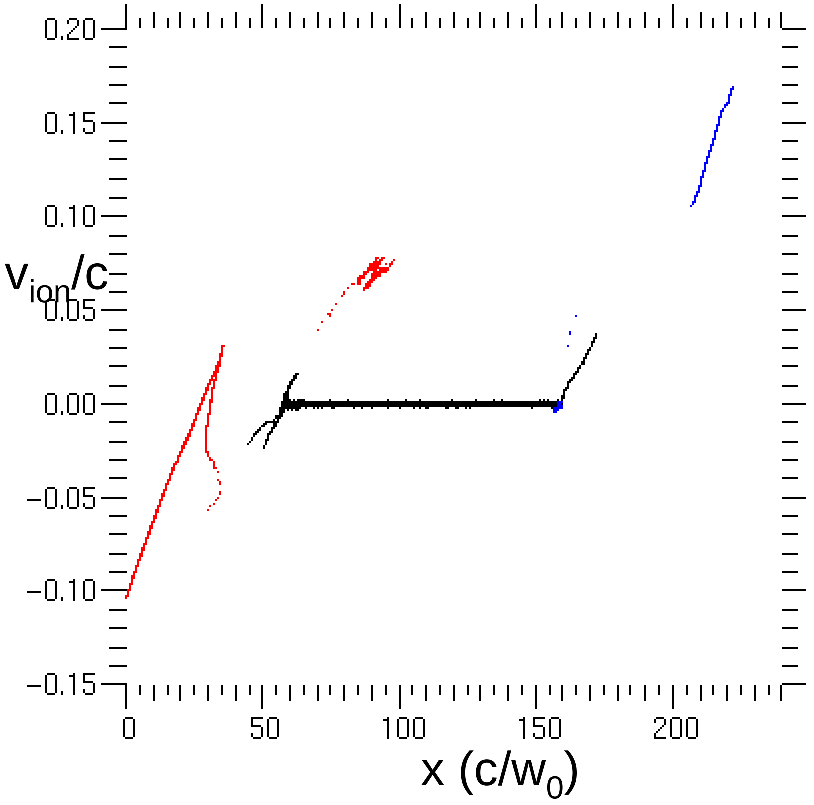

Vth/c = 0.1, n/ncr = 1.0

t = 0.04*1000 t = 0.04*5000 t = 0.04*8000

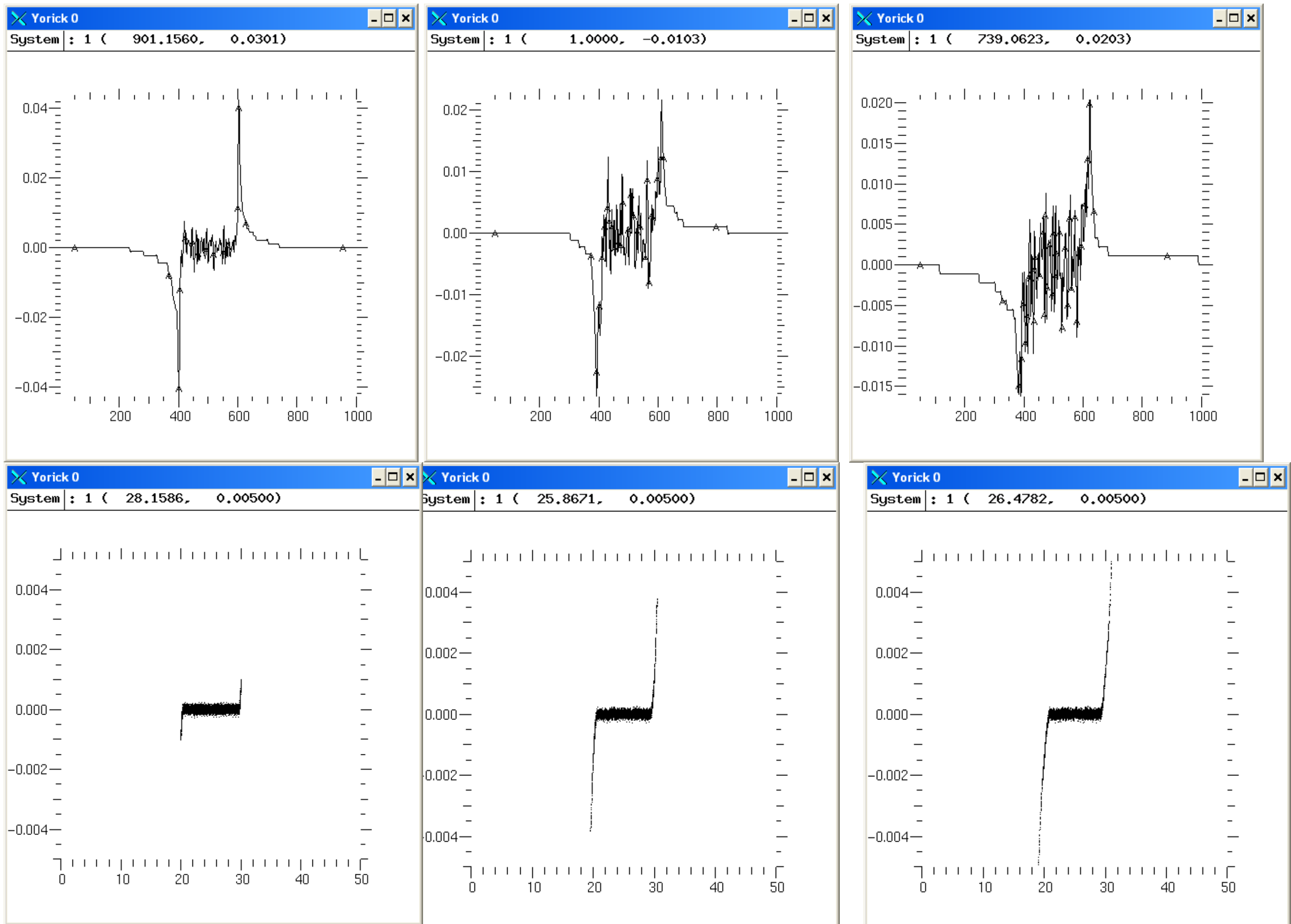

matt21 @ t = 500 fSec

Protons off the front:
0 MeV < E < 4 MeV

Protons off the back:
4.5 MeV < E < 10 MeV

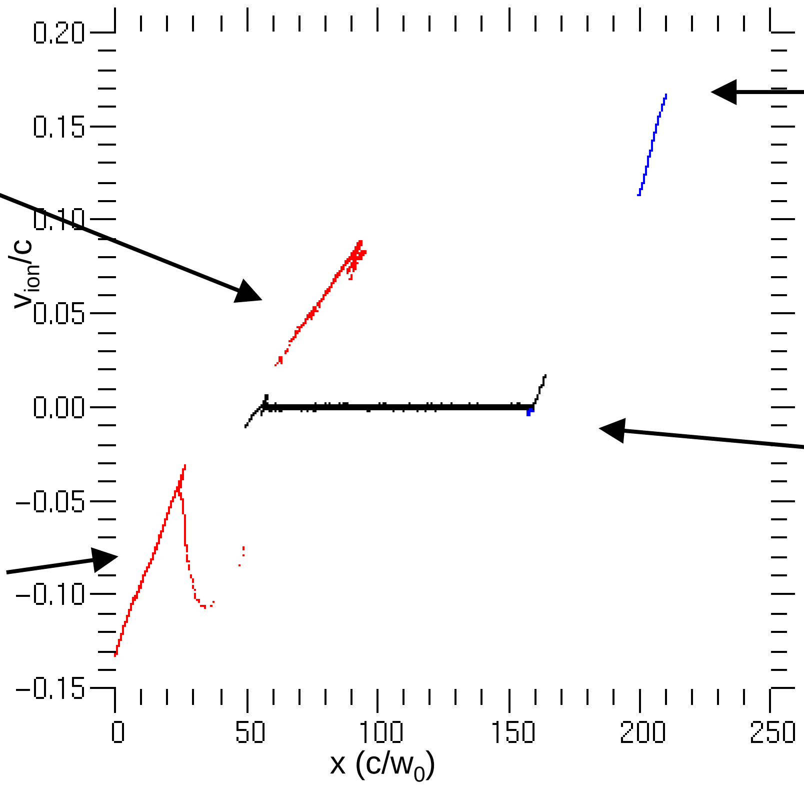

Bulk (heavy) ions

Protons off the front:
0 MeV < E < 4 MeV

scw 8/30/2004

Ion Acceleration Mechanisms in Ultra-Intense, Laser-Plasma Interactions

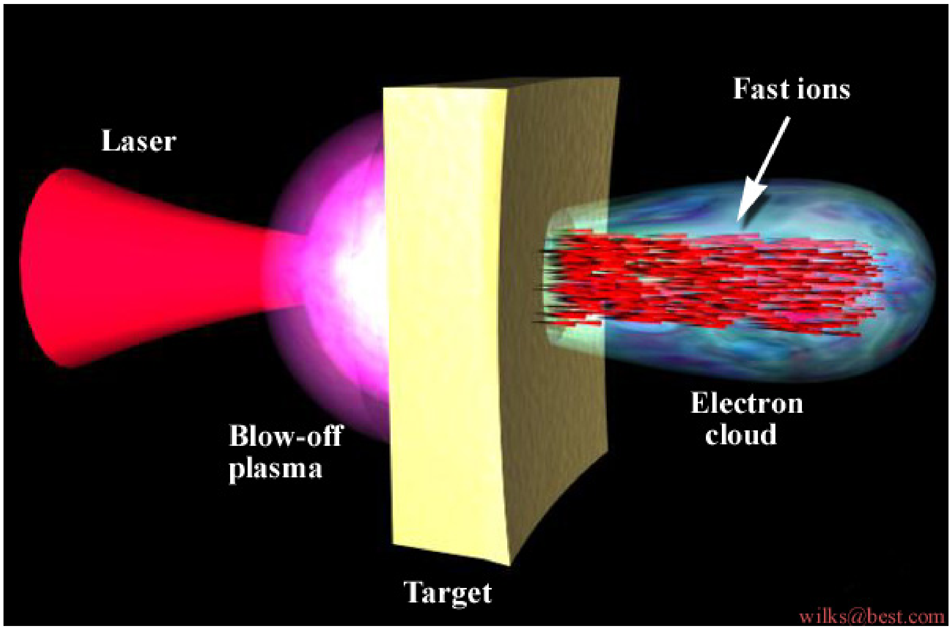

Scott C. Wilks, W. L. Kruer, T. Cowan, S. Hatchett, M. Key, B. Lasinski, A. B. Langdon, A. MacKinnon P. Patel, T. Phillips, P. Springer, R. Snavely

Lawrence Livermore National Laboratory
University of California
Livermore, CA 94550

and M. G. Haines

Imperial College of Science and Technology
UK, England, SW72BZ

For the American Physical Society, Division of Plasma Physics Meeting
Seattle, Washington
Nov. 15-19, 1999

This work was performed under the auspices of the US DOE under contract number: W-7405-ENG-48

Motivation: PetaWatt saw Copious Amounts of Ions off the Back of the Target.

Experimental Set-Up

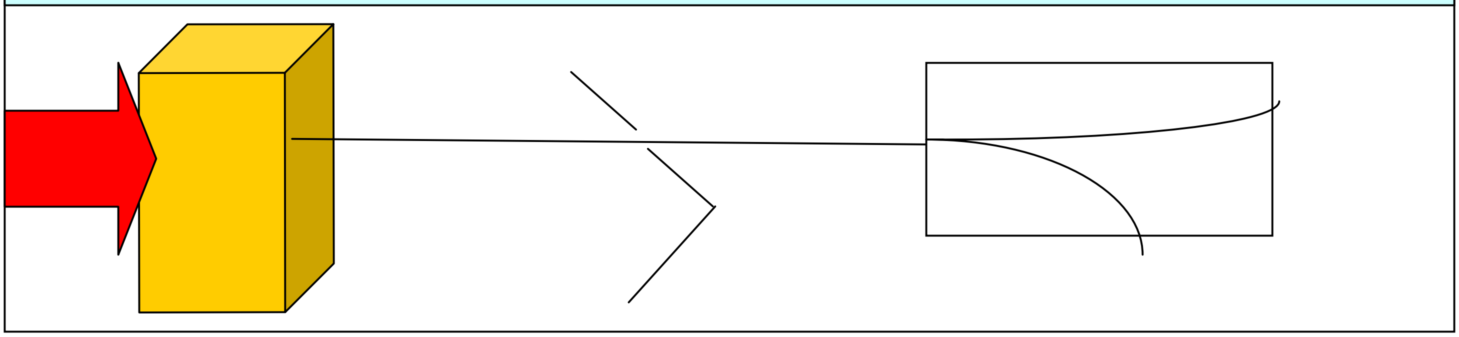

PetaWatt	Radiochromic Film	Ion/Electron Spectrometer
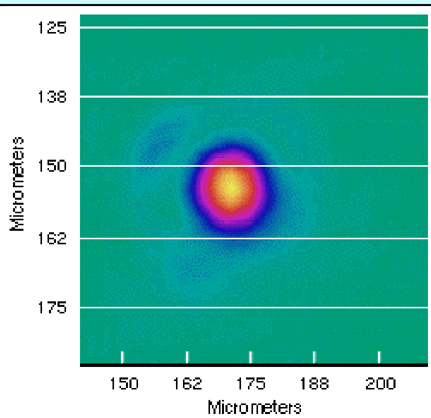	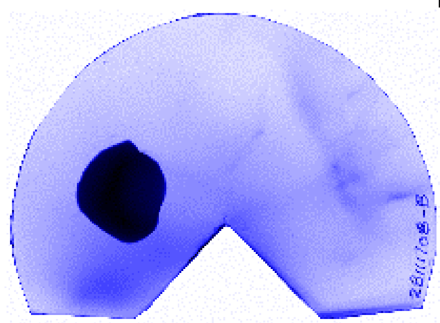	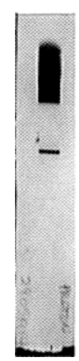

From these diagnostics, we determined that there were approximately $N_{ion}=3 \times 10^{13}$ protons[1] that come off the back in about a 400 micron spot[2], with energies up to about 50 MeV.

How can we explain these results?

1. R. Snavely, et. al. To be submitted PRL.
2. M. Roth, et. al. , to be submitted to PRL.

First Obvious Place to Look: Ions Created at Laser-Plasma Interface.

ION ACCELERATION MECHANISM #1

PetaWatt intensities could reach ~ 4 x 10^{20} W/cm^2. This can accelerate ions, via snowplow mechanism[2], to a couple MeV. Optimistic: $I\lambda^2=10^{21}$, $n/n_{cr}=50$, protons.

$$\frac{v_f}{c} = \sqrt{\left(\frac{n_{cr}}{n}\frac{Zm_e}{M_i}\frac{I\lambda^2}{2.7\times10^{18}}\right)} \approx 3MeV$$

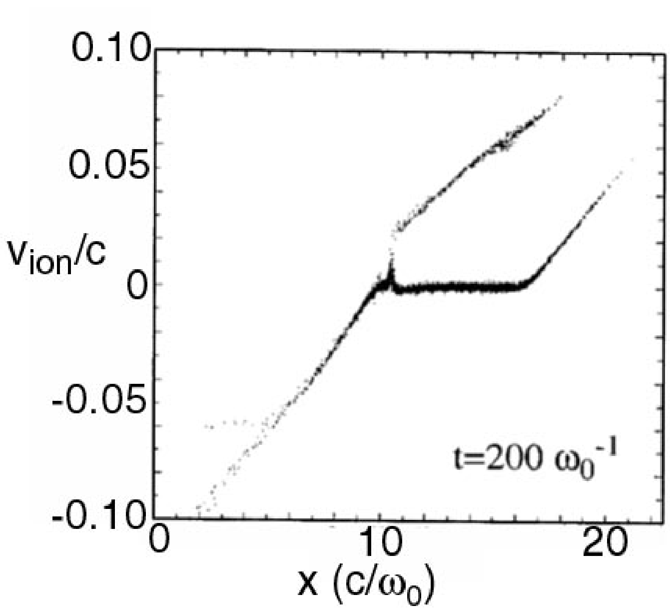

IS THIS THE MECHANISM?

Possible contribution, but: energy is too small and the angular divergence of the ion beam out the back is not consistent. Wedge target results kill it.

What was already known from Petawatt Experiments? Hot Electrons Produced.

Previous experimental work[1] on 100 Terawatt :hot electrons, agrees with predicted energies and levels[2].

$$T_{hot} \approx mc^2 \left[\sqrt{1 - \frac{I\lambda^2}{2.7 \times 10^{18}}} \right]$$

Electron spectrometer data from PetaWatt[3] showed that electron energies produced can exceed even these estimates: (~ 7 MeV effective T_{hots} for $I\lambda^2$=10^{20}).

Possibility: 10's of Joules of several MeV (~1-7 MeV) hot electrons are generated in the laser-plasma interaction region, and a large number are sent into and through the target.

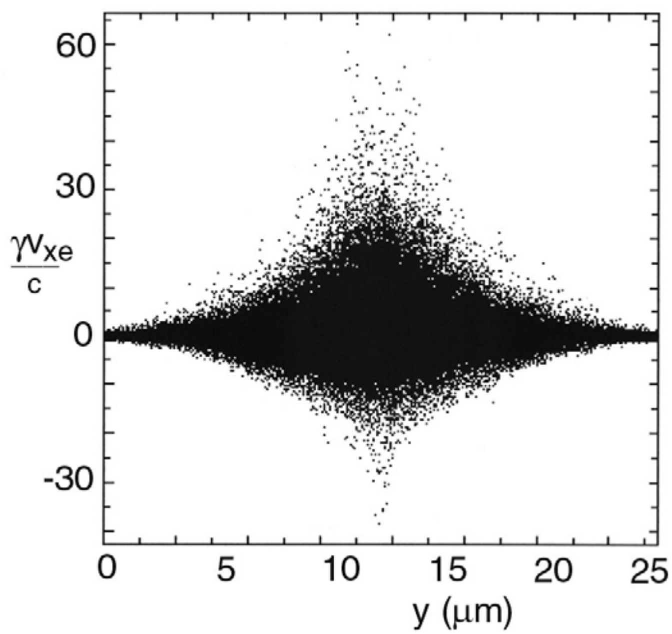

1. K. Wharton, et. al. PRL, (1998).
2. S. C. Wilks, et. al. IEEE (1997).
3. T. Cowan, et. al., PRL (1999).

Can these hot electrons go through the target, and accelerate ions off back?

Our model:

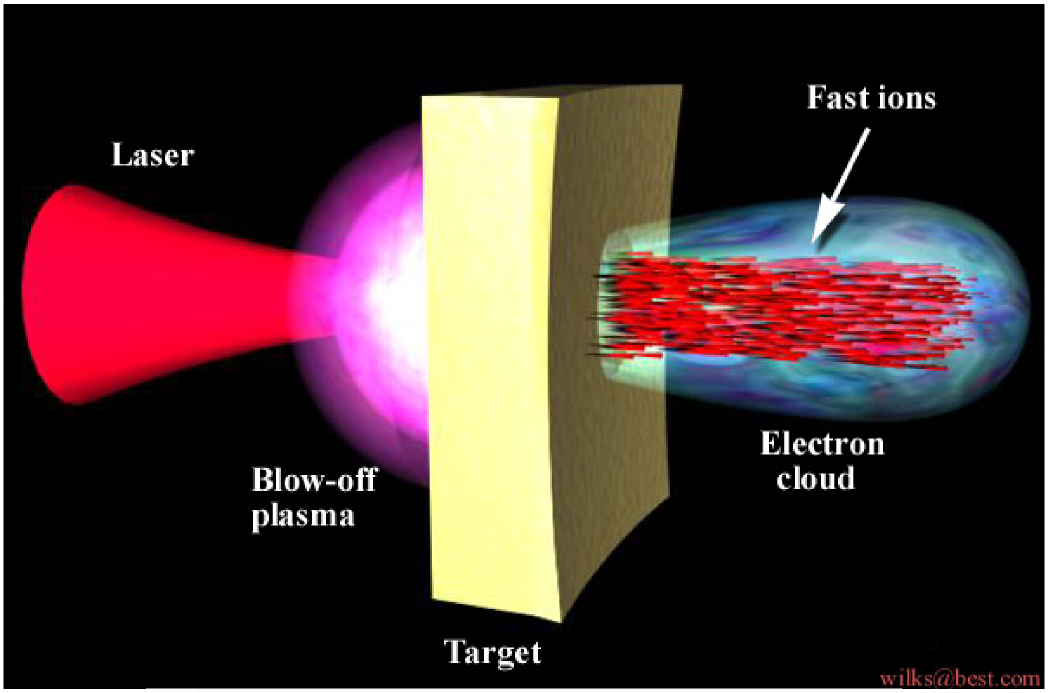

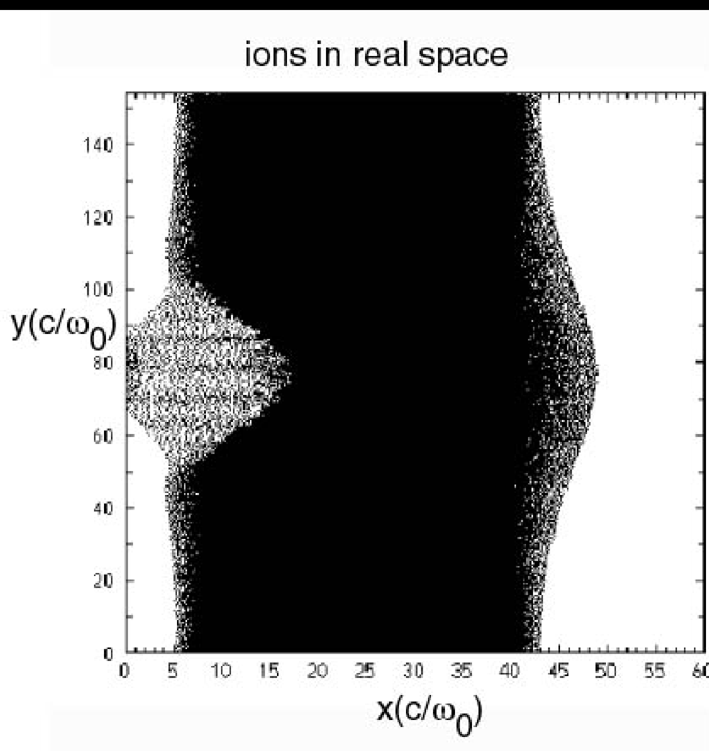

What causes these energetic ions off the back of the target?

Consider this simplified situation at back of target:

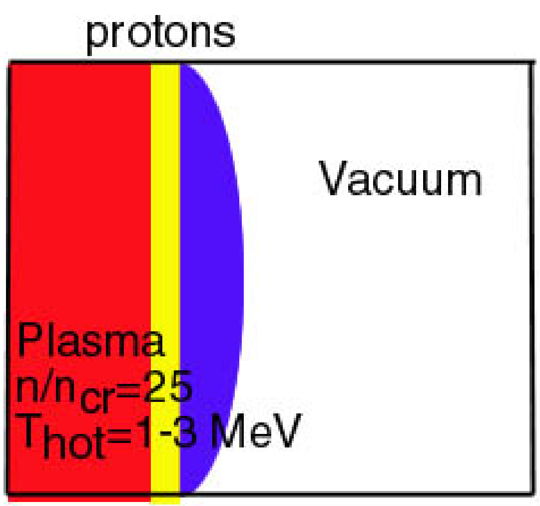

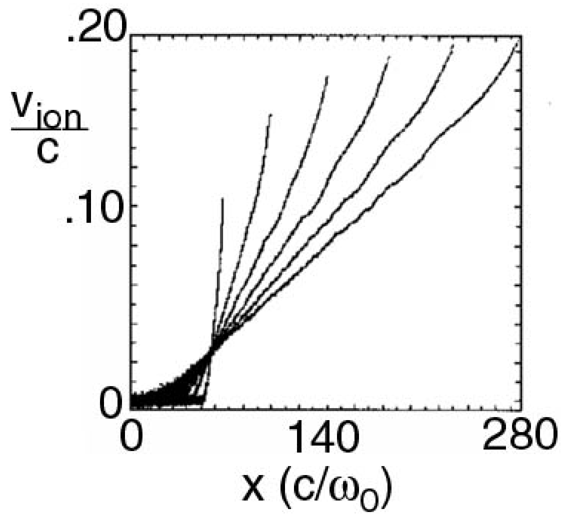

Similar to the much-studied, self-similar ion expansion solution, except Ln << l, MeV elecs. At t=0, and Te NOT constant.

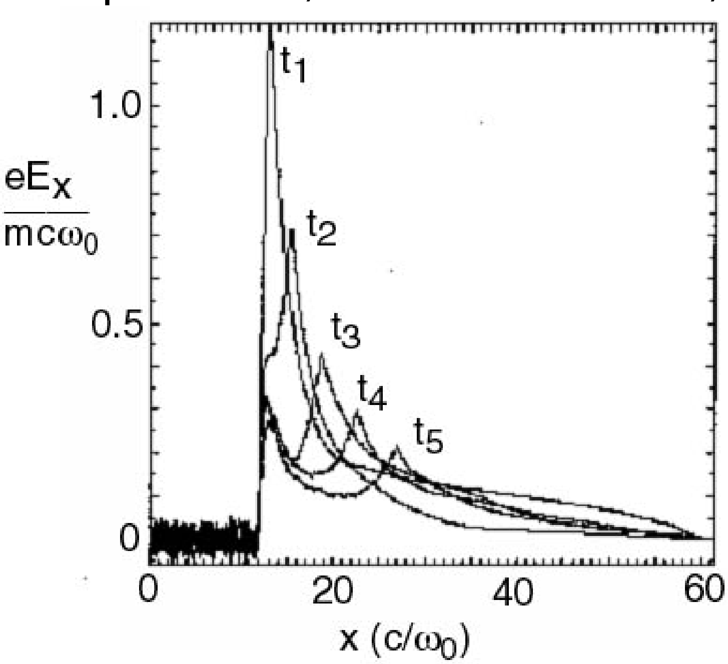

$$E = \frac{T_e}{eC_s t} = \frac{T_e}{eL_n}$$

$$E \approx 0.8\sqrt{\frac{n_{ef}}{n_{cr}}}\frac{T_e}{e\lambda_{De}}$$

Note: T_e NOT constant after laser shuts off. Electrons quickly cool.

Protons accelerated off back, as long as hot electrons present. Even for T_{hot}'s of ~ 1 MeV, 5 MeV ions are observed.

We find a strong dependence of E_{max} on the scale length of the plasma.

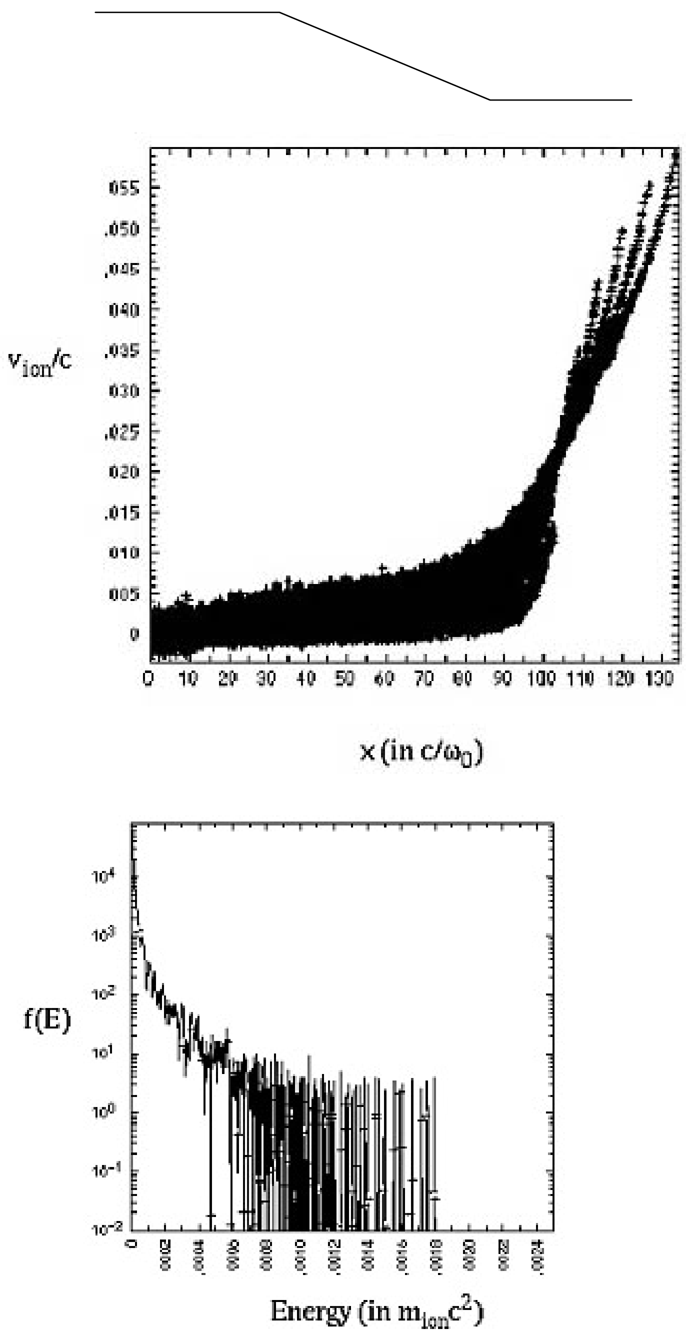

Fig. (6b) usp26 @ $\omega_0 t$=910, long scale length case, Max E_{ion} = 1.6 MeV.

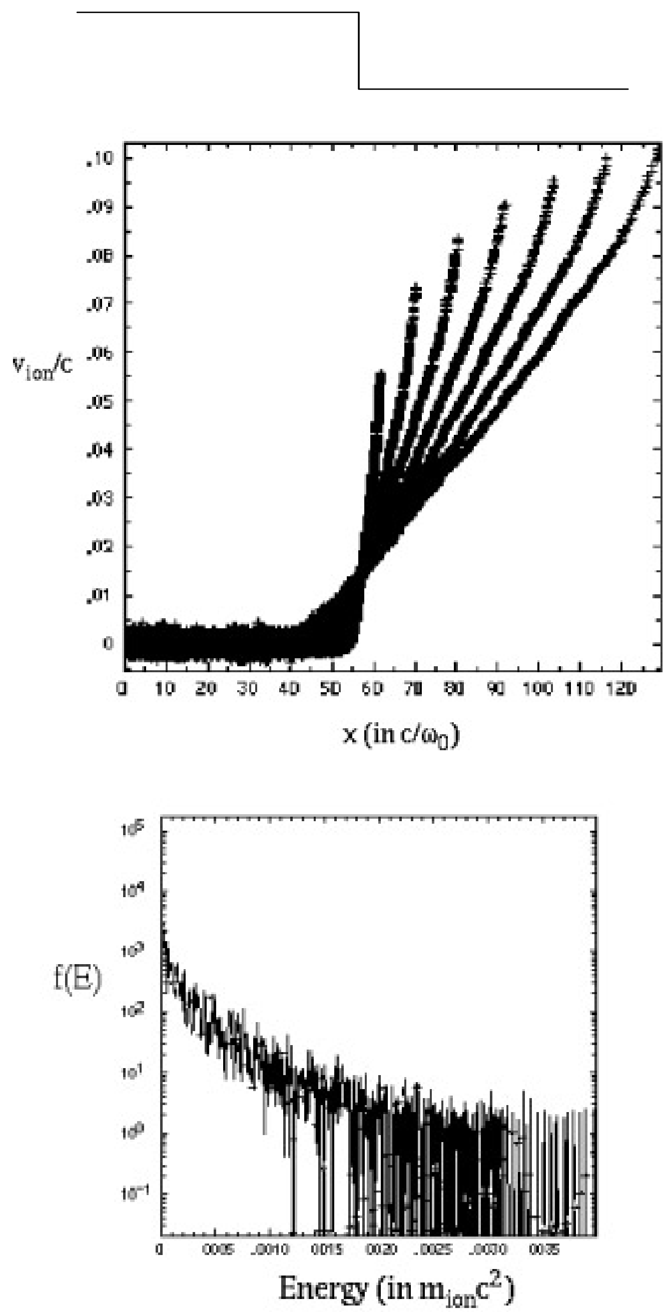

Fig. 3(b) usp27. Ion distribution function, for short density scalelength. Maximum ion energy is 5 MeV.

Sharper gradients => Higher Fields: Back of target sharp density profile. Not possible on front, due to prepulse.

What about the spatial distribution of the high energy ions?

What about 2-D? We use a 50 fSec, 4×10^{20} W/cm^2, r=2μm laser incident onto a 25 n/n_{cr} plasma. This generates the following hot electrons:

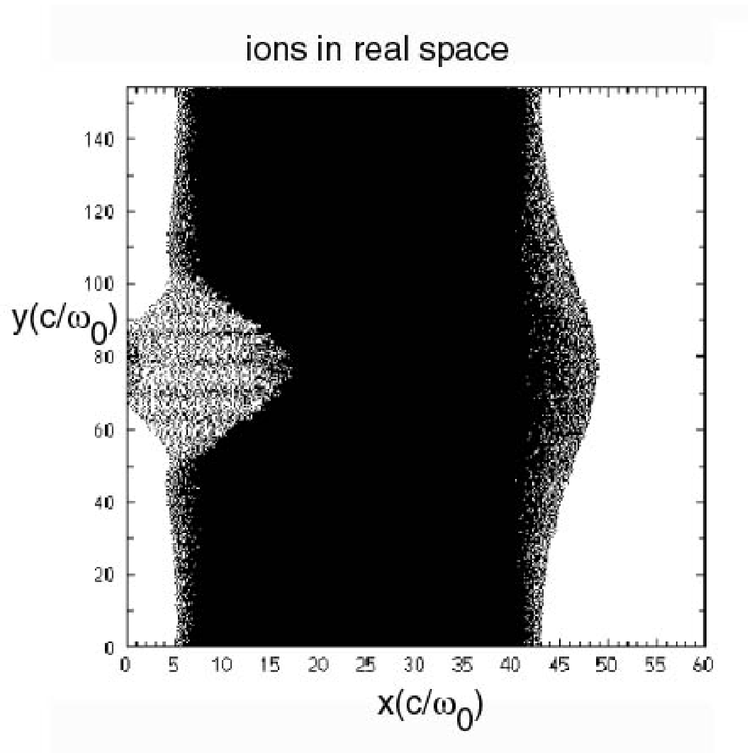

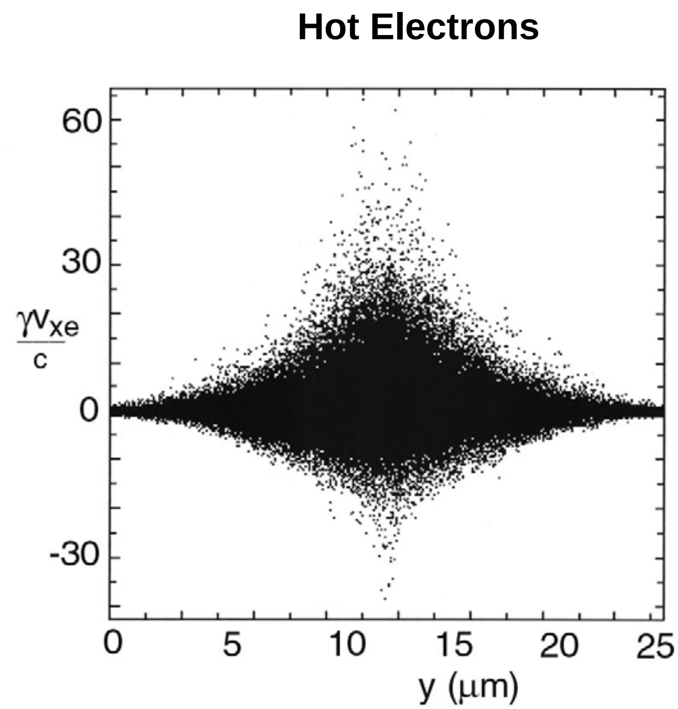

ion phase space

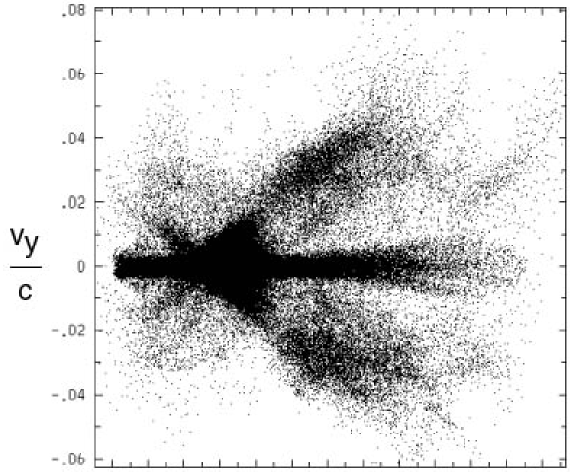

If we concentrate on ions off the back :

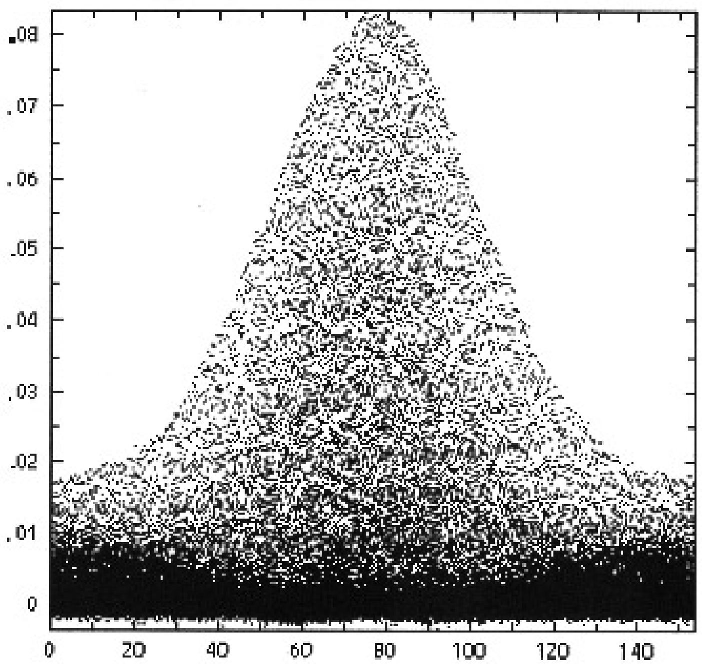

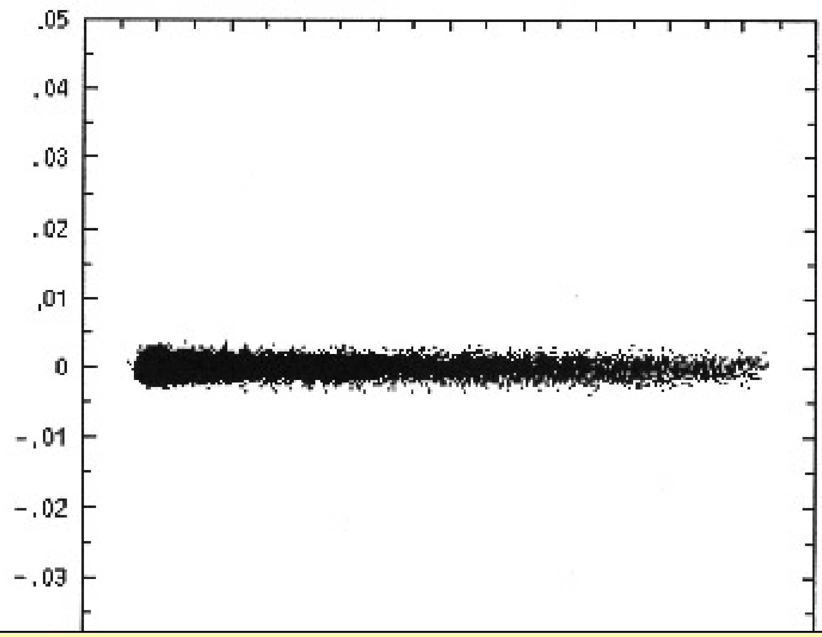

If this model is correct, one can imagine a "proton lens", by shaping the target.

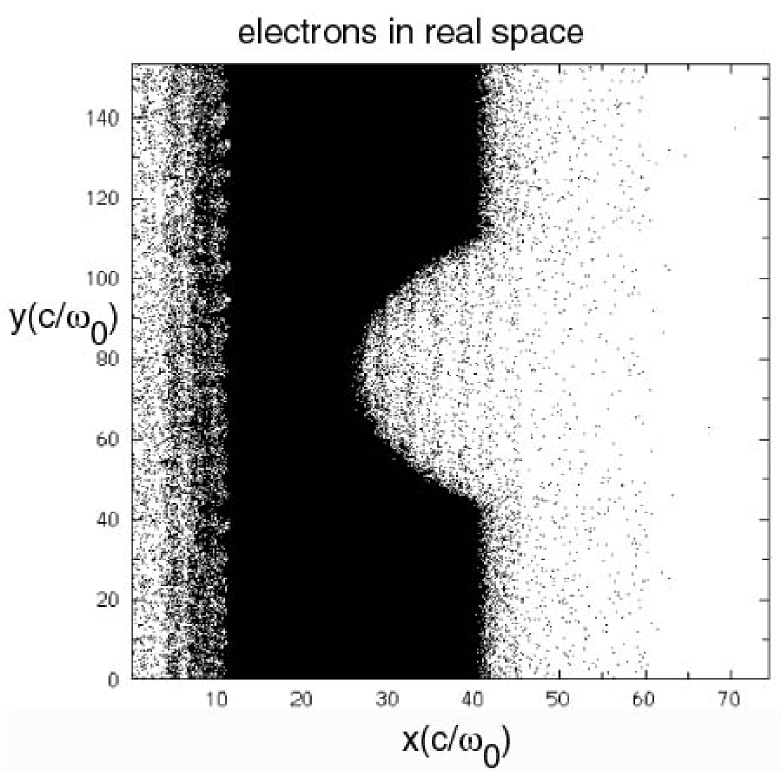

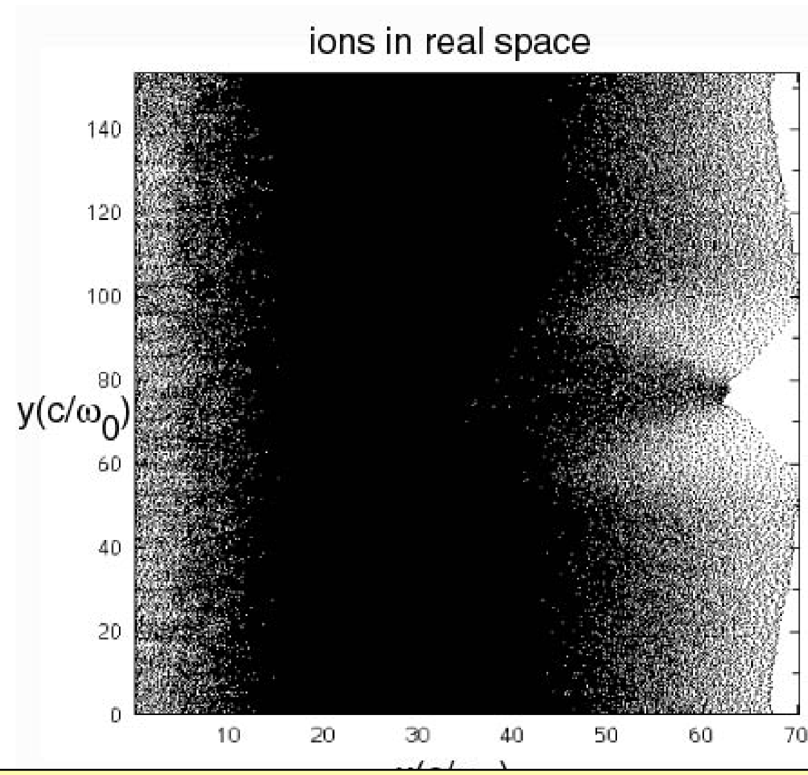

What are the limitations to this ion acceleration mechanism?

Maximum ion energy directly dependent on the electron energies.

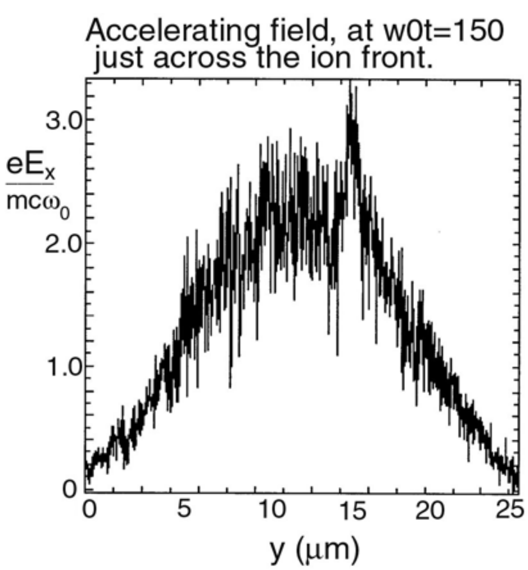

Scaling Laws for the ion energy, and efficiency.

Summary and Conclusions

By studying previous work on ion acceleration mechanisms, thinking about the hot electrons present, and doing ideal computer simulations, we came up with a possible explanation for the ions observed in the Petawatt experiments.

Properties of this ion acceleration mechanism:

1. Acceleration is normal to surface on back of target: typically occurs over a few micron distance.

2. Sharper density gradients give higher ion energies, for given electron distribution.
3. Maximum energy and number depend on electron energy distribution (total number, maximum energy.)
4. By shaping the back of the target, it may be possible to create an intense spot of energetic (~50 MeV) ions: less than a ½ micron in radius.